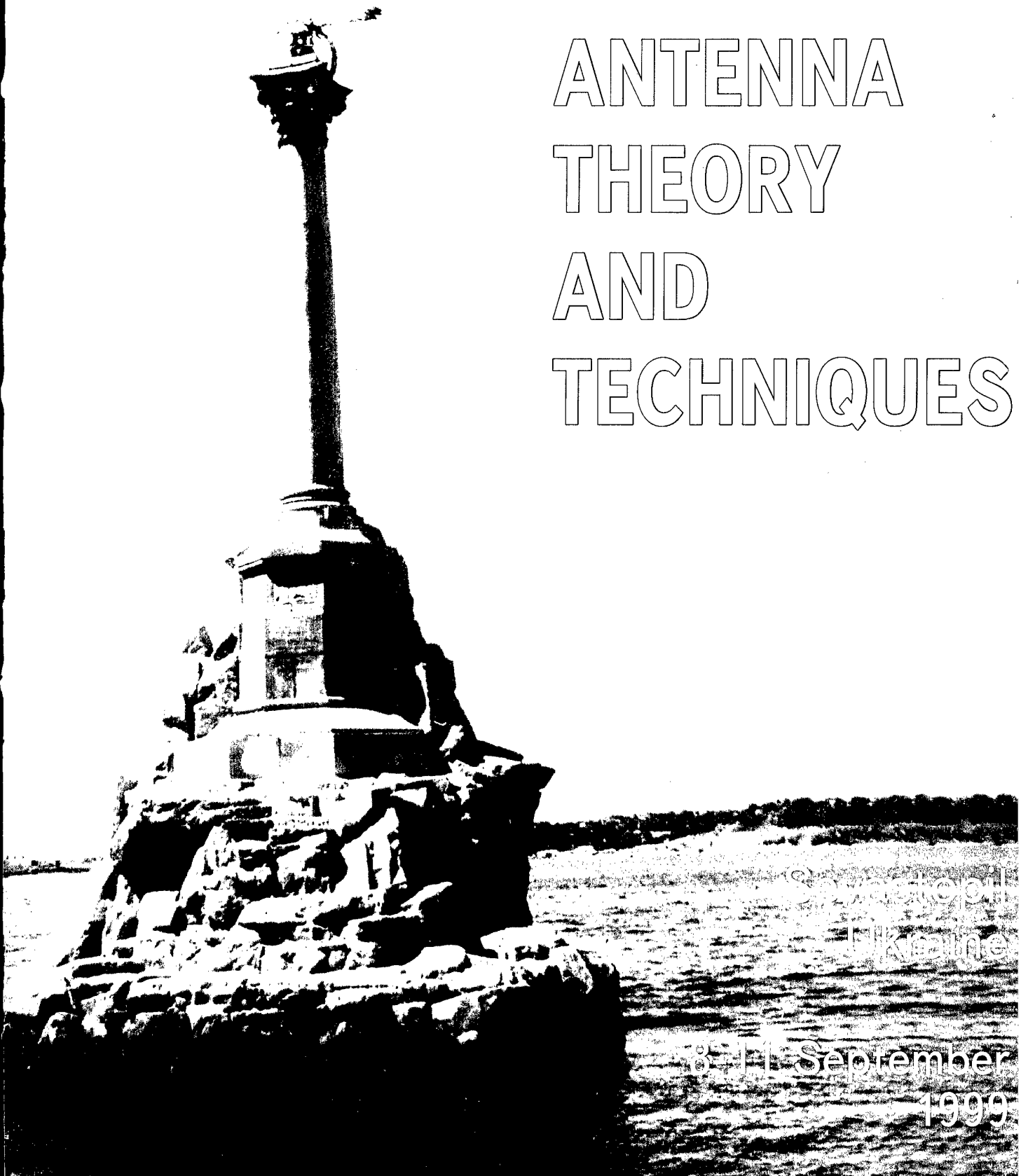
National Antenna Association
Ukraine

IEEE

Proceedings of IIIrd International Conference

ANTENNA THEORY AND TECHNIQUES



Ukraine

8-11 September
1999

REPORT DOCUMENTATION PAGE

Form Approved OMB No. 0704-0188

Public reporting burden for this collection of information is estimated to average 1 hour per response, including the time for reviewing instructions, searching existing data sources, gathering and maintaining the data needed, and completing and reviewing the collection of information. Send comments regarding this burden estimate or any other aspect of this collection of information, including suggestions for reducing this burden to Washington Headquarters Services, Directorate for Information Operations and Reports, 1215 Jefferson Davis Highway, Suite 1204, Arlington, VA 22202-4302, and to the Office of Management and Budget, Paperwork Reduction Project (0704-0188), Washington, DC 20503.

1. AGENCY USE ONLY (Leave blank)	2. REPORT DATE	3. REPORT TYPE AND DATES COVERED
	September 1999	8-11 September 1999 Final Report

4. TITLE AND SUBTITLE
Proceedings of the Third International Conference on Antenna Theory and Techniques.. 8-11 September 1999. Sevastopil, Ukraine.

5. FUNDING NUMBERS
N000-99-1-1033
F 61775-99-WF071

6. AUTHOR(S)
Multiple

7. PERFORMING ORGANIZATION NAME(S) AND ADDRESS(ES)
Sevastopil State Technical University
Sevastopil, Ukraine

8. PERFORMING ORGANIZATION REPORT NUMBER
ISBN 966-622-012-1

9. SPONSORING/MONITORING AGENCY NAME(S) AND ADDRESS(ES)
Office of Naval Research]
European Office
PSC 802 Box 39
FPO AE 09499-0039

10. SPONSORING/MONITORING AGENCY REPORT NUMBER

11. SUPPLEMENTARY NOTES
This work relates to Department of the Navy Grant issued by the Office of Naval Research International Field Office. The United States has a royalty free license throughout the world in all copyrightable material contained herein.

12a. DISTRIBUTION/AVAILABILITY STATEMENT
Approved for Public Release; Distribution Unlimited.
U.S. Government Rights License. All other rights reserved by the copyright holder.

12b. DISTRIBUTION CODE
A

12. ABSTRACT (Maximum 200 words)

ICCAT99 had over 200 contributed papers, grouped in topical areas about:

- General antenna theory- Reflector, lens and hybrid antennas, - Antenna Arrays, - Adaptive Antenna Arrays, - Low Gain antennas, printed antennas and antennas for mobile communications,- Broadband and multi frequency antennas, - Computational methods, - Antenna measurements, - Microwave components and circuits, fiber optical links, - Industrial and medical applications of microwave technologies.- Electromagnetics in high schools.
-
- See http://www.stel.sebastopol.ua/rt_sevgtu/icatt99.htm for a general conference overview.

The conference organizers include the National Antenna Association of the Ukraine, the National Technical University of Ukraine "Kiev Polytechnic Institute", IEEE AP/MTT/AES/ED/LEO/GRS-SS Joint Chapter, and Sevastopil State Technical Unversity.

13. SUBJECT TERMS
Antenna theory, Microwaves, Electromagnetics, Foreign reports

15. NUMBER OF PAGES

16. PRICE CODE

17. SECURITY CLASSIFICATION OF REPORT	18. SECURITY CLASSIFICATION OF THIS PAGE	19, SECURITY CLASSIFICATION OF ABSTRACT	20. LIMITATION OF ABSTRACT
UNCLASSIFIED	UNCLASSIFIED	UNCLASSIFIED	UL

Third International Conference on

Antenna Theory and Techniques

8-11 September 1999

Organizers

National Antenna Association of Ukraine

National Technical University of Ukraine "Kyiv Polytechnic Institute"

IEEE AP/MTT/AES/ED/LEO/GRS-SS East Ukraine Joint Chapter

Sevastopil State Technical University

Venue

20010808 130

Sevastopil State Technical University

Sevastopil, Ukraine

AQ F01-11-2213

CO-ORGANIZERS AND CO-SPONSORS

STATE COMMITTEE OF UKRAINE ON SCIENCE AND INTELLECTUAL PROPERTY

KHARKIV TECHNICAL UNIVERSITY OF RADIO ELECTRONICS

TERA LTD. (KYIV)

COMPANY "VEBER" (SEVASTOPIL)

ROMSAT LTD. (KYIV)

TERNOPIL STATE DESIGN BUREAU "PROMIN" (TERNOPIL)

We wish to thank the following for their contribution to the success of this Conference:

IEEE REGION 8 OFFICE

US AIR FORCE EUROPEAN OFFICE OF AEROSPACE R&D

OFFICE OF NAVAL RESEARCH INTERNATIONAL FIELD OFFICE

Proceedings of the Third International Conference on Antenna Theory and Techniques
ISBN 966-622-012-1

This material is based upon work supported by the European Office of Aerospace Research and Development, Airforce Office of Scientific Research, Airforce Research Laboratory under Contract No. F 61775-99-WF071.

This work relates to Department of the Navy Grant N 00014-99-1-1033 issued by the Office of Naval Research International Field Office. The United States has a royalty-free license throughout the world in all copyrightable material contained herein.

CHAIRMAN OF ICATT-99 Ya. S. Shifrin (Ukraine)

ICATT-99 TECHNICAL PROGRAM COMMITTEE

F. F. Dubrovka (Co-Chairman, Ukraine)

L. D.Bakhrakh (Co-Chairman, Russia)

J.-P. Daniel	(France)	V. F. Kravchenko	(Russia)
P. Edenhofer	(Germany)	L. M. Lobkova	(Ukraine)
A. S. Ilyinskiy	(Russia)	G. A. Morozov	(Russia)
K. Kagoshima	(Japan)	A. I. Nosich	(Ukraine)
T. Katagi	(Japan)	D. M. Sazonov	(Russia)
A. A. Kirilenko	(Ukraine)	H. Shigesawa	(Japan)
K. van 't Klooster	(Netherlands)	D. I. Voskresenskiy	(Russia)
D. J. Kozakoff	(USA)	V. I. Zamyatin	(Ukraine)
L. G. Kornienko	(Ukraine)		

ICATT-99 ORGANIZING COMMITTEE

A. G. Lukyanchuk	(Chairman)
V. I. Pravda	(Vice-Chairman)
A. G. Dudko	(Secretary&Editor)
N. G. Maksimova	(Secretary&Editor)

D. G. Afonin	V. G. Syrotyuk
A. N. Bratchikov	Ya. O. Rospopa
V. A. Katrich	V. I. Rudakov
V. I. Karpenko	P. P. Yermolov
A. M. Kupriy	M. S. Yurchenko

CONTENTS

National Technical University of Ukraine "Kyiv Polytechnic Institute" is not, as a body, responsible for the opinions expressed by individual authors or speakers

Page No

INVITED PAPERS

1 **Principal problems of the reflector antennas synthesis**
V. I. Andrianov, L. D. Bakhrakh, V. F. Los', A. Y. Makarov, V. B. Tarasov (Moscow, Russia)

3 **Fiber-optic technology for antenna signal transmission and distribution: present state and perspectives**
A. N. Bratchikov, D. I. Voskresensky and T. A. Sadekov (Moscow, Russia)

11 **Hot radiators in antenna measurements**
S. V. Butakova and K. A. Butakov (Kharkiv, Ukraine)

17 **An extremely fast-convergent iterative method of synthesis and its application to design of high performance antennas and microwave components**
F. F. Dubrovka (Kyiv, Ukraine)

27 **Modelling of printed antennas arrays for various applications**
J. P. Daniel (Rennes, France)

32 **Electronically tunable frequency selective surfaces for antenna applications**
P. Edenhofer, A. Alpaslan (Bochum, Germany)

36 **A low-loss and compact multi-sector antenna with distributed implicit RF beam switch**
K. Kagoshima (Japan)

41 **Technology for a quasi-GSO satellite communications system**
T. Katagi, R. Yonezawa, I. Chiba, S. Urasaki (Japan)

46 **The antenna sub-system for meteosat second generation satellites**
K. Van Klooster (Netherlands), M. Difausto, V. Santachiara, P. Carrati, A. Rosa, P. Russo (Roma, Italy), B. Robert (Cannes La Bocca, France)

49 **Modern methods of analysis and computation of antenna radomes**
D. J. Kozakoff (Marietta, USA)

55 **Atomic functions and numerical methods of the antennas theory synthesis solving problems**
V. F. Kravchenko (Moscow, Russia)

62 **Problems and new results of spectral estimation and antenna arrays superresolution techniques**
D. I. Lekhovitsky, D. V. Atamansky, I. G. Kirillov, P. M. Flexer (Kharkiv, Ukraine)

69 **A PC based program package FARFOR-99: improving our understanding of radiation from aperture antennas and antenna arrays**
D. M. Sazonov (Moscow, Russia)

72 **Adaptive antenna arrays with microwave signal processing**
Y. N. Sedishev, V. R. Khachaturov (Kharkiv, Ukraine)

80 **Radiation feature of space-wave-leaky mode on printed-circuit transmission lines**
H. Shigesawa and M. Tsuji (Kyoto. Japan)

GENERAL ANTENNA THEORY

85 **Plasma antenna. *Resume of Theoretical Research***
A. N. Almaliev, A. L. Gutman, B. G. Katsnelson, M. A. Shehalev (Voronezh, Russia)

87 **Excitation problem solution for the dielectric cylinder with thin cover**
A. V. Alpatova, N. N. Kisel', Yu. V. Yukhanov (Taganrog, Russia)

90 **About branching of the solutions of the phase synthesis problem of a linear antenna**
M. I. Andriychuk (Lviv, Ukraine)

93 **Surface and lateral waves of higher-order beam waves**
O. V. Bakumenko, N. A. Khizhnyak (Kharkiv, Ukraine)

95 **The model of grazing HF vertically polarized radio waves backscattering by sea surface waves**
G. N. Bondarchuk, I. I. Zarudnev, Y. A. Lupan, J. G. Mugenov, S. Y. Platonov (Kyiv, Ukraine)

98 **Transformation of wave beams at plane with oscillated anisotropic perturbation of surface impedance**
V. F. Borulko (Dnipropetrovsk, Ukraine)

101 **Reflection of surface wave and their coupling with wave beam at perturbated impedance plane**
V. F. Borulko, V. E. Ivanilov (Dnipropetrovsk, Ukraine)

104 **On the synthesis of antennas with an optimal ratio between the demand factor and the angle of concentration of the radiated/received power**
G. A. Evstropov, S. A. Smirnov (Moscow, Russia)

108 **Scattering plane electromagnetic wave by cruciform electrical dipole with a load**
D. D. Gabriel'yan, T. V. Peretyatko (Rostov-on-Don, Russia)

111 **The calculation of mutual coupling between dipoles in presence of impedance circular cylinder**
D. D. Gabriel'yan, M. Yu. Zvezdina (Rostov-on-Don, Russia)

113 **The influence of impedance surface of a circular cylinder on the dipole pattern**
D. D. Gabriel'yan, M. Yu. Zvezdina (Rostov-on-Don, Russia)

117 **Waves scattering on a system of fillets**
A. V. Golovchenko, G. I. Koshevoy, D. I. Yaresko (Kharkiv, Ukraine)

119 **Transient radiation from aperture antenna under non-synchronous excitation**
N. N. Kolchigin, S. N. Pivnenko (Kharkiv, Ukraine)

122 **Resonant transformation of the electric-dipole field into a circularly polarized field by means of a small dielectric sphere with the surface conductance along helical-type lines**
E. N. Korshunova, A. N. Sivov, and A. D. Shatrov (Moscow, Russia)

124 **Approximation of radiation patterns of antennas by entire functions of exponential type**
V. F. Kravchenko, E. G. Zelkin, V. V. Timoshenko (Moscow, Russia)

127 **Properties of Bragg diffraction of the second order in light and periodic structures interaction under dual Bragg angle**
L. F. Kupchenko, O. V. Efimova, Y. M. Plahov, V. B. Lobyrev, E. L. Cherkashina (Kharkiv, Ukraine)

129 **Property of intermediate diffraction regime near the second Bragg resonance under interaction of light with periodic structures**
L. F. Kupchenko, O. V. Efimova, Y. M. Plahov, V. B. Lobyrev, E. L. Cherkashina (Kharkiv, Ukraine)

131 **The α-properties of electromagnetic field fractal dipole**
I. V. Lysokon', V. M. Onufrienko (Zaporizhzhya, Ukraine)

133 **A sensor of the H-component of a pulse electromagnetic field of nanosecond duration**
A. A. Orlenko and P. V. Kholod (Kharkiv, Ukraine)

135 **Synthesis of antenna arrays with regard to the radiators mutual coupling and vector characteristics of electromagnetic fields**
L. Pasnak, P. Savenko (Lviv, Ukraine)

138 **Electromagnetic field of an antenna located near a sea tropospheric waveguide**
A. V. Polyarus, A. A. Koval, E. V. Tsekhmistrov (Kharkiv, Ukraine)

140 **The determined approach to calculation of radiolines in urban conditions**
L. I. Ponomarev, M. G. Alekseyenko, A. Y. Ganitsev (Moscow, Russia)

143 **On methods of solution to slot antennas synthesis problems**
Yu. Yu. Radtzig, M. A. Khavanova (Veliky Novgorod, Russia)

145 **An evaluation of the intensity of the electromagnetic field, reflected from the aerodynamic target in an above-water surface waveguide**
A. Samokhvalov (Kyiv, Ukraine)

148 **Theory of antennas with nonlinear elements and its application**
Y. S. Shifrin, A. I. Luchaninov, V. M. Shokalo (Kharkiv, Ukraine)

150 **Pseudodifferential equations method for solving problem of electromagnetic wave diffraction on conducting screens**
Yu. G. Smimov, A. A. Vartanov, M. Yu. Medvedik (Penza, Russia)

152 **Frequency and pulse responses of resonant objects buried in a dielectric, dispersive half-space**
O. I. Sukharevsky, G. S. Zalevsky (Kharkiv, Ukraine)

155 **Analytical representation of a spectrum of periodic solutions in a model of Majsner–Kronig–Penney in radiating system**
J. M. Terent'ev (Dnipropetrovsk, Ukraine)

158 **Radiation efficiency of coupled vertical dipole antennas located above a lossy half-space**
P. L. Tokarsky (Kharkiv, Ukraine)

160 **Radiation of waves by the fractal surface element**
E. I. Veliev (Kharkiv, Ukraine), V. M. Onufrienko (Zaporizhzhya, Ukraine)

162 **Use of an auxiliary sources method for calculation of the characteristics of antennas placed on impedance arbitrary shape bodies**
V. A. Voloshina, V. V. Shatskiy (Rostov-on-Don, Russia)

165 **Reflective properties of one-dimensional PBG dielectric structures with doubled quasi-periodicity of permittivity**
I. Y. Vorgul, A. G. Nerukh (Kharkiv, Ukraine)

167 **A multibeam impedance antenna synthesis**
Yu. V. Yukhanov, A. Yu. Yukhanov (Taganrog, Russia)

169 **About one method of determination of currents in the isolated antenna**
I. P. Zaikin, G. I. Koshevoy, D. I. Yaresko (Kharkiv, Ukraine)

171 **Modeling of non-coordinate electromagnetic problems**
Y. Zakharia (Lviv, Ukraine)

173 **Scattering of plane electromagnetic wave by impedance circular cylinder**
M. Yu. Zvezdina, A. S. Stepanov, V. V. Kharchenko, S. V. Chernov (Rostov-on-Don, Russia)

176 **Uniform asymptotic theory of electromagnetic diffraction by waveguide aperture**
A. A. Zvyagintsev, T. N. Demchenko, S. P. Phomushkin (Kharkiv, Ukraine)

REFLECTOR, LENS AND HYBRID ANTENNAS

179 **Cylindrical Luneberg lens analysis**
A. V. Boriskin, S. V. Boriskina and A. I. Nosich (Kharkiv, Ukraine)

181 **Account of effects of the irradiator's near zone in mathematical model of reflector antenna**
N. N. Gorobets, S. S. Vyazmitinova, A. I. Vyazmitinova (Kharkiv, Ukraine)

184 **Dual-reflector omnidirectional antenna for MMDS base stations**
O. S. Kim (Kyiv, Ukraine)

187 **Synthesis of the contoured radiation patterns of the dual-reflector antennas according to the prescribed magnitude patterns**
B. Podlevskyi and P. Savenko (Lviv, Ukraine)

190 **Dual-shaped symmetric reflector antenna with parabolic panels**
D. Y. Razdorkin, M. V. Romanenko (Rostov-on-Don, Russia)

192 **A conceptual approach to determine antennas gain loss in tropospheric-scatter communication systems**
V. I. Rudakov (Kyiv, Ukraine)

195 **A theoretical aspect of quick fadings autocompensation in tropospheric-scatter communication systems**
V. I. Rudakov (Kyiv, Ukraine)

198 **Features of radiation field formation of multibeam reflector antenna**
A. A. Savochkin (Sevastopil, Ukraine)

201 **Earth station antenna posts, created by design office "Promin"**
V. H. Syrotyuk, V. S. Pynylo, H. P. Khymych (Ternopil, Ukraine)

ANTENNA ARRAYS

204 **Underground phased antenna arrays as alternative to mast aerials of receiving radio**
S. M. Alekseev, A. V. Makaseev, A. G. Poshkov, B. V. Sosunov, N. G. Fitenko (St. Petersburg, Russia)

206 **The analytical approach to the computing of resonance effects for the diffraction at well reflecting gratings**
N. A. Balakhonova, A. V. Kats, I. S. Spevak (Kharkiv, Ukraine)

209 **Two-dimensional image retrieval**
K. P. Gaikovich, A. V. Zhilin (Nizhny Novgorod, Russia)

212 **Active phased antenna arrays radiating LFM pulse packet**
V. L. Gostuykhin, V. N. Trusov, A. V. Gostuykhin (Moscow, Russia)

214 **Limiting resolution of Capon method for correlated sources**
A. A. Kirillov, G. V. Serebryakov (Nizhny Novgorod, Russia)

217 **The accuracy of joint estimation of signal parameters of the antenna arrays in the case of non-gaussian interference**
Y. P. Kunchenko, V. A. Danyk, T. V. Prokopenko (Cherkassy, Ukraine)

219 **Apodization functions for antenna arrays with constructive-technological restrictions**
V. V. Lukin, A. V. Kabanov, N. N. Ponomarenko (Kharkiv, Ukraine)

222 **Coherence-reduced signal processing in large arrays**
A. Malekhanov (Nizhny Novgorod, Russia)

225 **Power optimization of the beam shared-forming monopulse arrays**
B. D. Manuilov, P. N. Bashly (Rostov-on-Don, Russia)

228 **Diagnostics of receiving hydroacoustic antenna arrays**
D. A. Orlov And V. I. Turchin (Nizhny Novgorod, Russia)

230 **Simulation of antenna array characteristics impact on objects image restoration**
I. Prudyus, L. Lazko, T. Holotyak (Lviv, Ukraine)

233 **Simulation of spatial-time signal processing in imaging systems with synthetic aperture**
I. N. Prudyus, A. T. Synyavskyy, V. P. Ostap (Lviv, Ukraine)

237 **Optically or electronically steerable mm-wave phased antennas array based on semiconductor structure**
V. Ya. Rogov, A. Yu. Grinev, A. E. Zaikin (Moscow, Russia)

239 **Pattern synthesis of antenna array with digital phase shifters**
N. V. Shcherbakov, I. V. Norinchuk (Kharkiv, Ukraine)

241 **The matrix models of digital antenna arrays with nonidentical channels**
V. I. Slyusar (Kyiv, Ukraine)

244 **A way of correction of DAA receiving channels characteristics using the heterodyne signal**
V. I. Slyusar (Kyiv, Ukraine)

246 **Analysis of the effect of geometric parameters of nonequidistant antenna array with unequal amplitude distribution on its working frequencies range**
S. I. Starchenko, A. Yu. Milovanov, I. V. Pleshivtsev (Tambov, Russia)

248 **Maximization of the power parameters of antenna arrays with suppression of the cross-polar radiation**
P. L. Tokarsky, A. M. Rybalko and A. V. Synepoop (Kharkiv, Ukraine)

251 **The influence of amplitude and phase perturbations of antenna array sensors on direction finding of narrow-band signals efficiency**
I. R. Urazgildiev, A. M. Vagapov (Kyiv, Ukraine)

254 **Uniform linear antenna array in superresolution mode by the modified unitary ESPRIT algorithm**
V. I. Vasilishin, A. N. Kolesnikov (Kharkiv, Ukraine)

256 **Synthesis of one-dimentional periodic perfectly conducting gratings**
L. G. Velychko (Kharkiv, Ukraine)

258 **Optimal combined processing of signals in multichannel synthetic aperture radars**
V. K. Volosyuk, S. E. Falkovich, V. M. Velasco Hererra, O. A. Gorbunenko (Kharkiv, Ukraine)

261 **Energy features of the surface E-wave scattering by a reflection antenna grating**
A. P. Yevdokimov, V. V. Krizhanovsky (Kharkiv, Ukraine)

264 **Space-time modulation of signals in a ring antenna array**
V. I. Zamyatin, O. V. Baturin, E. A. Tolokneyev (Kharkiv, Ukraine)

ADAPTIVE ANTENNA ARRAYS

266 **Measurement of signal informative parameters when its amplitude and phase are random in radar system with adaptive array**
S. T. Bagdasaryan, A. A. Belov, V. P. Ryabuha, V. A. Tarshin (Kharkiv, Ukraine)

269 **Analytical calculation of detection and resolution thresholds in antenna arrays using sample covariance matrix eigenvalue technique**
V. T. Ermolaev, A. A. Maltsev, K. V. Rodyushkin (Nizhny Novgorod, Russia), L. Lo Presti (Torino, Italy)

272 **Application of channeling principles of estimating weighting coefficients in antennas with adaptive spatial signal processing against the interference background**
A. U. Kobzev, V. R. Khachaturov (Kharkiv, Ukraine)

276 **Estimation of the influence of receiving-amplifying sections non-linearity on the adaptive antenna arrays efficiency**
Yu. Yu. Kolyadenko, V. V. Popovsky, A. G. Malitsky (Kharkiv, Ukraine)

279 **An efficiency of interference adaptive compensation in multipath propagation of radio waves**
L. Y. Komienko, O. A. Voitovich, V. P. Tischenko (Kharkiv, Ukraine)

282 **An adaptive compensation of partially polarized interferences in the presence of polarization differences in a frequency band**
L. G. Komiyenko, F. F. Mysik, S. Y. Polyakov (Kharkiv, Ukraine)

284 **Statistical characteristics of adaptive antenna arrays with independent reference-signals forming**
A. A. Maltsev, O. V. Poldin, A. M. Silaev (Nizhny Novgorod, Russia), L. Lo Presti (Torino, Italy)

287 **Experimental studying of influence of weight coefficients jitter on output signal of adaptive antenna array**
A. A. Maltsev, S. V. Zimina (Nizhny Novgorod, Russia)

290 **A robust adaptive antenna array for signals separation**
L. A. Marchuk, O. A. Nokhrin, A. N. Savelyev (Saint-Petersburg, Russia), L. A. Titarenko (Kharkiv, Ukraine)

293 **Adaptive antenna arrays with nonredundant apertures of the Mills cross type**
Y. N. Sedyshev, P. Y. Sedyshev, R. A. Kamaukh (Kharkiv, Ukraine)

297 **Method and algorithms of PAA RP synthesis adaptive to its elements failure**
Y. S. Shifrin, U. R. Liepin, L. V. Golovina (Kharkiv, Ukraine)

LOW-GAIN ANTENNAS
PRINTED ANTENNAS
ANTENNAS FOR MOBILE COMMUNICATIONS

299 **Radiation of the multi-mode slotted radiator**
V. Antyfeev, A. Borsov, A. Sokolov (Moscow, Russia)

301 **Small-sized dielectric split antenna of round cross-section**
V. Antyfeev, A. Borsov, A. Sokolov (Moscow, Russia)

303 **L-band antenna alternatives for the European mobile satellite (EMSAT) network**
G. de Balbine (Tarzana, USA)

304 **Optimization of characteristics of directivity of horn microwave band radiators**
A. A. Boichenko, I. I. Shumljansky (Odesa, Urkaine)

306 **A leaky-wave integrated antenna based on a prism coupled to a dielectric waveguide**
S. V. Boriskina and A. I. Nosich (Kharkiv, Ukraine)

308 **Matching and directivity features of waveguide radiator filled with dielectric**
A. A. Bulgakov, N. N. Gorobets, V. A. Lyaschenko (Kharkiv, Ukraine)

311 **On the estimation of electromagnetic characteristics of the system of dipole radiators in the logperiodic antenna**
L. G. Burova, Y. Y. Radtzig (Velikii Novgorod, Russia)

312 **Experimental investigation of horn antenna radiation**
O. O. Drobakhin, D. Yu. Saltykov (Dnipropetrovsk, Ukraine)

315 **Disk-on-rod-in-waveguide radiating element for dual-polarized broadband wide scanning array antennas**
R. F. Dubrovka (Kyiv, Ukraine)

318 **Directivity characteristics and radiation impedance of a circular frame placed around a cylinder of perfect conductivity**
G. A. Evstropov, A. I. Klimenko (Moscow, Russia)

321 **A reduction of log-periodic antennas dimensions**
E. V. Goremykin, G. I. Kostromitin (Taganrog, Russia)

324 **Mathematical model of radiation from open-ended circular waveguide**
N. N. Gorobets, L. V. Orlova, A. V. Shishkova (Kharkiv, Ukraine)

326 **Optimization of frequency performances of horn radiators**
A. A. Karpenko, I. I. Shumljansky (Odesa, Ukraine)

328 **The radiating properties of spiraphase reflector based on microstrip array**
A. O. Kasyanov (Taganrog, Russia)

331 **Investigation of parameters of loop oscillator with distribute reactive load**
E. N. Kayashova, V. G. Slyozkin (Sevastopil, Ukraine)

333 **Peculiarities of application of the induced EMF method for determination of helical antennas input impedance**
L. M. Lobkova, M. V. Ivashina, V. V. Golovin (Sevastopil, Ukraine)

335 **Estimation of the interaction impedance of the antenna array consisting of circular loops**
L. M. Lobkova, M. B. Protsenko, O. A. Posniy, M. V. Ivashina (Sevastopil, Ukraine)

337 **Radiation features of a flat z-antenna**
L. M. Lobkova, M. V. Ivashina, A. F. Rozvadovsky (Sevastopil, Ukraine)

339 **A coaxial spiral antenna with increased gain**
A. S. Mikryukoff, V. F. Korsak, Y. L. Maksimenko (Kyiv, Ukraine)

341 **About a new small-sized loop antenna with an isotropic radiation pattern**
V. V. Ovsyanikov (Dnipropetrovsk, Ukraine)

344 **Optimization of geometric and radiation parameters of a hemisphere helical antenna**
M. B. Protsenko, V. V. Molchanov (Sevastopil, Ukraine)

346 **The estimation of the radiation quality of the flat Archimedean spiral antennas**
M. B. Protsenko, I. V. Tankov (Sevastopil, Ukraine)

348 **An improving of energy radiation characteristics of an corner reflector antenna with Franklin antenna feed**
A. V. Seleznyov (Kyiv, Ukraine)

350 **Electrodynamic modeling of two-port C-band flat antenna**
B. V. Sestroretsky, A. V. Dorofeev, A. N. Savchenko, M. A. Drize, S. A. Ivanov (Moscow, Russia)

353 **Radiation characteristics of a multiple-arm conical helical antennas with two points excitation**
L. N. Stepanov, A.V. Lukyanchikov (Sevastopil, Ukraine)

355 **Means of radio–acoustic antennas interference immunity improving**
Yu. N. Ulyanov, V. S. Bedin, and S. V. Butakova (Kharkiv, Ukraine)

358 **Optimization of the polyhedral vehicle antenna array characteristics**
V. A. Voloshina, V. V. Shatskiy (Rostovs-on-Don, Russia)

360 **Electrodynamic parameters of narrow slots in a rectangular waveguide filled with three-layered dielectric. Theory and experiment**
L. P. Yatsuk, A. F. Lyakhovsky, A. A. Lyakhovsky (Kharkiv, Ukraine)

363 **About plane screen spirals near fields influence on radiation and scattering characteristics**
K. P. Yatzuk, R. R. Shvelidze (Kharkiv, Ukraine)

365 **Influence of diffraction effects on directivity of the corner antenna of arbitrary apex angle**
N. P. Yeliseyeva (Kharkiv, Ukraine)

368 **A multibeam hybrid printed antenna based on a strip periodic structure**
A. P. Yevdokimov, V. V. Krizhanovsky, P. N. Melezhik, and A. Ye. Poedinchuk (Kharkiv, Ukraine)

BROADBAND AND MULTIFREQUENCY ANTENNAS

371 **Multi-band electronically scanned antennas of santimeter and millimeter range waves**
N. A. Bei (Moscow, Russia)

374 **Dual-band antennas on the base of surface wave lines**
N. A. Bei, V. L. Khandamirov, A. A. Volkov, A. V. Panteleev (Moscow, Russia)

376 **Time-domain antenna studies for videopulse subsurface radars**
A. A. Boryssenko (Kyiv, Ukraine)

379 **Modeling the problem of pulse radiation from a slotted cone placed on the inhomogenous plane**
V. A. Doroshenko (Kharkiv, Ukraine)

382 **Effects of radiation pattern distortions of slot antennas with finite lateral metallization**
F. F. Dubrovka and V. M. Tereshchenko (Kyiv, Ukraine)

385 **A VHF-UHF logperiodic V-dipole TV antenna**
F. F. Dubrovka, O. M. Kupriy, V. V. Zaskalniy (Kyiv, Ukraine)

387 **Transient excitation of coaxial cone antenna**
A. N. Dumin, S. N. Pivnenko (Kharkiv, Ukraine)

390 **Propagation of short pulses in lossy long lines**
A. L. Gutman, A. N. Manko (Voronezh, Russia)

392 **Antenna system for georadar "Zond-10" consisting of a pair of curved loaded wideband dipoles**
S. A. Masalov, G. P. Pochanin, P. V. Kholod (Kharkiv, Ukraine)

395 **Novel approaches to the analysis and model synthesis of ultra-wide-band horn-type antennas**
A. O. Perov, Yu. K. Sirenko (Kharkiv, Ukraine), A. E. Yaldiz (Turkey)

397 **Multiband antennas on loop radiators**
Y. A. Rensh (Ekaterinburg, Russia)

400 **FDTD analysis of log-periodic flat dipole antennas**
A. E. Shrenk (Kyiv, Ukraine)

ANTENNA RADOMES AND ABSORBERS

403 **Millimeter wave characteristics of glass plastics for antenna covers**
E. E. Chigriai, V. V. Meriakri (Fryazino, Russia)

405 **A research of electromagnetic waves absorption in foam and layered structures**
L. A. Filinskiy, V. M. Morozov (Dnipropetrovsk, Ukraine)

408 **To asymptotics of a field of overreverberated beams in the aperture antenna with radome**
I. V. Sukharevsky, S. E. Vashinsky (Kharkiv, Ukraine)

COMPUTATIONAL METHODS

410 **Dissipation fields in flat waveguide with a triple bifurcation and dielectric filling**
V. Antyfeev, A. Borsov, A. Sokolov (Moscow, Russia)

413 **New method of aerials calculation**
V. V. Artemiev, V. L. Danilchuk, J. J. Radzig, S. I. Eminov (Novgorod, Russia)

415 **Analysis of microstrip antennas by numerical–analytical method**
V. V. Artemiev, S. I. Eminov, I. A. Jukovskaya (Novgorod, Russia)

417 **Propagation of the electromagnetic waves in double ring waveguide with dielectric layers**
A. V. Bezugliy, V. V. Khoroshun (Kharkiv, Ukraine)

419 **Method of regularization in numerical simulation of axially symmetric dielectric patch antenna excited by ved**
N. Bliznyuk, A. I. Nosich (Kharkiv, Ukraine)

421 **Rigorous calculation of active antennas**
V. L. Danilchuk (Novgorod, Russia)

423 **Numerical algorithm for calculating the electric characteristics of wire antennas used to analyse the electromagnetic compatibility parameters of a radio system**
A. S. Ilinski, I. V. Berezhnaya, O. Ju. Perfilov (Moscow, Russia)

426 **System of linear wires in anisotropic plasma**
E. A. Jatsenko, N. M. Jatsenko, N. A. Khizhnyak (Kharkiv, Ukraine)

427 **The solution of three – dimentional electrodynamic problems by the integral equation method**
V. M. Morozov, V. I. Magro (Dnipropetrovsk, Ukraine)

429 **Computer modeling of electromagnetic wave propagation in a time–varying medium**
A. G. Nerukh, K. M. Yemelyanov, F. V. Fedotov (Kharkiv, Ukraine)

432 **Equivalent surface impedance of slotted impedance load made as semi-cylindrical cavity for infinite array. The case of E-polarization**
B. M. Petrov, V. G. Koshkidko, O. V. Alpatova (Taganrog, Russia)

435 **Numerical solving of the integral equation for the elliptic loop antenna**
A. A. Schekaturin (Sevastopil, Ukraine)

438 **A CAD software for design and analysis of a rectangular microstrip antenna**
K. Y. Yazdandoost, D. C. Gharpure (Pune, India)

ANTENNA MEASUREMENTS

441 **Distorting influence of horn antenna on measurements by multifrequency radiointerferometer**
M. V. Andreev (Dnipropetrovsk, Ukraine)

445 **Method of estimation of requirements to the input information when determining antennas characteristics with near-zone methods**
O. D. Anohina, A. V. Nechosa (Kharkiv, Ukraine)

447 **About necessity of creation of the additional space sar calibration points and expedience of their integration into the international calibration net**
V. S. Blinov (Kharkiv, Ukraine)

449 **EM-properties measurement and error analysis of planar and convex surface samples using finite flange open-ended coaxial probe**
A.-K. A. Hassan, D. Xu, And Y. Zhang (Shanghai, China)

453 **Complex reflectivity meter in microwave paths**
L.Y. Ilnitskiy, L. V. Sibruk, M. I. Fuzik (Kyiv, Ukraine)

456 **The measurement of a power flow in two-mode waveguide with using galvanomagnetic transducers**
P. V. Ivkin (Kyiv, Ukraine)

459 **Radioholographic correlational measurements of large reflector antennas**
A. V. Kalinin (Nizhny Novgorod, Russia)

461 **Phase shift measurements for antenna systems**
L. D. Ogorodnijchuk (Kyiv, Ukraine)

464 **Requirements to the accuracy of PAA phase meters**
L. D. Ogorodnijchuk (Kyiv, Ukraine)

465 **Characteristics of antennas, recording systems and processing algorithms used in the radar systems for measuring projectile movement parameters at the time of shooting**
S. V. Porshnev (Nizhny Tagil, Russia)

468 **Statistical aspects of the theory for defining antenna characteristics by the field measurements in the near zone**
Y. S. Shifrin, V. A. Usin (Kharkiv, Ukraine)

MICROWAVE COMPONENTS AND CIRCUITS FIBER OPTIC LINKS

471 **Multireflector resonance systems in millimeter wave range**
D. G. Afonin, A. K. Malyshkin (Moscow, Russia)

473 **Active integrated antenna amplifier for handset receiver front end**
A. S. Andrenko, Y. Ikeda, M. Nakayama, K. Horiguchi, T. Fukasawa, O. Ishida (Japan)

476 **Numerical simulation of transverse-planar structures in waveguide**
R. V. Antipenko, S. E. Yukhno (Kyiv, Ukraine)

478 **The analysis of the irreciprocity of the signals delay of the antenna–feeder devices of active comparison systems**
V. V. Bavykina, Yu. A. Koval, O. L. Troshchin (Kharkiv, Ukraine)

480 **Creation of localized high intensity electromagnetic field pulses in open resonator**
I. N. Belobaba, D. M. Sazonov (Moscow, Russia)

482 **Phase stabilized fiber channel with remote heterodyning: spectral – noise analysis and experiment**
A. N. Bratchikov, D. I. Voskresenskii, T. A. Sadekov (Moscow, Russia)

487 **RF signal spectral analysis at the output of erbium doped fiber amplifier in the remote heterodyning mode**
A. N. Bratchikov, T. A. Sadekov (Moscow, Russia)

492 **Tunable waveguide bandpass filters with a near constant bandwidth**
F. F. Dubrovka and P. Ya. Stepanenko (Kyiv, Ukraine)

496 **Numerical algorithm for calculation of cavity microwave transducer of an aperture type**
Y. E. Gordienko, A. Y. Panchenko, A. A. Ryabukhin (Kharkiv, Ukraine)

498 **Multielement resonance diaphragms in microwave antenna-and-feeder devices**
V. A. Katrich, A. A. Shmat'ko (Kharkiv, Ukraine)

499 **The full-wave model for plane junction of waveguides with piecewise linear coordinate boundaries**
A. A. Kirilenko, D. Yu. Kulik, L. A. Rud', and V. I. Tkachenko (Kharkiv, Ukraine)

502 **Bandpass and lowpass filters on ridged waveguide sections**
A. A. Kirilenko, D. Yu. Kulik, L. A. Rud', and V. I. Tkachenko (Kharkiv, Ukraine)

505 **One- and two stopband rejection sections based on multiple rectangular aperture irises**
A. A. Kirilenko, L. P. Mos'pan (Kharkiv, Ukraine)

508 **Port reflectivity method in the theory of tees with iris inserts**
D. Y. Kulik (Kharkiv, Ukraine)

510 **FDTD analysis of metal plates in rectangular waveguide**
A. M. Kupriy, S. E. Martynyuk (Kyiv, Ukraine)

512 **High-power multiplexer for aerial feeder of TV and radio broadcasting transmitters**
A. N. Lishchenko, A. A. Boryssenko (Kyiv, Ukraine)

515 **Transfer characteristics of ultra high frequency devices based on two surface iron-yttrium garnet films**
M. I. Lyashenko, V. M. Talalaevskii, L. V. Chevnjuk (Kyiv, Ukraine)

517 **Application of MW delay lines in combined SAR calibration**
A. Y. Matveyev (Kharkiv, Ukraine)

520 **Millimeter wave devices based on dielectric, ferrite and semiconductor waveguides**
V. V. Meriakri, B. A. Murmuzhev, M. P. Parkhomenko (Fryazino, Russia)

522 **Studying of resonant rejecting and adsorbing cells based on sections of partially filled waveguides**
L. Minakova, L. Rud' (Kharkiv, Ukraine)

524 **Reconstruction of multiple rectangular aperture iris response by its complex natural oscillations**
L. P. Mos'pan (Kharkiv, Ukraine)

526 **Pulse current excitation of the rectangular resonator with distributed nonlinear loads**
D. V. Semenikhina (Taganrog, Russia)

528 **Tracts of Ku and C-band antennas for perspective communication satellites**
B. V. Sestroretsky, M. A. Drize, S. A. Ivanov, K. N. Klimov (Moscow, Russia)

534 **Aspects of implementing an optical fiber soliton sync-network for a complex of phased arrays**
A. S. Shcherbakov, A. Yu. Kosarsky, and V. N. Zvegintsev
(St. Petersburg, Russia)

536 **Experimental investigation of antenna characteristics of radioelectronic elements**
A. V. Timchenko, V. I. Chumakov, O. I. Kharchenko (Kharkiv, Ukraine)

539 **Rectangular waveguide filled with bianisotropic medium**
K. A. Vytovtov, I. V. Petrusenko (Dnipropetrovsk, Ukraine)

INDUSTRIAL AND BIOMEDICAL APPLICATIONS OF MICROWAVE TECHNOLOGIES

541 **Investigation of the complex permittivity of coals and oil products by the radiophysical methods**
S. V. Buharov, V. V. Ovsianicov, I. V. Petrusenko, A. G. Hundriga (Dnipropetrovsk, Ukraine)

544 **Rational technologies and microwave designs for gypsum binder, casein, fruits, vegetables and other food-stuffs**
A. I. Dokhov, V. V. Zhimov, N. E. Lukyanenko (Kharkiv, Ukraine)

545 **Back channel in digital MMDS**
A. I. Dolgonos, H. L. Baindurashvili (Russia), A. M. Voychinsky (USA)

547 **Influence of nonlinear capacitance of a microwave rectifying diode on rectenna characteristics**
A. I. Luchaninov, M. A. Omarov, A. A. Konovaltsev (Kharkiv, Ukraine)

548 **Transmission of an e-mail format signals in MF/HF ranges in a marine radio communication**
V. N. Martynkin, Y. V. Malyarenko (Odesa, Ukraine)

550 **Optimization of electromagnetic field excitation for microwave industrial and agricultural application**
G. A. Morozov, I. E. Sedelnikov (Kazan, Russia)

553 **Improvement of microwave equipment excitation efficiency using methods of focused arrays**
G. A. Morozov, O. V. Potapova, Y. E. Sedelnikov (Kazan, Russia)

556 **A modified microwave technology of heating and drying granular dielectrics**
V. I. Rudakov, A. V. Demchenko, Y. V. Zaichenko (Kyiv, Ukraine)

559 **About one way to decrease the directivity of rectenna spurious radiation**
V. M. Shokalo, A. A. Konovaltsev, Yu. A. Luchaninov (Kharkiv, Ukraine)

562 **Efficiency of power transmission system by a microwave beam with non-axial arrangement of transmitting and receiving apertures**
V. M. Shokalo, S. V. Sevsky, A. M. Rybalko, A. A. Konovaltsev (Kharkiv, Ukraine)

565 **Pulse high-power antibacterial irradiator**
S. N. Shostko, I. S. Shostko, U. F. Lonin, V. I. Chumacov, U. L. Novoselov, O. S. Shostko (Kharkiv, Ukraine)

568 **An increase of power efficiency of a microwave generator for microwave processing of materials**
V. I. Vodotovka, K. N. Gura, F. M. Repa (Kyiv, Ukraine)

ELECTROMAGNETICS IN HIGH SCHOOLS

571 **Problems of technique of organizing antenna laboratory course**
M. V. Andreev, O. O. Drobakhin, V. M. Morozov, D. Yu. Saltykov (Dnipropetrovsk, Ukraine)

573 **Architecture of the textbook "Antennas"**
L. Y. Ilnitskiy, L. V. Sibruk, M. I. Fuzik (Kyiv, Ukraine)

List of Authors

Page No.

Afonin D. G. 471
Alekseev S. M. 204
Alekseyenko M. G. 140
Almaliev A. N. 85
Alpaslan A. 32
Alpatova A. V. 87
Alpatova O. V. 432
Andreev M. V. 441, 571
Andrenko A. S. 473
Andrianov V. I. 1
Andriychuk M. I. 90
Anohina O. D. 445
Antipenko R. V. 476
Antyfeev V. 299, 301, 410
Artemiev V. V. 413, 415
Atamansky D. V. 62

Bagdasaryan S. T. 266
Baindurashvili H. L. 545
Bakhrakh L. D. 1
Bakumenko O. V. 93
Balakhonova N. A. 206
Balbine G. 303
Bashly P. N. 225
Baturin O. V. 264
Bavykina V. V. 478
Bedin V. S. 355
Bei N. A. 371, 374
Belobaba I. N. 480
Belov A. A. 266
Berezhnaya I. V. 423
Bezugliy A. V. 417
Blinov V. S. 447
Bliznyuk N. 419
Boichenko A. A. 304
Bondarchuk G. N. 95
Boriskin A. V. 179
Boriskina S. V. 179, 306
Borsov A. 299, 301, 410
Borulko V. F. 98, 101
Boryssenko A. A. 376, 512
Bratchikov A. N. 3, 482, 487
Buharov S. V. 541
Bulgakov A. A. 308
Burova L. G. 311
Butakov K. A. 11
Butakova S. V. 11, 355

Carrati P. 46
Cherkashina E. L. 127, 129
Chernov S. V. 173
Chevnjuk L. V. 515
Chiba I. 41
Chigriai E. E. 403
Chumakov V. I. 536, 565

Page No.

Daniel J. P. 27
Danilchuk V. L. 413, 421
Danyk V. A. 217
Demchenko A. V. 556
Demchenko T. N. 176
DiFausto M. 46
Dokhov A. I. 544
Dolgonos A. I. 545
Dorofeev A. V. 350
Doroshenko V. A. 379
Drize M. A. 350, 528
Drobakhin O. O. 312, 571
Dubrovka F. F. 17, 382, 492
Dubrovka R. F. 315
Dumin A. N. 387

Edenhofer P. 32
Efimova O. V. 127, 129
Eminov S. I. 413, 415
Ermolaev V. T. 269
Evstropov G. A. 104, 318

Falkovich S. E. 258
Fedotov F. V. 429
Filinskiy L. A. 405
Fitenko N. G. 204
Flexer P. M. 62
Fukasawa T. 473
Fuzik M. I. 453, 573

Gabriel'yan D. D. 108, 111, 113
Gaikovich K. P. 209
Ganitsev A. Y. 140
Gharpure D. C. 438
Golovchenko A. V. 117
Golovin V. V. 333
Golovina L. V. 297
Gorbunenko O. A. 258
Gordienko Y. E. 496
Goremykin E. V. 321
Gorobets N. N. 181, 308, 324
Gostuykhin A. V. 212
Gostuykhin V. L. 212
Grinev A. Yu. 237
Gura K. N. 568
Gutman A. L. 85, 390

Hassan A.-K. A. 449
Holotyak T. 230
Horiguchi K. 473
Hundriga A. G. 541

Ikeda Y. 473
Ilinski A. S. 423
Ilnitskiy L. Y. 453, 573
Ishida O. 473

Ivanilov V. E. 101
Ivanov S. A. 350, 528
Ivashina M. V. 333, 335, 337
Ivkin P. V. 456

Jatsenko E. A. 426
Jatsenko N. M. 426
Jukovskaya I. A. 415

Kabanov A. V. 219
Kagoshima K. 36
Kalinin A. V. 459
Karnaukh R. A. 293
Karpenko A. A. 326
Kasyanov A. O. 328
Katagi T. 41
Katrich V. A. 498
Kats A. V. 206
Katsnelson B. G. 85
Kayashova E. N. 331
Khachaturov V. R. 72, 272
Khandamirov V. L. 374
Kharchenko O. I. 536
Kharchenko V. V. 173
Khavanova M. A. 143
Khizhnyak N. A. 93, 426
Kholod P. V. 133, 392
Khoroshun V. V. 417
Khymych H. P. 201
Kim O. S. 184
Kirilenko A. A. 499, 502, 505
Kirillov A. A. 214
Kirillov I. G. 62
Kisel' N. N. 87
Klimenko A. I. 318
Klimov K. N. 528
Klooster K. 46
Kobzev A. U. 272
Kolchigin N. N. 119
Kolesnikov A. N. 254
Kolyadenko Yu. Yu. 276
Konovaltsev A. A. 547, 559, 562
Kornienko L. Y. 279
Korniyenko L. G. 282
Korsak V. F. 339
Korshunova E. N. 122
Kosarsky A. Yu. 534
Koshevoy G. I. 117, 169
Koshkidko V. G. 432
Kostromitin G. I. 321
Koval A. A. 138
Koval Yu. A. 478
Kozakoff D. J. 49
Kravchenko V. F. 55, 124
Krizhanovsky V. V. 261, 368
Kulik D. Yu. 499, 502, 508
Kunchenko Y. P. 217
Kupchenko L. F. 127, 129
Kupriy A. M. 385, 510

Lazko L. 230
Lekhovitsky D. I. 62
Liepin U. R. 297
Lishchenko A. N. 512
Lobkova L. M. 333, 335, 337
Lobyrev V. B. 127, 129
Lonin U. F. 565
Lo Presti L. 269, 284
Los' V. F. 1
Luchaninov A. I. 148, 547
Luchaninov Yu. A. 559
Lukin V. V. 219
Lukyanchikov A. V. 353
Lukyanenko N. E. 544
Lupan Y. A. 95
Lyakhovsky A. A. 360
Lyakhovsky A. F. 360
Lyaschenko V. A. 308
Lyashenko M. I. 515
Lysokon' I. V. 131

Magro V. I. 427
Makarov A. Y. 1
Makaseev A. V. 204
Maksimenko Y. L. 339
Malekhanov A. 222
Malitsky A. G. 276
Maltsev A. A. 269, 284, 287
Malyarenko Y. V. 548
Malyshkin A. K. 471
Manko A. N. 390
Manuilov B. D. 225
Marchuk L. A. 290
Martynkin V. N. 548
Martynyuk S. E. 510
Masalov S. A. 392
Matveyev A. Y. 517
Medvedik M. Yu. 150
Melezhik P. N. 368
Meriakri V. V. 403, 520
Mikryukoff A. S. 339
Milovanov A. Yu. 246
Minakova L. 522
Molchanov V. V. 344
Morozov G. A. 550, 553
Morozov V. M. 405, 427, 571
Mos'pan L. P. 505, 524
Mugenov J. G. 95
Murmuzhev B. A. 520
Mysik F. F. 282

Nakayama M. 473
Nechosa A. V. 445
Nerukh A. G. 165, 429
Nokhrin O. A. 290
Norinchuk I. V. 239
Nosich A. I. 179, 306, 419
Novoselov U. L. 565

Ogorodnijchuk L. D. 461, 464
Omarov M. A. 547
Onufrienko V. M. 131, 160
Orlenko A. A. 133
Orlov D. A. 228
Orlova L. V. 324
Ostap V. P. 233
Ovsyanikov V. V. 341, 541

Panchenko A. Y. 496
Panteleev A. V. 374
Parkhomenko M. P. 520
Pasnak L. 135
Peretyatko T. V. 108
Perfilov O. Ju. 423
Perov A. O. 395
Petrov B. M. 432
Petrusenko I. V. 539, 541
Phomushkin S. P. 176
Pivnenko S. N. 119, 387
Plahov Y. M. 127, 129
Platonov S. Y. 95
Pleshivtsev I. V. 246
Pochanin G. P. 392
Podlevskyi B. 187
Poedinchuk A. Ye. 368
Poldin O. V. 284
Polyakov S. Y. 282
Polyarus A. V. 138
Ponomarenko N. N. 219
Ponomarev L. I. 140
Popovsky V. V. 276
Porshnev S. V. 465
Poshkov A. G. 204
Posniy O. A. 335
Potapova O. V. 553
Prokopenko T. V. 217
Protsenko M. B. 335, 344, 346
Prudyus I. N. 230, 233
Pynylo V. S. 201

Radtzig Yu. Yu. 143, 311, 413
Razdorkin D. Y. 190
Rensh Y. A. 397
Repa F. M. 568
Robert B. 46
Rodyushkin K. V. 269
Rogov V. Ya. 237
Romanenko M. V. 190
Rosa A. 46
Rozvadovsky A. F. 337
Rud' L. A. 499, 502, 522
Rudakov V. I. 192, 195, 556
Russo P. 46
Ryabuha V. P. 266
Ryabukhin A. A. 496
Rybalko A. M. 248, 562

Sadekov T. A. 3, 482, 487
Saltykov D. Yu. 312, 571
Samokhvalov A. 145
Santachiara V. 46
Savchenko A. N. 350
Savelyev A. N. 290
Savenko P. 135, 187
Savochkin A. A. 198
Sazonov D. M. 69, 480
Schekaturin A. A. 435
Sedelnikov I. E. 550
Sedelnikov Y. E. 553
Sedyshev P. Y. 293
Sedyshev Y. N. 72, 293
Seleznyov A. V. 348
Semenikhina D. V. 526
Serebryakov G. V. 214
Sestroretsky B. V. 350, 528
Sevsky S. V. 562
Shatrov A. D. 122
Shatskiy V. V. 162, 358
Shcherbakov A. S. 534
Shcherbakov N. V. 239
Shehalev M. A. 85
Shifrin Y. S. 148, 297, 468
Shigesawa H. 80
Shishkova A. V. 324
Shmat'ko A. A. 498
Shokalo V. M. 148, 559, 562
Shostko I. S. 565
Shostko O. S. 565
Shostko S. N. 565
Shrenk A. E. 400
Shumljansky I. I. 304, 326
Shvelidze R. R. 363
Sibruk L. V. 453, 573
Silaev A. M. 284
Sirenko Yu. K. 395
Sivov A. N. 122
Slyozkin V. G. 331
Slyusar V. I. 241, 244
Smirnov S. A. 104
Smirnov Yu. G. 150
Sokolov A. 299, 301, 410
Sosunov B. V. 204
Spevak I. S. 206
Starchenko S. I. 246
Stepanenko P. Ya. 492
Stepanov A. S. 173
Stepanov L. N. 353
Sukharevsky I. V. 408
Sukharevsky O. I. 152
Synepoop A. V. 248
Synyavskyy A. T. 233
Syrotyuk V. H. 201

Talalaevskii V. M. 515
Tankov I. V. 346
Tarasov V. B. 1
Tarshin V. A. 266
Terent'ev J. M. 155
Tereshchenko V. M. 382

Timchenko A. V. 536
Timoshenko V. V. 124
Tischenko V. P. 279
Titarenko L. A. 290
Tkachenko V. I. 499, 502
Tokarsky P. L. 158, 248
Tolokneyev E. A. 264
Troshchin O. L. 478
Trusov V. N. 212
Tsekhmistrov E. V. 138
Tsuji M. 80
Turchin V. I. 228

Ulyanov Yu. N. 355
Urasaki S. 41
Urazgildiev I. R. 251
Usin V. A. 468

Vagapov A. M. 251
Vartanov A. A. 150
Vashinsky S. E. 408
Vasilishin V. I. 254
Velasco Hererra V. M. 258
Veliev E. I. 160
Velychko L. G. 256
Vodotovka V. I. 568
Voitovich O. A. 279
Volkov A. A. 374
Voloshina V. A. 162, 358
Volosyuk V. K. 258
Vorgul I. Y. 165
Voskresenskii D. I. 3, 482
Voychinsky A. M. 545
Vyazmitinova A. I. 181
Vyazmitinova S. S. 181
Vytovtov K. A. 539

Xu D. 449

Yaldiz A. E. 395
Yaresko D. I. 117, 169
Yatsuk L. P. 360
Yatzuk K. P. 363
Yazdandoost K. Y. 438
Yeliseyeva N. P. 365
Yemelyanov K. M. 429
Yevdokimov A. P. 261, 368
Yonezawa R. 41
Yukhanov A. Yu. 167
Yukhanov Yu. V. 87, 167
Yukhno S. E. 476

Zaichenko Y. V. 556
Zaikin A. E. 237
Zaikin I. P. 169
Zakharia Y. 171
Zalevsky G. S. 152
Zamyatin V. I. 264
Zarudnev I. I. 95
Zaskalniy V. V. 385
Zelkin E. G. 124
Zhang Y. 449
Zhilin A. V. 209
Zhirnov V. V. 544
Zimina S. V. 287
Zvegintsev V. N. 534
Zvezdina M. Yu. 111, 113, 173
Zvyagintsev A. A. 176

Computer Editor: Sergey Litvintsev

Signed for publishing on 10.08.99. Format 60×90/8, printer's sheets 75, circulation 200 copies.
Order N 18/99

Prepared and printed in Publishing House of "Izvestija VUZ. Radioelektronika".
Adress: 37, prospekt Pobedy, Kyiv, 252056, Ukraine
E-mail: radio@rtf.ntu-kpi.kiev.ua

PRINCIPAL PROBLEMS OF THE REFLECTOR ANTENNAS SYNTHESIS

V. I. Andrianov, L. D. Bakhrakh, V. F. Los', A. Y. Makarov, V. B. Tarasov

Moscow Scientific-Research Institute of Device Designing (MSRIDD)
Phone: (095) 249-22-41, 249-0704; fax: (095) 148-79-96

An idea to controlling the radiation field at changing medium parameters and a form of boundary surfaces initially has been proposed in optics, though the practical development it has gained in the antenna techniques, in particular, when developing reflector and lens antennas. A great deal of works were devoted to the expedient synthesis of reflector antennas (and generally to two-surface ones) in geometrical approximation. As a rule, forms of wave fronts with the distributions of electromagnetic field vectors prescribed on them had been used as the initial data, that is a certain continuously-unique conformity between points of these forms had been given.

The problem of transformation of the input wave front into the output one in two-surface axially symmetrical systems was solved long ago. However, in axially asymmetric antennas this problem accurate solvability had been denied [1]. This circumstance, nevertheless, did not make weaker the interest to the problem, taking into account high practical importance of asymmetric reflector antennas. Various practical methods of wave fronts transformation were published, and in a number of cases, approximations proved to be satisfactory. And although the problem had not been clarified theoretically, doubts in validity of conclusions of the work [1] appeared, what stimulated the theoretical investigations to be continued.

In the work [2], the rigorous proof was given of the accurate solution to the problem of transformation of wave fronts amplitude distributions in the general case of two-surface systems (reflectors and homogeneous lenses) with the aim to optimize their energetic characteristics.

At the same time in a lot of cases, the problem of accurate expedient transformation of the antenna polarization characteristics is of theoretical and practical interest as well.

On the example of homogeneous two-surface lens (a particular case of which at the reactive index $n = -1$ is a two-reflector antenna), the following theorem has been proved. If between two points of arbitrary wave fronts the continuously-unique conformity is given, there the two-surface lens produced from homogeneous isotropic material exists, that transforms

the input wave front into the output one. The proof is based on the existence inside medium of the normal straightforward congruence of beams under condition that the refracting surfaces of lens are not in the domain of the vector field caustic. Vectors of the refracted beams between lens surfaces are described by the Pfuff differential equations, which are integrated when the theorem conditions are satisfied. Thus, under given assumptions, an antenna of any complexity with optical feeding is equivalent to the generalized two-surface lens.

The proof of existence of the accurate geometrooptical solution is based on the normalized equation of energetic balance in different cross-sections of a beam-pipe. This equation does not depend, in particular, on polarization direction of the transformed field vectors, and therefore, has certain degrees of freedom. The latter means availability of arbitrary relation between parametrizations of both wave fronts, i.e. ambiguity of the solution to be obtained. In particular, this relation can represent limitations on a choice of symmetry type of the amplitude characteristics.

Prescription of additional requirements to transformation allows to eliminate the solution ambiguity. Just so in the work [3] is shown that the adding of the practically and theoretically important requirement of expedient transformation also of the antenna polarization characteristics (so-called the equation of polarization balance) leads to the closed, without degrees of freedom, system of equations to be solved with the known methods [4].

As an example, in 1996 there was treated the amplitude-polarization transformation of the far-field zone of an electric dipole (with a cross-polarization component sharply manifesting itself) into the homogeneous in amplitude and polarization field of plane wave in the antenna aperture. Such a transformation is of high applied importance, for example, in radio astronomy.

It is shown, that the equation of polarization balance imposes the rigorous conditions on a choice of the wave converter architecture (of the Gregorian or Cassegrain type). In this case, the reflector system realizing the specified transformation is to be asymmetric, and just of the Cassegrain type. It should be expected that the analogous conclusion will take place in the general case of the geometrooptical amplitude-polarization transformation of the input field into the output one as well.

REFERENCES

1. B. E. Keenber, "About two-reflector antenna", Radiotekhnika I elektronika, N 6, 1962 [in Russian].
2. L. D. Bakhrakh, V. B. Tarasov, "Accurate geometrooptical synthesis of two-surface lens and reflector antennas of general type", in Journal "Antennas", issue 1 (38), 1997 [in Russian].
3. L. D. Bakhrakh, V. B. Tarasov, "Expedient transformation of wave amplitude-polarization characteristics in two-reflector systems of general kind", Electromagnitnye volny I elektronnye systemy. V.1, No 1, 1996 [in Russian].
4. E. Kamke, "Handbook on differential equations in partial derivatives of the first order", M.: Nauka, 1966 [in Russian].

FIBER-OPTIC TECHNOLOGY FOR ANTENNA SIGNAL TRANSMISSION AND DISTRIBUTION: PRESENT STATE AND PERSPECTIVES

A. N. Bratchikov, D. I. Voskresensky and T. A. Sadekov

Moscow State Aviation Institute (MAI-Technical University)
Faculty of radioelectronics of flying vehicles. Division 406
Russia 125871 Moscow Volokolamskoye Sh., 4. E-mail: alexbrat@aha.ru

This paper reflects the state-of-the-art of a new and rapidly growing field [1], dealing with fiber-optic systems for antenna signal transmission. The two principal configurations of fiber-optic links with intensity modulation and direct photodetection (IMDD) are analyzed, using direct (DM) and external modulation (EM) of optical carrier by antenna signals. The basic system parameters of both configurations are compared: frequency bandwidth, insertion loss of RF signals, noise performance, linearity and dynamic range. The principal problems are formulated, which restrict wide applications of fiber-optic systems for antenna signal transmission in optically based antennas in radar and communication electronic complexes. The modifications of fundamental IMDD fiber link schemes are considered, providing successful solution of mentioned problems. Examples of practical IMDD fiber link applications are discussed.

INTRODUCTION

Development of modern high performance radar, communication and monitoring electronic complexes, utilizing antenna systems, including phased arrays, for air- and space-born applications, requires further decreasing of cost, mass, size and power supply; increasing the operational frequency, bandwidth, output power, sector and rate of spatial scanning.

Future antenna systems must have extended functional possibilities due to preliminary signal processing in space, time and spectral domain [2].

First the possibility of fiber- and integrated optic technology application in antenna technique was realized in [3] for phased arrays. At present, except of numerous review publications [4]-[5] and large number of papers, several monographs are issued in the new field by both antenna and fiber optic specialists [6]-[7].

There are three main fields in antenna technique, where fiber-optic and optoelectronic technologies find now successful application: (a) fiber- optic systems for antenna signal transmission and distribution; b) fiber-optic systems for beamforming and beamsteering in phased arrays and (c) fiber-optic systems for data processing.

This paper covers the first topic, dealing with fiber-optic systems for antenna signal transmission.

FIBER-OPTIC SYSTEMS FOR ANTENNA SIGNAL TRANSMISSION

This section considers the two principal IMDD fiber link configurations, using direct (DM) and external (EM) modulation of optical carrier by antenna signals [8]. The goal of such a consideration is to compare both DM and EM techniques in terms of main link figures of merit: bandwidth, loss, and noise performance in the form of signal-to-noise ratio (S/N), dynamic range and linearity.

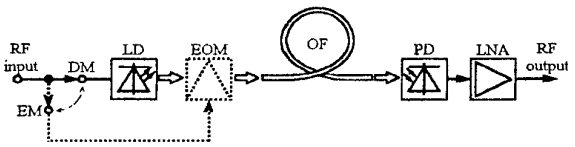


Fig. 1. The schematic of the two basic fiber-optic IMDD links with direct (DM) or external (EM) RF modulation of the optical carrier

The Fig. 1 shows the schematic of the two principle fiber-optic IMDD link configurations, united in the same hypothetical block diagram.

In the DM fiber link the antenna signal is imposed onto the laser bias current, yielding an intensity modulation of the optical beam. The EM based fiber link use a laser operated CW to drive an external optical modulator, which imposes the RF signal.

Frequency Bandwidth

In short single mode fiber links the bandwidth limitations are mainly due to modulation and photodetection processes.

Bandwidth limitations due to modulation: The bandwidth performance of DM fiber link modulating device is determined by the relative intensity noise (*RIN*) spectrum of the laser diode

$$RIN(f) = \langle \Delta P^2(f) \rangle / P_0^2 , \qquad (1)$$

where $\langle \Delta P^2(f) \rangle$ is the spectral density of the square of the optical power fluctuation and P_0 is the dc laser power. The frequency f of LD modulation is normally limited by the relaxation oscillation frequency f_r. The operating DM frequency has to be much less than f_r, because in the vicinity of f_r laser enters the self-

oscillating mode and instead of useful modulation imposes on optical carrier the relaxation oscillations. So maximum bandwidth of DM links is roughly 20 GHz, Fig. 2. The external modulator, that typically is in use in EM configuration Fig. 1 is an electrooptic travelling wave device, containing an optical waveguide structure in the form of Mach-Zehnder interferometer (MZI), embedded into $LiNbO_3$ substrate, over which a micro stripe electrode pattern is deposited. Accurate matching of optical and microwave phase velocities gives the 3-dB electrical bandwidth of 70 GHz. Simultaneous improvement of coupling the modulation signal onto the electrodes increased the bandwidth to 94 GHz.

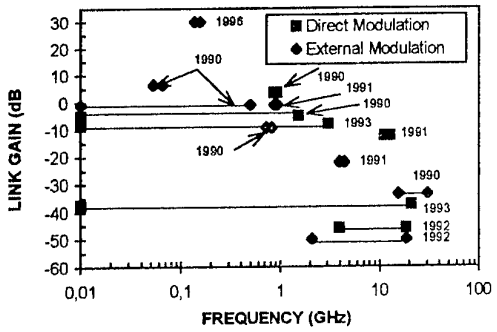


Fig. 2. Summary of DM and EM IMDD link gains (losses of RF signal) across frequency bands [8]

Bandwidth limitations due to photodetection: The photodetection bandwidth limitations are common for both DM and EM links with IDDD. Most of the photodetectors (PD) now have *p-i-n* semiconductor structure and operational wavelengths 1.3–1.55 μm. The Fig. 3. shows the summary of reported PD bandwidths versus responsivity.

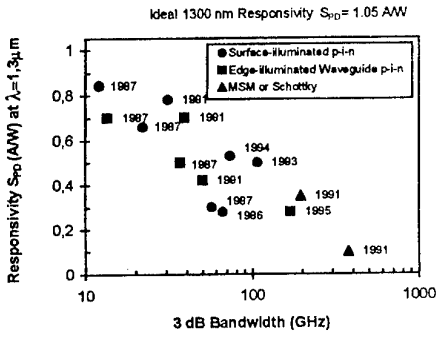


Fig. 3. Summary of reported PD bandwidths versus responsivity [8]

Insertion Loss

Fibers with transmission losses (0.2–0.5) dB/km are in competition with coaxial cables, metallic and dielectric waveguides with loss 120 dB/km, 1 and 0.5 dB/m, correspondingly. Insertion loss coefficient in *directly modulated* fiber link Fig. 1 is given by [1], [8] and one could estimate the order of loss coefficient magnitude $\alpha_{DM} = -(15 - 35)$ dB. The insertion loss of RF modulation power in the *external modulation* link is given by [1], [8] and is estimated to be about –(35-60) dB, that is approximately 30dB worse than α_{DM}.

Noise Performance

Signal-to-noise-ratio (SNR): In any IMDD link the total noise power at the PD output is contributed by: all components of LD noise (P_{LD}); short noise (P_{sh}), arising from the photodetection process; and thermal noise, arising from modulation device, PD and LNA (P_{th}) and also from ohmic losses in matching interfaces between input RF link and LD or EOM and between PD and output RF link. The Fig. 4 shows the dependence of $(SNR)^{-1}$ on photodetector current I_0 and link loss α_{DM}.

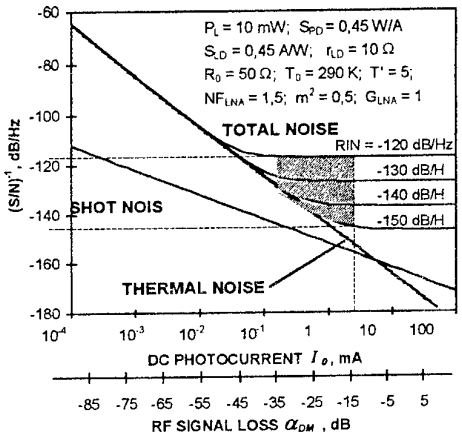


Fig. 4. Noise-to-signal ratio $(S/N)^{-1}$ dependence on dc photodetector current I_0 and loss α_{DM} for typical link parameters [1]

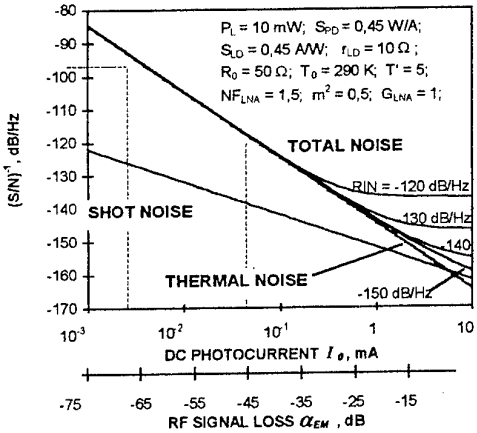


Fig. 5. Noise-to-signal ratio $(S/N)^{-1}$ dependence on dc photodetector current I_0 and loss α_{DM} for typical link parameters and $\kappa\alpha_{.4} = 0.01$ [1]

If operational bandwidth is, for example, ΔF = 1 GHz, SNR is estimated to be within 30-50 dB. The corresponding $(SNR)^{-1}$ dependence for EM is depicted in Fig. 5. If operational bandwidth is, for example, ΔF = 1 GHz, SNR is estimated to be within 10–30 dB.

Linearity

The nonlinearities are generated mainly in the optical source module and potentially in any amplifier, operating in large input signal mode. Thus the performance of the laser and external modulator must be examined to determine harmonic and intermodulation signal levels. In spectral domain the IMDD links look like narrow band passband RF filters with bandwidths less than one octave, so mentioned harmonics might be filtered in optical receivers with second harmonic suppression ratio more than 50 dB. That's why in narrow band IMDD links the primary measure of nonlinearity is the two-tone third order intermodulation products (IMP). The IMP level is typically measured at the link RF output for the two input RF signals at closely spaced frequencies f_1 and f_2. Interaction with nonlinear characteristics of LD or EOM leads to the appearance of not only higher harmonics of $f_{1,2}$, but also of intermodulation overtones of third-order at frequencies $2f_1 - f_2$ and $2f_2 - f_1$, inside link bandwidth.

In *direct modulation* IMDD fiber link nonlinear distortions appear mainly due to injection LD, which is *an active source* of *distortions* [9]. The third order intermodulation product (IMP) is shown to have the form

$$P_{2\omega_2-\omega_1} = \frac{2P_0 J_2(a_2) J_1(a_1)}{J_0(a_2) J_0(a_1)} \cos[(2\omega_2 - \omega_1)t], \quad (2)$$

where P_0 is time averaged photon density, $J_x(a_i)$ are the modified Bessel functions of the xth order and a_i, i = 1,2 are steady state solutions for output amplitudes of photon densities of both optical test signal components.

In *external modulation* IMDD fiber link nonlinear distortions appear mainly due to EOM, which is *a passive source of distortions* [9]. The third-order intermodulation product at frequency $2\omega_2-\omega_1$ may be estimated as follows

$$P_{2\omega_2-\omega_1} = P_{M\max} J_1(a) J_2(a) \cos\frac{\pi V_b}{V_\pi} \sin(2\omega_2 - \omega_1)t, \quad (3)$$

where $a = \pi v_m / V_\pi$, V_M is the applied voltage, V_π is the bias voltage V_b, required for 100% modulation or for full on-to-off optical switching.

Dynamic Range

If antenna signal consists of multiple RF carriers, the dynamic range (DR) of fiber link has the form of intermodulation-free DR (IMFDR). Following [8] and [9], the IMFDR is the maximum difference between the noise floor and the fundamental output power, which produces IMD term of equal amplitude to the noise floor. By another words, the IMFDR is the third order IMD-free range of input RF power for which the fundamental signal power at the link output is above the noise floor. It is important to note, that while the SNR_0 has the dimension of dB in 1Hz bandwidth (dB·Hz), the IMFDR, being measured in 1 Hz bandwidth, has the dimension of dB·Hz $^{2/3}$. If antenna signal consists of single RF carrier, the DR of fiber link has the form of compression dynamic range (CDR). The IMFDR of *direct modulated* IMDD fiber link depends on LD type used. The DM links on the basis of Fabry-Perot (FP) laser diodes has lower IMFDR, than that, based on DFB lasers, because DFB lasers have less RIN and more linear light-current dependence: $IMFDR_{FP} \approx 105$ dB·Hz$^{2/3}$, $IMFDR_{DFB} \approx 120$ dB·Hz$^{2/3}$. The techniques, which improve RIN by using an optical isolator and low back-reflection photodetector, permitted a FP laser link to have approximately the same IMFDR as the DFB laser link [8].

The IMFDR of an *external modulated* IMDD fiber link is dominated by the external modulator type used and average optical power. However, the IMFDR for EM fiber link using a standard Mach-Zhender modulator is about the same as for a DFB-based DM fiber link.

In practice experimental data is used to characterize both DRs in any concrete situation, Fig. 6.

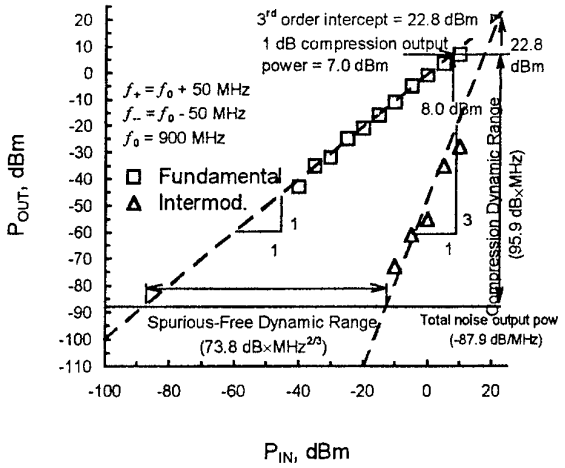


Fig. 6. Measured dynamic range of the experimental external modulated fiber-optic link at 900 MHz [9]

Direct vs. External Modulated Fiber Link: What Is Better?

To answer the question it is necessary to summarize the significant properties of both configurations:

- The unavoidable loss of the modulator always makes external modulation have 20–30 dB lower gain.
- In the EM link the post-amplifier and PD thermal noise are dominant compared with LD noise, the SNR is less compared with DM link.
- Direct modulation links operate at $f \langle f_r$, where laser's RIN is large.
- When large input signal level P_L must be accommodated, the DM fiber link will seriously degrade in *S/R* due to uncreased RIN.
- External modulated links can use lasers with $f \rangle\rangle f_r$. In this case, the laser contribution to the link noise can be negligibly small.

Summarizing the mentioned above conclusions, the traditional answer usually was [8], that of course, it is better to modulate LD directly, than to use it as optical source for external modulator.

However, small nonlinearities, high DR and possibility of link gain improvement make EM fiber link more and more attractive for numerous antenna applications.

MODIFICATIONS OF FUNDAMENTAL IMDD FIBER LINK CONFIGURATIONS

Modifications, Caused by the Problem of Frequency Bandwidth

Comparison of bandwidth limitations in IMDD fiber links due to modulation and photodetection processes shows, that while the latter may be done up to 350 GHz, modulation may be performed in considerably less bandwidth. The problem of modulation bandwidth can be principally solved by using the coherent method of remote heterodyning [10], where the classic modulation process is absent, but millimeter and even submillimeter harmonic signals can be obtained by interferention in PD active volume of the two optical carriers, shifted in frequency domain to the desired RF beat note reference [11]-[12].

Generation of the two offset tuned optical components: The main difficulties of this generation in practice are due to multifrequency character of LD output spectrum and random fluctuation of spectrum parameters due to natural and technical reasons. Natural fluctuations are connected with: (a) the single mode LD instability (mode hopping), caused by temperature and age effects and (b) quantum fluctuations of frequency and phase of optic field, which determine the line width of generated mode $\Delta\nu$ and instantaneous frequency inside $\Delta\nu$. Technical fluctuations are conditioned by high sensitivity of the frequency to the variations of LD temperature and pump current – 120 GHz/degr and (1–5) GHz/mA, respectively.

At present the mode hopping problem is successfully resolved by using the LD with distributed feedback (DFB) or distributed Bragg reflectors (DBR), where the boundary between *p*- and *n*- semiconductor areas for the whole length or only near the LD facets, respectively, has the corrugated form, supporting the stable single longitudinal mode generation [13]. The technical fluctuations of LD spectrum are eliminated by frequency etalon in the form of Fabry-Perot optical resonator or gas cell with super narrow transmission spectrum. Frequency stabilization is also performed by optoelectronic feedback systems, where the error signal, proportional to frequency shift, controls the LD temperature and pump current. Mentioned systems provide relative frequency instability of $(\Delta f / f_0) = 10^{-12} - 10^{-11}$ for 100 *s* [14]. Returning back to the effect of quantum frequency and phase fluctuations on relative frequency instability $(\Delta f / f_0)$ of the two off-set tuned LD, note, that instantaneous optic frequency of both LD randomly changes in the vicinity of their $\Delta\nu$. If both variations are independent, the beat frequency bandwidth, centered at differential frequency $f_0 = \nu_1 - \nu_2$ is twice an each LD bandwidth: $\Delta f = 2\Delta\nu$, otherwise, $\Delta f \to 0$ independently on $\Delta\nu$.

Semiconductor InGaAs lasers of DFB and FP types, operating at $\lambda = 1.5$ μm have $\Delta\nu = (10\text{-}300)$ MHz, that corresponds for $f_0 = 30$ GHz to the relative frequency instability $\Delta f / f_0 \sim (10^{-3} - 10^{-2})$ [15]. This value is not suitable for antenna applications in present electronic complexes, which require at least $\Delta f / f_0 \sim (10^{-4} - 10^{-6})$ [16]. To improve this performance, LD with less $\Delta\nu$ should be used or frequency and phase correlation should be introduced of both lasers. In one method of LD line width narrowing it locates inside high quality optical resonator: under weak coupling to resonator $\Delta\nu = 1$ MHz was obtained, that is corresponded to $\Delta f / f_0 \sim 10^{-4}$, and under strong coupling, respectively, $\Delta\nu = 15$ kHz and $\Delta f / f_0 \sim 10^{-6}$ [17]. Another method of beat signal line width narrowing is based on correlation improvement of phase (and frequency) fluctuations of both lasers by external injection locking of each LD as slave ones from master LD with much less $\Delta\nu$ [11]-[12].

For injection locking of two offset tuned LD, the master LD is modulated by harmonic signal with the frequency *F*, so that $2kF = f_0 = (\nu_1 - \nu_2)$, $k = 1, 2, \ldots$, . By this way output spectrum of master LD acquires components at frequencies of the two slave LD $\nu_{1,2} = \nu_0 \pm kF$, $k = 1, 2, \ldots$. Injection locking improves correlation of phase fluctuations in both lasers, leading to the narrowing of Δf independently of the $\Delta\nu$ values in each LD. By this method the values of Δf and $\Delta f / f_0$ were obtained as 20 MHz и 10^{-3}, respectively.

Better Δf narrowing may be obtained by injection locking of the two longitudinal modes inside DFB la-

ser: $\Delta f = 10$ kHz and $\Delta f / f_0 \sim 10^{-6}$ [18]. This method was also realized in fiber version of DFB laser [19], which is more convenient to conjugate with optical fiber, than conventional semiconductor LD. This structure with the two longitudinal modes detuned on $f_0 = \nu_1 - \nu_2 = 40$ GHz, provided $\Delta\nu = 900$ Hz and $\Delta f / f_0 \sim 0.5 \cdot 10^{-4}$ even without external injection locking [20].

To solve the bandwidth problem by coherent interferentional technique, it is necessary to ensure the narrowest line width of both single mode LD (or both modes in single LD), stable position of mode frequencies and high level of frequency and phase correlation between interacting optical components. Simultaneous application of mentioned methods [14] provides $\Delta f = 10^{-3}$ Hz, that is, $\Delta f / f_0 \sim 3.10^{-12}$.

Modifications, Caused by the Insertion Loss Problem

In the case of antenna signal distribution between M remote customers including modules of phased arrays, real loss in a single channel is 20lgM dB bigger than $\alpha_{DM,EM}$. Extra big loss limitation by ~25 of the number M_{max} of antenna channels, fed by single optic source, decrease SNR and dynamic range of distributed signals, require multistage electronic amplifiers, that complicates the total system, increases its mass, cost and power supply. As a result, fiber optic system may lose in competition with traditional microwave transmission systems. The insertion loss problem may be successfully resolved by modification of classic configurations Fig. 1 on the basis of erbium doped fiber amplifiers (EDFA). Compared with semiconductor optical amplifiers and non-linear (Raman) fiber amplifiers, EDFA have the advantages [21]: low insertion loss (< 1 dB) with more than 30 dB gain, which is insensitive to light polarization; more than 10 dBm saturation power; low crosstalk for several amplified signals; low insertion noise with the quantum limit level (3–4 dB); good reproducibility of spectral amplification dependence for all samples; low rippled and weakly temperature dependent gain as a function of wavelength. Disadvantages of EDFA: operates only at $\lambda = 1.5$ μm optical wavelength; requires additional components: optical pump source with output power 50–100 mW, selective optical coupler and optical isolators; can't be manufactured on integrated optic basis. A travelling wave EDFA schematics, presented in Fig. 7, contain three main elements: Er-doped fiber 4, selective optic coupler 2 and semiconductor laser pump source 1.

Optical isolators 3 and bandpass filters 5 provide the elimination of fiber end reflection effects on optic signal source operational mode and makes the filtration of the amplified spontaneous emission for SNR increasing, respectively. Reflection-type EDFA in Fig. 7b provides higher differential amplification θ (amplification in dB per 1 mW of pump power P_p) that gives more effective utilization of pump power but increases EDFA sensitivity to P_p fluctuations. Low threshold pump power P_{th}, required for total transparency of fiber, is typical for the reflection-type EDFA. For P_p = 18mW and θ = 1.1 dB/mW the reflection-type EDFA has G_{max} = 20 dB. Traveling wave EDFA under the same conditions provides only G = 2-3 dB and twice lower θ value.

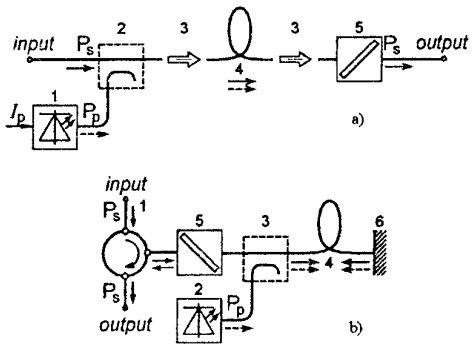


Fig. 7. Structural configurations of travelling wave (a) and reflection type Erbium-doped fiber amplifiers [21]

Modifications, Caused by the Problem of Phase Stability

The problem of phase stability is common for both DM and EM IMDD fiber links [1]. This problem arises every time when it is necessary to distribute in-phase harmonic signals (or digital signals without mutual delays) to several remote antennas of long base line radio interferometers, multipositional radars and modules of phased arrays. For mentioned above applications parasitic phase difference between adjacent channels should not exceed 1–5° [22]. The thermal sensitivity of modulation signal phase Φ is usually characterizing by the thermal phase sensitivity *(TPS)* coefficient

$$K_T^{\Phi} = \frac{d\Phi}{\Phi dT} . \qquad (4)$$

So, temperature variation ΔT causes at the output of fiber link the L -dependent parasitic phase shift

$$\Delta\Phi = \Phi K_T^{\Phi} \Delta T . \qquad (5)$$

For the fiber with silica core and polymer cladding $dN/NdT \approx 7 \cdot 10^{-6}$ 1/degr, $dL/LdT \approx (5 \cdot 10^{-7} - 3 \cdot 10^{-5})$ 1/degr, $(L/N)\partial N/\partial L \approx -0.22$, and the *TPS* value may be estimated as $K_T^{\Phi} \approx (7 \cdot 10^{-6} - 3 \cdot 10^{-5})$ 1/grad. If ΔT = 10 °K, L = 100 m and f_0 = 30 GHz, then $\Delta\Phi \approx$ (6.4–27.5) radians or (367–1576) degrees that exceeds the requirements for mentioned applications. Transformation of IMDD fiber link into phase stabilized ones requires link modification on the component [23], system [24] or/and structural [25] basis. Fiber channels, providing $\Delta\Phi$ = (1–5) degrees are usually called phase stabilized fiber links. The *structural method* of phase stabilized

fiber link modification [25] uses instead of traditional fiber length the extended optical filters, Fig. 8.

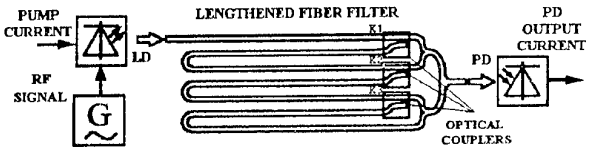


Fig. 8. Phase stabilized fiber optic link with lengthened transversal optical filter [25]

This method does not need neither complicated and costly phase stabilized fibers as in the component approach, nor the additional costly apparatus as in the system approach and stabilizes the electrical (for RF envelope) length of the fiber optic link over a wide range of environmental temperature. Structural method provides $K_T^{\Phi} \approx 2 \cdot 10^{-6}$, stabilizing the level of parasitic phase to $\Delta\Phi = \pm 1$ degrees for the environmental temperature range 15–100°C.

EXAMPLES OF PRACTICAL IMDD FIBER LINK APPLICATIONS

Transmission of Microwave Signals to and from a Satellite Antenna

The satellite and ground based fiber-optic distribution systems are used to transmit microwave signals from CPU to and from remote antennas located both on satellite board and on the ground [26]–[27]. In [28] the DM IMDD fiber link is used for the transmission of the 500-MHz C-band microwave signal spectrum to and from ground based 10-m satellite antenna, transmitting and receiving the 4 GHz signal from the AT&T Telstar T-302 satellite. Satellite signals, composed of typically 3-4 video signals, 1-2 sets of 60 Mbit/s QPSK signals and several sets of 3.088-Mbit/s QPSK signal, is transmitted over distances of up to 20 km with 1 dB or less of degradation in SNR for video and digital signals. The minimum reduction of *SNR* due to fiber link, expressed in noise figure ($NF = SNR_{in}/SNR_{out}$) was about NF = 2.5 dB under the APD's gain of 39 dB. The total IMD level, mainly generated by LD, was about –42 dBc under –5 dBm of input modulation power. The IMFDR and CDR, estimated on the basis of experimental data, were about 27.5 and 39 dB, respectively, that was acceptable for system operation.

Fiber-optic links provide meeting the phase noise and signal-to-noise specifications of modern radars [29]. In that work fiber channel was used remote the transmitter and antenna of the AN/SPQ-9B radar in transmit configuration. In [30] the same demonstration was performed to demonstrate the receive configuration, Fig. 9.

The AN/SPQ-9B radar specifications in receive channel gain, noise figure and compression dynamic range (CDR) are 0 dB, < 22 dB and > –8.5 dBm, respectively. Fiber-optic link with direct modulation, being implemented in radar configuration as shown in Fig. 9, offered –0.09 dB, 18 dB and –4 dBm, respectively. Fiber-optic link with external modulation offered 0.06, 16 dB and –10 dBm, respectively. The SNRs measured with DM and EM fiber links were slightly lower than that, measured for the baseline: 82.3 and 81.5 dB, respectively against 82.6 dB in baseline.

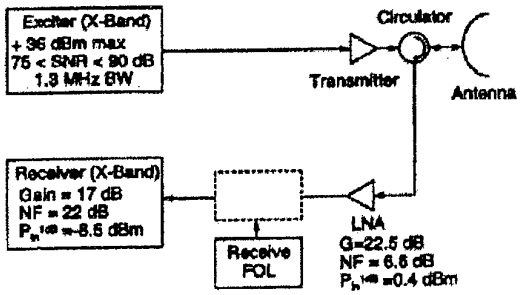


Fig.9. The simplified stuctural configuration of the AN/SPQ-9B Radar with the receiver fiber link [30]

The Indirect Phase Locking of Ka-Band Free Running Impatt Oscillator of Antenna Array Module

In accordance with remote data mixing configuration [31] the feed to each module is comprised of two fiber-optic links 100 m long, Fig. 10. The LD1 of fiber optic synchronizing link with 3 dB bandwidth of 6.3 GHz is directly modulated in a large signal mode by an 8dBm input power from a master oscillator at 3.246 GHz. In this mode of operation LD generates higher order harmonics, and the fourth order harmonic at 12.986 GHz is detected, amplified and used to subharmonically injection locking an IMPATT oscillator at 38.96 GHz, that is, on the twelfth harmonic of the master oscillator. A locking range of over 100 MHz was achieved. The fiber optic data communication link carries the 1GHz bandwidth communication signal and imposes it on Ka-band carrier in nonlinear mixer. The LD2 of data link with 3dB bandwidth of 1.6 GHz is modulated by FM signal at GHz with modulation index β = 0.85, providing the IMD level of D_{IMD} = –(28–9) dBc for m = 0.1–0.9.

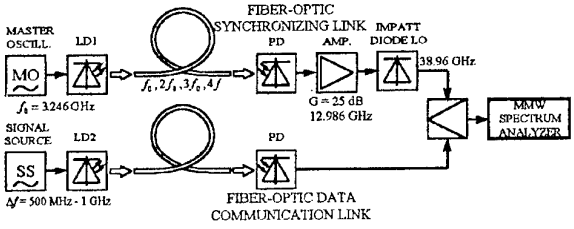


Fig. 10. Experimental set-up for indirect subharmonic synchronization of Ka-band IMPATT oscillator by S-band master oscillator [31]

Multichannel Transmission, Utilizing Er-Doped Fiber Amplifier

Optical Er^{3+}-doped fiber amplifiers (EDFA) are used in the frequency division multiplexing (FDM) system, Fig. 11 for distribution and transmission of 5 GHz-spaced, 16-channel IM signals at a bit rate of 622 Mbit/s. Four from sixteen DFB LDs, operating at $\lambda = 1543$ nm and stabilized in frequency at 5 GHz intervals, were intensity modulated by $LiNbO_3$ EOM with non-return-to-zero (NRZ) pseudo random code. The IM light beams were multiplexed and distributed by a 16×16 star coupler. Multiplexed signals at one of the output ports of a coupler were coupled to the EDFA with a length of 90 m. The 1.48 μm LD with output optical power of 80 mW were used as pump lasers. Optical isolators prevented EDFA from lasing.

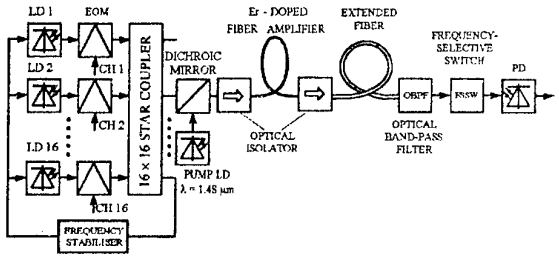


Fig. 11. Experimental set-up of 16-channel optical FDM distribution/transmission experiment utilizing Er^{3+}-doped fiber amplifier [32]

After transmission the 13 km-long single mode optical fiber the optical band-pass filter (OBPF) with 2 nm bandwidth absorbed the spontaneous emission of EDFA. The channel position in frequency domain is then selected by frequency selective switch (FSSW) providing the interchannel crosstalk less than –20 dB. A GaAs APD and FET circuit was used as the receiver for direct detection with single-channel sensitivity – 39.1 dBm, which is degraded by 1.1 dB to 38 dBm for 16-channel transmission. A signal gain of more than 15 dB per channel was achieved in the experiment. At the output of post APD amplifier the signal level was 1.0 dBm for single-channel transmission and –12.8 dBm for 16-channel transmission.

Fig. 12 illustrates another version of EDFA application in analog fiber-optic link [33]. A broadband and gain flattened EDFA is used with a flat amplification bandwidth of 54 nm by employing a parallel configuration/ The amplifier consists of 1.55 μm-band and 1.58 μm-band EDFA units. The input 13 channel signals to each EDFA unit and the output signals from the units were multiplexed and demultiplexed using 1.55/1.58 μm-band WDM coupler, respectively. The broadband fiber channel was shown to demonstrate the flat amplification for the signal wavelength regions of 1530 – 1560 nm and 1576–1600 nm with a gain non-uniformity of < 1.7 dB and a signal gain of 30 dB.

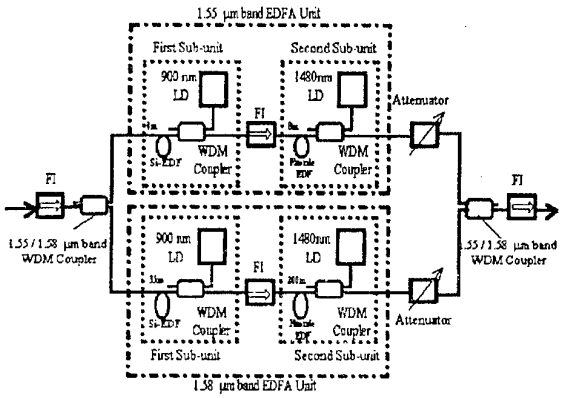


Fig. 12. Broad band and gain-flattened fiber link with Er^{3+} fiber amplifier [33]

SUMMARY

Optical fibers find now application in the three principal areas of antenna technique: (a) fiber-optic systems for antenna signal transmission and distribution; (b) fiber-optic systems for beamforming and beamsteering in phased arrays; (c) fiber-optic systems for data processing. The first topic, being the fundamental for all the rest ones is described here in detail. The two principal direct detection configurations are analyzed and compared, using direct and external intensity modulation of optical carrier by antenna signals. The principal problems are formulated, which restrict wide application of optically based antennas. The modifications of fundamental fiber link schemes are considered, providing successful solution of principal problems. Examples of practical fiber link applications are discussed.

REFERENCES

1. A. N. Bratchikov, "Optical fibers and antennas. (Invited paper) ", *Proc. 10-th International symposium on antennas, Nice, France*, pp.275-289, 1998.

2. D. I. Voskresensky, A. Yu. Grinev and E. N. Voronin, *Electrooptical Phased Arrays.* New-York: Springer Verlag ,1989.

3. J. R. Forrest, F. P. Richards, A. A. Salles and P. Varmish, "Optical fiber networks for signal distribution and control in phased array radars", *Proc. Int. Conf. "RADAR'82", IEE publ. No.216,* pp. 408-412, 1982.

4. A. Seeds, "Optical transmission of microwaves", in *The Review of Radio Science,* W.Stone, Ed. London, UK.: Oxford Univ. Press, 1996, pp. 325-360.

5. A. N. Bratchikov, "Fiber-ptic systems for phased array antennas", *Russian J. on Advances of Modern Radio Electronics*, No.7, pp. 3- 15, 1997.

6. H. Zmuda and E. N. Toughlian, *Photonic Aspects of Modern Radar*. Norwood, MA: Artech House, 1994.

7. N. A. Riza, Ed., *Selected Papers on Photonic Control Systems for Phased Array Antennas*, (SPIE Milestone Series), Bellingham, WA: SPIE, 1997.

8. C. Cox et al., "Techniques and performance of intensity- modulation direct-detection analog optical links", *IEEE Trans. Microwave Theory Tech.*, vol.45, pp. 1375-1383, Aug.1997.

9. A. S. Daryoush et al., "Interfaces for high speed fiber-optic links: analysis and experiment", *IEEE Trans. Microwave Theory Tech.*, vol. 39, pp.2031-2044, Dec. 1991.

10. A. N. Bratchikov, I. P. Glukhov, "Interferentional fiber links for microwave signal transmission", presented at the *XXIV Gen. Assembly, Int. Union Radio Sci.* Kyoto, Japan, Aug, 1993.

11. L. Goldberg et al., "35 GHz microwave signal generation with injection-locked laser diodes", *Electronic Letters.*, vol.21, no. 18, pp. 814-815, 1985.

12. K. Chang et al., "Microwave generation using sidebend locked lasers", *Proc. SPIE*, vol. 789, pp. 54-59, 1987.

13. K. Peterman, *Laser Diode Modulation and noise.* Norwood, MA: Kluwer, 1988.

14. Z. F. Fan and M. Dagenais, "Optical generation of a Megaherz-linewidth microwave signal usung semiconductor lasers and a discriminator-aided phased-locked loop", *IEEE Trans. Microwave Theory Tech.*, vol. 45, pp.1296-1300, Aug. 1997.

15. T. Kimura, "Coherent optical fiber transmission", *J. Lightwave Technol.*, vol. LT-5, pp. 414-428, Apr. 1987.

16. R. S. Raven, " Requirements for master oscillators for coherent radar", *Proc. IEEE*, vol. 54, pp. 237-243, Feb. 1966.

17. W. T. Tsang, Ed., *Semiconductor Injection Lasers*, (Lightwave Communication Technology Series, vol. 22), Orlando, FL: Academic Press, Inc., 1985.

18. D. Wake, C. R. Lima and P. A. Davies, "Optical generation of millimeter-wave signals for fiber-radio systems using a dual-mode DFB semiconductor laser", *IEEE Trans. Microwave Theory Tech.*, vol. 43, pp. 2270-2276, Sept. 1995.

19. M. Sejka rt al., "Distributed feedback Er^{3+}-doped fiber laser", *Electron. Lett.*, vol.31, pp. 1445-1446, 1995.

20. W. H. Loh and R. I. Laming, "1.55 μm phase shifted distributed feedback fiber laser", *Electron. Lett.*, vol.31, pp. 1440-1442, 1995.

21. A. N. Bratchikov and A. P. Sheremeta, "Optical amplifiers on the basis of Er-doped fibers: present state" in *Modeling, Measurement & Control, A.*: AMSE Press, Tassin-la-Demi-Lune, France, vol.54, no.3, pp.1-25, 1994.

22. M. I. Skolnik, Ed., *Radar handbook*, New York: McGraw-Hill, 1990.

23. T. Kimura et al., "New UV-curable primary coating material for optical fiber". *Electron. Lett.*, vol.20, pp. 201-202, 1984.

24. N. Shah and M. Shadaram, "Phase stabilization of reference sig-nals in analogous fiber optic links", *Electron. Lett.*, vol. 33, pp. 1164-1165, 1997.

25. A. N. Bratchikov, S. A. Garkusha, T. A. Sadekov, "Phase stabilized fiber channel for UHF signal distribution based on an extended optical filter", *Photonics and Optoelectronics,* vol.4, No.2, pp.79-83, 1997.

26. A. S. Daryoush et al., "High-speed fiber-optic links for distribution of satellite trafic", *IEEE Trans. Microwave Theory Tech.*, vol. 38, pp.510-517, May 1990.

27. W. Way and R. Wolff, "A 1.3μm 35 km fiber optic microwave multicarrier transmission system for satellite Earth stations," *J. Lightmave Technol.*, vol. 35, pp. 1325-1332, Sep. 1987.

28. J. E. Bowers et al., "Long distance fiber-optic transmission of C-band Microwave signals to and from a satellite antenna", *J. Lightwave Technol.*, vol.LT-5, pp.1733-1741, Dec., 1987.

29. J. E. Roman et al., "Photonic remoting of an SPQ-9B ADM ultra-high dynamic range radar, *IEEE Radar Conference, Dallas,TX,* 1998.

30. J. E. Roman et al., "Photonic remoting of the receiver of an ultra-high dynamic range radar, "*IEEE International microwave*

31. P. R. Daryoush, "Optical technology for spacecraft antennas", *Proc. SPIE*, vol.840, pp. 169-174, 1987.

32. H. Toba et al., "16 channel optical FDM distribution/transmission experiment uyilizing Er^{3+}-doped fiber amplifier", *Electron. Lett.*, vol.25, pp. 895-897, Jul. 1989.

33. M. Yamada et al., "Broadband and gain-flattened amplifier composed of a 1.55μm-band and a 1.58 μm-band Er^{3+}-doped fibre amplifier in a parallel configuration", *Electron. Lett.*, vol.33, No.8, pp. 710-711, April 1997.

HOT RADIATORS IN ANTENNA MEASUREMENTS

S. V. Butakova and K. A. Butakov

Box 10744, 310140, Kharkov, Ukraine.
Tel. +380 0572 272409

ABSTRACT

The properties of black body SHF models which are artificial sources of radio noise radiation and methods for antenna parameters measuring with the help of «hot» radiators (at radiation temperatures of 1000 ÷ 100000 K) are given. In the radiators it is possible to control dimensions of the radiating aperture, polarization and temperature of radiation. The hot radiators are certified by means of the national standard black body thermal model with the error not more than 2-4%.

ARTIFICIAL RADIATORS FOR ANTENNA MEASUREMENTS

The antenna parameters measured by classic methods at a narrow frequency band can be changed appreciably in case of the bandwidth broadens and the signal spectrum changes. Radiometric methods based on the use of artificial noise radiators allow to measure antenna parameters over a required frequency range of the investigated radiation.

Radiometric methods of the antenna measurements have been developed since the fifties on the basis of the use of radiation of both the heavenly bodies and the artificial radiator so-called «the black disk». It is a plate made of a microwave absorber material. The black disk is placed against a «cold» sky background in the far-field region or in the Fresnel region of a test antenna and signals received by the antenna from the sky and the disk are compared. A black disk radiation temperature is near the standard temperature (290 K). The black disk method is considered as one of the most exact those (the error is not more than 5-10% [1], 7-14% [2]). In this method it is necessary to direct the principal efforts towards accounting of external radiations (of local objects, of a background, re-reflections from the source and so on). The antenna pattern side lobes were registered by the black disk method at the level of 13-17 dB [3], 15-20 dB [4].

Consider the properties of the thermal radiator– *black disk.*

1. The disk is in the thermodynamic equilibrium with the environment at temperature T. The field on the radiating aperture of the disk has the correlation area $\sigma \geq \lambda^2/\pi$, where λ is the radiation midband wavelength.

2. The isotropic radiation (without interference effects) is formed near the geometric radiating surface, at the far-field distance R of the correlation area, $R \geq 2\sigma/\lambda$.

3. The radiation polarization is chaotic as a rule.

4. The noise power spectral density (NPSD) and the noise temperature of the isotropic radiation are determined by thermodynamic temperature T and emissivity ε (the absorption coefficient) of a material by $T_s = \varepsilon T$; $G = kT_s$; (as a consequence of Kirchhoff's and Rayleigh–Jeans' laws), where $k = 1.3806 \times 10^{-23}$ W/K/Hz (the Boltzmann's constant).

5. The radiation pattern is like Lambert's pattern, i.e. $T_s(\vartheta,\varphi) = \varepsilon(\vartheta,\varphi)T \cong \varepsilon T\cos\vartheta$.

There is no need of orienting precisely the radiator electrical axis on a receiving antenna.

6. An effective area of the radiating aperture is equal to the geometric area of the disk, i.e. $A_d = S_d$.

7. If the half-power beamwidth of a receiving antenna is larger than the angular size of the radiating aperture, a diffracted wave and a radiation pattern of a couple «disk–antenna» appear. In order to take into account this field it is necessary to introduce a diffraction correction for a noise temperature measurement of the disk [1, 2].

In radio astronomy of the Sun for the absolute calibration the standard field method is used. A standard field source comprises a calculated pattern horn with a calibrated transmitter [5]. For the transmitter power to be calibrated by the resistor thermal noise it is possible to change the calibrated transmitter by a calibrated noise generator. The noise temperature of that source is much more than 290 K. It is the «hot» radiator. The method of the standard field enables one to decrease the measurement error down to 1 %.

Consider the properties of the radiator in the form of *an directional antenna with a noise generator.*

1. The correlation area on the radiating aperture is equal to the antenna effective area A_e.

2.The isotropic radiation is formed at a far-field distance R_o of the antenna, $R_o \geq 2A_e/\lambda$.

3. The radiation polarization is determined by an eigenvector of the antenna polarization.

4. A monomode spectral radiance of the isotropic radiation is equal to $B = \varepsilon_1 kT_{ng}/2\pi$;

where $\varepsilon_1 = \eta\{1-[(SWR-1)/(SWR+1)]^2\}$,

T_{ng} is the noise generator radiation temperature; η is the antenna efficiency; the standing–wave ratio (SWR) in the antenna feed line describes a matching between the antenna and the noise generator. In the radiating aperture electrical centre $T_s = \varepsilon_1 T_{ng}$. T_s–distribution across the radiating aperture falls to its edges.

5. It is important to orient precisely the radiator electrical axis on the receiving antenna. The radiation pattern $T_s(\vartheta,\varphi)$ is determined by the antenna parameters.

6. The effective area of the radiator is equal to the effective area of the antenna, i.e. $A_r = A_e$.

7. It is necessary to take into account a secondary radiation pattern of a couple of antennas.

We see there is a large difference between the radiation pattern of the radiator in the form of the directional antenna with the noise generator and Lambert's pattern. Therefore, it is possible to attribute the value T_s only into a small solid angle round the antenna electrical axis. The angle has to be the same under conditions of the calibration and of the measurements of antenna parameters. When calibrating it is possible to place the receiving antenna only in the far-field region of the radiator.

Now let us consider properties of a radiator in the form of *an array of identical noise sources* consisted of low directional antennas with a matching noise generator. This is *a non-phased antenna array (NPAA).* [6,7]

1. The correlation area is equal to an effective area of the partial antenna, $\sigma_1 \geq \lambda^2/\pi$.

2. The isotropic radiation is formed at a far-field distance of the partial antenna, $R \geq 2\sigma_1/\lambda$.

3. The radiation polarization is determined by the sum of eigenvectors of the partial antenna polarization.

4. A monomode spectral radiance of the isotropic radiation is equal to $B = N\varepsilon_1 kT_{ng}/2\pi$; where N is the number of partial antennas in the NPAA.

On the radiating aperture $T_s = \varepsilon_1 T_{ng}$.

The T_s–distribution is nonuniform on the radiating aperture but if the NPAA intercepts the half-power beamwidth of the receiving antenna, the parameter «average radiation temperature $\overline{T}$ on the aperture» is used.

5. The radiation pattern $T_s(\vartheta,\varphi)$ of the NPAA is determined by that of a partial antenna by

$$T_s(\vartheta,\varphi) = \varepsilon(\vartheta,\varphi)\overline{T} \cong \varepsilon_1 F(\vartheta,\varphi)\overline{T}\,.$$

There is no need to orient precisely the radiator electrical axis on the receiving antenna.

6. The radiating aperture effective dimension $D_e = D_o + 2\rho_1$, where D_o is the radiating aperture geometrical dimension, the boundary of which passes over centres of the NPAA's external partial antennas and ρ_1 is the correlation radius of a radiating element.

$$\rho_1 = 0.5\sigma_1^{1/2} = \lambda(4\pi)^{-1/2} \cong 0.282\lambda.$$

7. It is possible to decrease appreciably a diffraction field at the NPAA's edges framing it within an absorber with the ambient temperature.

After comparing the listed above properties of the different artificial radiators of the radio noise we conclude that the radiation properties of a non-phased array of low directional identical noise sources are like those of the black disk, but such an array may give a much higher temperature when using plasma noise generators. Therefore, it is possible to carry out all the measuring procedures of the black disk method with the help of a «hot» NPAA, to achieve a larger dynamic range and a higher precision because external radiations can be neglected in comparison with NPAA's radiation. With the NPAA the antenna pattern side lobes are registered at the level of 30–40 dB [8].

It is possible to manufacture hot radiators NPAA with controlled aperture sizes, polarization and temperature of the radiation. A variant of such a radiator is shown in Fig. 1 [9]: the side view (a), the view of the radiating aperture (b). Serial semi-conductor noise generators 3 are connected through matching transformers 2 with slots 1. Over the slots plane there is net 4 of conductive tapes 5 which form cells 6 made in shape of the isosceles right-angled triangle (IRT). Each slot is placed along IRT's cathetus symmetrically relatively to net nearest knots and a tape plane. Tape width L is selected by the equation

$$L/a = 0.25/\{[(a/\lambda)^2 - 0.25]^{1/2} - [(a/\lambda)^2 - 0.5]^{1/2}\},$$

where a is IRT's cathetus length.

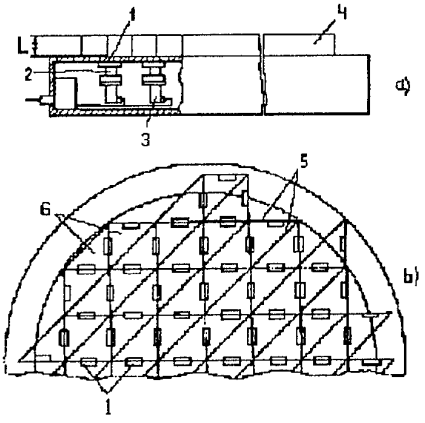


Fig. 1

If the net is mounted, then an elliptically polarized radiation has the right or left orientation when switching on the noise generators in rows or in columns. The radiation has a horizontal or vertical polarization by the

same switching without the net. One gets the chaotic polarization by switching on all the noise generators.

The hot radiators have enabled one to propose new methods for antenna diagnostics to be considered further.

METHODS FOR MEASURING ANTENNA PARAMETERS

Measurements of ohmic losses and efficiency

1. The method for measuring antenna ohmic losses is worked out on the basis of a noise passing through the antenna. A device for mesurements is given in Fig.2 [10]. Noise generator 1 and radiometer 2 are connected with inputs 4,5 of Y-circulator 3; test antenna 7 is connected with input 6 of the Y-circulator. Two absorber rings 8 adjoin a contour of the antenna aperture. Together with the antenna they form a cavity whose aperture is recovered by polarization matching assembly 9 and by well conducting metallic screen 10. Assembly 9 must be excluded when testing an antenna with a linear polarization.

In the device of Fig. 2 (without crosspiece 11) the noise generator is switched on and assembly 9 is controlled to get maximum signal U_1 of the radiometer. The signal covers the following path 1→4→3→6→7→8→9→10 ⇒9→8→7→6→5→2.

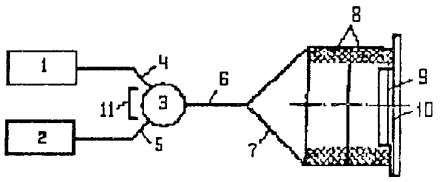


Fig. 2

Each ring partially absorbs waves on the path from the antenna to the screen and backwards and prevents parasitic resonant oscillations of the cavity.

When reflecting from screen 10 a mirror turn of an incident wave polarization ellipse takes place due to π–shift of phases of orthogonal linearly polarized components. In assembly 9 a polarization vector direction changes twice so that polarization vectors of the antenna and of the arrival wave appear to be matched.

In the device of Fig. 2 (without crosspiece 11) we leave one ring 8 and fix signal U_2. The first ring is replaced by the second one and signal U_3 is fixed. Noise generator 1 and the input of radiometer 2 are connected by setting crosspiece 11 between points 4.5. Signal T_{ng} is fixed. The following equations describe these procedures

$$\left.\begin{aligned} U_1 &= T_{ng}[k\eta^2(vw)^2 nR + q]; \\ U_2 &= T_{ng}[k\eta^2 v^2 nR + q]; \\ U_3 &= T_{ng}[k\eta^2 w^2 nR + q]; \end{aligned}\right\} \quad (1)$$

where η is the antenna ohmic loss factor to be defined; k,n,q are the certificate values of the Y-circulator transmission coefficients between arms 4→6, 6→5, 4→5; v, w are the transmission coefficients of the path «the antenna–the screen–the antenna» in the presence of one ring; R is a screen reflectivity. Taking into account that R = 1 we define η, v, w from the system of Eq (1). Let us determine η by

$$\eta = (1/vw)[(U_1 - qT_{ng})/(T_{ng} \times knR)].$$

According to this equation the total error of determination of ohmic loss factor η for antenna array ≈7 %, for lens antenna ≈ 9.5 %. Earlier there were no methods to define namely antenna ohmic losses being the principal part of antenna losses. In the proposed method antenna 7 is the part of the hot radiator structure as well as noise generator 1.

2. A device for the antenna efficiency direct mesurements is given in Fig. 3 [11]. Radiator 1 recovers an aperture of test antenna 2 connected with radiometer 3. Contact thermo-transformers are placed on the antenna surface. Noise temperature T_s and emissivity ε of the hot radiator are known. If the radiator is made as the NPAA, the apertures of the antenna and the radiator has to be placed at the distance R not nearer than the far field region of the radiating element.

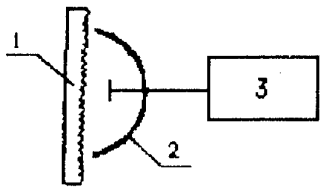


Fig. 3

In the device of Fig. 3 antenna real temperature T_a is measured by the thermo-transformers and radiometer reading T is recorded. There are following signals arriving to a radiometer input: 1) from the radiator with noise temperature T_s after passing through the antenna, 2) the antenna thermal radiation reflected by the radiator and falling on the antenna aperture, 3) the antenna thermal radiation in the direction of the radiometer.

$$T = \eta T_s + \eta(1 - \varepsilon)T_a + T_a(1 - \eta) \quad (2)$$

From the equation (2) we define the antenna efficiency by

$$\eta = (T - T_a)/(T_r - \varepsilon T_a). \quad (3)$$

If $T_s >> T_a$ (for the hot radiator) instead of (3) we can write

$$\eta = T/T_s \qquad (4)$$

When using the approximate formula (4) instead of (3) an error is not greater than 1% if T_s is 10 times T_a and not greater than 0.1% if T_s is 100 times T_a. The measurement error of the efficiency η does not exceed 4 %.

We note that direct methods of an antenna efficiency measurement have been absent to this day. The known indirect methods are very labourconsuming. They are based on measurements in the free space. According to the first method it is necessary to measure in the far field region or in the Fresnel region of the antenna. According to another one it is possible to combine black disk radiation measurements in the near field region and near field phasometric ones.

Measurements of gain and scattering coefficient

Owing to creation of the aperture radiators with autonomously switched elements (NPAA), methods of absolute measurements of antenna gain and scattering coefficient [12, 13] are worked out. It is possible to use the radiator of Fig. 1.

1. An equipment for gain measurements can be designed in two variants shown in Fig. 4: A) test antenna 1 is placed on a mast; B) antenna 1 is ground-based. The latter is directed towards radiator 2 with which control system 3 is connected. The antenna is connected with radiometer 4.

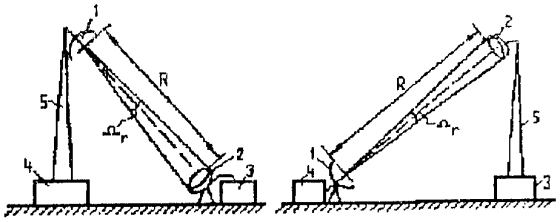


Fig. 4

The radiator has to be placed in the far field region or the Fresnel region of the antenna. In the latter case an parabolic antenna feed has to be carried off the focus. In the variant B it is recommended to place a phase centre of a highly directional antenna at a distance from the ground surface not smaller than the doubled height of the antenna. Angle of vision Ω_r of the radiator from the antenna has to be smaller than the antenna half-power beamwidth, i.e.

$$\Omega_r < \Theta_a \qquad (5)$$

In the equipment of Fig. 4 radiometer reading T_1 is recorded when the antenna is directed towards the radiator in which all the noise generators are switched on. Hot aperture area S_1 and its average noise temperature T_s are known.

Noise generators in the external hoop are switched off. ed off. The aperture area decreases to a known value S_2 and the noise tempereture does not change. Radiometer reading T2 is fixed. Every time when repeating operations of switching off noise generators in radiator external hoops a radiometer reading is fixed. We get a row of values The aperture area decreases to known value S_2 and the noise tempereture does not change. Radiometer reading T_2 is recorded. Every time when repeating operations of switching off noise generators in radiator external hoops a radiometer reading is recorded. The obtained row of values T_1, T_2, ...T_j,...,T_n, corresponds to the row of values of hot aperture areas S_1, S_2, ... S_j, ... S_n. The position of the radiator electrical axis does not change when switching off noise generators in the radiator external hoops.

All the noise generators are switched off and radiometer reading T_o is measured. We obtain the function $f(S) = \Delta T_j/S_j$, where $\Delta T_j = T_j - T_o$, extrapolate it in a spot $S = 0$ and write $f(S = 0) = \Delta T/S(S = 0)$. We define the antenna gain by

$$G = (4\pi R^2/T_s)\Delta T/S(S = 0). \qquad (6)$$

The G–definition error according to Eq. (6) is not more than 3.6 %.

2. For scattering coefficient measurement the equipment of Fig. 4 is used. The condition (5) is met. Antenna efficiency η is known. In the equipment of Fig. 4 radiometer reading T_1 is recorded when the antenna is directed towards the radiator in which all the noise generators are switched on. Hot aperture area S and its average radiation temperature T_s are known.

Each of two noise generators is switched off in chessboard manner. At this operation aperture area S does not change and the noise temperature decreases to known value T_s'. Radiometer reading T_2 is recorded.

We define the antenna energy scattering coefficient off the solid angle Ω_r by

$$\beta = 1 - (T_1 - T_2)/[\eta(T_s - T_s')]. \qquad (7)$$

The definition total error according to Eq. (7) is not more than (4.6–5.4) %.

Measurement of antenna pattern

In the radio astronomy a multiplicative interferometer is used for measuring an antenna pattern. Spaced antennas 4, 5 are connected with inputs of correlation radiometer 7. (See Fig. 5.) Antennas electrical axes are directed towards radio noise radiator 1 which is placed in far-field or Fresnel region of antennas. A phase difference of source 1 radiation is compensated in the antennas. A correlation function of a radiation received with the different turning angles of test antenna 4 and

with auxiliary non-scanning antenna 5 is recorded in the radiometer output. An radiometer output signal in the quadrature corresponds with a real component of an unknown pattern of antenna 4 and in the phase with a imaginary component of the same pattern [14, 15].

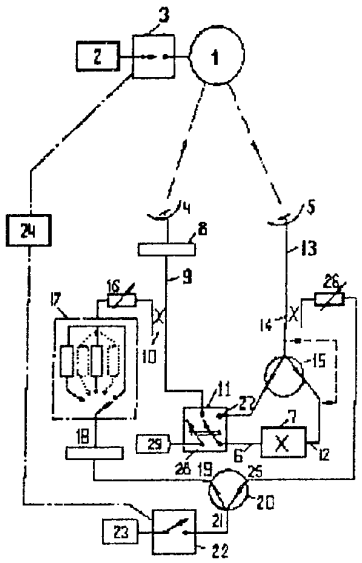


Fig. 5

After a correlation processing the larger the angle between the directions of a disturbance source and of radiator 1 and the greater product $B \times p$, where B is the radiometer bandwidth and p is the distance between the antennas 4,5 the weaker a disturbance signal becomes. The correlation reception expands the dynamic range by 10–15 dB in comparison with traditional methods of the antenna measurements by means of ordinary radio receivers.

Such antenna pattern measurements have a systematic error being stipulated by a nonlinearity of the correlation radiometer transfer characteristic and by the antennas' thermal noise. This error is estimated in [1] by

$$\sigma = 10 \ldots 16\%. \qquad (8)$$

A principle enabling to increase the measurement accuracy by eliminating the above mentioned error is described further and is illustrated by Fig. 5 [16]. Before the beginning of measurements electrical axes of the antennas are directed towards radiator 1. Power-supply 2 is switched on and commutator 3 is locked. Switchboard 11 is in the first position (terminal 27 is connected with input 6 of radiometer 7; terminal 28 and matched load 29 is connected with feed line 9), tee 15 is shunted by short-circuiting shown in Fig. 5 by means of a dotted line with arrows. Antennas 4,5 are connected consecutively with feed line 13 and each of them is turned to obtain the maximal signal of the radiometer indicator. A phase difference of source 1 radiation is compensated in the antennas by delay line 8.

The primary channel of radiometer 7 is calibrated. The switchboard 11 is in the first position. Commutators 3, 22 is switched synchronously in the opposite phase with the help of control system 24. Regulating attenuator 26 reading the equality of the radiometer readings is obtained when radiator 1 or noise generator 23 is switched on. Later attenuator 26 reading does not change.

The first measurement is carried out. Switchboard 11 is in the second position shown in Fig. 5. By means of regulating readings of attenuator 16 and delay line 8 and switching in magazine 17 of fixed calibrated attenuators, the equality of the radiometer readings is obtained when radiator 1 or noise generator 23 is switched on. The summary attenuation magnitude of attenuator 6 and magazine 17 (A_o) is fixed.

The ij-th measurement is carried out. Switchboard 11 is in the second position. Test antenna 4 is turned so that its electrical axis deflected from the direction towards radiator 1 by angles φ_i, ϑ_j. The first measurement is repeated and a summary attenuation magnitude of attenuator 6 and magazine 17 (A_{ij}) is fixed. We define the ij-th point of an antenna power pattern by

$$F(\varphi_i, \vartheta_j) = A_{ij}/A_o \qquad (9)$$

So in the known method [14,15] the correlation radiometer is used for direct reading. In the proposed principle [16] the radiometer functions as a comparator and readings are obtained with the help of the more accurate instruments that are attenuator 16 and magazine 17. It allows to compensate an measurement error being stipulated by a nonlinearity in the channels of the correlation radiometer and by the antennas non-identity (by their thermal noises). The point (9) definition error is smaller than 1.6% [17].

Measurement of a field amplitude and phase distribution (FAPD)

When a long proving ground is absent near-field techniques is used. In this method a probe antenna is used to samble the phase and amplitude, for two polarizations, of the radiated narrow-band field in the near region of the test antenna that is at a few wavelengths from its surface. The probe antenna scans over a well defined surface which can be for example a plane in front of the test antenna. From the measured FAPD an antenna pattern may be defined by means of the space Fourier transform. If an information about frequency properties of the antenna is necessary the same measuring process must be repeated for every required frequency.

Methods of defining FAPD in the required range of frequencies during one passage of the probe antenna are known. A wide-band pulse field is formed on the antenna aperture, field amplitude time dependences are recorded in space points of an antenna near region, the

time dependencies are transformed into the frequency domain by means of the frequency Fourier transform and then antenna patterns are calculated for required frequencies [18]. A measurement bandwidth is restricted by an upper frequency limit of a stroboscopic oscillograph (1–4 GHz). There is no possibility to test active receiving antennas which do not sustain pulse reactions.

The use of a noise signal instead of an pulse one removes mentioned restrictions. A functional diagram of a device for FAPD measuring in the required frequency range is shown in Fig. 6 [19]. Source 1 of a radio noise signal includes a serial semi-conductor noise generator with the radiation temperature ~200000 K, an amplifier with a bandwidth 3–4 GHz and a directional coupler. The first output of source 1 is connected with test directional antenna 2. Probe antenna 3 is supported by orientable frame 4. It is connected with the first input of two-channel receiver 5. The second output of source 1 is connected with the second input of receiver 5 through connecting line 7. Receiver 5 outputs are connected with inputs of correlometer 6. The correlometer includes one quantizator in every input circuit. Further there is a steerable delay line in one channel. Then both the channels are connected with a multiplier. To its output an integrator, a discrete memory circuit and a digital indicator are connected consecutively.

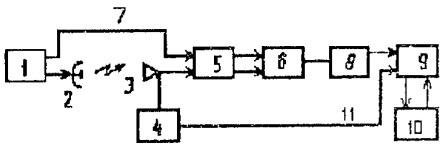


Fig. 6

With the correlometer output frequency Fourier transformer 8, memory circuit 9 and space Fourier transformer 10 are connected in series. Instead of positions 8,9,10 it is possible to use a computer with a corresponding software.

This method allows to widen a measurement work range close to millimeter waves. The minimum wavelength is defined by a value of a probe antenna doubled step. It can make up 4–5 mm when an error of a probe antenna setting in a required point is not more than 0.5 mm.

REFERENCES

1. N. M. Tseitlin, Antenna techniques and radio astronomy. Moscow: Soviet Radio, 1976. 350p. [in Russian].
2. L. N. Zahariev and A. A. Lemanski, The scattering of waves by «black bodies». Moscow: Soviet Radio, 1972.– 288 p. [in Russian].
3. V. I. Andrianov, L. D. Bakhrakh, I. V. Vavilova, V. G. Volkov, and K. I. Moguilnikova «Using the radiometric method for antenna measurements», Moscow: Antennas, no 18, 1973, 3-17 [in Russian].
4. A. P. Kurochkin, «State and perspectives of development of antenna external parameters measurement methods», Moscow: Antennas, no 30, 1982, 46-65 [in Russian].
5. A. Krüger, Introduction to Solar radio astronomy and radio physics.– D.Reidel publishing company. Dordrecht: Holland/Boston: USA. London: England. 1982.–469 p.
6. S. V. Butakova, «Antenna array», USSR author certificate no 786803. Feb.8,1977 (Priority). Bulletin izobretenii, no 5, 1982 [in Russian].
7. S. V. Butakova, «Aperture noise radiators in microwave radiometry», Moscow: Foreign radio electronics. Successes of advanced radio electronics, no 4, 1997, 3-26. 137 references [in Russian].
8. Ju. N. Seriakov, and R. I. Shabanov, «Calibration of radio noise radiation sources by using an antenna with the known gain», Moscow: Measuring techniques, no 7, 1982, 60-61 [in Russian].
9. S. V. Butakova, I. E. Jila, G. L. Kluzner, and A. F. Ljahovski, «Antenna array», USSR author certificate no 1241327. Aug.5,1983 (Priority). Bulletin izobretenii, no 24, 1986 [in Russian].
10. S. V. Butakova, K. A. Butakov, and N. M. Kuznetsov, «Device for defining the antenna ohmic losses», USSR author certificate no 1228044. March 24, 1983 (Priority). Bulletin izobretenii, no 16, 1986 [in Russian].
11. S. V. Butakova, K. A. Butakov, and L. P. Shelegov, «Method for defining the antenna efficiency», USSR author certificate no 924627. Nov. 24, 1978 (Priority). Bulletin izobretenii, no 16, 1982 [in Russian].
12. S. V. Butakova, and K. A. Butakov, «Method for measuring the antenna gain», USSR author certificate no 1037192. April 23, 1982 (Priority). Bulletin izobretenii, no 31, 1983 [in Russian].
13. S. V. Butakova, K. A. Butakov, and L. P. Shelegov, «Method for defining the antenna scattering rate», USSR author certificate no 1239645. July 24, 1984 (Priority). Bulletin izobretenii, no 23, 1986 [in Russian].
14. P. G. Smith, IEEE Trans., 1966. Vol. AP-14, no 1, 6-16.
15. F. Torres, A. Camps, J. Bara, I. Corbella, and R. Ferrero, «On-board phase and modulus calibration of large aperture synthesis radiometers: study applied to MIRAS.» IEEE Trans. on GRS. 1996. V.34, no 4. 1000-1009.
16. S. V. Butakova, K. A. Butakov, and N. I. Lecin, «Method for defining the antenna pattern», USSR author certificate no 1355949. Sept.23, 1985 (Priority). Bulletin izobretenii, no 44, 1987 [in Russian].
17. S. V. Butakova, and K. A. Butakov, «A correlation method of the antenna radiation pattern measurememt with the help of the artificial aperture source of SHF noise.» Moscow: Radio Engineering, 1995, no 6, 96-98 [in Russian].
18. D. M. Ponomaryov, V. I. Turchin, etc., «Method for defining the antenna pattern at a frequency range», USSR author certificate no 1415203. Bulletin izobretenii, no 29, 1988 [in Russian].
19. S. V. Butakova, K. A. Butakov, and V. I. Lesnikov, «Method for defining the amplitude and phase distribution of an antenna field at a frequency range», USSR author certificate no 1721547. Jan.3, 1990 (Priority). Bulletin izobretenii, no 11, 1992 [in Russian].

AN EXTREMELY FAST-CONVERGENT ITERATIVE METHOD OF SYNTHESIS AND ITS APPLICATION TO DESIGN OF HIGH PERFORMANCE ANTENNAS AND MICROWAVE COMPONENTS

F. F. Dubrovka

National Technical University of Ukraine "KPI", 2110-D, Faculty of Radioengineering,
Laboratory of Antennas and Telecommunications, 12 Politechnichna str., Kyiv, 252056, Ukraine
Tel./Fax: +380-44-241-7223, E-mail: dubrovka@ucl.kiev.ua

ABSTRACT

The paper presents an universal extremely fast-convergent iterative method of synthesis of physical objects and its application to synthesis of high performance antennas and microwave components. Due to the proper combining in each iteration a fast approximate analytic or parametric synthesis with rigorous analysis and introduction and the proper generating a new modified design objective in accordance with obtained differences between rigorously calculated characteristics of interest and actual design objectives, the iterative process is usually completed after a few optimization iterations.

INTRODUCTION

At present there is a variety of synthesis techniques applied in electromagnetic devices and other field engineering. Most of them use gradient information to find global optimum of a given function. The procedure of global optimum searching is often very time-consuming, if rigorous analysis of such devices is used.

The most versatile and precise method of diffraction synthesis of reflector antennas is proposed in [1]. When using this iterative method, the main reflector and subreflector profiles are represented in the form of expansion in Jacobi's functions, with subsequent gradient optimization of the expansion coefficients to obtain the required radiation pattern. At each iteration radiation pattern is calculated with taking into account of the near field, boundary diffraction, the subreflector supports, shading introduced by structures, etc. The method requires a large number of iterations and therefore is time-consuming that may be regarded as a disadvantage.

The problem is: how can most of guesswork be removed from synthesis and thus synthesis procedure can be made fast-convergent?

One possible way is using genetic algorithms [2], which have being extensively developed for electromagnetic systems during last years.

An another way is introduced in this paper and this way is a universal extremely fast-convergent iterative method of synthesis of physical objects.

As concerns synthesis of new dual-reflector antennas, this method of synthesis fits into the group of indirect methods since the purpose of the synthesis is not the radiation pattern itself but the required amplitude and phase distribution of the electromagnetic field in the aperture of the antenna main reflector. However, this fact does not impair the method potentialities and its practical value since we may consider the problem of relation between field distribution in the main reflector aperture and the radiation pattern in the angular sector adjacent to the main lobe as solved. But these are the near side lobes that present main difficulty, being of main concern to designers of antennas with a *prescribed* envelope of side lobes. The far side lobe level depends primarily (in the case of correct choice of the aperture field distribution) on the choice of the radiation angle of the subreflector edge, accuracy of the reflector surface, selection of the cross-section and location of the struts and on the antenna adjustment.

In the case of application of this synthesis method to improvement of performances of existing large dual-reflector earth station antennas to meet the current CCIR stringent requirements and to synthesis of high performance microwave components (filters, OMT, polarizers, rotators, etc.) as design objectives serve actual required characteristics like radiation pattern, VSWR, insertion loss, differential phase shift, et cetera. Recently, by using this method, a variety of high performance dual-reflector antennas and microwave components have been designed at the company "TERA" and Laboratory of Antennas and Telecommunications of National Technical University of Ukraine "KPI". At present some of the designed antennas and microwave components are in serial production. For example, updated 7 m and 3.66 m dual-reflector earth station antennas, that fully meet the CCIR requirements, are manufactured at state plant "Saturn" (Ternopil, Ukraine) and design office "Promin" (Ternopil, Ukraine) respectively.

A BRIEF OUTLINE OF THE METHOD

The block diagram of the method is shown in Fig. 1. It is assumed that *actual* required characteristics of a physical object under synthesis (e.g., amplitude and/or phase distributions, radiation patterns, frequency de-

pendencies of VSWR, insertion losses, phase shifts, etc.) serve as *actual* design objectives. In the first step these *actual* design objectives are used for an approximate synthesis (analytical or parametric) of the object design parameters (profiles, geometric parameters, dimensions, etc.) in the first iteration. As a result of the synthesis a set of the object design parameters (variables) is obtained. Then for the obtained design parameters, characterizing the object, an accurate (rigorous) analysis of the object is performed and the characteristics of interest are calculated. Next step in the first iteration includes evaluation of differences between the calculated and the actual required characteristics of the object. If the differences obtained exceed the permitted values then *new modified* (*false*) design objectives are generated in accordance with the following equation:

$$C_{k2}^{mr} = C_{k1}^{mr} - \left(C_{k1}^{c} - C_{k}^{ar}\right), k = 1,2\ldots, \qquad (1)$$

where C_{k2}^{mr} is a *new modified* required k-th characteristic of the object, which must be used for the approximate synthesis of the object parameters in the second iteration, C_{k}^{c} is a calculated k-th characteristic in the first iteration, C_{k}^{ar} is an *actual* required k-th characteristic and C_{k1}^{mr} is a modified required k-th characteristic in the first iteration (usually $C_{k1}^{mr} = C_{k}^{ar}$).

Generated in such a way *new modified* required characteristics serve as initial data for the approximate synthesis of the object parameters in the second iteration. Having performed the procedures like in the first iteration, in case the differences between the calculated and actual required characteristics exceed permissible values, we generate *new modified* design objectives which may be written as follows:

$$C_{k3}^{mr} = C_{k2}^{mr} - \left(C_{k2}^{c} - C_{k}^{ar}\right), k = 1,2\ldots. \qquad (2)$$

These *new modified* design objectives serve as initial data for the approximate synthesis of the object in the third iteration. After the i-th iteration is completed, in case the differences between the calculated and actual required characteristics exceed permissible values, we generate new modified objectives:

$$C_{k(i+1)}^{mr} = C_{ki}^{mr} - \left(C_{ki}^{c} - C_{k}^{ar}\right), k = 1,2\ldots, \qquad (3)$$

which define initial data for the approximate synthesis of the object in the $(i+1)$ iteration.

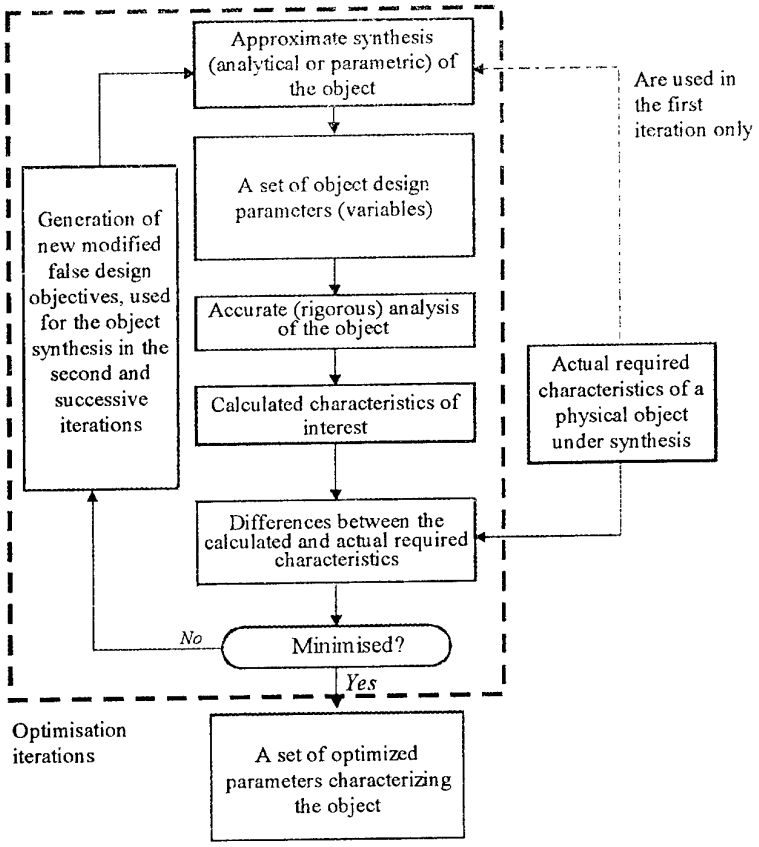


Fig. 1. Block diagram of the universal fast-convergent iterative synthesis technique for generation of optimum design parameters of a physical object with required characteristics

The iterative process continues until the differences between the calculated and *actual* required characteristics will be minimized to a given accuracy.

Thus, each iteration in this iterative method of synthesis includes four steps:

1. *approximate* (analytic or parametric) synthesis of a physical object, using *new modified* (*false*) design objectives (except the first iteration where *actual* design objectives are usually used) generated in accordance with equations (1) – (3);
2. accurate analysis of the synthesized object;
3. evaluation of differences between calculated and required characteristics;
4. generation of *new modified* design objectives in accordance with (1) – (3) which are to be used as initial data for synthesis in next iteration, if the obtained differences between the calculated and required characteristics are not minimized to a given accuracy.

The quintessence of this synthesis technique consists in the *proper combining* in each iteration a *fast rough synthesis* (analytic or parametric) with a *slow rigorous* analysis and *introduction* and the *proper generating* – in accordance with equations (1) – (3) *new modified* design objectives, i.e. *new modified* required characteristics, to be used in next iteration. Due to latter, already in the second iteration errors of an approximate synthesis of the object parameters are evaluated and the iterative procedure may be terminated. In the next sections we shall demonstrate an extremely fast convergence of this iterative method of synthesis in designing high performance dual-reflector earth station antennas and some microwave components.

APPLICATION OF THE METHOD TO DIFFRACTION SYNTHESIS OF MODERN HIGH PERFORMANCE DUAL-REFLECTOR ANTENNAS

In this section we shall concentrate on application of the method to diffraction synthesis of new modern high performance dual-reflector earth station antennas. As *actual* design objectives – *actual* required characteristics of a physical object under design – we take *actual* required amplitude and phase distributions of the electromagnetic fields in the aperture of an antenna main reflector under design. Correctness of this approach was discussed above. In this case the block diagram in Fig. 1 of the method is transformed to the block diagram in Fig. 2.

In the first iteration we initially perform the "rough" synthesis of geometry of the dual-reflector antenna based on *actual* required amplitude and phase distribution of the electromagnetic field yielding the *prescribed* characteristics of the antenna radiation. Then, for the obtained geometry of the antenna we carry out its rigorous analysis by diffraction theory methods. As a result, we obtain calculated amplitude and phase distributions of the electromagnetic field in the main reflector aperture. The amplitude and phase distributions are compared with *actual* required values, and their differences are evaluated. If the differences obtained exceed the permissible values then *new modified* (*false*) required distributions of the field in the main reflector aperture are generated using the equation (1), where now C_{k2}^{mr} are *new modified* required amplitude ($k = 1$) and phase ($k = 2$) distributions of the field in the main reflector aperture to be used for the synthesis in the second iteration, C_k^c are the calculated amplitude ($k = 1$) and phase ($k = 2$) distributions of the field in the first iteration, C_k^{ar} are *actual* required amplitude ($k = 1$) and phase ($k = 2$) distributions of the field in the aperture.

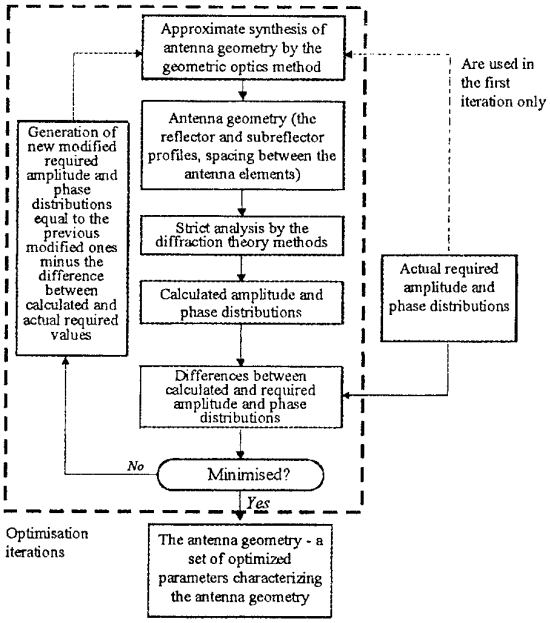


Fig. 2. Application of the method to diffraction synthesis of dual reflector antennas

The generated modified amplitude and phase distributions of the electromagnetic field in the main reflector aperture serve as a initial values for the synthesis of the antenna geometry in the second iteration. Having performed the procedure similar to those in the first iteration, after the second iteration (in the case when the differences between the calculated and actual required distributions for amplitudes and phases exceed the permissible values) we generate new modified required amplitude and phase distributions in the main reflector aperture for the third iteration in accordance with equation (2).

After implementation of the i-th iteration (if differences between the calculated and actual required amplitudes and/or phase distributions of the field in the aperture of the main reflector exceed the permissible values) we generate new modified amplitude and phase distributions in the main reflector aperture which determine initial values for the synthesis of the antenna geometry in the geometric optics approximation in the $(i+1)$ iteration, following the equation (3).

The iterative process continues until we minimize *to a given accuracy* the differences between the calculated by rigorous methods of the diffraction theory and the actual required distributions of amplitude and phase in the main reflector aperture.

Due to the *introduction* and proper generation of *new modified* required amplitude and phase distributions in the main reflector aperture no later than in the second iteration we can accurately evaluate the error of synthesis of the antenna geometry by the approximate method of geometric optics, and the iterative procedure may be terminated. Figure 3 demonstrates a case of extreme convergence of the method with the example of synthesis of geometry of a dual 3.66 m dual-reflector antenna with required uniform phase distribution in the main reflector aperture. It may be seen that after the first iteration the phase maximum deviation from the uniform pattern was 37°, and after the second iteration – less than 1°.

It is apparent that the most important part of the proposed method of synthesis which determines its accuracy is an accurate (rigorous) analysis of the dual-reflector antenna.

In order to achieve a high accuracy we carry out analysis of dual-reflector antenna as follows:

- feed horn analysis using mode matching technique or integral equation approach with taking into account a reaction of the free-space and the subreflector;
- determination of the spherical wave expansion coefficients for the electromagnetic field at the horn aperture;
- determination of the currents on the subreflector surface generated by an incident near field of the feed horn;
- determination of the fields near the main reflector surface by physical optics method using the subreflector currents assuming that the reflector is in the near field of the subreflector;
- determination of the currents on the main reflector surface generated by the subreflector currents;
- determination of the far-field of the main reflector by physical optics method;
- determination of the far-field radiation pattern of a dual-reflector antenna by superposition of the radiated far-fields by main reflector, subreflector and feed horn.

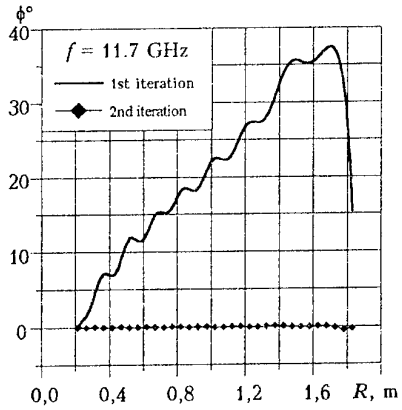


Fig. 3. Obtained phase distributions of the field in the main reflector aperture at each iteration

In order to obtain the overall generalized scattering matrix of feed horn we used mode-matching technique or integral equation method. At first horn is represented as a set of regular circular waveguide sections with longitudinal dimension much less than free space wavelength. The generalized scattering matrices of junctions between two waveguide sections are found and then they are combined with scattering matrices of regular circular waveguide sections. Having the overall generalized scattering matrix of the horn and an amplitude of the input mode it is easy to find amplitudes of incident modes in the horn aperture. By using moment method we obtain the scattering matrix of free space junction. Having calculated amplitudes of modes, reflected from the free space, and incident modes amplitudes it is possible to find total amplitudes of modes in the aperture. Amplitudes of electric and magnetic fields of m-th mode are obtained as follows:

$$\begin{aligned} A_2^{(m)} &= a_2^{(m)} + b_2^{(m)} \\ B_2^{(m)} &= a_2^{(m)} - b_2^{(m)} \end{aligned}, \qquad (4)$$

where $a_2^{(m)}$ is magnitude of m-th mode reflected from free space and $b_2^{(m)}$ is found from the following matrix equation:

$$[b_2] = [S_{21}]*[a_1] + [S_{22}]*[a_2], \qquad (5)$$

where a_1 is a column of incident amplitudes in the horn throat and S_{21} and S_{22} are elements of the horn generalized scattering matrix, which are matrices as well.

Spherical wave expansion (SWE) technique is used for calculation of the feed horn and the subreflector radiated fields at an arbitrary distance from the source. The coefficients of SWE are obtained by using orthogonality of the spherical waves functions and calculated fields at the horn aperture for the horn radiated fields and by using currents at the subreflector surface for the subreflector radiated fields. The integration over azimuth coordinate φ is performed analytically.

The currents at the subreflector and the main reflector surfaces are calculated by PO-method. Assumptions of infinitesimal thickness and infinite conductance of the surfaces are accepted. Far-field radiation pattern of the antenna on the whole is calculated using Kirchhoff-Huygens-Silver integral with analytic integration of the currents over azimuth coordinate φ.

Multiple reflections between feed horn and subreflector (including shading the subreflector by the horn) are taken into account using iterative procedure, where field a_s reflected from the subreflector is added to the of field a_0 reflected from the free space without influence subreflector:

$$a_2=a_0+a_s.$$

Obtained amplitude a_2 is used in (4) and after that a new value of field reflected from the subreflector will be found. This iterative procedure converges quite fast (only 3-5 iterations are necessary).

The main aperture blockage is introduced and correction for the first sidelobes is provided by zeroing the induced currents in the blocked region.

To illustrate the extreme convergence rate of the suggested method of diffraction synthesis of axially symmetric dual-reflector antennas (Fig. 3) we used an example of synthesis of antenna with uniform amplitude and phase distributions in the main reflector aperture. Our purpose was to produce the uniform phase distribution and, respectively, only one new modified design objective was generated.

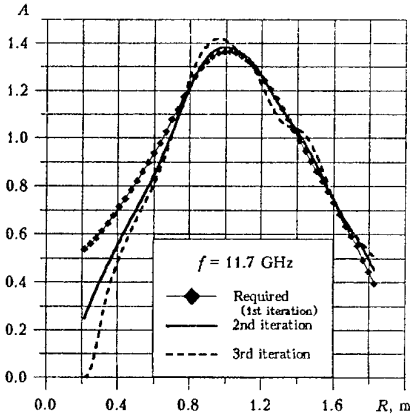


Fig. 4. Actual and modified required amplitude distributions of the field in the main reflector aperture, used in the iterative procedure

Consider now the more sophisticated case when we have to generate two modified functions simultaneously for two independent characteristics, namely, the amplitude and phase distributions of field in the main reflector aperture. The *actual* required amplitude distribution for the antenna whose main reflector diameter is 3.66 m and its subreflector diameter is 0.43 m is shown in Fig. 4 by a solid line with diamond-shaped marks. This amplitude distribution, together with uniform phase distribution, provides a level of side lobe envelope, meeting the current CCIR requirements for earth station antennas: 29-25 lgθ *(dBi)* in the angle sector 1...20 degrees (Fig. 5, solid line). In order to avoid exceeding side lobe peaks over the required envelope in the angle sector not covered by the subreflector, the angle of subreflector edge, seen from the phase center of the horn, was taken 25°.

All the amplitude distributions given below are obtained as normalized components of the aperture distribution of the field with the main polarization which have been averaged over two main planes. In this case the normalizing coefficient is so chosen that the normalized aperture distribution of the field is transmitting the same power as the unit uniform distribution written in the form $A(\rho) = 1$ at $r \le \rho \le R$ where r is the subreflector radius, and R is the main reflector radius. Then the normalizing coefficient

$$K = \sqrt{\frac{R^2 - r^2}{2\int_r^R A^2(\rho)\rho d\rho}}. \qquad (6)$$

Variations of the *modified* required amplitude and phase distributions of the field in the main reflector aperture at each iteration are presented in Figs. 4 and 6 while the corresponding distributions obtained are shown in Figs. 7 and 8. Note, that only three iterations were necessary to produce the *actual* required amplitude distribution of the field on the main reflector aperture. In order to get the *actual* uniform phase distribution on the main reflector aperture we had to perform an additional iteration in which we changed only the *modified* required phase distribution of the field while the *modified* required amplitude distribution remains the same as in the previous iteration.

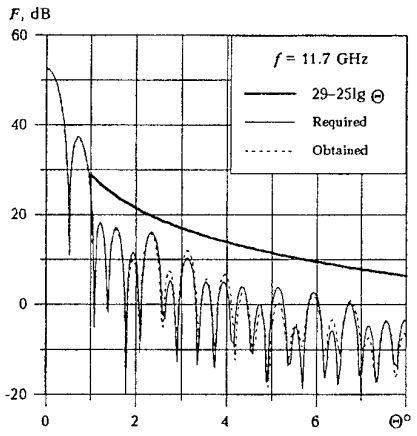


Fig. 5. Required and obtained far-field radiation patterns of the synthesized antenna

The dotted line in Fig. 5 corresponds to the radiation pattern of the antenna synthesized by this method. As

may be seen in the figure, the task of synthesis of the dual reflector antenna that produces *actual* required radiation pattern has been completely performed. Here the calculated efficiency of the antenna reaches 87.8% while maximum attainable value for the initial required distribution is 90%.

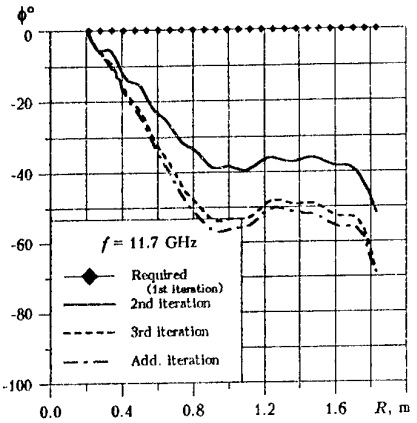


Fig. 6. Actual and modified required phase distributions of the field in the main reflector aperture, used in the iterative procedure

In addition, a comparison between the suggested method of synthesis and optimization using the correlation integral between the transmitted and received fields on reflectors' surfaces [3] has been made. One may see in Fig. 9 that the suggested method gives more close amplitude distribution to the actual required one, especially, at the edge of the main reflector aperture. The reason is that the correlation method of optimization is seeking a compromise between the required amplitude distribution and the power level flowing to the main reflector. This level arises from the finiteness of the steepness of the pattern of the field scattering by the subreflector in the direction of the main reflector edge [3].

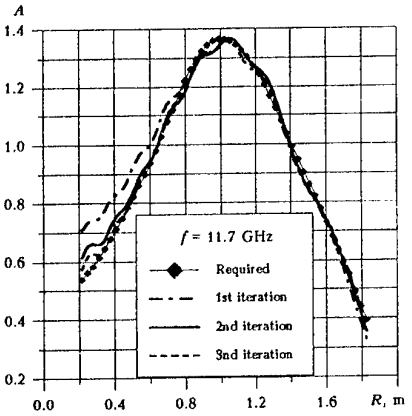


Fig. 7. Actual required and obtained in the iterative procedure amplitude distributions of the field in the main reflector aperture

By using the suggested method and the new field theory approach the optimized dual reflector omnidirectional antenna for MMDS base station (Fig. 10) has been developed.

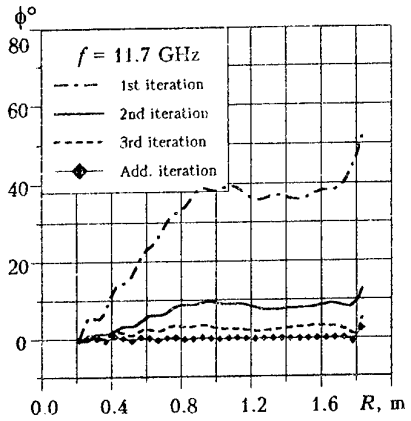


Fig. 8. Phase distributions of the field in the main reflector aperture obtained in the iterative procedure

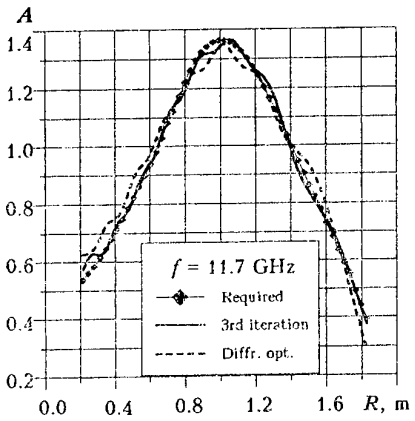


Fig. 9. Comparison of amplitude distributions of the field in the main reflector aperture

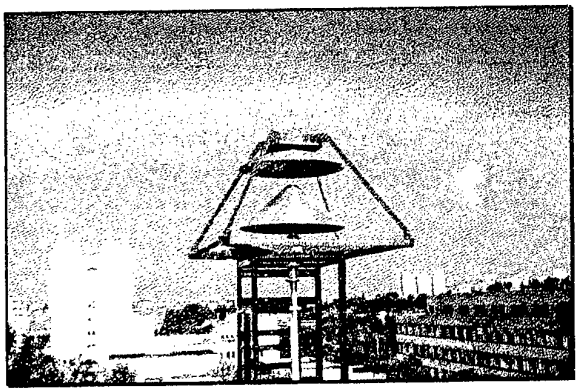


Fig. 10. Dual reflector omnidirectional antenna for MMDS base stations

APPLICATION OF THE METHOD TO IMPROVEMENT OF PERFORMANCES OF EXISTING LARGE DUAL REFLECTOR ANTENNAS

In this section we show how the suggested universal iterative synthesis technique may be applied to radiation pattern control of existing large dual-reflector antennas, namely, to reduction of their sidelobes in order to meet the current stringent CCIR requirements to earth station antennas.

In this case the block diagram in Fig. 1 is transformed to the block diagram, shown in Fig. 11. The main feature of this procedure is the fact that now in the first iteration we may also have accurate measured characteristics of interest and use the characteristics for generation C_{k1}^{mr} in equation (1) as follows:

$$C_{k1}^{mr} = C_k^{ar} - \left(C_{k1}^{e} - C_{k1}^{c}\right), k = 1,2\ldots, \qquad (7)$$

where C_{k1}^{e} is the measured k-th characteristic of the object under synthesis.

From this formula follows that in the first iteration actual required k-th characteristic is modified by a difference between measured and calculated k-th characteristic. Clearly, that only in the case, when this difference is negligible, $C_{k1}^{mr} \approx C_k^{ar}$. Therefore, there are several reasons for using the procedure in Fig. 11 for updating existing large dual reflector antennas:

- Experimental data for the existing antennas, that take account of manufacturing errors, main reflector and subreflector edge diffraction, strut diffraction, feed spillover and scattering of reflected power by feed, can be used in the first iteration.
- Second or third iteration would produce a correct result because the new modified design objectives are generated taking account of constant differences between accurate measured and non-rigorous calculated characteristics.
- Non-rigorous analysis can be actually used and nevertheless will give reliable results of the synthesis due to the reasons stated above.

It is necessary to note, that an antenna under design has to be near the required optimum. For instance, these ones are antennas that have been designed for maximum efficiency or for 32-25lg(θ) radiation pattern envelope.

In order to synthesize a new geometry of the feed system allowing for reduction of the side lobe envelope of already existing axially symmetrical dual-reflector antennas to the levels stipulated by the INTELSAT/EUTELSAT standards, an iterative procedure presented in Fig. 11 is used.

To prevent the elevation of the modified antenna radiation pattern arising from the side lobes compared to the standard envelope we have to generate such a distribution on the aperture of the main reflector which has a steeper decrease and a lower level at the shadow boundary of the subreflector and at the edge of the main reflector as compared to the already available version. It is known, however, that in order to obtain simultaneously the required amplitude and phase distribution on the main reflector (and, hence, the required radiation pattern), two surfaces are necessary. Thus, the variation of the amplitude distribution without changes of the phase one and with the use of geometrical optics may be achieved only by varying a feed radiation pattern if the profile of the main reflector remains unchanged. However, if we make the following assumptions: 1) the possibility for small deviations of phase; and 2) the antenna under optimization which has been designed by the geometric optics method, has a reserve of efficiency, which may be used for variations of the aperture distribution of field on the main reflector, then diminishing the level of the side lobes of the dual-reflector antenna may be achieved by simultaneous changing of the feed and the subreflector profile which provides much more freedom for optimization. In a less general case only the subreflector may be replaced.

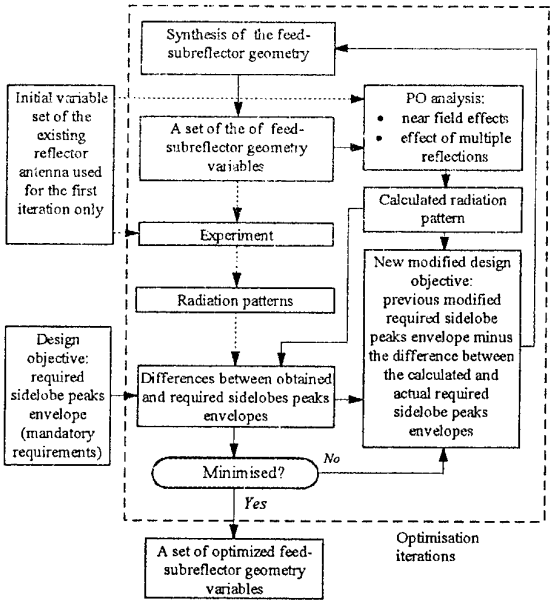


Fig. 11. Application of the iterative synthesis method to updating existing large dual reflector antennas. Dotted lines are related to the first iteration only

Eventually the procedure of synthesizing new geometry of a feed system was defined as follows:

1) choosing such a spacing between the feed horn which reduces the power spilling over the subreflector rim to the required level.

2) employing the above iterative method of diffraction synthesis of antennas except for the fact that, within the geometric optics approximation, we synthesize such an antenna that provides required amplitude and phase distribution with minimum deviation of the main reflector profile from the existing one. It is performed with the aid of an iterative procedure of fitting the distance between the main reflector and subreflector in the process of the geometric-and-optical synthesis.

3) performing the diffraction optimization of the subreflector profile (using the profile of the existing main reflector) based on Wood's iterative procedure [3] to obtain maximum uniformity of the phase distribution in the main reflector aperture.

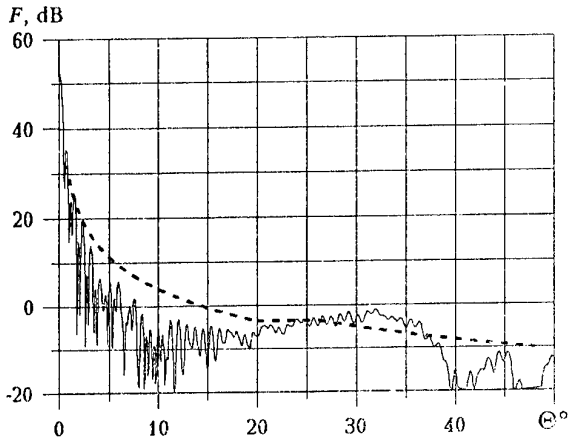


Fig. 12. Radiation pattern of the existing 3.66 m dual-reflector antenna

The method of diffraction optimization of subreflector used here is somewhat modified compared to that in [3]. Here the planar uniform wave in the main reflector aperture is replaced by the planar wave having the desirable amplitude distribution.

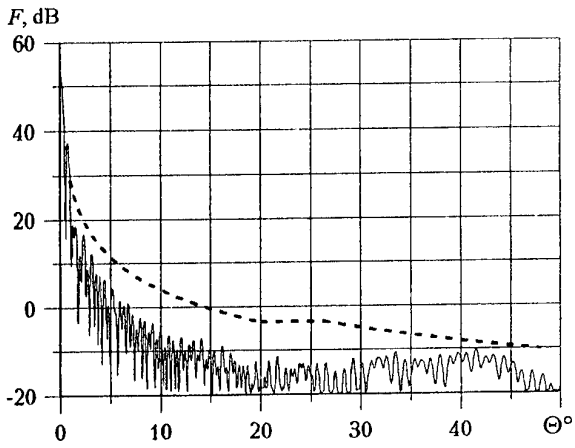


Fig. 13. Radiation pattern of the 3.66 m antenna after optimization of the feed system

As an illustration of applicability of the suggested fast-convergent method to improving the electric characteristics of already available large dual-reflector antennas let us consider the results of synthesis of a new feed system for existing 3.66 m Cassegrainian antenna.

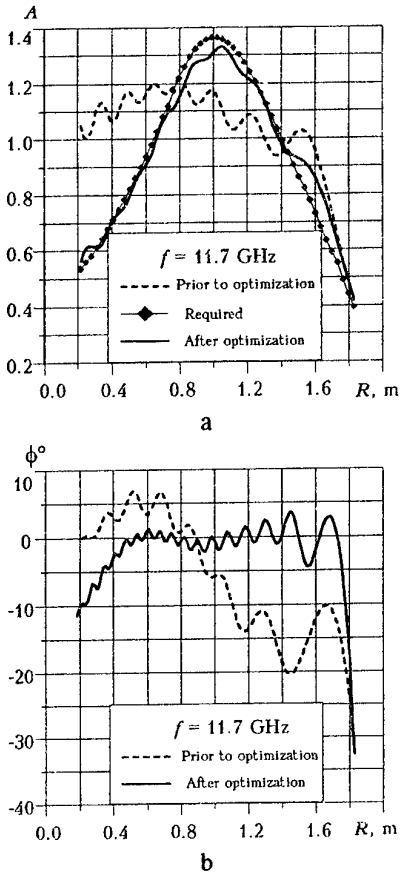


Fig. 14. Amplitude and phase distributions of the field in the main reflector aperture

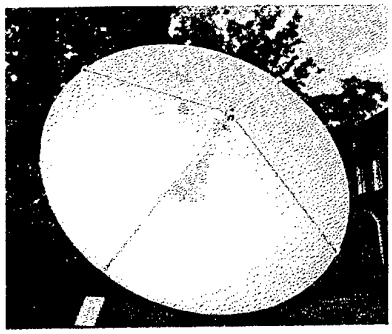


Fig. 15. Updated 3.66 m dual reflector antenna at the Ukrainian National Exhibition Center

The new feed system is designed to reduce the side lobe levels of the radiation pattern to the values permitted by CCIR standards for ground station antennas. The calculated radiation pattern of this antenna at frequency 11.7 GHz is shown in Fig. 12. This modified Cassegrainian antenna was designed using the geometric optics method to obtain maximum efficiency in the down-link frequency range of *Ku*-band (10.7...12.7

GHz). As may be seen from Fig. 12, several side lobes including those dealing with spillover of the power outside the subreflector, are elevated over the side lobe envelope permissible by the INTELSAT standard.

Optimization of this antenna was performed according to the method (Fig. 11). The amplitude distribution was identical to that used for the above synthesis of the antenna. The initial horn was replaced by the synthesized horn, providing the required characteristics in the whole *Ku*-band. The calculated radiation pattern of the updated antenna at frequency 11.7 GHz is presented in Fig. 13. Here one may see that the peaks of the side lobes do not exceed the side lobe envelope prescribed by INTELSAT, so the antenna may be employed in earth stations which use the space segments INTELSAT/EUTELSAT.

Figures 14a,b show, respectively, the amplitude and phase distributions of the field in the aperture of the antenna main reflector. After optimization the field amplitude distribution in the main reflector aperture has changed sharply (Fig. 14a) which caused decreasing the side lobe level. As a consequence, one could expect simultaneous decrease of the antenna efficiency. However, due to application of the diffraction optimization of the subreflector profile, the phase distribution became more uniform (Fig. 14b) and, as a result, the antenna efficiency remained as before the optimization. This synthesized 3.66 m transmit-receive earth station antenna (Fig. 15) is now under production at design office "Promin" (Ternopil, Ukraine).

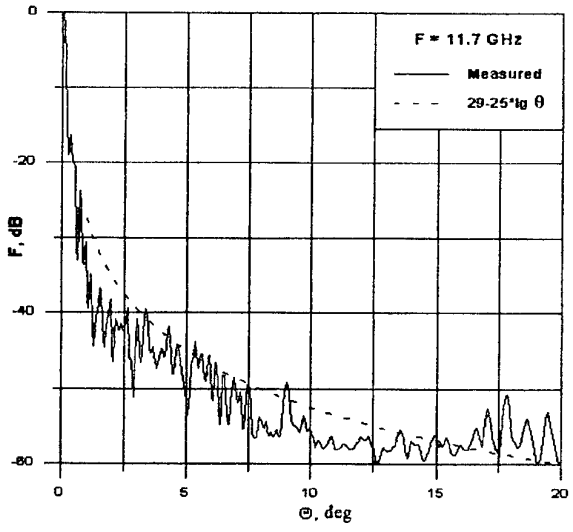


Fig. 16. Measured radiation pattern of the existing 7.0 m dual-reflector antenna

Another example of the improvement of electrical characteristics of existing large dual-reflector antennas to meet INTELSAT/EUTELSAT earth station requirements is a 7 m Ku-band Cassegrainian earth station antenna. Measured pattern of this antenna is shown in Fig. 16. This modified Cassegrain antenna was designed for maximal efficiency using GO-method. It is seen from Fig. 16, that several sidelobe peaks and we applied the iterative procedure (Fig. 11) and only one iteration has provided the required characteristics spillover exceed the INTELSAT sidelobe mandatory requirements.

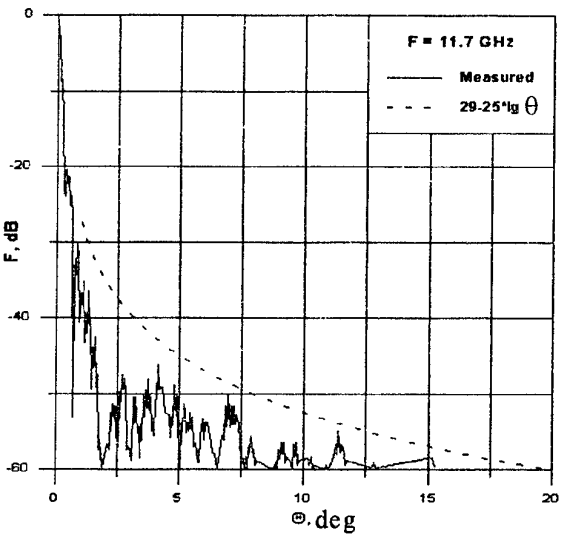


Fig. 17. Measured radiation pattern of the updated 7.0 m dual-reflector antenna

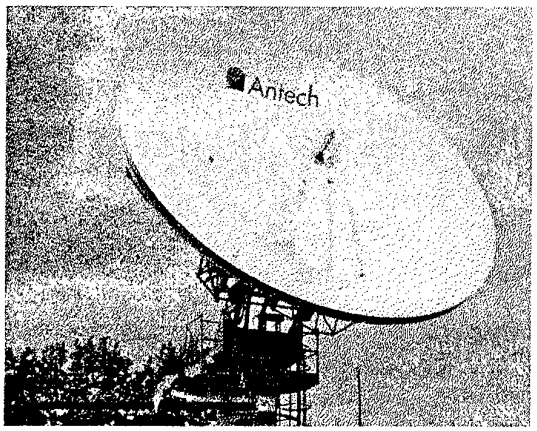


Fig. 18. Updated 7 m dual reflector antenna at Kyiv uplink station

Measured radiation pattern of the antenna is presented in Fig. 17, which confirms, that sidelobes peaks and spillover do not already exceed INTELSAT sidelobe mandatory requirements. Moreover, the efficiency remained the same due to Wood's iterative design. This antenna (Fig. 18) is manufactured at plant "Saturn" (Ternopil, Ukraine) and exported to European countries.

APPLICATION OF THE METHOD TO DESIGN OF SOME MICROWAVE COMPONENTS

This section presents results of application of the method to design some high performance microwave components. To start with, consider the synthesis of a wideband waveguide ridged polarizer. The problem was to synthesize the geometry of the ridges which provides the differential phase shift 90±2 degrees in the required frequency range (more than 10%). To solve the problem we have analyzed the irregular ridged waveguide structure, shown in Fig. 19.

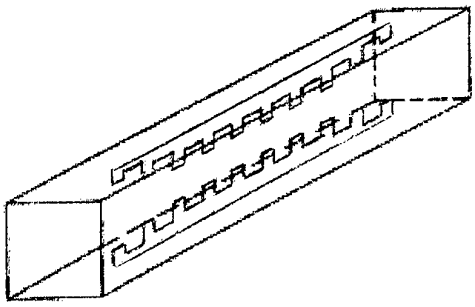


Fig. 19. A polarizer under design

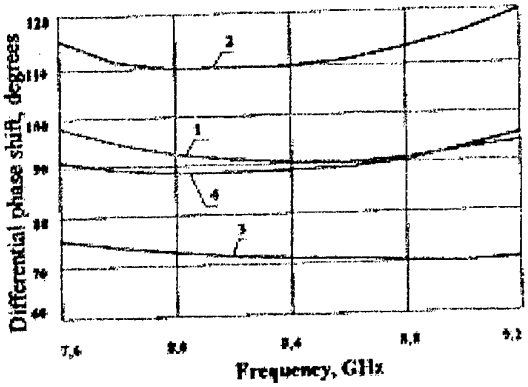


Fig. 20. Frequency dependence of VSWR of the polarizer in the iterative synthesis procedure

After the approximate synthesis, the polarizer geometry with differential phase shift characteristic close to the required one was obtained (curve 1 in Fig. 20). Then using rigorous analysis accurate differential phase shift characteristic for this geometry was obtained (curve 2 in Fig. 20). After the modifications of the input data in accordance with equation (1) and second iteration completion another geometry of the polarizer has been obtained. A differential phase shift characteristics corresponding to the new modified design objective and rigorous calculation for the determined geometry of the polarizer are shown in Fig. 20 (curve 3 and 4 accordingly).

By means of developed method we have also designed a unique high performance waveguide ridged rotator and tunable bandpass filters with near constant bandwidth. In particular, the unique rotator built prototype provides constant differential phase shift 180° over 20% frequency band and VSWR<1.15. It is worthy to note, that the new designed, developed, constructed and tested mechanically tunable waveguide narrow bandpass filter prototype has got all over the tuning frequency range 4.4...5.0 GHz near constant bandwidth 35 ± 2 MHz, insertion loss in pass band less than 1.3 dB, VSWR ≤ 1.4 and insertion loss values at frequencies $f_0 \pm 60$ MHz more than 50 dB and at $f_0 \pm 130$ MHz – more than 85 dB. The excellent performances of the filter has been achieved due to idea of the proper combining inductive and capasitive discontinuities and using in the iterative synthesis procedure the developed adequate mathematical model that base on generalized scattering matrices and exclude entirely a necessity of any adjusting the filter after the accurate fabrication.

CONCLUSION

This paper introduced the new highly efficient method of synthesis of physical objects. Contrary to most classical optimization methods a guesswork in this method is essentially reduced or fully removed. It has been shown that due to the proper combining in each iteration a fast approximate analytic or parametric synthesis with rigorous analysis and the proper generating a new modified design objective the iterative process is extremely fast-convergent. In practice only a few iterations are needed to complete the optimization procedure. The method was successfully applied to design of high-performance dual-reflector earth station antennas, antennas for MMDS base stations, log-periodic dipole antennas, septum OMTs, polarizers, rotators, filters, etc. Such important features of the method as very fast convergence, universality and reliability have been practically demonstrated. These appealing features, despite the fact that the method has not been mathematically proven yet, give a hope to the author that this method may become a popular design tool for practical synthesis of various electromagnetic and other devices.

REFERENCES

1. D.Duan, Y. Rahmat-samii. A generalized diffraction synthesis technique for high performance reflector antennas. IEEE Transactions on Antennas and Propagation, Vol. 43, №1, January 1995, pp. 27-39.

2. E. Michelssen, Y. Rahmat-samii, D.S. Weile. Electromagnetic system design using genetic algorithms in modern radio science. Oxford University Press, 1999, pp. 91-123.

3. P.J. Wood. Marconi review, Vol.35, № 185, pp. 121-138.

MODELLING OF PRINTED ANTENNAS ARRAYS FOR VARIOUS APPLICATIONS

J. P. Daniel

University of Rennes I. Laboratory "Antennes et Réseaux " UPRESA-6075 CNRS
Campus de Beaulieu, 35042 Rennes Cedex, France
e-mail: jean-pierre.daniel@univ-rennes1.fr

INTRODUCTION

The design of printed antenna arrays follows mainly two rules which are: first the choice of the elementary source and secondly the choice of the architecture of the array itself. At each stage the constraints of SWR, polarization, frequency bandwidth, the required patterns, the feeding network...need choices between conflicting requirements. Moreover the flexibility of the printed technology offers the possibilities of innovative radiating structures well suited to these various systems requirements (frequency, bandwidth, gain, size, patterns...). The paper shows first various printed sources developped in the Antenna Laboratory and classified through their bandwidth (from few % up to 50 % or more). The mutual coupling is a strong constraint for large bandwidth array but can be neglected in many cases when the distance between elements is large enough. Then different array architectures are presented for different kinds of patterns and bandwidth. Some of the arrays have received applications: for instance dual beam doppler radar for accurate measurements of speed [1].

THE RADIATING SOURCES

Sources with 1% to 5 % Bandwitdth:

The most common source is the patch printed on one dielectric layer of limited thickness. The shape can be rectangular, square, circular...and various feedings have been used (microstrip line, coaxial, electromagnetic coupling with slot for instance). Some examples are shown on Fig. 1. These patches can be modelized as resonant cavities which exhibit radiation losses (from edge magnetic currents) in addition to the dielectric, metallic and surface wave losses.

The corner fed patch has received a special interest because it provides a high input impedance (superposition of two degenerate modes (0.1) + (1.0)) well suited for serie's array [2]. The equivalent circuit is shown on the Fig. 2; it includes the resonant tank circuit which describes the radiating patch itself and a T discontinuity modelised by a transformer n_j and a_n inductance Lj . L_p takes into account the effects of the higher order modes. The input resistance has been plotted versus W_j/h in C, X, K bands and typical dielectric thicknesses (1.57 mm, 0.79 mm, 0.38 mm respectively).

Sources with 5% to 50 % or Higher Bandwitdth:

To increase the frequency bandwidth the main idea is to increase the thickness or to use mutual coupling effects between the different parts of the antenna as a beneficial consequence. Stacked corner fed patch can exhibit a larger bandwidth (typically 20 %) thanks to a parasitic patch of proper size and a correct air gap (typically 1 to 2 mm in X band).

However when a bandwidth up to 50 % or more is desired, the distance from the ground plane must be larger and can reach a quarter wave-length. Then the feeding structure has to support also this bandwidth and

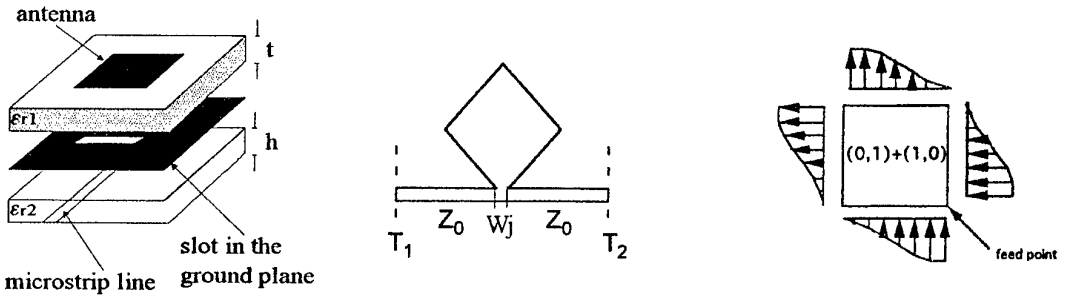
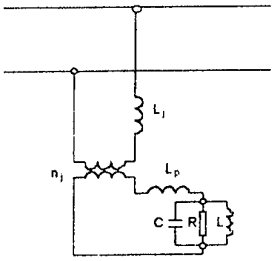
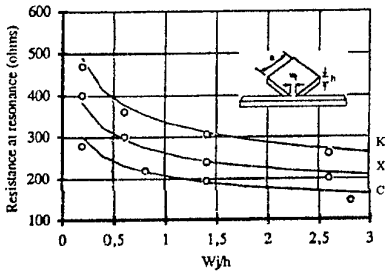


Fig. 1. Examples of microstrip patches and feedings: slot fed patch (a); corner fed patch and the field distribution at the edge (b)



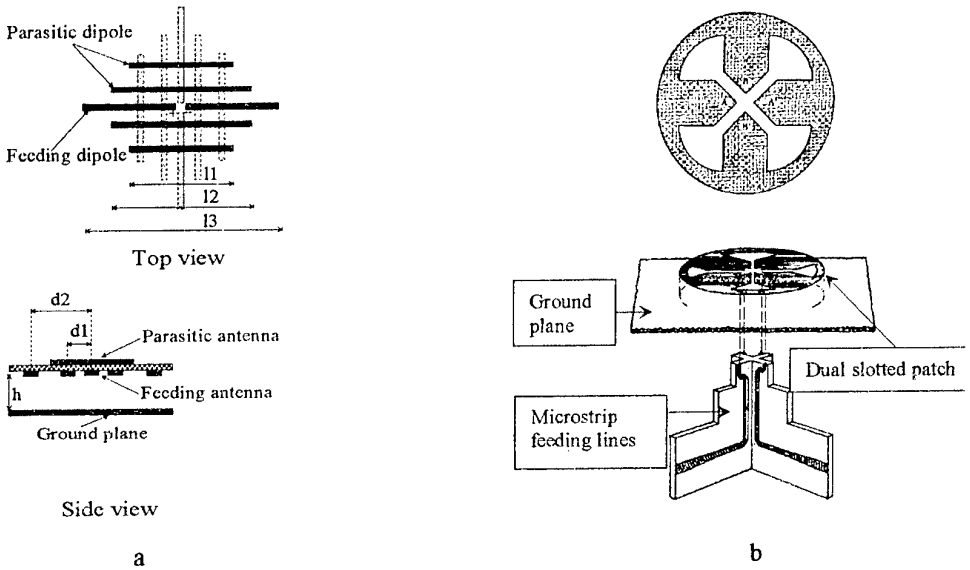
$$F_r = \frac{c}{\sqrt{\varepsilon_{ef}}\left(a - \frac{W_j}{2\sqrt{2}} + 2\Delta_a\right)}$$

$$R = 113\frac{\left(F_{r(GHz)}\right)^{0.354}}{\left(\frac{W_j}{h}\right)^{0.24}}$$



a b

Fig. 2. Corner fed square patches: equivalent circuit (a); variation of the resistance at resonance in C,X,K band (b)



a b

Fig. 3. Large bandwidth dual polarized printed antennas: sleeve dipoles (a); double slotted patch (b)

the baluns are often TEM lines such as coaxial cables or microstrip lines. Two examples of such antennas (both being dual polarised) are shown on Fig. 3 [3]. The first case is a double sleeve dipole with parasitics; the parasitic elements have been designed (lengths and positions) in order to increase the bandwidth. As the mutual coupling play a fundamental role a full wave analysis was necessary: here an integral equation on currents solved by a moment method has been used. The second antenna is a double slotted patch with linear slots ended by triangular slots. The current distribution shows that current lines exhibit loop shape and as a consequence the external dimensions remain small in the whole frequency band (50 %). The electromagnetic analysis leads to an integral equation solved by a moment method also.

THE ARRAYS

When the distance between elements is large enough (typically > 0.6 λ_0) the mutual coupling remains small; the antennas can be considered as being independant. The problem is reduced to the computation of the interferences of sources. However for given sources the architecture have to be defined in order to get the desired pattern (synthesis problem with constraints) or to choose proper pattern sources to increase or reduced some angular part of the array pattern. As an example the design of dual beam, multibeam, sector beam antennas is developped for narrow bandwidth. Large bandwidth arrays are considered after with an example.

Pattern Synthesis of Dual Beam Antenna with Low Side Lobes

Let us consider a linear array of $2N$ square patch antennas fed at theirs corners by a microstrip line, which is excited at its center by a coaxial probe (Fig. 4).

Amplitude distribution

If we keep a wavelength spacing between the elements, impedance transformers are necessary to obtain the given amplitude currents. To do this, a two-step quar-

ter-wave transformer can be used in each cell. The transformed admittance Y_i in the π_i' plane is given by

$$Y_i = \left(\frac{Y_{L2}}{Y_{L1}}\right) Y_{i+1} = n_i^2 Y_{i+1} \qquad (1)$$

where Y_{i+1} is the admittance of node $(i + 1)$, and Y_{L2} and Y_{L1} are the characteristic admittances of each quarter-wavelength transformer. If necessary, four quarter-wave transformers can be inserted when the spacing equals one wavelength.

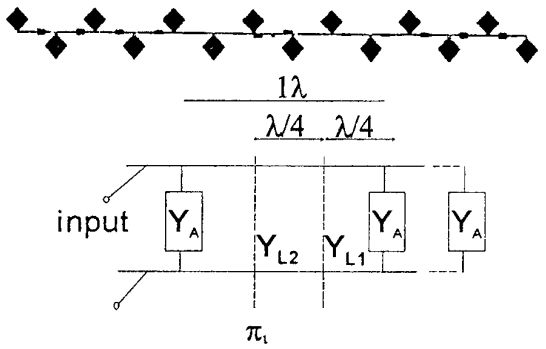


Fig. 4. Tapered linear serie's array and its equivalent circuit

When the input voltage leads to a unit current in the first element, the current distribution is readily obtained with the following relations:

$$\begin{aligned} I_0 &= Y_A V = 1 \\ I_1 &= n_1 Y_A V = n_1 \\ I_i &= n_i . n_{i-1} \ldots n_1 \end{aligned} \qquad (2)$$

It must be noticed that numerical synthesis methods have been developed [2],[3] in order to get the current distribution, taking into account the radiation pattern of the elementary sources.

Phase excitation:

A simple equal-phase excited dual-beam array can be made if the electrical length of the feeding line between two patches is a multiple of the guided wavelength [1]. Considering the patches located alternatively at each side of the feeding line (and as a result a 180° phase shift (Fig. 5)), the physical distance d_s between such sources will define the angular positions $\pm\theta_0$ of the two main lobes which are both located in the visible region:

$$\theta_0 = \arcsin\left(\frac{\lambda_0}{2d_s}\right) \qquad (3)$$

To reduce the beam tilt the first idea is to increase the distance. However if the distance is too large grating lobes appear and four beams are obtained (Fig. 6). If we consider a group of two "in phase sources" with a spacing $de = 0.64\lambda_0$, it exhibits a more directive pattern with two nulls which arise at $\lambda_0 = +55°$. If we consider an array (Fig. 5b) of such group of sources, it is clear that the null of the elementary source will cancel the grating lobe which stands at the same amplitude (Fig. 5b').

Pattern Synthesis of Sector Beam Antenna with Low Side-Lobes

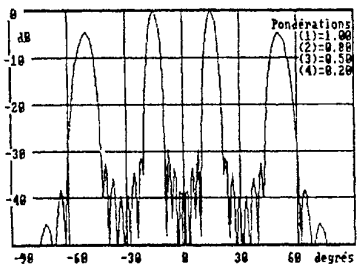
The problem is very similar to the previous one. It is well known that the far field is the Fourier transform of



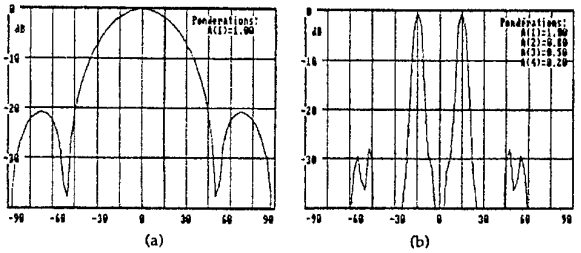
(a)
Tapered linear serie's array of square fed patch (with spacing *ds* = 1.93 λo)



(b)
Tapered linear serie's array of group of sources (with *de* = 0.64 λo and spacing *ds* = 1.93 λo)

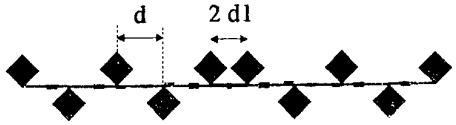


(a')
Pattern of tapered linear serie's array of square fed patch (with spacing *ds* = 1.93 λo)

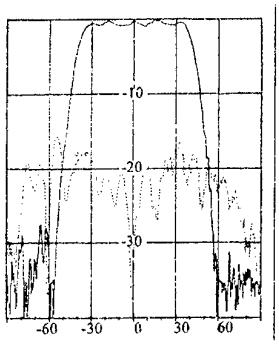


(b')
Pattern of a group of 2 sources (with *de* = 0.64 λo) and resultant pattern of the tapered linear serie's array (with spacing *ds* = 1.93 λo)

Fig. 5. Tapered linear serie's arrays and suppression of grating lobes

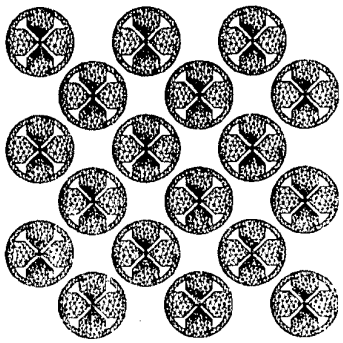


(a)
Tapered linear serie's array of square fed patches for sector beam of 90 °



(a')
Sector pattern of the tapered linear serie's array

Fig. 6. Tapered linear serie's arrays with a sectoral pattern



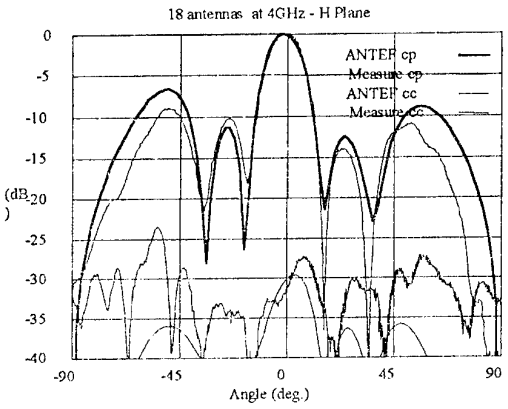


Fig. 7. Array of 2X9 dual polarized slotted antennas and the H plane pattern at 4 GHz. Distance between elements is 85 mm. One array is uniformly fed. The other is loaded

the antenna distributed excitation. Then a sector beam is obtained thanks to a $\sin(x)/x$ excitation. The amplitude distribution can be realized with quarter wave transformer and the 180° of phase shift (negative sign of $\sin(x)/x$) thanks to the alternate positions of the patch along the feeding line as before. If the feeding lines are simple straight printed lines on usual polymer substrate (with dielectric constant near 2) then the distance d = λ_g # 0.75 λ_0.The pattern of an array with such a distance is given by:

$$f(\theta) = \sum_{j=1} a_j \cos(2\pi(j-1/2)\frac{\lambda_g}{\lambda_0}\sin(\theta)) \qquad (4)$$

Whatever are a_j it is clear that $f(\theta)$ will be null when $\sin(\theta) = \frac{\lambda_0}{2\lambda_g}$ which is obtained for θ = 42° with classical polymers. To avoid this constraint and increase the sector beamwidth one solution is to reduce the distance $2d_1$ between the first elements. To reach 45° it was necessary to reduce d_1 down to $0.25\lambda_0$. A second important effect can come from the coaxial feeding point itself which often acts as parasitic source. To reduce this effect a small increase of the microstrip line width located in front the coaxial was enough to keep side lobe level smaller than –25 dB. The Fig. 6 shows the atructure and the result obtained for an array printed on polymer substrate (thickness = 0.8 mm, distribution: a_1 = 1, a_2 = –0.218, a_3 = 0.117, a_4= –0.082, a_5 = 0.074, d = 0.75λ_0 and d_1 = 0.25 λ_0).

These different pattern synthesis with equal or unequal spacings were performed using synthesis algorithms developed in the laboratory. They are mainly based on optimization process under constraints such as relaxation and simplex [4]. Mutual coupling is ignored in this case.

Pattern of Large Bandwidth Array (2-4 GHz)

The design of large bandwidth arrays is far more difficult and often needs a full wave analysis including all the mutual couplings [5]. The element pattern is not the same for all the radiating elements and active patterns

depend on the position in the full array. Here is shown the geometry of an two overlapped arrays of 9 elements each (one for emission and the other for reception) and the pattern of one of them for both polarization. Mutual coupling leads to distorsion and an increase of the side lobes. The numerical code ANTEF was used to solve this problem (10000 unknowns).

CONCLUSION

Various printed antenna arrays have been shown. Their designs need first the choice of a patch element. When the bandwidth requirement is limited to some percents then patch printed on one dielectric layer is enough. Moreover the limited bandwidth enables the designer to used serie's structures. Here two different kinds of patterns have been presented: directive multibeams and sector beam. Results of large bandwidth arrays have been also presented. Extensions of these flat printed structures have been studied for cylindrical geometries. Some arrays of square fed patches have also received commercial applications [1] and they will be presented at the conference.

REFERENCES

1. CRITT-CNRS French Patent n° 8712579P : "Antenne plaque microonde notament pour Radar Doppler", P. DUPUIS, J.P. DANIEL, J.L. ALANIC.
2. E. MOTTA CRUZ, J.P DANIEL : "Modèle d'Antenne Carrée Imprimée alimentée en Coin: Application aux Réseaux Linéaires", JINA-90, November 1990, Nice, France, pp. 297-300.
3. F. COLOMBEL: "Antennes à double polarisation et large bande. Application aux réseaux" Doctor Thesis of the University of Rennes I Janvier 1996, Rennes, France.
4. M. BOGUAIS : "Contribution à la Synthèse de Réseaux d'Antennes; Réalisations en Technologie Imprimée", Doctor Thesis of the University of Rennes I October 1986, Rennes, France.
5. P. POEY, X. BEGAUD "Electromagnetic analysis of dual polarized wide band antennas and arrays". PIERS 1998, 13-17 Juillet 1998.

ELECTRONICALLY TUNABLE FREQUENCY SELECTIVE SURFACES FOR ANTENNA APPLICATIONS

P. Edenhofer, A. Alpaslan

University of Bochum, Institute for High-Frequency Technique,
44780 Bochum/Germany,
E-mail: abbas@hf.ruhr-uni-bochum.de

ABSTRACT

An electronically tunable planar dipole grid deposited on a dielectric substrate is described. Such dipole grids can be used as active frequency selective (FSS) or polarization sensitive (PSS) surfaces in reflector antenna systems. It is shown how the resonance frequency of the surface can be tuned by changing the steering voltage or current of electronically tunable components such as varactor diodes or YIG films, respectively, implemented with each of the dipoles. The analysis of the problem is based upon a Floquet theory approach for double periodic structures. The resulting integral equation for the current distribution is numerically solved by the method of moment with Galerkin's weighting. The experimental investigations of the reflection- and transmission coefficient were performed by a waveguide simulation technique operating from 7 to 16 GHz. A dipole grid of size 40×25 mm^2 is deposited inside a tapered waveguide. Results show that the resonance frequency can be tuned around 9.85 GHz by a bandwidth of 7 % and around 10.1 GHz by 14 % in case of capacitive or inductive tuning, respectively.

INTRODUCTION

The concept of frequency selective surfaces have found many applications in microwave antenna systems like subreflectors in reflector antenna configurations or frequency windows in antenna radomes [1]. For communication and remote sensing satellites reflector antennas with single or multiple feed systems are prefered [2]. One particular disadvantage of a passive dichroic surface is that once designed and manufactured there is no possibility to change the reflection or transmission characteristics of the FSS/PSS. For many applications it would be desirable to have a controllable reflectivity or transmittivity levels at selected signal frequencies or/and polarization. In recent years there were many efforts to design such tunable surfaces. It was shown the possibility of changing the transmission response of a FSS by changing liquids within the substrate [3]. Similar results can be obtained for dipole grids printed on ferrite substrates which are biased by a DC magnetic field [4, 5]. Two arrays of dipoles positioned parallel and in close proximity to each other show a shift of the reflection response by varying the lateral distance [6]. This paper deals with the electronic shifting of the resonance frequency of a FSS. One advantage of such an *electronically tunable* surface is to be able to control the frequency response of a FSS at great distances (i.e. earth-satellite) for example by telecommand.

CURRENT DISTRIBUTION – INTEGRAL EQUATION

Fig. 1 shows the geometry of a two-dimensional periodic dipole grid in the *x-y* plane. Each planar dipole on the grid is loaded by equal lumped linear elements $Z_{L,i}$ at location i (homogenuous distribution). In order to calculate the current distribution on a single backscattering element we start from the surface impedance boundary condition [7]:

$$\vec{E}^{inc} + \vec{E}^{s} = Z_{L,i}\vec{J}_i , \tag{1}$$

where $\vec{E}^{inc}$ – incident electric fileld, $\vec{E}^{s}$ – scattered tangential electric field maintained by the surface current on the dipole, and $\vec{J}_i$ – induced current element at the location i of the lumped element. This implies that the total tangential electric field vanishes on the surface of the dipole and maintains a voltage drop across the lumped element. The scattered field $\vec{E}^{s}$ can be derived from the relationship

$$\vec{E}^{s} = -j\omega\mu\vec{A} + \frac{1}{j\omega\varepsilon}\nabla(\nabla\cdot\vec{A}) , \tag{2}$$

where $\vec{A}$ is the vector potential,

$$\vec{A} = \int_{-\infty}^{\infty}\int_{-\infty}^{\infty} G(\vec{r},\vec{r}')\vec{J}(\vec{r}')dx'dy' \tag{3}$$

with G denoting the free space Green's function and $\vec{J}$ the unknown surface current distribution. According to Floquet's theorem the current distribution on the surface can be expanded in a double infinite Fourier series

$$\vec{J}(x,y) = \frac{1}{F}\sum_{p=-\infty}^{p=\infty}\sum_{p=-\infty}^{p=\infty}\vec{J}^{\,per}(k_{xpq},k_{ypq})e^{-j(k_{xpq}x+k_{ypq}y)} \tag{4}$$

with Floquet modes p, q and k_{xpq}, k_{ypq} as propagation constants. $\vec{J}^{\,per}$ describes a function in spectral domain and is valid for each scattering element on the

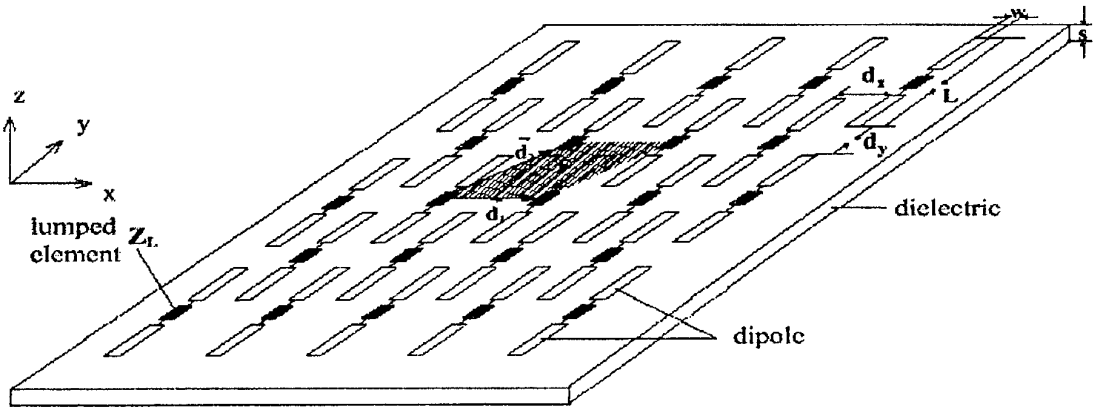


Fig. 1. Geometry of a two-dimensional planar dipole grid loaded by lumped elements Z_L with $\vec{d}_{1,2}$ as grid vectors, $d_{x,y}$ lateral-axial spacing and F the area of the unit cell

surface. For its calculation it is sufficient to integrate only over one element

$$\vec{J}^{per}(k_{xpq},k_{ypq}) = \int_{-L/2}^{L/2}\int_{-\omega/2}^{\omega/2} \vec{J}(x,y)e^{j(k_{xpq}x+k_{ypq}y)}dxdy . \tag{5}$$

The propagation constants for the geometry in Fig. 1 is given by

$$k_{xpq} = k_0 \sin\vartheta\cos\varphi + p\frac{\pi}{d_x},$$
$$k_{ypq} = k_0 \sin\vartheta\cos\varphi + (p+2q)\frac{2\pi}{L+d_y}. \tag{6}$$

Substituting (3) in (2) yields an integral equation for the current distribution. It is preferable to solve this equation in the spectral domain. In the spatial domain the scattered field is the convolution of the dyadic Green's function with the current distribution. In the spectral domain it simplifies to a multiplication of both Fourier transforms. After taking the inverse transform we obtain the equation for the unknown current distribution on a free-standing surface [8, 9]:

$$\begin{bmatrix} E_x^{inc} \\ E_y^{inc} \end{bmatrix} = \sum_{pq} \frac{1}{Fj\omega\varepsilon 2jk_{zpq}} \begin{bmatrix} k_0^2 - k_{xpq}^2 & -k_{xpq}k_{ypq} \\ -k_{xpq}k_{ypq} & k_0^2 - k_{ypq}^2 \end{bmatrix},$$
$$\begin{bmatrix} J_{xpq} \\ J_{ypq} \end{bmatrix} e^{-j(k_{xpq}x+k_{ypq}y)} = Z_{L,i} \begin{bmatrix} J_{x,i} \\ J_{y,i} \end{bmatrix}. \tag{7}$$

Here the z-component of the propagation vector is given by $k_{zpq} = (k_0^2 - k_{xpq}^2 - k_{ypq}^2)^{1/2}$ and the negative imaginary part is taken for $k_0^2 < k_{xpq}^2 + k_{ypq}^2$ (evanescent).

As an equivalent technical solution an inhomogeneous dipole grid (e.g. varying lateral distance/dipole length) turns out to achieve phase changes like a parabolically curved reflector (focusing effect) [10, 11].

NUMERICAL RESULTS

Equation (7) is numerically solved by using the method of moment and Galerkin's weighting. Expanding the unknown current in a series of orthonormal basis functions a matrix equation is derived. Because of the abruptly varying features of the current distribution due to the lumped elements, subdomain rooftop basis functions are chosen to represent the current adequatly. Fig. 2 shows the calculated copolar transmission coefficient for a capacitively center-loaded dipole grid with rectangular geometry ($\angle\ \vec{d}_1,\vec{d}_2 = 90°$). It is obvious that the resonance frequency ($\lambda/2$-resonance) of the surface can be shifted continuously from about 11.8 GHz to 9.2 GHz by varying the capacitively loading from 10 fF to 100 fF (e.g. by tuning of bias voltage of a varactor diode). Because of a minimum of the current distribution on the load location the λ-resonance is fixed at about 12.2 GHz.

EXPERIMENTAL INVESTIGATIONS

The measurements were made using a tapered waveguide simulator (aperture size 25×40 mm) with a calibrated frequency range from 7 to 16 GHz associated with varying the angle of incidence (TE_{10}-mode) from about 32° to 13° (Fig. 3). The measured frequency response from a small dipole grid size inside a waveguide simulator is equivalent to a free space experiment with a grid of infinite extent (twofold mirror principle). Given the efforts and complexity of manufacturing electronically tunable grids, this concept is considered to be an efficient and cost-effective solution.

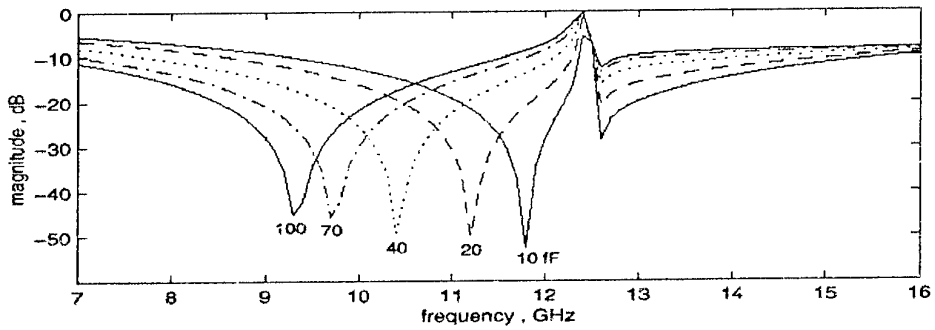


Fig. 2. Calculated copolar transmission coefficient for different capacitively loads varying from 10 fF to 100 fF (L = 23 mm; w = 0.5 mm; d_x = 4 mm; d_y = 2 mm)

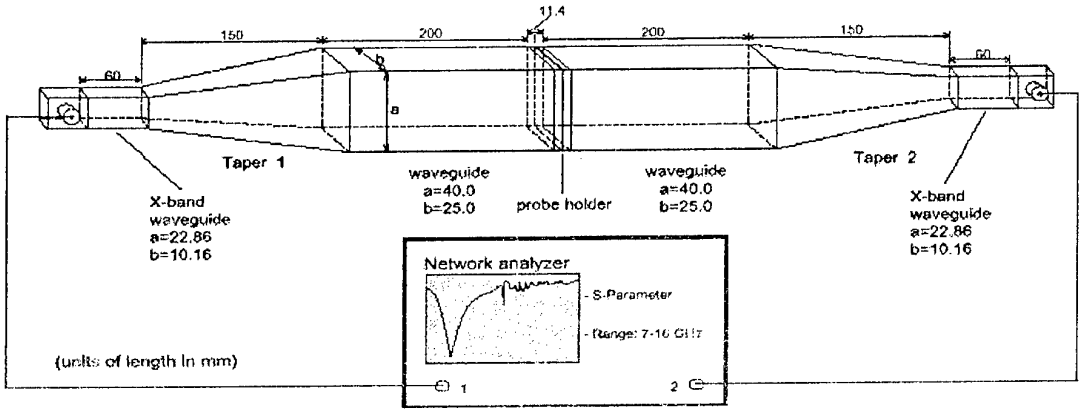


Fig. 3. Waveguide simulator with two tapered waveguides (aperture size 25×40 mm^2). Frequency range from 7 to 16 GHz (TE_{10}-mode). Measurement of reflection- and transmission coefficient (twofold mirror principle).

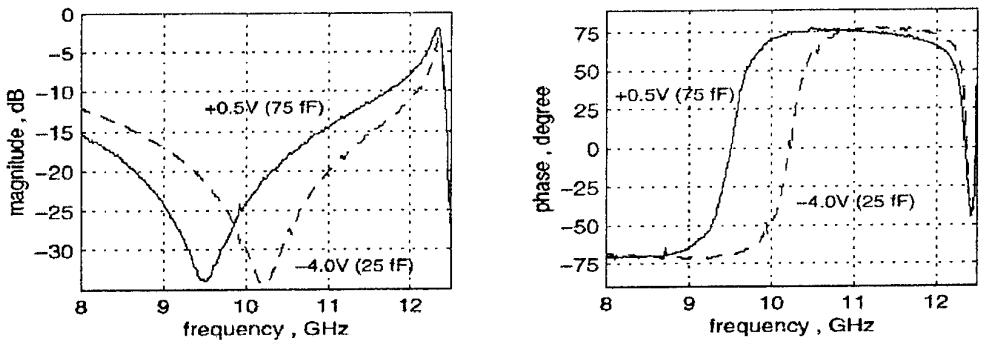


Fig. 4. Measured transmission coefficient (magnitude and phase) of an active dipole grid for two different DC voltages (–4 V → 25 fF; +0.5 V → 75 fF). Grid size: L = 23 mm; w = 0.5 mm; d_x = 4 mm; d_y = 2 mm on quartz substrate (ε_r = 3.8; tan $\delta = 10^{-4}$; s = 0.28 mm)

Tapering of the waveguide helps to minimize the problem of tolerances in positioning the dipole grid within the waveguide aperture. Fig. 4 shows the measured transmission coefficient response (magnitude and phase) of an active dipole grid (10 dipoles in one row) deposited on quartz substrate (ε_r = 3.8; tan $\delta = 10^{-4}$; s = 0.28 mm). Each dipole is center-bonded with a GaAs-varactor diode in chip form (dice). By tuning the diodes with a DC voltage from –4V to +0.5V (over two highly resistive meander lines) the resonance frequency could be continuously shifted by about 7 % (center frequency 9.85 GHz). In agreement with results from computer simulations (Fig. 2) the λ-resonance is fixed near by 12.2 GHz. The measured phase distribution (Fig. 4,

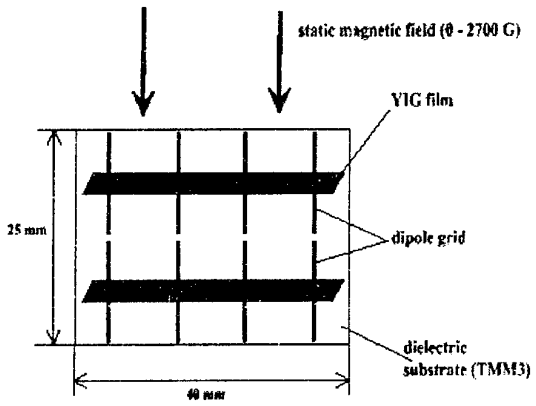


Fig. 5

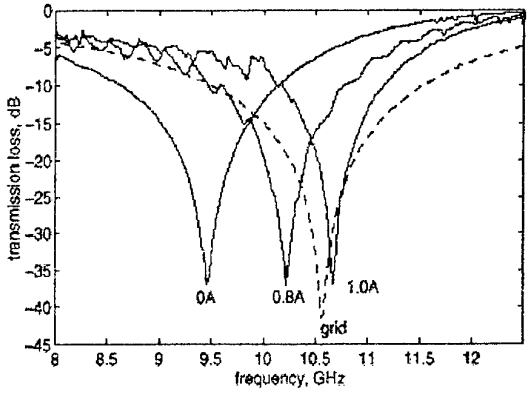


Fig. 6

Fig. 5. Geometry of a YIG-loaded 2 x 4-element dipole grid. Skewed terminations are to suppress multiple reflection of magnetostatic surface waves (MSSW) [12]. Position of the YIG film coincides with the maximum of the dipole current distribution.

Fig. 6. Experimental verification of shifting the resonance frequency of a YIG-loaded 2 x 4-element array (Fig. 5) by varying the steering current (0-1A) or transverse DC magnetic field (0.8A → 2200 G; 1A → 2700 G). Grid size: L = 11 mm; w = 0.5 mm; d_x = 8 mm; d_y = 1.5 mm on TMM3 substrate (ε_r = 3.27; tan δ = $1.6 \cdot 10^{-3}$; s = 0.5 mm)

right) shows that for a selected frequency, i.e. 10 GHz, it is possible to shift the phase from about –50° to 70°.

In case of inductive tuning two YIG films of size 36×5 mm^2 and thickness 300 μm were deposited across the 2×4-element array of dipoles (Fig. 5). Fig. 6 shows the shift of resonance frequency by varying the external DC magnetic field from 0 to 2700 G (0 to 1A steering current). At center frequency of 10.1 GHz a bandwidth of 14 % can be achieved.

ACKNOWLEDGEMENTS

This work was supported by Deutsche Forschungsgemeinschaft, DFG.

REFERENCES

1. Fasold, D. et al.: Elliptische Offset-Reflektorantennen mit Einfach- und Mehrfachspeisesystemen für Satellitenanwendungen. Kleinheubacher Berichte, Bd. 23 (1980), pp. 155-163.
2. Edenhofer, P.; Galka, M. and Habersack, J.: Polarisationstrennende Dipolgitter für offset- Reflektorantennen bei Nachrichten- und Fernerkundungssatelliten. ntz-Archiv Bd. 6 (1984), pp. 249-258.
3. Lima, A.C. de C.; Parker, E.A. and Langley, R.J.: Tunable frequency selective surface using liquid substrates. Electronics Letters, Vol. 30 (1994), pp. 281- 282.
4. Chang, T.K.; Langley, R.J. and Parker, E.A.: Frequency selective surfaces on biased ferrite substrates. Electronics Letters, Vol. 30 (1994), pp. 1193-1194.
5. Krug, J.: Oberächenwellengespeiste aktive Strahleranordnungen in planarer Technik mit Phasensteuerung. Ph.D. Dissertation, University of Bochum, 1983.
6. Lockyer, D. et al.: Coupled dipole arrays as reconfigurable frequency selective surfaces. Electronics Letters, Vol. 30 (1994), pp. 1258-1259.
7. Senior, T. B. A.: Impedance Boundary Conditions for Imperfectly Conducting Surfaces. App. Sci. Res., sec. B, Vol. 8 (1960), pp. 418-436.
8. Alpaslan, A.; Edenhofer, P.: Elektronisch verstellbare Dipolgitter als aktive Antennenre ektoren. Klein- heubacher Berichte, Bd. 41 (1998), pp. 548-555.
9. Alpaslan, A.; Edenhofer, P.: Electronically Tunable Frequency Selective Surfaces. International Symposium on Electromagnetic Theory, U.R.S.I., Thessaloniki, 25.-28. May 1998, Proceedings Vol. I, pp. 130- 132.
10. Noll, J.; Edenhofer, P.: Focusing Effects of Quasiperiodically Distributed Frequency Selective Structures. ICAP 91, IEE Conf. Publ. 333, London, 1991, pp. 632- 635.
11. Noll, J.: Quasiperiodische Verteilung von polarisationssensitiven und frequenzselektiven Strukturen für planare Antennenre ektoren. Ph.D. Dissertation, University of Bochum, 1994.
12. Krug, J.; Edenhofer, P.: Broadband Terminations for Magnetostatic Surface Waves. Electronics Letters, Vol. 19 (1983), pp. 971-972.

A LOW-LOSS AND COMPACT MULTI-SECTOR ANTENNA WITH DISTRIBUTED IMPLICIT RF BEAM SWITCH

K. Kagoshima

Department of Media & Telecommunications, Ibaraki University
316-8511 4-12-1 Nakanarusawa Hitachi, Japan
Tel: +81-294-38-5116 E-mail: kagosima@dmt.ibaraki.ac.jp

Abstract: A multi-sector beam antenna consisting of directional beam antennas and a beam selecting switch is effective for a terminal antenna of a broadband wireless access system and several antennas of this type have been used in the commercial services. In order to increase the channel capacity, higher frequencies such as Ku band, Ka band and millimeter waves are used or studied for the systems. In these high frequencies, the insertion loss of the beam selecting switch becomes large, therefore the antenna performances degrade. In this paper, a new type of the multi-sector antenna which has a distributed implicit RF switch is proposed for reducing insertion loss of the switch. The distributed implicit RF switch is composed of a Yagi-Uda antenna and diode switches in parasitic elements. Numerical calculations have been carried out to ensure the feasibility of the proposed antenna.

Keywords: multi-sector, RF switch, switch loss, distributed implicit switch, Yagi-Uda Antenna

INTRODUCTION

In the last decade of the 20th century, great changes have occurred in the telecommunication field. One is the change from telephone switching networks to digital networks which enable us to use various digital terminals such as personal computers (PC's). In other words, this is the coming of a multimedia era by the private LAN's and the Internet [1], [2]. People can send and receive various information, like data, images and videos, through computer terminals which have much more significant power than telephone terminals. The other one is the change from fixed communications to mobile communications. Especially, the advances in handheld telephone services have been changing our communication styles to be free from the restriction of the location [3].

The technological integration of computer terminals, digital networks and mobile communications have been creating new and enhanced communication services, and the demands for high speed systems in access networks are increasing to offer the comfortable multimedia mobile services. High speed wireless systems have appeared in the wireless LAN systems [4]. The Altair system [5] by Motorola and the VJ system [6] by NTT are the earliest systems of high speed wireless LAN and offer the date transmission rate of more than 10 Mbit/s, which is comparable to Ethernet. AWA [7] and wireless ATM systems [8] which present more flexible and wide-area services have been also investigating.

An antenna design for PC is one of the key technologies to realize the above high speed wireless access systems. In the Altair system and the VJ system, multi-sector antennas, which are consisted of several directional antennas and a beam selecting switch, are developed. This kind of antennas is effective to mitigate unwanted incident rays in the multipath environments such as indoor offices, and to access a basestation antenna from anypoint in the office. This is the different point from the antenna for a handheld telephone which has omnidirectional radiation pattern in the horizontal plane.

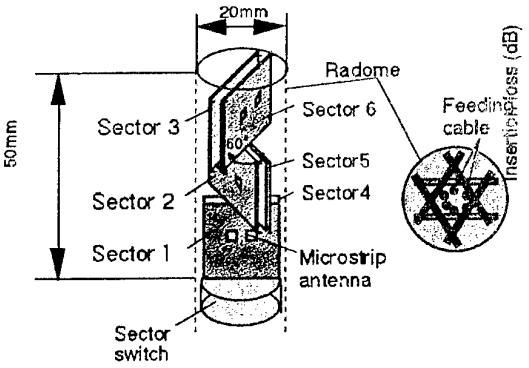


Fig.1. A rod-type 6-multisector Antenna (11)

In the Altair system and VJ system, wireless terminals are used to be fixed, although they can be transportable. Therefore, the antennas used in those terminals are not small enough to be installed at notebook PC's. In AWA systems, it is assumed that notebook PC's are used as wireless terminals and various types of antennas have been proposed to be installed at the handheld wireless terminals [10]. As shown in Fig. 1, a multi-sector antenna where its radiating elements made of patch antennas are arrayed vertically and confined in a rod. Prototypes of the antennas were manufactured at 20 GHz frequency band and measured data were reported [11]–[15]. The diameter and the length of the antenna is about 20 mm and 50 mm, respectively and it is feasible to be installed at the notebook PC. However, the

insertion loss of its RF switch is relatively high and it degrades the total antenna performance.

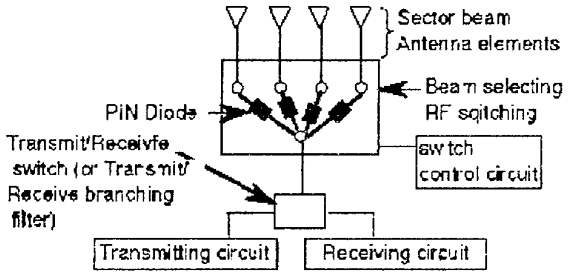


Fig. 2. Fundamental structure of a multi-sector antenna

In this paper, in order to reduce the insertion loss of the RF switch of the multi-sector antenna, a new configuration, which has the implicit RF switch instead of the conventional SPNT (Single Pole N Throw) switch, is proposed and fundamental analysis data are presented to ensure the validity of the proposed antenna. In section 2, a conventional multi-sector antenna is shown and its problem is pointed out. In section 3, the configuration of the proposed antenna ispresented, and numerical data of the antenna are described in section 4. Finally, conclude remarks are given in section 5.

A MULTI-SECTOR ANTENNA AND A BEAM SELECTING RF SWITCH

A multi-sector antenna is composed of some directional beam antennas, a beam selecting RF switch and a switch controller as shown in Figure 2. The SPNT switch is usually used as the beam selecting switch and one of the paths in the switch is active in selecting one of the beams. In transmitting, RF power directly passes through the active switch to the antenna element. Therefore, insertion loss tends to be large, especially when operating frequency becomes high. Figure 3 summarizes the insertion loss of the SPNT switches which were developed for the beam selecting switch of the multi-sector antenna [13]–[15]. As shown in Figure 3, insertion loss becomes about 2 to 3 dB around the frequency of 20 GHz and degrades communication characteristics considerably.

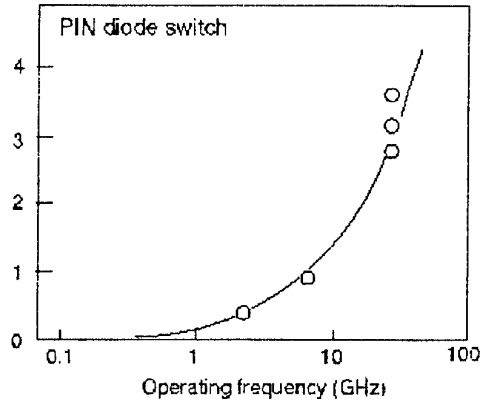
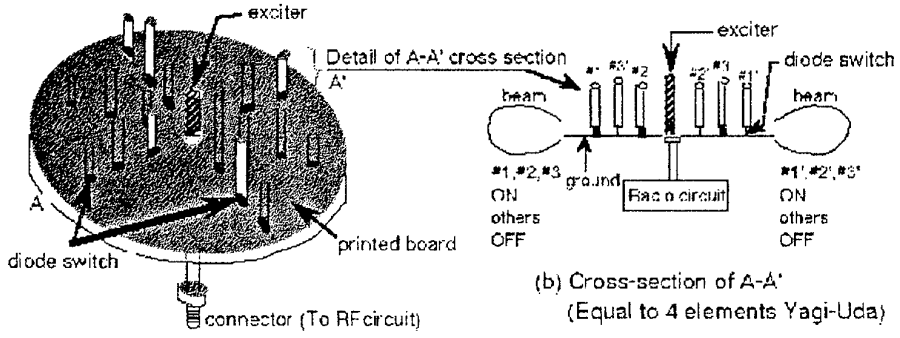


Fig. 3. Insertion loss of beam selecting switches

A good solution to reduce the insertion loss of the switch is to use diode devices with excellent RF performances. However, it is expensive or may be much power consuming. Then, in the next section, a new RF switch configuration is proposed where the beam selection is performed by the distributed implicit RF switch.

A MULTI-SECTOR ANTENNA WITH A DISTRIBUTED IMPLICIT RF SWITCH

A distributed implicit RF switch does not directly switch the RF power paths, but functionally creates a beam by altering the ON/OFF states of the switches which are positioned at the bottom of the wire elements. An example of the multi-sector antenna with a distributed implicit RF switch is shown in Figure 4. This is a case of a six sector beams antenna. The antenna consists of one center element which is fed by a feeding cable and surrounding parasitic elements. They are all on a circular ground plane and almost quarter wavelengths. A RF circuit (transmitter and/orreceiver) is directly connected to the center element of the an-



(a) whole antenna configuration

(b) Cross-section of A-A'
(Equal to 4 elements Yagi-Uda)

Fig. 4. A multi-sector beam antenna using distributed implicit RF switch

tenna which works as an exciter of a Yagi-Uda array. The elements around the center element have diode switches or other switching devices at the bottom of the elements.

By switching diodes properly, a directional beam is radiated to the desired direction. To clear how to realize the directional beams and to switch them, Figure 4(b) shows the elements arraged in one diameter where the Yagi-Uda arrays radiating directional beams to left-hand side or right-hand side are constructed depending on the ON/OFF state of the surrounding elements. The element, whose switch is OFF, is out of resonant condition. Therefore, induced current on it is very small. If the elements of #1, #2, and #3 are ON and the other elements are OFF, the antenna radiates towards left-hand side. On the contrary, if the elements of #1', #2' and #3' are ON and the others are OFF, the antenna radiates towards right. An antenna array, which radiates maximum to θ-direction or (θ+180)-direction, is arranged in the same diameter such as interleave manner, then the antenna can be constructed to be compact.

Beam direction control by switching the elements in a Yagi-Uda array has been reported by Preston, Thiel et al [16], [17]. However, in their papers, a SPNT RF switch was also used to switch beams as in the usual multi-sector antennas [16]. In the antenna proposed here, switches are distributed and placed at the bottom of the parasitic elements. Therefore, RF power does not pass through the diode switches directly. This is the principle why the insertion loss becomes small in this multi-sector antenna.

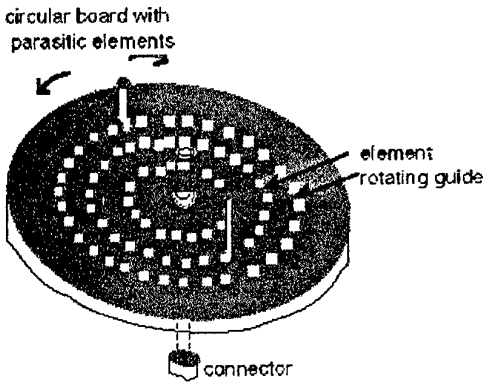
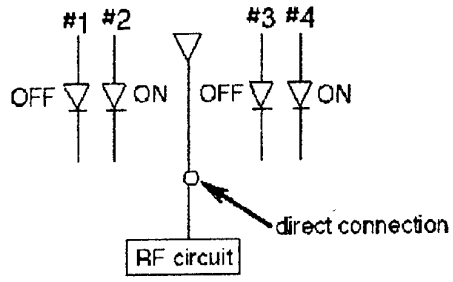


Fig. 5. A multi-sector beam antenna using mechanical implicit RF switch

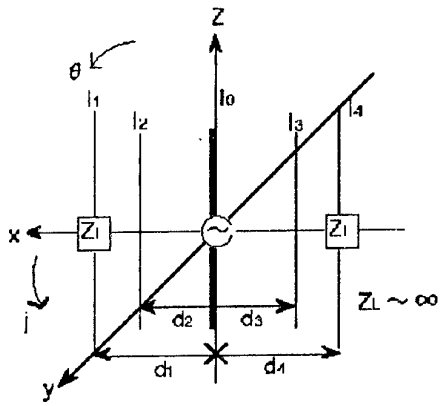
Figure 5 shows the mechanical beam steering antenna which is the alternative version of a low insertion loss multi-sector antenna. An exciter and a feeding cable are connected and fixed. A circular ground plane with parasitic elements rotates with an axis of the exciter. At the frequency of 20 GHz, the diameter of the ground plane is about 15 mm to 20 mm, therefore it is easy to rotate the ground plane.

NUMERICAL RESULTS

In order to ensure the feasibility of the antenna proposed in section 3, numerical calculations were carried out based on the antenna configuration shown in Figure 6. Although radiating elements with about a quater-wavelength in Figure 4, about half-wavelength elements are used in Figure 5 due to the assumption that the perfect image is produced by the ground plane. In this calculation model, a directive beam towards right-hand side or left-hand side is produced by a fixed exciter, a reflecting element and a directing element depending on the ON/OFF state of the switches, respectively.



(a) two-beam sector antenna consisting of 3 elements Yagi-Uda array



(b) coodinate system for analysis

Fig. 6. Antenna analysis model

Figure 7(a) and (b) show the radiation patterns when the maximum radiation is φ = 0°when elements of #2 and #4 are ON, and #1 and #3 are OFF. It is assumed that all diode switches work idealy, when a diode is ON or OFF. This means that the impedance at the center of each element is zero or infinite, respectively. Broken lines in Figure 7(a) and (b) mean the radiation patterns of a conventional three elements Yagi-Uda array. Radiation patterns of the proposed antenna agree well to those of the conventional Ygi-Uda array. Therefore, It is understood that the elements with OFF diodes do not influence to the total radiation pattern. The directivity of the proposed antenna is 9.0 dB, while the conventional Yagi-Uda array is 8.8 dB.

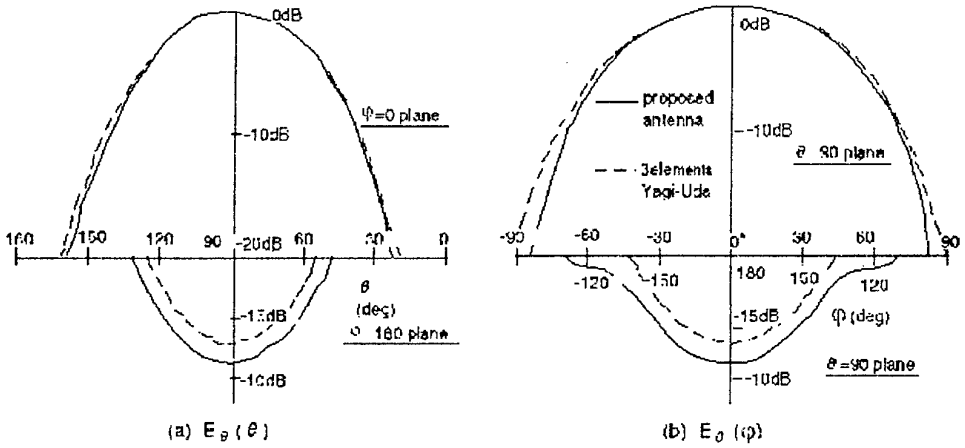


Fig. 7. Radiation pattern

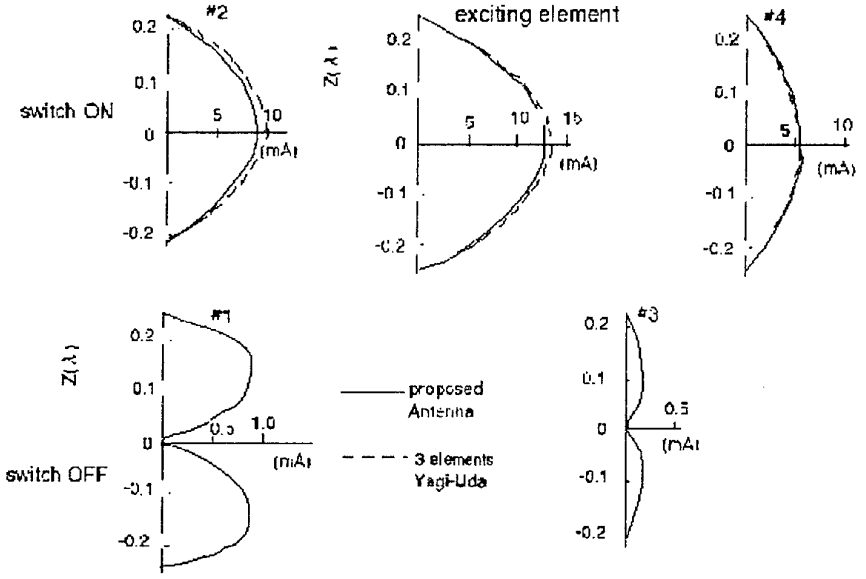


Fig. 8. Current distribution on the elements

Figure 8 shows the current distribution on each element of the proposed multi-sector antenna. In the figures of the elements with diode switches ON, current distributions of the conventional Yagi-Uda array with the same configuration are drown together with broken lines. The magnitude of induced currents on the elements with OFF switches are one-tenth or less to those of the elements with ON switches. From these current distributions, it is easy to understand that the radiation patterns of the proposed antenna are almost the same as those of the conventional Yagi-Uda array.

In the above calculations, attention was not paied to the impedance match, but it is not difficult to match the antenna impedance to the feeding circuit for all directive beams, because this antenna is rotationary symmetric. This is also the advantage of the proposed antenna.

CONCLUSION

A multi-sector beam antenna is promising antenna in a broadband wireless access system. However, when the operating frequency becomes high, the insertion loss of the sector switch increases. In this paper, in order to decrease the insertion loss, a new configuration of the multi-sector beam antenna was proposed and the feasibility was ensured by the numerical data, such as radiation patterns and current distributions. However, it is assumed that diode switches are ideal, so the more practical model should be considered. It is also neces-

sary to evaluated the total RF loss due to switches and compare quantitatively to that of the existing multi-sector antenna by experiments.

REFERENCES

1. H.Terada, "Information Network Evolutions into 21 century", IEICE (Japan), Vol.81, No.4, pp. 322-325, April, 1998.
2. S.Suzuki and H. Ishikawa, "A New Node System and Telecommunications Network for the Multimedia Era", NTT Technical Journal, Vol. 8, No. 9, pp. 8-16, Sept. 1996 (in Japan).
3. A. Nakajima and A. Kaiyama, "Evolution of Mobile Telecommunications Network" IEICE (Japan), Vol. 80, No. 4, pp. 338-343, April, 1997.
4. M. Tsukamoto, "Network Infrastructure for Mobile Computing", IEICE (Japan), Vol. 80, No. 4, pp. 338-343, April, 1997.
5. T. Tsutsumi and K. Ujiie, "Altair products of 19GHz radio LAN system," MWE'93 Microwave Workshop Digest PP201-206, Dec., 1993.
6. T. Shirato, T. Hanazawa, T. Okada and T. Maruyama, "A 19-GHz Band wireless LAN", NTT R&D, Vol. 45, No. 8, pp. 95-104, Aug. 1996 (in Japan).
7. H. Matsue, M. Umehira and A. Hashimoto, "Future trend of Broadband wireless Access Systems and their Core Technologies,' MWE'96 Microwave Workshop Digest, PP271-276 Dec., 1996.
8. A.S. Acampora, "Wireless ATM : A perspective on Issues and Prospects," IEEE Personal Communications Magazine, Vol. 3, No. 4, pp. 8-17, Aug. 1996.
9. T. Maruyama, K. Uehara and K. Kagoshima, " Design and Analysis of Small Multisector Antenna for Wireless LANs Based on Monopole Yagi-Uda Elements"' Electronics and Communications in Japan, Part 1, Vol. 81, No. 12, pp. 80-90, Dec., 1998 (Translated from Denshi Joho Tsushin Gakkai Ronbunshi, Vol.80-B-II-, No. 5, pp. 424-433, May, 1997).
10. K. Uehara, T. Seki and K. Kagoshima, "A Planner Sector Antenna for Indoor High-Speed wireless Communications," IEICE Trans. on Comm. Vol.E79-B, No. 12, pp. 1773-1777, Dec., 1996.
11. T. Seki, K Uehara and K. Kagoshima, "Rod Type Sector Antennas for High-Speed Wireless Communication"' Technical Report of IEICE, A·P96-169, pp. 19-24, Feb., 1997.
12. T. Seki et al, "6-Sector Terminal Antennas for ATM wireless Access System", Proceedings of the 1998 IEICE General Conference, B-5-290, Mar., 1998.
13. T. Seki et al, "A Rod-type Small 6-Sector Antenna for ATM Wireless Access System", Proceedings of the 1998 IEICE General Conference, B-5-291, Mar., 1998.
14. T. Seki et al, "A Small-Sized 6-Sector Terminal Antenna for ATM Wireless Access System", Proceedings of the 1998 IEICE General Conference, B-5-292, Mar., 1998.
15. T. Seki et al, "A 6-Sector Terminal Antenna Placed on the Face of a Hexagonal Prism for ATM Wireless Access System", Proceedings of the 1998 IEICE General Conference, B-5-293, Mar., 1998.
16. S.L. Preston, D.V. Thiel, T.A. Smith, S.G.O' Keefe and J.W. Lu,"Base-Station Tracking in Mobile Communicaitons Using a Switched Parasitic Antenna Array,"IEEE Trans. on Ant. & Prop. Vol. 46, No. 6, pp. 841-844, Jun., 1998.
17. D.V. Thiel, S.G.O'Keefe and J.W.Lu, "Electronic beam steering in wire and patch antenna systems using switched parastic elements," IEEE AP-S Symposium digest, pp. 534-537, Jul. 1996.

TECHNOLOGY FOR A QUASI-GSO SATELLITE COMMUNICATIONS SYSTEM

T. Katagi, R. Yonezawa, I. Chiba, S. Urasaki

Mitsubishi Electric Corporation
5-1-1 Ofuna, Kamakura, Kanagawa 247-8501, Japan
(tel) +81-467-2530 (FAX) +81-467-2519, e-mail: katagi@isl.melco.co.jp

Abstract: In this paper, a satellite communications system using a Quasi Geostationary Satellite Orbit (Quasi-GSO) is proposed. A 24-hour period Quasi-GSO system could give high quality communication to high latitude regions with its satellites observed from earth stations having high elevation angles. In this paper, a system concept and a deployable flat antenna with light weight antenna elements are described proposing it to be a good candidate for mobile communications satellite use.

Keywords: Quasi GSO, Satellite Communication, Deployable Antenna, Antenna Arrays, Multibeam Antenna

INTRODUCTION

In recent years, mobile communication has developed increasingly and there are more difficulties in coping with the growing demand of the users with limited channels. The Quasi-GSO system is fit for this demand having the ability to provide similar services that are now provided by GSO systems without causing the problems of frequency sharing with the GSOs. It also can provide high quality communication having high elevation angle seen from earth terminals in medium and high latitude regions. This feature is important especially in large cities with skyscrapers or in countryside with high mountains where terrestrial waves would not easily be reached. The details of the Quasi-GSO and its orbital parameters are described in section 2.

In section 3, the system concept is described in detail with the link budget. The proposed system is aimed for mobile communication with small and low powered earth terminals. In order to make the earth stations small and low power, the satellite antenna needs to be large and high power. This requirement calls for a fair amount of breakthrough in fundamental technologies such as element antennas, power feeding method and antenna deployment. Some of these technologies have been dealt with and are described in section 4 followed by conclusion.

QUASI-GSO[1]

In this section, the orbital parameters for the satellite orbit are described. A Quasi-GSO with 24-hour period is chosen for this system. Satellites in this orbit stay in a limited longitude position in respect to the earth. By using more than three satellites, seamless service of 24 hours a day could be possible while the operating satellite would be seen in a high elevation angle staying in an almost stationary position observed from the earth. Hence the earth station antennas do not need any tracking function. This is the reason this orbit system is called "Quasi-GSO".

Here, the orbit with the following parameters is used in this proposed system.

Table 1. Orbit parameters

Mean longitude	East 140 deg.
Orbit inclination	45 deg.
Perigee height	30000 km
Apogee height	42000 km
Period	24 hours

Figure 1 shows the ground trace of the satellite using this orbit system.

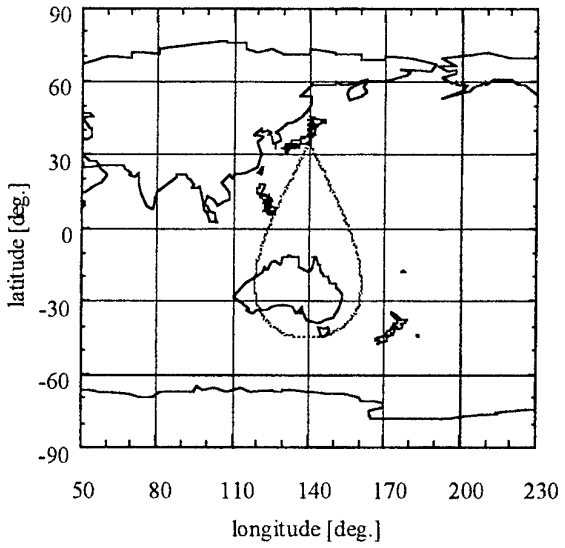


Fig. 1. Ground trace of Quasi-GSO satellite

The operating time of one satellite is 8 hours and by utilizing 3 satellites, the system can offer 24 hours a day service. This can be understood from Figure 2 that shows the elevation angle of the three satellites ob-

served from Tokyo. One can see at least one of the three satellites with more than 79 degrees elevation angle. Figure 3 is a skyward view showing the movement of one of the three satellites observed from Tokyo. The operating satellite stays in a limited portion in the sky and this is a characteristics that greatly resemble the GSO except that its elevation angle is fairly high.

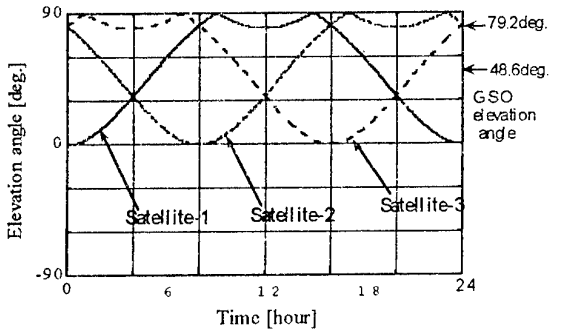


Fig. 2. Time variation of the elevation angle of the satellites observed from Tokyo

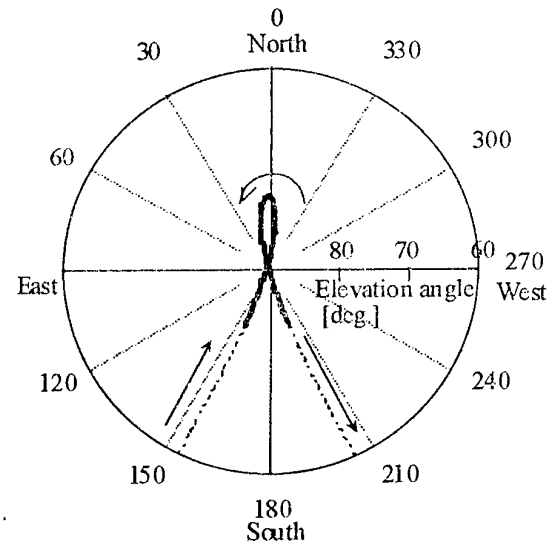


Fig. 3. Movement of a satellite observed from Tokyo (solid line corresponds to the operating time)

SYSTEM CONCEPT [2],[3]

In the proposed system, the satellite illuminates multiple beams to a certain area from high elevation angle so that the degradation due to shadowing effect can be reduced. When large aperture antennas are used for satellite antennas, high communication capacity can be attained using small size portable terminals as earth stations.

In an SCPC (Single Carrier per Channel) system, the antenna aperture can be determined from the required number of channels as follows. The number of beams (B) is,

$$B = \frac{C}{\left(F_d / C_W\right)}$$

where C is the required number of channels. F_d is the frequency bandwidth at one of the multibeams and C_w is the carrier signal frequency bandwidth.

The beam width in which the coverage area S [sr] illuminates is as follows.

$$\Theta = \sqrt{\frac{4S}{\pi B}}$$

Here, the antenna aperture D can be expressed as,

$$D = 60.2\frac{\lambda}{\Theta}$$

5.6 kbps digital voice service with carrier signal frequency bandwidth of 12.5 kHz is considered. When the carrier frequency is 2.5 GHz and the frequency band width of one of the multibeams is 7.5 MHz, the relation between the required number of channels and the antenna aperture could be calculated as shown in Fig. 4. For example, if an antenna of about 45 m^2 aperture size is used, 100,000 channels would be available.

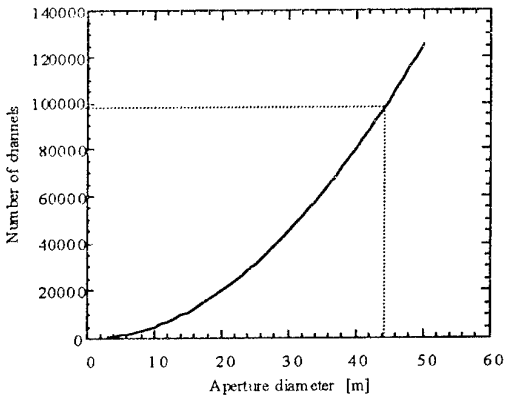


Fig. 4. Relation between the number of channels and antenna aperture

A system configuration of this system is shown in Fig. 5. To realize a 45 m^2 size antenna, conventional aperture antenna would not be a realistic choice. A flat panel antenna would be easier to make its aperture large. In this system, a large aperture phased array antenna is proposed for the satellite antenna to attain high power that makes it possible to achieve low power portable terminal.

In the proposed system, 100,000 digital voice channels could be provided by using 45m^2 phased array antenna. Three types of communication method have been taken

into consideration and the examples of the link budget are shown in Tables 2 and 3.

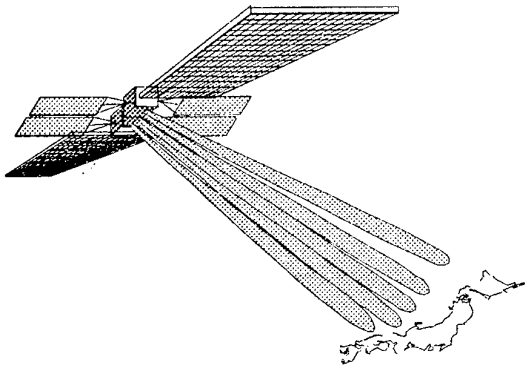


Fig. 5. System configuration

KEY TECHNOLOGIES

There are several technologies that need to be considered especially for space use. Some of the most important ones are described in this section.

DEPLOYABLE PHASED ARRAY[4],[5]

Antennas for space use should be small during launching of the satellite but need to be large after once they are out in space. A deployable antenna is a good candidate for this requirement. In order to deploy the antenna panels into 2-dimensional continuous plane, their fundamental structure should be composed of simple and loose mechanisms. The schematic deployment sequence is shown in Fig. 6. Since the axes of rotation of the panel joints are crossing normally, the deployment motion should be composed of two independent phases (The two phases are (1) to (2) and (3) to (4) in Fig. 6).

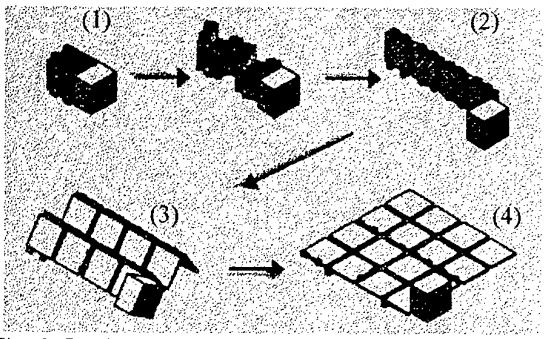


Fig. 6. Deployment sequence of the 2D-APAA structure

This type of structure often causes inaccuracy in its deployment, although the antenna is a phased array antenna that can control its beam electronically and thus the antenna structure need not be in accurate condition. This beam control can be realized by utilizing the digital beam forming technology and an estimation method of the antenna distortion.

LIGHT AND THIN ANTENNA PANEL[6]

To realize a large size deployable phased array antenna, the antenna panel with light weighted and thin structure has to be constituted. The conventional honeycomb material is too heavy for this system. Here, we propose an antenna with new material. The antenna configuration is shown in Fig. 7. The frame is made from CFRP. The dielectric plane on which antenna radiators are mounted is made with Kevlar fiber. In the first stage of its fabrication, the antenna is constructed at a temperature of 170 thermal degrees. The thermal expansion rate of these two materials is different and as the antenna is cooled to the steady thermal state, the frame made with CFRP expands and the antenna panel made with Kevlar fiber shrinks and consequently the desired plane configuration can be attained. A picture of the 4 by 4 sub-array panel is shown in Fig. 8.

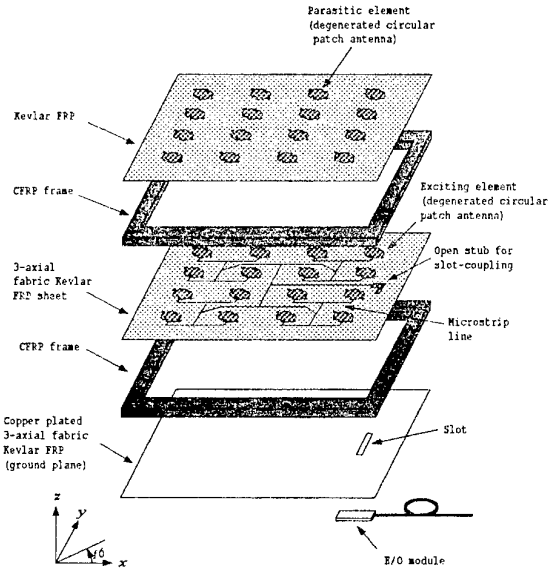


Fig. 7. Antenna configuration

The weight of this antenna panel becomes lighter than that of the conventional type, because there is no material besides the frame that is supporting the patch antennas over the earth conductor. At the present stage, the antenna panel has a weight of 300 g/m^2.

SMALL-SIZED HIGH EFFICIENCY LASER DIODE SUB-MODULE[7]

The proposed system requires flexible, lightweight, and low loss feeders to activate the deployable phased array antennas. A feasibility study on the application of fiber-optic links to microwave signal transmission has been done and we have developed a small-sized highly effi-

Table 2. Up link budget (frequency 2.5 GHz).

		SCPC/FDMA	TDMA	CDMA
Power of earth terminal	Average	16.2dBm (41.7mW)	16.8dBm (47.9mW)	13.5dBm (22.4mW)
	Maximum		37.8dBm (6.0W)	29.4dBm (871mW)
Gain of earth terminal		-2.2dBi	-2.2dBi	-2.2dBi
Free space loss		-192.0dB	-192.0dB	-192.0dB
Fading and rain scatter loss		-3.2dB	-3.2dB	-3.2dB
Feeding loss		-2.0dB	-2.0dB	-2.0dB
Power of arriving signal (C)		-122.7dBm	-101.1dBm	-123.4dBm
Noise power		-133.0dBm (B=7kHz)	-111.4dBm (B=1MHz)	-97.4dBm (B=25MHz)
CDMA gain		----------	----------	37.9dBm
Noise and interference (N+I)		-131.7dBm	-110.1dBm	-94.5dBm
Total C / (N + I)		9.0dB	9.0dB	9.0dB
Total Eb / (N0 + I0)		6.0dB	6.0dB	6.0dB
Desired Eb / (N0 + I0)		4.0dB	4.0dB	4.0dB
System Margin		2.0dB	2.0dB	2.0dB

Table 3. Down link budget (frequency 2.6GHz).

		SCPC/FDMA	TDMA	CDMA
Total power of SSP		63.7dBm (2.34kW)	64.3dBm (2.69kW)	61.0dBm (1.26kW)
Transmitting power at 1ch	Average	13.7dBm (23.4mW)	14.3dBm (26.9mW)	11.0dBm (12.6mW)
	Maximum		35.3dBm (3.39W)	26.9dBm (490mW)
Feeding loss		-1.5dB	-1.5dB	-1.5dB
Gain of satellite antenna		61.0dBi	61.0dBi	61.0dBi
Fading and rain scatter loss		-3.2dB	-3.2dB	-3.2dB
Free space loss		-191.5dB	-191.5dB	-191.5dB
Gain of earth terminal		-2.2dBi	-2.2dBi	-2.2dBi
Power of arriving signal (C)		-123.7dBm	-102.1dBm	-124.4dBm
Noise power		-134.0dBm (B=7kHz)	-112.4dBm (B=1MHz)	-98.4dB (B=25MHz)
CDMA gain		----------	----------	37.9dBm
Noise and interference (I)		-132.7dBm	-111.1dBm	-95.5dBm
Total C / (N + I)		9.0dB	9.0dB	9.0dB
Total Eb / (N0 + I0)		6.0dB	6.0dB	6.0dB
Desired Eb / (N0 + I0)		4.0dB	4.0dB	4.0dB
System Margin		2.0dB	2.0dB	2.0dB

cient laser diode sub-module. Fig. 9 shows the picture configuration of this module.

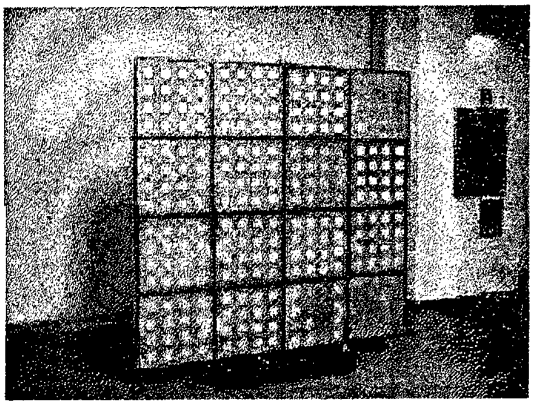


Fig. 8. 4×4 sub-array antenna panel

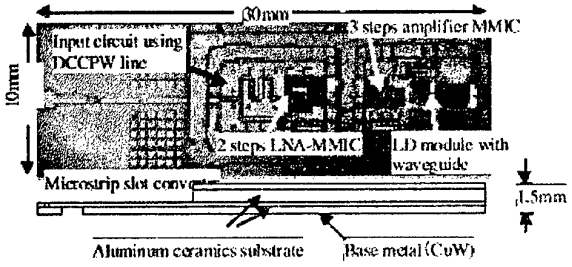


Fig. 9. Configuration of the module

CONCLUSION

We have proposed a new satellite communications system using Quasi-GSO satellites that mount deployable phased array antennas. In this system, the satellite illuminates multiple beams to a certain area from high elevation angle, so that the degradation due to shadowing effect can be reduced. When large aperture phased array antennas are used for satellite antennas, high communication capacity can be attained using small size portable terminals as earth stations.

REFERENCES

1. W. L. Pritchard et. al., "Satellite Communication Systems Engineering," Prentice Hall.
2. S. Mano and T.Katagi, "A method for measuring amplitude and phase of each radiation element of a phased array antenna," Trans. IECE Japan, J65-B, 5, pp.555-560 (May 1982).
3. S. Urasaki, T.Katagi et. al., "Inclined GEO satellite communication system with deployable phased array antenna," Proc. AP-S pp.24-28, 1998.
4. T. Katagi, et. al., "Large deployable active phased array antenna for satellite use," AIAA-94-1070 15th. Int. Communications Satellite Systems Conference, pp.1075-1084, Feb. 1994.
5. M. Tabata, et. al., "Conceptual study of a 2-D deployable active phased array antenna," 8 th. ICAST, Oct. 1997.
6. T. Takahashi, et. al., "Super lightweight planar array antenna with stretched structure for satellite communication systems," Proc. AP-S (to be presented in July 1999).
7. S. Kaneko, et. al., "Small-sized and highly efficient laser diode sub-modules for fiber-fed phased array antennas," Proc. CPT'99, pp. 59-60, Jan. 1999.

THE ANTENNA SUB-SYSTEM FOR METEOSAT SECOND GENERATION SATELLITES

K. van Klooster, M. DiFausto*, V. Santachiara*, P. Carrati*
A. Rosa, P. Russo**, B. Robert*****

ESA/ESTEC, Postbus22, Keplerlaan, 2200 AG Noordwijk, The Netherlands, kvtkloos@estec.esa.nl
*Alenia Spazio, Spa. Via Saccomuro 24, 00131 Roma, Italy, fax +39-06-4151-2389,
**Space Engineering, Via Berio 91, 00131 Roma, Italy, fax +39-06-2280739,
***Alcatel Space Industries, 100 Boulevard du Midi, 06156 Cannes la Bocca, France, fax +33-49292-3470

Abstract. The Meteosat Second Generation project (MSG) concerns a launch and operation of three new satellites in the coming years. MSG continues meteorological services, which are currently provided by the very successful first generation of satellites in the Meteosat Operational Program (MOP), operated by Eumetsat. MSG expands on the services offered by MOP by providing more frequently data in more observation bands, with higher resolution. The telecommunication system for the MSG satellite transmits the measured data to the primary ground station and receives and re-transmits pre-processed images and meteorological data from the latter station. It collects meteorological data from data collection platforms. The MSG satellite carries also a Search and Rescue transponder. The antenna sub-system has been specifically designed for the necessary functions and permits appropriate data throughput with the satellite spinning at a rate of 100 revolutions per minute. The antenna sub-system for MSG is explained, after a short general description

BACKGROUND

The first of two pre-operational Meteosat satellites was launched in 1977. Meteosat Operational Program was started in 1983 after this 'pre-operational' period with an agreement to launch three operational satellites. A prototype of a pre-operational satellite called P2, was also prepared and launched with the first ARIANE 4 launcher in 1988. One more satellite of the MOP type was launched in 1997 and continues service today in the so-called Meteosat Transitional Program (**MTP**). **ESA** [1] carried out the operations of Meteosat satellites (data collection, pre-processing and redistribution of meteorological information), until a new European organisation **Eumetsat** [2] took over the responsibility of these tasks in 1995. Eumetsat operates the MOP satellites and MTP, which continue services for another one and half year more, after which new **MSG** satellites shall take over with much more enhanced capabilities. ESA and Eumetsat are preparing this **MSG** program, with ESA responsible for procurement of the satellites. The first of the three **MSG** satellites is planned to enter services after commissioning in the year 2001 (launch the second half of 2000). **MSG** will have much more capabilities than **MOP**, as will be outlined below.

The **antenna subsystem** for **MSG** is the main subject, but first some more descriptive information is given for both **MOP** and **MSG** satellites. It assists to understand MSG antenna optimisations, decisions, implementation and functionality under specific constraints. Alenia Spazio in Roma is fully responsible for the MSG telecommunication payload, of which the antenna sub-system is a major part. Aerospatiale is the prime contractor for the satellite.

MOP AND MSG SATELLITES

A **MOP**-type satellite orbits the Earth at an altitude of 35.800 km, in geostationary orbit, thus leading to a satellite position above the equator on a fixed meridian. MOP is positioned on the Greenwich meridian. It is a spin-stabilised spacecraft, rotating at a speed of 100 revolutions per minute (100 RPM) and has its spin-axis perpendicular to the orbital plane. The primary payload for MOP is a high resolution three channel radiometer instrument, which images the Earth in less than half an hour in the three spectral bands (wavelength: 0.5–0.9 μm, 10.5–12.5 μm and 5.7-7.1 μm). One image line is taken over the Earth disc over a part of the revolution from +10° to −10° (as seen from the geostationary orbit). An image composed out of 2500 scan-lines results after 2500 revolutions, so 25 minutes.

The stored image line data are re-sampled and transmitted down to the Earth during remainder part of the 360° arc outside this ±10° interval.

The data are processed on the ground at a dedicated location (at Eumetsat in Darmstadt), where also other meteorological products are derived. Processed images with additional data are sent up again towards the satellite, which in turn redistributes data to users within the coverage zone. Much more info is found in [1] and [2]. Some data products are received in the Ukraine [3].

The satellite collects also meteorological data from remote (automatic) platforms within its coverage zone and relays this information to the central ground station (this is the so-called DCP mission).

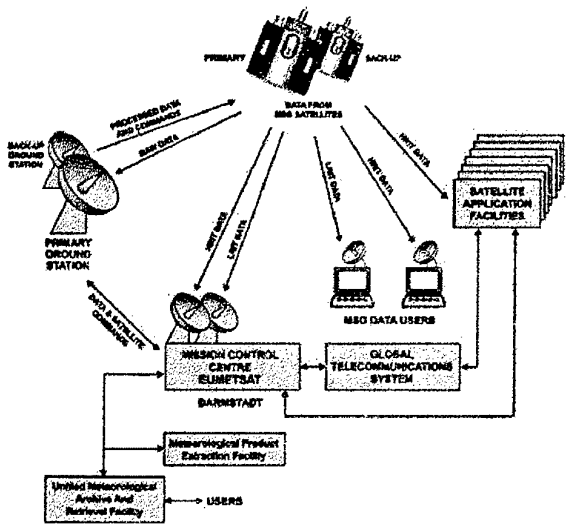


Fig. 1. MSG Mission Scenario with RF links for the raw radiometer data to the primary ground station (with back-up) and the up- and downlinks for the processed data to primary and secondary users (courtesy ESA)

A very broad basis has been created of experiences with the satellite, with its operations, with data processing and data utilisation, after more than 25 year. It provided a very good starting point for a configuration of a new satellite, the Meteosat Second Generation satellite.

MSG satellite will also be a spin-stabilised spacecraft, operating from a geo-stationary location. A number of enhanced capabilities are foreseen. The radiometer will generate images at double the speed, every 15 minutes, and will do this in 12 spectral bands, with a much better resolution (1 km for the visible channel, 3 km for other spectral channels). This permits to extract three-dimensional data about the atmospheric composition.

The reader is invited to estimate the pointing and localisation accuracy (1 km from 35800 km). The larger amount of data is also transmitted to the primary ground station of Eumetsat (in Usingen in Germany), from where processed data are transmitted up to the satellite again for re-distribution to primary and secondary users within the coverage [2]. Fig. 1 shows the link schema. MSG provides the data collection mission (DCP) with a larger number of channels than available on the MOP satellite. A Search and Rescue transponder is carried. It makes use of the UHF and L-band antenna for respectively reception (up) and transmission (down).

MSG is a much larger spacecraft than MOP, due to the enhanced capabilities with the much larger radiometer, the need for a longer lifetime and the associated supporting equipment. Fig. 2 shows the MOP spacecraft and the MSG spacecraft (left) with relative dimensions.

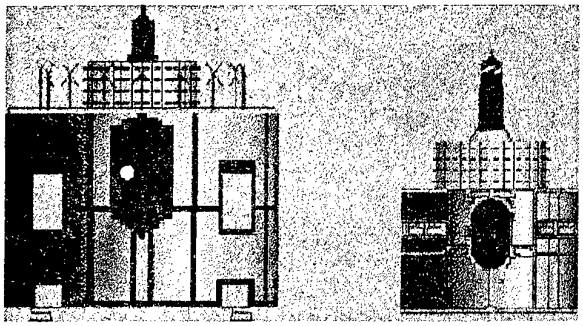


Fig. 2. MSG satellite (left) and MOP satellite at a similar scale (courtesy ESA)

Fig. 2 indicates also already a very important constraint for the antenna farm, located on top of the spacecraft. The height permitted for the antenna farm of MSG is relatively small, much less than the height available on top of the MOP satellite body. This is very important; it has led to many calculations to optimise the antennas for MSG in the presence of the satellite structure, as indicated below.

Conversion of the transfer orbit to the geostationary orbit is also different: MOP uses a solid fuel apogee boost motor to change from the transfer orbit to the geostationary orbit with one motor firing. MSG will use a set of two apogee boost motors, which use bi-propellant fuel. Three motor firings are planned to convert the transfer orbit to geostationary orbit (Fig. 3).

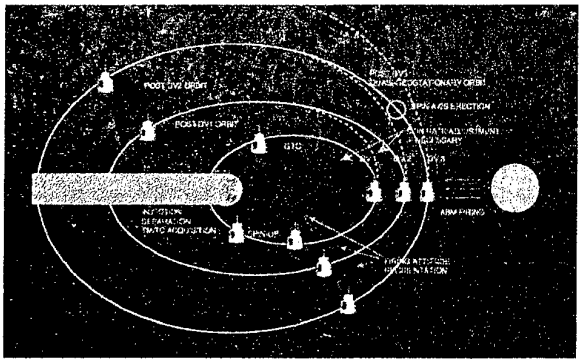


Fig. 3. From a high elliptic trasnfer orbit to a geostationary orbit. MSG will use three motor firings (courtesy ESA)

ANTENNAS USED FOR THE TELECOMMUNICATION SYSTEM

The telecommunication system of MSG has a number of tasks, each of which requires a particular antenna:

- Reception of telecommands and transmission of house keeping data. A dedicated (redundant) S-band transponder is used for this task, connected to a dedicated telemetry and telecommand antenna, (TT&C antenna), the antenna is not redundant

- Transmission of the measured radiometry data, coming from the data handling subsystem to the primary groundstation. The electronically despun antenna (EDA) is used for this task in L-band.
- Reception of pre-processed images with associated data. A toroidal pattern antenna is used, operating in S-band.
- Transmission to users, using the L-band EDA antenna for low resolution and high-resolution data.
- Receiving data from Data Collection Platforms (DCP). The Electronically Switched Circular array antenna is used (UHF-EDA at 402 MHz).
- Transmission of the DCP data, using the L-band EDA antenna.
- Receiving emergency messages (S&R or Search and Rescue). The UHF – EDA is used at 406 MHz.
- Transmission of S&R messages, using the L-band EDA antenna.

The antenna subsystem will be discussed in more detail and the first results will be presented, together with considerations related to decisions for solutions.

THE ANTENNA FARM FOR MSG

Alenia Spazio is responsible for design, manufacture and test of MSG-'s antenna subsystem (Fig. 4). The Engineering Model (Fig. 4) antennas permitted after detailed measurements to tune the parameters to an optimum for the Flight Model antennas, which is during July 99 right at the moment of writing this abstract under test at Alenia Spazio (It).

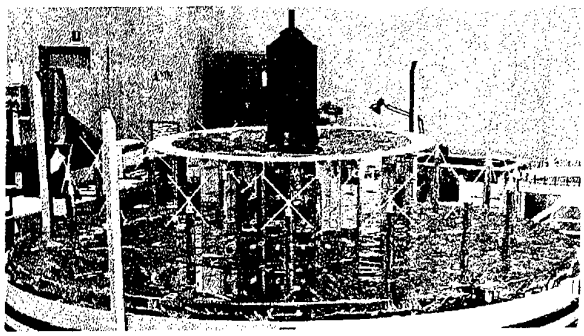


Fig. 4. MSG Antenna Farm, Engineering Model (courtesy Alenia Spazio / ESA)

The respective antennas are, going from top to bottom:

-1- TT&C antenna on top,

-2- S and L-band toroidal pattern antennas inside the black cylindrical radome,

-3- L-band Electronically Despun Antenna, using 32 columns, 4 dipole radiators in each column.

-4- UHF Electronically Despun Array, using 16 crossed dipole radiators, positioned in front of the L-Band EDA.

(The white vertical bars at 90 degree interval on the outer edge belong to ground support test equipment).

Very detailed analysis support has been provided by Space Engineering for all antennas and scattering analyses. The full paper will describe a number of the activities in detail. Also test results will be discussed.

REFERENCES

1. http://www.esa.int/, also under remote sensing, /msg
2. http://www.eumetsat.de/
3. http://www.cri.chernigov.ua/
4. "Antennas for Scientific and Remote Sensing Satel-lites", C.G.M.van't Klooster, N.E.Jensen, Invited paper, JINA Antenna Conference, 1990.
5. "Meteosat Antenna System" Nicolai, Alenia Spazio,
6. Alenia Revista, 1976.

MODERN METHODS OF ANALYSIS AND COMPUTATION OF ANTENNA RADOMES

D. J. Kozakoff

Millennium Corporation,
PMB#308-120, 2960 Shallowford Road,
Marietta, Georgia 30066, USA

ABSTRACT

A *radome*, an acronym coined from *radar dome*, is a structure placed over an antenna that protects the antenna from its physical environment. Ideally, the radome is radio-frequency (RF) transparent and does not degrade the electrical performance of the enclosed antenna. Today, radomes find wide applications in ground, maritime, aircraft, and missile electronic systems (Fig. 1.)

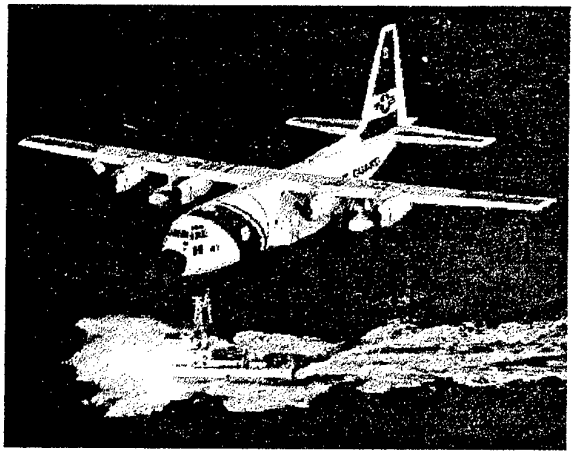


Fig. 1. Hercules Aircraft with Radome Enclosed Radar Antenna

Very early methods of radome evaluation were cumbersome, relying on the use of a nomograph (1, 2). With the advent of the personal computer (PC), geometric optics approaches based on PC computers were developed (3, 4). But with recent advances in the PC speed and capabilities, physical optics based surface integration approaches that previously required a mainframe computer can now be accomplished on a PC (5).

INTRODUCTION

During recent decades, rapid growth in the use of the electromagnetic spectrum has led to many improvements in the performance of electromagnetic sensors. Two examples of these improvements are (a) dual-polarized, wide band antenna systems for improved tracking and radar performance, and (b) very low side lobe antennas that provide ground clutter rejection for airborne radars that use pulse-Doppler modes, (c) SATCOM and other telecommunications antennas using frequency reuse (dual polarization.)

These sensors require more stringent radome performance than their predecessors because the antenna performance can be altered by radome effects on its radiation patterns. These efforts include, but are not limited to the following:

(1) Boresight error (BSE) and boresight error slopes (BSES)

(2) Increased antenna sidelobe levels Depolarization (folding of energy from one polarization sense to the other)

(3) Introduction of an insertion loss

(4) Flash lobe effects

Most modern approaches of radome analysis use ray tracing to describe propagation through the radome wall onto the receiving antenna aperture where integration produces the antenna port voltage. These methods use many approximations such as treating the radome wall at each ray intercept point as locally plane and also assuming parallelism between the inner and outer radome walls at each intercept point. These approximations introduce some error between the predicted and measured results.

Although a number of different radome electromagnetic analysis techniques are feasible, primarily the geometric optics (GO) and the physical optics (PO) approaches can be most easily implemented on a PC. Both transmit and receive formulations are possible.

GO treats the electromagnetic propagation as "light like" in behavior and, although approximate, is exact only in the limit of zero wavelength (infinite frequency.) However, it produces reasonably good results for radome enclosed antennas as small as five wavelengths in diameter. GO will not give good results near physical boundaries, but provides useful insights in those cases. We must consider three aspects to fully use GO; (a) ray reflections within the dome, (b) wave polarization, and (c) amplitude variations both along the ray path and through the reflections (6).

PO is based on Huygen's principle, which has been of fundamental importance to the development of electromagnetic wave theory. Huygen's principle states that each point on a primary wavefront can be considered as

a new source of secondary spherical waves, and that a secondary wavefront can be constructed as the envelope of these spherical waves. Thus, a spherical wave from a point source propagates as a spherical wave, whereas an infinite plane wave continues as a plan wave. The PO method is employed in surface integration formulations that produce reasonably good results for a radome-enclosed antenna less than a wavelength in diameter, and is generally a more robust modeling approach than GO.

Other radome approaches that are worthy of mention, but more difficult to model on a PC computer include the method of moments (MOM) approach (7) and the plane wave spectra (PWS) method (8, 9).

GEOMETRIC OPTICS (GO)

GO analysis approaches have conceptual simplicity combined with reasonable accuracy. The concept for receiving and transmitting formulations are illustrated in Fig. 2. Both receive and transmit formulations were researched (10) and were found to produce identical BSE prediction. However, the receiving application required greater computer run time.

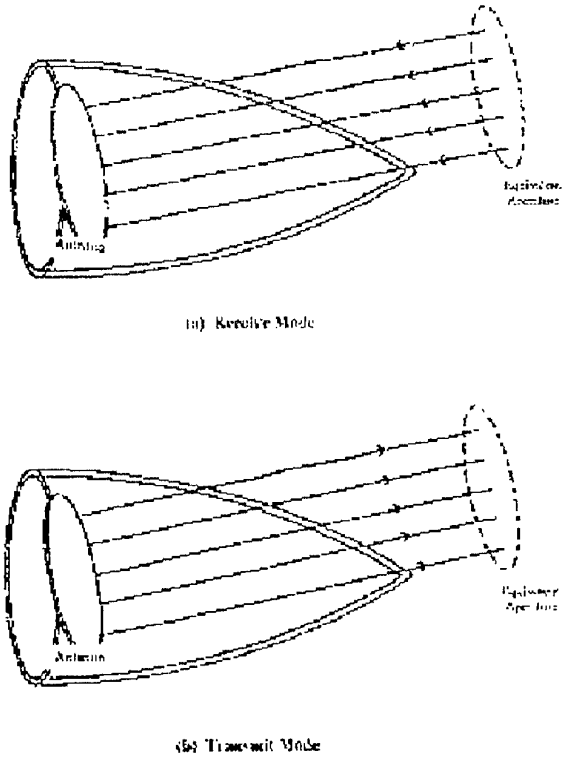


Fig. 2. GO Raytracing: Receiving Formulation (Top) Transmitting Formulation (Bottom)

GO Receiving Formulation

The GO receiving mode ray trace (Fig. 2 (a)) uses the direct rays incident on the aperture from a specified direction. The insertion voltage transmission coefficients based on flat-panel theory for both the parallel and perpendicular polarization are used to transform the plane wave fields associated with each ray from their values outside the radome to their values on the antenna aperture.

The receiving formulation finds the voltage at the antenna port when a plane wave is incident on a radome-enclosed antenna; this is sometimes referred to as a "backward ray trace." The complex antenna port voltage is obtained from the incident fields and the known characteristics of the antenna from the formula (11):

$$V_a = \iint F^a E^i T_W \, da$$

where E^i is the incident plane wave function; F^a is the complex valued receiving aperture distribution at point on the antenna surface; and T_W is the complex valued radome transmission coefficient at the ith ray intercept point. The integration over the differential antenna aperture "da"extends over the physical antenna surface area for which F^a has a significant contribution.

Usually, the radome is considered locally plane at each ray intercept point, which leads to small errors in the calculation of the transmission coefficient, T_W. The transmission characteristics of the radome wall for any given frequency, material type, number of layers, and layer thicknesses also depend on the angle-of-incidence θ (the angle between the propagation vector and the radome surface normal vector at the ray intercept point) and the apparent polarization of the incident wave with respect to the plane of incidence.

At each ray intercept point, it is customary to normally decomposed into components parallel and perpendicular to the plane-of-incidence prior to applying the respective transmission coefficients. Subsequently, the wave is reconstructed on the other side of the wall. For all cases, an equivalent transmission coefficient T_W can be defined. The calculation of T_W usually ignores multiple reflections within the radome wall and trapped waves. Some researchers (12) have observed that significant errors sometime occur by this omission.

The antenna aperture distribution can be found from probing the near field at several wavelengths from an actual antenna surface, and applying a backward propagation (Fourier transform) technique. Alternatively, it can be probed very close to the antenna aperture with a suitable probe.

GO Transmit Formulation

Early GO transmitting formulations modeled the antenna aperture as a collection of sources with arbitrary amplitude and phase. The collection of rays define an equivalent aperture outside of the radome whose amplitude and phase distribution incorporats the effect of the radome (Fig. 2 (b).) The fast Fourier transform

(FFT) of this distribution yielded the far-field radiation pattern of the radome-enclosed antenna.

In the transmitting mode, the antenna aperture distribution is projected through the radome wall to form an equivalent aperture outside of the radome. Each ray is modified by the amplitude and phase of its associated radome transmission coefficients, and the modified effective aperture distribution therefore includes the effect of the radome walls. Points forming the modified aperture distribution are related to the actual aperture distribution via:

$$F^e = T_W F^a$$

where, F^e is the complex valued transmit aperture distribution at a point on the equivalent aperture outside the radome. In this case, the equivalent aperture size is identical in size to the actual antenna aperture.

Assume that the antenna is in the x-y plane with the z-coordinate corresponding to the radome axis. We can obtain the normalized far-field antenna array pattern from the equivalent aperture on a PC via:

$$E_t = \frac{1}{MN}\sum_{m=1}^{M}\sum_{n=1}^{N} F^e_{mn} e^{-jk(x_m \sin\theta\cos\phi + y_n \sin\theta\sin\phi)}$$

here we assume that the external aperture is modeled with MN sample points so that $x_m = md_x$; $y_n = nd_y$; where d_x, d_y are the sample spacings in the x and y coordinate directions, respectively.

PHYSICAL OPTICS (PO)

In analyzing the performance of a radome-enclosed antenna system, the PO techniques generally offer higher computational accuracy than GO because of the necessary assumptions used with GO. For instance, GO makes the assumption that the EM wave propagates as a plane wave confined to a cylinder whose cross section the antenna aperture defines. However, in reality the field diverges.

For radomes smaller than about five wavelengths in diameter, the GO approach is too approximate and we must go to PO techniques. Integration over the radome surface with the Kirchoff-Fresnel integral yields better results to obtain the field at each point on the antenna aperture (Fig. (3).)

PO Receiving Formulation

To accomplish this integration, we use an external reference plane to reformulate an incident plane wave as a grid of Huygens's sources, and we then trace rays between that grid and each point on the antenna aperture (Fig. 3 (a).) Hence, the complex antenna antenna voltage is (12):

$$V_a = \iint F^a \{\iint E^i T_W \frac{e^{-jkr}}{r} ds\} da$$

where k is the wavenumber, r is the distance from any point on the external reference plane to a point on the antenna surface, and the integration over ds is over the external reference plane. The integration over the differential antenna aperture da extends over the antenna surface area for which F^a has significant contribution.

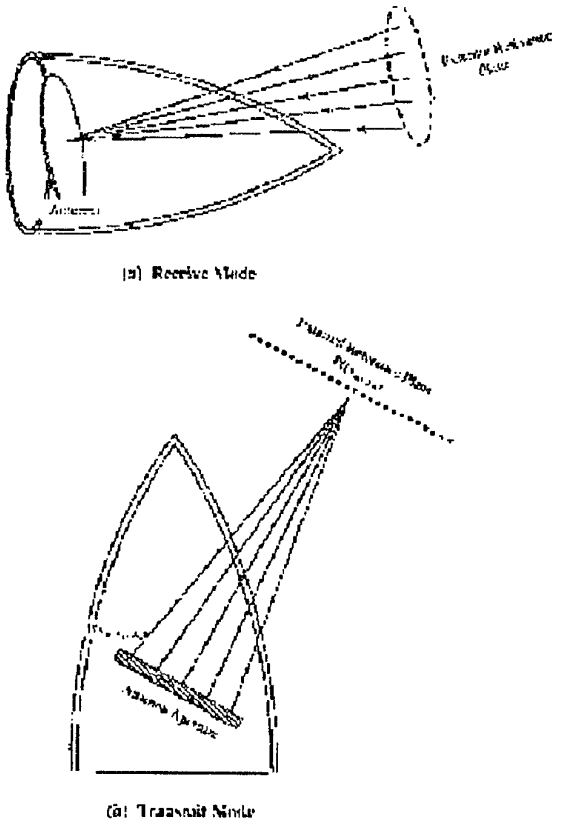


Fig. 3. PO Raytracing: Receiving Formulation (Top), Transmitting Formulation (Bottom)

PO Transmitting Formulation

In a PO transmitting formulation (Fig. 3 (b),) the following steps occur:

(1) We obtain the antenna near-field distribution on the inner radome surface.

(2) The transmission coefficients of the radome wall are applied to give the field on the exterior of the radome.

(3) We make a final transformation to the far field using a Fast Fourier Transform (FFT) technique.

A PC computer implementation of this transmit radome analysis technique uses PO for tracing the field from an antenna aperture through the radome wall to an external reference plane, where the contributions are col-

lected (13). Assuming that each point on the antenna aperture radiates as a Huygens's source, the complex distribution for each point on an external reference plane is:

$$F_e = \iint F_a \frac{e^{-jkr}}{r} da ,$$

here, the integration extends over the physical antenna surface area for which F a provides a significant contribution, and where the physical area forming the external reference plane is generally significantly larger than the physical area of the antenna. An exact solution corresponds to an infinite external plane, but this is not possible. Often, it is in the order of two to four times the physical area of the antenna. With a PC computer, the far field radiation pattern can be computed from the reference plane distribution in the identical manner it was for the GO transmitting case, previously.

Comparison of GO and PO Methods

The direct ray (GO) and surface integration (PO) methods differ primarily in the computation of the total transmission coefficient. With the PO method, the fact that the integration of a bundle of rays through the radome wall, as opposed to a single ray, more densely samples the curvature variation results in a more robust wall transmission model. Both the GO and PO methods use the flat-panel approximation to compute wall transmission coefficients at the ray intercept points and ignore both multiple internal reflections and trapped waves. Several researchers compared predicted with measured data for these two ray-trace methods. Overall, the researchers found that the surface integration was more accurate, especially for radomes that were small in wavelengths.

OTHER TECHNIQUES

Method of Moments (MOM)

Joy et al. (14) applied a two-dimensional method of moments (MOM) technique to a tangent ogive radome, based on the approach developed by Richmond (15–17). An integral equation for the electric field was solved by dividing the dielectric into cells that were small enough so that the electric field intensity was approximately uniform in each cell.

Also applying a MOM approach, Tricoles et al. (18) analyzed the EM fields scattered by a hollow cone, using two formulations. One was based on a scalar Green's function and the other on a tensor Green's function. The two are equivalent, but the procedures differ in the following ways:

(1) The scalar Green's function method decomposes the cone into circular cylinders, and subsequently decomposes the cylinders into angular sectors. The tensor Green's function method decomposes the cone into spheres.

(2) The number of cells differs because the cell sizes differ.

(3) Polarization dependance differs.

Tricoles et al. (19) applied the MOM technique to dielectric cylinders of arbitrary shape. Although sophisticated, the MOM is seems more difficult to apply to radome modeling than the other methods previously discussed. Very limited validation data appear in the technical literature at this time to compare its accuracy with the GO and PO methods. However, MOM may give a more robust solution to the effects of guided waves or scattering by a radome rain erosion tip.

Plane Wave Spectra

Paris developed a three-dimensional approach that could find the tangential fields on the outside radome surface because of horn antenna radiating inside the radome (20). Wu and Rudduck developed a three-dimensional method that used a plane wave spectrum representation to characterize the antenna (21). A discrete plane wave spectrum (PWS) is a complex vector array obtained from a Fourier transform of the near-field aperture and represents the radiating antenna properties. If an antenna aperture has $M \times N$ sample points, then the PWS contains MN plane waves. The PWS approach is illustrated in Fig. 4.

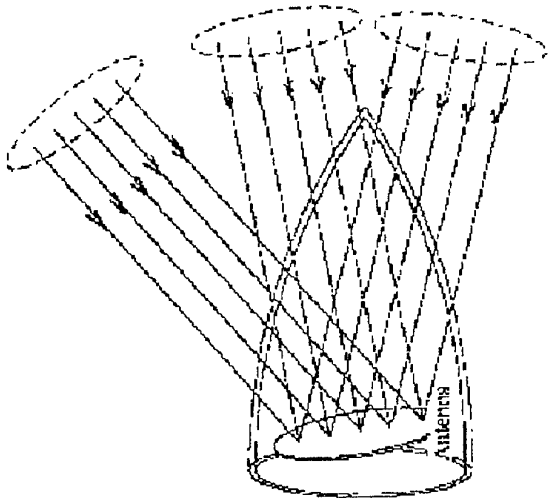


Fig. 4. Illustration of PWS Approach

Joy and Huddleston expanded on this idea by using a FFT to speed the computer calculations when applying a plane wave spectrum approach (22.) PWS is believed to give more accurate results than either GO or PO approaches discussed earlier. However, PWS requires considerably larger amounts of computer run time and cannot be implemented on a PC.

SOURCES OF RAY-TRACE COMPUTATIONAL ERROR

Ray-trace computational errors have several causes, including the following:

(1) Antenna modeling;

(2) Statistical wall variations;

(3) Internal wave reflections;

(4) Rain erosion tip modeling;

(5) Radome wall modeling.

Table 1 gives an assessment of additional factors contributing to radome performance computational accuracy. The internal reflections are a potentially significant source of computational error. In most radomes, it is safe to ignore rays that reflect off the radome wall more than once before striking the antenna because these multiple bounces produce insignificant energy. The mathematical modeling describing this error source is shown in Burks et al. (23).

Table 1

Parameters That Influence Prediction Accuracy

Category	Uncertainties
Antenna modeling	Antenna aperture distribution Polarization detail Physical detail
Statistical wall variations	Thickness variations Dielectric constant inhomogeneity Loss tangent uncertainty
Internal reflections	Back wall reflections Bulkhead reflections Multiple bounce Flashlobe
Tip modeling	Refraction
Wall model	Flat-panel assumption Anisotropic materials Variation of permittivity with temperature Adhesion layers Trapped waves

Many aircraft or missiles have a bulkhead plate between the radome and the vehicle body. If this bulkhead is not microwave-absorber treated, incoming rays can reflect off this surface and strike the backside of the antenna. The backlobe pattern of the antenna receives this reflection, causing boresight errors. Generally, bulkhead reflections will not have much effect until the angle-of-incidence of the incoming rays (with respect to the radome axis) becomes large. In actual applications, antenna gimbals and other electronic hardware may block some reflections from reaching the antenna. To evaluate the typical contribution of each of the ray bounce error contributors, we studied an A-sandwich tangent ogive radome with a fineness ratio of three. The antenna size was approximately 20 wavelengths at the operating frequency and the polarization was vertical. Using a GO receiving mode prediction model, we compared the measured elevation plane BSE data to predicted data. For this particular radome, when ignoring all internal reflection error sources, reasonably good correlation was seen between measured and predicted BSE data, but the predominant internal reflection error source was found to be bulkhead reflections.

Wall Model and Statistical Variations

Another source of computational error is the wall transmission model. In all current ray-trace solutions, the radome walls are approximated as locally plane at the ray intercept point because most radome walls are approximated as locally plane at the ray intercept point because most radome shapes are not separable coordinate surfaces, and differential equations cannot be used. The flat-panel approximation is not valid for thick, highly curved walls. For spherical radomes, Bloom et al. (24), attempted to compensate the transmission coefficient to account for wall curvature by use of a divergence factor (DF). Kozakoff (25) derived a solution applicable to ogive radome shapes. Geometric optics was used to trace the fields from the reference plane through the radome wall to a receiving monopulse antenna, where the wall transmissions on each ray collected. However, a DF derived from Snell's law for spherical shells accounted for the local wall curvature at each ray intercept point.

Most radome wall models assume that the dielectric and magnetic properties are homogeneous and isotropic with individual layers. This is not always true, and is another potential source of computational error and complication in the modeling. For instance, Kozakoff and Hensel (26) showed that the orientation of structural fibers in reinforced plastic radomes results in anisotropy of the electromagnetic medium that influences the modeling. To solve this type of problem, White and Banks (27) derived the wave equation into three components to deal with plane wave transmission and reflection from anisotropic materials. Guided waves were observed to propagate in radome walls by Tricoles and Rope (28), and are potential source of computational error. According to Ersoy and Ford (29), a radome performance degradation from the theoretical predictions also occurs from radome surface irregularities. Vorobyev (30) has applied statistical methods to manufacturing tolerances (on both dielectric constant and wall thickness) and related the manufacturing tolerances to the electrical performance of radomes.

REFERENCES

1. Kaplun, V.A., "Nomograms for Determining the Parameters of Plane dielectric Layers of Various Structure with Optimum Radio Characteristics," Radiotechnika I Electronika [in Russian], Part 2, Vol. 20, No. 9, 1965.
2. Zamyatin, V.I. et al, Antenna Fairings, V.I.Lenin Belorussian Publishing House [in Russian], 1980.
3. Bagby, J., "Desktop computer-aided Design of Aircraft Radomes," IEEE MIDCON '88 Conference Record, Western Periodicals Company, 1988.
4. Kaplun, V.A., et al, "Introduction to Computer Aided Design of Microwave Antenna Radomes," Radiotechnika i Electronika [in Russian], Vol 42, No. 2, 1987.
5. Kozakoff, D.J., "Analysis of Radome Enclosed Antennas," Artech House, Norwood MA, 1987.
6. Milligan, T.A., Modern Antenna Design, McGraw Hill Book Company, New York, 1988.
7. Tricoles, G. et al, "Analysis of Radomes by the Method of Moments Method," Proceedings of the 17 th Symposium on Electromagnetic Windows, Atlanta, Georgia, 1984.
8. Wu, D.C.F. and R.C.Rudduck, "Plane Wave Spectrum Surface Integration Technique for Radome Analysis," IEEE Transactions on Antennas and Propagation, AP-22, No.3, May 1974.
9. Joy, E.B. and G.K.Huddleston, "Radome Effects on Ground Mapping Radar," Final Report on Contract DAAH01-72-C0598, MICOM, Huntsville, Alabama, May 1973.
10. Tavis, M., "A Three-Dimensional Ray Tracing Method for Calculation of Radome Boresight Error and Antenna Pattern Distortion," TOR-0059 (56860), AD729811, Aerospace Corporation, May 1971.
11. Hayward, R.A., et al, "Accuracy of Two Methods for Numerical Analysis of Radome Electromagnetic Effects," IEEE International Symposium Digest on Antennas and Propagation, Seattle, Washington, June 1979.
12. Raz, S, et al, "Numerical Analysis of Antenna Radome Systems," Proceedings of the tenth III Convention in Israel, Tel Aviv, October 1977.
13. Israel, M.I., et al, "A Reference Plane Method for Antenna Radome Analysis," Proceedings of the fifteenth Symposium on Electromagnetic Windows, Georgia Institute of Technology, Atlanta, GA, 1980.
14. Joy, E.B., et al, "Comparison of Radome Electrical Analysis Techniques," Proceedings of the Fifteenth Symposium on Electromagnetic Windows, Georgia Institute of Technology, Atlanta, GA, 1981.
15. Richmond, J.H., "Scattering by Dielectric Cylinders of Arbitrary Cross Sectional Shapes," IEEE Transactions on Antennas and Propagation, Vol.AP-13, 1965.
16. Richmond, J.H., "The Calculation of Radome Diffraction Patterns," AD-423660, Department of Electrical Engineering, Ohio State University, 1966.
17. Richmond, J.H., "TE Wave Scattering by a Dielectric Cylinder of Arbitrary Cross Sectional Shape," IEEE Transactions on Antennas and Propagation, Vol.AP-14, 1966.
18. Tricoles, G., et al, "Wave Propagation Through Axially Symmetric Missile Radomes," AD-A106762 8, 1981.
19. Tricoles, G., et al, "Analysis of Radomes by the Method of Moment Method," Proceedings of the Seventh Symposium on Electromagnetic Windows, Georgia Institute of Technology, Atlanta, GA,1984.
20. Paris, D.T., "Computer Aided Radome Analysis," IEEE Transactions on Antennas and Propagation, Vol.AP-18, 1970.
21. Wu, D.C.F. And R.C.Rudduck, "Plane Wave Spectrum Surface Integration Technique for Radome Analysis," IEEE Transactions on Antennas and Propagation, Vol.AP-22, No.3, 1974.
22. Joy, E.B. and G.K.Huddleston, "Radome Effects on a Ground Mapping Radar," Final Report on Contract DAAH01-72-C-0598, MICOM, Huntsville, AL, 1973.
23. Burks, D.G., et al, "The Equivalent Source Concept Applied to the Analysis of Radome Performance," Proceedings of Southeastcon 78, IEEE Region 3 Conference, Auburn University, Auburn, AL, 1978.
24. Bloom, D.A., et al, "Comparison of Spherical Wave Ray Tracing and Exact Boundary Value Solutions for Spherical Radomes," Proceedings of the Seventeenth Symposium on Electromagnetic Windows, Georgia Institute of Technology, Atlanta, GA, 1984.
25. Kozakoff, D.J., "Geometric Optics Radome Analysis Wall Solution Incorporating the Effects of Wall Curvature," Proceedings of the SPIE OE/LASE 94 International Symposium, Los Angeles, CA, 1994.
26. Kozakoff, D.J. and J.Hensel, "Materials Implications of Millimeter Wave Radome Performance," Proceedings of the IEEE International Conference on Infrared and Millimeter Waves, Miami, FL, 1981.
27. White, D.J. and D.J.Banks, "Plane Wave Transmission and Reflection Coefficients for Anisotropic Sheets of Radome Materials," Proceedings of the Sixteenth Symposium on Electromagnetic Windows, Georgia Institute of Technology, Atlanta, GA, 1982.
28. Tricoles, G. and E.L.Rope, "Scattering of Microwaves by Dielectric Slabs and Hollow Dielectric Wedges," Journal of the Optics Society of America, Vol.55, No.11, 1988.
29. Ersoy, L., and D.Ford, "RF Performance Degradation due to Random Radome Surface Irregularities," IEEE Antennas and Propagation Society International Symposium Digest, 86CH2325-9, 1986.
30. Vorobyev, E.A., "Certain Production Criteria for Large Scale Monolithic Antenna Radomes," Izvestiya vuz Radioteknika [in Russian], Vol.9, No.3, 1966.

ATOMIC FUNCTIONS AND NUMERICAL METHODS OF THE ANTENNAS THEORY SYNTHESIS SOLVING PROBLEMS

V. F. Kravchenko

Institute of Radio Engineering and Electronics, Russian Academy of Sciences, ul.Mokhovaya 11
Moscow 103907, Russia, and Moscow Institute for Technology and Physics, Dolgoprudnyi, Moscow region 141700, Russia, tel: +7 (095) 921-48-37, fax: +7 (095) 925-92-41, e-mail: kvf@mx.rphys.mipt.ru

ABSTRACT

The work is devoted to analysis of Atomic Functions (AF) applications to principal problems of antennas theory. The analysis follows the result of the solution of some applied problems, such as is to determine the field of antenna in the far zone when the distribution of the current or the tangential components of the electromagnetics field on the surface of antenna is known, and of synthesis is to determine a current (or a field) in the antenna by means of radiation pattern in the zone, and boundary value problems of the antenna theory is to determine the field in antenna and surrounding area when excitation by outside sources and boundary conditions are known. In the second part of paper, the new algorithm for numerical solution of radiation pattern synthesis problems is proposed. A number of numerical examples were performed to illustrate the effectiveness of presented approach. Unique approximating properties of Atomic Functions (AF) let us apply more simple and effective method, which result in significant computational gain, and, hence, the solution requires less memory and run time.

INTRODUCTION

AF are widely used in different branches of computational physics and also in digital interpretation of measurements of signals and in regeneration of images. For the first time it is proposed to apply AF mathematical instrument to the antenna theory. The advantages of this principally new approach in analysis and synthesis of the antenna were shown, and also in boundary tasks of antenna theory. It was shown that AF in many cases are in the best agreement with the physical content of the antenna concept, and take possibility to construct simple and steady algorithms of calculation of their basic essential features.

It is known that a large role in approximation theory and numerical methods is played by algebraic and trigonometric (exponential) polynomials. This universal instrument of approximation has an essential flaw in practice – the "non-finiteness" of classical polynomials. In numerical realization, it is desirable to apply "local", i.e., finite functions, with carriers of small diameter, since in that case in the corresponding matrices the majority of elements are equal to 0, and the matrix is "rare" or even "ribbonlike", but at the same volume of computer operating memory it is possible to use an approximating subspace of high dimensionality and thus receive precise approximations. The widely used local spline functions are not universal in the sense that to obtain an optimal approximation function with better smoothness, higher degree splines are needed. Thus, the classical algebraic and trigonometric polynomials are universal, but not local, and splines are local, but not universal. The question arises of the construction of spaces for functions that would be simultaneously local and universal. The question arises of the construction of spaces for functions that would be simultaneously local and universal. At the same time, it is desirable that they be easily calculated. The functions discussed in more detail below are so simple and easy to use that it has proven expedient to fill a class of "elementary functions" with them.

The question arises: how are these functions constructed? We have in mind the fact that nonuniversal splines are conditioned by their already insufficient smoothness, which makes it necessary to consider infinitely differentiable finite functions. It is known that finite splines of the N-th degree are N-times folds of characteristic functions of intervals. These finite functions are infinitely repeated folds of characteristic functions of intervals. To obtain finite functions, the interval length should reach zero as quickly as possible. If $\varphi(x)$ is a sought-for function and $\varphi'(x)$ is its Fourier transform, then $\varphi'(x)=\prod_{k=1}^{\infty}\frac{\sin\alpha_k t}{\alpha_k t}$; here $\alpha_k>0$ and monotonically tends to zero, $\sum_{k=1}^{\infty}\alpha_k<\infty$. Out of all sequences $\alpha=|\alpha_k|$ tending monotonically to zero, we will pick those for which $\varphi(x)=\varphi_a(x)$ possesses good approximation properties. It is evident that the simplest and most convenient can be the function $\varphi(x)$ that corresponds to the geometric progression $\alpha_k=2^{-k}$. Such a choice of is at least logical. We will designate this function up(x). Consequently,

$$\mathrm{up}(x)=\frac{1}{2\pi}\int_{-\infty}^{\infty}e^{itx}\prod_{k=1}^{\infty}\frac{\sin t2^{-k}}{t2^{-k}}dt. \qquad (1)$$

The original results for the theory of AF were obtained at the end of 1970 by V. L. Rvachev. The first publication appeared in 1971 in [1]. The problem of the existence of the simplest and, to date, the most important

AF, up(x), originating with V. L. Rvachev in 1967 and solved by him jointly with Rvachev V. A., was a fundamentally new scientific result of the structural method suggested at the time by V. L. Rvachev for the solution of boundary value problems for equations in partial derivatives of mathematical physics. The functions up(x) discussed here appeared under the following circumstances. In 1967, V. L. Rvachev put forth the following problem [2]. If $\varphi(x)$ is a finite differentiable function, having one part rising and another falling (a "hump"), then its derivative $\varphi'(x)$ will consist of a "hump" and a "hole". Does a function $\varphi(x)$ exist for which the " hump" and the "hole". Does a function $\varphi(x)$ exist for which the "hump" and the "hole" of the derivative are similar to the "hump" of the function itself?

In the language of mathematics this means the following: does a finite solution, in which for definiteness we consider the carrier of $\varphi(x)$ to be the segment [−1; 1], exist? In this manner, V. L. Rvachev and Rvachev V. A. proved in a 1971 work the existence and uniqueness of such a finite solution with an interval equal to 1, and this is the function up(x).

Thus, at the same time that classical algebraic and trigonometric equations with constant coefficients, the function up(x) and other analogous functions satisfy equations of the form $Ly(x)=\lambda\sum_{k=1}^{m} c_k y(ax-bk)$, where $a > 1$, and L is linear differential operator with constant coefficients. These equations are close to linear differential equations with constant coefficients in the sense that here the Fourier transformations operates effectively for them as well. In the theory of AF are studied AF and similar functions, spaces created by AF, and also their application in approximation theory, mathematical analysis, the theory of differential functional equations in numerical methods, signal processing and image restoration, the statistical theory of knowledge of forms, boundary value problems of diffraction and scattering of electromagnetics waves, and problems of optimal control, analysis, and synthesis of antennas.

THE FUNCTION up(x)

The function up(x) [1–17] (Fig. 1) is defined from (1).

It has compact support [-1, 1] and is a solution of the functional-differential equation

$$y'(x) = 2y(2x + 1) - 2y(2x - 1). \qquad (2)$$

Approximation of various classes of differentiable functions by expressions of the form

$$\sum_{k=-\infty}^{\infty} c_k \mathrm{up}\left(\frac{x}{h} - k2^{-p}\right), \qquad (3)$$

for fixed p as $h \to 0$ was investigated earlier in [3, 14]. In this note we study the order of approximation of differentiable functions by means of linear combination of translates of the function up(x) in the form

$$\varphi(x)=\sum_{k=-\infty}^{\infty} c_k up(x-k\cdot 2^{-p}), \qquad (4)$$

as $p \to \infty$. It turns out that such approximations have a combination of properties not encountered with the classical trigonometric and algebraic polynomials and polynomial splines.

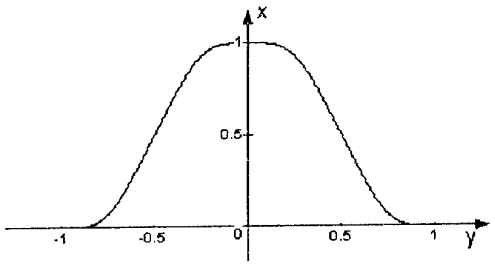


Fig. 1. Atomic function up(x)

Let $\{L_n\}$, n = 1, 2,..., be a sequence of subspaces of the space C[−1, 1] such that

$$\dim L_n = n,\ L_n \subset L_{n+1}.$$

Definition 1. The sequence $\{L_n\}$ is said to be approximately universal (a.u.) if for any natural number m and any $f(x) \in C^m$ [−1, 1]

$$\inf\left\|f-\varphi\right\|_{C[-1,1]} \le C_m n^{-m}\left\|f^{(m)}\right\|_{C[-1,1]}$$

for $n > n(m)$.

Definition 2. The sequence $\{L_n\}$ is said to be sequence with local basis (an l.b. sequence) if for any n there is a basis in L_n that consists of functions with compact supports whose diameters tend to 0 as $n \to \infty$.

Remark. For subspaces of C [−1, 1] used in numerical methods both the property and the existence of a local basis are important, one reason being that in this case the matrices of the corresponding algebraic systems turn out to be "thinly populated".

It is well known, that spaces of algebraic (trigonometric, in the periodic case) polynomials are a.u., but they do not have local bases. The spaces of polynomial splines do not have local bases, consisting of the B-splines of Schoenberg, but they are not a.u. However, if we consider a sequence of spline subspaces $\{L_n\}$ for which the degrees of the splines increase as $n \to \infty$, then we do not have the following condition, which is important from a practical point of view

$$L_n \subset L_{n+1}.$$

Theorem 1. There exist a sequence $\{L_n\}$, $L_n \subset C$ [−1, 1], such that:

a) $\dim L_n = n$,

b) $L_n \subset L_{n+1}$,

c) L_n is a subspace of space of linear combination of the form (4), where $p = [\log_2 n]$,

d) the sequence $\{L_n\}$ is a.u.,

e) $\{L_n\}$ is an l.b. sequence and the diameters of the supports of the functions in a local basis for L_n are equal to $(p + 2)\, 2^{-p}$.

STATEMENT OF THE PROBLEMS

1) In the antennas theory the following questions are considered:

(i) problem of analysis is to determine the field of antenna in the far zone when the distribution of the current or the tangential components of the electromagnetic field on the surface of antenna is known,

(ii) problem of synthesis is to determine a current (or a field) in the antenna by means of radiation pattern in the far zone,

(iii) boundary value problem of the antenna theory – determination the field in antenna and in surrounding area when the activation by outside source and boundary conditions are given.

AF can be successfully applied to solve all this problems. Consider one of them.

2) Problem 1. This problem is reduced to solving vector linear equation

$$LI = E, \tag{5}$$

where L is linear operator produced by Green's function of the medium antenna placed, I is current distribution (electrical magnetic current or polarization current) in antenna, E is field in far zone (usually considered a tangent components of electric or magnetic field to a sphere which radius is much more than the length of wave of light). To evaluate the advantages of applying AF to this problem lets consider one of the simplest following situations: analysis of the rectilinear antenna, which described by equation

$$E(u) = A \cdot \int_{-l}^{l} I(x) \cdot e^{-iux} dx, \tag{6}$$

where $E(u)$ is complex amplitude of the field in the far zone that is proportional to the radiation pattern of the antenna, $u = k\cos\theta$ (θ is the angle of aspect, which is reading from normal to the antenna, A is complex constant which is not depended upon the angle of observation, $2l$ is the length of the antenna, $I(x) = \mathrm{up}(x)$ is distribution of the current (electric, magnetic or current of polarization) in antenna that is placed along x axis of the Cartesian coordinate system. It is essential that $I(x)$ should be finite function of the x variable and should be differentiable, at last, two times (the low of the continuity of the current) and should be equal to zero on the end of the antenna. There in AF are very suitable to present function $I(x)$. Actually, AF are finite and nonanalytic functions on the segment, smoothly approaching to zero on the end of the segment. For example all this conditions are satisfied by function $\mathrm{up}(x)$. Same is referred to atomic functions of the higher orders. As it is known, when the segment [–l, l] is supplemented with infinity, the equation (2) can be considered as Fourier transform. Therefore when using AF relevant are their spectral properties.

The Fourier transform from AF $\mathrm{up}(x)$ i.e. the radiation pattern of allocation of a current $I(x) = \mathrm{up}(x)$ looks like

$$F[\mathrm{up}(x)] = \prod_{m=1}^{\infty} \frac{\sin u 2^{-m}}{u 2^{-m}}. \tag{7}$$

The Fourier transform of the AF belongs to class reactivity of entire functions of an exponential type of an extent not superior $2l$, descending on the material axis when $u \to \infty$ exponentially.

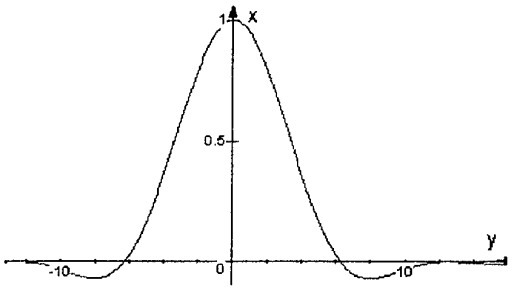


Fig. 2. Fourier transform from $\mathrm{up}(x)$

In other words a set of radiation patterns which correspond to AF has property to concentrate energy in a range of real angles $-k \le u \le k$. Representation of a current (field) in a uniform linear array (among them, in aperture) with the help of the main AF [10, 12] ensures a radiation pattern with quick descending side lobes. It allows constructing antennas with optimal radiation patterns.

The approximation of composite distribution of a current $I(x)$ with the help of AF is possible by a partition of length of the antenna $2l$ on $2N$ of cuts of length $D = l/N$ and representation function I(x) the following way

$$I(x) = \sum_{n=-2^N}^{2^N} C(n) \cdot \mathrm{up}\left(\frac{x/\Delta - n}{2^N}\right). \tag{8}$$

Thus, the radiation pattern will be introduced by the sum of the partial charts

$$E(u) = \sum_{n=-N}^{N} C(n) \cdot \prod_{k=1}^{\infty} \left(\frac{\sin(n\Delta/2^k)}{(n\Delta/2^k)}\right) \cdot e^{in\Delta}. \tag{9}$$

Thus, in the tasks of analysis of the theory of antennas a body of mathematics of AF allows to construct the constructive approach adequately representing analytical properties of these functions: finiteness, approaching to zero on the end, and concentration of a radiation energy in the area of physical observation angles (small reactance).

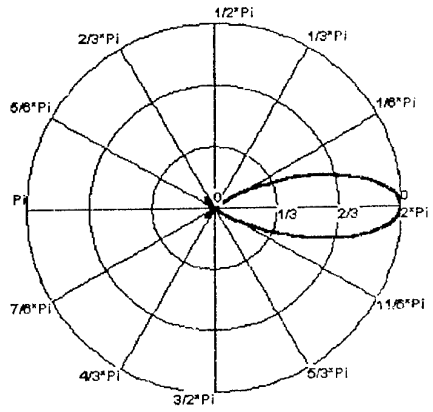


Fig. 3. Radiation pattern of allocation of a current $I(x)$ = up(x)

3) Problem 2. This problem is the inverse with the respect to the problem 1 and in the simplest case of the rectilinear antenna (6) it can be reduced to the solving of the integral equation of the 1st kind. As it was stated in the problem 1), the reduction of (6) to the form of bilateral Fourier transform requires complement of the $I(x)$ function with zero on the rest of x axis and some complement of the $E(x)$ function on the same interval without breaking the conditions of Wiener-Paley theorem. While using the AF for the representation of $I(x)$, there are no difficulties with the provision of the finiteness of $I(x)$ and with the progressing into the region of the superguided solutions, for avoiding of which one often refers to the methods of solution of incorrectly stated problems of mathematical physics. Consequently, the solution of the problem of antennas synthesis with the help of AF allows to suggest simple and stable algorithms for this class of problems.

4) Problem 3. The boundary value problems of antennas theory are, as a rule, solved with a Method of Moments (MoM), that is often called the generalized method of induced EMF. At the same time, from the boundary conditions there follows the equation $Z\,I = U$, where Z is a linear (impedance) operator, I is a sought distribution of the current (electric, magnetic or polarization) in the antenna, U is the given distribution of the primary (incident) field in the antenna. The important aspect of the MoM method is the choice of system of basic functions for decomposition of the sought current distribution. Formerly, for solving the problems of the antenna theory different systems of basic functions were used. The basic functions of subdomains upon the enough simplicity of the calculation of moments (reciprocal resistances or conductances) do not have the needed smoothness that often leads to errors upon solving the practical problems.

NUMERICAL APPROACH TO THE ANTENNAS SYNTHESIS BASED ON ATOMIC FUNCTIONS

The relative distribution of radiated power as a function of direction in space is the radiation pattern of the antenna. It is common practice to show planar sections of the radiation pattern instead of the complete three-dimensional surface. The two most important views are those of the principal E-plane and H-plane patterns. The E-plane patterns is a view of the radiation pattern obtained from a section containing the maximum value of the radiated field and in which the electric field lies in the plane of the chosen sectional view. In this paper we deal with E-plane radiation patterns.

Formulation

Radiation pattern of linear radiator is expressed in the form

$$F_\theta = \int_{-L/2}^{L/2} I(z) e^{ikz\cos\theta} dz \quad , \tag{10}$$

where L is the radiator's width and $I(z)$ is the current distribution in radiator. For numerical solution of the above integral equation Method of Moments is used. As basis functions we take shifts of AF [1-17]

$$f(z) = \sum_{-\infty}^{\infty} c_n f_n(z) = \sum_{n=-\infty}^{\infty} c_n up\left(z - n2^{-k}\right), \tag{11}$$

then

$$\begin{aligned} F_\theta &= \int_{-L/2}^{L/2} f_n(z) e^{ikz\cos\theta} dz = \\ &= \int_{-L/2}^{L/2} \sum_{n=-\infty}^{\infty} c_n up\left(z - n2^{-m}\right) e^{ikz\cos\theta} dz = \\ &= \sum_{n=-\infty}^{\infty} c_n \int_{-L/2}^{L/2} up\left(z - n2^{-m}\right) e^{ikz\cos\theta} dz = \\ &= \sum_{n=-\infty}^{\infty} c_n FT\left[up\left(k\cos\theta - n2^{-m}\right)\right] \end{aligned} \tag{12}$$

where FT[up(z)] is well known expression for Fourier transform of the function up(z) [1–3]

$$FT[up(z)](u) = \prod_{k=1}^{\infty} \frac{\sin\left(u \cdot 2^{-k}\right)}{u \cdot 2^{-k}}.$$

AF possess unique spatial-frequency features: finiteness in ordinary space and exponential localization in Fourier space. Let us consider the antenna with following current distribution $I(z)$ = up(z) shown in Fig. 1.

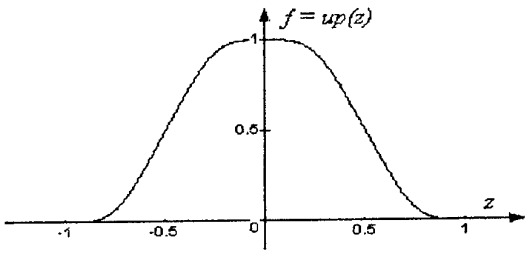


Fig. 4. Base function for current ductribution up(z)

Then according to (1) radiation pattern will have the form

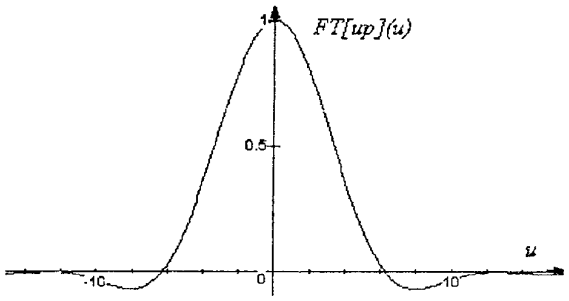


Fig. 5. Fourier transform of the function up(z)

or in the polar coordinate system

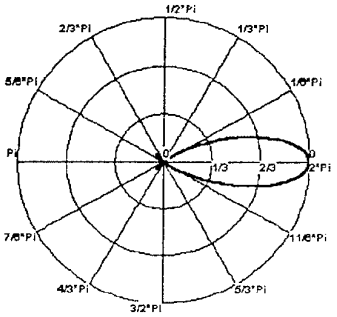


Fig. 6. Radiation pattern of allocation of a current $I(z) = up(z)$

Thus, we obtain the convenient antenna element with known current distribution and radiating pattern and, which is most important, with unique approximating properties.

NUMERICAL EXPERIMENTS

Representative computations are given to show the validity of the proposed method and to demonstrate its merits. We consider the following examples:

a) Linear antennas array.

b) Linear radiator.

For computation of Fourier transform of the up(z) $FT[up](u) = \prod_{m=1}^{\infty} \frac{\sin u2^{-m}}{u2^{-m}}$ we can use approximating formula

$$FT[up]_M(u) = \prod_{m=1}^{M} \frac{\sin u2^{-m}}{u2^{-m}},$$

where $M = 16$ is sufficient for requiring accuracy. The square error in this case

$$\varepsilon = \sqrt{2\int_0^{\infty} FT[up]^2(u) - FT[up]_M^2(u)du} = 0.5791 \cdot 10^{-9}.$$

Function up(z) equals to zero outside the [–1, 1] and is non-negative and even. Consequently, computing of up(z) on the [–1, 1] can be performed by means of Fourier series

$$up(z) = \frac{1}{2} + \sum_{k=1}^{\infty} FT[up](\pi k) \cdot \cos(\pi k z).$$

Linear antennas array

Directivity function for the linear antenna array can be define in the form

$$D(\theta, \psi) = D_0(\theta, \psi) \sum_{n=-N}^{N} I_n \exp(in(kd\cos\theta - \psi)),$$

where $D_0(\theta, \psi)$ is the element radiation pattern and $\sum_{n=-N}^{N} I_n \exp(in(kd\cos\theta - \psi))$ is the array factor. There are three common cases of radiation.

A. Normal radiation, $\psi = 0$

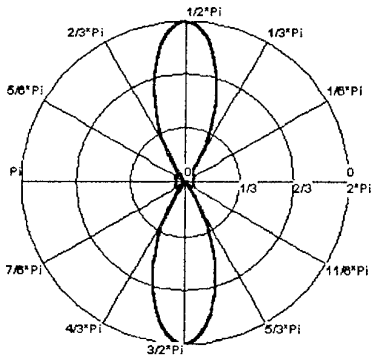


Fig. 7. Pattern of linear array of radiators for $I(z) = up(z)$, $\psi = 0$

B. Slope radiation, $0 < \psi < kd$

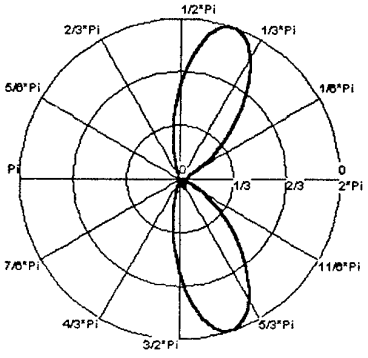


Fig. 8. Pattern of linear array of radiators with $I(z) = up(z)$, $\psi = \frac{\pi}{24}$

C. Axis radiation, $\psi \geq kd$

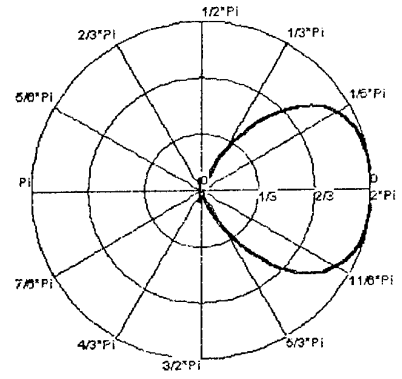


Fig. 9. Pattern of linear array of radiators

for $I(z) = up(z)$, $\psi = \frac{\pi}{8}$

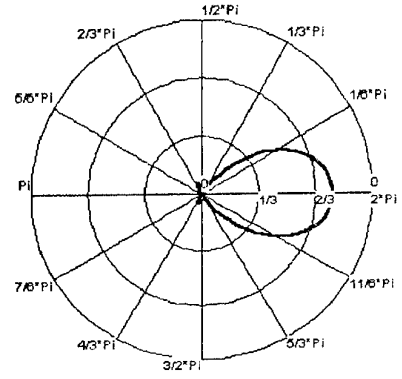


Fig. 10. Pattern of linear array of radiators

for $I(z) = up(z)$, $\psi = \frac{2\pi}{13}$

Linear radiator

Let us consider characteristics of linear radiator based on up(z). To show the effectiveness of the proposed approach we calculate same antennas characteristics of linear radiator with current distribution in form of up(z) to compare them with ones of widely used antennas.

The following antenna characteristics are of interest:

(i) Radiation pattern width $\Delta\theta_0$.

(ii) Radiation pattern width $\Delta\theta_{0.5}$ on half-power level. The half-power beam width is usually given for the principal E-plane patterns and is angular width between points at which the radiated power per unit area is one-half of the maximum.

(iii) Highest sidelobe level (in decibels) HSLL. Let θ_1, θ_2, ... be the local maximum angles of $D(\theta)$, distinct from θ_{main}. Then

$$HSLL = 10 \log \max_k \left| \frac{D(\theta_k)}{D(\theta_{main})} \right|^2$$

(iv) The so-called "usefulness factor" ν, which is defined by

$$\nu = \left| \int_{-L/2}^{L/2} I(z)dz \right|^2 \Big/ \int_{-L/2}^{L/2} |I(z)|^2 dz$$

and equals to the equivalent noise bandwidth.

Here FSLL is abbreviate for first sidelobe level, which is equal, in this case, to highest sidelobe level [5].

Further, we can also define other parameters:

(i) Overlap correlation: for the 50% overlap

$$OC = \int_0^{L/2} I(z)I(z-L/2)dz \Big/ \int_{-L/2}^{L/2} I^2(z)dz = 11.8\ \%.$$

(ii) Spurious amplitude modulation (SAM)

$$SAM = -10 \log \left| \frac{D(\pi/2)}{D(0)} \right|^2 = 1.21.$$

(iii) Maximum transformation loss (MTL)

$$MTL = 10 \log \nu + SAM = 3.29.$$

(iv) Asymptotic rate of sidelobe fall-off (in decibels per octave)

$$10 \log \lim_{|\theta| \to \infty} \left| \frac{D(2\theta)}{D(\theta)} \right|^2 = -\infty.$$

(v) Coherent gain

$$\left(\frac{1}{2} \int_{-L/2}^{L/2} I(z)dz \right)^{-1} = 0.5.$$

Such a physical set of parameters makes proposed numerical method effective and convenient, especially taking into account simplicity in definition of up(z).

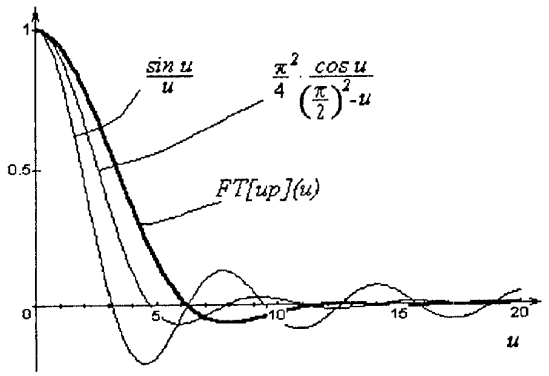


Fig. 11. Computed value of considered radiation patterns

CONCLUSION

The properties of the AF allows avoiding such errors, and as far as the partial radiation pattern are concentrated around zero, it guarantees the stability and exactness of calculation of field distribution in the far zone of the antenna, that is the first characteristic of

Table I
Characteristics of Radiator Based on up(z)

Current Distribution, $I(z)$	Array factor $F_c(u)$, $u = (kL/2)\cos\theta$	$\Delta\theta_0$	$\Delta\theta_{0.5}$	FSLL, dB	Factor $\nu = D/D_0$
I(z) = up(z)	$\prod_{m=1}^{M} \frac{\sin u 2^{-m}}{u 2^{-m}}$	$226^\circ \frac{\lambda}{L}$	$84^\circ \frac{\lambda}{L}$	-23.5	0.8085
I(z) = 1	sin u / u	$115^\circ \frac{\lambda}{L}$	$51^\circ \frac{\lambda}{L}$	-13.2	1
cos(π z / L)	$\frac{\pi^2}{4} \frac{\cos u}{(\pi/2)^2 - u^2}$	$172^\circ \frac{\lambda}{L}$	$67^\circ \frac{\lambda}{L}$	-23.0	0.81
$\cos^2(\pi z / L)$	$\pi^2 \frac{\sin u}{u(\pi^2 - u^2)}$	$229^\circ \frac{\lambda}{L}$	$83^\circ \frac{\lambda}{L}$	-32.0	0.667

any antenna by importance. The most attractive aspect is the application of AF in the theory of lattices of vibrator or slot antennas. Here the representation by AF is the most corresponding to the pattern of real distribution of the current in any transmitter, and consequently, it will yield the best convergence to the exact solution.

It was established that using AF as basis functions to far-field pattern approximation we obtain current distribution in the form of AF series. This result in sufficient computation gain and approximation accuracy. This algorithm can be further expanded to wide class of antenna synthesis problems.

REFERENCES

1. Rvachev, V. L. and Rvachev, V. A., On one finite function, Dokl. Akad. Nauk Ukr. SSR, Ser. A, no.8, pp. 705-707, 1971.
2. Rvachev, V. L. and Rvachev, V. A., Nonclassical methods of approximation theory in boundary value problems, Kiev: Naukova Dumka, 1979.
3. Rvachev, V. A., Compactly supported solutions of functional-differential equations and their applications, Russian Math. Surveys, vol. 45, no. 1, pp. 87-120, 1990.
4. Kravchenko, V.F., Rvachev, V.L., and Rvachev V.A., Mathematical methods for signal processing based on atomic functions, Journal of Communications Technology and Electronics, vol.40(12), pp.118-137, 1995.
5. Kravchenko, V.F., Rvachev, V.A, and Gulyaev Yu.V., Synthesis of weight windows on the basis of atomic functions, Doklady Mathematics, vol.51, no.3, pp.456-458, 1995.
6. Kravchenko, V.F. and Rvachev, V.A, Wavelet systems and their applications for signal processing, Zarubezhnaya Radioelectronica. Achievements in Modern Radioelectronics, no.4, pp.3-21, 1996.
7. Kravchenko, V.F. and Rvachev, V.A, Orthonormal wavelet systems based on atomic functions, Doklady Mathematics, vol.54, no.3, pp.824-826, 1996.
8. Kravchenko, V.F. and Rvachev, V.A Applications of atomic functions for solution boundary value problems in mathematical physics, Zarubezhnaya Radioelectronica. Achievements in Modern Radioelectronics, no.8, pp.6-22, 1996.
9. Kravchenko, V.F., Pustovoit, V.I, and Timoshenko, V.V. Atomic functions in processing of simple and compound signals, Radio and Communication Technology, vol.2, no.1, pp.25-31, 1997.
10. Kravchenko, V.F., Kuraev, A.A., and Rvachev, V.A, Atomic functions in optimal dynamic system control, Radio and Communication Technology, vol.2, no.9, pp.3-11, 1997.
11. Kravchenko, V.F. and Rvachev, V.A, Application of atomic functions to interpolation problems, Electromagnetic Waves and Electronic Systems, vol. 3, no. 1, pp. 10 - 20, 1998.
12. Kravchenko, V.F., Antenna pattern approximation and linear radiator synthesis based on atomic functions, Electromagnetic Waves and Electronic Systems, vol. 3, no. 1, pp. 40 - 47, 1998.
13. Kravchenko, V.F. and Rvachev, V.A, Atomic functions and its application to tasks of signal processing and boundary value problems, Proceedings of PIERS'98, Nantes, France, vol.3, p.1186, 13-17 July, 1998.
14. Kravchenko, V.F., Rvachev, V.L., and Rvachev,V.A, Applications of atomic functions to the boundary value problems, International Conference on Operator Theory and Its Applications to Scientific and Industrial Problems, Winnipeg, Canada, pp.51-52, October 7-11, 1998.
15. Kravchenko, V. F. and Zamyatin, A. A., Atomic functions and wavelet matrix transform approach for fast solution of electromagnetic integral equations in the boundary value problems of diffraction, Ibid. p.53, October 7-11, 1998.
16. Kravchenko, V. F. and Zamyatin, A. A., Approximation properties of Atomic Functions for Solving Integral Equations of Electrodynamics by the Method of Moments, Doklady Physics, vo44, no.4, pp.216-219, 1999.
17. Kravchenko, V. F. and Zamyatin, A. A., Application of atomic function to solving of electromagnetic integral equations, Zarubezhnaya Radioelectronica. Achievements in Modern Radioelectronics, no.3, pp.58, 1999.

PROBLEMS AND NEW RESULTS OF SPECTRAL ESTIMATION AND ANTENNA ARRAYS SUPERRESOLUTION TECHNIQUES

D. I. Lekhovitsky, D. V. Atamansky, I. G. Kirillov, P. M. Flexer

Kharkiv Military University - 6 Svoboda Square, Kharkiv, Ukraine
tel. +38-0572-437010

1. In recent research on AA theory one of the major issues is elaboration of methods for estimation of spatial spectrum of noise sources that could lower constraints of antenna's resolution stipulated by its limited aperture. List of the proposed up to now "superresolution" methods of spectral estimation is extremely long [1–6] and all-time continues to be supplemented.

But criteria and substantiations used for synthesis and analysis of these methods are rather heterogeneous, and conclusions on their efficiency and advantages are often based on either unrealistic assumptions about exact knowledge of the covariance matrix (CM) in array outputs or on "visual impressions [16]" about the forms of output effects realizations obtained by simulations.

Such a situation forces a number of problems to be put against the theory and engineering of spectral estimation based on AA. The most important of them may be formulated as follows.

A. Understanding of essence of the proposed "superresolution" methods of spectral estimation from the point of statistical resolution theory [7, 8] that determines potentialities and optimal resolution methods by statistical criteria that consider random nature of emissions and interference noises.

B. Determination of "the payment" for passing from the complicated optimal methods to more simple quasi-optimal ones and usage of non-statistical criteria (in particular, the Rayleigh criterion) for analysis and comparison of methods.

C. Determination and analysis of statistical characteristics of resolution, including the Rayleigh criterion as well, under real conditions of a priori undeterminacy that is overcome using the replacement of unknown CM with random estimation matrix, being formed on the basis of teaching samples of finite size. Classification of the methods by the level of requirements to the size of a teaching sampling, dependence of these requirements on the specificity of AA.

D. Substantiation of practical means for realization of superresolution spectral analysis methods, their unification and complexing that would enable to join advantages of different methods and to weaken their shortcomings.

The research on the above listed problems as well as on a number of other problems, are carried out in many countries, and by no means they can be considered as completed. The same considerations can be applied to the following description of some new findings on the above mentioned circle of problems.

2. The theory [7, 8] treats different types and criteria of resolution, and each of these types or their certain combination may be required to solve estimation problems of spatial spectrum of radiation. Nevertheless, the majority of known methods as well as a number of new ones may be obtained on the basis of the statistical theory of quasi-complete resolution-detection. According to this theory, n signals in the noise are considered to be resolved if the statistical characteristics of the detection (conditional probabilities of false alarm F and correct detection D) of each of them, in turn, being considered as useful, become worse due to the impact of the rest $(n-1)$ signals playing the role of interfering ones, in comparison with the case when there is only noise (without interference) not exceeding the given limits. Under such an assumption, the analysis of radiation spatial spectrum in the given sector (α_b, α_f) consists in testing of the hypotheses H_1 of presence or H_0 of absence of the source in the sequentially or parallel controlled "signal directions" $\alpha \in \alpha_b, \alpha_f$ on the basis of the processing of the input realization.

First, let us consider potentialities of the based on AA spatial resolution-detection of n sources of stationary noise radiation, assuming that the input realization is given by the sampling of size $K \geq 1$

$$\mathbf{Y} = \{\mathbf{Y}_i\}_{i=1}^{K}, \qquad \mathbf{Y}_i = N(\mathbf{0}, \mathbf{\Phi}),$$
$$\overline{\mathbf{Y}_i} = \mathbf{0}, \quad \overline{\mathbf{Y}_i \cdot \mathbf{Y}_i^*} = \mathbf{\Phi} \cdot \delta_{ij}, \quad i, j \in \mathbf{1}, K \tag{1}$$

of Gaussian mutually independent (δ_{ij}=0, $i \neq j$, δ_{ii}=1) M-dimensional vectors $\mathbf{Y}_i = \{y_l^{(i)}\}_{l=1}^{M}$ of complex amplitudes of M AA elements at K discrete time points, with equal M*M CM [3,5,8,9]

$$\mathbf{\Phi} = \{\varphi_{pq}\}_{p,q=1}^{M} = \overline{\mathbf{Y}_i \cdot \mathbf{Y}_i^*} = \mathbf{I}_M + \mathbf{G}(\beta) \cdot \mathbf{h} \cdot \mathbf{G}(\beta)^*, \quad i \in 1, K. \tag{2}$$

Here $\mathbf{I}_M$ is an identity M*M matrix that describes CM of mutually independent sensor noises, with a power

taken to be equal to one, $\mathbf{G}(\beta)=\{\mathbf{X}(\beta_\nu)\}_{\nu=1}^{n}$ is $M*n$ matrix with M-dimensional vectors

$$\mathbf{X}(\beta_\nu)=\left\{e^{j\cdot(l-(M+1)/2)\cdot\beta_\nu}\right\}_{l=1}^{M}, \qquad (3)$$
$$\beta_\nu=2\pi d\cdot\sin\theta_\nu/\lambda,\ \nu\in 1,n,$$

which describe phase distribution of source ν (from the direction θ_ν with respect to normal) as per the elements of uniform linear AA. Matrix $\mathbf{h}=diag\{h_\nu\}_{\nu=1}^{n}$ is $n*n$ diagonal matrix of mutually independent radiation powers, d and λ denote the inter-element distance and signal wavelength. The bar and asterisk (*) denote an average and the set of Hermitian transpose, respectively.

Under conditions of (1), (2) the H_1 hypothesis is true (or rejected in favour of H_0 hypothesis) if the statistics

$$\xi(\alpha)=\frac{1}{K}\cdot\sum_{l=1}^{K}\left|y_{\Sigma i}(\alpha)\right|^2, \qquad (4)$$
$$y_{\Sigma i}(\alpha)=\mathbf{Y}_i^{*}\cdot R_0(\alpha),\ R_0(\alpha)=\mathbf{\Phi}_0^{-1}\cdot\mathbf{X}(\alpha)$$

exceeds (or does not exceed) the threshold level

$$\omega(\alpha)=x_{tr}\cdot\sigma_0^2/K,\sigma_0^2=\overline{\xi_0(\alpha)}=\mathbf{R}_0^{*}(\alpha)\cdot\mathbf{\Phi}_0\cdot\mathbf{R}_0(\alpha). \quad (5)$$

In the equations (4), (5) $\mathbf{X}(\alpha)$ is the phase distribution vector of the (3) type of radiation from the "signal" direction α being analyzed, with the $h(\alpha)$ power, $\mathbf{\Phi}_0$ is the CM of $\mathbf{Y}_i$ vectors of the H_0 hypothesis, x_{tr}/K is the factor of threshold exceeding, over the mean value $\overline{\xi_0(\alpha)}$ of the pre -threshold statistics $\xi_0(\alpha)$ according to the H_0 hypothesis that ensures the prescribed probability of false alarm F, x_{tr} is the root of the equation

$$f(x_{tr})=F,\quad f(x)=\int_x^{\infty}p_a(x,1)\,dx=e^{-x}\cdot\sum_{i=0}^{K-1}x^i/i!, \qquad (6)$$

where $p_a(x,\sigma^2)$ is the Erlang distribution [10]

$$p_a(x,\sigma^2)=\left(\sigma^2\cdot(K-1)!\right)^{-1}\cdot\left(x/\sigma^2\right)^{K-1}\cdot\exp\left\{-x/\sigma^2\right. \qquad (7)$$

of the statistics $a=K\cdot\xi(\alpha)$ (4) with the paramcters of the form K and scale:

$$\sigma^2=\sigma_0^2=\overline{\xi_0(\alpha)},\quad \sigma^2=\sigma_1^2=\sigma_0^2(1+\mu)=\overline{\xi_1(\alpha)}, \qquad (8)$$

$$\mu=\overline{\xi_1(\alpha)}/\overline{\xi_0(\alpha)}-1=h(\alpha)\cdot\mathbf{X}^{*}(\alpha)\cdot\mathbf{\Phi}_0^{-1}\cdot\mathbf{X}(\alpha) \qquad (9)$$

according to H_0 and H_1 hypotheses respectively.

At that, the probability of the correct detection

$$D=f(x_{tr}/(1+\mu)) \qquad (10)$$

is determined by the parameter μ (9) that means a power signal/(interference + noise) ratio (SINR) and is maximized by an optimal linear processing at forming the weight sums $y_{\Sigma i}$ $(i\in 1,K)$ with the weight vector $\mathbf{R}_0(\alpha)$ (4).

In ordinary test case, with the two (n = 2) sources of equal power ($h_1=h_2=h$) at $\alpha=\beta_1$ (β_2) we obtain

$$\mu=q\cdot K_e,\qquad K_e=1-\frac{q}{1+q}\cdot|\rho|^2, \qquad (11)$$
$$\rho=\frac{1}{M}\cdot\mathbf{X}^{*}(\beta_1)\cdot\mathbf{X}(\beta_2)\approx\sin\pi\Delta/\pi\Delta\ ,$$

where $q=Mh$ is the signal/noise ratio (SNR) at the optimal linear processing of the "useful" signal when interfering ones are absent, $K_e\le 1$ is mentioned in the [1] "coefficient of energy usage of the "useful" signal" in the presence of, ρ is the coefficient of their spatial correlation, $\Delta=(\beta_2-\beta_1)/\Delta_0$ is the relative angular distance between the sources (in relation to the half width $\Delta_0=2\pi/M$, $M>>1$ of the in-phase AA radiation pattern as per the level of the first zeros).

From the equations (6)-(11) it follows that in the examining test situation the q value necessary to detect the "useful" signal against the background of noise and the interfering signal located at the angular distance Δ from the useful one, at the given values of F and D, should be equal to

$$q=\frac{(\mu-1)+\sqrt{(\mu-1)^2+4\mu\cdot(1-|\rho|^2)}}{2\cdot(1-|\rho|^2)}, \qquad (12)$$

where $\mu=x_{tr}/y-1$, and y are roots of the equations $f(y) = D$ of the (6) function.

In particular, at D = 0.5 and $F=10^{-6}$

$$\mu\approx\frac{a}{K}+b,\begin{cases}a\approx 15.7;\ b\approx 0.67; & 5\le K\le 20;\\ a\approx\ 22;\ b\approx 0.33; & K\ge 20.\end{cases} \qquad (13)$$

At spatial orthogonality of sources (Δ = 1, ρ = 0) K_e = 1, $\mu = q$, that is the energy of the "useful" signal is used entirely. At Δ < 1 ("superresolution" case) when the following assumption are reasonable

$$\rho\approx 1-\pi^2\Delta^2/6\approx 1-1.5\Delta^2, \qquad (14)$$
$$|\rho|^2\approx 1-3\Delta^2,\ 1-|\rho|^2\approx 3\Delta^2,$$

from the eq. (12) it is not difficult to obtain the following estimations

$$\Delta_B\ge\sqrt{(\mu-1)/3q}\ ,\ \mu\ge 3,\ \Delta_B\le 1/\sqrt{3}q,\ \mu\le 1 \quad (15)$$

of potentialities to resolution-detection of the two equal power noise sources, that is the minimum angular distance Δ_B between them when each one, in the presence of the second one, can be detected with the given sta-

tistical characteristics (F and D probabilities). So, at $D = 0.5$ and $F = 10^{-6}$ (see (13)) we obtain:

$$\Delta = \begin{cases} \Delta_B \geq 1/\sqrt{q} & \text{при} \quad K \leq 5; \\ \Delta_B \leq 0.577/q & \text{при} \quad K \geq 35, \end{cases} \qquad (16)$$

that corresponds well to the shown in Fig. 1 results of accurate calculations of $q = q(K,\Delta)$, by (12) and (11), at $K = 1$ known from [7].

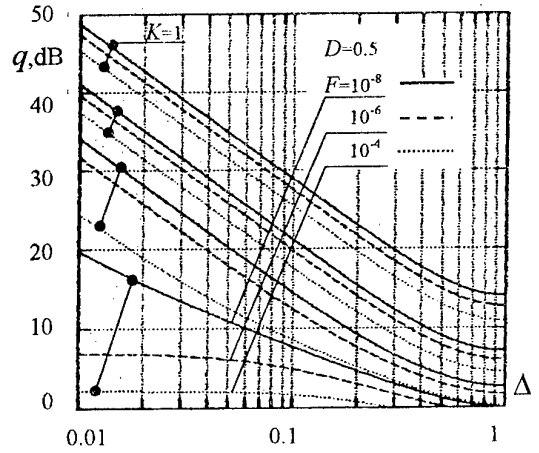


Fig. 1

Difference of the curves ordinates $r(K,\Delta) = q(K,\Delta) - q(K,1)$ (see Fig. 1) determines the power "payment for the superresolution" (in dB) of the two sources of equal power located at the angular distance $\Delta < \Delta_R$, being less than the Rayleigh limit $\Delta_R \approx 1$. For the models (1)-(3) this payment can't be reduced by any ways since it corresponds to the optimal processing of (4) and (5) under "ideal" conditions of the full a priori determinacy, that is exact knowledge at all values $\alpha \in \alpha_b, \alpha_f$ of the CM

$$\mathbf{\Phi} = \mathbf{\Phi}_0 \quad \text{и} \quad \mathbf{\Phi} = \mathbf{\Phi}_1 = \mathbf{\Phi}_0 + h(\alpha) \cdot \mathbf{X}(\alpha)\mathbf{X}^*(\alpha) \qquad (17)$$

in accordance with H_0 and H_1 hypotheses respectively.

3. In practice these CM are, as a rule, unknown. Instead of these, in accordance with the "adaptive Bayes's approach [11]", in the equations (4) and (5) certain random estimation matrices $\hat{\mathbf{\Phi}}$ are to be used, and proximity of the corresponding adaptive processing to the optimal one depends on the quality of these estimations.

However implementation of this approach for the considered problem of the spatial spectral analysis of the continuous noise sources has some fundamental restrictions. These are stipulated by high complication in obtaining classified "only interference" samplings (that is without "the signal") for all signal-bearing directions $\alpha \in \alpha_b, \alpha_f$ and, therefore, $\hat{\mathbf{\Phi}}_0$ estimation of CM according to H_0 hypothesis, and the adaptive weight vectors $\hat{\mathbf{R}}_0(\alpha) = \hat{\mathbf{\Phi}}_0^{-1}\mathbf{X}(\alpha)$ and thresholds $\hat{\omega}(\alpha)$ described by this estimation. That is why for all "superresolution" methods of spectral estimation, instead of "difficult to obtain" $\hat{\mathbf{\Phi}}_0$ matrix, $\hat{\mathbf{\Phi}}$ estimates $\mathbf{\Phi}$ are usually used being formed, in general, on basis of the teaching samplings of (1) and (2) types [1-6, 9, 12].

At such a substitution, for any unbiased estimates ($\overline{\hat{\mathbf{\Phi}}} = \mathbf{\Phi}$) the weight vector $\hat{\mathbf{R}}(\alpha) = \hat{\mathbf{\Phi}}^{-1}\mathbf{X}(\alpha)$ is formed, with a mean value of $\overline{\hat{\mathbf{R}}}(\alpha) = c(\alpha) \cdot \mathbf{R}_0(\alpha)$ that is proportional to the required weight vector $\mathbf{R}_0(\alpha)$ (4) [9,12], so that the SINR μ (9) retains unchanged (and highest possible) at the arbitrary $c(\alpha) \neq 0$ scale factors. But in this case the required threshold level $\hat{\omega}(\alpha)$ is still undetermined. This is the only explanation (and justification) of the universal prevalence of the non-statistical Rayleigh criterion, in accordance with that resolution is determined not by the results of comparison of the random value $\hat{\xi}(\alpha)$ with the threshold $\hat{\omega}(\alpha)$ in every point of the $\alpha \in \alpha_b, \alpha_f$ array, but by the depth of "the curve dips" between the peaks of $\hat{\xi}(\alpha)$ function at the α_b, α_f interval [5, 9, 12].

Principal impossibility to attain the limits (15) and (16) even at the extremely large size ($N \to \infty$) of the teaching sampling N is an unavoidable "payment" for this forced rejection of the adaptive implementation of all stages of (4) and (5) processing. One more consequence is that the "superresolution" methods, differing only in $c(\alpha)$ factors and fully equivalent as per statistical criteria of resolution-detection, may be substantially unequal as per the Rayleigh criterion. But it is the specificity of the $c(\alpha)$ scale factors that the differences of their majority [9]. Let us illustrate this by some examples directly leading to the known "superresolution" methods of spectral analysis.

4. Suppose instead of the "difficult to obtain" weight vector $\hat{\mathbf{R}}_0(\alpha) = \hat{\mathbf{\Phi}}_0^{-1}\mathbf{X}(\alpha)$ at the stage of the linear processing in the (4) the vector $\hat{\mathbf{R}}_C(\alpha) = c(\alpha) \cdot \hat{\mathbf{\Phi}}^{-1}\mathbf{X}(\alpha)$ is used, with the mean value

$$\overline{\hat{\mathbf{R}}}_C(\alpha) = \mathbf{R}_C(\alpha) = c(\alpha) \cdot \mathbf{R}(\alpha), \mathbf{R}(\alpha) = \mathbf{\Psi}\mathbf{X}(\alpha), \quad \mathbf{\Psi} = \{w_{pq}\}_{p,q=1}^{M} = \mathbf{\Phi}^{-1}. \qquad (18)$$

Due to (17) it is collinear to the $\hat{\mathbf{R}}_0(\alpha)$ vector (4). Thus stipulated independence of the SINR μ (9) on the factor $c(\alpha) \neq 0$ enables to subdue its selection to some additional requirements of "practical" nature. Sense of some these requirements become clear when put down the

mean value $S(\alpha)=\overline{\hat{\xi}(\alpha)}$ of the "prethreshold" statistical value $\hat{\xi}(\alpha)$ (4) in the form of the sum:

$$S(\alpha)=\overline{\hat{\xi}(\alpha)}=\mathbf{R}_C(\alpha)\cdot\mathbf{\Phi}\cdot\mathbf{R}_C(\alpha)= \\ =|c(\alpha)|^2\mathbf{X}^*(\alpha)\Psi\mathbf{X}(\alpha)=S_S(\alpha)+S_N(\alpha)+S_I(\alpha) \quad (19)$$

that represents the signal, noise, and interference components. For the first two components, according to the equations (2), (17) and (18), the following equalities are valid:

$$S_S(\alpha)=h(\alpha)\cdot|c(\alpha)|^2\left|\mathbf{X}^*(\alpha)\Psi\mathbf{X}(\alpha)\right|^2, \\ S_N(\alpha)=|c(\alpha)|^2\mathbf{X}^*(\alpha)\Psi^2\mathbf{X}(\alpha). \quad (20)$$

As an example, let us require for the signal transfer factor to be steady, that is the multiplier for the $h(\alpha)$ and $S_S(\alpha)$ values to be equal to one. Apparently, this requirement will be performed at

$$c(\alpha)=\left(\mathbf{X}^*(\alpha)\Psi\mathbf{X}(\alpha)\right)^{-1}.$$

In this case we have the following equation:

$$S(\alpha)=S_{ML}(\alpha)=\left(\mathbf{X}^*(\alpha)\Psi\mathbf{X}(\alpha)\right)^{-1} \quad (21)$$

and consequently, this function coincides with the spectral function (SF) of the generally known Capon "maximum likelihood" (ML) method [13, 1-6, 9, 12]. Fixation of the signal power means that in this case maximization of the SINR μ is ensured by minimization of the interference and noise power, and this explains the one more name of the Capon method – the method of minimum dispersion, as it has been used in [5].

Let us replace this requirement with the one of the noise component in the (19) equation to be constant at any angles $\alpha\in\alpha_b,\alpha_f$, that is $(S_N(\alpha)=1)$. It will be performed at

$$c(\alpha)=\left(\mathbf{X}^*(\alpha)\Psi^2\mathbf{X}(\alpha)\right)^{-1/2}=\left(\mathbf{R}^*(\alpha)\cdot\mathbf{R}(\alpha)\right)^{-1/2}.$$

At that, the function

$$S(\alpha)=S_{BL}(\alpha)=\frac{\mathbf{X}^*(\alpha)\Psi\mathbf{X}(\alpha)}{\mathbf{X}^*(\alpha)\Psi^2\mathbf{X}(\alpha)} \quad (22)$$

represents the SF of the Borgotti-Lagunas (BL) method [9].

Suppose now that $c(\alpha)=\sqrt{w_{mm}}/\mathbf{e}_m^*\Psi\mathbf{X}(\alpha)$, where $\mathbf{e}_m^*$ is the m-th ($m\in1,M$) row of the identity matrix $\mathbf{I}_M$. At such selection, the m-th ($m\in1,M$) element of vector $\mathbf{R}_K(\alpha)$ (18) is fixed at the level $\sqrt{w_{mm}}$, at all angles $\alpha\in\alpha_b,\alpha_f$, and the function

$$S(\alpha)=S_{MCA}(\alpha)=w_{mm}\mathbf{X}^*(\alpha)\Psi\mathbf{X}(\alpha)/\left|\mathbf{e}_m^*\Psi\mathbf{X}(\alpha)\right|^2, \quad m\in1,M \quad (23)$$

represents the SF of the "modified Capon's algorithm (MCA)" described in [15].

The (22) and (23) SF $S_{BL}(\alpha)$ and $S_{MCA}(\alpha)$ are bounded with the SF of the "heat noise (HN)" method [6] and "maximum entropy (ME)" method [1-6] by the following equalities:

$$S_{BL}(\alpha)=S_{HN}(\alpha)/S_{ML}(\alpha),\ \ S_{MCA}(\alpha)=S_{ME}(\alpha)/S_{ML}(\alpha).$$

The SF for the mentioned above methods have the following appearance:

$$S_{HN}(\alpha)=\left(\mathbf{X}^*(\alpha)\Psi^2\mathbf{X}(\alpha)\right)^{-1}, \\ S_{ME}(\alpha)=w_{mm}/\left|\mathbf{e}_m^*\Psi\mathbf{X}(\alpha)\right|^2,\ m=1\ \text{ or }\ m=M. \quad (24)$$

They may be derived from the (18) and (19) equations by means of $c(\alpha)$ multipliers' selection, but in such case their physical sense is not so evident.

In similar way, it is possible to come to many other methods including so called "eigenstructure" methods (Pisarenco, Bartlett, MUSIC, EV etc. [4, 5, 9, 12, 16]). Here, we will pay attention only to the methods based on the (21)–(24) equations, whose applications, in contrast to the "eigenstructure" methods, are not restricted to the processes with CM of $\mathbf{\Phi}$ type (2). We will notice consequences of induced refusal of the threshold processing and coming to estimations of resolution based on the Rayleigh criterion.

5. Two equipotent sources are considered to be resolved by Rayleigh's criteria if SF $S(\alpha)$ has two distinction maximum, that have coordinates α_i identifying to direction β_i on source i ($i\in1,2$). Parameters

$$\gamma_1=S(\alpha_i)/S(\alpha_m)\ \text{ or }\ \gamma=S(\beta_i)/S(\beta_m),i=1,2, \quad (25)$$

serve as a distinguishability index. These parameters describe relative "fall" depth in the midpoints $\alpha_m=(\alpha_1+\alpha_2)/2$ between maximum $S(\alpha)$ or $\beta_m=(\beta_1+\beta_2)/2$ between values $S(\alpha)$ in the points $\alpha=\beta_i\,(i=1,2)$. "Threshold" of the resolution, as usually, is set at the level $\gamma,\gamma_1\ge1$.

"Limiting" resolution capabilities correspond to hypothetical case of the exactly known CM $\mathbf{\Phi}$ (2). In this case requirements to SNR $q(\Delta)$ necessary for overcoming these are minimum. It is possible to show [15,17], that for the methods (21)–(24) they are bounded by curves (Fig. 2) for the "worse" Capon method (21) (curves 1,2,3) and for "better" one – MCA (23) (curves 4,5,6) at γ = 1 (curves 1,4) and γ = 2 (curves 2,5). Curves 3,6 characterize limits of $q = q_L$ at which sec-

ond derivatives $d^2S(\alpha)/d\alpha^2$ of corresponding SF $S(\alpha)$ equals zero in point $\alpha = \alpha_m$.

These SF have one maximum at $q \le q_L$ and sources are not resolved [12]. They start resolving if angular space between them is not less, than [15,17,18]

$$\Delta = \begin{cases} \Delta_L \ge 1.17/\sqrt[4]{q} & \text{for Capon's method (21),} \\ \Delta_L \ge 0.95/\sqrt[3]{q} & \text{for MCA (23).} \end{cases} \quad (26)$$

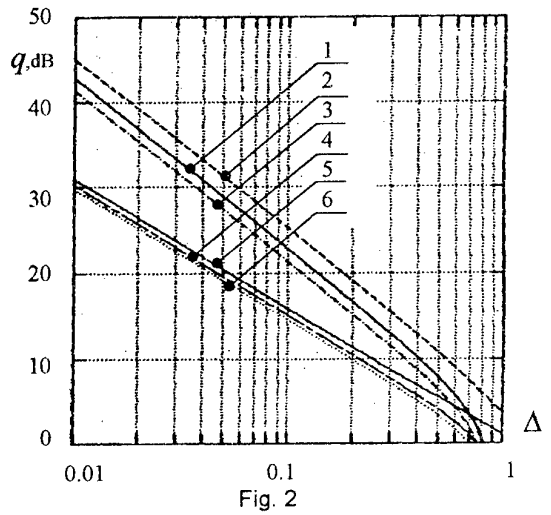


Fig. 2

From comparison of (26) with (15), (16) (Fig. 1 with Fig. 2) it follows that when using the Rayleigh criterion, the requirements to the energetics of resolved signals at small $\Delta \le 0.1$ increase by 10 to 20 and more dB.

6. Under real conditions of a priori unknown CM $\mathbf{\Phi}$ and of the use in the equations (21)-(24) of random matrix-estimates $\hat{\mathbf{\Phi}}$ instead of this unknown CM, the corresponding SF $\hat{S}(\alpha)$ are also random, as well as the parameters $\hat{\gamma}$ (25); so, the potential (Fig.1) and "limiting" (Fig.2) resolving characteristics are ensured only to certain probability that considers to be the most important characteristic of effectiveness. But analytical determination of this probability faces with rather great mathematical difficulties that have been overcome only partially. Below, some recent exact results are shown [17–20] in respect to practically most interesting cases when as the matrix $\hat{\mathbf{\Phi}}$ the following estimates have been used:

$$\hat{\mathbf{\Phi}} = N^{-1}\mathbf{A}, \mathbf{A} = \mathbf{Y}\mathbf{Y}^* = \sum_{i=1}^{N} \mathbf{Y}_i\mathbf{Y}_i^*, N \ge M, \quad (27a)$$

$$\hat{\mathbf{\Phi}} = N^{-1}\mathbf{B}, \mathbf{B} = (\mathbf{A} + \mathbf{A}_T)/2, N \ge (M+1)/2, \quad (27b)$$

These estimates have been formed on the basis of the N-dimensional sampling of the teaching vectors $\mathbf{Y}_i$ with the properties defined by (1). In this case the equation (27a) is maximum likelihood (ML) estimation of general type CM, and joint density thereof elements can be described by the Wishart complex distribution [14]. In the equation (27b) $\mathbf{A}_T$ denotes the matrix obtained from the matrix $\mathbf{A}$ by "turning-over" with regard to its secondary diagonal, and the estimation (27b) is, in general, the ML estimation of persymmetry CM that are typical in the wide range of centrosymmetrical AA. Joint density of its elements has been obtained in [20].

7. The random value normalized to its true one

$$\nu = N \cdot \hat{S}(\alpha)/S(\alpha) \quad (28)$$

for SF $S(\alpha) = S_{ML}(\alpha)$ (21) of the Capon method has the Erlang distribution $P_\nu(x,1)$ of (7) type in dependent on α, but with the following parameters of the form: $N - M + 1$ and $N - (M+1)/2 + 1$ for the estimations (27a) and (27b), respectively (for the estimation (27a) this result has been obtained in [14]). From this it follows that, if it was possible to determine the "difficult to obtain" (see item 3) threshold $\omega(\alpha)$ (5), the Capon method, even at the size of the teaching sampling

$$N = K + M - 1 \text{ or } N = K + (M+1)/2 - 1 \quad (29)$$

in the estimations (27a) or (27b), would have ensured the same parameters of resolution-detection (15) and (16) (see Fig. 1) as the optimal processing (4) and (5) of a K-dimensional sampling (1) under conditions of full a priori determinacy (see item 2). For the other methods, these parameters can be obtained at much greater requirements to the size (1-2 orders more) of the teaching sampling N.

As compared to SA methods based on Rayleigh's criterion, this advantage of the Capon method is not essential for selection of a spectral estimation method. In this case the selection should be based on the statistical characteristics of the random parameters $\hat{\gamma}$ (25) or, equivalently, on their standardized values

$$\nu = \hat{\gamma}/\gamma. \quad (30)$$

For the Capon method, the distribution density $p_\nu(x)$ of this parameter is described by the following equation [18]:

$$p_\nu(x) = \frac{\Gamma(2\delta+4)}{(\Gamma(\delta+2))^2}\left(1-|r|^2\right)^{\delta+2}\frac{x^{\delta+1}(1+x)}{\left((1+x)^2-4|r|^2x\right)^{\delta+2.5}}, \quad (31)$$

where Γ(z) is the gamma-function that is equal to (z-1)! for the integer variable $z \ge 1$; the quantity

$$r = \frac{\mathbf{X}^*(\alpha_1)\mathbf{\Psi}\mathbf{X}(\alpha_2)}{\left(\mathbf{X}^*(\alpha_1)\mathbf{\Psi}\mathbf{X}(\alpha_1)\cdot\mathbf{X}^*(\alpha_2)\mathbf{\Psi}\mathbf{X}(\alpha_2)\right)^{1/2}} \quad (32)$$

is a generalized coefficient of the spatial correlation of radiations from the directions α_1 and α_2, that is

$$\delta = N - M \quad \text{or} \quad \delta = N - (M+1)/2 \qquad (33)$$

for the estimations (27a) and (27b) respectively.

It can be shown that at any values of $|r| \le 1$ and $\delta \ge 0$ the distribution median of the function (31) is the point $x_0 = 1$. That is why the random parameter $\hat{\gamma}$ with the probability $P = 0.5$ is not less than γ that corresponds to the precise CM, and consequently, the curves 1, 2, 3 on the Fig. 2 describe not only "limiting" (see item 5) but also the actual resolution of the two sources of equal power that is ensured by the Capon method on the basis of the estimations (27), at any $\delta \ge 0$ with the probability $P = 0.5$.

For the other methods similar analogous accurate results are not known. In relation to this, Fig. 3 shows the experimental [19] plot of δ versus the probability $P(\hat{\gamma} \ge \gamma)$ of that the random parameter $\hat{\gamma}$ (25), is not less than the threshold $\gamma_0 = \gamma_{ML} \approx 2$ of the Capon method for the exactly known CM. As it comes out from the theory [17, 18], for the method (21) itself this probability equals to 0.5 already at $\delta = 0$, and at δ increasing does not change. As for this parameter, the methods (22)-(24), having substantially higher "limiting" (at $\delta \to \infty$]) resolution, are close to the Capon method or even worse. From this it follows that, if the size N of a teaching sampling is changed, it may be necessary to transfer from one method to another, or to their combination. Such a possibility should be envisaged at substantiation of the means of practical implementation of "superresolution" spectral estimation methods.

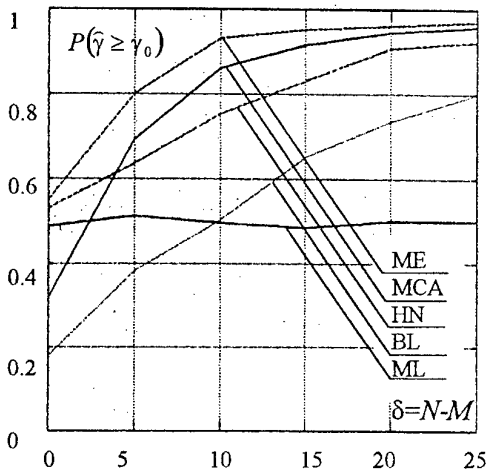


Fig. 3

8. The most promising way for the solution to these problems is the use of adaptive lattice filters (ALF) [1–4, 19, 21–24]. They enable to uniformly implement the methods (21)-(24), as well as a number of their varieties with practically useful properties [17, 19]. In this case, going from one method to the other as well as their combining is enabled by a mere re-commutation of the output signals at the ALF, but do not affect neither their internal structure nor the adaptation algorithms. The latter can be easily redesigned to take into consideration possible a priori information about the specificity of the AA, have high digital stability, and assure wide possibilities for re-distribution of time and hardware expenses [22-24]. It is also essential that, based on this, there can be formed adaptive systems solving not only the above discussed problems but also a wide range of the problems related to spatial-temporal processing of signals against a background of interference in radar systems utilising AA.

REFERENCES

1. S. Haykin, J. Litva and T.J. Shepherd (eds). Radar Array Processing. Springer-Verlag, Berlin, 1993.
2. Don H. Johnson and Dan E. Dudgeon. Array Signal Processing. Concepts and Techniques. Prentice-Hall, Englewood Cliffs, New Jersey, 1993.
3. H. Krim and M. Viberg "Two Decades of Array Signal Processing Research." IEEE Signal Processing Magazine, July 1996.
4. J. D. Shirman, V. N. Manzhos, D. I. Lekhovitsky "Some Stages and Problems of Theory and Technique of Radar Signals Resolution." Radiotekhnika, 1997, №1, pp.31-42 [in Russian].
5. S. L. Marple, Jr. "Digital Spectral Analysis with Applications." Prentice-Hall, Englewood Cliffs, New Jersey, 1987.
6. Drogalin V.V., Merkulov V.I., Rodsivilow V.A.. and oth. "DOA Estimation Algorithms base on Spectral Analysis Methods." Radiolokatsiya i Radiometriya, 1999, №1, pp.52-68 [in Russian].
7. J. D. Shirman "Statistical Analysis of the Optimal Resolution." Radiotekhnika i Elektronika, 1961, Vol. 6, № 8, pp. 1232 [in Russian].
8. J. D. Shirman "The resolution and Contraction of Signals." M.: "Sovietskoe Radio", 1974, 360 p. [in Russian].
9. J. Munier, G. Y. Delisle "Spatial Analysis in Passive Listening Using Adaptive Techniques." Proc. IEEE, Vol.75, pp.1458-1471, November 1987.
10. N. A. J. Hastings and J. B. Peacock "Statistical Distributions." Butterworth and Co (Publishers) Ltd, 1975.
11. G. V. Repin, G. N. Tartakovsky "Statistical Synthesis a Prior Uncertainty and Adapting of Information Systems." M.: "Sovietskoe Radio", 1977, 432 p. [in Russian].

12. V. V. Karavaev, V. V. Sasonov "Statistical Theory of the Passive Location." M.: "Radio and Svyaz' ", 1987, 240 p. [in Russian].

13. J. Capon "High Resolution Frequency – Wavenumber Spectrum Analysis." Proc. IEEE, Vol.57, pp.1408-1418, August 1969.

14. J. Capon and N. R. Goodman "Probability Distributions for Estimators of the Frequency - Wavenumber Spectrum." Proc. IEEE, Vol.58, pp.1785-1786, November 1970.

15. D. I. Lekhovitsky, S. B. Milovanov, V. M. Pishuchin, P. M. Flexer "Modified Capon's Algorithm for Problems of Spectral Analysis of Harmonic Space-Temporal Random Signals." Thesis's of All-Union School-Seminar "Designing of the Automatic and Control Systems for Complex Objects", Tuapse, October 1992 [in Russian].

16. S. M. Kay and C. Demeure "The High-Resolution Spectrum Estimator – A Subjective Entity." Proc IEEE, Vol.72, pp.1815-1816, December 1984.

17. D. I. Lekhovitsky, P. M. Flexer "Statistical Analysis of Resolvability of Adaptive Algorithms of Spectral Estimation." Thesis's of the Reports ISTC "Modern Radar", 1994, p. 164 [in Russian].

18. D. I. Lekhovitsky, P. M. Flexer "Statistical Analysis of Resolution of Quasiharmonic Spectral Estimating by the Capon's Method." Modern Radar, 1994, pp. 66-71 [in Russian].

19. D. I. Lekhovitsky, V. A. Doroshuk, A. A. Poberezhny "Theoretical and Experimental Research of Modern Quasiharmonic Spectral Estimation Algorithms." International Conference "Theory and Technique of Transmission, Admittance and Processing Information", Thesis of the Reports, Tuapse, 1995 [in Russian].

20. D. I. Lekhovitsky "On the Theory of an Adaptive Processing of Signals in Systems with the Central Symmetry of Receiving Channels." – Kharkov: Radiotekhnika, 1996, №100, pp.140-158 [in Russian].

21. D. I. Lekhovitsky "Generalized Levinson's Algorithm and Universal Lattice Filters." Izv. VUZov, Radiophizika, 1992, Vol.35, №9-10, pp.790-808 [in Russian].

22. D. I. Lekhovitsky, S. B. Milovanov, I. G. Kirillov "Universal Adaptive Lattice Filters. Adaptation at the Given of Correlation Matrix of Interference." The Manuscript in VINITI, Register №2127- B92, 1992 (Annotation. Izv. VUZov, Radiophizika, 1992.-Vol. 35.-№ 3-4) [in Russian].

23. D. I. Lekhovitsky, S. B. Milovanov, I. D. Rakov, B.G. Sverdlov "Universal Adaptive Lattice Filters. Adaptation at the Given Root of the Estimate Correlation Matrix." Izv. VUZov, Radiophizika, 1992, Vol. 35, № 11-12, pp. 969-991 [in Russian].

24. S. S. Kusin, D. I. Lekhovitsky "New Structure of the Lattice Filter and Adaptive Estimation Algorithm." M.: Radiotekhnika, 1989, №6, pp. 33-35 [in Russian].

A PC BASED PROGRAM PACKAGE FARFOR-99: IMPROVING OUR UNDERSTANDING OF RADIATION FROM APERTURE ANTENNAS AND ANTENNA ARRAYS

D. M. Sazonov

Moscow Power Engineering Institute, Krasnokasarmennaja 14,
111250, Moscow, Russia. Email: dsazonov@postman.ru

INTRODUCTION

Program package FARFOR-99 may be used as a powerful teaching tool in addition to the well-known antenna textbook [1] for technical university students and engineers. A very simple, universal and powerful model for wide class of antenna arrays, reflectors, lenses or hybrid antennas is presented. Both symmetrical and offset geometry are available. The feed arrays of hybrid antennas may have up to few hundreds independently placed and excited elements. The model has been realized in the program package FARFOR-99 for IBM-compatible personal computers. The advantages of the model have provided more than order decreasing in computation time, and program packages users can easily analyze and synthesize multi-element arrays, reflector and hybrid antennas practically in real-time mode. Using FARFOR-99 you can also reconstruct the antenna's far field from their near field measurements on planar surface. Advanced system of input and output design information, visual representation and program interface to popular graphic package SURPHER provide comfortable conditions for user-PC dialog. This report is accompanied by the demonstration of action FARFOR-99 tools in real time mode.

GENERAL CONSIDERATION

The design of modern Earth or board antenna systems for communication systems or radar is always connected with a large amount of pattern and secondary parameters computations. We carry to secondary parameters main beamwidth, directivity, gain, sidelobes, cross-polarization levels, etc. This computation is one of the most difficult and computer time consuming for electrically large reflector antennas and multi-element antenna arrays. So the problem of their computation optimization is serious and actual. The optimal strategy in fast computation of radiated fields is based on two principles. First principle is a decreasing of value of data, taking part in computation, to the low possible minimum. And, second principle is an increasing of the speed of computation by means of using the modern digital processing methods (Sazonov D., Sazonov M., [2]). The realization of such strategy was succeeded by the following tenets:

1. According to the limited spectrum function theory, the radiation field of the antenna is expressed as a series of its seldom complex samples. All intermediate field point values are the finite sums of Kotelnikov-Shannon series (with minimal number of coefficients). Thus, the only small part of pattern complex samples (about 20 %) is necessary for adequate field pattern presentation (Bucci and Franceschetti [3]). The other intermediate samples must born from this small part by means of fast interpolation procedures.
2. For fast computation of radiation field samples, the well-known aperture method was chosen. According to this method, radiated field is the two-dimensional Fourier transform from the amplitude-phase distribution the near (or equivalent) electromagnetic tangential field on planar surface. The position of aperture may be arbitrarily chosen near or on the real radiating surface.
3. For reflector, lens or hybrid antennas, the equivalent aperture distribution is found by applying a special method (a so-called "arranged ray tracing", Sazonov [4]). This method defines aperture field samples, which are lying in the nodes of prescribed grid. This grid is well matched with requirements of algorithm of computation the two-dimensional Fourier transform. Thus, continuous reflecting or radiating surface is modeled by hypothetical antenna array, having minimum of elements. Aperture blockage, causing by feed and supporting struts, is automatically taking into account by means of the appropriate algorithm.
4. After the set of fundamental complex samples of radiated field have been found by means of two-dimensional discrete Fourier transform with small dimensions. Other samples are constructed by means of Fourier interpolation technique [5] that is well known in digital signal processing. This technique replaces slow operations of summing and multiplying in Kotelnikov-Shannon series computation by fast convolution operations.

For computation both of two- and one-dimensional Fourier transforms the original algorithm of fast Fourier transform (FFT) is presented (Sazonov D. and Sazonov M. [2]). This is an inplace subroutine, which

runs more rapidly than traditional FFT-algorithms and gives additional advantages in the choosing of length of transform in one or both dimensions. The transform length is determined by product of several (up to five) mutually simple prime factors from prescribed set (2, 3, 4, 5, 7, 8, 9, 11 or 16).

PROGRAM PACKAGE SUMMARY

Now we have the common program packages FARFOR-99 for IBM-compatible personal computers under MS-DOS:

- Title: FARFOR-99, author: D.M. Sazonov
- Computer: IBM PC / AT, operation memory size: 640 kB
- Electron disk memory size: 6 MB
- Operation system: MS DOS 6.22
- Programming language: FORTRAN 77, MacroASSEMBLER
- Peripheral used: EGA/VGA monitor, dot/laser printer
- Package value: one 1.44 MB 3.50" diskette (include MS-DOS 6.22 files and EXE-files in archives).

This package serves for the aim of analysis and synthesis of the following antenna systems:

- **Planar antenna arrays** with rectangular or hexagonal grid of element's displacement in aperture. The aperture may have polygon contour (Fig. 1).

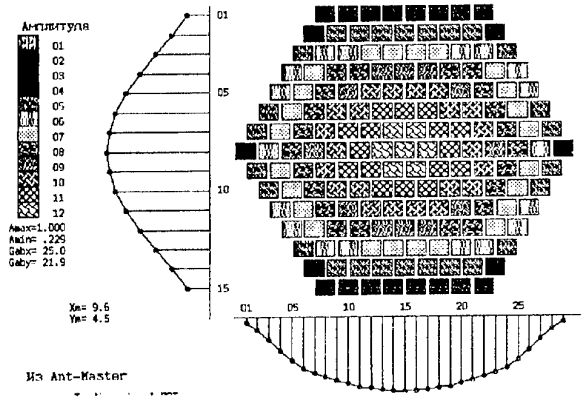


Fig. 1

Any possible type of element excitation (including that obtained from near-field measurements) is permitted. The elements may be the following: dipoles under screen, slots, rectangular or circular horns, endfire radiators, microstrip elements and other elements. It is possible to use model elements with prescribed radiation pattern and polarization

- **Single- or multi-panel mirror reflector antennas.** The antenna may have mirrors of any shape of second-order curve profiles (such as parabola, ellipse, etc.) and feed system with any possible radiation pattern and polarization performance. The position and orientation of feed system may be varied by the user. We can analyze a variety of aperture forms (circle, polygon, and ellipse) types. We can also to see on display the ray tracing in vertical plane. This gives the possibility to correct some input geometric parameters in necessary cases.
- **Hybrid reflector antennas** with feed arrays, having up to few hundreds elements of any type, displacement and excitation. There is the beautiful possibility to synthesize the antennas with contoured beams. It is possible to choose any one of two calculation modes in the program during the analysis or synthesis process: with prior summarizing of amplitude-phase distributions on the feed array, or with prior summing of partial pattern from each of the feed array elements.
- **Through-type and reflect-type holographic antennas** with plane transparencies. The FARFOR-99 can analyze and automatically synthesize antennas of such kinds.

For all of these antenna classes, the program package FARFOR-99 gives opportunities of studying the influence of random errors various kind in antenna geometry and excitation on the antenna performance.

Antenna synthesis may be fulfilled by means of FARFOR-99 by the user in interactive mode in the direction of intuition optimization. The convenient system of screen menu for data input/output with graphical and tabular representation of computation results has been created for these purposes. The initial data values may be taken for next optimization from more simple internal models, which were summarized from known antenna design experiences (like in expert systems).

It is possible in FARFOR-99 run mode to see the calculated antenna patterns (both co- and cross-polarized components) as a graph, or as a topographical map or as a surface view representation.

The excellent elaboration of all stages of computation algorithm made the cardinal computer time reducing possible. Practically we have the full absence of results waiting. The typical computational time per one antenna configuration prediction is no more than 20-40 sec for IBM 486 DX-2 or Pentium 100 MHz computer.

The modular architecture of FARFOR-99 tools easily allows modification and adaptation for many other antennas analysis/synthesis problems. This report is accompanied by the demonstration of action FARFOR-99 packages.

REFERENCES

1. Sazonov D.M., 1990, Microwave Circuits and Antennas (textbook in English), Mir Publishers, Moscow, p.p.502.
2. Sazonov D.M., Sazonov M.D., 1990, "Application of improved multivariate FFT algorithms in fast computations of EM-fields of antennas and scattering objects", *Thesis of Reports of Scientific Conference in Rostov (Yaroslavsky), Russia*, April 1990, 5--6.
3. Bucci O.M., Franceschetti G., 1989, "On the Degrees of Freedom of Scattered Fields", IEEE Trans. AP-37, 918-926.
4. Sazonov M.D., 1991, "Computation of GO-fields in reflector antennas in aperture grids with prescribed structure", *Radioelectronics and Communication Systems, Allerton Press.Inc.*, 33, No.3, 33--38.
5. Sazonov M.D., 1993, "Methods of interpolation of radiation fields in fast computation of reflector antennas", (in Russian), Radiotechnika, No. 4, pp.67 -- 73.

ADAPTIVE ANTENNA ARRAYS WITH MICROWAVE SIGNAL PROCESSING

Y. N. Sedishev, V. R. Khachaturov

Kharkov Military University
310043, Kharkov, sq. Svobody, 6, tel./fax (38) 0572 – 430740

The problems of design of signal aperture processing systems in adaptive antenna arrays (AAA) providing a receiving of wide-band signals at the background of multiple high-intensity jamming are considered.
It is shown that the basic approach to solve such problems is to combine the use of analog devices constructed with the aid of modern low-noise broad-band technologies of microwave and digital systems of signal processing and information storage.
The comparative analysis of variants of combined systems of aperture processing by the criterion of approximating their characteristics to the Wiener filter algorithm in a wide dynamic range of input signals and coordination of adaptation process with the rate of data arriving, updating and processing is carried out.

INTRODUCTION

For the last forty years the works on the theory development and practical application of adaptive arrays and antennas have been going on [1–3, 6]. Optimal processing of signals at the background of a stationary noise produced by non-correlated point sources of active interference with the accuracy up to α scale factor corresponds to a multichannel weight processing according to the Wiener filter algorithm:

$$W = \alpha R^{-1} \cdot S_0, \qquad (1)$$

where W is the weight factor vector; S_0 is the space vector of a desired signal in the antenna aperture providing the main beam formation; R^{-1} is the reciprocal correlation matrix of interference and internal noise received in N receiving channels.

Signal weight summation at N > M (where M is the number of interference sources) (1) maximizes the signal/ interference plus noise ratio (SNIR) minimizing the signal loss in the main beam and forming receiving zeros in the directions to the interference sources by the coherent compensation of their signals.

$$q_0 = S_0 \cdot W = S_0 \cdot R^{-1} S_0. \qquad (2)$$

For AAA with identical channels the moduli of the complex coefficients of the interchannel correlation outside the main diagonal R^{-1} depends on the total interference power/noise ratio and can be obtained like follows:

$$\rho = |\dot{\rho}| = \sum_{i=1}^{m} h_i \Big/ \sum_{i=1}^{m} h_i + 1, \quad h_i = \frac{P_i}{P_n} = \frac{\sigma_i^2}{\sigma_n^2}, \qquad (3)$$

where σ_i^2, σ_n^2 are the variances of the interference and noise, respectively.

For a quantitative estimation of the weight summation results we use the methods of reducing Hermitian matrices to the diagonal form through non-multiple eigenvalues and projection matrices [1, 2].

$$R = \sum_{i=1}^{m+1} \lambda_i P_i; \; P_i \cdot P_k = \begin{vmatrix} 1 & i = k, \\ 0 & i \neq k; \end{vmatrix} \; f(R) = \sum_{i=1}^{m+1} f(\lambda_i) P_i,$$

$$\lambda_1 \geq \lambda_2 .. \lambda_m, \qquad \lambda_{m+1} = \lambda_{m+2} = .. \lambda_N. \qquad (4)$$

$$\sum_{i=1}^{N} \lambda_i = N, \qquad m + 1 = \mu ..$$

Thus, the relation (2) is transformed to the following form:

$$q_0 = \sum_{i=1}^{m+1} \frac{1}{\lambda_i} S_0^* P_i S_0. \qquad (5)$$

From (4) and (5) it follows that if $m = 1$ and the array main beam position $S(\Delta)$ is changed the value q_0 can vary over a wide range from

$$q_{0max} = \frac{N}{1-\rho} \quad \text{to} \quad q_{0min} = \frac{N}{1-\rho+N_\rho} \approx 1,$$

at Raleigh resolution of m (N>m) sources of equal power

$$q_{0min} = \frac{N}{1-\rho+N_\rho/m} \approx m,$$

and, therefore, a potential gain of aperture processing varies over a range of

$$\frac{q_{0max}}{q_{0min}} = \frac{N}{m(1-\rho)}. \qquad (6)$$

From (6) it follows that the efficiency of broadband multiple interference aperture processing depends on receiving channel characteristic identity ($\lambda_N(1 - \rho)$

determines limiting opportunities of the coherent compensation) as well as on receiving channel redundancy in relation to the number of interference sources.

The degree of the modulus of the correlation coefficient approximation in real receiving channels, including array excites, to (3) is criterion of integral estimation of adaptation algorithm efficiency and technological perfection of processing equipment.

TO THE SELECTION OF AAA ADAPTATION METHOD FOR MICROWAVE SIGNAL PROCESSING

The quality of aperture processing is defined by the accuracy of setting the amplitude-phase distribution (APD) reduced to the antenna aperture. At the same time, the most of the known adaptation methods and devices provide weight summation at intermediate frequency or in digital processors after analog-to-digital conversion of signals at the outputs of multistage receivers [2]. In evaluating channel identity it is necessary to account both external and internal statistics of the antenna system. The identity difficulties increase with strengthening the requirements to a dynamic range of input signals and their relative broadbandness $\Delta f_s/f_0$. As applied to the use of digital methods it takes the form of the capacity of representing signals in the digital form and digital processor rapidity.

Besides, it is necessary to take into account additional quantization noise, which unlike internal noise cannot be considered as non-correlated one. It influences both the value of SNR and the accuracy of the weight vector calculation.

To estimate the gain in (6) it is necessary to take into account that an equivalent value of correlation coefficient modulus decreases due to non-identities of nonlinearities of the amplitude ($\rho_{\approx}$), amplitude-phase and phase-frequency ($\rho_{\Delta(\alpha,\varphi)}$) responses of receiving channels, differences of signal interchannel delay $\hat{R}^{-1}$ up to weight summator ($p_{\Delta\tau}$). Besides, errors in estimates of the reciprocal correlation matrix $\hat{R}^{-1}$ or the weight vector $\hat{W}$ in (1) also result in reduction of $\hat{\rho}$ proportional to $\rho_{\Delta W}$. Thus,

$$\hat{\rho} = \rho \cdot \rho_{\approx} \cdot \rho_{(\alpha,\varphi)} \cdot \rho_{\Delta\tau} \cdot \rho_{\Delta W} < \rho. \qquad (7)$$

From (7) it follows that for obtaining potential gains of the aperture optimum processing the operation of interference coherent compensation should be carried out in analog form in a broadband low-noise coordinated path at low signal level. In this case

$$\rho_{\Delta\alpha};\ \rho_{(\alpha,\varphi)};\ \rho_{\Delta\tau} \approx 1;\qquad \hat{\rho} = \rho \cdot \rho_{\Delta W}. \qquad (8)$$

For quantitative estimates at optional arrangement of interference sources and using the estimated values of $\hat{R}$ and $\hat{W}$ while processing we can use the following relations for SNIR at the processor output [6,9].

$$\hat{q}(\Theta) = \frac{(S^*_\Theta \hat{R}^{-1} S_\Theta)^2}{S^*_\Theta \hat{R}^{-1} R R^{-1} S_\Theta} = \frac{(S^*_\Theta \hat{W})^2}{W^* R W}, \qquad (9)$$

or, in accordance with (4)

$$\hat{q}(\Theta) = \left(\sum_{i=1}^{m} \frac{1}{\hat{\lambda}_i} S^*_\Theta P_i S \right)^2 \Bigg/ \left(\sum_{i=1}^{m} \frac{\lambda_i}{\hat{\lambda}_i} S^*_\Theta P_i S \right). \qquad (10)$$

It is obvious that the relation $\hat{q}/q_0$ defines the total losses of processing.

$$K_I(\Theta) = \frac{\hat{q}}{q_0} \le 1.$$

In the absence of adaptation $\hat{R} \to I$ and SNIR at the output

$$q_{na}(\Theta) = \frac{N^2}{S^*_\Theta R S_\Theta}. \qquad (11)$$

and the relation $q(\Theta)/q_{na}(\Theta)$ defines a relative gain if using non-adaptive PAA. Thus, its directivity pattern is determined by the Fourier transform for $W(\Theta_i)$

$$q(\Theta) = \dot{S}(\Theta) W(\Theta_i). \qquad (12)$$

At all variety of adaptive AAA algorithms two basic methods of the weight vector calculation are used:

- the method of direct determination of the correlation matrix by signal samples at the output of N-channel receiver with subsequent calculation of the weight vector in the digital form [1,2,4];
- the gradient method with N-channel negative correlation feedback (CNF) minimizing the noise at the output and forming in the stationary mode the vector of the form [1, 2]:

$$w = (I + \beta R)^{-1} S \approx \frac{1}{1+\beta} R^{-1} S; \qquad \beta >> 1,$$

where β is the amplification factor in a feedback circuit; I is the identity matrix.

Both the direct and gradient methods require much time for estimates of weight vector and large amplitudes of signals even if at one of correlator inputs. The direct method is practically non-realized at N>2 when using analog technologies, while the gradient methods admit both analog and digital realizations [6].

The advantage of the direct method is the opportunity of producing optimum amplitude-phase distributions in AAA aperture for signal receiving from any direction in a scanning sector. However, they do not work in the real time. The period of data updating affects essen-

tially the errors of the weight vector calculation, which depend on the time of interference stationarity and reduce $\rho_{\Delta W}$. In the practical application of direct methods it is necessary to take into account substantial computational expenses, which increase multiply with the number of channels.

The process of adaptation in gradient methods goes in real time and provides high calculation accuracy of the weight vector, though for one direction only; the speed of space scanning is limited by transients in a multichannel system with CNF. Besides, in the digital calculation of the weight vector and coherent weight summation the broadbandness is limited by the rapidity of digital elements. Therefore, in weight summation of analog signals at microwaves it is proposed to search reasonable trade off in combinations of direct and gradient methods, optimizing there contribution to the accuracy of the weight vector calculation ($\rho_{\Delta\omega} \to 1$), stabilization and reduction of transient time by the long-duration storage and updating information on $\hat{R}^{-1}$ or $\hat{W}(\Theta_i)$ for the preadaptation and fast correction of the weight vector for the direction of a useful signal arrival $S(\Theta_i)$.

The fulfillment of the listed conditions results in AAA structure which, to our mind, is versatile for a variety of applications and is given in Fig. 1.

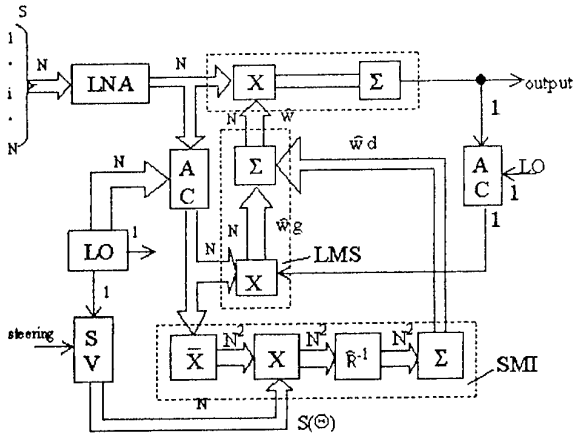


Fig. 1. Structural scheme of microwave weighting AAA signal processing

In the circuit of a linear AAA from the outputs of N-channel low-noise amplifier (LNA) with a pre-selector limiting a processing band, the low-level signals are applied to a weight summator. Through N-channel amplifiers-converters with ANGC the same signals are applied to multipliers of multichannel correlators of two processors: of direct calculation of interference matrix and gradient one.

Their dimensions are shown on the vector signal arrows. The vector sum of the weight vector estimates of two processors $\hat{W}_d$ and $\hat{W}_g$ providing more accurate amplitude-phase distribution $\hat{W}(\Theta_i)$ corrected by the gradient processor in the real time is applied to the weight summator control inputs.

Thus, the discrepancies of calculating the weight vector $\hat{W}_d(\Theta_i)$ appearing due to finite time of action and non-stationarity of interference are removed and the equalization of levels of various intensity interference provides a essential reduction of the transient time in a multichannel processor with CNF (Fig. 2).

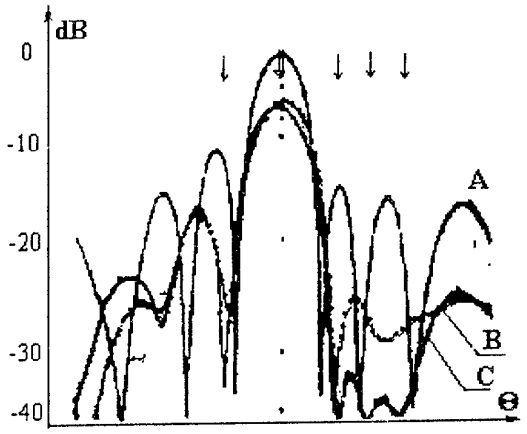


Fig. 2. Experimental patterns of 8-channel AAA. (A-linear AA, B-SMI-method, C-SMI+LMS method)

It should be noted that when constructing multichannel adaptive PAA with relative broadbandness up to 10% of is the redundancy of the number of summing channels has to be not less than 2–3. Gradient processor stability in a dynamic range is of special difficulty here. Its digital realization can require clock frequency of ADC (analog-to-digital converter) up to 0.5...1 GHz or division of total bandwidth into subchannels. The design of precision weight multipliers with low noise in various microwave ranges is not of less difficulty. However, the use of modern microwave technologies enables not only to solve these problems but also provide the construction of steady-state analog multichannel gradient processors with the weight vector calculation at high frequency. It can be achieved by using the properties of coherent parametric circuits with correlation feedback at non-linear reactances in adaptive antenna arrays.

APPLICATION OF GRADIENT PARAMETRIC PROCESSORS

The block-diagram of parametric processor for coherent weight summation is shown in Fig. 3.

The basis of each adaptation channel is a parametric non-regenerative converter (Fig. 4). At one of the combination frequencies of converter (ω_0) a narrowband integrating filter is connected. It provides a parametric

connection only between correlated components of exciting signals in channels and the sum of signals, converted to the frequency of summation filter (ω_Σ) with the aid of the reference signal vector components at the frequency (ω_0). Under the condition of smallness of the signals at the frequencies ω_0 and ω_Σ, $|U_s^i| >> |U_0|$ and $\omega_s + \omega_\Sigma = \omega_0$, oscillations, proportional to interchannel correlation coefficients, i.e. the weight vector components, are excited in the narrowband filter. Inverse conversion of these oscillations through a modulated reactance provides a closure of negative correlation feedback and interference coherent compensation in the filter F with the voltage differing from the initial oscillation by a factor of $(1 - \beta\rho/(1+\beta))$.

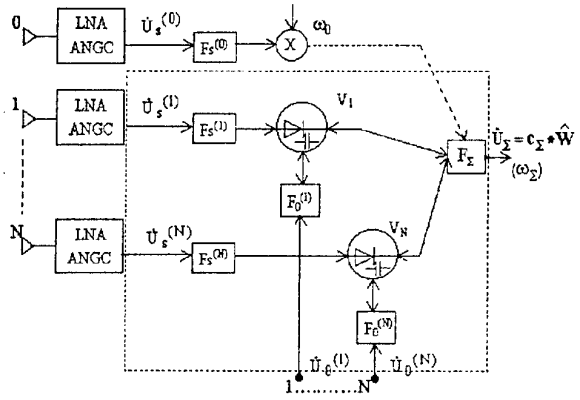


Fig. 3. Structural scheme of AAA with the adaptive parametric microwave processor

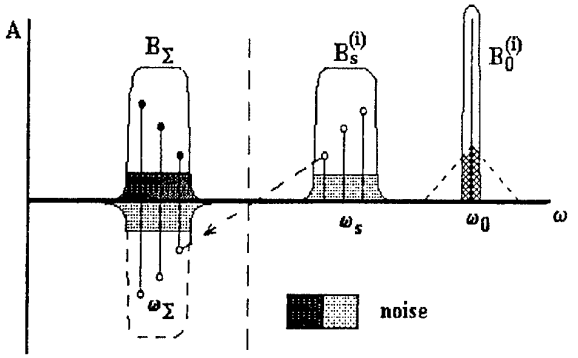


Fig. 4. Frequency diagram of the parametrical converter with a negative CFB

Non-linear capacities of parametric diodes (Fig. 3) are modulated by a signal set at the carrier frequency received by the array elements and amplified by a low-noise amplifier with AGCN to a desired level

$$\dot{U}_s^{(i)} = \sum_{k=1}^{m} \dot{U}_{sk} e^{j\varphi_k(i-1)} + U_{sn}, \qquad (13)$$

which can be represented as the sum of correlated and non-correlated components

$$U_s^{(i)} = U_{s1}^{(i)} + U_{s2}^{(i)}. \qquad (14)$$

Assuming that interference sources radiate Gaussian signals we suppose:

$$\overline{U_{si} * U_{s2}} = 0 \qquad \overline{U_s^{(i)} U_s^{*(i)}} = \sigma_s^2,$$

$$\rho_{il}^2 = \frac{\overline{U_s^{(i)} U_s^{(l)}}}{\sigma_s^2}. \qquad (15)$$

Correlation feedback availability enables to represent the *i*th non-linear capacity of the circuit in terms of a superposition of a constant component and two variable components $\dot{C}_{11}^{(i)} = \alpha \dot{U}_{s1}^{(i)}$, $\dot{C}_{12}^{(i)} = \alpha \dot{U}_{s2}^{(i)}$, where α is the slope of varicap capacity change.

In this case the analysis of gradient processor characteristics reduces to the analysis of the linear multiport properties (Fig. 5).

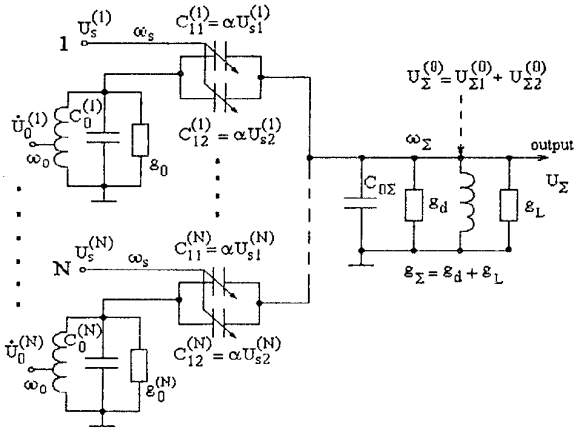


Fig. 5. Equvalent APP circuit

The scattering matrix S_s and the transfer operator T accounting for a multichannel circuit linearity (coherentness) can be obtained through its reciprocal normalized matrix of conductances Y_0:

$$S_s = I - 2\eta' Y_0^{-1} \eta'',$$

$$T = I - S = 2\eta' Y_0^{-1} \eta'' = 2\eta' \frac{\|a_{ij}\|}{|Y_0|} \eta'. \qquad (16)$$

Here, η', η'' are the diagonal matrices of conductances raised to the power 1/2 correcting for the losses in passive circuits of reference signal sources at the frequency ω_0 and the load frequency ω_Σ; $\|a_{ij}\|$ is the matrix consisting of algebraic complements of transposed matrix Y_0, $|Y_0|$ -is the matrix Y_0 determinant, I -is the identity matrix.

The matrix Y_0 in Fig. 6 relates the correlated and non-correlated signal components in receiving channels and signals of reference signal and load ω_Σ.

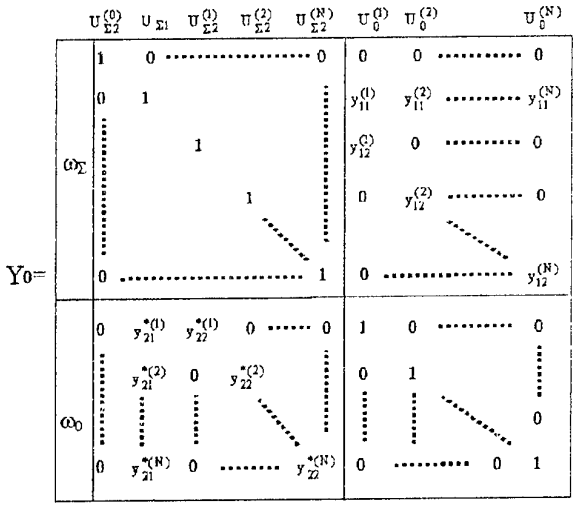


Fig. 6. Normalised matrix of conductances

Since the coupling between frequency components through a narrow-band filter-integrator is possible only for correlated components, the normalized conductance matrix consists of four block matrices: two identity matrices at the principal diagonal (I_{N+1} и I_N) and coupling coefficient matrices Y_{12}, Y_{21} of dimensions N*(N + 1) and (N + 1)*N, respectively.

If the signal from a separated channel is applied to the general summator then the total size I_{N+1} increases by one and becomes equal to (2N+2)*(2N+2). In this case the reference signal has the form of $S_0 = (1,0,0\ldots0)$ and AAA operates as an interference compensator [6, 7].

The lines $\{y_{11}^{(i)}\}_{N+1}$ in Y_{12} and the column $\{y_{11}^{*(i)}\}_{N+1}$ in Y_{21} enable coherent summation of correlated signals at the frequency ω_Σ and diagonal coefficient matrices in blocks Y_{12} and Y_{21} take into account non-coherent summation of thermal noise, which is proportional to the components of the weight vector.

The coefficients Y_{12}, Y_{21} for the equivalent circuit in Fig. 5 have the following form:

$$y_{11}^{(i)} = \frac{j\omega_\Sigma \alpha \dot{U}_{s1}^{(i)}}{(g_0 * g_\Sigma)^{1/2}},\quad y_{12}^{(i)} = \frac{j\omega_\Sigma \alpha \dot{U}_{s2}^{(i)}}{(g_0 * g_\Sigma)^{1/2}},$$

$$y_{11}^{*(i)} = \frac{j\omega_0 \alpha \dot{U}_{s1}^{(i)}}{(g_0 * g_\Sigma)^{1/2}}, y_{12}^{*(i)} = \frac{j\omega_0 \alpha \dot{U}_{s2}^{(i)}}{(g_0 * g_\Sigma)^{1/2}},$$

where g_0, g_Σ are resonance conductance of summing (ω_Σ) and integrating filters, respectively.

Using the rules of the block matrix determinant calculation it is possible to find the determinant, eigenvalues of matrix Y_0 and the transfer operator in a stationary mode providing for averaging in integrating filters for identical channels:

$$\det|Y_0| = I_{N+1}\left|I_N - \overline{Y_{12}Y_{21}}\right| = \left|I_N + \left\|\beta \cdot \dot{\rho}_{ij}\right\|\right|. \quad (18)$$

where

$$\text{где } \beta = \frac{\omega_0 \omega_\Sigma \alpha^2 \sigma_s^2}{g_0 g_\Sigma};$$

$$\dot{\rho}_{i,j} = \dot{\rho}^*_{i,j} = \left(\frac{U_{s1}^{(i)} U_{s1}^{*(j)}}{\sigma_s^2}\right)^{1/2}, \quad (19)$$

$$i, j = 1....N.$$

$$\left|\dot{Y}_0 - I_{2N+1}\lambda\right| = \left|I_{N+1}(1-\lambda)\right| * \left|I_N(1-\lambda) + \left\|\beta * \dot{\rho}_{ij}\right\|\right| = 0. \quad (20)$$

From (18, 20) it is seen that the properties of the multichannel parametric circuit under consideration are determined by the correlation matrix of input signals at the input and by the feedback depth. Normalized conductance matrix Y_0 has N + 1 multiple roots $\lambda = 1$ and, therefore, its rank is determined by the rank of the correlation matrix.

The transfer operator in a stationary mode to within the coefficients $1/1+\beta$ and the losses in circuits of an exciting signal source and a load is determined by the estimated value of the reciprocal correlation matrix

$$T = \eta' \hat{R}^{-1} \eta'' = \sum_{k=1}^{m} \frac{1}{\hat{\lambda}_k} \eta' P_k \eta''. \quad (21)$$

Here its minimum eigenvalues is

$$\lambda_\mu = \lambda_N = 1 - \frac{\beta}{1+\beta}\rho \quad (m < N).$$

Thus, under the action of the reference signal $S_0(\Theta)$ for reflected wave in a load circuit at the frequency ω_Σ $B=TS_0$. The transfer coefficient in power in view of (17), (19) and the frequency scale factor $\sqrt{\omega_\Sigma/\omega_0}$, when converting the reference signal U_o to the frequency ω_Σ in parametric converter, is equal to

$$K_{p,opt} = \frac{B^* B}{S_0^* S_0} = \frac{1}{N} \cdot \frac{\omega_\Sigma}{\omega_0} \cdot \frac{\beta^2}{(1+\beta)^2} \cdot \left[\sum_{k=1}^{m} \hat{\lambda}_k^{-1} S_0^* \eta' P_k \eta'' S_0\right]^2. \quad (22)$$

In the absence of interference $\hat{\lambda}_N = 1 + 1/\beta$ and

$$K_{p,opt} = N \cdot \frac{\omega_\Sigma}{\omega_0} \cdot \frac{\beta^2}{(1+\beta)^2} \cdot \eta'_0 \cdot \eta''_\Sigma \text{ where } \eta'_0 \cdot \eta''_\Sigma = \left[S_0^* \eta' P_k \eta'' S_0\right]^2, \quad (23)$$

which corresponds to the coefficient of internal noise power transfer in the N-channels non-regenerative frequency converter accounting for losses in filters.

The relations (22) within to a constant multiplier coincides with the numerator of expression (10) and at $\beta \to \infty$ with the relations (1), which points to an adequacy of the multichannel parametric circuit and the gradient adaptive aperture processing algorithm.

ESTIMATION OF THE INFLUENCE OF THE CORRELATION FEEDBACK DEPTH ON THE LOSSES OF THE APERTURE PROCESSING

The losses in signal processing at the output of AAA (Fig. 3) at the finite value of β can be obtained from (1), (9) and (10):

$$K_L = \frac{\hat{q}}{q_0} = \frac{\left(S_0^* \hat{R}^{-1} S_0\right)^2}{\left(S_0^* \hat{R} R S_0\right)\left(S_0^* R^{-1} S_0\right)} = \frac{\left(\sum_{k=1}^{m} \frac{1}{\hat{\lambda}_i} S_0^* P_i S_0\right)^2}{\left(\sum_{k=1}^{m} \frac{\lambda_i}{\hat{\lambda}^2} S_0^* P_i S_0\right)\left(\sum_{k=1}^{m} \frac{1}{\lambda_i} S_0^* P_i S_0\right)}. \quad (24)$$

If m = 1 then (4)

$$\lambda_1 = 1-\rho+N_\rho; \quad \lambda_N = 1-\rho; \quad \hat{\lambda}_1 = \frac{1+\beta\lambda_1}{1+\beta};$$

$$\hat{\lambda}_N = \frac{1+\beta\lambda_N}{1+\beta};$$

$$S_0^* P_1 S = NF^2(\varphi-\varphi_0); \; S_0^* P_N S = N[1-F^2(\varphi-\varphi_0)];$$

where $F^2(\varphi-\varphi_0) = \left[\frac{\sin\frac{N}{2}(\psi_0-\psi)}{N\sin\frac{1}{2}(\psi_0-\psi)}\right]^2$ –

is the value of the normalized pattern of AAA depending on angular distinctions in the directions of the signal and interference arriving and the value of K_L is equal to

$$K_L = \frac{\left[\hat{\lambda}_N F_{01}^2 + \hat{\lambda}_1(1-F_{01}^2)\right]^2}{\left[\hat{\lambda}_N^2 \lambda_1 F_{01}^2 + \hat{\lambda}_1^2 \lambda_N (1-F_{01}^2)\right]^2} \cdot \frac{\lambda_1\lambda_N}{\left[\lambda_N F_{01}^2 + \lambda_1(1-F_{01}^2)\right]} \le 1. \quad (25)$$

Since $\lambda_N << \lambda_1$, $\hat{\lambda}_i = \frac{1+\beta\lambda_i}{1+\beta}$; it can be shown that the value K_L is minimal (losses are maximal) at $F^2_{01} = 0.5$, which corresponds to the action of the interference coming from the direction corresponding to the half-width of AAA pattern. In this case

$$K_{Lmin} = \frac{N\beta^2(1-\rho)}{1+N\beta^2(1-\rho)}. \quad (26)$$

For m allowable radiation sources

$$K_{Lmin} = \frac{N\beta^2(1-\rho)}{m+N\beta^2(1-\rho)} = \frac{\frac{N}{m}\beta^2(1-\rho)}{1+\frac{N}{m}\beta^2(1-\rho)}. \quad (27)$$

From (27) we can make an important conclusion that losses of the weight vector estimation because of the CNF finite depth can be compensated by the redundancy of the number of channels with respect to the number of interference sources.

PROPERTIES OF MULTISTAGE ADAPTIVE PARAMETRIC PROCESSORS

The simplicity of adaptive elements enables to construct multistage parametric processors. A block-diagram of such a processor is shown in Fig. 7.

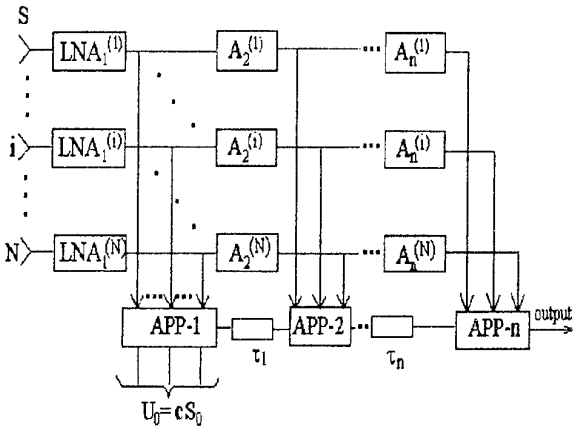


Fig. 7. AAA with multistage APP

The transfer operator of multistage APP can be obtained from (21)

$$T^{(n)} = T_1 T_2 \ldots . T_n.$$

At identical stages $T^{(n)} \neq T_1^n$ a sequential signal decorrelation occurs and the weighted noise appears in the summator of the first stage which cannot be considered non-correlated one for subsequent stades [9].

$$\rho_\upsilon = \sqrt{\frac{h}{1+h}}\sqrt{\frac{h+(\upsilon-1)\beta^{2(\upsilon-1)}}{h+(\upsilon-1)\beta^{2(\upsilon-1)}+(1+\beta)^{2(\upsilon-1)}}}, \quad (28)$$

where υ is the APP stage number.

In view of (28) the transfer operator of multistage APP can be written as follows

$$T^{(n)} = \sum_{k=1}^{m} \prod_{\upsilon=1}^{n} \hat{\lambda}_{k\upsilon}^{-1} \eta'^{\upsilon} P_k \eta''^{\upsilon}. \quad (29)$$

It is seen from (29) that the resulting estimate of eigenvalues $\hat{\lambda}_N^{(n)}$ is the product of their estimates in each stage of the filter. In the absence of correlated interference it is given by:

$$\rho_\upsilon = 0 \quad \text{и} \quad \hat{\lambda}_{k1} = 1 + \frac{1}{\beta}; \qquad \hat{\lambda}_{k2....n} = 1 \qquad (29a)$$

$$\text{и} \qquad K_p = N \cdot \frac{\omega_\Sigma}{\omega_0} \cdot \frac{\beta^2}{(1+\beta)^2} \cdot \eta_0'^{2n} \cdot \eta_\Sigma''^{2n}.$$

Therefore, the noise level is determined by the first stage with the reference signal in integrating filters.

Since the estimate $\hat{\lambda}_N$ differs from λ by $1/\beta$ the equivalent feedback depth of stage APP can be obtained as

$$\beta^{(n)} = 1/\hat{\lambda}_N^{(n)} - \hat{\lambda}_N.$$

The nature of changing $\hat{\lambda}^{(n)}$ and $\beta^{(n)}$ as functions of the feedback depth and the number of APP stages at the fixed value of λ_N is shown in Fig. 8.

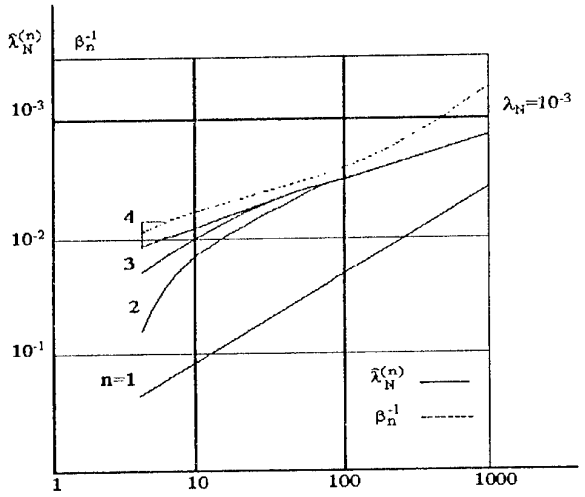


Fig. 8. Estimates of $\hat{\lambda}_N^{(n)}, \beta^{-1}$ in the multistage APP

The important moment is that at small $\beta = 10...100$ the use of two-stage processors approximating the estimate $\hat{\lambda}_N^{(n)}$ to the potential one by 6-8 dB, is the most effective. The losses of 3dB occur at $\beta^{-1} = \lambda_N$.

ADAPTATION ELEMENTS OF PARAMETRIC PROCESSORS

The adaptation element (AE) in APP is an electric circuit in the form of a series connection of the nonlinear reactance and high-Q filter. Possible variants of AE circuits are shown in Fig. 9.

The main task in selecting AE consists in ensuring the CNF depth, which is obtained from (18) and can be expressed through the equivalent filter Q-factors Q_0 and Q_Σ.

$$\beta = \frac{\omega_0 \omega_\Sigma \alpha^2 \sigma_s^2}{g_0 g_\Sigma} = a^2 Q_0 Q_\Sigma,$$

where a^2 is the square of the modulation parameter of AE non-linear capacity, which is equal to

$$a^2 = \frac{\alpha^2 \sigma_s}{C_0 C_{0\Sigma}},$$

where $C_0, C_{0\Sigma}$ are filter average capacities at the frequencies ω_0, ω_Σ, respectively.

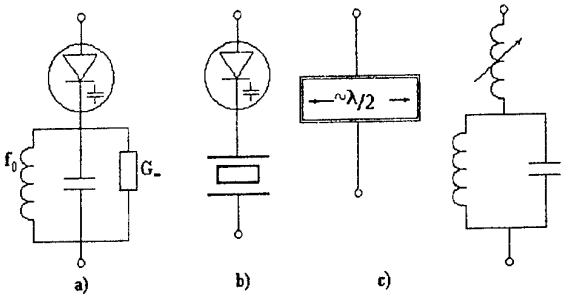


Fig. 9. Adaptive elements

Q-factor $Q_\Sigma \approx 10...20$ is determined by the spectrum width of processed signals and for existing varactors for obtaining $\beta >> 100$ it is quite promising to use high-Q resonators at volume and surface acoustic waves (Fig. 9b). When constructing microwave AE, conventional filters with tunnel-diode regenerative amplification have been effectively used (Fig. 9a).

The use of resonators based on the superconduction phenomena (Fig. 9c) makes it possible to enable Q-factor up to 10^6-10^7 in the microwave range. The film superconducting resonator having features of the nonlinear inductance and filter can be used as AE connecting the filters at the frequencies ω_S and ω_Σ and operates at superlow levels of input signals [8].

It is also interesting to use nonlinear reactances on superconductor-insulator-superconductor structures [8].

AE simplicity enables to construct multi-layered receiving systems for multichannal adaptive processors by using modern microwave technologies. As in the case of [5], the dimensions of a receiving adaptive structure will not exceed the aperture ones.

The tabulated results (Fig. 10) show the possibility to obtain a sufficiently high accuracy of the weight vector calculation in APP at the interference level in each channel up to –30 dB. Here the technical realization in various frequency ranges depends on availability of

suitable nonlinear reactances and possibility of technical implementation of high-Q filter-integrators.

Frequency, MHz			CFB	Number of channels	Number of stages	Time of estimations	Accuracy of estimations	Type AE
F_Σ	f_0	f_s	β	N	n	$t_{мкс}$	$\hat{\lambda}_N$	в
64	17	47	50	2	1	20	$5*10^{-3}$	в
54	17	37	10^4	2	3	10	$5*10^{-4}$	в
41	11	30	5000	4	2	50	10^{-3}	в
3000	90	2910	>100	2	1	2-4	$5*10^{-3}$	а,в
490	90	400	>100	4	1	2-4	$4*10^{-3}$	в

Fig. 10

CONCLUSIONS

The main advantage of the adaptive aperture microwave processing of space-correlated interferences is the possibility of achieving a high control accuracy of APD in AAA aperture that can provide a coherent compensation of a broadband interference practically up to the level of the internal noise in a wide dynamic range of input signals.

Solution of the interference coherent compensation problem and computation of the optimum weight vector can only be obtained when using adaptive parametric processors with correlated feedback. The developed theory of coherent parametric systems on nonlinear reactances allows reducing computations of processing multichannel systems to the calculation of multichannel linear electric circuits. The use of advanced low-noise microwave technologies, acoustoelectronic systems, resonant phenomena in solid body and properties of superconducting structures opens the way to creation of simple adaptation elements on non-linear superconductor-insulator-superconductor reactances with the level of the excitation less than one microwatt.

This enables to develop a microwave technology of adaptive multichannel processors the dimensions of which will not exceed the aperture dimensions at low energy consumption.

Thus, microwave gradient analog adaptive processors enable to provide a rational combination with digital processors of direct calculation of the weight vector and a microwave control. Such a combination simplifies the problems of the fast space scanning by accelerating the transients of inertial gradient systems and increases their stability.

Experimental studies of adaptive antenna models with microwave processing point to the necessity of further work development in this direction when constructing adaptive arrays in various waveranges.

The authors are grateful for help and close many- years' collaboration when developing works in this direction to professors A.V. Kobzev, A.P. Kondratenko.

REFERENCES

1. A. A. Pistolcors, O.S. Litvinov , *Introduction to the adaptive arrays theory*, M.: Science, 1991.
2. Hudson J.E. *Adaptive array principles*, L. Peregrinys, 1981.
3. Pat.3202930 US. -Intermediate frequency sidelobe canseller, P.W. Howells.Pabl.24.0865.
4. R. Nitzberg, "Computational precision requirements for optimal weights in adaptive processing", *IEEE Trans. Aerospace and Electron.Syst.*, 1980 Vol.16, N4, pp.418-425.
5. P. Jarmuszewski, Y.Shen, C.Laperle, J.Livta, "Four-Element Integrated Receiver Array for Digital Beecemforming", *URSI RADIO SCIENCE MEETING*, June 19-24, 1994. *Program and Abstracts the University of Washington Seattle*, Washington. p.186.
6. J.D. Shirman et al. , *Handbook on radio electronic systems* /J.D. Shirman ed. pp. M.: MACVIS, 1998.
7. Yu. N. Sedyshev et al., *The transceiver devises of the radio engineering systems P.2*, /Yu.N. Sedyshev ed., Kharkov, MREA, 1992.
8. V. F. Kravchenco, A. B. Kazarov, "The surface impedance superconductors and its application in the physics and engineering" // *FRE*, № 11, 1997.
9. Yu. N. Sedyshev, A. V. Kobzev, "The applicability of multichannel parametrical correlation filters for signal processing", *Questions of Radio electronics, Radar series*, №16, pp. 64-69, M., 1969.

RADIATION FEATURE OF SPACE-WAVE-LEAKY MODE ON PRINTED-CIRCUIT TRANSMISSION LINES

H. Shigesawa and M. Tsuji

Department of Electronics, Doshisha University
Tatara-Miyakodani 1-3, Kyotanabe, Kyoto 610-0321, Japan
(Tel.: +81-774-65-6357, Fax.: +81-774-65-6824, E-mail:hshigesa@mail.doshisha.ac.jp)

Abstract: We report here that, on printed-circuit transmission lines, the space-wave leaky mode, which radiates transmission power into both surface wave and space wave, propagates independent of both bound and surface-wave leaky modes. The wavenumber behavior, the vector-field plots and experiments show the evidence to this fact.

INTRODUCTION

Under usual circumstances for printed-circuit transmission lines, the guided dominant mode is purely bound at lower frequencies and then becomes leaky above some critical frequency as a surface-wave form on substrate [1,2]. This leaky mode is a slow wave, and we call it the ***surface-wave-leaky mode*** hereafter. At around the critical frequency, there exists the spectral-gap range or simultaneous-propagation range according to the structural dimensions of line cross section [3]. If there is the spectral gap, it separates clearly the ranges of both bound and leaky portions of the dominant mode each other, while such bound and leaky portions overlap when simultaneous-propagation effect occurs. Even in case of either, however, the bound-dominant-mode portion appears only below some critical frequency at which the dispersion curve for the dominant mode crosses the dispersion curve for the surface wave into which the leakage occurs.

On the other hand, it has been shown that there exists a new type of leaky mode, which leaks power at low frequencies in the forms of ***both*** the surface wave on substrate and the space wave above substrate. This leaky mode is a ***fast wave***, and we call it the ***space-wave leaky mode***. Then, this mode is understood as a solution in the cutoff range of some higher-order mode on printed-circuit lines [4-6]. Then, a ***question*** is caused. It is whether such a space-wave leaky mode can exist simultaneously with the bound dominant mode that has no cutoff frequency. To our knowledge, such a problem has not been examined so far. The purpose of this paper is provides the answer to this question.

In this paper, we show, for the first time, that the space-wave-leaky mode can propagate independent of the bound dominant mode at low frequencies even if it has no cutoff frequency. Therefore, there exists the frequency range in which both the space-wave-leaky mode and the bound dominant mode can propagate simultaneously. Furthermore, we show that, when the structural dimensions of line cross section are changed, there appears the frequency range, in which the bound dominant mode, the space-wave leaky mode and the surface-wave leaky mode propagate simultaneously. We show the numerical and experimental evidences here for these important facts.

CALCULATION RESULTS AND DISCUSSIONS

We consider here the conductor-backed coplanar strips as an example planar-transmission line, of which the cross-section is shown in Fig. 1 with the structural dimensions. Fig. 2 shows the bird-eye view of the line with the phase-constant vectors and radiation angles necessary for discussions, where β, k_s and k_0 mean the phase constants of the transmission mode, the surface wave and the free-space wave, respectively. The radiation condition into space wave are given, in good approximation, by $k_0 > \beta$. On the other hand, the relation $k_s > k_0$ is always held, so that the leakage condition into surface wave $k_s > \beta$ is always satisfied.

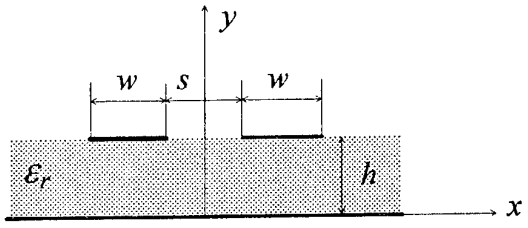
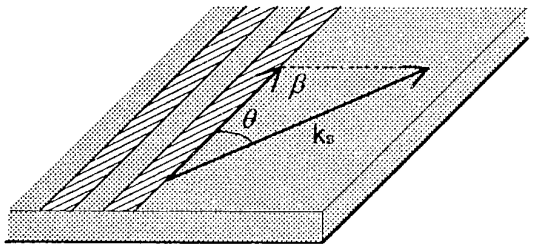


Fig. 1. Cross sectional view
of the conductor-backed coplanar strips

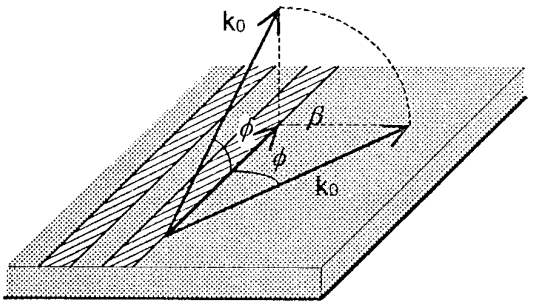
To find such a modal solution, we must carefully deform the integration path when the spectral-domain method is applied. Fig. 3 shows the integral path used in our calculations. This path first runs along the negative $Re[k_x]$ axis on the proper sheet (the negative $Im[k_y]$ plane), and then it cuts the branch cut to enter into the improper sheet (the positive $Im[k_y]$ plane), and again cuts the branch cut to come back on the proper sheet.

Fig. 4 shows the normalized phase and leakage constants when we select the strip width as $w/h = 1.0$. The other dimensions and ε_r are shown in the figure. The fine solid curve above the TM_0-surface-wave curve shown by the dotted curve is the bound dominant mode, and the space-wave leaky mode is obtained at low fre-

quencies as shown by the bold-solid curve. However, for this case of the strip width, the space-wave leaky mode is ***nonphysical*** because it takes the β/k_0 value larger than unity at all frequencies. But, it is clearly shown that the evolution of this solution exists independent of that of the bound mode. In addition to these solutions, we have here the surface-wave leaky mode solution as shown by the dot-broken curve, and this solution is physical only above the frequency f_{cr}. So, for $f > f_{cr}$, both the bound and surface-wave leaky modes propagate simultaneously.



(a)



(b)

Fig. 2. Angles θ and ϕ of leakage for the surface-wave leaky mode and the space-wave leaky mode, respectively

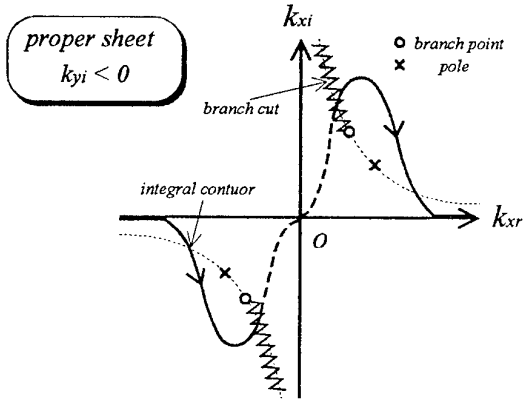
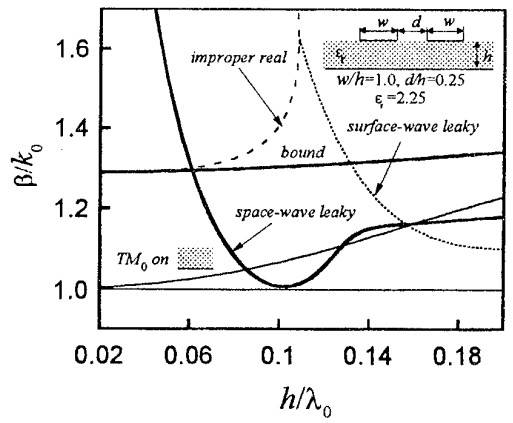


Fig. 3. Integral path for the space-wave leaky mode

To obtain the physical space-wave leaky mode, we make the strip width larger to w/h = 1.5. The result is shown in Fig. 5, where it is clearly shown that the space-wave leaky mode becomes physical between the critical frequencies f_{cr2} and f_{cr3}. Therefore, we can confirm for the first time that both the bound dominant mode and the space-wave leaky mode propagate ***simultaneously*** as physical modes even if the bound mode has no cutoff frequency. This fact certainly means that the space-wave leaky mode is a solution independent of the bound mode.

We further changed the strip width w/h from 1.5 to 2.0. Then the evolution of solutions changes as shown in Fig. 6. As for the space-wave leaky mode, its appearance does not significantly change from that of Fig. 5. However, this case shows the slight shift in both the critical frequencies f_{cr1} and f_{cr2} to lower and higher frequencies, respectively, so that the space-wave leaky mode can propagate simultaneously with ***both*** the bound and surface-wave leaky modes in the frequency range between f_{cr2} and f_{cr3}. Thus, we can conclude that the space-wave leaky mode is a solution ***independent*** of those of the bound mode and the surface-wave leaky mode.



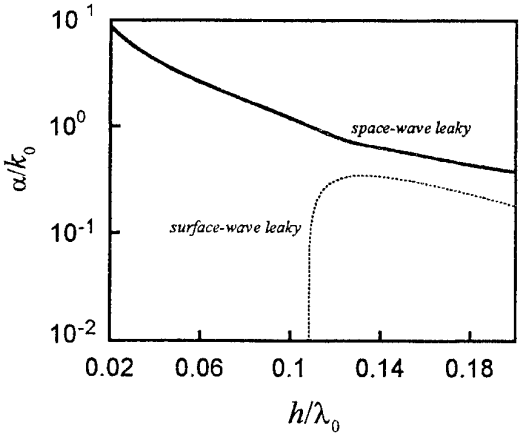


Fig. 4. Normalized phase and leakage constants as a function of the normalized frequency h/λ_0, when w/h is selected as 1.0

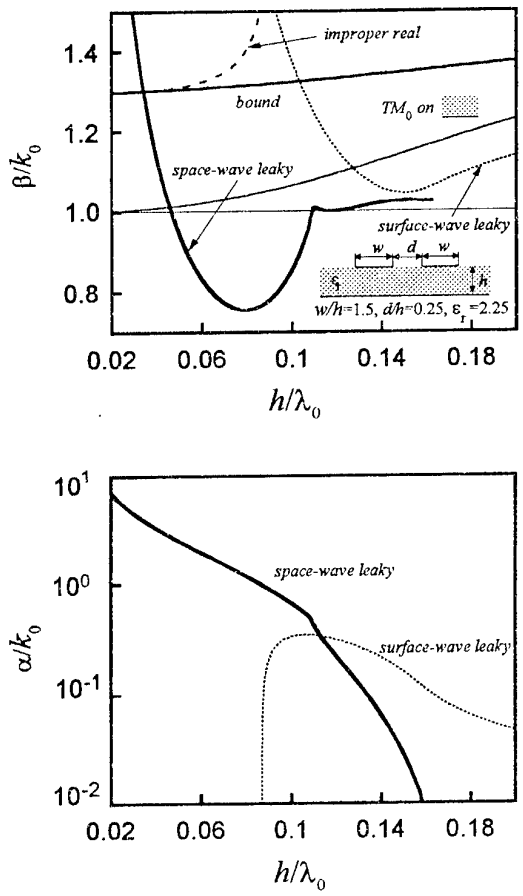


Fig. 5. Normalized phase and leakage constants as a function of the normalized frequency h/λ_0, when w/h is selected as 1.5

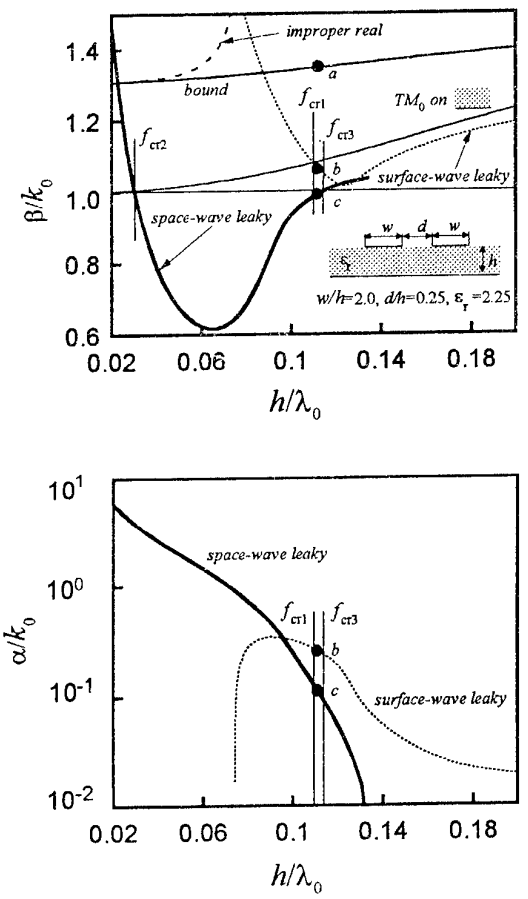


Fig. 6. Normalized phase and leakage constants as a function of the normalized frequency h/λ_0, when w/h is selected as 2.0

Next, we examine the modal nature of the space-wave leaky mode from the field behavior. As comparison, Fig. 7(a) and Fig. 7(b) show the plots of the vector-electric fields for the bound mode and for the surface-wave leaky mode at the frequencies marked *a* and *b* in Fig. 6, respectively. We show the plot for the space-wave leaky mode at the frequency marked *c* in Fig. 7(c). These plots are shown in the limited half area of the right-hand side of the line cross section. Fig. 7(a) shows certainly the field tightly bound to the strip, while the plot of Fig. 7(b) shows the field of the surface-wave leaky mode, which leaks power into the transverse direction only along the substrate with increasing amplitude. Let us next examine the space-wave leaky mode. It is expected that, when this mode becomes physical, the radiation occurs in a conical-horn shape above the substrate. Fig. 7(c) shows the result for this mode, and we can certainly see the radiation of the conical-horn shape resulted from both the space-wave leakage and the surface-wave leakage. At the same frequency corresponding to the points *a* and *c*, we have completely ***different*** field behaviors, so that we can confirm also from the field-nature point of view that the space-wave leaky mode can propagate as a physical mode independent of other types of physical mode.

EXPERIMENTS

To reinforce our numerical conclusions, we performed a set of experiments. The first experiment is the measurements of both the normalized phase constant β/k_0 and the normalized leakage constant α/k_0 over a wide frequency range, for the line with w/h = 1.45. In this case, the space-wave leaky mode is present simultaneously with the bound mode in the limited low-frequency range and also with the surface-wave leaky mode over a high-frequency range, respectively, as shown in Fig. 8. The round-open dots show the experimental results. The details of the measurement procedures employed are presented in [3]. Figure 8 shows that, although there are some difference in the measured data for the normalized leakage constant α/k_0, the measurements verify the propagation of the space-wave leaky mode independent of both the bound-dominant mode and the surface-wave leaky mode.

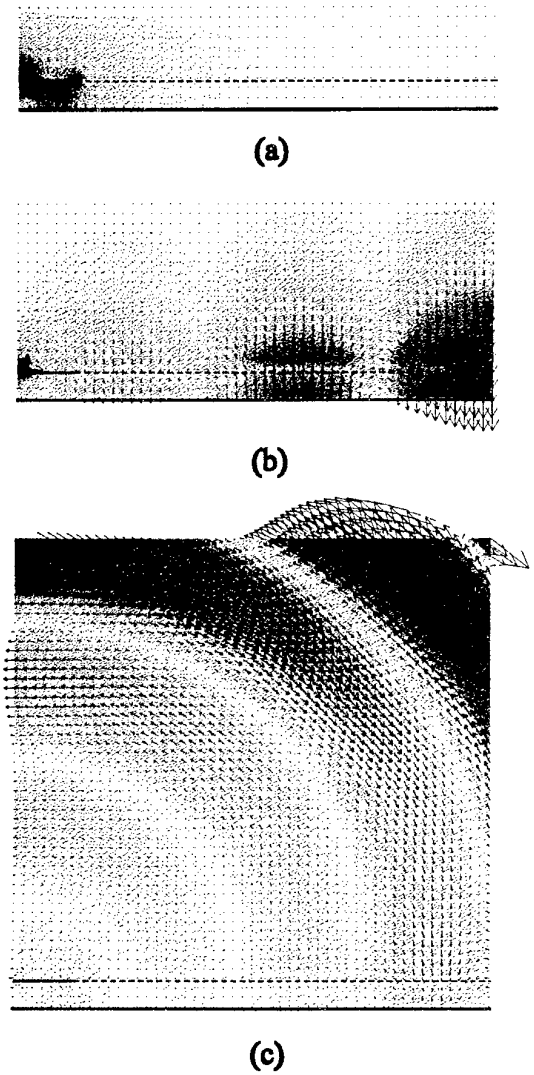


Fig. 7. Vector-field plots on the line cross section. Figures (a), (b) and (c) correspond to those obtained at point a, b and c marked in Fig. 6

The second experiment is the measurements of the radiation field of the space-wave leaky mode. The measured results are shown in Fig. 9. The measurements are taken in the near field, so that the radiation patterns are somewhat degraded. However, the radiation peaks at the different two frequencies are observed at the angles expected from the theoretical results.

CONCLUSIONS

We have reported here for the first time that the space-wave leaky mode can propagate as a physical mode independent of bound modes and surface-wave leaky modes. Although some researchers have been concerned in problems of the space-wave leaky mode [5,6], most of them have left unclearly the precise relations among the evolutions of the bound mode, the surface-wave leaky mode and the space-wave leaky mode. So,

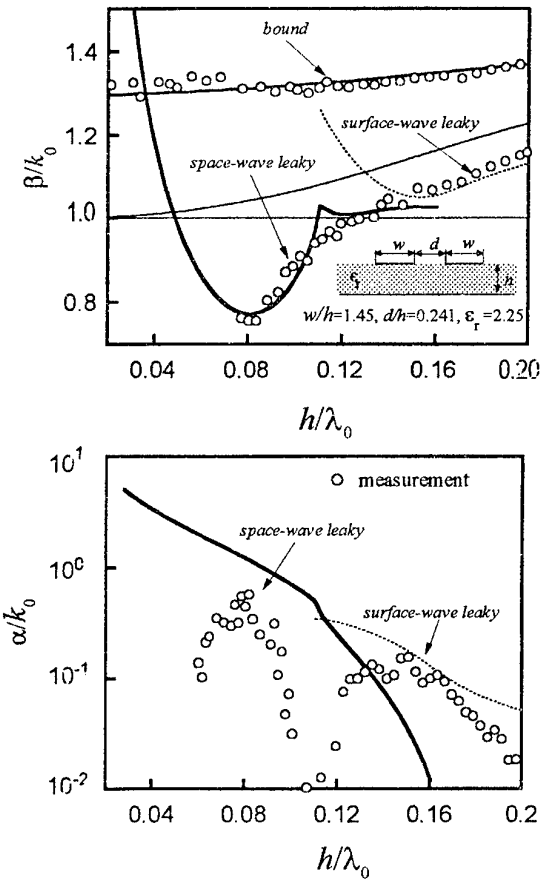


Fig. 8. Measured results (the round-open dots) for the β/k_0 and α/k_0 values when w/h = 1.45 and d/h = 0.241

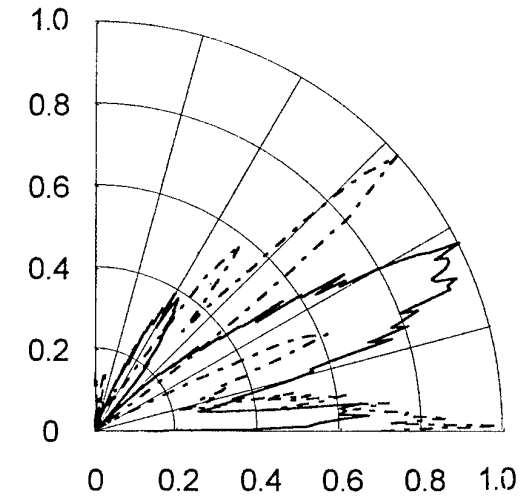


Fig. 9. Near-field patterns of the space-wave leaky mode at the normalized frequencies h/λ_0 = 0.0692 (solid curve) and 0.0831 (dot-broken curve) when w/h = 1.45 and d/h = 0.241

we present here several numerical and experimental evidences.

ACKNOWLEDGMENTS

This work was supported in part by a Grant-in-Aid for General Scientific Research (09650432) from the Ministry of Education, Science, Sports and Culture of Japan and by the Grants from the Research Center for Advanced Science and Technology, Doshisha University.

REFERENCES

1. H. Shigesawa, M. Tsuji and A. A. Oliner, "Conductor-backed slot and coplanar waveguide: Dangers and full-wave analysis," Digest of IEEE/MTT-S IMS 1988, pp. 199-202, 1988.
2. H. Shigesawa, M. Tsuji and A. A. Oliner, "Dominant mode power leakage from printed-circuit waveguides," *Radio Science*, vol. 26, pp. 559-564, Mar./Apr., 1991.
3. Tsuji, H. Shigesawa and A. A. Oliner, "Simultaneous propagation of both bound and leaky dominant modes on conductor-backed coplanar strips," Digest of IEEE/MTT-S IMS 1993, pp. 1295-1298, 1993.
4. K. A. Michalski and D. Zheng, "On the leaky modes of open microstrip lines," Microwave Opt. Tech. Lett., vol. 2, pp. 6-8, Jan. 1989.
5. A. A. Oliner, "Leakage from higher modes on microstrip line with application to antennas," Radio Science, vol. 22, pp. 907-912, Nov. 1987.
6. K. C. Tzuang and C. C. Lin, "Space-wave-type leaky mode carrying dominant-mode-like current distributions," Digest of IEEE/MTT-S IMS 1998, pp. 643-646, June 1998.

PLASMA ANTENNA
Resume of Theoretical Research

A. N. Almaliev, A. L. Gutman*, B. G. Katsnelson, M. A. Shchalev

Voronezh University, Universitetskaya sq.1, Voronezh,
* Voronezh State Forestry Engineering Academy, Timiryazeva 8, Voronezh,
ph. 0732-556-958, fax 0732-789-755, e-mail katz@mph.vsu.ru

Antenna is considered, a radiating element in which is a column of gas discharge. Possible gas mixes, ensuring required properties of a positive column, are analyzed. A conclusion and basic possibility of actualization of the specified antenna with sufficient efficiency of radiation are done

INTRODUCTION

The idea of an antenna, in which the basic radiating element is a plasma torch, is offered in works [1, 2]. In the referred papers an estimation of the characteristics of radiation from plasma, formed, for example, in the glow discharge at low pressure is performed. It is shown, that at rather low collision frequency it is possible, basically, to get acceptable efficiency of an such antenna, thus it is necessary to distinguish two cases — when the plasma rod on the properties is similar to conductor, and a case of dielectric -like plasma. Thus, the first case, which in our opinion has a higher efficiency, is considered in [3].

The stated below results of further research determine first, structure and parameters of gas mixes for the gas discharge to be realized and the achieving of necessary parameters of plasma and, secondly, by the numerical solution of the appropriate electrodynamic problems, characteristics of radiation of the plasma antenna.

PLASMA COLUMN AND OPTIMUM GAS MIXTURE

The positive column of the self maintained gas discharge, used for radiating a microwaves, is formed in radio-transparent tube, satisfying to a condition: $L >> a >> d$, where L, a are length and radius of tube, d is Debye length in plasma. At pressure lower 1 tor in the glow discharge rather low collision frequency ν is provided and, hence, small losses of the microwave energy take place. The plasma thus becomes non equilibrium: electron temperature is much greater than temperature of atoms ($T_e >> T_a$), it is assumed that the electrons' velocity distribution is maxwellian. Within the framework of some simplifying assumptions (the validity of the Thomson formula for probability of ionization, prevalence diffusion control for the gas discharge) it is possible to obtain the simple estimating formula for connection between of listed parameters of plasma:

$$\left(\frac{kT_e}{I}\right)^{1/2} \exp\frac{I}{kT_e} = \mathrm{Const}(pa)^2 \qquad (1)$$

Where I is potential of ionization of atoms, p is pressure in tube, k is Boltzmann's constant, the constant in the right part is expressed through the characteristic of a gas mixture — mobility of ions, concentration of mixture component and etc. and can be calculated for each specific case.

For such a category the distribution of free electrons concentration in a cross direction (coordinate r) is described by the Bessel function:

$$n_e(r) = n_e(0) J_0\left(2.405\frac{r}{a}\right) \qquad (2)$$

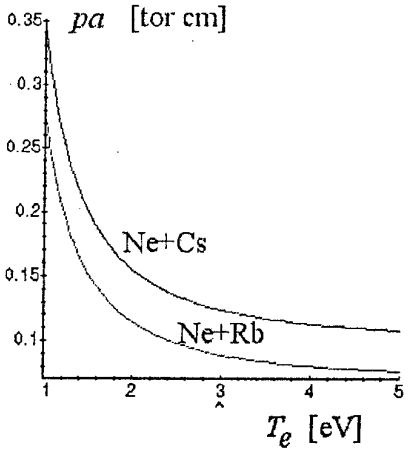


Fig. 1

The choice of a gas mixture is definined by the requirements of as lower collision frequency at as greater electron concentration. Such mixtures are known [4], and are used, in particular (personally), in MHD generators. Their structure is determined by the presence of a small part (up to 1 %) easily ionized additive. An example of a suitable mixture is for instance Ne + Cs in the ratio 0.995 + 0.005 or Ne + Rb in the ratio 0.99 + 0.01 Appropriate curves (the formula (1)) for the specified mixes are resulted in Fig. 1.

RADIATION OF THE CYLINDRICAL PLASMA VIBRATOR

Let's consider cylindrical coordinate system r,z,φ in the near zone of vibrator and spherical one R,θ,φ in far zone. For the electromagnetic field inside and outside of vibrator we have the following expressions:

In Out

$$E_z(r,z)=E_0I_0(k_1r)A(z), \qquad E_z(r,z)=\tilde{E}_0K_0(\kappa r)A(z),$$
$$H_\varphi(r,z)=-i\frac{k\varepsilon}{k_1}E_0I_1(k_1r)A(z), \quad H_\varphi(r,z)=-i\frac{k}{\kappa}\tilde{E}_0K_1(\kappa r)A(z),$$
$$E_r(r,z)=-i\frac{k_z}{k_1}E_0I_1(k_1r)A(z) \quad E_r(r,z)=-i\frac{k_z}{\kappa}\tilde{E}_0K_1(\kappa r)A(z) \tag{3}$$

where $k=\frac{\omega}{c}$, $A(z)=\frac{\sin k_z(L-z)}{\sin k_zL}$, $k_1=\sqrt{k_z^2-k^2\varepsilon}$, $\kappa=\sqrt{k_z^2-k^2}$. We will use also:

$k_1=\sqrt{\kappa^2+(1-\varepsilon)k^2}$, $k_z=\sqrt{\kappa^2+k^2}$, $I_0(x),I_1(x)$, $K_0(x)$, $K_1(x)$ are the Bessel functions.

Conditions of continuity for components of electromagnetic field give the following dispersion equation

$$\frac{K_1(\kappa a)}{\kappa aK_0(\kappa a)}+\frac{\varepsilon I_1(k_1a)}{k_1aI_0(k_1a)}=0, \tag{4}$$

from which we can obtain different components of wave vector. In turn, for the antenna radiation pattern (RP) we have

$$F(\theta)=\frac{N\sin\theta\cdot J_0(ka\sin\theta)}{1-\gamma^2\cos^2\theta}\sqrt{F_1^2(\theta)+F_2^2(\theta)},$$
$$F_1(\theta)=\cos(kL\cos\theta)-\cos(k_zL), \tag{5}$$
$$F_2(\theta)=\gamma\sin(k_zL)\cos\theta-\sin(kL\cos\theta).$$

$\gamma=k/k_z$, N is normalizing factor. Equivalent electrical and magnetic currents $\vec{I}_s^e(z)$, $\vec{I}_s^h(z)$, determining RP are equal to:

$$\vec{I}_s^e(z)=\frac{c}{4\pi}H_\varphi(a,z)\vec{e}_z=-i\frac{\omega\varepsilon}{4\pi k_1}\frac{E_0}{\sin k_zL}I_1(k_1a)\sin[k_z(L-z)]\vec{e}_z,$$
$$\vec{I}_s^h(z)=-\frac{c}{4\pi}E_z(a,z)\vec{e}_z=-\frac{c}{4\pi}\frac{E_0}{\sin k_zL}I_0(k_1a)\sin[k_z(L-z)]\vec{e}_z. \tag{6}$$

$\vec{e}_z$ is unit vector along z-axis. For our conditions $\omega<<\omega_p$ and

$$\left|\frac{I_s^e}{I_s^h}\right|\approx\frac{\omega\varepsilon}{ck_1}\approx\frac{\omega}{c}\frac{\omega_p^2}{\omega^2}\frac{c}{\omega_p}=\frac{\omega_p}{\omega}>>1 \tag{7}$$

Thus electrical surface current plays the main role and, thus, antenna is conductor-like.

Energy losses due to electron collisions in the plasma rod are determined by the equation:

$$\mathrm{Re}\left\{\frac{1}{2}\int_V\vec{j}\vec{E}dV\right\},\ \vec{j}=\sigma\vec{E},\ \sigma=\frac{\nu}{4\pi}\left(\frac{\omega_p}{\omega}\right)^2 \tag{8}$$

where σ is the plasma conductivity, integration is performed over plasma volume. Thus radiated power is

$$W_{rad}=\mathrm{Re}\left\{\frac{1}{2}\int_S\vec{E}\times\vec{H}d\vec{s}\right\} \tag{9}$$

here integration is performed over the closed surface in the far zone. An efficiency of antenna is

$$\eta=\frac{1}{1+\xi},\ \xi=\frac{\mathrm{Re}\left\{\frac{1}{2}\int_V\vec{j}\vec{E}dV\right\}}{\mathrm{Re}\left\{\frac{1}{2}\int_S\vec{E}\times\vec{H}d\vec{s}\right\}} \tag{10}$$

Below we present results of calculations for the mixture Ne+Rb at the temperature 3 eV, pressure 0.2 to at $a=0.5\,\mathrm{cm}$, $n_e=10^{12}\,\mathrm{cm}^{-3}$, $\omega_p=5.7\cdot10^{10}\,\mathrm{sec}^{-1}$, $\nu=1.2\cdot10^8\,\mathrm{sec}^{-1}$, $f_o=500\,\mathrm{MHz}$, $\varepsilon=-317-11.4i$, $L=\pi/2k_z\approx11.2\,\mathrm{cm}$.

Components of the wave vector are presented in the table

Ka	$\mathrm{Re}(k_1a)$	$\mathrm{Im}(k_1a)$	$\mathrm{Re}(k_za)$	$\mathrm{Im}(k_za)$	$\mathrm{Re}(k$	$\mathrm{Im}(k$
0.05	0.94	0.033	0.07	0.0006	0.04	0.00

For the given length of antenna, $\xi<0.1$ and its efficiency is $\eta\geq0.95=95\%$.

Taking into account energy losses due to matching device and transformation of a part of energy in plasma waves can decrease efficiency down to 60%.

CONCLUSION

The presented results allow to consider experimental setup for conductor-like antenna.

REFERENCES

1. A. L. Gutman, I. V. Narsky Antenna properties of plasma rod. Proc XXVII International Conference "Antenna theory and technique" 1994, p.58-61.
2. A. L. Gutman, I.V.Narsky Antenna properties of plasma rod. Proc. Of PIERS-95, Seattle, USA, 1995, p.151.
3. Gutman A.L., A.N.Almaliev, B.G.Katsnelson, M.A.Shehalev. Conductor like plasma antenna. Proc. Of XXV Conf. URSI, Toronto, Can. 1999.
4. Falkovsky N.I., Bozhko I.V., Troicky S.R., Glazkov N.I. Investigation of breakdown voltage in gaseus with easily ionized additive" - Teplofizika visokih temperatur . 1985, v.23, N2, p.247-252.

EXCITATION PROBLEM SOLUTION FOR THE DIELECTRIC CYLINDER WITH THIN COVER

A. V. Alpatova, N. N. Kisel', Yu. V. Yukhanov

Taganrog State University of Radio Engineering, department of Antennas and Radio Transmitters, TSURE, Nekrasovsky,44, GSP-17A, Taganrog, 347928, Russia,
phone (863-44) 6-17-33, fax (863-44) 6-50-19, e-mail: airpu@tsure.ru

INTRODUCTION

At present various electromagnetic radiation sources are widely used (for example, the cellular communication system operating at 450, 900 and 1800 MHz). Accordingly the interest to the problem of electromagnetic fields interaction with biological tissues has been increased. The inhomogeneous cylinder may be one of the possible biological structure models [1]. Such model investigation allows to take advantage of a strict solution of an electromagnetic problem. In resonance range (the specified frequency range) a method of eigenfunctions is usually used. In accordance with it fields are decomposed into infinite series of eigefunctions. The unknown expansion factors are determined from boundary conditions. However, for biological media (with large values of dielectric constants) expansion series converge extremely slowly. With a multiple eigenfunctions evaluation using appropriate direct or inverse recurrence formulas a significant error may occur. Diffraction problems in this case involve special combinations of cylindrical functions [2, 3]. In practice often it is important to know the electromagnetic field distribution inside a dielectric structure. The homogeneous dielectric cylinder with a thin cover may serve as a model of such structure. In this case it is possible to build equivalent homogeneous model utilizing two-sided second-order boundary conditions [4, 5].

PROBLEM FORMULATION

The infinite circular isotropic dielectric cylinder (Fig. 1) with a radius a, covered with a dielectric shell of a thickness $\tau = b - a$ is located in the free space. We'll consider a cylindrical coordinate system with Oz direction coincided with the cylinder axes. Complex dielectric and magnetic constants of the cylinder are introduced with the following functions

$$\varepsilon(r) = \begin{cases} \varepsilon_1, 0 < r < a \\ \varepsilon_2, a \le r \le b \end{cases}, \quad \mu(r) = \begin{cases} \mu_1, 0 < r < a \\ \mu_2, a \le r \le b \end{cases}$$

In the area V_1 the distribution of source electric currents with volume density $\vec{j}^{cm}$ is defined. The electric field strength at any point of space is to be determined.

PROBLEM SOLUTION

We'll take in mind that cover thickness τ is small as compared with the depth of field penetration into media $\tau < \delta$, where $\delta = 1/\alpha$, $k_2 = \beta - i\alpha = \omega\sqrt{\varepsilon_{a2}\mu_{a2}}$ is the wave factor of dielectric cover. The case of E-polarized wave will be considered now. To take into account a thin shell we'll make use of higher order boundary conditions (BC).

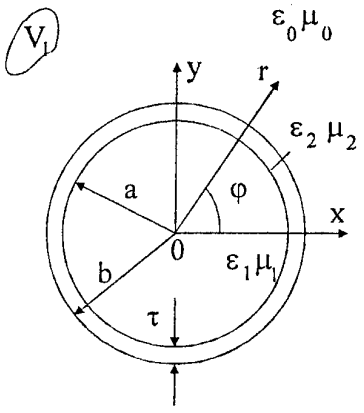


Fig. 1

Electric field intensity in the shell at $a \le r \le b$ is being expressed as Taylor series with only three components used in a vicinity of a point $a^+ = a + 0$.

At $r = b^- = b - 0$ it is possible to obtain

$$E_z(b^-, \varphi) \cong E_z(r, \varphi)\big|_{r=a^+} + \tau \frac{\partial}{\partial r} E_z(r, \varphi)\big|_{r=a^+} + \frac{\tau^2}{2} \frac{\partial^2}{\partial r^2} E_z(r, \varphi)\big|_{r=a^+} \quad (1)$$

It is assumed in expression (1) and further that time dependence is defined by factor exp(iωt). From (1), with the use of equality of tangent electric field components at $r = a$, $r = b$ and Helmholtz equation in polar coordinate system, the BC for tangent electric field component is being derived.

$$\left[1-\frac{k_2{}^2\tau^2}{2}-\frac{\tau^2}{2a^2}\left(\frac{\partial^2}{\partial\varphi^2}\right)\cdot\right]E_z(a^-,\varphi)+\left[\tau-\frac{\tau^2}{2a}\right]\times \quad (2)$$
$$\times\frac{\partial}{\partial r}E_z(r,\varphi)\Big|_{r=a^-}=E_z(b,\varphi)$$

where $E_z^n(r,\varphi)=E_z^s(r,\varphi)+E_z^i(r,\varphi)$ is a total field in the free space being equal to the sum of scattered and incident fields. When deriving (20) all derivatives by longitudinal coordinate z were concerned to be zero value (the two dimensional problem is under consideration).

Using Maxwell's equation expressed in cylindrical coordinate system, we'll obtain the second BC

$$\left[-k_2{}^2\tau-\frac{\tau}{a^2}\left(\frac{\partial^2}{\partial\varphi^2}\right)\right]\cdot\frac{1}{\mu_{a2}}\frac{1}{k_0}E_z(r,\varphi)\Big|_{r=a^-}+$$
$$+\left[1-\frac{\tau}{a}\right]\cdot\frac{1}{\mu_{a2}}\frac{1}{k_0}\frac{\partial}{\partial r}E_z(r,\varphi)\Big|_{r=a^-}= \quad (3)$$
$$=\frac{1}{\mu_0}\frac{1}{k_0}\cdot\frac{\partial}{\partial r}E_z^n(r,\varphi)\Big|_{r=b}$$

So, the approximate higher order BCs (2), (3) for tangent component of electric field have been formulated. They define the correlation between free space field ($r > b$) and field in interior cylinder ($r < a$).

Further derivation is carried out for the case when radiant is the infinite filament of an electrical current parallel to the cylinder axes. The filament is located in the free space at a point with coordinates r_0, φ_0 Its volume electrical current density is

$$\vec{j}=\vec{i}_z I_0\frac{1}{r_0}\delta(r-r_0)\delta(\phi-\phi_0).$$

The solution is realized by means of eigenfunction method [6] with application of the second order boundary conditions. As a result the following expressions for factors of expansion may be obtained (C_n, a_{n1} are the expansion factors of a scattered field in free space and total field in the cylinder)

$$C_n=\frac{H_n^{(2)}(k_0r_0)J_n'(k_0b)-\cdot\frac{B_n}{A_n}H_n^{(2)}(k_0r_0)J_n(k_0b)}{\frac{B_n}{A_n}H_n^{(2)}(k_0b)-H_n^{(2)'}(k_0b)},$$

$$a_{n1}=C_n\cdot\frac{H_n^{(2)}(k_0b)}{A_n}+\frac{H_n^{(2)}(k_0r_0)\cdot J_n(k_0b)}{A_n},$$

where

$$k_0=\omega\sqrt{\varepsilon_0\mu_0},$$

$$A_n=pJ_n(k_1a)+qJ_n'(k_1a) \qquad p=1-\frac{k_2^2\tau^2}{2}+\frac{\tau^2}{2a}\cdot n^2$$
$$B_n=\hat{p}J_n(k_1a)+\hat{q}J_n'(k_1a), \qquad q=k_1\cdot\left(\tau-\frac{\tau^2}{2a}\right)$$

$$\hat{p}=\left(-k_2^2\tau+\frac{\tau}{a^2}\cdot n^2\right)\frac{1}{k_0\mu_2}$$
$$\hat{q}=\frac{k_1}{k_0\mu_2}\cdot\left(1-\frac{\tau}{a}\right)$$

NUMERICAL RESULTS

The purpose of the numerical investigations was to define the possibility of application of the thin layer approximation presented above.

In Fig. 2 the spatial distribution of the absolute values of calculations relative error is depicted for the electric field intensity evaluated strictly and approximately in the structure with ka = 5.0, ε_1 = (5.,–i0.5), ε_2 = (1., –i0.0), kr_0 = 6 ($k=\omega\sqrt{\varepsilon_0\mu_0}$), $\varphi_0=0^0$.

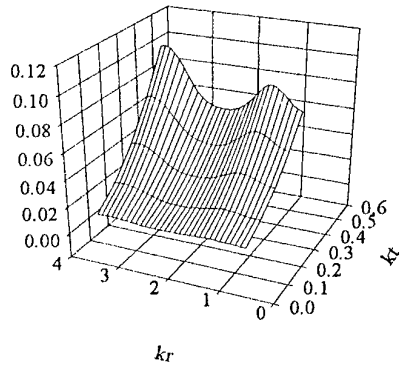


Fig. 2

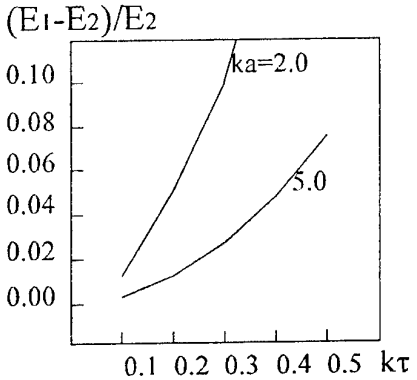


Fig. 3

Here E_1 , E_2 are the approximate and strict electric field values.

In Fig. 3 the relative error dependence of approximate and strict electric field intensity evaluation versus the shell thickness is presented for a structure with following parameters $\varepsilon_1 = (5., -i0.5)$, $\varepsilon_2 = (1., -i0.0)$, $kr_0 = 6$, $\varphi_0 = 0^0$ (graphs correspond to different cylinder radii).

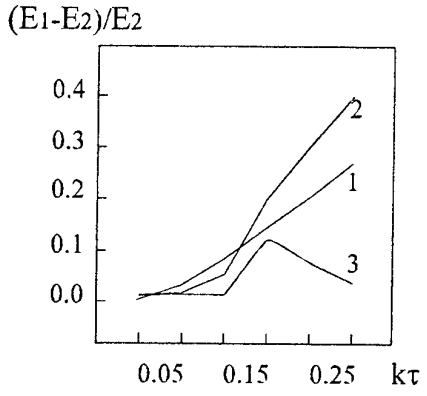


Fig. 4

In Fig. 4 graphs are shown ($ka = 2.5$, $\varepsilon_1 = (5.,-i0.1)$, $kr_0 = 6$, $\varphi_0 = 0^0$) for the different electric constants of the shell: $\varepsilon_2 = (20.,-i15.)$ (curve 1), $\varepsilon_2 = (20.,-i5.0)$ (curve 2), $\varepsilon_2 = (20.,-i0.0)$ (curve 3).

The result analysis outlines that reported approximation utilization depends upon the dielectric properties of a shell as well as on the cylinder radius. The satisfactory results for $ka = 2.5$ were obtained with cover thickness $k\tau < 0.15$.

REFERENCES

1. M. L. Rudakov. Models of biological objects at investigations of interactions with electromagnetic fields in a radio wave range. Zarubejnaja radioelectronika, 1998, №2, 68-75p. [in Russian].
2. V. V. Chechetka, A. I. Fedorenko. Excitation of multilayer cylindrical structure //Rassejanije elektromagnitnych voln, Taganrog, 1978. Is.2. [in Russian].
3. Vorontsov A. A., Mirovitskaya S. D. Specific functions of the scattering theory problems. Handbook. Moscow. Radio i Sviaz,1991. [in Russian].
4. D. L. Volakis, T. B. A. Senior. Application of a class of generalized boundary conditions to scattering on a dielectric half-plane with metal substrate. TIIER, May' 1989, v. 77, №5,176-186 p.
5. Rojas R. G., Al-hekail Z. Generalized impedance/resistive boundary conditions for electromagnetic scattering problems.-Radio Science, 1989, vol. 24, №1, pp.1-12.
6. G.T.Markov, A.F.Chaplin. Electromagnetic waves excitation. Moscow-Leningrad. Energija, 1967, 365 p.

ABOUT BRANCHING OF THE SOLUTIONS OF THE PHASE SYNTHESIS PROBLEM OF A LINEAR ANTENNA

M. I. Andriychuk

Pidstryhach Institute for Applied Problems of Mechanics and Mathematics
National Academy of Sciences of Ukraine, 3 "b" Naukova str., Lviv, 290601, Ukraine
Phone: +38-0322-651944, e-mail: andr@iapmm.lviv.ua

ABSTRACT

The phase synthesis problem of a linear antenna according to the prescribed amplitude radiation pattern in the variational statement is considered. The problem is reduced to a system of the nonlinear equations with respect to both the unknown phase distribution of current and the phase radiation pattern. The linear equation to determine the points of branching for the appropriate nonlinear equation is obtained. The investigation of this linear equation is carried out numerically. The results are presented for the even prescribed amplitude radiation pattern.

STATEMENT OF PROBLEM

In the process of the statement and solving the synthesis problem according to the prescribed amplitude radiation pattern (RP) it is necessary to solve the nonlinear equations of a various type. As a rule, these equations are nonlinear integral equations of the Hammerstein type [1]. The characteristic physical parameter of antenna is contained in the kernel of these equations and if it changes, except one solution, can appear other ones, that is the branching of solutions happens. The investigation of a number of these solutions and their properties is important not only in the theoretical plan, but also in the practical one, since it allows to select that solution, which satisfies the practical requirements to antenna in the best way.

As a rule, the following functional [2]

$$\kappa = \int_{-1}^{1} F(\xi)\,|f(\xi)|\,d\xi \Big/ \int_{-1}^{1} u(x)u^{*}(x)dx \qquad (1)$$

is used as a criterion of optimization in the process of solving the phase synthesis problem. Here $F(\xi)$ is the prescribed amplitude RP (real positive function), $|f(\xi)|$ is the module of the synthesized RP, ξ is the generalized coordinate, $u(x)$ is the current in antenna.

RP $f(\xi)$ and the current $u(x)$ are connected by the known relation [3]

$$f(\xi) = Au \equiv \int_{-1}^{1} u(x)e^{i\alpha x\xi}dx\,, \qquad (2)$$

that is, the solution of the direct problem (the analysis problem) is prescribed by the explicit formula. The operational form of the writing $f = Au$ in the formula (2) will be used in further for the shortcut of entries.

The function $u(x)$ is complex. Let's present it as $u = |u|e^{i\psi}$. The phase synthesis problem consists in a maximization of the functional (1) at the expense of choice of the function ψ named as the phase of current u. Thus, its amplitude $|u|$ is considered prescribed.

METHOD OF SOLUTION

From the condition of maximum of the functional κ it is possible to obtain a system of the nonlinear equations with respect to both the unknown phase distribution ψ of current and optimal phase RP φ [2]. Uniting this system in one equation, we obtain a nonlinear integral equation for determination of the function ψ.

Investigation of the number of solution of this nonlinear equation and the properties of these solutions can be carried out numerically, using this equation directly. For this end the method of successive approximation is used. The various types of initial approximations of the desired function ψ are prescribed (for example, the functions with various properties of evenness) to obtain the various solutions [4]. At small values of the characteristic parameter c the various types of the initial approximations lead to the same solution (accordingly, the value of κ is the same too). If the parameter c increases, then the new solutions appear. The values of functional κ are various at their solutions. Thus, investigating the behavior of κ at the various solutions, it is possible to determine the points of branching.

The analytical investigation of the number of solutions for the equations of such type is connected with the essential mathematical difficulties. Such investigation is carried out for the amplitude-phase synthesis problem for linear antenna in [5] and for linear array in [6].

At small values of parameter c, included in the kernel of the obtained nonlinear equation, there is the unique solution $\psi \equiv 0$ (in further, we name its trivial). If c increases, then at the certain its values, there can be appear the other solutions. The appropriate linear equation it is necessary to deduce for the determination

of these values of c, which are named as the points of branching. In accordance with the theory of branching the nonlinear equations [1], the points of branching can be such values of parameter c, at which except the trivial solution of the linear equation there are other eigenfunctions appropriating the eigenvalue $\lambda_n = 1$.

Since, in the neighborhoods of the points of branching the branching solutions are small, we write out a linear equation for small solutions. Let's the function γ is the small increment of the trivial solution ψ_0, the function η is the small increment of the phase pattern φ_0, appropriated to the solution ψ_0. For the functions γ and η we obtain the following system of the nonlinear equations [7]

$$\gamma = \mathrm{Re}\frac{A^*(F\eta\exp(i\varphi_0))}{u_0}, \qquad (3)$$

$$\eta = \mathrm{Re}\frac{A(|u|\gamma\exp(i\psi_0))}{f_0},$$

where $u_0 = |u|\exp(i\psi_0)$, $f_0 = Au_0$. The operator A^* is determined by the formula [2]

$$A^*g = \frac{c}{2\pi}\int_{-\infty}^{\infty} g(\xi)e^{-icx\xi}d\xi. \qquad (4)$$

To simplify the equations (3), we consider the case of the symmetric both the RPs F ($F(-\xi) = F(\xi)$) and amplitude of currents u ($|u(-x)| = |u(x)|$). The system (3) in this case can be written as

$$\gamma = \frac{A^*(F\eta)}{u_0}, \quad \eta = \frac{A(|u|\gamma)}{f_0}. \qquad (5)$$

For determination of the points of branching we consider the following eigenvalue problem

$$\lambda\nu = A^*(\frac{F}{f_0}w), \quad \lambda w = A(\frac{|u|}{u_0}\nu), \qquad (6)$$

where $w = \eta f_0$, $\nu = \gamma u_0$.

Substituting the first equation of (6) into its second one, we obtain one equation with respect to the function w

$$\lambda^2 w = A(\frac{|u|}{u_0}A^*(\frac{F}{f_0}w)). \qquad (7)$$

Taking into account the expressions for the operators A and A^*, this equation can be written as

$$\lambda^2 w(\xi) = \frac{c}{2\pi}\int_{-1}^{1}\frac{F(\xi')}{f_0(\xi')}K(c,\xi-\xi')w(\xi')d\xi', \qquad (8)$$

the kernel $K(c,\xi-\xi')$ has the form

$$K(c,\xi-\xi') = \int_{-1}^{1}\exp(icx(\xi-\xi'))\frac{|u(x)|}{u_0(x)}dx. \qquad (9)$$

The functions $f_0(\xi)$ and $u_0(x)$ are determined as follows

$$f_0(\xi) = \int_{-1}^{1}|u(x)|e^{icx\xi}dx, \qquad (10)$$

$$u_0(x) = \frac{c}{2\pi}\int_{-1}^{1}F(\xi)e^{-icx\xi}d\xi. \qquad (11)$$

Thus, investigating a behavior of eigenvalues of the equation (8) with the change of parameter c, we obtain the set of values $c_i, i = 1,2,3,...$, in which $\lambda_i = 1$ (at all values of c there is a trivial solution appropriated to $\lambda_0 \equiv 1$). Those values from the set of c_i, for which the eigenfunctions appropriated the $\lambda_0 = 1$ and $\lambda_i = 1$ are various, will be the points of branching.

NUMERICAL RESULTS

Determination of the eigenvalues of the equation (8) is carried out numerically. The results are presented for the prescribed amplitude RP $F(\xi) = \cos^2(\pi\xi/2)$ for two cases of the amplitude distribution of current in Fig. 1 and Fig. 2. In the first case ($|u(x)| \equiv 1$) in the point $c = 3.62$ the eigenfunctions corresponding the eigenvalues λ_0 and λ_1 are various, it means that this point is the point of branching. In the second case ($|u(x)| = \cos(\pi x/2)$) the point $c = 5.12$ is as the point of branching.

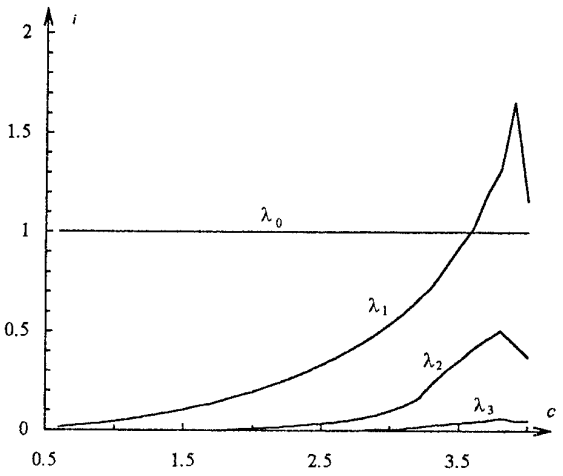


Fig. 1. The eigenvalues of the equation (8) in the case of constant amplitude of current ($|u(x)| \equiv 1$)

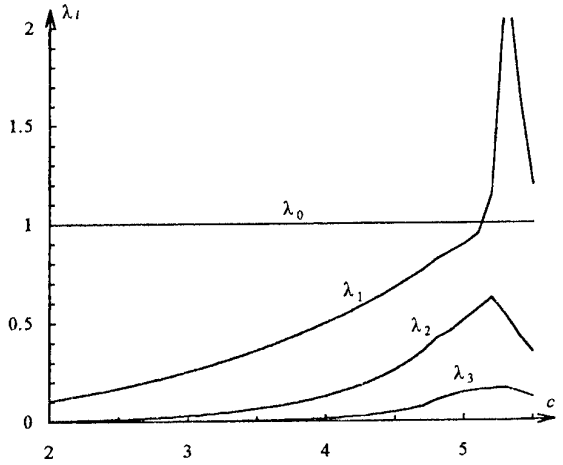


Fig. 2. The eigenvalues of the equation (8) in the case of variable amplitude of current ($|u(x)| = \cos(\pi x / 2)$)

REFERENCES

1. Veinberg M. M., Trenogin V. A. Theory of branching the solutions of the nonlinear equations. Moscow, Nauka Pub., 1969. 528 p. [in Russian].
2. Andriychuk M. I., Voitovich N. N., Savenko P. A., Tkachuk V. P. Antenna synthesis according to the amplitude radiation pattern. Numerical methods and algorithms. Kiev, Naukova Dumka Pub., 1993. 256 p. [in Russian].
3. Minkovich B. M., Yakovlev V. P. Antenna synthesis theory. Moscow, Sov. Radio Pub., 1969. 296 p. [in Russian].
4. Andriychuk M. I. "Investigation of the solutions of the nonlinear antenna synthesis problems". Proc. of Intern. Conf. on Math. Method in Electromagn. Theory (MMET-98). Kharkov, 1998, vol. 1, p. 127-129.
5. Voitovich N., Topolyuk Yu., Reshnyak O. "New closed solution of the linear antenna synthesis problem according to amplitude radiation pattern". Proc. of Intern. Conf. on Microwave & Radar (MIKON-98). Krakov, 1998, vol. 2, p. 304-307.
6. Voitovich N. N., Reshnyak O. O. "Closed solution of a nonlinear integral equation arisen in the antenna arrays synthesis theory". (DIPED-98). Lviv, 1998, p. 67-71.
7. Andriychuk M. I. "The analytical-numerical solution method of the nonlinear problems of the antenna phase synthesis". Proc. of III Intern. Seminar/Workshop on Direct and Inverse Problems of Electromagnetic and Acoustic Wave Theory (DIPED-98). Lviv-Tbilisi, 1998, p. 86-89.

SURFACE AND LATERAL WAVES OF HIGHER-ORDER BEAM WAVES

O. V. Bakumenko, N. A. Khizhnyak*

Kharkiv State University, Ukraine, Kharkiv-166, st. Lenina 3, ap. 73
*National Center - Kharkiv Institute of Physics and Technology

The problem of surface and lateral waves excitation on a plane isotropic boundary of dielectric media is considered. The uniform asymptotic for surface and lateral waves have been obtained by the integral representation of indecent beam field as a spectrum on plane waves.

Let us consider the narrow higher-order wave beam inclined to a boundary of dielectric media at an angle θ_0. Let source is located on distance h from a surface, the x axis coincides with the boundary.

The field of an incident beam can be presented as integrated decomposition on plane waves [1, 2, 5, 7]:

$$\psi_{in} = \frac{kw}{2\sqrt{\pi}} \int_{-\infty}^{+\infty} \Phi(\xi) \exp\left[ikx\xi + ik(h-z)\sqrt{1-\xi^2}\right] d\xi, \quad (1)$$
$$\xi = Sin(\theta)$$

where $\Phi(\xi) = \frac{(\xi-\xi_0)^p}{\cos^2(\theta_0)} \exp\left[-\frac{k^2w^2}{4\cos^2(\theta_0)}(\xi-\xi_0)^2\right]$ - the angular spectrum of a beam determined at $z=h$, p — the order of a beam.

Let relative refraction index n is less than 1.

The refracted field is:

$$\psi_t = \frac{kw}{2\sqrt{\pi}} \int_{-\infty}^{+\infty} \Phi(\xi) T(\xi) e^{\left[ikx\xi + ikh\sqrt{1-\xi^2} - ikz\sqrt{n^2-\xi^2}\right]} d\xi \quad (2)$$

$$T(\xi) = \frac{2m\sqrt{1-\xi^2}}{m\sqrt{1-\xi^2} + \sqrt{n^2-\xi^2}} \quad (3)$$

where: $T(\xi)$ - the plane wave factor of refraction.

In a case, when $\theta_0 > \delta$ (δ - the internal reflection angle) the refracted field is transformed to surface and lateral waves.

We make the following transformations to allocate the regular parts of integrand containing radicals [2]:

$$T(\xi) = \frac{2m\sqrt{1-\xi^2}}{m\sqrt{1-\xi^2} + \sqrt{n^2-\xi^2}} = T_1(\xi) + T_2(\xi)\sqrt{\xi-n}$$

where: $T_1(\xi) = \frac{2m^2\left(1-\xi^2\right)}{m^2-n^2-\left(m^2-1\right)\xi^2}$,

$$T_2(\xi) = -\frac{2im\sqrt{\left(1-\xi^2\right)(\xi+n)}}{m^2-n^2-\left(m^2-1\right)\xi^2}. \quad (4)$$

$$e^{\left[-ikz\sqrt{n^2-\xi^2}\right]} \equiv e^{\left[kz\sqrt{\xi^2-n^2}\right]} = \sum_{n=0}^{\infty} \frac{(kz)^l}{n!}\left(\xi^2-n^2\right)^{l/2}. \quad (5)$$

In a case, when the special points are located on great distance the asymptotical estimation of integral in expression (2) is [2, 5].

$$I = \int F(\xi) Exp[\rho f(\xi)] d\xi = I_S + I_B, \rho >> 1, \quad (6)$$

$$I_S = \sqrt{\frac{-2\pi}{\rho f''(\xi_0)}} F(\xi_0) Exp[\rho f(\xi_0)], \quad (7)$$

$$I_B = \frac{2\pi}{\partial(-\beta)} g(n) \left[\frac{-1}{\rho f'(n)}\right]^{\beta} e^{\left[\rho f(n) - \frac{i\pi}{2} - i\pi\beta\right]}, \quad (8)$$

I_S determine the surface wave, I_B determine the lateral wave.

In a case when $\theta_0 \sim \delta$, the stepdescent point ($\xi = \xi_0$) approaches the branchcut point ($\xi = n$) of the integrand. In this case it is impossible to use the classical formulas (7, 8).

The asymptotical representation can be found by using the expression for the Webber function [3, 4].

$$\tilde{I} = \int_{-\infty}^{\infty} d\xi (\xi-\xi_b)^{\beta} g(\xi) e^{\left[i\rho a(\xi-\xi_s)^2\right]} =$$

$$= \sqrt{2\pi}(2\rho a)^{-\frac{1+\beta}{2}} e^{\left[\frac{u^2}{4} + \frac{i\pi(1-\beta)}{4}\right]} \left\{g(\xi_b) D_{\beta}(u) + \right. \quad (9)$$

$$\left. + u^{-1}\left[g(\xi_s) - g(\xi_b)\right] D_{\beta+1}(u)\left[1 + O\left(\rho^{-1}\right)\right]\right\}$$

$$u = \sqrt{2\rho a}(\xi_b - \xi_s) Exp\left[-i\frac{3\pi}{4}\right].$$

For the estimates expression (6), it is necessary to make the following transformations:

$$f(\xi)=f(\xi_0)+\frac{f''}{2}\left[(\xi-\xi_0)+\frac{f'}{f''}\right]^2-\frac{f'^2}{2f''},$$
$$a=\frac{f''}{2i}\left[(\xi-\xi_0)+\frac{f'}{f''}\right]^2\frac{1}{\xi-\xi_0}. \quad (10)$$

Then: $I=Exp\left[-\rho\frac{f'^2}{2f''}\right]\int_{-\infty}^{\infty}d\xi(\xi-\xi_b)^{\beta}g(\xi)e^{\left[i\rho a(\xi-\xi_s)^2\right]}.$

We obtain uniform asimptotical estimate for the field in the bottom half-space.

$$\psi_t=\frac{kw}{2\sqrt{\pi}}\sum_{n=0}^{\infty}\frac{(kz)^{l+p}}{n!}(\xi+n)^{l+p/2}\sqrt{\frac{\pi}{\alpha}}T_1(n)(2\alpha)^{-1/4}\times$$
$$\times e^{\left[\frac{u^2}{4}+\frac{i\pi(1-\beta_1)}{4}\right]}D_{\beta_1}(u)e^{\left[-\frac{k^2}{4\alpha}(x-hTan(\theta_0))^2\right]}\times$$
$$\times\left[1+O\left(\frac{1}{kw}\right)\right]+\frac{kw}{2\sqrt{\pi}}\sum_{n=0}^{\infty}\frac{(kz)^{l+p}}{n!}(\xi+n)^{l+p/2}\times$$
$$\times\sqrt{\frac{\pi}{\alpha}}T_2(n)(2\alpha)^{-1/4}e^{\left[\frac{u^2}{4}+\frac{i\pi(1-\beta_2)}{4}\right]}\times$$
$$\times D_{\beta_2}(u)e^{\left[-\frac{k^2}{4\alpha}(x-hTan(\theta_0))^2\right]}\left[1+O\left(\frac{1}{kw}\right)\right],$$

where: $u=\sqrt{2\alpha}\left[\frac{k(h*tg(\theta_0)-x)}{2\alpha}-i(n-\xi_0)\right],$

$$\alpha=-\frac{k^2w^2}{4Cos^2(\theta_0)}+\frac{ikh}{2Cos^3(\theta_0)},\ \beta_1=\frac{n}{2},\beta_2=\frac{n+1}{2}.$$

Thus, the uniform asimptotical representation based on the integral representation of a higher-order beam allowing to estimate the excitation of surface and lateral waves on the boundary of dielectric media has been obtained.

REFERENCES

1. L. M. Brechovskih. Waves in layered media. Moscow, Academy of sciences USSR, 1957, 502 p. [in Russian].
2. O. A. Godin, L. M. Brechovskih. Acoustics of layered media. Moscow, Science, 1989, 416 p. [in Russian].
3. I. E. Kireev, K. A. Karpov. The tables of Webber function. Moscow. AS USSR, 1959, 344 p. [in Russian].
4. E. T. Uitecer, D. N. Vatson. A rate of the modern analysis. Moscow, 1963, 516 p. [in Russian].
5. L. Felsen, N. Markuvich. Radiation and dispersion of waves. Moscow, World, 1978, 534 p. [in Russian].
6. T. Tamir, B. Horovitzt. JOSA. 1971, vol. 61, ¹ 5, pp. 586-594.

THE MODEL OF GRAZING HF VERTICALLY POLARIZED RADIO WAVES BACKSCATTERING BY SEA SURFACE WAVES

G. N. Bondarchuk, I. I. Zarudnev, Y. A. Lupan, J. G. Mugenov, S. Y. Platonov

National Research Center of Defense Technologies & Military Security of Ukraine
Zip code 254119, 81, Melnikov str., Kyiv, Ukraine
Phone: [380] (044) 219-38-59

The new model of HF vertically polarized grazing radio wave backward scattered by agitated sea surface is based on the proposed analogy between the sea surface wave and statistically irregular system for electromagnetic wave channellisation. By comparison with the well known model of Barrick [1, 2] utilizing the mathematical methods of solid state physics the proposed model is more simple and obvious and its assumptions are in better correlation with the detected physical phenomena.

Both theories utilize as their base Pirson and Lounge-Higgins description of random sea surface [3]. But if Barrick theory composes such surface with the help of random sea wave amplitudes and random sea wave directions of propagation, the proposed theory adds to them the random variations of partial sea wave space period and uses the multiscale notion of sea agitation [4]. The proposed theory also utilizes the experimentally detected facts that:

- the sea waves with the length $L_i = (5...25)$ m comparable to the length of HF waves are always presented in oceans and developed to their maximum allowable heights limited by breaking [1,2,5]:

$$h_{inm} \le {}^{1}/_{\gamma} L_i , \qquad (1)$$

- and the random variations of the partial sea wave lengths are also limited by the magnitude [3]

$$\Delta L_i \le 0.35 L_i . \qquad (2)$$

Here i is index of partial wave and (n,m) – marked the space position of sea wave arbitrary crest on the detected area S.

Let's draw through the crest foots positioned on the limited sea area S the local virtual boundary surface and consider it to be plane due to the limited dimensions of aria and absolutely conductive due to the very high conductivity of sea water. The grazing vertically polarized wave will induce on the sea wave cones the surface currents I_{inm}. These currents together with their mirror reflections in virtual plane may by treated as dipoles with the lengths equal to double wave crest heights:

$$l_{inm} = 2h_{inm} \le {}^{2}/_{\gamma} L_i , \qquad (3)$$

and dipole moments:

$$\vec{p}_{imn} = \frac{\vec{n} \cdot I}{j\varpi} \cdot 2h_{inm} . \qquad (4)$$

The electromagnetic fare zone field reilluminated (scattered) by any dipole thus will be:

$$\vec{E}_{inm} = \sqrt{\frac{\mu}{\varepsilon}} \cdot \vec{H}_{inm} = \frac{\varpi^2 \mu^2}{4\pi} \vec{i}_y p_{imn} \frac{e^{j(\varpi t + kR_0)}}{R_0} \sin\beta , \qquad (5)$$

provided one choose the 0Y-axis parallel to $\vec{p}$ and R_0, β,γ, to characterize the scatter direction (Fig. 1).

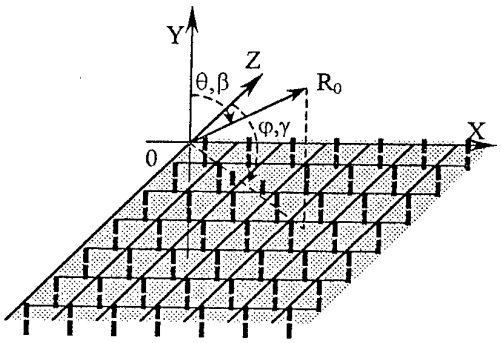


Fig. 1. The simplest square cell dipole array model and coordinate system choice

The crotches between sea wave crests are always filled by ripples thus the virtual plane can be considered to be rough and the electromagnetic field dispersed by this roughness must meet Leontovich boundary condition [6]. Therefore, it is only natural to model HF backscattering by the crests with the help of multitude of nearly regular arrays and supplement it with statistically irregular roughness to model the ripples in the crotches.

Let's illustrate the process of modeling with the help of the simplest square cell dipole array shown in Fig. 1.

Indicating the mean values of random variables h_{inm}, p_{inm}, L_{inm} for i-type developed partial sea wave as $\overline{h}_{inm}, \overline{p}_{inm}, \overline{L}_{inm}$ one can represent the far zone field dispersed by such array as:

$$\vec{E}(\theta,\varphi,\beta,\gamma) = C \cdot \exp\{j[(\varpi \pm \varpi_D)t + kR_0]\} \, {}^{1}/_{R_0} \times$$

$$\times \sum_{n=1,m=1}^{N,M} \begin{bmatrix} (\bar{p}_{yi} \pm \Delta_{nm} p_i) \times \\ \times \exp\left[k(n\bar{L}_i \pm \Delta_{nmz} L_i)(\sin\theta\cos\varphi + \sin\beta\cos\gamma)\right] \times \\ \times \exp\left[k(m\bar{L}_i \pm \Delta_{nmx} L_i)(\sin\theta\sin\varphi + \sin\beta\sin\gamma)\right] \end{bmatrix} + \bar{E}_r \tag{6}$$

where

ω_D is Doppler frequency shift due to the sea wave phase velocity V_{ph} equal to

$$\varpi_D = \frac{4\pi V_{ph}}{\lambda}\cos\varphi = \frac{2}{\lambda}\sqrt{\pi g\,\bar{L}_i}\cos\varphi\,; \tag{7}$$

g — gravity acceleration;

$$C = \frac{\varpi^2\mu^2}{4\pi}\sin\beta\,;$$

$\Delta_{nm}p_i$, $\Delta_{nmz,x}$ L_i — random Gaussian deviations from $\bar{p}_{yi}$, $\bar{L}_i$; θ,φ — the incident wave propagation angles; $N\times M$ — mean number of i-type sea wave crests within aria S perimeter ($N>>1$, $M>>1$) and $\bar{E}_r$ — the field scattered by ripples.

Let the incident plane vertically polarized electromagnetic wave propagates along the virtual plane in the direction parallel to square cell array column, that is in the direction of propagated sea wave. Furthermore let's assume that in the absence of strictly determined L_i Bragg scattering conditions:

$$\bar{L}_i = K\frac{\lambda}{2} \quad ,(K = 1,2,3...) \tag{8}$$

are satisfied for the average space period meaning - $\bar{L}_i$. Then the density of flow of backscattered power is characterized by: $\begin{matrix}\sin\theta\cos\varphi + \sin\beta\cos\gamma = 2,\\ \sin\theta\sin\varphi + \sin\beta\sin\gamma = 0\end{matrix}$ will be represented by the average real meaning of Umov-Pointing vector as:

$$\mathrm{Re}\langle\vec{\Pi}\rangle = \frac{1}{2}\mathrm{Re}\left[E_0 \times H_\varphi^*\right]\vec{i}_R = \mathrm{Re}\left\{\langle\vec{\Pi}_{dipole}\rangle \times \right.$$

$$\left. \times \sum_{n,m}^{\frac{N}{K},\frac{M}{K}} \sum_{\ell,s}^{\frac{N}{K},\frac{M}{K}} \begin{bmatrix} (1\pm\delta_{pmn})(1\pm\delta_{p\ell s}) \times \\ \times \exp\{j\frac{4\pi\bar{L}_i}{\lambda}[(n-\ell)\pm(\delta_{Lnmz} - \delta_{L\ell sz}]\} \end{bmatrix} \right\} =$$

$$= \mathrm{Re}\left\{\langle\vec{\Pi}_{dipole}\rangle \sum_{n,m}^{\frac{N}{K},\frac{M}{K}} \sum_{\ell,s}^{\frac{N}{K},\frac{M}{K}} \begin{bmatrix} (1\pm\delta_{pmn})(1\pm\delta_{p\ell s}) \times \\ \times \exp\{\pm j2\pi K(\delta_{Lnmz} - \delta_{L\ell sz}\} \end{bmatrix} \right\} \tag{9}$$

Here:

$\langle\vec{\Pi}\rangle$ is the average meaning of Umov-Pointing vector;

$$\delta_{pnm} = \frac{\Delta_{nm} p_i}{\bar{p}_{iy}}, \quad \delta_{Lnmz} = \frac{\Delta_{nmz} L_i}{\bar{L}_i}, \tag{10}$$

and

$$\overline{\Pi}_{dipole} = \frac{\varpi\left(\frac{2\pi}{\lambda}\right)^3 \bar{p}_{iy}^2}{32\pi^2 R_0^2 \varepsilon}\cdot\vec{i}_z, \tag{11}$$

coincides for fare zone with its real meaning.

As to the deposition of the ripples to the scattered energy it is negligibly small. That was shown by direct solution of the boundary problem at Leontovich condition. Thus the power arising and scatterring by the array cells (the crotches) due to the fields induced by nearby dipoles is negligible small as well.

The

$$\mathrm{Re}\left\{\exp\left[\pm j2\pi K(\delta_{Lnmz} - \delta_{L\ell sz})\right]\right\} = 1 -$$

$$-\frac{1}{2}(2\pi K)^2(\delta_{Lnmz} - \delta_{L\ell sz})^2 + \ldots \approx$$

$$\approx 1 - 0.2 + 5\cdot 10^{-3}\ldots$$

even for $(\Delta\delta_L)_{\max} = 0.35$, so one can readily establish the intensities of Doppler spectrum resonant lines by calculating the root mean square value of (9). For independent δ_{pnm} and δ_{Lnm} it is equal to:

$$\mathrm{Re}\langle\vec{\Pi}\rangle_{rms} = \langle\vec{\Pi}\rangle_{dipol}\frac{1}{K^4}N^2M^2[(1-4(\pi K)^2\sigma_L^2) + \sigma_h^2] \tag{12}$$

where, because of (4),

$$\sigma_h^2 = \sigma_p^2 = \left\langle \frac{K^2}{MN}\sum_{n,m}^{\frac{N}{K},\frac{M}{K}}\delta_{pnm}^2 \right\rangle$$

$$\sigma_L^2 = \left\langle \frac{K^2}{MN}\sum_{n,m}^{\frac{N}{K},\frac{M}{K}}\left(\delta_{Lnmz}^2\right) \right\rangle \tag{13}$$

From (12) it is clear that intensities of the resonant lines in Doppler spectrum relate to one another as $1/K^4$ (where K are their numbers) and the dispersion of L_i directly reduce the intensity of resonant lines, while the dispersion of the sea wave heights enlarge Doppler spectrum background. Thus Doppler first order spectrum may be written as:

$$\left(\mathrm{Re}\left(\overline{\Pi}\right)\right)_{rms} = \left\langle\overline{\Pi}\right\rangle_{dipole}\left\{\frac{N^2M^2}{K^4}\times\right.$$
$$\left.\times\left[1-2(\pi K)^2\sigma_L^2\right]\cdot\delta\left(\varpi\pm\sqrt{K}\sqrt{\frac{4\pi}{\lambda}g}\right)+\sigma_h^2\frac{N^2M^2}{K^4}\right\}, \quad (14)$$

where $\delta(\omega)$ is Dirack δ-function.

The enlargement of the sea wave space period dispersion even in the limits (3) may course the distraction of all resonant maximums (besides, the first) when

$$4(\pi K)^2\sigma_L \geq 1, \quad (15)$$

The background in these cases will transform into:

$$\frac{N^2M^2}{K^4}\left[\left(4(\pi K)^2\sigma_L^2-1\right)+\sigma_h^2\right] \quad (16)$$

The typical experimental Doppler spectrum of electromagnetic wave backscattered by agitated sea surface is shown in Fig. 2.

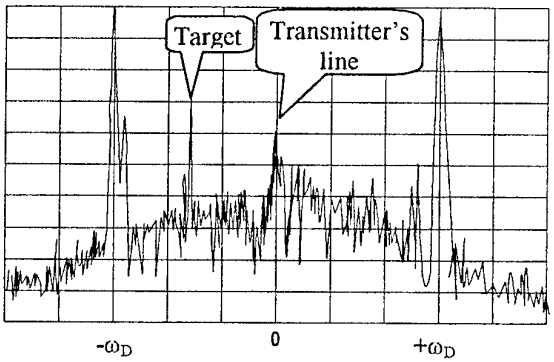


Fig.2. The experimental Doppler spectrum of backscattering from limited area of Black sea (strong wind weather conditions)

If to denote through G the array gain and through σ_S the S aria cross-section for backscattering then σ_S may be easily calculated as $\sigma_S = GS$. The gain efficient of the equivalent plane array having the same area S and sited normally to the virtual surface can be readily write for resonant lines Doppler spectrum [7]:

$$G = G_{cell}\frac{MN}{K^2}\left(1-\left|\Gamma(\varpi)\right|^2\right). \quad (17)$$

As in array cell is sited the only dipole and the scattering coefficient:

$$\left|\Gamma(\varpi)\right|^2 \cong 4(\pi K)^2\sigma_L^2$$

takes in the consideration omnidirectional scattering and partly dipole interactions so with the accuracy to background level:

$$G_{cell} \cong G_{dipole}\left(1-4(\pi K)^2\sigma_L^2\right). \quad (18)$$

The cell area S is equal to $\lambda^2K^2/4$ thus:

$$G_{dipole}\left(\frac{\lambda^2K^2}{4}\right)\cdot\left(1-4(\pi K)^2\sigma_L^2\right)\cdot\left(\frac{\lambda^2K^2}{4}\right)^{-1} =$$
$$= \sigma_{dipole}\left(\frac{\lambda^2K^2}{4}\right)^{-1}\left(1-4(\pi K)^2\sigma_L^2\right) =$$
$$= \sigma_0\left(1-4(\pi K)^2\sigma_L^2\right)$$

where σ_0 is maximum specific cross-section so that

$$\sigma_S = \sigma_0\left(1-4(\pi K)^2\sigma_L^2\right)S \quad (19)$$

Dipole dimension being limited by $h_{inm} \leq \frac{L_{inm}}{7} \leq \frac{\lambda}{14}$ upon the virtual plane the dipole must be Raleigh scatterer with the cross-section

$$\sigma_{dipole} = 4.44\cdot10^4\left(\frac{h_{inm}}{\lambda}\right)^4 h_{inm}^2 \quad (20)$$

Thus for $K = 1$:

$$\sigma_0 = 17.6\cdot10^4\left(\frac{1}{14}\right)^6 = 2.2\cdot10^{-2} \quad , \quad (21)$$

or nearly –17dB.

This corresponds with the results of the experimental measurements and Barrik's calculations [1, 2].

For present or foreseen weather conditions one can estimate the mean magnitude of the developed sea wave heights by the Douglas scale [5] and their periods from (1) and thus calculate by the help of the model the passive interferencies maximum intensity for over-the-horizon radar naval route.

REFERENCES

1. D. E. Barrick. First – Order Theory and Analysis of MF/HF/VHF Scatter from the Sea.// IEEE Transactions On Antennas and Propagation, 1972, Vol. AP – 20, No.1, pp 2-10.
2. D. E. Barrick, J. M. Headrick, R. W. Bogle, D. D. Crombie. Sea Backscatter at HF: Interpretation and Utilization of the Echo.// Proceedings of the IEEE, 1974, Vol. 62, No. 6 pp 673 – 680.
3. Kononkova G.E. Dynamics of sea waves, Moscow, Moscow State Univ., 1969, 206 p. [in Russian].
4. Zjukov B.S. Physical principles of remote sensing. Earth exploration from space. Moscow, VINITI AS USSR, 1987, p. 6 – 87 [in Russian].
5. Handbook on radar engineering. Edit. By Scolnik M. Volume 1., Moscow, Sov.Radio, 1976, 456 p. [in Russian].
6. Bass F.G., Fuks I.M. Wave sacattering by statistically rough surface, Moscow, Nauka, 1972, 424 p. [in Russian].
7. Microwave scanning antennas, edited by Hansen R.C., Academic press New-York & London 1966 pp.490.

TRANSFORMATION OF WAVE BEAMS AT PLANE WITH OSCILLATED ANISOTROPIC PERTURBATION OF SURFACE IMPEDANCE

V. F. Borulko

Dept. of Radiophysics, Dniepropetrovsk State Univ.,
13 Naukovy St., Dniepropetrovsk 320625 Ukraine
Tel: 38 0562 7254592, Fax 38 0562 465523 E-mail: garry@rff.dsu.dp.ua

INTRODUCTION

The consideration of electromagnetic wave propagation in irregular waveguiding structures usually assumes either smooth variation of medium parameters [1] or their rigorously periodical perturbation [2, 3]. Combination of smooth and oscillated parameter perturbations leads to additional peculiarities of Bragg scattering [4]. Anisotropy of parameters causes coupling of waves with different polarization [3]. In the present paper the mutual transformation of waves in open guided structures has been theoretically considered using a complex form [4] of the asymptotic method of Krylov, Bogoliubov and Mitropolsky (KBM) [5]. The influence of surface waves on scattering TM and TE wave beams by a surface with spatially oscillated anisotropic surface impedance has been analyzed. For some types of perturbations analytical solutions to coupled-wave equations with the KBM method have been obtained and expressions for perturbed wavenumbers of eigenwaves have been derived. Comparisons with some known in literature results have been done. In general case the differential equations with slowly varying coefficients are rather easily integrated numerically. Longitudinal distributions of wave complex amplitudes describe a combination of different physical phenomena in the considered structure.

METHOD OF ANALYSIS

If a volume wave falls on a surface with spatial variation of parameter it could expect that scattered field would essentially differ from mirror reflected one only under strong distortion of boundary shape. But if the incident wave can excite surface wave propagating in the structure a reflected wave would be essentially differed from the mirror one even if a surface perturbation amplitude is small. In the paper physical effects of coupling of paraxial wave electromagnetic TM and TE beams incident on a surface with spatially oscillated surface anisotropic impedance and TM surface wave propagating along this surface are theoretically investigated. This electromagnetics problem is also important when we consider transmitting antennas that transform the surface wave into the volume one by nonperiodical diffraction grating or receiving antenna that transform plane wave or wave beam into surface wave. When perturbation amplitudes are small, the consideration of such a structure is usually carried out by expansion in space Floquet harmonics or by perturbation method based on overlapping integrals [2]. The first approach is limited by rigorously periodical perturbation functions; the second one does not allow obtaining higher approximations.

In the present work the asymptotic method [4] based on ideas of KBM method [5] has been used. Oscillated anisotropic perturbations are expressed as sum of sinusoidal components with small amplitudes smoothly varying along longitudinal coordinate. Heat loss is taken into consideration by introducing small real part of impedance. Amplitudes of incident TM and TE wave beams are smoothly varied across the beam. The same small parameter β is used for all small values and as smoothness parameter. For the case when $\partial/\partial x \equiv 0$, all components of electromagnetic field are expressed in terms of x component of magnetic and electric fields H_x and E_x. The potential functions $H(y,z) \equiv H_x$ and $E(y,z) \equiv E_x$ are determined by the solution of the following boundary-value problem:

$$\frac{\partial^2 H}{\partial z^2}+\frac{\partial^2 H}{\partial y^2}+k^2 H=0,\qquad \frac{\partial^2 E}{\partial z^2}+\frac{\partial^2 E}{\partial y^2}+k^2 E=0, \tag{1}$$

$$\left(\frac{\partial H}{\partial y}+w_H H+w_{HE}\frac{\partial E}{\partial y}\right)\Bigg|_{y=0}=0,\qquad \left(E+w_E\frac{\partial E}{\partial y}-Z_{xx}H\right)\Bigg|_{y=0}=0, \tag{2}$$

where parameters w_H, w_{HE} and w_E are expressed through components of surface impedance tensor $\mathbf{Z}$. Impedance parameters as functions of longitudinal coordinate are supposed to be expressed in a form of sums of spatial harmonics of perturbation and unperturbed constant values. In the present paper we assume that unperturbed impedance tensor has only nondiagonal components, so the following expressions are valid:

$$w_H = i\omega\varepsilon Z_{zx} = w_{H,0} + \beta\sum_j w_{H,j}(\beta z)\exp(i\chi_j z) - i\beta^2 w_{H,0}'',$$

$$w_E = iZ_{xz}/(\omega\mu) = w_{E,0} + \beta\sum_j w_{E,j}(\beta z)\exp(i\chi_j z),$$

$$w_{HE} = \varepsilon Z_{zz}/\mu = \beta\sum_j w_{HE,j}(\beta z)\exp(i\chi_j z),$$

$$Z_{xx} = -\beta\sum_j w_{EH,j}(\beta z)\exp(i\chi_j z),$$

where χ_j is a wavenumber of the jth spatial harmonics of the perturbation, $w_{H,j}$, $w_{E,j}$, $w_{HE,j}$ and $w_{EH,j}$ are amplitudes of these harmonics. Alongside with longitudinal coordinate z we introduce a "smooth" variable $\zeta = \beta z$ (values which are functions of ζ smoothly vary along z). The Bragg resonant coupling of a surface wave and TM and TE wave beams occurs, when the wavenumber mismatch $\eta = k_z + \chi_p - h$ becomes small. Here k_z is a longitudinal wavenumber of beams, h is a longitudinal wavenumber of the surface wave, and p is the number of a spatial harmonic of the perturbation ensuring Bragg coupling.

The solution to the boundary-value problem (1), (2) will be searched as an asymptotic series on orders of small parameter β

$$\begin{aligned} H &= a_s\exp(-ihz - w_{H,0}y) + \beta a_H(\zeta + \beta y k_z/k_y)\exp(-i(k_z z - k_y y)) + \Gamma_H\beta a_H(\zeta - \beta y k_z/k_y)\exp(-i(k_z z + k_y y)) + \\ &+ \beta u_1(a_s, k_z z, hz, \chi z, \zeta, y) + \beta^2 u_2(a_s, k_z z, hz, \chi z, \zeta, y) + \ldots, \\ E &= \beta a_E(\zeta + \beta y k_z/k_y)\exp(-i(k_z z - k_y y)) + \Gamma_E\beta a_E(\zeta - \beta y k_z/k_y)\exp(-i(k_z z + k_y y)) + \\ &+ \beta v_1(a_s, k_z z, hz, \chi z, \zeta, y) + \beta^2 v_2(a_s, k_z z, hz, \chi z, \zeta, y) + \ldots, \end{aligned} \tag{3}$$

where $\Gamma_H = (ik_y + w_{H,0})/(ik_y - w_{H,0})$ and $\Gamma_E = (ik_y w_{E,0} + 1)/(ik_y w_{E,0} - 1)$ are the reflectivities of plane waves from an undisturbed impedance plane, $k_y = \sqrt{k^2 - k_z^2}$, a_H and a_E are distributions of amplitudes of wave beams, u_n and v_n (n = 1, 2,...) are 2π-periodic versus $k_z z$, hz and $\chi_j z$ functions to be found. Complex amplitude a_s of the surface wave pursuant to ideas of Krylov-Bogoliubov-Mitropolsky asymptotic method is determined by a following differential equation:

$$\frac{da_s}{dz} = \beta B_1(a_s, \zeta, \alpha) + \beta^2 B_2(a_s, \zeta, \alpha) + \ldots, \tag{4}$$

where $\alpha = \eta z$ is phase mismatching from the resonance, B_n (n = 1,2,...) are 2π-periodic versus α functions fitted from a condition of absence of infinitely increasing addends (when $z \to \infty$ and $\eta \to 0$) in u_n and v_n. Substituting the expansion (3) into the equation (1) and the boundary conditions (2) using (4) and equating expressions at identical orders of β, we obtain a sequence of boundary-value problems for u_n and v_n. These boundary-value problems are solved at the "frozen" values of a_s and parameters that are functions of ζ and βy.

In the second approximation on small parameter value B_2 can be obtained as

$$B_2 = a_s A_2 + \exp(-i\eta z)(a_H G_{2,H} + a_E G_{2,E}), \tag{5}$$

where

$$A_2 = -iw_{H,0}\left\{\sum_j \left[w_{HE,j}w_{EH,-j}ik_{-j}/(ik_{-j}w_{E,0} - 1) - w_{H,j}w_{H,-j}/(ik_{-j} - w_{H,0})\right] - iw''_{H,0}\right\}/h$$

and $G_{2,H} = 4w_{H,-p}k_y w_{H,0}/[(2h + \eta)(ik_y - w_{H,0})]$, $G_{2,E} = 4w_{HE,-p}k_y w_{H,0}/[(2h + \eta)(ik_y - w_{H,0})]$.

Solving the equation (4) using (5) it is possible to find a variation of amplitude of the surface wave along longitudinal coordinate z. Then we obtain the field, radiated from the surface.

THE PHYSICAL EFFECTS

Real part of A_2 describes the attenuation caused by heat losses and leaking energy of surface wave into energy of volume spatial harmonics. Parameters $G_{2,H}$ and $G_{2,E}$ characterize transformation energy of falling TM and TE wave beams into energy of the surface wave. For lossless impedance, value $|G_{2,H}|$ does not change when changing directions of waves propagation or polarity of ferrite magnetization. But value $|G_{2,E}|$ can change essentially in these cases. Special choice of corrugation tilt and magnetization ensures non-zero value of $G_{2,E}$ for only one propagation direction and zero one for opposite direction. General field radiated from impedance plane in mirror direction is composed of unperturbed reflected wave and pth volume spatial harmonic excited by scattering surface wave on the surface impedance perturbation.

In simple particular case of strictly sinusoidal disturbances and strictly plane falling wave we can write the expression for complex amplitude of surface wave a_s

$$a_s = -\exp(-i\eta z)\left(a_H G_{2,H} + a_E G_{2,E}\right)/(A_2 + i\eta/\beta^2)$$

Some physical effects observed in the structures with perturbed isotropic surface impedance have been discussed in [6]. Anisotropy of perturbation allows to couple waves with different polarization. Gyrotropy of impedance causes nonreciprocity of reflection tensor. In particular case the considered structure can serve as circulator concerning incident and reflected TM and TE plane waves.

Distortion of rigorous exponentiality of perturbations and incident wave changes physical pattern in principle – the amplitude of a surface wave varying from " minus infinity " enters into operation. In this case the solution of the equation (4) has a form:

$$a_s(z) = \exp\left(\int_{-\infty}^{z} \beta^2 A_2 dz\right)\left[a_s(-\infty) + \int_{-\infty}^{z} \beta^2 \left(a_H G_{2,H} + a_E G_{2,E}\right)\exp\left(-i\eta z - \int_{-\infty}^{z} \beta^2 A_2 dz\right) dz\right]$$

The considered structure can be used as nonreciprocal reflector, transmitting or receiving antenna. It is very important that antenna patterns for reception and transmission are essentially different. Special choice of parameters allow to use the structure as circulator concerning surface waves and TE wave beams.

CONCLUSIONS

Combination of various perturbations considered above can secure extremely wide possibilities of wave transformations. Asymptotic methods based on method of Krylov, Bogoliubov and Mitropolsky have wider field of applications than Floquet or coupled-wave methods. Formulas obtained in the work can be used for analysis of radio-wave scattering by structures with small surface nonperiodically oscillated perturbations of parameters and for designing reflectors and leaky-wave antennas or nonreciprocal devices which combined some functions.

REFERENCES

1. M. Babich, V. S. Buldyrev *Short-wavelength diffraction theory (Asymptotic methods).* New York: Springer, 1991.
2. C. Elashi, "Waves in active and passive periodic structures: A review," *Proc. IEEE*, vol. 64, pp.1666-1698, Dec. 1976.
3. K. Araki and T. Itoh "Analysis of periodic ferrite slab waveguides by means of improved perturbation method" *IEEE Trans. Microwave Theory Tech.*, vol. MTT-29, pp. 911-916. Sept. 1981.
4. V. F. Borulko "Waves in nonregular rectangular waveguide with helical corrugation gyrotropic filling " *in Proc. of the 16th URSI Int. Symp. on Electromagnetic Theory.* - Thessaloniki (Greece), 1998. - pp. 54-56.
5. N. N. Bogolyubov, Yu. A. Mitropolsky, *Asymptotic Methods in the Theory of Nonlinear Oscillations.* New York 1961,
6. V. F. Borulko, V. E. Ivanilov "Coupling of wave beam with surface wave at oscillated perturbation of surface impedance" *in Proc. of XXVIII Moscow International Conference "Antenna theory and techniques".* - Moscow. - 1998. - P. 180-183 [in Russian].

REFLECTION OF SURFACE WAVE AND THEIR COUPLING WITH WAVE BEAM AT PERTURBATED IMPEDANCE PLANE

V. F. Borulko, V. E. Ivanilov

Dept. of Radiophysics, Dniepropetrovsk State Univ.,
13 Naukovy St., Dniepropetrovsk 320625 Ukraine
Tel: 38 0562 7254592, Fax 38 0562 465523 E-mail: garry@rff.dsu.dp.ua

INTRODUCTION

In open periodic waveguiding structures Bragg scattering can be observed in different forms [1]. Type of the wave transformation depend on from a value of perturbation period. If a perturbation wavenumber is twice as large as longitudinal wavenumber of surface wave, then coupling of two surface waves with opposite propagation directions occurs, that is reflection of surface waves is observed [2]. If a wavenumber of the perturbation is equal to difference of longitudinal wavenumbers of surface and volume waves then a coupling of these waves secures, that is why we can obtain output of radiation from structure [3]. Open inhomogeneous structures become more interesting and useful when parameter perturbation is not periodic. If amplitudes of spatial harmonics of perturbation are not constant, input of incident radiation into open waveguide is possible [4]. It is theoretically and practically important to consider combination of these phenomena [5]. Such a combination is more easily achieved for not equidistant wavenumbers of perturbation space harmonics.

In the present paper physical effects of coupling of waves at plane with spatially oscillated surface impedance are theoretically investigated. A combination of two processes is investigated. The first process is reflection of surface waves propagating along impedance surface. The second process is an input-output coupling of incident paraxial wave electromagnetic beam with both surface waves. This electromagnetics problem is important for consideration of devices combining functions of antenna and microwave generator.

METHOD OF ANALYSIS

In the present work an asymptotic method [6] based on ideas of KBM method [7] has been applied. Oscillated perturbation is assumed to be expressed as sum of sinusoidal components with small amplitudes smoothly varying along longitudinal coordinate. Heat loss is taken into consideration by introducing of small real part of impedance. Incident wave beam amplitude is smoothly varied across beam. The same small nondimensional parameter β is used for all small values and as smoothness parameter. For the case of TM-waves all components of electromagnetic field are expressed in terms of x component of magnetic field H. The function $H(y,z) \equiv H_x$ is determined by the solution of the following boundary-value problem:

$$\frac{\partial^2 H}{\partial z^2}+\frac{\partial^2 H}{\partial y^2}+k^2 H=0, \qquad (1)$$

$$\left\{\frac{\partial H}{\partial y}+\left[w+\beta\sum_j w_j(\beta z)\exp\left(i\chi_j z\right)+\right.\right.$$

$$\left.\left.+\beta^2\sum_{j,l} w_{j,l}(\beta z)\exp\left(i\chi_j z+i\chi_l z\right)\right]H\right\}\Big|_{y=0}=0, \qquad (2)$$

where βw_j and $\beta^2 w_{j,l}$ are amplitudes of the perturbation harmonics, and χ_j are their wavenumbers.

The Bragg resonant coupling of each surface wave and wave beam occurs, when the wavenumber mismatches $\eta_{v,s} = k_z + \chi_{pv(s)} - h_s$ (s = 1, 2) become small. Here k_z is a longitudinal wavenumber of the beam, h is a longitudinal wavenumber of the surface wave, and pv(s) is integer-value function that coincide with the number of a spatial harmonic of the perturbation ensuring Bragg coupling. The Bragg reflection of a surface wave is observed if wavenumber mismatches $\eta_{S,s,l} = -2h_s - \chi_l - \chi_{ps(s,l)}$ are close to zero. Combinational resonance for reflection process is considered because in this case reflection and radiation have the same order of influence on the amplitudes of the surface waves.

The solution of the boundary-value problem (1), (2) will be searched as an asymptotic series on orders of small parameter β

$$\begin{aligned} H=\sum_{s=1}^{2} a_s\exp\left(-ih_s z-wy\right)+\beta a_H\left(\zeta+\beta y k_z/k_y\right)\times \\ \times\exp\left(-ik_z z+ik_y y\right) \\ +\Gamma\beta a_H\left(\zeta-\beta y k_z/k_y\right)\exp\left(-ik_z z+k_y y\right)+ \\ +\beta u_1\left(a_1,a_2,k_z z,hz,\chi z,\zeta,y\right)+ \\ +\beta^2 u_2\left(a_1,a_2,k_z z,hz,\chi z,\zeta,y\right)+\ldots, \end{aligned} \qquad (3)$$

where $k_y = \sqrt{k^2 - k_z^2}$ is transverse wavenumber of the beam, $\zeta = \beta z$ is a «smooth» variable (values that are functions of ζ smoothly vary along z). $\Gamma = \left(ik_y + w\right)/\left(ik_y - w\right)$ is the reflection coefficient of a plane wave from an undisturbed impedance plane, a_H is distribution of amplitude of the wave beam,

u_n (n = 1, 2,...) are 2π-periodic versus $k_z z$, $h_s z$ and $\chi_j z$ functions which are being a subject to determination. Complex amplitudes a_s of the surface waves pursuant to ideas of the Krylov-Bogoliubov-Mitropolsky asymptotic method is determined by the following differential equations:

$$\frac{da_s}{dz} = \beta B_{s,1}(a_1, a_2, \zeta, \alpha) + \\ + \beta^2 B_{s,2}(a_1, a_2, \zeta, \alpha) + ..., \quad (4)$$

where $\alpha = \eta z$ are phase mismatches from the resonances, B_n (n = 1,2,...) are 2π-periodic versus α functions fitted from a condition of absence of infinitely increasing addends (when $z \to \infty$ and $\eta \to 0$). in u_n.

Substituting the expansion (3) into the equation (1) and the boundary conditions (2) utilizing (4) and equating expressions at identical orders of β, we obtain a sequence of boundary-value problems for u_n. These boundary-value problems is solved at the «frozen» values of a_s and parameters that are functions of ζ and $\beta\gamma$.

As the first approximation on a small parameter the solution has a form

$$u_1 = \sum_{s=1}^{2} a_s \sum_j w_j \exp(-ih_s z + i\chi_j z - ik_{s,j} y)/(ik_{s,j} - w), \\ B_1 = 0, \quad (5)$$

where the transversal wavenumbers k_{sj} of spatial harmonics of the field are determined from the relations

$$k_{sj}^2 = k^2 - (-h_s + \chi_j)^2,$$

$\mathrm{Re}(k_{s,j}) > 0$, if $\mathrm{Re}(k_{s,j}^2) > 0$ (radiated harmonics),

or $\mathrm{Im}(k_{s,j}) < 0$, if $\mathrm{Re}(k_{s,j}^2) < 0$ (surface harmonics).

Total radiated field consists of three parts – the first part is undisturbed reflected field, the second and the third ones are volume space harmonics exited by scattering of forward and backward surface waves on perturbations of the surface impedance. It is necessary to pay attention to that if $\eta = 0$ the pv(1)-th volume harmonic associated with the forward surface wave and the pv(2)-th volume harmonic associated with the backward surface wave are radiated in the same direction as mirror reflected beam. Proceeding from this, it is possible to enter the resultant amplitude $\beta a_{H,R}$ for field radiating in a mirror direction by the formula

$$\beta a_{H,R} = \beta a_H \Gamma + \sum_{s=1}^{2} a_s \exp\frac{(-i\eta_{V,s} z)\beta w_{\mathrm{pv}(s)}}{(ik_{s,\mathrm{pv}(s)} - w)} \quad (6)$$

In the second approximation on small parameter value $B_{s,2}$ can be obtained as

$$B_{s,2} = a_s A_{s,2} + \exp(-i\eta_{V,s} z) G_{s,2,V} + \\ + \sum_l \exp(-i\eta_{S,s,l} z) G_{s,2,S,l} \quad (7)$$

where

$$A_{s,2} = iw\left\{\sum_j w_j w_{-j} / (ik_{s,j} - w) - w_{0,0}\right\} / h,$$

$$G_{s,2,V} = 4a_H w_{-\mathrm{pv}(s)} k_y w / [(2h_s + \eta_{V,s})(ik_y - w)],$$

$$G_{s,2,S,l} = -ia_{3-s} 2w_{\mathrm{ps}(s,l)} w_l w / [(2h_s + \eta_{S,s,l})(ik_{3-s,l} - w)],$$

Solving the equation (4) using (7) makes possible to find change of amplitude of the surface wave along longitudinal coordinate z. Then we define the field radiated from the surface in a mirror direction with the formula (6) and for unmirror waves from the formula (5).

Obtained solution is valid for small and not small values of η. So we do not need to splice resonant and non-resonant asymptotics.

THE PHYSICAL EFFECTS

Imaginary part of $A_{s,2}$ is a perturbed addition to the phase coefficient of propagation of the sth surface wave. Real part of $A_{s,2}$ describes the attenuation caused by heat losses and leaking of energy of surface wave into energy of volume spatial harmonics. Parameters $G_{s,2,V}$ characterize transformation energy of incident TM wave beam into energy of the forward or backward surface wave. Parameters $G_{s,2,S,l}$ determine intensity of the reflection process of the surface waves.

In simple particular cases of strictly sinusoidal disturbances and strictly plane falling wave we can obtain analytical solutions of equation system in exponential forms. If the incident volume field is absent we find the expression for eigenwaves and eigen wavenumbers. Each eigenwaves consist of both surface waves and small additional space harmonics. Each of these harmonics has surface or radiated nature. Perturbed longitudinal wavenumber has an imaginary part caused not only by heat and radiation losses but also by Bragg reflection. If the incidentplane wave is available amplitudes of exited surface waves are derived from system of algebraic linear equations. If one of the values $\eta_{V,s}$ or both of them become small, the amplitudes of surface waves sharply raised. In this case waves radiated from impedance plane are far from being similar to unperturbed ones.

If the perturbation amplitudes are not constant physical processes in considered structure become more complicated and interesting. The amplitudes of surface wave going from «infinities» must be taken into account. If only one surface wave is exited an analytical solution of system of differential equation (4) can be obtained [8]. It has been shown that for input-output of cophased wave beams not only the amplitude of the perturbation harmonics [4] but also its phase must be proper chosen. In general case this system can be integrated by numerical method.

CONCLUSIONS

Non-periodic perturbations considered above provide rich possibilities for different types of transformations of surface waves and volume wave beams. Asymptotic methods based on method of Krylov, Bogoliubov and Mitropolsky allow to obtain solution common for resonant and non-resonant bands. Presented approach can be developed for theoretical analysis of other open inhomogeneous waveguiding structures. Obtained formulas can be especially useful for designing of devices which combine functions of reflectors and leaky-wave antennas.

REFERENCES

1. C. Elachi, "Waves in active and passive periodic structures: A review," *Proc. IEEE*, vol. 64, pp. 1666-1698, Dec. 1976.
2. Li Zong-Weng, Zhang Wen-Xun, «Design and performance of the millimeter wave DBR Gunn oscillators» *IEEE MTT-S. 1986 Intern. Microwave Symp. Dig.* pp. 531-534. 1986.
3. S. Erkin, N. S. Chang, H. Maheri, and M. Tsutsumi, «Characteristics of millimeter-wave radiation in a corrugated ferrite slab structure» *IEEE Trans. Microwave Theory Tech.*, vol. MTT-36, pp. 568-575. March. 1988.
4. M. K. Barnoski, *Introduction to Integrated Optics.* New York and London. 1974.
5. B. S. Song, T. Itoh, «A distributed feedback dielectric waveguide oscillator with a built leaky-wave antenna» *IEEE MTT-S. 1986 Intern. Microwave Symp. Dig.* pp. 217-219. 1979.
6. V. F. Borulko, "Polarization and mode conversions in nonperiodically corrugated waveguides with a gyrotropic filling," in *Proceeding of the 1995 URSI International Symposium on Electromagnetic Theory* (St. Petersburg, Russia) May, 1995, pp. 729-731.
7. N. N. Bogoliubov, Yu. A. Mitropolsky, *Asymptotic Methods in the Theory of Nonlinear Oscillations.* New York 1961.
8. V. F. Borulko, V. E. Ivanilov «Coupling of wave beam with surface wave at oscillated perturbation of surface impedance» *in Proc. of XXVIII Moscow International Conference "Antenna theory and techniques".* - Moscow (Russia). pp. 180-183. 1998.

ON THE SYNTHESIS OF ANTENNAS WITH AN OPTIMAL RATIO BETWEEN THE DEMAND FACTOR AND THE ANGLE OF CONCENTRATION OF THE RADIATED/RECEIVED POWER

G. A. Evstropov, S. A. Smirnov

SC NPK NIIDAR,
107258, Moscow, 1st Buchvostova str., 11/12,
tel. 963-93-09, E-mail: paradox@gorodtsk.msk.ru

The demand factor (K_k) introduced in [1] is equal to the ratio between the power radiated by an antenna in some solid angle to the total radiated power. If we define the solid angle as the angle corresponding to the lobe of the radiation pattern (RP), then the demand factor is uniquely defined by the diffusing factor (K_r; $K_k = 1-K_r$) which is equal to the ratio of the power radiated in the direction of the side lobes to the total radiated power [2]. In general, both the demand factor and the angle of concentration have independent values. In [3] it was shown that the power, received by an antenna of a radiometric research station (RMS) under realistic conditions does not depend on the antenna size and is proportional to K_k, and the solid angle (Ω_k) coincides with the angular discrimination of the RMS. The values are similar for radar installations with continuous radiation [4] with a fixed system of radiation pattern on reception, and also in some active radio ecological stations.

A study of the existing literature (partlially cites in [3], [11]) has shown that antenna arrays with rectangular or circular apertures are frequently used in RMS's and aforementioned radar instalations (RI). Radiation pattern are symmetric in the main planes and are axially symmetric for circular aperture. In this work we will address apertures of this types.

The relation of K_k and Ω_k with other characteristic of the antenna are investigation detail in [3]. When using results of [5] and [6] in [3], it was also shown that in order to estimate the influence of random errors on the value K_k one can use formula for the fall of falling with respect to the directive gain of the antenna.

In order to ensure the best characteristic for RMS's and certain RI's the value of K_k must be at its maximum, and Ω_k must be as small as possible. The leads to a contradiction and we have two optimal synthesis problems:

1) calculating the distribution in an antenna aperture to ensure the maximum of K_k for a given Ω_k;

2) calculating the distribution in the aperture minimizing Ω_k for a given K_k.

This problems of finding the conditional extremum of K_k or Ω_k are considered in the present work.

PRELIMINARY CONSIDERATIONS

In general, these problems can be solved using the method of synthesis, or the method of partial diagrams of RP [12]. In this method, the RP in question is represented as a sum of partial RP's with unknown excitation factors, and the amplitude distribution is represented as a sum of partial distributions, i.e.

$$F(\theta,\varphi) = \sum_{i=1}^{n} z_i F_i(\theta,\varphi)$$

and

$$f(x,y) = \sum_{i=1}^{n} z_i f_i(x,y)\,. \qquad (1)$$

The demand factor, K_k, is defined by the ratio between the power P_κ which is radiated by the antenna in the corresponding angle Ω_k, and the total power P_Σ, i.e. $K_k = P_\kappa / P_\Sigma$.

The powers are proportional to the integrals of the squared absolute value of the total RP in the corresponding angles. They are quadratic forms [10] with respect to the excitation factors.

If we assume that partial RP's are real functions, Then we can show that the optimal value of K_κ is achieved if coefficients z_i take real values, i.e. $z_i = x_i$. The fact that z_i's are real is also confirmed by results of the related studies [7, 8 and 13]. Using the conventional notations for quadratic forms, we can write:

$$P_\kappa = A(x,x) = \sum_{i,j=1}^{n} A_{i,j} x_i x_j\,;$$

$$P_\Sigma = B(x,x) = \sum_{i,j}^{n} B_{i,j} x_i x_j \qquad (2)$$

The coefficients are defined as

$$A_{i,j} = \int_{\Omega_k} F_i(\theta,\varphi) F_j(\theta,\varphi)\, d\Omega \quad \text{and}$$

$$B_{i,j} = \int_{\Omega_\bullet} F_i(\theta,\varphi) F_j(\theta,\varphi)\, d\Omega \qquad (3)$$

As a result of this relations, the problems are reduced to finding the unknown coefficients which lead to the maximal value of K_κ (minimal value of Ω_κ) for a given Ω_κ (K_κ). As it was mentioned before, these are problems of finding a conditional extremum and they can be solved by the method of Lagrangean multipliers [14]. However, for the first problem it is more convenient to use some results from the theory of quadratic forms [10].

SOLUTION OF THE FIRST PROBLEM

First we will remind the reader of some relevant results from the theory of quadratic forms [10].

A real quadratic form $A(x,x)$ takes stationary values on those vectors from a unit sphere which are eigenvectors of the matrix A, The stationary values of the quadratic form are equal to the eigenvalue of the matrix A The maximal (minimal) stationary value corresponds to the largest (smallest) eigenvalue. Two real quadratic forms $A(x, x)$ and $B(x, x)$ define a bundle of quadratic forms $A(x, x)$-$\lambda B(x, x)$, where λ is a parameter. If the form $B(x, x)$ is positive definite, then the bundle is called a regular bundle. The equation A-$\lambda B = 0$ is called the characteristic equation of the bundle of forms. A characteristic equation always has n real roots (characteristic numbers) which correspond to the principal vectors $x^k = (x_1^k, x_2^k \ldots x_n^k)$, where $k = 1,2...n$. The smallest (largest) characteristic number λ_1 (λ_n) is equal to the minimum (maximum) of the ratio of the forms.

If the partial RP's are orthogonal, then the total radiated power is equal to the sum of the squares of the excitation factors up to a constant coefficient d_o. $B(x, x)$ can be reduced to its normal form by means of dividing the forms $A(x, x)$ and $B(x, x)$ by d_o. Next, we can assume that $B(x, x) = 1$ and deduce that the demand factor is equal to $A(x, x)$. Therefore, by the first extremal property of quadratic forms, $K_{\kappa\, max} = \lambda_{\max}$, where $\lambda_{\max}$ – is the largest eigenvalue of the matrix A which corresponds to the quadratic form $A(x, x)$, and the vector of excitation factors is equal to the eigenvector of the matrix which corresponds to the largest eigenvalue.

If the partial RP's are not orthogonal and the form B is not of the normal type, then for the calculation we can use the second extremal property of quadratic forms (a bundle of forms). In this case, the maximum of the ratio of the forms is equal to the largest characteristic number of the bundle of forms, and the vector of excitation factors is equal to the principal vector corresponding to this characteristic number.

SOLUTION OF THE SECOND PROBLEM

The problem is now finding the unknown vector x which leads to the minimum value of Ω_k with a given K_k. The solution can be obtained by using the Lagrange's method [14]. Namely, we can write down the functional

$$\Phi = \Omega_k + \lambda \left(\sum_{i=1}^{n} x_i - 1\right), \qquad (4)$$

where λ is the Lagrangean multiplier. Ω_k can be determined from the equation $L = A(x, x) - K_k B(x, x) = 0$.

After differentiating equation (5) with help of [14] we obtain the system of equations

$$\sum_{k=1}^{n}(A_{i,k} - K_k B_{i,k})x_k + \lambda \sum_{i,k=1}^{n} F_i(U_k)F_k(U_k)x_i x_k = 0,$$

$$i = 1,2...n \qquad (5)$$

The system of equations contains a term which is the same for all the equations. It is the the second term which is a sum multiplied by the unknown λ. We can replace this product by a new unknown μ and finally get

$$\sum_{i=1}^{n=1}(A_{i,j} - K_k B_{i,k})x_i + \mu = 0; \sum_{i=0}^{n=1} x_i = 1; A(x,x) - K_k B(x,x) = 0 \qquad (6)$$

where we took into account the equation $L = A(x, x) - K_k B(x, x) = 0$ which defines the implicit function Ω_k.

PARTIAL RADIATION PATTERNS AND DISTRIBUTIONS

For the types of antennas considered here, we can restrict ourselves with the case where the RP's only depend on one angle. Then the K_k for rectangular apertures is equal to the product of the K_k for two linear antennas. The K_k for a circular aperture can be obtained directly.

Radiator Lattice

For our system of partial RP's we chose the RP's of two symmetrical radiators, i.e.

$$F_i(u) = \cos((i + \frac{1}{2})u) \quad \text{or} \quad F_i(u) = \cos(iu) \qquad (7)$$

corresponding to an even or an odd number of radiators, $u = kd\sin\theta$. Here θ is the angle with respect to the aperture, d is the radiator step, k is the wave number and i=0,1,2... $n-1$.

In this case, the currents in the radiators are equal to a half of the excitation factors for $i \neq 0$. The current in the zeroth radiator is equal to the excitation factor (for an odd number of radiators).

Continuous Distribution with a Linear (Rectangular) Aperture

$$F_i(u) = \varepsilon_i\left(\frac{\sin(u - i\pi)}{u - i\pi} + \frac{\sin(u + i\pi)}{u + i\pi}\right),$$

$$\varepsilon_i = \begin{cases} 1/2, i = 0 \\ 1, i > 0 \end{cases}, f_i(y) = \cos(\frac{\pi i}{l} y) \qquad (8)$$

$i = 0,1,2 \ldots n-1$; $u = kl\sin\theta$ (l is a half of the lenght of antenna).

Circular Aperture [9]

$$F_i(u) = \frac{2J_1(u)}{J_0(\alpha_i) - J_2(\alpha_i)}(\frac{1}{u-\alpha_i} + \frac{1}{u+\alpha_i});$$

$$f_i(t) = J_0(\alpha_i t), t = \frac{r}{a} \qquad (9)$$

where $u = ka\sin\theta$, $J_m(z)$ is a Bessel's function, a –is the aperture radius, α_i are roots of the Bessel's function, i.e. $J_1(\alpha_i) = 0$.

RESULTS AND SOME STUDIES OF OPTIMAL DISTRIBUTION

Using the method outlined above we calculated the dependencies of K_k on U_k and U_k on K_k. In our calculations we considered rectangular apertures. For continuous distributions we studied both rectangular and circular apertures.

Let us assume that the angle U_k is normalized with respect to the width of the antenna at the zeroth level and the distribution is uniform in the aperture. Then the analysis of our results shows that the optimal dependence of K_k on the angle U_k, is universal and does not depend on the size or the type of the aperture as they vary over a wide range. Moreover, it does not depend on which parameter is given and which is being varied. Such optimal dependence is presented in Table 1. Using this table one can determine the optimal value for U_k given K_k and vice versa. Note that the optimal distribution is obtained more easily using the method of the first problem for personal computer and results of [15].

Table 1

U_k	0.5	0.6	0.7	0.8	0.9
K_k	0.612	0.74	0.835	0.900	0.932

U_k	1.0	1.1	1.2	1.3
K_k	0.967	0.982	0.990	0.995

In the work we also investigate the optimal amplitude of the distributions and the RP for antennas of the type mentioned above. For instance, the optimal RP's for a rectangular aperture are given in Fig. 1. The notation P_{snm} corresponds to the normalized U_k =1,3; P_{s1m}- to U_k = 1; P_{s2m}- to U_k = 0.7, and P_{tm}- to a unifor distribution.

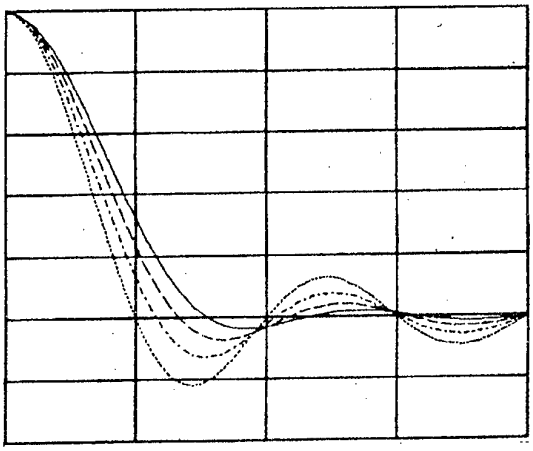


Fig. 1 Optimal radiation patterns

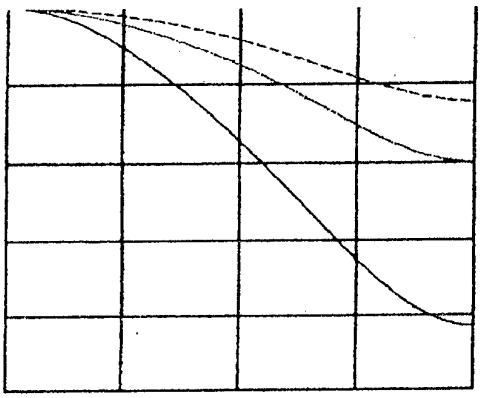


Fig. 2 Optimal amplitude distributions

REFERENCES

1. L. D. Bachrach, S.D. Krimenetsky, Radiating system synthesis, Publisher "Sov. Radio", M., -1974, 232 p.
2. A. A. Kuzmin, E.A. Solomonovitch, Radio astronomical methods of measurement of parameters of antennas, M.: Sov. Radio, 1964, 184 p.
3. D. I. Voskresensky, G.A. Evstropov, S.A Smirnov, Specificity of antennas of radiometre for definition of environment parameters: demand factor and angular discrimination, M., Bulletin MAI, Vol. 5, No.1 1998, p. 62-68.
4. G. A. Evstropov, A.I. Klimenko, Distance resolution for continuous -radiation-radar and antenna characteristics// Proceedings of the XXVII Moscow International Conference on Antenna Theory and Technology, 22-24 September 1998, Moscow, Russia, M., 1998, part 243-245.
5. Ya. S. Shifrin, Problems of statistical theory of antennas, Publisher "Sov. Radio", M., 1970, 383 p.

6. D. M. Sazonov, Antennas and devices of super high frequency, Publisher "Higher school", M., 1988, 432 p.

7. N. G. Mironenko, Synthesis of an antenna of the finite aperture, radiating maximum share of power in the given solid angle of space. "Radio Engineering", Vol. 22, No. 4 - 1967, p. 43-49.

8. B. A. Evstropov, G. A. Evstropov, V. D. Korotkov, About one method of synthesis of linear lattices with maximum directive gain, Radio Engineering and Electronics, 1967, Vol. XII – No. 4, p.591-599.

9. B. M. Minkovitch, V.P. Yakovlev, Theory of synthesis of antennas, Publisher "Sov. Radio", M., 1969, 294 p.

10. F. R. Gantmacher, Theory of matrixes, Publisher "Science", M., 1967, 575 p.

11. G. A. Evstropov, S.A. Smirnov, On calculation optimum aperture field providing maximum concentration of power in a given solid angle // Proceedings of the XXVII Moscow International Conference on Antenna Theory and Technology, 22-24 September 1998, Moscow, Russia, M., 1998, part 357-360.

12. E. G. Zelkin, V.G. Sokolov, Methods of synthesis of antennas, Publisher "Sov. Radio", M., 1980, 294 p.

13. A. N. Yuriev, Synthesis of antennas with the minimum level of side radiationl, "Radio Engineering and Electronics", Vol. XV, No. 1, 1970, p. 29 - 37.

14. G. M. Fichtengoltc, Cource of differential and integral calculus. M.: Science, 1969, Vol., 607 p.

15. MATHCAD 6.0 PLUS, Financial, engineering and scientific calculations in Windows 95 environment, translation from English, M., Information-publishing house "Filin", 1996, 712 p.

SCATTERING PLANE ELECTROMAGNETIC WAVE BY CRUCIFORM ELECTRICAL DIPOLE WITH A LOAD

D. D. Gabriel'yan, T. V. Peretyatko

Rostov Military Institute of Missile Corps,
Rostov-on-Don, 344027, Russia

The problem of scattering the plane electromagnetic wave by antenna array is not only of theoretical urgency, but also of practical importance. The solution to this problem for the case of linear dipole is considered in a number of papers, for example in [1-4]. However, the solution to the considered problem for the case of other types of radiators is of interest as well. One of such types of radiators includes, for example, cruciform electrical dipoles.

The aim of the report is solution to the problem of scattering the plane electromagnetic wave by a cruciform dipole.

Let's discuss the symmetrical cruciform electrical dipole excited by the incident plane electromagnetic wave. The direction of wave falling is θ_0, φ_0. The vector of electric field strength in the incident wave has only θ- or φ- component. The dipole arms are oriented along axes Ox and Oy. The dipole arm length is ℓ and the radius is a. The center of the dipole is at point 0 with coordinates x_0, y_0. The load connected to dipole is W. It is needed to find the current distribution in dipole arms. The geometry of the problem is presented in Fig. 1.

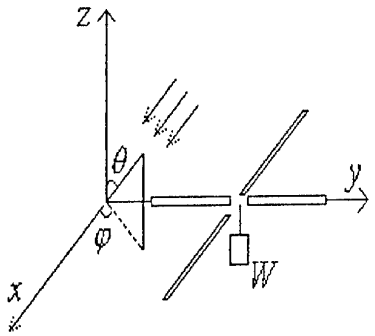


Fig. 1. Problem geometry

The scattered electric field should satisfy the Helmgoltz equation and the condition of radiation. When solving the problem, we take into account the boundary conditions for electric field on the dipole surface. The tangential component of the electric field must be equal to zero. In this case we obtain the following equation [2]

$$\begin{cases} E_x(\vec{r}) + E_x^{cm\chi}(\vec{r}) = I^{\chi}(\vec{r}) W\delta(\vec{r}) \\ E_y(\vec{r}) + E_y^{cm\chi}(\vec{r}) = I^{\chi}(\vec{r}) W\delta(\vec{r}) \end{cases}, \quad \chi = \theta, \varphi \qquad (1)$$

where

$$\begin{cases} E_x(\vec{r}) = E_{xx}(\vec{r}) + E_{xy}(\vec{r}) \\ E_y(\vec{r}) = E_{yy}(\vec{r}) + E_{yx}(\vec{r}) \end{cases}$$

In the expression (1) $E_{s\xi}$ is the contribution of current along s-arm of dipole to E_ξ-component of the electric field strength (s = x, y, ξ = x, y).

Let the unknown current distribution in the dipole be presented as superposition of the basic functions, which turn to be equal to zero at ends of the dipole arms.

$$\vec{I}^{\chi}(\vec{r}) = \vec{I}_x^{\chi}(\vec{r}) + \vec{I}_y^{\chi}(\vec{r}), \qquad (2)$$

$$\vec{I}_x^{\chi}(\vec{r}) = \vec{i}_x \sum_{m'_x=1}^{\infty} \{A_{m'_x}^{x\chi} \cos(\frac{\pi(m'_x - 0.5)(x' - x_0)}{\ell}) + B_{m'_x}^{x\chi} \sin(\frac{\pi m'_x x'}{\ell})\} \delta(y' - y_0)\delta(z')$$

$$\vec{I}_y^{\chi}(\vec{r}) = \vec{i}_y \sum_{m'_y=1}^{\infty} \{A_{m'_y}^{y\chi} \cos(\frac{\pi(m'_y - 0.5)(y' - y_0)}{\ell}) + B_{m'_y}^{y\chi} \sin(\frac{\pi m'_y y'}{\ell})\} \delta(x' - x_0)\delta(z')$$

Taking into account expressions

$$E_x^{cm\chi}(\vec{r}) = E_0 \exp(ikx\sin\theta\cos\varphi) \times \begin{cases} \cos\theta\cos\varphi & \text{for } \chi = \theta \\ -\sin\varphi & \text{for } \chi = \varphi \end{cases}$$

$$E_y^{cm\chi}(\vec{r}) = E_0 \exp(ikx\sin\theta\sin\varphi) \times \begin{cases} \cos\theta\sin\varphi & \text{for } \chi = \theta \\ \cos\varphi & \text{for } \chi = \varphi \end{cases} \qquad (3)$$

where E_0 is the electric field strength in the incident wave front.

From (1) there follows the system of two integral equations for currents in the dipole arms, placed along axes Ox and Oy.

$$E_{\xi\xi}(\vec{r}) = (k^2 + \frac{\partial^2}{\partial\xi^2}) \int_V I_\xi^{\chi}(\vec{r}) \tilde{G}(\vec{r}, \vec{r}'(\xi)) dr' \qquad (4)$$

$$E_{s\xi}(\vec{r}) = \frac{\partial^2}{\partial\xi\partial s}\int_V I_s^{\chi}(\vec{r})\tilde{G}(\vec{r},\vec{r}'(\xi))dr' \qquad (5)$$

$$\xi = x, y, \quad s = y, x$$

If we insert an operator of partial derivatives as integrand and perform integration by parts, we exclude the second derivative. Going from the double integrals to unitary ones permits to decrease the number of calculations.

The solution to the system of integral equations with the help of the Bubnov-Galerkin method enables to reduce this system to the following system of linear algebraical equations

$$\begin{cases} \sum\limits_{m_x^l=1}^{M_x}\{A^x C_{m_x}^{m_x^l} + B^x D_{m_x}^{m_x^l}\} + \sum\limits_{m_y^l=1}^{M_y}\{A^y F_{m_x}^{m_y^l} + B^y H_{m_x}^{m_y^l}\} = S_{m_x}^{\chi} \\ \sum\limits_{m_x^l=1}^{M_x}\{A^x D_{m_x}^{m_x^l} + B^x G_{m_x}^{m_x^l}\} + \sum\limits_{m_y^l=1}^{M_y}\{A^y H_{m_x}^{m_y^l} + B^y P_{m_x}^{m_y^l}\} = T_{m_x}^{\chi} \\ \sum\limits_{m_x^l=1}^{M_x}\{A^x F_{m_y}^{m_x^l} + B^x H_{m_y}^{m_x^l}\} + \sum\limits_{m_y^l=1}^{M_y}\{A^y C_{m_y}^{m_y^l} + B^y D_{m_y}^{m_y^l}\} = S_{m_y}^{\chi} \\ \sum\limits_{m_x^l=1}^{M_x}\{A^x H_{m_y}^{m_x^l} + B^x P_{m_y}^{m_x^l}\} + \sum\limits_{m_y^l=1}^{M_y}\{A^y D_{m_y}^{m_y^l} + B^y G_{m_y}^{m_y^l}\} = T_{m_y}^{\chi} \end{cases} \qquad (6)$$

The coefficients of the system of linear algebraical equations are determined as follows

$$C_{m_\xi}^{m_\xi^l} = -iW_0\{(1-(\frac{\pi(m_\xi^l-0.5)}{\ell})^2)\int_{-\ell+\xi_{0'}}^{\ell+\xi_{0'}}\int_{-\ell+\xi_0}^{\ell+\xi_0}\cos(\frac{\pi(m_\xi^l-0.5)(\xi'-\xi_{0'})}{\ell})\times$$

$$\times\cos(\frac{\pi(m_\xi-0.5)(\xi-\xi_0)}{\ell})\tilde{G}(\vec{r},\vec{r}'(\xi'))d\xi'd\xi +$$

$$+\frac{\pi(m_\xi^l-0.5)}{\ell}\sin(\pi(m_\xi^l-0.5))\int_{-\ell+\xi_0}^{\ell+\xi_0}\cos(\frac{\pi(m_\xi^l-0.5)(\xi-\xi_0)}{\ell})\times$$

$$*(\tilde{G}(\vec{r},\vec{r}'(\ell+\xi_{0'}))+\tilde{G}(\vec{r},\vec{r}'(-\ell+\xi_{0'})))d\xi -$$

$$-\frac{iW}{W_0}\int_{-\ell+\xi_0}^{\ell+\xi_0}\cos^2(\frac{\pi(m_\xi-0.5)(\xi-\xi_0)}{\ell})d\xi\},$$

$$D_{m_\xi}^{m_\xi^l} = -iW_0\{(1-(\frac{\pi m_\xi^l}{\ell})^2)\int_{-\ell+\xi_{0'}}^{\ell+\xi_{0'}}\int_{-\ell+\xi_0}^{\ell+\xi_0}\sin(\frac{\pi m_\xi^l(\xi'-\xi_{0'})}{\ell})\times$$

$$\times\cos(\frac{\pi(m_\xi-0.5)(\xi-\xi_0)}{\ell})\tilde{G}(\vec{r},\vec{r}'(\xi'))d\xi'd\xi -$$

$$-\frac{\pi m_\xi^l}{\ell}\int_{-\ell+\xi_0}^{\ell+\xi_0}\cos(\frac{\pi(m_\xi^l-0.5)(\xi-\xi_0)}{\ell})(-1)^{m_\xi^l}\times$$

$$\times(\tilde{G}(\vec{r},\vec{r}'(\ell+\xi_{0'}))-\tilde{G}(\vec{r},\vec{r}'(-\ell+\xi_{0'})))d\xi\},$$

$$F_{m_\xi}^{m_s^l} = -iW_0\int_{-\ell+s_0}^{\ell+s_0}\int_{-\ell+\xi_0}^{\ell+\xi_0}\frac{\pi(m_s^l-0.5)}{\ell}\frac{\pi(m_\xi^l-0.5)}{\ell}\sin(\frac{\pi m_s^l(s-s_0)}{\ell})*$$

$$\times\sin(\frac{\pi(m_\xi-0.5)(\xi-\xi_0)}{\ell})\tilde{G}(\vec{r},\vec{r}'(s))dsd\xi$$

$$H_{m_\xi}^{m_s^l} = -iW_0\int_{-\ell+s_0}^{\ell+s_0}\int_{-\ell+\xi_0}^{\ell+\xi_0}\frac{\pi m_s^l}{\ell}\frac{\pi(m_\xi^l-0.5)}{\ell}\cos(\frac{\pi m_s^l(s-s_0)}{\ell})\times$$

$$\times\sin(\frac{\pi(m_\xi-0.5)(\xi-\xi_0)}{\ell})\tilde{G}(\vec{r},\vec{r}'(s))dsd\xi$$

$$G_{m_\xi}^{m_\xi^l} = -iW_0\{(1-(\frac{\pi m_\xi^l}{\ell})^2)\int_{-\ell+\xi_{0'}}^{\ell+\xi_{0'}}\int_{-\ell+\xi_0}^{\ell+\xi_0}\sin(\frac{\pi m_\xi^l(\xi'-\xi_{0'})}{\ell})\times$$

$$\times\sin(\frac{\pi m_\xi(\xi-\xi_0)}{\ell})\tilde{G}(\vec{r},\vec{r}'(\xi'))d\xi'd\xi -$$

$$-\frac{\pi m_\xi^l}{\ell}\int_{-\ell+\xi_0}^{\ell+\xi_0}\sin(\frac{\pi m_\xi^l(\xi-\xi_0)}{\ell})(-1)^{m_\xi^l}\times$$

$$\times(\tilde{G}(\vec{r},\vec{r}'(\ell+\xi_{0'}))-\tilde{G}(\vec{r},\vec{r}'(-\ell+\xi_{0'})))d\xi -$$

$$-\frac{iW}{W_0}\int_{-\ell+\xi_0}^{\ell+\xi_0}\sin^2(\frac{\pi m_\xi(\xi-\xi_0)}{\ell})d\xi\},$$

$$P_{m_\xi}^{m_s^l} = -iW_0\int_{-\ell+s_0}^{\ell+s_0}\int_{-\ell+\xi_0}^{\ell+\xi_0}\frac{\pi m_s^l}{\ell}\frac{\pi m_\xi}{\ell}\cos(\frac{\pi m_s^l(s-s_0)}{\ell})\times$$

$$\times\cos(\frac{\pi m_\xi(\xi-\xi_0)}{\ell})\tilde{G}(\vec{r},\vec{r}'(s))dsd\xi \qquad (7)$$

where Green's function is determined as

$$\tilde{G}(\vec{r},\vec{r}') = (4\pi)^{-1}\exp(-ikr)/kr$$

$$r = ((x'-x_0)^2+(y'-y_0)^2+(z'-z_0)^2+a^2)^{1/2}$$

$k = 2\pi/\lambda$ is the wave number.

The right part of the system is presented in the following form

$$\begin{Bmatrix} S_{m_x}^{\varphi} \\ T_{m_x}^{\varphi} \end{Bmatrix} = (-1)^{m_x+1}2E_0\cos\theta_0\sin\varphi_0\exp(ikx\sin\theta_0\cos\varphi_0)\times$$

$$\times\begin{Bmatrix} \frac{\pi(m_x-0.5)}{\ell} & \frac{\cos(k\ell x\sin\theta_0\cos\varphi_0)}{-(\sin\theta_0\cos\varphi_0)^2+(\frac{\pi(m_x-0.5)}{\ell})^2} \\ i\frac{\pi m_x}{\ell} & \frac{\sin(k\ell x\sin\theta_0\cos\varphi_0)}{-(\sin\theta_0\cos\varphi_0)^2+(\frac{\pi m_x}{\ell})^2} \end{Bmatrix} \qquad (8)$$

$$\begin{Bmatrix} S^{\varphi}_{m_x} \\ T^{\varphi}_{m_x} \end{Bmatrix} = (-1)^{m_x+1} 2E_0(-\sin\varphi_0)\ \exp(ki x \sin\theta_0 \cos\varphi_0) \times$$

$$\times \begin{Bmatrix} \frac{\pi(m_x-0.5)}{\ell} & \frac{\cos(k\ell x \sin\theta_0 \cos\varphi_0)}{-(\sin\theta_0\cos\varphi_0)^2 + (\frac{\pi(m_x-0.5)}{\ell})^2} \\ i\frac{\pi m_x}{\ell} & \frac{\sin(k\ell x \sin\theta_0 \cos\varphi_0)}{-(\sin\theta_0\cos\varphi_0)^2 + (\frac{\pi m_x}{\ell})^2} \end{Bmatrix} \quad (9)$$

The expressions (7 – 9) completely describe the system of linear algebraical equations (6) and permit to find the current distribution inside the cruciform electric dipole, load by W. The case of the plane wave falling from direction θ_0, φ_0 is considered here. Then the scattering properties are defined simply. The control of computed results correctness and reliability of relations was performed by the comparison with the known data [1], [3], [4]. Calculated values of input resistance and current distribution coincide with the results in [1], [3].

These relations can be used for calculation of the pattern of scattering for the cruciform electric dipole for various parameters of the problem.

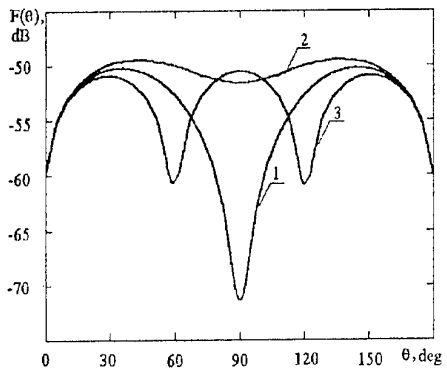


Fig. 2. The patterns of scattering for various loads W

At calculation the cruciform electrical dipole with ℓ = 0.25λ and a = 0.0025λ is considered. The results of calculations are presented in Fig. 2 by curves 1–3. The direction of incidence is defined by $\theta_0 = 90^0$, $\varphi_0 = 0^0$ and the electric field strength has θ-component. The value of load is W = 1+1170i Ohm. This value permits to obtain the pattern of scattering with null in the incidence direction. The curve 1 illustrates the pattern of scattering for nominal frequency, whereas curves 2 and 3 — for frequencies differed by +5% and -5%, respectively.

The mentioned curves are normalized to a maximum value of scattering field of electrical vibrator with consistent load.

The obtained results allow to conclude, that the characteristics of scattering of such a dipole are rather sensitive to parameters of the problem.

Thus, the mentioned expressions allow to investigate the characteristics of scattering for various applications.

REFERENCES

1. *Tang, T., Gunn, M.W.* "Current distribution on a Receiving Dipole Antenna", IEEE Trans., Antennas and Propag., V.AP-29, no.5, pp.817- 822, September 1981.
2. *Ponomarev, L.N., Shatalov, A. V.* "Rasseyanie electromagnitnoi volny periodicheskoiy reshetkoi vibratorov s sosredotochennymi i raspredelennymi nagruzkami" (The scattering of the plane electromagnetic wave by periodical array of dipoles with a concentrated and distributed loads), Ser. Radioelektronika, vol.29, 1986, no.2, pp.58-63.
3. *Popichenko V. A.* "Ob upravlenii diagrammoi rasseyaniya vibratora v rezhime priema pri pomoshchi izmeneniya ego nagruzok" (About control pattern of scattering of dipole under conditions of receiving with the change of its loads), Antenny, vip. 35 - Moscow: Radio i svyaz', 1988, pp.43-49 [in Russian].
4. *Brikker, A. M., Zernov, N. A.., Martynova, T. E., Shkil, V. M.* "Rasseyanie electromagnitnoy volny vibratornoy antennoy pri proizvolnykh uglakh padeniya"(The scattering of electromagnetic wave by dipole antenna with an arbitrary angle of incidence), Radiotekhnika i elektronika, vol.43, 1998, no.5, pp.574-579 [in Russian].

THE CALCULATION OF MUTUAL COUPLING BETWEEN DIPOLES IN PRESENCE OF IMPEDANCE CIRCULAR CYLINDER

D. D. Gabriel'yan, M. Yu. Zvezdina

Rostov Military Institute of Missile Corps, 344027 Rostov-on-Don, 27 Russia
E-mail: zvezd@jeo.ru

The calculation of mutual coupling between dipoles is one of the important problems taken into account in analysis of antenna arrays. The wide using of antennas on cylindrical surfaces with impedance characteristics dictates urgency of problem considered in this paper.

Let's consider two thin longitudinal dipoles placed near impedance circular cylinder with radius a. The length of dipoles is l (Fig.1). The centers of dipoles have coordinates $\vec{r}=\{r,\varphi,z\}$ and $\vec{r}'=\{r',\varphi',z'\}$. For calculating mutual coupling between two dipoles we use following expression [1]

$$Z_{12}^{mut}=-\frac{1}{|I_0|^2}\int_l \vec{j}_1(\vec{r}')\,\vec{E}_{12}(\vec{r},\vec{r}')\,dl\,, \qquad (1)$$

where $\vec{j}_1$ is the current distributed along first dipole; $\vec{E}_{12}$ is the electric field strength at and parallel to first radiator due to the current in the second dipole; I_0 is the terminal currents of dipoles.

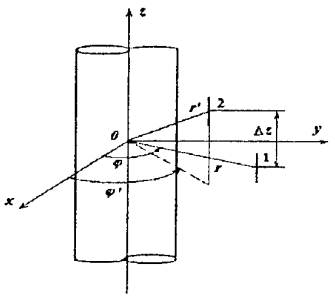


Fig. 1. Problem geometry

Parallel component (z-component) of electrical field $\vec{E}_{12}$ is defined as [1]

$$E_{12}=\frac{W_0}{4\pi k}(k^2+\partial^2/\partial z^2)\int_l j_2(z')\times \qquad (2)$$
$$\times\int_\Gamma \Re(\kappa\vec{r},\kappa\vec{r}')\exp[-i\gamma|z-z'|)\,d\gamma\,dz'\,,$$

where $\kappa^2=k^2-\gamma^2$; $k=2\pi/\lambda$ is wave number; λ is wavelength; W_0=120π Ohm is free-space impedance; i is imaginary unity;

$$\Re(\kappa\vec{r},\kappa\vec{r}')=\frac{1}{2}\sum_{p=0}^{\infty}\varepsilon_p\cos[p(\varphi-\varphi')]\times$$
$$\times\left\{\Re_p(\kappa r,\kappa r')+\Re_p^*(\kappa r,\kappa r')\right.,$$
$$\Re_p(\kappa r,\kappa r')=H_p^{(2)}(\kappa r)\left(J_p(\kappa r')-a_p H_p^{(2)}(\kappa r')\right),$$
$$a_p=\frac{\left\{\frac{\kappa}{k}J_p(\kappa a)+iZ_N\,J_p'(\kappa a)\,D1_p^e(\kappa a)\right\}}{\frac{\kappa}{k}H_p^{(2)}(\tilde{k}a)+iZ_N\,H_p^{(2)'}(\kappa a)\,D2_p^e(\kappa a)},$$
$$D1_p^e(\kappa a)=1+K_p^e(\kappa a)\frac{J_p(\kappa a)}{J_p'(\kappa a)},$$
$$D2_p^e(\kappa a)=1+K_p^e(\kappa a)\frac{H_p^{(2)}(\kappa a)}{H_p^{(2)'}(\kappa a)},$$
$$K_p^e(\kappa a)=\left(\frac{p\gamma}{k\kappa a}\right)^2\left[\frac{H_p^{(2)'}(\kappa a)}{H_p^{(2)}(\kappa a)}-iZ_N\frac{\kappa}{k}\right]^{-1},$$

$Z_N = Z/W_0$ is surface impedance, normalized by the free-space impedance; $J_p(\cdot)$,$J_p'(\cdot)$ are the Bessel function of order p and its derivation; $H_p^{(2)}(\cdot)$, $H_p^{(2)\,\prime}(\cdot)$ are the Hankel function of second kind of order p and its derivation; ε_p is the Neumann number. The contour of integration in (2) has branch between points $\gamma = k$ and $\gamma = 0$ on real axis and branch from point $\gamma = 0$ to $\gamma = k - i\infty$ on imaginary semi-axis of complex plane γ [1,2].

From expressions (1) and (2) we get complete expression to calculate mutual impedance between two longitudinal dipoles

$$Z_{12}^{mut}=-\frac{iW_0}{4\pi}\int_\Gamma\int_{-l}^{l}\int_{-l}^{l} j_1^3(kz)\,j_2^3(kz')\,\Re(\kappa\vec{r},\kappa\vec{r}')\times \qquad (3)$$
$$\times\left\{\left(k^2+\partial^2/(\partial z)^2\right)\exp[-i\gamma|z-z'|]\right\}dz\,dz'\,d\gamma\,.$$

Using substitution $\gamma = k\alpha$ we transform ratio (3) to the following form

$$Z_{12}^{mut}=-\frac{W_0 i}{4\pi}\int_1^{1-i\infty}\Re(kr[1-\alpha^2]^{1/2},kr'[1-\alpha^2]^{1/2})\times \qquad (4)$$
$$\times T_{zz}\,d\alpha\,,$$

in which $T_{zz}=\int_{-l}^{l}\int_{-l}^{l} j_1(z)\,j_2(z')\exp[-ik\alpha|z-z'|]\,dz\,dz'$.

For realizable current distributions expressed in terms of expansion on series the function T_{zz} can be calculated analytically. For the rule of current distribution in dipoles described by expressions $j_1(z)=\sin[k(l-|z|)]$ and $j_2(z')=\sin[k(l-|z'-\Delta z|)]$ function T_{zz} is presented in papers [1–4].

For the rule of current distribution in dipoles defined by expressions $j_1(z)=\cos\left((\pi(m-0.5)z)/l\right)$ and $j_2(z')=\cos\left((\pi(m'-0.5)(z'-\Delta z))/l\right)$ (m, m' are order of harmonic of current in the first and second dipoles correspondingly; $\Delta z<0$) T_{zz} has following form

$$T_{zz}=\frac{(-1)^{m+m'}(1-\alpha^2)}{\left([\frac{\pi(m-0.5)}{l}]^2-\alpha^2\right)\left([\frac{\pi(m'-0.5)}{l}]^2-\alpha^2\right)}\times \quad (5)$$

$$\times\begin{cases}\frac{\pi(m-0.5)}{l}\frac{\pi(m'-0.5)}{l}\{\exp[-ik\alpha(2l-\Delta z)]+\\ +\exp[-ik\alpha(2l+\Delta z)]+2\exp[ik\alpha\Delta z]-2i\alpha\times\\ \times\frac{\pi(m'-0.5)}{l}\sin\left(\frac{\pi(m-0.5)\Delta z}{l}\right) & \text{at } 0\le|\Delta z|<2l,\\ \frac{\pi(m-0.5)}{l}\frac{\pi(m'-0.5)}{l}\exp[ik\alpha\Delta z]\times\\ \times\left(\exp[-ik\alpha l]+\exp[ik\alpha l]\right)^2 & \text{at } |\Delta z|\ge 2l.\end{cases}$$

If we use the current distribution described by formula $j_1(z)=\sin\left((\pi mz)/l\right)$ and $j_2(z')=\sin\left(\frac{\pi m'(z'-\Delta z)}{l}\right)$ then the expression for T_{zz} may be written as

$$T_{zz}=\frac{(-1)^{m+m'}(1-\alpha^2)}{\left([\frac{\pi m}{l}]^2-\alpha^2\right)\left([\frac{\pi m'}{l}]^2-\alpha^2\right)}\times \quad (6)$$

$$\times\begin{cases}\frac{\pi m}{l}\frac{\pi m'}{l}\{\exp[-ik\alpha(2l+\Delta z)]-\exp[-ik\alpha(2l-\Delta z)]+\\ +2\exp[ik\alpha\Delta z]-2i\alpha\left\{\frac{\pi m'}{l}\sin\left(\frac{\pi m\Delta z}{l}\right)-\frac{\pi m}{l}\times\right.\\ \left.\times\sin\left(\frac{\pi m'\Delta z}{l}\right)(1-\exp[-2ik\alpha l]\right\} & npu\ 0\le|\Delta z|<2l,\\ (-1)\frac{\pi m}{l}\frac{\pi m'}{l}\times\left(\exp[-ik\alpha(l+\Delta z)]-\right.\\ \left.-\exp[ik\alpha(l-\Delta z)]\right)^2 & npu\ |\Delta z|\ge 2l.\end{cases}$$

It is interest to analyze the case where the current distribution rules in dipoles have different forms. It is clear that the expression described T_{zz} retains form in interchanging the current distribution rule $j_1(z)$ on $j_2(z')$ and $j_2(z')$ on $j_1(z)$ conversely. In using current distribution rules $j_1(z)=\cos\left((\pi(m-0.5)z)/l\right)$ and $j_2(z')=\sin\left((\pi m'(z'-\Delta z))/l\right)$ we derive the following expression

$$T_{zz}=\frac{(-1)^{m+m'}(1-\alpha^2)}{\left([\frac{\pi(m-0.5)}{l}]^2-\alpha^2\right)\left([\frac{\pi m'}{l}]^2-\alpha^2\right)}\times \quad (7)$$

$$\times\begin{cases}\frac{\pi(m-0.5)}{l}\frac{\pi m'}{l}\{\exp[-ik\alpha l][1-\exp[-ik\alpha(l-\Delta z)]]-\\ -\cos\left(\frac{\pi(m-0.5)\Delta z}{l}\right)[1-\exp[-ik\alpha(l+\Delta z)]]\}-\\ -i\alpha[\frac{\pi m'}{l}\sin\left(\frac{\pi(m-0.5)\Delta z}{l}\right)[1+\\ +\exp[-ik\alpha(l+\Delta z)]]-\frac{2\pi(m-0.5)}{l}\sin\left(\frac{\pi m'\Delta z}{l}\right)\times\\ \times[1+\exp[-2ik\alpha l]]] & \text{at } 0\le|\Delta z|<2l\\ \frac{\pi(m-0.5)}{l}\frac{\pi m'}{l}\exp(ik\alpha\Delta z)\times\\ \times\left(\exp[2ik\alpha l]-\exp[-2ik\alpha l]\right) & \text{at } |\Delta z|\ge 2l.\end{cases}$$

The relations (5)–(7) describe function T_{zz} on the first branch of contour of integration between points [1,0] on real axis. The expressions for T_{zz} on the second branch of contour of integration can be derived from (5)–(7) by substitution α on $-i\alpha$.

In general case the current distributions in dipoles are described by superposition of given harmonics. The calculation of mutual coupling is performed to solution of system linear algebraic equations. The coefficients of matrix are defined by formula (4) in which function T_{zz} is determined previously. Obtained analytical presentation of T_{zz} in integral (3) permits to reduce considerably required calculations.

REFERENCES

1. *Aizenberg, G.Z., Yampol'skii, V.G., and Tereshin, O.N.*, Antenny UKV (Ultrashort Wave Antennas), Moscow: Svyaz', 1977, vol.1.
2. *Kravtsov, V.A., Kravtsova, G.V.* "Vzaimnie soprotivleniya prodolnikh vibratorov (The mutual coupling between longitudinal dipoles near circular cylinder)", Radiotekhnika, V.33, pp.85-90, February 1978
3. *Yashin, B.A.* "Analiz i raschet sobstvennogo i vzaimnogo soprotivlenii prodolnikh vibratorov vblizi idealno provodyashchego cilindra (Analysis and calculation of the self-impedance and the mutual impedance the longitudinal dipoles near perfectly conducting circular cylinder)", Tr. NII radio, pp.71-76, April 1988.
4. *Kravtsov, V.A., Kravtsova, G.V., and Ulasik, O.L* "Vzaimnoye vliyaniye vibratornikh antenn, raspolozhennikh na ellipticheskom cilindre (Mutual coupling of antenna of dipoles near elliptic cylinder), Radiotekhnika, V.43, pp.65-70, June 1988.

THE INFLUENCE OF IMPEDANCE SURFACE OF A CIRCULAR CYLINDER ON THE DIPOLE PATTERN

D. D. Gabriel'yan, M. Yu. Zvezdina

Rostov Military Institute of Missile Corps, 344027 Rostov-on-Don, 27 Russia
E-mail: zvezd@jeo.ru

The problem of solving the volumetric vector pattern for electric dipole disposed near by the impedance circular cylinder is high priority from different points of view. This is confirmed by a great number of papers of the given theme, for example [1–5].

The purpose of the report is to study the influence of impedance surface of circular cylinder on the pattern of the arbitrary-oriented electric dipole disposed near it.

Using the equivalent surface current theorem one obtains the expression for the pattern of the electric dipole as [1]

$$\vec{\chi}\vec{E}(\theta,\varphi) = \int_V \vec{J}^{\,e}(\kappa\vec{r}')\vec{E}_\chi(\theta,\varphi;\kappa\vec{r}')d\vec{r}' . \qquad (1)$$

$$(\chi = \theta,\varphi)$$

In the relation (1) $\vec{E}_\chi(\theta,\varphi;\kappa\vec{r}')$ is the solution of the diffraction problem for the plane electromagnetic wave on circular impedance cylinder of radius a in the point where radius vector is $\vec{r}'$; plane electromagnetic wave arrives from direction θ,φ. Vector $\vec{E}$ in the front of wave has only χ-component; $\vec{J}^{\,e}(\kappa\vec{r}')$ is a vector of current density distribution in dipole.

In the incident wave only vector $\vec{E}$ or $\vec{H}$ has a longitudinal component which may describe in the quasi-3D approximation as

$$\begin{Bmatrix} E_z^{inc}(\theta,\varphi;\kappa\vec{r}') \\ H_z^{inc}(\theta,\varphi;\kappa\vec{r}') \end{Bmatrix} = E_0 \begin{Bmatrix} 1 \\ W_0^{-1} \end{Bmatrix} \exp(-ikz\cos\theta)\times \qquad (2)$$

$$\times \sum_{n=-\infty}^{\infty} \exp[-in(\varphi-\varphi_0)] J_n(\widetilde{\kappa}r') H_n^{(2)}(\widetilde{\kappa}r),$$

where $\widetilde{k} = k\sin\theta$; the top and lower rows correspond to the cases of calculating θ- and φ-component of the pattern; E_0 is the amplitude of the electric field strength in the front of the incident wave; $W_0 = 120\pi$ Ohm is the free-space impedance; $k = 2\pi/\lambda$ is the wave number; λ is the wavelength in the free space; i is imaginary unity; $J_n(\cdot)$, $H_n^{(2)}(\cdot)$ are the Bessel function and the Hankel function of the second kind of order n respectively. Figure 1 shows the problem geometry. The time dependence factor $\exp(i\omega t)$ is omitted.

In the scattering field in general case of the impedance circular cylinder the longitudinal components have both E- and H-fields. The scattering field we shall find in the form [3, 4]

$$\begin{Bmatrix} E_z^s \\ H_z^s \end{Bmatrix} = \sum_{n=-\infty}^{\infty} \begin{Bmatrix} a_n \\ b_n W_0^{-1} \end{Bmatrix} C_n(\theta,\varphi), \qquad (3)$$

where $C_n(\theta,\varphi) = E_0 \exp(-ikz\cos\theta)\times$

$$\times \exp[-in(\varphi-\varphi')] H_n^{(2)}(\widetilde{k}r') .$$

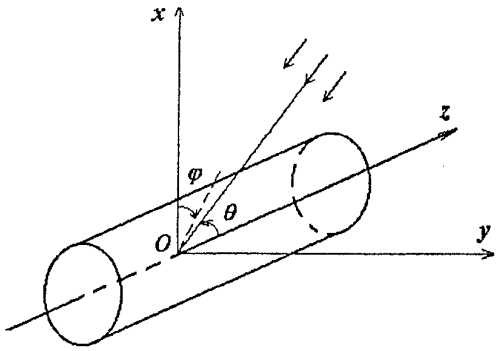


Fig.1. Problem geometry

The transversal components of the electromagnetic field can be obtained using the ratio [1]

$$E_\varphi = \frac{1}{\widetilde{k}^2}\left\{ ikW_0 \frac{\partial H_z}{\partial r} - \frac{k\cos\theta}{r}\frac{\partial E_z}{\partial \varphi} \right\}, \qquad (4)$$

$$E_r = -\frac{1}{\widetilde{k}^2}\left\{ \frac{ikW_0}{r}\frac{\partial H_z}{\partial \varphi} + k\cos\theta \frac{\partial E_z}{\partial r} \right\},$$

$$H_\varphi = -\frac{1}{\widetilde{k}^2}\left\{ \frac{k\cos\theta}{r}\frac{\partial H_z}{\partial \varphi} + \frac{ik}{W_0}\frac{\partial E_z}{\partial r} \right\},$$

$$H_r = -\frac{1}{\widetilde{k}^2}\left\{ -k\cos\theta \frac{\partial H_z}{\partial r} + \frac{ik}{W_0 r}\frac{\partial E_z}{\partial \varphi} \right\}.$$

The impedance boundary condition of form [6] is to be satisfied on the surface ($r' = a$) of circular cylinder

$$\begin{cases} E_z = Z H_\varphi \\ E_\varphi = -Z H_z \end{cases}, \qquad (5)$$

where Z is the surface impedance.

Under the E_θ-wave diffraction let E_z^t denote a longitudinal component of the total electric field strength and H_z^c is a longitudinal cross polarized component of the scattered magnetic field strength (the given components is equal to zero in the incident field). Under H_θ-wave diffraction write H_z^t for a longitudinal component of the total magnetic field strength and E_z^c for a longitudinal component of the scattering electric field strength (the given component equals to zero in the incident field). With the introduction of the given notation the total fields for the diffraction problem may be written in the form

$$E_z^t(\theta,\varphi) = A_0 \sum_{n=-\infty}^{\infty} \exp[-in(\varphi-\varphi')] \times \quad (6)$$

$$\times \left\{ i^n J_n(\widetilde{\kappa} r') + a1_n H_n^{(2)}(\widetilde{\kappa} r') \right. ,$$

$$H_z^c(\theta,\varphi) = A_0 \sum_{n=-\infty}^{\infty} \exp[-in(\varphi-\varphi')]\, b1_n H_n^{(2)}(\widetilde{\kappa} r') \quad (7)$$

for the E_θ-wave and

$$H_z^t(\theta,\varphi) = B_0 \sum_{n=-\infty}^{\infty} \exp[-in(\varphi-\varphi')] \times \quad (8)$$

$$\times \left\{ i^n J_n(\widetilde{\kappa} r') + b2_n H_n^{(2)}(\widetilde{\kappa} r') \right. ,$$

$$E_z^c(\theta,\varphi) = B_0 \sum_{n=-\infty}^{\infty} \exp[-in(\varphi-\varphi')]\, a2_n H_n^{(2)}(\widetilde{\kappa} r') , \quad (9)$$

for the H_θ-wave (E_φ-polarization).

In relations (6)–(9) the following notation has been introduced: $A_0 = E_0 \sin\theta$; $B_0 = H_0 \sin\theta$, as well as the asymptotic of the Hankel function is used for large argument values

$$H_n^{(2)}(\kappa r) = \sqrt{\frac{2}{\pi\kappa r}} i^n \exp(-i\pi/4 - i\kappa r);$$

$$a1_n = \frac{i^n \left\{ J_n(\widetilde{ka}) + \dfrac{iZ_N}{\sin\theta} J_n'(\widetilde{ka}) D1_n^e(\widetilde{ka}) \right\}}{H_n^{(2)}(\widetilde{ka}) + \dfrac{iZ_N}{\sin\theta} H_n^{(2)'}(\widetilde{ka}) D2_n^e(\widetilde{ka})},$$

$$b1_n = -\frac{nW_0 \cos\theta}{\widetilde{ka}} \frac{i^n J_n(\widetilde{ka}) - a_n H_n^{(2)}(\widetilde{ka})}{H_n^{(2)'}(\widetilde{ka}) - iZ_N \sin\theta\, H_n^{(2)}(\widetilde{ka})},$$

$$a2_n = Z \frac{n\cos\theta}{\widetilde{ka}\sin\theta} \frac{i^n J_n(\widetilde{ka}) - b_n H_n^{(2)}(\widetilde{ka})}{H_n^{(2)}(\widetilde{ka}) + \dfrac{iZ_N}{\sin\theta} H_n^{(2)'}(\widetilde{ka})},$$

$$b2_n = \frac{i^n \left\{ J_n'(\widetilde{ka}) - iZ_N \sin\theta\, J_n(\widetilde{ka}) D1_n^h(\widetilde{ka}) \right\}}{H_n^{(2)'}(\widetilde{ka}) - iZ_N \sin\theta\, H_n^{(2)}(\widetilde{ka})\, D2_n^h(\widetilde{ka})} .$$

$Z_N = Z/W_0$ is the surface impedance, normalized by the free-space impedance; $J_n'(\cdot)$, $H_n^{(2)\prime}(\cdot)$ are the derivations of the Bessel function of order n and the Hankel function of the second kind of order n, respectively;

$$D1_n^e(\widetilde{ka}) = 1 + K_n^e(\widetilde{ka}) \frac{J_n(\widetilde{ka})}{J_n'(\widetilde{ka})},$$

$$D2_n^e(\widetilde{ka}) = 1 + K_n^e(\widetilde{ka}) \frac{H_n^{(2)}(\widetilde{ka})}{H_n^{(2)'}(\widetilde{ka})},$$

$$K_n^e(\widetilde{ka}) = \left(\frac{n\cos\theta}{\widetilde{ka}} \right)^2 \left[\frac{H_n^{(2)'}(\widetilde{ka})}{H_n^{(2)}(\widetilde{ka})} - iZ_N \sin\theta \right]^{-1},$$

$$K_n^h(\widetilde{ka}) = \left(\frac{n\cos\theta}{\widetilde{ka}} \right)^2 \left[\sin\theta + iZ_N \frac{H_n^{(2)'}(\widetilde{ka})}{H_n^2(\widetilde{ka})} \right]^{-1}.$$

We shall pursue a study of the influence of the impedance properties for the circular cylinder surface on the pattern of the dipole disposed near by it on the model of differently-oriented electric dipoles.

For the longitudinal electric dipole the vector of the current density distribution has the form

$$\vec{J}^e(\kappa r') = \vec{z}\, \delta(z')\delta(\varphi-\varphi')\delta(r'-r)/r .$$

In this case the relations for the θ- and φ-components of the pattern may be written as

$$F_0(\theta,\varphi) = \widetilde{\kappa} l \sum_{n=0}^{\infty} \varepsilon_n i^n \cos[n(\varphi-\varphi')] \times \quad (10)$$

$$\times \left\{ J_n(\widetilde{\kappa} r') - a1_n H_n^{(2)}(\widetilde{\kappa} r') \right. ,$$

$$F_\varphi(\theta,\varphi) = \widetilde{\kappa} l \sum_{n=0}^{\infty} \varepsilon_n i^n \sin[n(\varphi-\varphi')] \times \quad (11)$$

$$\times a2_n H_n^{(2)}(\widetilde{\kappa} r'),$$

where ε_n is the Neumann number.

For the case circumferential electric dipole the vector of the current density distribution has the form

$$\vec{J}^e(\kappa r') = \vec{\varphi}\, \delta(\varphi')\delta(z')\delta(r'-r)/r .$$

Under such current distribution the relations for the θ- and φ-components of the pattern are defined by expressions

$$F_0(\theta,\varphi) = \frac{2\kappa l \cos\theta}{\widetilde{\kappa} r'} \sum_{n=1}^{\infty} i^n n \sin[n(\varphi-\varphi')] \times \quad (12)$$

$$\times \left\{ J_n(\widetilde{\kappa} r') - a1_n H_n^{(2)}(\widetilde{\kappa} r') \right\} -$$

$$-\kappa l \sum_{n=0}^{\infty} \varepsilon_n i^n \sin[n(\varphi-\varphi')]\, b1_n H_n^{(2)}(\widetilde{\kappa} r'),$$

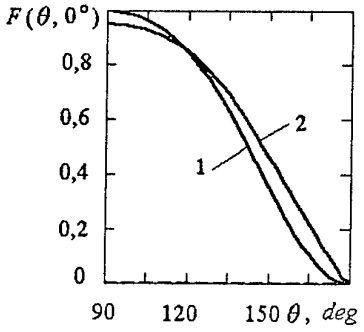


Fig. 2

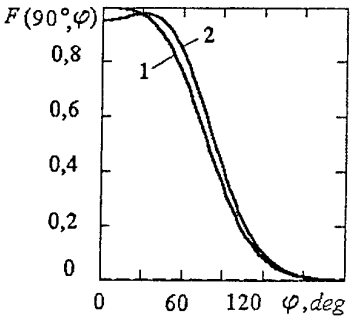


Fig. 3

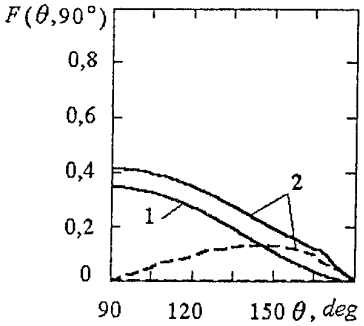


Fig. 4

Fig. 2. The conic sections of the θ-component for the volumetric pattern by the surface plane φ = 0° (1 – perfectly conducting cylinder; 2 – impedance cylinder)

Fig. 3. The conic sections of the θ-component for the volumetric pattern by the surface plane θ = 90° (1 – perfectly conducting cylinder; 2 – impedance cylinder)

Fig. 4. The conic sections of the θ-component for the volumetric pattern by the surface plane φ = 90° (1 – perfectly conducting-cylinder; 2 – impedance cylinder)

$$F_{\varphi}(\theta,\varphi) = -\widetilde{\kappa} l \sum_{n=0}^{\infty} \varepsilon_n i^n \cos[n(\varphi-\varphi')] \times \quad (13)$$
$$\times \left\{ J_n'(\widetilde{\kappa} r') - b2_n H_n^{(2)'}(\widetilde{\kappa} r') \right\} -$$
$$- \frac{2\kappa l \cos\theta}{\widetilde{\kappa} r'} \sum_{n=1}^{\infty} i^n n \cos[n(\varphi-\varphi')] a2_n H_n^{(2)}(\widetilde{\kappa} r') .$$

For the radial electric radiator the vector of the current density distribution has the form

$$\vec{J}^{e}(\kappa r') = \vec{r}\,\delta(r')/r\,\delta(\varphi-\varphi')\delta(z') .$$

The relations for the θ- and φ-components of the volumetric pattern of the radial electric dipole disposed near the circular impedance cylinder are described as

$$F_{\theta}(\theta,\varphi) = \widetilde{\kappa} l \cos\theta \sum_{n=0}^{\infty} \varepsilon_n i^n \cos[n(\varphi-\varphi')] \times \quad (14)$$
$$\times \left\{ J_n'(\widetilde{\kappa} r') - b2_n H_n^{(2)'}(\widetilde{\kappa} r') \right\} +$$
$$+ \frac{\kappa l}{\widetilde{\kappa} r'} \sum_{n=0}^{\infty} \varepsilon_n i^n n \cos[n(\varphi-\varphi')] b1_n H_n^{(2)}(\widetilde{\kappa} r') ,$$

$$F_{\varphi}(\theta,\varphi) = \frac{2\kappa l \cos\theta}{\widetilde{\kappa} r'} \sum_{n=1}^{\infty} i^n n \sin[n(\varphi-\varphi')] \times \quad (15)$$
$$\times \left\{ J_n(\widetilde{\kappa} r') - a1_n H_n^{(2)}(\widetilde{\kappa} r') \right\} +$$
$$+ \kappa l \cos\theta \sum_{n=0}^{\infty} \varepsilon_n i^n \sin[n(\varphi-\varphi')] a2_n H_n^{(2)'}(\widetilde{\kappa} r') .$$

More detailed numerical investigations have been carried out for the longitudinal electric dipole disposed at distance of 0.25λ from the surface of the circular cylinder of radius $a = 2\lambda$. The sections of the θ-component for the volumetric pattern are illustrated in Fig. 2–4. On them curve 1 denotes the results corresponding to the volumetric pattern sections of perfectly conducting cylinder surface, curve 2 – normalized surface impedance $Z_N = 0.3i$ [7]. Solid lines correspond to the base component of the volumetric pattern and dashed ones to the cross-polarized component.

The plots in Fig. 2–4 permit to analyze the influence of the surface impedance magnitude on the base component of the longitudinal dipole. At the same time the longitudinal radiator near the circular impedance cylinder acquires a φ-component of the pattern as well. However the magnitude of the latter for the considered value of the surface impedance does nit exceed 8% from the amplitude of the base component.

The investigations conducted show that the surface impedance changes not only the form of the pattern but the structure of the dipole patterns as well.

REFERENCES

1. *Wait, J.R.* Electromagnetic Radiation from Cylindrical Structures, Oxford: Pergamon, 1959.

2. *Markov, G.T. and Chaplin, A.F.*, Vozbuzdenie electromagnitnykh voln (Excitation of Electro-

magnetic Waves), Moscow: Sovetckoe Radio, 1969.

3. *Vasil'ev, E.N.*. Vozbuzdenie tel vrascheniya (Excitation of bodies of revolution) Moscow: Radio i sviaz, 1987.

4. *Gabriel'yan, D.D., Zvezdina, M.Yu.* "Radiation of Linear Antenna Parallel to an Impedance Circular Cylinder", Acoustical Physics, V.43, pp.471-473, April 1997.

5. *Kumar A., Shastry S.V.K.* "Radiation from dipoles in the presence of dielectric-coated circular cylinder", J. Inst. Electron. and Telecommun. Eng., V.31, pp.184-189, June 1985.

6. *Vaganov, R.B., Katsenelenbaum, B.Z.,* Osnovy teorii difraktsii (Foundations of Diffraction Theory), Moscow: Nauka, 1982.

7. *Baranchugov, E.A., Zatsepin, P.M. and Komarov, S.A.* "Quasitrekhmernaya zadacha difraktsii ploskoiy elektromagnitnoiy volny na impedansnoiy lente" (Quasi-three-dimension Problem of Diffraction of a Planar Electromagnetic Wave by Impedance Strip), Radiotekhnika i elektronika, V.43, pp.1291-1295, November 1998.

WAVES SCATTERING ON A SYSTEM OF FILLETS

A. V. Golovchenko, G. I. Koshevoy, D. I. Yaresko

State aerospace university named after N. E. Zhukovsky
17 Chkalov Street, Kharkov, Ukraine, 310070, tel. 8-0572-442-361

The problemof scattering of flat linearly polarized wave on a system of absolutey thin ideally conducting fillets with parallel edges comes to two scalar boundary value problems [1]. It is Dirichlet's problem (in the case of a falling *E*-polarized incident wave) and Neumann's problem (in the case of *H*- polarization) for the two-dimensional Helmholtz equation on a system of segments located arbitrarily (Fig. 1).

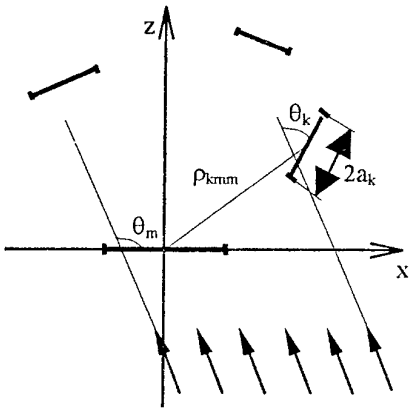


Fig. 1. The cross-section of the considered structure

In both cases the systems of integral equations of the first kind can be obtained, in which the addends connected with some considered m fillet (or a segment that does not differ here) are chosen containing the difference kernel as Hankel's function, having a logarithmic singularity under coincidence of arguments. The rest addends contain regular kernels and following the work [2], systems of integral equations can be represented as:

$$(e_1)\quad \int_{-a_m}^{a_m} \varphi_m(t) H_0^{(1)}(k|x-t|)dt = f_m^e(x) + \sum_{k=1,k\neq m}^{N} \int_{-a_k}^{a_k} \varphi_k(t) R_k^e(k;x,t)dt,\ |x| < a_m$$

$$(h_1)\quad \int_{-a_m}^{a_m} \phi_m(t) H_0^{(1)}(k|x-t|)dt = A_m \cos kx + B_m \sin kx + \frac{1}{k}\int_0^x \sin k(x-t)\left[f_m^h(t) + \sum_{k=1,k\neq m}^{N} \int_{-a_k}^{a_k} \phi_k(\xi) R_k^h(k;x,\xi)d\xi\right]dt,\ |x| < a_m$$

$$m = 1, 2, \ldots, N$$

Here the unknown values of the function $\varphi_m(x)$ and $\phi_m(x)$ from an electrodynamic point of view have the meaning of a surface electric current on m fillet flowing in parallel and perpendicular to its edge; $f_m^{e,h}(x)$ — known complex-valued functions, difined by the incident electromagnetic wave on the system; A_m and B_m are determined by conditions on the fillet edges; $\phi_m(\pm a_m) = 0$.

Moreover, it is known that transversal component decreases on an edge as $\rho^{1/2}$, ρ is the distance from the edge, and longitudinal component of surface current density has a rooted singularity while approaching to the edge of the fillet. These circumstances should be taken into account both for numerical realization of the known methods, and for deriving asymptoticses.

Among numerical methods it is necessary to mark a method described in the work [3], which is well mathematically grounded, but quite labour-consuming during its realization. Here it is proposed a little other, more simple, but less justified method of solution of integral equations such as a convolution. Its idea consists in selection of logarithmic singularity in the kernel with its further elimination at the expense of obvious analytical solution of the elementary singular equation with the difference logarithmic kernel. Let's explain this method in application to the problemof scattering of E - polarized wave on one fillet, which can be represented as the integral equation

$$\int_{-1}^{1} \varphi(t) H_0^{(1)}(\kappa|x-t|)dt = -4i,\ |x| < 1$$

As

$$H_0^{(1)}(z) = \frac{2i}{\pi}\left[\sum_{k=1}^{\infty} \frac{(-1)^k z^{2k}}{2^{2k}(k!)^2}\left(\ln\frac{\gamma z}{2i} - \sum_{m=1}^{k}\frac{1}{m}\right) + \ln\frac{\gamma z}{2i}\right],$$

then the singularity is selected very simply

$$\int_{-1}^{1} \varphi(t)\ln|x-t|dt = -2\pi - \varphi\ln\frac{\gamma z}{2i} - \sum_{k=1}^{\infty}\frac{(-1)^k}{2^{2k}(k!)^2}\int_{-1}^{1}\varphi(t)\kappa^{2k}|x-t|^{2k}\left[\ln\frac{\gamma z}{2i}|x-t| - \sum_{m=1}^{k}\frac{1}{m}\right]dt$$

By designating the right-hand term through $f(x)$, the solution of this equation with regard for singularity on the edge can by written down as [4]:

$$\varphi(x)=\frac{-1}{\pi^2\sqrt{1-x^2}}\int_{-1}^{1}\left[\frac{\sqrt{1-y^2}}{x-y}f'(y)+\frac{f(y)}{\sqrt{1-y^2}\cdot\ln 2}\right]dy.$$

Using this, eliminate the singularity:

$$\varphi(x)=\frac{2\pi+\varphi\ln\frac{\gamma\kappa}{2i}}{\pi\sqrt{1-x^2}\ln 2}+\sum_{k=1}^{\infty}\frac{(-1)^k\kappa^{2k}}{2^{2k}(k!)^2}\int_{-1}^{1}\frac{\varphi(t)}{\sqrt{1-x^2}}\times$$

$$\times\int_{-1}^{1}\frac{\varphi(t)}{\sqrt{1-x^2}}\left[\frac{\sqrt{1-y^2}}{x-y}|y-t|^{2k-1}\left(2k\left(\ln\frac{\gamma\kappa|y-t|}{2i}-\sum_{m=1}^{k}\frac{1}{m}\right)\right)\times\right.$$

$$\left.\times Sign(y-t)+\frac{|y-t|^{2k}}{\sqrt{1-y^2}\ln 2}\left(\ln\frac{\gamma\kappa|y-t|}{2i}-\sum_{m=1}^{k}\frac{1}{m}\right)\right]dt.$$

This is an integral equation of the second kind. It is convenient for realization of a long wave asymptotics, which takes place when $\kappa=ka<<1$. The principal term of this asymptotics is connected to the first addend and reduces to expression $\varphi_0(x)=\frac{-2}{\ln\frac{\gamma\kappa}{4i}\sqrt{1-x^2}}$, which completely coincides with a known classical outcome (see, for example, [1]).

The same method in case of H-polarization reduces to the following asymptotic expression for transversal current in a fillet:

$$\phi_m(x)=i\kappa_m\sqrt{1-\left(\frac{x}{a_m}\right)^2}M_m\sin\theta_m 2\left\{1+\right.$$

$$+i\kappa_m\frac{x}{a_m}\cos\theta_m-\kappa_m^2\left[\frac{1}{4}\ln\frac{\gamma\kappa_m}{4i}-\frac{5}{24}+\frac{\cos^2\theta_m}{12}+\right.$$

$$+i\frac{\pi}{4}\sum_{n\neq m}^{N}R(k\rho_{km})\frac{a_k^2M_k\sin\theta_k}{a_m^2M_m\sin\theta_m}+$$

$$\left.\left.+\frac{1+2\cos^2\theta_m}{12}\left(\frac{x}{a_m}\right)^2\right]+\ldots\right\}$$

$$\kappa_m=ka_m,\quad |x|<a_m.$$

Here

$$R(k\rho)=\left[H_0^{(1)}(k\rho)-2\frac{H_1^{(1)}(k\rho)}{k\rho}\right]\frac{z_{km}\cdot z_{mk}}{\rho^2}-$$

$$-\frac{H_1^{(1)}(k\rho)}{k\rho}\cos\alpha_{mk}.$$

This expression supposes passage to the limit to one fillet. The expression, obtained under it, in case of an orthogonal falling $\left(\theta_m=\frac{\pi}{2}\right)$ completely coincides with reduced in the monography [1], that testifies to regularity of obtained outcomes. The reduced asymptotic expression takes into account electromagnetic interaction between separate fillets: it is ensured with an addend with sum in square brackets. In other words, the influence of availability of adjacent fillets to transversal current on m fillet is exhibited only as single-error correction $(\kappa_m)^3$, at that k fillet renders the influence on m fillet under $\theta_k\neq 0$. In the case when $\theta_k=0$ this influence is exhibited in addends of the higher order.

REFERENCES

1. H.Henl, A.Mawer, K.Vestfal. Theory of diffraction. Moscow, "Mir" publ., 1964, 428 p. [in Russian].
2. Koshebvoy G.I. "On wave diffraction on a system of fillets". Proc. VIII Int. Symp. MDOZMF '99 [in Russian].
3. Sologub V.G. "on solution of one integral equation of convolution-type with finite integrating limits". Zhurnal vychislitelnoy matematiki i matematichesloy fiziki. 1971, N 4, pp.837-854 [in Russian.
4. Gahov F.D. Eqghenvalue problems. Moscow. "Nauka" publ., 1977, 640 p. [in Russian].

TRANSIENT RADIATION FROM APERTURE ANTENNA UNDER NON-SYNCHRONOUS EXCITATION

N. N. Kolchigin, S. N. Pivnenko

Kharkov State University, 4, Svobody sq., Kharkov, 310077, Ukraine
Tel: +38-0572-457257; e-mail: Nicolay.N.Kolchigin@univer.kharkov.ua

INTRODUCTION

A number of papers has been devoted to the thorough theoretical investigation of radiation characteristics of aperture antennas under synchronous transient excitation [1-3]. At the same time, a few works was directed to the problem of non-synchronous excitation of such antennas [4]. In this work, we describe a general problem of radiation from a rectangular aperture excited with transient signal of arbitrary time dependence and amplitude distribution of a current density over aperture taking into account arbitrary non-synchronous function of excitation.

SOLUTION TO THE PROBLEM

A rectangular aperture with sizes of $2a \times 2b$ is situated in the plane $z = 0$ of Cartesian coordinate sistem X, Y, Z. The center of the aperture is in the point $x = 0$, $y = 0$ (Fig. 1).

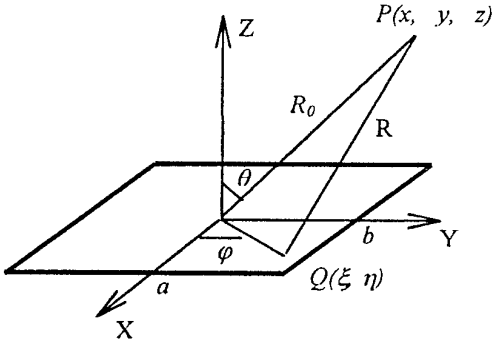


Fig. 1. Geometry of the problem and coordinate systems

Due to linearity of the problem we consider a case of aperture excitation with a current of single polarization. Assume the vector of current density to be directed along Ox axis. Then the magnetic field vector has components H_y and H_z. For simplisity we consider only H_y field component

$$H_y(\omega, x, y, z) = \\ = \frac{-1}{4\pi}\iint I_x(\omega, \xi, \eta)\,(ik + \frac{1}{R})\,\frac{z\,e^{-ikR}}{R^2}\,d\xi d\eta \qquad (1)$$

Here x, y, z are coordinates of the observation point P; ξ, η are coordinates of the point Q at the aperture; $k = \omega/c$, c is the speed of light. A distance between the observation point $P(x, y, z)$ and the point $Q(\xi\ \eta, 0)$ at the aperture is $R = ((x-\xi)^2 + (y-\eta)^2 + z^2)^{1/2}$; $I_x(\omega, \xi, \eta)$ is a Fourier image of a time function of excitation.

Consider a general type dependence of current density over the aperture in the form

$$I(t, \xi, \eta) = A(\xi, \eta) f(t - t_d(\xi, \eta)), \qquad (2)$$

where $A(\xi\ \eta)$ is a function of amplitude distribution of current density over the aperture, $t_d(\xi\ \eta)$ is a function of time delay over the aperture and $f(t)$ is an arbitrary time function. Taking into consideration (2) and changing to the time domain we obtain

$$H_y(t, x, y, z) = \\ = -\frac{1}{4\pi}\int_{-a}^{a}\int_{-b}^{b} A(\xi, \eta)\left(\frac{1}{c}\dot{f}\left(t - \frac{R}{c} - t_d(\xi, \eta)\right) + \right. \qquad (3) \\ \left. + \frac{1}{R} f\left(t - \frac{R}{c} - t_d(\xi, \eta)\right)\right)\frac{z}{R^2}\,d\xi\,d\eta.$$

In this formula the first item describes the field of radiation while the second item describes the static field of the current. In an expression for the electric field, one more item is present due to a static field of a charge.

In the near zone (Fresnel zone) the expression for R can be represented as a summation $R \cong R_0 + \frac{\xi^2 + \eta^2}{2R_0} - \frac{x\xi + y\eta}{R_0}$, where $R_0 = (x^2 + y^2 + z^2)^{1/2}$ is a distance from the aperture center to the observation point. Neglecting the magnetostatic item, which decreases with distance as $1 / R^3$, we obtain the field in the Fresnel zone ($R_0 >> a$):

$$H_y(t, x, y, z) = -\frac{z}{4\pi R_0^2 c}\int_{-a}^{a}\int_{-b}^{b} A(\xi, \eta) \times \\ \times \dot{f}\left(\tau - t_d(\xi, \eta) - \frac{\xi^2 + \eta^2}{2R_0 c} + \frac{x\xi + y\eta}{R_0 c}\right) d\xi\,d\eta. \qquad (4)$$

In the Fraunghopher zone ($R_0 >> a^2 / 2cT$, where T is a pulse duration):

$$H_y(t,x,y,z) = -\frac{z}{4\pi R_0^2 c}\int_{-a}^{a}\int_{-b}^{b} A(\xi,\eta)\times \times \dot{f}\left(\tau - t_d(\xi,\eta) + \frac{x\xi + y\eta}{R_0 c}\right) d\xi\, d\eta. \quad (5)$$

In this formulas is designated $\tau = t - R_0/c$.

Obtained expressions (4) and (5) describe the radiation field of the aperture antenna under arbitrary amplitude and time excitation subject to arbitrary distribution of time delay of excitation over the aperture. Expressions (4) and (5) differ from corresponding expressions in [1] by presence of the additional item $t_d(\xi,\eta)$ in the argument of function $\dot{f}$. The general expression for the time delay function allows to consider a variety of particular cases such as linear delay, spherical delay and more complicated cases of the time delay function.

For particular case when the amplitude distribution and the time delay are varied along ξ-coordinate:

$$I(t,\xi,\eta) = I(t,\xi) = A(\xi) f(t - t_d(\xi)), \quad (6)$$

we obtain an expression for the field in the far zone as a single integral over ξ:

$$H_y(t,x,y,z) = \\ = -\frac{z}{4\pi y R_0}\int_{-a}^{a} A(\xi)\left[f\left(\tau - t_d(\xi) + \frac{x\xi}{R_0 c} + \frac{yb}{R_0 c}\right) - f\left(\tau - t_d(\xi) + \frac{x\xi}{R_0 c} - \frac{yb}{R_0 c}\right)\right] d\xi. \quad (7)$$

There is a finite difference under the integral between delayed excitation functions corresponding to left and right boundaries of the aperture (along Oy axis) which can be replaced in the plane Ox ($y = 0$) with a time derivative:

$$H_y(t,x,0,z) = \\ = -\frac{bz}{2\pi R_0^2 c}\int_{-a}^{a} A(\xi)\dot{f}\left(\tau - t_d(\xi) + \frac{x\xi}{R_0 c}\right) d\xi. \quad (8)$$

For the case of the linear time delay along the Ox axis it is convenient to choose the function $t_d(\xi)$ in the form: $t_d(\xi) = (nT/a)\xi$. Substituting into expression (8) the explicit form of $t_d(\xi)$ and assuming $A(\xi) = 1$ after integration over ξ we obtain the field in the plane Ox as follows

$$H_y(t,x,0,z) = -\frac{bz}{2\pi R_0^2 c}\frac{1}{B}\left(f(\tau + Ba) - f(\tau - Ba)\right), \quad (9)$$

where $B = x/R_0 c - nT/a$. Expression (9) is a finite difference which transforms into time derivative under condition $B \to 0$:

$$H_y(t,x,0,z) = -\frac{abz}{\pi R_0^2 c}\dot{f}(\tau). \quad (10)$$

The condition $x/R_0\ \tilde{n} - nT/a = 0$ determines a turn angle of the radiated field beam. Taking into account the equality $x/R_0 = \sin\theta$, which is correct in spherical coordinate system, we obtain an expression relating angle θ of beam turn, parameter n and relationship $\tilde{n}T/2a$ between space duration $\tilde{n}T$ of the pulse and the aperture dimension $2a$:

$$\sin\theta = 2n(cT/2a). \quad (11)$$

It is follows from (11) that for a constant value of $\tilde{n}T/2a$ sinus of the turn angle is directly proportional to the parameter n and vise versa, for a constant value of n and aperture dimension $2a$ sinus of the turn angle is directly proportional to the space duration $\tilde{n}T$ of the pulse.

For a general case of a spherical time delay describing excitation of TEM-horn antenna, the function $t_d(\xi,\eta)$ has the following form [4]:

$$t_d(\xi,\eta) = (\rho^2 + \xi^2 + \eta^2)^{1/2}/c - \rho/c, \quad (12)$$

where ρ is a radius of a sphera (TEM-horn length). In this case an expression for radiated field can not be obtained in the Fresnel zone in explicit form and we exploited the expression (4) for numerical calculations.

SPACE-ENERGY CHARACTERISTICS OF RADIATED FIELD

Consider space-energy characteristics of the aperture antenna under non-synchronous excitation. Define the total energy of radiated pulse as [1]

$$E = 120\pi\int_{-\infty}^{\infty}\left|H_\varphi(t)\right|^2 dt. \quad (13)$$

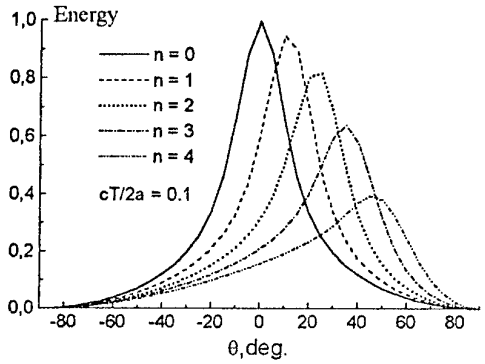
For the case of a linear delay the time delay function is chosen in the form $t_d(\xi) = (nT/a)\xi$. It was shown above that in the far zone ($R_0 >> a^2/2cT$) in the plane Ox the expression for the radiated field is obtained in the explisit form. It allowed analysing directly the expression (11). Fig. 2 shows a dependence of the normalized energy of the radiated field on an observation angle θ ($\varphi = 0$, E-plane) for several values of parameter n of the linear time delay at $cT/2a = 0.1;\ 0.03$. Time dependence of the excitation function is chosen as a gaussian function; $2a = 2b = 0.2$ m, $R_0 = 3$ m.

Consider the case of a spherical function of the non-synchronous aperture excitation. The function of the time delay is chosen in the form (12). All calculation were performed according to (4) for gaussian time dependence of the excitation function and for $2a = 2b =$ 0.2 m. In Fig. 3 dependencies of normalized energy of the radiated pulse on the radius of the spherical time delay ρ at various distances R_0 from the aperture and for $cT/2a = 0.1;\ 0.03$ ($\theta = 0$, $\varphi = 0$) are shown.

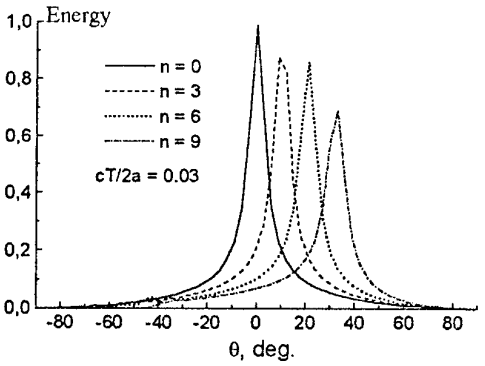
It is seen from the figure that the change of ρ results in the shift of the energy focus point along the Oz axis. Each value of ρ corresponds to some distance R_0 for which a maximum of energy is observed. It is also seen that $R_0(\max) = |\rho|$.

CONCLUSION

Solution to the problem of transient radiation from the aperture antenna is obtained in a general form taking into account an arbitrary function of non-synchronous excitation of a current density over the aperture. The solution is obtained in an explicit form for the case of a linear function of non-synchronous excitation. Dependence of the pulse energy focus point location on the value of a spherical time delay parameter is found.

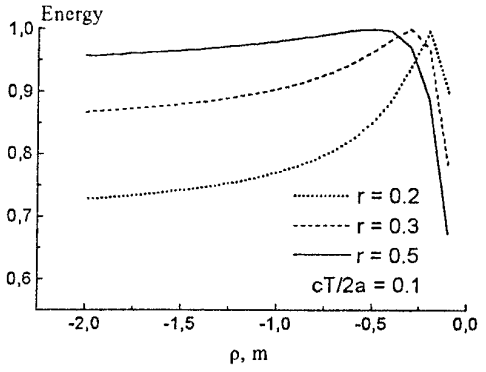


a)

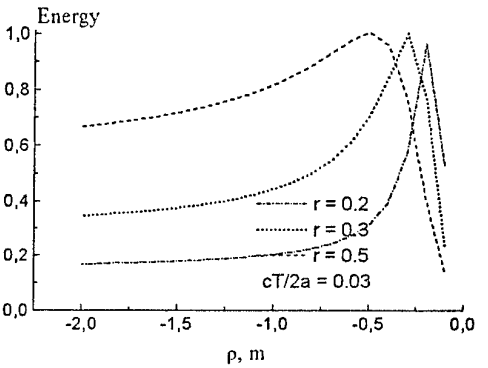


b)

Fig. 2. Dependence of normalized energy of radiated pulse on the observation angle θ



a)



b)

Fig. 3. Dependence of normalized energy of radiated pulse on the radius of the spherical time delay ρ.

REFERENCES

1. Sodin L. G. "Pulsed radiation of antenna". Radiophysics and radioastronomy. - 1997. - Vol.2, N1. - P.5-15 [in Russian].

2. Heyman E., Melamed T. "Certain considerations in aperture synthesis of ultrawideband short-pulse radiation". IEEE Trans. Antennas Propagat. - Apr. 1994. - Vol. 42. - P. 518-525.

3. Kolchigin N.N.,Pivnenko S.N., and Lomakin V.M "Influence of lossesin dielectric half-space on characteristics of reflected pulsed 3D wave beam". Radiophysics and radioastronomy. - 1997. - Vol.2, N3. - P.318-322 [in Russian].

4. Lisitsyn V. P., Domashenko G. D., Utkin M. I. "Transient electromagnetic field of TEM-horn array" Radiotekhnika i elektronika. - 1992. - Vol.37, N11. - P.1954-1959.

RESONANT TRANSFORMATION OF THE ELECTRIC-DIPOLE FIELD INTO A CIRCULARLY POLARIZED FIELD BY MEANS OF A SMALL DIELECTRIC SPHERE WITH THE SURFACE CONDUCTANCE ALONG HELICAL-TYPE LINES

E. N. Korshunova, A. N. Sivov, and A. D. Shatrov

Institute of Radio Engineering and Electronics, Russian Academy of Sciences,
1 Vvedenskii sq., Fryazino, Moscow region, 141120 Russia
Tel: (095) 526 9266 Fax: (096) 7029572 e-mail: ask138@ire216.msk.su

Resonant transformers of the spatial and polarization strtuctures of electromagnetic waves are known that employ semitransparent surfaces with anisotropic conductance [1, 2]. Here, we consider the problem of excitation of a dielectric sphere with the electric dipole located at its center and directed along the z axis (Fig. 1).

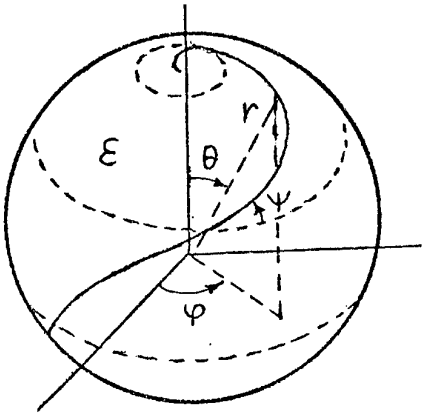


Fig. 1

The sphere surface is characterized by anisotropic conductance along the lines with constant pitch angle ψ. On the surface $r = a$, the following two-sided Vladimirskii boundary conditions hold

$$E_\theta^- = E_\theta^+, E_\varphi^- = E_\varphi^+, E_\varphi = \nu E_\theta,$$
$$H_\varphi^- - H_\varphi^+ = \nu\left(H_\theta^- - H_\theta^+\right). \qquad (1)$$

Here, the signs "+" and "–" refer to the domains $r \le a$ and $r \ge a$, respectively, and $\nu = \tan\psi$. For definiteness, the helical lines are assumed to be right ($\nu > 0$). Electromagnetic fields in the problem considered are axially symmetric ($\partial/\partial\varphi \equiv 0$) and expressed in terms of the electric U and magnetic V Hertzian potentials by the formulas

$$E_\theta^- = \frac{1}{kr}\frac{\partial^2 U^-}{\partial(kr)\,\partial\theta}, \quad E_\varphi^- = \frac{i}{kr}\frac{\partial V^-}{\partial\theta},$$

$$H_\theta^- = \frac{1}{kr}\frac{\partial^2 V^-}{\partial(kr)\,\partial\theta}, \quad H_\varphi^- = -\frac{i}{kr}\frac{\partial U^-}{\partial\theta}. \qquad (2)$$

$$E_\theta^+ = \frac{1}{k\sqrt{\varepsilon}}\frac{1}{r}\frac{\partial^2 U^+}{\partial(k\sqrt{\varepsilon}r)\,\partial\theta},$$

$$E_\varphi^+ = \frac{i}{k\varepsilon}\frac{1}{r}\frac{\partial V^+}{\partial\theta},$$

$$H_\theta^+ = \frac{1}{k\sqrt{\varepsilon}}\frac{1}{r}\frac{\partial^2 V^+}{\partial(k\sqrt{\varepsilon}r)\,\partial\theta},$$

$$H_\varphi^+ = -\frac{i}{kr}\frac{\partial U^+}{\partial\theta}.$$

The source field of the exciting electric dipole is expressed in terms of the Hertzian potential

$$U_0^+ = h_1^{(2)}(k\sqrt{\varepsilon}r)\cos\theta, \qquad (3)$$

where $h_1^{(2)}$ is the Riccatti–Hankel function of the second kind. We represent the Hertzian potentials for the total field inside and outside the sphere as follows:

$$U^+ = U_0^+ + A^+ j_1(k\sqrt{\varepsilon}r)\cos\theta,$$
$$U^- = A^- h_1^{(2)}(kr)\cos\theta, \qquad (4)$$
$$V^+ = B^+ j_1(k\sqrt{\varepsilon}r)\cos\theta,$$
$$V^- = B^- h_1^{(2)}(kr)\cos\theta.$$

Here, j_1 is the Riccatti–Bessel function. The unknown amplitudes $A^\pm$ and $B^\pm$ are determined from (4) subject to the boundary conditions (1). For example, we obtain the following expression for the external field

$$A^- = ij_1 h_1^{(2)} \Big/ \left[\nu^2\left(\sqrt{\varepsilon}j_1' h_1^{(2)} - j_1 h_1^{(2)'}\right)j_1' h_1^{(2)'} + \left(j_1' h_1^{(2)} - \sqrt{\varepsilon}j_1 h_1^{(2)'}\right)j_1 h_1^{(2)}\right], \qquad (5)$$

$$B^- = -i\nu\frac{h_1^{(2)'}}{h_1^{(2)}}A^-. \qquad (6)$$

In these formulas, j_1 and j_1' are the functions of the argument $k\sqrt{\varepsilon}a$, while $h_1^{(2)}$ and $h_1^{(2)'}$ are the functions of the argument ka. Thus, the external field is a superposition of the electric- and magnetic-dipole fields that are oriented along the axis z and have the amplitudes A^- and B^-.

It is essential that the sphere with helical conductance is characterized by a low-frequency resonance. This resonance was first observed in the problem of scattering of a plane wave by such a sphere in [3]. In this work, the following approximate formula was obtained for the resonance frequency for $k\sqrt{\varepsilon}a \ll 1$

$$ka \approx \nu\sqrt{\frac{6}{\varepsilon+2}}. \qquad (7)$$

At the resonant frequency, the radiated power is maximal. When $ka \ll 1$, formula (6) reduces to

$$B^- \approx i\frac{\nu}{ka}A^-. \qquad (8)$$

Formula (8) implies that the radiated field is polarized counterclockwise irrespective of the magnitude of ε, provided that

$$ka \approx \nu. \qquad (9)$$

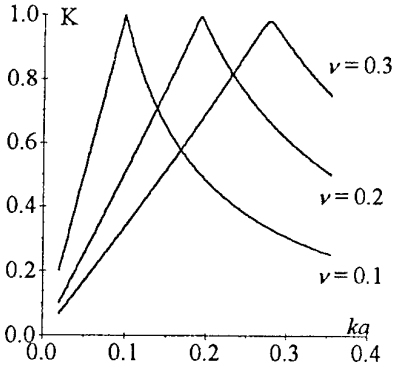


Fig. 2

Figure 2 represents the functions of ellipticity factor K versus frequency for various ν. These functions are derived from (6). The figure shows that the maximum values of K are close to unity, and the positions of these values are well described by the approximate formula (9). As is seen from (7) and (9), for the circularly polarized field to be radiated at the resonant frequency, it is necessary that $\varepsilon = 4$.

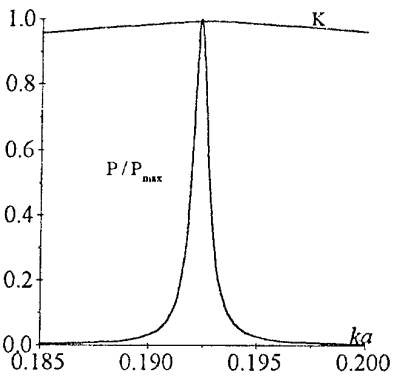


Fig. 3

Figure 3 demonstrates the energy and polarization characteristics of the transformer analyzed as functions of frequency for $\nu = 0.2$ and $\varepsilon = 4.2$. The radiated power is defined as

$$P = \left|A^-\right|^2 + \left|B^-\right|^2. \qquad (10)$$

Figure 3 represents the normalized values P/P_{max}, where $P_{max} = 5.4 \times 10^3$ (in free space, the electric dipole would radiate the power $P = 1$).

ACKNOWLEDGMENTS

This work was supported by the Russian Foundation for Basis Research, project no. 98-02-16197.

REFERENCES

1. Elektrodinamika antenn s poluprozrachnymi poverkhnostyami. Metody konstructivnogo analiza (Electrodynamics of Antennas with Semitransparent Surfaces: Methods for Constructive Analysis), Katsenelenbaum, B.Z. and Sivov, A.N., Eds., Moscow: Nauka, 1989.

2. Katsenelenbaum, B.Z., Sivov, A.N., Chuprin, A.D., and Shatrov, A.D., A New Type of Linear-to-Circular Polarization Transformers Based on a Three-Grating Transmission Resonator, Radiotekhnika i Elektronika, 1994, vol. 39, no. 11, p. 1681.

3. Shevchenko, V.V., Diffraction on Small Chiral Particle, Radiotekhnika i Elektronika, 1995, vol. 40, no. 12, p. 1777.

APPROXIMATION OF RADIATION PATTERNS OF ANTENNAS BY ENTIRE FUNCTIONS OF EXPONENTIAL TYPE

V. F. Kravchenko, E. G. Zelkin, V. V. Timoshenko

Institute of Radio Engineering and Electronics, Russian Academy of Sciences,
ul. Mokhovaya 11, Moscow 103907
Tel.: (095) 921-48-37, Fax: (095) 925-92-41, e-mail: kvf@mx.rphys.mipt.ru

INTRODUCTION

One of the central problems in the theory of synthesis of antennas is the question of the approximation of the specified direction diagram (RP) by entire functions of an exponential type; i.e., we are given functions of class W_σ [1]. In fact, if the specified RP belongs to these functions, the problem of synthesis has an exact solution. It is known [2] that in practice the required RP of an antenna usually does not belong to these functions; therefore, they can acquire various forms. In this case, the problem of synthesis has no exact solution and the question of its approximate solving may be posed. Moreover, it will be possible to define the distribution of a current (field) on an aperture ensuring a specific RP with a required accuracy.

STATEMENT OF PROBLEM

In [2], the following method for approximation was proposed. Its idea lies in the fact that the specified RP can be approximated by polynomials $P_k(z)$ of sufficiently high degree. By the theorem of Weierstrass [1], this procedure can be realized with any degree of accuracy. Further, we can multiply these polynomials by auxiliary functions $U_m(z)$, which include the following properties:

(i) The functions $U_m(z)$ belong to the functions of the class W_σ;

(ii) The functions $U_m(z)$ on the real axis under $z \to \infty$ are infinitestimals of order $o\left(1/z^m\right)$, where $m > k$;

(iii) On the part where we specify the RP, under an increase in the number m, the functions $U_m(z)$ tend to one; i.e., there exists such an m for any ε_1 $|1-U_m(z)| < \varepsilon_1$, in the domain $-L/\lambda \le z \le L/\lambda$ RP, where L is the antenna length and λ is the wavelength.

The production of the functions $P_k(z)U_m(z)$ belongs to the functions of the class W_σ, and therefore there exists an APD current on the antenna aperture that ensures the specified RP.

Since $|R(z)-P_k(z)| < \varepsilon_2$, then

$$|R(z)-P_k(z)U_m(z)| \le |R(z)-R(z)U_m(z)| + \\ +|R(z)U_m(z)-P_k(z)U_m(z)| < |R(z)|\varepsilon_1 + |U_m(z)|\varepsilon_2. \quad (1)$$

The conditions $|R(z)| \le 1$ and $|U_m(z)| \le 1$ for any m on the part $-L/\lambda \le z \le L/\lambda$ are fulfilled; therefore, $|R(z)-P_k(z)U_m(z)| \le \varepsilon_1 + \varepsilon_2, m > k$. Analogous statements are also applied if the trigonometric polynomial $T_k(z)$ is used as an approximation function. Thus, the RP obtained will belong to the class W_σ and are realized. They can be subsequently presented in the form of a Kotel'nikov series [2]

$$R_s(z) = \sum_m R_s(z_m) S(z - z_m), \quad (2)$$

where

$$S(z) = \sin(\sigma z)/\sigma z, \\ z_n = \pi n/\sigma. \quad (3)$$

In [2], a function presented as a Fourier transformation of a cosine function of the degree m was proposed as the auxiliary function $U_m(z)$:

$$U_m(z) = \frac{1}{2\pi}\int_{-\pi}^{\pi} e^{izy}\left[\frac{\Gamma^2(m/2+1)}{m!}\left(2\cos\frac{y}{2}\right)^m\right]dy, \quad (4)$$

where $\Gamma(\alpha)$ is the gamma-function. Under an even m,

$$U_m(z) = \frac{\sin \pi z}{\pi z \prod_{p=1}^{m}\left(1-\frac{z^2}{p^2}\right)}, \quad (6)$$

while under an odd m,

$$U_m(z) = \frac{\cos \pi z}{\prod_{p=1}^{m}\left(1-\left(\frac{2z}{2p+1}\right)^2\right)}. \quad (7)$$

Both functions belong to the class W_π. At the point $z = 0$, they have a maximum equal to one. The first zero is at the points $z = m/2+1$. At all points at which $z = n$ and $n \le m$

$$U_m(n)=\frac{(m!)^2}{(m+n)!\,(m-n)!}. \qquad (8)$$

The functions $U_m(n)=0$ at the points where $z=n$ and $n>m$. The choice of the number m tends to one at the given part at any degree of accuracy and approximates the specified RP with the required accuracy.

The application of the functions $U_m(z)$ as auxiliary functions is not always expedient. In such cases, when the relation L/λ is great, the polynomials $P_k(z)$ must be of high degree. Since $m>k$, the functions $U_m(z)$ slowly tend to zero outside the part $L/\lambda \le |z| \le m$.

ATOMIC FUNCTIONS

A different auxiliary function, lacking the above flaws and presented as a Fourier transformation of atomic functions (AF), was proposed in [3–5]. A large family of AF exists. The simplest of them is denoted by $up(y)$, which is the solution to the differential equation

$$dup(y)/dy = 2up(2y+1)-2up(2y-1). \qquad (9)$$

The Fourier transformation of the function $up(y)$ has the following form

$$Up(z)=\frac{1}{2\pi}\int_{-\infty}^{\infty} e^{iyz}up(y)dy=\prod_{p=1}^{\infty}\frac{\sin z2^{-p}}{z2^{-p}}. \qquad (10)$$

The function $up(y)$ is infinitely differentiable, finite, and satisfying the following properties

$$\begin{aligned} &(a)\ 0\le up(y)\le 1,\ up(-y)=up(y),\\ &(b)\ \sum_{k=-\infty}^{\infty} up(y-k)\equiv 1. \end{aligned} \qquad (11)$$

The function $Up(z)$ was used as an auxiliary function in the approximation of the specified RP. After approximation, the RP obtained will be minimal outside the part $-L/\lambda \le z \le L/\lambda$.

In [4,5] the AF $\Xi_n(y)$ was used in the solution of the problem of synthesis. Its Fourier transformation has the following form:

$$K_n(z)=\prod_{p=1}^{\infty}\frac{\sin z(n+1)^{-p}}{z(n+1)^{-p}}. \qquad (12)$$

Under $m=1$, $\Xi_1(y)=up(y)$.

At the present time, the following approximating functions $R_s(z)$ and their corresponding distributions of current (field) along the antenna $f_s(y)$ have been studied:

A. The polynomial approximations

$$R_s(z)=K_n(\alpha z)\sum_{m=0}^{k}a_m z^m, \qquad (13)$$

$$f_s(y)=\alpha\sum_{m=0}^{k}(-i/\alpha)^m a_m \Xi_n^{(m)}(y/\alpha). \qquad (14)$$

B. The approximation of the trigonometric polynomials

$$R_s(z)=K_n(\alpha z)\sum_{m=-\beta(1-\alpha)/\alpha}^{\beta(1-\alpha)/\alpha} a_m e^{-i\beta z m}, \qquad (15)$$

$$f_s(y)=\sum_{m=-\beta(1-\alpha)/\alpha}^{\beta(1-\alpha)/\alpha} a_m \Xi_n\left(\frac{y-\beta m}{\alpha}\right). \qquad (16)$$

C. Approximation of shifts and contractions of the following functions $K_n(z)$:

$$R_s(z)=\sum_m a_m K_n(\alpha(z-\beta m)), \qquad (17)$$

$$f_s(z)=\Xi_n\left(\frac{z}{\alpha}\right)\sum_m a_m e^{-i\beta y m}. \qquad (18)$$

The choice of the parameters α,β, a_n and these functions are determined by the methods of approximation (mean square, uniform, and pointwise) in [3–5].

NUMERICAL EXPERIMENT

The diagrams of RP synthesized by the method of multiparametric regularization (MR) [4] (dashed line) and by the method of AF (solid line), using formula (15), in the mean square approximation of a narrow sector of the RP are shown in Fig. 1.

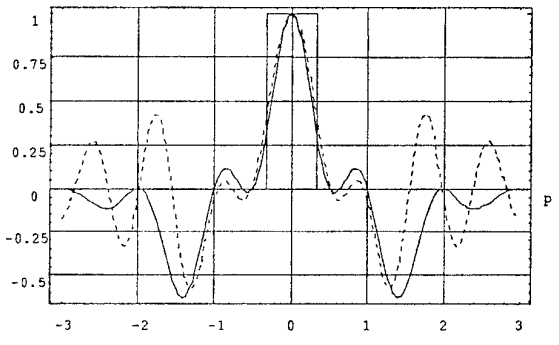


Fig. 1. Diagrams of synthesized RP

The numerical experiment (Table 1) showed that the application of these functions in problems of the synthesis of specified RP yield a higher degree of accuracy than traditional methods and improve other integral parameters of antennas (factor of directivity (FD), factor of reactivity (FR), mean square of error (MSE)).

Table 1

Integral parameters of the RP in Fig. 1

Method	FD	FR	MSE
AF	7.83357	1.66184	0.0358387
MR	7.05728	8.42549	0.105041

Diagrams of the required cosecant RP (dashed line) and the synthesized Kotel'nikov series (2) (solid line) under the parameters $\sigma = 2\pi$ are shown in Fig. 2.

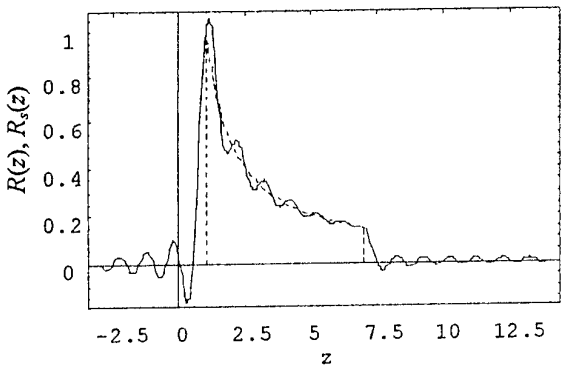


Fig. 2. Approximation of cosecant RP by the Kotel'nikov series

In Fig. 3, the AF method using formula (17) was employed to synthesize RP for the same cosecant RP under the parameters $n = 1, \alpha = 2\pi, \beta = 1, a_m = R(m)$.

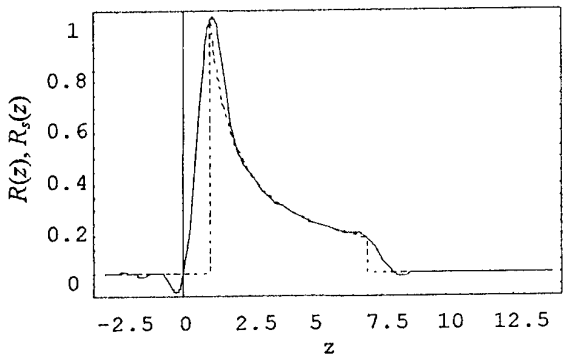


Fig. 3. Approximation of cosecant RP by the AF method

CONCLUSION

Thus, in this work a new method for the synthesis of linear antennas was proposed and substantiated. As shown by the numerical experiment, this method is more effective than traditional ones. It may be extended to a wide class of problems on the analysis and synthesis of radiating systems: plane apertures and arrays, and the synthesis of phased antenna arrays.

REFERENCES

1. Akhiezer, N. I., Lecture on Approximation Theory, Moscow: Nauka, 1965.

2. Zelkin, E. G. and Sokolov, V. G., Methods of Synthesis of Antennas, Moscow: Sov. Radio, 1980.

3. Kravchenko, V. F., Antenna Pattern Approximation and Linear Radiator Synthesis Based on Atomic Functions, Electromagnetic Waves and Electronic Systems, 1998, vol. 3, no. 1, pp. 40–47.

4. Kravchenko, V. F. and Timoshenko, V.V., Atomic Functions in the Theory of the Analysis and Synthesis of Linear Antennas, Electromagnetic Waves and Electronic Systems, 1999, vol. 4, no. 5.

5. Kravchenko, V.F., Pustovoit, V.I., and Timoshenko, V.V., Spectral Properties of Atomic Functions and the Approximation of Direction Diagrams of Linear Antennas, Doklady Physics, 1999 (in press).

PROPERTIES OF BRAGG DIFFRACTION OF THE SECOND ORDER IN LIGHT AND PERIODIC STRUCTURES INTERACTION UNDER DUAL BRAGG ANGLE

L. F. Kupchenko, O. V. Efimova, Y. M. Plahov, V. B. Lobyrev, E. L. Cherkashina

Kharkov military university,
Svoboda square, 6, Kharkov, 310043, Ukraine

The researchers' interest in studying properties of higher order diffraction components under Bragg diffraction is due to the fact that the second order diffraction components has angular dispersion that is twice as large and the third order - three times as large as that of the first order [1]. Appearance of higher order diffraction components is due to multiple light scattering by three-dimensional periodic structures and therefore they have higher angular and spectral selectivity. Apparently this gives an opportunity of constructing the new class of devices which use light diffraction on periodic structures which differ from devices using ordinary Bragg diffraction. Here under periodic structures we mean three-dimensional (volumetric) phase gratings created in dielectric transparent medium by ultrasonic traveling wave or the gratings produced in photorefractive crystals by holographic methods [2].

Analytic expressions allowing to investigate light diffraction at ultrasonic wave not only of the diffraction first order occurring at interaction under Bragg angle but Bragg diffraction of higher orders under interaction angles that are multiple of Bragg angle are obtained in [3]. It is shown that besides of higher selectivity and angular dispersion the higher order components have additional properties consisting in that the value of diffraction efficiency in satisfying Bragg synchronism conditions for each of the orders depends not only on the value of relative refraction coefficient change $\Delta n/n$ but on diffraction grating period (at constant values of interaction length l and light wave number k) [4].

Formerly this property was not verified experimentally and is the subject of investigation in present work. Usually under diffraction efficiency one understood the ratio of amplitude square of diffracted components to incident radiation amplitude:

$$|\psi_i|^2 = |E_i/E_0|^2,$$

where $i = 1, 2...$

For comparative analysis of the properties of the first and the second order diffraction components we'll present diffraction efficiency expressions of each of the orders in the form [3]. Remind that expression data are obtained under assumption of small Ritov parameter values ($q << 1$) which are observed in the domain of sound low power and high frequency values:

$$|\psi_1|^2 = \frac{1}{1+\gamma_1^2}\sin^2\left(\frac{\Delta n}{n}\frac{kl}{2}\sqrt{1+\gamma^2}\right) \quad (1)$$

$$|\psi_2|^2 = \frac{1}{1+\gamma_2^2}\sin^2\left[\left(\frac{\Delta n}{n}\right)^2\frac{kl}{2}\left(\frac{k}{k_0}\right)^2\sqrt{1+\gamma^2}\right] \quad (2)$$

where $\gamma_1 = \varepsilon_1/2q$; $\gamma_2 = \varepsilon_2/q^2$; $q = \Delta n/n\ (k/k_0)^2$;

$$\varepsilon_1 = 1+\frac{2k\sin\theta}{k_0};\ \varepsilon_2 = 2\left(1+\frac{k\sin\theta}{k_0}\right);$$

k and k_0 are wave numbers of light and ultrasound. Relative derangements ε_1 and ε_2 defines the closeness of the angle θ, between plane optical wave and acoustical wavefront, to Bragg angle θ_B and dual Bragg angle θ_{2B}, respectively.

As it seen from expressions (1) and (2), maximum diffraction efficiency for each of the diffraction orders can be ensured under satisfying the following two conditions: first, when relative derangement parameter is equal to zero ($\varepsilon_1 = 0$ or $\varepsilon_2 = 0$), and second, when sine argument of each of the expressions reaches $\pi/2$, i.e. under conditions:

$$(\Delta n/n)kl/2=\pi/2; \quad (3)$$

$$(\Delta n/n)^2(k/k_0)^2kl/2=\pi/2; \quad (4)$$

The expressions (3) and (4) include three factors: the first one is proportional to relative refraction coefficient change $\Delta n/n$ of grating, the power of which corresponds to diffraction order number $i = 1, 2...$; the second factor is proportional to the ratio of light and ultrasound wave numbers k/k_0 with the power degree equal to $2j$ ($j = 0; 1$) and the third one is equal to the product of light wave number by interaction length $k \cdot l$.

In the experiment the periodic phase structure was created with the use of traveling sound wave. One of the properties of the second order diffraction component has been verified that can be formulated now in the following way. If light and ultrasound interaction occurs under dual Bragg angle and synchronism conditions $\varepsilon_2 = 0$ are satisfied then for obtaining a certain value of diffraction efficiency at higher ultrasound frequency it is necessary to ensure a greater value of

refraction index modulation depth than at a lower ultrasound frequency.

The experimental investigations of diffraction efficiency of the second order in light and ultrasound interaction under dual Bragg angle were carried out with the use of isotropic diffraction in acoustic conductor made of dense flint TF-7. As it known, this material has relatively low acoustooptical properties that required to increase high frequency voltage at ultrasound exciter and for exclusion of exciter overheat there have been formed short ultrasound pulses of duration 30 mcs and pulse-repetition frequency of 1 kHz. Acoustic wave power was controlled on the value of electric voltage at piezoconverter. At the experiment the length of light and ultrasound interaction was $l \approx 0.6$ cm and laser operating at the wavelength $\lambda = 0.633$ mcm was used as a radiation source.

In Fig. 1 there are presented the calculated dependencies of diffraction efficiency for the second order component on optical density of ultrasound grating at fixed values of ultrasound frequency $f_0 = 70$ MHz, $f_0 = 80$ Mhz, $f_0 = 90$ Mhz, and the measured values of diffraction efficiency. The comparative analysis of theoretical and experimental investigation results has manifested their good agreement. Actually from charts it follows that the value of diffraction efficiency of the second order diffraction component under satisfying Bragg synchronism conditions $\varepsilon_2 = 0$ depends not only on grating optical density but on its period. In order to obtain certain value of diffraction efficiency of the second order at a higher ultrasound frequency it is necessary to increase optical density of ultrasound grating (tension at ultrasound exciter).

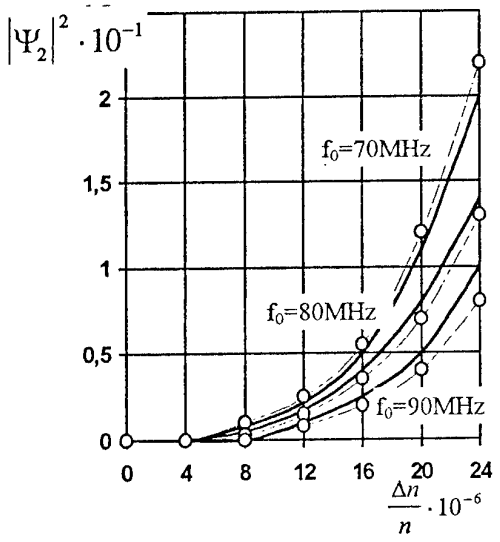


Fig. 1. Calculated dependencies of diffraction efficiency (solid curves) of the second order component on grating optical density and on its frequency in light and grating interaction under dual Bragg angle and experimental dependencies (dotted curves)

REFERENCES

1. Balakshiy V.I., Krilov I.P., Kulish T.G. Experimental investigation of higher orders of acoustooptical interaction // Optica i spectroscopiya. - 1998. - v.84, ¹2. - p.269-273 [in Russian].

2. Kupchenko L.F., Kosmina M.B., Vdovenkov V.Y. and others. Bragg resonance of the second and third order on volumetric holographic structures // Ukrainian physical journal. -1988. - v.33, ¹ 10. - p.1469-1474 [in Russian].

3. Zilberman G.E., Sidorov I.I., Kupchenko L.F. To the theory of light diffraction on ultrasound // Radiotekhnika i elektronika. - 1982. - v.27, ¹2. - p.241-247 [in Russian].

4. L.F.Kupchenko, Y.M. Plahov, A.M. Reznichenko, N.A. Kovalyov, O.V. Efimova. Properties of high order Bragg resonances under light diffraction on periodic structures. Second international Conference on Antenna Theory and Techniques. 20-22 May 1997. Kyiv, Ukraine, p.20-21.

PROPERTY OF INTERMEDIATE DIFFRACTION REGIME NEAR THE SECOND BRAGG RESONANCE UNDER INTERACTION OF LIGHT WITH PERIODIC STRUCTURES

L. F. Kupchenko, O. V. Efimova, Y. M. Plahov, V. B. Lobyrev, E. L. Cherkashina

Kharkov military university,
Svoboda square, 6, Kharkov, 310043, Ukraine

Under "the second Bragg resonance" we'll mean such interaction conditions of light with volumetric (three-dimensional) periodic phase gratings when interaction takes place under dual Bragg angle and here the second and zeroth diffraction orders will be the most essential. If besides of the second and zeroth orders of diffraction there is the first order component, i.e. the three-wave diffraction condition is realized, then such a regime we'll call the intermediate one.

It is stated that transition from two-wave to three-wave intermediate regime is connected with the Rytov parameter value of $q = (\Delta n/n)(k/k_0)^2$ (where $\Delta n/n$ is the relative change of grating optical density; k and k_0 are wave numbers of light in medium and of grating). If $q \le 0.1$ then the diffraction efficiency value of the first order component $|\psi_1|^2 = E_1/E_0|^2$ (where E_1 and E_0 are amplitudes of the first order diffraction component and incident wave, respectively) is, as a rule, substantially less than diffraction efficiency of the second order component $|\psi_2|^2 = |E_2/E_0|^2$, and if $q \approx 0.3 \div 0.4$, then their values are close and the Bragg diffraction intermediate regime is realized near the second Bragg resonance. Depending on grating period and its optical density the first and the second order components compete with each other (Fig. 1).

It has been found advantageous to determine such parameter values of light and volumetric periodic grating interaction $\Delta n/n$ and $k_0 = 2\pi/d$ (where d is the grating period) at which an intermediate three-wave diffraction condition ($q \approx 0{,}3$-$0{,}4$) goes into a two-wave one, and this work is devoted to investigation of this property. The fact is that the higher orders of diffraction have large angular dispersion. This allows to hope that on their basis the devices with characteristics different from the known ones will be constructed. However the higher orders of diffraction, including the second one, have more angular and spectral selectivity. Thus the investigation of intermediate diffraction regime properties near the second Bragg resonance, with less selectivity but with dispersion two times greater in comparison with the first resonance, is of certain practical interest.

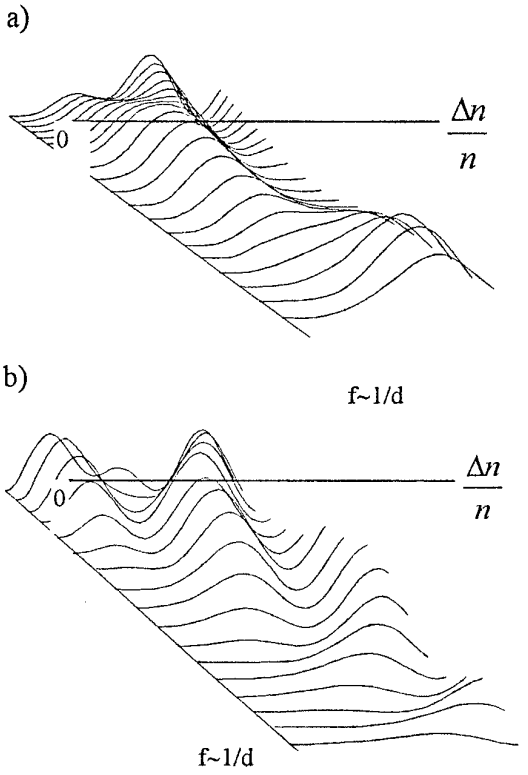


Fig.1 Graphs of dependence of diffraction efficiency of a) the second order diffraction and b) the first order diffraction on a change of $\Delta n/n$ and $f \sim 1/d$ near the second Bragg resonance.

In the present work the case of interaction of plane wave with three-dimensional grating which can be constructed by using ultrasonic wave in dielectric or by holographic methods in photorefractive crystals is considered. The problem is formulated as follows: using obtained earlier expressions for the second order diffraction component calculated for the case of light interaction with ultrasonic wave under dual Bragg angle, the interaction parameters are to be found at which this component is maximum. Then an amplitude is to be found of the first order component of diffraction occurred under dual Bragg angle too, as well as interaction conditions are to be revealed under which this amplitude is minimum. Combined solution of two equations will permit to obtain interaction conditions ensuring the maximum of the second order diffraction at optimum value of the first order diffraction.

Diffraction efficiency for the second order diffraction is determined by the following expression:

$$|\psi_2|^2 = \frac{1}{1+\gamma_2^2}\sin^2\left[\left(\frac{\Delta n}{n}\right)^2 \frac{kl}{2}\left(\frac{k}{k_0}\right)^2 \sqrt{1+\gamma^2}\right], \quad (1)$$

where $\gamma^2=\varepsilon_2^2/q^4$;

$$\varepsilon_2 = 2\left(1+\frac{k\sin\theta}{k_0}\right);$$

l is the interaction length.

Maximum of diffraction level in the second order $|\psi|^2 = |\psi|^2_{max}$ is realized if the relative derangement $\varepsilon_2 = 0$ and sine argument in (1) is equal to $\pi/2$. Hence:

$$k_{01} = \left(\frac{\Delta n}{n}\right) k\sqrt{\frac{kl}{\pi}}, \quad (2)$$

The analytical expression for field amplitude E_1 is found using the method of continued fractions [2]. The method intends to determine diffraction component amplitudes and phases with the help of the dispersal equation that is an algebraic one, its power is defined by the number of waves under consideration. It is quite intricate to obtain the analytical expression for a light field in intermediate diffraction regime because the dispersal equation without assumptions is of 5-th power.

However, assumpting that interaction of light with ultrasound occurs under dual Bragg angle

$$\theta_{2B} = \arcsin k_0/k$$

for complete Bragg synchronism conditions we succeeded in obtaining the expression for a field amplitude of the following form:

$$E_1 = \frac{2q}{\sqrt{8q^2+1}}\sin\left(\frac{k_0^2 l}{2k}\sqrt{8q^2+1}\right) \quad (3)$$

Since in the expression (3) a periodic function is present, it isn't difficult to find an expression for a wave number of sound at which the minimum energy transfer into the first order diffraction occurs, i.e.

$$|\psi_1|^2 = |\psi_1|^2_{min}.$$

Then:

$$k_{02} = \sqrt[4]{\frac{16\pi^2 k^2 m^2}{l} + 8\left(\frac{\Delta n}{n}\right)^2 k^4}, \quad (4)$$

where $m = 1, 2, 3....$

Using simultaneously (2) and (4) let us define conditions under which the second order component for an intermediate regime is maximum. In Fig. 2 the curves 2, 3 and 4 represent interaction conditions - ultrasound frequency and relative change of medium refraction index in

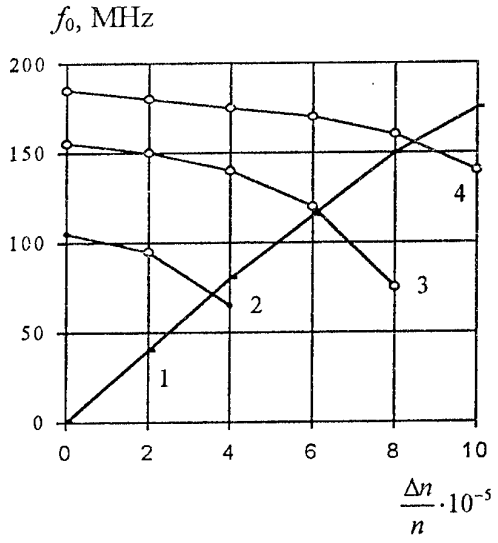


Fig.2. The graph of determining acoustooptical interaction parameters - the frequency of ultrasound f_0 and the optical density of ultrasonic grating $\Delta n/n$.

ultrasonic field under which the first order value is minimum. In contrast, the curve 1 represents interaction conditions under which the second order diffraction efficiency value is maximum. It is obvious that curve intersection points allow to find the required values of grating frequency and optical density. The graphs are plotted for the case when the sound conductor is made of the glass TF-7 where the velocity of ultrasound propagation V = 3630 m/s, the interaction length l = 0.6 cm and the wavelength of light radiation λ = 0.633 mcm.

In conclusion, we note that the investigated property of intermediate diffraction regime near the second Bragg resonance in our opinion can be explained by the fact, that in interaction of light with grating under dual Bragg angle the value of the second order diffraction depends not only on the optical density of grating $\Delta n/n$ and the product kl but on the relation k/k_0.

REFERENCES

1. Zilberman G.E., Sidorov I.I., Kupchenko L.F. To the theory of light diffraction on ultrasound // Radiotekhnika i elektronika. - 1982. - v.27, '2. - p.241-247 [in Russian].
2. Zilberman G.E., Kupchenko L.F. Light propagation through ultrasound beam in homogenous dielectric // Radiotekhnika i elektronika. - 1977. - v.82, '8.- p.1551-1556 [in Russian].

THE α-PROPERTIES OF ELECTROMAGNETIC FIELD FRACTAL DIPOLE

I. V. Lysokon', V. M. Onufrienko

Zaporizhzhya State Technical University,
Zhukovsky Str., 64, Zaporizhzhya ,330600, SP-39, Ukraine
(0612)644046, e-mail: onufr@zstu.zaporizhzhe.ua

INTRODUCTION

The Hertz's dipole is known as variant of the scheme, which ensures a heavily radiation at a rather small connected part of an energy. For mathematical simulation of such dipole usually use the idealized elementary electrical vibrator, which is located in a boundless homogeneous isotropic nonconductive medium. The vibrator is represented as wires, short on a comparison with a wavelength, from a constant on all it to length by amplitude and phase of a current. In an inconsistency with this classical model there is a practical problem creation of a vibrator with amplitude and phase of a current, which are constant on all it to length. Nor it is obviously possible to supply presence of a material medium with properties of a homogeneity and nonconductivity.

Proceeding from fractal representations about a structure of a current in a conductor and field in semiconductor medium, we enter α-characteristics of electromagnetic field and we create differintegral model of electrical vibrator.

In the present work we use the concept of fractional calculus [1], [2] which allows most completely to map fractal properties of the real physical object [3] – [6].

CONSTRUCTION THE FRACTAL DIFFERINTEGRATIVE MODEL OF DIPOLE

The electromagnetic field of Hertz's dipole can be expressed as follows [7]

$$\dot{\vec{H}}_m(\vec{r})=\frac{1}{4\pi}\cdot\int_V\left(\frac{1}{|\vec{r}-\vec{r}'|^2}+\frac{i\dot{k}}{|\vec{r}-\vec{r}'|}\right)\cdot\left[\dot{\vec{j}}_m^{cm}(\vec{r}'),\vec{r}_{oq}\right]\cdot e^{i\dot{k}|\vec{r}-\vec{r}'|}dV' \quad (1)$$

$$\dot{\vec{E}}_m=\frac{1}{i\omega\dot{\varepsilon}}\cdot rot\dot{\vec{H}}_m .$$

The expression (1) is fair for case of distribution of an indirect current in some area of space V. Outside of radiant area V conductive currents are absent. The expressions (1) for off-site ideal linear current in the near zone of a radiation in a polar frame will look like the following (see, for example, [7])

$$\dot{E}_r=-\frac{i\cdot I_m^{cm}\cdot l}{2\pi\omega\varepsilon_a r^3}\cdot\cos\theta\cdot e^{i(\omega t-kr)},$$

$$\dot{E}_\theta=-\frac{iI_m^{cm}l}{4\pi\omega\varepsilon_a r^3}\cdot\sin\theta\cdot e^{i(\omega t-kr)} \quad (2)$$

$$H_\varphi=\frac{I_m^{cm}l}{4\pi\cdot r^2}\sin\theta\cdot e^{i(\omega t-kr)} .$$

If a continuous line on a regular site of it to cover with a polygonal line with segments Δl_n, and on a fractal part to enter a measure of the Hausdorff with coating of a polygonal line, the expansion of a curve will be determined by the formula (see, for example, [8])

$$L=\lim_{\Delta l_n\to 0}\sum\Delta l_n+\lim_{\Delta l_m\to 0}\sum\frac{M(\Delta l)^\nu}{\Delta l_m^{\nu-1}} .$$

Let's consider α-characteristic (differintegral, $0<\alpha<1$) with respect to the θ (see [2], [6], [7])

$$(I^\alpha f)(x)\equiv\frac{1}{\Gamma(\alpha)}\int_a^x\frac{f(t)}{(x-t)^{1-\alpha}}dt,\ x>a,\ \alpha>0 . \quad (3)$$

We are bounded with reviewing only of simple harmonic motions of a source current. We obtain, applying formula (3) to (2), expressions for α-characteristics of electrical field component E_θ, E_r of a vibrator

$$\dot{E}_{m\theta}=\frac{-1}{\Gamma(\alpha)}\cdot\frac{i\cdot l\cdot e^{-i\cdot k\cdot r}}{4\pi\omega\varepsilon r^3}\cdot\int_0^\theta\frac{I_m^{cm}\sin(\theta')}{(\theta-\theta')^{1-\alpha}}d\theta',$$

$$\dot{E}_{mr}=\frac{-1}{\Gamma(\alpha)}\cdot\frac{i\cdot l\cdot e^{-i\cdot k\cdot r}}{4\pi\omega\varepsilon r^3}\cdot\int_0^\theta\frac{I_m^{cm}\cos(\theta')}{(\theta-\theta')^{1-\alpha}}d\theta' .$$

Introduction of α-characteristics can be argued with reviewing of a new physical and mathematical model, to which there corresponds the following statement of the task about a radiation of the Hertz's dipole: the electrical dipole has a geometric fractal structure. It attracts a modification of a current magnitude in direction of an angle 0 under the law:

$$I_m^\alpha=\frac{1}{\Gamma(\alpha)}\cdot\frac{I_m^{cm}}{(\theta-\theta')^{1-\alpha}}$$

CALCULATION OF THE DIAGRAMS α-CHARACTERISTICS OF THE VIBRATOR FIELD

The greatest interest represents a field of a vibrator in near wave zone ($r >> l$, $l << \lambda$, $2\pi r << \lambda$). In this zone

the fractality of a vibrator renders the greatest influence on emitted by it a field.

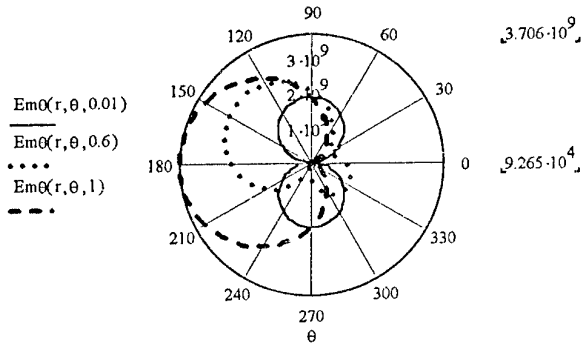


Fig. 1. α - characteristics θ - component of an electrical field of the dipole of a Hertz in a polar frame for various values α

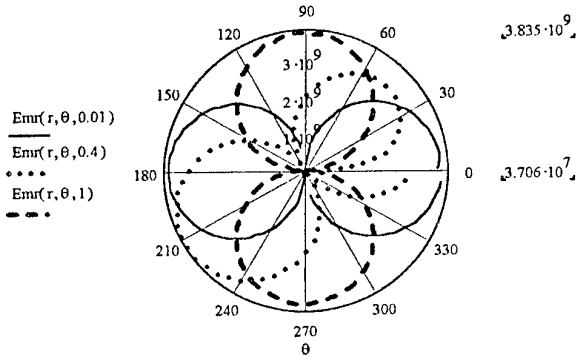


Fig. 2. α-characteristics r-component of an electrical field of the dipole of a Hertz in a polar frame for various values α

CONCLUSION

In classical statement the task about a radiation of the electrical Hertz's dipole reduces in outcomes, which will not be agreed dates of an experimental research of such model in actual mediums. In the report is constructed the differintegral model of an electrical vibrator on the base of fractal representations about a current structure in a conductor and field in the semiconductor medium.

The α-characteristics of the vector field component E_θ and E_r are obtained. These characteristics have allowed to define α-component electromagnetic fields by the emitted dipole. In wave zone the graphs of a field amplitude strength association from direction to a viewpoint are obtained. Thus the full coincidence α-characteristics with usual components of field strength is marked.

In a considered medium with fractal performances the presence of a dipole radiation in the direction its axe (on a classical mathematical model this mark radiation is absent).

Is underlined on a possibility of deriving of new outcomes connected to reviewing of processes of wave distributions in mediums to fractal properties.

REFERENCES

1. Samko S.G., Kilbas A.A., Marichev O.I. Integrals and derivatives of the fractional order and their applications, Minsk, Nauka i tekhnika, 1987, 688 p. [in Russian].

2. Engheta N. On the Role of Fractional Calculus in Electromagnetic Theory// IEEE Antennas & Propagation Magazin.-Vol.39.- No. 4, August 1997.- P.35-46.

3. Fractals in physics// Proc. of the YI Int. simposium on fractals in physics (Triest, Italy, 9-12 July, 1985).

4. Zeldovich Ya.B., Sokolov D.D. Fractals, similarity, intermediate asymptotics // YFN, 1985, v.146, №3, P.493-506 [in Russian].

5. Onufrienko V. On "α-features" of electrical waves above impedance plane// Conference Proceedings 12 International Conference on Microwaves & Radar. Krakov, Poland, May 20-22, 1998.- Vol.1.- P.212-215.

6. Onufrienko V. New Description of Spatial Harmonics of Surface Waves, Conference Proceedings. 1998 International Conference of Mathematical Methods in Electromagnetic Theory (MMET - 98), Ukraine, Krakov, June 2 – 5, 1998. Vol. 1, pp. 219 – 221.

7. Nikolsky V.V. Electrodynamics and radio wave propagation, Moscow, Nauka, 1973 [in Russian].

8. Feder E. Fractals. Transl. From Engl., Moscow, Mir, 1991, 254 p. [in Russian].

A SENSOR OF THE H-COMPONENT OF A PULSE ELECTROMAGNETIC FIELD OF NANOSECOND DURATION

A. A. Orlenko and P. V. Kholod

Usikov Institute of Radiophysics and Electronics, National Academy of Sciences of Ukraine
ul. Proskury 12, Kharkov 310085, Ukraine
tel.: 38-0572-44-84-70, e-mail: orlenko@ire.kharkov.ua, kholod@ire.kharkov.ua

INTRODUCTION

Precise measuring of the field patterns in the far and near zone of a radiator is an important factor in developing video pulse radiators. It is known that the wave resistance $Z = E/H$ in the near zone of an electromagnetic field radiator depends on the location of the observation point and varies by different laws subject to the transmitting antenna design [1]. Thus, to obtain a precise field image, the electric and magnetic field components must be recorded separately.

This investigation is aimed at developing a sensor with a uniform amplitude-frequency characteristics in a wide frequency band for measuring the magnetic component of the video pulse fields.

GENERAL DESCRIPTION

In the paper [1], H. Harmuth has formulated the relations between the distortion of the received signal shape and the degree of matching between sensor's radiation resistance R_R and the load resistance R_L. The minimum distortion of the received signal shape is reached at $R_L << R_R$ for magnetic field.

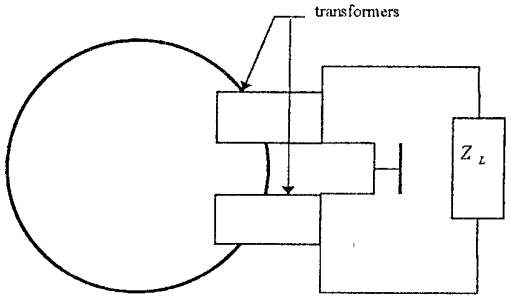
The suggested magnetic field sensor was developed by employing the results of papers [1–5]. This sensor is the Hertz magnetic dipole designed as a loop 40 mm across loaded through a transformer with a transformation factor of 1 : 10 at the input resistance of the differential amplifier (Fig. 1). The differential amplifier is established by the transformer circuit current-voltage. A zero-tending input resistance of such differential amplifier allows matching the loop radiation resistance with the load resistance to comply with the condition of the minimum distortion of the received signal shape $R_L << R_R$. The output resistance of the differential amplifier was selected to meet the requirement of matching between the sensor output resistance and the input resistance of the recorder and made 50 Ω.

The sensor characteristics were measured at a TEM-chamber-based system [6]. These systems are usually applied for generating quickly increasing reference electromagnetic pulses. The strength of the magnetic field in the center of the *TEM*-chamber is conditioned by the voltage between the strip-line conductors and the strip-line wave resistance and can be calculated by a formula

$$H = kU_1 / 4Zh$$

$$k = (1 + U_{out} / U_{in}) / 2,$$

where U_1 is the resistance between the strip-line conductors, Z is the strip-line wave resistance and h is the separation between the strip-line conductors.



Z_L – input resistanse of the amplifier.

Fig. 1. Circuit of the antenna-Hertz's magnetic dipole

The measurements were performed by applying a pulse signal with the front duration of 2 ns and pulse duration of nearly 12 ns (Fig. 2 a). The pulse was generated by the source G5-78. This signal was sent through a matching symmetrizing transformer to the *TEM*-chamber. After passing the TEM-chamber, the pulse signal arrived through the transformer at the oscilloscope input (Fig. 2 c) for controlling the parameters of the reference signal. The sensor under investigation was located in the center of the TEM-chamber. The signal received by the sensor was sent to the oscilloscope input. The oscilloscope was synchronized by sync pulses from generator.

Fig. 2 b shows a reaction of the sensor towards the magnetic field pulse travelling through the TEM - chamber.

The degree of the signal distortion was estimated by comparing the signal shape at the generator output, at the *TEM*-chamber output and at the output of sensor's amplifier. The results demonstrated that, while measuring the parameters of the magnetic field pulse, the received signal shape differed slightly from the reference signal in the center of the *TEM*-chamber.

In addition, we examined the limits of the time parameters of pulses that can be recorded by this sensor. The measurements revealed that a peak decreased by about 10 % with the pulse duration being less than 1 μs, the time of increase and decrease of the measured pulse, at the level of 0.1 U_{max} was 1.7 ns.

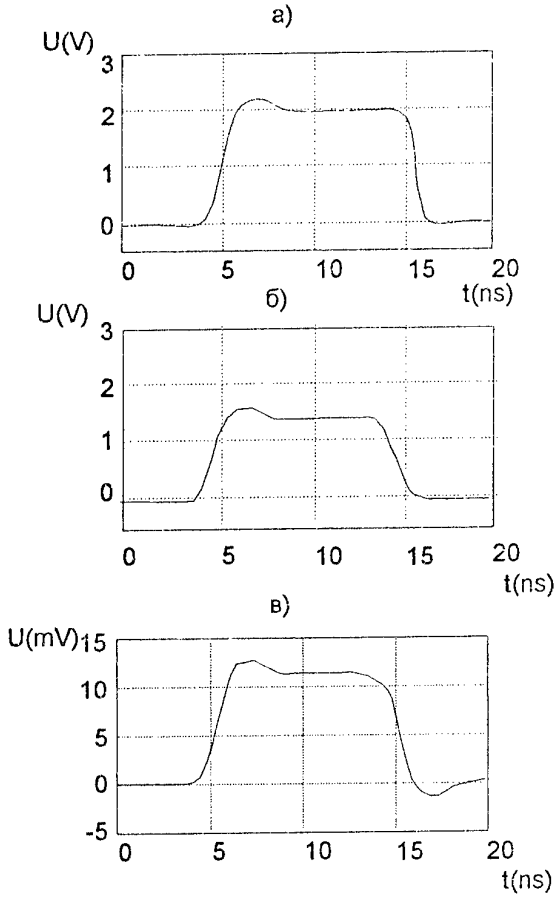


Fig. 2. Estimation of signal shape distortion
a) signal at the input of the *TEM*-chamber;
b) signal from the magnetic Herz dipole antenna;
c) signal at the output of the *TEM*-chamber;

The sensitivity of the sensor was determined as a relation between the resistance at the sensor output and the strength magnitude of the corresponding field component in the center of the *TEM*-chamber. The sensitivity of the sensor of the electromagnetic field H-component was 0.24 V/(A/m).

CONCLUSIONS

The measurements have demonstrated that the magnetic field sensor can receive the pulse signals with the increase time more than 1.7 ns and the pulse duration, at the level of 0.1 U_{max}, less than 1 μs. It is applicable in the experimental investigations of antennas for measuring the amplitude and shape of the *H*-component of the pulsed electromagnetic field.

REFERENCES

1. H. F. Harmuth, and S. Ding-Dong. Antennas for nonsinusoidal waves: Sensors //IEEE Trans., Vol.EMS-25, No.2, 1983, p.107-115.

2. Х.Ф. Хармут. Теория секвентного анализа. - М.: Мир, 1980. (H.F. Harmuth. Theory of sequent analysis).

3. Х.Ф. Хармут. Несинусоидальные волны в радиолокации и связи. М.: Мир, 1984. (H.F. Harmuth. Nonsinusoidal waves in radars and radio communication)

4. H. F. Harmuth. Antennas and waveguides for nonsinusoidal waves. - N.Y. Academic Press, 1984.

5. M. A. Stunchly, H. LePonche, D.T. Gibbons and A. Thanssandote. Active magnetic field sensor for measurements of Transients //IEEE Trans., Vol.33, No. 4, Nov, 1983, p. 275-280.

6. Вопросы излучения и измерения нестационарных электромагнитных полей. Сборник научных трудов. НИИ физико-технических и радиотехнических измерений. М., 1980. (Problems of radiation and measurements of transient electromagnetic fields).

SYNTHESIS OF ANTENNA ARRAYS WITH REGARD TO THE RADIATORS MUTUAL COUPLING AND VECTOR CHARACTERISTICS OF ELECTROMAGNETIC FIELDS

L. Pasnak, P. Savenko

Institute of Applied Problems of Mechanics & Mathematics of NASU
3b Naukova St., 290601, Lviv, Ukraine, phone: +380 (0322) 65-19-79
E-mail: savenko@iapmm.lviv.ua

ABSTRACT

The nonlinear synthesis problems of antenna arrays according to the given amplitude radiation pattern (RP) are solved by the method which regards the mutual coupling of radiators. The mutual coupling is taken into account by solving the boundary problem of the high-frequency electrodynamics on the multi-connected areas. The variational formulation of problems is considered. It is reduced to solving the nonlinear integral or matrix equations – the Euler equations. The numerical algorithm of solving for optimum generation minimization sequence, which weakly convergences to the point of the local minimum is developed. The branching of solutions in the case of linear vibrators synthesis, is investigated by the methods of nonlinear analysis [1]. The number of solutions to these problems and their qualitative characteristics are dependent on both the electrical size of the array and the properties of the given RP.

FORMULATION OF THE PROBLEM

The antenna under consideration consists of a system of ideal-conduction radiators placed in the infinite homogenous isotropic media. There are a lot of publications where analysis problems of the radiator or array of radiators are investigated. The method of integral equations [3-6] is the most resulting approach for solving the antenna array's analysis problem. Thus, the systems of linear integral Hallen and Poklington equations are usually used for solving the numerous practical analysis problems of linear vibrators and different kinds of spiral radiators.

The system of integral equations for abstract radiators in the operator form can be written as:

$$B\vec{J} = \vec{E}^{cm}. \qquad (1)$$

Here B is a linear matrix-integral operator from the Hilbert space $H_j = L^2_{(\overline{S}_1)} \oplus L^2_{(\overline{S}_2)} \oplus \cdots \oplus L^2_{(\overline{S}_N)}$, of functions which are integratiable with square to the Hilbert space $H_E = L^2_{(\overline{G}_1)} \oplus L^2_{(\overline{G}_2)} \oplus \cdots \oplus L^2_{(\overline{G}_N)}$. The functions of current distributions $\vec{J} = \{J_{\tau_1}(s_1), J_{\tau_2}(s_2), \ldots, J_{\tau_N}(s_N)$ (with regard to the mutual coupling of radiators) belong to the space H_j, the functions of the extrinsic electric field $\vec{E}^{cm} = \{E^{cm}_{\tau_1}(s_1), E^{cm}_{\tau_2}(s_2), \ldots, E^{cm}_{\tau_N}(s_N)$ belong to the space H_E.

The system (1) is the Fredholm system of linear integral equations of 1st type and the problem of finding the solutions is incorrect. But the kernels are of Green's type, that have the peculiarity. This makes it possible to apply the self-regularization for finding the stable solutions [2]. The direct numerical methods, based on the interpolation and collocation methods, are most elaborated one for solving the integral equations of the first type with the logarithm peculiarity in the kernel.

Let's assume there are the regularization algorithm for finding the stable solutions of the system (1) and it has the form:

$$\vec{J} = \widetilde{B}^{-1}\vec{E}^{cm}. \qquad (2)$$

Here $\widetilde{B}^{-1}$ is the linear limited operator from H_E to H_J.

The vector radiation pattern of the antenna array can be written as:

$$\vec{f}(\vartheta,\varphi) = f_\vartheta(\vartheta,\varphi)\vec{e}_\vartheta + f_\varphi(\vartheta,\varphi)\vec{e}_\varphi. \qquad (3)$$

Here $\vec{e}_\vartheta, \vec{e}_\varphi$ are the unit orts of the spherical system. Using the linear integral operator $A = \{A_\vartheta, A_\varphi$, RP can be written as:

$$\vec{f} = A\vec{J} \equiv A_\vartheta \vec{J}\vec{e}_\vartheta + A_\varphi \vec{J}\vec{e}_\varphi. \qquad (4)$$

Operator $A: H_j \to C_f$, where $C_f = C_{(\overline{\Omega})} \oplus C_{(\overline{\Omega})}$ is a complex space of the continued vector-functions with uniform and mean-square metrics, $\overline{\Omega} \in R_2$ is some two-dimensional region. The form and properties of A operator depend on the type of radiators as well as on the geometry of antenna array. Using (2), (4) the synthesis RP is defined as:

$$\vec{f} = A\widetilde{B}^{-1}\vec{E}^{cm},\ f_{\vartheta,\varphi} = A_{\vartheta,\varphi}\widetilde{B}^{-1}\vec{E}^{cm}. \qquad (5)$$

The above formulas determine the direct dependence of RP on the exstrinsic electric field.

The problem of synthesis is considered as the minimization problem of the following functional:

$$\sigma_\alpha = \left\| F_\vartheta - \left| A_\vartheta \tilde{B}^{-1} \vec{E}^{cm} \right| \right\|_2^2 + \left\| F_\varphi - \left| A_\varphi \tilde{B}^{-1} \vec{E}^{cm} \right| \right\|_2^2 + \alpha \left\| \vec{E}^{cm} \right\|_2^2. \quad (6)$$

on the Hilbert space H_E. The first two terms in (6) are the mean-square components deviation of the synthesis amplitude pattern from the given RP, and the last summand puts a limitation on the norm of electric field, α is a parameter of regularization.

THE BASIC SYNTHESIS EQUATIONS

The minimization of functional σ_α is reduced to solving the Euler equations for $\vec{E}^{cm}$:

$$\alpha \vec{E}^{cm} + \left(A_\vartheta \tilde{B}^{-1}\right)^* A_\vartheta \tilde{B}^{-1} \vec{E}^{cm} + \left(A_\varphi \tilde{B}^{-1}\right)^* A_\varphi \tilde{B}^{-1} \vec{E}^{cm} = \left(A_\vartheta \tilde{B}^{-1}\right)^* F_\vartheta e^{i \arg A_\vartheta \tilde{B}^{-1} \vec{E}^{cm}} + \left(A_\varphi \tilde{B}^{-1}\right)^* F_\varphi e^{i \arg A_\varphi \tilde{B}^{-1} \vec{E}^{cm}} \quad (7)$$

Equation (7) is a nonlinear one with the Hammerstein type operator in the right-hand part and with a linear operator in the left part of equation. Using the operators $A_\vartheta \tilde{B}^{-1}$ and $A_\varphi \tilde{B}^{-1}$ to the both sides of expression (7) and taking into account formula (5), we obtain the system of nonlinear operator equations with respect to the components of RP:

$$\begin{aligned} &\alpha f_\vartheta + A_\vartheta \tilde{B}^{-1}\left(A_\vartheta \tilde{B}^{-1}\right)^* f_\vartheta + A_\vartheta \tilde{B}^{-1}\left(A_\varphi \tilde{B}^{-1}\right)^* f_\varphi = \\ &= A_\vartheta \tilde{B}^{-1}\left(A_\vartheta \tilde{B}^{-1}\right)^* F_\vartheta e^{i \arg f_\vartheta} + A_\vartheta \tilde{B}^{-1}\left(A_\varphi \tilde{B}^{-1}\right)^* F_\varphi e^{i \arg f_\varphi}, \\ &\alpha f_\varphi + A_\varphi \tilde{B}^{-1}\left(A_\vartheta \tilde{B}^{-1}\right)^* f_\vartheta + A_\varphi \tilde{B}^{-1}\left(A_\varphi \tilde{B}^{-1}\right)^* f_\varphi = \\ &= A_\varphi \tilde{B}^{-1}\left(A_\vartheta \tilde{B}^{-1}\right)^* F_\vartheta e^{i \arg f_\vartheta} + A_\varphi \tilde{B}^{-1}\left(A_\varphi \tilde{B}^{-1}\right)^* F_\varphi e^{i \arg f_\varphi}. \end{aligned} \quad (8)$$

Operators $A_\varphi \tilde{B}^{-1}\left(A_\vartheta \tilde{B}^{-1}\right)^*, A_\varphi \tilde{B}^{-1}\left(A_\varphi \tilde{B}^{-1}\right)^*$ are self-adjoin and positively half-determined.

In a general case, the analytical and numerical investigations of solutions to the equations (7), (8) are very complicated. However, considering the Euler equations in the operator form makes it possible to apply the methods of the nonlinear functional analysis and to construct the general numerical algorithms. The existence of solutions to the equations (7), (8) is proved by the following theorem:

Theorem 1. *Let $A: H_J \to \tilde{L}_f$ be a linear compact operator and $\tilde{B}^{-1}: H_E \to H_J$ be a linear boundary operator. Then functional σ_α has a minimum at some point $\vec{E}_*^{cm} \in H_E$. and the equation (7) in the space H_E and equation (8) in the space C_f both have at least one solution.*

We note two important properties of the systems (8):

1. If f_ϑ, f_φ are solutions of the system (8), then complex-adjoint functions $\overline{f_\vartheta}, \overline{f_\varphi}$ are the solutions of the system too.

2. If f_ϑ, f_φ are solutions of system (8), then functions $f_\vartheta e^{i\gamma}$, $f_\varphi e^{i\gamma}$ (where j is the arbitrary constant) are the solutions too.

THE NUMERICAL SOLVING OF THE SYNTHESIS PROBLEM

In the base of the iteration process of finding the solutions to equation (7) we put the implicit scheme of successive approximation method:

$$\begin{aligned} &\alpha \vec{E}_{p+1}^{cm} + \left(A_\vartheta \tilde{B}^{-1}\right)^* A_\vartheta \tilde{B}^{-1} \vec{E}_{p+1}^{cm} + \left(A_\varphi \tilde{B}^{-1}\right)^* A_\varphi \tilde{B}^{-1} \vec{E}_{p+1}^{cm} = \\ &= \left(A_\vartheta \tilde{B}^{-1}\right)^* F_\vartheta e^{i \arg A_\vartheta \tilde{B}^{-1} \vec{E}_p^{cm}} + \left(A_\varphi \tilde{B}^{-1}\right)^* F_\varphi e^{i \arg A_\varphi \tilde{B}^{-1} \vec{E}_p^{cm}}, \\ &(p = 0,1,2,\ldots). \end{aligned} \quad (9)$$

Here p is the iteration number. The following theorem is actual for the sequence $\left\{\vec{E}_p^{cm}\right.$ from (9):

Theorem 2. *The sequence $\left\{\vec{E}_p^{cm}\right.$ which is generated by the iterative process (9) is a relaxation for the functional σ_α, that is*

$$\sigma_\alpha(\vec{E}_{p+1}^{cm}) \le \sigma_\alpha(\vec{E}_p^{cm}) \quad (10)$$

for $p = 0,1,2,\ldots$

With respect to (10) and taking into account the limitation of functional σ_α from below we obtained the convergent sequence $\left\{\sigma_\sigma^{(p)}\right\} = \left\{\sigma_\alpha(\vec{E}_p^{cm})\right.$.

We numerically investigated the synthesis of the 5-elements antenna for the conical-spiral radiators with two arms. The tops of cones are located along the axis OX with crosselement distance 0.5λ. The amplitude RP is given in the area $\Omega = \{\vartheta \in [0, \pi/6], \varphi \in [0, 2\pi]$ by the expression $F_\vartheta(\vartheta, \varphi) = F_\varphi(\vartheta, \varphi) = |\cos(3\vartheta)|$. The linear system of the integral equations of the Poklington type is used for solving the analysis problem:

$$\sum_{m=1}^{N}\int_{S_m} J_{\tau_m}(s_m)\Big[k^2 G(s_n,s_m)\cdot(\vec{s}_n,\vec{s}_m)-\frac{\partial G(s_n,s_m)}{\partial s_n \partial s_m}\Big]ds_m = -i\frac{k}{W}E^{cm}_{\tau_n}(s_n) \qquad (11)$$

$$(n=\overline{1,N}).$$

Here s_m is a parameter equal to the length of the wire from its beginning; $J_{\tau_m}(s_m)$ is a component of the current vector at the point s_m tangential to the axis of the m-th radiator; k is the wave number; $\vec{s}_m$ is the unit vector tangential to the axis of the m-th radiator at the point s_m; $G(s_n,s_m)$ is Green's function; $E^{cm}_{\tau_n}(s_n)$ is a component of the outside current vector at the point s_n tangential to the axis of the m-th radiator; W is the wave resistance.

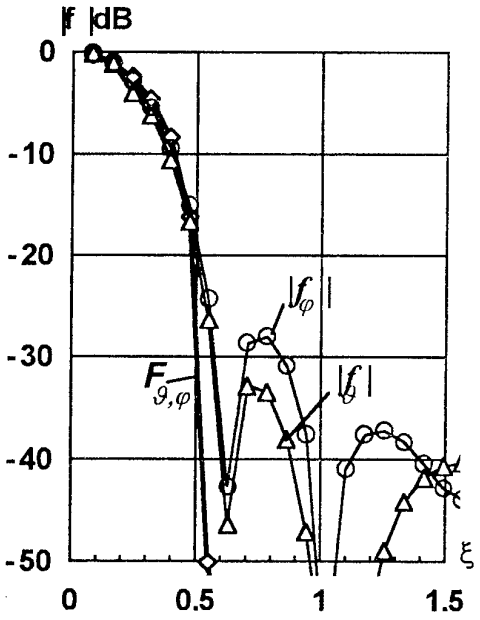


Fig. 1.

The numerical solving of the synthesis problem, with respect to (7), is reduced to finding the solutions of the nonlinear algebraic system of equations. On the base of equation (9) we design the iterations process. The results of synthesis are shown in the plane $\varphi = 0°$ in Fig. 1.

CONCLUSION

The described above problem of synthesis and the method of its solving take into account the vector character of electromagnetic field. They admit the generalization of synthesis on other types of antenna arrays, for example the conform array. The iteration process for numerical finding the minimum points of the functional is constructed. It generates the minimization sequence, which weakly converges to one of the points of local minimum.

REFERENCES

1. Chaplin A.F. Analysis and synthesis of the antenna arrays. Lvov 1987, 179 p.
2. Dmitriev V.I., Sereda P.P. Mathematical models and method of the integral equation in the theory of the spiral antenna. // Numerical methods and programming. Moscow, MGU, 1980.
3. Savenko P.O. About existence solutions of the synthesis problem of the radiating system for the given amplitude RP. // Mathematics methods and phys.-mech. fields. – 1995. V.38, p. 72-78.
4. Andriychuk M.I., Voitovich N.N., Savenko P.A., Tkachuk V.P. The antenna synthesis according to the amplitude radiation pattern. Numerical methods and algorithms. Kiev, Naukova Dumka Publ. 1993 [in Russian].

ELECTROMAGNETIC FIELD OF AN ANTENNA LOCATED NEAR A SEA TROPOSPHERIC WAVEGUIDE

A. V. Polyarus*, A. A. Koval, E. V. Tsekhmistrov

Kharkov Military University, Svoboda sq., 6, Kharkov, 310043, Ukraine
*phone (0572) 16-78-80. E-mail: polyarus@hotmail.com

The character of radio waves propagation when detecting low flying targets over a sea surface essentially depends on the distribution of temperature, pressure, humidity of air and hence on the height distribution of refractive index. Typical height dependences of the modified refractive index M on height h above the Black sea measured by refractometer are shown in Fig. 1 for July (curve 1) and August (curve 2). An example of a the mentioned diurnal dependence is given in Fig. 2. The regular measurements were accomplished in a height range from 0 to 30 meters and the separate measurements- up to heights of several kilometers. When analyzing the curves (Fig. 1, 2) we can deduce that they M (h) have the characteristic breaks showing an possibility of near-the-surface and elevated tropospheric waveguide occurrence. Maximum tropospheric waveguide heights didn't exceed 200...1500 meters.

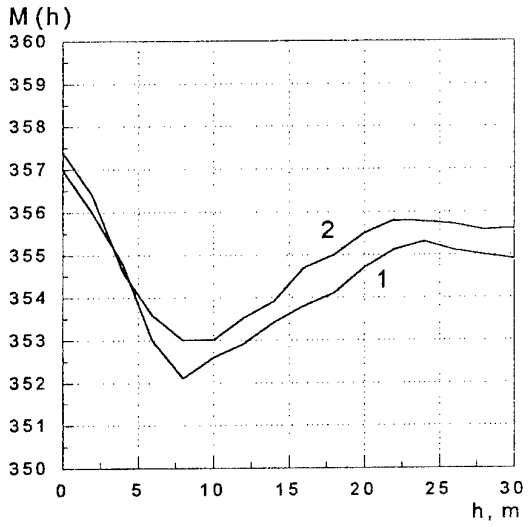


Fig. 1

The theory of radio waves propagation near Earth surface has been presented in a number of scientific works, for example, in [1]. But insufficient attention was paid to questions of low flying targets radar in these cases because of irregularity of tropospheric waveguides. We carried out the analysis of a radar channel consisting of coastal (ship) radar, tropospheric waveguide and low flying target over the sea surface. The exact calculation of electromagnetic field in a radar channel is impossible in a case like that since the tropospheric refractive index and the conductivity randomly depend on height and distance, and character of the radio wave scattering by a target or sea surface is, as a rule, unknown.

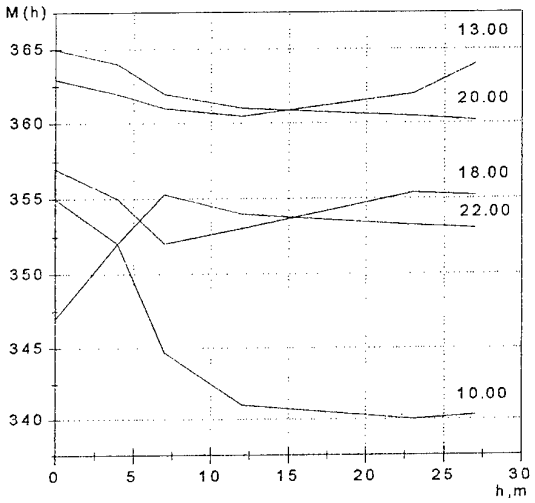


Fig. 2

The exact solution of the electromagnetic problem for a simplified mathematical model of radar channel can be found in some conditions. In this case the troposphere is assumed to be spherically-stratified with a conductivity equal to zero. Sea surface is represented as a perfectly conducting spherical one with the radius equal to the one of the Earth, and the target as an object, shaped as a perfectly conducting sphere shaped as with a known scattering diagram.

Mathematical description of an electromagnetic excitation of a sea tropospheric waveguide is an extremely difficult task. In [2] we have presented the approximate method of the analysis of a radar channel. The main attention was given to calculation of an electromagnetic field inside of tropospheric waveguide by the geometrical optics method. It was shown that electromagnetic wave, radiated by a radar in the antenna beam can propagate in follow ing ways: a) by steps, being reflected from the sea surface at each step and staying inside tropospheric waveguide (in this case we shall name all jumping trajectories as the first-type trajectories); b) purely by waveguide mechanism, staying inside the tropospheric waveguide and not falling on the sea surface (the second-type trajectories); c) leaving the tropospheric waveguide (trajectories of the third type).

During electromagnetic waves propagation, various trajectory transformations of one type into another are probable.

The results of experiments do not show strong echo from near zone, that should be inherent for waves propagating along trajectories of the first type. However signals reflected from large distances were being frequently detected. As it has turned out, the azimuth-distance dependences of the received signals intensity were similar to a relief of the opposite coast of the sea. One of characteristic radar portraits of the opposite sea coast is given in Fig. 3. It is easy to see that the detection of the signals reflected from an opposite coast is possible if radiowaves propagate along the second type trajectories.

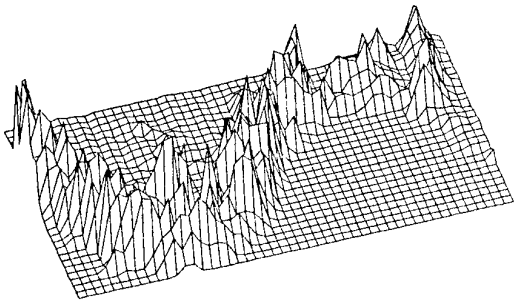


Fig. 3

The signals level measurements were carried out inside tropospheric waveguides by two antennas mounted above a sea surface respectively, at heights 5 and 25 meters at a distance from radar up to 90 kilometers. The average results of measurements are shown in Fig. 4. From the analysis of curves we can deduce that near to a sea the surface electromagnetic wave in a layer of thickness of less than 20...25 meters can propagate up to large distances. It is evident that radar of ships and low flying target is possible under some conditions. The best conditions for radar were since May till November.

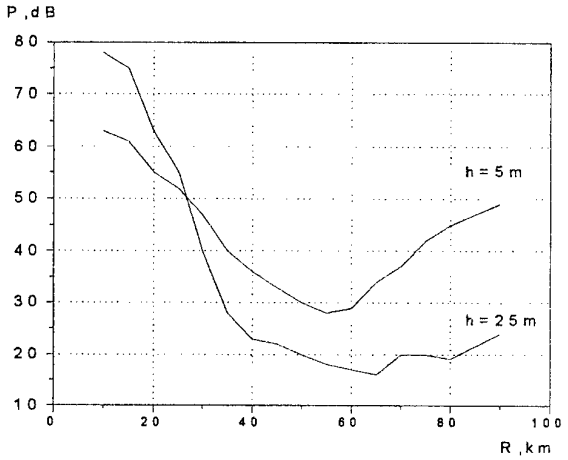


Fig. 4

It is confirmed by Fig. 5 where the distribution in months of average intensity of the signals reflected from an opposite coast is presented. When determining this parameter the cases were taken into account when the signals were not registered in general.

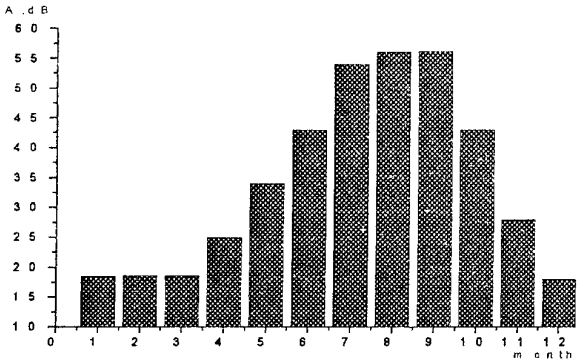


Fig. 5

Experiments require significant efforts and time. The calculation of an electromagnetic field by the method of geometrical optics shows in a number of cases excess sensitivity of the received results to changes of the input data, that is why, this method isn't universal. The solution of Maxwell's equations with respect to a tropospheric waveguide model results in the differential equation of the second order in partial derivatives with the right part. Its approximate solution by known methods requires significant expenses of a computer resource and not always leads to the steady results. The simplifications of the differential equation, for example, refusal of the taking into account of radiator characteristics and preservation of the physically reasonable boundary conditions are possible. In this case the differential equation can be solved by using the separation of variables. The application of the integral equations method for the problem of an electromagnetic field in tropospheric waveguide computation is also possible. These and many other problems await for further investigation.

REFERENCES

1) V. A. Fock. The problems of diffraction and propagation of electromagnetic waves.- Moscow: Sov. radio, 1970.- 520 p. [in Russian].

2) A. V. Polyarus, A. A. Koval, V.V. Fatafutdinov. Mathematical method of the analysis of "radar-tropospheric waveguide-low flying target over sea surface" radar channel.- 1998 International conference on mathematical methods in electromagnetic theory, volume2.-Kharkov, Ukraine, June 2-5, 1998. -pp. 880...882.

THE DETERMINED APPROACH TO CALCULATION OF RADIOLINES IN URBAN CONDITIONS

L. I. Ponomarev, M. G. Alekseyenko, A. Y. Ganitsev

Moscow State Aviation Institute (engineering university MAI)
125871, Russia, Moscow, Volokolamskoe shosse, 4;
Tel: (095) 1584152; Fax: (095) 1581697
E-mail: ponomarev@iname.com, almagen@iname.com

Up to now, the problem of electromagnetic field calculation in urban environment is topical. It is due to both intensive development of a mobile radio communication means and problems of electromagnetic compatibility of radioelectronic means provision. There are different approaches to the solution of this task — determined [1–6], statistical [7–9], and also complex [10]. However, accuracy of offered methods in a number of cases is insufficient.

In Fig. 1a is shown the example of urban building. The letters "BS" on it mark base station, "MT" — mobile telephone. In Fig. 1b,c are shown sideways and from above view on urban building, direction of the basic waves falling from BS (within the framework of the geometrical theory of diffraction approach) on top and lateral edges (TE and LE) of the buildings, in a point of an arrangement MT. At modeling the following assumptions were used. Each building was simulated by the thin screen with height and length equal to height and length of a building. In that it was supposed, that the primary wave from BS is spherical, and polarization of the antenna BS is vertical. The distance from BS up to the nearest building is those, that it is a front of a spherical wave, falling on it, on TE and LE locally flats. In that the directions of locally flat waves fall on TE and LE of screens lay in planes, normal (or near to normal) for TE and LE. The waves formed in result of diffraction on TE and LE of buildings, are locally cylindrical. The structure of a terrestrial surface between buildings is such, that a cylindrical waves after reflection remains locally cylindrical. Only the complex amplitude of the reflected wave is changed.

With distribution from BS to MT the signal try a multiple diffraction on TE and LE of screens, as shown in Fig. 1a,b. On an antenna MT there come waves, scattered TE and LE n and $n + 1$ buildings. The waves, incident on these buildings, were considered as a sum of a direct field and fields formed in a result of consistent diffractions on TE and LE of all previous buildings. The registration repeated multiple overreflections and diffractions between buildings did not give noticeable modifications of modeling results. The diffraction on upper and side edges of a screen was considered as a diffraction on edge of a conducting half-plane [11].

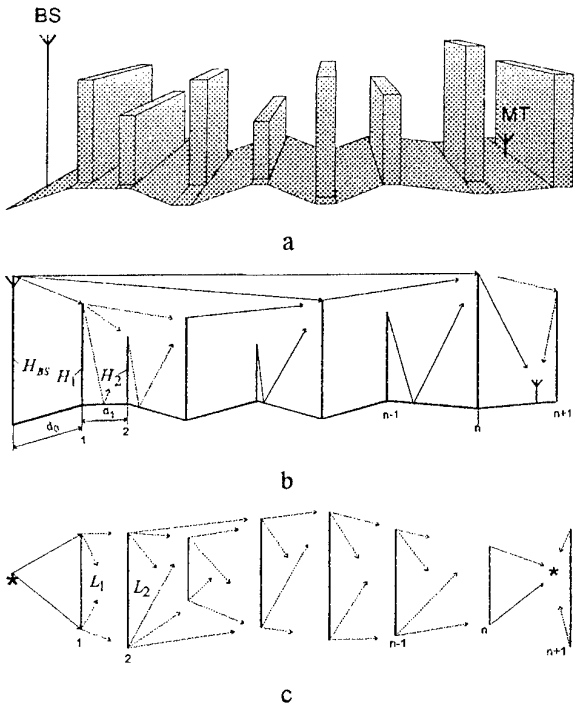


Fig. 1

From Fig. 1 b,c it can be seen, that basic channels of propagation of an electromagnetic field UHF in city are the following:

1. in free space above roofs of buildings;

2. a result of a diffraction on roofs of standing one after another buildings;

3. a result overreflection from of a terrestrial surface;

4. a result of a diffraction on lateral edges of buildings.

A sequence of buildings with a height $H_1 = H_2 = ... = H_n = 30$ m and length $L_1 = L_2 = ... = L_n = 150$ m and with a distance between them $d_1 = d_2 = ... = d_n = 100$ m was considered in this model. Analyze has shown, that if the antenna BS is above the level of buildings' roofs ($H_{BS} = 40$ m), basic propagation paths are above roofs and channel through upper edges of buildings. The signal strength by other propagation path is more than 50 dB below [12]. If the antenna BS is located below than level of buildings roofs ($H_{BS} =$

20 m), basic the channel through upper edges of buildings is, and the signals from other channels are less basic on 15 dB and more.

For such sequence of buildings is accounted and analyzed dependencies of losses from number of buildings, height and length of buildings, distance between them, height of antenna BS rise, position of antenna MT [12].

For an evaluation of an accuracy of the developed model the experimental researches were carried out. For this purpose the site of urban building in Moscow is choose, shown in Fig. 2. The objects of scattering 1-10 represented 5-storied houses by a height approximately 18m. Between houses located the high trees, which crowns were at a level of buildings roofs.

The measurements of power signal level were carried out by a mobile radio telephone with spiral — dipole antenna at 869 MHz. The reception antenna located vertically at the height 1.6 m. The transmission power was 2 W. The antenna of the transmitter located at the height 45 m. The location of the antenna is depicted by an asterisk in Fig. 2. The direction of pattern maximum is depicted in Fig. 2 greasy arrow.

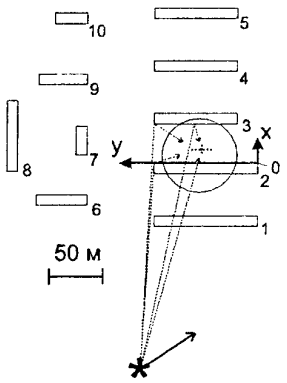
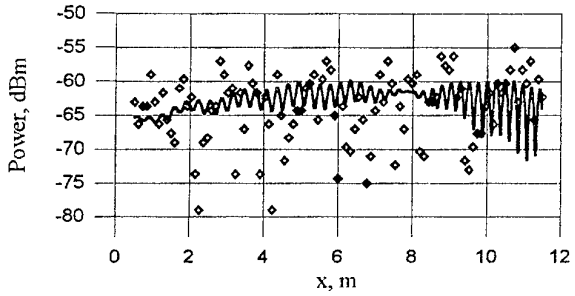


Fig. 2

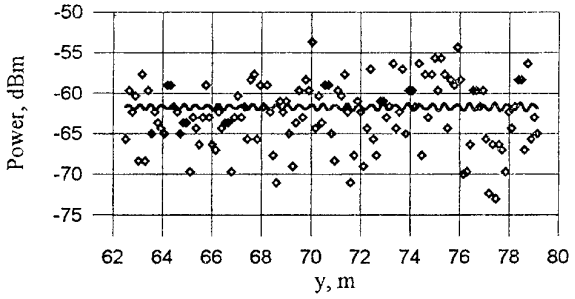
The measurements were carried out in space area between 2 and 3 buildings (the route is shown by a dotted line in a circle) with an interval 0.1 m along a line parallel axis OX, parallel axis OY and along a line parallel axis OZ, directed perpendicularly plane of figure.

The experimental and calculated data were compared with. At that the fields, scattered lateral edges of buildings 6–10 were estimated. They have appeared more than 30 dB less of signals level coming through roofs and left LE of the buildings 1–3. The signal coming through right LE of buildings 1–3 because of consistent diffractions on these edges was more than 20 dB less above-stated signals. Thus, basic channels in the given example have appeared paths through a roof and left LE of buildings 1–3.

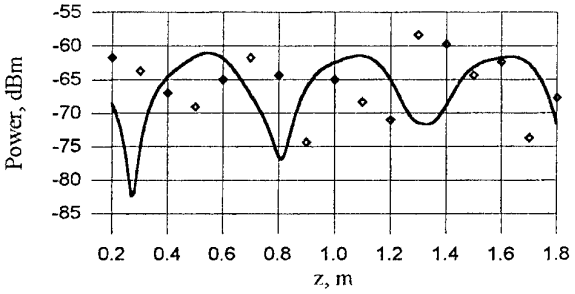
The results of calculated and experimental data comparison are depicted in Fig. 3 a,b,c (the solid lines show theoretical results, squares - experimental data). As it is visible from figures, the rather good correspondence of average level calculated and experimental results is observed. So, arithmetic mean value of difference between calculated and experimental data along a line parallel axis OX is equal 1.6 dB, along a line parallel axis OY – 1.4 dB, and along a line parallel axis OZ — –0.4 dB. The arithmetic mean value of difference on all samples is equal 1.4 dB. The mean square deviation of difference between calculated and experimental data is equal respectively 5.3 dB, 4.0 dB, 7.7 dB and 4.9 dB.



a



b



c

Fig. 3

Thus, the developed algorithm allows to calculate strength of an electromagnetic field for sites of a radioline, by which the explained above assumptions are applicable. It can be used as a fragment of the more general determined approach. This approach allows to calculate strength of a field and created BS in arbitrary area with a high degree of accuracy. One may be use

for frequency planning, optimization of the arrangement BS, to solve tasks of electromagnetic compatibility and series of other adjacent tasks.

REFERENCES

1. Beresina L.N., Piven I.V.: " Modelling of radiowave propagation for a urban radio communication ", Theory and engineering of radio communication, 1993, no. 2.
2. Maciel L.R., Bertoni H.L., Xia H.H.: " Unified approach to prediction of propagation over buildings for all ranges of base station antenna height ", IEEE Trans. Veh. Technol., 1993, 42, no. 1.
3. Ashok Ranade: "Local access radio interference due to building reflections", IEEE Transactions on Communications, 1989, 37, no. 1.
4. Neve M.J., Rowe G.B.: "Mobile radio propagation in irregular cellular topographies using ray methods", IEE Microwaves, Antennas and Propagat., 1995, 142, no. 6.
5. Brown P.G., Constantinou C.C.: " Investigation on the prediction of radiowave propagation in urban microcell environments using ray-tracing methods ", IEE Microwaves, Antennas and Propagat., 1996, 143, no. 1.
6. M.F. Catedra, F. Saez de Adana, O. Gutierrez. Efficient ray-tracing techniques for three-dimensional analyses of propagation in mobile communications: application to picocell and microcell scenarios.–IEEE Antennas and Propagat. Magazine, 1998, vol. 40, no. 2.
7. Ponomarev G.A., Telpuhovsky E.D.: "UHF propagation in town ", Tomsk: "Rasko", 1991.
8. Warakin L.E.: "Statistical model of multiray UHF propagation in town ", Radio Engineering, 1989, no. 12.
9. Hata M.: "Empirical formula for propagation loss in land mobile radio services", IEEE Transactions on Vehicular Technology, 1980, 29, no. 3.
10. Panchenko V.E., Gaynutdinov T.A., Erohin G.A., Kocherschevsky V.G., Shorin O.A.: "Combination of statistical and determined methods of account radio field in urban conditions ", Electric Communication, 1998, no. 4.
11. Borovikov V.A., Kinber B.E. "Geometric theory of diffraction ", Ì.: Communication, 1978.
12. Ponomarev L.I., Alekseyenko M.G., Ganitsev A.Y.: "The determined approach to calculation of urban radiolines for cellular systems of communications ", Antennas, 1999, no. 1.

ON METHODS OF SOLUTION TO SLOT ANTENNAS SYNTHESIS PROBLEMS

Yu. Yu. Radtzig, M. A. Khavanova

173000, Veliky Novgorod, Nov STU of Yaroslav Mudry,
St-Petersburgskaya str., 41, FTSP, tel.(816-22)11-68-91
fax (816-22)-24110, E-mail: theorphy@info novsu.ac.ru

It is known that nowadays antennas are widely used both as separate weakly directed radiators, particularly at superhigh-speed aircraft, and as elements of phasing antenna (PAA).

At first consider the problem of synthesis of a slot antennas. It is useful to present this problem as two separate problems, i. e. An internal and an external ones.

While the external problem consists in determination of the amplitude-phase distribution of a field in exposing an antenna in the prescribed radiation pattern, the internal problem consists in estimating the function of sources that realize the amplitude-phase distributions of a field that were found as a solution of the first problem. Thus, the external problem is the problem of synthesis of the radiation pattern, while the internal problem is that one of synthesis of the field amplitude-phase distribution.

A lot of papers of Russian and foreign authors are devoted to solution of the external problem. One can find an information at most of them, for example, in the well-known monograph [1], and we won't dwell on this problem.

Consider in more details solution of the internal problem. It is necessary for that firstly to investigate functions of sources and distribution of voltage that is generated hereby along the slot. As it is known, such a connection is written as an integral-differential equation. It is not difficult to generalize this equation for the case of a curvilinear slot, and not only on the plane screen [2].

The problem of analysis consists in determination of field distribution in a slot on the prescribed function of excitation. For the narrow slot of length L and width d, it is necessary to determine stress distribution between the slot edges. The numerical-analytical method [3] proved to be the most effective for this purpose. Hereabout the first field (function of excitation) is prescribed (preset) precisely, possibly in a kind of an infinite series. The numerical-analytical method reveals physics of the processes which take place in the excited field. It proves to be the most essential when solving equations for moderately thin, medium, and electrically wide slot antennas. The indicated method turned out to be well generalized for the case of curvilinear, bucolic, and impedance slot antennas, as well as systems of the mentioned antennas and the antennas situated near the medium interface.

High efficiency of numerical-analytical methods has been demonstrated for the antennas considered in publications. The possibility to attain any preset precision is shown [4].

Separately there are considered problems of integral-differential equations solution for infinitely thin slot antennas, when the slot latitude can be unlimitedly lessened down to zero. The specific difficulties of such equations solution have been revealed.

THE ELECTROMAGNETIC ANALYSIS OF SLOT ANTENNAS

Knowledge of the electric and magnetic currents on a surface of the antenna plate enables one to determine the antennas main electrodynamic characteristics: input conductance, radiation power, electromagnetic field in far and near zones [2].

There are also discussed problems of parametric synthesis of antennas to achieve the optimal coordination in a frequency range or to obtain the required radiation pattern. A successful solving of the parametric synthesis problems is caused in many respects by high efficiency of the numerical-analytical method for integral-differential equations solution.

PROBLEMS OF INTERNAL SYNTHESIS OF SLOT ANTENNAS

It is possible, on the base of integral relations between functions of excitation and stress in a slot, to conduct the detailed investigation of methods of solving the problem of synthesis of the amplitude-phase distribution of a field in slot antennas [5].

The main integral relation between stress and function of sources is presented in the operator form, and functions of stress and sources are considered as elements of complex-valued Gilbert spaces. The properties of the integral operator of the considered problem of synthesis are studied. It is shown that it is a quite continuous operator in Gilbert space. The properties of function of sources on a complex plane and a material axis are considered as well. For solving the considered integral problem of synthesis, the apparatus of regulation of the incorrectly set problems of mathematical physics is

used [1]. This apparatus allows to consider the stable solution of the synthesis problem and estimate this stability. There is found the necessary connection between the pre-set stress reproduction error in a slot and the error of realization of function of sources, due to which this stress is generated.

The found continuous function of sources is in general difficult for practical realization. Therefore there are proposed methods of substitution, with a high precision degree, of the continuous function of excitation, for the system of discrete sources that are convenient for practical realization. Such a substitution proves to be possible when solving the integral problem of synthesis by methods of regularization. For this purpose the right hand part of the specially obtained integral relation of the second type, connecting stress and function of sources, is substituted by the approximate expression with the help of various quadrature formulae. There are considered in detail the separate kinds of quadrature formulae that allows to construct different schemes of discrete excitation of slots (in the equidistant points; in the non-equidistant points, when the less realization error is ensured; and in the non-equidistant points that ensure reproduction of the "base" of continuous function of sources, etc.).

The entire order of solving the internal problem of synthesis is described in detail, and examples of its solution for linear circular and elliptical slots are given. Realization of solving the problem of synthesis of the field amplitude-phase distribution in slot antennas is made with the system of symmetrical strip lines with the common earthed plates. It is shown that the system of discrete sources, electric currents, is to be reproduced most efficiently with the set of symmetrical strip lines with common earthen plates, in one of which the curvilinear radiating slot is cut through. The approximation limits are determined that are given by the proposed methods when realizing the pre-set amplitude-phase distribution of a field in a slot. Under the chosen scheme of excitation, the necessary current amplitudes are ensured by the discrete system of central strips and the power divider that are built in the strip system, and phases are chosen for the point of excitation. The matching conditions are ensured in the excitation points. As a result a theory is constructed as well as its practical realization, for solving the entire problem of synthesis of slot antennas with an arbitrary configuration.

REFERENCES

1. L. D. Bakhrakh., S. D. Kremenetsky. Synthesis of radiating systems (Theory and methods of calculation). M.: Sov.radio, 1974, pp. 232 [in Russian].
2. Yu. Yu. Radtsig. Dissertation for Doctorate degree. Kazan, 1971, pp. 332 [in Russian].
3. Yu. Yu. Radtsig., S. I. Eminov, etc. Calculation of slot and dipole antennas basing on numerical-analytical technique// Tez. dokl. III Vseros. Nauchno-techn. Konf. Kazan', 1994, pp.114-115 [in Russian].
4. E. I. Nefedov, Yu. Yu. Radzig, S. I. Eminov.

1. Regularization of integral equations of slot and dipole antennas. Doklady RAN, 1995, V.344, No.4, pp.477-478 [in Russian].
5. Yu. Yu. Radtsig, M. A. Khavanova. On the solution to the internal boundary electromagnetic problem for slot radiators by non-linear programming // Vestnik Novg. Gos. Univ. Ser.: Estestvennye nauki, 1998, No.10, pp.58-59 [in Russian].

AN EVALUATION OF THE INTENSITY OF THE ELECTROMAGNETIC FIELD, REFLECTED FROM THE AERODYNAMIC TARGET IN AN ABOVE-WATER SURFACE WAVEGUIDE

A. Samokhvalov

Central Research Institute of Armament and Military Engineering
of the Armed Forces of Ukraine
4, Andrushchenko Str., Kiev - 135, tel. (044) 271-62-45

There are works [1] considering the theoretical principles of radio waves propagation in above-water surface tropospheric waveguide, but till now a practical evaluation for methodical calculations of actual above-water surface tropospheric waveguides has not been carried out yet.

Therefore the purpose of the present paper is to describe a method allowing to determine not only a field in the middle of tropospheric waveguide, but a power of a signal reflected from a target being at low altitude in the middle of tropospheric waveguide as well.

Let's the antenna be a receiving-transmitting one and creates in tropospheric waveguide formed by the phenomenon of a superrefraction in above-water tropospheric layers a complicated enough picture of rays represented in a Fig. 1, with a lot of rereflections and caustics, that is stipulated by focusing abilities of smoothly - inhomogeneous troposphere [1].

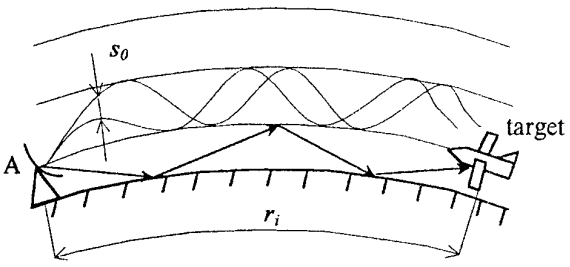


Fig. 1. Above-water surface tropospheric waveguide

Then all the electromagnetic waves can be presented as N-data-flow tubes with azimuth circular width equal to $\varphi_{0.5p}$, i.e. width of the radiation pattern (RP) of radar-tracking station (RTS) antenna in the azimuth plane at half power level.

Within the limits of each data-flow tube rays trajectories are considered to be of the same type according to the strategy of choosing a minimal number of tubes being optimum [1,2] and depending on a required accuracy of radio channel characteristics according to Fig. 1.

The cross-section of the ith data-flow tube can be determined [1, 2] as:

$$S_{ij} \approx r_i \cdot \varphi_{0.5p} \cdot \Delta h_i , \qquad (1)$$

where r_i — distance from RTS up to the ith view point in tropospheric waveguide; $\varphi_{0.5p}$ — antenna RP width at half power level; Δh_i – minimal distance between two trajectories, which create the ith data-flow tube at distance r_i.

Let's assume that each ith data-flow tube is excited by a partial source of radio waves, radiated by RTS with power p/N and gain equal to a product $G'_m F^2(\alpha,\varphi)$, where G'_m — gain of partial RP, and $F^2(\alpha,\varphi)$ — RP with respect to RTS antenna.

Then power flow density in each data-flow tube is [1]

$$P_{N_i} = \frac{PG_m F^2(\alpha,\varphi)}{Nr_i \varphi_{0.5p} \Delta h_i} \qquad (2)$$

If the target is at distances r_i less than the distance of the first hop, then the power a signal reflected from the target the RTS receiver's input taking into account radio waves in the ith data-flow tube is determined by method [1, 2]

$$P_{r_i} = A_r \frac{PG_m A_{ef\,m} F^2(\alpha,\varphi)}{Nr_i \Delta\varphi_{0.5p} \Delta h_i} \sigma(x_i), \qquad (3)$$

where A_r — factor of radio waves propagation proportional to a signal attenuation according to the radar-tracking equation [1] according to Fig. 1,

$$P_{r_i} = \frac{PG^2\lambda^2\varphi\tau c \sec\theta}{(4\pi)^3 R^3}\sigma_0 ,$$

for small q (angle of meeting with sea surface), and

$$P_{r_i} = \frac{PG^2\lambda^2 h\varphi}{(4\pi)^3 R^3 \sin\theta}\sigma_0 ,$$

for large q, where P_t — impulse power of the transmitter; G – antenna gain; λ — wavelength; R — distance up to the target; φ — RP width in an azimuth plane at half power level; h – beam width in a vertical plane at half power level; t — pulse duration; q — angle of RP axis RP with respect to azimuth; c — velocity of radio waves propagation; σ_0 — mean equivalent reflecting

surface of sea plot of reflection; $\sigma(x)$ — effective surface of target scattering in limits of the ith data-flow tube; $A_{ef\,m}$ — maximum value of effective square of RTS receiving antenna.

Then the amplitude of an electric field intensity E_{mi} in each data-flow tube is approximately determined according to [1] as:

$$E_{m_i} = \sqrt{\frac{240\pi\, PG_m F^2(\alpha_i, \varphi)}{N r_i \Delta\varphi_{0,5p} \Delta h_i}} \qquad (4)$$

For multiple reflection of radio waves it is necessary to take into account a reflection square

$$\sigma_0 = \frac{\pi \Delta\varphi^0_{0,5p}}{360}\left(r^2_{kl_i} - r^2_{nl_i}\right) \qquad (5)$$

and radiation polarization $|R_{0z}|^2$, and for certain glazing angle (θ_0 is small or large) the power of reflection is determined by expression

$$P_{ref1_i} = \frac{PG_m F^2(\alpha_i, \varphi)}{N r_i \Delta\varphi_i \Delta h_i} \frac{\pi \Delta\varphi^0_{0,5p}}{360}\left(r^2_{kl_i} - r^2_{nl_i}\right)\left|\dot{R}_{v,h}\right|. \quad (6)$$

Taking into account $r_i = \frac{r_{kl_i} + r_{nl_i}}{2}$, the expression (6) will be the following

$$P_{ref1_i} = \frac{PG_m F^2(\alpha_i, \varphi)}{N \Delta h_{ref1_i}}\left(r_{kl_i} - r_{nl_i}\right)\left|\dot{R}_{v,h}\right|, \qquad (7)$$

where Δh_{ref1i} — minimum distance between two trajectories creating the ith data-flow tube at the end of the first hop, that is at distance r_{nli} along a ray.

It is necessary to mark, that on the second hop the extension of a data-flow tube in an azimuth plane is continuing. Linear beam width in the given plane is:

$$\Delta L_{2i} = \Delta\varphi_{0,5p}(r_{1i} + r_{2i}), \qquad (8)$$

where r_{2i} — distance from a plot of reflection (end of the first hop) up to the target, which is within the limits of the second hop.

Linear beam width for the pth hop in limits of the ith data-flow tube is:

$$\Delta L_{pi} = \Delta\varphi_{0,5p} \sum_{l=1}^{p} r_{li}\,, \qquad (9)$$

where the distance along ray r_{li} is similar to distance r_{2i} or r_{1i}.

The full cross-section of the ith data-flow tube on the second hop:

$$S_{2i} \approx \Delta L_{2i} \Delta h_{2i}\,, \qquad (10)$$

where Δh_{2i} — minimum distance between two trajectories creating the ith data-flow tube for the second hop.

This distance to present dimensions of plot of radio waves reflection after the first hop should be such to allow emerging of a various kind of trajectories "interlacings", that is boundaries of the focussing and defocussing. For correct separation it is necessary a line AB (Fig. 1) to divide into m_2 parts, each of which creates a reflected wave propagating in the second hop within limits of ray tube of the same type. In this case:

$$\Delta h_{2i} = \sum_{n_2=1}^{m_2} \Delta h_{in_2}\,, \qquad (11)$$

where n_2 — number of ray tubes for the second hop. Thus, in limits of the ith ray tube for the second hop m_2 ray tubes with the cross-section

$$S_{in_2} \approx \Delta L_{2i} \Delta h_{in_2} \qquad (12)$$

and distance between two nearest trajectories of this handset Δh_{in_2} will be chosen.

The similar separation is necessary to carry out for each consequent hop. For the p-the hop

$$S_{in_2 - n_p} \approx \Delta L_{pi} \Delta h_{in_2 - n_p} \qquad (13)$$

In (13) indexes in Δh characterize numbers of ray tubes, which were allocated fron the ith tube for the first hop, that is from the ith ray tube for the second hop n_2 of tubes were allocated, on the third — n_3 of tubes, etc., for the pth hop — n_p of tubes. Totally there are m_1 of tubes for the first hop, for the second — m_2, for the $p$tht — m_p. Total number of ray tubes for p hops is

$$\prod_{u=1}^{p} m_u\,.$$

The cross-section of the ith ray tube with number α for the pth hop is:

$$S_{in2\ldots n(p-1)\alpha} \approx \Delta L_{pi} \Delta h_{in2\ldots n(p-1)\alpha} \approx$$
$$\approx \Delta\varphi_{0,5p} \Delta h_{in2\ldots n(p-1)\alpha} \sum_{l=1}^{p} r_{li}\,. \qquad (14)$$

Analogous to (7) the power of a signal reflected from sea surface in any data-flow tube can be determined. Knowing the power of signal distributed on the known tube's (14) the power flow density can be easily determined by dividing power by cross-section square.

So, for example, in the tube with number n_2 for the second hop the power flow density is

$$S_{ni_{n2}} = \frac{P_{ref1i}}{S_{in2}}, \qquad (15)$$

where P_{ref1i} and S_{in2} are determined by (7) and (14).

The power of the signal reflected from sea surface after passing the second hop is

$$P_{refn2} = \frac{P_{refn1i}}{S_{in2}} S_{refn2} \left|R_{vhp2}\right|^2 \gamma, \qquad (16)$$

where: γ — factor taking into account pattern of secondary radio waves scattering by sea surface; S_{refn2} — square of reflection surface at the end of the second hop in data-flow tube with number n_2; $\left|R_{vhp2}\right|$ — reflectivity module for vertically and horizontally polarized radio waves for plot of reflection in the given data-flow tube.

The value $S_{\text{ref } n2}$ is determined similarly to $S_{\text{ref } n1i}$ (5).

Analogous to (16) reflected signal power can be determined for any hop. Knowing a cross-sectional square of data-flow tube it is easy to determine the power flow in any section of this tube. If to multiply it by ESS of the target being in this section, the power of reflected signal can be easily determined by known method. Here it is supposed that tropospheric above –water surface waveguide, as a quadruple, is reciprocal: signal scattered from the target propagates in direction of RTS on the same path, which it has passed from RTS to the target.

Thus, detecting signal reflected from the target RTS operator can, relatively to point, determine only azimuth of the target. But, however, the target can be low-altitude or high-altitude, and the elevation angle in both cases can be identical.

The indicated technique allows to evaluate operatively strength electromagnetic field intensity in any point of a line for superrefractional radio waves propagation, but disregarding return radio waves scattering due to a state of sea surface.

REFERENCES

1. Shirman Ya. D., Manzhos V.H. Theory and technique of radar data processing at the background of interferences. – Moscow, Radio i Sviaz, 1981.
2. Radar Handbook. Editor-In-Chief Merrill J. Skolnik. McGraw-Hill Book Company, 1970.

THEORY OF ANTENNAS WITH NONLINEAR ELEMENTS AND ITS APPLICATION

Y. S. Shifrin, A. I. Luchaninov, V. M. Shokalo

Kharkov State Technical University of Radio Electronics
Prospekt Lenina 14, Kharkov 310726, Ukraine
e-mail: shifrin@kture.kharkov.ua

The report presents the results of the research carried out in the Kharkov State Technical University of Radio Electronics (KhTURE) for about twenty years and aimed at developing the theory and techniques of a new class of antennas – antennas with nonlinear elements (ANE).

The need to research effects in the antennas including elements with a nonlinear characteristic had appeared due to a few reasons. The main one was the expansion of the scope of tasks, accomplished with the to-date radio electronic systems, that had led to emergence of a new type of antennas, whose functioning is inherently connected to the presence of nonlinear elements (NEs). These are rectennas, antenna-mixers, antenna-multipliers, antenna-generators and antenna-amplifiers.

The presence of NEs in an antenna causes the appearance of new spectral components in its response and the dependence of antenna characteristics and parameters on the input excitation level. The mentioned effects complicate sufficiently the analysis and lead to the necessity of computation of output ANE parameters at every frequency (working, harmonic and combination) for different levels of the input excitation.

At the time of beginning the ANE research at KhTURE (1980) the ANE theory was weakly developed. There was a number of simulating models and analysis methods of antennas with lumped NEs, which were suitable for the research of highly exceptional ANE types and based on a number of simplifying assumptions. Antennas with the distributed nonlinearity were almost unexplored, the development of such antennas used to be carried out only experimentally.

The mentioned circumstances defined the goal of the research at KhTURE, namely, the creation of the sufficiently general theory of antennas suitable for the adequate analysis of the settle regime of the whole variety of antennas including NEs with lumped and distributed parameters, as well as the application of the developed theory to investigation of specific ANE types.

The main achievements in developing the theory of antennas with lumped and distributed NEs are following.

For the antennas with lumped NEs:

- the general mathematical model convenient for analysis of a wide class of ANE is proposed. This model is given by the set of equations of state (ES) and output equations as well as equations for computation of the external antenna parameters. The model allows to investigate all nonlinear effects connected with forming of new spectral components in ANE response as well as with a nonlinear dependence of ANE characteristics on the input excitation level;
- the two-level iteration method of numerical solving the set of equations of state extending, in compare with a traditional one, the possibilities of ANE analysis is developed. The proof of this method convergence is obtained. The convergence of low and high level iteration procedures is investigated. The modified high level iteration procedure converged with any parameters of linear and nonlinear ANE subcircuits is proposed. The ways of taking into account the properties of the ANE linear subcircuit for increasing the analysis algorithm efficiency are substantiated;
- the method of analytical ES solving is proposed. This method is based on the use of the Volterra series in matrix presentation and allows to build the so-called structure ANE model, i.e. the model describing the antenna in terms of input-output.

For antennas with distributed NEs:

- the mathematical model of the antenna with distributed NEs is developed. This model is given: in the spatial-time region by the nonlinear integral equations (NIEs) for electric or magnetic field defined relatively to instant values of current density on the surface of a nonlinearly conducting radiator; in the spatial-frequency region by the set of NIEs defined relatively to complex amplitudes of frequency harmonics of the surface current density. These NIEs are the sets of the equations of state and, as in the case of antennas with lumped NEs, allow to take into account forming of new frequency components in the spectrum of the antenna response as well as the dependence of antenna parameters on the excitation level;

- the sets of integral equations for a number of specific types of antennas with distributed NEs are obtained taking into account the antenna geometric properties, that allows to simplify the NIEs and, as a result, to increase their solving efficiency;
- the methods of solving the set of NIE based on dividing the set into linear and nonlinear parts are developed. This dividing allows to use the method of linear integral equations for defining the linear part parameters and to take into account the nonlinear properties of ANE with methods of solving the equation of state developed for antennas with lumped NEs.

In general the developed ANE theory forms the sufficient basis for investigation and developing of various types of the antennas with NEs, for solving the task of diffraction on a body with lumped and distributed NEs.

The efficiency of the developed theory has been proved by its application to solving a number of important tasks of to-date radio engineering. The originality of a number of new ANE types is confirmed by the Certificates of authorship and patents. The most investigated are the nonlinear effects in systems of wireless power transmission. The report presents results of the first in Ukraine experiment on wireless power transmission and investigations of one ANE type – the large aperture rectenna.

PSEUDODIFFERENTIAL EQUATIONS METHOD FOR SOLVING PROBLEM OF ELECTROMAGNETIC WAVE DIFFRACTION ON CONDUCTING SCREENS

Yu. G. Smirnov, A. A. Vartanov, M. Yu. Medvedik

Dept. of Mathematics, Penza State University, Krasnaya, 40, 440017, Penza, Russia
E-mail: math@diamond.stup.ac.ru

STATEMENT OF THE PROBLEM

In the following we study the electromagnetic scattering problem for a bounded screen. The surface of the screen is assumed to be infinitely thin and perfectly conducting. Let Ω be the two-dimensional bounded surface in R^3 with the smooth boundary $\partial\Omega$ outside a finite set of singular points. Let consider boundary value problem for Maxwell equations

$$rotE = ikH,\ rotH = -ikE \text{ in } R^3,\ \mathrm{Im}k \geq 0, k \neq 0, \quad (1)$$

$$E_t = -E_t^0 \text{ on } \Omega, \quad (2)$$

$$r\left(\frac{\partial E}{\partial r} - ikE\right) \to 0,\ r\left(\frac{\partial H}{\partial r} - ikH\right) \to 0 \text{ as } r := |x| \to \infty \quad (3)$$

$$E, H \in L^2_{loc}\left(R^3\right), \quad (4)$$

where E_t^0 are the tangential electric components of the incident electromagnetic field E^0, H^0. It is supposed that the sources of incident field lie away from the screen and, hence $E_t^0\big|_\Omega \in C^\infty\left(\overline{\Omega}\right)$.

For the functions E, H it is required that $E, H \in C^2\left(R^3 \setminus \overline{\Omega}\right)$, $E_t \in C\left(R^3 \setminus \partial\Omega\right)$. The static case $k = 0$ is not considered because it leads to the well elaborating Dirichlet or Neumann scalar problems for the Laplacian.

The uniqueness of the solution to (1)–(4) holds because for $\mathrm{Im}k \geq 0, k \neq 0$ the homogenous problem (1)–(4) has at most the trivial solution. The problem (1)–(4) can be reduced to the vector pseudodifferential equation

$$Lu := \left(gradA(Divu) + k^2 Au\right)\Big|_t = f, \quad x \in \Omega, \quad (5)$$

where A denotes the integral operator

$$Au = \int_\Omega \frac{\exp\left(ik|x-y|\right)}{|x-y|} u(y) ds, \quad (6)$$

$f := 4\pi k E_t^0\big|_\Omega$ and Div is the tangential divergence on Ω. Here, the tangential vector u is the so-called current density on Ω. In this case the fields $E, H \in C^2\left(R^3 \setminus \overline{\Omega}\right)$ are obtained by formula

$$E = ik^{-1}\left(gradA_1(Divu) + k^2 A_1 u\right),\ H = rotA_1 u;\ k \neq 0,$$

$$A_1 u = \frac{1}{4\pi}\int_\Omega \frac{\exp\left(ik|x-y|\right)}{|x-y|} u(y) ds; \quad x = \left(x_1, x_2, x_3\right).$$

The purpose of this work is to extend the method of pseudodifferential equations to the electrodynamic screen problem.

PSEUDODIFFERENTIAL EQUATIONS FOR SCREEN PROBLEM

Taking into account (6) the equation (5) can be rewritten as the vector pseudodifferential equation on manifold Ω

$$Grad\Delta^{-1/2}(Divu) + k^2\Delta^{-1/2}u = f. \quad (7)$$

Note that the principal symbol of equation (7) is degenerated. In order to study the equation (7), the Sobolev space W is introduced in accordance with the asymptotic behaviour of the solution u near the edge $\partial\Omega$. Define the space of distributions W as the closure of $C_0^\infty(\Omega)$ in the norm

$$\|u\|_W^2 = \|u\|_{-1/2}^2 + \|Divu\|_{-1/2}^2.$$

One can show that

$$W = \left\{u \in \widetilde{H}^{-1/2}\left(\overline{\Omega}\right) : Divu \in \widetilde{H}^{-1/2}\left(\overline{\Omega}\right)\right\},$$

where the Sobolev space $\widetilde{H}^s\left(\overline{\Omega}\right)$ is denoted in the usual way. The space W has the following important property. Let W_1 and W_2 be subspaces of W such that

$$W_1 := \left\{u \in W; Divu = 0\right\}, W_2 := \left\{u \in W; Rotu = 0\right\},$$

where Div and Rot are the tangential divergence and rotor on Ω. The space W may be decomposed into the direct sum of the closed subspaces W_1 and W_2: $W = W_1 \oplus W_2$. By using the method of quadratic forms one can show that it is possible to consider L as a bounded operator $L : W \to W'$, where, W' denotes antidual space for

$$W : W' = \left\{u\big|_\Omega : u \in H^{-1/2}(M), Rotu \in H^{-1/2}(M)\right\},$$

where M is the closed surface such that $\overline{\Omega} \in M$.

Theorem 1. *For* $\mathrm{Im}k \geq 0$ *and* $k \neq 0$ *there are exactly one solution of the equation (8):*

$$L(k)u = f,\ u \in W,\ f \in W' \qquad (8)$$

Moreover, it is established the limiting absorption principle. Let $\mathrm{Im}k \geq 0$, $k \neq 0$. Then the bounded operator-function $L^{-1}(k): W' \to W$ exists and depends analytically with respect to k in the neighbourhood of every real point $k_0 \neq 0$. This implies

Theorem 2. *Let* $\mathrm{Im}k \geq 0$, $\mathrm{Im}k_0 > 0$, $k_0 \neq 0$ *and* $f(k) \xrightarrow{W'} f(k_0)$ *weakly as* $k \to k_0$. *Then* $u(k) \xrightarrow{W} u(k_0)$ *strongly as* $k \to k_0$, *where* $u(k)$ *and* $u(k_0)$ *solve the problems* $L(k)u(k) = f(k)$ *and* $L(k_0)u(k_0) = f(k_0)$.

THE BEHAVIOR OF THE FIELDS NEAR A CORNER

Consider a singular point $P \in \partial\Omega$, where $\partial\Omega$ consists of two arcs of two smooth curves intersecting transversally at the singular point. If $\alpha(P)$ is the interior angle of the tangent cone to Ω at $P \in \partial\Omega$, then $\alpha(P) = \pi$ if P is a regular point and $0 < \alpha(P) < 2\pi$, $\alpha(P) \neq \pi$ for singular points. Let $f \in C^{\infty}(\overline{\Omega})$. We apply the regularity theory for equation (2) to determine the values β of the critical exponent for singularities of the solution $|u| \leq Cr^{-\beta}$ near the corner point P, where r is the distance to the point P:

α/π	0.	0.0500	0.1161	0.1250
$\tau(\alpha)$	1.0000	0.8705	0.8350	0.8317

α/π	0.2500	0.3750	0.5000	0.6250
$\tau(\alpha)$	0.7820	0.7384	0.6956	0.6517

α/π	0.7500	0.8750	0.9000	0.9500
$\tau(\alpha)$	0.6057	0.5561	0.5456	0.5423

α/π	1.0000	1.1250	1.2500	1.3750
$\tau(\alpha)$	0.5022	0.4448	0.3799	0.3073

α/π	1.5000	1.6250	1.7500	1.8750	2.0000
$\tau(\alpha)$	0.2277	0.1444	0.0702	0.0281	0.

THE GALERKIN METHOD IN THE VECTOR 3D CASE

The expounded above theory lays a firm ground for work with the electric field integral equation $Lu = f$. Since L possesses the Fredholm property, for non-resonant wave number values we may assume that L is a continuously invertible operator. This is automatically fulfilled if all these screens are open.

Consider an n-dimensional space $V_n \subset W$ and let us approximate u by an element $u_n \in V_n$. The Galerkin method suggests that u_n is sought from the Galerkin equations

$$(Lu_n, v) = (f, v) \quad \forall v \in V_n. \qquad (9)$$

These equations define a finite dimensional operator $L_n: V_n \to V_n'$, where V_n' is antidual to V_n.

The principal difficulty with the electric field equation (8) consists in that L is no strongly elliptic. However, we are now able to propose some Galerkin schemes, which are guaranteed to converge.

Theorem 3. *Let the electric field integral equation (8) be such that the operator* L *is invertible, and assume that* n*-dimensional subspaces*

$$V_n^1 \subset W_1 \text{ and } V_n^2 \subset W_2$$

possess the approximation property in W_1 *and* W_2 *respectively. Then the Galerkin method on subspaces* $V_n \equiv V_n^1 + V_n^2$ *is guaranteed to converge.*

The scattering of the plane wave with $k = 1$ on the sphere of radius 1 is considered. The comparison of our method with the Rao-Wilton-Glisson one is given in the following table:

The Rao-Wilton-Glisson Method

The number of unknowns	72	162	288	450
The relative error	0.151	0.108	0.100	0.098

Our Method

The number of unknowns	144	324	576	
The relative error	0.100	0.048	0.028	

REFERENCES

1. Rao S. M., Wilton D. R. and Glisson A. W. (1982) Electromagnetic scattering by surfaces of arbitrary shape. *IEEE Trans. on Antennas and Propagat. AP-30, No. 3,* 409–418.
2. Ilyinsky A. S., Smirnov Yu. G. Electromagnetic wave diffraction by conducting screens. *VSP, Holland, Utrecht, 1998.*

FREQUENCY AND PULSE RESPONSES OF RESONANT OBJECTS BURIED IN A DIELECTRIC, DISPERSIVE HALF-SPACE

O. I. Sukharevsky, G. S. Zalevsky

Kharkov military university
maidan Svobody 6, Kharkov 310043, Ukraine

INTRODUCTION

The problem of numerical modeling of electromagnetic frequency and pulse responses from resonant perfectly conducting and dielectric objects, which are located in a dielectric lossy, dispersive half-space, are considered. An electrically short antenna is used for the object illumination. The magnetic dipole is utilized as the model of such antenna. The numerical modeling results for the perfectly conducting and dielectric ellipsoids, buried in the ground are demonstrated in the paper.

BASIC CALCULATING RELATIONS

The model applicable to the considered problem is shown in Fig. 1. The electromagnetic field source is the located inside free half-space V_1 ($\varepsilon_1 = 1$) magnetic dipole with vector-moment $\vec{p}^{a1}$. Inside a bottom lossy, dielectric half-space V_2 ($\varepsilon_2 = \varepsilon_2' + i\varepsilon_2''$), bordering on V_1 along the plane L, there is located object V_3 ($\varepsilon_3 = \varepsilon_3' + i\varepsilon_3''$) with the surface Σ. The problem consists in calculating of electromagnetic field scattered by the system "boundary L- object V_3" at arbitrary point of half-space V_1.

In [1], there were obtained integral equations for the equivalent current densities on the surface of the considered object V_3 and integral relations, which permit to calculate field scattered by the object at any point of half-space V_1.

For the case of perfectly conducting object ($\varepsilon_3'' \to \infty$), there has been obtained the Fredgolm integral equation of the second kind for the $\vec{J}^e$ - electric current densities on the object's surface:

$$\left\| \begin{matrix} \vec{p}_2^{\,0} \\ -\vec{p}_1^{\,0} \end{matrix} \right\| \cdot \left(\vec{J}^e(Q_0) - 2\vec{J}_d^e(Q_0) \right) =$$

$$= \frac{-2}{i\omega} \int_\Sigma \left\| \begin{matrix} \vec{E}_d^m(Q|Q_0, \vec{p}_1^{\,0}) \\ \vec{E}_d^m(Q|Q_0, \vec{p}_2^{\,0}) \end{matrix} \right\| \cdot \vec{J}^e(Q)\,ds, \; (Q_0 \in \Sigma), \quad (1)$$

where Q_0, Q are the observation and integration points, respectively, $\vec{J}_d^e$ are densities of electric currents induced by the same sources, that the $\vec{J}^e$, but in the object absence. The kernel of integral equation (1) is the electric field intensity $\vec{E}_d^m(Q|Q_0, \vec{p}^{\,0})$ of magnetic point source located at Q_0. This field takes into account the presence of boundary L. Mutually perpendicular unit vectors $\vec{p}_1^{\,0}, \vec{p}_2^{\,0}$, tangential to the surface Σ at the point Q_0, indicate the orientation of magnetic vector-moment of auxiliary point source.

For the dielectric object, there has been obtained the system of surface Fredgolm's integral equations of the second kind for the $\vec{J}^e, \vec{J}^m$ - equivalent electric and magnetic current densities, respectively:

$$\begin{cases} \left\| \begin{matrix} \vec{p}_2^{\,0} \\ -\vec{p}_1^{\,0} \end{matrix} \right\| \cdot \left(\vec{J}^m(Q_0)(\varepsilon_2 + \varepsilon_3) - 2\vec{J}_d^m(Q_0)\varepsilon_3 \right) = \\ = \frac{2}{i\omega} \int_\Sigma \left\{ \left\| \begin{matrix} \Delta\vec{H}_d^e(Q|Q_0, \vec{p}_1^{\,0}) \\ \Delta\vec{H}_d^e(Q|Q_0, \vec{p}_2^{\,0}) \end{matrix} \right\| \cdot \vec{J}^m(Q)\varepsilon_3 + \right. \\ \left. + \left\| \begin{matrix} \Delta\vec{D}_d^e(Q|Q_0, \vec{p}_1^{\,0}) \\ \Delta\vec{D}_d^e(Q|Q_0, \vec{p}_2^{\,0}) \end{matrix} \right\| \cdot \vec{J}^e(Q) \right\} ds, \\ \left\| \begin{matrix} \vec{p}_2^{\,0} \\ -\vec{p}_1^{\,0} \end{matrix} \right\| \cdot \left(\vec{J}^e(Q_0) - \vec{J}_d^e(Q_0) \right) = \\ = \frac{1}{i\omega} \int_\Sigma \left\{ \left\| \begin{matrix} \Delta\vec{H}_d^m(Q|Q_0, \vec{p}_1^{\,0}) \\ \Delta\vec{H}_d^m(Q|Q_0, \vec{p}_2^{\,0}) \end{matrix} \right\| \cdot \vec{J}^m(Q) + \right. \\ \left. + \left\| \begin{matrix} \Delta\vec{E}_d^m(Q|Q_0, \vec{p}_1^{\,0}) \\ \Delta\vec{E}_d^m(Q|Q_0, \vec{p}_2^{\,0}) \end{matrix} \right\| \cdot \vec{J}^e(Q) \right\} ds, \end{cases} \quad (2)$$

$$(Q_0 \in \Sigma).$$

The kernels of the system of the integral equation (2), are the differences of the fields of electric

$$\Delta\vec{H}_d^e = \vec{H}_{d2}^e - \frac{\varepsilon_2}{\varepsilon_3}\vec{H}_{d1}^e, \; \Delta\vec{D}_d^e = \vec{D}_{d2}^e - \vec{D}_{d1}^e$$

and magnetic

$$\Delta\vec{H}_d^m = \vec{H}_{d2}^m - \vec{H}_{d1}^m, \; \Delta\vec{E}_d^m = \vec{E}_{d2}^m - \vec{E}_{d1}^m$$

vector point sources, which take into account the influence of boundary L. Here $\vec{D}_{d\,1(2)}^e = \varepsilon_0\varepsilon_{2(3)}\vec{E}_d^e$. Indices 1, 2 indicate the different parameters of dielectric media.

After solving equations (1), (2), the electromagnetic field can be calculated at any points of half-space V_1 scattered by the object using formulae:

$$i\omega\vec{p}^{a1}\cdot\left(\vec{H}(Q_0)-\vec{H}_d^m(Q_0)\right)= =-\int_\Sigma \vec{E}_d^m(Q|Q_0,\vec{p}^{a1})\cdot\vec{J}^e(Q)ds\,,\ (Q_0\in V_1) \quad (3)$$

in the case of perfectly conducting object, and

$$-i\omega\vec{p}^{a1}\cdot\left(\vec{H}(Q_0)-\vec{H}_d^m(Q_0)\right)=\int_\Sigma\{\Delta\vec{H}_d^m(Q|Q_0,\vec{p}^{a1})\cdot\vec{J}^m(Q)+ +\Delta\vec{E}_d^m(Q|Q_0,\vec{p}^{a1})\cdot\vec{J}^e(Q)\}ds\,,\ (Q_0\in V_1) \quad (4)$$

in the case of dielectric object.

The developed numerical calculating algorithm, based on relations (1–4) permits to obtain frequency responses of the objects buried inside dielectric half-space. The pulse responses of considered objects can be calculated by applying of Fourier transform to the obtained frequency functions. Below, the numerical modeling results for a number of particularly cases are demonstrated.

CALCULATION RESULTS

In accordance with the proposed algorithm, the intensity of the magnetic field scattered by various objects located in the ground has been calculated. In this paper, frequency and pulse responses of perfectly conducting and dielectric ellipsoids are presented. The objects were illuminated by ultra-wideband signal with uniform discrete spectrum from 100 to 1000 MHz. Interval between the spectrum lines has been 50 MHz. For object illumination and scattered field receiving, there were used electrically short loop antennas A_1, A_2. Magnetic dipoles with vector-moments $\vec{p}^{a1}, \vec{p}^{a2}$ oriented along axis OX (see Fig. 1) were utilized as the model of used antennas. The dipoles height above the ground was h_a = 50 cm. Magnetic intensity of the incident upon the plane L electromagnetic wave, was 1 A/m. Objects were located at a depth h = 8 cm in the ground (gray loam with humidity 10%, density 1.2 g/cm^3). The plots of the magnitude $|H_x(f)|$ of the electromagnetic field scattered at receiving point are shown in Fig. 2, 3.

In Fig. 2a is shown frequency response of perfectly conducting ellipsoid and in Fig. 2b of dielectric (ε_3 = 2.2) ellipsoid with half-axes: a = b = 7.25 cm, c = 3.8 cm. Half-axes a, b, c are in parallel to X, Y, Z coordinate axes, respectively. Frequency dependencies incorporating responses from ellipsoids buried in the ground and reflection from boundary L are depicted by solid lines. Response induced by air-ground interface in the object absence is shown by dash line. Further, in Fig. 3 are shown frequency responses of perfectly conducting (Fig. 3a) and dielectric (Fig. 3b) buried ellipsoids which take not into account the component caused by the air-ground interface reflection.

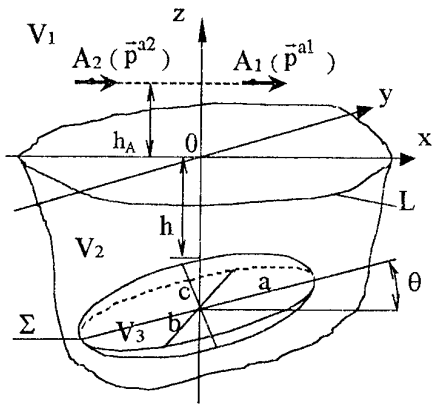
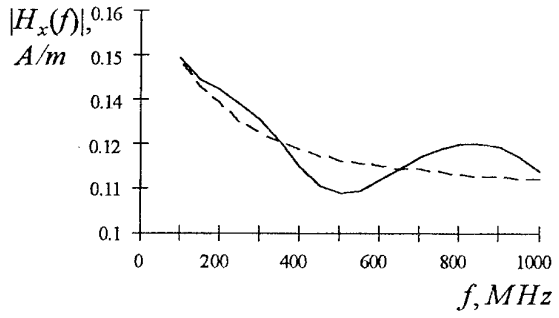
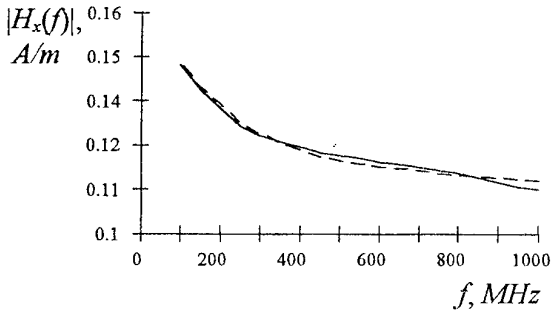


Fig. 1

In Fig. 3c are depicted frequency responses from dielectric ellipsoid with parameters corresponding to Fig. 3b, but for the case, when ellipsoid is rotated at angle θ = 10° in the plane XOZ (Fig. 1).



a



b

Fig. 2. x_{a1}=20 cm, x_{a2}= –30 cm, y_{a1}=y_{a2}=0, —— entire field, – – – field in the object absence

As seen in Fig. 3, the form of frequency responses weekly depends on relative position of antennas A_1, A_2 and object. Only amplitude of responses changes substantially. At 400–1000 MHz responses of perfectly conducting object have the steady state. The same de-

pendencies for the dielectric ellipsoid have the qualitatively distinction. For the case of $\theta = 10°$ the intensity of responses increases at frequencies 600–800 MHz and decreases in band of 900–1000 MHz. With approach the receiving point to object's center, the difference caused by ellipsoid orientation changing becomes less substantially.

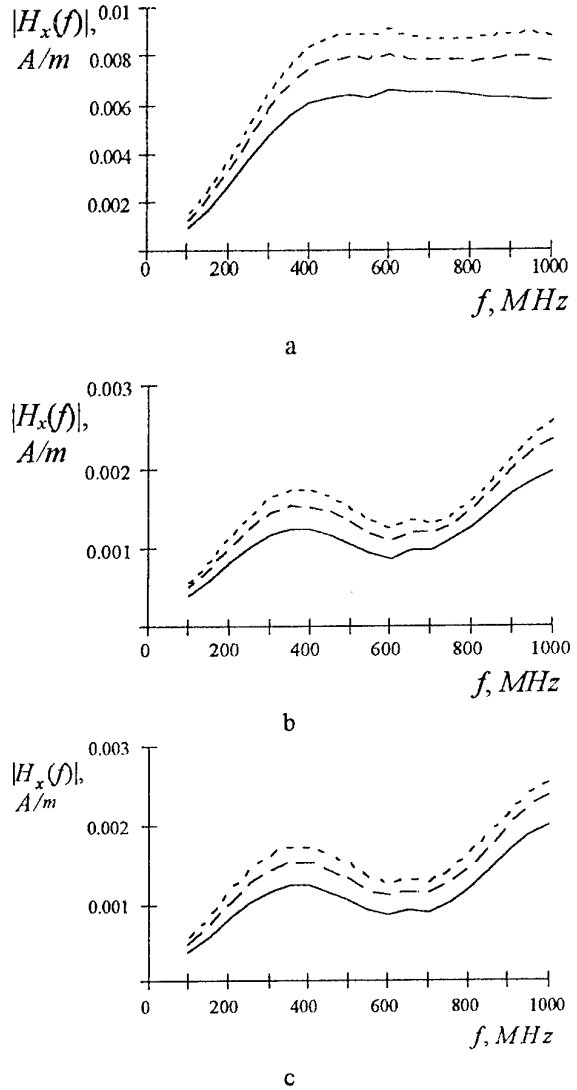


Fig. 3. $y_{a1}=y_{a2}=0$, —— $x_{a1}=0$, $x_{a2}=-50$ cm, – – – $x_{a1}=10$ cm, $x_{a2}=-40$ cm, - - - - $x_{a1}=20$ cm, $x_{a2}=-30$ cm

In Fig. 4a, 4b are depicted the pulse responses of perfectly conducting and dielectric ($\varepsilon_3 = 2.2$) ellipsoids, respectively. The time-domain responses were obtained with the inverse Fourier transform of considered below frequency functions (Fig. 3a, 3b). In Fig. 4 the pulse amplitude is shown in relative units.

Comparison of time-domain responses of buried objects and of objects in free space shows that the dispersive ground substantially changes the form of pulses. Maximum amplitude of pulses from buried objects decreases in ratio 5.7 and 5 for perfectly conducting and dielectric ellipsoids, respectively.

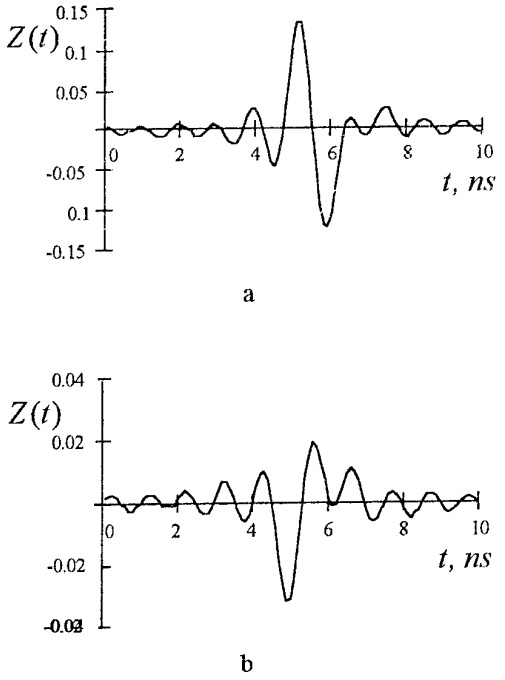


Fig. 4. $x_{a1} = 0$, $x_{a2} = -50$ cm, $y_{a1} = y_{a2} = 0$

Thus, the created algorithm, which based on the considered relations, enable to obtain space, frequency and pulse electromagnetic responses of objects of resonant dimensions, which are located inside a dielectric lossy, dispersive half-space. The shape of considered objects, their orientation, relatively to half-spaces interface, electric parameters ε,σ of objects material can be arbitrary.

The obtained algorithm can be applied for numerical modeling of the electromagnetic fields scattered from the group of buried objects.

REFERENCES

1. O. I. Sukharevsky, G. S. Zalevsky. Electromagnetic Waves Scattering by Resonant Objects Buried in a Dielectric Half-Space (In Russian)// Radiofizika i Radioastronomiya. 1998, vol. 3, No. 1, p. 37-42.

ANALYTICAL REPRESENTATION OF A SPECTRUM OF PERIODIC SOLUTIONS IN A MODEL OF MAJSNER–KRONIG–PENNEY IN RADIATING SYSTEM

J. M. Terent'ev

Dnipropetrovsk State University
Radiophysics department, Dnipropetrovsk State University,
Dnipropetrovsk-50, 320625, Ukraine, tel. 43–36–30

The wide application of a Majsner–Kronig–Penney (MKP) model is explained by analogy between distribution of waves in periodic structures, phenomenon of parametrical instability of oscillatory systems, electron properties in a crystal potential field, by a likeness of the differential equations and possibility to present solutions by elementary functions [1–5]. Characteristic features of the zonal theory, such as prohibited and permitted power bands, superficial condition have clear analogies for electromagnetic and sound waves in stratified–periodic medium and for parametric instabilities of a oscillatory system [5, 6].

In a model MKP system parameters are piece–continuous function, that is physical properties of each layer of a multilayer structure are fixed, whereas the sequence of layers is assumed to be periodic. It allows from elementary solutions, corresponding to separate layers, to construct a translation matrix connecting solutions at the beginning and at the end of one period of a mentioned sequence and, taking advantage of the Floquet theorem, to obtain the dispersing equation for waves (oscillations) in a system.

The implicit character of description obtained in a model MKP, not hindering numerical account of waves in concrete periodic systems, hampers the analysis of common properties of a spectrum, that is represented obvious by comparison to the well investigated properties of solutions used for a solution of the same physical problems of the equation the Mathieu [7, 8]. The closed representation for a spectrum in a MKP model is known only for the essentially simplified case of a comb of the Dirac [9].

In the present work the analytical representation of a spectrum of periodic solutions of a model Majsner-Kronig-Penney for a two-layer periodic structure is reduced to:

$$\ldots a\,b\,a\,b\,a\,b\,a\,b\ldots \tag{1}$$

containing layers a and b differed in physical parameters. The solution uses a symmetry of a system enabling to compare a matrixes of transformations obtained for period with a center, in the middle of the layer a and, accordingly, layer b.

The differential equation of a MKP model present as follows:

$$\frac{d^2}{dx^2}\Psi+(e-h_i)\Psi=0\,; \qquad i=1,2 \tag{2}$$

the index i accepts here is of two possible values 1 and 2, corresponding to reduced values of a potential in layers a and b. Introducing thicknesses of layers l_1 and l_2, and assuming satisfaction of conditions:

$$k_i^2=e-h_i\geq 0 \tag{3}$$

for a phase symmetrically located concerning a layer a period we shall obtain a matrix of transformations with the elements:

$$a_{11}=\cos\phi_1\cos\phi_2-\frac{1}{2}\left(\frac{k_1}{k_2}+\frac{k_2}{k_1}\right)\sin\varphi_1\sin\varphi_2 \tag{4}$$

$$a_{22}=\cos\phi_1\cos\phi_2-\frac{1}{2}\left(\frac{k_1}{k_2}+\frac{k_2}{k_1}\right)\sin\varphi_1\sin\varphi_2$$

on a principal diagonal. Conditions of existence of the periodic:

$$a_{11}=a_{22}=1 \tag{5}$$

and the antiperiodic:

$$a_{11}=a_{22}=-1 \tag{6}$$

solutions of the differential equation (2) taking into account unimodularity requires for such solutions of a vanishing even of one of the nondiagonal elements of a matrix of transformation:

$$a_{12}=\frac{1}{k_2}\left\{\sin\varphi_2\cos\varphi_1+\right.$$
$$\left.+\frac{\sin\varphi_1}{2}\left[\cos\varphi_2\left(\frac{k_1}{k_2}+\frac{k_2}{k_1}\right)-\left(\frac{k_1}{k_2}-\frac{k_2}{k_1}\right)\right]\right\} \tag{7}$$

and

$$a_{21}=-k_2\left\{\sin\varphi_2\cos\varphi_1+\right.$$
$$\left.+\frac{\sin\varphi_1}{2}\left[\cos\varphi_2\left(\frac{k_1}{k_2}+\frac{k_2}{k_1}\right)+\left(\frac{k_1}{k_2}-\frac{k_2}{k_1}\right)\right]\right\} \tag{8}$$

The eigenvectors have then for such matrices the form:

$$(0;1)^T \text{ and } (1;0)^T \tag{9}$$

This is accordance with solutions having on the boundaries of a phase zero and accordingly zero derivative. For a matrix of transformations constructed under condition of coincidence of a center of a phase with a middle of the layer b it is obtained:

$$b_{11}=b_{22}=a_{11}=a_{22} \tag{10}$$

that means coincidence of conditions of existence of periodic and antiperiodic solutions. For the nondiagonal elements of a matrix of transformations it is obtained:

$$b_{12}=\frac{1}{k_1}\left\{\sin\varphi_1\cos\varphi_2+\right.$$
$$\left.+\frac{\sin\varphi_2}{2}\left[\cos\varphi_1\left(\frac{k_1}{k_2}+\frac{k_2}{k_1}\right)+\left(\frac{k_1}{k_2}-\frac{k_2}{k_1}\right)\right]\right\} \tag{11}$$

and

$$b_{21}=-k_1\left\{\sin\varphi_1\cos\varphi_2+\right.$$
$$\left.+\frac{\sin\varphi_2}{2}\left[\cos\varphi_1\left(\frac{k_1}{k_2}+\frac{k_2}{k_1}\right)-\left(\frac{k_1}{k_2}-\frac{k_2}{k_1}\right)\right]\right\} \tag{12}$$

By rather simples angular transformation (6) we shall obtain analytical representation for two sequences of antiperiodic solutions:

$$\frac{k_1}{k_2}=\operatorname{tg}\frac{\varphi_1}{2}\cdot tg\ \frac{\varphi_2}{2} \tag{13}$$

and

$$\frac{k_1}{k_2}=\operatorname{ctg}\frac{\varphi_1}{2}\cdot ctg\ \frac{\varphi_2}{2} \tag{14}$$

From the equation (5) two series of solutions for periodic solutions of the differential equation (2) follow:

$$\frac{k_1}{k_2}=-\operatorname{ctg}\frac{\varphi_1}{2}\cdot\operatorname{tg}\frac{\varphi_2}{2} \tag{15}$$

and

$$\frac{k_1}{k_2}=-\operatorname{tg}\frac{\varphi_1}{2}\operatorname{ctg}\frac{\varphi_2}{2} \tag{16}$$

Each of transcendental equations (13–16) determines a gang of parameters at which the considered the differential equation has a periodic or antiperiodic solution. At fixed geometry of a periodic structure, using the analogy with theory of the equation Mathieu, is possible to state, that obtained equations determine eigenvalues e_j , $j=1,2...$; For analysis of the form of solutions we shall present nondiagonal elements of a matrix of transformations as:

$$a_{12}=\frac{1}{k_2}\cdot\left(\frac{k_1}{k_2}-\operatorname{ctg}\frac{\varphi_2}{2}\cdot\operatorname{ctg}\frac{\varphi_1}{2}\right)\times$$
$$\times\left(\frac{k_1}{k_2}+\operatorname{ctg}\frac{\varphi_2}{2}\operatorname{tg}\frac{\varphi_1}{2}\right) \tag{17}$$

and

$$a_{21}=-k_2\cdot\left(\frac{k_1}{k_2}-\operatorname{tg}\frac{\varphi_2}{2}\cdot\operatorname{tg}\frac{\varphi_1}{2}\right)\cdot$$
$$\left(\frac{k_1}{k_2}+\operatorname{ctg}\frac{\varphi_1}{2}\operatorname{tg}\frac{\varphi_2}{2}\right) \tag{18}$$

Like this we shall obtain:

$$b_{12}=\frac{1}{k_1}\cdot\left(\frac{k_1}{k_2}-\operatorname{tg}\frac{\varphi_2}{2}\cdot\operatorname{tg}\frac{\varphi_1}{2}\right)\times$$
$$\times\left(\frac{k_1}{k_2}+\operatorname{ctg}\frac{\varphi_2}{2}\operatorname{tg}\frac{\varphi_1}{2}\right) \tag{19}$$

and

$$b_{21}=-k_1\cdot\left(\frac{k_1}{k_2}-\operatorname{ctg}\frac{\varphi_2}{2}\cdot\operatorname{ctg}\frac{\varphi_1}{2}\right)\times$$
$$\times\left(\frac{k_1}{k_2}+\operatorname{ctg}\frac{\varphi_1}{2}\operatorname{tg}\frac{\varphi_2}{2}\right) \tag{20}$$

Refusing from restrictions (3) on a domain of e definition, we shall introduce:

$$\chi^2=h_1-e;\ \alpha=\chi\cdot l_1;$$
$$k^2=e-h_2;\ \varphi=k\cdot l_2; \tag{21}$$

Hence, the conditions of existence of an antiperiodic solution will be:

$$\frac{\chi}{k}=\operatorname{tg}\frac{\varphi}{2}\cdot\operatorname{th}\frac{\alpha}{2} \tag{22}$$

and

$$\frac{\chi}{k}=-\operatorname{ctg}\frac{\varphi}{2}\cdot\operatorname{cth}\frac{\alpha}{2} \tag{23}$$

whereas conditions, at which the periodic solution is realized have the form

$$\frac{\chi}{k}=-\operatorname{ctg}\frac{\varphi}{2}\cdot\operatorname{th}\frac{\alpha}{2} \tag{24}$$

and

$$\frac{\chi}{k}=\operatorname{tg}\frac{\varphi}{2}\cdot\operatorname{cth}\frac{\alpha}{2} \tag{25}$$

The conterminous diagonal elements of matrices of transformations $a_{11}=a_{22}=b_{11}=b_{22}$ pass into

$$\mathrm{ch}\alpha\cdot\cos\varphi+\frac{1}{2}\cdot\left(\frac{\chi}{k}-\frac{k}{\chi}\right)\cdot\mathrm{sh}\,\alpha\cdot\sin\varphi \qquad (26)$$

The nondiagonal elements of a matrix of transformations on a phase with a center in a layer *a*:

$$a_{12}=\frac{1}{k}\cdot\left\{\sin\varphi\ \mathrm{ch}\alpha+\right.$$
$$\left.+\frac{1}{2}\mathrm{sh}\alpha\left[\cos\varphi\left(\frac{k}{\chi}-\frac{\chi}{k}\right)+\frac{k}{\chi}+\frac{\chi}{k}\right]\right\} \qquad (27)$$

and

$$a_{21}=-k\cdot\left\{\sin\varphi\ \mathrm{ch}\alpha+\right.$$
$$\left.+\frac{1}{2}\mathrm{sh}\alpha\left[\cos\varphi\left(\frac{k}{\chi}-\frac{\chi}{k}\right)-\frac{k}{\chi}-\frac{\chi}{k}\right]\right\} \qquad (28)$$

Nondiagonal components of a matrix of transformations with a phase which center in a layer *b*:

$$b_{12}=\frac{1}{\chi}\cdot\left\{\cos\varphi\ \mathrm{sh}\alpha+\right.$$
$$\left.+\frac{1}{2}\sin\varphi\left[\mathrm{ch}\alpha\left(\frac{\chi}{k}-\frac{k}{\chi}\right)+\frac{k}{\chi}+\frac{\chi}{k}\right]\right\} \qquad (29)$$

and accordingly:

$$b_{21}=-\chi\cdot\left\{\cos\varphi\ \mathrm{sh}\alpha+\right.$$
$$\left.+\frac{1}{2}\sin\varphi\left[\mathrm{ch}\alpha\left(\frac{\chi}{k}-\frac{k}{\chi}\right)-\frac{k}{\chi}-\frac{\chi}{k}\right]\right\} \qquad (30)$$

As well as earlier, the nondiagonal elements of a matrix of transformation can be presented as permitting to set periodic solutions in the elementary aspect - with the help of unit vectors of the entry conditions in a center of a layer *b*:

$$a_{12}=\frac{1}{k}\cdot\left[\left(\frac{\chi}{k}+\mathrm{ctg}\frac{\varphi}{2}\cdot\mathrm{th}\frac{\alpha}{2}\right)\times\right.$$
$$\left.\times\left(\frac{\chi}{k}+\ \mathrm{ctg}\frac{\varphi}{2}\cdot\mathrm{cth}\frac{\alpha}{2}\right)\right] \qquad (31)$$

and

$$a_{21}=-k\cdot\left[\left(\frac{\chi}{k}-\mathrm{tg}\frac{\varphi}{2}\cdot\mathrm{th}\frac{\alpha}{2}\right)\times\right.$$
$$\left.\times\left(\frac{\chi}{k}-\mathrm{tg}\frac{\varphi}{2}\cdot\mathrm{cth}\frac{\alpha}{2}\right)\right] \qquad (32)$$

or in a center of a layer *a*:

$$b_{12}=\frac{1}{\chi}\cdot\left[\left(\frac{\chi}{k}+\mathrm{th}\frac{\alpha}{2}\cdot\mathrm{ctg}\frac{\varphi}{2}\right)\cdot\left(\frac{\chi}{k}-\mathrm{th}\frac{\alpha}{2}\cdot\mathrm{tg}\frac{\varphi}{2}\right)\right] \qquad (33)$$

and

$$b_{21}=-\chi\cdot\left[\left(\frac{\chi}{k}+\mathrm{cth}\frac{\alpha}{2}\cdot\mathrm{ctg}\frac{\varphi}{2}\right)\cdot\left(\frac{\chi}{k}-\mathrm{cth}\frac{\alpha}{2}\cdot\mathrm{tg}\frac{\varphi}{2}\right)\right] \qquad (34)$$

The obtained results by an equal image are applied for each of the mentioned above areas of use of the Majsner-Kronig-Penney model.

REFERENCES

1. Yakubovich V. A., Starzinskii G. M. Paranetric resonance in linear system.–Moscow. Nauka, 1987-328 p. [in Russian].
2. Shmidt G. Parametric oscelations.–Moscow. Mir, 1978-336 p. [in Russian].
3. Zaiman Dz. Principles of the theory rigid bould.–Moscow. Mir, 1974-472 p. [in Russian].
4. Yariv A., Yuh P. Optics of waves in cristal.-Moscow. Mir, 1987-616 p. [in Russian].
5. Chechulin S. L. Parametric oscillation and stability of periodic driving.- L.:LGU.1983-220 p. [in Russian].
6. Bass F. G., Bulgakov A. A., Teterov A. P., – High-frequency properties is semiconducting with Grating.-Moscow. Nauka, 1989-288 p. [in Russian].
7. Manual on special functions. // M. Abpamovich and И.Stigan. Moscow. Nauka.1979. 832 p. [in Russian].
8. Whittaker, Э.Т., Watson Дж. Н. a Rate of the modern analysis, V.2.-Moscow. Physmatgiz, 1964-516 p.
9. Ulianov V. V. Problems on a quantum mechanics and quantum statistics.– Kharkov. Vysshaya shkola 1979, 216 p.

RADIATION EFFICIENCY OF COUPLED VERTICAL DIPOLE ANTENNAS LOCATED ABOVE A LOSSY HALF-SPACE

P. L. Tokarsky

Kharkiv State Technical University of Radio Electronics
14, Lenin Av., Kharkiv, 310726, Ukraine
Phone: +380 572 409 430, Fax: +380 572 409 413, E-mail: shifrin@kture.kharkov.ua

INTRODUCTION

The study of properties of an antenna placed over a lossy half-space occupies an important place in the antenna theory. However, despite the long list of publications on the subject, the influence of the ground parameters on the antenna element interaction coupling and the antenna arrays efficiency have not been adequately investigated. In this paper, a rigorous impedance approach to analysis radiation efficiency of the coupled dipole antennas, placed near the air-ground interface, is developed.

THEORY

Consider an array made of two perfectly conducting symmetric dipoles located in a close proximity to the plane interface between two media (Fig. 1).

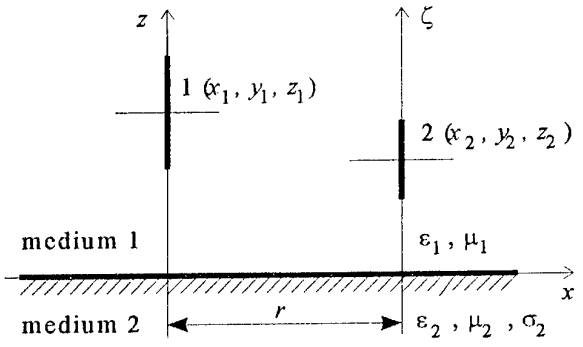


Fig. 1

The dipoles 1 of length $2l_1$ and 2 of length $2l_2$ are centered, respectively, at the points (x_1, y_1, z_1) and (x_2, y_2, z_2) of the Cartesian coordinate system. Both are vertically oriented with respect to the interface. The medium 1 (air), where the dipoles are placed, of permittivity ε_1, permeability μ_1 and conductivity $\sigma_1 = 0$ occupies the upper half-space $z > 0$. The medium 2 (earth) with electrical parameters $(\varepsilon_2, \mu_2, \sigma_2)$ occupies the lower half-space $z < 0$. While the dipoles are lossless, the presence of the lossy medium 2 allows us to consider this radiating structure as dissipative. Indeed, the dipole input power P_{in} is completely radiated and, hence can be represented as a sum $P_{in} = P_\Sigma + P_d$. Here P_Σ is the power radiated into the upper half-space, i.e. the useful power, and P_d is the power transmitted through the interface and dissipated in the ground, i.e. the lost power of the radiating structure [1]. The antenna array efficiency, $\eta = P_\Sigma / P_{in}$, can be found in the impedance approach that allows expressing all required powers through the input currents of dipoles [2], viz.

$$P_{in} = \sum_{m=1}^{N}\sum_{n=1}^{N} P_{mn} = \sum_{m=1}^{N}\sum_{n=1}^{N} I_{0m} R_{mn} I_{0n}^{*};$$

$$P_{\Sigma,d} = \sum_{m=1}^{N}\sum_{n=1}^{N} P_{\Sigma,dmn} = \sum_{m=1}^{N}\sum_{n=1}^{N} I_{0m} \Re_{\Sigma,dmn} I_{0n}^{*},$$

where $P_{\Sigma mn}$ is the mutual radiation power and P_{dmn} is the mutual lost power [3]; $R_{mn} = \mathrm{Re}\{Z_{mn}\} = \Re_{\Sigma mn} + \Re_{dmn}$; Z_{mn} is the self ($m = n$) or mutual ($m \neq n$) impedance between the m-th and n-th dipoles; $\Re_{\Sigma mn}$ is the mutual radiation resistance and $\Re_{dmn}$ is the mutual loss resistance; I_{0n} is the input current amplitude of the n-th dipole; N is the number of array elements. As was shown in [3], the resistances $\Re_{\Sigma mn}$ and $\Re_{dmn}$ are generally complex-valued quantities with $\Re_{\Sigma,dmn} = \Re_{\Sigma,dnm}^{*}$, $\mathrm{Im}\{\Re_{\Sigma mn}\} = -\mathrm{Im}\{\Re_{dmn}\}$. Let us present the mutual impedance as a sum $Z_{21} = Z_{21\infty} + \Delta Z_{21}$, where $Z_{21\infty}$ is the mutual impedance between the dipoles over a perfectly conducting ground; ΔZ_{21} is a correction term that takes into account the real parameters of the ground. Since the impedance $Z_{21\infty}$ is well known, we will determine only the correction term, ΔZ_{21}, using the induced EMF method [2]

$$\Delta Z_{21} = -\frac{1}{I_{01} I_{02}^{*}} \int_{z_2 - l_2}^{z_2 + l_2} \Delta E_{1z}(\zeta) I_{2z}^{*}(\zeta) d\zeta,$$

where $I_{2z}(\zeta)$ is the current distribution on the dipole 2; ΔE_{1z} is a some part of the electromagnetic field due to the dipole 1. Representation of the ΔE_{1z} as a spectrum of plane waves [4] yields

$$\Delta Z_{21} = -j \frac{Z_{c1}}{4\pi k_1} \int_0^{\infty} \mathrm{J}_0(\nu r) s_2^{*}(\nu) s_1(\nu) T_\varepsilon(\nu) \times$$

$$\times \exp\{-\gamma_1 (z_1 + z_2)\} \frac{\nu^3}{\gamma_1} d\nu,$$

where

$$T_\varepsilon(\nu)=2\gamma_2/(\gamma_2+\tilde{\varepsilon}_2\gamma_1/\varepsilon_1);\ k_{1,2}=\omega\sqrt{\tilde{\varepsilon}_{1,2}\mu_{1,2}};$$

$$\gamma_{1,2}=\sqrt{\nu^2-k_{1,2}^2};\ \tilde{\varepsilon}_{1,2}=\varepsilon_{1,2}\left(1-j\sigma_{1,2}/\omega\varepsilon_{1,2}\right);\ J_0(x)$$

is the zeroth-order Bessel function; $Z_{c1}=\sqrt{\mu_1/\varepsilon_1}$; the time dependent factor is $\exp(j\omega t)$; $r=\sqrt{(x_2-x_1)^2+(y_2-y_1)^2}$ is the distance between the dipole axes; $s_{zn}(\nu)=\frac{1}{I_{0n}}\int_{-l_n}^{l_n} I_{nz}(z)\exp(\gamma_1 z)dz$ is the Fourier transform of the current on n-th dipole. For a dipole with a sinusoidal current distribution, the Fourier transform is

$$s_{zn}(\nu)=2k_1\left(\operatorname{ch}\gamma_1 l_n-\cos k_1 l_n\right)/\left(\nu^2\sin k_1 l_n\right),$$

while for a Hertzian dipole of the same length, it is $s_{zn}(\nu)=2l_n$.

We determine now the mutual resistances $\Re_{\Sigma 21}$ and $\Re_{d21}$ by the Poynting's vector method as $\Re_{\Sigma,d21}=2P_{\Sigma,d21}/I_{01}I_{02}^*$, where the mutual powers are

$$P_{\Sigma,d21}=\frac{1}{4}\int_{S_{\Sigma,d}}\left\{\left[\vec{E}_1,\vec{H}_2^*\right]\vec{s}^0\right)+\left(\left[\vec{E}_2^*,\vec{H}_1\right]\vec{s}^0\right)\Big\}ds.$$

Here $\vec{E}_n,\vec{H}_n$ are the electromagnetic field due to the n-th dipole at the surfaces S_Σ or S_d; and $\vec{s}^0$ is the unit outward normal to the surface $S_{\Sigma,d}$. Let S_Σ be a hemisphere of radius $R\to\infty$ covering the upper half-space and S_d be the plane separating the two media ($z=0$). After inserting the spectral representation for the fields into the latter equation, we can finally obtain the desired expressions for the unknown resistances in the following form

$$\Re_{d21}=\frac{jZ_{c1}}{16\pi k_1\varepsilon_1}\int_0^\infty\left[\frac{\tilde{\varepsilon}_2}{\gamma_2}-\frac{\tilde{\varepsilon}_2^*}{\gamma_2^*}\right]J_0(\nu r)s_{z2}^*(\nu)\times$$

$$\times s_{z1}(\nu)|T_\varepsilon(\nu)|^2\exp\left\{-\gamma_1^* z_2-\gamma_1 z_1\right\}\nu^3 d\nu;$$

$$\Re_{\Sigma 21}=\frac{Z_{c1}k_1^2}{8\pi}\int_0^{\pi/2}J_0(\nu_0\rho)\Phi_1(\theta)\Phi_2^*(\theta)\sin\theta d\theta,$$

where

$$\Phi_n(\theta)=s_{zn}(k_1\sin\theta)\sin\theta\left[2\cos(k_1 z_n\cos\theta)-\right.$$
$$\left.-T_\varepsilon(k_1\sin\theta)\exp(-jk_1 z_n\cos\theta)\right];$$

(R,θ,φ) are spherical coordinates.

NUMERICAL RESULTS

Fig. 2 shows the efficiency of the array of the two collinear half-wave vertical dipoles with a sinusoidal current distribution ($|I_{01}/I_{02}|=1$) versus E-plane scan angle at 6 MHz. The dipoles 1 and 2 are centered at distances $\lambda/2$ and λ from the interface respectively.

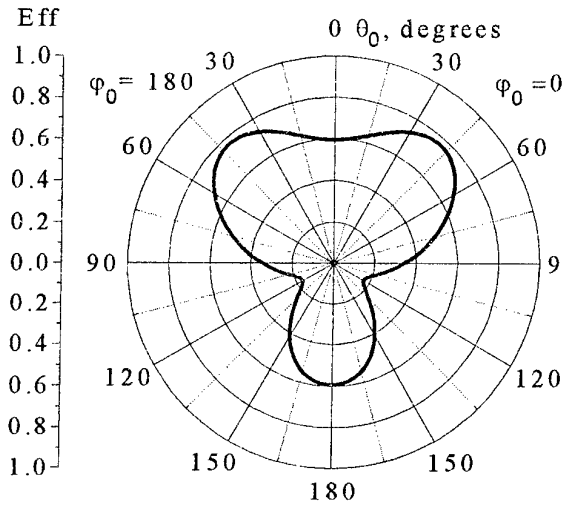


Fig. 2

The parameters of the ground are $\varepsilon_2/\varepsilon_1=10$, $\sigma_2=0.01(\Omega\cdot m)^{-1}$, $\mu_2/\mu_1=1$. As can be seen, the antenna efficiency ranges from 0.17 to 0.77 when the beam is scanned within the elevation plane. The efficiency of the in-phase excited array, whose beam is pointing along the interface, is about 0.34. The value can be increased more than twice by choosing the beam-pointing angle equal to $\theta_0\approx 45°$.

In addition, the results of computation in this way of the efficiency of the single Hertzian and half-wave dipoles is compared with the similar results in [1]. The agreement between the two data sets is excellent.

CONCLUSION

The approach proposed can be useful for development of various antenna structures over the earth, especially of antenna arrays for HF communication systems.

REFERENCES

1. P. M. Hansen, «The Radiation Efficiency of a Dipole Antenna Located Above an Imperfectly Conducting Ground», *IEEE Trans. on Antennas and Propagation*, vol. AP-20, no.11, pp.766-770, 1972.

2. D. M. Sazonov, «Microwave Circuits and Antennas», Mir Publishers Moscow, 1990.

3. P. L. Tokarsky, «Mutual Coupling in a System of Radiators with Joule Losses», *Radiotekhnika i Elektronika*, vol. 31, no. 9, pp.1717-1723, 1986. (In Russian). English translation: *Soviet Journal of Communications Technology and Electronics*, no. 3, pp. 9-14, 1987.

4. G. T. Markov, A. F. Chaplin, «Excitation of Electromagnetic Waves», Moscow: Energiya, 1967 [In Russian].

RADIATION OF WAVES BY THE FRACTAL SURFACE ELEMENT

E. I. Veliev, V. M. Onufrienko*

Institute of Radiophysics and Electronics, National Academy of Sciences
Ulitsa Proskury, 12, Kharkov, 310085, Ukraine
e-mail: veliev@dut.kharkov.ua
* Zaporizhzhya State Technical University,
Zhukovsky Str., 64, Zaporizhzhya ,330600, SP-39, Ukraine
(0612)644046, e-mail: onufr@zstu.zaporizhzhe.ua

INTRODUCTION

The principle of the Huygens in classical statement ("each point of a wavefront set starts to a radiant of a spherical wave, and the position of front is as a superposition of elementary spherical waves") is inexact. At addition of elementary waves there should be still front behind of primary, that it is necessary frequently artificially to ignore [1].

The statement of the problem about a radiation of the fractal surface element enables to estimate presence of front of a radiation behind of initial front.

FORMULATION

The electromagnetic field $\vec{E},\vec{H}$ is represented as superposition of two fields $\vec{E}_1,\vec{H}_1$ (from electrical radiant) and $\vec{E}_2,\vec{H}_2$ (from magnetic radiant)

$$\vec{E}=\vec{E}_1+\vec{E}_2,$$
$$\vec{H}=\vec{H}_1+\vec{H}_2.$$

The electrical and magnetic fields $\vec{E}_1,\vec{H}_1$ are determined through a vector potential $\vec{A}$:

$$\vec{A}=\frac{1}{4\pi}\int_V \mu\,\vec{j}^{\,e}(\vec{r}')G(\vec{r},\vec{r}')dV'; \qquad (1)$$

$$\vec{H}_1=\frac{1}{\mu}rot\vec{A},\quad \vec{E}_1=-\frac{i\omega}{k^2}(grad\,div\vec{A}+k^2\vec{A}). \qquad (2)$$

The fields $\vec{E}_2,\vec{H}_2$ are determined by the similar formulas in view of a duality principle.

The solution of the task as a fractal potential is formal can to arise, if in the formula (1) to consider: a) distribution of radiant on volume (surface, line) with a fractal structure; b) distribution of a fractal current in volume (on a surface, on a line); c) fractal distribution of electromagnetic parameters of a medium [2]. We mark that the generalization of this problem is possible after input in reviewing of a fractal Green function.

EQUIVALENT SOURCE. α - FEATURES

The surface-current density, which does not take volume, is determined as

$$\vec{j}=\lim_{\Delta l\to 0}\vec{n}_0\frac{\Delta I}{\Delta l}, \qquad (3)$$

($\vec{n}_0$ — unit vector indicating direction of driving of charges; Δl — element of an outline, which is intersected by a current ΔI). In case of an ideal continuous medium the limit-passage in (3) reduces in a usual derivative, and the integration restores a current I.

The unambiguity of a derivative (3) is absent for fractal ("thick") surface element $\Delta S=\Delta x\Delta y$.

The use of arc-coating L of a polygonal line with links Δl_i reduces in the degree law of increase of length of a polygonal line $L_{\Delta l_i}$ at a diminution of a link Δl_i (see [3]):

$$L_{\Delta l_i}=\frac{M_\nu}{\Delta l_i^{\nu-1}} \qquad (4)$$

(M_ν — the Hausdorff-measure with dimensionality ν, which depends on geometric properties of a fractal point set of a curve). Length of a polygonal line $L_{\Delta l_i}$ will be final in case, when the Hausdorff measure as $M_\nu=M\times(\Delta l)^\nu$, is determined on Δl_i ($M\to\infty$ - amount of links of coating with length Δl on Δl_i).

The limit process (4)

$$\lim_{\Delta l\to 0}\frac{M\times(\Delta l)^\nu}{\Delta l_i^{\nu-1}}$$

we consider as a fractional differential of an arc

$$d^\alpha l=(D^\alpha)l\,dl^\alpha=\frac{1}{\Gamma(2-\alpha)}\frac{dl^\alpha}{l^{\alpha-1}},$$

where $(D^\alpha)l$ — fractional differintegral (definition see, for example, in [4], [5]); $\Gamma(.)$ — gamma function of the Euler.

We consider, that $\Delta x<<\lambda, \Delta y<<\lambda$ (λ — wavelength), and the fractal element exhibits itself as the population is orthogonal oriented of electrical and magnetic emitters with the elements of currents on links with fractal properties:

$$d^\alpha I^e=(D^\alpha)j^e dy^\alpha=-(D^\alpha)H^s dy^\alpha,$$
$$d^\alpha I^m=(D^\alpha)j^m dx^\alpha=-(D^\alpha)E^s dx^\alpha.$$

The surface-current fractal density are connected with fields α - features [6] $(D^{\alpha})H^{s}, (D^{\alpha})E^{s}$

on the element ΔS

$$(D^{\alpha})\vec{j}^{e} = [\vec{z}_0, (D^{\alpha})H^{s}] = -\vec{x}_0(D^{\alpha})H^{s},$$
$$(D^{\alpha})\vec{j}^{m} = [(D^{\alpha})E^{s}, \vec{z}_0,] = -\vec{y}_0(D^{\alpha})E^{s},$$

and $(D^{\alpha})E^{s} = W(D^{\alpha})H^{s}$, where W — wave resistance.

CALCULATION OF A LONG-FIELD

Amplitudes of vectors α - features of a long-field $(D^{\alpha})\vec{E}^{\partial}, (D^{\alpha})\vec{H}^{\partial}$ $(r >> \lambda)$ (under conditions $r >> \Delta x$, $r >> \Delta y$, $G(r,r') \approx exp(-ikr)/r = G^{\partial}(r)$) is defined from (1) and (2):

$$(D^{\alpha})\vec{H}_1^{\partial} = \frac{ik}{4\pi}\int_{\Delta S^{\alpha}}[(D^{\alpha})\vec{j}^{e}(r'), \vec{r}_0^{\partial}]G(\vec{r},\vec{r}')dS^{\alpha'} \approx$$
$$\approx \frac{ik}{4\pi}[-\vec{x}_0(D^{\alpha})H^{s}, \vec{r}_0]G^{\partial}(r)\Delta S^{\alpha}.$$

In a spherical frame (r,θ,φ) is obtained

$$(D^{\alpha})H_1^{\partial} \approx \frac{ik}{4\pi}(D^{\alpha})H^{s}G^{\partial}(r)\Delta S^{\alpha}(\vec{\theta}_0 \sin\varphi + \vec{\varphi}_0 \cos\theta\cos\varphi).$$

Are similarly determined $(D^{\alpha})H_2^{\partial}$, $(D^{\alpha})E_1^{\partial}$ and $(D^{\alpha})E_2^{\partial}$.

In total, electromagnetic field $\vec{E},\vec{H}$ in long zone is restored for fractal ("thick") on θ surface element after application fractional calculation to

$$(D^{\alpha})\vec{E}^{\partial} = (D^{\alpha})(\vec{E}_1^{\partial} + \vec{E}_2^{\partial}), (D^{\alpha})\vec{H}^{\partial} = (D^{\alpha})(\vec{H}_1^{\partial} + \vec{H}_2^{\partial})$$

with

$$\vec{E}^{\partial} \approx R(\theta)(\vec{\theta}_0 \cos\varphi - \vec{\varphi}_0 \sin\varphi);$$
$$\vec{H}^{\partial} \approx \frac{1}{W}R(\theta)(\vec{\theta}_0 \sin\varphi + \vec{\varphi}_0 \cos\varphi), \qquad (6)$$

where

$$R(\theta) = \frac{ik}{4\pi}E^{s}\Delta S(\frac{\theta^{-\alpha}}{\Gamma(1-\alpha)} + \cos(\theta + \alpha\frac{\pi}{2})G^{\partial}(r).$$

Directivity pattern of fractal the Huygens element:

$$F_{\alpha}(\theta) = \frac{1}{2}(\frac{\theta^{-\alpha}}{\Gamma(1-\alpha)} + \cos(\theta + \alpha\frac{\pi}{2})). \qquad (7)$$

At $\alpha = 0$ the formula (6) and (7) give a classical outcome of a radiation of the smooth Huygens element.

In Fig. 1 the polar pattern $F_0(\theta)$ and $F_{\alpha}(\theta)$ $(\alpha = 0.1)$ accordingly classical and fractal Huygens elements represented.

In Fig. 2 the polar pattern $F_{\alpha}(\theta)$ and $F_{zw}(\theta, \varphi = 0)$ of generalized Huygens element are compared (is applied in the theory of antennas (see, for example, [1])) (ratio of a wave resistance to a surface impedance W equally 0.25).

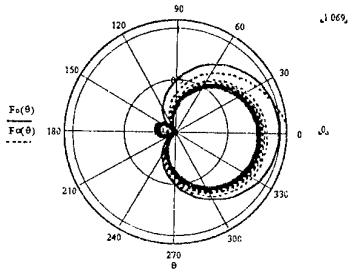


Fig. 1

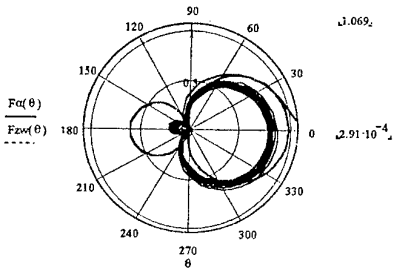


Fig. 2

CONCLUSION

The approach, represented in work, to calculation of fractal performances on a coordinate θ of the Huygens element can be generalized on case others (till r,φ) distributions of geometric singularities on a surface.

The practical interest in the theory of antennas represents a radiation of the generalized Huygens element in a fractal medium.

The analysis of a modification of radiation performance of the fractal element in a comparison with ideal element enables to define a degree of a surface fractality.

REFERENCES

1. V.V.Nikolsky. Electrodynamics and wave propagation, Moscow, Nauka, 1973 [in Russian].
2. Veliev E., Onufrienko V. Fractal Electrical and Magnetical Radiators //Symposium Proceedings MSMW-98, Kharkov, Ukraine, September 15-17, 1998,V.1, pp. 357-359.
3. Feder E. Fractals. Tnransl. From Engl., Moscow, Mir, 1991, 254 p. [in Russian].
4. Samko S.G., Kilbas A.A., Marichev O.I. Integrals and derivatives of fractional order and their application. Minsk: Nauka i tekhnika, 1987, 688 p. [in Russian].
5. Engheta N. On the Role of Fractional Calculus in Electromagnetic Theory// IEEE Antennas & Propagation Magazin. -Vol. 39. -No. 4, August 1997.- P.35-46.
6. Onufrienko V. On "α-features" of electrical waves above impedance plane//Conference Proceedings 12 International Conference on Microwaves & Radar. Krakov, Poland, May 20-22, 1998, Vol.1, P. 212-215.

USE OF AN AUXILIARY SOURCES METHOD FOR CALCULATION OF THE CHARACTERISTICS OF ANTENNAS PLACED ON IMPEDANCE ARBITRARY SHAPE BODIES

V. A. Voloshina, V. V. Shatskiy

Rostov Military Institute Missile Corps, Rostov-on-Don, 344027, Russia

The mathematical model, algorithm and radiation problem solution results of the cavity-backed low-directional antenna are described, its numerical research characteristics are discussed in the report.

The generalized model of the antenna is shown in Fig. 1.

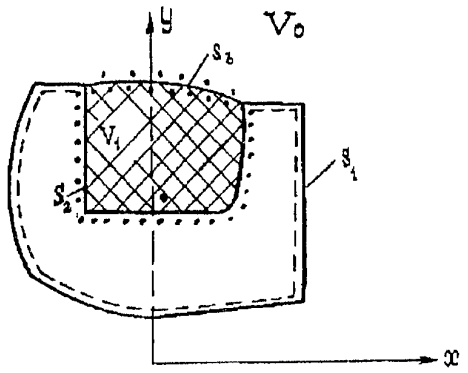


Fig. 1

The metallic constructive elements (including segments S_1 and S_2) of arbitrary configurations are assumed to be impedance or perfectly conducting. The dielectric elements occupy the volume V_1 with relative permittivity ε_1 and permeability μ_1, that is bounded by an surface of arbitrary configuration, including segments S_2 and S_3. The antenna is in the volume V_0 with permittivity ε_0 and permeability μ_0 or in the dielectric volume.

The electrical and magnetic antenna fields with longitudinal components in volume V_0 and V_1 satisfy the two-dimensional Helmholtz's equation and in volume V_0 they must satisfy the radiation conditions on infinity and the boundary conditions. These expressions have form [2]

$$du(x,y)/dn - i\alpha u(x,y) = 0 \qquad (1)$$

for surface segments S_1 and S_2,

$$u_i(x,y)|_{s_3} = u_j(x,y)|_{s_3}, \qquad (2a)$$

$$P_i du_i(x,y)/dn\,|_{s_3} = P_j du_j(x,y)/dn\,|_{s_3} \qquad (2b)$$

for surface segment S_3,

where $u = E_z, \alpha = kW/Z_0, P_i = \mu_i^{-1}, P_j = \mu_j^{-1}$

for E-polarization,

$$u = H_z, \alpha = kZ_0/W, P_i = \varepsilon_i^{-1}, P_j = \varepsilon_j^{-1}$$

for H-polarization, W is a metal impedance; Z_0 is the wave impedance of the free space.

The mathematical model of the radiation system is constructed with the use of an auxiliary sources method [1], according to which inside a body at a distance Δ from surfaces S_1, S_2, S_3 the auxiliary sources are entered as a filament of electrical or magnetic currents with unknown complex amplitudes A_n. The sources volume current density is represented as

$$j_{6cn} = i_z \sum_n A_n \delta(x - x_n)\delta(y - y_n). \qquad (3)$$

The numbers of the sources located close to surfaces S_1, S_2, S_3, equal N_1, N_2, $2N_3$ respectively (N_3 sources are placed in volume V_0 above dielectric segment S_3).

The T-electrical filament currents (for E-polarization) or T magnetic filament currents (for H-polarization) are considered as the field exciting sources. These currents with the known complex excitation amplitudes D_t are placed arbitrarily in volume V_1. The exciting current density is defined as

$$j_{cm} = i_z \sum_t D_t \delta(x - x_t)\delta(y - y_t) \qquad (4)$$

According to [1], we shall write down expressions for definition of electrical and magnetic fields strength in volume V_0 (observation point P (x_p, y_p) $\in V_0$) in the following form

for E-polarization:

$$u(x_p, y_p) = -i\mu_0\{\sum_{n_1} A^1_{n_1} G(k_0 p, k_0 q_{n_1}) + \sum_{n_3} A^3_{n_3} G(k_0 p, k_0 q_{n_3})\}, \qquad (5)$$

for H-polarization:

$$u(x_p, y_p) = -i\varepsilon_0\{\sum_{n_2} B^1_{n_2} G(k_0 p, k_0 q_{n_2}) + \sum_{n_3} B^3_{n_3} G(k_0 p, k_i q_{n_3})\}. \qquad (6)$$

In a similar manner the fields strength expressions can be written down for volume $V_1(P(x_p,y_p) \in V_1)$

$$u(x_p, y_p) = -i\mu_i\{\sum_{n_2} A^2_{n_2} G(k_0 p, k_0 q_{n_2}) + \sum_{n_3} A^3_{n_3} G(k_1 p, k_1 q_{n_3}) + \sum_t D_t G(k_1 p, k_1 q_t)\} \quad (7)$$

for E-polarization,

$$u(x_p, y_p) = -i\varepsilon_i\{\sum_{n_2} B^2_{n_2} G(k_1 p, k_1 q_{n_2}) + \sum_{n_3} B^3_{n_3} G(k_1 p, k_1 q_{n_3}) + \sum_t D_t G(k_1 p, k_1 q_t)\} \quad (8)$$

for H-polarization.

In expressions (5)–(8) $G(k_i p, k_i q_n) = H_0^{(2)}(k_i r_{pq})$ is the Green's function of the 2-D free space, that connects the coordinates of observation points (x_p, y_p) and coordinates of sources points (x_q, y_q) for medium with parameters ε_i, μ_i, $k_i = 2\pi(\varepsilon_i \mu_i)^{1/2}/\lambda$ is the wave number in the i-th volume, λ is the wave-length.

The auxiliary sources with unknown complex amplitudes can be found from the solution of linear algebraic equations system. This system is formed by imposing boundary conditions [1, 2] on surfaces S_1, S_2, S_3 on fields determined by dependencies (5) – (8).

It is necessary to emphasize, that the collocation points number on each of a contour segments should be equal to the appropriate auxiliary sources number. Thus, the total order of solved system is defined as $NS = N_1 + N_2 + 2N_3$, and the matrix of the equations system is square.

The radiation pattern is calculated by (5) or (6) when an observation point has moved off to infinity.

The calculating algorithm developed on the basis of the expressions (5)–(8) is realized as the universal program allowing to solve a wide range of tasks.

The computer program correctness was controlled by comparison of the obtained results with the known literature data [1, 3, 4].

So, transformation of the model considered above in an angled-reflector antenna, reflector of which has finite thickness, has allowed not only to obtain coincidence with good accuracy of results [4], but also to extend a research scope. In addition to latter results [4] of the angle-reflector antenna radiation pattern dependencies on the source angular position, on linear sizes of the reflector and its thickness, and also on the reflector surface impedance are investigated.

Curves, shown in Fig. 2, characterize the radiation pattern maximum dependence on the source allocation concerning coordinate axes. As one would expect, the calculation results shows that the asymmetrical source location leads to displacement of the radiation pattern maximum. The same effect can be achieved at various values of the reflector surfaces impedance. The angle-reflector antenna radiation pattern are shown in Fig. 3, at which the surface 1 has the impedance $Z = 533–533i$, the surface 2 is produced from a perfectly conducting metal (curve 1), and the curve 2 corresponds to a reverse case.

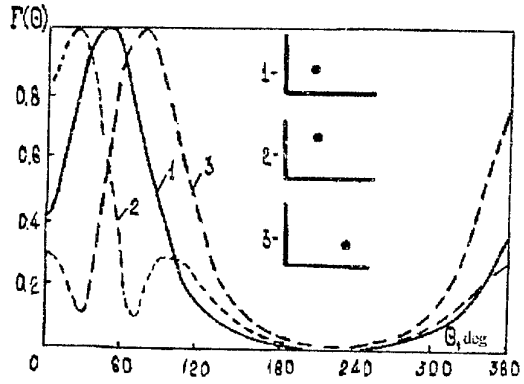


Fig. 2

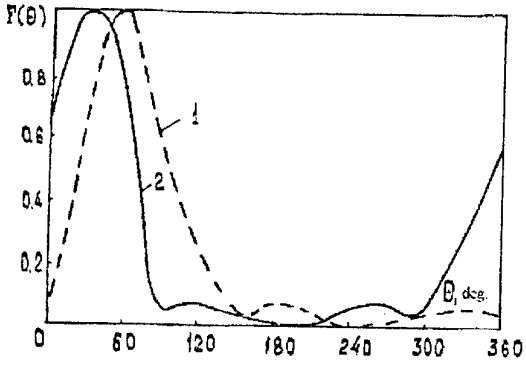


Fig. 3

Introduction of the third wall (model in Fig. 4) allows expanding possibilities to control both the radiation pattern width and its maximum position, what is illustrated with the dependencies curves given in Fig. 4.

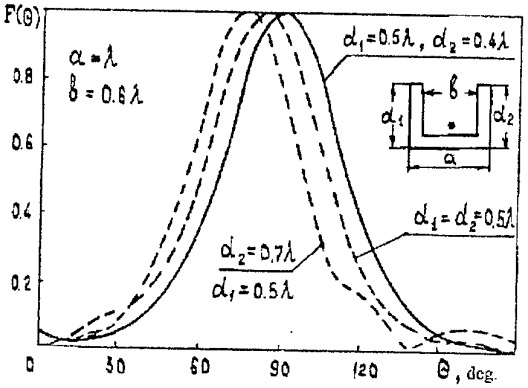


Fig. 4

The additional possibilities occur when the cavity-backed antenna is filled by a dielectric with relative

permittivity ε. For example, radiation patterns are shown in Fig. 5 for various values ε.

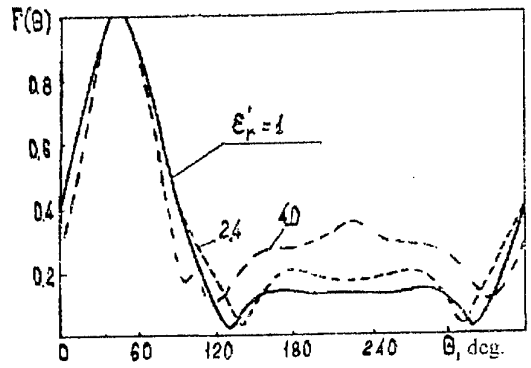


Fig. 5

For fixing dielectric in the resonator the fastening elements, usually metallic, are made. The radiation pattern behavior for various sizes of fixing metal ledges is shown in Fig. 6. If the width of the ledges $b' = b'' << \lambda$, then the radiation pattern is slightly narrowed and the outer side lobes grow, and for the symmetrical ledges, that cut down a surface of radiation, these changes become more noticeable with increase of the size b'.

Thus, the considered mathematical model of a radiation system implemented on a basis of the cavity-backed antenna allows to calculate the characteristics of the low-directional antennas of complex shapes. The given examples demonstrate radiation pattern variation possibilities of the considered antennas over a wide range.

The results of investigations are generalized on revolution bodies. As auxiliary sources rings of an electrical current with azimuth (along a ring) and meridian (in parallel tangent to body forming) direction of a current here are used. In a case of a metal-dielectric revolution body the system of the linear algebraic equations for definition of required complex amplitudes m-azimuth harmonic of auxiliary sources consists of twelve subsystems, four of which correspond to impedance segments on boundaries metal–free space and metal– dielectric.

The program is tested by the known solutions using an eigenfunctions method for metal and dielectric sphere excited by electrical dipoles, and for metal sphere with an annular slit antenna. The distinction of the calculating radiation pattern of two methods does not exceed unit of the fourth significant digit of the amplitude and 0.2 degree of a phase. Forming line body of revolution, that is approximated by segments of direct lines and arches of circles, can be arbitrary configuration.

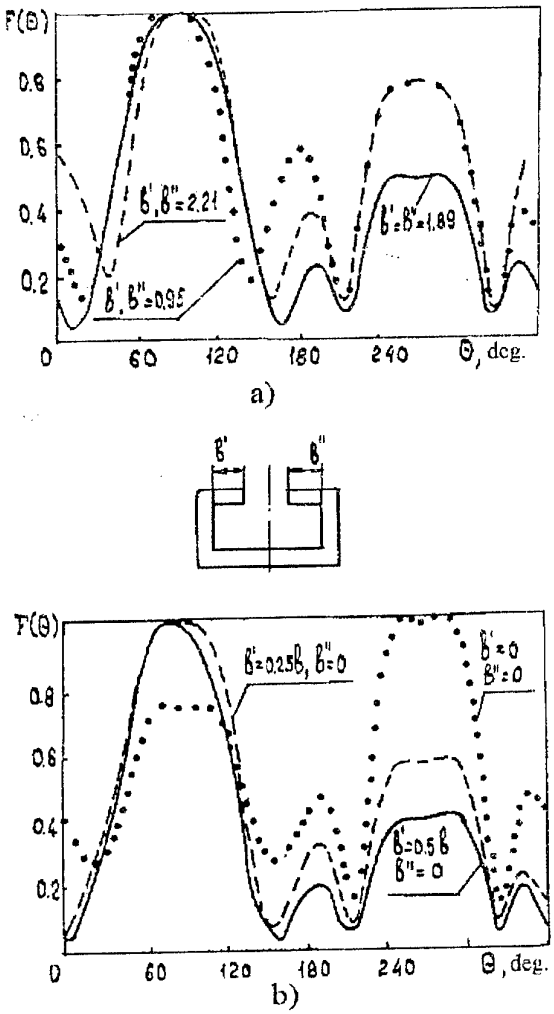


Fig. 6

REFERENCES

1. *Malakshinov N.P., Erikhov V.G.* "About one numerical method of the diffraction problems solution", in book: Antenny.- vyp.25, Moscow: Svyaz, 1977, p.53-65, [in Russian].
2. *Galishnikova G.D., Il'inskii A.S.* " The numerical methods in diffraction problems", Moscow: MGU, 1987. -208 p, [in Russian].
3. *Vasilyev E.N., Sedel'nikova Z.,V., Seregina A.R.* " Diffractions and excitation electromagnetic waves in dielectric and layered bodies of revolution" in book: sbornik nauchno-metodicheskikh statei po prikladnoi elektrodinamike. Moscow, Vysshaya shkola, vyp.6, 1983, p.15-84, [in Russian].
4. *Zakharov E.V., Pimenov Yu. V.* "About angle reflector influenceon the radiation pattern of a linear radiator", Radiofizika (Izv. Vyssh. Uchebn. Zavedenii), vol. XVIII, 1975, № 3, p. 418-424, [in Russian].

REFLECTIVE PROPERTIES OF ONE-DIMENSIONAL PBG DIELECTRIC STRUCTURES WITH DOUBLED QUASI-PERIODICITY OF PERMITTIVITY

I. Y. Vorgul, A. G. Nerukh*

Kharkov State University,
4 Svoboda Sq., Kharkov, 310077, Ukraine
* Kharkov Technical University of Radioclectronics,
14 Lenin Av., Kharkov, 310726, Ukraine

INTRODUCTION

In the last years research activities on Photonic Band-gap (PBG) structures as artificial periodic and quasi-periodic structures whose transmission properties exhibit frequency bands where the propagation of electromagnetic waves is forbidden [1], becomes one of the most actual direction in compact design of wireless communication systems. It is known also that such structures can display properties of bandpass filters by disruption of the periodicity [2]. The microstrip patch antenna is one of the most prefered structures for low cost and compact design. PBG technology is considered as a promising new solution to the problems of the antennas limitations for high frequencies such as narrow bandwidth, low gain and surface wave losses [3].

In spite of impressive progress in the new and emerging area of PBG engineering in recent years, their development by increasing complexity of the structures (as, for example, dual periodicity) toward the improved model is still actual. The criteria for such an optimization are the gap width and shape (preferably a rectangular-like one) as well as the structure dispersion and simplicity of their fabrication.

In this paper we propose a planar structure as a dielectric layer with double-quasi-periodical permittivity for using as a reflector or planar antenna substrate. An additional complexity of the structure allows to obtain high reflection for a wide band or sharp resonances on defined frequencies as well as a sufficient reflected field phase shift for some parameters combinations. A case of an abrupt temporal change of the permittivity in such structures is also considered showing an appearance of additional frequencies in the reflected field.

PROBLEM FORMULATION AND SOLUTION

The considered dielectric layer $0 \le x \le a$ has a permittivity mathematically determined by

$$\varepsilon(x)=\sum_{n=0}^{N}\left(\alpha-\left(\frac{1}{\beta}\right)^{n}\right)\left[\theta(x-an)-\theta(x-a(n+1))\right]+$$
$$+\sum_{m=0}^{M}\left(\gamma-\left(\frac{1}{\eta}\right)^{m}\right)\left[\theta(x-bm)-\theta(x-b(m+1))\right], \quad (1)$$

being essentially a superposition of two quasi-periodical structures with the composing layers widths equal to a and b, correspondingly, and slight deviation of the layers permittivity from the periodical ones (like that shown in Fig. 1, a).

The problem was solved based on integral equations for electromagnetic fields in non-stationary media [5]. There are some advantages in using this approach even for stationary structures because the method is based on Volterra integral equation which can be solved by iterations with improved convergence unlike Friedholm's and singular equations. So we can easily control the obtained results acccuracy. Initial point of the problems solutions are Volterra integral equations [5] which can be obtained from Maxwell equation for the electrical component of electromagnetic field obtained by Green's function of corresponding wave equation with all non-stationarities picked up at its right hand part. In the considered 1D case it has the following form

for the internal field ($x > 0$, $t > 0$)

$$E_{in}(t,x)=E_0(t,x)-\theta(vt-x)\int_{t-x/v}^{t}dt'j(t',x-v(t-t'))-$$
$$-\theta(x-vt)\int_{0}^{t}dt'\,j(t',x-v(t-t'))-\int_{0}^{t}dt'\,j(t',x+v(t-t')),$$

and for the external field ($x < 0$)

$$E_{ex}(t,x)=B(t,x)-\theta(vt+x)\int_{0}^{t+x/v}dt'\,j(t',v(t-t')+x) \quad (2)$$

where $j(t,x)=\dfrac{\partial}{\partial x}\left[\dfrac{\varepsilon_2(t,x)-\varepsilon_1}{\varepsilon_1}E_{in}(t,x)\right]$ for dielectric medium, θ is Heaviside step function and $v = c/\sqrt{\varepsilon}$.

Analytical iteration formula for the reflected field determined by the layer permittivity distribution was obtained. The iteration algorithm was realized as a computer program enabling one to investigate band-gap and filtering properties of the considered structures reflection for transient and stationary (as a long-time approximation for the transient one) cases.

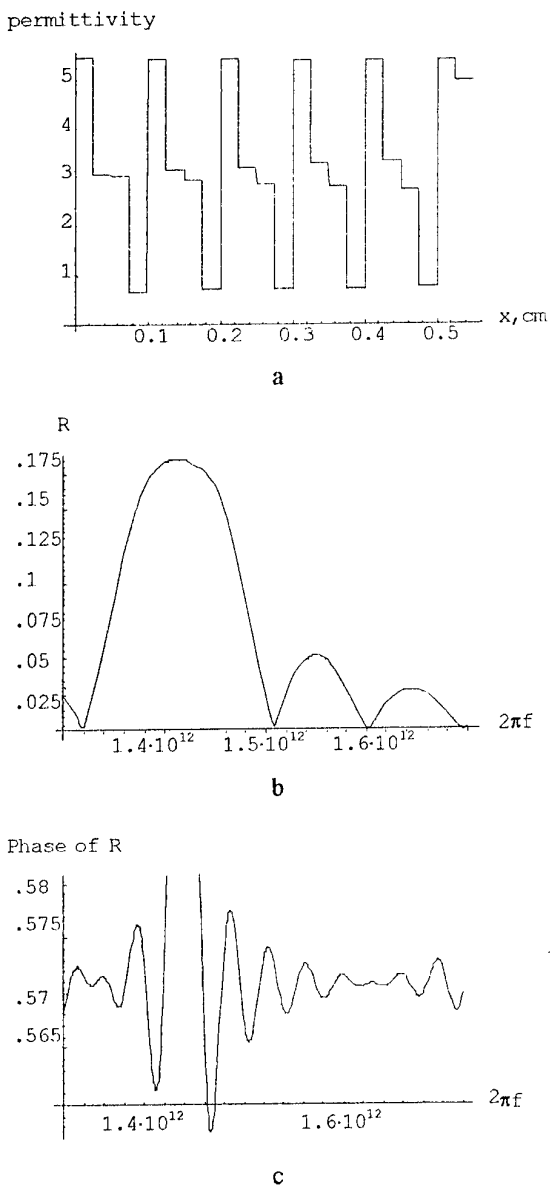


Fig. 1. Permittivity profile in the layer (a); reflection coefficient amplitude in dependence on the incident wave frequency (b); reflection coefficient phase, equal to π at its maximum (c)

CALCULATION RESULTS

Calculation for different layer parameters showed that for big deviation of the structure permittivity from one of the periodic structure the reflection coefficient oscillates slightly about the value, which is not appropriate neither for anti-reflection coating nor for a good reflector.

For small deviations of the structure from the periodical one it is possible to choose such structure parameters which provide good filtering and band-gap characteristics of it (see Fig. 1).

In a case when there is an abrupt change of the composing layers permittivity at zero time moment, the reflected field contains in addition to the stationary one a component of low frequency with time-reducing amplitude. The frequency value depends only on the composing layers width being almost independent on their permittivity values, which determines however this wave amplitude.

REFERENCES

1. E. Yablonovich, *J. Opt. Soc. Am. B*, N 10, 1993, pp.283-295.
2. H. J. De Los Santos, "On the design of photonic bandgap crystal filters", Proc.1998 URSI Symp, Atlanta, 1998, p.121.
3. Y. Qian, R.Coccioli, D.Sievenpiper, V.Radisic, E.Yablonovitch and T.Itoh. «A microstrip patch antenna using novel photonic band-gap structures». Microwave J., January 1999, p.66-76.
4. A. G. Nerukh, N.A.Khizhnyak, *Modern problems of transient macroscopic electrodynamics.* (in Russian) Test-Radio Publ., Kharkov, 1991.
5. I. Yu.Vorgul, A.G.Nerukh, "Inverse problems for media with transient conductivity", *Microwave and Optical Technology Letters,* v. 19, issue 3, 1998, pp. 148-150.

A MULTIBEAM IMPEDANCE ANTENNA SYNTHESIS

Yu. V. Yukhanov, A. Yu. Yukhanov

Taganrog State University of Radio Engineering
44 Nekrasovsky, GSP-17A, Taganrog, 347928 RUSSIA

Nowadays as multibeam antennas (MBA) hybrid antennas, spherical reflector antennas and antennas array are widely used. However, their sophisticated construction and considerable size imply some certain difficulties when used with moving vehicles. In the paper, a method of multibeam impedance reflector antenna (MBIA) synthesis is offered. It could be interesting that the reflector form can be arbitrarily conform: e.g. it can be plain, or it can be combined with the vehicle surface. This could open the possibility to construct the MBIA of a smaller size.

Let's consider the solution of a two-dimensional problem. Let in the unlimit isotropic space the infinitely long and along the homogeneous cylinder with partially differentiable surface S and the normal section contour ρ is located (Fig. 1). It is excited with the system of M longitudinal threads radiating the co-phase magnetic current with the radiation patterns (RP) $\Phi_m(\varphi)$.

It is necessary to find the distribution law of the impedance Z, such as to provide the antenna with the required multibeam RP. We shall see the impedance as purely a reactive one $Z = iX$, to avoid the undesirable losses.

The traditional approach to solve a synthesis problem was the way of minimising the gap between the required and realised antenna RP in the required angle sector with one on the linear programming methods. In our case it would be rather complicated because of the complex law of the impedance $Z = iX$ distribution.

The synthesis method we propose in the paper is, to put it briefly, as follows. It is known that the round cylinder with the radius a in the environs of its top with the aperture of $r = a\sqrt[4]{\lambda/a}$ is of the same focusing features as the parable with the focus distance $a/2$, if the radiator is located at the distance of $f = a/2$ from the top. Strictly speaking, phase abberations in that aperture do not exceed $\pi/2$, and thus we can consider it as a co-phase. So if we move the radiator along the arc of the circumference with the $a/2$ radius, or if we put the radiator array along the arc, we can maintain the beam swinging regime in the wide angle sector, and produce a multibeam RP as well.

To design the MBIA we shall require for its reflector S to possess the scattering possibilities identical to those of an ideally conductive round cylinder S_0 with a radius of a (Fig. 1).

As the aperture of a reflector antenna with a sharp RP is large in comparison with the emitting EMW, we shall use a method of physical optics to solve the problem. In this case the field dissipated with the impedance cylinder S in an arbitrarily chosen point p will be [1], [2]

$$H^s_{mz}(p) = \frac{2}{\pi}\int_S \frac{\cos\gamma_n \cos\gamma_0}{\cos\gamma_n + \cos\gamma_0}\frac{\cos\gamma - Z}{\cos\gamma_0 + Z} I_m \frac{e^{-ik(R_{nm}+R_{pq})}}{\sqrt{R_{nm}R_{pq}}} dS, \quad (1)$$

where γ_n, γ are angles constituted by the rays connecting the observation point and the source point, and the normal in the point of integrating (see Fig. 1); γ_0 - the reflection angle of the incident field in the current point of the impedance surface S.

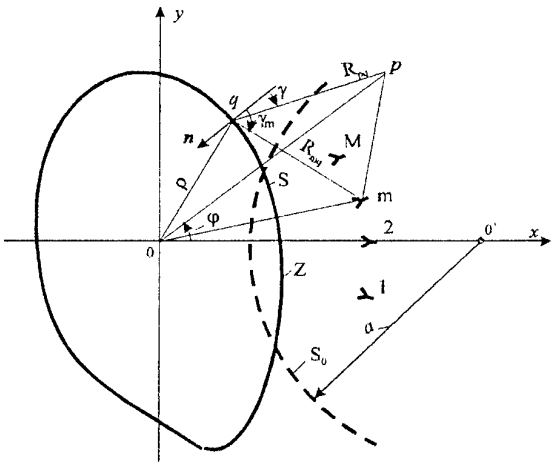


Fig.1

The surface impedance Z we shall find from the equivalence of the field reflected by the impedance reflector under synthesis excited with the given distribution of the radiators and that of the ideally conductive cylinder S_0, excited by the radiators distributed upon the arc of the circumference with the radius $a/2$ in the $0'$ point (on the S_0 cylinder axis).

For the observation point p co-located with the $0'$ point (Fig. 1) the ratios for the dissipation fields of the S and S_0 cylinders, consequently after (1), will be:

$$H^s_z(0) = \frac{2}{\pi}\int_S \frac{\cos\gamma_0 - Z}{\cos\gamma_0 + Z} U \frac{e^{-ik\rho}}{\sqrt{\rho}} dS, \quad (2)$$

$$H^{s}_{z0}(0') = \frac{2}{\pi}\int_{S_0} \cos\Gamma U_0 \frac{e^{-ika}}{\sqrt{a}} dS, \qquad (3)$$

where $U = \sum_{m=1}^{M} \frac{\cos\gamma_n \cos\gamma_0}{\cos\gamma_n + \cos\gamma_0} \Phi_m I_m \frac{e^{ikR_{nm}}}{\sqrt{R_{nm}}}$;

$$U_0 = \sum_{m=1}^{M} \Phi_m I_{0m} \frac{e^{ikR_{nm}}}{\sqrt{R_{nm}}}.$$

The $Z = iX$ impedance distribution law can be obtained explicitly from the subintegral sentences (2) and (3) equivalence, provided that the angular dimensions of the S and S_0 cylinders from $0'$ point are to be equal

$$X = \cos\gamma_0 tg\{0.5[u - u_0 + k(a-\rho)]\} \qquad (4)$$

where $u = \arg(U)$; $u_0 = \arg(U_0)$.

Thus we have find the required impedance distribution.

E.g. the MBIA with a plain reflector S with $2L$ width, irradiated with the radiators with the RP

$$\Phi_m = \cos^N(\varphi - \psi_m),$$

where ψ_m is the RP m-th beam direction, the radiators being located upon the direct line parallel to S at the distance of h.

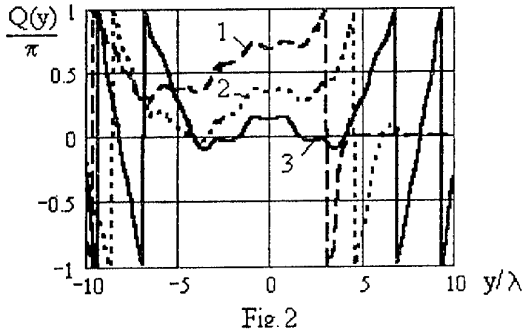


Fig. 2

Let's choose a cylindrical coordinate system in such a way as to provide the coincidence of z axis with the $0'$ axis of the S_0 cylinder under imitation. We put the S reflector at the distance of $2h$ from the $0'$ axis so that to provide the coincidence of the normal to its centre with x axis. We take the cylinder radius to be equal to $2h$. The corrugated structure, realizing the required impedance distribution law, permits for the antenna to display five beams within the angle sector of $\pm 20^0$, reflector size being $L = 10\lambda$, $h = 5\lambda$, $a = 10\lambda$ ($\lambda = 1$), $N=8$ and $I_m = I_0 = 1A/м$.

The distribution of the integrands (3) of Q_m phase for the rays -20^0 (curve 1), -10^0 (curve 2), and 0^0 (curve 3) are sketched in Fig. 2. One can see that the reflector surface phase for the each ray does not exceed the admissible deviation (0.5λ) along the considerably long intervals that are able to form the required RP.

The impedance reflector antenna m-th ray RP diagram can be calculated with the formulation:

$$F_m(\phi) = \frac{2}{\pi}\int_L \frac{\cos\gamma_{nm}\cos\gamma_0}{\cos\gamma_{nm} + \cos\gamma_0} \frac{\cos\gamma - Z}{\cos\gamma_0 + Z} * \qquad (5)$$
$$* I_m \Phi_m(y) H_0^{(2)}(kR_{nm}) e^{iky\sin\phi} dy,$$

At the Fig. 3 the RPs for all five beams of the antenna under synthesis are shown. The beams are corresponding to the radiators positions coordinated ($x=-5\lambda$, $y=\pm 1.89\lambda$) (curves *1,5*), ($x=-5\lambda$, $y=\pm 0.88\lambda$) (curve *2,4*) and ($x=-5\lambda$, $y=0$) (curve *3*).

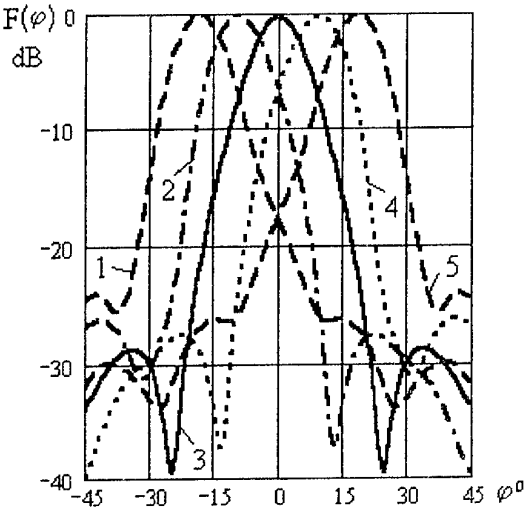


Fig. 3

As it can be seen, all the rays RP are practically identical, the differences in the amplification factors do not exceed *0.1 dB* the sidelobe level is 23-28 dB and can be regulated with the radiators RP form.

Thus, the theoretical investigations and numerical calculations verify the relevance of the proposed method of synthesis of MBIA with the impedance reflector of the arbitrary form. The calculation results obtained can be used either as the exemplary solution, or as the first approximation, bearing in mind the possible optimisation with the more strict methods of electrodynamics.

REFERENCES

1. *Yukhanov Yu.V.* Analysis and Synthesis of Impedance Plane//In 1998 International conference on Mathematical Methods in Electromagnetic Theory. MMET*98/Conference Proceedings. Kharkov, Ukraine, June 2-5, 1998. Vol.1.C. 118-120.

2. *Yukhanov Yu.V.* Synthesis of a Mirror Antenna with Impedanse Reflector// Proceedings of the 28 Moscow International Conference on Antenna Theory and Technology. Moscow, Russia, September 22-24, 1998. C. 384-387.

ABOUT ONE METHOD OF DETERMINATION OF CURRENTS IN THE ISOLATED ANTENNA

I. P. Zaikin, G. I. Koshevoy, D. I. Yaresko

State aerospace university named after N. E. Zhukovsky
17 Chkalov Street, Kharkov, Ukraine, 310070, tel. 8-0572-442-361

PROBLEM ACTUALITY

A success in the field of a miniaturization of modern radio electronics are so great, that the sizes of majority of devices have reached practically limited values. Unfortunately, this does not concern fully one of the major elements of radio engineering systems-antennas radiating or receiving of electromagnetic waves, the sizes of which depend on the frequency of oscillation and should exceed or be commensurable with a wavelength.

There are not less than ten ways of miniaturization of antennas.

The offered method of determination of currents in the antenna concerns to the most perspective way of miniaturization, namely to application of dielectrics and ferrite as envelopes (covers) of antenna.

STATEMENT OF THE PROBLEM

While determine currents on the cylindrical antenna of final length in an isolating envelope with a dielectric permeability ε more than one we'll proceed from an integral equation obtained in [1]:

$$\int_{-1}^{1}\varphi(t)R(x-t)dt = C\cos\kappa x - \frac{i}{2}\sin\kappa|x|, |x|<1; \quad (1)$$

Here we have $\varphi(t)$ as the required function, proportional to longitudinal component density of the surface current on the cylinder, the kernel integral equation being equal to the following:

$$R(u)=\frac{1}{\pi}\left[\oint_{C\kappa(\kappa,0)}+\int_{2\kappa}^{\infty}\right]\frac{\zeta_\varepsilon J_0(\alpha\zeta_1)}{\zeta_1{}^2K(w)}\cos wu\,dw, \quad (2)$$

$$\zeta_\varepsilon=\sqrt{\kappa^2\varepsilon-w^2},\ \zeta_1=\zeta_\varepsilon \text{ at } \varepsilon=1,\ \kappa=kh,\ \alpha=\frac{a}{h},$$

$$K(w)=\varepsilon J_0(\alpha\zeta_1)\frac{D_1(w)}{D_2(w)}-J_1(\alpha\zeta_1)\frac{\zeta_\varepsilon}{\zeta_1},$$

$$D_1(w)=\zeta_\varepsilon H_1^{(1)}(\beta\zeta_1)HJ_{01}(\zeta_\varepsilon)-\varepsilon\zeta_1 H_0^{(1)}(\beta\zeta_1)HJ_{11}(\zeta_\varepsilon),$$
$$D_2(w)=\zeta_\varepsilon H_1^{(1)}(\beta\zeta_1)HJ_{00}(\zeta_\varepsilon)-\varepsilon\zeta_1 H_0^{(1)}(\beta\zeta_1)HJ_{10}(\zeta_\varepsilon),$$

$$i\cdot HJ_{mk}(\zeta_\varepsilon)=H_m^{(1)}(\beta\zeta_\varepsilon)J_k(\alpha\zeta_\varepsilon)-J_m(\beta\zeta_\varepsilon)H_k^{(1)}(\alpha\zeta_\varepsilon), \quad (3)$$

$\beta=\frac{b}{h}$, a and b are radiuses of the cylindrical antenna and isolating envelope, correspondingly, $2h$ — length of the antenna (isolating envelope in the given mathematical model is infinite).

RESEARCH FROM THE KERNEL OF THE INTEGRAL EQUATION

The first integral in terms of the kernel represents a half of deduction of am intergrand function, which has a simple pole in a point $w=\kappa$, that is

$$\oint_{C\kappa(\kappa,0)}\frac{\zeta_\varepsilon J_0(\alpha\zeta_1)}{\zeta_1{}^2K(w)}\cos wu\,dw=\frac{-\pi i\sqrt{\varepsilon-1}B_{00}\cos\kappa u}{2\varepsilon B_{01}-\alpha\kappa\sqrt{\varepsilon-1}B_{00}}.$$

Here $B_{mk}=HJ_{mk}\left(\kappa\sqrt{\varepsilon-1}\right)$ are of real values, which can be easily proved by transition from Hankel's functions in expression (3) to cylindrical Bessel's and Neumann's functions.

The term in (2), representing an improper integral can be represented as two terms:

$$\int_{2\kappa}^{\infty}=\int_{2\kappa}^{\kappa\sqrt{\varepsilon}}+\int_{\kappa\sqrt{\varepsilon}}^{\infty}. \quad (4)$$

Numerically-analytical research of intergrand function $\frac{\zeta_\varepsilon J_0(\alpha\zeta_1)}{\zeta_1{}^2K(w)}$ in a range of modification w from 2κ up to $\kappa\sqrt{\varepsilon}$, for various ε, is shown in Fig. 1. It testifies that there are no problems with the first integral.

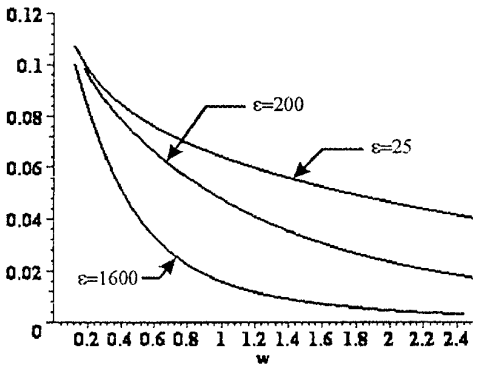


Fig. 1. Dependence of intergrand function on various ε

As analytical asymptotic research shows, the second integral, provides logarithmic singularities to the difference kernel of the equation (1) at coincidence of the arguments. It also confirms numerical calculationpresented in Fig. 2. It is necessary to point out here that the expression of intergrand function was expressed not through cylindrical functions but through the functions of purely imaginary argument:

$$I_n(w)=J_n(iw)/i^n,\ \mathrm{K}_n(w)=\frac{\pi i}{2}e^{in\frac{\pi}{2}}H_n^{(1)}(iw),$$

namely

$$\frac{\zeta_\varepsilon J_0(\alpha\zeta_1)}{\zeta_1{}^2K(w)}=\frac{\xi_\varepsilon I_0(\alpha\xi_1)}{\xi_1[\xi_\varepsilon I_1(\alpha\xi_1)-\varepsilon\xi_1 I_0(\alpha\xi_1)D(w)]}, \quad (5)$$

where $\xi_\varepsilon=\sqrt{w^2-\kappa^2\varepsilon}\ge 0, \xi_1=\xi_\varepsilon$ under $\varepsilon=1$,

$$D(w)=\frac{\xi_\varepsilon K_1(\beta\xi_1)KI_{01}(\xi_\varepsilon)-\varepsilon\xi_1K_0(\beta\xi_1)KI_{11}(\xi_\varepsilon)}{\xi_\varepsilon K_1(\beta\xi_1)KI_{00}(\xi_\varepsilon)-\varepsilon\xi_1K_0(\beta\xi_1)KI_{10}(\xi_\varepsilon)},$$

$$KI_{mk}(x)=K_m(\beta x)I_k(\alpha x)-(-1)^{m+k}I_m(\beta x)K_k(\alpha x).$$

Thus,

$$\frac{\zeta_\varepsilon J_0(\alpha\zeta_1)}{\zeta_1{}^2K(w)}\cos wu=\frac{1}{\varepsilon+1}\frac{\cos wu}{\sqrt{w^2-\kappa^2}}+$$

$$+\left[\frac{\xi_\varepsilon I_0(\alpha\xi_1)}{\xi_\varepsilon I_1(\alpha\xi_1)-\varepsilon\xi_1 I_0(\alpha\xi_1)D(w)}-\frac{1}{\varepsilon+1}\right]\frac{\cos wu}{\xi_1}. \quad (6)$$

Integral from the first term

$$\int_{\kappa\sqrt{\varepsilon}}^{\infty}\frac{\cos wu}{\sqrt{w^2-\kappa^2}}dw=\int_{\sqrt{\varepsilon}}^{\infty}\frac{\cos\kappa ux}{\sqrt{x^2-1}}dx= \quad (7)$$

$$=-\frac{\pi}{2}N_0(\kappa u)-\int_1^{\sqrt{\varepsilon}}\frac{\cos\kappa ux}{\sqrt{x^2-1}}dx,$$

where

$$N_0(\kappa u)=\frac{2}{\pi}\left[I_0(\kappa u)\ln\frac{\gamma\kappa u}{2}-\sum_{k=1}^{\infty}(-1)^k\frac{(\kappa u)^{2k}}{2^{2k}(k!)^2}\sum_{m=1}^{k}\frac{1}{m}\right].$$

The term in expression (6) for large w behaves not worse than $\frac{1}{w^2}$, thick ensures absolute convergence of an improper integral In Fig. 3 the character of behavior of the second term multiplied on w^2 under modification of value w for various thickness of a dielectric insulator of an antenna is shown.

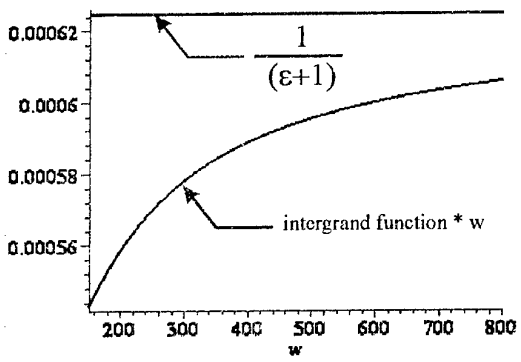


Fig. 2. Behaviour of intergrand function at large w

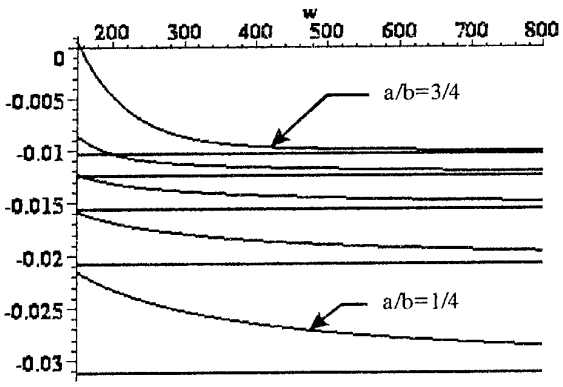


Fig. 3. A behaviour of the second term of the expression (6) for various values of interior and exterior diameters of an insulator of an antenna on large w

As it follows from the graphs, being also confirmed by the asymptotics, this termfor want of large w is proportional to $\frac{b}{a(\varepsilon+1)\cdot w^2}$.

So, the difference kernel of the equation (1) has a logarithmic singularity under coincidence of the arguments, therefore here the method of discrete singularities [2] can be successfully applied with suitable choice of quadrature knots $\tau_k=\cos\frac{\pi(2k-1)}{2n}, k=1..n$ and points of collocation $t_m=\cos\frac{\pi m}{n}, m=1..n-1$. Besides as it can be seen from the formulas (6) and (7), this singularity is selected as usual log, that allows to convert it, obtaining an integral equation of the second kind.

REFERENCES

1. Zaikin I.P., Zelenskiy A.A., Koshevoy G.I. "Investigation of currents in isolated antenna of finite length". Radiotechnika. 1988. V.90 [in Russian].

2. Gandel Yu. V. "Method of discrete singularities in electrodynamics problems". Voprosy kibernetiki. Moscow. USSR Acad, of Sciences Publ. 1986. Pp.166-183 [in Russian].

MODELING OF NON-COORDINATE ELECTROMAGNETIC PROBLEMS

Y. Zakharia

Radio Engineering Faculty, State University "Lvivska polytechnika",
12 S.Bandery Str. 290646, LVIV, UKRAINE
Phone: (380-322) 72-37-25

Estimation of excited or diffracted field by an element arranged in surrounded structure forms an electromagnetic problem. In the case, when the field tensions of an element could be written in the different coordinate system than the structure field tensions, the electromagnetic problem is considered as a non-coordinate problem. Direct transformation of one coordinate system into another often makes the analysis more difficult. Physical modeling of the element allows to write this field tensions in the structure-coordinate system.

For conducting elements field investigation some modeling principles by means of current filaments are proposed [3–5, 7]. Using these methods it is necessary additionally estimate the current filaments density, that gives the result independently from filament density. Simultaneously the singularity of the corresponding Green function must be avoided. In the analysis of the inner electromagnetic problems field radiated by filaments is expressed by means of infinite, slowly convergent series. The sum of such series always is found not exactly. Using moment method this error leads to ill-conditioned system of linear algebraic equations. Solution of such equations demands the iterative procedure. In general case the surface patch model is used [2, 6]. The surface of element is replaced by small flat triangle or rectangular conducting patches. It is difficult to find the appropriate basic functions for that model [6].

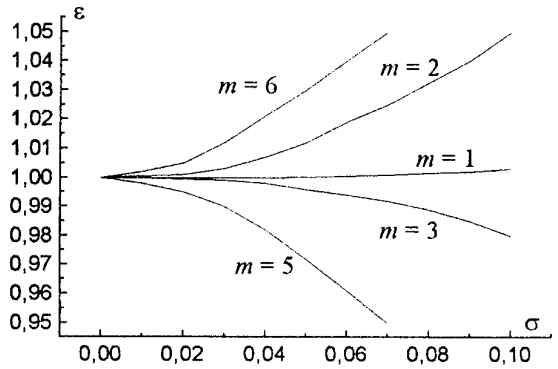


Fig. 1

An alternative principle of modeling is reviewed below using an example of diffraction on a cylindrical element. It is assumed, that the axis of element is parallel to one coordinate of rectangular system of general structure. The surface of conducting cylinder is replaced by narrow conducting strips. Quantity of strips is defined by perimeter of cylinder and width of the strip. Current density distribution on the strip width is accepted as uniform. However such strip remains as a non-coordinate. Two projections of non-coordinate strip on two coordinate of rectangular system that is orthogonal to the axis are formed. The idea of the proposed modeling follows from concept of tensor Green function [1]. It is confirmed below, that the field of two conducting orthogonal coordinate strips coincides with the field of sufficiently narrow non-coordinate strip. The advantages of the mentioned method are the next: 1) quantity of strips for any model is more less than number of necessary filaments in filament-model under the condition of the same accuracy of field tensions estimation (it is unnecessary to find the number of strips); 2) in the analysis the normal modes of the rectangular structure-coordinate system could be used (this allows differentiate the corresponding Fourier series); 3) Fourier series describing the field of narrow strip are fast convergent (that circumstance facilitates calculation of the sum of series and improves the accuracy of calculations); 4) usage of moment method permits to obtain well conditioned system of lower order equations.

Choice of strip-width (w) for an strip model is realized by comparison of the field tensions radiated from filament model of non-coordinate strip with the field tensions of equivalent orthogonal coordinate-strips. We consider the case, when the strip is placed between the broad walls of rectangular waveguide (A-width of the guide wall). The strip-width is arranged under the angle 45° to the transverse coordinate of the widther wall of waveguide. The dependence of ratio (ε) of the field tension of coordinate-strips model to the field of non-coordinate strip from non-coordinate strip width ($\sigma = w/A$) is showed on the Fig. 1. Number of current filaments for the non-coordinate -strip-model was chosen for any width W. It is evident, that the current density distribution in the filament model is non-uniform along the strip-width. As follows from figure, for sufficient narrow strip ($\sigma < 0.03$) amplitudes of electrical tensions are equal even for high order of normal modes (m). For greater σ the ratio ε deflects from unity. This deflection has different sign for odd and even normal modes and reduces the error of series sum calculation.

Implementation of considered above non-coordinate modeling is based on usage of boundary conditions on the surface of two orthogonal conducting coordinate-

strips. The resulting field is a sum of tensions radiated by both coordinate-strips. Singularity of Green function demands to accept a finite thickness of coordinate-strips. This method was used for analysis of exciting and diffraction on the non-coordinate wire-elements in waveguides, of thick waveguide obstacles, non-coordinate wide strip, etc.

REFERENCES

1. Collin Robert E. Field theory of guided waves. McGraw-Hill book comp., London, 1960. P. 591.
2. Glisson Allen W., Wilton Donald R. Simple and efficient numerical methods for problems of electromagnetic radiation and scattering from surfaces/IEEE Trans. on AP, vol.28, N 5, sept., 1980. Pp.
3. Jarem John M. A multifilament method-of-moments solution for the input impedance of a probe-excited semi-infinite waveguide/IEEE Trans. on MTT, vol. 35, N 1, Jan. 1987. Pp.14-19.
4. Leviatan Yehuda, Li Ping G., Adams Arlon T., Perini Jose. Single post inductive obstacle in rectangular waveguide/IEEE Trans. on MTT, vol.31, N 10, Oct. 1983. Pp. 806-812.
5. Leviatan Yehuda, Schaffer Gad S. Analysis of inductive dielectric posts in rectangular waveguide/IEEE Trans. on MTT, vol. 35, N 1, Jan. 1987. Pp. 48-59.
6. Rao Sadisava M., Wilton Donald R. Glisson Allen W. Electromagnetic scattering by surfaces of arbitrary shape/IEEE Trans. on AP, vol. 30, N 3, May 1982. Pp.
7. Model' A. M., Savitskiy A. Yu. Diffraction of H_{10} wave of a rectangular waveduide on an array of circular inductive rods. Radiotekhnika, No. 4, 1986. p. 13-18.

SCATTERING OF PLANE ELECTROMAGNETIC WAVE BY IMPEDANCE CIRCULAR CYLINDER

M. Yu. Zvezdina, A. S. Stepanov, V. V. Kharchenko, S. V. Chernov

Rostov Military Institute of Missile Corps, 344027 Rostov-on-Don, 27 Russia
E-mail: zvezd@jeo.ru

It is well known that the radio absorbing materials cover on the bodies for the changing their scattering characteristics. That causes some diffraction problems. One of them is the study of particularities of scattering plane electromagnetic wave in the case of oblique incident and Leontovich-Schukin boundary conditions on the cylindrical surface. This problem is not sufficient studied.

There are a lot of papers devoted to the problems of scattering of a plane electromagnetic wave by a circular impedance cylinder, but the results shown in these works do not expose regularities caused by a surface impedance on the circular cylinder and oblique incidence of the electromagnetic wave, for example [1–3].

The purpose of this report is the investigations of scattering regularities of scattering of oblique incident plane electromagnetic wave by infinite impedance circular cylinder.

Let the plane electromagnetic wave irradiates an infinite impedance circular cylinder with radius a; the direction of incoming is shown by angle θ, φ (Fig. 1). In the front of this wave the vector of electric or magnetic field strength has projection on the Oz axes. It might be written in quasi-3D approach as

$$\begin{Bmatrix} E_z^i \\ H_z^i \end{Bmatrix} = \begin{Bmatrix} E_0 \\ iE_0 W_0^{-1} \end{Bmatrix} \sin\theta \exp(-ikz\cos\theta). \qquad (1)$$

In this formula E_0 is the electric field amplitude; $W_0 = 120\pi$ Ohm is the free-space impedance; $k = 2\pi/\lambda$ is the wave number; λ is the wavelength; i is imaginary unit. The time dependence factor $\exp[-i\omega t]$ is omitted.

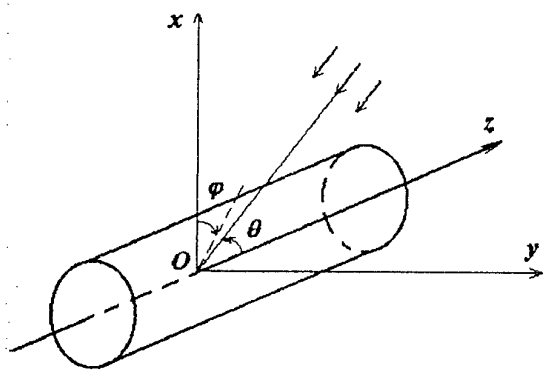


Fig. 1. Problem geometry

In general case there are longitudinal components of both electric field strength and magnetic one in scattering wave. We will study these components in the form [3, 4]

$$\begin{Bmatrix} E_z^s \\ H_z^s \end{Bmatrix} = \sum_{n=-\infty}^{\infty} \begin{Bmatrix} a_n \\ b_n W_0^{-1} \end{Bmatrix} C_n(\theta,\varphi), \qquad (2)$$

where

$$C_n(\theta,\varphi) = E_0 \exp(-ikz\cos\theta) \times \exp(-in\varphi) H_n^{(2)}(\tilde{k}r);$$

$\tilde{k} = k\sin\theta$; $H_n^{(2)}(\cdot)$ is Hankel function of the second kind of order n.

It is easy to notice that the functions E_z^s and H_z^s satisfy the Sommerfeld radiation conditions as well as Helmholtz equation [3,4].

Transversal components of electromagnetic field may be defined when using the expressions [3]

$$E_\varphi = \frac{1}{\tilde{k}^2}\left\{ ikW_0 \frac{\partial H_z}{\partial r} - \frac{k\cos\theta}{r}\frac{\partial E_z}{\partial \varphi} \right\}, \qquad (3)$$

$$E_r = -\frac{1}{\tilde{k}^2}\left\{ \frac{ikW_0}{r}\frac{\partial H_z}{\partial \varphi} + k\cos\theta \frac{\partial E_z}{\partial r} \right\},$$

$$H_\varphi = -\frac{1}{\tilde{k}^2}\left\{ \frac{k\cos\theta}{r}\frac{\partial H_z}{\partial \varphi} + \frac{ik}{W_0}\frac{\partial E_z}{\partial r} \right\},$$

$$H_r = -\frac{1}{\tilde{k}^2}\left\{ k\cos\theta \frac{\partial H_z}{\partial r} - \frac{ik}{W_0 r}\frac{\partial E_z}{\partial \varphi} \right\}.$$

The impedance boundary conditions [6]

$$\begin{cases} E_z = Z H_\varphi \\ E_\varphi = -Z H_z \end{cases} \qquad (4)$$

should be met on the surface of circular cylinder ($r = a$). In formula (4) Z is the surface impedance.

The solving of system (4) for electromagnetic field components, described by formulas (1)-(3), enables to write the following equations for coefficients a_n and b_n in quasi-3D approach

$$a_n = \frac{i^n\left\{ J_n(\tilde{k}a) + \frac{iZ_N}{\sin\theta} J_n'(\tilde{k}a) D1_n^e(\tilde{k}a) \right\}}{H_n^{(2)}(\tilde{k}a) + \frac{iZ_N}{\sin\theta} H_n^{(2)'}(\tilde{k}a) D2_n^e(\tilde{k}a)}, \qquad (5)$$

$$b_n = -\frac{nW_0 \cos\theta}{\tilde{k}a} \frac{i^n J_n(\tilde{k}a) - a_n H_n^{(2)}(\tilde{k}a)}{H_n^{(2)'}(\tilde{k}a) - iZ_N \sin\theta H_n^{(2)}(\tilde{k}a)}$$

for the wave with E-polarization and

$$a_n = Z\frac{n\cos\theta}{\tilde{k}a\sin\theta} \frac{i^n J_n(\tilde{k}a) - b_n H_n^{(2)}(\tilde{k}a)}{H_n^{(2)}(\tilde{k}a) + \frac{iZ_N}{\sin\theta} H_n^{(2)'}(\tilde{k}a)}, \quad (6)$$

$$b_n = \frac{i^n \left\{ J_n'(\tilde{k}a) - iZ_N \sin\theta J_n(\tilde{k}a) D1_n^h(\tilde{k}a) \right\}}{H_n^{(2)'}(\tilde{k}a) - iZ_N \sin\theta H_n^{(2)}(\tilde{k}a) D2_n^h(\tilde{k}a)}$$

for the wave with H-polarization.

In formulas (5) and (6) $Z_N = Z/W_0$ is the surface impedance, normalized by the free-space one; $J_n(\cdot)$, $J_n'(\cdot)$ are the Bessel function of order n and its derivation; $H_n^{(2)}{}'(\cdot)$ is the derivation of Hankel function of the second kind of order n;

$$D1_n^e(\tilde{k}a) = 1 + K_n^e(\tilde{k}a)\frac{J_n(\tilde{k}a)}{J_n'(\tilde{k}a)},$$

$$D2_n^e(\tilde{k}a) = 1 + K_n^e(\tilde{k}a)\frac{H_n^{(2)}(\tilde{k}a)}{H_n^{(2)'}(\tilde{k}a)},$$

$$D1_n^h(\tilde{k}a) = 1 - K_n^h(\tilde{k}a),$$

$$D2_n^h(\tilde{k}a) = 1 - K_n^h(\tilde{k}a),$$

$$K_n^e(\tilde{k}a) = \left(\frac{n\cos\theta}{\tilde{k}a}\right)^2 \left[\frac{H_n^{(2)'}(\tilde{k}a)}{H_n^{(2)}(\tilde{k}a)} - iZ_N \sin\theta\right]^{-1},$$

$$K_n^h(\tilde{k}a) = \left(\frac{n\cos\theta}{\tilde{k}a}\right)^2 \left[\sin\theta + iZ_N \frac{H_n^{(2)'}(\tilde{k}a)}{H_n^2(\tilde{k}a)}\right]^{-1}.$$

It is not hard to notice that the formulas (5), (6) can be transformed to well known regularities for particular causes of perfectly conducting cylinder surface ($Z_N = 0$) or wave incidence in the transversal plane ($\theta = \pi/2$).

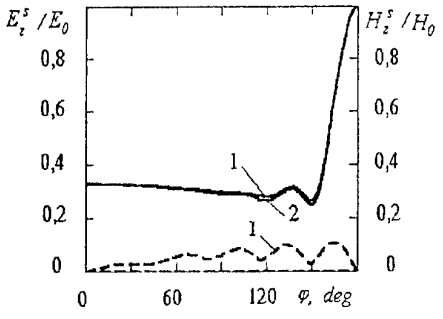


Fig. 2. The conic section of volumetric scattering pattern E_z^s – and H_z^s – field components for case of exciting circular cylinder by electromagnetic wave with E-polarization ($\theta = 60°$)

The formulas (5), (6) confirm the well-known aspect that the azimuth regularities of scattering pattern of oblique incident wave for perfectly conducting circular cylinder might be obtained according to the following algorithm [3,4]: correction of cylinder radius by coefficient $\sin\theta$; calculation of scattering pattern are realized in transversal plane. But this algorithm become incorrect for the case of impedance surface, because coefficients in numerators and in denominators in expressions for a_n and b_n are the functions both surface impedance and angle θ for waves with E- and H-polarization. The appearance of cross polarization component is in principle as well.

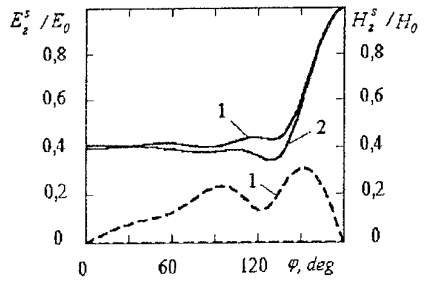


Fig. 3. The conic section of volumetric scattering pattern E_z^s – and H_z^s – field components for case of exciting circular cylinder by electromagnetic wave with E-polarization ($\theta = 30°$)

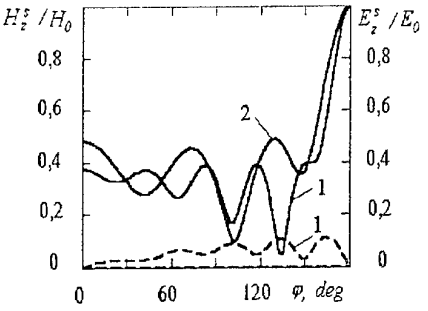


Fig. 4. The conic section of volumetric scattering pattern E_z^s – and H_z^s – field components for case of exciting circular cylinder by electromagnetic wave with H-polarization ($\theta = 60°$)

Figures 2–5 corroborates of the report aspects. These figures show the results of scattering pattern studies by different methods for cylinder with radius $a = 2\lambda$ and surface impedance $Z_N = 0.3i$. The value of surface impedance has been taken from [7]. The solid curves display the conic sections of the volumetric scattering pattern of main component obtained according to quasi-3D approach (curves 1) and to the 2D algorithm (curves 2). The dash curves display conic sections of the volumetric scattering of cross component. Figures 2 and 3 show the conic sections with the angles $180°-\theta$ of the volumetric scattering pattern of plane E-

polarization wave incoming from direction $\theta = 60°$ and $\theta = 30°$ respectively. Figures 4 and 5 show similar functions for case of wave with *H*-polarization.

The comparison of curves 1 and 2 in Fig. 2 and 3 shows that difference between quasi-3D approach results and 2D-algorithm results is insignificant for main component for case of the wave with *E*-polarization This difference is considerable for the case of the wave with *H*-polarization. The latter is confirmed comparison of curves 1 and 2 in Fig. 4 and 5. As it should be expected the pattern difference increases with the angle θ decreases.

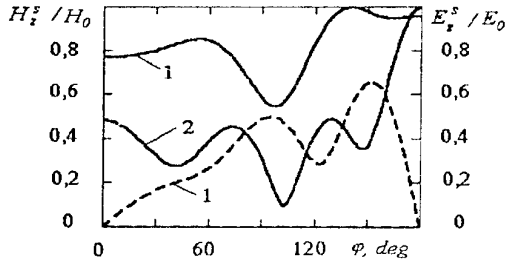


Fig. 5. The conic section of volumetric scattering pattern E_z^s – and H_z^s – field components for case of exciting circular cylinder by electromagnetic wave with *H*-polarization ($\theta = 30°$)

Thus, these the obtained expressions permit to define the main regularities caused by the oblique incident plane electromagnetic wave scattering and to investigate the scattering pattern for various value of cylinder radius, the surface impedance and the wave incident angle.

REFERENCES

1. *Graglia, R.D., Uslenghi, P.L.E., Vitiello, R., and D'Elia, U.* "Electromagnetic scattering for oblique incidence of impedance bodies of revolution", IEEE Trans. Antennas and Propag., V.43, pp.11-26, January 1995.
2. *Syed, Hasnain H., Volakis, J.L.* "High-frequency scattering by a solution a smooth coated simulated with generalized impedance boundary conditions", Radio Sci., V.26, pp.1305-1314, May 1991.
3. *Wait, J.R.*, Electromagnetic Radiation from Cylindrical Structures, Oxford: Pergamon, 1959.
4. *Zakhar'ev, L.N., Lemanskii, A.A., and Shcheglov, K.S.* Theory of Surface Antennas. Moscow: Sovietskoe Radio, 1969.
5. *Markov, G.T. and Chaplin, A.F.* Excitation of Electromagnetic Waves. Moscow-Leningrad: Energia, 1967.
6. *Vaganov, R.B., Katsenelenbaum, B.Z* Foundations of Diffraction Theory. Moscow: Nauka, 1982.
7. *Baranchugov, E.A., Zatsepin, P.M. and Komarov, S.A.* Quasi-three-dimension Problem of Diffraction of a Planar Electromagnetic Wave by Impedance Strip, Radiotekhnika i elektronika, V.43, pp.1291-1295, November 1998.

UNIFORM ASYMPTOTIC THEORY OF ELECTROMAGNETIC DIFFRACTION BY WAVEGUIDE APERTURE

A. A. Zvyagintsev, T. N. Demchenko, S. P. Phomushkin

Kharkov state university,
Kharkov, Liberty square 4. (057"2"-457319)

In this work the diffraction problem of an electromagnetic field by the plane-parallel waveguide aperture is solved by the uniform asymptotic theory of diffraction (UAT). The problem is reduced to the solution of the model problem – diffraction between two perfectly conducting half-planes. The solution found is valid both at the distance and near the shadow boundaries of the incident and reflected fields. In the distance it turns into the solution of the geometrical theory of diffraction (GTD). However it is not determined close to edges and other caustics.

The geometrical theory of diffraction is an effective method of the analysis and calculation of distribution, radiation and scattering wave fields. Its field of application is rather wide: engineering of antennas and tracts of ultrahigh frequencies, millimeter and infra-red ranges, and also the problem of distribution and scattering of waves in inhomogeneous media and in the complicated form profiles. Though GTD is created as the asymptotic theory which is used when a characteristic size of the problem is much greater than the wavelength, but the experience of GTD calculation shows, that it yelds reliable results up to the order of a about λ [1].

The form in which the GTD solution is found is an asymptotic expansion of the Maxwell's equations for $k \to \infty$. The GTD algorithm allows to find a main term, and sometimes some succeedents of this expansion. However, from the practical point of view, the most serious restriction is the GTD statement, that the field is infinite at the shadow boundaries of incident and reflected fields (denote them as $SB^{i,r}$). This difficulty occurs as a result of the boundary layer availability in an asymptotic solution of the differential equation [2].

For overcoming the difficulties connected with the shadow boundaries near $SB^{i,r}$, the method called "uniform asymptotic theory of diffraction on the shadow boundaries" (UAT) was developed. Based on the postulated expression for the geometrical optics field (GO), including the Fresnel integral, UAT gives the unique expression, which is valid at $SB^{i,r}$ boundaries intersections as well, thus, avoiding some difficulties connected with the availability of several expressions for the field, inherent to the boundary layer method [3].

Basing on the statement of the problem, we have solved two model diffraction problems: by the perfectly conducting half-plane and slot between two half-planes. It is not difficult to notice that the diffraction problem by aperture of the plane-parallel waveguide is reduced to the problem of the diffraction by the slot.

In this work the following symbols are accepted: 1) the temporary factor looks like $\exp(-i\omega t)$ and it is omitted; 2) the diffraction problem is always reduced to the two-dimensional case (there is no modification on an y - axis); 3) the transversal magnetic (TM) wave (nonzero components of the field H_y,E_x,E_z) and transversal electrical (TE) wave (E_y,H_x,H_z) are denoted by two symbols u and t, respectivly for TM $u = H_y$ and $t = +i$, for TE $u = E_y$ and $t = -i$.

STATEMENT OF THE PROBLEM

The geometry of the plane-parallel waveguide is represented in Fig. 1. $\Sigma_1 u \Sigma_2$ are two perfectly conducting half-planes parallel each other. The distance between them equals 2a. The single mode extending in the waveguide, drops on the aperture from $z = \infty$ and has the form:

$$\mathrm{TM}: \mathrm{H}_y^n(x,z) = 2\cos(\xi_n(x+a))\exp(i\beta_n z),\ n = 0,1,2\ldots; \quad (1)$$

$$\mathrm{TE}: \mathrm{E}_y^n(x,z) = 2\cos(\xi_n(x+a))\exp(i\beta_n z),\ n = 1,2,3\ldots, \quad (2)$$

where $\xi_n = n\pi/2a$ is the transverse wave number and $\beta_n = \left(\kappa^2 - \xi_n^2\right)^{1/2}$ is the longitudinal wave number.

The TM-wave expression also contains the TEM mode ($n = 0$).

The incident field can be safely decomposed into its two plane wave components and, with the help of prescribed u and τ, both polarizations of the incident field may be written as

$$u^i = u_+^i + u_-^i; \quad (3)$$

$$u_+^i = \exp i(\xi_n(x+a) + \beta_n z); \quad (4)$$

$$u_-^i = \tau \exp i(-\xi_n(x+a) + \beta_n z). \quad (5)$$

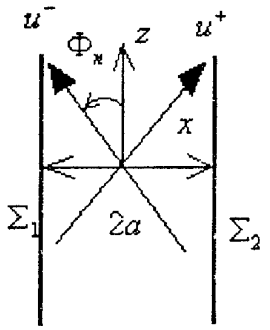


Fig. 1. Geometry of the plane-parallel waveguide

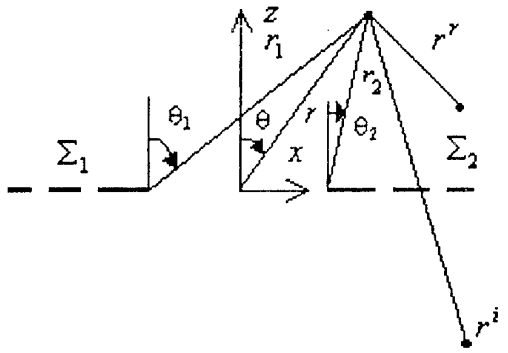


Fig. 2. Coordinates of the view point

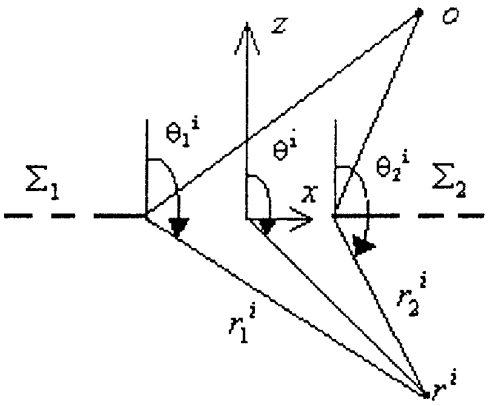


Fig. 3. Coordinates of the source

On the other hand, the expressions u_+^i (u_-^i) represent the plane wave propagating at the angle Φ_n ($-\Phi_n$) with respect to the z -axis:

$$\Phi_n = \sin^{-1}\left(n\pi/2\kappa a\right). \tag{6}$$

Notice that u_-^i represents incident fields for the wedge W_1, while u_+^i corresponds to the field reflected from W_1. For the second wedge W_2 the roles of u_+^i (u_-^i) are reversed.

DIFFRACTION BY THE SLOT

Consider the aperture formed by two perfectly conducting half-planes, which are irradiated with the incident field U^i. It is necessary to determine a high-frequency asymptotic solution for the entire field U^t at the viewpoint. Geometrically we have three rays, which are radiated by the source one and the direct ray and two diffracted rays converged in the viewpoint (look at Fig. 2, 3). As the slot is formed by two half-planes, the entire field U^t for it can be received by combination of fields for each half-plane.

The solution for field emitted from the slot, will be of the following form:

$$u^t = u^g + u^d; \tag{7}$$

$$u^g = \left[F\left(\xi_{s1}^i\right) - \hat{F}\left(\xi_{s1}^i\right) + F\left(\xi_{s2}^i\right) - \hat{F}\left(\xi_{s2}^i\right) - 1\right]u^i(r) +$$

$$+\left[F\left(\xi^r\right) - \hat{F}\left(\xi_{s1}^r\right) + F\left(\xi_{s2}^r\right) - \hat{F}\left(\xi_{s2}^r\right)\right]u^r(r). \tag{8}$$

The indices 1, 2 concern the first and second half-plane respectively, where

$$\xi_{1,2}^i = \sqrt{2kr_{1,2}}\sin\left(\frac{1}{2}\psi_{1,2}^i\right);$$

$$\xi_{1,2}^r = \sqrt{2kr_{1,2}}\sin\left(\frac{1}{2}\psi_{1,2}^r\right);$$

$$\psi_{1,2}^i = \theta_{1,2} + \pi - \theta_{1,2}^i; \psi_{1,2}^r = \theta_{1,2} - \pi + \theta_{1,2}^i.$$

$$u^d = g(kr_1)\left[\chi\left(\psi_1^i\right) + \tau\chi\left(\psi_1^r\right)\right]\cdot u^i(x=-a, z=0) +$$

$$+ g(kr_2)\left[\chi\left(\psi_2^i\right) + \tau\chi\left(\psi_2^r\right)\right]\cdot u^i(x=a, z=0), \tag{9}$$

where U^i, U^r were determined earlier.

$g(kr) = \frac{1}{\sqrt{8\pi kr}}\cdot\exp\left[i\left(kr + \frac{\pi}{4}\right)\right]$ is a cylindrical wave factor; $\chi\left(\psi^{i,r}\right) = \cos ec\left(\frac{1}{2}\psi^{i,r}\right)$ is the diffraction coefficient for an indefinitely thin screen [2]; $F(\xi) = \exp\left(i\pi/4\right)\Big/\sqrt{\pi}\int_{\xi}^{\infty}\exp\left(ix^2\right)dx$ is the Fresnel integral and $\hat{F}(\xi) = \frac{\exp\left[i\left(\xi^2 + \frac{\pi}{4}\right)\right]}{2\pi\xi}\cdot\sum_{n=0}^{\infty}\Gamma\left(n+\frac{1}{2}\right)\cdot\left(i\xi^2\right)^{-n}$ is the asymptotical series.

RESULTS

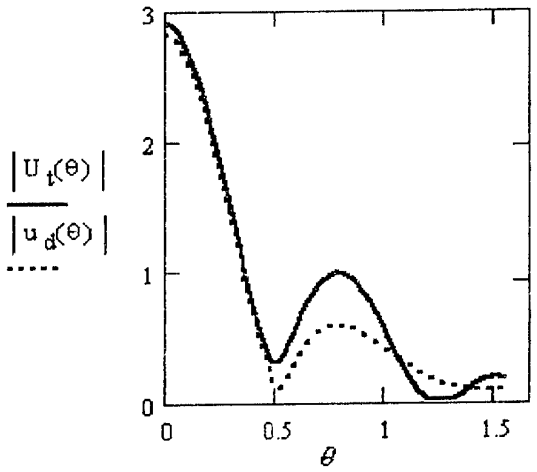


Fig.4 Dependence of the UAT and GTD fields on θ
(n = 0, τ = 1, r = 2a)

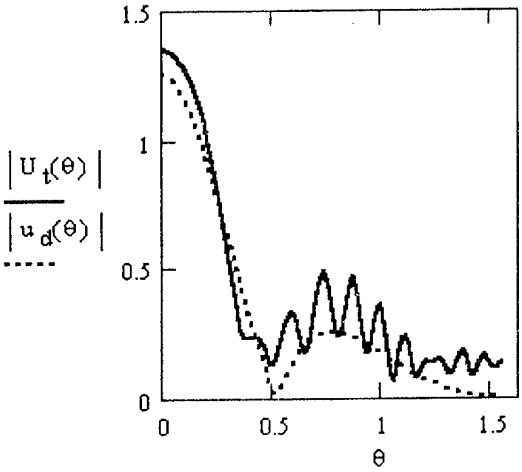


Fig.5 Dependence of the UAT and GTD fields on θ
(n = 0, τ = 1, r = 10a)

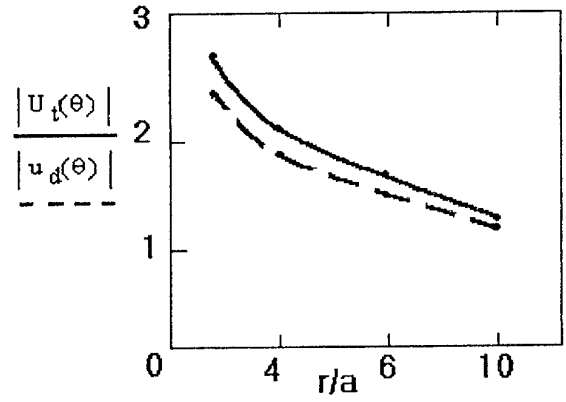


Fig.6 Dependence of the UAT and GTD fields on r/a
(θ = 0.01, n = 0, τ = 1)

CONCLUSIONS

In this work the attempt has been made to determine the entire field after the diffraction of an electromagnetic field by the plane-parallel waveguide aperture with the UAT up to the order of $k^{-1/2}$. The entire field solution is determined by equation (7). It is valid everywhere, except for the fields which are near edges and other caustics. Far from the shadow boundaries this solution turns into GTD results. The complete confirmation of the theory is impossible until the strict asymptotic solution of the model problems is obtained. The solutions are presented by the special asymptotic series, including the Fresnel integral. This solution is valid near to the shadow boundaries. The approximation can be presented as the adding of a transitional field to the GTD-solution. For the case, when the diffraction occurs at the edge of the thin screen UAT improves GTD results. UAT makes more precise the GTD solution at the shadow boundaries, where GTD is discontinuous. With the UAT the systematic approach is carried out to calculate all the terms, the order of which is higher than $k^{-1/2}$ (with respect to the incident field). UAT does not give positive outcomes on caustics, where it predicts indefinitely large fields.

Thus, by using the solution of the modeling problems, UAT allows to simulate fields created by more complicated objects and to calculate them fast and effective with the help of a computer.

REFERENCES

1. B.A.Borovicov, Б.Е.Kinber " The Geometric theory of diffraction ", Moscow, Svyaz', 1978, 248 pages [in Russian].
2. J.B. Keller " Diffraction by aperture " J. Apple. Phys., 1957, v. 28, № 4, p. 570 - 579.
3. R.G. Koumjian, P.G. Pathak " Uniform geometrical diffraction for an edge in a perfectly conducting surface ", IEEE, 1974, v. 62, № 11, p. 1448 - 1461.

CYLINDRICAL LUNEBERG LENS ANALYSIS

A. V. Boriskin, S. V. Boriskina and A. I. Nosich*

Radiophysics Dept., Kharkov State University,
Svobody Sq.4, Kharkov 310077, Ukraine
* Institute of Radiophysics and Electronics, National Academy of Sciences,
Kharkov 310085, Ukraine

ABSTRACT

The radiation pattern of a circularly-layered dielectric lens is computed using the series solutions and recurrent formulas for cylindrical functions with complex arguments. The Complex Source Point (CSP) beam is taken as a 2D model of a beam field. Unlike the well-known classical approximation for a plane wave scattering from a layered circular cylinder the proposed approach enables one to obtain a numerically accurate solution of the discussed problem.

INTRODUCTION

Dielectric lens [1] finds an application in various frequency ranges for various purposes. In the optical range, lenses are used as focusing devices for a laser beam at the input to a fiber. In the radio-frequency range, lenses are used in the design of indoor local communication systems and scanning mounted antennas on the civil and military ground equipment.

The main advantage of the used approach is that the CSP field is an exact solution of the Helmholtz equation with respect to the coordinate of the observation point [2]. Here, we recall that Gaussian beam, which is commonly used as a model of the beam field, does not satisfy it. Therefore the accuracy of results obtained by such an approximate method can not be estimated.

As a 2D model of the lens, a circularly-layered dielectric cylinder is considered. The values of the dielectric constants of the layer materials are chosen in accordance with a Luneberg Lens (LL) law:

$$\varepsilon_i = \left[2 - \left(r_j / r_m\right)^2\right]^{-1}, \quad r_j = \left(r_i + r_{i-1}\right)/2 \qquad (1)$$

The CSP is located and oriented as shown in Fig. 1.

METHOD OF ANALYSIS

Due to the axial symmetry of the studied LL scatterer problem the solution can be written in terms of the series of cylindrical functions. On applying the boundary conditions sequentially, starting from the boundary between the two most inner layers up to the outer ones and expressing the scattered field via the incident field, one can obtain the following expression for the field outside the lens:

$$U_m^{sc} = \sum_{n=-\infty}^{\infty} \gamma_{mn} H_n\left(k_m r_{cs}\right) \cdot e^{-in\varphi_{cs}} H_n\left(k_m r\right) \cdot e^{-in\varphi}, \qquad (2)$$

where H_n is the Hankel function of the 1st kind.

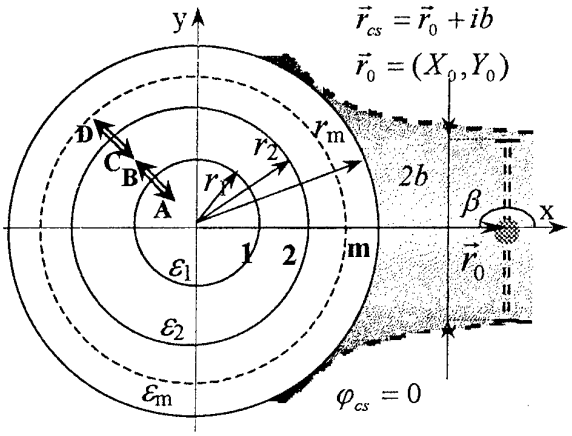


Fig. 1. A beam-fed coaxially-layered dielectric lens. Angles φ_{cs} and β determine the CSP location and beam orientation, respectively.

The coefficient γ_{mn} is determined by using the following recurrent formulas:

$$\gamma_{0n} = 0, \qquad (3)$$

$$\theta_{in} = \theta_{in}\left(\gamma_{(i-1)n}\right) = \frac{\gamma_{(i-1)n} H_n\left(k_i a_i\right) + J_n\left(k_i a_i\right)}{\alpha_i\left(\gamma_{(i-1)n} H_n'\left(k_i a_i\right) + J_n'\left(k_i a_i\right)\right)}, \qquad (4)$$

$$\gamma_{in} = \gamma_{in}\left(\theta_{in}\right) = \frac{J_n\left(k_{i+1} a_i\right) - \theta_{in}\alpha_{i+1} J_n'\left(k_{i+1} a_i\right)}{\theta_{in}\alpha_{i+1} H_n'\left(k_{i+1} a_i\right) - H_n\left(k_{i+1} a_i\right)}. \qquad (5)$$

where J_n is the Bessel function.

Here, the index i runs the values from 1 to m (m is the number of layers); $k_i = k\sqrt{\varepsilon_i}$; $r_{cs} = r_0 + ib$; parameter α_i depends on the polarization and equals: $\alpha_i = (\varepsilon_i)^{1/2}$ or $(\varepsilon_i)^{-1/2}$ in the case of E- or H-polarization respectively.

The axial symmetry of the boundary conditions enables one to solve the equations separately for each value of index n [3].

The directivity of the incident CSP beam depends on the parameter kb as it is seen from the asymptotic expression for CSP field in the far zone:

$$U_0 = H_0^{(1)}\left(k\left|\vec{r} - \vec{r}_{cs}\right|\right), \quad U_0 \approx \sqrt{2/i\pi kr}\, e^{ikr} e^{kb\cos(\varphi - \beta)} \quad \text{for } r \to \infty \qquad (6)$$

By using the above expressions for the fields in the exterior domain, the radiated-field characteristics were calculated. A fast algorithm for the calculation of cylindrical functions with complex arguments, based on the recurrent technique (forward one for Neumann and backward for the Bessel functions) was used [4].

RESULTS OF ANALYSIS

The most interesting questions to be answered are: location of the focus of LL, dependence of LL directivity on the CSP location, its directivity and the number of layers.

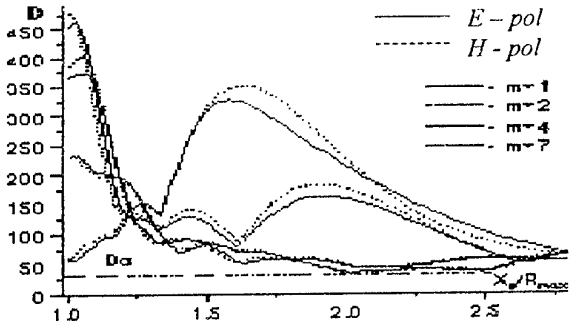


Fig.2. Directivity of LL versus the CSP location $kb = 2$ ($D_0 = 30.35$), $R_{max} = 41.9$ *, $Y_0/R_{max} = 0$, $\beta = 180$, D_0 is the directivity of CSP in the free space.

As it is seen from Fig. 2 the focal ring of LL has finite thickness, whose value, as well as its location depend on the number of layers taken into account: the more layers the narrower the focal ring and the nearer its location to the outer lens surface. Our analysis showed that at least 3-layer cylinder can be considered as a lens, and the optimal number of layers is 7-8. The curves in Fig. 2 were plotted for the fixed CSP beam-width parameter kb, but the dependence on kb is another interesting question.

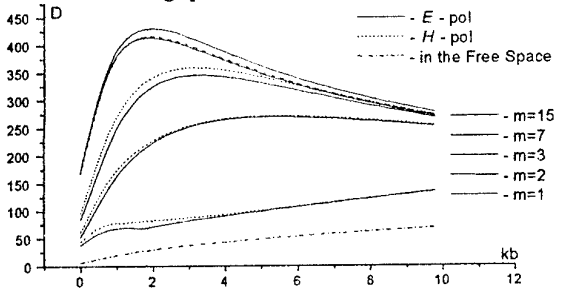


Fig. 3. Directivity of LL versus beam-width parameter

In Fig. 3, a non-monotonic behavior is well seen. Following Fig. 4, where the power level decreasing the optimal corresponds to LL "edge" illumination of -8 to -10 dB depending on the number of layers.

The most complete information on the lens effect can be obtained from the Fig. 5.

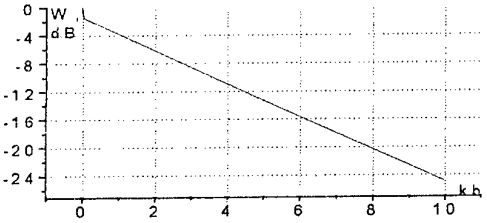


Fig. 4. Power level decreasing in the beam cross-section at the width of the outer surface radius r_m and at the distance of X_0 $X_0/R_{max} = 1.05$, $Y_0/R_{max} = 0$, $R_{max} = 41.9$, $\beta = 180$

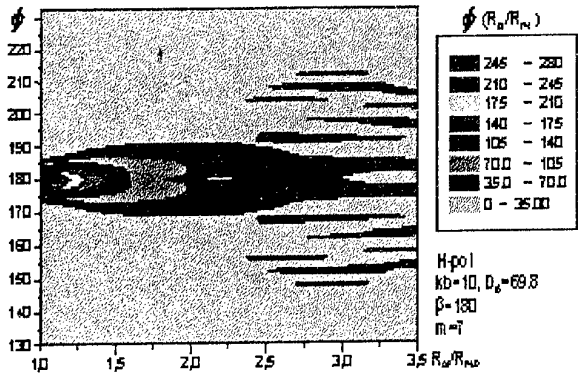


Fig. 5. Directivity of LL system versus the observation point and the CSP location on the lens optical axis. $Y_0/R_m = 0$, $R_m = 41.9$

It is well seen that the focus is located nearby the outer surface of the lens but one has to remember that in fact the focal area is not a point but a coaxial ring. Besides, Fig. 5 shows the degradation of the directivity when move away from the focus.

CONCLUSIONS

In this paper the series solution of the CSP beam-fed 2D dielectric Luneberg lens diffraction problem has been obtained. The numerically accurate results are presented for the both polarization cases and for the different lens and beam parameters. They show that a 3 to 7-layer lens fed with a -10 to -8 dB edge illumination provides a ten-fold improvement of directivity.

REFERENCES

1. H. Mieras, 'Radiation pattern computation of a spherical lens using Mie series', *IEEE Trans. on Antenna & Propagation*, vol. ap-30, no.6, pp. 1221-1224, Nov. 1982.
2. G. A. Suedan and E.V. Jull, 'Beam diffraction by a half-plane and a wide slit', *IEEE Trans. on Antenna & Propagation*, vol.AP-35 , pp.1077-1083, 1987.
3. A. V. Boriskin 'Two-dimensional beam excitation of a circular dielectric shell', Proc. Int. Conf. MMET-98, v.2, pp.525-527.
4. C. F. Du Toit, 'The numerical computation of Bessel functions of the first and second kind for integer orders and complex arguments', *IEEE Trans. on Antenna & Propagation*, vol.38, no.9, pp.1341-1349, 1990.

ACCOUNT OF EFFECTS OF THE IRRADIATOR'S NEAR ZONE IN MATHEMATICAL MODEL OF REFLECTOR ANTENNA

N. N. Gorobets, S. S. Vyazmitinova, A. I. Vyazmitinova

Kharkov State University,
4, Svoboda Sq., Kharkov, p.o.310077, Ukraine
Phone: 0572-45-71-75, Fax: 0572-47-18-16; E-mail: Nikolay.N.Gorobets@univer.kharkov.ua

The method of physical optics is employed to analyze the major electrodynamics characteristics of a reflector antenna in a form of a parabolic cylinder, which is irradiated by the field of a filament of an in phase magnetic current, and a spherical reflector, which is irradiated by the field of a Hertzian horizontal dipole. The irradiator field is written in an explicit form and can be calculated with a prescribed accuracy in an arbitrary space point, including the case of small electrical dimensions of the focal distance. Proceeding from the above, an influence of the effects of the irradiator's near zone on the results of calculating the radiation pattern of a reflector antenna was analyzed.

Nowadays, the reflector antennas with electrically small focal distances are widely used in practice. It can be caused mainly to the trend to minimize the mass and dimension parameters of the antenna and, besides, such antenna has advanced electrodynamics characteristics in comparison with "long focal" ones, e.g. a lower side lobes level. The most wide-spread technique of calculating the reflector antennas is the method of physical optics. As a rule, the calculations of the irradiator field are based on approximate solutions of the corresponding electrodynamics problems, which yields good results in most cases. But, uncontrolled errors occur in a case when the reflector is placed in the intermediate or even in the near zone of the irradiator. In this view, the problem of accounting the effects conditioned by placing the reflector in the near zone of the irradiator can be considered as a valid one.

This paper considers the mentioned problem taking as an example two simple model problems of electrodynamics, for which quite complete results of analysis through the rigorous numerical-analytical method are known. One of these problems is that about excitation of an idealized conductive parabolocylindrical reflector by the field of a linear in phase magnetic current. The second problem considers scattering of the Hertzian dipole field by a spherical reflector.

1. The components of the field of the magnetic current filament in terms of the cylindrical coordinate system will be written as [1]:

$$E_\varphi = \chi_1 H_1^{(2)}(kr); H_z = \chi_2 H_0^{(2)}(kr);$$
$$E_r = E_z = 0; H_r = H_\varphi = 0, \qquad (1)$$

where $H_0^{(2)}(x), H_1^{(2)}(x)$ are cylindrical Hankel's functions of the zero and first orders of the argument $x = kr$ describing a diverging cylindrical wave at $x \to \infty$.

Writing the source field as (1) we can calculate the both components with a prescribed accuracy in an arbitrary space point. Implementing the calculation algorithm for various intervals of argument variations, we used the following function representations of $J_n(x), Y_n(x)$ [2] in terms of which $H_0^{(2)}(x), H_1^{(2)}(x)$ were expressed, at $x \in (0, 10]$:

$$J_0(x) = \sum_{k=0}^{\infty}((x^2/4)^k/k!)(-1)^k;$$

$$J_1(x) = (x/2)\sum_{k=0}^{\infty}(-1)^k(x^2/4)/(k!(k+1))!;$$

$$Y_0(x) = (2/\pi)\ln(x/2)J_0(x) -$$

$$(1/\pi)\sum_{k=0}^{\infty}\psi(k+1)*\{1+(-1)^k(x^2/4)^k/(k!k!)\}$$

For the case of $x \geq 10$ we employed the polynomial approximation that provides the value of the absolute error module $|\varepsilon| \leq (1.6 \div 9)*10^{-8}$ [2]:

$$J_0(x) = x^{-1/2} f_0 \cos\theta_0;$$
$$Y_0(x) = x^{-1/2} f_0 \sin\theta_0; J_1(x) = x^{-1/2} f_1 \cos\theta_1,$$

where the values $f_o, \theta_o, f_1, \theta_1$ are given in paper [2]. The values of the function $Y_1(x)$ both in the first and the second intervals of the argument variations were calculated from the relation specified by the wronskian $W\{J_0(x), Y_0(x)\}$ taking the form:

$$Y_1(x) = (\, J_1(x)Y_0(x) - 2/(\pi x)\,)/J_0(x).$$

On the other hand, the functions $H_n^{(1)}(x)$ and $H_n^{(2)}(x)$ at $x >> n$ and $x \to \infty$ have very simple asymptotic expansions [2]:

$$H_n^{(1)}(x) \approx \sqrt{(2/\pi x)}\exp(i(x - n\pi/2 - \pi/4));$$
$$H^{(2)}{}_n(x) \approx \sqrt{(2/\pi x)}\exp(-i(x - n\pi/2 - \pi/4)),$$

which is the reason for writing the source field with an accuracy up to the constant factor as

$$H_z \approx \sqrt{(2/\pi x)e^{-i(x-3\pi/4)}},$$

where $x = kr$, $k = 2\pi/\lambda$, and r is the distance between the source and the reflector.

Thus, placing the irradiator somewhat away from the reflector and calculating the irradiator field either by precise or asymptotic formulas, it can be seen, how the often occurring inaccuracy of the electrodynamics model of the irradiator field influences the calculations of mirror antenna characteristics. As it was shown by a numerical experiment, in the case of small focal distances corresponding to the argument value of the Hankel function $H_0^{(2)}(x)$ x = 5; 10; 15,..., the radiation pattern obtained for different representations of the irradiator field do not coincide even within the principal directional lobe. A precise representation gives a narrower principal lobe and a number of strongly pronounced side lobes. On the contrary, the asymptotic representation provides fluent dependence of the relative radiation power of antenna on the azimuthal angle, and the side lobes occur only at $x \geq 10$ (see Fig. 1a).

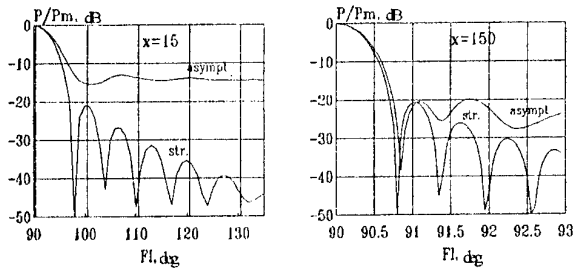


Fig. 1. Radiation pattern of a single-mirror antenna for various representations of the source field

Beginning from the point $x = 30$, the both radiation patterns converge within the main lobe and at $x \geq 50$ describe it practically in the same way up to the level of (-12...-15) dB. The near side lobes can be seen more clearly at the "asymptotic" radiation pattern, the side lobes maximums are close to these of the maximums of the near side lobes of the "precise" radiation pattern. Further expansion of the minimal distance between the irradiator and the reflector is accompanied by convergence of the side lobes (x = 100, 150), but the minimums that separate the principal lobe from the first side one and the first lobe from the second one, remain not deep even at x = 150 (Fig. 1b), i.e. a phenomenon is present, that is usually explained by square phase errors, as well as by non-optimal amplitude distribution of the irradiator field in the antenna radiating aperture. In the case considered, the two reasons are valid by calculating the radiation pattern with application of both the asymptotic and precise representation of the irradiator field, still the "precise" radiation pattern shows the minimums much more clearly. Hence, the inaccuracy of the representation of the irradiator field is one of the reasons for "delays" of the minimums of the antenna radiation pattern.

2. The field of the Hertzian dipole placed at the beginning of the spherical coordinate system with a dipole moment oriented along the polar axis will be written as:

$$E_r = -\frac{1}{ix\sin\theta}\frac{\partial}{\partial\theta}\left(H_\varphi \sin\theta\right),$$
$$E_\theta = \frac{1}{ix}\frac{\partial}{\partial r}\left(rH_\varphi\right), H_\varphi = ph_1^{(1)}(x)\sin\theta$$

where $x = kr$; p is module of the dipole moment, θ is a polar angle, $h_1^{(1)} \equiv j_1(x) + iy_1(x)$ is Hankel's spherical function. In order to estimate the distance between the Hertzian dipole and the far field zone, the amplitudes and phases of the cross components of the electrical and magnetic fields were calculated in the plane perpendicular to the dipole moment, i.e. in the case of $\theta = 90^o$. Calculations indicated, that the relation between the amplitudes of electric and magnetic fields near the Hertzian dipole has a complex feature: $|E_\theta| > |H_\varphi|$, when $R/\lambda < 0.17$; $|E_\theta| < |H_\varphi|$, when $0.17 < R/\lambda < 0.6$; $|E_\theta| = |H_\varphi|$, when $R/\lambda > 0.6$ and beginning in $R/\lambda > 0.53$ the amplitudes of the both components decrease inversely as the first power of distance (see Fig.2a). In Fig.2b curve 1 corresponds to the dependence of $\arg E_\theta$ on R/λ; curve 2- dependence of $\arg H_\varphi$ on R/λ and curve 3- dependence of the phase difference of the E_θ и and H_φ components on distance R/λ.

In the case of $R > 0.25\lambda$, the phase difference of the E_θ и and H_φ components does not depend on the distance between the irradiator and the control point, and the edge of the far zone can be assumed $R > 0.53\lambda$. These results match quite well with the results of paper [3] and ascertain them.

The radiation pattern of the spherical reflector was calculated by the approximate method of physical optics and a rigorous method [4]. Comparing the calculation results, it should be noted, that the method of physical optics provides a precise solution in the main lobe field, and the assumption that the currents in the shadow zone are zero is valid for the first side lobes. Thus, Fig. 3 shows the radiation patterns for the "quasi-resonance" band, when the dimensions of the diffraction structure are comparable with the wavelength, the cut angle $\theta_0 = 120^o$, and the irradiator is in the paraxial focus at a distance $br = 0.4 * r_0$ from the origin of coordinates. Results obtained by the rigorous method are marked with (+) [4].

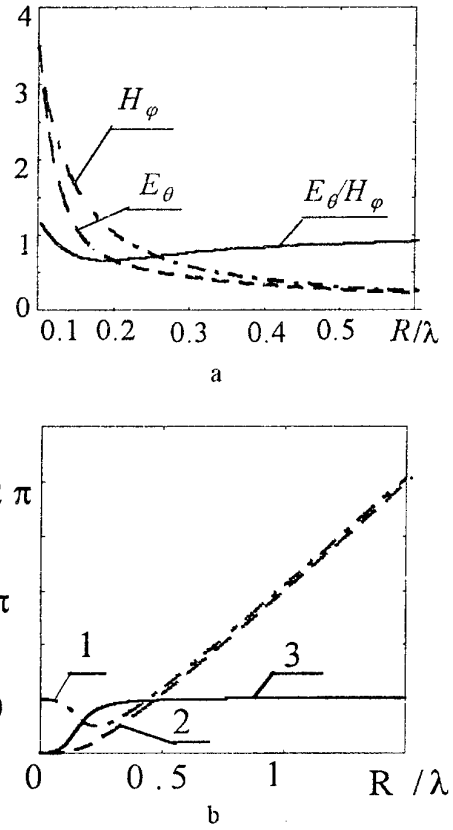
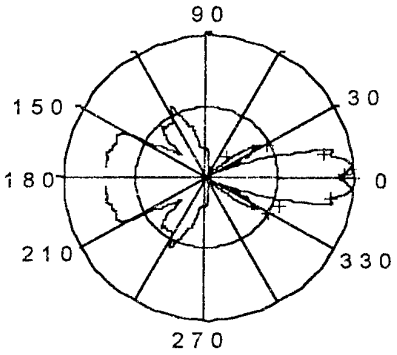
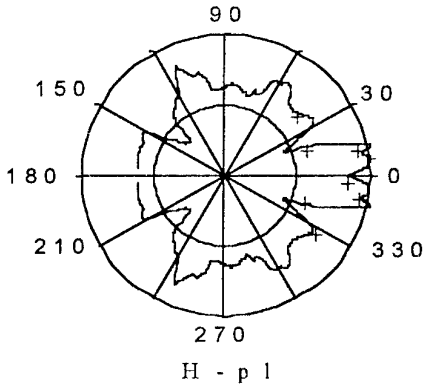


Fig. 2. Dependence of the amplitudes and phases components of electric and magnetic fields on distance





$\theta_0 = 120^0, \lambda_0 = 0.6283 * r_0, br = -0.4 * r_0$

Fig. 3. Radiation pattern of the spherical reflector for the quasi-resonance band

3. The results of numerical analysis of major characteristics of a reflector antenna show, that the accuracy of representation of the irradiator field with the reflector being placed in the near zone strongly influences the accuracy of calculating the radiation pattern, especially in the field of the side lobes. At the same time, with the reflector being disposed from the irradiator at a distance not less than $r_{\min} \approx (4...5)\lambda$, the approximate representation of the irradiator field provides a correct description of the principle lobe of the radiation pattern up to the level of (-12...-15) dB. Taking $r_{\min} \geq 20\lambda$, we obtain the asymptotic representation of the irradiator field describing the correct form and the level of the first side lobe. The problem of scattering of the Hertzian dipole field by a spherical mirror in Kirchhoff's approximation by a rigorous representation of the source field, a calculating algorithm for efficient analyzing a large scope of data was developed and implemented in the up-to-date software MatLab (version 4.2, 5.0). The algorithm was tested for carrying out the limit transitions. The obtained results confirm, that the developed algorithm can be applied as a working instrument while examining the electrodynamical characteristics of reflector antennas.

REFERENCES

1. G. T. Marcov, B.M. Petrov, G.P. Grudinskaya. Electrodynamics and wave propagation -Moscow. Sov.Radio, 1979, 376 p. [in Russian].

2. Handbook of mathematical functions with formulas, graphs and mathematical tables (Russian trans. By M.Abramowitz and I.Stegun) Moscow. Nauka 1979, 832 p.

3. N. N.Gorobets. Characteristic properties of the wave processes in the near zone of sensors of electric and magnetic field. In: "Methods and equipment of measurements in the field of electromagnetic compatibility" Vinnitsa, 1991, pp. 95-100 [in Russian].

4. I. A.Vyazmitinov. Diffraction of the concentrated source fields at an open spherical screen with the axial symmetry. Abstract of theses for Ph.D. in Physics and Mathematics. Rostov-na-Donu, 1990, 23 p. [in Russian].

DUAL-REFLECTOR OMNIDIRECTIONAL ANTENNA FOR MMDS BASE STATIONS

O. S. Kim

National Technical University of Ukraine "KPI", Laboratory of Antennas and Telecommunications,
2110D, Radio Engineering Faculty, Polytekhnichna st., 12, Kyiv, 252056, Ukraine
Tel/Fax: 380-44-2417223 e-mail: alex_kim@ucl.kiev.ua

INTRODUCTION

Multichannel Multipoint Distribution System (MMDS) along with cable net represent the most convenient way to distribute TV and radio signals over a small area. Asynchronous access to the Internet can also be realized via MMDS. MMDS base-stations, covering a circle area, employ antennas, that produce omnidirectional radiation patterns in the azimuth plane. Common methods of achieving a uniform azimuth distribution are using arrays of surface slots on a circular or coaxial waveguide, arrays of vibrators, etc. Another way is a dual-reflector omnidirectional antenna, which consists of a waveguide feed, sub- and main reflectors, shaped to produce the prescribed elevation pattern. The antenna axisymmetry along with properly designed feed ensure azimuthal omnidirectionality. Such antenna has a number of advantages: high gain, shaped elevation pattern, vertical and horizontal polarizations at the same time. TM_{01}, TE_{01} as well as H_{11} excitation may be utilized.

A new mathematical model of such antennas, allowing VSWR calculation, has been given in [1]. In this paper the results of design, simulation and measurement of the dual-reflector omnidirectional antenna for MMDS (11.7–13.5 GHz) are presented.

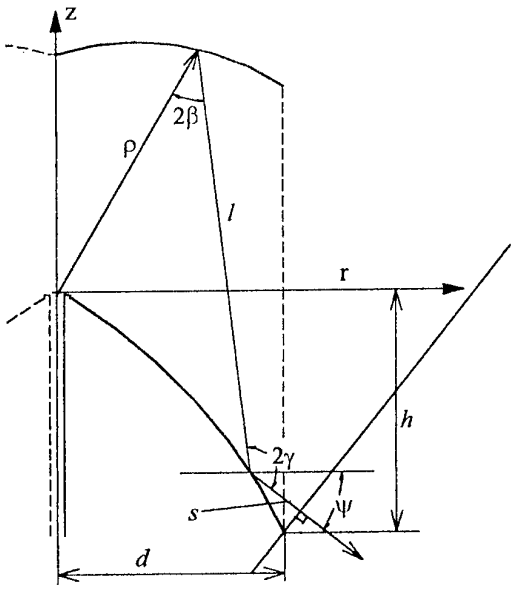


Fig. 1

ANTENNA DESIGN

Dual-reflector omnidirectional antenna (Fig. 1) is a kind of dual-reflector axisymmetrical antennas and therefore can be synthesized using well known geometrical optics principles (see, for instance, reference 2). The only difference is that the aperture is a cylinder. Under the definitions of the Fig. 1 the expressions [1] are transformed as follows:

$$c = \rho + l + s, \tag{1}$$

$$z = f(\theta), \tag{2}$$

$$\frac{1}{\rho}\frac{d\rho}{d\theta} = \frac{r\cos(\theta) + z\sin(\theta)}{l + \rho + r\sin(\theta) - z\cos(\theta)}, \tag{3}$$

$$r^2\cos\psi - 2r\left(d\cos\psi + (h+z)\sin\psi\right)\cos\psi + \\ + \left(d\cos\psi + (h+z)\sin\psi\right)^2 = s^2, \tag{4}$$

where c is the constant path length. Equation (2) defines the transformation law of the feed energy into the aperture distribution. A solution of the system (1)–(4) leads to the subreflector $\rho(\theta)$ and main reflector $r(z)$ cross sections.

To illustrate the synthesis technique, dual-reflector omnidirectional antenna has been designed for MMDS operating in 11.7–13.5 GHz frequency range. Since TM_{01} + TE_{01} excitation can not guarantee the expected antenna radiation pattern equivalence on the orthogonal polarizations then H_{11} excitation has been chosen. The antenna feed is an open circular waveguide with an axial slot in the aperture, which symmetries the feed pattern and at the same time prevents from the induced current on the external feed surface. The radiation pattern of the feed, computed using Mode Matching Technique, is presented in Fig. 2. The design procedure [3] has been applied to the reflector profiles synthesis in order to obtain the maximum antenna for the given feed pattern.

ANTENNA INVESTIGATION

The entire antenna has been analyzed using the field theory approach (FTA) [4]. It has to be noticed that applied technique gives the complete electromagnetic characteristics of the antenna, including radiation pattern and VSWR. The designed antenna has been

manufactured at the Ternopil's design office "Promin" (Fig. 3).

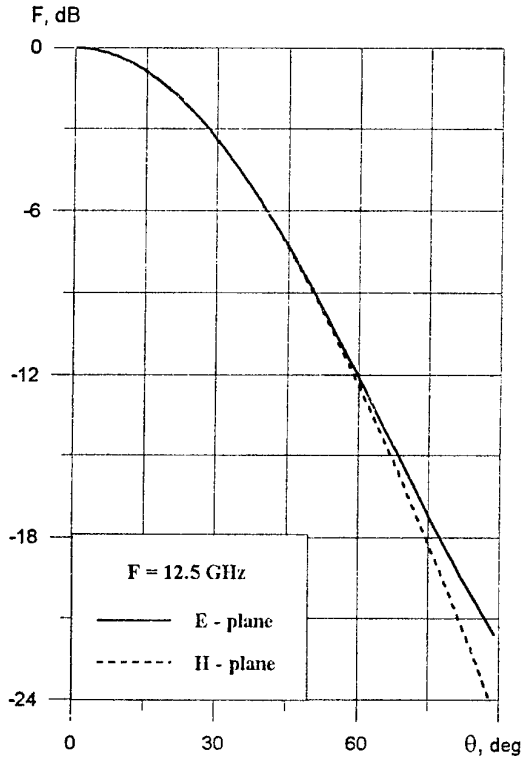


Fig. 2



Fig. 3

The antenna's VSWR versus frequency is shown in Fig. 4. A good agreement between computed (dashed line with crosses) and measured (solid line) characteristics of the experimental antenna is demonstrated. Fig. 5 contains a comparison between the measured and FTA simulated radiation patterns. It can be seen that the theoretical technique gives accurate main lobe and fist sidelobe as well as wide angle prediction.

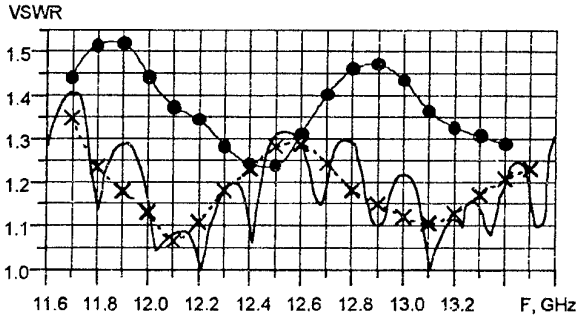


Fig. 4

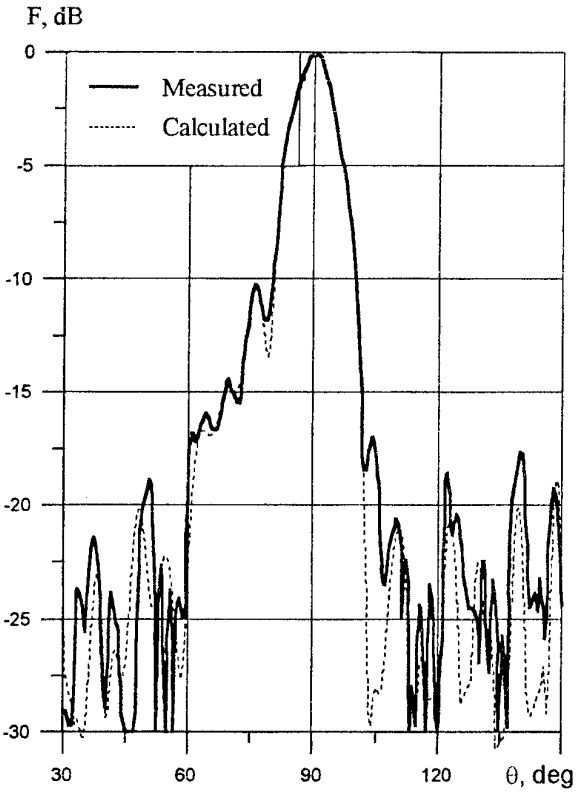


Fig. 5

DISCUSSION

The synthesis procedure for dual-reflector omnidirectional antenna has been proposed earlier by Norris [4]. It employs a parabolic subreflector and shaped main reflector. Under $m = 0$ excitation in this case the antenna's VSWR is mainly determined by interior feed matching, because of the null radiation along the axis, which lowers the subreflector reaction. However, when H_{11} excitation is used the particular consideration must be given to the subreflector reaction. It is obvious, that properly shaped subreflector, unlike conventional paraboloid, will improve antenna matching characteristics. This is demonstrated in Fig. 4, where H_{11} FTA simulated VSWR is presented for the omnidirectional system, synthesized by Noris's method (solid line with

circles). Both geometries, previously described (solid line) and Noris's (dashed line), are shown in Fig. 6. The same feed horn, feed angle and main reflector height are used. It is interesting to notice, that Noris's method gives a conventional conic section for main reflector profile, when the maximum gain is required.

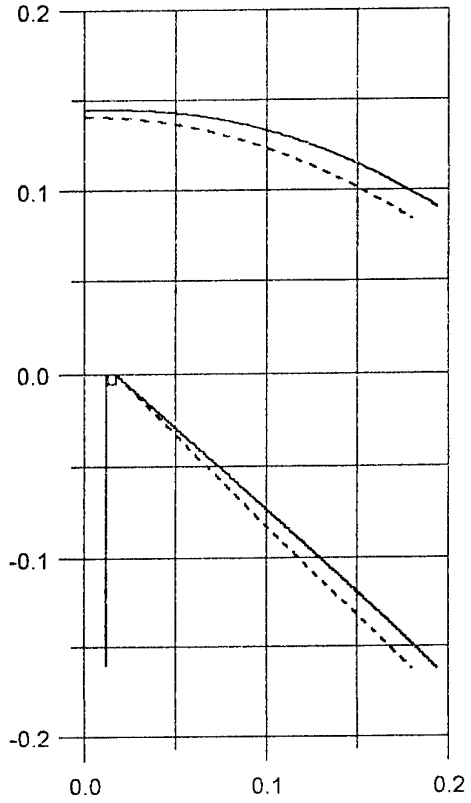


Fig. 6

REFERENCES

1. Dubrovka F. F., Kim O. S. A new mathematical model of omnidirectional dual-reflector antennas// Radioclektronika (Izvestiya VUZ). – 1999. – Vol.42. – N6. – P.3-16. [in Russian; translation into English: Radioelectronics & Communication Systems, V.42, no.6, 1999].

2. Galindo V. Design of dual-reflector antennas with arbitrary phase and amplitude distributions // IEEE Trans. – 1964. – Vol. AP-12. – No.4. – P. 403–408.

3. Dubrovka F.F., Dubrovka R.F., Kim O.S. A highly efficient iterative method of diffraction synthesis of axially symmetric dual-reflector antennas for satellite information systems. Part 1: The theory// Radioelektronika (Izvestiya VUZ). – 1998. – Vol.41. – N7. – P.9-21. [in Russian; translation into English: Radioelectronics & Communication Systems, V.41, no.7, 1998, pp. 5–13].

4. Norris A.P., Waddoup W.D. A millimetric wave omnidirectional antenna with prescribed elevation shaping // Internet. Conf. On Antennas and Propagation, 1985: IEE Conf. Proc. N.Y. 1985. – P.141–145.

SYNTHESIS OF THE CONTOURED RADIATION PATTERNS OF THE DUAL-REFLECTOR ANTENNAS ACCORDING TO THE PRESCRIBED MAGNITUDE PATTERNS

B. Podlevskyi and P. Savenko

Institute of Applied Problems of Mechanics &Mathematics of NASU,
3-b Naukova Str. Lviv, 290601 Ukraine
tel.: +380 (0322) 65-19-79, e-mail: podlev@iapmm.lviv.ua

ABSTRACT

The problem of synthesis of the contoured radiation patterns of spacecraft reflector antenna with classic and non-classic reflectors and array feed are considered. The variational formulation of the synthesis problem according to the given magnitude pattern and nontraditional forms of apertures are used. The mean-square deviation of given and synthesized magnitudes is chosen as optimization criterion. It permits to improve the approximation quality of the magnitudes, to influence by a certain mean on polarized properties of synthesized radiation patterns, and also to satisfy set additional requirements.

INTRODUCTION

For formation of zonal receive-transmitting antennas beams of modern satellite communication systems, reflector spacecraft contoured reflector antennas systems had been used. These can have various configurations, but the requirement to ensure covering a certain region of the ground with a given factor of amplification in whole service region is usually laid for everyone. For this purpose the antenna beam of a given shape (contoured beam), consisting of several narrow compound beams generated by separate element of the feed array is used.

In this work one approach to the solution of synthesis problem of the contoured radiation patterns dual-reflector antennas according to the prescribed magnitude pattern is proposed. It consists in determination of the amplitude-phase distribution (APD) on the elements of the feed array. Freedom of choice of the phase radiation pattern is used as the additional possibility for improvement the approximation quality of the synthesized amplitude pattern to the given.

STATEMENT OF THE PROBLEM

The design of a dual-reflector antenna consisting of two nonsymmetrical offset reflectors and feed array is considered. It is supposed that the subreflector is placed in the far zone in relation to separate feed element and in the near zone in relation to the main reflector and to the feed array as a whole.

Let a field (partial radiation pattern) in the far zone be described by the coordinates of the satellite antenna: the angle of elevation ϑ and the angle of azimuth φ. It is assumed, that the partial radiation pattern of the n-th separate beam in the point of observation (ϑ_j,φ_j), exciting by the unit level of power and zeroth phase, can be presented by the complex vector $(\mathbf{f_n}(\vartheta,\varphi) = f_n^{\vartheta}(\vartheta,\varphi)\mathbf{i}_{\vartheta} + f_n^{\varphi}(\vartheta,\varphi)\mathbf{i}_{\varphi}.)$.

The feed array in our research can have general configuration in the sense that the position and orientation of the n-th feed element is specified independently. Besides, the excitation coefficients and the type of radiation (a $\cos^p\vartheta$ feed) might also varying from element to element [1].

Having designated through I_j the complex factor of excitation of n-th feed element, electromagnetic field of all system is considered as a sum of the partial fields, and the total radiation pattern is written as

$$\mathbf{F}(\vartheta,\varphi) = \mathbf{AI} = \sum_{n=1}^{N} I_n \mathbf{f_n}(\vartheta,\varphi),\ \mathbf{A}: H_I \to H_f, \qquad (1)$$

where H_I and H_f are the Hilbert spaces with the inner products $(\cdot,\cdot)$ and norms $\|\cdot\|$

$$(\mathbf{I},\mathbf{I}) = \sum_{n=1}^{N} I_n I_n^*,\ \|\mathbf{I}\|_{H_I}^2 = (\mathbf{I},\mathbf{I}), \qquad (2)$$

$$(\mathbf{f_1},\mathbf{f_2}) = (f_1^{\vartheta}, f_2^{\vartheta}) + (f_1^{\varphi}, f_2^{\varphi}) =$$

$$= \iint_S \left\{ f_1^{\vartheta}(\vartheta,\varphi)\left[f_2^{\vartheta}(\vartheta,\varphi)\right]^* + f_1^{\varphi}(\vartheta,\varphi)\left[f_2^{\varphi}(\vartheta,\varphi)\right]^* \right\} \sin\vartheta \cdot d\vartheta d\varphi, \qquad (3)$$

respectively, N is a quantity of feed elements and S is a surface of the main reflector.

The value $\mathbf{f_n}(\vartheta,\varphi)$ can be determined for all points of observation inside a service zone and outside of it with the help of the physical optics methods, i.e.

$$\mathbf{f_n}(\vartheta,\varphi)=\frac{2}{\pi}\iint\limits_S[\mathbf{n}\times H_{\mathbf{n}}]\exp(ik(\mathbf{r},\mathbf{r}'))ds,$$

where $\mathbf{n}$ is the unit vector normal to surface S and pointing to the subreflector, $\mathbf{r}'$ is a vector of the point of integration on the reflector, $\mathbf{r}$ is a vector of the point of observation, $\eta = 120\pi$, $\mathbf{H_n}$ is a vector of the magnetic field near the surface of the main reflector and is determined with the help of the relation (see, for example [1])

$$\mathbf{H_n}=\mathrm{rot}\left(\frac{1}{4\pi}\iint\limits_{S_m}\mathbf{J_n}\frac{\exp(-ik\rho)}{\rho}dS_m\right),$$

i. e. taking into account a real distance between the reflectors ρ and the whirlwind (vortex) character of the fild between the reflectors. Here S_m is a surface of the contrreflector and $\mathbf{J_n}$ is a vector of the formed current on it.

Assume also that in some region Ω of angles ϑ and φ the magnitude pattern $\mathbf{F_0}$ is given by their components F_0^{ϑ} and F_0^{φ}. Outside this region we shall believe $\mathbf{F_0}=\mathbf{0}$ (i.e. $F_0^{\vartheta}=F_0^{\varphi}=0$).

Taking into account this assumption, the problem of synthesis of the contoured beam reflector antenna can be concisely formulated in the following form. At a known geometry of the feed array and the partial radiation patterns of the separate radiators of array it is required to determine the amplitudes and phases of excitation of the radiators (a vector of excitation of the feed elements $\mathbf{I}=\{I_1,I_2,..,I_N\}$). The designing problem is essentially nonlinear one and can possess non-unique solution. In this situation, one needs means to search the "best" (or the "optimum") solution in terms of some criterion. The mean-square deviation of synthesized and given amplitude radiation patterns in some region Ω is used as criterion of optimization. Thus, the problem of synthesis consists in a finding vector $\mathbf{I}$, which minimizes the functional [2]

$$\sigma=\left\|\mathbf{F_0}-|\mathbf{F}|\right\|^2_{H_f}+\beta\|\mathbf{I}\|^2_{H_I}, \qquad (4)$$

where $\beta > 0$ is some real parameter.

BASIC EQUATION AND ALGORITHM OF THE SOLUTION

The condition of stationarity of the functional σ leads to the equation

$$\beta\mathbf{I}=\mathbf{A}^*(\overline{\mathbf{F_0}\cdot e^{i\arg\mathbf{F}}}-\mathbf{F}), \qquad (5)$$

in which

$$\overline{\mathbf{F_0}\cdot e^{i\arg\mathbf{F}}}=\left\{F_0^{\vartheta}\cdot e^{i\arg\mathbf{F}},F_0^{\varphi}\cdot e^{i\arg\mathbf{F}}\right\}.$$

Here $\mathbf{A}^*$ is an operator which is an adjoint to operator $\mathbf{A}$ in the identity sense

$$(\mathbf{AI},\mathbf{F})_{H_f}=(\mathbf{I},\mathbf{A}^*\mathbf{F})_{H_I}. \qquad (6)$$

Substituting (1) in (5) we obtain the Euler's operator equation relatively to $\mathbf{I}$:

$$\beta\mathbf{I}=-\mathbf{A}^*\mathbf{A}\mathbf{I}+\mathbf{A}^*\mathbf{A}(\overline{\mathbf{F_0}\cdot e^{i\arg\mathbf{F}}}), \qquad (7)$$

and using (2), (3) for the operator $\mathbf{A}^*$ we obtain the correlation

$$\mathbf{A}^*\mathbf{F}=\iint\limits_{\Omega}\left\{\left[f_n^{\vartheta}(\vartheta,\varphi)\right]^*F^{\vartheta}(\vartheta,\varphi)+\left[f_n^{\varphi}(\vartheta,\varphi)\right]^*F^{\varphi}(\vartheta,\right\}\sin\vartheta\cdot d\vartheta d\varphi \qquad (8)$$

It permits to write the equation (7) in extented form. So, taking into account (8) from (7) we obtain the nonlinear system of algebraic equations relatively to $\mathbf{I}$:

$$\beta I_n=\sum_{m=1}^{N}b_{nm}I_m=q_n(\mathbf{I}),\ n=1,2,..,N, \qquad (9)$$

where b_{nm} and q_n are defined with the help of the formulas

$$b_{nm}=\iint\limits_{\Omega}\left\{\left[f_n^{\vartheta}(\vartheta,\varphi)\right]^*f_m^{\vartheta}(\vartheta,\varphi)+\left[f_n^{\varphi}(\vartheta,\varphi)\right]^*f_m^{\varphi}(\vartheta,\varphi)\right\}\sin\vartheta\cdot d\vartheta d\varphi, \qquad (10)$$

$$q_n=\iint\limits_{\Omega}\left\{F_0^{\vartheta}(\vartheta,\varphi)\left[f_n^{\vartheta}(\vartheta,\varphi)\right]^*e^{i\arg F^{\vartheta}}+F_0^{\varphi}(\vartheta,\varphi)\left[f_n^{\varphi}(\vartheta,\varphi)\right]^*e^{i\arg F^{\varphi}}\right\}\sin\vartheta d\vartheta d\varphi$$

The components of vector $\mathbf{I}$ to be found enter in a system (9) nonlinearly only while defining q_n. It permits to construct iterative process of solution of the system in a form

$$\mathbf{I}^{(\nu)}=(\beta\mathbf{E}+\mathbf{B})^{-1}q(\mathbf{I}^{(\nu-1)}), \qquad (11)$$

where ν is a number of iterations, $\mathbf{B}$ is a matrix, the elements of which do not depend on $\mathbf{I}$, $\mathbf{E}$ is a unit matrix, $q(\mathbf{I})$ is a vector of the right part of equation (9). Thus, the iterative process is reduced to the process in which the inverse matrix $(\beta\mathbf{E}+\mathbf{B})^{-1}$ is calculated once and it is multiplied on the vector $q(\mathbf{I})$ which is calculated on each iteration, that saves a time of the solution.

Analysis of this equations show that they can have the solution both in class of synphased radiation patterns and in classes of complex functions. The questions of

definition of the quantity optimal solutions and their quality characteristics, have a sufficiently difficult character and are based on the methods of the nonlinear analysis.

CONCLUSION

The offered approach and developed algorithm permits to solve the problems of synthesis of the contoured radiation patterns for any forms of hybrid antennas. Besides, the accepted statement of a problem has the following means:

Freedom of choise of the phase radiation pattern is used for improvement of the approximation quality of the synthesized amplitude patterns to the given.

- The mean-square deviation of the components of synthesized and given amplitude patterns permit to take into consideration the polarized properties of the radiation pattern. In particular, in a case of circular polarization we have

$$\left|F_0^{\vartheta}(\vartheta,\varphi)\right| = \left|F_0^{\varphi}(\vartheta,\varphi)\right| \text{ and}$$

$$\arg F_0^{\vartheta}(\vartheta,\varphi) = \arg F_0^{\varphi}(\vartheta,\varphi) + \pi / 2 .$$

- The second summand in the optimization criterion ensures the realizing of the solution to be found.

- The radiation patterns can be synthesized for the antennas with nonsymmetrical offset reflectors. In particular, the various cuttings from a paraboloidal reflector such as ellipse, circle, rectangular, square, sector, etc can be used.

- The feed system can comprise an array of general configuration. The each element of the feed array can have own, diferent from others, radiation pattern which can be calculated using formulas or measured data

Thus, such an approach can be used for designing the satellite antennas communication systems for covering certain territory.

REFERENCES

1. Datsyk, M.M., Podlevskyi, B.M., Savenko, P.A. *Calculation radiation patterns for singl- and dual-reflector antennas.* Lviv: Inst. of Appl. Probl. of Mech. and Math. National Acad. of Scien. of Ukraine. Preprint no.10, 1990 [in Russian].

2. Andriychuk, M.I., Voitovich, N.N., Savenko, P.A. and Tkachuk, V.P. *Synthesis of antennas according to the prescribed amplitude pattern.* Kyiv: Naukova dumka, 1993 [in Russian].

DUAL-SHAPED SYMMETRIC REFLECTOR ANTENNA WITH PARABOLIC PANELS

D. Y. Razdorkin, M. V. Romanenko

Rostov Research Institute of Radio communication,
Rostov -on-Don, Russia, Nansena 130, ph. 34-07-44

The optimization algorithm of the dual reflector antenna with the main reflector, typed from parabolic panels ensuring the maximal value of the aperture efficiency is considered.

The modern multiband antennas for earth station of satellite communication systems should have a high aperture efficiency in all frequency ranges simultaneously. The optimality of electrical parameters for such antennas is provided with wide use of axial symmetrical dual-shaped reflector antennas. The mathematical problem of using geometrical optics (GO) to synthesize such surfaces was solved for the rotationally symmetric case in 1962-1964 [1], [2]. Later the GO synthesize algorithm was elaborated for the existing parabolic antenna's modification [3]. In this case the aperture efficiency was increased by the subreflector surface modification and subreflector's location only. Then there are the insignificant phases errors and the optimal amplitude distribution in the main reflector's aperture.

However such a modification isn't sufficient for the multiband antennas with the large ratio of the high and lower frequency ($f_H / f_L = 2 \div 3$). If subreflector is optimized for the lower frequency, the aperture phases errors are as significant as for high frequency. The diameter of the subreflector optimized for high frequency is small for lower frequency, and in this case the diffraction losses are essential.

In this paper the optimization algorithm for the parabolic reflector's surface is considered on the basis of the classical Cassegrain antenna, by the criterion of the maximal aperture efficiency achievement with the use of the main reflector, whose surface is formed by parabolic panels located in N of circles. An auxiliary condition imposed on a choice of the resulting surface shape, was restriction on radial moving of units of fastening of panels to the main reflector's load-bearing carcass.

As it is known the dual-shaped reflector antenna has the theoretical maximum possible aperture efficiency η_a, equal to unit. The traditional task of the updating symmetric dual reflector antenna with the given surface form of the main reflector (Fig. 1) is solved by the replacement of existing subreflector with reflector from dual-shaped antenna, ensuring the maximum value of the aperture efficiency [3]:

$$\max(\eta_a(\beta)), \qquad (1)$$

where β is the irradiation angle of the main reflector edge. This optimization method provides the minimization of the aperture phases errors, occurred as a result of the use of the main reflector with the given surface $Z_0(x)$.

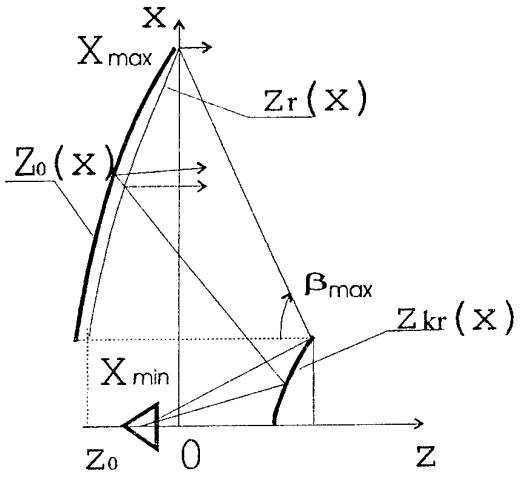


Fig. 1. Traditional partial modification antenna

The theoretical profile of the dual-shaped antenna's main reflector should satisfy the condition

$$\max_{x \in [X_{\min}, X_{\max}]} \left(z_T(x) - \frac{(x - X_{\min})^2}{4F} \right) < \partial_{\max}, \qquad (2)$$

where $\partial_{\max}$ is the maximum deviation of the theoretical synthesized profile $z_T(x)$ of the main reflector from the initial parabolic one, F is the focal length of the initial parabolic main reflector $Z_0(x)$.

The optimization of the main reflector surface z_{opt} was carried out by the parabolic panels packing in such a manner that to minimize the maximum deviation of the resulting surface from the surface $z_T(x)$ of the main reflector profile in the theoretical dual-shaped antenna:

$$\min_{x \in [X_{\min}, X_{\max}]} \left(\Delta_{\max} \left(z_T(x) - z_{opt} \right) \right), \qquad (3)$$

where $X_{\min}, X_{\max}$ are the boundary coordinates of the main reflector.

The algorithm for the calculation of the dual-shaped reflector antenna profiles of surfaces was described in [4]. The theoretically designed profile of the main reflector in this antenna was approximated by the polynomial curve:

$$z_T = z_0 + \sum_{i=0}^{N} A_i (x - x_0)^i, \qquad (4)$$

where A_i are the approximation coefficients of the calculated points of the dual-shaped antenna's main reflector, (x_0, z_0) is the internal edge coordinate of the calculated main reflector surface.

The resulting surface profile is defined as the function

$$z_{opt} = \mathrm{F}(z_i(x), x'_{0i}, z'_{0i}, \theta_i), \qquad (5)$$

where $z_i(x)$ is surface profile of the i-th parabolic panel, (x'_{0i}, z'_{oi}) is the panels joints coordinate of the optimized reflector, θ_i is the turning angle of the i-th panel relatively to its initial location (Fig. 2).

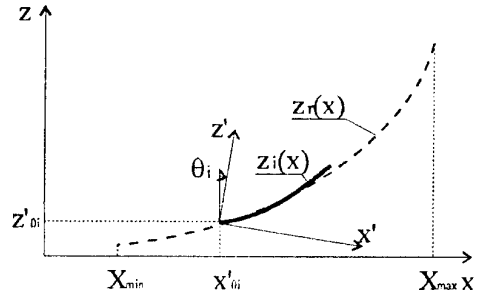


Fig. 2. The transfer of the i-th panel in the optimal location

The piecewise-parabolic profile of the initial reflector is determined by the ratio

$$z_i = z_{0i} + \frac{(x - x_{0i})^2}{4F}, \qquad (6)$$

where (x_{0i}, z_{oi}) is the initial coordinate of the panel's joints, $i = 0,...N$ is the panel's number, N is the number of the forming profile panels.

The solution of multiparametrical task of the surface optimization was carried out in two stages:

1. Choice of an optimum profile of the main reflector's theoretical surface, satisfying the condition (2);
2. Optimization of the parabolic panels arrangement ensuring minimization of the panel surface from theoretical deviation.

The maximum deviation of the curvature of the theoretical surface from the parabola is observed on periphery of the main reflector. Therefore the optimization of the panels location is carried out from choice of the peripheral panel location. For other panels the optimization of its location is reduced to overlapping the external edge of the panel with the previous panel internal edge and to the solution of an one-parametrical task of finding the turning angle of the coordinates system relatively to this point .

For the Cassegrain antenna with $F/D = 0{,}45$ and size of the aperture $D/\lambda = 216$ in the bottom range of frequencies it was possible to reduce a deviation of the theoretical profile from the resulting surface one up to $\Delta_{\max} = 0{,}072\lambda$.

REFERENCES

1. B. Y. Kinber, "On two reflector antennas," *Radio Eng. Electron. Phys.*, vol. 6, June 1962.
2. V. Galindo. "Design of dual reflector antennas with arbitrary phase and amplitude distribution," *IEEE Trans. Antennas Propagat*, vol. AP-12., pp. 403-408, July 1964.
3. V. P. Bandukov, A. M. Pokras, "Highly effective irradiating system for dual-reflector antennas", Trudy NII Radio, 1970, vol. 2, pp. 87-95 [in Russian].
4. M.V. Romanenko "The uniform approach to dual-shaped symmetrical reflector systems"(in Russian), "Antennas, radiocommunication and means" (ICARSM-97), Proceeding of the III International Conference, Voronezh-May-97, pp. 204-214.

A CONCEPTUAL APPROACH TO DETERMINE ANTENNAS GAIN LOSS IN TROPOSPHERIC-SCATTER COMMUNICATION SYSTEMS

V. I. Rudakov

Central Rescarch and Development Institute of Armament and Military Engineering,
Kiev - 135, str. Andrushenko, 4, tel. 271-62-45

The antennas gain (GA) loss (for antennas with GA = 40–45 dB) in tropospheric-scatter communication (TSC) systems is determined by a mechanism of long distance tropospheric radio waves propagation (LDTRWP) [1] and affects TSC systems power potential that determines noise immunity of these systems [2, 5] and fade margin [3, 4].

To calculate more accurately a power potential of TSC system it is necessary to consider more correctly a varying signal level at input of TSC system receiver, i.e. to calculate more accurately level of antennas gain loss — ΔG_{GA}. But for this it is necessary to simulate fragmentarily some parameters of antennas and troposphere determining value — ΔG_{GA}. Moreover it is necessary to formalize and algorithmize calculating antennas gain loss for definite problems of determining power potential of TSC systems.

At the moment according to [2], there is no formalized correlation for signal level varying at output of TSC system receiver and antennas gain of such systems, and, as a result, for antennas gain loss — ΔG_{GA} [3].

Thus, the present paper is devoted to a conceptual approach to formalize problem of determining the correlation between signal level and level of antennas gain loss — ΔG_{GA} of TSC system with the help of a conceptual model "antenna-troposphere-antenna" (Fig. 1) for LDTRWP mechanism [2].

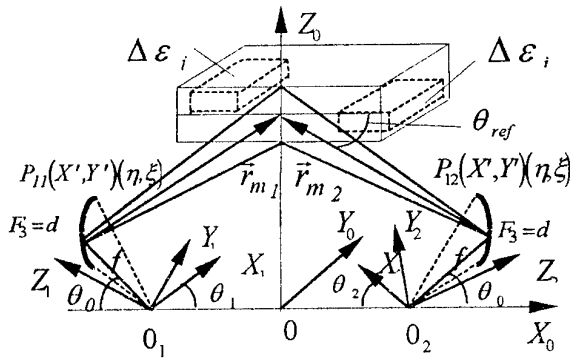


Fig.1. A conceptual model "antenna-troposphere-antenna"

Then, the electric field in focal region of antenna is determined [3] as follows.

$$E_m = \frac{-i\pi dB\tau E_n |g| \exp\left\{\frac{g}{\Delta\varepsilon_0}(H-H_1)\right\}}{16 f\lambda \sin^2\theta_m \left(\frac{g}{\Delta\varepsilon_0} + i\frac{4\pi}{\lambda}\sin\theta_m\right)} \times$$

$$\times \frac{\sin\left(\frac{B\tau^2}{B+\tau^2}U'\right)}{\frac{B\tau^2}{B+\tau^2}U'} \exp\left(\gamma R_0 + \frac{B\tau^2}{B+\tau^2}\right) \qquad (1)$$

Introducing $V_{MOD} = |E_m / E_n|$, the expressions for tropospheric wave attenuation in the focal region of antenna with respect to coordinates X, Y, Z for corresponding focal planes of antenna aperture have been obtained as follows [3]:

$$V_{MOD_X} = \frac{-i\pi dB\tau |g| R_{E_{eg}}^3}{8 f R^3 (1-\xi)^3} \exp\left\{\frac{gR^2(1-\xi)^2}{8R_{E_{eg}}\Delta\varepsilon_0}\right\} \times$$

$$\times \left\{2\frac{I_1(U)}{U} + i\frac{U}{\tau}\tan\frac{\theta_0}{2}\frac{I_2(U)}{U}\cos\Phi_2\right\}; \qquad (2)$$

$$V_{MOD_Y} = \frac{-i\pi dB\tau |g| R_{E_{eg}}^3}{8 f R^3 (1-\xi)^3} \exp\left\{\frac{gR^2(1-\xi)^2}{8R_{E_{eg}}\Delta\varepsilon_0}\right\} \times$$

$$\times \left\{2\frac{I_1(U)}{U} + i\frac{U}{\tau}\tan\frac{\theta_0}{2}\frac{I_2(U)}{U}\cos\Phi_2\right\}; \qquad (3)$$

$$V_{MOD_Z} = \frac{-i\pi dB\tau |g| R_{E_{eg}}^3}{8 f R^3 (1-\xi)^3} \exp\left\{\frac{gR^2(1-\xi)^2}{8R_{E_{eg}}\Delta\varepsilon_0}\right\} \times$$

$$\times \left\{-\frac{U}{\tau}\frac{I_2(U)}{U}\cos\Phi_2\right\}. \qquad (4)$$

The calculation results for layer formations in troposphere with asymmetric dependence of $\Delta\varepsilon_{ij}$ variation in the layer are shown in Fig. 2. The obtained results characterize mean-statistic values of tropospheric wave attenuation (V_{trop}) in the focal region of antenna and angles of tropospheric wave arrival (ϕ_{trop}) corresponding to a distorted wave front in antenna aperture, i.e. its difference from a plane one [2, 3]. This is equivalent to antenna feed displacement in the focal region on some value ΔCM_{trop}. Determining this value dependence on time it is possible to determine varying in time value of

antenna gain — G_{GA}, for example, that has been determined experimentally in [3] and which daily variations have been $0.01–0.03G$ (standard value G = 30 dB, R = 200 km, λ = 6.4 cm).

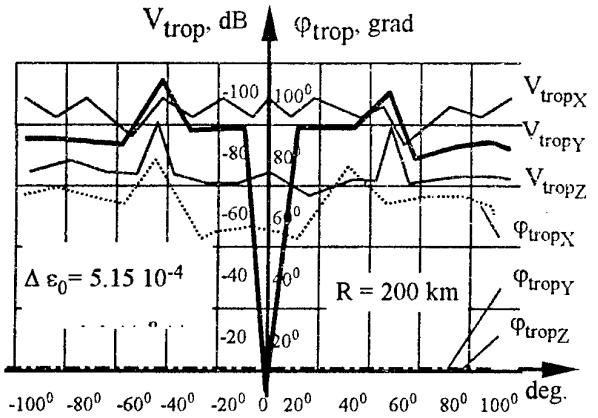


Fig. 2. Mean-statistic variation of the antenna focal tropospheric spot

Then taking into account standard antenna gain G antenna gain loss ΔG_{GA} is determined as [3]

$$\Delta G_{GA} = G - G_{GA} \tag{5}$$

for reflector antennas that have a profile describing by the law [2-4]

$$Y^2 = nfx. \tag{6}$$

Introducing the mean-statistic function of feed displacement from the focus due to troposphere influence as $\beta(X,Y,Z)$ [3, 4], it can be determined as

$$\beta(X,Y,Z) = -\frac{ka^2}{2f^2}\frac{\Delta CM_{trop}}{1+a^2/4f^2}. \tag{7}$$

The calculation results for $\beta(X,Y,Z)$ are shown in Fig. 3.

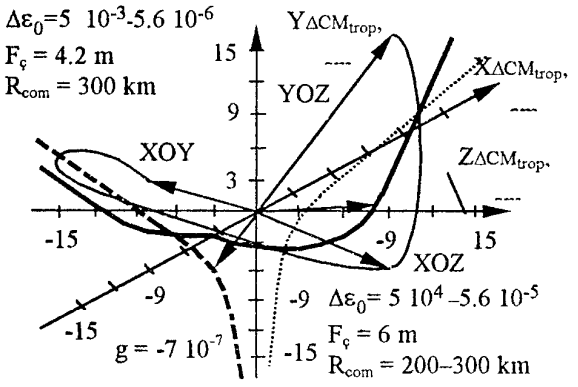


Fig. 3. Calculated "displacement" of the feed through tropospheric influence

They confirm the main principle of the conceptual approach to determine ΔG_{GA}: it is possible to "recover" the standard antenna gain during receiving fluctuating tropospheric wave if antenna feed is displacing in the antenna focal region according to complex trajectories (see Fig. 3) simultaneously in three planes [3]. Under this the correlation between antenna gain loss level and tropospheric wave field is determined as [3]

$$E_Z(X,Y) = \iint_{\sigma_{par}} V_{MMD_0}\{R,\theta,(F)\}K_Z(\xi,\eta)d\xi d\eta + \alpha \iint_{\sigma_{feed}} V_{MOD_{ref}}\{R, \theta,(F)\}K_Z(\xi,\eta,X',Y')K_Z(\xi,\eta,X,Y)d\xi d\eta \tag{8}$$

where η,ξ — coordinates in a paraboloid plane; X,Y — coordinates in a feed plane; X',Y' — coordinates of the system: feed plane-paraboloid plane.

And the power of the signal being received by feed [3] is determined [3] as

$$I_{tr_{feed}}(Z) = \left(1-|\alpha|^2\right)\left|\iint_{\sigma_{feed}} MOD_{ref}\{R,\theta,(F)\}\times K_z(\xi,\eta,X',Y')K_Z(\xi,\eta,X,Y)d\xi d\right|^2 \tag{9}$$

and considering some assumptions [2,3]

$$I_{tr_{feed}}(Z) = B\left|E_{tr}(X,Y)\right|^2, \tag{10}$$

where $B = \sigma_{feed}(1-|\alpha|^2)$; $\alpha = \alpha_{feed} + \alpha_{par}$.

According to [3]

$$I_{tr_{feed}} = B\left|V_{MMD}\{R,\theta,(F)\}\right|^2\left[1+2ACos\left(\frac{2K}{1+\gamma^2}\times \Delta CM_{trop}+\varphi_1\right)Sin\left(\frac{2K\gamma^2}{1+\gamma^2}\Delta CM_{trop}+\varphi_2\right)\right]. \tag{11}$$

The calculation results are shown in Fig. 4.

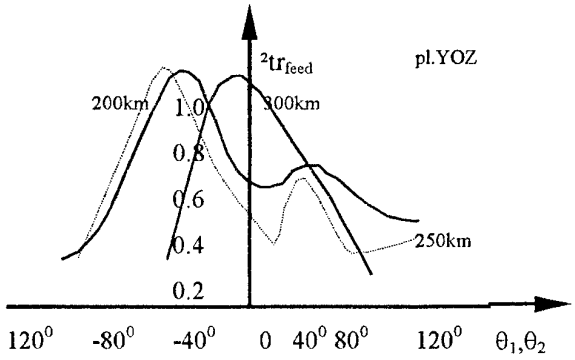


Fig. 4. Energy distribution in feed aperture

Then ΔG_{GA} is determined as [2,3,5]

$$\Delta G_{GA} = \frac{A}{B}, \qquad (12)$$

then: $A = \left(1 - |\alpha|^2\right) \times$

$$\times \left| \iint_{\sigma_{feed}} \frac{V_{MMD}\{R,\theta,(F)\}K_Z(\xi,\eta,X,Y)}{\left[1 - \alpha\sigma_{feed}K_Z(\xi,\eta,X,Y)K_Z(\xi,\eta,X',Y')\right]} \times \right.$$

$$\left. \times K_Z(\xi,\eta,X',Y')K_Z(\xi,\eta,X,Y)d\xi d\eta \right|^2;$$

$$B = \left| \iint_{\sigma_{par}} V_{MMD}\{R,\theta,(F)\}K_Z(\xi,\eta)d\xi d\eta + \right.$$

$$+ \alpha \iint_{\sigma_{feed}} V_{MMD_{refe}}\{R,\theta,(F)\}K_Z(\xi,\eta,X',Y')$$

$$\left. K_Z(\xi,\eta,X,Y)d\xi d\eta \right|^2 .$$

The calculation results of determining the energy re-distribution between feed and antenna for formulae mentioned above are shown in Fig. 5.

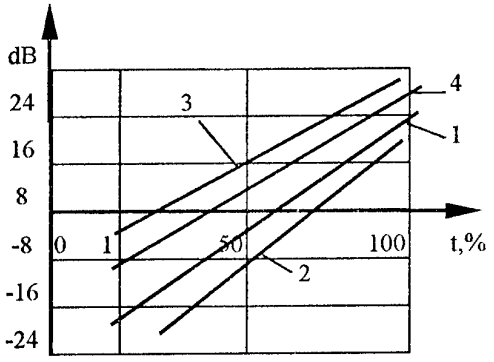


Fig. 5. Calculation distributions of signal levels equivelent $\Delta G_{GA_{\min}}$ и $\Delta G_{GA_{\max}}$

CONCLUSIONS

1. Distributions 1 and 2 in Fig. 5 determine the variation of signal level received by antenna, and are similar to Rayleigh law [3]

$$\rho\left(A_{trop}\right)_{feed-par} = \frac{A_{trop}}{\sigma} e^{-\frac{A_{trop}^2}{2\sigma^2}} . \qquad (13)$$

i.e. they correspond to a minimum of $\Delta G_{GA_{\min}}$.

2. Distributions 3 and 4 in Fig. 5 represent integral distributions of two signals having equal medians, both of which distributed according to Rayleigh law [2–5], i.e. they correspond to a maximum of $\Delta G_{GA_{\max}}$.

3. Fig. 6. shows intervals of varying ΔG_{GA} with respect to maximum and minimum of approximating straight lines necessary to calculate power potential of TSC system.

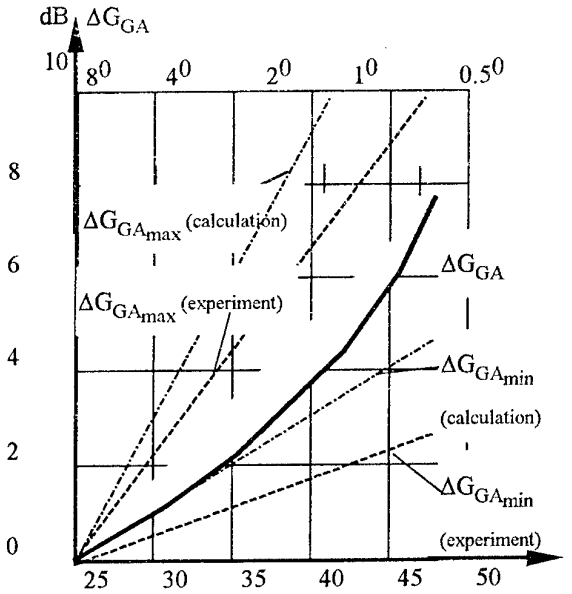


Fig. 6. Calculation values $\Delta G_{GA_{min}}$ and $\Delta G_{GA_{max}}$ for TSC systems

The results represented in the present paper permit, according to [3, 5], to confirm the main principles of the conceptual approach to determine antennas gain loss, namely: developing the conceptual model "antenna-troposphere-antenna"; determining the variation of mean-statistic value ΔCM_{trop}; determining the quasi-optimum trajectories of feed displacement to recover standard antenna gain; determining the formalized antenna gain loss $-\Delta G_{GA}$; determining maximum and minimum values of ΔG_{GA} in order to calculate more accurately the power potential of TSC system [5].

REFERENCES

1. Shifrin Y.S. The questions of statistical theory antennas, M, Sov. radio, 1970 [in Russian].

2. Rudakov V.I. Determination of the optimum radiation patters of antennas of tropospheric-scatter communications systems, STC LETI, issue. 8, Leningrad, 1978 [in Russian].

3. Rudakov V.I., Galkin A.P. Auth. sert. N118791, VPI, Vladimir, 1978 [in Russian].

4. Rudakov V.I. On possibility of using phase array of tropospheric scatter communication systems, STC LETI, issue. 7, Leningrad, 1978 [in Russian].

5. Rudakov V.I., Loman V.I., Nystyrenko I.K. Method of struggle with fadings signals in radio links TSC (Aut. sert. N 4431247/09/06357), KHMSC, Kiev, 1989 [in Russian].

A THEORETICAL ASPECT OF QUICK FADINGS AUTOCOMPENSATION IN TROPOSPHERIC-SCATTER COMMUNICATION SYSTEMS

V. I. Rudakov

Central Research and Development Institute of Armament and Military Engineering,
Kiev - 135, str. Andrushenko, 4, tel. 271-62-45

A problem of autocompensators are actual not only for tropospheric-scatter communication (TSC) systems [1–5]. Due to the complexity of is solving [1–3] the present paper considers only the one theoretical aspect of the problem of quick fading autocompensation in TSC system, namely, that one that concerns the formalization of the correlation between quick fading margin and antennas gain loss ΔG_{GA} in order to stabilize automatically a standard power fading margin in TSC systems [1–3]. Under this, the evaluation of necessary fading margin in TSC system is done with respect to informational reliability according to condition [1-5]

$$10\lg\frac{n_{0med}}{n_{0i}} \langle 10\lg\frac{n_{0medi}}{n_{kriti}} \qquad (1)$$

where

$$n_{okriti} = \sqrt{\frac{J(r)}{(L-1)!\,2P_{0er}}}\ \text{[1–3]}; \qquad (2)$$

$$n_{omed} = A_{par}\,\Phi\left(\frac{G_1 G_2}{\Delta G}\right)\ \text{[1–5]}; \qquad (3)$$

$$G_1 = G_2 = \left(\frac{\pi d_A}{\lambda}\right)^2 g_A \exp\left[-\left(\frac{4\pi\bar{\Delta}}{\lambda}\right)^2\right]\eta\ \text{[2-3]} \qquad (4)$$

$$\Delta G_{GA} = \frac{A}{B},\ \text{[1–3]} \qquad (5)$$

where:

$$A = \left(1-|\alpha|^2\right)\times$$

$$\times\left|\iint_{\sigma_{feed}} \frac{V_{MMD}\{R,\theta,(F)\}K_Z(\xi,\eta,X,Y)}{\left[1-\alpha\sigma_{feed}K_Z(\xi,\eta,X,Y)K_Z(\xi,\eta,X',Y')\right]}\times\right.$$

$$\left.\times K_Z(\xi,\eta,X',Y')K_Z(\xi,\eta,X,Y)d\xi d\eta\right|^2;$$

$$B = \left|\iint_{\sigma_{par}} V_{MMD}\{R,\theta,(F)\}K_Z(\xi,\eta)d\xi d\eta + \alpha\iint_{\sigma_{feed}} V_{MMD_{refe}}\{R,\right.$$

$$\left.\theta,(F)\}K_Z(\xi,\eta,X',Y')K_Z(\xi,\eta,X,Y)d\xi d\eta\right|^2.$$

Well known [1–3], that in modern TSC systems an effective way to create fading margin while receiving fluctuating signals is an increases in diversity order (L) of receiving signal channels, frequency, time diversities or their combination [1–3]. This increase the total level of receiving signals. According to [1–5], for example, for TSC systems with angle diversity it is impossible to obtain decorrelated space receiving channels without narrow radiation patterns (RP) of different diversity beam width equal to $0.1^0 - 0.3^0$ [1–3].

Thus, to formalize the correlation between fading margin and antenna gain loss it is considered a theoretical aspect of quick fading autocompensation in TSC systems with angle diversity formed when two antennas in TSC systems are joined according to two-element radio interferometer (RI) scheme (see Fig. 1).

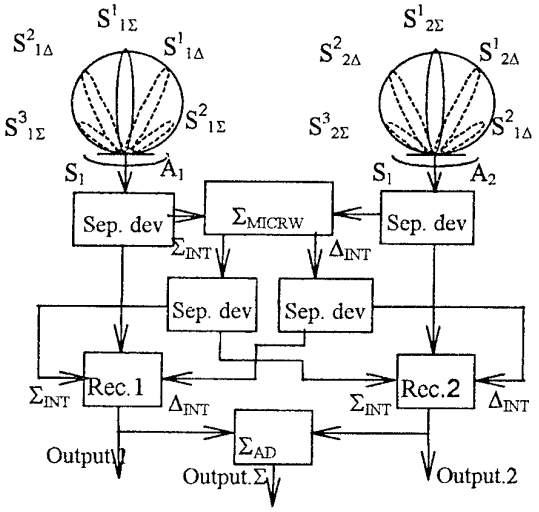


Fig.1. A scheme of an angle diversiry TSC system

Such antennas joining [1–3] is possible due to common heterodyne in a receiver for preselective signal processing in the event when the latters have been received by two spatially diversed antennas [1–3]. Then median levels of receiving signals n_{omed} (1) are determined according to [1–5] by the mean-median levels of receiving signals n_{omed} (1) are determined, according to [1–5] by the mean-median levels of interferometric components

$$n_{med}\left(\sum\nolimits_{\Sigma,\Delta}^{INT}\right) = \frac{1}{2}\left[S^1_{1\Sigma} + S^2_{1\Sigma} + S^3_{1\Sigma} - S^1_{1\Delta} - S^2_{1\Delta}\right]+$$
$$\left[S^1_{1\Sigma} + S^2_{1\Sigma} + S^3_{1\Sigma} - S^1_{1\Delta} - S^2_{1\Delta}\right]+$$
$$\left[S^1_{2\Sigma} + S^2_{2\Sigma} + S^3_{2\Sigma} - S^1_{2\Delta} - S^2_{2\Delta}\right]+$$
$$+\left[S^1_{2\Sigma} + S^2_{2\Sigma} + S^3_{2\Sigma} - S^1_{2\Delta} - S^2_{2\Delta}\right] \qquad (6)$$

where $S^m_{n\Sigma}$, $S^m_{n\Delta}$ — sum and difference interferometric components (m, n = 1,2....,k).

The sum $(\sum)$ and difference (Δ) interferometric signal components are determined by multi-beam RP in Fig. 1, according to [1–3] for RI with base size equal to 70–100 λ, and lobes width $0.15^0 - 0.3^0$.

A correlation function for amplitude fluctuations of tropospheric waves received by two RI antennas determines the relation between signals amplitudes S_1 and S_2 and sum-difference interferometric components levels [1–3]

$$\frac{\langle S_1(x)S_2(x+\Delta)\rangle}{\langle\delta^2\rangle r_0 R} = \frac{\langle \int_0^R \delta(r_2)dr_2 \int_0^R \delta(r_1)dr_1 \rangle}{\langle \delta^2 \rangle r_0 R} \quad (7)$$

Then the mutual correlation function for amplitude fluctuations $S_1(V_{MOD1}\{r_1\theta_1(\Phi)\}$ and $S_2(V_{MOD2}\{r_2\theta_2(\Phi)\}$ is determined according to [1–3] as

$$C(r_{12}) = \frac{\langle V_{MOD1}\{r_1,\theta_1,(\Phi)\}V_{MOD2}\{r_2\theta(\Phi)\}\rangle}{\langle V^2_{MOD1}\{R,\theta,(\Phi)\}\rangle} \quad (8)$$

The calculation simulation and experimental results [1–5], for example, for R = 200 km and space correlation radii ρ^*_r = 1.4 – 10 m determine signals mutual correlation values that are equal to 0.01 and 0.0002 for $S^m_{n\Sigma}$ and 0.05 and 0.1 for $S^m_{n\Delta}$ [1–3]. These results confirm that there is weak correlation between space signals received by interference RP lobes of RI. In this event in TSC system automatically, at any rate, the 4-order angle diversity in TSC system automatically, at angle diversity in azimuth and tilt planes is «formed», and interferometric components sum level at adder output in Fig. 1 is determined according to [1–5]

$$\sum\nolimits^{RI}_{output} = \sum_{i=1}^{n}\left[\prod_{i=1}^{m}\left(\sum_i S^i_{1\Sigma} + \sum_i S^i_{2\Sigma} + \right.\right.$$

$$\left.\left. + \sum_i S^i_{3\Sigma} - \sum S^i_{1\Delta} - \sum S^i_{1\Delta}\right)\right] + \sum_{j=1}^{n}\left[\prod_{i=1}^{m}\left(\sum_i S^i_{1\Sigma} + \right.\right. \quad (9)$$

$$\left.\left. \sum_i S^i_{2\Sigma} + \sum_i S^i_{3\Sigma} - \sum_i S^i_{2\Delta} - \sum_i S^i_{2\Delta}\right)\right]$$

The correlation function is determined as a mean-value with respect to product of signals proportioning to the gain of the antennas G_1 and G_2

$$B(\tau) = S_1(t)S_2(t) \quad (10)$$

The $B(\tau)$ has to be presented as a product of amplitude $B_a(\tau)$ and phase $B\varphi(t)$ fluctuations [1–3]

$$B(\tau) = \overline{S}^2\left(1 + \frac{Ra}{4} + \sum_{n=2}^{\infty}\frac{[(2n-3)!!]^2 Ra^{2n}}{2^{2n}(n!)^2}\right)\times$$

$$e^{-2\sigma^2_\varphi[1-R\varphi]}\cos\omega_0\tau \quad (11)$$

Then the gain loss for RI antennas with multi-beam RP is determined through relative stationary in time value ΔG^{RI}_{GA}, according to [1-3]

$$\Delta G^{RI}_{GA} = \frac{\overline{S}^2\left(1 + \frac{Ra}{4}\sum_{n=1}^{\infty}\frac{[(2n-3)!!]^2 Ra^{2n}}{2^{2n}(n!)^2}\right)}{\ln D/D_0}\times$$

$$\times e^{-2\sigma^2_\varphi[1-R\varphi]}\cos\omega_0\tau \quad (12)$$

where D and D_0 – relative sizes of irregularities scales in scatering tropospheric volume [1–5].

It has been also established that in the event signals S_1 and S_2 at the input of TSC system with two-element RI are distributed accoding to Rayleigh law, at adder receivers outputs (see Fig. 1) the following distributions laws will occur: for difference components — a generalised Rayleigh law [1–3], and for sum component — thee parametric one [1–3].

Now according to (1–5) it is necessary to evaluate a power quick fading margin in TSC system with RI. For this it is necessary to obtain an integral distribution law for total (sum) power being intercepted by two element RI aperture in 10, 50 and 90 % of observation time with respect to the level of a long-term median [1–3] as follows

$$P(0<W_\Sigma<t) = \int_0^t P(W)dW = C\int_0^t e^{-\frac{W}{2\delta^2}}W^{-1}dW \quad (13)$$

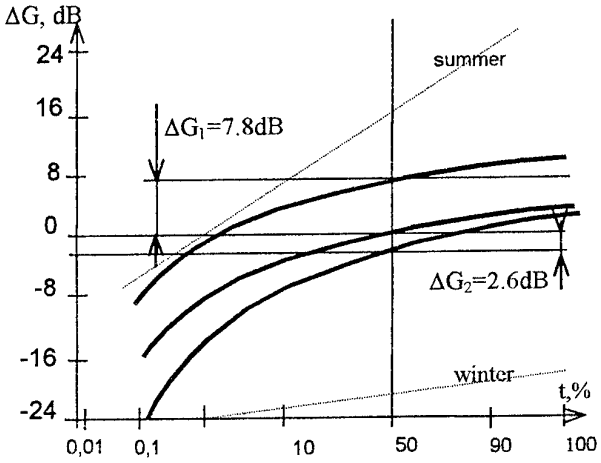


Fig.2. An advantage in signal level with respect to long-term median

The calculation results are shows in Fig. 2. The values ΔG_1 end ΔG_2 present an advantage in sum signal level

obtained automatically with respect to the level of long-term median, that is distributed according to Rayleigh law for quick fading in TSC systems with two-element RI, ensuring 4-order angle diversity in azimuth and tilt planes [1-3]. This advantage in mentioned time observation slots is 2.6 – 7.8 dB for quick fading [1–3]. Calculating the information reliability with respect to the condition (1) it has been taken into account that for every of the receiving diversity channels quick fading are described by Rayleign distribution law for envelopes of sum signals being received. In this case condition (1) is true for calculated data shown in Table 1.

Table 1

Evaluation of informational reliability for TSC systems with two-element RI

№	TSC system type	TSC systems without RI $Y<Y_{cirti}$	TSC systems with RI $Y<Y_{criti}$
1	AN/TRC-66	8.63<5.12	9.82<11.7
2	AN/TRC-66A	16.45<20.85	17.60<30.4
3	AN/TRC-80	7.04<6.05	8.13<10.4
4	AN/TRC-90	18.3<15	19.5<21.9
5	AN/TRC-90A	12.85<10.70	14.0<15.0
6	AN/TRC-90B	20.18<17.98	21.3<26.8
7	AN/TRC-97	3.77<7.83	11.5<16.7
8	H-3112/N-3122	21.52<20.9	23.5<27.5
9	FM 1970	21.59<21.9	21.6<21.9

CONCLUSION

The formalization of correlation between fading margin (quick fadings) and antennas gain loss in TSC systems has been based on the correspondence of receiving mode with definite channel number to signal receiving for RI with multibeam RP whose antennas A_1 and A_2 have an integral directivities each greater then RP of separate antennas A_1 and A_2 due to directivity increase of RI RP lobes.

REFERENCES

1. Rudakov V. I., Loman V.I., Nystyrenko I.K. Method of struggle with fadings signals in radio links TSC, Aut. sert.№4431247/09/061357, KHMS, Kiev, 1989, [in Russian].
2. Rudakov V.I., Galkin A.P., Aut. sert. №118791, VPI., Vladimir, 1978 [in Russian].
3. Galkin A.P., Rudakov V.I., Tarakankov S. P., Aut. sert., №114561, VPI, Vladimir, 1978 [in Russian].
4. Rudakov V.I. On possiblity of using phase array of tropospheric scatter communication systems, STC, LETI, issue 7, Leningrad, 1977 [in Russian].
5. Rudakov V.I. Determination of the optimum radiation patterns of antennas of troposheric-scatter comunication systems, STC, LETI, issue 8, Leningrad, 1978 [in Russian].

FEATURES OF RADIATION FIELD FORMATION OF MULTIBEAM REFLECTOR ANTENNA

A. A. Savochkin

Sevastopol State Technical University,
Streletskaya bukhta, Sevastopol-53, 335053, Ukraine
Ph: +38(0692) 23-51-52, e-mail: rt.sevgtu@stel.sebastopol.ua

INTRODUCTION

Development of communication and broadcasting satellite systems all over the world is a spesific characteristics of the last decade. It resulted in appearance of system with multiple application of frequencies and systems with channels separation on the basis of spatial selection. So, for example, receiving satellite television broadcasting there are two interesting practical situations such as:

- Receiving of TV broadcasting signals from two or more satellites on one multibeam antenna (the angular separation of radiation pattern (RP) maxima is usually insignificant). The solution of such a problem is possible with the use of a reflector parabolic antenna with offset feeds displaced in relation to the focal point.
- Receiving of TV broadcasting signals from one satellite, but in two various ranges, for example Ku-range (10.7... 12.7 GHz) and C-range (3.6... 4.2 GHz). In this case a reflector parabolic antenna is widely used. In the focal area of such an antenna there are two independent feeds for operation in two various ranges. These feeds are offset ones in relation to the real focal point of the antenna.

The development of such antennas and the investigation of their radiation features represent rather urgent problem. This paper is devoted to the problem solution.

BASIC PART

The analysis of multi-beam reflector antennas in the first approximation can be carried out, considering radiation features of separate reflector antennas with the appropriate arrangement of feeds in relation to the reflector focal point. But for this purpose it is necessary to realize a mathematical model of the antenna taking into consideration possible offsets of the feed with respect to the focal point.

Improvement of reflector antennas engineering promotes the favours development of analysis methods of such systems. Today there are many methods for calculation of reflector antennas. Among them we can highlight the surface currents method (SCM) (or the current method). It is used jointly with an approximation of physical optics, according to which the currents on " illuminated" part of the reflector surface are calculated by the following expression

$$\bar{J}_S = 2\left[\bar{n}_0, \bar{H}\right],$$

where $\bar{n}_0$ is the normal unit vector to the reflector surface; $\bar{H}$ is the magnetic component vector of the feed field near the reflector surface.

According to SCM electrical components of the field in the far-field zone are determined by the expression

$$\bar{E} = -j\omega\mu\frac{e^{-jkr}}{4\pi r}\int_S \left[\bar{r}_0, \left[\bar{r}_0, \bar{J}_S\right]\right] \exp\left[jk\left(\bar{r}_0, \bar{r}_s\right)\right] dS, \quad (1)$$

where ω is the circular frequency of electromagnetic oscillations; μ is the magnetic permeability of a medium; $k = 2\pi/\lambda$ is the wave number; λ is the wave length; r is the length of the radius-vector of the observation point; $\bar{r}_0$ is the unit vector of the observation point; $\bar{r}_S$ is the radius-vector of the reflector surface point; S is the reflector surface.

Taking into account a lot of characteristic properties of multibeam reflector antennas, SCM is more suitable for calculation of such antennas.

Note, that the solution of the problem is complicated by the following conditions:

- in calculation it is necessary to use several coordinate systems (a system connected with the reflector axes, a system connected with the feed, a system of the observation point);
- the integration (1) generally should be carried out in nonsymmetric limits (i.e. the equation of the reflector edge is to be determined).

However, from the author's point of view the system connected with the reflector axes is more convenient for the integration (1), owing to that in this case it is not required to recalculate the reflector surface element, only the reflector and the normal vector features are to be recalculated. The integration is carried out within constant limits.

The geometry of the described problem is shown in Fig. 1, where: Δ_1 is the value of orthogonal offset of the feed; Δ_2 is the one of axial offset. Thus, the surface point of the reflector is described by the coordinates (θ;

φ; ρ) in the axial system and (θ*; φ*; ρ*) in the system of the feed. Therefore, it is required to establish correlation of these systems (see Fig. 2).

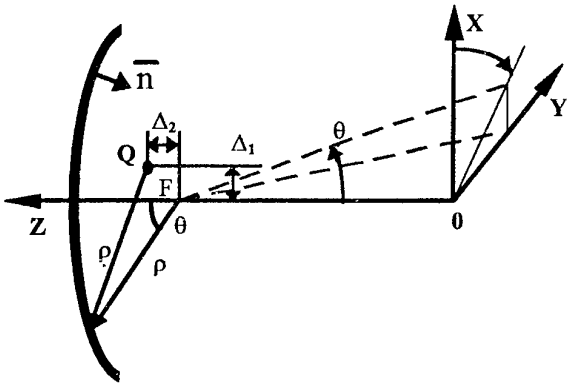


Fig. 1. Scheme of feed offset

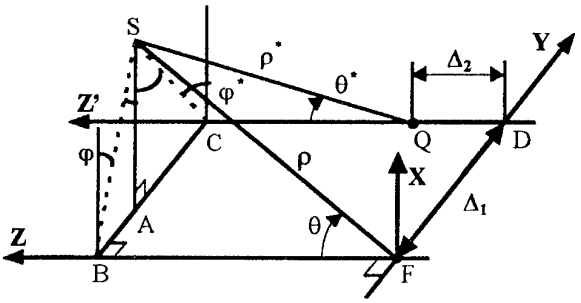


Fig. 2. On calculation of coordinates correlation

According to Fig. 2 one can determine coordinates of an arbitrary point of the reflector surface for the feed system as follows

$$\rho^* = \sqrt{(\rho\cos\theta - \Delta_2)^2 + (\rho\sin\theta)^2 + \Delta_1^2 - 2\Delta_1\rho\sin\theta\sin\varphi};$$

$$\theta^* = \arccos\frac{\rho\cos\theta - \Delta_2}{\rho^*};$$

$$\varphi^* = \arccos\frac{\rho\sin\theta\cos\varphi}{\sqrt{(\rho\sin\theta)^2 + \Delta_1^2 - 2\Delta_1\rho\sin\theta\sin\varphi}},$$

where $\rho = 2f/(1 + \cos\theta)$; f is the focal distance of the parabolic reflector.

While calculating the distribution of the surface current density it is necessary to determine the magnetic component vector of the field created by the feed near the reflector surface. For this we need to know polarization characteristics of the feed.

For a horn antenna feed the polarization characteristic is assumed equivalent to Huygens's element. Then, for field polarization along the X in the accepted systems (see Fig. 1), it is possible to note an expression for the feed field in the far-field zone

$$\overline{E} = E_0\, e^{-jk\rho^*} F\left(\theta^*, \varphi^*\right)\left(\overline{\theta}\cos\theta^*\cos\varphi^* - \overline{\varphi}\sin\varphi^*\right), \quad (3)$$

where E_0 is the maximum value of the field density created by the feed in the far-field zone at the distance ρ^*; $F(\theta^*;\varphi^*)$ is the normalized amplitude of the feed pattern.

In this paper the case of the antenna feed as an uniform round platform is considered. The feed pattern is calculated on the basis of Kirchhoff's formula with account of reflectivity from aperture. [1]. In a first approximation such a technique allows to consider a wide class of aperture feeds with a round aperture (a conic horn, an open-ended circular waveguide).

According to [2], the value E_0 is determined as follows

$$E_0 = \frac{1}{\rho^*}\sqrt{60\, P_\Sigma\, D_O},$$

where P_Σ is the entire power of the feed; D_O is the directivity factor of the feed.

For the described feed the distribution of surface currents is determined by the expressions:

$$\left.\begin{aligned} J_{x,y,z} &= \frac{\sqrt{60P_\Sigma D_{ОБЛ}}}{\rho^*}\exp\left(-jk\rho^*\right)F\left(\theta^*,\varphi^*\right)f_{x,y,z}; \\ f_x &= \sin\frac{\theta}{2}\sin\varphi\sin\theta^*\sin\varphi^* + \cos\frac{\theta}{2}\cos\theta^*; \\ f_y &= -\sin\frac{\theta}{2}\cos\varphi\sin\theta^*\sin\varphi^*; \\ f_z &= -\sin\frac{\theta}{2}\cos\varphi\cos\theta^*. \end{aligned}\right\} \quad (4)$$

From (1), (2) the analytical expression for radiation field of reflector is obtained:

$$\overline{E} = -j\omega\mu\frac{\exp(-jkr)}{4\pi r}\left[\overline{r}_0,\left[\overline{r}_0,\overline{I}\right]\right];$$

$$I_{x,y,z} = \sqrt{60P_\Sigma D_{ОБЛ}}\,2f^2\int_0^{2\pi}\int_0^{\theta_0}\frac{F(\theta^*,\varphi^*)}{\rho^*}f_{x,y,z}\frac{\sin\frac{\theta}{2}}{\cos^4\frac{\theta}{2}}\times$$

$$\times\exp\left\{jk\rho^*\left[\sin\theta^*\sin\theta'\cos\left(\varphi^*-\varphi'\right)-\cos\theta^*\cos\theta'-1\right]\right\}d\theta d\varphi,$$

where θ_0 is the coordinate of the reflector edge in the axial coordinate system.

The presented model enables to determine radiation characteristics of reflector antennas in an arbitrary point of space, but usually the pattern section in the offset plane of the feed is of the most interest because this section is characterized by more significant values of RP distortions.

On the basis of the presented procedure the special program with calculation of radiation features was created in the Visual Fortran 5.0 language.

In the paper as an example the reflector antenna is represented wich the following values of parameters,

describing the geometry of the system: F = 0.495 m; λ = 0.0265 m; the aperture diameter D_a = 1.09 m. The results are given for the case of the orthogonal offset (modification Δ_1) and for the axial offset of the feed (modification Δ_2).

CONCLUSION

From author's point of view the presented technique of the radiation features analysis of reflector antennas can be used at the development and the research of multi-beam reflector parabolic antennas, including reflector antennas with small offset of the pattern maxima and reflector antennas intended for operation in various ranges.

REFERENCES

1. Microwave antennas and devices. Calculation and projection of antenna arrays and their radiating elements / Edited by. D.I.Voskresenkij. -Moscow: Sov. radio, 1972. -320 p.

2. Ajzenberg G.Z., Iampolskij V.G., Tereshin O.N. UHF Antennas - Moscow: Svyaz, 1977. -672 p.

EARTH STATION ANTENNA POSTS, CREATED BY DESIGN OFFICE "PROMIN"

V. H. Syrotyuk, V. S. Pynylo, H. P. Khymych

Ternopil State Design Office "Promin"
38, Tekstylna vul.,Ternopil,Ukraine
Tel/fax /0352/22-75-03

In the process of development of mobile telecommunication systems a specific aggregate, namely, an antenna post, has been constructed. The antenna post comprises feed, receive-transmitt, control, life supporting, guidance and energy supply subsystems.Depending on purpose tasks the number of subsystems is changed.

Ternopil State Design Office "Promin" in cooperation with the Laboratory of Antennas and Telecommunications of the National Technical University of Ukraine "KPI" have created and tested antenna posts for earth stations of different types in C- and Ku- band.

The design is based on a modified dual reflector Cassegrain antenna. To meet the INTELSAT/EUTELSAT requirements concerning with radiation patterns at a principal and cross polarization the synthesis of amplitude and phase field distribution at aperture of the main reflector has been realized.

At present the following projects have been realized by the Design Office "Promin":

1. Antenna posts with the main reflector of diameter 12 m and 7 m for central earth stations of satellite telecommunication systems.

2. Antenna posts with the main mirror diameter 5 m and 3.66 m for operation in regional receive and transmit earth stations.

3. Offset antenna posts with reflectors of equivalent diameter 2.4 m and 1.8 m for operation in regional and customer earth stations or points of the satellite telecommunications. This class of antennas is developed in a single and dual reflector variants.

4. Guidance systems, tracking and control systems are realized on the modern element basis with a computer information processing including self-diagnosis of executive mechanisms and a whole system.

Concerning an antenna system with reflector diameter equivalent to 2.4m, it should be noted that the antenna was designed and developed by the dual reflector Gregory type scheme, as well. This antenna type allows to decrease cross-polarization radiation level to –35 dB (single reflector antenna only to –28 dB). Radiation pattern of such antenna ensures the required INTELSAT/EUTELSAT standards. Field distribution at the reflector aperture is asymmetric, thus to reduce cross-polarization component, created by the asymmetric main reflector and sub-reflector, the known condition was used.

As can be seen in Fig. 1 in order to to reduce the offset angle Qd of the main reflector one can increase the aperture angle 2Q3m.

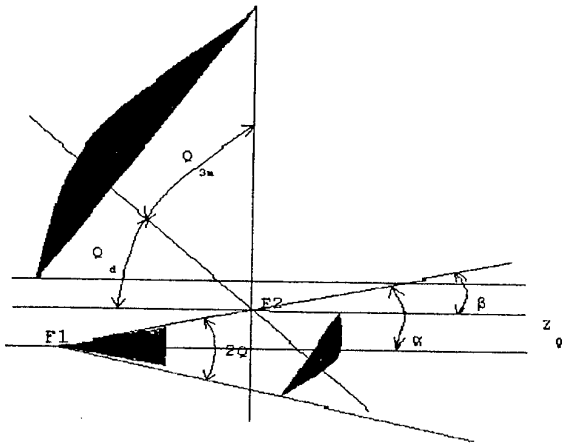


Fig. 1

Unlike Cassegrain scheme, the Gregorian scheme has sub-reflector with real focus and gives the following advantages:

- one can increase the sub-reflector size, that will cause reduction of spill over the edges of the main reflector and sub-reflector,
- ability to correct phase center shift of primary feed in regard to frequency and provide a large operating bandwidth.

The primary feed is a corrugated feed that provides in a wide frequency range a symmetric radiation pattern with low side lobe level, low cross-polar radiation level (less than minus 40 dB) and absence of phase center astigmatism.

According to the design a primary feed is movable on the main bar relative to the sub-reflector. The sub-reflector is a synthesized quasiellipsoid, which is movable relative to the main reflector and the primary feed. The main reflector is made of four steel panels, providing antenna installation on high buildings without any lifting mechanisms usage. An independent hanging fastening system of the power bar with the secondary

Table 1

Performance specifications	Antenna diameter				Table 1	
Electrical	1.8 m	2.4 m	3.6 m	5.0 m	7.0 m	12.0 m
Frequency, 3.625–4.225GHz			yes	yes	yes	yes
5.925-6.425 GHz			yes	yes	yes	yes
8.0 – 8.4 GHz				yes	yes	
10.7 – 12.75 GHz	yes	Yes	yes	yes	yes	yes
14.0 – 14.5 GHz	Yes	Yes	yes	yes	yes	yes
12.75-13.5 GHz			yes	yes	yes	
17.3-18.1 GHz			yes	yes	yes	
17.3- 21.3 GHz			yes	yes		
29.0-30.0 GHz			yes			
Midband Gain ($\pm$ 0.2 dB)						
3.625-4.225 GHz			41.4 dBi	43.8 dBi	46.8 dBi	51.3 dBi
5.925-6.425 GHz			45.6 dBi	48.0 dBi	51.2 dBi	53.6 dBi
8.0 – 8.4 GHz				50.8 dBi	53.9 dBi	
10.7-12.75 GHz	44.8 dBi	47.5 dBi	50.9 dBi	53.1 dBi	56.5 dBi	60.9 dBi
14.0-14.5 GHz	47.2 dBi	49.7 dBi	53.1 dBi	55.5 dBi	58.9 dBi	62.8 dBi
12.75-13.5 GHz			52.2 dBi	54.9 dBi	57.9 dBi	
17.3 – 18.1 GHz			55.1 dBi	57.8 dBi	60.3 dBi	
17.3 – 21.3 GHz			55.4 dBi	58.0 dBi		
29.0 – 30.0 GHz			59.3 dBi			
Antenna noise temperature						
10 elevation, K (receive)	< 50	<50	< 50	< 50	< 70	< 70
VSWR	1.3 : 1 Max.					
Cross- Polarization	- 30 dB	- 30 dB	-35 dB	- 35 dB	- 35 dB	- 35 dB
Side lobe Envelope , Co-Pol						
$1^0 < \Theta < 20^0$	29 – 25 Log Θ dBi					
$20^0 < \Theta < 26.6^0$	- 3.5 dBi					
$26.6^0 < \Theta < 48^0$	32 – 25 Log Θ dBi					
$\Theta > 48^0$	- 10 dBi					
Polarization	Orthogonal linear, orthogonal circular					
Antenna Optics	Offset	Offset				
Mechanical						
Mount type	Elevation over azimuth					
Reflector material	Steel	Steel	Aluminium			
Elevation range	+5...+45	+5...+45	0...45	5...70	0...+85	0...90
Elevation tracking					+/- 14	
Azimuth range	+/- 70	+/- 70	+/- 170	+/- 70	+/- 105	+/- 270
Azimuth tracking	+/- 10	+/- 10	+/- 15		+/- 15	
Weight of antenna, kg	150	220	450	1500	11930	22000
Antenna type	prime focus, Gregory		Dual –reflector shaped Cassegrain			
Control	Elevation and azimuth jacks Remote control unit .Step-track servo system					
Environmental performance						
Wind loading operational	108 km/h	108 km/h	108km /	108 km/h	90 km/h	90 km/h
Survival	180 km/h					
Temperature	-50^0 C ... +55^0 C					

antenna system is realized (Fig. 2). This design approach allows removal of the load and deformation of the main reflector.

Main technical specifications of the antenna posts are presented in the Table 1. There is information about Ka-band antenna system in the Table 1, as well. It should be noted, that making the antenna posts for

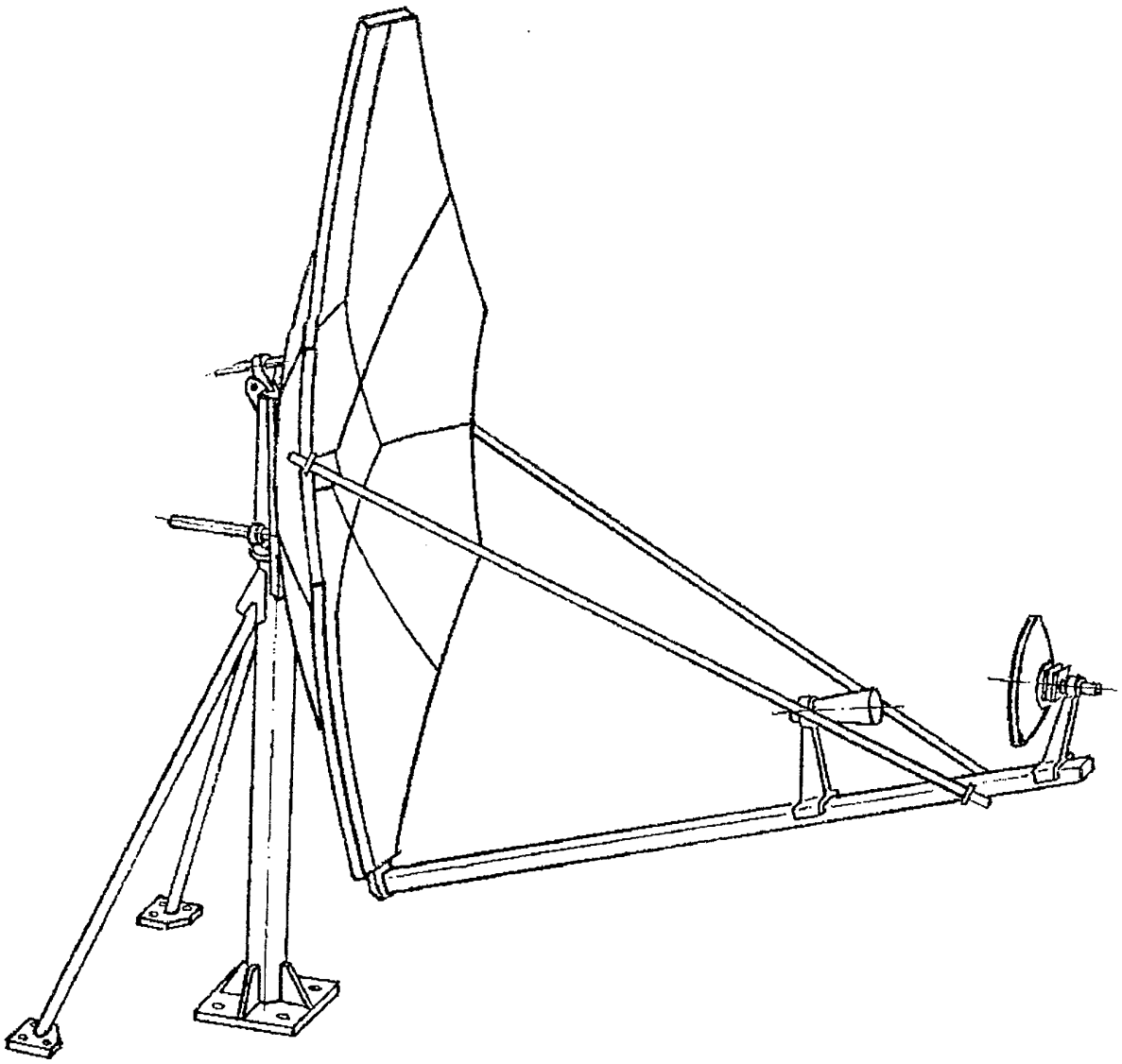


Fig. 2

operation in this perspective frequency band is connected with some difficulties in fabrication of main reflectors, providing accuracy of their reproduction and adjustment. In Ku-band the RMS deviation of the main reflector profile 0.25-0.3 mm from theoretical is acceptable, while in Ka-band RMS 0.15 mm is required. This requirement puts forward corresponding requirements on reflector design, technologies of its production. At present the Design Office "Promin" has developed a documentation and directive technology for the antenna system with the main reflector diameter 3.66 m for operation in Ka-band. Besides a corresponding technological equipment providing necessary accuracy for the main reflector production has been fabricated. Also, the works on the production of the antenna system itself have been started.

UNDERGROUND PHASED ANTENNA ARRAYS AS ALTERNATIVE TO MAST AERIALS OF RECEIVING RADIO

S. M. Alekseev, A. V. Makaseev, A. G. Poshkov, B. V. Sosunov, N. G. Fitenko

St. Petersburg department of state communication inspection military telecommunication university
194064, St. Petersburg, Tikhoretsky prospekt, 3,
tel. 556-93-95, fax. 325-80-39, E-mail: sosunov@dom.spb.ru

Signal and noise power ratio at the receiver input is defined by known expression:

$$\frac{P_c}{P_{uu}} = \frac{\Pi}{\kappa \cdot \Delta f}\left[\frac{\lambda^2 D \xi_n \cdot F^2(\theta,\varphi)}{4\pi\left(T_я + T_0\dfrac{1-\eta_a\eta_\phi}{\eta_a\eta_\phi} + T_{np}\dfrac{1}{\eta_a\eta_\phi\xi_c}\right)}\right], \quad (1)$$

where k = 1,38·10^{-23}W/(Hz·K^0) — a Boltzmann constant; Δf — a frequency band; Π — a Pointing vector value of an incident wave; λ — a wavelength; $F^2(\theta,\varphi)$ — a normalized antenna pattern by power in the direction of the wave arrival with angles of azimuth φ and elevation θ; ξ_n — a polarizing transfer coefficient by power; ξ_c — coefficient of antenna and load matching by resistance; η_a, η_f — antenna and feeder efficiency; D — directivity; $T_я$ - a temperature of external sources of noise; T_{np} - a noise temperature of the receiver; T_0 = 293° — a standard temperature.

The requirements on the maximal coverage scope of frequency bands and receiving angles lead to the necessity to use a set of antenna types with various standard sizes occupying (taking into account existing norms) antenna fields of a significant area (up to 10 hectares and more).

The possibility of creation of antennas meeting the stated requirements with small sizes is based on use of new technical designs. They are characteristic for a class of underground antennas (UA) which have found application in a number of special areas of radio communication.

It is of fundamental importance in comparison with usual upsurface antenna that UA reacts both on horizontally polarization wave and on the field with a vertical polarization. Thus, it appears to be a universal antenna for receiving waves with an arbitrary polarization.

The disadvantage of UA is their smaller efficiency that is caused by a set of factors connected with the features of operation under a layer of the ground.

A minimal allowable efficiency of the receiving antenna-feeder path may be defined if the required signal/noise ratio is referred to one provided by an ideal antenna-feeder arrangement (AFA), for which, as the $\eta_a = \eta_f = \xi_c = 1$, it follows from expression (1):

$$\left(\frac{P_c}{P_{uu}}\right)_0 = \frac{\Pi\lambda^2 D}{4\pi\kappa\Delta f\left(T_я + T_{np}\right)} . \quad (2)$$

When designing a real antenna, allowable value of signal/noise ratio deterioration should be given at the expense of a mismatch and losses in AFA:

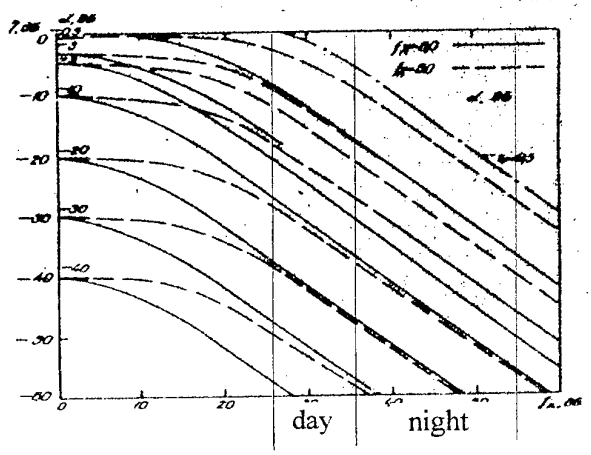
$$\alpha = \frac{P_c / P_{uu}}{\left(P_c / P_{uu}\right)_0} . \quad (3)$$

The value of coefficient α stipulates the requirement to a minimally allowable efficiency of the receiving antenna, obtained from the formulas (1-3):

$$\eta_{don.} = \frac{\alpha\left(T_0 + T_{np}/\xi\right)}{\alpha T_0 + T_{np}\left(1-\alpha\right) + T_{np}} . \quad (4)$$

For smaller efficiency the signal/noise ratio at the receiver input will be worsened.

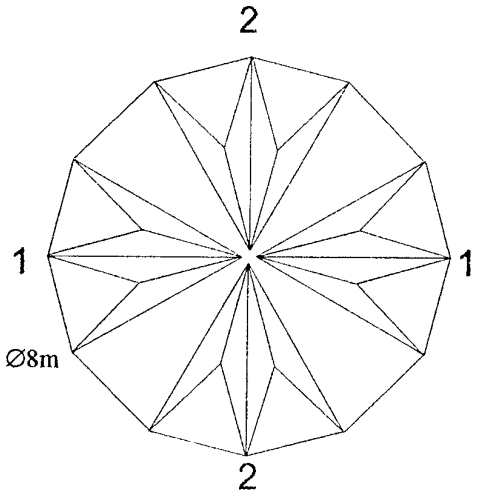
Let us consider the dependence of receiving antenna efficiency on a relative level of external noise ($F_a = T_я/T_0$) at different α values calculated using expression (4). The solid curves correspond to a receiver with a high sensitivity ($T_{np} = 6T_0$), dash curves – to a receiver with a small one ($T_{np} = 60T_0$). A dash-dot curve illustrates the influence of the lowered antenna matching with a receiver raising requirement to efficiency.

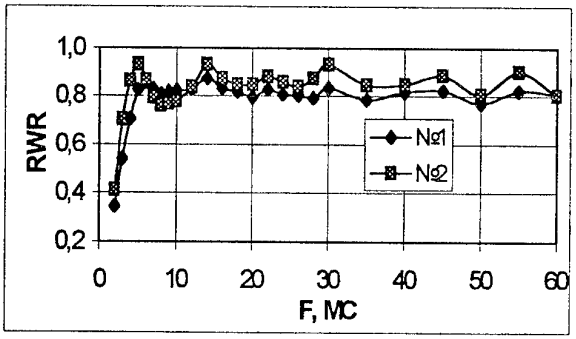


The plot allows to determine allowable values of receiving antenna efficiency in various interference

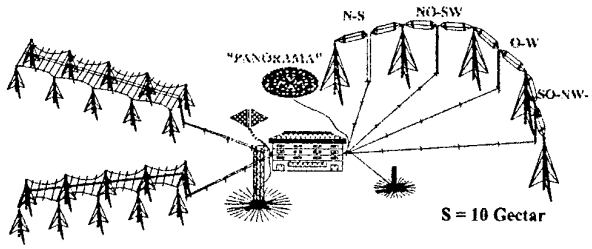
situations when the parameters α are given. The vertical lines set aside the areas of typical f_a values in a HF band for day and night conditions. For example, for α = -3 dB at daytime the efficiency should be not less that –17 dB.

The developed UA represents two orthogonal vibrators. Its wide band and lowered losses are provided by the arrangement of arms from several conductors radiating outwards like a fan at the angle of 60°, the external ends of the conductors being connected by the ring shunt.

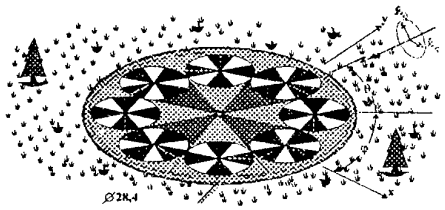


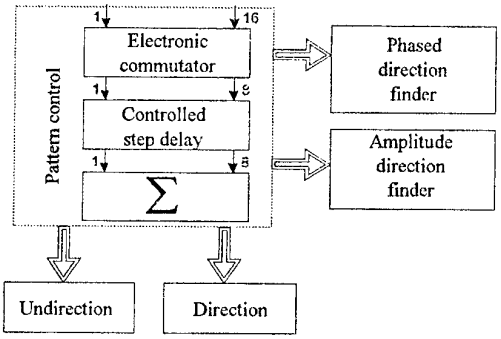


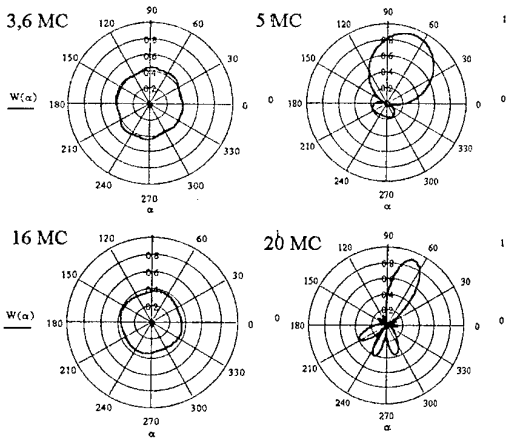
Provision of UA electronic control with a high efficiency are achieved by application of phased antenna arrays on the basis of the described element.



The phased array "Panorama", satisfying the listed requirements, is created. The platform required for accommodation of "Panorama" is less 900m^2, so significant economy of ground resources is created in such a way. There is no need in service during a guarantied (15-20 years) service life.







THE ANALYTICAL APPROACH TO THE COMPUTING OF RESONANCE EFFECTS FOR THE DIFFRACTION AT WELL REFLECTING GRATINGS

N. A. Balakhonova, A. V. Kats, I. S. Spevak

Kharkiv Military University,
e-mail: jenya<pinvest@ mailbox.Kharkov.ua>
P.O. Box 8847, 310002 Kharkiv, Ukraine. Tel.: +380 572 43-27-90 (home), 40-28-73 (office)

The electromagnetic radiation scattering by diffraction grating possesses many peculiarities under condition of resonance diffraction $|\vec{k}_t + m\vec{g}| \approx k$, where $\vec{g}$ is the grating wavevector, $\vec{k}_t$ is tangential wavevector's component of the incident wave, m is integer. E.g., these are great increase of the resonance spectra amplitude, transformation of polarization, suppression of specular reflection. These phenomena have the same nature as well-known Wood anomalies, and they are caused by resonance of the grazing spectra and eigenmode of a highly conductive surface — the surface electromagnetic wave (SEW). Many works in recent years have been devoted to experimental and theoretical investigations of resonance diffraction (see, e.g., [1-3]). In order to explain strong resonance effects complicated numerical calculations are used [4, 5]. The essential simplification is made in this paper. It is based on modified perturbation theory (see [6, 7]).

GENERAL DESIGNATION

Let a plane electromagnetic wave

$$\vec{E}(\vec{r},z,t) = \vec{E}\exp[\mathrm{i}(\vec{k}_t\vec{r} + k_z z - \omega t)], \qquad (1)$$

be incident upon the surface $z = \zeta(\vec{r})$, where $\zeta(\vec{r}) = \sum_{m=-\infty}^{\infty}\zeta_m[\exp(\mathrm{i}\,m\vec{g}\vec{r})]$, $\vec{r} = (x,y)$, the axis z is directed inside the material. The dielectric constant $|\varepsilon| >> 1$ and the surface impedance $\xi = 1/\sqrt{\varepsilon} = \xi' + i\xi''$ ($\xi' > 0$, $\xi'' < 0$) modulus is very small for the highly conducting surfaces. Total field $\vec{E}$ above the surface $z = \zeta$ may be represented as a sum of the incident $\vec{E}(\vec{r},z,t)$ and diffracted waves.

$$\vec{E}_m(\vec{r},z,t) = \vec{E}_m\exp[\mathrm{i}(\vec{k}_{mt}\vec{r} + k_{mz}z - \omega t)]. \qquad (2)$$

Here $\vec{k}_{mt} = \vec{k}_t + m\vec{g}$, $k_{mz} = \sqrt{k^2 - k_{mt}^2}$, $k = \omega/c$, $\mathrm{Re}(k_{mz})$, $\mathrm{Im}(k_{mz}) \le 0$ due to the radiation conditions; index $m = 0$ corresponds to the mirror reflected wave, $k_{0z} = -k_z$.

Each of the waves can be represented as a sum of linearly polarized components: $\vec{E}_n = \sum_{\sigma=\pm}\vec{e}_n^{\sigma}E_n^{\sigma}$. Here $\vec{e}_n^{+}$ is polarization ort in the n-th wave propagation plane $(\vec{e}_z, \vec{k}_n)$ and $\vec{e}_n^{-}$ is the one perpendicular to it. The polarization amplitudes are linear functions of the incidence wave polarization components: $E_n^{\sigma} = \sum_{\sigma'=\pm}R_n^{\sigma\sigma'}E^{\sigma'}$. From the impedance boundary conditions on the surface $z = \zeta$ and Maxwell equations one obtains infinite set of linear equations for the transformation coefficients $R_n^{\sigma\sigma'}$

$$\sum_{m,\sigma'}D_{nm}^{\sigma\sigma'}R_m^{\sigma'\sigma''} = V_n^{\sigma\sigma''},\ n = 0, \pm 1,\ \pm 2, \ldots. \qquad (3)$$

The matrix elements $D_{nm}^{\sigma\sigma'}$ and right-hand side coefficients $V_n^{\sigma\sigma'}$ are expressed as grating depth power series. If resonance doesn't occur expansion of diagonal (both in the diffraction order numbers and polarization indices) elements of the matrix starts from the value of the order of unity: $D_{nn}^{--} = \beta_n + \xi_0$, $D_{nn}^{++} = 1 + \beta_n\xi_0$. Non-diagonal ones $D_{nm}^{\sigma\sigma'}$ are linear in ζ, $D_{nm}^{\sigma\sigma'} \sim \zeta_{n-m}$. Here the $\beta_n = -k_{nz}/k$ are propagation constants, $\mathrm{Re}(\beta_n) \ge 0$, $\mathrm{Im}(\beta_n) \ge 0$. The resonance appears when for one of the diffracted waves, e.g. the r-th one, $|D_{rr}^{--}| = |\beta_r + \xi_0| << 1$. If resonance doesn't occur, all non-diagonal elements of the matrix are small in comparison with diagonal ones. Thus the system solution can be represented as power series of grating depth. In resonance occurrence the series begin to diverge even for the small depth value. However, if one exploits both grating depth and impedance smallness the solution may be obtained analytically in simple explicit form also for the resonance case (see [6, 7]).

RESULTS

Let us present the solution for the resonance diffraction, assuming that the grating is a harmonic one ($\zeta(\vec{r}) = a\cos(\vec{g}\vec{r})$, $a = 2\zeta_1 = 2\zeta_{-1}$, $2a$ is grating depth) and resonance occurs in the first order diffracted wave ($r = 1$). In the plane geometry case (the plane of incidence is perpendicular to grating grooves) the resonance takes place if incidencte wave has non-vanishing p component (in plane geometry the SEW is excited by p - polarization wave). The transformation coefficient are of the form:

$$R_1^{--} = -2i\kappa\mu/D, \quad R_0^{--} = R_0 - 2(\kappa\mu)^2/(D\beta_0), \qquad (4)$$
$$D = \beta_1 + \xi + (\beta_0^{-1} + \beta_2^{-1})\cdot(\kappa\mu)^2,$$

where $\kappa = g/k$, $\mu = ka/2$, $R_0 = (\beta_0 - \xi)/(\beta_0 + \xi_0)$.

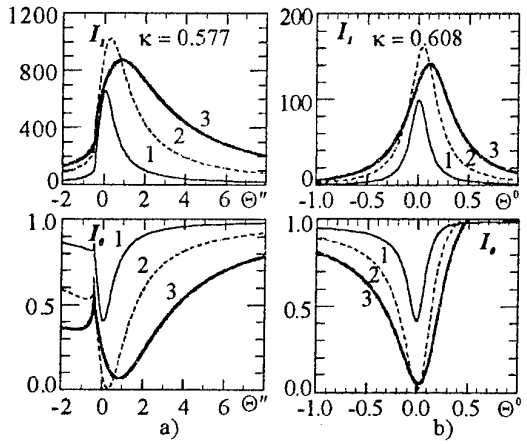


Fig. 1

The quantities $I_1 = \left|R_1^{--}\right|^2$ and $I_0 = \left|R_0^{--}\right|^2$ are proportional to the waves intensities. They are fast functions of the propagation constant β_1. Therefore, other variables, that describe diffraction can be assumed as constants. Thus the I_1 maximum corresponds to the denominator $|D|$ minimum with respect to β_1

$$\beta_1' = 0, \ \beta_1'' = -\xi'' + (\vec{\alpha}_1\vec{\kappa})^2 |\mu|^2 / \beta_2'', \qquad (5)$$

where $\vec{\alpha}_m = \vec{k}_{mt}/k$. The expression (5) represents the resonance condition which is written for arbitrary oriented grating, for plane geometry $(\vec{\alpha}_1\vec{\kappa}) = \kappa$. The condition (5) is close to the transformation coefficient branch point: $\beta_1 = 0$ and $\theta = \theta_0$, $\sin\theta_R = 1 - \kappa$, corresponding to the Rayleigh anomaly because of the small values of the grating depth and impedance. The peak of I_1 on the resonance curve (5) depend nonmonotonously on the grating depth and reaches it's maximum value for $a = a_{opt} = 2\sqrt{\xi'\beta_0}/g$.

Sharp increasing of I_1 influences nonresonance spectra, in particular the mirror reflected wave. If resonance doesn't occur, reflection coefficients from surface with small impedance are close to unity. In resonance case the total suppression of specular reflection (TSSR) may occur.

The condition of I_0 vanishing is equivalent to two real equations. One of them coincides with (5) and the other has the form

$$\xi' - (\kappa\mu)^2/\beta_0 = 0. \qquad (6)$$

It follows from the equation (6) that the TSSR condition corresponds to the same grating depth a_{opt} as I_1 maximum. For other values of a the mirror reflection suppression isn't complete, see Fig. 1. In Fig. 1 the I_1 and I_0 dependences on the angle of incidence $\Theta = \theta - \theta_0$ ($\theta_0 = 25°$) for different sinusoidal gratings on the Ag surface are presented. Cases à) and b) correspond to $\lambda = 10$ μm, $\xi = 8.8\cdot10^{-4} - 1.87\cdot10^{-3}\cdot i$, $a_{opt} = 0.156$ μm (Θ — in seconds of arc) and $\lambda = 632.8$ nm, $\xi = 5.54\cdot10^{-3} - 0.25\cdot i$, $a_{opt} = 23.5$ nm (Θ — in degrees). The curves 1, 2, 3 correspond to the grating depths $a_n = 0.5\cdot n\cdot a_{opt}$ for $n = 1, 2, 3$ respectively. The grating depth increasing, widths of the curves I_0 and I_1 increase. In the point $\Theta = \Theta_R = -\xi''^2/(2\cos\theta_0)$ corresponding to the Rayleigh's anomaly the curves have infinite derivatives, see Fig. 1,a). The Fig. 1,b) corresponds to greater value of $|\xi''|$ and therefore the Rayleigh's anomaly point $\Theta_R \approx -2°$ is not present at the plot.

In general geometry, i.e. for arbitrary grating orientation, the variation of the incident radiation wavelength (or angle of incidence, grating depth and period) leads not only to the fast changes in speculary reflected wave amplitude but to the fast polarization changes as well. The transformation coefficients describing the specular reflected wave take the following form:

$$\begin{aligned} R_0^{++} &= -1 + 2D^{-1}\beta_0\kappa^2|\mu|^2\sin^2\phi, \\ R_0^{+-} &= -R_0^{-+} = D^{-1}\kappa^2|\mu|^2\sin 2\phi, \\ R_0^{--} &= 1 - 2(\beta_0 D)^{-1}\kappa^2|\mu|^2\cos^2\phi, \\ D &= \beta_1 + \xi + (\vec{\alpha}_1\vec{\kappa})^2|\mu|^2\left(\beta_0^{-1} + \beta_2^{-1}\right), \end{aligned} \qquad (7)$$

where $\phi = \hat{\vec{k}_t\vec{g}}$ denotes the angle between vector $\vec{g}$ and the plane of incidence. The non-diagonal coefficients $R_0^{+-} = -R_0^{-+}$ describe transformation of polarization from p- to s- component and vice versa. We'll analyze the coefficient $\Re = |R_0^{-+}|^2$. $\Re$ is the function of two variables namely the angle of incidence θ and the angle ϕ, i.e. $\Re = \Re(\theta, \phi)$, Fig. 2[1], if wavelength and grating parameters (the depth a and period d) are

[1] Because lack of the space the calculation of the resonance conversion are presented for the optical range only. This allows to compare the calculations with experimental data [2]. With wavelength increase the results do not change qualitatively. The only thing that the impedance $|\xi|$ decrease causes is the resonance width decrease.

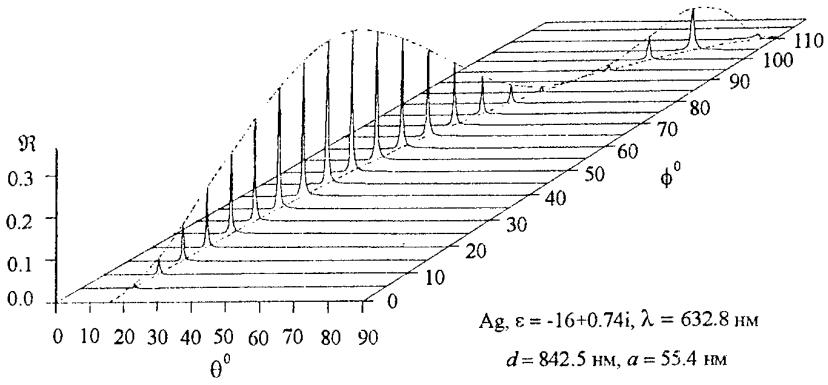


Fig. 2

fixed. The transformation coefficient has maximum at the line (5). Excluding the angle of incidence θ from $\Re(\theta,\phi)$ with the help of the approximate resonance condition (5) $\beta_1'' = -\xi''$, one obtains the maximum values of $\Re$ as the function of the grating orientation angle ϕ, $\rho(\phi) = \Re_{max}$, Fig. 3:

$$\rho(\phi) = |\mu|^4 [\xi' + B|\mu|^2]^{-2} \sin^2 2\phi, \qquad (8)$$

where

$$B = B(\phi) \equiv \frac{[\kappa \sin^2\phi + X\cos\phi]^2}{\sqrt{-(\xi'')^2 - \kappa^2\cos 2\phi + 2X\cos\phi}},$$

$$X = \sqrt{1 + (\xi'')^2 - \kappa^2 \sin^2\phi}, \quad \kappa = \lambda/d.$$

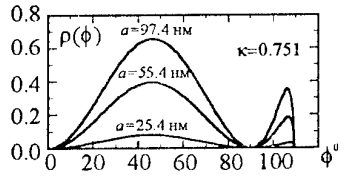


Fig. 3

The results of the conversion coefficient computing are presented in Figs. 2-4. The values of parameters correspond to the experiments [2, 4]. In the experiments the ϕ range was $0° \le \phi \le 90°$. Note, that results of our calculations are in excellent accordance with experimental data. The discrepancy is less than 1% without any fitting of the parameters. Note also that for $0° \le \phi \le 90°$ $B = B(\phi)$ is approximately constant and ρ behaves as $\rho \sim \sin^2 2\phi$. The effect of polarization conversion may be observed in the range $90° \le \phi \le 110°$ also (the upper ϕ value corresponds to the grazing angle of incidence and depends on $\kappa = \lambda/d$ value). In this range the $\rho = \rho(\phi)$ differs essentially from the $\sin^2 2\phi$ dependence due to changes in $B(\phi)$.

The monotonic increase of $\rho(\phi)$ with the grating depth increase is worth noting. The increasing is limited by saturation for $ka >> \xi_0'$.

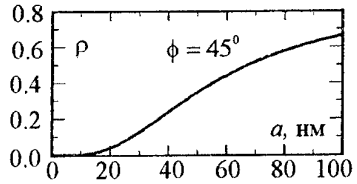


Fig. 4

CONCLUSIONS

The method presented allows to compute analytically the transformation coefficients $R_n^{\sigma\sigma'}$ and to investigate the strong resonance effects caused by SEW excitation on highly reflective surface. It is limited by small enough values of grating depth, but deals with arbitrary profile gratings. The results obtained are in good accordance with experimental data and allows to explain all patterns observed. The method allows to provide very simple calculations of various effects that makes it perspective for technical applications. Therefore, it is of interest for the designing of elements for receiving (transmitting) systems and radiation transformers with special properties, in particular, with to the wavelength, polarization and angle of incidence selectivity.

REFERENCES

1. Hutley M.C., Maystre D. // Opt. Commun. 1976. V. 19, № 3, P. 431-436.
2. Bryan-Brown G.P., Sambles I.R, Hutley M.S. // J. of Modern Optics. 1990. V. 37, N 7. P. 1227 - 1232.
3. E.G. Loewen, E. Popov. Diffraction gratings and applications. N-Y: Marcel Dekker Inc., 1997, 601 p.
4. Electromagnetic theory of gratings, Ed. by R. Petit Springer-Verlag, Berlin, 1980.
5. Elsten S.I., Bryan-Brown G.P., Sambles I.R. // Phys. Rev. B. 1991. V. 44, N 12. P. 6393 - 6400.
6. Kats A.V., Spevak I.S. . Diffraction of the electromagnetic waves. Kharkiv: KMU, 1998. 178 p. [in Ukrainian].
7. Kats A.V., Pavitskiy P. D. Spevak I.S. // Izv vuzov. Radiofizika. 1992. V. 35, № 3-4. pp. 234 – 245 [in Russian].

TWO-DIMENSIONAL IMAGE RETRIEVAL

K. P. Gaikovich, A. V. Zhilin

Institute for Physics of Microstructures RAS GSP-105,
Nizhny Novgorod, Russia, 603600, Nizhny Novgorod, Russia, 603600,
Phone: 8312 327920, Fax: 8312 675553, E-mail: gai@ipm.sci-nnov.ru

INTRODUCTION

Tikhonov's method is applied for the solution of image deconvolution inverse problem in two-dimensional case. It appeared possible to improve the resolution beyond the aperture limit. The case of many-beam synthetic aperture radiometers (SAR) measurements is also considered. The method is applied to improve the resolution of radiobrightness image of oil spills on lakes. Data have been obtained from helicopter-borne radiometer measurements of thermal radio emission. The problem of the retrieval of true radiobrightness distribution by two-dimensional distribution of measured antenna temperature is very important in radioasrtonomy as well as in remote sensing, especially in the case of SAR measurements. The antenna temperature distribution is a two-dimensional convolution of radiobrightness distribution and antenna pattern as a kernel of the integral. If the kernel is a known function, it is possible to formulate the deconvolution inverse problem to retrieve the true radiobrightness image by measured antenna temperature distribution.

The deconvolution inverse problem consists of the solution of Fredholm integral equation of the 1-st kind, and it is well known that this problem is ill-posed. To solve such a problem it is necessary to use additional (*a priori*) information about the exact solution. This information determines a regularization method. There are various approaches: statistical (maximum entropy) [1], iterative [2], singular systems analysis [3]. In the present paper Tikhonov's method of generalized discrepancy is applied, which uses the common information about the exact solution as a function [4]. It is supposed that the exact solution belongs to the set of square-integrable functions with square-integrable derivatives. The results of numerical simulation give us the retrieval accuracy at various levels of the refraction error.

PROBLEM FORMULATION

The relationship between antenna temperature and radiobrightness distribution can be written as

$$\mathrm{K_h}T_b = \int_{-\infty}^{+\infty}\int_{-\infty}^{+\infty} K_h(x-s,y-t)\,T_b(s,t)\,ds\,dt = T_a^{\delta}(x,y), \quad (1)$$

where $K_h(w,W)$ is the antenna pattern (kernel), T_a^{δ} is measured antenna temperature, and $T_b(s,t)$ is the radiobrightness to be found. The measure δ of the error of measured antenna temperature (measurement errors) and measure h of the kernel error satisfy to

$$\left\|T_a^{\delta}-T_a\right\|_{L_2}\le\delta,\quad \left\|\mathbf{K}-\mathbf{K}_h\right\|_{W_2^2\to L_2}\le h, \quad (2)$$

where T_a corresponds to the exact solution. According to generalized discrepancy method, the approximate solution T_b^{α} of equation (1) minimizes the generalized discrepancy functional

$$\mathbf{M}_{\alpha}[T_b]=\left\|\mathbf{K}_hT_b-T_a^{\delta}\right\|_{L_2}^2+\alpha\left\|T_b\right\|_{W_2^2}^2 \quad (3)$$

at the condition

$$\left\|\mathbf{K}_hT_b^{\alpha}-T_a^{\delta}\right\|_{L_2}^2=(\delta+h\left\|T_b^{\alpha}\right\|)^2.$$

The use of Fourier transform permits to obtain the exact solution of the convolution-type equations in the form:

$$T_b^{\alpha}(s,t)=\frac{1}{4\pi^2}\cdot \int_{-\infty}^{+\infty}\int_{-\infty}^{+\infty}\frac{\tilde{K}_h^*(\omega,\Omega)\tilde{T}_a^{\delta *}(\omega,\Omega)e^{i\omega s+i\Omega t}\,d\omega\,d\Omega}{L(\omega,\Omega)+a[1+(\omega^2+\Omega^2)^2]} \quad (4)$$

where

$$\tilde{K}_h^*(\omega,\Omega)=\tilde{K}_h^*(-\omega,-\Omega),$$

$$L(\omega,\Omega)=\left|\tilde{K}_h(\omega,\Omega)\right|^2,$$

$$\tilde{T}_a^{\delta}(\omega,\Omega)=\int_{-\infty}^{+\infty}\int_{-\infty}^{+\infty}T_a^{\delta}(x,y)e^{i\omega x-i\Omega y}\,dx\,dy, \quad (5)$$

$$\tilde{K}_h(\omega,\Omega)=\int_{-\infty}^{+\infty}\int_{-\infty}^{+\infty}K_h(u,w)\,e^{i\omega u-i\Omega w}\,du\,dw. \quad (6)$$

The main preference of Tikhonov's method consists of the uniform convergence of the retrieval error to zero at mean square convergence of measurement errors. The closed form of the exact solution (4) and the possibility

to use Fast Fourier Transform (FFT) codes permits to make very efficient algorithm. Its accuracy has been investigated in numerical simulations. It appeared possible to retrieve images beyond the aperture resolution limit.

RESULTS OF NUMERICAL SIMULATIONS

The most interesting results have been obtained in the case of image retrieval by multi-beam SAR data. For more compact presentation, an example was selected, in which two-beam antenna pattern $K_h(w,W)$ coincides with two-modal initial radiobrightness distribution $T_b(s,t)$. (see, in Fig. 1). In the Fig. 2 the corresponding distribution of antenna temperature distribution (observed image) $T_a(x,y)$ from (1) is given. It is possible to see that the two maxima of true T_b distribution are indistinguishable in observed image T_a.

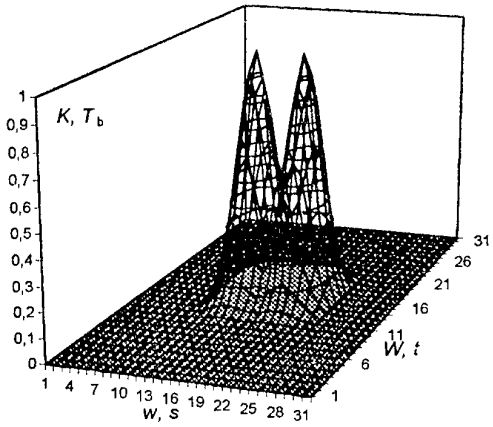


Fig. 1. Antenna pattern and initial radiobrightness distribution, in conventional units

The approximate solution (4) is shown in Fig.3,4 at two different values of simulated measurement error δ (with respect to T_a, in integral L_2 - space). The Tikhonov's method of image retrieval permits to distinguish two-modal structure of initial distribution even at comparatively low measurement accuracy.

There is an opinion that it is impossible to resolve two point sources if they are inside diffraction resolution limit because the spectra of real antennas are bounded and it is impossible to resolve frequencies beyond maximum frequency. But one has no periodic structure in the case, for example, of two point sources, and it is possible to use known information about the exact solution including its specific character at high frequencies.

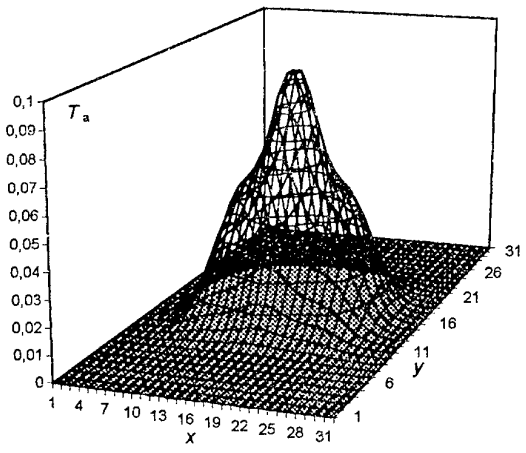


Fig. 2. The corresponding observed image

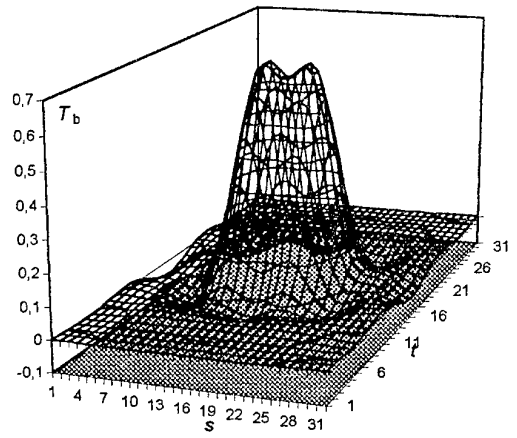


Fig. 3. Retrieved image at error level 1%

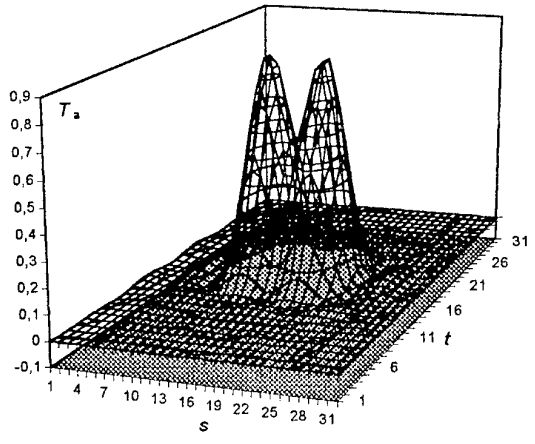


Fig. 4. Retrieved image at error level 0.01%

EXPERIMENTAL RESULTS

The method has been applied to improve the resolution of radiobrightness image in the case of helicopter-borne radiometer measurements of thermal radio emission cm of oil spills on lakes at wavelength 3 cm [5]. The size of antenna pattern footprint was about 20 m. It was impossible to improve the resolution using large apertures because montage conditions on helicopter, and it was impossible to improve it by means of measurements at lower heights because of influence of propeller wind on oil spills.

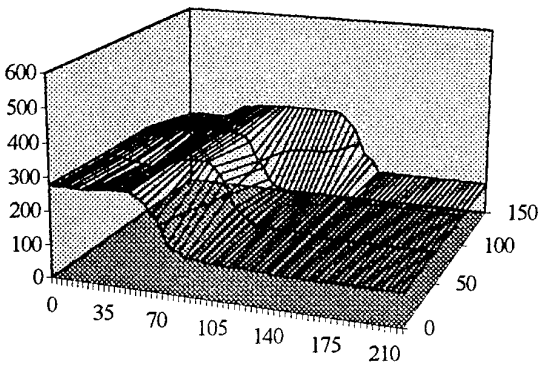


Fig. 5. Measured radiobrightness distribution

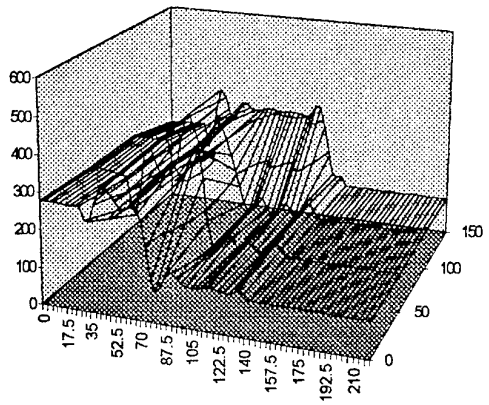


Fig. 6. Retrieved radiobrightness distribution

The only possibility was to solve inverse problem using high sensitivity of radiometer (about 0.1 K). One can see that the retrieved radiobrightness distribution contains more thin details of structure, and these details have been observed visually as thin folds across wind direction.

REFERENCES

1. Frieden B.R., Wells D.G. Journal Opt. Soc. America, 1978, v.68, *No.*1, pp.93-103.
2. Tan Sze M. Month. Not. Radio Astron. Soc., 1986, v.1, No.4, pp. 971-1001.
3. F.Bardaty, M.Mongiardo, D.Solimini. Proceedings of IGARSS'86 Symp. (Zurich, 8-11 Sept. 1986), 1986, ESA Publ. Division, pp.595-598.
4. Tikhonov A.N., Goncharsky A.V., Stepanov V.V., Yagola A.G. Numerical method for the solution of ill-posed problems. Moscow, Nauka, 1990.
5. K.P.Gaikovich, A.V.Troitsky, L.M.Snopik. Helicopter radiometer measurements of thin lake ice and oil spills on lakes and soil. Radiophysics and Quantum Electronics, 1995, vol.38, *No.*11, pp.719-726.

ACTIVE PHASED ANTENNA ARRAYS RADIATING LFM PULSE PACKET

V. L. Gostuykhin, V. N. Trusov, A. V. Gostuykhin

Moscow State Aviation Institute. MAI, 4, Volokolamskoe shosse, Moscow, 125871, Russia
Tel.: (095) 158-4740. Fax: (095) 158-1697. Email: antenna@mai.ru

As known [1], active antennas arrays are widely used nowadays because of the significantly improving of a number of radiosystem's performances. It is usually assumed that the APAA is radiating continuously or as if continuously. Thereby the problems of modulating signal's radiating of APAA aren't investigated. When modulated signals are considered it is very important to choose the approach to modulation method: in exciter on ir ending cascades of active modules.

The goal of the work — the investigation of technology non-stability factors' influence on the APAA performances (radiated power, side-lobe level, etc.) for the case of LFM radio-pulse signals.

Let us consider the radiating of periodic packet of LFM pulses by N-channel APAA [1], consisted of the distributing system of synchronizing signal, active modules (AM) — for example n-cascade amplifiers, phase-shifters with phase cancellation or controlled delay lines for two methods of modulation — in exciter or in AM.

The complex envelope of input signal of pulse amplifying AMs is:

$$a_n(t) = a_n \sum_{r=-\infty}^{\infty} u_1(t - \delta_n - rT), \qquad (1)$$

where a_n is the complex coefficient with phase controlled by phase shifter; $u_1(t) = rect(t/\tau)\exp(j\pi\alpha t^2)$ is the complex envelope of LFM pulse [2]; τ - pulse duration; α is steepness of LFM performance; $T = 2\pi / \Omega_T$ — pulses' period; δ_n — the delay in controlling delay line (if used); r is a sum index.

Then the average power spectrum of the complex envelope of the radiated field (the array factor) for the ensemble of similar APAAs is [1]

$$\left\langle W_F(\Theta,\varphi,\Omega)\right\rangle = \sum_{nn'}\sum_{qq'} D_{qn}^{-1} D_{q'n'}^{-1} \times \times \left\langle H_n \overset{*}{H}_{n'}\right\rangle \frac{2\pi}{|\alpha| T^2} a_n a_{n'}^{*} \times \times e^{-j\Omega(\delta_n - \delta_{n'})} e^{jk(\bar{\rho}_n - \bar{\rho}_{n'})} \times \times rect\left(\frac{\Omega}{2\pi\alpha\tau}\right) \sum_{r=-\infty}^{\infty} \delta(\Omega - r\Omega_T), \qquad (2)$$

where $D_{qn}, D_{q'n'}$ are elements of square matrix $[D]$ that describes the multiple coupling of radiators; $\bar{k}$ is a wave vector that is directed to the point of view; Ω is the modulation's circular frequency; $\bar{\rho}_n, \bar{\rho}_{n'}$ are radius-vectors of radiators n and n'; $\left\langle H_n \overset{*}{H}_{n'}\right\rangle$ are average values of AMs' transfer function.

If APAA is controlled by the delay lines with random errors of its lines, then the transfer coefficient of AM will be

$$H_n = H_0 e^{j\frac{\omega_0+\Omega}{C_0}(l_n+\delta l_n)}, \qquad (3)$$

where ω_0 — average resonance frequency; C — the velocity of light; $l_n = -\bar{k}_0 \bar{\rho}_n$ is length of the delay line for phasing in maximum radiation's direction $\bar{k}_0$; δl_n — errors in length of delay lines (distribution on normal law with zero average value and the disperse of σ_l^2).

The average value of transferring functions (3) is

$$\left\langle H_n \overset{*}{H}_{n'}\right\rangle = \begin{cases} |H_0|^2, & n = n'; \\ |H_0|^2 e^{j\frac{\omega_0+\Omega}{C_0}(l_n - l_{n'})} \times & \\ \times e^{-\left(\frac{\omega_0+\Omega}{C_0}\right)^2 \delta_l^2}, & n \neq n'. \end{cases} \qquad (4)$$

For average APAA power spectrum with controlling delay lines we have (adding (4) to (2) and after integrating over frequency Ω) the relation for reducing of average radiated power comparatively to maximum power,

$$\left\langle P(\Theta_0,\varphi_0)\right\rangle_{dl} \Big/ P_{\max}(\Theta_0,\varphi_0) \cong 1 - \sigma_\varphi^2$$

and increasing of the omnidirectional radiation (for $\bar{k} = \bar{k}_0$ and small σ_l^2).

$$\Delta R \cong |F_1^H(\Theta_0,\varphi_0)|^2 \frac{1}{N} \sigma_\varphi^2,$$

where $\sigma_\varphi = \frac{\sigma_l}{C_0}\omega_0 = \sigma_l \frac{2\pi}{\lambda_0}$; $\left|F_1^H\left(\Theta,\varphi\right)\right|$ is normalized pattern of a APAA single radiator; N — the number of APAA radiators.

So, for the base of LFM signal $|\alpha|\tau^2 = 50$ and square average deviations of delay lines' length $\sigma_\varphi = 25^0$, the average power in maximum radiation's direction $\overline{K}_0$ will be decreased to 1 dB.

For the case of creating LFM pulses in APAA exciter the active modules are operating in amplifying regime. As it is known [3] this regime is less effective than the above modulation regime.

On the other hand, the modulation in the end of cascades, as more powerful, can produce the additional deterioration of APAA performances because of scattered AMs' parameters and the difficulty of modulating signals' syn-phasing in AM in process of signal's distribution.

So, taking into account only the time fluctuations of pulses' appearance in AM ($\sigma_\varphi = \sigma_l \frac{\omega_0}{C_0} = 0$) decreasing the average power and increasing of omnidirectional radiation will be

$$\frac{\left\langle P\left(\Theta_0,\varphi_0\right)\right\rangle_{\text{d.l.}}}{P_{\max}\left(\Theta_0,\varphi_0\right)} \cong 1 - \frac{1}{3}\left(\pi|\alpha|\tau^2\right)^2\left(\frac{\sigma_\nu}{\tau}\right)^2,$$

$$\Delta R \cong \left|F_1^H\left(\Theta,\varphi\right)\right|^2 \frac{1}{N}\frac{1}{3} \times \left(\pi|\alpha|\tau^2\right)^2\left(\frac{\sigma_\nu}{\tau}\right)^2,$$

where $\sigma_\nu = \sigma_l / C_0$ are the standard deviations of times of pulses' appearance in different AMs.

The above formulas allow to calculate, that APAA is very sensitive to the deviations of time delays of pulses with LFM, and for the equal standard deviation, for example $\sigma_\nu/\tau = 5\cdot10^{-3}$, the average radiated power is reduced on 6,5 dB for two times signal's base increasing.

The additional value for side-lobe level in described case of random delays (time appearance of pulses) significantly depends on the signal's base and in equal conditions increases with $|\alpha|\tau^2$. For example, for $\sigma_\nu/\tau = 0.01$ (standard deviations of delays is 1% of the pulse duration) and the base $|\alpha|\tau^2 = 100$, radiators' number $N = 21$ the additional value is 8.1 dB.

The numerical relation between APAA output performances and modulation parameters is determined for random deviations of performances of active modules and distribution system of modulating signal. This relation allows to choose the correct modulation regime when APAA is designed.

REFERENCES

1. V. L. Gostuykhin, V. N. Trusov, K. G. Klimachev, U. S. Danich. Active phased antenna arrays / Edited by V. L. Gostuykhin. Moscow, Radio and communication, 1993 [in Russian].
2. The reference book on radio-radar / Edited by M. Skolnic. Vol 1. New-York, 1970.
3. Radio-transmitting devices. High-school textbook. / L. A. Belov, M. V. Blagoveshensky., B. M. Bogachev. Moscow, Radio and communication, 1982 [in Russian].

LIMITING RESOLUTION OF CAPON METHOD FOR CORRELATED SOURCES

A. A. Kirillov, G. V. Serebryakov

Research Institute of Applied Mathematics and Cybernetics, Nizhny Novgorod State University,
10 Ul'janov st., Nizhny Novgorod, 603 005, Russia
fax: +7 8312 39 04 11, e-mail:gvs@focus.nnov.ru

INTRODUCTION

Use of the optimum/adaptive beamforming (so called, Capon method) in bearing estimation of closely located sources has become very popular due to its superresolution properties [1–4]. It has been shown that this method is capable of resolving two independent sources which are separated by an angle which is of the order of one standard beamwidth (SBW) and sometimes less. However, when some sources are fully or highly correlated (coherent), i.e. when one source is a scaled and delayed replica of another source, this method encounters significant difficulties concerning with signal cancellation effect [2, 3, 6, 7]. Note that coherent sources appear frequently in practical problems. A well-known example is the phenomenon of multipath propagation.

The purpose of this paper is to obtain analytical estimation of the potential capability for adaptive beamforming in the presence of correlation between the sources as a function of coherence coefficient, signal power and the parameters of the optimum processor. Our resolution analysis is based on the assumption that the covariance matrix of the received signal will be determined rigorously by averaging over an infinite period of time, thus enabling us to obtain an estimate of the limiting ability of resolution.

SIGNAL MODEL

Assume that L narrow-band correlated (partially or fully) sources radiation is incident on a linear array consisting of N equidistant omnidirectional sensors, and the directions of receiving (DOP's) from these sources are $\{\theta_1, \theta_2,\ldots, \theta_L\}$ with respect to the array normal. The output of the k-th sensor can be expressed as

$$x_k(t) = \sum_{l=1}^{L} s_l(t) \exp\{-j(k-1)u_l\} + \eta_k(t), \qquad (1)$$

where $s_k(t)$ denotes the signal radiated by the l-th source as observed at the sensor one, and $\eta_k(t)$ is an additive sensor noise, which is assumed to be a zero-mean stationary random process which is independent from sensor to sensor. The interelement phase delay is given by $u_l = (2\pi d/\lambda) \sin\theta_l$, where d denotes the spacing of the sensors, θ_l is the DOA of the l-th source, and λ is the wavelength of the narrow-band signals. We shall be confined to the assumption that the received signals have plane wave fronts. In matrix notation, the array signal vector can be expressed as

$$\mathbf{x}(t) = \mathbf{A}\,\mathbf{s}(t) + \eta(t), \qquad (2)$$

where $\mathbf{x}(t)$ is given by

$$\mathbf{x}^{T}(t) = \{ x_1(t), x_2(t),\ldots, x_N(t)\},$$

where (T) denotes transposition and $\mathbf{A}$ is a matrix N x P with l-th column equal to

$$\mathbf{a}_k = \{ 1,\exp(-j\,u_k),\ldots,\exp(-j(N-1)\,u_k)\}.^{T}$$

The Nxl vectors $\{\mathbf{a}_1,\ldots,\mathbf{a}_l\}$ are called the directive vectors of the sources. The vectors $\mathbf{s}(t)$ and $\eta(t)$ are defined similarly to $\mathbf{x}(t)$.

The array covariance matrix can now be expressed as

$$\mathbf{R} = \langle \mathbf{x}(t)\,\mathbf{x}+(t)\rangle = \sigma_\eta^2\,\mathbf{I} + \mathbf{ASA}^{+} \qquad (3)$$

where $\mathbf{S}=\langle \mathbf{s}(t) + \mathbf{s}(t)\rangle$ denotes the source covariance matrix, σ_η^2 is the variance of the additive noise, $\mathbf{I}$ is a unit matrix, and (+) represents the complex conjugate transpose. The Capon algorithm estimates the spatial frequencies of the L radiators by finding the L maxima of a functional $P(\theta)$ (it is well-known that this is the output power of the optimum/adaptive beamformer)

$$P(\theta) = (S(\theta)^{+}\,\mathbf{R}^{-1}\,S(\theta))^{-1}, \qquad (4)$$

where $S(\theta)$ is a vector of direction with elements $S_k = \exp\{j(k-1)u\}$, where $u = (2\pi d/\lambda)\sin\theta$, and θ is the bearing angle. To simplify our work we restrict our analysis to the case of the two sources. The covariance matrix of the received signal can be written as

$$R = \sigma_\eta^2\,I + \sigma_1^2\,S_1S_1^{+} + \sigma_2^2\,S_2\,S_2^{+} + \\ + \sigma_1\,\sigma_2\,\{\rho\,S_1\,S_2^{+} + S_2\,S_1 + \rho^*\}, \qquad (5)$$

where σ_l^2 is a variance of l-th signal, and S_l is a direction vector of l-th signal. S_l is given by

$$S_l = [\,1,\exp\{ju_l\},\ldots,\exp\{j(N-1)u_l\}]^{T}\ l = 1,2.$$

The coefficient of correlation between signals is defined as follows: $\rho = |\rho|\exp(j\varphi)$, where $|\rho|$ and φ represent an amplitude and phase of the correlation factor. The angle φ is equal to the average phase shift between signals at the coordinate origin. The phase difference between two correlated signals is a function of the location distance of the array from the sources. It can be easily shown that the amplitude of correlation coeffi-

cient lies between 0 and 1. When the signals differ by only a constant deterministic phase and amplitude, they are fully correlated, i.e. $|\rho| = 1$. This situation can arise, for example, when multiple propagation paths (with fixed differences in path length) exist between a single source and the array. For simplicity, we consider the phase-centered arrays, which exhibit symmetry through the origin. By using a well-known matrix identity, the inverse covariance matrix can be expressed as

$$\mathbf{R}^{-1} = (1/\sigma_\eta^2)\{\mathbf{I} - (1/\alpha)[\nu_1(1+N\nu_2(1-|\rho|^2)\mathbf{S}_1\mathbf{S}_1^+ - (N\nu_1\nu_2(1-|\rho|^2)f(\Delta u) - \sqrt{\nu_1\nu_2}\,|\rho|\exp(j\varphi))\mathbf{S}_1\mathbf{S}_2^+ - (N\nu_1\nu_2(1-|\rho|^2)f(\Delta u) - \sqrt{\nu_1\nu_2}\,|\rho|\exp(-j\varphi))\mathbf{S}_2\mathbf{S}_1^+ + \nu_2(1+N\nu_1(1-|\rho|^2)\mathbf{S}_2\mathbf{S}_2^+]\}, \quad (6)$$

where $\nu_{1,2} = \sigma_{1,2}^2/\sigma_\eta^2$, $f(\Delta u) = \sin(N\delta u/2)/(N\sin(\Delta u/2))$, Δu denotes the normalized angular separation between the two sources and is given by $\Delta u=(2\pi d/\lambda))(\sin\theta_1 - \sin\theta_2)$, $\alpha = 1+N(\nu_1+\nu_2)+N^2\nu_1\nu_2(1-|\rho|^2)(1-f(\Delta u)^2)+2N|\rho|\sqrt{\nu_1\nu_2}\,f(\Delta u)\cos\varphi$. From (4) and (6) the output power of the optimum beamformer when the signals are correlated can be expressed as

$$P(\theta) = (\sigma_\eta^2/N)\{1-(1/\alpha)(N\nu_1(1+N\nu_2(1-|\rho|^2))f_1^2 - 2N(N\nu_1\nu_2(1-|\rho|^2)f(\Delta u) - \sqrt{\nu_1\nu_2}\,|\rho|\cos(\varphi))f_1f_2 + N\nu_2(1+N\nu_1(1-|\rho|^2))f_2^2)\}^{-1}, \quad (7)$$

where

$$f_1 = \sin(N(u-u_1)/2)/(N\sin((u-u_1\})/2)),$$
$$f_2 = \sin(N(u-u_2)/2)/(N\sin((u-u_2)/2)).$$

Using this exact expression for output power of the optimum/adaptive beamformer we can study any scenario for two-source.

RESOLUTION OF SOURCES

When the sources are resolved, the beam energy evaluated at target bearing must be larger than the beam energy evaluated between the target bearings. The vector of between targets observation direction, $\mathbf{S}_0$ is defined to have the elements $S_{0k} = \exp\{j(k-1)(u_1+u_2)/2\}$. The criterion used for resolution of the sources is that the ratio of on-target to between-target beam energies exceeds a threshold value of 1 (Rayleigh resolution limit). We shall consider the case when two sources to be resolved are of equal strength ($\nu_1 = \nu_2 = \nu$). Then the threshold of resolution is defined by the condition

$$P(\theta_i) / P((\theta_1+\theta_2)/2)\} = \{\mathbf{S}_0^+\mathbf{R}^{-1}\mathbf{S}_0\}/\{\mathbf{S}_i^+\mathbf{R}^{-1}\mathbf{S}_i\} < 1,\ i=1,2. \quad (8)$$

Then, using (7), from (8) we obtain the following exact formula

$$1+2N\nu+N^2\nu^2(1-|\rho|^2)(1-f(\Delta u)^2)+2N|\rho|\nu\cos\varphi\,(f(\Delta u)-f(\Delta u/2)^2)+2N^2\nu^2(1-|\rho|^2)f(\Delta u)f(\Delta u/2)^2-2N\nu(1+N\nu(1-|\rho|^2))f(\Delta u/2)^2 > 1+N\nu(1-f(\Delta u)^2). \quad (9)$$

The complexity of expression (9) prevents a clear ratio, coherence, and bearing separation on resolving capability. To gain its understanding, assume that the sources are localized in the main lobe and that the angular separation between them is very small compared to the beamwidth of the array. Then, expanding the functions $f(\Delta u)$, $f(\Delta u/2)$ in an exponential series over Δu, we retain the first four terms of the expansion

$$f(\Delta u) = 1 - (N\Delta u)^2/6 + (N\Delta u)^4/120 + (N\Delta u)^6/5040,$$
$$f(\Delta u)^2 = 1 - (N\Delta u)^2/3 + 2(N\Delta u)^4/45 + 16(N\Delta u)^6/5040,$$

Substituting these approximations in (9) for minimal angular separation Δu_{min} we obtain (after some algebraic transformation)

$$\Delta u_{min} = 8.71\,((1+|\rho|\cos\varphi)/(N^5\nu(1-|\rho|^2))^{1/4} \quad (10)$$

One can see that minimal angular separation is a function of the magnitude and phase of the coherence as well as input signal-to-noise ratio. From the expression (10) for resolvent array SNR, the minimum SNR which results in resolved sources can be write as

$$N\nu_{min} = (8.71/(N\Delta u))^4(1+|\rho|\cos\varphi)/(1-|\rho|^2) \quad (11)$$

As it can be seen from (11) the resolvent *SNR* of two plane correlated waves is inversely proportional to the fourth power of the angular separation, indicating that the minimal *SNR* increases much faster than the angular separation decreases. We can see that the this method is capable of resolving arbitrarily closely lcated source bearings if the input *SNR* is high enough. As the amplitude of the coherence increases, the resolvent *SNR* increases. The loss of the resolvent *SNR* due coherence between sources can be expressed as

$$g = \frac{SNR}{SNR_{|\rho|=0}} = \frac{1}{1-|\rho|}$$

For example, for $|\rho| = 0.99$ the resolvent *SNR* is greater by 20 dB than for uncorrelated sources. For coherent signals ($|\rho| = 1$) the source covariance matrix becomes singular and the array cannot resolve the sources for any value of the input *SNR*. An interesting result from (11) is that the resolvent *SNR* has minimum for $\varphi = \pi$. The relationship between resolvent *SNR* and φ indicates that the resolving power of Capon method is determined by the location of the array. In particular, the array located at the maximum of the interference pattern ($\varphi = 0$) exhibits a resolving power lower than the array at the minimum of the interference pattern ($\varphi = \pi$). The maximum gain in the resolvent *SNR* which can be achieved by changing the position of the adaptive array is determined by the quantity $(1+|\rho|)/(1-|\rho|)$. Moreover, we noted follows. The resolving power of optimum beamforming for correlated sources may be greater than that for uncorrelated sources if the following condition is satisfied

$$(1+|\rho|\cos\varphi)/(1-|\rho|^2) < 1.$$

The explanation of this effect is follow. For uncorrelated sources the output power of optimum beamformer for the between-sources observation direction is defined by depth of the nulls in the directions of the signals. Hereat the null depth decreases with decreasing angular separation between sources and output power increases. For correlated sources there is the other mechanism of the forming of the output signal. In this case the output power for the between-sources observation direction is defined also by the sum of the coherent components of received signals. This sum is determined by the coherence amplitude and phase only. For the array located at the minimum of the interference pattern ($\varphi = \pi$) these components are subtracted and for highly correlated sources, and the actual array output signal is really just a noise due the signal cancellation effect. Therefore the output power for highly correlated sources for the between-sources observation direction is less than that for uncorrelated sources. Of course, the output power for the observation direction on the source for highly correlated signals is also less than for weak correlated sources. But the resolving power is defined by a mutual relation of these values. Note that the gain at the resolvent *SNR* for array located in the minimum of the interference pattern is given by $1/(1+|\rho|)$ and for coherent sources it is about 3 dB. The effect of resolving the coherent sources in accordance with our criterion (8) for $\varphi = \pi$ when using the adaptive beamforming was apparently firstly detected in [5] by computer investigations. However, it was shown in this work, that for these correlation amplitude and phase, bias of the bearing estimates increases.

We have done the extensive computer simulations to support our theoretical analysis.

CONCLUSIONS

In this paper we analyzed the potential capability for optimum/adaptive beamforming to estimate the bearings of two closely located radiating equal-energy correlated sources. Analysis shows that it depends on the coherence amplitude. We showed that the resolution capability depends on the location of the array and is better for array located at the minimum of interference pattern due the complex structure of the received field at this point.

AKNOWLEDGMENTS

This work was supported in part by INTAS grant (#96-2352) and RFRB grants (#99-02-16401, #98-01-16273).

REFERENCES

1. J. Capon,"High-resolution frequency-wavenumber spectrum analysis," *Proc.IEEE*, **57**(1969), 1408-1418.
2. W.Gabriel," Spectral analysis and adaptive array superresolution techniques," *Proc. IEEE*, **68**(1980), 654-666.
3. S.De Graaf and D.H.Johnson ,"Capability of array processing algorithms to estimate source bearings," *IEEE Trans. Acoust., Speech,Signal Processing*, **ASSP-33** (1985), 1368-1379.
4. H.Cox,"Resolving power and sensitivity to mismatch of optimum array processor," *JASA*, **54** (1973), 771-785.
5. W.White ,"Angular spectra in radar applications," *IEEE Trans. Aerospace Electron.Syst.*, **AES-15** (1979), 895-899.
6. A.Cantoni and L.C.Godara, "Resolving the directions of sources in a correlated field incident on an array," *JASA*, **67** (1980), 1247-1256.
7. T.Shan and T.Kailath, "Adaptive beamforming for coherent signals and interference," *IEEE Trans. Acou st., Speech, Signal Processing*, **ASSP-**33(1985), 527-536.

THE ACCURACY OF JOINT ESTIMATION OF SIGNAL PARAMETERS OF THE ANTENNA ARRAYS IN THE CASE OF NON-GAUSSIAN INTERFERENCE

Y. P. Kunchenko, V. A. Danyk, T. V. Prokopenko

Cherkassy Institute of Engineering and Technology
460 Shevchenko Blvd., Cherkassy, 257006, Ukraine
Phone: 380(0472)435171, fax: 380(0472)433190
E-mail: ykunchen@chiti.uch.net

ABSTRACT

The dispersions of joint estimation of the parameters of harmonic signal are presented in the article. Array's sensors receive the signal at the background of non-Gaussian interference. It's presumed, that estimation are calculated by the method of polynomial maximisation for order equal to S = 1, 2, 3,4. It's shown that for non-Gaussian interferences the dispersions of joint estimations can be significantly smaller than the dispersions of estimations in the case of Gaussian interference.

INTRODUCTION

In the majority of works devoted to synthesis of the meters of the parameters of a signal received by an array, it's assumed, that interference in every sensor of the array is Gaussian [1]. However, Gaussian interference is often considered as an idealisation of real interference, so the synthesis of the signal parameters meters for non-Gaussian interferences and investigation of their accuracy characteristics are of great scientific and practical interest.

Using the moments or cumulants of higher orders presents one of the perspective directions of non-Gaussian interference description. Using them, linear and nonlinear algorithms of parameter estimation are researched [2]. In most cases to find the estimations the method of maximum likelihood is used, which is based on another description of interference, and due to this the cumulants of the order higher then the fourth are not taken into account [3]. In this research it is presumed that for finding the estimations the method of a polynomial maximisation is used [3,4], which allows to take into account the thin structure of interference presented by the cumulants of higher orders, and to use them in an optimal way during synthesis of various meters. It's shown that for non-Gaussian interference the dispersion of joint estimation of a vector parameter can be significantly smaller than the dispersion of joint estimation found by the method of maximum likelihood for Gaussian interference. It's also shown that dispersion of estimation decreases with the polynome order increasing.

STATEMENT OF A PROBLEM AND METHOD OF ITS SOLVING

Let there is a q-element equidistant array of receiving sensors, on which there is incident real flat wave. Let's consider, that from the output of the p-th sensors of the arrays the discrete sample $\vec{x}_{(p)} = \{x_{1(p)}, x_{2(p)}, \ldots, x_{n(p)}\}$ of volume n of an additive mixture of a useful harmonic signal $s_{v(p)}(\vec{\vartheta})$ and non-Gaussian of a interference $n_{v(p)}$ is made, i.e.

$$x_{v(p)} = s_{v(p)}(\vec{\vartheta}) + n_{v(p)}, \; v = \overline{1,n}, \; p = \overline{0,(g-1)}$$

where $\vec{\vartheta}$ — vector of the dimension g of unknown signal parameters. Let $En_{v(p)} = 0$, the dispersions is equal to χ_2, and the cumulant of the i-th order interference is equal to χ_i, i = 3,4....

In this case, each sample value $x_{v(p)}$ is described by sequence of initial moment $m_{iv(p)}(\vec{\vartheta})$ of the i-th order h dependent on vector parameter $\vec{\vartheta}$. It is necessary, for the sample $\vec{x}_{(p)} = \{x_{1(p)}, x_{2(p)}, \ldots, x_{n(p)}\}$, using moments $m_{iv(p)}(\vec{\vartheta})$ of higher orders to find and to investigate a joint estimation of parameter $\vec{\vartheta}$.

To find the estimation it is possible to use the method of a polynomial maximisation [4,5], according to which the estimations are obtained by joint solving equation system

$$\sum_{p=0}^{g-1}\sum_{v=1}^{n}\sum_{i=1}^{s} h^{(p)}_{iv(m)}(\vec{\vartheta})\left[x_v^i - m_{iv(p)}(\vec{\vartheta})\right]\Big|_{\vec{\vartheta}=\hat{\vec{\vartheta}}} = 0, \; m = \overline{1,g},$$

where coefficients $h^{(p)}_{iv(m)}(\vec{\vartheta})$ are found from the solution of the linear algebraic equations system

$$\sum_{j=1}^{s} h^{(p)}_{jv(m)}(\vec{\vartheta}) F^{(p)}_{(i,j)v}(\vec{\vartheta}) = \frac{\partial}{\partial \vartheta_m} m_{iv(p)}(\vec{\vartheta}),$$

$$p = \overline{0,1-q}\,,\ v = \overline{1,n}\,,\ i = \overline{1,s}\,,\ m = \overline{1,g}\,.$$

$$F^{(p)}_{(i,j)v} = m_{(i+j)v(p)}(\vec{\vartheta}) - m_{iv(p)}(\vec{\vartheta}) m_{jv(p)}(\vec{\vartheta})$$

Thus the variational matrix of estimation $V_{sn(q)}(\vec{\vartheta})$ is equal to an inverse matrix $J_{sn(q)}$ of the extracted information quantity, with elements

$$J^{(m,r)}_{sn(q)}(\vec{\vartheta}) = \sum_{p=0}^{q-1}\sum_{v=1}^{n}\sum_{i=1}^{s} h^{(p)}_{iv(r)}(\vec{\vartheta}) \frac{\partial}{\partial \vartheta_m} m_{iv(p)}(\vec{\vartheta})$$

The dispersions of estimation of component of vector parameter lie on a diagonal of a variational matrix.

RESULTS

We shall consider the case when the order of a stochastic polynome is $s = 1$. In this case variational matrix of estimation will be equal to

$$V_{1n(q)} = J^{-1}_{1n(q)}$$

where the elements of a matrix $J_{1n(q)}$ are equal to

$$J^{(m,r)}_{1n(q)} = \sum_{p=0}^{q-1}\sum_{i=0}^{s}\sum_{v=1}^{n} \frac{\partial}{\partial \vartheta_m} m_{iv(p)}(\vec{\vartheta}) \frac{\partial}{\partial \vartheta_r} m_{iv(p)}(\vec{\vartheta})$$

When $s = 2$ variational matrixes will be equal to

$$V_{2n(q)} = q_{21} V_{1n(q)} \qquad (1)$$

From expression (1) it is clear, that at $s = 2$ dispersions of the found estimation will be less than at $s = 1$ in q_{21} times, where

$$q_{21} = 1 - \frac{\gamma_3^2}{\gamma_4 + 2} \qquad (2)$$

From the formula (2) it is clear, that the decreasing of a dispersion depends on a coefficient of skewness γ_3 and coefficient of excess γ_4.

When $s = 3$

$$V_{3n(q)} = q_{31} V_{1n(q)}\,,$$

where the factor of decreasing q_{31} is equal to

$$q_{31} = 1 - \frac{\gamma_4^3 + 2\gamma_4^2 - 3\gamma_4\gamma_3^2 + 9\gamma_3^4 + 6\gamma_3^2}{9\gamma_4^2 + 24\gamma_4 + 9\gamma_4\gamma_3^2 - 18\gamma_3^2 + 12}\,.$$

When $s = 4$

$$V_{4n(q)} = q_{41} V_{1n(q)}\,,$$

where q_{41} is equal to

$$q_{41} = 1 - \frac{34\gamma_4^5 + 76\gamma_4^4 + 168\gamma_4^3 + 48\gamma_4^2 + \rightarrow}{306\gamma_4^4 + 888\gamma_4^3 + 1968\gamma_4^2\gamma_4 - 1188\gamma_4^2\gamma_3^2}$$

$$\rightarrow \frac{+852\gamma_4^2\gamma_3^2 + 426\gamma_4^3 - 1512\gamma_4\gamma_3^4 + 360\gamma_4\gamma_3^2 - \rightarrow}{-594\gamma_4^3\gamma_3^2 + 2268\gamma_4\gamma_3^4 - 360\gamma_4\gamma_3^2 -}$$

$$\rightarrow \frac{-270\gamma_4^2\gamma_3^2 + 1296\gamma_3^6 - 216\gamma_3^4 + 144\gamma_3^2}{-324\gamma_3^6 - 216\gamma_3^4 - 1296\gamma_3^2 + 288}$$

At increase of the order of stochastic polynome the dispersion of the obtained estimations decreases.

ACKNOWLEDGEMENT

This work was supported by Grant N 96-2353.

REFERENCES

1. Zhuravlev A.K., Lukoshkin A.P., Poddubnij S.S., Processing of signals in adaptive antenna arrey. Leningrad university, 1983.-240 p. [in Russian].
2. Cardoso J.-F. and Moulines E., Asimptotic performance analysis of direction - finding algorithms based on fourth-order cumulants, IEEE Trans. Signal Processing, vol. 43, pp. 214-224, Jan-1995.
3. Gershman A.B., Bohme J.F. Pseudorandomly generated estimator banks: a new resampling scheme for improving the threshold performance of second and higher - order direction finding methods, Proc. of the Second Inter. Conf. on Antenna Theory and Thechnigues, Kyiv, Ukraine, 1997, pp. 43-50.
4. Kunchenko Y.P., Lega Y.G., Estimation of parameters of random variables by the a method of polynomial maximization, Kyiv: Naykova dumka, 1992.-180 p. [in Russian].
5. Kunchenko Y.P. Estimation of parameters of a vectorial random variable by the method of polynomial maximization, Proceedings 9-th National Scientific Symposium "Metrology and metrology Assurance' 99", Bulgaria, 1999.

APODIZATION FUNCTIONS FOR ANTENNA ARRAYS WITH CONSTRUCTIVE-TECHNOLOGICAL RESTRICTIONS

V. V. Lukin, A. V. Kabanov, N. N. Ponomarenko

State Aerospace University, Department 504, 310070 Kharkov, Ukraine

INTRODUCTION

For multielement antenna arrays (MAA) the desired characteristics of the corresponding pattern are often provided by means of the proper selection or optimization (synthesis) of an apodization function (AF), i.e. an amplitude distribution represented in a sampled manner [1]. However, for some types of MAA not all the known apodization functions (also called weighting windows for digital signal processing applications) [2] can be implemented. The reasons are the constructive and technological restrictions. They are originated by different factors depending upon the type of MAA under consideration. In particular, for wave-guide-slot antennas the desirable amplitude distribution is provided by means of varied displacement of slots in the wide wall of waveguide in respect to its axis. In this case the minimal distance of the slot to the axis is not less than some value predetermined by geometrical dimensions of the slots, wavelength and the requirements to antenna solidity [3]. Similar reasons take place for patch MAAs. In general, the factors mentioned above lead to restricting an available range of apodization function value variation. If it is represented in a normalized way then AF values can not be less than typically 0.1–0.2. That is why below we consider several possible solutions applicable for described constructive technological restrictions. In addition, we propose some new AFs having rather good characteristics of the corresponding patterns.

AVAILABLE SOLUTIONS

Among a wide set of weighting windows described in [2] we have selected only those ones that for which the AF $w(x)$ satisfied the following conditions

$$w(x) \geq a_{\min}, \; x \in [-L/2; L/2],$$

$$\max\{w(x)\}=1; \; w(x)=0; \; x \notin [-L/2; L/2], \qquad (1)$$

where L is the one-dimensional ($1-D$) array physical length, x denotes the coordinate on antenna axis. For MAA it is supposed that the interelement distance Δx is not larger than half-wavelength $\lambda/2$. Then the array pattern is defined as

$$G(\theta) = \left| \int_{-L/2}^{L/2} w(x) e^{-j\frac{2p}{l} x SINq} \right|^2, \qquad (2)$$

where θ is the angle coordinate.

The expressions that describe some apodization functions contain the parameters determining the AF appearance and the corresponding pattern characteristics. The examples of such AFs are presented in Table (items 1-4). For such AFs the parameter α values are adjusted in such a manner that $a_{\min}$ is not less than some predetermined value. Generally, the larger α the lower maximal side lobe level (MSLL) and the large the pattern main lobe width (MLW). It is a common tendency that the pattern MLW increases with reduction of MSLL. For items 1-4 in Table $a_{\min} = 0.1$. An example of such window and the corresponding pattern is presented in Fig. 1–2. These are the Kaiser-Bessel window ($a_{\min} = 0.1$ when the pattern MSLL equals to –28 dB) and the corresponding response (See Fig. 1 and Fig. 2, respectively).

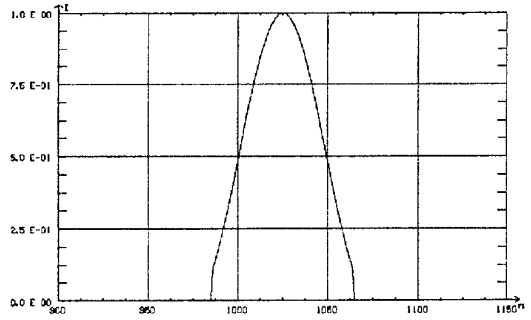


Fig. 1. The Kaiser-Bessel window (apodization function providing $a_{\min}$=0.1)

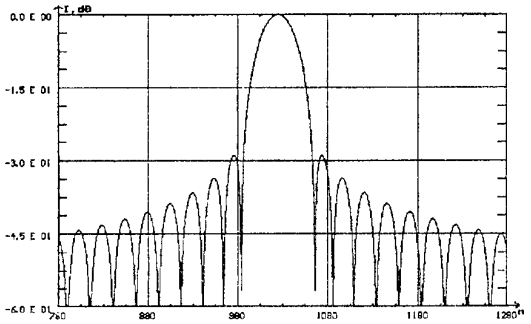


Fig. 2. The corresponding pattern with MSLL equal to –28 dB

As there are different ways to determine and describe the pattern parameters we consider below and give in Table the following characteristics of patterns:

- the pattern MSLL expressed in dB;
- the pattern MLW by the first zeroes expressed in degrees (for $N = 80$, $\Delta x = \lambda/2$);
- the relative MLW $\delta\theta_{0.5}/\delta\theta_{D\text{-}Ch}$ determined by the level -3dB and normalized by the MLW of the Dolph-Chebyshev pattern with the same MSLL.

As it is seen from Table the Poisson window produces too large MSLL and it is not an appropriate solution for many practical application. Considerably better trade-off of pattern parameters is provided by the Gauss AF, so is quite good solution. The MSLL of Kaiser-Bessel pattern is not low enough, however, in some cases it is also an appropriate solution especially taking into account the other advantages like relatively narrow main lobe and minimization of the ratio of energies contained in the pattern side lobes and its main lobe. Let us remind that the Kaiser-Bessel AF was optimized just according to this criterion. The Abel-Cauchy-Poisson window is characterized by too wide main lobe, so, to our opinion, it is not worth applying it in practice.

For all these AFs the corresponding patterns are characterized by a regular structure of the side lobes and decreasing behavior of their envelope. It can be seen, for example, in Fig. 2. While getting the pattern plots presented in this paper and evaluating the pattern parameters we added the sample of AF by zero values in order to make the pattern interpolation [4] and to ensure the high accuracy of obtained estimations of the measured parameters. For derivation of the pattern the algorithms of fast Fourier Transform were used. They were implemented by software package LIPHAR designed by our group [5].

A very good result is provided by two-component Nuttal-Harris-Blackman window with the weights $a_0 = 0.55$ and $a_1 = 0.45$ ($a_{\min} = 0.1$). This ran us into idea to analyse the windows generally expressable as

$$w(x, L) = a_p + a_w w_k(x, L_w / L), \qquad (3)$$

where a_p is the amplitude of pedestal ($a_p \geq a_{min}$), $a_p + a_w = 1$, L_w is the length where $w_k(x, L_w/L) \neq 0$, $L_w \leq L$.

In the considered case the optimization task can be solved in a similar manner as it was done in our paper [6]. Varying the parameter $a_w = 1 - a_p$, the type of the window $w_k(x)$ (or selecting it among known ones) and the ratio L_w/L one can get an optimal solutions by minimizing the response MSLL. This task was also performed by software LIPHAR. The obtained results are given in items 6–12 of the Table.

Obviously, the window "Riss on pedestal" ($a_{min} = 0.17$) is a rather good solution when the constructive-technological limitations are strict, i.e. a_{min} value are rather large. The window "Boman on pedestal" provides the MSLL appropriate for many practical applications for strict constraints but the array pattern MLW is to wide.

A very interesting results are got for the window "*cos* on pedestal". For larger a_{min} (compare items 8 and 9) the better pattern MSLL is ensured due to possible variation of L_w/L. The results for the window "cos^3 on pedestal" are not too good because of rather large MLW. An example of optimized AF "*cos* on pedestal" (item 9) is given in Fig. 3. The corresponding pattern is presented in Fig. 4.

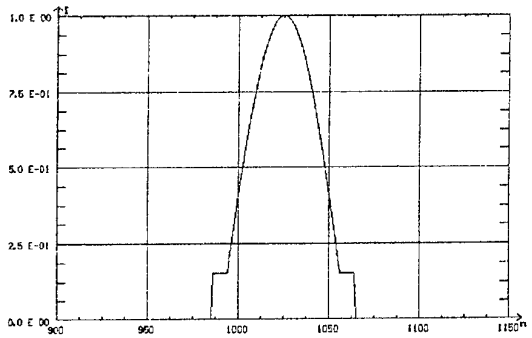


Fig. 3. Optimized AF "*cos* on pedestal" (item 9 in Table), $a_{min} = 0.15$

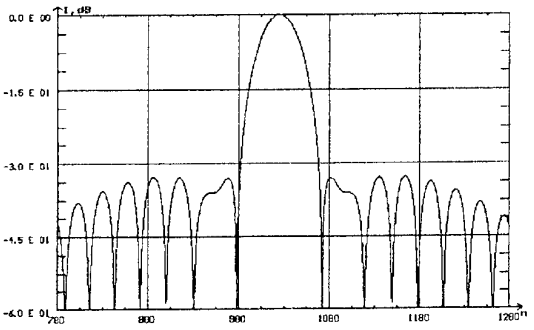


Fig. 4. The pattern corresponding to AF "*cos* on pedestal"

The optimization appears itself in the fact that several side lobes located close to the main lobe have practically equal maximal amplitudes and just they determine the pattern MSLL. The pattern side lobes have irregular structure and with further increasing of $|\theta|$ the side lobe envelope slightly reduces.

Finally, depending upon the trade-off of requirements to the response MSLL and MLW the windows "Kaiser-Bessel on pedestal" (item 12 in Table) and "cos^2 on pedestal" (item 10, it is very similar to Nuttal-Harris-Blackman one [7]) can be the appropriate solutions as they provide the low MSLL and rather small MLW.

Table

The parameters of apodization functions and the corresponding pattern main characteristics for $N = 80$, $\Delta x = \lambda/2$

Item	Apodization function type and its parameters	MSLL, DB	zero-level MLW, degrees	$\delta\theta_{0.5}/\delta\theta_{D\text{-}Ch}$
1	Gauss, $\alpha_G = 2.2$	-34.6	5.84	1.27
2	Poisson, $\alpha_p = 2.3$	-18.3	5.61	1.71
3	Kaiser-Bessel (for MSLL = -28dB)	-28.0	4.70	1.16
4	Abel-Cauchy-Poisson, $\alpha_{ACP} = 3$	-31.1	10.78	2.53
5	Nuttal-Harris-Blackman, $a_0 = 0.55$, $a_1 = 0.45$	-39.8	5.62	1.09
6	Riss on pedestal 0.17, $L_w/L = 0.75$	-30.6	5.16	1.20
7	Boman on pedestal, 0.17 $L_w/L = 1$	-35.7	8.81	1.86
8	*cos* on pedestal 0.1, $L_w/L = 1$	-22.0	4.84	1.32
9	*cos* on pedestal 0.15, $L_w/L = 0.77$	-32.9	5.28	1.19
10	cos^2 on pedestal 0.1, $L_w/L = 0.97$	-39.9	6.07	1.18
11	cos^3 on pedestal 0.1, $L_w/L = 1$	-34.4	8.47	1.84
12	Kaiser-Bessel (with initial. MSLL = -40dB) on pedestal 0.1	-36.0	5.84	1.17

CONCLUSIONS

It is shown that the constructive-technological restrictions determined by the MAA type and restrictions imposed on available AF characteristics can essentially narrow the set of weighting windows applicable in practice. At the same time they limit the reachable parameters of patterns. However, some AFs and, in particular, those ones proposed and optimized in this paper can serve as appropriate solutions for considered practical situations. The obtained results demonstrate that potentially the pattern MSLL within the limits -30...-40 dB can be provided. The MLWs of these patterns are only 15–20 % larger than for Dolph-Chebyshev patterns having the same MSLL.

REFERENCES

1. Problems of antennas engineering / Edit. By L.D.Bakhrakh, D.I.Voskresenskij, Moscow, Radio i sviaz, 1989, 368 p. [in Russian].
2. Harris F.J. On the use of windows for harmonic analysis with the discrete Fourier transform, Proceedings IEEE. - 1978. Vol.66, No 1, pp.51-83.
3. Zelensky A.A. Lukin V.V., Anukhin I.P. Apodized array pattern analisis and synthesis for spatially independent and correlated error influence under constructive and technological restrictions, in Proceedings of PIERS'94, Noordwijk, Netherlands, June 1994, pp.440-443.
4. Ifeachor E.C., Jervis B.W., Digital Signal Processing: A Practical Approach, 1993, Addison-Wesley Publishers, Ltd.
5. Gorbunenko B.F., Lukin V.V. Program package for computer-aid design of multielement antenna systems // Trudy nauchno-tech. Konferenciji "Perspektivy razvitija i primenenija sredstv VT dlia modelirovanija I avtomatizirovannykh issledovanij", Moscow, 1991, P. 160-161 [in Russian].
6. Lukin V.V., Saramaki T., Step-like weighting windows for DSP in spectral analysis and antenna arrays, in Proceedings of 1996 IEEE Digital signal Processing Workshop, Loen, Norway, Sept. 1996, pp. 362-365.
7. Nuttal A.H. Some windows with very good side lobe behavior, IEEE Trans. ASSP, Vol.29, No. 1, 1981, pp. 84-91.

COHERENCE-REDUCED SIGNAL PROCESSING IN LARGE ARRAYS

A. Malekhanov

Institute of Applied Physics, Russian Academy of Science
46 Uljanov Street, 603600 Nizhny Novgorod, Russia
tel/fax: +7 (8312) 36 7804, e-mail: almal@hydro.appl.sci-nnov.ru

INTRODUCTION

Long-range (electromagnetic, acoustic) signal propagation in random-inhomogeneous environments is well known to lead to loss of the signal coherence in space, time and frequency, which results from stochastic effects of multiple signal scattering. From an application point of view in radar and sonar, an important issue is to optimize the signal processing techniques and, therefore, to decrease in part or even to minimize a coherence-induced degradation of the processor performances.

Following the general idea of spatial-temporal processing factorization, we restrict ourselves to the study of coherence effects in the spatial domain, which is of primary interest in large-array beam-forming. The problem of array processing under the conditions of reduced signal coherence was studied earlier by several authors [1-4] on the basis of a general theory of random signal detection [5] but without invoking specific models for the channels of propagation. In our recent papers [6,7] we developed an effective approach of combined consideration of the signal coherence and array signal processing for long-range sound propagation in underwater sound channels. A distinctive feature of this study is incorporating realistic models of the signal coherence to predict the coherence effects on the array beam-pattern and gain for several types of linear and quadratic array processors, the optimal ones included. In the comparative analysis of array processors, we exploit, as a basic technique, the eigenvalue-eigenvector decomposition of the signal covariance matrices. Generally, this approach can be effectively used for various detection criteria including the maximum likelihood (ML) and maximum signal-to-noise (SNR) ones. Our particular interest concerns the small-signal asymptotics of the ML detection performance, which is a reasonable choice for long-range signal reception against the noise background.

In this paper, we give a short introduction to large-array processing of partially coherent, or spatially random signals with emphasis on optimal linear and quadratic beamformers.

BACKGROUND AND FORMULATIONS

Generally, the problem of array signal processing is to detect a signal source and/or to estimate unknown source or transmission parameters. In both cases, one possible strategy is to optimally process the outputs of array elements (sensors) according to a predetermined statistical criterion. In this respect, the ML processor is well known to be of fundamental importance because it is optimal for a variety of detection and estimation criteria [5]. Conventional array beamformers such as those used for plane-wave source detection or bearing estimation in radar [8,9] are derived under the key assumptions of a time-invariant and spatially homogeneous transmission channel between a source and sensors. In realistic long-range channels, however, such assumptions are not generally adequate. Therefore, a principal issue arises, which is to examine the effects of random inhomogeneities perturbing a regular signal wavefield and causing its coherence loss.

In the recent two decades several important developments have been made in this direction. First, the coherence effects on the array beampattern [10] and the detection performance [1-3] were examined by the use of some (exponential-type) models of the plane-wave signal coherence. Second, more relevant models of the multimode signal coherence were used to predict the array beampattern degradation and to compare SNR loss for several linear and quadratic beamformers, conventional plane-wave beamformers (PWBF) and the optimal ones included, in random-inhomogeneous multimode waveguides [4,6,7]. Following these works, we outline below basic for-mulations for the optimal large-array processing of partially coherent signals with emphasis on small-signal consideration.

The signal of interest and the noise background are both assumed to be zero-mean, mutually uncorrelated and Gaussian random processes. The detection problem is formulated as a two-hypothesis alternative:

$$\mathbf{x} = \mathbf{s} + \mathbf{n}, \quad \text{or} \quad \mathbf{x} = \mathbf{n},$$

where $\mathbf{s}$ and $\mathbf{n}$ are, respectively, the N-dimensional signal and noise vectors of the Fourier-transformed data vector $\mathbf{x}$ received by the N-element array of arbitrary configuration.

In general, the data vector can be processed in quadratic form to obtain the detection statistic d by

$$d = \mathbf{x}^{\mathrm{T}} \mathbf{A} \mathbf{x}^{*}, \qquad (1)$$

where $\mathbf{A}$ is an arbitrary ($N \times N$) matrix, and the superscripts "$^{\mathrm{T}}$" and "*" denote transpose and complex conjugate, respectively.

For the ML criterion, the optimal matrix $\mathbf{A}_{\mathrm{opt}}$ is expressed by

$$\mathbf{A}_{\text{opt}} = \mathbf{M}_{\text{n}}^{-1} - (\mathbf{M}_{\text{s}} + \mathbf{M}_{\text{n}})^{-1}. \quad (2)$$

Here, $\mathbf{M}_{\text{s}}$ and $\mathbf{M}_{\text{n}}$ are the spatial covariance mat-rices of the signal and noise, respectively, which are defined for a random vector $\mathbf{x}$ as $\mathbf{M}_{\text{x}} = \langle \mathbf{x}^{*}\mathbf{x}^{\text{T}} \rangle$.

Under the small-signal condition which is a rea-sonable assumption for long-range signal propagation and pow-erful noise interference, the detection performance can be characterized by the deflection q of the detection statistic d, which is also known as the detection index [5,9] or output SNR [1-4]:

$$q = \frac{\langle d(\mathbf{s}+\mathbf{n}) \rangle - \langle d(\mathbf{n}) \rangle}{\left\{ \langle d^2(\mathbf{n}) \rangle - \langle d(\mathbf{n}) \rangle^2 \right\}^{1/2}}. \quad (3)$$

The optimal small-signal matrix from Eq. (2) and de-flection from Eq. (3) are given, respectively, by

$$\mathbf{A}_{\text{opt}} = \mathbf{M}_{\text{n}}^{-1}\mathbf{M}_{\text{s}}\mathbf{M}_{\text{n}}^{-1}, q_{\text{opt}} = \left\{ \text{Tr}(\mathbf{M}_{\text{n}}^{-1}\mathbf{M}_{\text{s}})^2 \right\}^{1/2}. \quad (4)$$

An important point is here the fact that Eq. (4) can be derived alternatively by direct maximizing the deflec-tion q (3) for *arbitrary* signal statistics. There-fore, the choice of the maximum deflection, or SNR criterion is quite reasonable for the case of weak and unknown (non-Gaussian) signals in the Gaussian noise back-ground, when the ML criterion is general-ly not appli-cable to give the optimal processor [5].

The deflection, or the SNR (3) can be used to compare directly the array gain and the gain loss for different beamformers. The array gain G is defined as the out-put SNR normalized to the input SNR q_0, and the gain loss δ as the gain normalized to the number of array elements:

$$G = \frac{q}{q_0}, q_0 = \frac{\text{Tr}(\mathbf{M}_{\text{s}})}{\text{Tr}(\mathbf{M}_{\text{n}})}, \delta = \frac{G}{N}. \quad (5)$$

ARRAY BEAMFORMERS

A general structure of a quadratic beamformer (QBF) can be described clearly using the processor matrix (1) in factorized form as $\mathbf{A} = \mathbf{W}\mathbf{W}^{+}$, where $\mathbf{W}$ is an $(N \times R)$ weight matrix consisting of vector-rows $\mathbf{w}_p$ $(p = 1,2,...,R, 1 \le R \le N)$, and the superscript "+" de-notes conjugate transpose. This structure consists, therefore, of the matrix filter $\mathbf{W}$ followed by an R-channel quadratic processor. Its weight-square-sum output is obtained directly as a *quadratic* function of the input vector $\mathbf{x}$ by

$$y_{\text{QBF}} = \sum_{p=1}^{R} \left| \mathbf{w}_p^{\text{T}}\mathbf{x} \right|^2. \quad (6)$$

Each partial channel of QBF is a linear beamformer (LBF) characterized by the corresponding array weight vector $\mathbf{w}_p$. As distinct from QBF, the LBF weight-sum output is obtained as a *linear* function of the input vector by

$$y_{\text{LBF}} = \mathbf{w}^{\text{T}}\mathbf{x}, \quad (7)$$

where $\mathbf{w}$ is an arbitrary $(N \times 1)$ weight vector. This is a conventional choice for array signal processing with numerous applications in radar and sonar.

Comparing these beamforming schemes we conc-lude that QBF is an incoherent combination of R partial LBFs and reduces to LBF in the particular case of $R = 1$. A choice of the weight vector $\mathbf{w}$ and matrix $\mathbf{W}$ in the LBF and QBF schemes, respectively, determines directly the output processor performan-ces for given (measured or simulated) signal and noise covariance matrices.

We turn now to the optimal QBF and LBF which are of particular interest in examination of the coherence-induced effects on large-array signal processing. For the optimal QBF, the partial weight vectors and SNR are given by [4]

$$\mathbf{w}_p = \lambda_p^{1/2}\mathbf{M}_{\text{n}}^{-1}\mathbf{m}_p^{*}, p = 1,2,..., r = \text{rank}(\mathbf{M}_{\text{s}}), \quad (8)$$

where λ_p and $\mathbf{m}_p$ are the eigenvalues and eigenvec-tors of the signal matrix $\mathbf{M}_{\text{s}}$, respectively.

As follows from Eq. (8), the number R of partial LBFs in the optimal QBF is exactly the signal rank. There-fore, the linear structure can be optimal if and only if the signal matrix $\mathbf{M}_{\text{s}}$ is the rank-one matrix. This conclusion is extremely important for our study because the signal coherence and the signal rank are intrinsi-cally interrelated: the rank r increases with the array length N as compared to the signal coherence length N_{c} (where N_{c} is the dimensionless coherence length expressed in element spacing units).

The optimal LBF exhibits, in its turn, the ultimate coherence-induced limitation for all possible LBFs. Its weight vector and SNR are given by the following ei-genvalue-eigenvector problem:

$$q_p\mathbf{v}_p = \mathbf{M}_{\text{n}}^{-1}\mathbf{M}_{\text{s}}\mathbf{v}_p, p = 1,2,..., r. \quad (9)$$

The largest eigenvalue q_1 gives the maximum SNR, and the corresponding eigenvector $\mathbf{v}_1$ gives the opti-mal weight vector: $\mathbf{w}_{\text{opt}} = \mathbf{v}_1$. Moreover, the eigen-values (9) give the optimal SNR q_{opt} (4).

It follows from Eqs. (8), (9), that in the case of the rank-one signal matrix, both the optimal QBF and LBF reduce to the well-known steady-state adaptive beamformer (noise prewhitening beam-former followed by the matched-signal filter) [8,9] which is, therefore, the optimal scheme to process the perfectly coherent signal against the noise interference.

For the purpose of emphasizing the signal coherence effect, we point out a particular case of spatially white

noise. In this case, the optimal QBF scheme is the incoherent λ_p-weighted combination of the partial filters matched to the signal eigencomponents $(\lambda_p, \mathbf{m}_p)$ (8), while the optimal LBF matches the most powerful eigencomponent $(\lambda_1, \mathbf{m}_1)$. There-fore, an additional gain Q of the optimal QBF is determined only by the signal eigenvalues:

$$Q = \frac{G_{\mathrm{QBF}}}{G_{\mathrm{LBF}}} = \frac{\left\{\sum_{p=1}^{r} \lambda_p^2\right\}^{1/2}}{\lambda_1}, \quad 1 \le Q \le r^{1/2}. \qquad (11)$$

In practice, only the largest eigenvalues and an "effective" signal rank r_{eff} (defined as their number) are of real importance for estimation of the QBF performance, while the contribution of the higher order eigenvalues can be ignored.

Thus, the following characteristics of the received signal are the most important ones with application to the optimal large-array processors: the first (lar-gest) eigenvalue λ_1, the effective rank r_{eff}, and the quadratic gain Q from Eqs. (8)-(11). All of them are determined by the signal eigenvalues and, therefore, are intrinsically interrelated.

The physical parameter related to the signal eigenvalues is the ratio N_c / N which can be estimated by direct measurements using the array. For the case of a coherence-degraded signal, $N_c / N << 1$,

the following estimates are of interest:

$$\lambda_1 \approx \frac{N_c}{N}, r_{\mathrm{eff}} \approx \frac{N}{N_c}, Q \approx r_{\mathrm{eff}}^{1/2} \approx \left(\frac{N}{N_c}\right)^{1/2}. \qquad (12)$$

DISCUSSION

The general formulations outlined above have been effectively exploited by several authors to simulate the optimal processors and to consider suboptimal (quadratic and linear) techniques by the use of exponential-type models for the signal cohe-rence [1,2]. In our papers [4,6,7] the theory has been developed by incorporating a model of multimode signal and simulations of the modal covariance effects on array beamforming. Two intrinsic factors, the modal covariances and the mode orthogonality, were shown to affect mutually optimal array beam-forming and detection performance. For example, the signal rank is considerable, $r_{\mathrm{eff}} \approx M$, if the signal-carrying modes (M is their number) are weakly correlated and the array length is sufficient for their shapes orthogonality or spatial resolution. This means that the coherence effects depend intrinsically on the array configuration in a channel and the array length.

Moreover, the beamforming techniques are very different from the point of view of environmental robustness. The PWBF gain can dramatically vary as a function of the source and environmental parameters, but an obvious advantage of the PWBF techniques is their comparative simplicity. They do not require a preprocessing procedure to estimate the signal eigenspace, and their performance can easily be controlled by reforming the beampattern.

As distinct from the PWBF, the optimal beamformers require the signal eigenvalue-eigenvector analysis. The full-optimal QBF reduces significantly the coherence-induced gain loss, however, at a cost of increased processor complexity: the number of its partial weight-sum channels is equal to the number of the largest signal eigenvalues. The reason to follow such a complicated scheme is only the signal coherence degradation at large distances from a source, or the case of $r_{\mathrm{eff}} >> 1$. Under these conditions, the additional gain Q (11) is considerable.

Therefore, *a priori* estimation from Eq. (12) is the key point of the optimal processor performance/ complexity analysis in the coherence-degraded environments. The most essential and pronounced feature of the optimal QBF is the increase of the gain function $G(N)$ for all array lengths without a "saturation" plateau. The latter, in turn, is an intrinsic feature of the optimal LBF.

ACKNOWLEDGMENTS

This work was supported in part by the Russian Foundation for Basic Research under Grant ¹ 96-15-96592.

REFERENCES

1. H. Cox, *J. Acoust. Soc. Amer.*, 1973, vol. 54, pp. 1743-1746.
2. D. R. Morgan and T. M. Smith, *Ibidem*, 1990, vol. 87, pp. 737-747.
3. L. Laval and Y. Labasque, in *Underwater Aco-ustics and Signal Processing*, L. Bjorno, Ed. Dordrecht, The Netherlands: D. Reidel, 1981, pp. 41-70.
4. A. I. Malekhanov and V. I. Talanov, *Sov. Phys. Acoust.*, 1990, vol. 36, pp. 496-499.
5. H. L. Van Trees, *Detection, Estimation and Modulation Theory, Part I.* New York: Wiley, 1968.
6. E. Yu. Gorodetskaya, A. I. Malekhanov, and V. I. Talanov, *Sov. Phys. Acoust.*, 1992, vol. 38, pp. 571-575.
7. E. Yu. Gorodetskaya, A. I. Malekhanov, A. G. Sazontov, and N. K. Vdovicheva, *IEEE J. of Ocean Eng.*, 1999, vol. 24 (in press).
8. Ya. D. Shirman and V. N. Manzhos, *Theory and Techniques of Signal Processing in Radar.* Moscow: Radio i Svyaz', 1981 [in Russian].
9. R. A. Monzingo and T. W. Miller, *Introduction to Adaptive Arrays.* New York: Wiley, 1980.
10. Ya. S. Shifrin, *Radiotekhn. i Electron.*, 1990, vol. 35, pp. 1345-1360 [in Russian].

POWER OPTIMIZATION OF THE BEAM SHARED-FORMING MONOPULSE ARRAYS

B. D. Manuilov, P. N. Bashly

The Rostov military Institute of Rocket
Troops 24a, Oktyabrya an., Rostov-on-Don, 344027
E-mail: chernat@don.sitek.net

Maximization of signal - to noise and interference relation (SNIR) or an energy optimization is one of the trends in the optimization of array integral parameters.

In spite of the defining role of the SNIR in providing an accuracy of the monopulse radar systems there are no published papers on the energy optimization for the monopulse arrays.

The purpose of the present paper is the development of the energy optimization method for the total-difference, beam-shared-forming monopulse arrays, that is for such arrays, in the channel of each radiator of which there is one device of a complex weighing J_n (n = 1, 2...N). In such arrays forming of two beams of the monopulse group is provided by the way of using two adders, the inputs of which are connected with the devices of complex weighing through the fixed shift-phasers, providing a progressive increasing (for the first beam) or decreasing (for the second beam) phase shift.

The problem of the energy optimization is formulated as follows. It is necessary to find N-dimensional vector-column $|J\rangle$ for the complex currents amplitudes in the radiators which maximizes the ratio q of the signal power in the aggregate channel to the sum of the noise and interference power in the first and the second beams of the monopulse group, that is

$$\max_{|J\rangle} q = \frac{P_s^{\Sigma}}{(P_{ns}+P_{in})^{(1)}+(P_{ns}+P_{in})^{(2)}}, \qquad (1)$$

where in assumption of unit load it is accepted that

$$P_s^{\Sigma} = \left|f^{\Sigma}(\Theta_o)\right|^2 = f^{\Sigma *}(\Theta_o)\cdot f^{\Sigma}(\Theta_o), \qquad (2)$$

$$(P_{ns}+P_{in})^{(\nu)} = \frac{1}{2\pi}\int_{-\pi/2}^{\pi/2} f^{(\nu)*}(\Theta) f^{(\nu)}(\Theta) T(\Theta) d\Theta, \qquad (3)$$

$$f^{(\nu)}(\Theta) = f(\Theta \pm \Delta\Theta), \ \nu = 1, 2. \qquad (4)$$

$T(\Theta)$ is a noise distribution function determined by the following expression

$$T(\Theta) = \begin{cases} a_o^k & \text{at } \Theta_{\text{in k}}^{\min} \le \Theta \le \Theta_{\text{in k}}^{\max} \\ 1 & \text{otherwise} \end{cases},$$

where a_o^k - is a relative level of the k-th interference,

$\Theta_{\text{in k}}^{\min}$ and $\Theta_{\text{in k}}^{\max}$ are the lower and upper boundaryis of the spatial distribution of the k-th interference.

The upper sign in the expression (4 corresponds to $\nu = 1$. Denote the unnormalized pattern of the system excited by current $|J\rangle$ by the function $f(\Theta)$:

$$f(\Theta) = \sum_{n=1}^{N} f_n(\Theta)\cdot J_n = (f)\cdot|J\rangle. \qquad (5)$$

(f) means here the for N-dimensional vector-row of the unnormalized pattern $f_n(\Theta)$ of the system excited by the current of a unit amplitude at the $n-$th input. Also

$$f^{\Sigma}(\Theta) = f^{(1)}(\Theta) + f^{(2)}(\Theta), \qquad (6)$$

where Θ_0 is the boresight angle,

$2\Delta\Theta$ is the angle of the beam spread of the monopulse group,

and is a sign of a complex conjugation of the scalar magnitude and the Hermite matrix conjugation.

Taking into account that

$$f(\Theta \pm \Delta\Theta) = \sum_{n=1}^{N} f_n(\Theta)\cdot J_n \cdot e^{\mp j\Psi_n}, \qquad (7)$$

where $$\Psi_n = \frac{2\pi}{\lambda} x_0 \left(n - \frac{N+1}{2}\right)\sin\Theta, \qquad (8)$$

λ, x_0 - are the wavelength and array spacing, relatively, and introducing the designation

$$\bar{f}_n(\Theta) = f_n(\Theta)\cdot 2\cos\Psi_n, \qquad (9)$$

we obtain from (6) taking into account (4) at $\Theta = \Theta_0$ the following:

$$f^{\Sigma}(\Theta_0) = \sum_{n=1}^{N} \bar{f}_n(\Theta_0) J_n = \left(\bar{f}(\Theta_0)\right)\cdot|J\rangle. \qquad (10)$$

Taking into consideration (2), we can write

$$P_s^{\Sigma} = |J\rangle^{*}\left[A^{\Sigma}(\Theta_0)\right]J\rangle, \qquad (11)$$

where $\left[A^{\Sigma}(\Theta_0)\right]=\left(\bar{f}(\Theta_0)\right)^{*}\left(\bar{f}(\Theta_0)\right)$ - is the square matrix of the N-th order with elements

$$a_{mn}=\bar{f}_m^{*}(\Theta_0)\bar{f}_n(\Theta_0). \qquad (12)$$

Similarly we can write

$$\left(P_{ns}+P_{in}\right)^{(\nu)}=|J\rangle^{*}\left[B^{(\nu)}\right]J\rangle, \qquad (13)$$

where $\left[B^{(\nu)}\right]$ - is the square matrix of the N-th order with elements

$$b_{mn}^{(\nu)}=\frac{1}{2\pi}\int_{-\pi/2}^{\pi/2}f_m^{*}(\Theta)\cdot f_n(\Theta)\cdot e^{\pm j(\Psi_m-\Psi_n)}T(\Theta)d\Theta\,. \qquad (14)$$

Taking into account (12) and (13) and introducing the designation

$$[B]=\left[B^{(1)}\right]+\left[B^{(2)}\right], \qquad (15)$$

from (1) we obtain

$$q=\frac{|J\rangle^{*}\left[A^{\Sigma}(\Theta_0)\right]J\rangle}{|J\rangle^{*}[B]J\rangle}\,. \qquad (16)$$

As matrices $\left[A^{\Sigma}(\Theta_0)\right]$ and $[B]$ are the Hermite ones, then q is the ratio of the Hermite shapes.

The Hermite shapes introduced in (16) define the bundle of the shapes $|J\rangle^{*}\left[A^{\Sigma}(\Theta_0)\right]J\rangle-q|J\rangle^{*}[B]J\rangle$ which is regular as shape $|J\rangle^{*}[B]J\rangle$ is defined positively due to being caused by its physical nature.

Maximum of (16) is egual to the greatest characteristic number of the shape bundle and this maximum is reached only for the principal vector of the bundle corresponding to this number.

The optimal current vector (the complex weighting coefficients) is found from

$$|J\rangle_{\text{opt}}=[B]^{-1}\left(\bar{f}(\Theta_0)\right)^{*}, \qquad (17)$$

And the functional maximum realized in this case is defined by the relation

$$q_{\max}=\left(\bar{f}(\Theta_0)\right)[B]^{-1}\left(\bar{f}(\Theta_0)\right)^{*}. \qquad (18)$$

Numerical simulation of the power optimization according to the suggested method was carried out on the specimen of the 19-component antenna array of isotropic elements arranged with 0.5λ spacing. The receiver direction of the desired signal is $\Theta_0 = 20°$.

In Fig. 1 one can see the total $f^{\Sigma}(\Theta)$ (dashed line) and the difference $f^{\Delta}(\Theta)$ (solid line) pattents optimized at the interference distribution function of the following form:

$$T(\Theta)=\begin{cases}10^5 & \text{at } 35^{o}\le\Theta\le 40^{o}\\ 1 & \text{otherwise}\end{cases}.$$

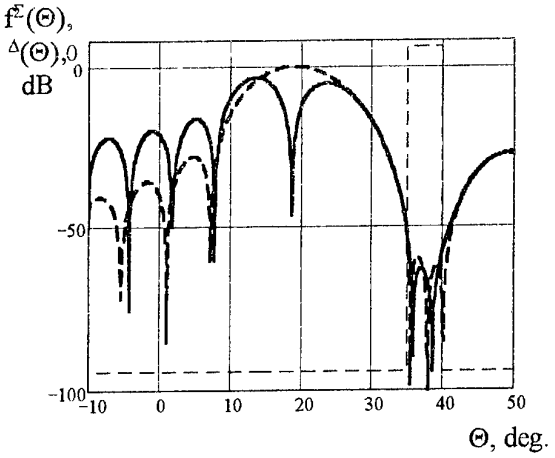


Fig. 1

It follows from Fig.1 that the gaps with the level < -60 dB are formed in the whole sector of the interference distribution and in the total and difference pattern and in this case the directive gain in the aggregate channel of the optimised antenna array decreases by 0,7 dB and SNIR in the aggregate channel increases from -5.8 dB to 10.7 dB.

At the same time it is necessary to note that thefunctional maximum (1) defined by expression (18) is equal to 12.5 dB while its magnitude before the optimization was equal to -14.5 dB.

While the gap forming the boresight shift arises both in the total and difference patterns. The shift magnitude reaches almost 10 % of the principle maximum width of the total pattern in the considered specimen.

One of the ways to compensate the boresight shift while forming the gaps in the pattern is to form a gap not only in the interference direction but in the direction symmetric to it in the generalized coordinate with respect to the radar boresight.

Anexample of the array parameter optimization with allowance for the dummy interference is shown in Fig. 2. In this case the interference distribution function has the form:

$$T(\Theta)=\begin{cases}10^5 & \text{at } 35°\le\Theta\le 40°\\ 10^5 & \text{at } 2.4°\le\Theta\le 6.3°\\ 1 & \text{otherwise}\end{cases}.$$

All the designations here are the same as in Fig. 1.

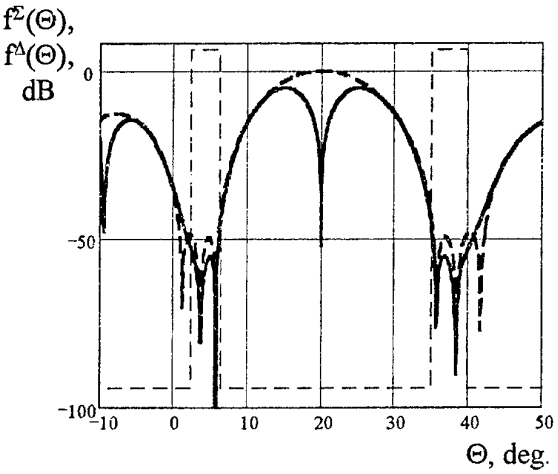


Fig. 2

The result analysis has shown that the introduction of the dummy iterference, symmetrical in the generalized coordinate with respect to the radar boresight eliminates the boresight shift both in the total and difference pattern, and in this case an additional reduction of the directive gain by 0.5 dB and SNIPR in the aggregate channel by 2.3 dB takes place.

The developed method of the power optimization for the monopulse antenna arrays for the maximum criterion of the ratio of the signal power in the aggregate channel to the sum of the powers in each of the beams of the monopulse group is efficient and permits to carry out the spatial filtering of the interfering signals received from the certain directions.

Modification of function $T(\Theta)$ by the dummy interference permits to compensate the boresight shift arising at the gap forming.

Functional (1) can be used also in the adaptive beam-shared-forming monopulse antenna arrays.

DIAGNOSTICS OF RECEIVING HYDROACOUSTIC ANTENNA ARRAYS

D. A. Orlov and V. I. Turchin

Institute of Applied Physics RAS
46 Uljanova Str., 603600 Nizhny Novgorod, Russia
Tel.: (8312) 384274. Fax: (8312) 365976. E-mail: orlov@hydro.appl.sci-nnov.ru

INTRODUCTION

Any experiment performed with the use of receiving hydroacoustic antenna arrays requires solving the important problem of determining their various characteristics after array deployment.

Transfer coefficients of array hydrophones, that relate acoustic pressure at the hydrophone input with voltage at the output, are an example of such characteristics. After array deployment, these coefficients may differ considerably from the values measured under laboratory conditions (before array deployment). The problem of measurement of transfer coefficients of low-frequency arrays after array deployment has not been fully investigated. In the case of arrays with flexible or semi-rigid deployment, solution of the important problem of determining their profile in horizontal or vertical planes is needed. Besides for many applications in is necessary to estimate bottom parameters in the region of array deployment must be performed.

To solve the problems mentioned, a complex method was developed. This method uses a source of tonal acoustic signal with changing frequency and a precise hydrophone with a known transfer coefficient. It is assumed that the transfer coefficients of array hydrophones are not considerably dependent on frequency, the source is monopole (its radiation level is the same in various directions) and the precise hydrophone has a uniform spatial beam pattern. The realization of the proposed method also enables to determine whether a multibeam substance model is suitable under natural conditions. In this model, an acoustic signal from a source of tonal signal is modeled as the sum of the direct signal and multiple reflections at the surface and bottom.

EXPERIMENTAL SETUP

The method described below was applied to the hydroacoustic data obtained in the framework of the expeditions of the Institute of Applied Physics RAS to Sankhar Lake, Vladimir region (1997 and 1998). All the results demonstrated below were obtained from the data collected during these expeditions.

The method proposed consists in the following. At a small distance from a horizontal or vertical antenna array, a precise hydrophone with the known transfer coefficient and a source of tonal signal with changing frequency are placed at a given distance from each other (Fig. 1).

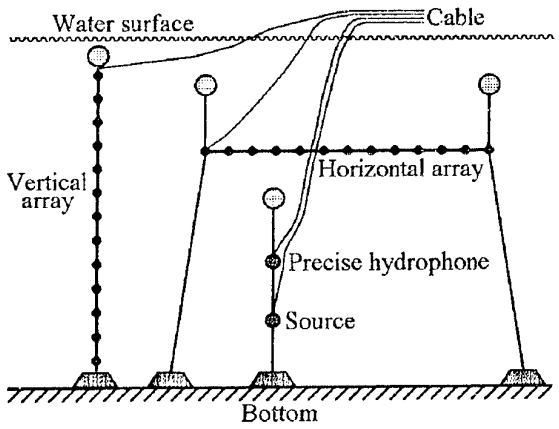


Fig. 1. Scheme of the experiment

The source is excited by the frequency stepped signal in a certain frequency range. For each frequency, the received signal is filtered by a narrow-band filter with the center frequency equal to the frequency of radiation, and the resulting complex amplitudes of the signals from the precise hydrophone and from each of the array hydrophones are recorded. Thus, the signal at the processing input represents the dependence of the received signal on the hydrophone number and frequency.

TRANSFER COEFFICIENTS

The proposed technique of determining the transfer coefficients of array hydrophones consists in the comparison of the signal received by the precise hydrophone with the signal received by each of the array hydrophones. For such a comparison, it is necessary to separate the direct signal and the reflections from the surface, from bottom, and multiple reflections from the surface and bottom. In order to achieve this aim, the Fourier transform of the initial dependence of the complex signal on frequency can be used each hydrophone. This operation transforms the initial dependence on the hydrophone number and frequency to the dependence on the hydrophone number and time delay, so that the impulses corresponding to the direct signal, as well as multiple reflections at the surface and bottom, are obtained. A characteristic dependence of signal amplitude in the "hydrophone number – time delay" plane in the case of a horizontal array is represented in Fig. 2. The first three rays – the direct ray (1) and the rays reflected

by the surface (2) and bottom (3) – are clearly visible in this picture.

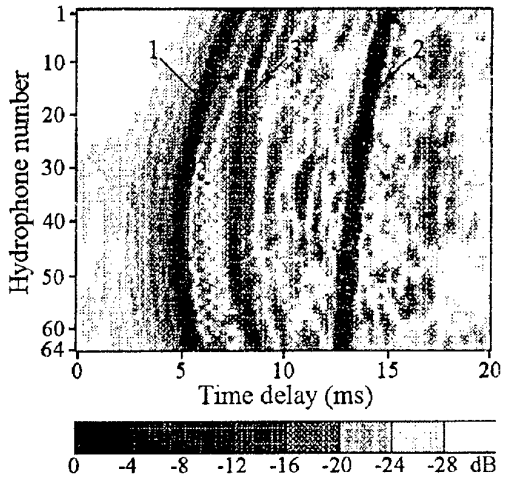


Fig. 2. Received signal versus time delay and hydrophone number for a horizontal array

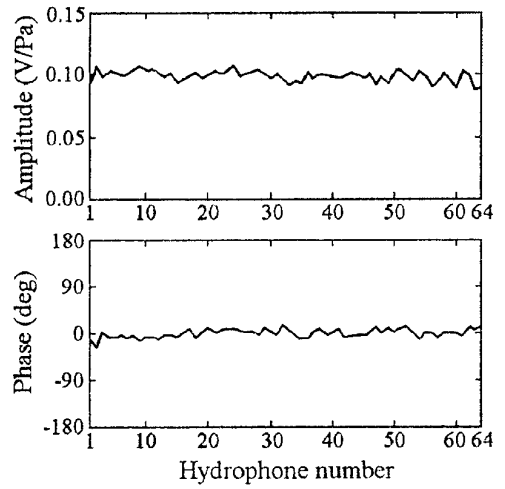


Fig. 3. Amplitude and phase of the transfer coefficients

Separated in such a way, the direct ray can be used for determining the transfer coefficients of the array hydrophones. The maximum positions corresponding to the direct signal allow (know the sound velocity in water) to determine the distances from the source to each hydrophone. Then, upon finding the signal at the maxima and knowing both the precise hydrophone transfer coefficient and the distances from the source to both the precise hydrophone and the array hydrophones, one can calculate the transfer coefficients of the array hydrophones. Since the procedure of ray separation has at its input the signal over a wide frequency range, the transfer coefficients calculated in this way represent the averaged values in the given frequency range. An example of dependence of transfer coefficients amplitude and phase on the hydrophone number obtained according to the descibed above procedure is demonstrated in Fig. 3.

ARRAY PROFILE

To solve the second problem – determination of the array profile – one can use the direct ray and the ray reflected by the surface (separated with the help of the procedure described above). In particular, the profile of a horizontal array can be modeled as a chain line with three unknown parameters (for example, the depths of the array edges and its flexure), and these parameters can be estimated by means of the MRSE method proceeding from the arrival times of the direct ray and the ray reflected by the surface. An example of restored profile of a horizontal array is given in Fig. 4.

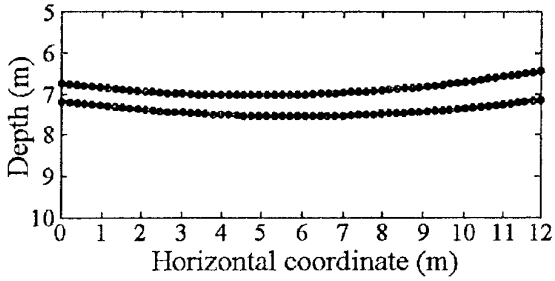


Fig. 4. Shape of a horizontal array (for two deployments)

BOTTOM PARAMETERS

For an estimation of the bottom parameters, the direct and bottom-reflected rays can be used. The ratio of signal amplitude in maxima corresponding to the direct and bottom-reflected rays gives an estimate of the bottom reflection coefficient for the angle of incidence corresponding to the locations of the source and of each of the array hydrophones. Thus, having chosen an appropriate source location, one can obtain the dependence of the reflection coefficient on the angle of incidence in the range wide enough to estimate (for example, by the MRSE method) the bottom parameters – density and sound velocity – for a chosen bottom model, for instance, for the model of liquid bottom, where the reflection coefficients are given by the Fresnel formula.

CONCLUSION

The use of the described method for the determination of the transfer coefficients of array hydrophones and array profile has shown its efficiency. Since the bottom of the lake where the experiment was performed had rather complex structure (most likely, it represented ground with a layer of silt on it), it was not possible to determine the contributions of ground density and sound velocity in ground to the reflection coefficient.

ACKNOWLEDGMENT

The work was supported by Russian Foundation of Basic Research under Grant 96-15-96603.

SIMULATION OF ANTENNA ARRAY CHARACTERISTICS IMPACT ON OBJECTS IMAGE RESTORATION

I. Prudyus, L. Lazko, T. Holotyak

State Univetrsity «Lvivska Polytechnika», 12 S.Bandery Str., Lviv, 290646, Ukraine
E-mails: {iprudyus, t.holotyak}@polynet.lviv.ua; lazko@postmark.net

Remote sensing systems development permits to improve their informative parameters, i.e. increase probability of target detection/recognition, spatial resolution, etc. This paper deals with passive type of remote sensing systems or with radiometry imaging systems.

These modern systems require high spatial resolution that could be satisfied by two ways: 1) usage of improved antenna systems or 2) signal or image processing methods applications. Impact of antenna system on image formation quality is rather high though the influence of this system on parameters of image formation system in general.

Problem of aperture geometry impact on image formation process was investigated in [1] Therefore, in this paper problem of aperture field distribution and phase distribution influence on image formation/restoration will be considered.

Image formation in remote sensing system could be written by means of the following integral equation

$$g(\theta,\varphi)=\iint_{\Omega} h(\theta',\varphi')f(\theta',\varphi',\theta,\varphi)d\theta' d\varphi', \qquad (1)$$

where g is a received image, f is an original image, h is a direction function of receiving system, θ, φ are the spatial coordinates.

For radiometry imaging system with spatially invariant direction function of receiving system above equation could be rewritten as follow

$$g(\theta,\varphi)=\iint_{\Omega} h(\theta',\varphi')f(\theta-\theta',\varphi-\varphi')d\theta' d\varphi', \qquad (2)$$

or in matrix form

$$\mathbf{g}=\mathbf{H}*\mathbf{f}, \qquad (3)$$

where **H** depends on aperture amplitude and phase distribution.

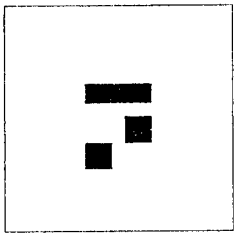


Fig. 1. Test image

Impact of the amplitude distribution will be considered on the base of the following example. Three different types of amplitude field distributions (Fig. 2) will distort test image (Fig. 1).

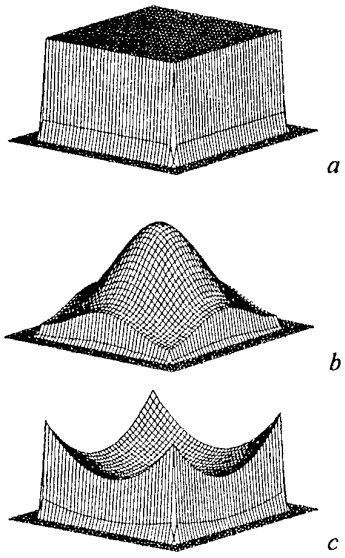


Fig. 2. The amplitude field distribution:
(a) uniform; (b) cos-distribution; (c) with valley

Distribution (b) and (c) were defined according to the following equations, respectively

$$I(x,y)=\cos\left(2\pi\frac{x}{L_x}\right)\cos\left(2\pi\frac{y}{L_y}\right), \qquad (4)$$

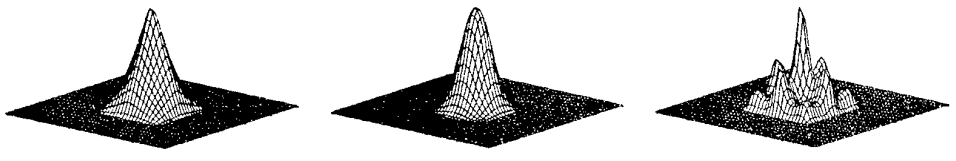
$$I(x,y)=\left((1-a)+a\left(\frac{x}{L_x}\right)^2\right)\left((1-a)+a\left(\frac{y}{L_y}\right)^2\right), \qquad (5)$$

where x, y are coordinates in antenna aperture, parameter a determines the valley of the field distribution and was chosen $a = 0.7$.

Spatial spectra of the corresponding aperture for radiometry imaging systems are the Fourier transform from power direction pattern and are shown in Fig. 3.

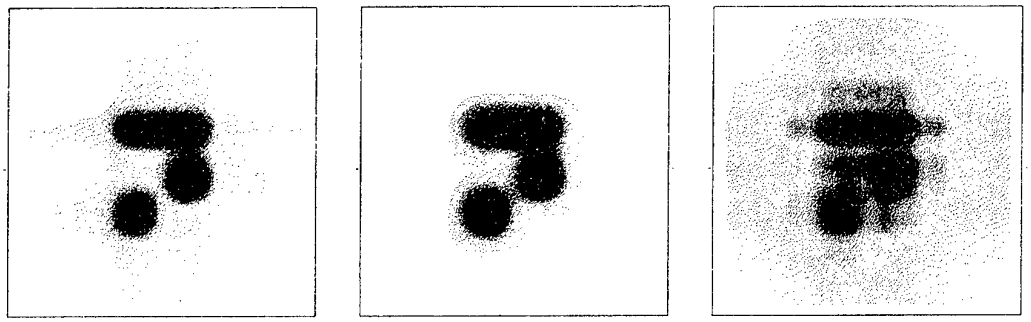
Results of image formation by antennas are presented in Fig.4.

Obtained results permit to conclude that aperture that has distribution with valley (case (c)) satisfies the pre-



a b c

Fig. 3 Spatial spectra for apertures with different amplitude distribution:
(a) uniform; (b) cos-distribution; (c) with valley



a b c

Fig. 4. Image formation by antennas with different aperture distributions:
(a) uniform; (b) cos-distribution; (c) with valley

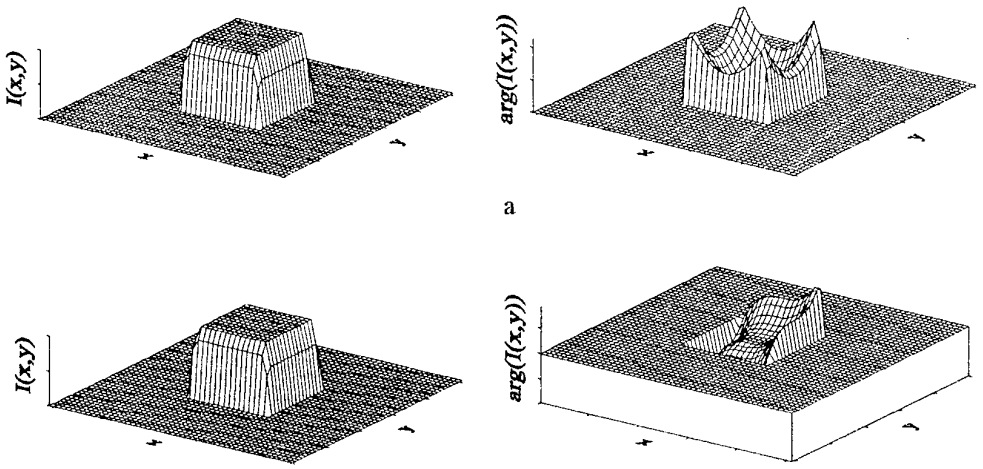


Fig. 5. Amplitude and phase distributions for quadratic (a) and cubic (b) phase distortions

serving of image element details and form that can be explained by structure of high frequency part of antenna spatial spectrum (less suppression of high spatial frequencies in comparative with another cases).

Problem of phase distribution in antenna aperture is also actual, especially in radiometry imaging system with synthesised aperture. Main role in image formation plays quadratic and cubic phase distributions.

Quadratic phase distortions characterise near zone systems and are named as defocusing. They can be expressed according to the following equation

$$I(x,y) = I_0 \exp\left(-j\Phi_2\left(\left(\frac{2x}{L_x}\right)^2 + \left(\frac{2y}{L_y}\right)^2\right)\right), \quad (6)$$

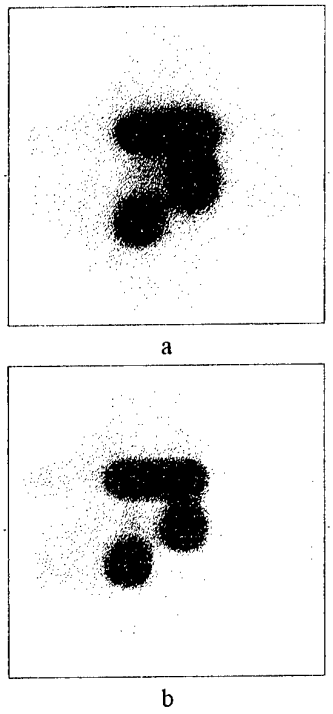
where I_0 is field amplitude distribution (uniform), Φ_2 is maximum phase deviation on aperture border.

Cubic phase distortion is written by the following expression

$$I(x,y) = I_0 \exp\left(-j\Phi_3\left(\left(\frac{2x}{L_x}\right)^3 + \left(\frac{2y}{L_y}\right)^3\right)\right). \quad (7)$$

Both kinds of phase distortions for the case of uniform amplitude distribution are shown in Fig. 5.

Fig. 6 presents the results of test image formation by means of antenna with mentioned phase distributions.



a

b

Fig. 6. Image formation by antennas with quadratic (a) and cubic (b) phase distributions

In this paper influence of amplitude and phase distribution on image formation process in radiometry imaging systems was investigated. Results of carried out simulation could be applied for real antenna array analysis.

REFERENCES

1. I. Prudyus, S. Voloshynovskiy, T. Holotyak. Sparse antenna array in radar imaging systems // Proceedings of 3rd International Conference on Telecommunications in Modern Satellite. Cable and Broadcasting Services, TELSIKS'97, Nis, Yugoslavia, October 8-10 1997, V. 1. pp.46-49.
2. I. Prudyus, S. Voloshynovskiy, T. Holotyak. Investigation of spatial antenna system characteristics in active and passive imaging system // Proceedings of International Conference on Modern Problem of Telecommunications, Computer Science end Engineer Training, TCSET'98, Lviv, Ukraine, February 23-28, 1998, pp.124-125.
3. I. Prudyus, S. Voloshynovskiy, T. Holotyak. Mathematical models and spatial characteristics of coherent and incoherent imaging systems // Proceedings of 3rd International Symposium MSMW'98, Kharkiv, Ukraine, September 15-17, 1998, pp. 562-564.
4. I. Prudyus, S. Voloshynovskiy, T. Holotyak. Comparative analysis of continuum antennas and sparse arrays with signal processing in remote sensing problems. // Proceedings of the Second International Conference on Antenna theory and techniques, Kyiv, Ukraine, May 20-22, 1997, pp. 183-185.

SIMULATION OF SPATIAL-TIME SIGNAL PROCESSING IN IMAGING SYSTEMS WITH SYNTHETIC APERTURE

I. N. Prudyus, A. T. Synyavskyy, V. P. Ostap

State University "Lvivska Polytechnika" Radio Engineering Faculty
Lviv 29646, S.Bandery Str., 12, Ukraine Tel.: (0322) 72 37 25
E-mail: sinat@polynet.lviv.ua

The principle of synthesizing of the apertures is widely known and is effectively used in radar imaging systems [1–3]. The synthetic apertures enable to get a narrow radiation pattern (RP), that improves a resolution of the radar system. If in ordinary antenna systems the shaping of a RP occurs instantly and depends on mutual arrangement of radiating elements and parameters of their excitation, than in synthetic aperture the shaping of a RP is carried out in time by a relocating of the elementary antenna carrier and is provided by the appropriate spatial-time processing in the system.

Depending on the type of an antenna channel single-station radar systems and coherent multistaion radar systems are distinguished. The mathematical simulation of such systems allows effectively to develop, analyze and optimize algorithms of a received radar information processing.

For radar systems, which work on the single-station principle with angular scanning by a RP the simple and effective model is developed [4]. In such systems the quality of the obtained image is defined in a greater degree by properties of spatial filtering of the antenna, namely by parameters of the RP. In such model it is inexpedient to take into account time process. Mathematically, such model is represented by convolution of a spatially distributed scattering ability (SA) with point spread function (PSF), which is dependence on spatial coordinates.

In space and airborne active radar imaging systems with coherent processing – synthesizing of the aperture at the expense of relocating of the elementary antenna carrier are most often used [3]. The principle of such systems activity consists in probing of researched objects from different points of a space, and appropriate consequent coherent summation of the received signals. The systems in which the relocation trajectory is close to linear are most often used. Schematically, the principal of their activity is shown in the Fig. 1. The advantage of such systems over single-station ones consists in their ability to provide by far higher resolution.

A special feature of the simulation of radar systems with coherent processing is their impossibility to represent separately spatial and time processes. Analytically relation between a function, which specifies a spatially distributed SA $Q(x,y)$ of a researched object and the resulting raw image $I(x,y)$ will be called the mathematical model of the system.

The well-known methods of a simulation of such systems based on the Radon transformation [5] do not allow to specify completely the processes at the synthesizing aperture and is their simplified mathematical models.

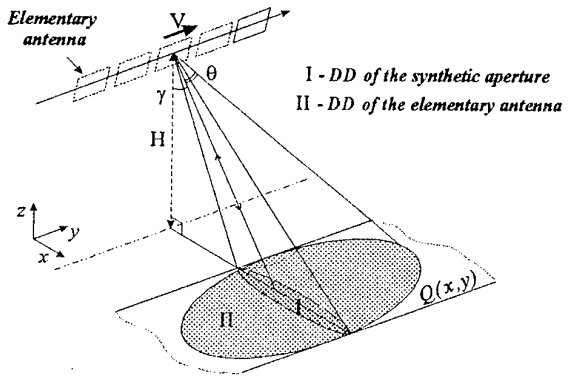


Fig. 1. Synthesizing of the apertures in radar imaging systems

At created the model, plane character of researched objects, isotropic scattering of points and an absence of secondary reflection on a surface of the objects are assumed. Then echo-signal $\dot{s}_{echo}(t)$ from a direction θ is convolution SA $Q(\tau,\theta)$ in the direction with a probe signal $\dot{s}_{probe}(t)$:

$$\dot{s}_{echo}(t,\theta) = \dot{W}(\theta)\int_0^{\infty} Q(t-\tau,\theta)\cdot \dot{s}_{probe}(\tau)d\tau . \quad (1)$$

A coefficient $\dot{W}(\theta)$ is defined by spatial filtering features of the radiating elementary antenna, losses K at a wave propagation and complex coefficient, which depends on a Doppler shift $\Omega_{Doppler}(\theta)$ in given direction

$$\dot{W}(\theta) = K\cdot \dot{F}_{rad.}(\theta)\cdot e^{-j\Omega_{Doppler}(\theta)t}, \quad (2)$$

where $\dot{F}_{rad}(\theta)$ – RP of the elementary radiating antenna.

The such systems feature consists in this, that there is the Doppler shift, which depends on a propagation direction of the signal is caused by the carrier velocity V:

$$\Omega_{Doppler}(\theta) = \frac{2\omega_o}{c} \cdot V \cdot \sin(\theta), \qquad (3)$$

where ω_o – carrier frequency of a signal probe; c – velocity of a wave propagation.

The received signal in the i-th position of probing is defined:

$$\dot{S}_i(t) = \int_{-\pi/2}^{\pi/2} \dot{F}_{rec.}(\theta) \cdot \dot{s}_{echo}(t,\theta)\, d\theta, \qquad (4)$$

where $\dot{F}_{rec.}(\theta)$ – RP of the elementary receiving antenna. Then for spherical coordinate system, which has a center in i-th position of probing, the signals on an output of a receiver are defined by the expressions (1), (2) and (4):

$$\dot{S}_i(t) = K \cdot \int_{-\pi/2}^{\pi/2} \int_{0}^{\infty} \dot{F}_{rec}(\theta) \cdot \dot{F}_{rad}(\theta) \times \qquad (5)$$

$$\times \dot{Q}^i(t-\tau,\theta) \cdot \dot{S}_{probe}(\tau) \cdot e^{-j\tau\left(\omega_o + \Omega_{Doppler}(\theta)\right)} d\tau\, d\theta,$$

where $\dot{S}_{probe}(t)$ – complex envelope of a probe signal; $\dot{Q}^i(t,\theta)$ – spatially distributed SA of a researched object, which is represented in a spherical coordinate system with a center in i-th position of probing.

The resulting radar information is represented by the set $\dot{S}_i(t)$ of the received samples in different positions of probing.

The process of synthesizing of the aperture consists in coherent summation of the received samples. The signal of the synthetic aperture, which consists of $(2N+1)$ elements, is could analytically represented by a sum of the complex samples with appropriate weighting coefficients $\dot{C}_j$:

$$\dot{U}_k(t) = \sum_{j=k-N}^{k+N} \dot{C}_j \dot{S}_j(t). \qquad (6)$$

The coefficients $\dot{C}_j$ are by an equivalent of distribution of a current in the synthetic aperture. If a law of variation of the coefficients is provided to be necessary we can form the different RP in the synthetic aperture, define a direction of a lobe of the RP, or focus of the RP on a defined distance.

The expressions (5) and (6) represents an analytical model of radar imaging system. A resulting raw image $I(x,y)$ correspondes to the set of the complex variables $\dot{U}_{k,l}$, which are defined in discrete samples of a time $l = t/\Delta t$.

The created model (5) and (6) represents relationship between two coordinate systems:

- movable spherical coordinate system, where it is convenient to describe the spatial-time features of the radar receiving and transmitting channel;
- stationary rectangular coordinate system, where the spatially distributed SA of a researched object is represented.

A numerical simulation requires to use interpolation methods at a transition between both of this discretization grids in the appropriate coordinate systems.

The linearity of the model (5) and (6) gives possibility to characterize of radar systems with synthetic aperture by a point spread function (PSF) [6]. The created model was used for the search of a response of the system at SA by way of the unit impulse. It is assumed, that an envelope of the probe signal has a form of the gaussian pulse.

The processes in a far zone and fresnel zone needs to be precisely separated in the radar systems with synthetic aperture. Results of the research denote a variation of a form of spatial-time point spread function, which depends on the coordinates of a researched object:

- the far zone is defined by a phase incursion at the aperture edges at the expense of the change of range, which is less than $\pi/4$;
- the fresnel zone is defined by a phase incursion at the synthetic aperture edges at the expense of the change of range, which is more than $\pi/4$.

In the far zone the quadratic phase incursion do not result in the significant degradation of a resolution. The coherent optimal summation can be performed without a compensation of the phase incursions. The result of synthesizing of the aperture, which is composed of 5 elementary antennas is represented by the spatial-time PSF and the RP of the radar system in the Fig. 2.

An enhancement of effective width of the synthetic aperture gives rise to an apparition of significant quadratic phase incursion. At the coherent summation of the received signals the existing of the phase incursions and the time delay should is compensated by choosing of the appropriate coefficients $\dot{C}_j$ for the reception of a high resolution in the fresnel zone. The spatial-time PSF and the equivalent RP is represented in the Fig. 3 for synthetic aperture, which composed with 100 ele-

mentary antennas and the phase incursion is compensated at the coherent processing.

Without the compensation of the phase incursion the extension of the RP of synthetic aperture is passed. It is represented by the Fig. 4.

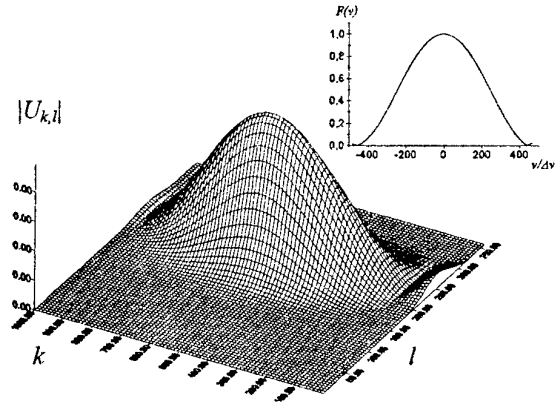


Fig. 2. The spatial-time PSF and the RP at the synthesizing of the aperture with 5 elementary antennas

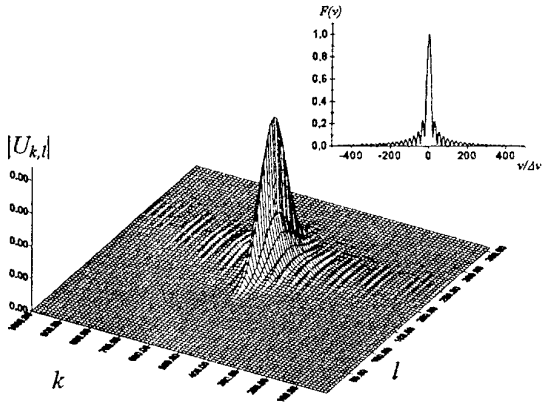


Fig. 3. The spatial-time PSF and the RP at the synthesizing of the aperture with 100 elementary antennas and the compensated phase incursion

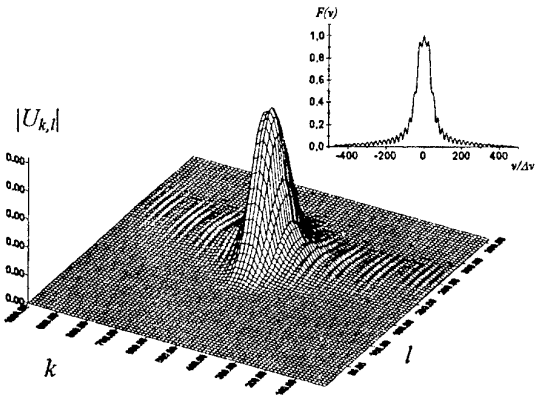


Fig. 4. The spatial-time PSF and the RP at the synthesizing of the aperture with 100 elementary antennas without compensation of the phase incursion

The results of the simulation processes at the radar imaging are represented in the Fig. 6, 7 for the test model SA (Fig. 5) by the radar systems with synthetic aperture and coherent spatial-time processing.

The possibility of an obtaining of the narrow enough RP of the synthetic aperture at the expense of optimal spatial-time processing with compensation of the quadratic phase incursion and time delays is confirmed by the results of the simulation. It is allows to provide the high resolution of the radar imaging systems with synthetic aperture and obtain a high quality radar images.

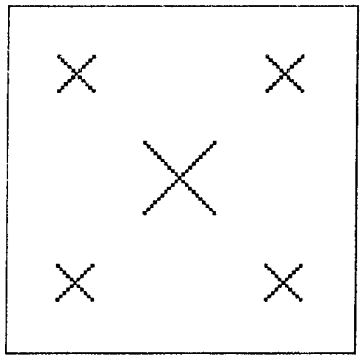


Fig. 5. The model SA $Q(x,y)$

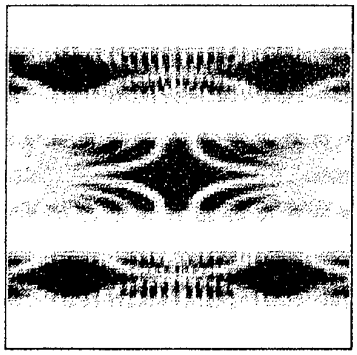


Fig. 6. The obtained raw radar image $I(x,y)$ by synthetic aperture with 5 elementary antennas

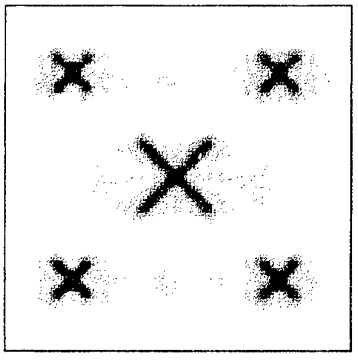


Fig. 7. The obtained raw radar image $I(x,y)$ by synthetic aperture with 100 elementary antennas

REFERENCES

1. N. I. Burenin. Radars with synthetic aperture, Moscow, Sov. Radio, 1972 [in Russian].
2. V. V. Karavajev, V. V. Sazonov. Principles of synthetic antennas theory, Moscow, Sov. Radio, 1974 [in Russian].
3. A. P. Reutov, B. A. Mikhajlov, G. S. Kondratenko, B. V. Bojko, Radars of side looking, Moscow, Sov. Radio, 1970 [in Russian].
4. I. Prudyus, S. Voloshynovskiy, T. Holotyak, "Investigation of Spatial Antenna System Characteristics in Active and Passive Imaging System,"/ *Proc. TCSET'98*, Feb. 1998.
5. Martin Lindberg, "Radar Image Processing with the Radon Transform", No 1997-05/ISSN 0347-2809.
6. M. D. Desai, W. K. Jenins, "Convolution Back-projection Image Reconstruction for Splotight Mode Synthetic Aperture Radar" / IEEE Trans. on Image Processing, 1992.

OPTICALLY OR ELECTRONICALLY STEERABLE MM-WAVE PHASED ANTENNAS ARRAY BASED ON SEMICONDUCTOR STRUCTURE

V. Ya. Rogov, A. Yu. Grinev, A. E. Zaikin

Moscow State Aviation Institute. MAI, 4, Volokolamskoe shosse, Moscow, 125871, Russia
Tel.: (095) 158-4740. Fax: (095) 158-2977 or (095) 928-8187. Email: antenna@mai.ru
Phazotron-NIIR JSC. 1, Elektrichesky per., Moscow 123557, Russia
Phone: (095) 253-1636. Fax: (095) 253-0495. E-mail: voha @ centro.ru

This paper presents results of thecomplex researches of Phased Array Antennas (PAAs) for the MMW-band's short-wave subband based on the nontraditional approach to designing the anrenna's aperture when using multilayer semiconductor structures with optically or electronically steerable electrophysical parameters.

The MMW PAAs (30 to 300 GHz) are analyzed, which are based on the similarity principle (extension of the cm-wave antenna design principles to the MMW antenna system design principles), on using of steerable lens antennas, on surface-to-volume wave conversion effect, on using of a steerable impedance aperture. In addition, gallium-arsenide and indium phosphide technologies for monolithic PAAs containing the antenna, phasing and TR modules combined on a single ship are analyzed. To design electronically scanned Antenna Arrays (AAs) of the MMW-band's short-wave subband (λ = 2 to 4 mm), it is reasonable to use the nontraditional approch in which the steerable impedance aperture is used to form AA elements and to steer electromagnetic field. This aperture is realized as a multilayer semiconductor structure on which the antenna array structure with a required amplitude-phase distribution is formed under the steering optoelectronic effect.

When analyzing interaction of microwave field with the semiconductor structure, the boundaries of employing the classical macroscopic approach using electrophysical parameters ε, μ, σ are determined. The cutoff frequency up to which the macroscopic approach may be used corresponds to the submillimeter wave band. Analysis of interaction of the semiconductor structure with a steering optical emission (electron flow) showed that the optical emission level $I > 1$ W/cm^2 (electron flow density $j > 0.1$ mA/cm^2) is needed for forming and steering the antenna aperture's elements based on the semiconductor structure. The described forming and steering method is reasonable throughout a wave band of about 1 mm to 4 cm.

For the MMW PAA with linear and elliptical polarizations, base radiators-phase shifters are proposed which may be formed through using the array antenna's semiconductor aperture via combining the processes of steering electronically and optically the electrophysical parameters of the semiconductor structure with a technology of forming the array antenna elements (radiators-phase shifters) on the aperture. A "negative" method of array antenna element forming was studied which decreases the steering optoelectronical system power by a factor of 10 to 50. In this case, the array antenna efficiency η = 0.35 to 0.45; it is suitable for multielement array antennas throughout the MMW-band's short-wave subband (2 to 4 mm).

A field-emission cathode steering system (Fig. 1), an electron-beam steering system (with dot (symbol) recording), and an optical steering system are discussed for the selected array antenna design and its semiconductor aperture's physical and electrodynamical characteristics. Analysis of the steering systems' characteristics have shown that these systems may be used for forming and steering the AA elements throughout the MMW-band's short-wave subband.

Algorithmization of a base task of electromagnetic scattering by steerable impedance structures built on the basis of a semiconductor dipole with a steerable stub ("positive" forming method) and of a slot in a semiconductor structure ("negative" forming method) which form constituent parts of the AA was carried out. The algorithmization includes: formulation of the scattering task as a functional equation with more exactly defined boundary conditions in regard to the steerable elements' currents and the task solving by iteration methods (simple iteration method, minimum error method, steepest descent method) with selected stopping rules.

An aplication program package, developed in accordance with the developed algorithm and tested, made it possible to analyze how main parameters and characteristics of the impedance dipole with the steerable stub ("positive" forming method) and of the slot in the impedance structure ("negative" forming method) which form parts of the AA depend on dimensions of the elements, on geometrical and electrophysical parameters of the semiconductor structure, and on the scan angle. In addition, the application package made it possible to carry out parametric optimization of such structures for the purpose of eliminating the effect of AA "blinding". The proposed array antennas designed on the basis of optically steerable impedance structures make it possible to obtain, due to a finite conductivity of the semiconductor structure, an efficiency of about 0.75 for the "positive" method of AA element forming

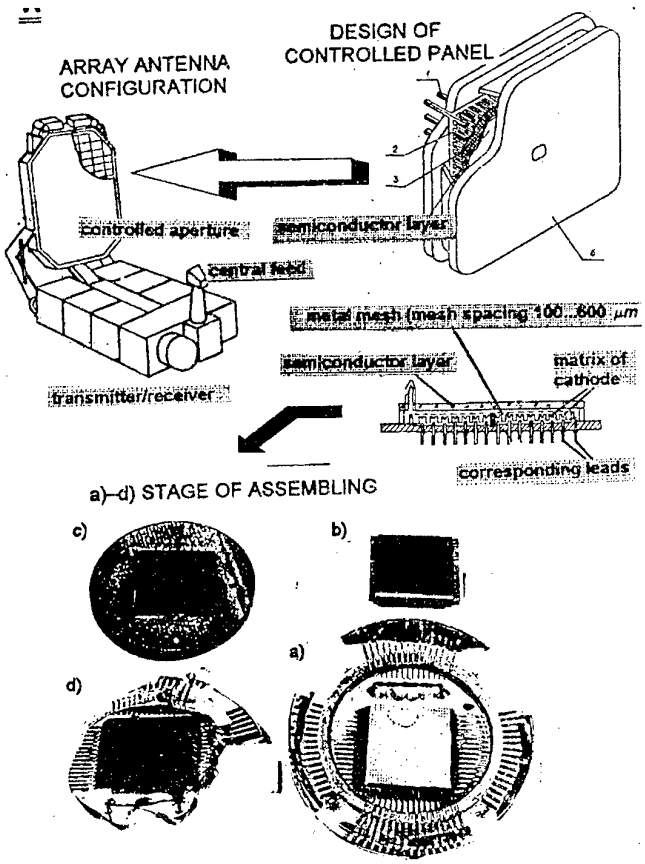


Fig. 1. Design of Steerable PAA with Field-Emission Cathode Control System

and of about 0.35 to 0.45 for the "negative" AA element forming method which reduces the optoelectronic steering system power by a factor of 10 to 50. This is acceptable for multielement AAs throughout the MMW-band's short-wave subband (2 to 4 mm).

An experimental setup using an optical steering system and a steerable semiconductor (cadmium sulphide) aperture was developed and the following parameters and characteristics were measured in a frequency band of 26.8 to 37.6 GHz: the semiconductor-structure's reflection coefficient for different values of the steering light flux intensity, the semiconductor structure's and the array antenna's patterns and gains (for the "positive" and "negative" forming methods) for different values of the steering light flux intensity. The array antenna's efficiencies were determined. Due to heat loss caused by the semiconductor aperture's impedance behaviour, the efficiencies were $\eta POS = 0.6$ to 0.65 and $\eta NEG = 0.6$ to 0.32, respectively. Design values of the efficiencies were 0.68 and 0.3, respectively. Design values of the efficiencies were 0.68 and 0.3, respectively (design values for silicon are 0.75 and 0.45), which is quite acceptable for multielement AAs in the MMW band's short-wave subband (2 to 4 mm).

Technical solutions which can be used to implement phased array antennas for the MMW-band's short-wave subband (2 to 4 mm) make it possible both to improve functional capabilities and characteristics of electronic systems for traditional applications (search and fire-control short-range radars, communications systems, metrology and others) and to extend the field of non-traditional applications (short-range radio-vision systems, runway monitoring systems etc.).

REFERENCES

1. Grinev A. Yu., Zaikin A. E. Electrodynamical Analyses of Millimeter Waveband PAA with Optical and Electron-Beam control, //Radiotechnika i Electronika, 1996, v.41, ¹5, pp. 633-638 [in Russian].

2. Grinev A. Yu., Zaikin A. E. Opto(electron)-controlled VHF Band Array Antennas //Radiotechnika, 1995, ¹8, pp.21-25 [in Russian].

3. Grinev A. Yu., Zaikin A. E. VHF Band Phased Array Antennas with Optical and Electron-beam Control System, //Izv. vuzov Radioelectronika, 1993, v.35, ¹5, pp. 3-17 [in Russian].

PATTERN SYNTHESIS OF ANTENNA ARRAY WITH DIGITAL PHASE SHIFTERS

N. V. Shcherbakov, I. V. Norinchuk

Kharkov Military University, Svoboda sq., 6, Kharkov, 310043, Ukraine
Tel. (0572) 40-41-41 add. 2-85

One of the problems in the design work of phased arrays is the one taking into account phase shifter discreteness. Usually this problem is solved by means of finding the required continuous phase distribution and subsequent its rounding-off according to phase shifter discreteness. Such an approach is very simple but it often leads to non-optimal results, especially in the case of large shifter discreteness. Therefore, the problem arose to find the so-called discrete methods of phase synthesis that would allow to take into account the problem discrete nature more efficiently. From the mathematical point of view, these are the methods of finding the extremums of quite complicated functions in discrete space of search. Nowadays there is no the developed technique of such a task solving so it can be solved by different methods. In this paper it is proposed to use genetic algorithms (GA) to solve the problem of discrete phase synthesis because just these algorithms can easily be applied to the problems of optimization for complicated, multiextreme, nondifferentiable functions as well as for discrete search space [1]. The work is intended to show the advantages of the discrete phase synthesis method in comparison with classical method of continuous solution rounding-off and to investigate the possible ways of more rational computation when using genetic algorithm for phased array synthesis.

The process of optimal solution search in GA resembles the nature evolution process. As in animate nature, natural selection, reproduction and mutations occur in GA's. But the evolution direction of optimization object is specified by the researcher. The genetic algorithm used in this work is based on the proposed in [2] real-coded GA modified for the discrete phase synthesis task.

Note that in general case the problem of antenna synthesis consists of two stages:

1.The synthesis criterion selection.

2.The optimization criterion problem solution according to the selected criterion.

Let's consider the possibility of applying GA to the optimization problem solution on some test example. As an criterion we'll select the characteristic for synthesis tasks requirement to reduce the sidelobe level (SLL) in some specified sector. The task of reducing SLL in the sector of angles $5° \le \theta \le 8°$ of equidistant antenna array with the number of elements $N = 100$ and the distance between elements $d = 0.7 \cdot \lambda$ was considered as a test one:

$$\min_{\vec{\varphi}} \max_{\theta \in \Omega} \left| F(\theta, \vec{\varphi}) \right|, \qquad (1)$$

where $\vec{\varphi}$ is a phase distribution vector; $F(\theta, \vec{\varphi})$ is the normalized antenna array pattern; Ω is the given area in the sidelobe sector.

Consider the results of optimization problem (1) solution for different phase shifter bit capasity and compare them with the results obtained by rounding-off continuous solving the phase synthesis problem. In Table 1 the results are presented of solving this problem by discrete method for different discreteness by five GA starts with the number of iterations $N_{iter} = 500$.

Table 1

Start number	1	2	3	4	5
SLL, dB $\Delta\varphi = 45°$	-34.4	-36.9	-38.9	-36.1	-31.7
SLL, dB $\Delta\varphi = 90°$	-36.1	-37.3	-36.1	-36.1	-34.7
SLL, dB $\Delta\varphi = 180°$	-35.8	-35.9	-34.3	-33	-35.9

For a faster convergence in all starts each vector of initial population phase distribution was formed with the GA with the small number of iterations ($N_{iter} = 50$). For comparison Table 2 gives five solutions obtained by the method of continuous synthesis rounding-off. When comparing we can see that even the worst result of discrete synthesis exceeds the best result of rounding-off method by 3 dB for the discreteness $\Delta\varphi = 90°$ and by 4.3 dB for $\Delta\varphi = 180°$. When solving such a complex multiextreme tasks it is very difficult to find a global extremum. At the same time the results can be farther or closer to a global extremum. It is clear that the closer the results of optimization methods to a global extremum the better the method is. In order to evaluate approximately the considered phase synthesis methods we'll define the mean value of attained sidelobe level in the specified SLL sector given by

$$SLL_{mean} = \frac{\sum_{i=1}^{n} SLL_i}{n}, \qquad (2)$$

where SLL_i is the sidelobe level in the specified angle sector attained in i-th start of optimization algorithm (for deterministic optimization method all the values of SLL_i are equal); n is the number of starts.

Table 2

Start number	1	2	3	4	5
SLL, dB Continuous synthesis	-38.4	-35.9	-39.5	-34.9	-39.8
SLL, dB $\Delta\varphi = 45°$	-28.9	-33.3	-38	-29.9	-38
SLL, dB $\Delta\varphi = 90°$	-22.4	-31.6	-31.7	-31.7	-31.7

Table 3 presents the values of SLL_{mean} obtained by the discrete synthesis and rounding-off methods. From the data analysis it follows that the mean value of SLL in given sector obtained by the discrete phase synthesis method is less than the one obtained by the rounding-off method by 2 dB for the discreteness $\Delta\varphi = 45°$, by 6.3 dB for $\Delta\varphi = 90°$ and by 10.5 dB for $\Delta\varphi = 180°$.

Table 3

Discreteness	SLL_{mean} (dB) by rounding-off method	SLL_{mean} (dB) by discrete method
$\Delta\varphi = 45°$	-33.6	-35.6
$\Delta\varphi = 90°$	-29.8	-36.1
$\Delta\varphi = 180°$	-24.4	-34.9

Since GA's drop in a class of stochastic methods of global optimization the achievement of an optimal solution is of probability character. It means that probability of the best result attainment increases with the number of iterations. Taking into account this and also the fact that to perform such calculations it is necessary to have relatively much time (about an hour and a half when using AMD K6/233 MHz) the problem of accelerating the algorithm becomes of high priority. Therefore, some attempts were made to improve the results of discrete synthesis. These attempts were executed in several directions. The first direction is to increase the population size. Calculations were carried out for $N_{pop} = 10,20,30,40$. The number of iterations was chosen such that it could provide the approximate equality of computation total time. The result essential improvement was not achieved.

The second direction was connected with sequential discreteness reduction. Here at first the problem of discrete synthesis for $\Delta\varphi = 180°$ is solved. Such a solution we have already obtained and it is in the last line of the Table 1. Using each of the obtained results for initial population formation the problem of discrete phase synthesis for $\Delta\varphi = 90°$ has been solved. The obtained results in turn were used when forming the initial populations to solve the problem with the discreteness $\Delta\varphi = 45°$. For discreteness $\Delta\varphi = 90°$ the best result was reduced by 0.3 dB and for $\Delta\varphi = 45°$ – by 0.8 dB with approximately the same computation time.

And the third direction is to split the array into n blocks in which the phase values are assumed to be equal. Gradually reducing the values of n (10, 5, 1 with discreteness $\Delta\varphi = 90°$) we proceed to initial problem. The results obtained in such a way didn't exceed the previous results.

Thus, the analysis of told above enables to draw the following conclusions. In most cases the results obtained by discrete phase synthesis method are noticeably (to 10 dB) better than the results of continuous solution rounding-off. And the advantage from using discrete method becomes more noticeable with discreteness increase.

It is shown that solving a discrete phase synthesis problem with sequential discreteness reduction gives as a whole some improvement (to 0.8 dB). The antenna array division into blocks with an equal phase distribution allows to reduce substantially computation time of one GA iteration. Reducing the block dimensions gradually we obtain satisfactory results with essential economy in time. This permits either to increase the total number of iterations to attain more qualitative solution or to use such an algorithm variant to solve the problems of large dimensions (up to 1000 elements in array).

Unfortunately, even applying GA to the solution of optimization problems the authors didn't succeed in finding global extremums at each stage of solving test example. Nevertheless the results obtained by the proposed method firstly have higher stability as compared to the method of rounding-off and secondly they are close enough to optimal results.

REFERENCES

1. Daniel S. Weille and Eric Michielssen, "Genetic algorithm optimization applied to electromagnetics: a review", IEEE Trans. Antennas Propagat.,vol. 45, pp. 343-351, March 1997.

2. Keen-Keong Yan and Yilong Lu, "Sidelobe reduction in array-pattern synthesis using genetic algorithm", IEEE Trans. Antennas Propagat.,vol. 45, pp. 1117-1121, July 1997.

THE MATRIX MODELS OF DIGITAL ANTENNA ARRAYS WITH NONIDENTICAL CHANNELS

V. I. Slyusar

Central Research and Development Institute of Armament and Military Engineering
Kiev, Andruschenko Street, 4, e-mail: swadim@777.com.ua

The modern technology of radar and mobile communications systems is adaptive digital beam forming. When considering the multicoordinate digital beam forming in radar and communication systems with nonidentical channels of antenna arrays there is a problem of compact matrix record of the receiving channels responses. To solve the given problem it is proposed to operate with a special type of the matrices product, named by the author as "penetrated" and "generalized face-splitting" products.

According to the definition [1], for p×g-matrix A and p×gn-matrix B with p×g-blocks ($B=[B_n]$) their penetrated face-splitting product $A \boxdot B$ is the p×gn-block-matrix $[A \circ B_n]$, where "$\circ$" -a symbol of Adamar splitting, B_n — is a p×g-block of matrix B:

$$A \boxdot B=[A\circ B_1 \,|\, A\circ B_2 \,|\cdots|\, A\circ B_n \,|\cdots] \text{ or } A \boxdot B=\begin{bmatrix} A\circ B_1 \\ \hline A\circ B_2 \\ \hline \vdots \\ \hline A\circ B_n \\ \hline \vdots \end{bmatrix}.$$

The example:

$$A=\begin{bmatrix} a_{11} & a_{12} \\ a_{21} & a_{22} \\ a_{31} & a_{32} \end{bmatrix},\quad B=\begin{bmatrix} B_1 \\ \hline B_2 \\ \hline B_3 \end{bmatrix}=$$

$$=\left[\begin{array}{cc} b_{111} & b_{121} \\ b_{211} & b_{221} \\ b_{311} & b_{321} \\ \hline b_{112} & b_{122} \\ b_{212} & b_{222} \\ b_{312} & b_{322} \\ \hline b_{113} & b_{123} \\ b_{213} & b_{223} \\ b_{313} & b_{323} \end{array}\right],\quad A \boxdot B=\left[\begin{array}{cc} a_{11}\cdot b_{111} & a_{12}\cdot b_{121} \\ a_{21}\cdot b_{211} & a_{22}\cdot b_{221} \\ a_{31}\cdot b_{311} & a_{32}\cdot b_{321} \\ \hline a_{11}\cdot b_{112} & a_{12}\cdot b_{122} \\ a_{21}\cdot b_{212} & a_{22}\cdot b_{222} \\ a_{31}\cdot b_{312} & a_{32}\cdot b_{322} \\ \hline a_{11}\cdot b_{113} & a_{12}\cdot b_{123} \\ a_{21}\cdot b_{213} & a_{22}\cdot b_{223} \\ a_{31}\cdot b_{313} & a_{32}\cdot b_{323} \end{array}\right].$$

As an example, the response of three-coordinate flat digital antenna array of R×R elements can be written down through penetrated face-splitting product of matrices as (without noise):

$$U = \dot{a}\cdot(Q \boxdot F)=\dot{a}\cdot[Q\circ F_1 \,|\, Q\circ F_2 \,|\cdots|\, Q\circ F_r \,|\cdots],$$

where $\dot{a}$ — is a complex signal amplitude,

$$Q=\begin{bmatrix} \dot{Q}_{11}(x,y) & \dot{Q}_{12}(x,y) & \cdots & \dot{Q}_{1R}(x,y) \\ \dot{Q}_{21}(x,y) & \dot{Q}_{22}(x,y) & \cdots & \dot{Q}_{2R}(x,y) \\ \vdots & \vdots & \vdots & \vdots \\ \dot{Q}_{R1}(x,y) & \dot{Q}_{R2}(x,y) & \cdots & \dot{Q}_{RR}(x,y) \end{bmatrix}$$

is the matrix of the directivity characteristics of primary channels in azimuth and elevation angle planes (can not be factorized),

$$F=\left[\begin{array}{ccc|c|ccc} \dot{F}_{111}(\omega) & \cdots & \dot{F}_{1R1}(\omega) & \cdots & \dot{F}_{11G}(\omega) & \cdots & \dot{F}_{1RG}(\omega) \\ \vdots & \cdots & \vdots & & \vdots & \cdots & \vdots \\ \dot{F}_{R11}(\omega) & \cdots & \dot{F}_{RR1}(\omega) & \cdots & \dot{F}_{R1G}(\omega) & \cdots & \dot{F}_{RRG}(\omega) \end{array}\right]$$

is the block-matrix of amplitude-frequency characteristics meanings $\dot{F}_{nmg}(\omega)$ of G filters for R×R nonidentical receiving channels ($\dot{F}_{11g}(\omega)\neq\dot{F}_{rrg}(\omega)$);

$$Q\circ F_g=\begin{bmatrix} \dot{Q}_{11}(x,y)\dot{F}_{11g}(\omega) & \cdots & \dot{Q}_{1R}(x,y)\dot{F}_{1Rg}(\omega) \\ \dot{Q}_{21}(x,y)\dot{F}_{21g}(\omega) & \cdots & \dot{Q}_{2R}(x,y)\dot{F}_{2Rg}(\omega) \\ \vdots & \vdots & \vdots \\ \dot{Q}_{R1}(x,y)\dot{F}_{R1g}(\omega) & \cdots & \dot{Q}_{RR}(x,y)\dot{F}_{RRg}(\omega) \end{bmatrix},$$

U – block-matrix of voltages of the channels responses.

To select a single source on four coordinates (azimuth, elevation angle, frequency and range) the response of digital antenna array can be written down through generalized face-splitting product or generalized transposed face-splitting product (the theory of face-splitting products is presented in [1–4]). According to the definition, for block-matrices $A=[A_{ij}]$ and $B=[B_{ig}]$ with p×g- blocks their generalized face-splitting product $A \tilde{\boxdot} B$ is the block-matrix

$$[A_{ij} \boxdot [B_{i1}\ B_{i2}\ \cdots\ B_{ig}\ \cdots]].$$

The example:

$$A \tilde{\boxdot} B=\begin{bmatrix} A_{11} & A_{12} & \cdots & A_{1T} \\ A_{21} & A_{22} & \cdots & A_{2T} \\ \vdots & \vdots & \cdots & \vdots \\ A_{P1} & A_{P2} & \cdots & A_{PT} \end{bmatrix} \tilde{\boxdot} \begin{bmatrix} B_{11} & B_{12} & \cdots & B_{1G} \\ B_{21} & B_{22} & \cdots & B_{2G} \\ \vdots & \vdots & \cdots & \vdots \\ B_{P1} & B_{P2} & \cdots & B_{PG} \end{bmatrix}=$$

$$=\left[\begin{array}{ccc|c|ccc} A_{11}\boxdot[B_{11} & \cdots & B_{1G}] & \cdots & A_{1T}\boxdot[B_{11} & \cdots & B_{1G}] \\ A_{21}\boxdot[B_{21} & \cdots & B_{2G}] & \cdots & A_{2T}\boxdot[B_{21} & \cdots & B_{2G}] \\ \vdots & & & \vdots & \vdots & & \\ A_{P1}\boxdot[B_{P1} & \cdots & B_{PG}] & \cdots & A_{PT}\boxdot[B_{P1} & \cdots & B_{PG}] \end{array}\right].$$

The alternative to the above considered is a generalized transposed face-splitting block-matrices product:

$$A \tilde{\blacksquare} B = \left[A_{ij} \circledcirc \begin{bmatrix} B_{1j} \\ B_{2j} \\ \vdots \\ B_{Gj} \end{bmatrix} \right].$$

For example, it can be written down:

$$A \tilde{\blacksquare} B = \begin{bmatrix} A_{11} & A_{12} & \cdots & A_{1T} \\ A_{21} & A_{22} & \cdots & A_{2T} \\ \vdots & \vdots & \cdots & \vdots \\ A_{Pi} & A_{P2} & \cdots & A_{PT} \end{bmatrix} \tilde{\blacksquare} \begin{bmatrix} B_{11} & B_{12} & \cdots & B_{1G} \\ B_{21} & B_{22} & \cdots & B_{2G} \\ \vdots & \vdots & \cdots & \vdots \\ B_{P1} & B_{P2} & \cdots & B_{PG} \end{bmatrix} =$$

$$= \left[\begin{array}{c|c|c|c} A_{11} \circledcirc \begin{bmatrix} B_{11} \\ B_{21} \\ \vdots \\ B_{P1} \end{bmatrix} & A_{12} \circledcirc \begin{bmatrix} B_{12} \\ B_{22} \\ \vdots \\ B_{P2} \end{bmatrix} & \cdots & A_{1T} \circledcirc \begin{bmatrix} B_{1G} \\ B_{2G} \\ \vdots \\ B_{PG} \end{bmatrix} \\ \hline \vdots & \vdots & \cdots & \vdots \\ \hline A_{P1} \circledcirc \begin{bmatrix} B_{11} \\ B_{21} \\ \vdots \\ B_{P1} \end{bmatrix} & A_{P2} \circledcirc \begin{bmatrix} B_{12} \\ B_{22} \\ \vdots \\ B_{P2} \end{bmatrix} & \cdots & A_{PT} \circledcirc \begin{bmatrix} B_{1G} \\ B_{2G} \\ \vdots \\ B_{PG} \end{bmatrix} \end{array}\right].$$

The response of four-coordinate flat digital antenna array with R×R nonidentical channels can be present as (without noise):

$$U = \left(Q \circledcirc \left\{ S \tilde{\square} F \right\}\right) \cdot \dot{a} = Q \circledcirc \left[S_1 \circledcirc F \,|\, S_2 \circledcirc F \,|\cdots|\, S_T \circledcirc F \right] \cdot \dot{a},$$

where

$$S = \left[\begin{array}{ccc|c|ccc} S_{111}(z) & \cdots & S_{1R1}(z) & \cdots & S_{11T}(z) & \cdots & S_{1RT}(z) \\ \vdots & \cdots & \vdots & & \vdots & \cdots & \vdots \\ S_{R11}(z) & \cdots & S_{RR1}(z) & & S_{R1T}(z) & \cdots & S_{RRT}(z) \end{array}\right]$$

is the matrix of the responses of single signal in T range gates (all channels have nonidentical radio impulse curve $S_{11t}(\omega) \neq S_{rrt}(\omega)$).

The alternate to considered above variant of analytical model of four-coordinate radar with flat digital antenna array is

$$U = \left(Q \circledcirc \left\{ \tilde{S} \tilde{\blacksquare} \tilde{F} \right\}\right) \cdot \dot{a} = Q \circledcirc \left[\begin{array}{c} S_1 \circledcirc \tilde{F} \\ \hline \vdots \\ \hline S_T \circledcirc \tilde{F} \end{array} \right] \cdot \dot{a},$$

where

$$\tilde{S} = S^R = [S_1 \,|\cdots|\, S_T]^R = \left[\begin{array}{c} S_1 \\ \hline \vdots \\ \hline S_2 \end{array} \right] = \left[\begin{array}{ccc|c|ccc} S_{111}(z) & \cdots & S_{1R1}(z) & \cdots & S_{11T}(z) & \cdots & S_{1RT}(z) \\ \vdots & \cdots & \vdots & & \vdots & \cdots & \vdots \\ S_{R11}(z) & \cdots & S_{RR1}(z) & & S_{R1T}(z) & \cdots & S_{RRT}(z) \end{array}\right],$$

$$\tilde{F} = F^R = [F_1 \,|\cdots|\, F_G]^R = \left[\begin{array}{c} F_1 \\ \hline \vdots \\ \hline F_2 \end{array} \right] = \left[\begin{array}{ccc|c|ccc} F_{111}(\omega) & \cdots & F_{1R1}(\omega) & \cdots & F_{11G}(\omega) & \cdots & F_{1RG}(\omega) \\ \vdots & \cdots & \vdots & & \vdots & \cdots & \vdots \\ F_{R11}(\omega) & \cdots & F_{RR1}(\omega) & & F_{R1G}(\omega) & \cdots & F_{RRG}(\omega) \end{array}\right],$$

"R" is the symbol of block-rotation (this new block-matrix operation is proposed by author).

With the considered matrices models, on the basis of Neudecker's matrix derivative [3,4] an information Fischer's block-matrix, describing the accuracy of joint estimation of angular coordinates, range and frequency, is obtained:

$$I = \frac{1}{\sigma^2} \cdot \left[\begin{array}{c|c} P^T \cdot P & a^* \cdot P^T \cdot \dfrac{\partial P}{\partial Y} \\ \hline \dot{a} \cdot \left(\dfrac{\partial P}{\partial Y}\right)^T \cdot P & \left(\dfrac{\partial P}{\partial Y}\right)^T (\dot{a} a^* \cdot 1_{RRTG}) \dfrac{\partial P}{\partial Y} \end{array}\right],$$

where 1_{RRTG} — a unit matrix of dimension R×R×T×G, $\frac{\partial P}{\partial Y}$ — Neudecker's derivative of matrix P on vector Y formed of unknown estimations of angular coordinates, range and frequency of sources,

$$P = Q \circledcirc \left\{ S \tilde{\square} F \right\} \text{ or } P = Q \circledcirc \left\{ \tilde{S} \tilde{\blacksquare} \tilde{F} \right\}.$$

To analyse multistatic radar systems the following matrix model (without noise) can be used:

$$U = \left(\begin{bmatrix} Q_1 \\ Q_2 \\ \vdots \\ Q_P \end{bmatrix} \tilde{\square} \begin{bmatrix} S_{11} & \cdots & S_{T1} \\ \vdots & \vdots & \vdots \\ S_{1P} & \cdots & S_{TP} \end{bmatrix} \tilde{\square} \begin{bmatrix} F_{11} & \cdots & F_{G1} \\ \vdots & \vdots & \vdots \\ F_{1P} & \cdots & F_{GP} \end{bmatrix} \right) \cdot \dot{a},$$

$$\begin{bmatrix} Q_1 \\ Q_2 \\ \vdots \\ Q_P \end{bmatrix} = \left[\begin{array}{ccc|c|ccc} \dot{Q}_{111}(x,y) & \cdots & \dot{Q}_{1R1}(x,y) & \cdots & \dot{Q}_{11T}(x,y) & \cdots & \dot{Q}_{1RT}(x,y) \\ \dot{Q}_{211}(x,y) & \cdots & \dot{Q}_{2R1}(x,y) & & \dot{Q}_{21T}(x,y) & \cdots & \dot{Q}_{2RT}(x,y) \\ \vdots & & \vdots & & \vdots & & \vdots \\ \dot{Q}_{R11}(x,y) & \cdots & \dot{Q}_{RR1}(x,y) & & \dot{Q}_{R1T}(x,y) & \cdots & \dot{Q}_{RRT}(x,y) \\ \hline \dot{Q}_{11P}(x,y) & \cdots & \dot{Q}_{1RP}(x,y) & & \dot{Q}_{11G}(x,y) & \cdots & \dot{Q}_{1RG}(x,y) \\ \dot{Q}_{21P}(x,y) & \cdots & \dot{Q}_{2RP}(x,y) & & \dot{Q}_{21G}(x,y) & \cdots & \dot{Q}_{2RG}(x,y) \\ \vdots & & \vdots & & \vdots & & \vdots \\ \dot{Q}_{R1P}(x,y) & \cdots & \dot{Q}_{RRP}(x,y) & & \dot{Q}_{R1G}(x,y) & \cdots & \dot{Q}_{RRG}(x,y) \end{array}\right],$$

$$S_{tp} = \begin{bmatrix} S_{11tp}(z) & \cdots & S_{1Rtp}(z) \\ \vdots & \cdots & \vdots \\ S_{R1tp}(z) & \cdots & S_{RRtp}(z) \end{bmatrix},$$

$$F_{gp} = \begin{bmatrix} F_{11gp}(\omega) & \cdots & F_{1Rgp}(\omega) \\ \vdots & \cdots & \vdots \\ F_{R1gp}(\omega) & \cdots & F_{RRgp}(\omega) \end{bmatrix},$$

$$U_{gtp} = \left(Q_p \circ S_{tp} \circ F_{gp}\right) \cdot \dot{a},$$

P is a number of radar position.

In the general case, for multiple signals the modeling concept, based on using of block generalized face-splitting product (symbol "$\tilde{\circledcirc}$") and block generalized transposed face-splitting product (symbol "$\tilde{\circledast}$") can be proposed. According to the definition,

$$A\ \tilde{\circledcirc}\ B=\left[A_{bg}\ \tilde{\square}\ B_{bk}\right]_{dn},\quad A\ \tilde{\circledast}\ B=\left[A_{bg}\ \tilde{\blacksquare}\ B_{kg}\right]_{dn}.$$

The example:

$$A=\left[\begin{array}{cc|cc} A_{111} & A_{121} & A_{112} & A_{122} \\ A_{211} & A_{221} & A_{212} & A_{222} \end{array}\right],$$

$$B=\left[\begin{array}{cc|cc} B_{111} & B_{121} & B_{112} & B_{122} \\ B_{211} & B_{221} & B_{212} & B_{222} \end{array}\right],\quad A\ \tilde{\circledcirc}\ B=$$

$$=\left[\left[\begin{array}{cc} A_{111} & A_{121} \\ A_{211} & A_{221} \end{array}\right]\tilde{\square}\left[\begin{array}{cc} B_{111} & B_{121} \\ B_{211} & B_{221} \end{array}\right]\middle|\left[\begin{array}{cc} A_{112} & A_{122} \\ A_{212} & A_{222} \end{array}\right]\tilde{\square}\left[\begin{array}{cc} B_{112} & B_{122} \\ B_{212} & B_{222} \end{array}\right]\right],$$

$$A\ \tilde{\circledast}\ B=$$

$$=\left[\left[\begin{array}{cc} A_{111} & A_{121} \\ A_{211} & A_{221} \end{array}\right]\tilde{\blacksquare}\left[\begin{array}{cc} B_{111} & B_{121} \\ B_{211} & B_{221} \end{array}\right]\middle|\left[\begin{array}{cc} A_{112} & A_{122} \\ A_{212} & A_{222} \end{array}\right]\tilde{\blacksquare}\left[\begin{array}{cc} B_{112} & B_{122} \\ B_{212} & B_{222} \end{array}\right]\right].$$

The model of four-coordinate radar with flat digital antenna array in multisignal case can be written as:

$$U=\left(Q\ \tilde{\circledast}\left(S\ \tilde{\circledast}\ F\right)\right)\left(A\otimes 1_R\right),$$

where A is the vector of complex amplitudes of signals of I sources,

$$Q=\left[Q_1\ Q_2\ \cdots Q_M\right],\ Q_m=\left[\begin{array}{ccc} Q_{11}(x_m,y_m) & \cdots & Q_{1R}(x_m,y_m) \\ \vdots & \cdots & \vdots \\ Q_{R1}(x_m,y_m) & \cdots & Q_{RR}(x_m,y_m) \end{array}\right]$$

$$S=\left[\begin{array}{ccc} S_1 & S_2 & \cdots\ S_M \end{array}\right],$$

$$S_m=\left[\begin{array}{ccc} S_{111}(z_m) & \cdots & S_{1R1}(z_m) \\ \vdots & \cdots & \vdots \\ S_{R11}(z_m) & \cdots & S_{RR1}(z_m) \\ \hline S_{11T}(z_m) & \cdots & S_{1RT}(z_m) \\ \vdots & \cdots & \vdots \\ S_{R1T}(z_m) & \cdots & S_{RRT}(z_m) \end{array}\right],$$

$$F=\left[\begin{array}{ccc} F_1 & F_2 & \cdots\ F_M \end{array}\right],\ F_m=\left[\begin{array}{ccc} F_{111}(\omega_m) & \cdots & F_{1R1}(\omega_m) \\ \vdots & \cdots & \vdots \\ F_{R11}(\omega_m) & \cdots & F_{RR1}(\omega_m) \\ \hline F_{11G}(\omega_m) & \cdots & F_{1RG}(\omega_m) \\ \vdots & \cdots & \vdots \\ F_{R1G}(\omega_m) & \cdots & F_{RRG}(\omega_m) \end{array}\right],$$

1_R is a unit matrix of dimension R; $\otimes$ — symbol of Kronecker's- products of matrixes.

REFERENCES

1. Slyusar V. I. The family of the face-splitting matrices products and its characteristics// Kibernetika i sistemny analiz. - 1999.- ¹ 3. - to be published [in Russian].
2. Slyusar V. I. New operations of matrices product for applications of radars, in Proc. Direct and Inverse Problems of Electromagnetic and Acoustic Wave Theory (DIPED-97), Lviv, September 15-17, 1997, P. 73-74 [in Russian].
3. Slyusar V. I. Accuracy of linear digital antenna array at joint estimation of range and angular coordinate of M sources, in Proc. ICATT—97, Kyiv, May 1997.- P. 110 – 111.
4. Slyusar V. I. The face-splitting matrix products in radar applications.// Radioelectronika. -1998. - ¹ 3. - P. 71 - 75 [in Russian].

A WAY OF CORRECTION OF DAA RECEIVING CHANNELS CHARACTERISTICS USING THE HETERODYNE SIGNAL

V. I. Slyusar

Central Research and Development Institute of Armament and Military Engineering,
Kiev-135, Andrushenko Str., 4, tel. 271-62-45

Usually a problem of correction of a digital antenna array (DAA) channels characteristics is solved by applying an external pilot-signal or additional diversing of control signal with respect to radio frequency.

To minimize the hardware expenditures it is proposed to use unnominal heterodyne operational mode, which consists in changing the excitation conditions in a control period so to cause the generation of parasitic broadband or multimode signals. At the same time it is necessary to provide stable arising of intermediate frequency oscillation at mixer's output. In the event of a narrow pass band of intermediate frequency amplifiers such signal is quite suitable for equalization of complex transfer characteristics of receiving channels.

As a correction procedures it is proposed to use a method [1], according to which the correction process is consisted in weighing the digital voltages in receiving channels be complex weight coefficients which quadratic components have been calculated for a set of N readings

$$\alpha^c_{rq} = \frac{\sum\limits_{i=1}^{N} V^c_{rq_i} a^c_i + \sum\limits_{i=1}^{N} V^s_{rq_i} a^s_i}{RQ \sum\limits_{i=1}^{N} \left(V^{c^2}_{rq_i} + V^{s^2}_{rq_i} \right)},$$

$$\alpha^s_{rq} = \frac{\sum\limits_{i=1}^{N} V^c_{rq_i} a^s_i - \sum\limits_{i=1}^{N} V^s_{rq_i} a^c_i}{RQ \sum\limits_{i=1}^{N} \left(V^{c^2}_{rq_i} + V^{s^2}_{rq_i} \right)},$$

where α^c_{rq}, α^s_{rq} — quadratic components of correction coefficient of the rqth primary DAA channel situated in the rth row of qth column,

$$V^c_{rq_i} = U^c_{rq_i} \cos(x_r + x_q) + U^s_{rq_i} \sin(x_r + x_q)$$

$$V^s_{rq_i} = U^s_{rq_i} \cos(x_r + x_q) - U^c_{rq_i} \sin(x_r + x_q)$$

$$x_r = \frac{2\pi}{\lambda} d_r \left(r - \frac{R+1}{2} \right) \sin\beta \cdot \cos\varepsilon$$

$$x_q = \frac{2\pi}{\lambda} d_q \left(q - \frac{Q+1}{2} \right) \sin\beta \cdot \sin\varepsilon$$

$U^c_{rq_i}$, $U^s_{rq_i}$ — quadratic components of response of the rqth primary DAA channel in the ith time interval, x_r, x_q — generalized coordinates of calibrating source with respect to DAA normal, λ — wavelength of calibrating source carrier, d_r, d_q — the distance between array's elements in a row and in a column correspondingly, R, Q — number of array's elements in a row and in a column, β, ε — angle coordinates of the calibrating source with respect to DAA normal,

$$a^c_i = \frac{1}{RQ} \sum_{r=1}^{R} \sum_{q=1}^{Q} \left\{ U^c_{rq_i} \cos(x_r + x_q) + U^s_{rq_i} \sin(x_r + x_q) \right\},$$

$$a^s_i = \frac{1}{RQ} \sum_{r=1}^{R} \sum_{q=1}^{Q} \left\{ U^s_{rq_i} \cos(x_r + x_q) - U^c_{rq_i} \sin(x_r + x_q) \right\}.$$

In the considered case the expressions for the correction coefficients can essentially become simpler if the calibrating source (heterodyne) is placed in the array plane.

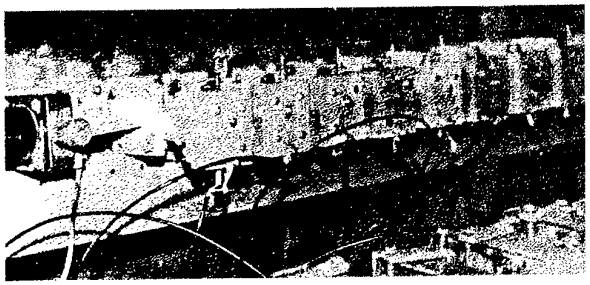


Fig. 1

The proposed approach has been tested on a working model of the 8-element digital antenna array made in 1989 by a team of scientists of the former Academy of Anti-aircraft Defence of Ground Forces (Kiev) headed by Dr. Sci. Prof. V.A.Varjukhin. An appearance of model's elements is shown in Fig. 1-4. Fig. 1 shows a microwave part of the array with a heterodyne block (to the left). A set of the digital receiving modules is shown in Fig. 2 (to the left). Fig. 3 shows the outputs of digital filters of quadratures diversing, from which signals are applied to a buffer storage and adapter of the central computer (Fig. 4).



Fig. 2

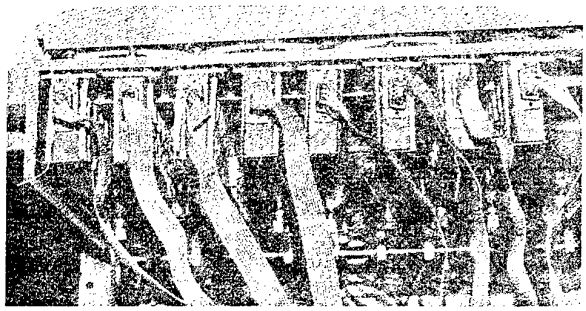


Fig. 3

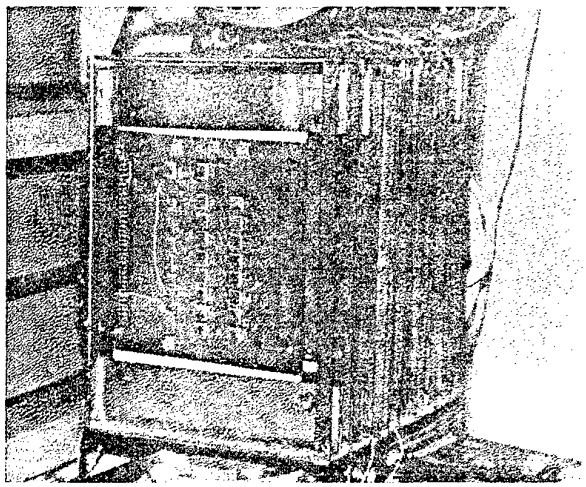


Fig. 4

The experimental results have confirmed the effectiveness of the proposed method of promt correction. But however, the problem of technological optimization of reliable heterodyne changing over into unnominal operational mode and its reset requires further investigations.

REFERENCES

1. Patent of Russ. Fed. N 2103768 H 01 Q3/36, G 01 R 29/10. A way of amplitude-phase characteristics correction of primary channels of plane digital antenna array. Slyusar V.I., Pokrovskij V.I., Sakhno V.F., priority 16.10.92, publ. 27.01.98.

ANALYSIS OF THE EFFECT OF GEOMETRIC PARAMETERS OF NONEQUIDISTANT ANTENNA ARRAY WITH UNEQUAL AMPLITUDE DISTRIBUTION ON ITS WORKING FREQUENCIES RANGE

S. I. Starchenko, A. Yu. Milovanov, I. V. Pleshivtsev

Tambov military air force engineering institute 392006, Tambov -6, Tambov MAFEI

ABSTRACT

In this paper the analysis of the effect of geometric parameters of unequidistant antenna array (AA) with the irregular amplitude distribution on its working frequencies range is presented. The coefficient of working frequencies range overlapping [1] was selected as criterion of optimization.

FORMULATION OF A TASK

Under certain conditions in equidistant AA it is possible an existence of parasitic interference lobes of higher order together with a main lobe. Their position relatively to the area of real angles depends on a distance between elements in lengths of waves and on a value of phase shift between currents in adjacent elements. Appearance of the lobes in the high-frequency area of AA working range is especially possible with deviation of the main lobe from a orthogonal position to AA.

The most effective way to overcome the parasitic interference lobes is the use of the unequidistant AA. The coordinates of elements play a particular role in diffraction lobes corruption. This paper presents numerical results of the analysis of the influence of elements coordinates in unequidistant antenna array with unequal amplitude distribution on its scanning sector in different range of frequencies [1].

In order to find out the coordinates of elements in an unequidistant AA a principle of power equivalence between an equidistant AA with irregular current distribution and an unequidistant AA with uniform current distribution was used [2]. The number of elements N in an original equidistant AA is equal 31, a distance between them is equal to a half of a original wavelength (d = λ/2). In this case a coordinate of n element in the unequidistant AA is determined by the expression

$$x_{un} = d\left[n-(N_x-1)/2\right]+\frac{d}{N_x I(x_n)}\int_{-L/2}^{L/2} \mathrm{I(x)}\,dx, \quad (1)$$

where $I(x_n)$ is a current in element number n of the original equidistant AA; L is a length of the original equidistant AA, $L = d\ (N - 1)$; $I(x)$ is a current distribution along a original equidistant AA.

Thus, distances between adjacent elements of the unequidistant AA are inversely proportional to values of currents in appropriate elements of the original equidistant AA. Using in (1) various types of current distributions it is possible to get various unequidistant AAs.

In this work unequidistant antenna arrays were analyzed, obtained by the following two kinds of current distribution in a original equidistant AA:

- a current distribution "cosine to the m power on a pedestal"

$$I(x_n)=\Delta+(1-\Delta)\left[\cos(\pi x_n/n)\right]^m; \quad (2)$$

- distribution like a "parabola to the s power on pedestal"

$$I(x_n)=1-(1-\Delta)(\pi x_n/n)^s, \quad (3)$$

where Δ is a value of relative amplitude of a current on equidistant AA edges; under solution of the task of optimization the area of its change lies within the limits of $0 < \Delta < 1$; m and s are exponents, the range m lies in bounds $1 \le m \le 4$, and the exponent s was of two values: 2 and 4.

Using expressions (1)...(3), coordinates of unequidistant equiamplitude synphased AA elements were determined. Then the unnormalized pattern was

$$f(\theta)=\sum_{n=1}^{N} I(x_{un})\exp\left[j(2\pi/\lambda_w)x_{un}\cos(\theta)\right], \quad (4)$$

where λ_w is the working wavelength, investigated when solving the task of optimization varied in limits of $0.2\lambda < \lambda_w < \lambda$ that is the range of work frequencies with an overlapping coefficient equal to 5; N is the number of elements in unequidistant AA, in general less than numbers of elements in the equidistant antenna array; $I(x_{un})$ is a current amplitude in nth element of the unequidistant antenna array.

After normalizing and taking the logarithm (4), the angle at which the parasitic interference lobe of any order other than zero exceeding a level –10 dB with respect to a main lobe was determined. It enables to find out the area of scanning beam actual angles of the unequidistant AA and range of working frequencies, providing one main lobe only. This results are presented in Table 1.

Table 1

Overlapping Coefficient		1	2	3	4	5
		Scanning sector				
Amplitude distribution in equidistant antenna array	Cosine	±90°	±36°	±36°	±24°	±22°
	Cosin. Sq.	±90°	±45°	±37°	±28°	±22°
	Cosin. Cub	±90°	±43°	±29°	±23°	±22°
	Cosin. Fo.	±90°	±43°	±38°	±28°	±22°
	Parabola	±90°	±51°	±34°	±28°	±21°
	Parab. Sq.	±90°	±54°	±34°	±23°	±23°

Table 2

Overlapping Coeficient		1	2	3	4	5
		Amplitude distribution in unequidistant AA				
Amplitude destribution in nonequidistant antenna array	Cosine	Cosine Sq	Parabola S	Parabola S	Parabola S	Cosine
	Cosine Sq	Cosine	Parabola S	Parabola S	Parabola S	Cosine
	Cosine Cub	Parabola	Parabola S	Parabola	Cosine	Parabola
	Cosine Fo.	Cosine	Cosine	Parabola S	Parabola S	Parabola S
	Parabola	Cosine Sq	Parabola S	Parabola S	Parabola S	Parabola S
	Parabola Sq	Cosine Sq	Parabola S	Parabola S	Parabola S	Cosine

The scanning sectors of the unequidistant antenna array presented in Table 1 might be produced only with the particular amplitude distribution, since not all types of distributions are capable to ensure them. Table 2 presents combinations of amplitude distributions in equidistant and unequidistant antenna arrays represented by scanning sectors given in Table 1.

CONCLUSION

Analysis of Table 1 and 2 allows to conclude the following:

1. When reducing a relative current amplitude on edges of equidistant antenna array a scanning sector of unequidistant antenna array increases, herewith every type of amplitude distribution in equidistant antenna array have value of pedestal under which scanning sector will be maximum. Changing of a value of relative current amplitude on unequidistant antenna array edges considerably influences on scanning sector at overlapping coefficient greater than unit i.e. maximum scanning sector can exist, depending on the type of amplitude distribution, both under greater and under small pedestals.
2. In general, the decreasing of relative current amplitude on edges of unequidistant antenna array leads to the worse results i.e. the suppression of parasitic interference lobes weakens because the influence of elements on AA edges is diminished.

REFERENCES

1. I.A.F. Chaplin Analysis and synthesis of antenna arrays, Lviv, "Vyscha shkola", 1987.
2. A.S. Lavrov, G.B. Reznikov Antenna and feeding devices, Kiev, KVIAVU, 1969.

MAXIMIZATION OF THE POWER PARAMETERS OF ANTENNA ARRAYS WITH SUPPRESSION OF THE CROSS-POLAR RADIATION

P. L. Tokarsky, A. M. Rybalko and A. V. Synepoop

Kharkiv State Technical University of Radio Electronics,
14, Lenin Ave, Kharkiv, 310726, Ukraine
Phone: +380 572 409 430, Fax: +380 572 409 413, E-mail: shifrin@kture.kharkov.ua

INTRODUCTION

Polarization isolation of antennas is among the widely used methods for providing electromagnetic compatibility of various radio and electronic facilities. However, it turns out to be efficient in the only case when the cross-polar radiation of the antennas has sufficiently low level. Suggested in this paper is a method for optimizing the current distribution in an antenna array to provide its high performance along with suppression of the power radiated by cross-polar waves.

THEORY

In order to optimize the power characteristics of an arbitrary antenna array we introduce a functional $K(\vec{u}_0)$

$$K(\vec{u}_0) = \gamma R^2 \overline{S(\vec{R}_0)} / \overline{P}, \qquad (1)$$

that generalizes basic integral parameters of the antenna array (e.g., directive gain, gain, signal-to-noise ratio etc.) and takes into account the random errors in the its current distribution. Here $\overline{S(\vec{R}_0)}$ is a magnitude of the Poynting's vector; $\overline{P}$ is a power, e.g. the array input power, the radiation power, etc. depending on the physical meaning of the parameter K, $\vec{R}_0 = \vec{u}_0 R$ is the radius vector of the observation point in the far-field region; γ is a constant factor; and the bar denotes the averaging operator.

The cross-polar radiation power can be characterized by the mean polarization loss factor (PLF) [1,2], $\overline{a}_c$, defined as the ratio of the power radiated by cross-polar waves $\overline{P}_c$ to the total radiation power, $\overline{P}_\Sigma$, of the array

$$\overline{a}_c = \overline{P}_c / \overline{P}_\Sigma. \qquad (2)$$

Mathematically, the optimization problem in the present formulation can be reduced to maximization of the functional

$$K_{\max}(\vec{u}_0) = \max_{\overline{a}_c \le a_{c\lim}} \gamma R^2 \overline{S(\vec{R}_0)} / \overline{P}, \qquad (3)$$

where $a_{c\lim}$ is the limiting value of PLF.

We assume that the current amplitudes on the radiator inputs are random quantities, which can be expressed as [3]: $i_n = x_n(1 + c_n + jd_n)$, for $n = \overline{1,N}$, where N is the number of array elements; $x_n = \alpha_{0n}\exp(j\phi_n)$ corresponds to the current of the n-th element, with an amplitude α_{0n} and a phase ϕ_n in the absence of errors; c_n and d_n are the centered normal random quantities with statistics as follows: $\overline{c_n^2} = \overline{d_n^2} = \sigma_n^2/\alpha_{0n}^2$; $\overline{c_m d_n} = 0$; and $\overline{c_m c_n} = \overline{d_m d_n} = Q_{mn}/\alpha^2$; Q_{mn} is the correlation coefficient between the random errors of the m-th and the n-th array elements. Here we consider the ratio $\alpha_{0n}/\sigma_n = \alpha$ as a given constant for all radiators.

We express the powers involved in Eqs (1)-(3) through input currents of the radiators and write them in terms of the Hermitian forms whose matrices are the resistance matrices of the antenna array [2]. Thus, the optimization problem can be formulated (3) in the following matrix form

$$K_{\max}(x\rangle) = \max_{x\rangle \in X} \gamma \frac{\left|\langle \vec{f}(\vec{u}_0)x\rangle\right|^2 + \langle x^* \mathbf{A} x\rangle}{\langle x^* \mathbf{A} x\rangle},$$

$$X = \left\{ x\rangle \left| \frac{\langle x^* \mathbf{C} x\rangle}{\langle x^* \mathbf{D} x\rangle} \le a_{c\lim} \right. \right\},$$

where $x\rangle$ is the column-matrix of the desired deterministic currents distribution of the array; $\langle \vec{f}(\vec{u})$ is the row- matrix of the normalized vectorial directional pattern of the array elements [4]; the asterisk denotes the complex conjugate; A, B, C and D are the positive-definite or positive-semidefinite Hermitian matrices, whose elements are defined as follows

$$A_{mn} = \left(\vec{f}_m^*(\vec{u}_0)\vec{f}_n(\vec{u}_0)\right)Q_{mn},\ B_{mn} = r_{mn}\left(1 + \frac{2}{\alpha^2}Q_{mn}\right),$$

$$C_{mn} = r_{mn}^{cc}\left(1 + \frac{2}{\alpha^2}Q_{mn}\right),\ D_{mn} = r_{\Sigma mn}\left(1 + \frac{2}{\alpha^2}Q_{mn}\right).$$

Here $r_{mn} = \mathrm{Re}(z_{mn})$, z_{mn} are elements of the normalized impedance matrix of the antenna array [4]; r_{mn}^{cc} are $r_{\Sigma mn}$ elements of the normalized radiation resistance matrices (r_{mn}^{cc} characterize the interaction be-

tween the array elements due to the radiated cross-polar waves only, while $r_{\Sigma mn}$ takes into account the radiated waves of the both polarization [2]).

The optimal current distribution across the antenna array has been found by the method of the Lagrangian undetermined multipliers and as a result the following nonlinear equation with respect to $x\rangle$ has been obtained

$$x\rangle = \left[\mathbf{B} - p\left(\mathbf{C} - a_{c\lim}\mathbf{D}\right) + \frac{2\mathbf{A}}{\alpha^2 K(x\rangle)}\right]^{-1} f^*(\vec{u}_0)\rangle . \quad (4)$$

The magnitude of p can be determined from an auxiliary equation, which it is easy to obtain by substituting $x\rangle$ given by Eq.(4) into Eq.(2), viz.

$$\langle x^*\mathbf{C}x\rangle / \langle x^*\mathbf{D}x\rangle = a_{c\lim}, \quad (5)$$

For the solution of the Eq.(4) we suggest the following iterative procedure

$$x^{(n+1)}\rangle = \left[\mathbf{B} - p^{(n+1)}\left(\mathbf{C} - a_{c\lim}\mathbf{D}\right)\right]^{-1} \times$$
$$\times \left(f^*(\vec{u}_0)\rangle + \frac{2}{\alpha^2 K\left(x^{(n)}\rangle\right)}\mathbf{A}x^{(n)}\rangle \right),$$

where $x^{(1)}\rangle = \left[\mathbf{B} - p^{(1)}\left(\mathbf{C} - a_{c\lim}\mathbf{D}\right)\right]^{-1} f^*(\vec{u}_0)\rangle$ is the initial approximation and p is determined from the Eq.(5) at each iteration step.

It should be noted, that the algorithm suggested converges rapidly when $\alpha > 1$, and normally two or three steps provide the acceptable calculation accuracy.

NUMERICAL RESULTS

The proposed method was used to maximize the directivity of a normal-firing antenna array radiating circularly polarized waves, with its PLF being constrained. The array is made of seven thin half-wave cross-dipoles, located at the center point and at the vertices of a regular hexagon of side $d = 0.7\lambda$.

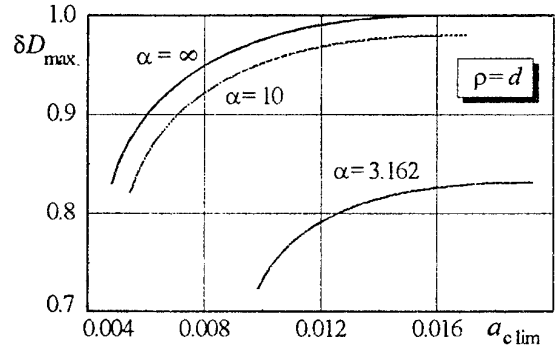
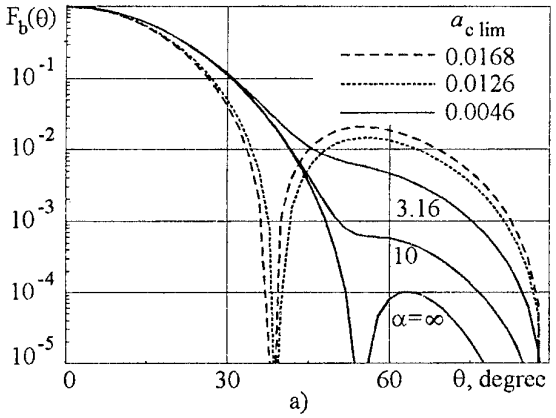


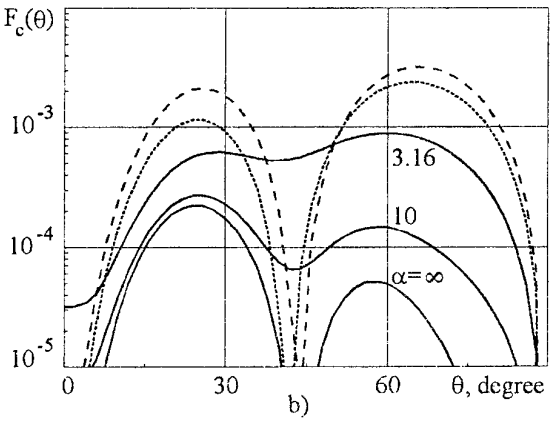
Fig. 1

Fig. 1 shows the ratio $\delta D_{\max} = \overline{D}_{\max}/D_{0\max}$ as a function of the tolerable PLF value $a_{c\lim}$ for the several values of the parameter α. Here $D_{\max}$ is the maximum value of the antenna array directivity with the specified PLF; and $D_{0\max}$ is the unconstrained directivity maximum in the absence of the random errors ($\alpha = \infty$). The correlation coefficient has been chosen in the Gaussian form, viz.: $Q_{mn} = \exp[-d_{mn}^2/\rho^2]$, where d_{mn} is the distance between the m-th and the n-th array elements; and ρ is the correlation distance of errors. As can be seen from the plots, the optimization of antenna array excitation allows to achieve an appreciable decrease of PLF with a slight reduction of the directivity.

Effect of the limiting of PLF level on the co-polar and cross-polar power directivity patterns of the antenna array is illustrated in Fig. 2, a,b. The represented curves are calculated for the several PLF values in the absence of the random errors ($\alpha = \infty$), and for different errors values at $a_{c\lim} = a_{c\min} = 0.0046$.



a)



b)

Fig. 2

CONCLUSION

The results obtained allow to conclude that method developed can effectively be applied to design of antenna arrays characterized by suppressed level of the cross-polar radiation.

REFERENCES

1. B. A. Panchenko and V. D. Oshivalov, «Polarization Losses of Turnstile Dipole Antennas», Raditekhnika, no. 5, pp. 62 – 63, 1987 [in Russian].
2. P. L. Tokarsky, «Impedance approach to Analysis of Polarization Losses in Antenna Arrays», Radiotekhnika i Electronika, vol. 37, no. 8, pp. 1388 – 1395, 1992 [in Russian]. English translation: *Soviet Journal of Communications Technology and Electronics*, no. 16, pp. 17-23, 1992.
3. L. A. Rondinelli, «Effects of Random Errors on the Performance of Antenna Arrays of Many Elements», *IRE National Convention Records*, vol. 9, pt. 1, pp. 174-188, 1959.
4. D. M. Sazonov, «Basics of the Matrix Theory of Antenna Arrays», Proceeding of the Seminar of the Soviet Higher School on Applied Electromagnetics, Vysshaya shkola Publishers Moscow, Issue no.6, pp. 111 – 162, 1983 [in Russian].

THE INFLUENCE OF AMPLITUDE AND PHASE PERTURBATIONS OF ANTENNA ARRAY SENSORS ON DIRECTION FINDING OF NARROW-BAND SIGNALS EFFICIENCY

I. R. Urazgildiev, A. M. Vagapov

National Scientific and Research Center of Defensive Technologies and Military Security of Ukraine
81 Melnikova st., Kiev-119, Ukraine, 252119. Ph. (044) 211-64-77, fax (044) 213-04-31
E-mail ildar@pson.ntu-kpi.kiev.ua

The amplitude and phase perturbations (APP) of antenna array sensors are the basic sources of the errors arising while estimating the narrow-band signals direction arrival (DOA). The analysis of the APP influence on the quality of estimation is performed by statistical simulation technique as a rule. The given method has broad capabilities, however, when simulating the array with a large number of sensors the using of this one requires essential computing costs. In this connection there is a necessity in obtaining analytical representations connecting the DOA estimation errors with the APP parameters of array sensors. The aim of the given paper is the getting of canonical representations for mean value and variance of DOA estimation errors as well as the matching of obtained relations with statistical simulation results.

Consider an array of N sensors. The noiseless array output can be expressed as a complex vector $x(t)$ [1-3]

$$x(t) = V(\Theta)\, s(t), \qquad (1)$$

where $s(t)$ is a $M\times 1$ vector which denotes the complex envelopes of the M narrow-band signals. The elements of $s(t)$ are assumed to be independent Gaussian distributed random variables with zero mean. $V(\Theta)$ is a $N\times M$ matrix whose columns are the direction vectors $v(\vartheta_m)$ with parameters $\Theta = [\vartheta_1, \ldots, \vartheta_M]$ denoting the angles of arrival of the M signals. It is assumed that the nth element of vector $v(\vartheta_m)$ is defined as

$$v_n(\vartheta_m) = a_n \exp\{j2\pi d_n \sin\vartheta_m/\lambda + \varphi_n\},$$

where a_n , φ_n are the real random values of amplitude and phase perturbations of nth array sensor respectively; d_n is the sensor spacing; λ is a wavelength. Random values a_n , φ_n we will assume to be statistically independent with mean values

$$E\{a_n\} = 1,\ E\{\varphi_n\} = 0 \qquad (2)$$

and variances

$$\mathrm{var}\{a_n\} = E\{\delta a_n{}^2\} = S_a^2,$$
$$\mathrm{var}\{\varphi_n\} = E\{\delta\varphi_n{}^2\} = S_p^2, \qquad (3)$$

where

$$\delta a_n = a_n - 1,\ \delta\varphi_n = \varphi_n;$$

E denotes the expectation operator.

The set of complex exponents $exp\{j2\pi d_n \sin\vartheta_m/\lambda\}$, $n = 1\ldots N$, we will denote as a $N\times 1$ vector $u(\vartheta_m)$.

The unknown canonical representation for mean value and variance of DOA estimation errors manages to be received only for an one-signal situation, when the maximum likelihood DOA estimator coincides to the maximum of a function [1–3]

$$R(\vartheta, \boldsymbol{a}, \boldsymbol{f}|\vartheta_0) = P_0\left|\boldsymbol{u}(\vartheta)^H \boldsymbol{v}(\vartheta_0)\right|^2 =$$
$$= P_0\left|\sum_n a_n \exp\left\{j[\theta_n - \theta_n^0 + \varphi_n]\right\}\right|^2,$$

where P_0, ϑ_0 are the power and angle of arrival of the received signal; a, f are the $N\times 1$ vectors of amplitude and phase perturbations respectively; ^{H} denotes conjugate transpose; $\theta_n^0 = 2\pi d_n \sin\vartheta_0/\lambda$.

The estimation of parameter $\tilde{\vartheta}_0$ is the solution of an equation

$$\frac{\partial R(\vartheta, \boldsymbol{a}, \boldsymbol{f}|\vartheta_0)}{\partial\vartheta} = 0.$$

Let's introduce the denotation

$$F(\vartheta, \boldsymbol{a}, \boldsymbol{f}|\vartheta_0) = \frac{\partial R(\vartheta, \boldsymbol{a}, \boldsymbol{f}|\vartheta_0)}{\partial\vartheta}.$$

For obtaining the canonical representation for mean $E\{\tilde{\vartheta}_0\}$ and variation $\mathrm{var}\{\tilde{\vartheta}_0\}$ we will expand $F(\vartheta, a, f|\vartheta_0\}$ in a neighborhood of true parameter ϑ_0 and zero APP into Taylor series. Limiting by the first terms of series we can obtain

$$F(\vartheta, \boldsymbol{a}, \boldsymbol{f}|\vartheta_0) = F(\vartheta_0, \boldsymbol{1}, \boldsymbol{0}) + \sum_{n=1}^{N}\frac{\partial F}{\partial a_n}\Big|_{(\cdot)}\delta a_n +$$
$$+\sum_{n=1}^{N}\frac{\partial F}{\partial\varphi_n}\Big|_{(\cdot)}\delta\varphi_n + \frac{\partial F}{\partial\vartheta}\Big|_{(\cdot)}\delta\vartheta,$$

where $\delta\vartheta = \vartheta - \vartheta_0$; $(\cdot) = (\vartheta_0, 1, 0)$; 1, 0 are the $N\times 1$ vectors of units and zeroes. By virtue of that $F(\vartheta, a, f|\vartheta_0\} = 0$ and $F(\vartheta_0, 1, 0\} = 0$ for an DOA estimation error we have

$$\delta\vartheta = \tilde{\vartheta}_0 - \vartheta_0 = -\frac{\sum_{n=1}^{N}\left[\frac{\partial F}{\partial a_n}\Big|_{(\cdot)}\delta a_n + \frac{\partial F}{\partial\varphi_n}\Big|_{(\cdot)}\delta\varphi_n\right]}{\frac{\partial F}{\partial\vartheta}\Big|_{(\cdot)}}. \qquad (4)$$

By meaning (4) random and statistically independent parameters a_n, φ_n and taking into account (2), (3), we will obtain the following expressions:

$$E\{\tilde{\vartheta}_0\} = \vartheta_0, \tag{5}$$

$$\mathrm{var}\{\tilde{\vartheta}_0\} = \frac{S_a^2 \sum_{n=1}^{N}\left(\frac{\partial F}{\partial a_n}\Big|_{(\cdot)}\right)^2 + S_p^2 \sum_{n=1}^{N}\left(\frac{\partial F}{\partial \varphi_n}\Big|_{(\cdot)}\right)^2}{\left(\frac{\partial F}{\partial \varphi_n}\Big|_{(\cdot)}\right)^2}. \tag{6}$$

As it follows from (5) the presence of small sensor's APP doesn't result in the bias of estimator. For obtaining the explicit representation for a variance it is necessary to calculate partial derivatives included in (6). By executing all the necessary transformations we can obtain the following canonical representation

$$\mathrm{var}\{\tilde{\vartheta}_0\} = \left(\frac{S_p \lambda}{2\pi\sqrt{N}\sigma_d \cos\vartheta_0}\right)^2, \tag{7}$$

where

$$\sigma_d^2 = \frac{1}{N}\sum_{n=1}^{N} d_n^2 - \left(\frac{1}{N}\sum_{n=1}^{N} d_n\right)^2.$$

We will name the parameter σ_d as an effective root-mean-square size of the array aperture.

From the representations obtained follows that in a one-signal situation and in the presence of small APP the variance of DOA estimation error is proportional to the variance of phase perturbations and is inversely proportional to the effective root-mean-square array aperture size multiplied by the number of sensors, the variance being independent on the level of amplitude perturbations.

Computer simulations have been carried out to compare the experimental root-mean-square error (RMSE) of DOA to that of theoretical one, which was calculated as

$$RMSE = \sqrt{\sum_{m=1}^{M} \mathrm{var}\{\tilde{\vartheta}_m\}},$$

where $\mathrm{var}\{\tilde{\vartheta}_m\}$ is calculated according to (7). In all experiments to follow, a uniform linear array of $N = 8$ sensors with half-wavelength spacing have been assumed. A total of 200 independent simulation runs were performed to obtain each simulated point. The randomly generated vectors a, f have been renewed in each simulation run. The random parameters φ_n, a_n were supposed to be normal (Gaussian) and lognormal random values respectively [3]. For each DOA estimator tested, the experimental RMSE is calculated as

$$RMSE = \sqrt{\frac{1}{M}\frac{1}{L_{runs}}\sum_{m=1}^{M}\sum_{l=1}^{L_{runs}}\left[\tilde{\vartheta}_m(l) - \vartheta_m\right]^2},$$

where $\tilde{\vartheta}_m(l)$ is the estimate of the mth DOA achieved in the lth run.

The theoretical and experimental RMSE's of DOA estimation versus the phase perturbation level S_p is depicted on Fig. 1.

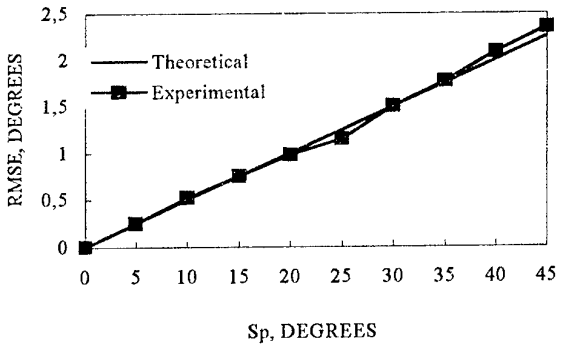


Fig. 1. Experimental and theoretical RMSE's of DOA estimation versus the standard deviation of phase perturbations S_P. Simulations with the one Gaussian source for the scenario ($\vartheta_1 = 10^0$)

The simulation results have shown that the analytical values (5), (7) describe RMSE quite precisely for the standard deviation of phase perturbation $S_P = 0...45^\circ$ and more.

In case of the number of signals presence equations (5), (7) can be used for the description of the DOA estimation errors when the signals have rather essential distinctions on parameter ϑ, that is when we can consider vectors $u(\vartheta_i)$, $u(\vartheta_j)$ mutually orthogonal:

$$u(\vartheta_i)^H u(\vartheta_j) \approx \| u \| \delta_{ij},$$

where $\| \cdot \|$ denotes vector norm; δ_{ij} is the Kronecker delta. The decreasing of the angular distance between the signals results in increasing the estimator bias and variance as well as the deterioration of resolution. Experimental and theoretical RMSE's of DOA estimation versus the angular distance $d\vartheta$ between two sources for fixed $S_P = 5^\circ$ and different S_a are depicted on Fig. 2. In this experiments we consider the signal scenario

$$\vartheta_1 = 10^0, \ \vartheta_2 = \vartheta_1 + d\vartheta.$$

Thus, in the approximation of small APP, representations (5), (7) describe the mean value and variance of orthogonal signals DOA estimation error quite completely. Obtained representations show that when receiving of orthogonal signals the basic bottom of estimator errors is the phase perturbations. At this the signal DOA estimators are unbiased and their variances are proportional to a variance of phase perturbations

and do not depend on amplitude perturbations. The influence of the latter ones became is rather to be significant in case of close spaced signals. Amplitude perturbations result in increasing the errors and decreasing the resolution. The obtained representations can be used for simulation of antenna array with a large number of sensors.

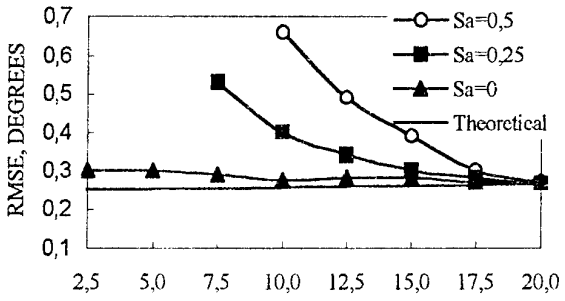


Fig. 2. Experimental and theoretical RMSE's of DOA estimation versus the angular distance $d\vartheta$ between two sources for fixed $S_P = 5^\circ$. Simulations with Gaussian sources for the scenario ($\vartheta_1 = 10^0$, $\vartheta_2 = \vartheta_1 + d\vartheta$)

REFERENCES

1. A. Vagapov. ML Estimates of Bearings and Shapes of Linear Independent Signals. Radioengineering and electronic. 1989. №10, - p.2094-2102.

2. Ziskin, M. Wax. Maximum likelihood localization of multiple sources by alternating projection. IEEE Trans. Acoust., Speech, Signal Processing, vol. 36, pp. 1553-1560, 1988.

3. R. Monzingo, T. Miller. Introduction to Adaptive Arrays. John Wiley and Sons, Inc., New York, 1980.

UNIFORM LINEAR ANTENNA ARRAY IN SUPERRESOLUTION MODE BY THE MODIFIED UNITARY ESPRIT ALGORITHM

V. I. Vasilishin, A. N. Kolesnikov

Kharkov Air Force Institute of Pilots
Klochkovskaya str., 228, Kharkov, 310165, Ukraine
tel.(057-2)30-82-18

The passing to the phased arrays based multichannel systems with digital signal processing is one of the ways to increase the radar signal processing efficiency. In such systems there is a possibility to measure parameters of several simultaneously located objects, when the angular spacing between them is smaller than the radar array beamwidth, i.e. in superresolution mode.

One of directions of superresolution algorithms synthesis bases on using the eigenvalues and eigenvectors of covariance matrix (CM) of a signals and noise mixture, received by the array. The interest to this algorithms (named in technical literature as eigensrtucture based (EB)) is due to the high accuracy of the obtaining with them of measurement estimates. However, realization of the EB algorithms is hampered by requirement of $O(M^3)$ (where M denotes the number of sensors) complex multiplication operations for CM eigendecomposition. For a wide class of antenna arrays with central – symmetrical sensor disposition the reduction problem of computational complication can be solved by way of nonsingular linear transformation (for example, an unitary transformation) of such arrays CM. In view of CM specific symmetry in this case (so-called persymmetry), CM might be transformed to real-valued symmetric matrix, that causes reduction more than by half of required for CM eigendecomposition the computation load.

Among a number of EB algorithms, such as MUSIC, Root-MUSIC (RM), Min-NORM the special interest represents ESPRIT algorithm, as having the high quality parameters it requires the least operations number for implementation among the indicated algorithms. Notice, that for algorithm realization it is necessary for the antenna system to comprise two identical subarrays [1]. The special case of such an antenna system is the uniform linear array (ULA), which it is possible to consider as consisting of two subarrays, the first of them comprises $M-1$ first sensors and the one — of last $M-1$ sensors. The analysis of the given algorithm efficiency shows [1] that the better accuracy can be achieved when displacing subarrays more than by one sensor, i.e. by 2, 3 and so on.

In this connection it is of interest to modify Unitary ESPRIT algorithm [2] for subarrays displacement more than by one sensor. Consider a ULA consisting of M identical elements, located symmetrically with respect to the array phase center. Each element is excited by narrow-band signals of V sources, located in the far-field of array. The thermal noises in the processing tracts are considered statistically independent on each other and on signals. The directions of arrival (DOA) of signals are to be determined. The data model in details is considered in [1, 2] and consequently, we present only values of need for a further setting of a material.

The array input vector can be expressed by

$$\mathbf{x}(t) = \mathbf{A}(\theta)\mathbf{s}(t) + \mathbf{n}(t), \qquad (1)$$

where $\mathbf{A}(\theta) = [\mathbf{a}(\theta_1),\ldots,\mathbf{a}(\theta_V)]$ is $M \times V$ matrix whose columns $\mathbf{a}(\theta)$, which are array response vectors, correspond to the $V \times 1$ DOA vector $\theta = [\theta_1,\cdots,\theta_V]^{\mathrm{T}}$, $\mathbf{s}(t)$ is a vector of source complex envelope, $\mathbf{n}(t)$ is an additive spatial white noise vector, $(\cdot)^{\mathrm{T}}$ denotes transpose. The covariance matrix of $\mathbf{x}(t)$ is

$$\mathbf{R} = E[\mathbf{x}(t)\mathbf{x}^{\mathrm{H}}(t)] = \mathbf{A}(\theta)\mathbf{S}\mathbf{A}^{\mathrm{H}}(\theta) + \sigma^2\mathbf{I}, \qquad (2)$$

where $\mathbf{S} = E[\mathbf{s}(t)\,\mathbf{s}^{\mathrm{H}}(t)]$ is CM of sources, σ^2 is the array channel noise variance, $\mathbf{I}$ is an identity matrix, $(\cdot)^H$ denotes hermitian transpose. The eigendecomposition of CM $\mathbf{R}$ is of the following form

$$\mathbf{R} = \mathbf{E}_s\Lambda_s\mathbf{E}_s^{\mathrm{H}} + \mathbf{E}_n\Lambda_n\mathbf{E}_n^{\mathrm{H}}, \qquad (3)$$

where $\mathbf{E}_s = [\mathbf{e}_1,\cdots,\mathbf{e}_V]$ and $\mathbf{E}_n = [\mathbf{e}_{V+1},\cdots,\mathbf{e}_M]$ are signal and noise subspace eigenvectors matrices, respectively, Λ_s is $V \times V$ diagonal matrix that contains V largest eigenvalues in descending order and diagonal elements of Λ_s are σ^2.

The consistent estimates of eigenvalues and eigenvectors might be obtained by means of eigendecomposition of the sampled CM

$$\hat{\mathbf{R}} = \frac{1}{N}\sum_{t=1}^{N}\mathbf{x}(t)\mathbf{x}^{\mathrm{H}}(t) = \hat{\mathbf{E}}_s\hat{\Lambda}_s\hat{\mathbf{E}}_s^{\mathrm{H}} + \hat{\mathbf{E}}_n\hat{\Lambda}_n\hat{\mathbf{E}}_n^{\mathrm{H}}, \qquad (4)$$

where $\hat{V} \times \hat{V}$ and $(M-\hat{V}) \times (M-\hat{V})$ diagonal matrices $\hat{\Lambda}_s$ and $\hat{\Lambda}_n$ contain $\hat{V}$ and $M-\hat{V}$ signal and noise subspace eigenvalues, respectively. The columns of the $M \times \hat{V}$ matrix $\hat{\mathbf{E}}_s$ and $M \times (M-\hat{V})$ matrix $\hat{\mathbf{E}}_n$ contain the corresponding eigenvectors, and $\hat{V}$ is an estimate of sources number, which can be obtained by using one of known methods, such as AIC and MDL [1].

The essence of an unitary transformation (UT) method is in the array data or CM conversion, described by the following expression

$$\mathbf{U}_{2K} = (1/\sqrt{2})\begin{bmatrix} \mathbf{I}_K & j\mathbf{I}_K \\ \widetilde{\mathbf{I}}_K & -j\widetilde{\mathbf{I}}_K \end{bmatrix} \quad \Rightarrow \quad \mathbf{y}(t) = \mathbf{U}^H\mathbf{x}(t)$$

$$\text{or } \mathbf{R}_u = E\left[\mathbf{y}(t)\mathbf{y}^H(t)\right] = \mathbf{U}^H\mathbf{R}_x\mathbf{U}, \qquad (5)$$

in which also the matrix $\mathbf{U}$ for even sensor number (i.e for $M = 2K$) is determined, and $\widetilde{\mathbf{I}}_K$ is an $M \times M$ exchange matrix with ones on its antidiagonal and zeros elsewhere. Matrix $\mathbf{U}$ is a sparce unitary matrix, that determine the transformation method name (i.e. UT method). It is possible to show, that due to persymmetry of $M \times M$ hermitian CM $\mathbf{R}$ the product $\mathbf{U}^H\mathbf{R}\mathbf{U}$ is real-valued and symmetric (as is known, eigenvalues and eigenvectors of a real-valued symmetric matrix are real). Therefore calculation of the eigendecomposition of matrix $\mathbf{U}^H\mathbf{R}\mathbf{U}$ requires only real calculations. In practice, as the sampled CM $\hat{\mathbf{R}}$ is hermtitian but generally not persymetric, it is necessary to take the real part of the matrix $\mathbf{U}^H\hat{\mathbf{R}}\mathbf{U}$ for UT method to be implemented.

The sequence of steps, describing realization of modified Unitary ESPRIT algorithm is presented below:

1) compute $\hat{\mathbf{E}}_s$ via $\hat{V}$ largest eigenvectors of matrix $\mathrm{Re}(\mathbf{U}^H\hat{\mathbf{R}}\mathbf{U})$ or largest singular vectors of $\{\mathrm{Re}(\mathbf{y}(t)),\mathrm{Im}(\mathbf{y}(t))\}$;

2) compute $(M-\widetilde{m}) \times M$ matrices $\mathbf{K}_{1(\widetilde{m})} = \mathrm{Re}(\mathbf{T})$ and $\mathbf{K}_{2(\widetilde{m})} = \mathrm{Im}(\mathbf{T})$, where $\mathbf{T} = \mathbf{U}^H_{M-m}\mathbf{J}_{2(\widetilde{m})}\mathbf{U}$; $\mathbf{J}_{1(\widetilde{m})} = [\mathbf{I}_{M-\widetilde{m}} \ \mathbf{0}_{(M-\widetilde{m})\times\widetilde{m}}]$, $\mathbf{J}_{2(\widetilde{m})} = [\mathbf{0}_{(M-\widetilde{m})\times\widetilde{m}} \ \mathbf{I}_{M-\widetilde{m}}]$ are selection matrices [1, 2], and subscript $\widetilde{m}$ in a paranthesis indicates accordance of the matrices to a certain displacement value $\widetilde{m}$, measured in the number of sensors, i.e 1, 2, etc;

3) solve the $(M-\widetilde{m}) \times \hat{V}$ matrix equation $(\mathbf{K}_{1(\widetilde{m})}\hat{\mathbf{E}}_s)\Psi = \mathbf{K}_{2(\widetilde{m})}\hat{\mathbf{E}}_s$ and calculate eigenvalues $\lambda_i, i = 1,\ldots,\hat{V}$ of $\hat{V} \times \hat{V}$ real-valued matrix Ψ;

4) compute the spatial frequency estimates as $\omega_i = c\,\mathrm{arctg}(\lambda_i)$, $i = 1,\cdots,\hat{V}$, where $c = 2/\widetilde{m}$.

To assess the performance of modified Unitary ESPRIT the following simulations were carried out. Two uncorrelated sources with angular coordinates $\theta_1 = 10°$, $\theta_2 = 13°$ impinged on $M = 12$ -elements ULA with half -wavelength element spacing. For each of L = 500 trials, N = 40 snapshots were taken. The root-mean square (rms) error of the first source ($\theta_1 = 10°$) DOA estimate is calculated and displaced in Fig. 1 as a function of signal-to-noise ratio (SNR). The dashed-and-dotted line is rms error for unitary TLS-ESPRIT algorithm with the maximum overlapping of subarrays [2], i.e. $\widetilde{m} = 1$, and dashed and solid lines correspond to rms error for $\widetilde{m} = 2$ and $\widetilde{m} = 3$, respectively. The double dotted line is rms error for RM algorithm with use of UT method.

As follows from the lines analysis, for unitary ESPRIT the maximum overlapping of subarrays it is not the best and for considered case algorithm possesses minimum rms in the case of subarray displacement by 3 elements. Notice, that the significant increase of subarray displacement can cause the decrease of algorithm performance due to reduction of subarray aperture. Also the magnitude of $\widetilde{m}$ determines the range of DOA's in which there are no ambiguities [1]. However, even if ambiguities problem is occurs, the using of the ideas of Jonson approach [3] allow to save the domination of modified Unitary ESPRIT over the initial algorithm.

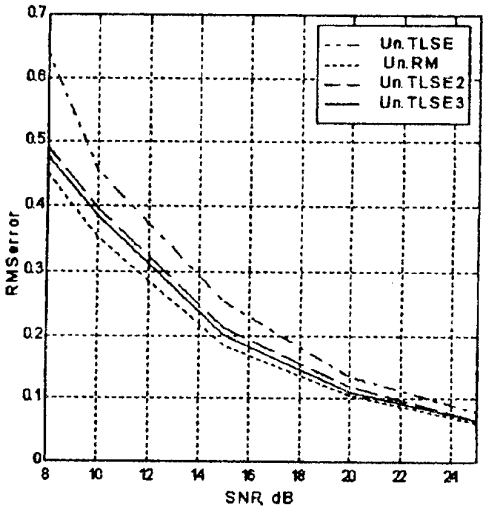


Fig. 1

Thus ULA in superresolution mode by modified Unitary ESPRIT algorithm is presented. The using of the latter permits to improve the quality parameters (in comparison with initial Unitary ESPRIT algorithm) when the signal direction finding under superresolution.

REFERENCES

1. Ottersten B., Viberg M., Kailath T. Performance analysis of the total least squares ESPRIT algorithm // IEEE Trans. on Signal Processing.-1991.-vol.39, N5.-pp.1122-1135.
2. Zoltowski M.D., Haardt M., Mathews G.P. Closed-form 2-D angle estimation with rectangular arrays in element space or beamspace via unitary ESPRIT // IEEE Trans. Signal Processing.-1996.-vol.44, N2.-pp.316-328.
3. Jonson R.J, Miner G.E. An operational system implementation of the ESPRIT DF algorithm // IEEE Trans. on AES. -1991. -vol.27, N1.-pp.159-166.

SYNTHESIS OF ONE-DIMENTIONAL PERIODIC PERFECTLY CONDUCTING GRATINGS

L. G. Velychko

Institute of Radiophysics and Electronics, National Academy of Sciences of Ukraine,
12 Acad. Proskura st., Kharkov, 310085, Ukraine.
Phone: 38(0572)448557; fax: 38(0572)441105; e-mail: sirenko@ire.kharkov.ua

INTRODUCTION

The modern electrodynamic theory of gratings represents a unique collection of analytical and experimental results providing a rather full physical picture of the processes in resonant wave scattering under conditions of complex dispersion laws (including nonclassical ones). By now the reliable mathematical methods oriented to both qualitative and numerical analysis are developed and evaluated [1–4]. A large body of anomalous and resonant phenomena are revealed and investigated [1, 5, 6]. Justified recommendations have been elaborated for their use in spectroscopy, antenna engineering, optics, electronics, acoustics, solid state physics, millimeter and submillimeter radio engineering, etc. In total, all these results constitutes the necessary basis for posing and solving practically important inverse problems. However, a number of challenging mathematical problems arises in their solution [7]. Sometimes they are significantly different from that in direct problems. Certain of them are considered in the present work devoted to the synthesis of one-dimensional periodic perfectly conducting gratings.

FORMULATION OF THE PROBLEMS [6-8]

A direct problem is to determine some electrodynamic characteristics of the structure with the given material and geometric parameters from a knowledge of incident field. In inverse problems the parameters of the grating and the sources are unknown (in full or in part) and are to be determined. The information on the electrodynamic characteristics is the input one. The type of inverse problem and the possible methods for its solution are governed by a bulk and exactness of the input data. It is commonly accepted to classify inverse problems in three groups: the diagnostics or visualization problems (electrodynamic characteristics of the real object and the incident field are known, the parameters of the structure are to be determined); the synthesis problems (the construction of structures capable of realizing the given electrodynamic characteristics); and the optimization problems (a general topology, a type of the structure, and the sources are known; a number of particular geometric and material parameters are to be determined, which result in attainment of scattering characteristics closely approximating the given ones). The questions arising in solving these problems are differentiated respectively. Thus, for example, the question about existence of the solution does not arise in diagnostics problems with exact scattering data. The main problem here is to chose the size of input data set allowing one to determine the solution uniquely. Accumulation of analytical results of this kind (the uniqueness theorems) [6, 7] for a variety of practical situations is important also for a proper posing and for the construction of reliable algorithms of the solution of synthesis problems, where the solvability becomes the most essential issue. The solution, in a classical sense, does not need to exist. However, the construction of a generalized (regularized) solution is possible, if the input data set is supplemented to the size that ensure the uniqueness of the solution in the ideal case of exact input data. The first part of the report centers on this problem and the relevant results.

SIMPLE ALGORITHMS FOR SOLVING SYNTHESIS PROBLEMS [9, 10]

In the second part of the report, the novel methods of attack of synthesis problems for perfectly conducting gratings with an arbitrary profile are presented. These approaches are based on the idea of quasilinearization of integral relations of potential theory and allow one to obtain satisfactory analytical and numerical results in both long wavelength and partly resonance frequency regions (with respect to the typical dimensions of the grating, like grating period or depth). The complex amplitudes of spatial harmonics of a scattered field given in a frequency range or (and) in a range of angles of incidense of a plane E-polarized wave act as an input data set (incomplete and inexact). The final algorithms realize the standard Newton-Kantorovich linearization method and Lavrent'ev α-regularization. The self-closed scheme for obtaining "good" initial approximations is constructed; in some instances one can use the resulting approximations as solutions proper of synthesis problems.

MODEL SYNTHESIS OF QUASI-OPTICAL DEVISES WITH SELECTIVE GRATING-MIRRORS

An investigation of dispersive properties of diffraction gratings has revealed a diversity of interesting phenomena from the standpoint of their practical implementation. However, the use of gratings as selective elements

in resonance quasi-optical devices is substantially restricted by the complexity of the initial analysis of a designed unit. This analysis must meet two requirements. On the one hand, it has to take into account all key operating parameters of separate elements and, on the other hand, to judge the effectiveness of the system as a whole. This is the general problem of *model synthesis* in the design of resonance quasi-optical systems. The solution of this problem is divided naturally into the following conceptually independent steps. The first one is the construction of the electrodynamic model accounting for analytically an influence of scattering inhomogeneities varying in wave size. The second step is the formation of the input data set for the synthesis of dispersive elements, such as gratings, and the last one is the solution of relevant inverse problems. The last part of the report is concerned with the results guided by key problems of the model synthesis of such resonance quasi-optical systems as efficiently absorbing and rescattering coatings, plane pattern-forming structures and open dispersive resonators with a considerably rarefied spectrum. A number of new analytical results allowing one to construct the adequate models as well as the results of computational experiments showing the potentialities of the approaches and methods under discussion are presented here.

REFERENCES

1. Shestopalov V. P., Litvinenko L. N., Masalov S. A. and Sologub V. G. 1973 *Wave Diffraction on Gratings* (Kharkov: Kharkov State University Press) [in Russian].
2. Petit R (ed) 1980 *Electromagnetic Theory of Gratings* (Berlin: Springer).
3. Shestopalov V. P., Kirilenko A. A., and Masalov S. A. 1984 *Matrix Convolution Equations in Diffraction Theory* (Kyiv: Naukova Dumka) [in Russian].
4. Shestopalov V. P., Tuchkin Y. A., Poyedinchuk A. Y., and Sirenko Y. K. 1997 *New Methods for Solving Direct and Inverse Problems in Diffraction Theory. Analytical Regularization of Boundary Value Problems in Electrodynamics* (Kharkov: Osnova).
5. Shestopalov V. P., Kirilenko A. A., Masalov S. A., and Sirenko Y. K. 1986 *Resonance Wave Scattering Vol 1 Diffraction Gratings* (Kyiv: Naukova Dumka) [in Russian].
6. Shestopalov V. P. and Sirenko Y. K. 1989 *Dynamic Theory of Gratings* (Kyiv: Naukova Dumka) [in Russian].
7. Velychko L. G. 1997 Inverse diffraction problems for the plane periodic gratings *PhD Thesis* Institute of Radiophysics and Electronics, Kharkov [in Russian].
8. Sirenko Y. K. and Velychko L. G. 1996 Inverse two-dimensional boundary value problems in diffraction theory *Zarubezhnaja Radioelektronika. Uspekhi Sovremennoy Radioelektroniki* **2** №2 [in Russian].
9. Sirenko Y. K. and Velichko L. G. 1999 Diffraction grating profile reconstruction: simple approaches to solving applied problems *Electromagnetics* **19** № 2.
10. Sirenko Y. K., Velychko L. G., and Karacuha E. 1999 Synthesis of perfectly conducting gratings with an arbitrary profile of slits *Inverse Problems* **15** № 2.
11. Velychko L. G. 1997 Model Synthesis of latticed Absorbing and Pattern-Forming Structures *Preprint 97-1* Institute of Radiophysics and Electronics, Kharkov [in Russian].

OPTIMAL COMBINED PROCESSING OF SIGNALS IN MULTICHANNEL SYNTHETIC APERTURE RADARS

V. K. Volosyuk, S. E. Falkovich, V. M. Velasco Hererra, O. A. Gorbunenko

State Aerospace University "Kharkov Aviation Institute", department 501,
Chkalova str. 17, Kharkov-310070 Ukraine.
E-mail victor@ai.kharkov.ua

Abstract. Meeting the increased complication of the problem of surfaces remote sensing with the synthesis aperture radar (SAR) use, requiring more high level of resolution and the need in performing of the multiparametric measurements, the necessity of the multichannel SAR construction appears, which could receive signals in the different frequency bands, of different polarization, from different directions etc.

In the proposed paper the algorithms of such a combined processing are examined. These algorithms were synthesized by the solving of the optimization problems. They include the classic operations of the aperture synthesis and operations of the adaptive signal whitening, operations of the Earth covers parameters and statistical characteristic calculation as well

INTRODUCTION

Nowadays, great attention is paid to the design and software of the combined multichannel SAR. In such SARs the signals are received in some frequency bands, of some types of polarization, from different directions of survey (multifrequency, multipolarization, multiangle SAR). In these systems, when forming images in one of the channels, it is expedient to use the auxiliary information available in signals received in other channels. Mostly, such an information is of statistical nature and has the form of the mutual correlation's between the signals passing in different channels. Especially, such SARs are required for solving the multiparametric problems of measuring the different electrophysical and biological parameters of the Earth covers and the statistics of their irregularities as well.

In the proposed paper the optimization of the received signal processing is examined, beginning from the moment of the signal registration by the antenna and ending by the parameters and statistical characteristics of the Earth covers $\vec{\lambda}(\vec{r})$ formation. The algorithm of the specific radar (scattering) cross section (RCS), $\sigma^0(\vec{r})$, formation is considered as a particular case. Parameters $\vec{\lambda}(\vec{r})$ and $\sigma^0(\vec{r})$ are assumed as functions of the surface coordinates $\vec{r}=(x,y)\in D$ (or $\vec{r}=(x,R_0(y))$, R_0 is the distance). Such functions are the surface images (maps). The humidity, root-mean-square of the irregularity altitude, components of the microterrain power spectra, the field of the near-the-water-surface oceanic wind velocity etc. Are parameters $\vec{\lambda}(\vec{r})$ to be measured. The function RCS $\sigma^0(\vec{r})$ shows the surface image in scatterometric SAR.

Usually, the problem of parameters $\vec{\lambda}(\vec{r})$ measurement is the problem of the secondary data processing of SAR.

In our paper the united algorithms represent the entire scope of processing. However, in the conclusion the peculiarities of dividing the single algorithm into the stages of primary ($\sigma^0(\vec{r})$ imaging) and secondary processing (obtaining the information about parameters $\vec{\lambda}(\vec{r})$) are treated.

THE PROBLEM AND ITS SOLUTION

The equation of observation (the signal model in the antenna output) we shall write in the following form:

$$\vec{u}(t)=\mathrm{Re}\,\vec{\dot{S}}(t,\vec{\lambda}(\vec{r}))\exp(j\varpi_0 t)+n(t),\ \vec{u}(t)=\left\|u_k(t)\right\|,$$

$$\vec{\dot{S}}(t,\vec{\lambda}(\vec{r}))=\left\|\dot{S}_k(t,\lambda(\vec{r}))\right\|,\ \vec{n}(t)=\left\|n_k(t)\right\|,$$

$$k=\overline{1,K},t\in(0,T), \qquad (1)$$

where $\dot{S}_k(t,\lambda(\vec{r}))$ is the complex amplitude of the useful signal reflected by the surface and received by the antenna.

The correlation matrix of the received signal is of the following form:

$$\underline{R_u}(t_1,t_2)=\left\langle\vec{u}(t_1)\vec{u}^T(t_2)\right\rangle\approx\frac{1}{2}\mathrm{Re}\,\rho(t_1-t_2)\times$$

$$\times\int_D\underline{\sigma^0}(\vec{r},\vec{\lambda}(\vec{r}))\dot{S}_0(t_1,\vec{r})\dot{S}_0^*(t_2,\vec{r})d\vec{r}+\frac{N_0}{2}\delta(t_1-t_2), \qquad (2)$$

where $\underline{\sigma^0}(\vec{r},\vec{\lambda}(\vec{r}))$ is the scattering covariation matrix whose main diagonal consists of specific RCS (when signals of vertical, horizontal and crossed polarization types are received, such a matrix consists of 4x4 elements).

$$\underline{\sigma^0}(\vec{r},\vec{\lambda}(\vec{r}))\cdot\rho(t_1-t_2)=$$

$$= \int_D \left\langle \dot{\vec{F}}(\vec{r},\lambda(\vec{r}),t_1)\dot{\vec{F}}^{+}(\vec{r}\lambda(\vec{r}),t_2)\right\rangle \exp(-\vec{q}_{\perp}\Delta\vec{r})d\Delta\vec{r},$$

$$\rho(0)=1;\ \underline{N_0}/2 = diag(N_{0k}/2); \qquad (3)$$

$\vec{q}_{\perp}$ is the horizontal projection of the reverse scattering vector; "T", "+",< > are the signs of transposition, Ermit connection and statistical averaging, respectively.

In the beginning we shall examine the optimization problem solution by the use of maximum likelihood method. Calculating the variational derivative of the likelihood functional and putting it equal to zero, $\delta P[\vec{u}(t)/\vec{\lambda}(\vec{r})]/\delta\lambda_M(\vec{r}) = 0$, we shall obtain the following set of the integral equations:

$$\frac{1}{4}\int_D \dot{\underline{\Psi}}_W(\vec{r},\vec{r}_1)\underline{\sigma}^0[\vec{r}_1,\vec{\lambda}(\vec{r}_1)\dot{\Psi}^{*}_W(\vec{r},\vec{r}_1)d\vec{r}_1 +$$

$$+\frac{1}{2}\int_0^T \dot{\underline{S}}_W(t,\vec{r})\underline{N}_0\dot{\underline{S}}^{*}_W(t,\vec{r})dt = \dot{\vec{Y}}^{+}_{out}(\vec{r})\dot{\vec{Y}}_{out}(\vec{r}). \quad (4)$$

Where $\vec{Y}_{out}$ is the vector, whose components are the optimal output effects of the multichannel SAR:

$$\vec{Y}_{out} = \int_0^T\int_0^T \underline{W}(t_1,t_2,\lambda(\vec{r}))\vec{u}(t_2)\dot{S}^{*}_0(t,\vec{r})dt_1dt_2; \quad (5)$$

$$\dot{\underline{S}}_W(t,\vec{r}) = \int_0^T \underline{W}(t,t_1,\lambda(\vec{r}))\dot{S}_0(t_1,\vec{r})dt_1, \qquad (6)$$

is the matrix of signals;

$$\underline{\Psi}_W(\vec{r},\vec{r}_1) = \int_0^T\int_0^T \underline{W}(t_1,t_2,\lambda(\vec{r}))\dot{S}_0(t_1,\vec{r})\dot{S}^{*}_0(t_2,\vec{r})dt_1dt_2, \quad (7)$$

is the matrix indeterminacy function (Woodward function) which defines SAR's resolution.

One of the basic operations, performed in such a multichannel SAR with the received signals, is the operation of the output effect $\vec{Y}_{out}(\vec{r})$ forming.

The operation of the output effect $\vec{Y}_{out}(\vec{r})$ forming comprises adaptive whitening (decorrelation) of the received signals with the weight matrix $W(t_1,t_2,\vec{\lambda}(\vec{r}))$, which depends on the measured values of $\vec{\lambda}(\vec{r})$ and signal optimal filtration with the weight function $\dot{S}_0(t,\vec{r})$. In the absence of decorrelating adaptive filter $W(t_1,t_2,\vec{\lambda}(\vec{r}))$, the output effect $\vec{Y}_{out}(\vec{r})$ forming operation coincides with the classic one of the aperture synthesis with the focused signal processing

$$\vec{Y}_{out}(\vec{r}) = \int_0^T \vec{u}(t)\dot{S}_0(t,\vec{r})dt.$$

The measurement errors of parameters $\vec{\lambda}(\vec{r})$ as well as of specific RCS $\underline{\sigma}^0(\vec{r})$ of the operator track, which is inverse to the Fisher operator are as follows:

$$\rho = \int_D Spur\underline{F}^{-1}(\vec{r}_1,\vec{r}_2)\,|_{\vec{r}=\vec{r}_1=\vec{r}_2}\,d\vec{r},$$

where

$$\underline{F}^{-1} = -\left\| \frac{\delta \ln P(\vec{u}(t)/\vec{\lambda}(\vec{r}))}{\delta\lambda_{\mu}(\vec{r}_1)\delta\lambda_{\nu}(\vec{r}_2)} \right\|^{-1} \approx$$

$$\approx 4\left\| \sum_{k=1}^{K} \frac{\partial\sigma^0_k(\vec{r}_1,\lambda(\vec{r}_1))}{\partial\lambda_{\mu}} \frac{\partial\sigma^0_k(\vec{r}_2,\lambda(\vec{r}_2))}{\partial\lambda_{\nu}} \left|\Psi_{Wk}(\vec{r}_1,\vec{r}_2)\right|^2 \right\|^{-1}. \quad (8)$$

Here $\rho = \infty$ that indicates incorrectness of the solution to the problem (insolvency of valuations). But, if we exclude from the consideration function $\dot{\underline{\Psi}}_{WK}$, all the same the research of a matrix is of great significance as it helps to examine matrix $\underline{F}^{-1}$ and to find such sensing conditions (frequencies, polarization types, and observation angles) when the errors of the measurements are minimum.

As an example, Fig. 1 shows the dependencies of root-mean-square errors of estimation of permittivity ε and angle θ when joint measurement of these parameters takes place. The graph are plotted for the smallscale surface model in the case of the oscillations of vertical and horizontal polarization. In this case, the following values of model parameters were assumed: $2/T\Delta F = 10^{-6}$, $\varepsilon = (5,10,20,40,80)$.

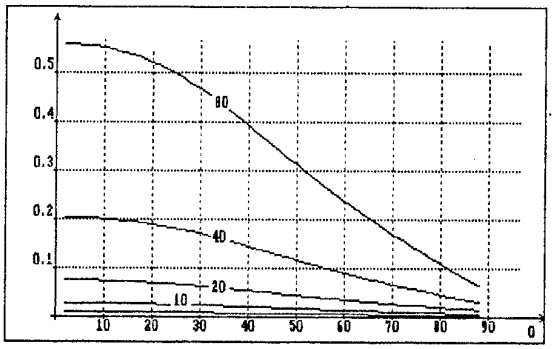


Fig. 1

The regularized solution to the problem can be obtained with the use of the APM method if, for example, the

correlation matrix $\underline{R}_{\lambda}(\vec{r}_1,\vec{r}_2)=\left\langle\vec{\lambda}(\vec{r}_1)\vec{\lambda}^T(\vec{r}_2)\right\rangle$ or $\underline{R}_{\sigma^0}(\vec{r}_1,\vec{r}_2)=\left\langle\vec{\sigma}^0(\vec{r}_1)\vec{\sigma}^{0T}(\vec{r}_2)\right\rangle$ is known. Examining the equality $\delta P[\vec{\lambda}(\vec{r})/\vec{u}(t)]/\delta\lambda_{\mu}(\vec{r})=0$ we obtained, in gaussian approximation, the algorithm for the functions $\vec{\lambda}(\vec{r})$ finding (and, in particular, functions $\underline{\sigma}^0(\vec{r})$, if assume $\partial\sigma_k^0/\partial\lambda_{\mu}=\partial\sigma_k^0/\partial\sigma_k^0=1$).

We can find the total complexing of the processes in this algorithm that are received by different receiving channels. This was achieved not only by the mutual links of the scattered fields prescribed by the correlation matrix $R_{uk}[t_1,t_2,\lambda(\vec{r})]$ elements and, in particular, taking into account all the covariation scattering matrix $\underline{\sigma}^0[\vec{r},\vec{\lambda}(\vec{r})]$ elements, but also by using the a-priori statistical links between $\lambda_{\mu}(\vec{r})$ parameters which we can be given by the elements of the correlation functions matrix $\underline{R}_{\lambda}(\vec{r}_1,\vec{r}_2)=\left\langle\vec{\lambda}(\vec{r}_1)\vec{\lambda}^T(\vec{r}_2)\right\rangle$.

One of the essential operations in the equations which provides the estimates consistency is the smoothing of the first component which consists of the output effects $\vec{Y}_{out\Sigma}$ by the weight functions (windows) defined by the elements of correlation functions matrix $\underline{R}_{\lambda}(\vec{r}_1,\vec{r}_2)$.

The structural scheme of the system corresponding to this algorithm is shown in Fig. 2.

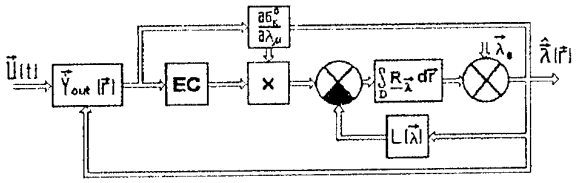


Fig. 2

CONCLUSION

In spite of the complication of the proposed algorithms one can see the possibility of their essential simplifying if it is known a-priori that the interval of the functions $\sigma_k^0[(\vec{r}),\vec{\lambda}(\vec{r})]$ and $\vec{\lambda}(\vec{r})$ substantial alternation is considerably less than the interval of the output effect $\vec{Y}_{out}(\vec{r})$ correlation which, in the absence of decorrelating transforms of the functions $U_k(t)$ with the weight matrix $\underline{W}(t_1,t_2)$, is approximately equal to the indeterminacy (Woodward) function

$$\left|\dot{\Psi}_W(\vec{r}_1,\vec{r}_2)\right|=\left|\int_0^T\dot{S}_0(t,\vec{r}_1)\dot{S}_0^*(t,\vec{r}_2)dt\right|$$

width, and, in the presence of decorrelating transform, it can be considerably reduced and be equal to the indeterminacy function $\left|\dot{\Psi}_W(\vec{r}_1,\vec{r}_2)\right|$ width. Since the processes $U_k(t)$ are assumed to be gaussian so the processes $\dot{\vec{Y}}^T{}_{out}(\vec{r})\dot{\vec{Y}}_{out}(\vec{r})$, in each sections $\vec{r}$, are scattered by χ^2 law. But if the proposed algorithms are used the output effects would be effectively normalized by their smoothing with $\underline{R}_{\lambda}(\vec{r}_1,\vec{r}_2)$ operator. Under condition that the sampling values of the SAR's output effects are taking in intervals equal to or more than the correlation interval, one can use the non-linear filtration apparatus or the Kalman one of filtration of Markov gaussian fields against the discrete white noise background modeling the output effect $\vec{Y}_{out}(\vec{r})$ fluctuations.

The proposed methodology of the surface imaging and parameters estimation can serve as theoretical foundation for the new generation of measuring multichannel scatterometric SAR design with high resolution and measuring accuracy. Such a methodology can be applied for the statistical synthesis of the multichannel passive systems and combined active-passive systems as well.

REFERENCES

1. Volosyuk V.K., Kravchenko V.F., Ponomaryov V.I., "Optimal evaluations of electrophysical parameters for models of scattering covers in remote sensing", *Doklady Akademii Nauk (Soviet Reports of Acad. Sci. USSR)*, vol.319, No5, pp.1120-1124, 1991 [in Russian].

2. Volosyuk V.K., Kravchenko V.F., Falkovich S.E., "Optimization of estimates of spatially-distributed parameters for electrodynamic models of surfaces in inverse interpretation problems of active remote sensing", *Doklady Akademii nauk SSSR (Soviet Reports of Acad. Sci. USSR)*, vol.322, No 2, p.277-280, 1992 [in Russian].

3. S.E. Falkovich, V.I.Ponomaryov, Yu.V.Shkvarko, *Optimal reception of space-time signals in radiochannels with dissipation*, Sovetskoe radio, Moscow, 1989 [in Russian].

ENERGY FEATURES OF THE SURFACE E-WAVE SCATTERING BY A REFLECTION ANTENNA GRATING

A. P. Yevdokimov, V. V. Krizhanovsky

The A.Ya. Usikov's Institute of Radiophysics and Electronics NASU
Ul. Proskury 12, Kharkov 310085 Ukraine,
Ph.: 38 (0572) 44 83 26, fax 38 (0572) 44 11 05, e-mail: yevdok@ire.kharkov.ua

The theoretical and experimental researches on electromagnetic scattering from diffraction gratings of different types, including open transmission lines (OTL), revealed that the millimeter-wave open electrodynamical structures providing the basis for functional components and units, feature high efficiency, which makes it possible to get over a series of technological problems and reduce the cost of new designs, especially in the field of antenna technology.

Facilities utilizing the conversion of the surface waves of a periodic scatterer into the volume waves were found to be a quite successful approach in the realization of the electrodynamical schemes of the SHF and EHF electromagnetic sources[1]. First used in the modeling of physical processes in diffraction radiation oscillators, this effect extended its application area and gave rise to a new line in the development of antenna arrays [2].

The research on surface-wave scattering from a diffraction grating revealed that the electrodynamical system of this kind is capable of forming a highly directional radiation in space, and the OTL (in particular, variously shaped dielectric waveguides) serves there for the surface-wave source. The antenna arrays of this kind rest on the holographic principles and have the two basic functional components, namely, OTL in the form of a dielectric waveguide and diffraction grating (e.g., comb) which is parallel to the OTL lateral surface. By varying characteristics of the diffractive elements associated with the slow-wave field in the OTL one can attain a high directivity, wide-range scanning, and efficiency no worth than 90 ... 95 percent. The polarization of the produced radiation depends both on the oscillation type excited in the OTL and the scatterer construction.

A large body of the data obtained [2] enables us to develop various antenna systems for different purposes. The designs exhibit technological effectiveness, wide-range application, and great variety of the electrodynamical schemes. The developed antennas have found use in both aircraft/spacecraft equipment and ground-based (both fixed and mobile) complexes [3, 4].

The electrodynamical system of the suggested antenna is given in Fig. 1. A surface wave P_i transmitted by surface-wave line 2 is scattered by periodic structure 1 in the form of a reflecting diffraction grating with the dominant mode of E type. This wave type choice is determined by the necessary horizontal polarization of the antenna. The surface - wave line represents a ridged dielectric waveguide. The study involves teflon (ε = 2.05) and quartz-glass (ε = 3.9) ridged waveguides. The waveguide geometry provides the wave slowing factor U = 1.2 for teflon and 1.5 for quartz. The wave slowing factor $U = \gamma/k$ is determined by a minimum transmission loss in a single - mode operation.

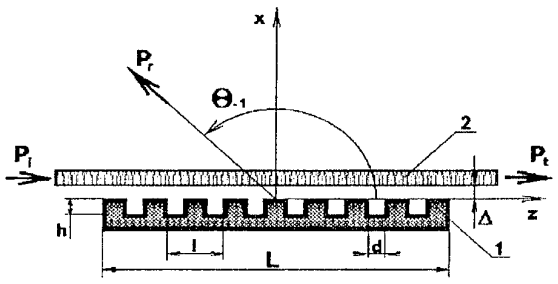


Fig. 1

The diffraction grating is placed over the surface-wave line to be at a distance Δ and remains in its field. If a surface wave with propagation constant γ travels in the ridged dielectric waveguide and locks in phase synchronism with another wave scattered by the grating and having propagation constant k, then

$$k\ell\cos\theta_n - \gamma\ell = 2\pi n, \qquad (1)$$

where ℓ is the grating period. The scattered field direction is given by the angle θ_n which the wave vector $\vec{k}$ makes with the Oz axis; $\vec{k}$ therewith belongs to the xOz plane.

Radiation condition (1) holds only for negative n , and for a single - mode operation n is taken to be - 1. The absence of the second-order harmonic with n = - 2 is ensured by the constraint $\ell < \frac{2\lambda}{U+1}$. In our case, the fields of the single scatterers add up in phase in the direction θ_{-1} :

$$\theta_{-1} = \arccos\left(U - \frac{\lambda}{\ell}\right). \qquad (2)$$

The power characteristics of the diffraction gratings in the E case were previously estimated for the gratings much wider than the waveguide ridge. The attenuation of the transmitted power P_t is shown in Fig. 2 as the function $(-10\ \ell g P_t/P_i) = f(\Delta)$. The aim was to reach a sufficient attenuation of the transmitted power of the signal at a maximum possible spacing Δ between the grating and the ridged waveguide. To this end, the gratings of different groove depth were examined. As mentioned before, the considered electrodynamical scheme represents a holographic-type antenna where the diffraction grating acts as a hologram. The only difference is that the grating scattered field contains no positive harmonics because of the impractibility of condition (1). In this case, the zeroth harmonic corresponds to the transmitted power P_t. In the acting antenna, P_t is close to zero. In our scheme when condition (1) holds for the sole harmonic with $n = -1$, the scattered field contains no virtual image. Contrary to the optical hologram, the diffraction grating efficiency can reach 90 ... 95 percent. This means that a right choice of the parameters of a single scatterer can provide the control of the power take-off along the aperture.

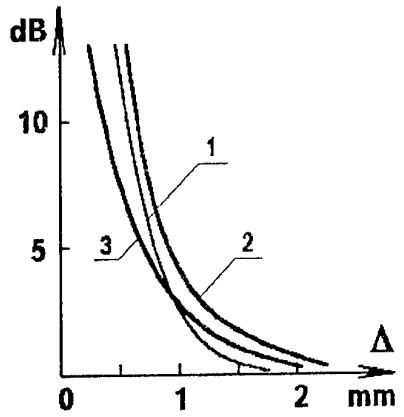


Fig. 2

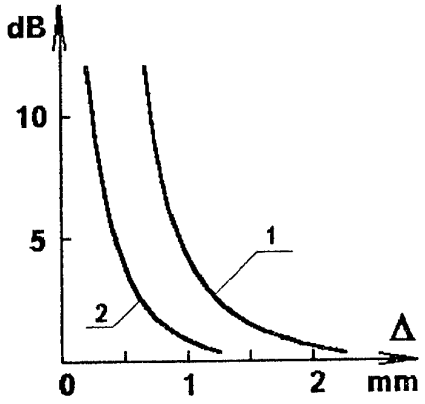


Fig. 3

The dependence $(-10\ \ell g P_t/P_i) = f(\Delta)$ is plotted for the wide gratings with groove depth 0.47 mm (curve 1, Fig. 2), 0.7 mm (curve 2), and 0.85 mm (curve 3) for the grating length 120 mm, groove width 1 mm, and grating period 3 mm ; the wave slowing factor is U = 1.2. A groove depth of 0.7 mm is seen to be the most close to the resonance value at the working frequency 76.5 GHz and wave slowing factor U = 1.2, so it offers the highest efficiency. With a length 240 mm and Δ = 0.75 mm, this grating provides the power take-off P_t more than 97 percent or 15 dB.

The measurements of various narrow gratings comparable in width with the waveguide ridge, which is 2 mm wide in the teflon waveguide and 1.5 mm in the quartz one, have revealed the most efficient geometry of the grooves measuring 0.75 mm in depth and 0.5 mm in width. The grating length is 100 mm and width is 1 mm. The transmitted power $(-10\ \ell g P_t/P_i) = f(\Delta)$ is plotted in Fig. 3 with curves 1 for the teflon waveguide and 2 for the quartz one. One can see that the antenna involving the teflon waveguide can be built with any technological difficulties because the chosen diffraction grating 300 mm long with Δ = 0.75 mm produces more than 30 dB of the power take-off. So this grating in combination with the teflon waveguide exhibits the desired amplitude - phase distribution in the aperture which makes possible a side-lobe level 25 dB. In view of that the quartz waveguide produces a large slowing factor, the antenna on its basis is also possible but requires more accuracy, which evidently rises its cost.

Up to now, many features of diffraction of an inhomogeneous plane wave by a grating of an arbitrary but finite length are not revealed. This is because of lack of a satisfactory mathematically rigorous theory for the electrodynamical system of this kind (Fig. 1). In this connection we suggested an algorithm [5, 6] calculating such antenna characteristics as amplitude distribution in aperture and antenna efficiency. This algorithm takes into account two types of the coupling - uniform and wedge-shaped - occurring between the dielectric waveguide and grating. The uniform coupling occurs in a space Δ separating the dielectric waveguide and grating as shown in Fig. 1. The wedge-shaped one occurs when the space Δ between the waveguide and grating is extended by an additional space δ introduced in front of them in between.

The input calculation data are found from the only one experiment performed for the desired dielectric waveguide and relevant grating in the uniform - coupling operation. In so far as the calculation is based on the coupled-wave approximation [7], the agreement between the calculations and measurements may be sought only with gratings no shorter than 10 λ .

The radiation pattern calculations are made in the conventional way using the Fresnel–Kirchhoff integral for the far-field radiation. The applied method of the pattern calculation takes no account of the grating action on the wave phase velocity in the dielectric waveguide as well as it does not take into consideration the change of the effective cross section of the waveguide in the grating presence. This makes the coupling coefficient dependent on the waveguide-grating space. Therefore long gratings associated with sufficiently large Δ and δ are preferable.

Two open transmission lines in the form of the ridged dielectric waveguide with an exiting units were investigated in the present work. Periodic scatterers reflection in type were optimized at horizontal polarization. Energy and polarization characteristics of these scatterers are investigated. Radiation patterns are calculated and compared with an experimental ones.

ACKNOWLEDGMENT

This work was supported in part by DaimlerChrysler under the contract G005830106.

REFERENCES

1. S. D. Andrenko, N.D. Devyatkov, V.P. Shestopalov. Millimeter wave antenna arrays. - Doklady AN SSSR, 1978, vol.240, No.6, pp.1340-1343.
2. A. P. Yevdokimov and V.V. Krizhanovsky. A new line in antenna array technology. - Izv. VUZov. Radioelektronika, 1996, vol.39, No.9-10, pp.54-61.
3. S. D. Andrenko, A.P. Yevdokimov, Krizhanovsky, S.A. Provalov, and Yu.B. Sidorenko. The scanning antenna of airborn radiometric complex. - Radiophysical methods and means of the environment investigations in the mm wave region. Kyiv: Naukova Dumka, 1988, pp.154-160.
4. V. P. Shestopalov, A.I. Kalmykov, A.P. Yevdokimov, et al. Complex researches of the Earth environment by radiophysical method. - Doklady AN SSSR, 1985, vol. 284, No.1, pp. 98-102.
5. A. P. Yevdokimov, V. V. Krizhanovsky, and Yu.B.Sidorenko. Calculation of radiation pattern of a radiating system "Dielectric waveguide - Grating". - The Ist Ukrainian simposium "Physics and Technology of MM and SubMM Radiowaves". Kharkov, October 15-17, 1991, p. 325.
6. V. V. Krizhanovsky, S. A. Provalov, and Yu. B. Sidorenko. Power charakteristics of a system "Dielectric waveguide - Grating". - Radiophysics and Electronics of the MM and SubMM Wave Range. Kharkov, 1991, p.p. 104-113.
7. Integrated Optics. Edited by T.Tamir/ Springer-Verlag Berlin Heidelberg, New York, 1975.

SPACE-TIME MODULATION OF SIGNALS IN A RING ANTENNA ARRAY

V. I. Zamyatin, O. V. Baturin, E. A. Tolokneyev

Kharkov Military University, 310043, Kharkov, Svoboda Sq. 6.
Tel. 0572-40-41-41 (2-87, 4-30), 0572-45-60-27

The rise of reguirements to quality of the information circulating in radioelectronic system (RES) and rate of its exchange led to the fact that traditional circuits of antenna construction have practically exhausted their resources. The use of phased antenna arrays, i.e. the systems with spatial phase-time modulation (or filtration) of signal has sufficiently raised the efficiency of RES. However at present in a number of cases this is deficient so far. One of the methods of further increase of system capabilities is the use of a more complex multiparametric joint, space-time, frequency and phase modulation of radiated signals. Therefore the publications devoted to the discussion of space-time characteristics of antenna radiation with such a modulation appear in the literature more frequently. But it is true, that in these works the characteristics of linear (or plane) antennas [1, 2] are considered and practically there are no publications on multiparametric modulation in the ring (cylindrical) radiating systems.

The purpose of this work is the discussion of space-time characteristics in a far-zone field on a ring antenna array with multiparametric modulation of signals. The consideration is carried out on the example of "superfast" circular scanning organization (with the frequency to several per cent from the carrier).

So suppose we have a ring antenna of radius R working at the middle circular frequency ω_0. It is required to determine the modulation type of signals (space – time distribution (STD), amplitude–phase and frequency ones of signals) needed for energizing the antenna so that to form in a far zone the narrow-beam pattern rotating without shape change with circular frequency Ω.

We can distiguish two basic modes of scanning in such arrays. Briefly they can be described as follows:

1. Each radiator (emitter) is energized by its signal, but such one that the resulting narrow-beam pattern performs circular scanning.
2. The system of partial patterns is created each of which is energized by its signal so that the resulting narrow-beam pattern performs circular scanning.

In the first mode it is necessary to energize each radiator of circular antenna array (CAA) by its own signal. To define the signal type for energizing radiator the reciprocity principle can be used. In the work [5] it is defined that each element of CAA with coordinate (R,α) must be energized by the current

$$I(\alpha,t)=I_m\cdot e^{j\left[\omega t+\frac{\omega}{C}R\cdot\cos(\alpha-\varphi(t))\right]},$$

where R is antenna radius, α is angular position of radiator, C is light velocity, $\varphi(t)$ is dependence of rotation angle of the pattern main maximum on time; i.e. by harmonics of frequency ω with phase modulation $\Phi(t)=(\omega R/C)\cdot\cos(\alpha-\varphi(t))$ or corresponding frequency modulation $\Phi'(t)$. In particular, for circular scanning by narrow-beam with a constant angular velocity Ω STD has to be of a form

$$I(\alpha,t)=I_m\cdot e^{j\omega t(1+\frac{\Omega}{C}R\cdot\sin(\alpha-\Omega t))},$$

i.e. the currents that are frequency-modulated according, to the law $\sin(\alpha-\Omega t)$ with the same carrier frequency ω and frequency modulation index $K=R\Omega/C$ and delayed (under the law of modulation) by the value of angular position of the element α are fed into antenna elements. It is the tolerable value of K that limits an angular velocity of scanning. In this case the far-zone field is described within a constant factor (space-time directional response) by a formula

$$f(\varphi,t')=\int_{\varphi-\alpha_{max}}^{\varphi+\alpha_{max}} f_0(\alpha-\Omega t)\cdot f_0(\alpha-\varphi)\times e^{j\omega_0\left(t'-\frac{R}{C}(\cos(\alpha-\Omega t')-\cos(\alpha-\varphi))\right)}d\alpha,$$

where $t'=r/C$, r is the distance to an observation point, f_0 is the element of antenna radiation, C is the light velocity.

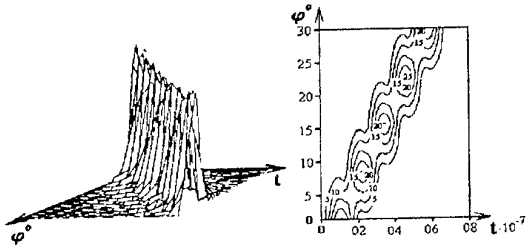


Fig. 1 Signal amplitude STD in a far zone

Thus for scanning CAA with constant velocity it is necessary to use signals that are frequency-modulated according to harmonic law and delayed by the time equal to the product of angular position of an element α_n by angular velocity of scanning.

In the second of considered models in the simplest case when circular fan of narrow-beam patterns is formed by a pattern-forming circuit, scanning is carried out by their sequential commutation during survey period [4].

If the set of partial non-narrow-beam patterns is formed, each input of PFC (pattern-forming circuit) is energized by its own signal the addition of which results in narrow pattern formation with circular scanning. For example, if a Butler scheme is used as a pattern-forming circuit (PFC), the set of partial patterns will be formed corresponding to angular harmonics, i. e. to each input of PFC corresponds amplitude-phase distribution (APD) of the form

$$A_m(\alpha_n) = A_m \cdot e^{j2\pi m\alpha},$$

where m is the angular harmonic number.

In its turn CAA radiators are energized by the currents

$$I_m = A_m(\alpha) \cdot e^{j\omega_0 t} = A_m \cdot e^{j2\pi m\alpha + j\omega_0 t},$$

then the partial patterns of the form [4] will be formed as

$$f_m(\varphi) = C_m \cdot A_m \cdot e^{j2\pi m\varphi},$$

where C_m is a complex constant.

As a result of summation of a sufficient number of partial patterns, the narrow-beam one is formed in space.

Circular movement of maximum in an antenna plane can be provided by different harmonic phase change, i.e. each PFC input must be energized at its frequency $\omega_0 + n \cdot \Omega$ and the resulting pattern will be of the form

$$f_m(\varphi) = \sum_m A_m \cdot e^{j2\pi m(\varphi + \Omega t)}.$$

In the pattern-forming circuits not only sine harmonic functions but more simple distribution functions can be formed, for example, the functions corresponding to discrete angular dependencies of the form sign(sin(mα)) or sign(cos(mα)). Then in antenna pattern the APD`s are formed of the following form

$$A_{my}(\alpha_n) = sign[\cos(m \cdot \alpha)] + j \cdot sign[\sin(m \cdot \alpha)],$$

as a result, the partial patterns are formed

$$f_{my}(\varphi) = \sum_m sign[\cos(m \cdot \alpha)] \cdot \cos(\alpha - \varphi) \cdot e^{j\omega\frac{R}{C}\cdot\cos(\alpha-\varphi)} +$$

$$+ j \cdot \sum_m sign[\sin(m \cdot \alpha)] \cdot \cos(\alpha - \varphi) \cdot e^{j\omega\frac{R}{C}\cdot\cos(\alpha-\varphi)}.$$

Fig. 2 presents the form of partial patterns at $A_m = sign[\cos(m\alpha)]$, $m = 1$ и $m = 3$.

Then for realization of SFS (superfast scanning) the signal of the form given below must be fed at each input

$$U_m(t) = U_0[sign(\cos(m \cdot \Omega \cdot t))] \cdot e^{j\omega_0 t} +$$
$$+ U_0 \cdot [j \cdot sign(\sin(m \cdot \Omega \cdot t))] \cdot e^{j\omega_0 t}.$$

Here all radiating elements are powered by signals with the same amplitude, whereas phases of these signals change in time stepwise by π, according to the functions $sign[\cos(m\alpha)]$ and $sign[\sin(m\alpha)]$.

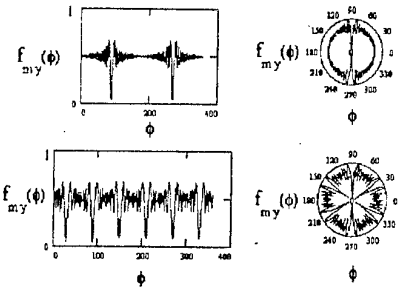


Fig. 2. The form of partial patterns at APD corresponding to function $sign[\cos(m\alpha)]$

Summary pattern is a narrow-beam one (at a sufficient number of harmonics) and is shown in Fig. 3.

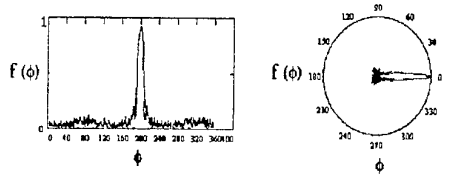


Fig. 3. Summary pattern

CONCLUSION

Joint space-time, frequency and phase modulation of signals in ring antennas enable to obtain a number of new effects, for example, to carry out circular SFS.

To attain the same effect at different modes of spatial energizing it is necessary to apply different signals to the inputs of pattern-forming circuit (PFC).

In all cases the laws of space-time modulation can be found by specified space-time responses in a far-zone field from reciprocity principle.

REFERENCES

1. Ginzburg V.M. Formirovanie i obrabotka izobragheniy v realnom vremeni. Metodi bistrogo skanirovaniy. Moscow: Radio & Sviaz, 1986 [in Russian].
2. Korostelev A.A. Prostranstvenno-vremennay teoriy radiosistem. Moscow: Radio & Sviaz, 1987 [in Russian].
3. Voskresenskiy D.I., Ponomarev L.I., Filippov V.S. Vipuklie skanirouschie antenni. Moscow: Sov. radio, 1978 [in Russian].
4. B.Sheleg A Matrix-Fed Circular Array for Continuous Scanning // Proceedings of the IEEE. Volume 56 numbers 11, November 1968.
5. Zamyatin V.I,.Baturin O.V, Tolokneyev E.A. Sverhbistroe skanirovanie loochem kolcevoy antennoi reshetki. Radiotekhnika All-Ukr. Sci. Interdept. Mag. 1999. N 109 [in Russian].

MEASUREMENT OF SIGNAL INFORMATIVE PARAMETERS WHEN ITS AMPLITUDE AND PHASE ARE RANDOM IN RADAR SYSTEM WITH ADAPTIVE ARRAY

S. T. Bagdasaryan, A. A. Belov, V. P. Ryabuha, V. A. Tarshin

The Kharkov military university,
maidan Svobody 6, Kharkov 310043, Ukraine

The different approaches to synthesis (method of a maximum likelihood) of non-tracking measurers of informative parameters of a signal against noise background are known. Frequently, likelihood ratio (LR) is averaged by uninformative parameters of a signal (initial phase and amplitude) and than, likelihood equation of small dimension is constructed, relatively only informative parameters [3, 4]. The latter is achieved also by using different methods of a preliminary maximization of the LR by uninformative parameters [1,2,5], or joint use of an averaging (over an initial phase) and maximization over amplitude. When averaging the LR one assumes, that the initial phase of a signal β has the uniform distribution within the interval $(0, 2\pi)$. However, the real distribution β is unknown and depending on models of the targets is described by the wide class of probability densities[3].

In the report it is shown, that the estimation of informative parameters of a signal against a noise background does not depend on indeterminacy of its random initial phase. It is noted, that the obtained algorithm of measurement is reduced to the one based on a preliminary maximization of the LR by uninformative parameters, and it is more preferable than the algorithm based on averaging indicated parameters. The comparison of algorithms is carried out with reference to the task of measuring a receiving direction of a signal by the radar with an adaptive array against a noise hum of external spatially correlated interference.

Let's assume, that the active radar with an array receives quasi-deterministic signal against internal noise hum and interfering oscillations from external source. Thus, the LR $L(\vec{\alpha}, b, \beta)$ depends on informative parameters $\vec{\alpha}$, random amplitude b and initial phase β of a signal and looks like

$$L(\vec{\alpha}, b, \beta) = \exp\left\{ \mathrm{Re}\left(b\dot{Z}(\vec{\alpha}) e^{-j\beta} \right) - b^2 \frac{q^2(\vec{\alpha})}{2} \right\}, \quad (1)$$

where

$$\dot{Z}(\vec{\alpha}) e^{-j\beta} = \frac{1}{2} \int_{-\infty}^{\infty} \vec{\dot{Y}}^{T}(t) \vec{\dot{R}}^{*}(t, \vec{\alpha}, \beta) dt$$

is a complex weight integral;

$$\vec{\dot{Y}}(t) = \vec{\dot{X}}(t, \vec{\alpha}_c) e^{j\beta_c} + \vec{\dot{N}}_{\text{П}}(t, \vec{\vartheta}) + \vec{\dot{N}}_{\text{Ш}}(t),$$

$\vec{\dot{R}}(t, \vec{\alpha}, \beta) = \vec{\dot{R}}(t, \vec{\alpha}) e^{j\beta}$ are vectors of complex amplitudes of received oscillations and weight processing, respectively; τ,* are signs of a transposition and complex conjugation; $\vec{\dot{X}}(t, \vec{\alpha}_c), \vec{\dot{N}}_{\text{П}}(t, \vec{\vartheta}), \vec{\dot{N}}_{\text{Ш}}(t)$ are vectors of complex signal amplitudes, external spatially correlated interference and internal noise, respectively; $q^2(\vec{\alpha})$ is a power signal-to-jamming ratio.

From (1), performing a maximization over amplitude b, we shall obtain the log of the LR

$$\ln L(\vec{\alpha}, \beta) = \left[\mathrm{Re}\, \dot{Z}(\vec{\alpha}) e^{-j\beta} \right]^2 \Big/ 2q^2(\vec{\alpha}).$$

Then the estimations $\hat{\vec{\alpha}}$ of informative parameters $\vec{\alpha}$ are determined from the system of equations

$$\frac{\partial}{\partial \alpha_i} \frac{\left[\mathrm{Re}\, \dot{Z}(\vec{\alpha}) e^{-j\beta} \right]^2}{2q^2(\vec{\alpha})} = 0 \text{ at } \vec{\alpha} = \hat{\vec{\alpha}}. \quad (2)$$

Using a relation $\mathrm{Re}\,\dot{A} \cdot \mathrm{Re}\,\dot{B} = \frac{1}{2}\mathrm{Re}(\dot{A}\dot{B}^{*}) + \frac{1}{2}\mathrm{Re}(\dot{A}\dot{B})$ and introducing a designation $\dot{Z}_{\text{Н}}(\vec{\alpha}) = \frac{\dot{Z}(\vec{\alpha})}{q(\vec{\alpha})}$, we shall reduce the equations (2) to the form

$$\mathrm{Re}\left[\dot{Z}'_{\text{Н}}(\vec{\alpha}) \dot{Z}^{*}_{\text{Н}}(\vec{\alpha}) \right] + \mathrm{Re}\left[\dot{Z}'_{\text{Н}}(\vec{\alpha}) \dot{Z}_{\text{Н}}(\vec{\alpha}) e^{-j\beta} \right] = 0 \quad \text{at } \vec{\alpha} = \hat{\vec{\alpha}}, \quad (3)$$

where $\dot{Z}'(\vec{\alpha}) = \frac{\partial \dot{Z}(\vec{\alpha})}{\partial \alpha_i}$.

From complex equality $\dot{A} = s + jp = 0$ it follows, that $s = p = 0$. Therefore, (3) is contained in the ratio

$$\dot{Z}'_{\text{Н}}(\vec{\alpha}) \dot{Z}^{*}_{\text{Н}}(\vec{\alpha}) + \dot{Z}'_{\text{Н}}(\vec{\alpha}) \dot{Z}_{\text{Н}}(\vec{\alpha}) e^{-j2\beta} = 0 \text{ at } \vec{\alpha} = \hat{\vec{\alpha}}, \quad (4)$$

where functions 1, $e^{-j\beta}$ are linearly independent for all values β within an interval $(0, 2\pi)$. Therefore, (4) it is possible, if

$$\dot{Z}'_{H}(\vec{\alpha})\dot{Z}^{*}_{H}(\vec{\alpha}) = 0 \text{ or } \mathrm{Re}\left[\dot{Z}'_{H}(\vec{\alpha})\dot{Z}^{*}_{H}(\vec{\alpha})\right] = 0$$

$$\text{at } \vec{\alpha} = \hat{\vec{\alpha}}, \qquad (5)$$

$$\dot{Z}'(\vec{\alpha})\dot{Z}(\vec{\alpha}) = 0 \text{ at } \vec{\alpha} = \hat{\vec{\alpha}}. \qquad (6)$$

Technically it is convenient to implement (5), which can be presented as the other expression

$$2\ \mathrm{Re}\left[\dot{Z}'_{H}(\vec{\alpha})\dot{Z}^{*}_{H}(\vec{\alpha})\right] = \left(Z^{2}_{H}(\vec{\alpha})\right)' = \left(\frac{Z^{2}(\vec{\alpha})}{q^{2}(\vec{\alpha})}\right)' = 0$$

$$\text{at } \vec{\alpha} = \hat{\vec{\alpha}}, \qquad (7)$$

or

$$\frac{\left(Z^{2}(\vec{\alpha})\right)'}{Z^{2}(\vec{\alpha})} - \frac{\left(q^{2}(\vec{\alpha})\right)'}{q^{2}(\vec{\alpha})} = 0 \text{ at } \vec{\alpha} = \hat{\vec{\alpha}}, \qquad (8)$$

where $Z_{H}(\vec{\alpha}) = \left|\dot{Z}_{H}(\vec{\alpha})\right|$.

From (5), (7) and (8) it follows, that the maximum likelihood estimates of informative parameters $\vec{\alpha}$ of signal against a noise background do not depend on its random phase and are determined over a maximum of square modular value of a normalized weight integral $Z^{2}_{H}(\vec{\alpha}) = \dfrac{Z^{2}(\vec{\alpha})}{q^{2}(\vec{\alpha})}$. It is equivalent to the equation

$$Z^{2}_{H}(\vec{\alpha}) = \max_{(\vec{\alpha})} Z^{2}_{H}(\vec{\alpha}). \qquad (9)$$

The preliminary maximization (1) over a random initial phase β and amplitude b also leads to (9). Actually, due to relation

$$\max_{(\beta)} \mathrm{Re}\left[\dot{Z}(\vec{\alpha})e^{-j\beta}\right] = Z(\vec{\alpha})$$

and at a maximizing value $b = Z(\vec{\alpha})/q^{2}(\vec{\alpha})$ from (1) we have a log of the LR

$$\ln L_{1}(\vec{\alpha}) = \frac{Z^{2}_{H}(\vec{\alpha})}{2}, \qquad (10)$$

which depends only on informative parameters $\vec{\alpha}$.

LR $L(\vec{\alpha})$ obtained by a statistical averaging (1) over random amplitude b and initial phase β gives a uniform sufficient statistics for the problem solution of a detection and measurement. However, obtained algorithm of measurement differs from (7), (8). So, let's assume, that in (1) initial phase has a uniform distribution $p(\beta) = 1/2\pi$, $\beta = \overline{0,2\pi}$, and amplitude has the Rayleigh distribution $p(b) = 2be^{-b^{2}}$ $b > 0$. Then, averaging (1) over β and b, we obtain

$$\ln L(\vec{\alpha}) = \frac{q^{2}(\vec{\alpha})Z^{2}_{H}(\vec{\alpha})}{4\left(1+q^{2}(\vec{\alpha})/2\right)} - \ln\left(1+q^{2}(\vec{\alpha})/2\right). \qquad (11)$$

According to (11) estimations $\hat{\vec{\alpha}}$ of informative parameters are calculated from the system of equations

$$\left[\frac{q^{2}(\vec{\alpha})Z^{2}_{H}(\vec{\alpha})}{4\left(1+\dfrac{q^{2}(\vec{\alpha})}{2}\right)} - \ln\left(1+\frac{q^{2}(\vec{\alpha})}{2}\right)\right]' = 0 \text{ at } \vec{\alpha} = \hat{\vec{\alpha}}. \qquad (12)$$

From (12) it is seen, that only in the case of measurement of non-power parameters against a background of internal noise, when $\left[q^{2}(\vec{\alpha})\right]' = 0$, the full identity of (7) and (12) follows.

Further, we shall execute the comparative analysis of algorithms (7), (9) and (11), (12) with reference to the problem of finding direction $(\vec{\alpha} = \psi)$ of signal receiving with the random amplitude and initial phase at effect on a radar with an adaptive linear equidistant array (with the number of elements M = 10, placed at a distance $\lambda/2$, where λ is the wavelength) of active masking interference from m of dotted sources. For a case of the interference effect from one source (m = 1) dependencies of $\ln L(\psi)$ (averaged over N = 75 samples) are shown in Fig. 1 according to (11) and $Z^{2}_{H}(\psi)$, where ψ is an expected direction of receiving of a signal, that is expressed in parts of a halfwidth of the array directivity pattern on a zerothlevel. Here the arrows indicate directions of signal receiving ($\psi = 0$), effect of interference ($\psi = 0.5$), as well as their relative h_c and h_i excess over a background level. At $\psi = 0$ a value of a signal-to-jamming ratio $\tilde{q}(\psi)$ in the output of the device of adaptive procedure also is indicated. For interfering situation depicted in Fig. 1, curves $\mathrm{Re}\left[\dot{Z}'_{H}(\psi)\dot{Z}^{*}_{H}(\psi)\right]$ and $(\ln L(\psi))'$ corresponding to equations (7) and (12) are shown in a Fig. 2. From Figs. 1, 2 it is seen, that a maximum of curve $Z^{2}_{H}(\psi)$ and zeroth value of curve $\mathrm{Re}\left[\dot{Z}'_{H}(\psi)\dot{Z}^{*}_{H}(\psi)\right]$ coincide with a true receiving direction of a signal, and maximum of curve $\ln L(\psi)$ and zero of curve $(\ln L(\psi))'$ are biased, relatively to a true receiving direction of a signal ($\psi = 0$). The latter means, that when averaging LR over random amplitude and initial phase, the direction of receiving is measured with the systematic bias. At effect interference from one source with $h_i = 30$ dB such an error takes place for a difference of directions of signal receiving ($\psi = 0$) and a source of interference

$\Delta\psi \le 0.7$. Under complicated interfering situation the systematic bias of measurement over a maximum $\ln L(\psi)$ is possible for values $\Delta\psi > 0.7$ as well. It is illustrated in Fig. 3, where the curves $Z_н^2(\psi)$ and $\ln L(\psi)$ are plotted for the case when the interference from four sources influence on the first side lobe of array directivity pattern. Let's mark also, that the variance of a measurement error of a direction of a signal receiving over a maximum $Z_н^2(\psi)$ in different interfering situations is less, than over a maximum $\ln L(\psi)$.

CONCLUSIONS

1. It is shown, that the system of equations of a likelihood (7) or (8) for estimations of informative parameters of a signal against a noise background does not depend on indeterminacy of a random initial phase. It is equivalent to the known equations, obtained by preliminary maximization of the LR over amplitude and initial phase of a signal. Thus the estimations of parameters are evaluated over a maximum of a normalized weight integral.
2. The obtained algorithms have been used for the particular case of a receiving signal direction measurement in the radar system with an adaptive array, on which the active masking interference affects. The results of simulation show, that the estimation of direction of signal receiving by a maximum of a normalized weight integral is unbiased, whereas by a maximum of LR, obtained after averaging over a phase and amplitude, can be displaced.

REFERENCES

1. Devis R.C., Brenan L.E., Reed I.S. Angle estimation With adaptive arrays in external noise fields.-IEEE Trans. 1976, vol. AES-12, .) 2, p.179-186.
2. Repin, V.G. and G.P. Tartakovsky. Statisticheskiy sintez pri apriornoy neopredelennosti i adaptatsiya informatsionnykh sistem (Statistical Synthesis in the Case of a priori Uncertainty and Adaptation of Information Systems), Sovetskoye Radio Press, Moscow, 1977.
3. Kulikov, Ye.I. and A.P. Trifonov. Otsenka parametrov signala na fone pomekh (Evaluation of Signal Parameters Against a Noise Background), Sovetskoye Radio Press, Moscow, 1978.
4. Shirman, Ya.D. and V.N. Manzhos. Teoriya i tekhnika obrabotki radiolokatsionnoy informatsii na fone pomekh (Theory and Technique of Processing Radar Data on Noise Background), Radio i Svyaz Press, Moscow, 1981.
5. Zuravlev A.K., Lukoshkin A.P. and S.S. Poddubny. Obrabotka signalov v adaptivnykh antennykh reshetkakh (Signal processing in adaptive array), Leningrad university Press, Leningrad, 1983.

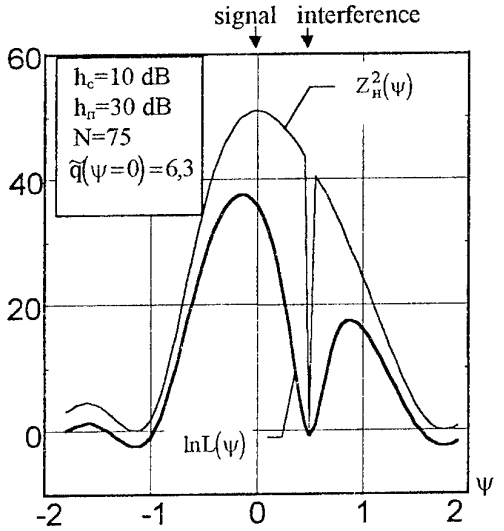


Fig. 1

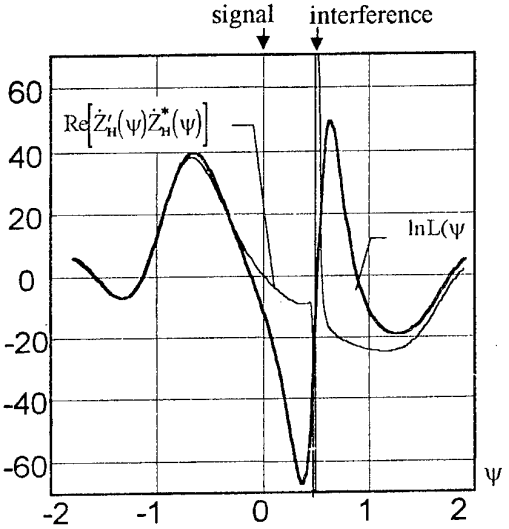


Fig. 2

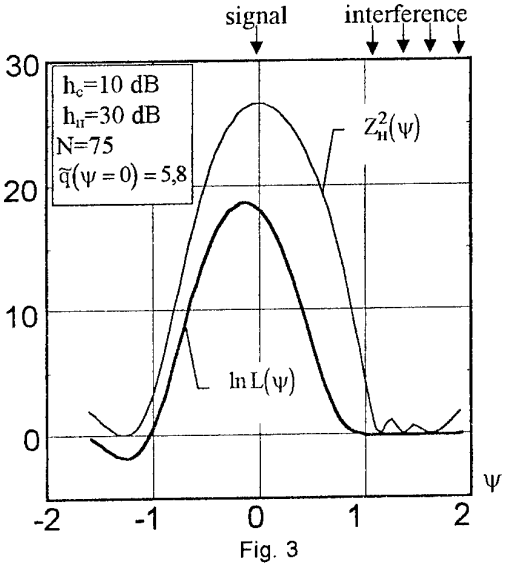


Fig. 3

ANALYTICAL CALCULATION OF DETECTION AND RESOLUTION THRESHOLDS IN ANTENNA ARRAYS USING SAMPLE COVARIANCE MATRIX EIGENVALUE TECHNIQUE

V. T. Ermolaev, A. A. Maltsev, K. V. Rodyushkin, L. L. Presti*

Department of Statistical Radiophysics, Nizhny Novgorod State University,
603600, Nizhny Novgorod, Gagarin Ave. 23, e-mail maltsev@rf.unn.runnet.ru
* Dipartimento di Elettronica, Politecnico di Torino,
Corso Duca degli Abruzzi 24, 10129 Torino, Italy, e-mail lopresti@polito.it

ABSTRACT

Different algorithms based on the consideration of eigenvectors and eigenvalues of the sample covariance matrix are widely used for signal detection and estimating the number of sources. But classic eigenvalue technique makes difficult the evaluation of the thresholds for eigenvalues at given false alarm probabilities. To find these thresholds, it is necessary to know eigenvalue distribution functions of the sample covariance matrix. For some important tasks of signal detection and signals resolution the knowledge of statistical characteristics of only two maximum eigenvalues is enough for the appropriate choice of the thresholds.

In this work the cumulative distribution function (CDF) for the first (maximum) eigenvalue of the sample correlation matrix has been found in explicit form for case when only internal noise presents (for the null hypothesis in detection task). Also the approximate CDF of the second eigenvalue has been found for asymptotic case of one powerful external signal (for the null hypothesis in resolution task).

INTRODUCTION

Detection and resolution of signals may be made by the analysis of the first and the second eigenvalues of sample correlation matrix of array signals [1–3]. The procedure of detection and resolution consists in comparison the eigenvalues with appropriately chosen thresholds.

At the beginning the first (maximum) eigenvalue is compared with the detection threshold λ_D which value for Neyman-Pearson's criterion is calculated for given probability of false detection (P_{FD}). If the first eigenvalue exceeds this threshold, then the decision about the external sources presence is accepted (the null hypothesis of detection task is rejected).

At the next step the second eigenvalue is compared with the second threshold λ_R which value is calculated for given probability of false resolution (P_{FR}). If the second eigenvalue exceeds the threshold then the decision about presence of two or more external signal sources is accepted.

It is obvious that for calculation of the thresholds λ_D and λ_R the statistical characteristics of two maximum eigenvalues of the sample covariance matrix are necessary. In the present report a rigorous analytical expression for the first eigenvalue the cumulative distribution function (CDF) is derived. For the second eigenvalue we find an approximate formula in asymptotic case of large external signal-to-noise ratio (SNR). Both results are obtained for N-sensors narrow-band antenna array of any geometry and L statistically independent snapshots of data vector observed. It is assumed that signals of interest and internal noise background are zero-mean, mutually uncorrelated, complex Gaussian random processes.

CUMULATIVE DISTRIBUTION FUNCTION OF MAXIMAL EIGENVALUE IN CASE OF SIGNAL ABSENCE

We consider the array of N elements. Let $X = [x_1, x_2, \ldots, x_N]^T$ denotes the signal vector, $M = < XX^+ >$ denotes correlation matrix of array signals. It is assumed that internal noise of array elements is white, uncorrelated, Gaussian noise with zero-mean value and variation equal to 1.

Consider the sample correlation matrix $\hat{M}$ calculated on the base of L snapshots:

$$A = \sum_{i=1}^{L} X_i X_i^+, \quad \hat{M} = \frac{1}{L} A \tag{1}$$

Here X_i, i = 1,...,L are snapshots of random vector X. It is known that in case of $L \geq N$ the random Hermitian matrix A has the Wishart distribution. In our case of signal absence $M = E$ because the matrix A distribution can be written as:

$$P(A) = C(N,L)[\det(A)]^{L-N} e^{-Sp(A)}$$
$$C(N,L)^{-1} = \pi^{N(N-1)/2} \prod_{i=1}^{N} (L-i)! \tag{2}$$

The matrices A and $\hat{M}$ can be represented in the following form:

$$A = \sum_{i=1}^{N} \rho_i U_i U_i^{+}, \quad \hat{M} = \sum_{i=1}^{N} \lambda_i U_i U_i^{+} \qquad (3)$$

where U_i are eigenvectors, ρ_i and λ_i are eigenvalues of matrices A and $\hat{M}$.

As seen from (2) the matrix A distribution function depends only on eigenvalues ρ_i of this matrix. Hence, according to [4], the joint probability density function (PDF) of matrix A eigenvalues ρ_i is written as:

$$P(\rho_1, \rho_2, \ldots, \rho_N) = C_3(N,L) \prod_{i=1}^{N} \rho_i^{L-N} e^{-\rho_i} \prod_{i>j}^{N} (\rho_i - \rho_j)^2$$

$$C_3(N,L) = \frac{N1}{\prod_{i=1}^{N} (L-i)!\, i!},$$

$$\rho_1 \geq \rho_2 \geq \ldots \geq \rho_N \geq 0 \qquad (4)$$

Here $\rho_1, \rho_2, \ldots, \rho_N$ are matrix A eigenvalues sorted by decreasing. If condition $\rho_1 \geq \rho_2 \geq \ldots \geq \rho_N \geq 0$ is not fulfilled then $P(\rho_1, \rho_2, \ldots, \rho_N) = 0$.

For finding the CDF $F(\rho) = P\{\rho_1 < \rho\}$ of the random matrix A maximal eigenvalue ρ_1, it is necessary to integrate the (4) over other eigenvalues:

$$F(\rho) = C_3(N,L) \int_0^{\rho} d\rho_1 \int_0^{\rho_1} d\rho_2 \ldots \int_0^{\rho_{N-1}} \prod_{i=1}^{N} (\rho_i^{L-N} e^{-\rho_i}) \prod_{i>j}^{N} (\rho_i - \rho_j)^2 d\rho_N \qquad (5)$$

Because the subintegral function does not vary when any couple of variable ρ_i, ρ_j are interchanged, the equation (5) can be rewritten as:

$$F(\rho) = \frac{C_3(N,L)}{N!} \int_0^{\rho} d\rho_1 \int_0^{\rho} d\rho_2 \ldots \int_0^{\rho} \prod_{i=1}^{N} (\rho_i^{L-N} e^{-\rho_i}) \prod_{i>j}^{N} (\rho_i - \rho_j)^2 d\rho_N \qquad (6)$$

To simplify the equation (6), consider the product $\prod_{i>j}^{N} (\rho_i - \rho_j)^2$. It can be represented as the square of Vandermonde's determinant [5] and written as:

$$\prod_{i>j}^{N} (\rho_i - \rho_j)^2 = \begin{vmatrix} 1 & \rho_1 & \rho_1^2 & . & \rho_1^{N-1} \\ 1 & \rho_2 & \rho_2^2 & . & \rho_2^{N-1} \\ . & . & . & . & . \\ 1 & \rho_N & \rho_N^2 & . & \rho_N^{N-1} \end{vmatrix}^2 \qquad (7)$$

The determinant of the NxN matrix can be represented as the sum of $N!$ transpositions:

$$\prod_{i>j}^{N} (\rho_i - \rho_j)^2 = \left(\sum_{s \in S_N} (-1)^{d(s)} \prod_{i=1}^{N} \rho_i^{s(i)-1} \right)^2 = \sum_{s_1 \in S_N} \sum_{s_2 \in S_N} (-1)^{d(s_1)+d(s_2)} \prod_{i=1}^{N} \rho_i^{s_1(i)+s_2(i)-2} \qquad (8)$$

So the function $F(\rho)$ is equal:

$$F(\rho) = \frac{C_3(N,L)}{N!} \sum_{s_1 \in S_N} \sum_{s_2 \in S_N} (-1)^{d(s_2)+d(s_2)} \int_0^{\rho} \int_0^{\rho} \ldots \int_0^{\rho} \prod_{i=1}^{N} \rho_i^{L-N+s_1(i)+s_2(i)-2} e^{-\rho_i} d\rho_1 \ldots d\rho_N \qquad (9)$$

It is seen that the multidimensional integral (6) has transformed to the sum of the product of one-dimensional integrals, each of them is incomplete gamma function. The gamma function can be written as the following integral:

$$\gamma(\alpha, x) = \int_0^{x} e^{-t} t^{\alpha-1} dt \qquad (10)$$

Using (10), the equation (9) becomes:

$$F(\rho) = \frac{C_3(N,L)}{N!} \sum_{s_1 \in S_N} (-1)^{d(s_1)} \sum_{s_2 \in S_N} (-1)^{d(s_2)} \prod_{i=1}^{N} \gamma(L-N+s_1(i)+s_2(i)-1, \rho) \qquad (11)$$

After some not complicated reduction this equation can be rewritten as the following determinant:

$$F(\rho) = C_3(N,L) \det[b_{i,j}(\rho)],$$
$$b_{i,j}(\rho) = \gamma(L-N-1+i+j, \rho) \qquad (12)$$

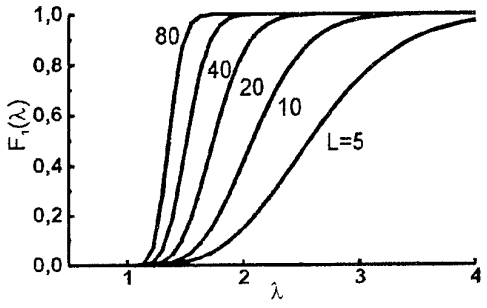


Fig. 1. The first eigenvalue cumulative density function for $N = 5$ and different L

Using the relationship between λ_i and ρ_i and equation (12) the CDF $F_1(N,L,\lambda)$ of the maximum eigenvalue of the sample correlation matrix $\hat{M}$ of the array internal noise can be written as:

$$F_1(N,L,\lambda) = \det\left[\frac{\gamma(L-N+i+j-1,L\lambda)}{\Gamma(L-N+i)\Gamma(j)}\right], \quad (13)$$

where $\Gamma(i)$ is gamma function. In Fig. 1 the CDF's calculated by formula (13) for $N = 5$ and different L are shown.

THE SECOND EIGENVALUE DISTRIBUTION FUNCTION IN CASE OF THE ONE SIGNAL PRESENCE

Now we find the CDF $F_2(N,L,\lambda)$ of the second eigenvalue in case of one high power external signal presence. In this case the correlation matrix of input array signals equals

$$M = E + \nu SS^+, \quad (14)$$

where S is the phase-vector which depends on signal wave-front, array geometry and has been normalized as $|S|^2 = N$, ν is the signal power. We assume that the internal noise has unit power.

It can be shown that in case of $\nu >> 1$ the maximum eigenvalue ρ_1 is independent of other eigenvalues $\rho_2, \rho_3, \ldots, \rho_N$ and the joint probability density function of matrix A eigenvalues is

$$P(\rho_1,\rho_2,\ldots,\rho_N) = C\left[\rho_1^{L+N-2} e^{-\frac{\rho_1}{1+N\nu}}\right] \left[\prod_{i=2}^{N} \rho_i^{L-N} e^{\rho_i} \prod_{i>j>1}^{N} (\rho_i - \rho_j)^2\right] \quad (15)$$

where C is normalization factor, the first factor in square brackets is the maximum eigenvalue PDF, and the second factor in square brackets is joint PDF of the other eigenvalues.

Comparing the second part of equation (15) with the matrix A eigenvalues PDF in case of external signal absence (4), it is seen that joint PDF of *N-1* small eigenvalues in case of one signal presence (14) can be written through the PDF of the $N-1$ eigenvalues of the sample matrix A calculated for $(N-1)$-element array with $L-1$ snapshots in case of only internal noise presence. Therefore, the CDF $F_2(N,L,\lambda)$ of the second eigenvalue in case of one large power signal presence can be expressed through the CDF $F_1(N,L,\lambda)$ (13)

$$F_2(N,L,\lambda) = F_1(N-1,L-1,\lambda\frac{L}{L-1}) \quad (16)$$

Figure 2 depicts the theoretical curve of the second eigenvalue CDF calculated by (16) (solid line). Also in this figure the calculated curves of the second eigenvalue CDF for different signal power ν = 0.25, 1, 4 (dashed lines) are depicted. It is seen that for $\nu > 4$ the numerically calculated curves practically coincide with theoretical CDF.

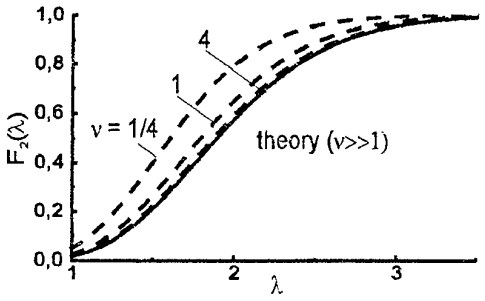


Fig. 2. The second eigenvalue cumulative density function for $N = 5$ and $L = 5$

This work was supported by grants INTAS No.96-2352, RFFI No. 96-15-96718, RFFI No. 97-02-16525.

REFERENCES

1. V.V. Karavaev, V.V. Sazonov, *Statistical theory of passive location*, Moscow, Radio and communication, 1987.

2. H. B. Lee, Fu Li, ``An eigenvector technique for detecting the number of emitters in a cluster'', *IEEE Trans. Signal Processing*, vol.42, no.9, Sept. 1994.

3. A. A. Maltsev, V. T. Ermolaev, K. V. Rodushkin, ``Detection characteristics of antenna array using the maximum eigenvalue of the sample correlation matrix as solving statistic'', *Proceedings of International Conference JINA98*, Nice, November 1998.

4. V. L. Girko, *Spectral theory of random matrices*, Moscow, Nauka, 1988.

5. G. A. Korn, T. M. Korn, *Mathematical handbook for scientists and engineers*, N.Y., McGrow-Hill, 1961.

APPLICATION OF CHANNELING PRINCIPLES OF ESTIMATING WEIGHTING COEFFICIENTS IN ANTENNAS WITH ADAPTIVE SPATIAL SIGNAL PROCESSING AGAINST THE INTERFERENCE BACKGROUND

A. U. Kobzev, V. R. Khachaturov

Kharkov Military University, 310043 Kharkov, Svoboda Sq. 6.
Tel/Fax: +380 572 43-07-40

INTRODUCTION

Nowadays among all known algorithms of adaptive antenna (arrays) functioning the algorithms with gradient adaptation and their modification method is of the highest efficiency as for convergence rate, computational expenses and a degree of proximity to optimal conditions [1]. Here the vector of weighting summation coefficients $\mathbf{K}(t)$ of signals $\mathbf{Y}(t)$ received by antenna elements is determined through a gradient estimate which for discrete representation of processes is equal to $\mathbf{grad}_j = \mathbf{Y}_j y_{0j}^*$, where $\mathbf{Y}_j = \mathbf{Y}(t_j)$, $\mathbf{K}_j = \mathbf{K}(t_j)$, $y_{0j} = \mathbf{K}_j^* \mathbf{Y}_j$ is the oscillation in the adaptive antenna output. Here and further the representation of signals in the form of complex envelopes is used. The sign " * " denotes Hermitian conjugacy. A dimensionality of vectors is determined by the number of antenna elements N. The weighting coefficients at each adaptation step are set in accordance with the iteration procedure

$$\mathbf{K}_{j+1} = \mathbf{K}_j + \mu \mathbf{grad}_j, \qquad (1)$$

where μ is the value which determines the convergence rate and the algorithm stability.

A gradient method is considered as the complex one in hardware realization due to the fact that along with N channels of weighting summation $y_{0j} = \mathbf{K}_j^* \mathbf{Y}_j$ it is necessary to have the same number of parallel channels for gradient estimation. The hardware complexity and bulkiness increase if weighting summation is carried out at a sufficiently high carrier frequency. Since multiplication y_{0j} by Y_j^* can be implemented only at lower frequencies, it is necessary to introduce N mixers with circuits of heterodyne voltages and amplifiers at intermediate frequency into the set of N additional channels.

Some works are known (for example, [2, 3]) where the variants are proposed of constructing adaptive antennas with interference compensation in sidelobes of the radiation pattern without additional channels of signals $\mathbf{Y}(t)$ transformation and amlification. There the channels of weighting summation and the channels of weighting coefficients estimation are combined at once at a carrier frequency, are transformed and amplified in a common tract and then are divided at a low intermediate frequency, and the gradient vector is estimated. The channel combination is provided due to the fact that the elements of weighting multiplication play also the role of modulator of received signals. The degree of spectrum expansion at the expense of modulation under certain conditions may be sufficiently less than the number of channels N. This favours simplification of the adaptive processing equipment. Such variants of antenna construction are better to be called antennas with channeling. In the above-mentioned works there were shown the possibilities of adaptive processing realization with frequency or time channelling as applied to sidelobe supression systems and only for an algorithm with accelerated gradient.

The purpose of this work is to generalize the known results on adaptive antennas with channeling, to extend channeling principle to other algorithms and variants of their construction and to define requirements to basic parameters of processing devices.

PRINCIPLES OF CHANNELING

Unlike channeling in multichannel systems of data transfer where all transmitted signals of message are restored at receiving side, in adaptive antennas upon channeling and subsequent channel division it is sufficiently to preserve and restore only interchannel correlation connections. Exactly the noted circumstance permits to simplify the processing equipment and to keep the possibility of gradient estimating. At first let's consider the details of such a channeling on the example of adaptive antenna array with equivalent elements (Fig. 1). Here double arrows show connections between multichannel elements. Vector $\mathbf{S}$ gives the direction of expected useful signal reception.

Let external interference be a stationary "white" noise. Interference spectrum is limited in preselection filters (PF) at carrier frequency, with passband Δf_{PF}. The vector signal arrives at control inputs of weighting multipliers

$$\mathbf{W}(t) = \mathbf{K}(t) m_0(t) + \mathbf{V}(t) m_1(t), \qquad (2)$$

where scalar modulating functions $m_0(t)$ and $m_1(t)$ are orthogonal at the interval $T > t_k = 1/\Delta f_{PF}$ (t_k is the

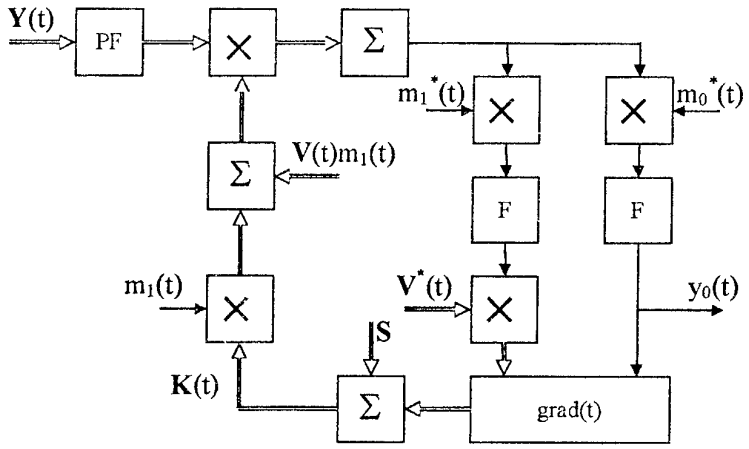


Fig. 1. Adaptive system with channeling of estimating weighting coefficients $\mathbf{K}(t)$

interval of interference correlation), $\mathbf{V}(t)$ is the periodic function of spatial modulation of the period T_V, which consists of the sequence N of orthonormal vectors $\mathbf{V}_k\ (k=1...N)$. Each vector $\mathbf{V}_k$ acts in the time interval $(k-1)t_V < t < kt_V$. Therefore the period is equal to $T_V = Nt_V$. Vectors $\mathbf{V}_k$ can be selected arbitrarily. The necessary condition is only their orthogonality $\mathbf{V}_k^*\mathbf{V}_k = 1;\ \mathbf{V}_k^*\mathbf{V}_j = 0,\ (k \neq j)$. All modulating signals are formed with processing equipment. In the output of antenna summator we'll have

$$y_\Sigma(t) = \mathbf{K}^*(t)\mathbf{Y}(t)m_0^*(t) + \mathbf{V}^*(t)\mathbf{Y}(t)m_1^*(t) = \\ = y_0(t)m_0^*(t) + y_V(t)m_1^*(t) \qquad (3)$$

Functions $m_0(t)$ and $m_1(t)$ are selected so that components in (2) do not have frequency or time coverage. In the first case we can speak about frequency channeling while in the second case — about time channeling. Thus, in the case of frequency channeling it is necessary to select $m_0(t) = 1,\ m_1(t) = \exp\{2\pi f_m t\},\ f_m > \Delta f_{PF}$, and then the component spectra (3) are displaced from one another by the value of f_m. Under time channeling these functions are non-overlapped periodic sequences of videopulses with the length of $t_m < t_k/2$ and then the signals (3) in the output acquire amplitude-pulse modulation.

After shifting to intermediate frequency and amplifying in a wideband amplifier (these circuits are not shown in Fig.1) the sum components (3) are divided by multiplying $y_\Sigma(t)$ by $m_0^*(t)$ and $m_1^*(t)$ and passed through main selection filters (F) with the band equal to the width of useful signal spectrum Δf_S. Since usually $\Delta f_S << \Delta f_{PF}$, then the processes with the amplitude-pulse modulation turn into the continuous process. In the outputs of filters F the processes $y_0(t)$ and $y_V(t)$ are formed. Then the vector signal $\mathbf{Y}_M(t) = \mathbf{V}(t)y_V(t) = \mathbf{P}(t)\mathbf{Y}(t)$, where matrix $\mathbf{P}(t) = \mathbf{V}(t)\mathbf{V}^*(t)$ is generated.

We'll show that under certain conditions on signal product $y_0(t)\mathbf{Y}_M(t)$ the gradient vector $\mathbf{grad}(t)$ can be evaluated. For time interval $(k-1)t_V < t < kt_V$ the equality $\mathbf{Y}_M(t) = \mathbf{P}_k\mathbf{Y}(t)$, where $\mathbf{P}_k = \mathbf{V}_k\mathbf{V}_k^*$, is valid. Due to the orthogonality of vectors $\mathbf{V}_k$ the matrices $\mathbf{P}_k$ have the properties of projection matrices

$$\mathbf{P}_k^2 = \mathbf{P}_k;\ \ \mathbf{P}_k\mathbf{P}_k^* = \mathbf{P}_k;\ \ \mathbf{P}_k\mathbf{P}_j = \mathbf{0},\ \ (k \neq j); \\ \mathbf{P}_1 + \mathbf{P}_2 + ... + \mathbf{P}_N = \mathbf{E}.$$

Here $\mathbf{0}$ is the zero matrix, $\mathbf{E}$ is the unit matrix. Therefore, if we denote $\mathbf{P}_j = \mathbf{P}(t_j)$ then

$$\sum_{j=1}^{T_V} \mathbf{P}_j = \mathbf{E}. \qquad (4)$$

Let us proceed to discrete processes and determine the vector of sample correlation coefficients $\mathbf{G}$ between the processes $y_0(t)$ and $\mathbf{Y}_M(t)$ on condition that a correction step of weighting coefficients and the number of samples averaged over one step are equal to the period of spatial modulation T_V. Then under fixed vector $\mathbf{K}_r$ we have

$$\mathbf{G}_r = \frac{1}{T_V}\sum_{j=r}^{r+T_V} \mathbf{Y}_{Mj}y_{0j}^* = \frac{1}{T_V}\sum_{j=r}^{r+T_V} \mathbf{P}_j\mathbf{Y}_j\mathbf{Y}_j^*\mathbf{K}_r. \qquad (5)$$

Taking into account the last property of projection matrix (4), the average value of vector $\mathbf{G}$ under specified conditions is $M\{\mathbf{G}\} = \mathbf{R}\mathbf{K}_r$ ($\mathbf{R}$ is the interference correlation matrix) what agrees with the gradient [1].

So the vector $\mathbf{G}$ on the average corresponds to the gradient and therefore can be used for correcting weighting coefficients. Therefore, we can recommend the algorithm of adaptive processing (1), where $\mathbf{grad}_r = \mathbf{G}_r$.

The gradient algorithm of the form (1) has the limited range of stability [1], and is considered only as a simple example of using the channeling method. In principle, nothing is changed if the other known types of adaptive algorithms are used. For example, for extending the range of stability the vector of sign functions $\mathbf{sign}(\mathbf{Y}_{Mj})$ can be used instead of vector $\mathbf{Y}_{Mj}$. In this case the algorithm becomes equivalent to the procedure with an ideal noise limiter $\mathbf{Y}(t)$ in a feedback circuit [1]. It is also possible to realize the accelerated gradient algorithms [1]. For this purpose, the gradient must be formed according to the rule

$$\mathbf{grad}_r = \frac{\sum_{j=r}^{r+T_V} \mathbf{Y}_{Mj} y_{0j}^*}{\sum_{j=r}^{r+T_V} (y_{Vj})^2}. \qquad (6)$$

Finally, the possibility of using the algorithm with estimating and subsequent conversion of the interference correlation matrix is not excluded. The sample correlation matrix of multidimensional process $\mathbf{Y}_M(t)$ is equal to

$$\mathbf{R}_M = \frac{1}{K}\sum_{j=1}^{K} \mathbf{P}_j \mathbf{Y}_j \mathbf{Y}_j^* \mathbf{P}_j^*. \qquad (7)$$

When $K = nT_V$ (n is an integer) the mean value of this matrix coincides with matrix $\mathbf{R}$.

Channeling is also applicable in adaptive antennas with selected main receiving channel when the interference suppression is realized in sidelobes of the radiation pattern of the main antenna at the expense of using N additional low-directional antennas.

TECHNICAL POTENTIALITIES

As it follows from the above-stated, the parameters of modulating signals $m_0(t)$ and $m_1(t)$ depend on passband Δf_{PF} of filter PF and its selectivity. Thus, upon frequency-division multiplexing and rectangular (ideal) frequency response of this filter, the frequency f_m can be selected as equal to Δf_{PF}. For the cases of real responses the frequency f_m must be increased so that component spectra (3) did not overlap. If interference is always narrow-band then selection of modulating signal parameters is made proceeding from their spectrum width. The period T_V of modulating function $\mathbf{V}(t)$ can also expand oscillation spectrum $y_V(t)$, and it affects the algorithm convergence rate. Therefore, the value T_V is to be selected proceeding from trade-off requirements. For example, we can assume $T_V = N/\Delta f_S$. In such a case spectrum expansion is negligible, but it is to be expected that adaptation rate decreases by a factor of N in comparison with proceeding without channeling what is natural payment for simplification of adaptation equipment. The form of orthogonal vectors $\mathbf{V}_k$ doesn't play a particular role. As an example, it can be offered to choose vectors $\mathbf{V}_k$ so that they were lines of Butler matrix. In work [3], the function $\mathbf{V}(t)$ is the set of signals with phase manipulation $(-\pi,+\pi)$ and orthogonal modulating functions in each channel.

As it follows from channeling principle, upon adaptive summation of signals at sufficiently high carrier frequency when passband of filters PF can be of several dozens of MHz, specific requirement are placed for control circuits of devices for weighting multiplication and modulation. As such devices, as a rule, the quadrature modulators which must have operating frequency band in control input not less than $2\Delta f_{PF}$, are used. To corroborate technical potentialities of channeling let's note that Hewlett Packard produces quadrature modulators in the form of microcircuits for operating frequency range up to 2.5 MHz with passband in control circuit from 0 to 700 MHz. All main operations on computation of weighting coefficients or correlation interference matrix can be performed with the help of microprocessor facilities. It will permit to create universal devices of adaptive processing with flexible modification of algorithms and their parameters.

SIMULATION RESULTS

Simulation of adaptive system for interference suppression in sidelobes in which there were 4 additional channels with low-directional antennas was carried out. Interference of the type "white noise" from two sources act on sidelobes of the main antenna with the level of abut –30dB producing interference/noise ratio in the output of key channel of about 25dB. Interference was passed through forming filters with Gaussian frequency response and with time constant equal to 16 samples. The period of modulating function $m_1(t)$ was equal to 8 samples and T_V = 8 samples. The orthogonal vectors $\mathbf{V}_k$ were formed according to the rule

$$\mathbf{V}_k^T = 0.5\left\{1^k \quad j^k \quad -1^k \quad -j^k\right\}$$

where $k = 1, 2, 3, 4$; j is the unit imaginary number.

The algorithm with an ideal limiter of interference envelope in the feedback circuit was simulated. Simulation has shown that before correction of weighting

coefficients there is no necessity to realize preliminary averaging in accordance with the formula (5). Such an averaging takes place automatically as a result of the iterative procedure.

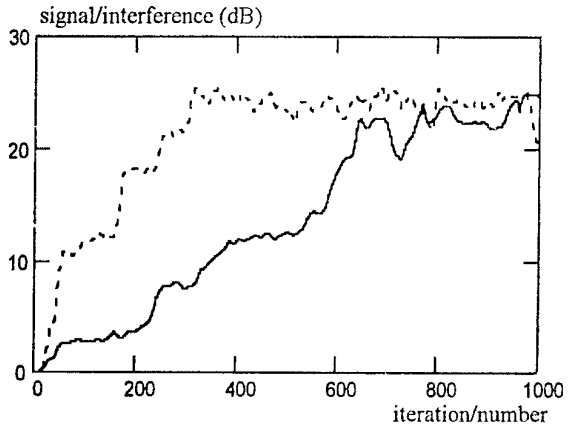


Fig. 2. The process of setting signal/interference ratio in system with channeling (——) and without channeling (.....)

In Fig. 2 solid lines represent the plots of trasients for signal/interference ratio in the output under zero initial conditions of weighting coefficients $K_1,\ldots,K_4$ in adaptive antenna with frequency channeling. Dotted lines show similar dependencies for the algorithm without channeling. As it seen from the figure, the channeling results in delaying transients approximately by a factor of N ($N = 4$ is the number of channels with adaptive tuning). The efficiency of interference compensation in steady state for algorithms under consideration differs slightly. System simulation with time channeling jave shown that their characteristics differ a little from systems with frequency channeling.

CONCLUSION

The presented results allow to hope for simplification of adaptive antenna (antenna arrays) equipment at the expense of using channeling of weighting coefficient estimation. The payment for simplification is the reduction of internal performance that in some practical cases can be found acceptable.

REFERENCES

1. R.A.Monzingo and T.W.Miller. Introduction to Adaptive Arrays. Hughes Aircraft Company Fullerton, California. 1980.
2. Kaitsuka. Interference Compensation system. U.S.Patent 4384366, May, 1983.
3. M.H.Myers. Adaptive Processing Apparatus. U.S.Patent 4442433, April, 1984.

ESTIMATION OF THE INFLUENCE OF RECEIVING-AMPLIFYING SECTIONS NON-LINEARITY ON THE ADAPTIVE ANTENNA ARRAYS EFFICIENCY

Yu. Yu. Kolyadenko, V. V. Popovsky, A. G. Malitsky

Kharkov State Technical University of Radio Electronics
Prospekt Lenina 14, Kharkov, 310166, Ukraine
Phone: +380 572 409320, Fax: + 380 572 409113

The adaptive antenna arrays (AAA) still remain one of the most effective means of concentrated interference control, for when applying them there is no need to change regimes of radio lines, whereas a level of interference suppression attains tens of dB [1–3].

In the same time, a number of authors [1, 3] point to the AAA efficiency sharp loss due to non-linearity in receiving sections.

Let's estimate quantitatively these losses for types of nonlinearity inherent for receiving-amplifying sections, i.e. limiters.

The fact that a great deal of real processes and fields may be approximated with a required accuracy by the markov ones is common in use [4]. The question on accordance of random processes and fields with markov ones is unambiguously connected with their presentation in the form of equations of state:

$$\frac{\partial \bar{x}(t,r)}{\partial t} = F(\bar{x},t,r) + G(\bar{x},t,r)\bar{\xi}(t,r), \qquad (1)$$

where $\bar{x}(t,r)$ is a vector of state depending on time and spatial coordinate r; $F(\bar{x},t,r)$, $G(\bar{x},t,r)$ are, in a general case, the matrix functions representing a state and an excitation of the field; $\bar{\xi}(t,r)$ gives rise to the vector white gaussian field with a zero mean and an unit level.

In lots of cases in practice the initial presentation of the random field can be reduced directly to a model of the vector random process. Under assumption of the absence of spatial dynamics, as well as in the case of isotropic propagation, the equation is simplified and takes the form:

$$\frac{d\bar{x}(t)}{dt} = F(\bar{x}(t),t) + G(\bar{x}(t),t)\bar{\xi}(t) \qquad (2)$$

With the help of the equation of state (2) we obtain the N-dimensional space-time random process.

In the input of the receiver-amplifier we shall consider an additive process as follows:

$$\bar{X}(t) = \bar{X}_s(t) + \bar{X}_{\text{int}}(t) + \bar{X}_n(t), \qquad (3)$$

where indices s, int, n are applied to signal, concentrated interference and white gaussian noise, respectively.

In receivers-amplifiers the weight factors are denoted as $w(t)$, other amplifying elements have the characteristic of the smoothed limiter, what is described by the function:

$$y(x) = \sqrt{\frac{2}{\pi}} \int_0^{x/l\sigma} e^{-\frac{x^2}{2}} dx, \qquad (4)$$

where x is the input signal with the dispersion σ^2; l is the parameter pointing to the feature of the function nonlinearities, α defines the dip angle of the curve. At $l \to 0$ the function (4) turns into the expression for the ideal symmetrical limiter. $l = k^{-1} = tg^{-1}\alpha$, k is an element gain. At $l \to \infty$ the function (4) tends to the abscissa. Fig. 1 shows a family of the symmetrical limiter characteristics at l = 0.5...5.

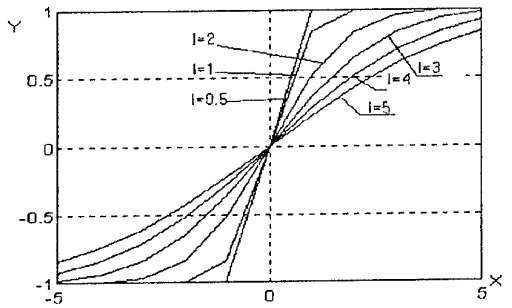


Fig. 1

It can [5] be shown that in order to provide operation at linear part, it is required for a value of the input signal of P_{inp} not to exceed a certain threshold of linearity and not to be within a saturation zone. At saturation zone boundary values of $\pm b$ this corresponds to inequality $kP_{inp} < b$. Replacing k with $1/l$, we obtain: $bl > P_{inp}$. It can be shown that at $bl > P_{inp}$ the nonlinearity is practically insignificant, and in this case one considers the system as linear. When P_{inp} increases, the nonlinearity starts to manifest itself and at

$bl \cong P_{inp}$ leads to the deformation of power spectral density both of signals and interferences, especially in the high-frequency region. One can say that the latter is a zone of the moderate influence of the nonlinearity, where the ordinary for communication channels gaussian distribution density of a random input signal keeps its unimodal form. At the continued P_{inp} increase, that is at $bl < P_{inp}$ the nonlinearity affects tremendously and the distribution density appears to be bimodal.

Let's analyze a standard algorithm of space-time signal processing in these regions and compare it with the potentially attainable variant.

We shall investigate AAA with N elements, in the inputs of which the multidimensional random process (3) is prescribed. Assume, the introduced multidimensional processes are stationary, with zero expectations, and their correlation matrices are known:

$$R_i(\tau) = M(\vec{X}_I(t)\vec{X}_I^T(t-\tau)), \qquad (5)$$

where I is a signal, an interference and a noise.

When passing through the nonlinear element (NE) (1) the signal is distorted, and its correlation functions change as well. Then the correlation matrices in the output of the nonlinear system will accordingly be [1]:

$$B(\tau) = \frac{2}{\pi}\arcsin\frac{R(\tau)}{1+I^2} \qquad (6)$$

Formulate the task of finding the weight factors of the N-dimensional space-time filter ensuring the optimal filtration of multidimensional signal. The weighted signal looks like:

$$\hat{S}(t) = H(\overline{X}(t)), \qquad (7)$$

where $H(\overline{X}(t))$ is a certain nonlinear functional transformation as, for example:

$$H(\overline{X}(t)) = \overline{W}^T f(x(t)), \qquad (8)$$

where $\overline{W}$ is the weight factors vector (WFV) to be found of the optimal N-dimensional spatial filter; $f(\bullet)$ is the nonlinear transformation of signal.

It is evident that any estimation differs from the true signal and an error of filtration occurs:

$$\varepsilon(t) = S(t) - H(\overline{X}(t)) = S(t) - \overline{W}^T f(x(t)). \qquad (9)$$

Since this error is a random function, so some statistical characteristic $\varepsilon(t)$ should serve as the criterion of optimality of the operator $H(\overline{X}(t))$, for example, the dispersion of signal estimation error:

$$\sigma^2 = M([S(t) - \overline{W}^T f(x(t))]^2) = \\ = M(S^2(t) - 2\overline{W}^T R_{xc} + \overline{W}^T B_{xx}\overline{W}). \qquad (10)$$

Now the task is reduced to minimization of σ^2 over all components of vector $\overline{W}$. We find the minimum of function σ^2 solving the equation:

$$\nabla_{\overline{W}}(\sigma^2) = 2B_{xx}\overline{W} - 2R_{xc} = 0, \qquad (11)$$

where $\nabla_{\overline{W}}(\sigma^2)$ is a gradient of root mean square error.

Solving this equation, we obtain

$$\overline{W}_{onm} = B_{xx}^{-1}R_{xc} \qquad (12)$$

The algorithm (12) has been analyzed for the three-dimensional linear equidistant AAA.

Fig. 2 shows the plots of the power signal P_s to interference P_{int} ratio in the AAA output versus the interference input angle at different ratios of these powers and the following input data: $I = 1$, $P_s / P_n = 20\ \partial B$, an input angle of signal is $\varphi_s = 10^o$. For the analysis there have been selected such signal-interference situations that correspond to the three considered above cases: $kP_{inp} < b$, $bl \cong P_{inp}$ and $bl < P_{inp}$.

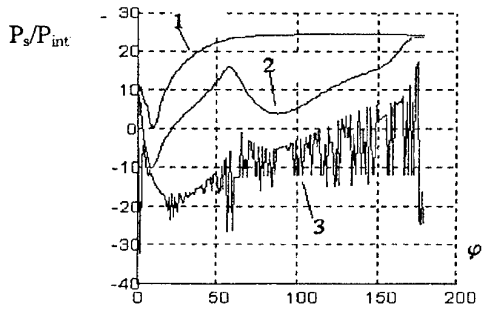


Fig. 2

Curve 1 is associated with $P_{\text{int}} / P_s = 0$ dB and $bl > P_{inp}$, that is the receiving-amplifying section may be treated as linear, what agrees with the potentially attainable efficiency of AAA. From this plot it follows that in the AAA output P_s / P_{int} reaches 20...25 dB at the difference between input angles of signal and interference of more than 40°. In the case of these angles coincidence, and $\varphi_s = \varphi_{\text{int}} = 10^o$, the efficiency falls down to zero, what is stipulated by the AAA blindness effect.

Curve 2 conforms with $P_{\text{int}} / P_s = 10\,dB$ and $bl \approx P_{inp}$. In this case the noticeable influence of the nonlinearity is exhibited, the efficiency loss at some interference input angles runs into 20 dB.

Curve 3 is plotted for $P_{\text{int}}/P_s = 20\,dB$ and $bl < P_{inp}$. Here the obtained results differ from the desired ones for a linear system both qualitatively and quantitatively. The system is in the unstable state, its behavior gains unforeseen character, and the bifurcation effect manifests itself. This can be as a result of the bimodal distribution density in the output of the nonlinear element.

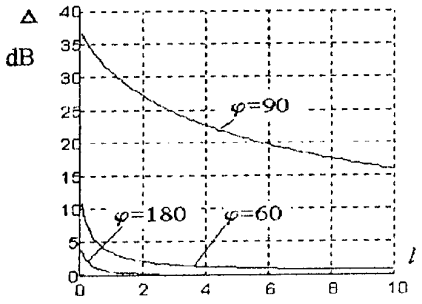


Fig. 3

Consider more thoroughly the boundary case of $P_{\text{int}}/P_s = 10\,dB$ for extremum interference input angles of $\varphi_{\text{int}} = 60^o, 90^o, 180^o$. For this let's study the NE influence depending on l, if comparing ratios P_s/P_{int} in the AAA output in the absence of NE (the linear AAA) and in its presence: $\Delta = (P_{s\,l}/P_{\text{int}\,l}) - (P_{s\,n}/P_{\text{int}\,n})$, where $P_{s\,l}/P_{\text{int}\,l}$ is the signal-interference-noise-ratio (SINR) in the output of the linear system, $P_{s\,n}/P_{\text{int}\,n}$ is the one in the system output taking into account nonlinear distortions.

As is seen from charts presented in Fig. 3, at interference input angles $\varphi_{\text{int}} = 60^o\ u\ 180^o$ the losses due to nonlinear distortions are from 3 to 6 dB and with the increase of parameter l they tend to zero. Along with this, there observed such interference input angles $\varphi_{\text{int}} = 90^o$ at which even significant increase of l does not yield positive results, and the losses constitute from 15 to 35 dB.

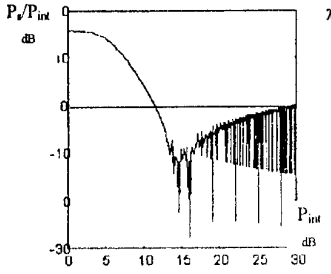


Fig. 4

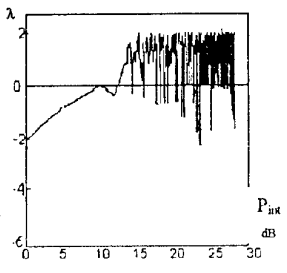


Fig. 5

Consider in detail the behavior of the dynamic system in the bifurcation zone. In Fig. 4 plots P_s/P_{int} versus P_{int} are presented at $l = 1$ and $P_s/P_n = 20$ dB. As is seen from the chart, the unstable state does not appear abruptly and in no time. Initially, the efficiency smoothly descends, and when reaching a certain threshold value of $P_{\text{int}} \approx 15$ dB loses its stability. Its state turns to be chaotic.

One of quantitative characteristics of the chaotic behavior is the Lyapunov index [6]:

$$\lambda(P_{\text{int}}) = \lim_{N\to\infty} \frac{1}{N} \ln \left| \frac{df^N(P_{\text{int}})}{dP_{\text{int}}} \right|, \qquad (13)$$

the plot of which is shown in Fig. 5. This index characterizes a degree of exponential run away of neighbouring points.

One distincts a bifurcation regime, where the Lyapunov index is always negative (it becomes equal to zero only at points of bifurcation), and a chaotic regime, where the majority of values λ are positive, what indicates the chaotic behavior. Such a behavior is interrupted with r-windows, where $\lambda < 0$.

CONCLUSIONS

The carried out investigations show that in the general case availability of NE in the receiving-amplifying sections leads to losses. These ones depend on both nonlinearity nature and the input signal level. One can separate two characteristic zones connected with the single- and bimodal density of the a posteriori probability distribution after NE. In the first zone, the more is the level of the input signal the less is the advantage of the AAA use (which decreases from 25...35 dB practically down to zero). In the second zone, the bimodal distribution results in the algorithm instability and chaotic behavior of the system.

REFERENCES

1. A. P. Rodimov, V. V. Popovsky. Statistical theory of polarization-temporal signal and interference processing. - Moscow: Radio i svyaz'. 1984. - pp. 272 [in Russian].
2. V. K. Grishin, F. A. Zhivopistsev, V. A. Ivanov. Physical experiment mathematical processing and interpretation.- Moscow: Isd-vo Moskovskogo Universiteta, 1988 - pp. 318 [in Russian].
3. A. R. Levin. Theoretical foundations of statistical radio engineering. - the 3rd publication developed and completed. - Moscow: Radio i svyaz', 1989. - 656 pp. [in Russian].
4. V. I. Tikhonov , Statistical radio engineering . - Moscow: Radio I svyaz', 1982, pp. 623 [in Russian].
5. Non-linear stochastic model of telecommunications signal spatial-time processing / Yu.Yu. Kolyadenko // Radiotetekhnika. All-Ukr. Mag. 1999. N. 109 [in Russian].
6. G Shooster Deterministic chaos: Introduction. Transl. from Eng. M. Mir, 1988 – pp 240 [in Russian].

AN EFFICIENCY OF INTERFERENCE ADAPTIVE COMPENSATION IN MULTIPATH PROPAGATION OF RADIO WAVES

L. Y. Kornienko, O. A. Voitovich, V. P. Tischenko

Kharkov Military University, Svoboda sq. 6,
Kharkov, 310043, Ukraine, telephone (0572) 329-845

Adaptive antenna arrays usually function in radio wave multipath propagation, occurred, for example, due to reflection from local objects and underlaying surface. In frequency identity of microwave receiving channel paths the multipath effect is one of the most serious factors limiting the efficiency of interference compensation. The latter depends on correlation degree of direct and reflected interference radio waves [1] which is defined not only by the relation of interchannel time delay and correlation interval but by radio wave reflection and reception conditions.

The object of this report is to analyse the influence of interference radio waves reflected from underlaying surface on efficiency measures of interference one-channel autocompensator at small elevation angles, i.e., mirror reflection is the prevailing one. Reception conditions are simulated by giving directed properties and heights of antenna size of main and compensating channels, having identical relative passbands.

Using the method of reflective treatment, we can obtain the following expression for the coefficient of narrowband stationary interference suppression

$$K_S = 1\Big/\left[1-\frac{q_0 q_1}{(1+q_0)(1+q_1)}|\rho|^2\right], \qquad (1)$$

where

$$|\rho|^2 = \frac{\left|\exp(-j\omega_0 t_\Omega)\operatorname{sinc}\pi B t_\Omega + T_1\exp(-j\omega_0 t_{\Omega_0})\operatorname{sinc}\pi B t_{\Omega_0} + \right.}{\left[1+|T_0|^2+2\operatorname{Re}T_0\exp(-j2\omega_0\tau_0)\operatorname{sinc}2\pi B\tau_0\right]}$$

$$\frac{\left.+T_0^*\exp(j\omega_0 t_{\Omega_0})\operatorname{sinc}\pi B t_{\Omega_0} + T_0^* T_1\exp(j\omega_0 t_\Omega)\operatorname{sinc}\pi B t_\Omega\right|^2}{\left[1+|T_1|^2+2\operatorname{Re}T_1\exp(-j2\omega_0\tau_1)\operatorname{sinc}2\pi B\tau_1\right]} \qquad (2)$$

is the square of modules of interchannel interference correlation coefficient;

$$q_i = \frac{N_\Omega A_{Ei} f_i^2(\Theta-\Theta_M^i)}{N_w}(1+|T_i|^2 + 2\operatorname{Re}T_i\exp(-j2\omega_0\tau_i)\sin c2\pi B\tau_i)$$

is interference/noise ratio in power at the outputs of main ($i = 0$) and compensating ($i = 1$) channels.

In the given expression $\omega_0 = 2Bf_0$, f_0, B are average frequency and passband of receiving channels with effective areas A_{Ei} and normalized antenna patterns $f_i(\Theta)$ oriented at angles Θ_M^i, Θ is an elevation angle of interference source;

$$T_i = R(\Theta) f_i(-\Theta-\Theta_M^i)\Big/ f_i(\Theta-\Theta_M^i),$$

where $R(\Theta)$ is a reflectivity factor; $\tau_i = \frac{h_i \sin\Theta}{c}$ is a time delay of interference radio waves at the inputs of principal ($i = 0$) and auxiliary ($i = 1$) channels with heights of antenna phase centers rise h_0 & h_1, c is a velocity of light; $\frac{N_\Omega}{N_w}$ is ratio of interference spectral power densities and internal noise;

$$t_\Omega = \tau_0 - \tau_1, \quad t_{\Omega_0} = \tau_0 + \tau_1, \quad \operatorname{sinc}x = \sin x\Big/x.$$

Under antenna phase center coincidence ($h_0 = h_1$) and identical conditions of radio wave receiving ($T_0 = T_1$) the value $|\rho|^2 = 1$. The complete correlation of direct and reflected radio waves is provided also with the help of narrowband, in space-time sense, systems for which the products of bandwidth by maximum interchannel delay time is much less than 1. For wideband systems $|\rho|^2 \to 0$. In real conditions $0 \langle |\rho|^2 \langle 1$.

Let's consider the typical case when direct and horizontally reflected polarized interference radio waves are received by highly directive principal antenna on sidelobes with slowly decreasing envelope so that $T_0 \approx -1$, and highly directive auxiliary antenna is oriented by maximum on interference source and reflected wave is received on sidelobes of the level of –13 dB. Then $T_1 \approx -0.05$.

In Fig. 1 a-c the dependencies on the angle Θ of limiting suppression factor $K_{LS} = \frac{1}{\left[1-|\rho|^2\right]}$, suppression factor (1) and using energy $K_U = \frac{K_S}{(1+q_0)}$ for relative spectral power density of direct interference wave, equal to 40 dB in the main input and 50 dB in the auxiliary one the autocompensator are presented. Passband is 0,2%, $h_1 = 15\lambda_0$, $h_0 = 20\lambda_0$ (curve 1) and $h_0 = 30\lambda_0$ (curve 2), λ_0 is the wave length corresponding to the

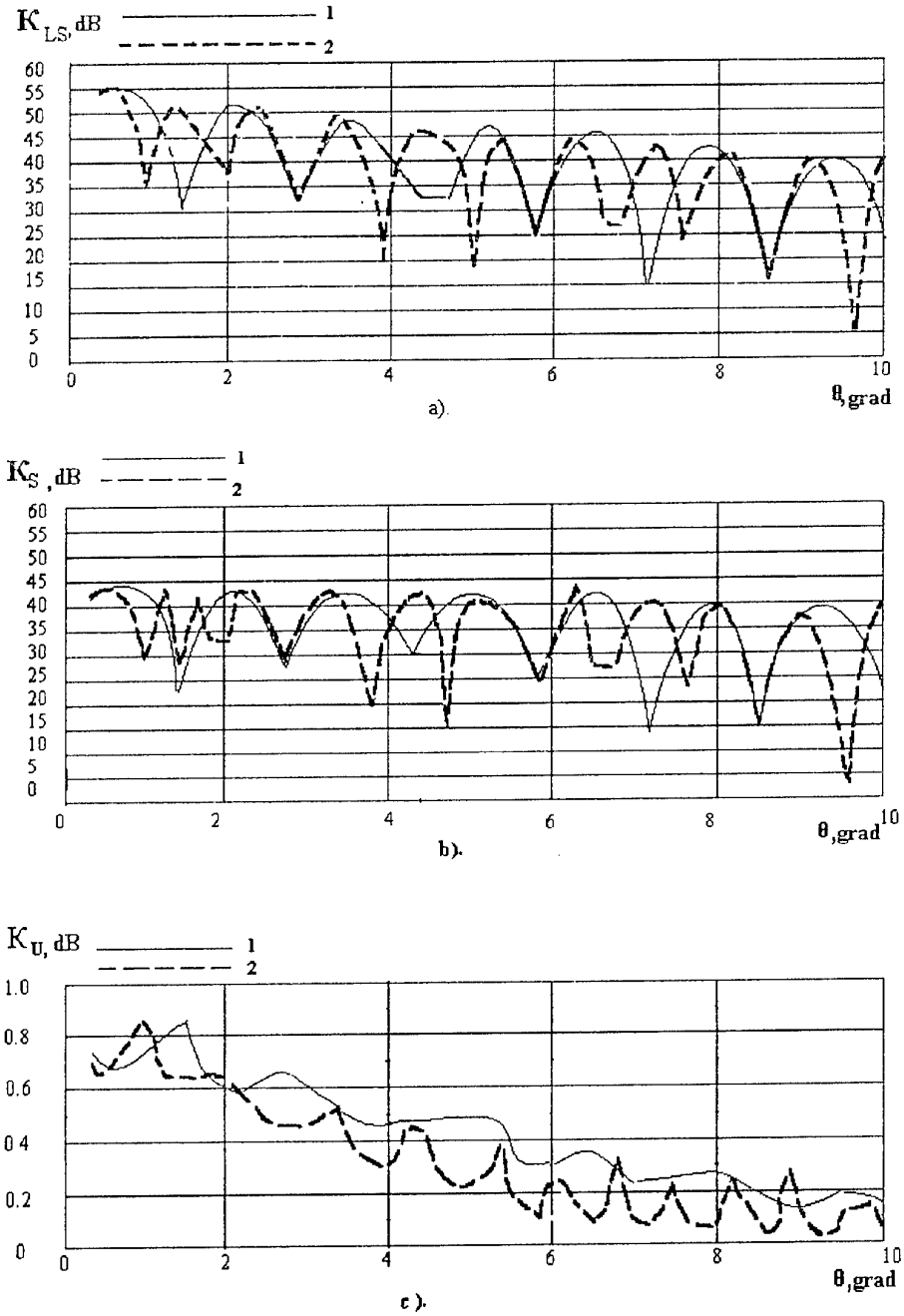


Fig. 1

carrier. The 10 dB excess of direct wave interference power in auxiliary channel is due to using highly directive antenna. The dependence of K_S on Θ is of multilobe nature conditioned by the presence of zeros in interferential factor of the main antenna. In these directions frequency responses of principal and auxiliary (without marked dips in interferential factor) channels essentialy differ. The suppression factor is maximum in the directions close to the values of the main antenna interferential factor maximum at the carrier, since in these directions interference reception conditions by main and auxiliary channels are more identical. The change of antenna phase center separation weakly affects on maximum value K_{LS} because in the considered case the value of interchannel radio wave delay remains much less than the interference correlation

interval $\tau_K \approx \frac{1}{B}$ in receiving channels. The increase h_0 has resulted in dip number increase and position displacement of maxima and minima in K_{LS}/Θ dependence. K_U-on-Θ dependence is of oscillating nature, angular positions of maxima and minima don't coincide with maxima and minima positions of K_S. The value K_U has maximum values in directions corresponding to minimum values of K_S in those cases, when due to antiphase combination of direct and reflected waves in principal channel the resulted power of interference oscillations becomes commensurable with K_S. As a whole, because of interference residual power increase, K_U decreases with Θ rise. So when $\Theta = 8 \div 10°$ $K_U < 0.2$, that corresponds to reducing target detection range by 30 % with the given probability.

REFERENCE

1. A.A. Pistolkors, O.S. Litwinov. Introduction into the theory of adaptive systems. -Moscow: Nauka, 1991, 200 pp. [in Russian].

AN ADAPTIVE COMPENSATION OF PARTIALLY POLARIZED INTERFERENCES IN THE PRESENCE OF POLARIZATION DIFFERENCES IN A FREQUENCY BAND

L. G. Korniyenko, F. F. Mysik, S. Y. Polyakov

Kharkov Military University, sq. Svobody, 6,
Kharkov, 310043, Ukraine, ph. (0572) 329-845

The influence of the non-identities of the basic and supplementary channels' characteristics on the efficiency of self-balancing potentiometers (SBP) of interferences explicitly enough is analysed in the literature, including the books [1, 2]. The interferences by virtue of one or other reasons [3] frequently are partially polarized. The features of the adaptive compensation of interferences are studied in [3, 4]. In this paper [5] the influence of the polarization differences of antennas on the efficiency of the SBP is investigated, but the research is carried out in a narrow-band approximation. In the present paper the influence on a limiting suppression factor of one-channel SBP of polarization differences of antennas in a frequency band is studied.

The marginal suppression factor $K_{\Pi P} \approx \left[1-|\rho|^2\right]^{-1}$ is completely determined by an interchannel correlation ρ coefficient of oscillations in the basic and supplementary receiving channels.

Recording responses in the outputs of the main antenna (MA) and supplementary antenna (SA) on the effect of the partially polarized interferences that are shown with respect to Stokes' theorem as a sum of completely polarized (CP) and unpolarized (UP) components, after a series of transformations it is possible to obtain the following expression for the square module of the correlation coefficient

$$\rho^2(\vec{u})=\frac{\left|\int \exp[j\omega\tau]\left[n\xi^*_{AO}\xi_{A1}+0.5(1-m)\vec{P}^*_{AO}\vec{P}_{A1}\right]df\right|^2}{\int\left[n\left|\xi_{AO}\right|^2+0.5(1-m)\right]df\int\left[n\left|\xi_{A1}\right|^2+0.5(1-m)\right]df}, \quad (1)$$

where τ is an interchannel lag of a flat partially polarized interference radio wave with a polarization degree m, decreasing with an orth direction $\vec{u}$; $\vec{P}_{Ai}(\vec{u},f)=(\vec{i}_0+\mu_{Ai}\vec{i}_\varphi)\ (1+|\mu_{Ai}|^2)^{-0.5}$, i = 0,1, is the polarization vector MA (i = 0) and SA (i = 1) on the frequency f with phasors $\mu_{Ai}(\vec{u},f)$; $(\vec{i}_\theta,\vec{i}_\varphi)$ are the orths of a spherical coordinate system, $\xi_{Ai}(\vec{u},f)=\vec{P}_{Ai}\vec{P}_B$ is the polarization factor of coordination of the antenna and an incident wave component with the polarization vector. The integrating in (1) is performed in limits f_0-0,5Π_0 ,f_0+0,5Π_0], f_0, Π_0 is the average frequency and the bandwidth of receiving channels.

From (1) it follows that the compensation of interferences (m = 1) is influenced by the degree of polarization misalignment of antennas and the incident wave in the frequency band. For compensation of interferences (m = 0) it is important to ensure the identity of polarizable — frequency characteristics (PFC) of antennas. In the narrow-band approximation for CP interferences ρ = 1 without regard for dependence on the polarization ratio of antennas and the incident wave. For UP interferences $\rho^2=\left|\vec{P}^*_{AO}\vec{P}_{A1}\right|^2$ the value is determined by the differences of polarizations of antennas at the medium frequency. SBP with orthogonally polarized antennas is unsuitable for suppression of UP interferences.

Usually, the polarization differences of SBP antennas are insignificant and consequently it is possible to put $\mu_{Ai}(f)=|\mu_{Ai}(f_0)|\exp[j\xi_i+t_i(\omega-\omega_0)]$, where ξ_i, t_i, respectively, phase shift on the average frequency and a difference of group lags of orthogonal components of the ith antenna. Substituting the $\mu_{Ai}(f)$ values in (1) it is easy to obtain an analytical expression for ρ^2.

Let the supplementary antenna on the average frequency have a circular polarization that is matched to the polarization of a CP interference component. The polarization differences of antennas on the average frequency are determined by the values $\mu=|\mu_{AO}|$ and $\xi=\xi_1-\xi_0$. In the absence of these differences μ = 1, ξ = 0, and at τ = 0 and $2\pi\Pi_0 t_i << 1$ we have

$$K_S = 10\lg(1+m) - 20\lg|t_1-t_0|\omega_0 - 10\lg(\Pi_0^2/24f_0^2).$$

Hence it follows that K_S decreases with the growth of the passband width, decreasing at m a change from 1 to 0 by 3dB. At identical PFC (t_1 = t_0) the interference is completely suppressed. At $\omega_0 t_1$ = –9.03 and $\omega_0 t_0$= – 6.73 (that corresponds to standard sizes of polarizers SA as a phasing section and MA as a system of parallel plates), and change Π_0/f_0 from 0.01 up to 0.05 the values of K_S for CP interference changes from 49.6 dB down to 35.6 dB. Thus, even the small differences of polarizations of antennas in the frequency band at $(\omega-\omega_0)/\omega_0$ = 0.05 elliptic coefficients $r_{\ni 0}$ = 0.709, $r_{\ni 1}$ =

0.626), result in an noticeable weakening of SBP compensatory capabilities. The presence of polarization differences on the average frequency results in the further decrease of K_S, in particular, for its slightly polarized interferences. For example, at $\mu = 1$, $\xi = 10^0$ and $\Pi_0/f_0 = 0.05$ for $m = 1$ the value $K_S = 35.3$, and for $m = 0 - K_S = 21$ dB.

In the presence of mismatching of phase centers of antennas the additiondl limiting factor for K_S becomes a value of interchannel lag of interferences oscillations that grows with the increase of angle of the fiat front in the incident wave. In Fig. 1. the charts of K_S vevsus angle θ are shown at an interval between phase centers of antennas $10\lambda_0$, $\Pi_0/f_0 = 0.05$, $\mu = 0.9\,\xi = 10^0$ for CP ($m = 1$) and UP ($m = 0$) in cases a) when antenna polarization does not depend on frequency ($t_0 = t_1 = 0$) curves 1, 1'; б) PFC of antennas are identical ($\omega_0 t_1 = \omega_0 t_0 = -8{,}53$) - curves 2,2 '; в) for considered types of polarizers curves 3, 3 '. If antenna polarization does not depend on frequency, then for the CP of interferences the difference in polarizations at the mean frequency are unessential and

$$K_S = \left[1 - \left|\sin c\,\pi\,\Pi_0\,\tau\right|^2\right]^{-1}.$$

For UP interferences, the form of the law of polarizations change depending on frequency does not play a role, relevant is only the presence of polarization differences, which for the curves 1 ', 2 ' are only at the mean frequency, and these differences are determining that is comtirmed by curve 3.'

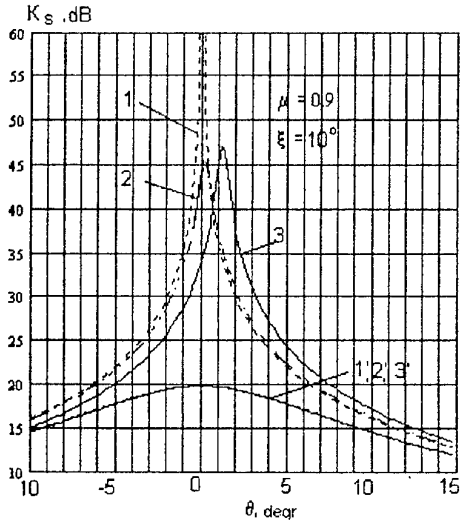


Fig. 1

The presence of maxima for the curves 2 and 3 is explained by that for the corresponding angles θ there is a compensation of delays.

In this area K_S is of greater importance, than under action of each of the factors separately.

At $\theta > 10^0$ the main limiting factor is the interchannel delay, which, however, in its effect is commensurable with effect of polarization differences for interferences. (see the value of K_S for $\theta = 0$). Therefore effect of a cancellation of lags slightly influences on K_S under effect of UP interferences.

Thus, the polarization – frequency differences of antennas represent severe factor limiting SBP efficiency, in particular, under effect of weakly polarized interferences. It requires thorough analysis of PFC antennas, detection and removals of causes leading to in their differences. It is possible to apply the adaptive tuning of polarization of the supplementary antenna [5].

REFERENCES

1. R. A. Monsingo, T.Y. Miller. Adaptive antenna avvays. The introduction in the theory. Transl. from Engl.- M: Radio i svyaz, 1986.- 448 p. [in Russian].

1. Y. I. Losev, A. T. Berdnikov, E.Sh. Goihman, B.D. Sizov. Adaptive compensation of handicapes in communication channels. Under red. Y.I.Losev.- M: Radio i svyaz, 1988.- 208 p. [in Russian].

2. A. P. Rodionov,V.V. Popovskiy. The statistical theory of a polarization - temporary signal processing and handicapes in communication circuits. M: Radio i svyaz , 1984.- 272 p. [in Russian].

3. L. G. Korniyenko, Y.A. Kolos. Adaptive antenna arrays with the controlled space-polarization characteristics under conditions of partially polarized waves. Antenny. № 36.- M: 1989, Radio i svyaz, p.p. 12-23.

4. L.G. Korniyenko, Y.A. Kolos. S.A. Maltsev Efficiency of suppression by the self-balancing potentiometer of partially - polarized radio waves in the presence of polarization distinctions of antennas of the basic and supplementary channels. Radio tekhnika i elektronika XXXIV, №2 1989.p.p. 321-326 [in Russian].

STATISTICAL CHARACTERISTICS OF ADAPTIVE ANTENNA ARRAYS WITH INDEPENDENT REFERENCE-SIGNALS FORMING

A. A. Maltsev, O. V. Poldin, A. M. Silaev, L. L. Presti*

Department of Statistical Radiophysics, Nizhny Novgorod State University,
603600, Nizhny Novgorod, Gagarin Ave. 23, e-mail maltsev@rf.unn.runnet.ru
*Dipartimento di Elettronica, Politecnico di Torino,
Corso Duca degli Abruzzi 24, 10129 Torino, Italy, e-mail lopresti@polito.it

ABSTRACT

Adaptive antenna array communication system is considered that receives phase-manipulated signal in a background of Gaussian interferences and internal noise. Reference signal is formed by nonlinear inertialess transformation of the array output. It is shown that weight coefficients vector that minimizes mean square error between reference and output signals also provides maximum of output signal-to-noise ratio (SNR). Statistical characteristics of adaptive array in stationary regime are investigated for different schemes of reference signal forming. Theoretical results are confirmed by computer simulation.

INTRODUCTION

In many practical situations the design of adaptive antenna array for radio-communication systems is made difficult by the fact that the directions of arrival of useful signal and interferences are a priori unknown. Therefore to adjust antenna array weight coefficients, as a rule, algorithms are used that minimize the mean square error (MSE) between output signal and some reference ("desired") signal [1–4]. When there is no a priori known reference signal in the received message, a problem arises to find an optimal way to form the "desired" signal in the receiver [5, 6]. In the present paper we investigate statistical characteristics of receiving phase-manipulated signals in adaptive array when different schemes of reference signal forming are used. It is shown that specific design of nonlinear element used to form reference signal does not influence on the output signal-to-noise ratio (the output SNR) of adaptive antenna array. By computer simulation the main statistical characteristics of adaptive array were investigated for different interference scenarios. The relationship between useful signal power, output SNR, error probabilities and input SNR are found.

PROBLEM STATEMENT AND ANALYTICAL RESULTS

A functional diagram of N-element narrow-band adaptive array with independent reference signal forming is shown in Fig. 1. Assuming that a distance between array elements is of order half a wavelength and neglecting the delay of the signals envelopes and phases, we can write N-dimensional vector of complex amplitudes at the sensor elements outputs as a sum:

$$\vec{x}(k) = s(k)\vec{S} + \sum_{i=1}^{J} f_i(k)\vec{\Psi}_i + \vec{\eta}(k), \qquad (1)$$

where $s(k)$, $f_i(k)$ describe the time variations of the complex amplitudes of the signal and i-th interference; J is a total number of interferences; $\vec{\eta}(k)$ is the additive internal noise of antenna elements; $\vec{S}$, $\vec{\Psi}_i$ are wavefront vectors (phasor vectors) of the useful signal and i-th interference [1-4].

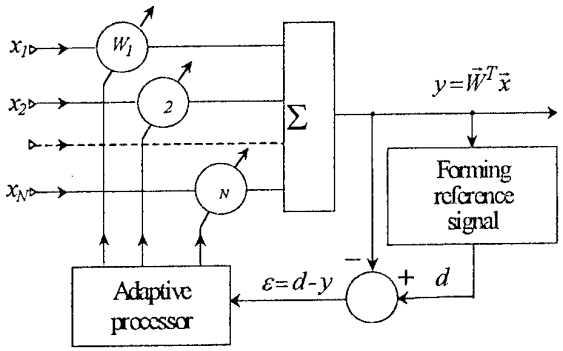


Fig. 1

We assume that samples of interferences and noise at different instants are statistically mutually independent and have complex Gaussian distributions with zero mean values and mutual covariance functions of the form

$$\left\langle f_i^*(k) f_l(k) \right\rangle = D_i \delta_{il}, \quad \left\langle \eta_m^*(k) \eta_n(k) \right\rangle = D_\eta \delta_{mn},$$

where δ_{il}, δ_{mn} are Kronecker delta ($i,l = \overline{1,J}$; $m,n = \overline{1,N}$); D_η is the internal noise power; D_i is the power of i-th interference. The phase-manipulated signal of interest is described by the sequence $s_0(k) = a_s s(k)$, where a_s is a complex constant that characterizes the signal power $\left\langle |s_0(k)|^2 \right\rangle = |a_s|^2 = D_s$. In each step $s(k)$ with equal probability takes one of M values $\exp(j2\pi n/M)$, $n = \overline{0,M-1}$, that are uniformly distributed over the unit circle in complex plane.

The output signal of the adaptive array can be represented as a sum of useful signal and interference-noise components:

$$y(k) = \vec{W}^T \vec{x}(k) = A_s s(k) + \xi(k), \qquad (2)$$

where $\vec{W}$ is a weight coefficients vector; "T" denotes transposition; $A_s = a_s \vec{W}^T \vec{S}$ is an amplitude of useful signal at the array output; a sequence $\xi(k) = \sum_{i=1}^{J} f_i(k) \vec{W}^T \vec{\Psi}_i + \vec{W}^T \vec{\eta}(k)$ is a sum of Gaussian interferences and noises. The useful signal power at the output equals $P_s = |A_s|^2 = D_s |\vec{W}^T \vec{S}|^2$, the output power of interferences and noises is determined by variance of $\xi(k)$, i.e. $P_n = D_\xi = \vec{W}^+ R_n \vec{W}$, where $R_n = D_\eta I + \sum_{i=1}^{J} D_i \vec{\Psi}_i^* \vec{\Psi}_i^T$ is the spatial covariance matrix of interferences and noise at the adaptive array input; I is identity matrix; "$*$" and "+" denote complex and Hermitian conjugation, respectively.

As well known [2], the maximum of the SNR $\rho = P_s / P_n$ at the array output is obtained with weight vector

$$\vec{W}_{MSNR} = c R_n^{-1} \vec{S}^*, \qquad (3)$$

where c is arbitrary complex nonzero coefficient. In this case $\rho_{\max} = \rho_0 = D_s \vec{S}^T R_n^{-1} \vec{S}^*$. In the receiving array of radio-communication systems the directions of arrival of useful signal and interferences are usually a priori unknown, and therefore matrix R_I and phasor vector $\vec{S}$ are a priori undetermined. So it is impossible to apply the solution (3) directly. In practice to adjust weight coefficients the algorithms are used that minimize the MSE between the processed signal $y(k)$ and reference signal $d(k)$:

$$J = \left\langle \left| \vec{W}^T \vec{x}(k) - d(k) \right|^2 \right\rangle = \min. \qquad (4)$$

Here angle brackets $\langle \ldots \rangle$ denote an averaging over statistical ensemble of signals $\vec{x}(k)$. If the sequence $s(k)$ is a priori known at receiver, then as the reference signal may be taken the sequence $d_0(k) = s(k)$. In this case, as seen from equation (3), the optimal with respect to minimum MSE criterion the weight vector

$$\vec{W}_0 = a_s^* R_{xx}^{-1} \vec{S}^* = a_s^* R_n^{-1} \vec{S}^* / (1 + \rho_0) \qquad (5)$$

is also optimal with respect to maximum SNR criterion. In practice often $s(k)$ is not known a priori, so the problem arise to form $d(k)$ directly in the array.

One of most known and applied in practice way to generate reference signal is nonlinear inertialess transformation of the antenna array output $d(k) = g[y(k)]$. In paper [5] was shown, that when the function $J = \left\langle |y - g(y)|^2 \right\rangle$ has a minimum at some $\vec{W} = \vec{W}_0$, this weight vector $\vec{W}_0$ also provides maximum SNR at the adaptive array output, i.e. $\vec{W}_0$ can be represented as (3) for any nonlinear transformation $d = g(y)$.

COMPUTER SIMULATION RESULTS

For adaptation of the adaptive array weight coefficients to the minimum of the quality functional (4) there was used standard gradient LMS algorithm [2,3]:

$$\vec{W}(k+1) = \vec{W}(k) + \mu \vec{x}^*(k) \left[d(k) - \vec{W}^T(k) \vec{x}(k) \right]. \qquad (6)$$

Here μ is the feedback gain. The reference signal $d(k)$ was obtained in two ways. In the first case it was done by using the formula:

$$d_1(k) = \exp(j 2\pi n / M), \ \varphi_n \le \arg y(k) \le \varphi_{n+1}, \qquad (7)$$

where $\varphi_n = \pi(2n-1)/M$, $n = \overline{0, M-1}$; $\arg y(k)$ is argument of complex number $y(k)$. In the second case it was worked out as:

$$d_2(k) = y(k) / |y(k)| = \arg y(k). \qquad (8)$$

Detailed theoretical analysis of the algorithms (6), (7) or (6), (8), shows [6] that generated reference signal $d(k)$ contains a component that is correlated with the useful signal $s(k)$. Using this component the weight vector $\vec{W}$ adapts, forming maximum of the adaptive array pattern in direction of useful signal arrival and minimum of it. in directions of interferences. This causes, in its turn, a significant suppressing interferences power at the array output and, therefore, leads to increase of correlation between $d(k)$ and $s(k)$. Besides it, nonlinear transformation of type (7) or (8) performs function of stabilizing weight coefficients in algorithm (6) preventing weight vector from becoming zero or infinite.

Computer simulation was made for the antenna array that consists of four omnidirectional sensor elements located at the vertices of a square with half-wavelength diagonals. The useful phase-manipulated signal with four positions ($M = 4$) of power $D_s = 10$ arrived from the direction of one of the diagonals of the square. The interference signal of power $D_1 = 10$ arrived at the angle $\alpha = 60°$ to the direction of useful signal arrival. In addition, complex white noise of power $D_\eta = 1$ was present in each antenna element. For adjusting weight coefficient vector there was used gradient adaptive

algorithm (6) with feedback gain $\mu = 10^{-3}$ and initial value $\vec{W}(0) = (1,1,1,1)^{\mathrm{T}}$.

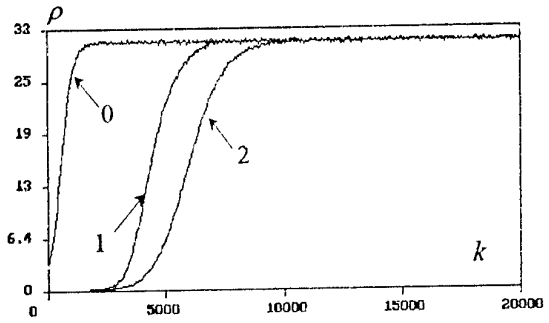


Fig. 2

Fig. 2 depicts the curves of the output SNR $\rho = P_s/P_n$ convergence to its stationary value on condition that in algorithm (6) there were applied the ideal reference signal $d_0(k) = s(k)$ (curve 0), the signals of type (7) (curve 1) and (8) (curve 2).

Results of simulation that characterize interference suppression in stationary regime are presented in Fig. 3–5. In Fig. 3, 4 the steady state patterns of array are depicted. In Fig. 5 the relationships are shown between the output SNR ρ and the input ratio of interference power to useful signal power D_I/D_s with $D_\eta = 1$, $D_s = 10$ for theoretically optimal solution (5) (curve 0) and for stationary weight vectors (6), (7) (curve 1).

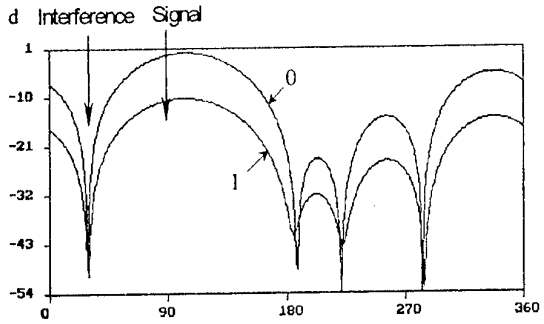


Fig. 3. The adaptive array pattern:
0 – for optimal weight vector (5); 1– for stationary optimal weight vectors of algorithms (6) or (7)

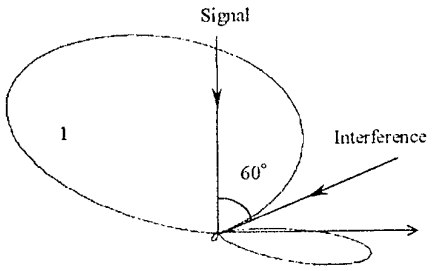


Fig. 4. The array cardioid pattern

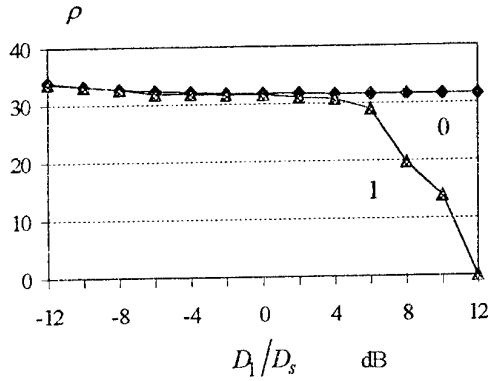


Fig. 5. The output signal-to-noise ratio

This material is based upon work supported by grants INTAS No. 96-2352, RFFI No. 96-15-96718, RFFI No. 97-02-16525.

REFERENCES

1. J. D. Shirman, V. N. Manzhos, Theory and technique of processing radar information in the background of noise, Moscow, Radio i svjaz, 1981.

2. R. A. Monzingo, T. W. Miller, Introduction to adaptive arrays, New York, John Wiley, 1980.

3. B. Widrow, S. Stearns, Adaptive signal processing, Englewood Cliffs, N.J., Prentice-Hall, 1985.

4. A. A. Pistolcors, O. S. Litvinov, Introduction to the adaptive array theory, Moscow, Nauka, 1991.

5. S. V. Ignatenko, A. A. Maltsev, A. M. Silaev, ``Analysis of Statistical Characteristics of Adaptive Antenna Array with Independent Reference-Signal Generation`` Izvestiya vuzov - Radiofizika, 1991, vol . 34, No. 10–12, pp. 1159 – 1169.

6. S. V. Ignatenko, A. A. Maltsev, A. M. Silaev, ``Analysis of Schemes of Independent Reference-Signal Generation in Adaptive Antenna Array with Phase-manipulated Signals``, Radiotekhnika i Elektronika, 1993, vol. 38, No. 5, pp. 877 – 888.

EXPERIMENTAL STUDYING OF INFLUENCE OF WEIGHT COEFFICIENTS JITTER ON OUTPUT SIGNAL OF ADAPTIVE ANTENNA ARRAY

A. A. Maltsev, S. V. Zimina

Faculty of radiophysics, Nizhny Novgorod State University
Gagarin ave. 23, 603600 Nizhny Novgorod, Russia
tel. 8(312) 65-61-53, e-mail maltsev@rf.unn.runnet.ru

INTRODUCTION

It is well known that weight coefficients jitter in adaptive arrays does not allow to obtain a theoretical limit of the quality criterion [1, 2].

Sometimes the weight vector jitter phenomena is called a control-loop noise, because it is a consequence of using noisy gradient estimates [1]. In the real-time application, it is not feasible to smooth the gradient estimates sufficiently to remove the effect of weight fluctuations because of lack of time for smoothing. Note, that the adapted weight coefficients act as integrators. So accumulation of estimating error produces a weight vector valued random walk effect. The deviation of the weight vector sets up changes in the output signal characteristics and directional pattern of the antenna [3].

Statistical analysis of weight jitter influence on the characteristics of adaptive systems is very complicated. Many authors studied weight jitter phenomena, using different assumption about statistical features of input signals and statistical dependence between input signal vector and weight vector [4 – 10].

As has been shown in papers [4, 5], for signals with uncorrelated samples the noise of weight coefficients always leads to increasing the output power in adaptive system. Conclusion about increasing of the adaptive antenna additional output power was obtained also in the works [1, 6] too, where theoretical analysis was carried out for adaptive antenna with continuous gradient algorithms.

Statistical analysis of weight vector jitter in the adaptive array with gradient algorithms for the input signals with correlated samples was carried out in papers [7–10]. There it has been shown that an influence of weight coefficients fluctuations depends on value of coefficient of correlation between samples of input signals and can cause either increasing or decreasing ("overcompensation") effect of the output signal power comparing with the case when signal is processed with an optimal, constant weight vector.

Thus weight jitter influence on adaptive array characteristics is an equilibrium condition balanced between the gradient error, samples correlation and statistical dependence between weight vector and input signals.

In this paper there are presented computer simulation results that are aimed to checking these theoretical conclusions of the article [10].

PROBLEM STATEMENT AND SOLUTION

We consider N-element narrow-band antenna array with linear constraints on the radiation pattern. Discrete gradient algorithm for the weight vector $\vec{W}$ of the adaptive array is described by N-dimension vector equation [10, 11]:

$$\vec{W}(k+1) = \mathbf{P}\{\vec{W}(k) - \mu\vec{X}^*(k)\vec{X}^T(k)\vec{W}(k)\} + \vec{W}_q \quad (1)$$

where: $\vec{X}(k) = \vec{S}(k) + \vec{\xi}(k)$ is a vector of input signal that is a sum of useful signal $\vec{S}(k)$ and interference $\vec{\xi}(k)$ ($<\vec{S}(k)>=0, <\vec{\xi}(k)>=0$); μ is coefficient of adaptation; $\vec{W}_q$ is a vector of complex weight coefficients that corresponds to "desired" radiation pattern with no interference at the environment.

In Eq. (1) $\mathbf{P} = \mathbf{I} - \mathbf{C}(\mathbf{C}^+\mathbf{C})^{-1}\mathbf{C}^+$ is a projection matrix (matrix filter in adaptive antenna control-loop), providing the multiple linear constraints on spatial characteristics of the adaptive array; $\mathbf{I}$ is an identity matrix; $\mathbf{C} \equiv [\vec{C}_1, \vec{C}_2, ..., \vec{C}_L]$ is $[N \times L]$- matrix of constraints, which columns are linear-independent vectors of constraints $\vec{C}_l$; L is number of constraints; signs *, + and T denotes operations of complex conjugate, Hermitian's conjugate and transposition, respectively.

We consider the narrow-band adaptive array with correlation matrix of the input signals of the form:

$$\mathbf{R}_{xx}(k, k+n) \equiv <\vec{X}^*(k)\vec{X}^T(k+n)> = \mathbf{R}_{xx} r^{|n|},$$

where r is a coefficient of correlation between samples of input signals, $\mathbf{R}_{xx}$ is a spatial part of the correlation matrix of input signals.

In [10] in assumption of small parameter μ and applying the theory of perturbations, there was obtained an expression for the power of output signal $<|Z|^2>_{CT} = <|\vec{W}^T(k)\vec{X}(k)|^2>_{CT}$ taking into account the weight vector jitter phenomena:

$$<|Z|^2>_{CT} = \{1 + \frac{1}{2}\mu \frac{1-3r^2}{1-r^2} Sp(\mathbf{PR}_{xx})\} <|Z|^2>_0 . (2)$$

The term $<|Z|^2>_0 = \vec{W}_{CT}^{+} \mathbf{R}_{xx} \vec{W}_{CT}$ is a power of signal in adaptive array output with constant stationary value $\vec{W}_{CT}$ of the weight vector (without jitter).

The second term in the formula (2) takes into account weight jitter phenomena. As seen from the theoretical formula, the output power depends on value of correlation coefficient r : at $r < 1/\sqrt{3}$ the power is increasing (misadjusment effect, [5]), and at $r \geq 1/\sqrt{3}$ the power is decreasing ("overcompensation" effect).

RESULTS OF COMPUTER SIMULATION

In this section we present computer simulation results that illustrate the theoretical expression (2).

There was considered seven-element narrow-band adaptive array with half-wavelength spacing, working with gradient algorithm (1) with the single linear constraint (L = 1) on the radiation pattern. In this case matrix $\mathbf{C}$ has dimension $[N \times 1]$ and it is equal to $\mathbf{C} \equiv \vec{C}_1 = \vec{S}^*$, where $\vec{S}$ is a phasor vector of a useful signal wave front:

$$\vec{S} = [1, \exp\{-j\pi \sin\theta_S\}, ..., \exp\{-j(N-1)\pi \sin\theta_S\}]^T .$$

In the considered case projection matrix had a form:

$$\mathbf{P} = \mathbf{I} - \frac{1}{N} \vec{C}_1 \vec{C}_1^{+} .$$

It was assumed, that adaptive array received useful signal and interference with correlated samples. The input signals were formed by filtering two independent Gaussian "white" noise processes. It gave a possibility to obtain different coefficients correlation between samples of input signals. Angles of arrival of the useful signal and interference were equal to $\theta_S = 0^0$; $\theta_\xi = 45^0$, respectively. The power of interference was taken 100 times as much as a power of useful signal (20 dB). Power of the internal noise ("white" gaussian noise) in each adaptive array channel was taken equal to 0.1 (-10 dB) of the useful signal power.

To verify the formula (2) we made the comparison the theoretical value of $M = \frac{1}{2}\mu \frac{1-3r^2}{1-r^2} Sp(\mathbf{PR}_{xx}) \cdot 100\%$ with corresponding empirical characteristic

$$M = \frac{<|Z|^2>_{CT} - <|Z|^2>_0}{<|Z|^2>_0} \cdot 100\% .$$

The adaptive array output signal power was measured by means of time averaging the realization of output random process. The length of the realization was chosen equal to $2 \cdot 10^3 \tau_x$, where τ_x is an auto correlation time of input signals (measured in discrete time samples). $\vec{W}_{CT}$ served as initial weight coefficients, which was obtained by means of numerical iterative solution by Gauss-Zeidel method (with accuracy $\varepsilon = 10^{-10}$) of a stationary theoretical equation.

In this investigation we are studied a transition from increasing of additional output power for signals with uncorrelated samples ("misadjasment effect", [5]) to quality different weight jitter phenomena, which leads to "overcompensation" effect. For this aim investigation of samples correlation influence of the input signals on the value of relative changing of the output power (M) was carried out.

In Fig. 1 the value of M is plotted versus the r (coefficient of correlation between input signals samples) for the case of adaptation coefficient $\mu = 10^{-3}$.

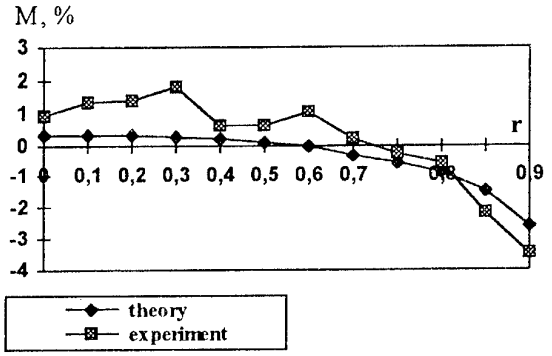


Fig. 1

From comparison of theoretical and experimental curves in the Fig. 1 it is seen, that weight vector jitter influence on the output power depends on the value of samples correlation of the input signals: at $r \leq 0.735$ the output power of the signal is greater than the "minimum" power (power that was obtained without taking into account the weight vector jitter), at $r > 0.735$ there is an "overcompensation" effect, i.e. output power becomes less than "minimum" power. Some differences between theoretical and experimental data are stipulated by limited time of averaging at the obtaining of values "overcompensation" power and presence of noise in adaptive array channels.

In Fig. 2 and Fig. 3 the theoretical and empirical values of M versus μ are plotted for two different values of r. From the Fig. 2 it is seen, that in the case of high samples correlation of the input signals (r = 0.9) there is rather a good agreement of the theoretical and experimental results. Note, that "overcompensation" effect reduces weight jitter. Because of this, theory and computer simulation results coincide, when μ is rather large. In the case of uncorrelated samples (r = 0, Fig. 3)

the additional output power increases. It leads to increasing weight jitter intensity and the emergence of divergence between theory and experiment. It is necessary to stress, that formula (2) was obtained in the first Born's approximation. When μ is not small, Born's approximation is not applicable and it is necessary to use high order approximations.

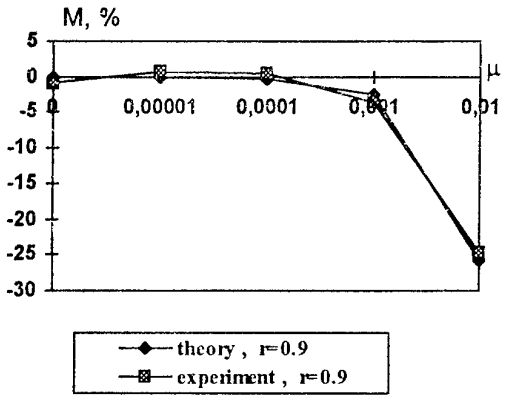


Fig. 2

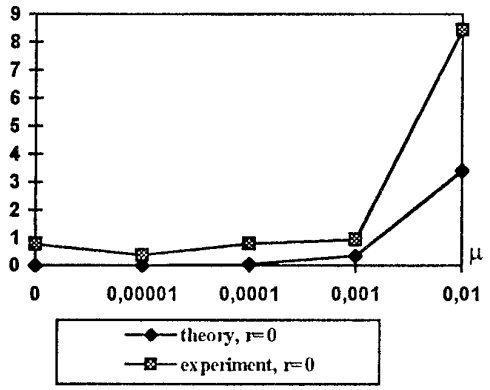


Fig. 3

The research carried out has confirmed outcomes of the theoretical analysis and has shown, that in adaptive array with gradient algorithms the weight coefficients jitter can lead to increasing the output signal power, as well as to its decreasing.

The work was carried out under the support of the Russian foundation of fundamental research (RFFI grants No. 97-02-16525, No. 96-15-96718) and International Association for the promotion of cooperation with the scientists from the New Independent States of the former Soviet Union (INTAS grant No. 96-2352).

REFERENCES

1. L. E. Brennan, E. L. Pugh, I. S. Reed, "Control - loop noise in adaptive array antennas", *IEEE Trans.*, 1971, vol. AES-7, No. 2, pp. 254-262.
2. B. Widrow, J. M. McCool, "A comparison of adaptive algorithms based on the methods of steepest descent and random search", *IEEE Trans.*, 1976, vol. AP - 24, pp. 615 - 637.
3. J. E. Hudson, *Adaptive array principles*, London, IEE, 1991.
4. B. Widrow et. al., "Stationary and non stationary learning characteristics of the LMS adaptive filter", *Proc. IEEE*, 1976, vol. 64, No. 8, pp. 1151 - 1162.
5. B. Widrow, S. Stearns, *Adaptive signal processing*, Englewood Cliffs, N. J., Prentice-Hall, 1985.
6. V. V. Fedinin, "Statistical analysis of multichannel adaptive system with correlation loops", *Radiotekhnika i Elektronika*, 1982, vol. 27, No. 8, pp. 1548-1553.
7. A. A. Mal'tsev, I. E. Pozumentov, "Statistical characteristics of adaptive antenna arrays with constraints", *Izvestiya. Vuzov - Radiofizika*, 1981, vol. 24, No. 5, pp. 577 - 585.
8. Y. L. Su, T. J. Shan, B. Widrow, "Parallel spatial processing: a cure for signal cancellation in adaptive arrays", *IEEE Trans.*, 1986, vol. AP -34, No. 3, pp. 347 - 355.
9. A. A. Mal'tsev, "Analysis of characteristics of adaptive antenna arrays at account rapid parameters fluctuations", *Izvestiya vuzov - Radiofizika*, 1987, vol. 30, No. 8, pp. 1013 - 1022.
10. S. V. Ignatenko, A. A. Maltsev, "Adaptive antenna arrays statistical characteristics in processing of discrete signals with correlated samples", *Izvestiya vuzov - Radiofizika*, 1994, vol. 37, No. 12, pp. 1532 - 1545.
11. R. A. Monzingo, T. W. Miller, *Introduction to adaptive arrays*, New York, John Wiley, 1980.

A ROBUST ADAPTIVE ANTENNA ARRAY FOR SIGNALS SEPARATION

L. A. Marchuk, O. A. Nokhrin, A. N. Savelyev, L. A. Titarenko*

Military telecommunication university,
Tikhoretsky prospect 3, 194064 Saint-Petersburg, Russia, Tel: 007/8125569425
* Kharkov State University of Radio Electronics,
Kharkov, Lenin avenue, 14, 310726, Ukraine, Tel 038/0572409385

ABSTRACT

A method of synthesis of adaptive antennas arrays (AAA) control algorithms, ensuring separation of independent non-Gaussian signals under conditions of a priory unknown spacing of signal sources and characteristics of antenna array (AA), is proposed. Algorithms have a low sensitivity to calculation errors, random fluctuations of amplitudes and phases of signals in the outputs of array elements and spatial evolutions of the object, were AAA is located.

INTRODUCTION

AAAs, providing separation of the signals with coinciding (close) carrier frequencies and varying with direction of arrival (DOA) may be used for the solution of many practical problems. In particular, in mobile telecommunication systems such AAAs enable one to realize a multiple access with a spatial separation of channels, supression of co-channel interference, etc. However, there are several serious problems of adaptive spatial separation (ASS) application in practice. The main one is connected with the development of blind ASS algorithms not employing model assumption about DOA of signals, AA structure and characteristics.

The problem of blind ASS algorithms synthesis is the topic of discussion in many publications, such as [1–3]. Some of them are devoted to the special case of two-element AA, in the others restrictions are imposed on time structure of signals or AA characteristics. In addition, known non-parametric ASS algorithms are extra sensitive to the number of samples, computation errors and other implementation restrictions.

In the paper rather general criterion of separation is proposed and synthesized blind ASS algorithms are presented, ensuring signal/noise+interference ratio (SINR) in the given vicinity of potentially achievable values under conditions of various implementation restrictions. We used only weak assumptions on independence and non-Gausian nature of input signals.

PROBLEM FORMULATION

Consider M-elemental AAA of an arbitrary configuration receiving narrowband in space and time context signals against a Gaussian noise background. Therefore, disregarding mutual coupling effect of antennas, we shall present signals and noise in the outputs of antenna elements (AE) as M-dimensional vector

$$X(t) = \mathbf{D}\, S_L(t) + N(t), \qquad (1)$$

where $S_L(t) = [s_1(t)\ s_2(t)\ \dots\ s_L(t)]^T$ is L-dimensional vector; $s_i(t)$ is a complex envelope of the i-th source signal; $\mathbf{D} = [V_1\ V_2\ \dots V_L]$ is the (N×L) matrix; $V_i = [a_{1i}\exp(j\varphi_{1i})\ a_{2i}\exp(j\phi_{2i})\dots a_{Mi}\exp(j\phi_{Mi})]^T$; a_{ki} is a normalized complex gain of the k-th AE in the DOA of the i-th signal; ϕ_{ki} is a phase shift of the i-th signal at the k-th AE due to the space structure of AA relatively it is phase center point; $N(t)=[n_1(t)\ \dots\ n_M(t)]^T$ is M-dimensional vector of thermal noise; T denotes the transposition.

Assume that signals $s_1(t)$, ..., $s_L(t)$, emitted by spatial dispersed sources, are independent non-Gaussian random processes with symmetrical probability density functions, and the elements of noise vector $n_i(t)$, $i = \overline{1,L}$, are joint Gaussian centralized random processes. Besides, we shall consider DOA of the signals to be a priori unknown, and vectors V_i do not allow scalar paramertization such as $V(\theta_i)$, where θ_i is DOA of the i-th signal.

Taking into account these restrictions, we shall decompose the problem of algorithms synthesis into two particular tasks:

Finding estimations $\hat{V}_i$ of each vector V_i, $i = \overline{1,L}$.

Constructing on the basis of $\hat{V}_i$ estimations of separating weight vectors (WV) satisfying condition

$$\eta(W_i) \geq \eta_{0i} - \Delta\eta_i \ \forall\, V_i \in \mathbf{G}_{vi},\ i = \overline{1,L} \qquad (2)$$

where W_i is SINR in the i-th output of AAA; η_{0i} is potentially achievable SINR value; $\Delta\eta_i$ is the admissible decrease of SINR; $\mathbf{G}_{vi} = \left\{ \hat{V}_i \,\middle|\, \left\| \hat{V}_i - V_i \right\| \leq \delta_{vi} \right\}$; $\delta_{vi} \in R_+$; $\|\cdot\|$ denotes the Hermitian norm.

SYNTHESIS OF ALGORITHMS

Using (2), we shall formalize the first partial task as the problem of estimating the matrix **D**

$$\hat{\mathbf{D}} = f\{X(t)\} \qquad (3)$$

where $\hat{\mathbf{D}}$ is the estimate of $\mathbf{D}$; $X(t)$ is the input vector; $f\{\cdot\}$ is some operator, ensuring fulfilment of the condition $\mathbf{D}^{+}\mathbf{D} = \mathbf{TP}$, where $\mathbf{T}$ is a diagonal matrix, $\mathbf{P}$ is the permutation matrix; "+" denotes the pseudo-inversion.

It is easy to show that the energetic criteria, characteristic for correlation theory, can not be used for the solution of the problem (3). Actually, in correlation approach any estimate can be obtained as a result of correlation matrix $\mathbf{R}_{XX} = \mathrm{E}\{X(t)X(t)^{\mathrm{H}}\}$ analysis. where $\mathrm{E}\{\cdot\}$ is the mean, H denotes Hermitian conjugation. This matrix always can be reduced to a diagonal form, for instance $\mathbf{B}\mathbf{R}_{XX}\mathbf{B}^{\mathrm{H}} = \mathbf{T}$, where diagonalizing matrix $\mathbf{B}$ can be unitary. Consequently, $\mathbf{R}_{XX} = \mathbf{B}^{-1}\mathbf{T}\mathbf{B}$, $\mathbf{R}_{XX}^{-1} = \mathbf{B}^{\mathrm{H}}\mathbf{T}^{-1/2}\mathbf{T}^{-1/2}\mathbf{B}$, i.e. with the accuracy up to a diagonal matrix $\mathbf{T}^{-1/2}$ the diagonalizing matrix $\mathbf{B}$ is the square root of $\mathbf{R}_{XX}$, and, as it is known decomposition $\mathbf{R}_{XX}^{-1} = \mathbf{R}^{-1/2}\mathbf{R}^{-1/2}$ is not the single one [4].

Therefore, we shall denote $y_i = W_i^{\mathrm{H}}X(t), i = \overline{1,L}$ and use the theorem:

Theorem 1. The necessary condition of mutual independence of signals in the output of AAA is the equality to zero of all the cumulant functions, including more than one variable (mutual cumulant functions) of vector $Y = \left[y_i \quad \dots \quad y_L\right]^{\mathrm{T}}$.

The proof of theorem 1 is based on decomposition of natural logarithms of characteristic functions $\Phi_Y(V) = \mathrm{E}\left\{\exp\left(jV^{\mathrm{H}}Y\right)\right\}$ $\Phi_{y_i}(U_i) = \mathrm{E}\left\{\exp(jU_i^{*}y_i)\right\}$, (where "*" denotes the complex conjugation) into Taylor series under condition of coefficients equality with corresponding powers.

Note, that since according to the condition, the input signals $s_i(t)$, $i = \overline{1,L}$, are mutually independent, so theorem 1 indeed determines the necessary conditions of the (3) solution. However, in practice we can not minimize all mutual cumulant functions of vector Y. So, taking into account the assumption of the symmetry of input signals probability density functions, we shall restrict ourselves by the minimum even value of cumulant function order and present the condition of matrix $\hat{\mathbf{D}}$ finding as follows

$$\mathrm{cum}\left(y_i, y_j^{*}, y_k, y_l^{*}\right) = 0, \quad i, j, k, l = \overline{1,L} \qquad (4)$$

where $\mathrm{cum}(\cdot,\cdot,\cdot,\cdot)$ is a cumulant function of 4-th order; $(i, j, k, l) \notin \{i, j, k, l \,|\, i = j = k = l\}$; $y_i = W_i^{\mathrm{H}}X(t)$; W_i is the i-th column of matrix $\mathbf{D}^{+}$.

Replacing cumulant functions with corresponding estimations and solving the system of non-linear equations (4), we can estimate the elements of $\mathbf{D}^{+}$ (a separating matrix). In this case matrix $\hat{\mathbf{D}}$ can be defined as pseudo-inverse one $\hat{\mathbf{D}}^{+}$ At the same time on the basis of [1] the solution of system of non-linear equations can be replaced with joint diagonalization of appropriately formed cumulant matrices. It is necessary to note, that such a substitution directly determines the elements of matrix $\hat{\mathbf{D}}$ (the mixing matrix).

Starting discussion of the second partial task we note, that the finding of separating WV is possible by various algorithms, for example, by projection algorithms [4]

$$\hat{W}_{0i} = \hat{\mathbf{P}}_i\hat{V}_i, \quad i = \overline{1,L} \qquad (5)$$

where $\hat{\mathbf{P}}_i = \hat{\mathbf{B}}_i\left(\hat{\mathbf{B}}_i^{\mathrm{H}}\hat{\mathbf{B}}_i\right)^{-1}\hat{\mathbf{B}}_i^{\mathrm{H}}$;

$$\hat{\mathbf{B}}_i = \left[\hat{V}_1 \quad \hat{V}_2 \quad \dots \quad \hat{V}_{i-1} \quad \hat{V}_{i+1} \quad \dots \quad \hat{V}_1\right].$$

But algorithm (5) just as the one realizing criterium of SINR maximum $\hat{W}_i = \beta\hat{\mathbf{R}}_{XX}^{-1}\hat{V}_i$ where β is a normalizing coefficient, $\hat{\mathbf{R}}_{XX}$ is the estimate of correlation matrix $\mathbf{R}_{XX}$, does not ensure satisfying of robustness condition.

However, it is easy to show, that in case of projection WV (5) the limiting relation is valid

$$\lim_{\alpha\to o}\hat{W}_{0i} = \lim_{\alpha\to o} Q_{\mathrm{N}}\left(\lambda_{\mathrm{N}}\left(\hat{\mathbf{R}}_{ii} - \lambda\left(\hat{\mathbf{R}}_{\Sigma i} + \alpha\mathbf{I}\right)\right)\right), \qquad (6)$$

where $\hat{\mathbf{R}}_{\Sigma i} = \sum_{l=1, j\neq i}^{L}\hat{\mathbf{R}}_{jj}$; $\hat{\mathbf{R}}_{jj} = \hat{V}_j\hat{V}_j^{\mathrm{H}}$; $Q_{\mathrm{N}}\left(\lambda_{\mathrm{N}}(\cdot)\right)$ - eigenvector, corresponding to maximum eigenvalue λ_{N} of matrix pencil $\hat{\mathbf{R}}_{ii} - \lambda\left(\hat{\mathbf{R}}_{\Sigma i} + \alpha\mathbf{I}\right)$; $\mathbf{I}$ is a unit matrix; $\alpha \in \mathrm{R}_{+}$.

Taking into account (6) by analogy with [5] we shall present the robust algorithm of ASS as

$$W_i = Q\left(\lambda_{\max}\left(F_1\left\{\hat{\mathbf{R}}_{ii} - \lambda\hat{\mathbf{R}}_{\Sigma i}\right\}\right)\right), \quad i = \overline{1,L}, \qquad (7)$$

where $F_1\{\cdot\}: \mathbf{TL}_i(\mathrm{C}) \to \mathbf{SL}_i(\mathrm{C})$ is some contracting operator; $\mathbf{TL}_i(\mathrm{C}) = \left\{\hat{\mathbf{R}}_{ii} - \lambda\hat{\mathbf{R}}_{\Sigma i} \,\middle|\, \hat{\mathbf{R}}_{ii} \in \mathbf{G}_{vi}, \lambda \in \mathbf{R}_{+}\right\}$;
$\mathbf{SL}_i(\mathrm{C}) = \left\{\mathbf{B} \in \mathbf{RL}_{\mathrm{N}}(C) \,\middle|\, \left|\angle\left(Q(\lambda_{\max}(\mathbf{B})), W_{0i}\right)\right| \le \gamma_{0i}\right\}$;

$\angle(\cdot,\cdot)$ is a generalized angle between two vectors in complex Euclidian space; $\mathbf{RL}_{\mathrm{N}}(C)$ is a set of Hermitian non-negatively defined matrices; $Q\left(\lambda_{\max}(\mathbf{B})\right)$ is an eigenvector, corresponding to maximum eigenvalue of matrix $\mathbf{B}$; $\gamma_{0i} \in \mathrm{R}_{+}$.

Replacing the task of contracting operator synthesis with the one of finding this operator's image in subspace $SL_i(C)$, $\|\mathbf{B}\|_F$, where $\|\mathbf{B}\|_F$ denotes Frobenius matrix norm, and using results of [6], after not difficult considerations we conclude that algorithm satisfying condition (1) can be presented as

$$W_i = Q\left(\lambda_{max}\left(\lambda_i \mathbf{A}_i - \sum_{j=1, j\neq i}^{L} \lambda_j \mathbf{A}_j\right)\right), \quad i = \overline{1,L}, \qquad (8)$$

where $\left(\mathbf{A}_j\right)_{kk} = \left(\hat{V}_j \hat{V}_j^H\right)_{kk}$; $\left(\mathbf{A}_j\right)_{kl} = \rho_{kl}\left(\hat{V}_j \hat{V}_j^H\right)_{kl}$; $\rho_{kl} = \rho_{lk} \in]0 \ldots 1]$; $\lambda_j \in R_+$.

Eigenvector $Q\left(\lambda_{max}(\cdot)\right)$ can be found by traditional methods of linear algebra (Jakobi's, Hausholder's etc.). At the same time, algorithms (8) can be presented as globally converging recurrent procedures

$$W_i(k+1) = P_r\left\{ W_i(k) + \mu_k\left(\lambda_i \mathbf{A} - \sum_{j=1, j=i}^{L} \lambda_j \mathbf{A_j}\right) W_i(k)\right\}, \qquad (9)$$

where μ_k is a step constant; $P_r\{\cdot\}$ is a projector to unitary hypersphere. Matrices $\mathbf{A}_j$ and scalars λ_j included in algorithms (8), (9) are chosen on the basis of a minimax approach (maximum possible value of estimation error and maximum value of interference-to-noise ratio).

MODELING RESULTS

For illustration of robust algorithms ASS efficiency in Fig.1 experimental dependencies of output SINR on the input signal-noise ratio are shown. When modeling we assumed that M=5, L=3. Taking into account an evident AAA symmetry, we restrict ourselves by examining only one AAA output (signal $s_1(t)$ is the one to be found, $s_2(t)$ and $s_3(t)$ are interferences). Moreover, we used the following assumptions on signal-interference conditions and AA characteristics: - AA is linear and equidistant, an inter-element distance is $d=m_1/2$ (m_1 is a wavelength of $s_1(t)$); - AEs are identical and non-interacting; - DOAs of the signals $s_1(t)$, $s_2(t)$ and $s_3(t)$ are defined relatively to a normal to AA, $\theta_1 = 30°$, $\theta_2 = 50°, \theta_3 = 85°$; carrier frequencies of all signals are equal; - input SINRs are $10\lg(P_2/\sigma_n^2) = 20$ dB (P_1, P_2 are powers of the second and the third signals, σ_n^2 is a dispersion of Gaussian noise.

Vectors, characterizing signals spatial structure were estimated by solving a system of nonlinear equations (4) with the following errors: $\delta_{v1} = \left\| \hat{V}_1 - V_1 \right\| \le 1.293$, $\left\| \hat{V}_2 - V_2 \right\| \le 0.997$, $\left\| \hat{V}_3 - V_3 \right\| \le 0.196$. Elements of matrices $\mathbf{A}_1$, $\mathbf{A}_2$, $\mathbf{A}_3$ and coefficients $\lambda_1, \lambda_2, \lambda_3$ were defined with

$$\Delta\eta_1 = 0.9 \text{ dB}; \ \delta_{v\,max} = 1.3;$$
$$\max(10\lg(P_i/\sigma_n^2)) = 40 \text{ dB}.$$

The dependence 1 (Fig. 1) corresponds to algorithm (9) and dependence 2 - to algorithm (5). For comparison in Fig. 1 the potentially achievable value of output SINR (dependence 3) is also shown. The dependencies (Fig. 1) show, that efficiency of ASS, realized according to algorithm (9) is close to potentially achievable in rather wide class of signal-interference conditions and is weakly dependent on input SINR.

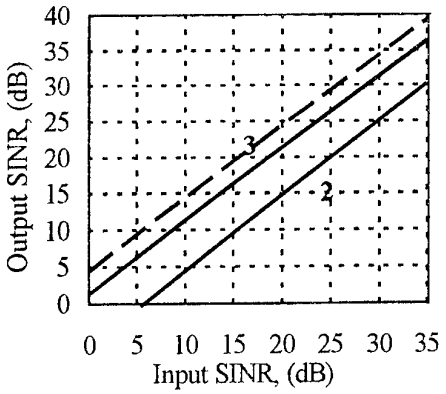


Fig. 1

REFERENCES

1. Cardoso J.F., Souloumias A. "Blind beamforming for non-Gaussian signals", IEEE Proceedings - F, Vol. 140, № 6, pp. 362-377, December, 1993.
2. Yellin D., Weinstein E. "Multichannel signal separation: methods and analysis", IEEE Trans, Signal Processing, Vol. 44, № 1, pp. 106-118, January 1996.
3. Marchuk L.A., Venskauskas K.K, Ivanov V.A. "A polynomial-based approach to design of a small adaptive antenna array for blind separation of sources", in Proceedings 1998 AP-S International symposium and USNC/URSI national radio science meeting, July 21-26, 1998, Atlanta, USA.
4. Ph. R. Gantmakher, "Matrix theory", Science, Moscow, 1988.
5. Marchuk L.A., Efimov A.V "Algorithms of adaptive space separation of signals and interferences." Radio Electronics and Communications systems." Izvestia VUZ Radioelectronika, vol. 39, № 6, pp. 38-46, 1996.
6. Marchuk L.A., Giniyatullin N.F., Venskauskas K.K. "A novel approach to robust sensor array processing", in Proceedings 1997 IEEE AP-S International symposium and URSI radio science meeting, July 13-18, 1997, Canada, Montreal.

ADAPTIVE ANTENNA ARRAYS WITH NONREDUNDANT APERTURES OF THE MILLS CROSS TYPE

Y. N. Sedyshev, P. Y. Sedyshev, R. A. Karnaukh

Kharkov Military University
310043, Kharkov, sg. Svobody - 6, tel./fax (38) 0572 – 430740

The block diagrams of multiplicative antennas with nonredundant apertures of the Mills cross type using a combination of autocompensation of interference and self-focusing modes are considered. The possibilities of application of such antennas in the direction finding of a radiation source (RS) are analyzed. It is shown that the combination of two mutually perpendicular adaptive linear antenna arrays can provide a correct evaluation of two angular coordinates.

Recently in the theory and engineering of antenna arrays (AAs), there have appeared and are actively advancing the adaptive methods of signal processing that enable one to increase essentially the angular resolution of the non-correlated radiation sources (RS) in comparison with traditional methods of scanning by an AA beam and output power evaluation. By using these methods which are frequently called the "superresolution" methods (Capon's method, thermal noise, MUSIC, Root-music etc.), it is possible to determine angular coordinates of RS in one plane β (ε) with high accuracy. For measuring the second angular coordinate of each RS, a highly directive scanning antenna can be used, but it requires much time, survey coordination, and does not solve the problem of a joint measurement of two angular coordinates because of a high probability of false bearings.

Two main principles of constructing two-dimensional direction finder with false bearing elimination on the basis of linear adaptive AAs of the Mills cross type are analyzed.

The Mills cross is a system with empty aperture. Here, the fact that, in a passive system, the pattern is determined not by the aperture itself but by the autocorrelation of subapertures is used more completely. The Mills cross represents an example of nonredundant apertures realization in which the number of degrees of freedom is equal to $N^2 - N$, where N is the number of receiving elements [2]. This is of great importance for adaptive systems of aperture processing. Taking into account that for optimum aperture processing of signals from each RS at the back-ground of others it is necessary tj have their number not greater than N – 1 (N – 1 is the number degrees of freedom of antenna array), the advantage of application of antenna systems of the Mills cross type becomes obvious.

It is also known that the Mills cross pattern is equivalent to a product of patterns of antenna arrays forming the cross by the voltage, i. e. :

$$P_{output} \approx F_1(\beta,\varepsilon)\cdot F_2^*(\beta,\varepsilon) + F_1^*(\beta,\varepsilon)\cdot F_2(\beta,\varepsilon), \quad (1)$$

where $F_1(\beta,\varepsilon)$ and $F_2(\beta,\varepsilon)$ are the pattern's of arrays forming the Mills cross; * denotes the operation of the complex conjugation.

In principle cross-shaped antennas can achieved the same accuracy of measurement as a plane one of the same dimensions [1].

In the first case, the principle of constructing a two-dimensional direction finder on the basis of multiplication of signals by an adaptive linear AA with Capon's "superresolution" algorithm in the azimuthal plane and multibeam dynamic antenna in the elevation plane in correlation identification of two-dimensional bearings is proposed.

The simplified block diagram of such a direction finder is given in Fig. 1. In Fig. 1, the new notation is introduced: DAA is the dynamic antenna array; LAAA is the linear adaptive AA with processing unit ensuring memorizing and restoring optimum azimuth gain-phase distribution (APD) on each RS by means of ranging their power; CC is the computer of coordinates; Ec is the electronic commutator; FP is the Fourier-processor; AD is the adaptive detector; CSEFB is the correlation system of elimination of false bearings; WR is the weight regulator.

In briefly, we note the main moment in the operation of such a direction finder. The azimuth channel produces the information on all RS, and the priorities of their servicing. Then we find the weight coefficients $W_i(\beta_i)$ and $W_j(\beta_j)$ corresponding to the pattern values of all RS in azimuthal plane, where

$$W_i(\beta_i) = \hat{\Phi}^{-1}\cdot S_i(\beta_i), \quad (2)$$

$$W_j(\beta_j) = \hat{\Phi}^{-1}\cdot S_j(\beta_j), \quad (3)$$

where $Si(\beta_i)$ the vector of expected signals of the interfering ith RS from the ith azimuth value; S_j (β_j) is the vector of expected signals of the jth RS under bearing from the jth azimuth value, $\hat{\Phi}^{-1}$ is the estimate of

reciprocal correlation matrix of interference in the azimuth direction-finding channel.

It can be shown that in such a system the power at the correlator output is equal:

$$P_{output} \approx \sum_{i=1}^{m} \rho_i \,, \qquad (4)$$

where ρ_i is the cross correlation coefficient.

The expression (4) has global maxima in joint evaluation of angular coordinates. The excess of the threshold corresponding to the level of summary signal of the CSEFB channel at the expense of using a stringent limited can serve as a criterion of identification.

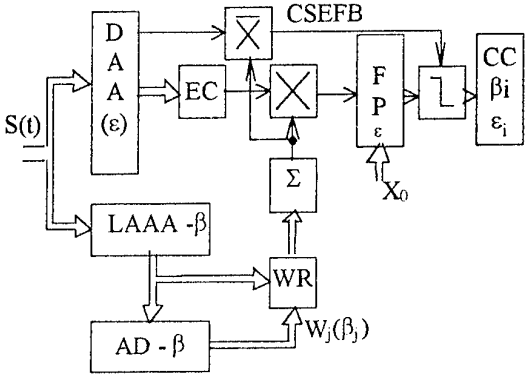


Fig. 1. Phase-locked AA of a two-dimensional direction finder with the correlation identification

The expression for the signal intensities of the RS under bearing at the background of all interfering RSs at the threshold device output has the form like follows:

$$P_{out.cor.} = \frac{H_j^2\left[F_k^2(\varepsilon_j) - 1/N^2\right]F_j^2(\beta_j)}{\sum_{i=1}^{m} H_i\left[F_k^2(\varepsilon_i)+1\right]\sum_{i=1}^{m} H_i F_j^2(\beta_j)}, \qquad (5)$$

where $F_k^2(\varepsilon_i)$ is the squared pattern of dynamic AA; k is the number corresponding to the direction of the pattern maximum; H_i is the interference/noise ratio (of the interfering RS); H_j is the signal/noise ratio (SNR) (of the RS under bearing); N is the number of antenna array elements. Thus the background level hindering the identification on each interfering RS is determined by the formula:

$$P_{out.background} = \frac{H_i^2\left[F_k^2(\varepsilon_i) - 1/N^2\right]F_j^2(\beta_j)}{\sum_{i=1}^{m} H_i^2\left[F_k^2(\varepsilon_i)+1\right]\sum_{i=1}^{m} H_i F_j^2(\beta_i)}, \qquad (6)$$

The relations (5), (6) enable one to estimate the identification efficiency at any energy relation in channels. The application of such a scheme enable one to determine unambiguously two-dimensional bearings on RS but this requires a correlation system of elimination of false bearing (CSEFB).

Consider an antenna of the Mills cross type, which consists of two linear adaptive AAs normal to each other. The field polarization is the same for both AAs. In such a system, it is possible to define two angular coordinates of RS if one of AA's of the cross (the azimuthal one) evaluates the RS azimuth on the basis of one of the algorithms of "superresolution" type and the elevation linear AA is a self-focusing antenna array (SFAA).

The block diagram of such a system is given in Fig. 2. It's operation consists in the following. The azimuthal channel produces information on the position of all RSs and their priorities. The most powerful RS has the highest priority. Further, output signal of the azimuthal AA is fed to the main channel of the elevation SFAA as a reference signal $S_\beta(t)$. Any signal received by the elements of elevation SFAA passes through the corresponding amplifiers K1,..., Kn (with controlled amplification factors and phases) and then enters the summator forming the output signal of the array $S_\varepsilon(t)$. Further the output signal of the elevation AA $S_\varepsilon(t)$ is compared to the reference one $S_\beta(t)$, and the error signal $\Delta(t)$ is fed to the input of the feedback system: the device of the weight coefficients control (DWCC), regulating the complex weights Kn. Any received signal which is not presented in $S_\beta(t)$ is perceived as an error signal and the feedback system regulates the weight coefficients to eliminate it from the output signal. As a result the antenna pattern maximum is determined in the direction of reference signal, and the pattern zeroes in other directions. The elevation adaptive AA is focused at the signal of the azimuthal channel. Removing this signal in a steady — state mode of APD at the DWCC output and subjecting it to a further processing in the Fourier-processor (FP) and CC (computer of coordinates), we can obtain the RS elevation angle value from the given azimuth direction. The advantage of such a system is that it does not requite using a special scheme for measurement identification. The measurement coordination occurs automatically at the expense of elevation SFAA properties.

SNR at the output is determined by the following expression:

$$Q = \frac{P_s}{P_n} = \frac{\nu_s \cdot N \cdot F^2(u)}{1 + \nu_s \cdot N \cdot (2 + \nu_s \cdot N)\cdot\left[1 - F^2(u)\right]}, \qquad (7)$$

where ν_s is the signal power received by a signal element and expressed through the power of its own noise; $F(u)$ is the normalized antenna pattern; N is the number of elements; $u = \frac{2\pi}{\lambda} d \sin\vartheta$.

In the adaptation, the pattern width at half-power reduces by a factor of 0.81 $\nu_s N$, i.e. in proportion to the

received signal power. The more powerful signal, the greater the narrowing of main maximum. The main maximum sharpening increases the accuracy of determining the signal arrival direction, i.e. the array direction-finding ability. At large values of N, we can suppose, with sufficient accuracy, $F(u)=\frac{\sin 0.5Nu}{N\sin(0.5u)}\approx\frac{\sin x}{x}$, $x=\frac{Nu}{2}$ and the zone width where the signal power exceeds the noise power $x\approx\sqrt{3/(3+vN)}$. For comparison, $x\approx 1.40$ in the case of non-adaptive pattern [3].

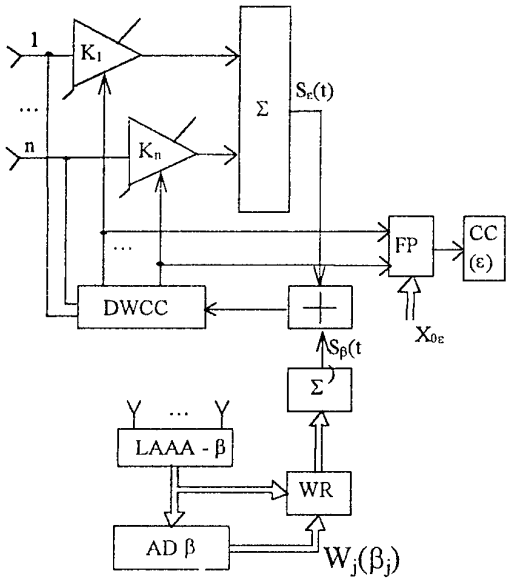


Fig. 2. PAA of a two-dimensional direction finder with a self-focusing

Consider now the possibility of application of an antenna of the Mills cross type in multipositional system.

The usage, in one of the receiving stations of a multipositional antenna system of the Mills cross type consisting of two SFAAs enable one to implement joint measurement of two coordinates and to assure automatical survey coordination in the angular coordinates by diversity receiving station. In Fig. 3, a diagram in which every subsystem of the Mills cross is SFAA is represented. As a reference signal for the cross subarrays, a LAAA signal from one of the receiving stations evaluating the azimuth of all RS using one of the "superresolution" algorithms, their ranging and assuring the memorizing and restoration of the optimum azimuth APD on each RS under bearing is used. The constant delays by $2\tau_b$ are introduced in order to compensate the delay. The cross SFAA is focused at the signal of RS for which the delay is compensated in the line of changing delay and it is extracted at simultaneous suppression of the interfering RS oscillation. Thus, an automatic coordination of space survey is realized. In the direction of this RS the pattern maximum is determined and in the other interfering RSs, the pattern gaps are formed. By removing them in the steady-state of APD from the subarrays and subjecting to further processing in FP and CC, it is possible to determine the angular coordinates of the selected RS (ε,β) from the removed unit (RU). Besides, if in one of the processing units the oscillation difference is to be measured, i. e. Use a goniometrical-difference-distance measuring technique, it is possible to calculate the RS coordinates, and a redundant measurements presence will result in a higher accuracy of coordinate determination [4].

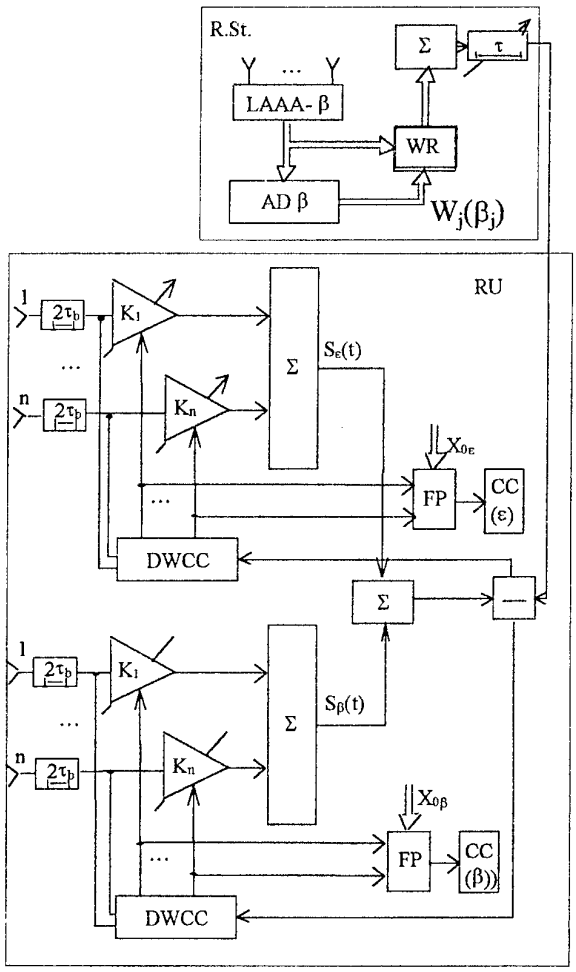


Fig. 3. Multidimensional direction finder in a diversity reception system

In Fig. 4, the results of PAA operation simulation of two-dimensional direction finder with CSEFB are presented. From Fig. 4, it is seen that when changing the azimuthal position of the RS under bearing (in the left part of the graph) we have a steady estimate of its angular position. At coincidence of azimuth directions of the RS under bearing and the interfering one, a coordinate measurement of two RSs is assured. The model is developed for two AAs consisting of 8 elements and two RSs.

The results of experimental investigations are presented in Fig. 5. Here a new notation is introduced: A is the initial pattern of linear adaptive AA of the Mills cross type; B is the pattern restored in APD on the basis of the Caypon algorithm; C is the focused pattern of linear adaptive AA. The arrows show the directions to the interfering RSs. The double arrows show the directions to RS under bearing. RS power values (counting from left to right) are respectively: 20, 10, 20, 10, 10, 20 dB. As it is seen from Fig. 5, the maxima of restored and focused patterns have one global maximum in the direction to RS under bearing while in the direction of the other five interfering RSs the pattern zeroes (gaps) are formed.

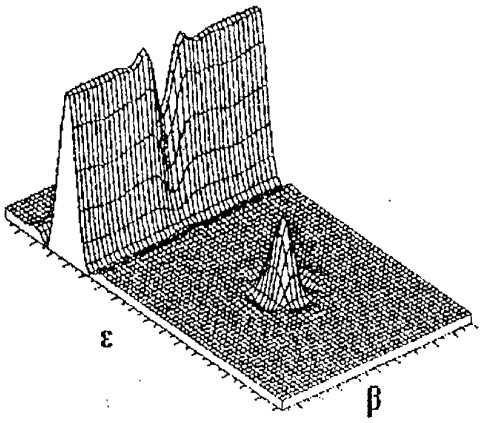


Fig. 4

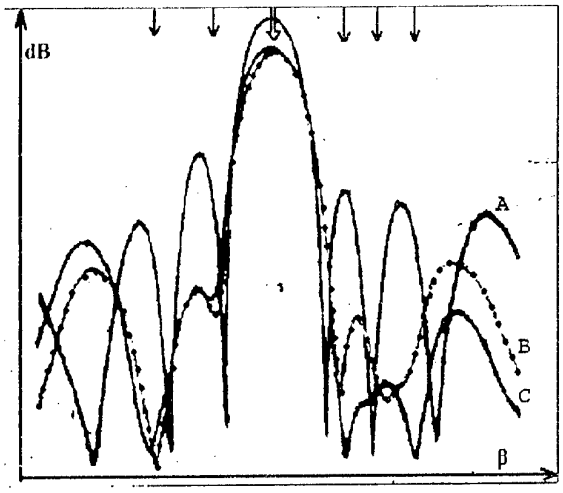


Fig. 5

Thus, the construction of two-dimensional direction finders based on adaptive AAs with nonredundant apertures of the Mills cross type ensures one-to-one measurement of the RS angular coordinates. The use of SFAA in the Mills cross structure in the case of a multipositional reception enable one to determine unambiguously the angular coordinates of RS in automatic space survey.

REFERENCES

1. Antennas: (State-of-the-art and Problems). Edited by L.D. Bahrah, D.I. Voskresensky.-M.: Soviet Radio, 1979.
2. V.V. Karavayev, V.V. Sazonov. Statistic theory of passive radars. M.: Radio i Svyaz, 1986.
3. A.A. Pistolkors, O.S. Litvinov. Introduction to the Theory of Adaptive Arrays. - M.: Nauka, 1991.
4. V.S. Chernyak. Multipositional Radars - M.: Radio i Svyaz, 1993.

METHOD AND ALGORITHMS OF PAA RP SYNTHESIS ADAPTIVE TO ITS ELEMENTS FAILURE

Y. S. Shifrin, U. R. Liepin*, L. V. Golovina*

Kharkov State Technical University of Radioelectronics, Lenin Av., 14, Kharkov 310166,
Ukraine, Tel.(38) 0572 409430, Fax.: (38) 0572 409113, E-mail: shifrin@kture. kharkov. ua;
*Kharkov Military University, Svoboda Sq.,6, Kharkov 310043, Ukraine, Tel.: (38) 0572 404141

Algorithms of PAA adaptation for technical conditions and algorithms of self focusing under failure of a part of the beam control system (BCS) executive elements or under non-excitation of a number of channels become low-efficient. The reason is that the restoration of the calculated (non-disturbed) amplitude-phase distribution (APD) in the rest of the controlled channels doesn't mean achieving the aims of adaptation for the integral criteria, for example, scattering coefficient minimum.

In the case, when the array has uncontrolled or non-excited channels, the APD synthesis problem is to be solved for a remained serviceable part of the array in order to provide significantly more improved values of the chosen array qualitative indices than of the array with failures under calculated APD.

The aim of this paper is to consider the method and algorithms of such a APD synthesis problem solution in the real time.

The idea of the offered method consists in the following. Within the regime of the functional control of the radio technical system (RTS) with PAA one of the diagnostics algorithms defines non-excited and uncontrolled channels. This information is stored and used for PAA modeling and APD in it under the action of the standard control signals on the BCS executive elements calculated for the array phasing in the given direction. The adaptive synthesis, i.e. the APD adaptation for the failures appeared in the array (which can not be overcome by electrical methods), is implemented not for the array itself but for its mathematical model used in the BCS.

Such traditional indices as attainment of directive gain (DG) maximum, scattering coefficient minimum or some others can be chosen as the model adaptation criteria. Application of the depth of nulls, being restored in the directions corresponding to the non-disturbed APD, to the RP adaptive synthesis as the quality criterion is new in the offered method. At first it is merely an intuitive premise, later on it was completely verified by the simulation, modeling the synthesis process.

The following can be used as the model adaptation algorithms when realizing the synthesis:

the gradient adaptation algorithms by the criterion of attaining maximum (minimum) of the chosen array quality index;

the algorithms of nulls formation in the direction of nulls of the calculated (ideal) RP.

The paper presents the results of the tests of both types of the algorithms for the simulation models.

Fig. 1 shows RP $F_a(g)$ (a solid line) obtained as a result of adaptation of the phase distribution by the criterion of attaining the DG maximum in the eight-channel Dolph-Chebyshev array. Here and in the other figures the ideal RP $F_0(g)$ are shown with dashed lines and RP $F(g)$ are shown with dotted lines corresponding to the APD before the adaptation (for Fig. 1 two channels "set" by the phase by ± 0.5 rad, for the rest the compensated distortions with a standard deviation (SD) amounted to 0.2 rad).

Figs. 2 and 3 show the results of the adaptive synthesis when forming the difference RP in 16-elemental (Fig. 2) and 32-elemental (Fig. 3) arrays by the algorithms forming the gaps in the nulls direction of the ideal RP: in the 16 channel array - by the algorithm based on defining the coefficients of the spatial spectrum of the APD forming the gaps only in the places of even nulls of the ideal RP, in the 32 channel array - by the algorithm of the direct inversion of the correlation matrix, that forms the gaps in the direction of all nulls of the ideal RP.

The initial APD for both arrays are characterized by a faulty state of 25 % of the channels (lack of excitation in 15 – 20 % of the channels plus uncontrolled state by phase in 5...10 % of the channels). In the controlled channels the distortions of the APD with SD are within 0.2.

The results of statistical tests of the indicated types of algorithms carried out by the authors allow to formulate recommendations for their application when solving the adaptive synthesis problems:

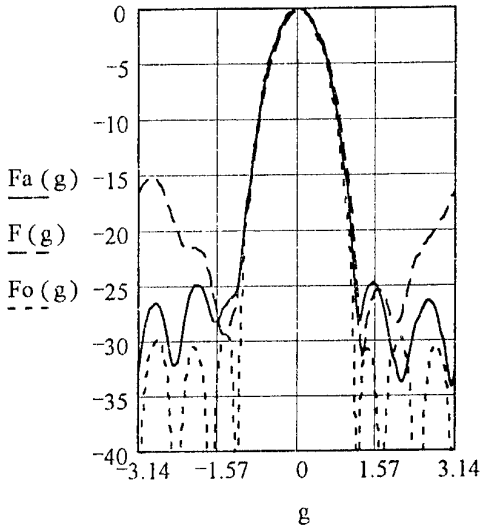


Fig. 1

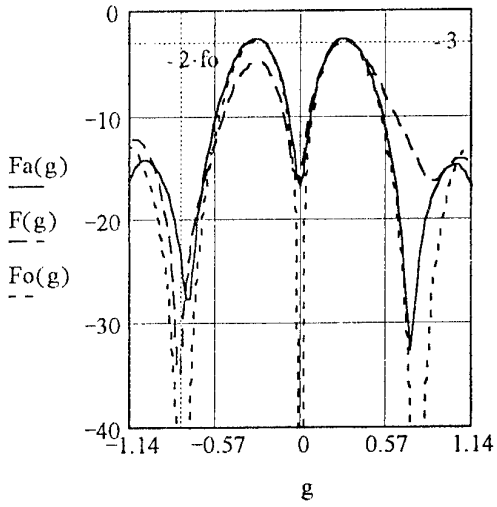


Fig. 2

the gradient algorithms of synthesis of phase distribution, ensuring the maximum DG, function successfully in arbitrary combinations of the phase shifter (PS) failures in 25% of the array elements. An appreciable deterioration in adaptation (as compared to the algorithms of gaps formation in the RP) is observed when part of channels is not excited. The reason is in the absence of possibilities to change the amplitude distribution;

the synthesis algorithms based on the nulls restoration operate successfully with arbitrary combinations of the PC failures and the non-excited channels (up to 20 %). An appreciable deterioration in adaptation is observed in the presence of the APD distortions in the controlled channels as well. The reason is that in this case the depth of the gaps being formed by the adaptive algorithm decreases noticeably.

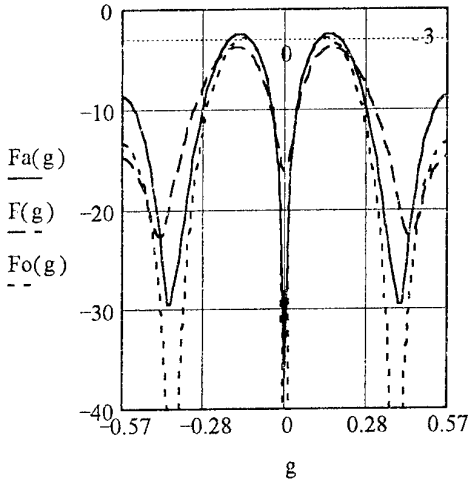


Fig. 3

The influence of APD distortions over the whole aperture manifests itself. But this shortage is easily removable by the successive application of two algorithms: first, the adaptation for the distorted APD and then the nulls restoration of the ideal RP.

In conclusion it should be noted, that going to the synthesis on the array model makes the synthesis results precision dependent on the diagnostics precision and on the used array model precision. But these shortages can be overcome by making the requirements to the diagnostics precision and the array model precision more rigid.

The arguments in favour of going to the synthesis on the array model are as follows:

the adaptation time doesn't depend neither on the intensity of received signals nor on PS inertiality but on the processors speed ;

the procedures of diagnostics and synthesis through the array adaptation can be realized in the regime of the RTS control and in the process of the main operation it remains only to recover the results of the adaptation from the memory.

In the RTS with a limited number of the RPs being formed (for example, in the surveillance raiders) it allows to carry out adaptation for every new array phasing in the real time.

RADIATION OF THE MULTI-MODE SLOTTED RADIATOR

V. Antyfeev, A. Borsov, A. Sokolov

Moscow, Russia

Usage of the multi-mode slotted radiator (MSR) as discrete radiators of multi-element uniform linear arrays is offered the exterior is adduced in a Fig. 1. MSR having a relative simplicity of a design provides a capability of forming of the funnel-shaped polar pattern (PP).

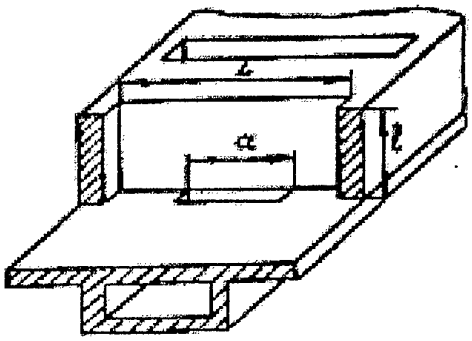


Fig. 1. The multi-mode slotted radiator

The offered equivalent circuit of MSR (Fig. 2) completely describes its impedance properties. The calculation of parameters of an equivalent circuit and radiator PP requires consideration of a number of internal and external problems of an electrodynamics having essential differences. In accordance with fact, it is possible practically in any case to present the solutions of the Maxwell equations determining an electromagnetic field in closed area, by decompositions on eigenwaves, for which the discrete spectrum of eigenvalues is characteristic. In a case of unlimited area the spectrum of eigenvalues becomes continuous.

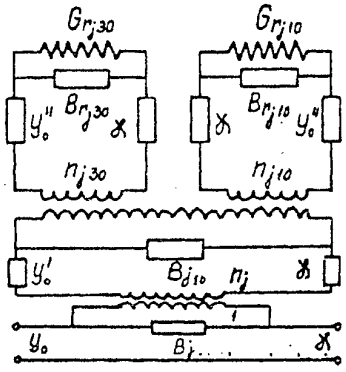


Fig. 2. The equivalent circuit of the multi-mode slotted radiator

It was routined, that for PP definition of the MSR whose aperture is excited by a combination of waves such as H_{30} and H_{10}, and also for calculation of their reflectance's, it is necessary to consider a problem of the aperture's radiation excited generally by a wave such as H_{po} (where p = 1, 3, 5... – any odd number) [1].

Opposite to closures, which all characterized by the discrete spectrum of eigenwaves, the representation of a field in unlimited transversal area assume an air of a continuous spectrum and is described by a Fourier integral by the solution of a bivariate wave equation in open area:

$$\varphi(x,z)=\frac{1}{2\pi}\int_{-\infty}^{\infty}\phi(\alpha)\exp(-j\alpha x)\exp(-\gamma x)d\alpha$$

Where $\phi(\alpha)$ is spectral amplitude of a plane wave; $\gamma=\sqrt{\alpha^2-k^2}$.

The definition of $\phi(\alpha)$-function is the basic moment in problems of finding out of a radiation field in open areas. The analysis of modification of the generalized wave-guide frame with a triple bifurcation [1], in which the dimension L→ ∞, has allowed to determine ϕ-value in an obvious view. In particular, for frame without dielectric filling:

$$\phi=\sqrt{\frac{1}{2\pi k\rho}}\cdot|\sin\theta|\times \frac{L(\gamma_{pa})\cdot L(-k\cos\theta)}{(-k\cos\theta+j\gamma_{pa})\cdot\sqrt{(j\gamma_{pa}+k)\cdot(k-k\cos\theta)}}\times \exp\left(j\left[k\rho-\frac{\pi}{4}\right]\right)\frac{p\pi}{a}\exp\left[-j\frac{ka}{2}|\sin\theta|\right],\quad k\rho\to\infty \qquad (1)$$

Where θ is equatorial angle, $\gamma_{pa}=\sqrt{\left(\frac{p\pi}{a}\right)^2-k_a^2}$,

$k_a=k\sqrt{\varepsilon_a}$, $k=\frac{2\pi}{\lambda}\sqrt{\varepsilon_0\mu_0}$,

$$L(\alpha)=\sqrt{\cos\frac{ka}{2}}\exp\left\{\frac{j\alpha a}{2\pi}\left[1-C+\ln\left(\frac{\pi}{ka}\right)+j\frac{\pi}{2}\right]\right\}\times\exp\left[\frac{j\gamma a}{2\pi}\ln\left(\frac{\alpha-\gamma}{k}\right)\right]\times\prod_{n=1}^{\infty}\left(1+\frac{\alpha}{j\gamma_{na}}\right)\exp\left(j\frac{\alpha a}{n\pi}\right).$$

These ratios allows to calculate PP of the MSR aperture's radiation, which is excited by wave such as H_{po} (where p is an odd index), and to calculate amplitude

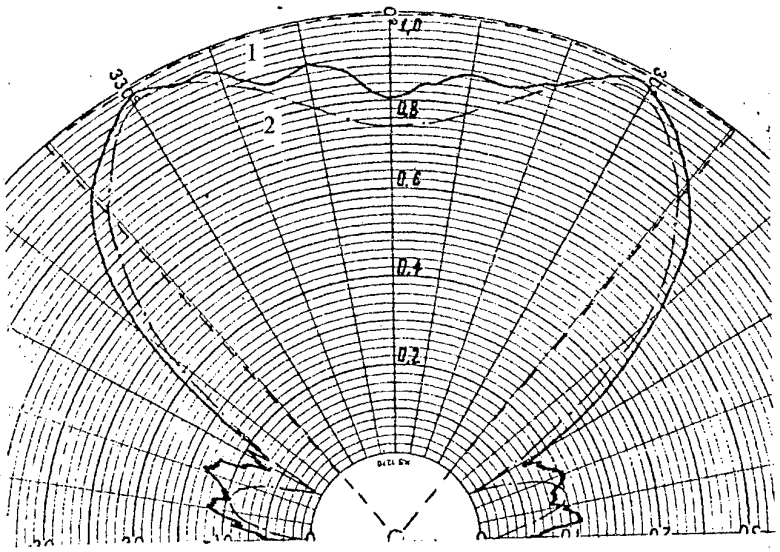


Fig. 2.
Experimental (1) and computational (2) PP of MSR (L = 2.4λ, a = 0.65λ)

and phase reflectances and transformations of waves in aperture. In process of calculation of parameters of the equivalent circuit of the multi-mode slotted radiator excited by a combination of waves such as H_{30} and H_{10} it is necessary to consider not only complex reflectances of this type of waves, but also transformation ratios of a H_{30}-wave into H_{10}-wave and H_{10}-wave into H_{30}-wave, which can propagate in A-area.

The results of calculations of relations of amplitudes and phases of reflectances depending on the length of aperture are adduced. The analysis of the obtained results has shown, that firstly, the amplitudes of reflectances descend faster with increase of length of aperture and at $\Lambda = 2.0 + 2.4\lambda$ — are insignificant, and secondly, the transformation ratios on the value in a number of cases surpass reflectances. At filling of aperture of a slot by the dielectric with low values of a permittivity $\varepsilon = 1.2 \ldots 2.4$, some increase of values of aperture's reflectances is observed. Thus the filling by the dielectric has a bit influence on the PP shape.

The obtained results are in good compliance with conclusions of [2–3], in which the problems of radiation of the open end of flat hollow waveguide and those one with dielectric filling were considered. With the purpose of check of theoretical outcomes the experimental researches of multi-mode slotted radiators made from the standard waveguide of 3.4×7.2 mm cross-section, which dwarfed broad wall has transversal rectangular narrow cutted slots of length 0.65 and 0.75λ. The changeable nozzles have allowed the change of length of a beaming slot stepwise from 1.8 up to 2.4λ.

As an example, funnel-shaped PP of the multi-mode slotted radiator with L = 2.4λ, a = 0.65λ, obtained as a result of measurements, is adduced in a Fig. 2. For matching experimental sector PP (1) and computational PP (2) is adduced. It is clear that the good identity of theoretical and experimental result takes place, but at some values of the sizes a and L more essential differences were observed, depending on inaccuracies of manufacturing and assembly of the radiator.

REFERENCES

1. Antyfeev V., Borsov A., Sokolov A. The fields of dissipation in the flat waveguide with a triple bifurcation and dielectric filling. The article in the given collection.

2. Vainstein L. The theory of diffraction and method of factorization. -M.: Soviet radio, 1966.

3. Voskresensky G., Zhukov S. Radiation of the open end of the flat waveguide with dielectric filling. - Radiotechnics and electronics, 1976, V.21, I. 12, pp. 2608-2614.

SMALL-SIZED DIELECTRIC SPLIT ANTENNA OF ROUND CROSS-SECTION

V. Antyfeev, A. Borsov, A. Sokolov

Moscow, Russia

The main imperfection of dielectric antennas marked in large length of a dielectric rod becomes an essential obstacle of use of these antennas as quality weak-directional independent antennas and as units of complex antenna arrays. So in 8 mm wave band length of dielectric rod indispensable for forming of the directional PP having width 25–30° on a half-power level, approximately will make of 5–6 wavelengths, i.e. 40–50 mm, and the design requirements admit length of a protuberance no more than 12–15 mm (1.5–1.9λ).

Therefore, the problem of substantial improvement of directional properties of a dielectric rod feel a rather actual, that will allow to use for forming of PP in width 25-30° at a level of lateral radiation not superior 18–20 dB, dielectric antennas of length no more than 2λ.

For improvement of directional properties of short dielectric antennas excited by the basic wave, usage of a flat metal inset into a dielectric rod from the waveguide aperture to the end of a rod is offered (Fig. 1).

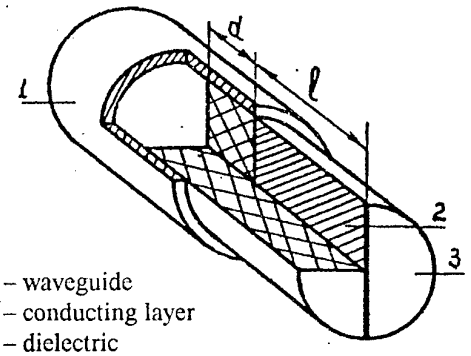


Fig. 1. Dielectric split antenna

As the conducted researches have shown [1], for the description of emitting properties of short dielectric antennas having round cross-section and excited by wave such as H_{11}, it is possible to take advantage of a method of equivalent surface currents if to enter a correcting factor into expression for a field pattern lengthwise of dielectric rod. Pursuant to this method components of electrical fields of radiation of a dielectric split antenna having round cross-section and excited by H_{11}-wave in spherical coordinate system is possible to obtain as:

$$E_\theta = \frac{E_0}{\rho_0}\left[jk(n_Z - \cos\theta)\right]\cdot J_1(k_1\rho_0)\cdot I_{10}^{*}\cdot I_{20},$$

$$E_\phi = E_0\cdot k_1^2\cdot J_1(k_1\rho_0)\cdot I_{10}\cdot I_{20}.$$

Here ρ_0 is radius of dielectric rod, J_1 (k_1, ρ_0) — Besselian function of the first kind and of the first order, E_o — scale factor. The integral multiplicands I_{10}, I_{10}^{*} and I_2, determining directional properties of the antenna, are determined by a kind of a correcting function ω(z), which one in pursuant to [1] is selected as:

$$\omega(z) = d + (1-d)\sin\left(\frac{\pi r}{e}\right).$$

Then, the integral multiplicands can be presented as:

$$I_{10} = J_0(k\rho_0\sin\theta) - \sum_{\upsilon=1}^{\infty}\left\{J_{2\upsilon}(k\rho_0\sin\theta)\times\right.$$
$$\times\frac{\upsilon\sin(2\nu\phi)+\cos\left[2\nu\left(\phi+\frac{\pi}{4}\right)\right]}{\nu^2-1} + jJ_{2\upsilon-1}(k\rho_0\sin\theta)\times$$
$$\left.\times 2\frac{(2\nu-1)\cos[(2\nu-1)\phi]+2\sin[(2\nu-1)(\phi+\pi/4)]}{(2\nu-3)(2\nu+1)}\right\},$$

$$I^{*}_{10} = J_0(k\rho_0\sin\theta) + \sum_{\upsilon=1}^{\infty}\left\{J_{2\upsilon}(k\rho_0\sin\theta)\times\right.$$
$$\times\frac{\nu\sin[2\nu(\phi+\pi/4)]\cos(2\nu\phi)}{\nu^2-1} + jJ_{2\upsilon-1}(k\rho_0\sin\theta)\times$$
$$\left.\times 2\frac{(2\nu-1)\cos[(2\nu-1)(\phi+\pi/4)]+2\sin[(2\nu-1)\phi]}{(2\nu-3)(2\nu+1)}\right\},$$

$$I_{20} = \frac{ld}{2}\left\{\frac{\frac{\pi}{2}\cdot\left(\frac{1-d}{d}\right)\cdot\cos\left[\frac{kl}{2}(n_z-\cos\theta)\right]}{\left(\frac{\pi}{2}\right)^2-\left[\frac{kl}{2}(n_z-\cos\theta)\right]^2}+\right.$$
$$\left.+\frac{\sin\left[\frac{kl}{2}(n_z-\cos\theta)\right]}{\frac{kl}{2}(n_z-\cos\theta)}\right\}\times\exp\left[j\frac{kl}{2}(n_z-\cos\theta)\right]$$

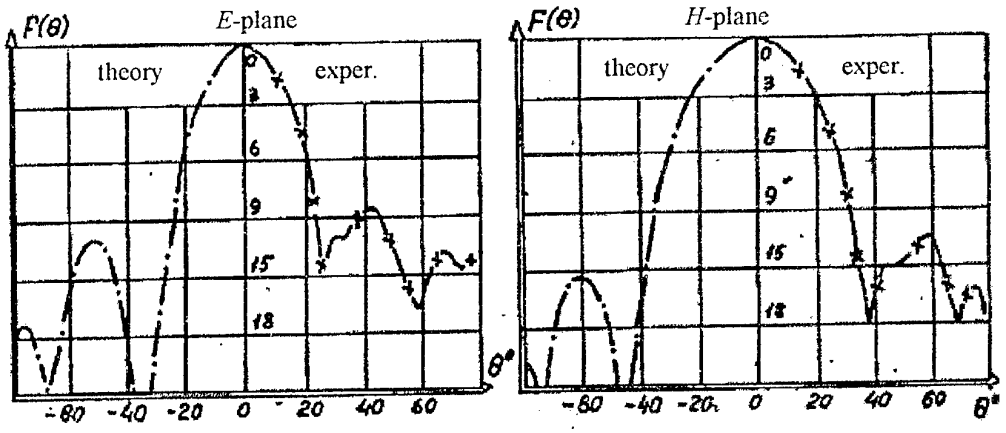


Fig. 2.
PP of dielectric split antennas having length 2.0λ and diameter 0.92λ and $\varepsilon_r = 2.6$, obtained by theoretical and experimental methods

The analysis of factors I_{10}, I_{10}^{*} and I_2 has shown, that first and second one take into account the contribution into PP the allocation of a field pattern lengthwise of rod, and I_2 — on its cross-section. Improvement of an aerial directivity is reached by introduction of a thin conducting stratum on a shaft axle in parallel to E-vector. The increase of ε_z without changing of cross-sectional dimensions and dielectric constant of a rod also results in increase of a directivity of the dielectric antenna and in H and E- planes.

The value of variable ε_z (n_z) was determined as the solution of a transcendental secular equation. Then the expressions for factors I_{10}, I_{10}^{*} and I_2 can be presented as series which convergence provide a behavior of Besselian functions at small values of real argument and descending of each member of a series with increase of an index.

Limiting by consideration of 10 members of a series, PP of dielectric split antennas having length 1.6λ; 2.0λ; 2.4λ and diameter 0.92λ and $\varepsilon_r = 2.6$ were calculated at values of parameters $\varepsilon_z = 1.31$ and $d = 1.0$ in H-plane ($\phi = \pi/2$) and I-plane ($\phi = 0$). PP calculated were compared to experimental data of measurement of directional properties of antennas of the same geometrical sizes, which one have shown good conformity by correct selection ε_z and d. In a Fig. 2 PP of dielectric antennas having length 2.0λ and diameter 0.92λ and ε_r = 2,6 obtained by means of theoretical and experimental method are shown.

REFERENCE

1. Kuhn R. Microwave antennas. M. Sudostroenye, 1970.

L-BAND ANTENNA ALTERNATIVES FOR THE EUROPEAN MOBILE SATELLITE (EMSAT) NETWORK

G. de Balbine

IDLtech
Tarzana, California 91356, USA
idltech@ix.netcom.com

The EMSAT network is a new pan European mobile telephone/fax/data/messaging service offered by Eutelsat using the EMS payload on the Italsat F2 GEO satellite at 16.4 E and the equipment developed for the Optus network in Australia. It is designed primarily for professional applications such as fleet management involving either land transports or commercial fishing boats.

As part of the acceptance testing of the EMSAT services, our efforts have included selecting and testing those components best suited for operation in Europe. Of all components, mobile antennas have proven to be the most critical. Because mobile antennas only offer moderate gains, the network operates in a power limited mode. The satellite L-band power has to be adjusted to compensate for each mobile's antenna performance, using only as much as is necessary to guarantee a good quality of service. This power adjustment is in fact done on a call be call basis, using the last known location of the mobile to also compensate for edge of coverage roll off. The gains of the mobile antennas therefore determine network capacity. To be fair, either the call charge should factor in the specific gain of each antenna or all antennas should have roughly similar gains which would then exclude a mix of omnidirectional and directional antennas.

But achieving an adequate gain over a large range of satellite elevations is not the only criterion. There are many other criteria that are important but often discounted:

- physical characteristics (size and weight)

- ease of installation in view of masking at low elevation angles

- manual vs. automatic antenna adjustment and the risk of erroneous or forgotten adjustments

- automatic antenna type reporting for satellite power adjustment

- coupling of position reporting with power management

- time to acquire and, more importantly, time to reacquire after an obstacle,

- quality of the tracking algorithm particularly for 2 and 3 axis antennas and the risk of false locks,

- mechanical vs. electronic dithering

- autonomous versus externally controlled pointing and the impact of voice activation on antenna pointing,

- resistance to severe environments particularly at sea, including the choice of sealed vs. unsealed antennas,

- and last but not least, the cost of the resulting antenna.

Using examples from actual testing, we shall examine the alternatives which we explored to arrive at a good mix of antennas.

OPTIMIZATION OF CHARACTERISTICS OF DIRECTIVITY OF HORN MICROWAVE BAND RADIATORS

A. A. Boichenko, I. I. Shumljansky

270029 Odessa-29, Didrihsona St. 4, OSMA
Tel. (0482) 32-11-43 E-mail: root@ osma.odessa.ua

There have been several stages in development of the horn antennae (HA). The initial period was characterized by employing straight HA. The antennae of this type are still used nowadays. They were followed by stepped-shape horns. Another type of horn was that with corrugated walls. As compared with similar flat-wall antennae these horns should be preferred for being able to provide symmetrical circular space patterns and practically stable main-lobe width even when the operating frequency changes two-fold. Also, their beam patterns practically do not have back or side lobes. And, finally, at the next stage, the employment of horns of curved configuration came into practice.

Consider the publications on general theoretical problems. [1] discusses the horn with a rounded flange, which facilitates the analysis of the boundary effects. Suggested in [2] is the method of calculating the horn beam pattern in plane E by making use of the Sommerfeld-Pauli conception of diffraction. The author of the work notes a satisfacting matching of the results of the analysis with experimental data. But the author's reference to thin and thick-wall horn radiators is hardly acceptable, as the thickness of the horn walls has no effect on the antenna pattern. In this case it is a matter of how wide is the edge of the horn aperture flange. An importance of the research is narrowed as the author discusses only the simplest class of straight horn antennae.

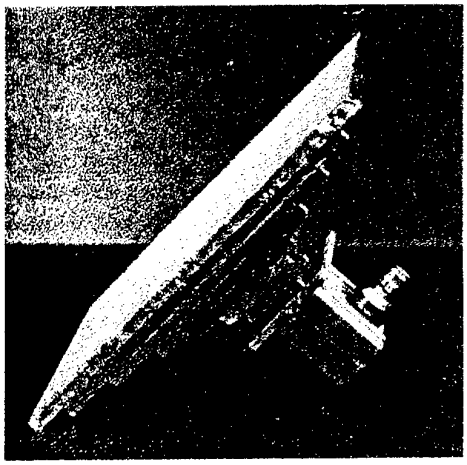


Fig. 1

It is assumed hereinafter that the shape generating elements of various types of horn antenna are described in terms of different mathematical functions.

The horn antennae and the waveguide coupling are of interest not only as the most common elements of microwave band systems. They are used as well to solve some related problems as regards the field structure and horn configuration design. Therefore the conclusions and data obtained for a certain device are used, where possible, for similar devices. It should be noted, however, that the horn antennae and waveguide adapters are for different purpose (hence tolerances, dimensions, etc.), which certainly leads to substantial differences in calculating specific equipment.

In this scientific work a six-step horn antenna was investigated. Its inlet and outlet dimensions are 90×45 mm and 368×394 mm respectively which, in terms of wavelengths, corresponds to $0.90\lambda_0 \times 0.45\lambda_0$ and $3.68A_0 \times 3.24A_0$ where λ_0 = 100 mm. Maximum permissible mismatch factor $|r|n$, ax = 0.07. The pyramidal horn was made of dielectric (foam plastic, n = 1.14) with metallized side surface. The stepped horn input was flange-coupled with the feeding waveguide. The cross-section of the first step of the horn was equal to that of the feeding waveguide, which was excited by an SHF oscillator via coaxial cable. The cross-sections and lengths of the subsequent steps provided matching with the proceeding steps. A general view of this stepped horn is shown in Fig. 1 and its design is shown in Fig. 2. Method of calculation from [3] was used. The experimental investigations of stepped radiator beam patterns were carried out in 5.5×7.5 m room on a test bed, and the measurements was recorded by a strip-chart recorder. To reduce the reflections inside the room, a part of the wall surfaces was covered with absorbing material.

The receiving and transmitting antennas were placed at a height of 2 m above the floor and at a distance equal to 3.5 m each from the other. The investigated horn antenna was operating as a receiver.

The source of HF oscillations was an oscillator with a klystron. The oscillator was coupled with the feeder by means of a simplified oscillator section. The klystron was modulated by rectangular pulse having relative pulse duration of 1:2 and pulse-recurrence rate F = 1000 Hz.

Via absorptive attenuators and a matching device, HF oscillations were supplied to the transmitting antenna and radiated in the direction of the investigated antenna. A pyramidal HA from the field intensity meter

set was used as transmitting antenna. The high directivity (2θ = 20°) of the transmitting antenna provided almost complete elimination of the reflections from the room walls. A non-uniformity of the field amplitude along the flare of the investigated HA totaled less than 2 % w.r.t. power, and a non-uniformity of the phase – less than 15 % which ensured a sufficient accuracy of measurements for the considered problem. The transmitting antenna-feeder system was mounted on a rotary stand which allowed to change the polarization of radiation through 90° to obtain beam patterns in electrical and magnetic planes by turning the whole system about the longitudinal axis.

The operating wavelength was measured with a wave meter. The coaxial cable connecting the system with the wave meter was used also to periodically connect to the system power meter employed for amplitude calibration of the indicator.

The HA under investigation was rotated in the horizontal plane through a rotation gear arranged on the bench. The antenna was coupled with the detachable curved waveguide section by means of a rotary joint. The dimensions of the section were selected so that the receiving and transmitting antennae were at the same level and the center of the receiving antenna aperture (being close to its conventional phase center) was located on the axis of rotation. To measure the beam pattern in the electrical plane a bent section was used, with its vertical portion being twisted along the axis at an angle equal to 90°.

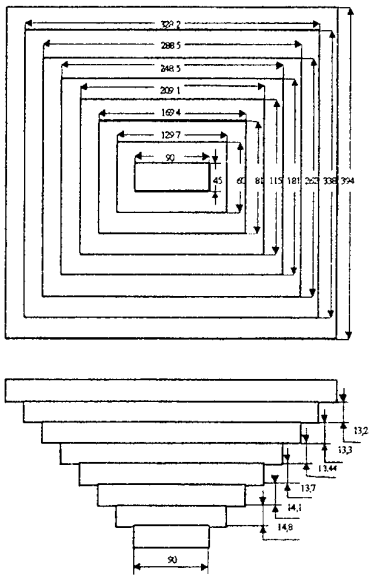


Fig. 2

Fig. 3 presents also the beam patterns of a Pyramidal stepped horn (solid curves) and that for a straight horn with similar aperture and $|r|_{max}$ (dash curves) in a magnetic plane for intermediate frequencies of the operating frequency range.

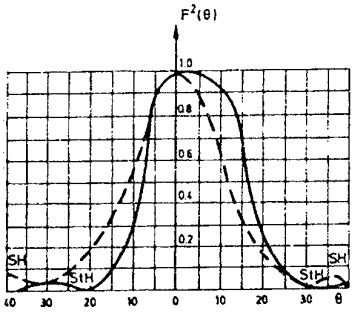


Fig. 3

It follows from the graphs that in the H-plane the pyramidal stepped horn has a wider flattop pattern than a HA with straight generants. It can be also easily noticed that the application of stepped structure allows to preserve observed interferential maximum of the side lobes, which important for the application of such horns in the antenna arrays with wide scan angle. However, having narrow scan sectors, the stepped horns are perfectly suitable, the more so, that the stepped structure allows to reduce the longitudinal dimension of the horn by approximately 30% as compared with the straight horns, for the same other conditions.

In the described HA the envelope of the steps corresponds to the Chebyshev waveguide transition which results in a wider operating range.

Thus, the following recommendations can be shaped:

1. In the synthesis of stepped horns a rather effective method for designing the stepped waveguide adapters is that based on the circuit theory.

2. When designing the stepped horns, the presented here graphs and experimental data would be practiccal use.

REFERENCES

1. Kinber B.E. On Diffraction of Electromagnetic Waves on Concave Surface of Circular Cylinder. Radioengineering and Electronics. 1961. V. 6.

2. Russo P. M., Rudduck R. C., Peters L.J. A Method for Computing E-Plane Patterns of horn Antennas //IEEE Tr. On Antennas and Propagation. -1965. - №3. –P.219-225.

3. Shumlyanskiy I. I. Horn Radiators of Complex Configuration. - Singapore-London: "World Scientific", 1993. -172 P.

4. Shumlyanskiy I. I. Horn Radiators with Stepped and Curved Generants. Kiev: Vysha Skola Publishers, 1986. pp. 147.

A LEAKY-WAVE INTEGRATED ANTENNA BASED ON A PRISM COUPLED TO A DIELECTRIC WAVEGUIDE

S. V. Boriskina and A. I. Nosich*

Radiophysics Department, Kharkov State University, Svobody Sq. 4, Kharkov, 310077, Ukraine,
tel: 380-(572)-335787, fax: 380-(572)-377380, e-mail: mybox@public.kharkov.ua
* Institute of Radio Physics and Electronics NASU, Proskury St. 12, Kharkov, 310085, Ukraine
tel, fax: 380-(572)-377380, e-mail: alex@emt.kharkov.ua

Dielectric prisms are widely utilized in the design of the millimeter wave and optical functional components, which are used in communication systems [1, 2]. Dielectric prisms coupled to open dielectric waveguides can also be used as versatile leaky-wave antennas due to their ability to convert a waveguide surface wave to a beam [2]. Among their advantages are low weight, low losses, simple coupling technique and high radiation efficiency. For any given prism configuration and wavelength, the radiation angle of a beam varies with the surface mode number. If a waveguide supports several higher-order modes, the output far-field radiation pattern has several well-defined beams corresponding to these modes.

To study the characteristics of the leaky-wave integrated prism antenna, we propose to use the method of analytical regularization [3], based on the inversion of the free-space circular-cylinder part of the singular integral operators. Consider a problem of a dielectric waveguide surface wave radiation through the dielectric prism placed over the waveguide (Fig. 1). The total field can be characterized by the single scalar function U, which represents either E_z or H_z component, depending on the polarization, and must satisfy the Helmholtz equation, with corresponding coefficients in each material, and the boundary conditions. At infinity, a modified radiation condition is to be satisfied:

$$U^{rad}(\vec{r}) - U^{inc}(\vec{r}) \underset{r\to\infty}{\approx} \sqrt{\frac{2}{i\pi kr}} e^{ikr} \begin{Bmatrix} \Phi^{E(H)}(\varphi), & y > -b \\ 0, & -(b+d) < y < -b \end{Bmatrix} + \sum_{n=1(0)}^{Q^{E(H)}} \begin{Bmatrix} T_n^{E(H)}, & x > 0 \\ R_n^{E(H)}, & x < 0 \end{Bmatrix} V_n^{E(H)}(y) e^{ih_n|x|} \tag{1}$$

Here, $Q^{E(H)}$ is the total number of the higher-order guided modes supported by the slab waveguide at the given frequency. Function $\Phi^{E(H)}(\varphi)$ is the radiation pattern of the prism, numbers $T_n^{E(H)}$ and $R_n^{E(H)}$ are the mode conversion coefficients.

First, the fields inside and outside the dielectric prism are presented in the integral form as surface potentials over the prism contour. To do so, we should describe a prism contour L_p by a closed curve of the Lyapunov type L_s, i.e. a curve without the edges or points of infinite curvature κ. To this end, we characterize the prism cross-section by the following function:

$$\begin{aligned} y &= \frac{c_p}{2}\left(1+\frac{2x}{a_p}\right), -a_p \le x \le 0 \\ y &= \frac{c_p}{2}\left(1-\frac{2x}{a_p}\right), 0 \le x \le a_p \\ y &= -\frac{c_p}{2}, -a_p \le x \le a_p \end{aligned} \tag{2}$$

Functions (2) are further parameterized and expressed in terms of the Fourier series:

$$\begin{aligned} x(t) &= \sum_{m=-N_f}^{N_f} x_n e^{imt}, \quad y(t) = \sum_{m=-N_f}^{N_f} y_n e^{imt} \\ x_m &= \frac{1}{2\pi}\int_0^{2\pi} x(t)e^{-imt}dt, \quad y_m = \frac{1}{2\pi}\int_0^{2\pi} y(t)e^{-imt}dt \end{aligned} \tag{3}$$

The more terms of the Fourier series taken into account, the closer the contour to the triangle. It should be mentioned that the curvature of such an approximation contour has finite values at all the points of the contour.

Then, by using the boundary conditions on the prism contour, a set of the first-kind integral equations is obtained, for the unknown densities φ and ψ:

$$\begin{aligned} &\int_{L_s} \varphi^{E(H)}(\vec{r}_s) G_\varepsilon^{E(H)}(\vec{r},\vec{r}_s) dl_s - \\ &- \int_{L_s} \psi^{E(H)}(\vec{r}_s) G_0^{E(H)}(\vec{r},\vec{r}_s) dl_s = U^{inc}(\vec{r}) \\ &\frac{1}{\alpha}\frac{\partial}{\partial n}\left\{ \int_{L_s} \varphi^{E(H)}(\vec{r}_s) G_\varepsilon^{E(H)}(\vec{r},\vec{r}_s) dl_s - \right. \\ &\left. - \int_{L_s} \psi^{E(H)}(\vec{r}_s) G_0^{E(H)}(\vec{r},\vec{r}_s) dl_s \right\} = \frac{\partial}{\partial n} U^{inc}(\vec{r}) \end{aligned} , \tag{4}$$

where $G_\varepsilon^{E(H)}$ is the E-(H-) type Green's function of the homogeneous medium with permittivity ε_p, and $G_w^{E(H)}$ is the Green's function of the halfspace bounded by a grounded dielectric slab.

On extracting and analytically inverting circular-cylinder parts of the integral operators, these equations are converted into the Fredholm second-kind infinite-matrix equations:

$$\varphi_m H_m^{(1)}(ka\sqrt{\varepsilon_p})J_m(ka\sqrt{\varepsilon_b}) - \psi_m H_m^{(1)}(ka)J_m(ka) + \sum_{n=-\infty}^{\infty} A_{mn}^{shape}\varphi_n - \sum_{n=-\infty}^{\infty}\left(B_{mn}^{slab} + B_{mn}^{shape}\right)\psi_n = e_m \quad (5)$$

$$\varphi_m\left(\frac{ka\sqrt{\varepsilon_p}}{\alpha}H_m^{(1)}(ka\sqrt{\varepsilon_p})J_m'(ka\sqrt{\varepsilon_p}) + \frac{i}{\pi}\right) - \psi_m\left(kaH_m^{(1)'}(ka)J_m(ka) - \frac{i}{\pi}\right) + \sum_{n=-\infty}^{\infty}\left(ka\sqrt{\varepsilon_p}C_{mn}^{shape} - \frac{i}{\pi}L_{m-n}\right)\varphi_n - \sum_{n=-\infty}^{\infty}\left(ka\left(D_{mn}^{slab} + D_{mn}^{shape}\right) + \frac{i}{\pi}L_{m-n}\right)\psi_n = ka\tilde{e}_m \quad (6)$$

Here, φ_n, ψ_n and $e_n, \tilde{e}_n$ are the unknown Fourier coefficients of the unknown density functions and the functions in the right-hand parts of the integral equations, respectively; J_n, H_n are the Bessel and Hankel functions, respectively, and the prime is for the derivative with respect to the argument; the coefficients L_m is determined by the cylinder cross-section shape:

$$L_m = \frac{a}{2\pi}\int_0^{2\pi}\frac{1}{L(t)}e^{-imt}dt\ ,\ L(t) = \sqrt{\left(\frac{dx}{dt}\right)^2 + \left(\frac{dy}{dt}\right)^2}\ . \quad (7)$$

Matrix elements A_{mn}^{shape}, B_{mn}^{shape}, C_{mn}^{shape}, D_{mn}^{shape} are the Fourier coefficients of the regular functions formed as the differences between the Green's function (or their derivative) values at the initial contour and at the circular contour. Coefficients B_{mn}^{slab} and D_{mn}^{slab} appear due to the presence of the waveguide.

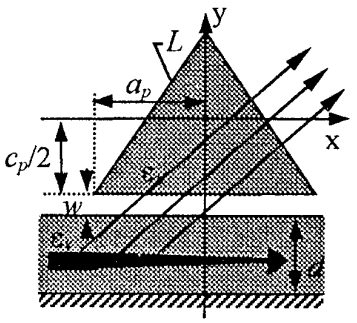


Fig.1. Leaky-wave prism antenna

Obtaining the Fredholm second-kind infinite-matrix equations is possible due to the fact that, for a circular scatterer, all the singular operators can be diagonalized in terms of the integer-index azimuthal exponents. By using the set of the latter as expansion basis, in the discretization of arbitrary-shape operator via Galerkin scheme, we combine the discretization and semi-inversion. The resulting Fredholm second-kind matrix equation is solved numerically with guaranteed accuracy.

To fill in the matrix, it is necessary to calculate cylindrical functions and the Fourie double-series expansion coefficients A_{mn}^{shape}, B_{mn}^{shape}, C_{mn}^{shape}, D_{mn}^{shape}. The center of gravity of the algorithm based on this regularized matrix equation is shifted to numerically accurate and efficient computation of the double Fourier-series expansion coefficients of the regular parts of the kernels of integral operators. To this end, we use the Double Fast Fourier Transform with the weighting coefficients [4].

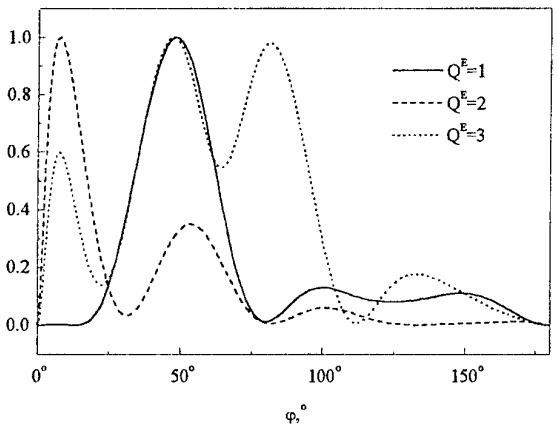


Fig. 2. Normalized radiation patterns for a prism placed over a multimode dielectric slab, E-polarization. kc_p=3, a_s/c_s=1, ε_b=ε_s=2.13, w/c_p=0.0005, a) d/c_p=2 (Q^E=1), b) d/c_p=6 (Q^E=2), c) d/c_p=10 (Q^E=3)

Based on the proposed method, highly efficient algorithm of modeling the leaky-wave antenna has been developed. Radiated power, mode conversion coefficients and radiation efficiency have been calculated as a function of the dimensionless frequency parameter, as well as several radiation patterns (Fig. 2). The results have been validated by checking the power conservation law.

REFERENCES

1. E. I. Nefedov, Diffraction of Electromagnetic Waves from Dielectric Structures, Moscow, Nauka, 1979 [in Russian].

2. R.G. Hunsperger, Integrated Optics. Theory and Technology, Berlin:Springer-Verlag, 1995, pp. 93-105.

3. A. I. Nosich, "The Method of Analytical Regularization in Wave Scattering and Eigenvalue Problems", IEEE Antennas Propagat. Magazine, 1999, vol.42, no.3.

4. D. F. Elliot, K.R. Rao, Fast Fourier Transforms: Algorithms, New York: Academic Press, 1982.

MATCHING AND DIRECTIVITY FEATURES OF WAVEGUIDE RADIATOR FILLED WITH DIELECTRIC

A. A. Bulgakov, N. N. Gorobets*, V. A. Lyaschenko*

Institute of Radiophysics and Electronics NAS of Ukraine
E-mail: bulgakov@ire.kharkov.ua,
Institute of Radiophysics and Electronics, National Academy of Sciences,
Ul. Akademika Proskury 12, Kharkov 310085, Ukraine,
Tel: +38-(0572)-448323
* Kharkov State University, E-mail: Nikolay.N.Gorobets@univer.kharkov.ua,
310077, Kharkov-77, Svobody sq. 4, Tel.: +38-(0572)-457175

ABSTRACT

Matching of a waveguide radiator filled by dielectric and free space has been studied theoretically. Algorithms and programs for the computer analysis of an electrical conductance and susceptance of a waveguide aperture have been developed. Reflectivities of the H_{m0} wave modes of a waveguide from the radiator aperture have been analyzed.

There is no exact radiation theory of a waveguide aperture. It is shown in [1] that an electromagnetic model [2] of a rectangular waveguide aperture with an infinite flange allows describing identically the radiation from waveguide radiator apertures. In this work, both electrical conductance, susceptance, and reflectivities from a waveguide aperture are investigated. The waveguide is filled by a perfect dielectric, which is characterized by the permittivity ε_1; the free space has the permittivity ε_2. It is assumed that the H_{m0} mode is incident on the aperture of the waveguide.

In order to obtain an integral equation for the electrical field on the aperture of the waveguide radiator, we have to satisfy the boundary condition for the tangential components of the electromagnetic field. There is no need to solve this integral equation because we can obtain an expression for the normalized conductance of the waveguide aperture by means of variational methods:

$$Y_m = \frac{i}{\pi ab\gamma_{m0}} \cdot \left[k^2 - \left(\frac{m\pi}{a}\right)^2 \right] \cdot \int_0^a\int_0^a\int_0^b\int_0^b \mathrm{d}x\,\mathrm{d}x'\,\mathrm{d}y\,\mathrm{d}y' \times \sin\frac{m\pi}{a}y \sin\frac{m\pi}{a}y' G(x,y,x',y')$$

$$+ \frac{i}{\pi ab\gamma_{m0}} \frac{m\pi}{a} \int_0^a\int_0^b\int_0^b \mathrm{d}x\,\mathrm{d}x'\,\mathrm{d}y' \sin\frac{m\pi}{a}y' \times \left\{ G(x,0,x',y') - \cos m\pi G(x,a,x',y') \right\},$$

where

$$k = k_0\sqrt{\varepsilon_2},\ k_0 = \frac{2\pi}{\lambda},\ \gamma_{m0} = \sqrt{k_0^2\varepsilon_1 - \left(\frac{m\pi}{a}\right)^2},$$

$$G(x,y,x',y') = \frac{\exp\left[-ik\sqrt{(x-x')^2+(y-y')^2}\right]}{\sqrt{(x-x')^2+(y-y')^2}},$$

λ is the free-space wavelength, a,b are the waveguide width and height, x,x' and y,y' are the coordinates along the wider and the narrower walls, respectively.

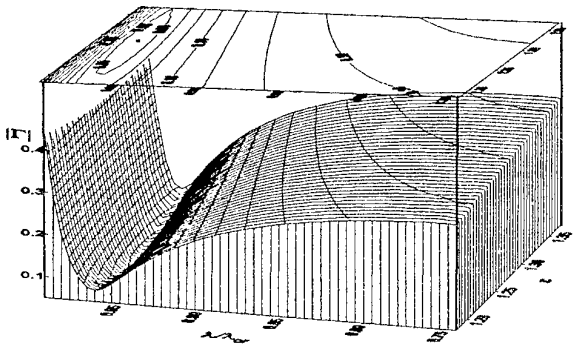


Fig. 1

This expression has been used to calculate $\mathrm{Re}\,Y_m$ and $\mathrm{Im}\,Y_m$ for the waveguides with the different ratios of the sides a and b and different values of ε_1 and ε_2. The H_{10}, H_{20}, H_{30} modes were assumed to be incident on the aperture of the waveguide. After calculating the complex permittivity of the aperture, we have evaluated the reflectivity Γ. In Fig. 1, computed results for the reflectivity $|\Gamma|$ of the H_{10} mode are shown. The waveguide radiator has the cross-section $a \times b = 23 \times 10$ mm $(b/a = 0.435)$. For a better insight, a reflectivity relief versus ε_1 and the ratio λ/λ_{cr} is given. The cutoff wavelength has been determined taking into account due to the dielectric permittivity. As it is seen, for the standard cross-section waveguide there is a region with a minimum value of the reflectivity $|\Gamma| < 0.06$. On the top of Fig. 1, there is a cartographic projection, i.e. the curves of the equal values of the

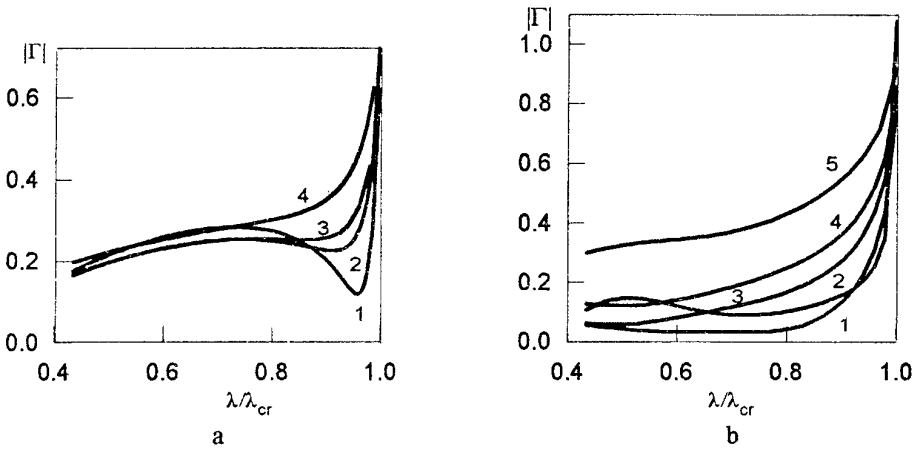


Fig. 2. Reflectivity of H_{10} mode versus λ/λ_{cr}. $\varepsilon_1 = 1$, ε_2:
a) $b/a = 0.435, 1 - \varepsilon_2 = 0.9; 2 - \varepsilon_2 = 1.1; 3 - \varepsilon_2 = 1.2; 4 - \varepsilon_2 = 1.5$.
b) $b/a = 1.1 - \varepsilon_2 = 0.9; 2 - \varepsilon_2 = 2; 3 - \varepsilon_2 = 1.2; 4 - \varepsilon_2 = 1.5; 5 - \varepsilon_2 = 3$.

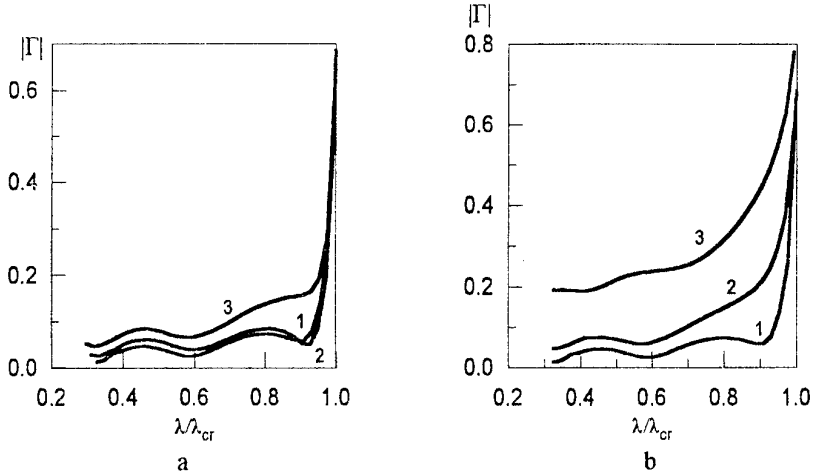


Fig. 3. Reflectivity of H_{30} mode versus λ/λ_{cr}. $a/b = 0.435$:
a) $\varepsilon_2 = 1, 1 - \varepsilon_1 = 1; 2 - \varepsilon_1 = 1.1; 3 - \varepsilon_1 = 1.2$;
b) $\varepsilon_1 = 1, 1 - \varepsilon_2 = 1; 2 - \varepsilon_2 = 1.1; 3 - \varepsilon_2 = 2$.

reflectivity. One can see that there is a region where $|\Gamma| \leq 0.025$ if $\varepsilon_1 \approx 1.29$. As it has been shown in [1], the reflectivity of a 'low' waveguide principal mode ($b/a < 0.4$) turns out to be greater than 0.4 in a single-mode operation band. Thus, our investigations have shown that the dielectric filling of such a kind does not improve the matching of the waveguide radiator with free space in the waveband $\lambda/\lambda_{cr} = 0.3 \div 0.995$.

Besides, the exterior permittivity effect on the radiator characteristics has been studied. In Fig. 2, the reflectivities versus λ/λ_{cr} for the different values of ε_2 are depicted. Curves in Fig. 2a correspond to the $a/b = 0.435$ waveguide; dependences in Fig. 2b correspond to the $b/a = 1$ one. One can see that, in comparison to the case $\varepsilon_2 = 1$, the reflectivity decreases in the case of a small value of permittivity $\varepsilon_2 \sim 1.1 \div 1.2$ and a large value of the ratio $\lambda/\lambda_{cr} > 0.9$. In addition, there is an improvement of the radiator band features. It is known [1] that the rectangular waveguide aperture with the size ratio $b/a = 1$ has the reflectivity less than 0,1 in the band $(0.2 \div 0.8)\lambda/\lambda_{cr}$. As it is seen in Fig. 2b, if the exterior dielectric has the permittivity $\varepsilon_2 > 1.3$, the free space matching deteriorates but it turns out possible to improve the band features (to the point $\lambda/\lambda_{cr} \cong 0.9$), although the value of $|\Gamma|$ increases.

We have also investigated the problems of the H_{20} and H_{30} modes incident on the aperture of the waveguide radiators. The conductance and the reflectivities have been calculated. In Fig. 3, the plots show the results calculated for the H_{30} mode in the $b/a = 0.435$ waveguide. The curves in Fig. 3a correspond to $|\Gamma| = f(\lambda/\lambda_{cr})$ dependences, different permittivities ε_1 and the free-space permittivity $\varepsilon_1 = 1$. One can see that the reflectivity $|\Gamma|$ depends strongly on ε_1 and ε_2. Such an analysis has been carried out for the H_{20} mode as well. The reflectivity is less than 0.1 in the cases of the $b/a = 0.435, b/a = 1$ waveguides, when the radiation from an empty waveguide into the free space is studied. The 'low' waveguide is characterized by $|\Gamma| < 0.2$ in the case of $\lambda/\lambda_{cr} = 0.2 \div 0.5$ and $|\Gamma| \sim 0.2 \div 0.35$ in the band $0.55 \div 0.98$. Filling waveguides by dielectric increases the reflectivity.

Still besides, we have studied the directivity features of the waveguide radiators as a function of the dielectric filling.

REFERENCES

1. Gorobets N.N., Lyaschenko V.A. Matching Analysis of Microwave Band Waveguide and Horn Antennas. Proceedings Crimiko-97. Sevastopol, 1997., Vol. 2, pp. 504-505.

2. Levin L. Advanced Theory of Waveguides. 1954, 215 p. [in Russian].

ON THE ESTIMATION OF ELECTROMAGNETIC CHARACTERISTICS OF THE SYSTEM OF DIPOLE RADIATORS IN THE LOGPERIODIC ANTENNA

L. G. Burova, Y. Y. Radtzig

Yaroslav Mudryi Novgorod State University
St. Petersburg Str. 41, 173000, Velikii Novgorod
tel: (816-22) -11-68-91, fax: (816-22)-24110, e-mail: theorphy @ info novsu.ac.ru

Logperiodic antennas are widely used for construction of super-wideband antenna systems [1]. A logperiodic antenna is a system of discrete radiators (dipoles or slots), whose every subsystem forms the directivity diagram in its frequency band. The number of overlapping bands depends both on the general number of radiators in the logperiodic array and on the constructive parameters of arrays. Unfortunately, existing methods of estimating electromagnetic characteristics of such antennas have a very rough character due to mathematical complexities that can occur. In general, their construction is done experimentally, when one has to obtain the given characteristics of radiation and broad-band matching by a trial-and-error method.

In the paper a rigorous method is proposed to analyze a subsystem of the logperiodic array consisting of several dipoles. The method is based on the use of the numerical analytical method that was first offered to analyze dipole and slot radiators [2-3]. For the analysis of director antennas, this method was used in paper [4], where the rigorous analysis of a system of active and passive radiators was performed.

It is also possible to extend this method to our case. The numerical-analytical method belongs to hybrid ones [3] and guarantees the least loss of accuracy in calculations. Here, the known integral operator [2] is chosen to calculate a current distribution along the dipole. The solution for the current distribution, which allows obtaining all the other electromagnetic parameters of the radiator, is found partially by Galerkin numerical method, and partially analytically:

$$LI = e,$$

where L is the integral operator with the logarithmic singular kernel; I is the current distribution to be found, e is the known excitation function.

Thus, it is possible to obtain accurate solutions of the following problems:

-determination of the required number of basis functions in the current expansion according to Galerkin method;

-calculation of the system characteristics versus the dipole length and thickness;

-determination of the solution convergence rate with parameter changes.

Similar problems for the director dipole antennas were treated in [5], where the high efficiency of the method proposed was shown. It is expedient to extend this solution to the analysis of strip logperiodic dipole and slot antennas. With this, dipole antennas are made on the basis of nonsymmetrical lines and slot antennas, or on the basis of strip lines. In the SHF and EHF ranges these lines are made by modern technology methods, and they are small-sized constructions, which can be successfully placed on any mobile engineering (aircraft, automobile, etc.).

The array elements are chosen, as a rule, with the length L being close to $\lambda/2$ (λ is the wavelength). The limitation of the working range of a dipole logperiodic antenna at low frequencies is conditioned by the increase of dimensions (which is especially inadmissible in strip systems), and at high frequencies, by accuracy of manufacturing a construction (which is very important in themicrowave ranges). At present, for strip logperiodic structures with the use of modern technology methods, overlapping of the working ranges of the order of 20:1 is attained [5].

REFERENCES

1. V. Ramzey, Frequency-independent antennas, Moscow. Mir, 1968 [in Russian].
2. Yu.Yu. Radtzig, S.I. Eminov, et al., Proc. of III Russian Scientific and Technical Conference, Kazan, 1994, pp. 114-115 [in Russian].
3. E.I. Nefedov, Yu.Yu. Radtzig, S.I. Eminov, Doklady RAN, 1995, vol. 344, no. 4. pp. 477-478 [in Russian].
4. I.L. Orlov, Yu.Yu. Radtzig, S.I. Eminov, Dep. B VINITI № 500-B96, 16.02.96 [in Russian].
5. I.L. Orlov, Ph.D. Dissertation, Novgorod, 1996 [in Russian].

EXPERIMENTAL INVESTIGATION OF HORN ANTENNA RADIATION

O. O. Drobakhin, D. Yu. Saltykov

Dnepropetrovsk State University,
13, per. Nauchny, 320625, Dnepropetrovsk, tel. (0562) 46-79-95

Horn antennas are widely used in different practical applications. They serve as feed antennas in many types of more complex constructions of antennas. The horn antennas are powerful means of high energy technology, they are used as applicators in medical purposes. The horn antennas are the most popular probing device in non-destructive testing. The horn antennas are also important tools of standards of power gain. In all applications the information about of space distribution of electromagnetic field is very important. For instance in medical and technological applications knowledge of field distribution allow ones to control the depth of heating that is very important for success of operation. The feature of these applications is use of near-field wave. Information about longitudinal distribution of field serves for increasing accuracy in non-destructive testing due to more accurate calibration at the same distances for structure under test and metallic standard mirror. Usually they cannot be positioned in the same place under technological process and displacement courses error in calibration and therefore errors in dielectric constant and thickness. Power gain can be measured using metallic plate but this approach is simple only for far-field zone, for Fresnel zone a few sets of measurements at a few distances are need. This circumstance determines importance of the field description.

TECHNIQUE OF PROCESSING

Measurements have been carried out in frequency range 17 – 25.5 GHz. Waveguide with cross-section 11×5.5 mm was used. Two horns with length 99 mm and aperture size 46.5×47 mm (horn 1) and with length 200 mm and aperture size 82×83 mm (horn 2) were tested. Both of them have reflection in throat in 1.5 – 2 times greater than in aperture plane. Reflectivity for metallic plate situated 20 cm from aperture against frequency are presented in Fig. 1 (horn 1) Fig. 2 (horn 2). Corresponding time-domain signals are displayed in Fig. 3, 4. Consideration of experimental data for metallic plate positioned in different distance shows that measured dependence contains many ripples. The course of this phenomenon is presence additional discontinuities in a horn.

Let us analyze amplitude reflectivity $A(\omega)$ in presence two reference reflections r_1 and r_2 with time delay t_1 and t_2 from structure under test (SUT) with complex reflectivity $R(\omega)$. Then $A(\omega)$ is given by

$$A(\omega) = k|r_1\exp(+j\omega t_1) + r_2\exp(+j\omega t_2) + R(\omega)|^2 = k\{|r_1|^2+|r_2|^2+|R(\omega)|^2+r_1^*R(\omega)\exp(-j\omega t_1) + r_1R^*(\omega)\exp(j\omega t_1) + r_2^*R(\omega)\exp(-j\omega t_2) + r_2R^*(\omega)\exp(j\omega t_2) + r_1^*r_2\exp[j\omega(t_2-t_1)] + r_1r_2^*\exp[-j\omega(t_2-t_1)]\}. \quad (1)$$

For horn, experiments show that the autocorrelation function $r_A(t) = F^{-1}\{|R(\omega)|^2\}$ ($F^{-1}\{\ \}$ — the inverse Fourier transform) is more powerful than cross-correlation functions $r_R'(t) = F^{-1}\{r_1^*R(\omega)\exp(-j\omega t_1)\}$ and $r_R''(t) = = F^{-1}\{r_2^*R(\omega)\exp(-j\omega t_2)\}$ if reflection of metal plate is measured. For SUT's with reflectivity 0.2–0.3, these functions are comparable. For SUT's with reflectivity approximately equals 0.05, cross-correlation functions are dominated. Similar to open-ended waveguide preliminary processing in form $1 - A / (k_2|r_0|^2)$ with $|r_0|^2 = |r_1\exp[j\omega(t_2-t_1)]+r_2|^2$ is impossible due to small values in $|r_0|^2$. Autocorrelation function of horn $k|r_0|^2$ is subtracted from experimental data $A(\omega)$ which are square of modulus of sum of horn reflection (reference signal) and SUT reflection.

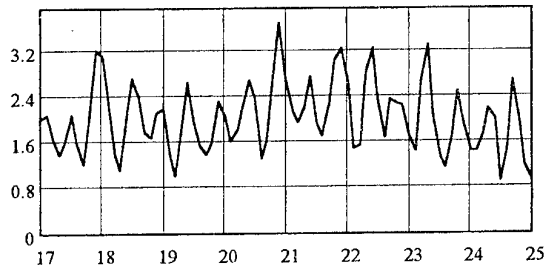


Fig. 1

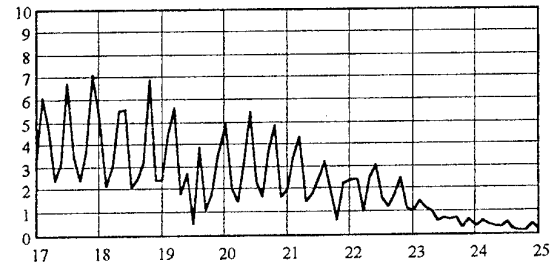


Fig. 2

After subtraction $k|r_0|$ from $A(\omega)$ we have

$$A'(\omega) = k\{|R(\omega)|^2+r_1^*R(\omega)\exp(-j\omega t_1) + r_1R^*(\omega)\exp(j\omega t_1) + r_2^*R(\omega)\exp(-j\omega t_2) + r_2R^*(\omega)\exp(j\omega t_2)\}. \quad (2)$$

Cross-correlation functions $r_R'(t)$ and $r_R''(t)$ are not overlapping if t_1, t_2 and $|t_1-t_2|$ are greater than time of propagation in SUT. For SUT time-domain signal extraction, any cross-correlation function $r_R'(t)$ or $r_R''(t)$ can be used. If only cross-correlation $r_R'(t)$ is used, situation can be simplified. The conditions for time intervals must be realized only for reference discontinuity r_1, the first in the horn. Thus the length of horn must be longer than SUT electrical thickness. For metal plate this requirement can be satisfied very simply. The latter requirement can be relaxed if impulse function of SUT has tendency to decrease. Effect of cross-function overlapping is negligibly small in this case.

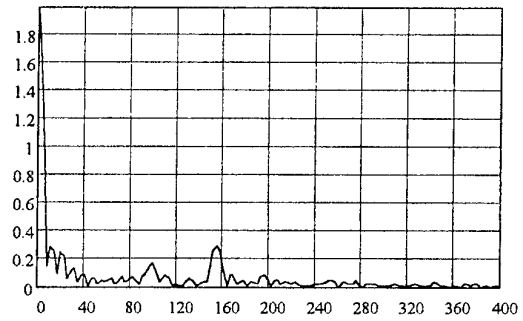


Fig. 3

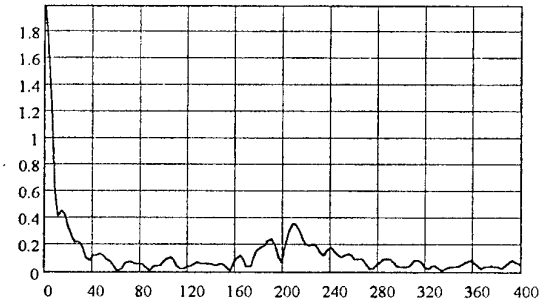


Fig. 4

Measurements are multifrequency ones. After Fourier transformation time-domain signal is obtained. We can analyze some peaks. The peak at $t = 0$ is proportional to $F^{-1}\{k|R(\omega)|^2\}$. After square rooting modulus of average value of $k|R(\omega)|$ is obtained. This approach is appropriate if frequency property of reference reflection is not optimal thus the error of modulus reconstructed from cross-correlation function is rather large. Another appropriate situation is one then autocorrelation is greater than any cross-correlation functions but under real conditions all spurious reflections form their proper autocorrelation functions. Spectra of all these functions have identical support thus informative autocorrelation function is corrupted. Trend due to calibration displacement course error as well. Practical significance of this approach lies in situation then additional signals are absent or rather small. Cross-correlation function produces peak that is proportional to average value of reflectivity. As result of the experimental investigation the amplitude of peak corresponding to reflection from metal surface versa distance between aperture and reflector has been obtained. Fig. 5, 6 shows result for cross-correlation peak and Fig. 7, 8 shows data for autocorrelation peak. Data for horn 1 are presented in Fig. 5, 7, data for horn 2 are presented in Fig. 6, 8. Non-monotonic behavior for horn 2 coursed by near-field measurements and complicated summation of reflections from cutoff sections in the horn. Data for peak corresponding to reflection from frontier surface of single layer dielectric structure such as ST-16 and plexiglass are presented in Fig. 9 (horn 1) and Fig. 10 (horn 2). More monotonic behavior is due to less level of reverberations.

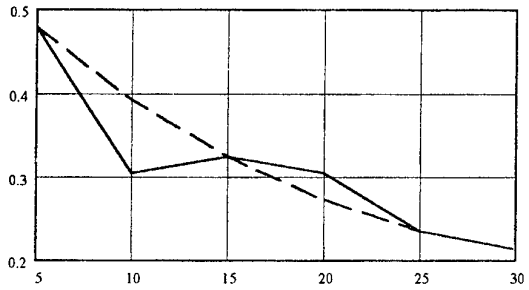


Fig. 5

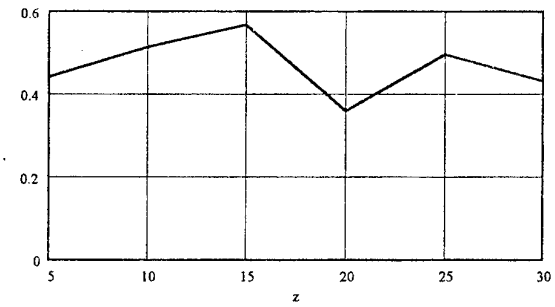


Fig. 6

Models of circular and elliptic gauss beams have been used for experimental data approximation. Approximation process consists of two steps. The first step was interpolation of experimental data by rational function of different orders according to gauss beam model, the second step was calculation of gauss beam parameters such as waist position and radius using correspondence of different models of gauss beam and coefficients of rational functions. For circular gauss beam function is $R(z) = 1/\sqrt{z^2 + b^2}$ where $b = \frac{\pi}{\lambda}\rho_0^2$ is confocal parameter and ρ_0 is minimal radius of beam, z is longitudinal coordinate. Thus $b^2 = a_0/a_1$ where a_0, a_1 are the coefficients of function $\left(a_0 + a_1 z^2\right)^{-\frac{1}{2}}$. For model of circular gauss beam with waist displacement in form

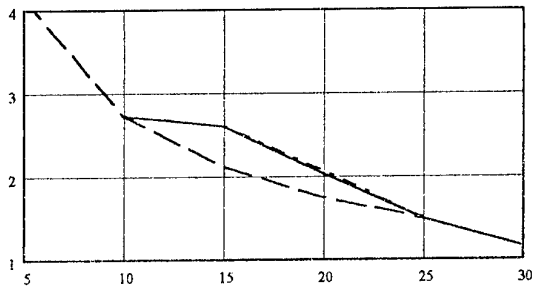


Fig. 7

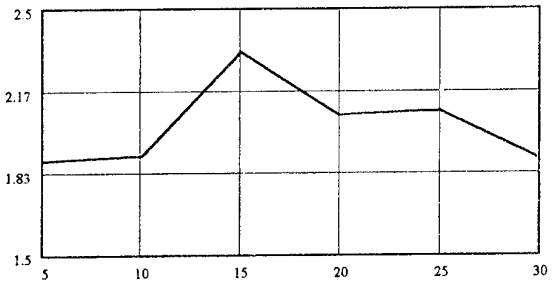


Fig. 8

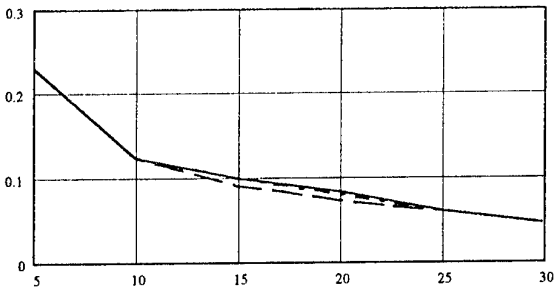


Fig. 9

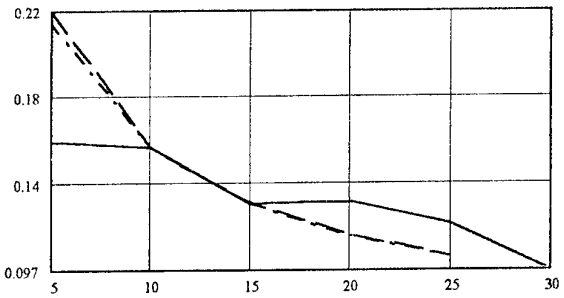


Fig. 10

$R(z)=1/\sqrt{(z-z_0)^2+b^2}$ beam parameters can be searched as $b^2=a_0/a_1-a_1^2/4a_2^2$, $z_0=a_1/2a_2$, where a_0, a_1, a_2 are coefficients of rational function $\left(a_0+a_1z^2+a_2z^4\right)^{-\frac{1}{2}}$ and z_0 is displacement of waist position from the aperture plane, positive value corresponds to the displacement in direction to the horn throat. For elliptical gauss beam it is true $R(z)=1/\sqrt{\left(z^2+b_x^2\right)\left(z^2+b_y^2\right)}$ with confocal parameters b_x and b_y in planes $x0z$ and $y0z$. b_x and b_y can be calculated using the coefficients of function $\left(a_0+a_1z^2+a_2z^4\right)^{-\frac{1}{4}}$ according to

$$b_x=\frac{1}{2}\left[\frac{a_1}{a_2}\pm\sqrt{\left(\frac{a_1}{a_2}\right)^2-4\frac{a_0}{a_2}}\right]$$

and

$$b_y=\frac{1}{2}\left[-\frac{a_1}{a_2}\pm\sqrt{\left(\frac{a_1}{a_2}\right)^2-4\frac{a_0}{a_2}}\right].$$

At last for elliptical gauss beam with non-uniform of waist displacement in planes $x0z$ and $y0z$ $R(z)=1/\sqrt{\left((z-z_{0x})^2+b_x^2\right)\left((z-z_{0y})^2+b_y^2\right)}$ has place. The values of beam parameters can be determined using the roots of polynomial of fourth order.

The results of approximation are presented in Fig. 3 –5 by dashed line for circular beam and by dot-and-dash line for elliptic beam.

CONCLUSION

Coincidence of model and experimental data was improved with growing of the number approximation parameters of gauss beam from circular to elliptic with waist displacement. For horn 1 mean square values were 1.2 % for metal plate, 1 % for St-16, 0.8 % for plexiglass. For horn 2 these values were 6.5 %, 0.8 %, 0.3 % correspondingly.

DISK-ON-ROD-IN-WAVEGUIDE RADIATING ELEMENT FOR DUAL-POLARIZED BROADBAND WIDE SCANNING ARRAY ANTENNAS

R. F. Dubrovka

National Technical University of Ukraine "KPI", Laboratory of Antennas and Telecommunications,
2110D, Radio Engineering Faculty, Polytekhnichna st., 12, Kyiv, 252056, Ukraine
Tel/Fax: 380-44-2417223 e-mail: dubrovka@ucl.kiev.ua

INTRODUCTION

Dual polarized broadband wide scanning arrays are found to be of great interest for application in modern and future radars and satellite telecommunications systems. Designing such arrays puts on the array element two contradictory requirements: minimization of cross-section of the element aperture and decreasing its cut-off frequency.

In the paper a combined disc-on-rod in cylindrical waveguide radiating element ("disk-on-rod-in-waveguide") as a potential candidate for the arrays is studied.

OUTLINE OF THEORY

Longitudinal section of the disk-on-rod-in-waveguide radiating element is shown in Fig. 1. Analysis of radiation characteristics of the array element is based at the mathematical model [1, 2] developed for a generalized longitudinally irregular axisymmetrical radiating element with taking into account an influence of free-space, that is, a reflection of waveguide modes at the aperture.

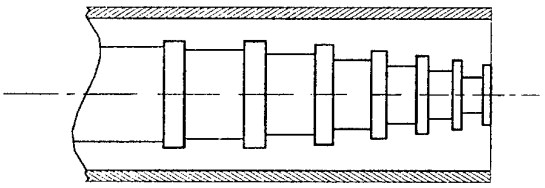


Fig. 1

At first, the initial geometry of the radiating element is divided into sections of regular coaxial waveguides. Using mode-matching technique the generalized scattering matrix of the element is found. Knowing the general scattering matrix of the element and a amplitude of exciting mode at the throat of the element it is possible to find field distribution at the element aperture in terms of coaxial waveguide modes. After that amplitudes of modes excited by electromagnetic waves reflected from the free space are found using moment method. Summing amplitudes of the incident and reflected modes, more accurate field distributions at the radiating element aperture and at its throat are determined. Hence, it is possible to find an accurate VSWR value and a radiation pattern of the radiating element. The radiation pattern is determined as a Fourier transformation of the tangential electrical components of the coaxial waveguides modes at the element aperture.

THEORETICAL AND EXPERIMENTAL RESULTS

Measurements of radiation characteristics (including crosspolarization) of the disk-on-rod-in-waveguide element were performed in the unechoic chamber. Comparision of theoretical and experimental results confirmed that the mathematical model [1,2] describes this radiating element with a fairly good accuracy.

Radiation pattern of the radiating element looks like Huygens element one. The main crosspolar radiation maxima are in planes inclined at angle 45° to the cardinal *E*- and *H*-planes. There are two possible ways to create the broadband antenna array element with low crosspolar radiation level:

Decreasing of overall crosspolarization lobes of the radiation pattern due to an optimal profile of the corrugated conductor.

Forcing the crosspolar radiation peaks out an operating angle sector.

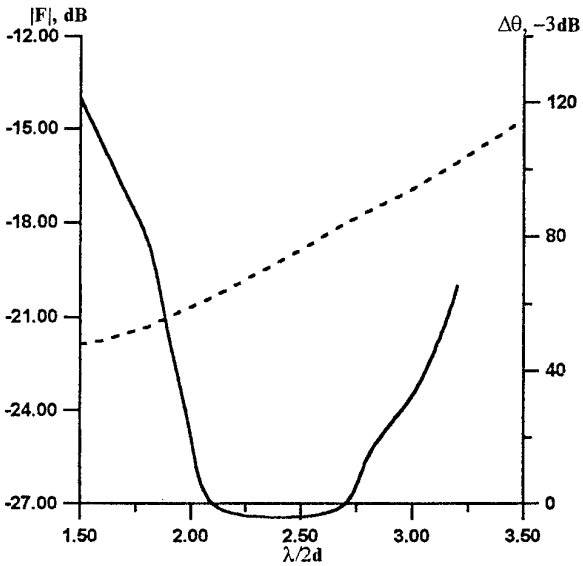


Fig. 2

The main complexity in the array element synthesis is necessity to meet the contrary requirements to a broad frequency bandwidth and a wide scanning angle of the array.

To cover octave frequency bandwidth a compact radiating element (aperture diameter is equal $0.4\lambda_L$, where λ_L is the lowest operating frequency) was synthesized. Peak values of crosspolar radiation level in the scanning sector and beamwidth values versus normalized wavelength are presented in Fig. 2. It can be seen that the radiating element half-power beamwidth is not less than 60° in a frequency range 40 %. This is a crucial point to meet the requirements to wide-angle scanning. In order to cover initial settings to the scanning sector crosspolar radiation maxima were forced out the angle sector ±45°.

Experimental verification of radiation characteristics of the synthesized radiating element was carried out. The radiating element excitation in the frequency range 5.0...10.0 GHz was realized by a symmetrical antiphase exciter. VSWR < 1.3 has been achived.

Typical measured radiation patterns of the synthesized radiating element are presented in Fig. 3. Here the bold line represents radiation pattern in *E*-plane, the thin line — in *H*-plane and dush-dot line — crosspolar radiation pattern in the intercardinal plane. Radiation characteristics of the element in the operating frequency range are given in Fig. 4.

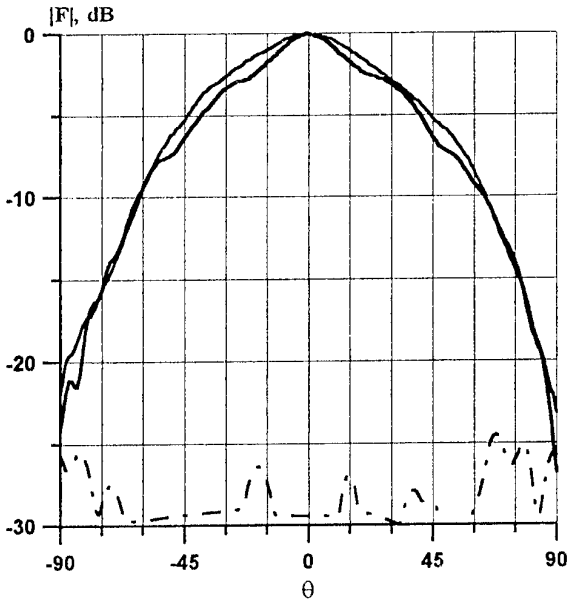
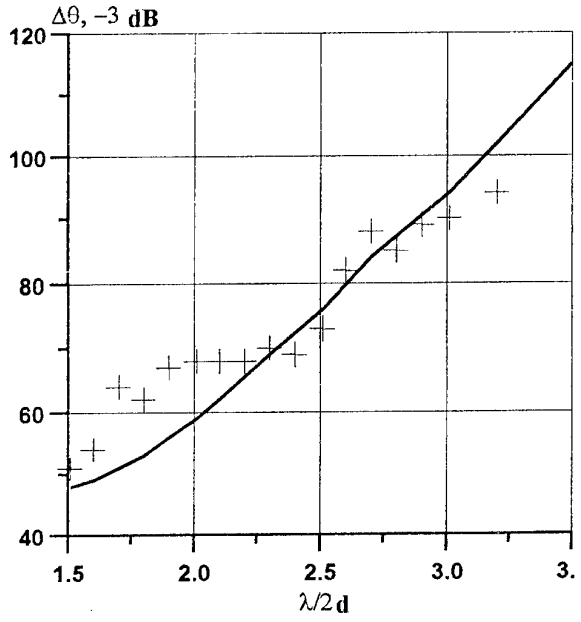


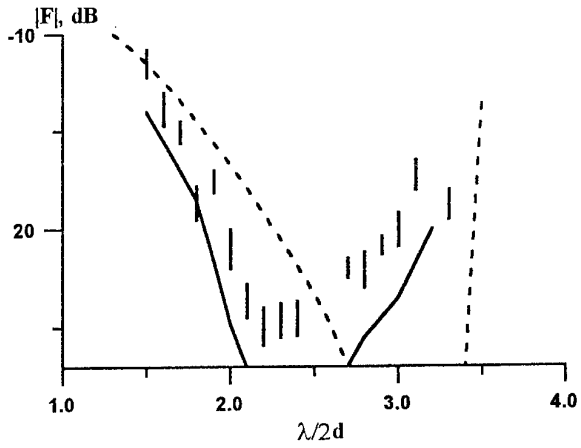
Fig. 3

Fig. 4a demonstrates half-power beamwidth frequency response: solid line represents theoretical data, crosses represent experimental ones.

Solid line in the Fig. 4b represents calculated peak values of crosspolarization in the scanning sector (±45°) in the frequency range. Dush line in the figure represents peak values of crosspolarization calculated by using the periodical structure theory [3]. Vertical bars represent measured data. Comparing the results in Fig. 4 one can conclude that the moment method solution [1] is much more accurate than that of the periodical structure theory [3].



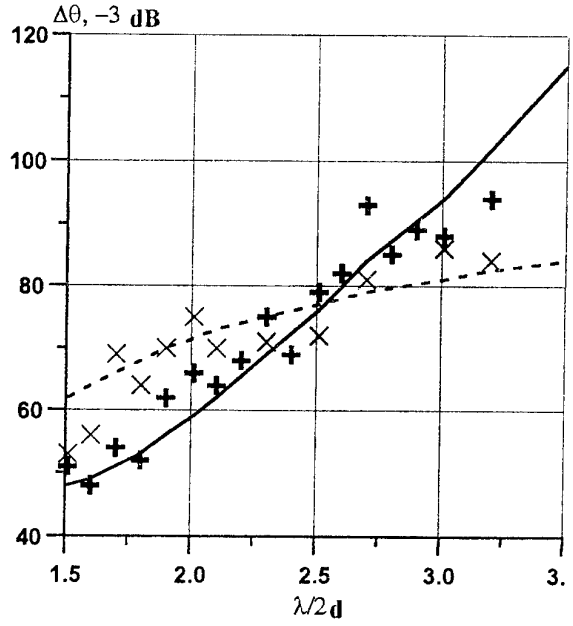
a



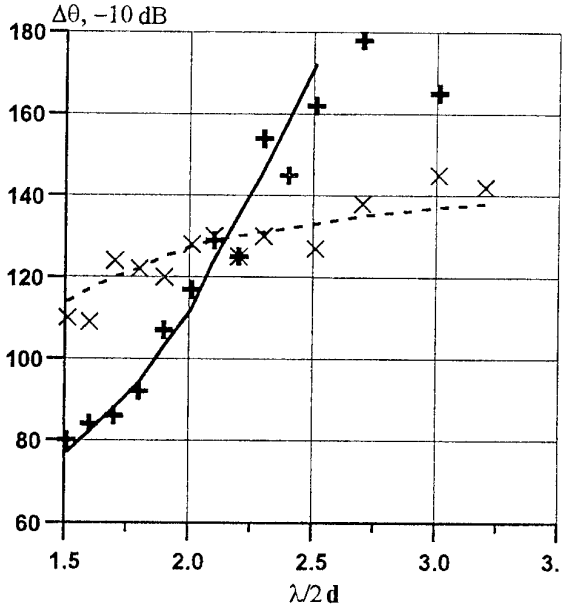
b

Fig. 4

Theoretical and measured values of −3 dB and −10 dB beamwidths for *E*- and *H*-plane are shown in Fig. 5. Measured data in *E*-plane and *H*-plane are marked by crosses and inclined crosses respectively. Theoretical results are shown by solid line (*E*-plane) and dushed line (*H*-plane). One can see that the calculated beamwidth values agreed fairly well with experimentally determined values.



a



b

Fig. 5

CONCLUSIONS

Disk-on-rod-in-waveguide radiating element is definitely a good choice for broadband polarizationally invariant antenna array applications due to a small cross-section and octave frequency bandwidth capability. It has been established that the developed technique allows one to predict radiation characteristics of such elements reasonably well, whereas periodical structure approach gives poor results in prediction of crosspolar radiation pattern. By using the developed theory and a theory of the finite antenna array composed of the disk-on-rod-in-waveguide elements one can design finite polarizationally invariant broadband wide angle scanning antenna arrays.

REFERENCES

1. R.F. Dubrovka. Analisys of finite antenna arrays composed of open-ended axisymmetrical lognitudinally irregular structures, Izvestia VUZov Radioelectrinica, vol. 39, pp. 50-64, October 1996.

2. R.F. Dubrovka. Theoretical and experimental investi-gations of finite antenna arrays composed of disk-o-cone radiating elements, Proc. of the 2nd Int. Conf. on Antenna Theory and Techniques, Kyiv, Ukraine, pp. 62-64, 1996.

3. F.F. Dubrovka, V.A. Lenivenko. Synthesis of disk-on-rod antennas. Izvestia VUZov Radioelectrinika, vol. 38, pp. 29-34, May 1993.

DIRECTIVITY CHARACTERISTICS AND RADIATION IMPEDANCE OF A CIRCULAR FRAME PLACED AROUND A CYLINDER OF PERFECT CONDUCTIVITY

G. A. Evstropov, A. I. Klimenko

Research Institute of Long- Distance Radio Communication
11/12, 1 Bulvostova St. Moscow 107258, Russia
Phone: (095) 963-93-09

Circular, rhombic, square and rectangular loop antennas are widely used in practice, especially as receiving TV antennas [1–3]. The radiation impedance of a circular loop antenna is equal to 132 Ω, whereas the impedance of a square antenna is 122 Ω. This matches quite well a 75-Ω cable and allows one to use a double loop (z-antennas for TV program reception). When using square loop antennas with sides a and b, it is possible to change the radiation impedance and, as a consequence, the input impedance in the wide range from 30 Ω to 300 Ω. When the height of the loop is small (small values of b), the antenna becomes a folded dipole antenna. The polarization of the loop antenna radiation in the principal planes coincides with the direction of the electrical field at the input terminals.

Lately, as the number of TV broadcast stations has been growing rapidly, loop antennas have become used as TV transmitting antennas. The most widely used ones are horizontally polarized loop antennas with the loop in the vertical plane. In order to obtain a sufficiently uniform azimuth radiation pattern (RP), two perpendicular loops are usually used with a quadratic drive.

It is useful to note that double loops are not the most optimal ones from the point of view of construction. For instance, the vertical step of circular loops turns out to be $t = \lambda/\pi$ (λ is the wave length) whereas for the best gain KND, the optimal step is $t = 2.3\ \lambda/\pi$. The gain of one double loop is $D = 4.6$ dB, the gain of an optimal step loop is $D = 7.3$ dB and the gain of a single loop is 3.3 dB. As a uniform azimuth RP is formed, the gain is reduced by 3 dB.

A horizontally polarized transmitting antenna with an ideal azimuth uniformity can be built using a horizontal circular loop. For a single loop, the RP in the horizontal plane is $f1 = (\varphi) = \cos\varphi$. For two parallel loops rotated around the common vertical axis by the angle of $\pi/2$ and driven quadratically, we get $f(\varphi) = \exp(i\varphi)$, i.e. $|f(\varphi)| = 1$.

It is convenient to place a horizontal circular loop around a metal tube which can possibly have a different primary purpose. In order to fix the loop in place one can use a metal stick attached by one end to the loop at the zero potential point and by the other end — to the tube. The driving cable can be directed through the stick to the opening in the loop. The centers of the opening and the metal stick must be placed along one diameter of the ring.

In order to calculate directional characteristics we will assume that the circumference of the loop is equal to the wavelength, and the field distribution in the ring is given by

$$I = I_0 \cos(k r_1 \Psi), \tag{1}$$

where $k = 2\pi/\lambda$ is the wave number, and ψ is the angular coordinate of the element of the ring. We assume here that in the Cartesian coordinate system, the ring is situated in the x-z plane, and the axis of the infinite cylinder (the tube) coincides with the y-axis. The azimuth angles ψ and φ are measured with respect to the x-axis. The angle θ is measured with respect to the plane of the ring. If the ring is placed in a free space, then we can use well known techniques [4] to obtain the following expressions for the field components in the far field

$$E_\varphi = 30\pi I_0 (J_0(kr_1\cos\theta) - J_2(kr_1\cos\theta))\cos\varphi \frac{\exp(-ikR)}{R} \tag{2}$$

$$E_\theta = 30\pi I_0 (J_0(kr_1\cos\theta) + J_2(kr_1\cos\theta)) \times \sin\theta\sin\varphi \frac{\exp(-ikR)}{R}$$

The radiation impedance is obtained by means of integrating the squared absolute values of the above expressions with $I_0 = 1$ over a share of radius R, and then adding the two results. Now we turn to the problem with a cylinder. There, one must consider the problem of finding the excitation of the special domain bounded by a cylinder of perfect conductivity, by a coaxial ring of electric current. We assume here that the side of the current ring is infinitely thin, i.e. it can be represented by a δ-function, and the coordinate y is a constant and equal to 2 δ. To solve the problem, we split the space into two cylindrical domains: one between the conducting cylinder and the ring (domain i) and the other - outside the ring (domain e). Since the size of this publication is limited and some of the expressions are quite cumbersome, we will only outline the most important steps of the calculation and present the results. We represent the solution in each of the domains as a su-

perposition of E- and H- waves along the y-axis by analogy with the coaxial representation of a field. Then the longitudinal components of the fields in domains i and e are expressed as

$$\left.\begin{aligned} H_y^i &= (A^i e)x^2(J_1(xr)+B\mu Y_1(xr))\sin\varphi e^{-ik\beta y} \\ H_y^i &= (A^i \mu)x^2(J_1(xr)+B\mu Y_1(xr))\cos\varphi e^{-ik\beta y} \\ H_y^e &= (A^e e)x^2(H_1^{(2)}(xr)\sin\varphi e^{-ik\beta y} \\ H_y^e &= (A^e \mu)x^2(H_1^{(2)}(xr)\cos\varphi e^{-ik\beta y} \end{aligned}\right\} \quad (3)$$

for each value of β. Here J_1, Y_1 $H_1^{(2)}$ cylindrical functions

$$x^2 = k^2(1-\beta^2) \quad (4)$$

The constants B are determined from the boundary conditions on the cylinder ($r = r_0$):

$$E_y(r_0) = E_\varphi(r_0) = 0$$

The constants A are obtained from the continuity of E_y, E_φ, H_φ, for $r = r_1$ and from the fact that the difference between $H_y^{(e)}$ and $H_y^{(i)}$ for $r = r_1$ is equal to the external current density (1). In order to satisfy the latter boundary condition, we represent the circular current along the y-axis analytically in terms of the Fourier transform

$$I(y) = \int_{-\infty}^{\infty} \frac{I_0}{2\pi}\frac{\sin k\beta\delta}{k\beta\delta}e^{-ik\beta y}dk\beta \quad (5)$$

where sin $((k\beta\delta)/k\beta\delta)$ is the Fourier transform of the external current along the y-axis. Then the boundary condition for H_y becomes

$$H_y^e(r1) - H_y^i(r1) = \frac{I_0}{2\pi}\frac{\sin k\beta\delta}{k\beta\delta}e^{-ik\beta\delta} \quad (6)$$

After determining the coefficients A, the field in the e-domain can be obtained by integrating the expressions for E_φ and H_φ (see (3)) in beta. The far field can be calculated from this integral by the method of stationary phase. As a result, we get

$$H_\varphi = -i30\pi\frac{\sin(k\delta\sin\theta)}{\beta\delta\sin\theta}(J_0(kr_1\cos\theta - J_2(kr_1\cos\theta) - \frac{J_0(kr_0\cos\theta)-J_2(kr_0\cos\theta)}{N_0(kr_0\cos\theta)-N_2(kr_0\cos\theta)}(N_0(kr_1\cos\theta - N_2(kr_1\cos\theta)\cos\varphi\exp(ikR)/R \quad (7)$$

$$H_\varphi = \frac{i}{4}\frac{\sin(k\delta\sin\theta)}{k\delta\sin\theta}(J_0(kr_1\cos\theta + J_2(kr_1\cos\theta) + + \frac{J_1(kr_0\cos\theta)}{N_1(kr_0\cos\theta)}(N_0(kr_1\cos\theta + N_2(kr_1\cos\theta))\times \sin\theta\sin\varphi\exp(-ikR)/R \quad (8)$$

As $\delta\to 0$ and $r_0 \to 0$, the expressions obtained here coincide with the results for the fields radiated by a thread and a circle in a free space (2) if we take into account that $E_\theta = Z_0 H_\varphi$. The resistance impedance and the gain are obtained from these formulae in a way similar to the case of a ring in a free space.

Our calculations show that the radius of the cylinder strongly influences the radiation level of component E_φ in the plane of the ring, compared to the axial radiation. It also affects the radiation impedance (RΣ) and the gain. The corresponding results are given in the Table.

Kr_0 (times)	RΣ (Ω)	Fφ (0) (times)	KND (dB)	Fφ(0)*KND (dB)
0.0001	132	0.65	3.5	-0.3
0.001	132	0.65	3.5	-0.3
0.2	118	0.62	3.8	-0.4
0.3	101	0.58	4.2	-0.5
0.4	81	0.52	4.8	-0.8
0.5	59	0.44	5.7	-1.3
0.6	39	0.35	6.8	-2.1
0.7	22	0.26	8.2	-3.6

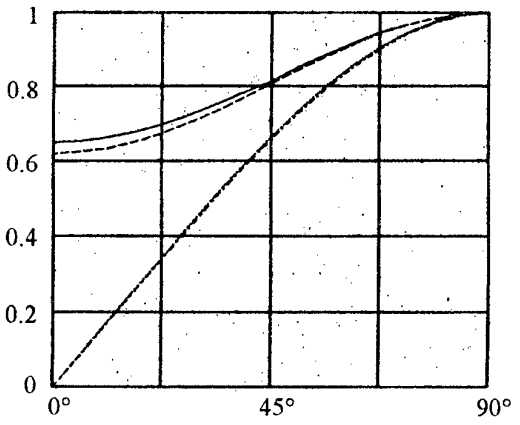


Fig.

The radiation impedance of 75 Ω is obtained for kr_0 = 0.43. The impedance of 50 Ω corresponds to kr_0 = 0.545. The diagram of Fφ (θ) is normalized so that it is equal to 1 for θ = π/2. The values of Fφ(θ) for kr_0 = 0.001 coincide with the values of the RP in a free space up to three decimal digits. The values of the RP for kr_0 = 0.001 and kr_0 = 0.2 are given in the Fig. In this antenna, the horizontal polarization is the operating one. However, as it follows from the pictures, it has a great significance as the observation point gets close to the

cylinder axis. The maximum of the operating polarization is also in the direction $\theta = \pi/2$. For an antenna it is usually required that the maximum lies in the direction $\theta = 0$. Both the axial and the spurious radiation can be reduced to a small value if rings are composed into a lattice. For instance, a two level lattice of rings in a free space leads to the gain of 2.7 dB (with respect to the isotropic radiation) for a uniform azimuth RP and the optimal step of $kt = 4$.

A four level lattice gives 6.8 dB with the optimal step of $kt = 5$.

REFERENCES

1. Karl Rothammel. Antennas. M: "Boyanich", Sanct-Peterburg, 1998, 650 s.
2. K. Kharchenko.YKV antennas. M.:.DOSAAF. Moscow, 1969, 110 s.
3. I. N. Sidorow. Televizionnis antennas. Lenizdat, Sanct-Peterburg, 1996.
4. Spravochnic po antennoi tekhnice. Tom 1. M/: "Padiotekhnica", Moscow, 1997, 249s.

A REDUCTION OF LOG-PERIODIC ANTENNAS DIMENSIONS

E. V. Goremykin, G. I. Kostromitin

Taganrog State University of Radio Engineering, Department of Antennas and Radio Transmitters, TSURE, Nekrasovsky, 44, GSP-17A, Taganrog, 347928, Russia,
phone (863-44) 6-17-33, fax (863-44) 6-50-19, e-mail: airpu@tsure.ru

ABSTRACT

The effects of dielectric substrate and impedance loads of vibrators on the dimensions of log-periodic antennas are investigated. The equations for impedance matrix of feeder, input impedance and gain of the log-periodic antennas are presented. Numerical results for the log-periodic and Uda-Yagi antennas are included. Effect of impedance loads on the parameters of log-periodic antennas is examined.

INTRODUCTION

The reduction of antenna dimensions is a large problem because the antennas determine weight-dimensions parameters of a device as a whole. The antennas with gain (8 – 12) dB and good matching in frequency band (10 – 30) % or arrays formed of such elements are necessary for VHF communications (service communication, cellular communication, the mobile telephones, etc.). The antennas used in this frequency range must have smaller dimensions with the same gain, therefore, the actual problem is a development of methods to reduce antennas dimensions.

Antennas of a travelling wave have the largest gain. There are three types of dipole antennas of a travelling wave – a wave channel antenna (Uda-Yagi) (AWC), a log-periodic dipole antenna (LPDA) and antenna of a travelling wave (ATW). At the moment AWC has the greatest application, however LPDA has advantages on electrical performances and dimensions. The LPDA also has design shortages.

The design shortages of LPDA are eliminated with a replacement of a twin feed line by its printed analog. The second variant is a completely printed antenna for eliminating design shortages, but in this case wind resistance will increase.

The principal requirements to a dielectric substrate used in LPDA are high mechanical strength and small wave losses. The dielectric on a basis of glass-fibre materials is widespread, but it has large losses and unstable relative permittivity ε_r. For dielectric on a basis of glass-fibre material СТФТ-2-35 damping factor ~ 3.9 dB/m on frequency 900 MHz, permittivity $\varepsilon_r \sim 4.8$ are experimentally determined.

The LPDA has basic advantage: practical lack of restrictions on frequency band and lack of the elements of set-up. The second advantage is smaller dimensions on a comparison with AWC of an identical gain [5].

THEORY

The parameters of LPDA (Fig. 1) are determined by an equation [1], and corrected during calculation. The purpose of calculation is determination of current distribution along vibrators of the LPDA. The current distribution determines the radiation pattern (RP), input impedance (Z_{in}) and gain of LPDA.

LPDA and AWC are analyzed [2] by solving Hallen's integral equations systems in view of wave losses in a dielectric.

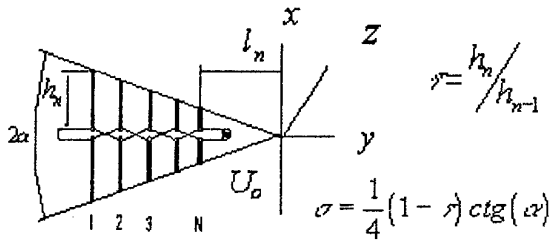


Fig. 1. Geometry of LPDA

The wave losses in a dielectric are taken into account in the parameters of the feeder. A matrix of the loss-free feeder $[Z^{\Phi}]$ it is easier to determine as $[Z^{\Phi}] = [Y^{\Phi}]^{-1}$. A conductivity matrix $[Y^{\Phi}]$ is given as [1]:

$$Y^{\Phi}_{N,N} = -\frac{i}{W}\mathrm{ctg}[k(l_{N-1} - l_N)];$$

$$Y^{\Phi}_{1,1} = -\frac{i}{W}\{\mathrm{ctg}[k(l_1 - l_2)] + \mathrm{ctg}\frac{kh_1}{2}\};$$

$$Y^{\Phi}_{n,n} = -\frac{i}{W}\{\mathrm{ctg}[k(l_{n-1} - l_n)] + \mathrm{ctg}[k(l_n - l_{n+1})]\}, \quad (1)$$

$$n = 2,3,\ldots,N-1;$$

$$Y^{\Phi}_{n,n+1} = Y^{\Phi}_{n+1,N} = -\frac{i}{W}\frac{1}{\sin[k(l_n - l_{n+1})]};$$

$$n = 1,2,\ldots,N-1;$$

where l_n – distance from geometric top of an antenna to the n-th vibrator.

The required wave resistance of the feeder W is determined from [1] and then it is updated.

The strip width of the feeder b, thickness of a dielectric substrate d, relative permittivity ε_r and strip thickness Δ [3,4] is given as

$$b \approx \frac{d}{2}\left(\frac{200\pi}{W\sqrt{\varepsilon_r}} - 1\right)\left(1 - \frac{2\Delta}{d}\right);$$

$$\varepsilon_{ef} \approx \frac{\varepsilon_r + 1}{2} + \frac{\varepsilon_r - 1}{2\sqrt{1 + 5\frac{d}{b}}}, \qquad (2)$$

where ε_{ef} – effective permittivity.

Factor k is given as [4] $\kappa = \beta - i\alpha$,

$$\beta = \frac{2\pi\sqrt{\varepsilon_{ef}}}{\lambda\sqrt{2}}\sqrt{\sqrt{1 + (\mathrm{tg}\delta_{ef})^2} + 1};$$

$$\alpha = \frac{2\pi\sqrt{\varepsilon_{ef}}}{\lambda\sqrt{2}}\sqrt{\sqrt{1 + (\mathrm{tg}\delta_{ef})^2} - 1}, \qquad (3)$$

where $\mathrm{tg}\delta_{ef} = \mathrm{tg}\delta\left[1 + \left(\sqrt{1 + 5\frac{hd}{bf}} - 1\Big/\varepsilon_r\left(\sqrt{1 + 5\frac{hd}{bf}} + 1\right)\right)\right]^{-1}$.

The conductivity matrix of the feeder with wave losses is given as:

$$Y^{\Phi}_{N,N} = \frac{1}{Wz(l_{N-1} - l_N)}; \quad Y^{\Phi}_{1,1} = \frac{1}{W}\left[\frac{1}{z(l_1 - l_2)} - \frac{1}{z(h_1/2)}\right];$$

$$Y^{\Phi}_{n,n} = \frac{1}{W}\left[\frac{1}{z(l_{n-1} - l_n)} + \frac{1}{z(l_n - l_{n+1})}\right], \quad n = 2,3,..,N-1; \qquad (4)$$

$$Y^{\Phi}_{n,n+1} = Y^{\Phi}_{n+1,n} = \frac{1}{W\sinh[(\alpha + i\beta)(l_n - l_{n+1})]}, n = 1,2,..,N-1;$$

in which $z(l)$ is input resistance of short circuit of a feeder with losses [5]:

$$z(l) = \frac{\sinh(2\alpha l) + (\alpha/\beta)\sin(2\beta l) - i[(\alpha/\beta)\sinh(2\alpha l) - \sin(2\beta l)]}{\cosh(2\alpha l) + \cos(2\beta l)}. \qquad (5)$$

The input impedance expressed through parameters of the feeder is given as:

$$Z_{in} = V_N = Z^{\Phi}_{N,N} - \sum_{m=1}^{N} Z^{\Phi}_{N} \quad {}_{m}\sum_{\mu=1}^{Q} I^{\mu}_{m}\varphi^{\mu}_{m}(0). \qquad (6)$$

Antenna gain ($D(\theta,\varphi)$) is given as:

$$D(\theta,\varphi) = \frac{|f(\theta,\varphi)|^2}{30\mathrm{Re}(Z_{in})(I_N(0))^2}. \qquad (7)$$

Antennas with narrow frequency band have been analyzed. These antennas have no vibrators longer then 0.6λ. For RP, Z_{in} and gain calculations we have used one single basis function of current distributions.

NUMERICAL RESULTS

We compared LPDA and AWC which have an identical gain (D ~ 10 dB) in frequency band, determined by a level VSWR < 1.5 in a range 900 MHz.

AWC with a band of operational frequencies (VSWR ≤ 1.5, F_{middle} = 900 MHz) 856 – 932 MHz consists of 7 vibrators and has length of 588 mm. The input resistance of antennas is 50 Ohm.

LPDA consists of 9 vibrators (τ = 0.9661; σ = 0.12) and has 300 mm length.

The current distribution along antennas are presented in Fig. 2 (in all figures the curves for LPDA are above, for AWC - below).

In Fig. 3 a shaped line correspond to the LPDA without wave losses, continuous – with wave losses.

The wave losses in a dielectric reduce gain of LPDA on ~ 1 dB (Fig. 3).

Calculations showed that LPDA is almost twice shorter then AWC at an approximately identical gain. LPDA has more uniform current distribution (Fig. 2) that increases the contribution of each vibrator to RP pattern.

The second reason of a reduction of dimensions of LPDA is a small level of side lobes (Fig. 4), that allows to obtain larger gain at an identical RP width.

Calculations showed that for diminution of length of an antenna it is necessary to provide uniform current distribution along an antenna. LPDA ensures the best current distribution today.

Length of vibrators influences on sizes of an antenna.

The longest vibrator in LPDA is shorter then $\lambda_{max}/2$. Calculation of current distributions taking into account three modes gives the greater shortening.

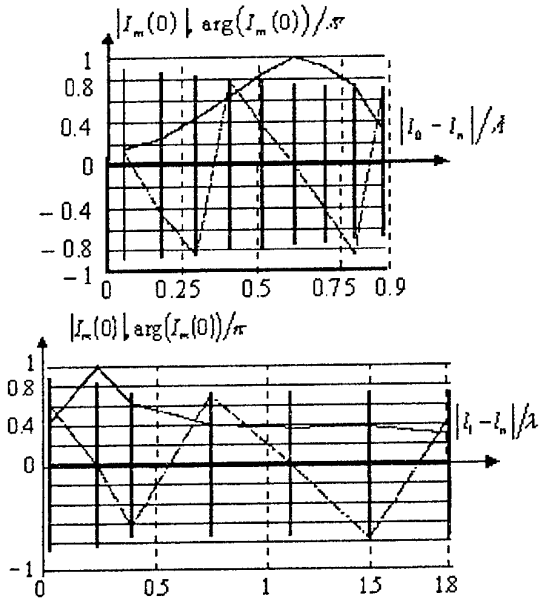


Fig. 2. Relative long and currents distribution of researched antennas (solid line – distribution of amplitude, shaped – current phase distribution)

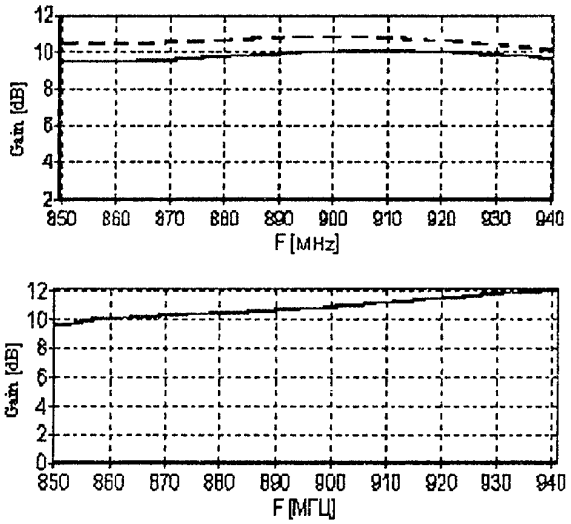


Fig. 3. A gain dependence on frequency ($D(\theta,\varphi)$)

With growth of τ, σ, ε_r shortening is increasing and making (8–15) %, and for the printed antennas – up to 30 % from $\lambda_{max}/2$. Therefore, a transversal size of LPDA is less than appropriate size of AWC. Physics of this effect is transparent: more short vibrators are closer to a point of a feed and radiate a basic part of an energy and the energy does not reach resonance vibrators.

For LPDA vibrators length reduction methods, useds in LW, MW and SW antennas, that is various form capacity loads on the ends of vibrators such as short inductance, etc., can be used.

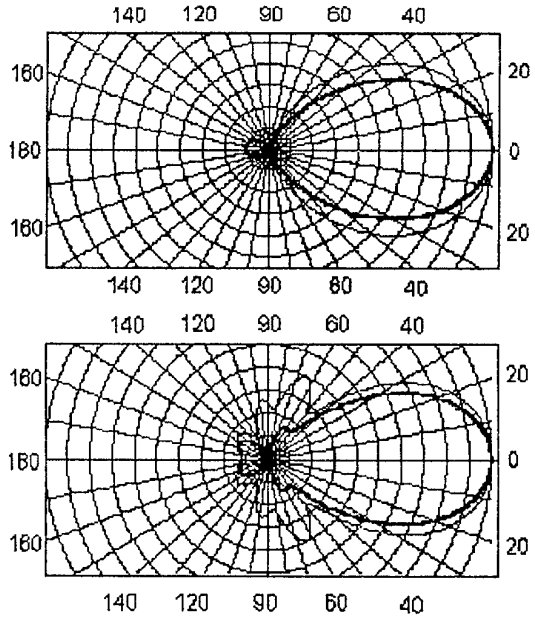


Fig. 4. The researched antennas radiation patterns

The capacity loads are most convenient tot ensure more uniform current distribution along a vibrator.

The limits of an integration to evaluate the influence of not-radiating capacity loads have been cosen taking into account the shortening, and the own input reactivity of short vibrators was equated to an own full reactivity. RP of a short vibrator was calculated strictly. Simultaneously experimental models of printed antennas with T-figurative loads were experimentally investigated.

Vibrators shortening changes a gain of LPDA differently in an association with τ and σ. At $\tau < 0.8$ shortening leads to a contraction of active zone that worsens a gain, but reduces length of an antenna. The increase in τ compensates a contraction of active zone and allows to obtain at initial length a former gain.

At increase in τ up to ~ 0.9 the active zone of LPDA vary weakly with shortening but gain a little bit decrease at the expense of a vacillation of a phase velocity along an antenna. At further increase in τ the active area with shortening extends a little but at the expense of a vacillation of a phase velocity gain a little bit decreases. At small σ shortening of vibrators does not almost influence on gain. The experimental outcomes are a little bit better than calculated, gain decrease is not more than on 0.5 dB.

The shortening reached 30–40 %. In printed antennas shortening reached 2 times and more.

The research outcomes showed that LPDA with a microstrip feed line and short vibrators is probably the most small-sized antenna even when using of dielectric with wave losses.

REFERENCES

1. *Carrel R.*, 1961 IRE Internat. Conv. Rec., pt. 1, 67-75 (1961).
2. *Wiriga B.A., Poluhin T.A., and other.* Phase lattices with wide band, Collection of scientific - methodical papers on an applied electrodynamics (issue 4).- Moscow, Vyschaja Shkola, 1980. – 240 p.
3. *Wolman W.I.,* Manual on calculation and designing a microwave strip devices, Radio i Sviaz - Moscow, 1982.
4. Designing and calculation of strip devices / Ed. by Kovalev I. S. - Moscow: Sov. Radio, 1974.
5. *Goremykin E.V., Kostromitin G.I.,*. Log-periodic antennas for UHF communications. Rostov Military Institute of Rocket Forces, 10,11 December, 1998, Rostov-on-Don.

MATHEMATICAL MODEL OF RADIATION FROM OPEN-ENDED CIRCULAR WAVEGUIDE

N. N. Gorobets, L. V. Orlova, A. V. Shishkova

Kharkov State University,
4 Svobody sq., 310077 Kharkov, Ukraine

The mathematical model of radiation from open-ended circular waveguide, operating on dominant-mode wave H_{11} has been developed. The simple approximation formulas allowing to calculate the power pattern for dominant-mode range on the whole observation-space, and also for one-mode range, as well as for multimode waveguide up to the level –12 dB have been obtained in *E*- and *H*- plane. It has been shown that the approximation relative error for the first case does not exceed 3 % in the main lobe of radiation pattern and for the second case it does not exceed 4 %.

FORMULATION OF THE PROBLEM

The waveguide radiators operating on the wave of dominant-mode H_{11} are widely used in the modern Microwave engineering as the elements of antenna arrays and as the feeds of narrow-beam reflector and lens antennas. The calculation accuracy of the power, phase and polarization reflector antenna characteristics is evaluated to a marked degree by calculation accuracy of the feed characteristics. The rigorous solution to the radiation problem from open-ended circular waveguide calculated by method from [1] is well correlated with experimental data. In addition, these characteristics clearly interpret the physical processes of diffraction on the open-ended waveguide, namely: the reflection of dominant-mode wave excited in waveguide and the appearances of the higher-order waves transformed from the base wave H_{11} in some frequency bands, in particular, the transformation H_{11} wave into E_{1n} and H_{1k}, that allows to investigate the effect of higher-order waves on radiation characteristics. It should be note, that Vainshtain method seems to be the only possibility to extend the range of the radiation theoretical investigation. The well-known aperture techniques [2] not only forbid to obtain the radiation characteristics for multimode waveguide but also give the results different from those of the experimental ones.

But, in spite of all the obvious advantages of the rigorous theory, it is very difficult to use it in practice. It connected with cumbersome and complicated calculation formulas. The problem can be solved, if the computations carried out are approximated by simple functions with some beforehand assumed accuracy.

APPROXIMATE MODEL

In narrow-beam reflector antennas the radiation power on the edge of reflector usually has a level of about –10 dB from the maximum directed power. This level is lower than the mentioned above one in antenna systems with more strict requirement to the side and back levels. It's about –12 dB. Therefore, it is appropriate to obtain the simple approximate formulas for calculation of the power pattern at the radiation range of the main lobe up to the level –12 dB concerning the radiation maximum in *E*- and *H*- plane in a wide frequency range. Thus, in present paper the approximation functions of two variables, where the first one is connected with directivity of the radiator (θ angle) and the second one is connected with the waveguide diameter ($x = 2\pi a/\lambda$ is the undimensional wave number, a is the waveguide radius and λ is the wavelength) have been derived.

The approximation formulas for pattern normalized to the radiation power at the major radiation maximum have been determined in this case as follows:

$$P_E(\theta, x) = \exp\{-E_1(x)\, Z\, [1+ E_2(x)\, Z]\}, \qquad (1)$$

$$P_H(\theta, x) = \exp\{-H_1(x)\, Z\, [1+ H_2(x)\, Z]\},$$

where $Z = \sin^2(\theta/2)$.

$$E_1 = -0.364\ x^{1/2} + 2.364\ x + 0.412\ x^2,$$
$$E_2 = 0.415\ x^{1/2} - 0.963\ x + 0.211\ x^2, \text{ for } x < 3.832;$$
$$E_1 = -9.8\ x^{1/2} + 7.3\ x + 0.43\ x^2,$$
$$E_2 = -0.84\ x^{1/2} - 0.38\ x + 0.24\ x^2,\ 3.832 < x \le 7.016;$$
$$E_1 = 0.909\ x^2 + 2.938,$$
$$E_2 = 0.189\ x^2 - 2.7,\ 7.016 < x \le 10.173;$$
$$E_1 = 0.9215\ x^2 + 2.294\ 1,$$
$$E_2 = 0.185\ x^2 - 2.417,\ 0.173 < x \le 13.324;$$
$$E_1 = 0.934\ x^2 + 0.1645,$$
$$E_2 = 0.178\ x^2 - 1.132,\ 13.324 < x \le 16.471;$$
$$E_1 = 0.951\ x^2 - 4.2073,$$
$$E_2 = 0.175\ x^2 - 0.4039,\ 16.471 < x \le 18.$$
$$H_1 = 0.41(x + 1.86)^2,$$
$$H_2 = 0.1(x - 3.34)^2,\ 2 < x \le 5.33;$$
$$H_1 = 0.56(x + 0.86)^2,$$
$$H_2 = 0.76\ x - 3.85,\ 5.33 < x \le 8.536;$$
$$H_1 = 0.645(x + 0.27)^2,$$
$$H_2 = x\,(0.06\ x - 0.18),\ 8.536 < x \le 11.706;$$
$$H_1 = 0.586(x + 0.89)^2,$$
$$H_2 = 0.18(x - 8.64)^2 + 4.16,\ 11.706 < x \le 14.864;$$

$$H_1 = 17.94(x - 6.76),$$

$$H_2 = 0.31(x - 11.47)^2 + 7.55,\ 14.864 < x \le 18.016.$$

From comparison of the results obtained by means of the approximation formulas and that found from the rigorous theory some conclusions have been made. The calculation relative error of the power characteristics computed by approximate formulas (1) up to the level -12 dB does not exceed 3 %. It is true for one-mode range where $1.9 < x < 3.832$ except the case $x = 1.9$ (the beginning of the operating frequency range), where relative error reaches 4.5 %. At the rest range of the x values up to the 18 inclusive the error does not exceed 3 %.

Approximate formulas for angels $\theta_E = \theta_E(x)$, $\theta_H = \theta_H(x)$ determining the application limits of approximation (1) as for the variable θ have been obtained. These formulas are important for practical application of the formulas (1).

In the E-plane: (2)

$$\theta_E = 33.1/(x - 1.55) + 46.7,$$
$$2.0 \le x \le 2.6,\ 78° < \theta_E \le 120°;$$
$$\theta_E = 213.6/x - 5.05,$$
$$2.6 < x \le 3.83,\ 52° < \theta_E \le 78°;$$
$$\theta_E = 280.1/x + 2.19x - 35.5,$$
$$3.832 < x \le 7.016,\ 25° < \theta_E \le 51°;$$
$$\theta_E = 178.5/x + 0.045x - 1.32,$$
$$7.016 < x \le 13.324,\ 13° < \theta_E \le 25°;$$
$$\theta_E = 190/x + 0.07x - 2.53,$$
$$13.324 < x \le 18.0,\ 9° < \theta_E \le 13°.$$

In the H-plane:

$$\theta_H = 79.85/x - 5.45x + 55.7,$$
$$2 < x \le 5.33,\ 42° < \theta_H \le 87°;$$
$$\theta_H = 263.3/x + 0.805x - 12.1,$$
$$5.331 < x \le 8.536,\ 26° < \theta_H \le 42°;$$
$$\theta_H = 236.6/x + 0.13x - 3.15,$$
$$8.536 < x \le 18,\ 12° < \theta_H \le 26°.$$

The maximum relative error of formula (2) given above does not exceed 1.3 %.

Since the formulas (1, 2) approximate the normalized pattern, the approximation formulas for relation the power in the main maximum to the power, which excites the wave radiator have been derived.

$$P_{max}/P_A = 0.3838x - 0.4058 \text{ for } x < 3.832;$$

$$P_{max}/P_A = 0.0676x^2 + 0.133 \text{ for } 3.832 < x \le 18. \quad (3)$$

The error of approximation (3) does not exceed 1 %.

For the case of one-mode waveguide performance, widely used in practice, the approximation formulas have been obtained not only to the level -12 dB, but also at the whole observation space in E- and H-planes.

$$P_E(\theta, x) = [\Sigma A_j(x)\cos(j - 1)\theta]^2, j = 1...7, \quad (4)$$

$$P_H(\theta, x) = [\Sigma B_j(x)\cos(j - 1)\theta]^2,$$

where

for pattern in E-plane:

$$E_1 = 0.7238/x - 0.04065x + 0.1997,$$

$$E_2 = x(0.51878 - 0.05806x)^2,$$

$$E_3 = -0.369/x + 0.345,$$

$$E_4 = -0.09436 + 0.05446x,$$

$$E_5 = 0.1375/x + 0.03341x - 0.11317,$$

$$E_6 = 0.05584/x + 0.01784x - 0.07396,$$

$$E_7 = 0.005;$$

for pattern in H-plane:

$$H_1 = 0.58735/x - 0.01245x + 0.14037,$$

$$H_2 = x(0.5426 - 0.0612x)^2,$$

$$H_3 = 0.28918 - 0.30353/x + 0.3525/x^2,$$

$$H_4 = -0.14104/x + 0.03962x - 0.02466,$$

$$H_5 = (0.2593 + 0.0825x)^3/x,$$

$$H_6 = 0.2025/x + 0.033x - 0.17653,$$

$$H_7 = ((-0.99157 + 0.60226x)/x^2)^2.$$

These formulas are very useful when using the waveguide radiator as weakly directive antenna.

CONCLUSION

The mathematical model of radiation from the open-ended circular waveguide excited by H_{11} dominant-mode wave have been developed in a wide frequency bandwidth, where $1.81 < x < 18$. For the case of one-mode range $1.81 < x < 3.832$ the calculation was carried out for all observation angles. The relative error of approximation for such a case does not exceed 3 %, but for the whole frequency range $1.81 < x < 18$ up to the level -12 dB this error does not exceed 4 %.

REFERENCES

1. Vainshtain L.A. Theory of diffraction and factorization method. Moscow, Soviet Radio Publish, 1966 [in Russian].

2. Fradin A.Z. Ultrahigh frequency antennas, Moscow, Soviet Radio Publish, 1957 [in Russian].

OPTIMIZATION OF FREQUENCY PERFORMANCES OF HORN RADIATORS

A. A. Karpenko, I. I. Shumljansky

270029 Odessa-29, Didrihsona str. 4, OSMA
tel. (0482) 32-11-43,e-mail: root@ osma.odessa.ua

The main advantages of horn radiators (HA) are flat gain over the frequency range, simplicity of construction and reliability in service. From these qualities the high passband response is the most important one for being extremely essential factor for raising the information carrying capacity of radio lines in different applications. The antenna passband response is determined quantitatively by the range of frequencies within which the antenna parameters are within certain limits. Sometimes the antenna passband response is determined by the mismatch factor which represents the reflected wave to incident wave amplitude ratio. The mismatch factor specifies the antenna passband response by the antenna input impedance. It is assumed also that the antenna directivity (shape and width of the main lobe, level of the side lobes) for a wide frequency range varies within the acceptable limits. However, it is, as a rule, rather difficult to formulate a criterion for passband response on the beam pattern characteristics. In each particular case one should proceed from the application of a corresponding radio technical equipment.

Unfortunately, an accurate theory, even for simplest types of HAc, has not yet been developed, which complicates the investigation of the antennae and the determination of their electrical parameters such as mismatch factors and beam patterns.

In absence of an rigorous theory, approximate techniques have to be used in the HA analysis and design.

As it has been already mentioned, a great role in studying the horn antennae belongs to experiments. From the number of papers on this point [1, 4] which deal with the HA passband response investigation.

Paper [1] considers a special case of uniform HA with a pentagonal aperture not similar to the horn throat. Such complication of the design should, to the author's opinion, improve the antenna pattern over a wide frequency band. The characteristics of measured in the antenna ntar-field radiation seem to corroborate the author's suppositions. However, the far-zone antenna pattern turns out to be worse than that of conventional horn antennae.

Considered in [2] are exponential and parabolic horns. The presented review of horn antennae resembles a listing of arbitrarily selected types of horns without any relation to the problems for which these antennae are solved. Some of the considered types do not have any advantages as compared with simpler types of the horns. As the envelopes are restricted only to parabolic and exponential shape, optimal conditions with respect to mismatch factor and other technical parameters can hardly be provided.

Paper [3] is certainly correct in assessing the advantages of curved shapes. A construction is suggested consisting of two conducting curved plates which do not form a complete horn. However, the qualitative estimation of the mismatch factor, pattern and other technical parameters of the radiator is not given.

Described in [4] are experimental techniques to solve the problem of synthesizing the horn system. Thereby, the horn shaping element is not varied or optimized, and the required effect is reached by changing the position of some waveguide sections in the throat of the horn system. The antenna has a narrow field of application. As no expression for the internal structure of the field or horn characteristics and parameters are presented, the advantages of the suggested system cannot be duly evaluated.

Here one suggests consideration of stepped horns, bear in mind that the horn with steps number tending to infinity is transformed into a curve horn.

A six-step horn antenna was investigated, with inlet and outlet dimensions being equal to 90×45 mm and 368×394 nun respectively which, in terms of wavelengths, corresponds to $0.90\lambda_0 \times 0.45\lambda_0$ and $3.68\lambda_0 \times 3.24\lambda_0$ where λ_0 = 100 mm. Maximum permissible mismatch factor $|\Gamma|_{max}$ = 0.07. The pyramidal horn was made of dielectric (foam plastic, n = 1.14) with metallized side surface. The stepped horn input was flange-coupled with the feeding waveguide. The cross-section of the first step of the horn was equal to that of the feeding waveguide, excited by microwave oscillator via coaxial cable. The cross-sections and lengths of the subsequent steps provided matching with the proceeding steps.

In Fig. 1 with solid line the measured VSWR within the frequency band operating is shown. For a medium frequency f_0 = 3000 MHz, the $VSWR_{diel}$ = 1.3. Taking into consideration the VSWR dependence on the dielectric refractive index, the VSWR can be found for the same HA filled with air:

$$VSWR_{air} = \frac{VSWR_{diel}}{n} = \frac{1.3}{1.14} = 1.14.$$

In this case the reflectivity is

$$\Gamma = \frac{\text{VSWR}-1}{\text{VSWR}+1} = \frac{1.14-1}{1.14+1} \cong 0.066,$$

which does not exceed the rated value of $|\Gamma|_{max} = 0.07$. As it should have been expected, for operating frequencies $f < f_0$ the mismatch factor increases appreciably, remaining within the permissible limits. The explanation of this fact is that for lower frequencies the HA length turns out to be insufficient, and the optimality condition is thus violated.

For comparison, shown with dash line Fig. 1 is the VSWR for a similar horn antenna with straight generating line.

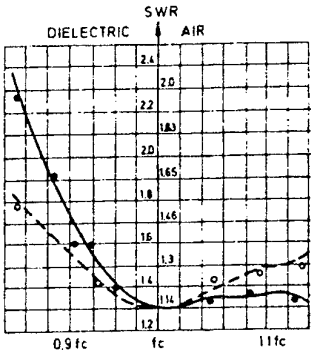


Fig. 1

It can be also easily noticed that the application of stepped structure permits to preserve the VSWR in a wider frequency band (see Fig. 1).

In the described HA the envelope of the steps corresponds to the Chebyshev waveguide transition which results in a wider operating range.

Calculations have been performed also for other types of stepped horns as well for different numbers of steps and different values of maximum permissible mismatch factor. Plotted on the basis of these calculations are graphs of $l(n)$ against $|\Gamma|_{max} = 0.02$ (Fig. 2), $l(\Gamma)$ against n = 20 (Fig. 3), and $\Gamma(n)$ (Fig. 4). In Figs. 2-4 the curves 1 correspond to *H*-sectoral stepped horn, curves 2 - to *E*-sectoral horn, and curves 3 - to the pyramidal horn with dissimilar inlet and outlet cross-sections.

The main results of the performed investigations can be summarized as follows. Within a given operating wave band and constant mismatch factor and the inlet and outlet dimensions, the increase of the number of steps *"n"* results in increasing the horn length to a certain limiting value l_{lim}, as it can be seen from Fig. 2. Starting from $n = 6$ for *H*-sectoral SH, n = 7-8 for pyramidal horn and $n = 9$ for *E*-sectoral stepped horn the longitudinal dimension of the horn antenna which ensures required mismatch factor for the given frequency band remains practically unchanged. The limitation of the number of steps facilitates a fabrication of the SH. The exception is a SH with dissimilar cross-sections at input and output, whose $l(n)$ function is monotonically increasing being however very slightly different from the linear one.

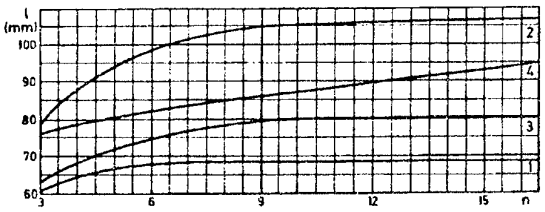


Fig. 2

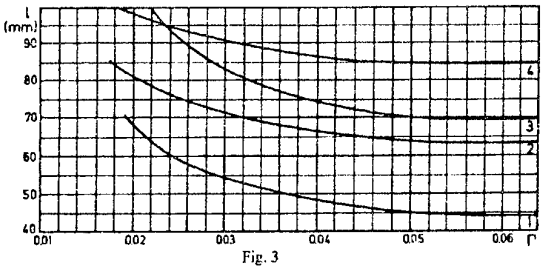


Fig. 3

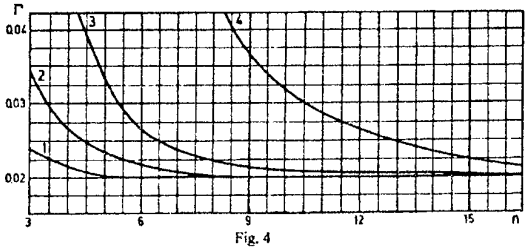


Fig. 4

Displayed in Fig. 3 is the required length of the horn at a certain mismatch factor. It follows, in particular, from the figure that for $\Gamma > 0.05$ the required length of an optimal stepped horn of any type does not practically change.

The graphs in Fig. 4 allows to assess how many steps should have one or an other type of SH to provide the given maximum permissible value of the mismatch factor. It follows from this figure that at a certain mismatch factor the maximum number of steps would belong to pyramidal stepped horns with dissimilar inlet and outlet cross-sections.

Figs. 2-4 illustrate that for similar other conditions the *E*-sectoral horn will be the longest one.

REFERENCES

1. Brueckmann H., Hagaman B. Horn Antennas for HF Long-Range Communication. IRE Tr. 1960. AP 16. N. 9 pp. 523-526.
2. USP 2283935, Cl. 343-778, pbld. 26.05.42.
3. WGP 1101535, Cl. 21, Subcl. a^4, Gr. 46, Subgr. 01, pbld, 1966.
4. Fr. Pat. 1290275, Cl. HOIQ, pbld. 01.03.61.
5. Shumlyanskiy I. I. Horn Radiators of Complex Configuration. - Singapore-London: "World Scientific", 1993. - 172 P.
6. Shumlyanskiy I. I. Horn Radiators with Stepped and Curved Generating Line. Kiyv: Vyssha Shkola Publishers, 1986. pp.147 [in Russian].

THE RADIATING PROPERTIES OF SPIRAPHASE REFLECTOR BASED ON MICROSTRIP ARRAY

A. O. Kasyanov

Dept. of Antennas and Radiotransmitting Devices,
Taganrog State Univ. of Radioengineering, Russia

Abstract. The phased array composed from microstrip radiators is considered. This array can be applied as radiation focusing spiraphase system. The lack of traditional phase shifters ensures good cost, technological and constructive characteristics of spiraphase arrays in a microwave range. Antenna construction and mathematical model are considered. This device permits to realize a focussing of antenna feed field by a microstrip antenna array. The microstrip element shape is arbitrary. The structure contains controlled elements (crystal diodes). These array electrodynamic characteristics are controlled by diodes. The mathematical model is obtained by integral equation method. Microstrip radiators current distribution and radiating properties are investigated. The numerical results can be used to develop antennas with optimum parameters.

INTRODUCTION

The microstrip antennas attract attention of the developers due to their numerous advantages. However any single printed antenna has a low directivity. Microstrip arrays have not this defect. Such arrays experimental researches and measuring of their parameters are complex and expensive procedures. This circumstance causes significant interest to creation of mathematical models of arrays. The purpose of the present work is the development of a mathematical model by an antenna array. This antenna consists of microstrip reradiators. They have arbitrary shape. The placements of printed reradiators are determined by a rectangular grid nodes. Such choice has allowed us to eliminate grating lobes in the antenna array pattern. Our mathematical model allows to investigate such microstrip reradiators, which contain the controllable elements. These elements are applied to expand an antenna array scanning angles sector. Each controllable element is simulated by the conducting probe with an impedance load. An impedance distribution on the probe is necessary given. Proposed mathematical model is based on the periodical structures conception and integral equation system solution. The vector integral equations are formulated by Lorentz lemma. The application of periodicity condition has allowed to reduce the solution area to one Floquet channel. The magnetic current density distribution on the array aperture and the electrical currents in controllable elements are determined from integral equation system based on the boundary conditions. The moment method is used for integral equation numerical solution. The subsectional rooftop function set is used for magnetic current approximation. By solving an integral equation, we define the magnetic and electrical currents distributions. Now we can determine a radiation fields of printed reradiator and other important parameters of considered antenna array. Microstrip reradiators current distribution and radiating properties are investigated. The numerical results can be used to develop antennas with optimum parameters.

THEORY

We shall consider radiation focusing spiraphase system [1] (Fig. 1). This antenna consists of microstrip reradiators. The numerical analysis demonstrates a novel means of achieving cophasal far-field radiation for a circularly polarized microstrip with elements having variable rotation angles. To explain the concept of this array we shall refer to following principle [2]. It is known that if a circularly polarized antenna element is rotated from its original position by ψ rad, the phase of the element will be either advanced or delayed (depending on the rotation direction) by the same ψ rad. Hence, the technique of rotating circularly polarized elements to achieve the required phases for a conventional array to scan its beam has been previously demonstrated [3]. Thus we can achieve a wavefront transformation. It means, that this structure has focusing properties.

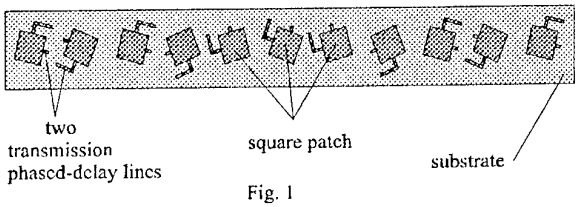


Fig. 1

MATHEMATICAL MODEL

The mathematical model foundation for the microstrip structures is made in accordance with the concept of infinite periodic arrays. Such approach is reasonable because of consideration the multielement arrays with rather complicated element structure. An alternative way of modelling may be based on the basis of so called "element by element method" with taking into account mutual coupling between array elements. This way may become much more difficult because of necessity to solve large sized system of integral equations.

FORMULATION

The boundary problem is formulated as follows. Flat periodic element arrangement array consists of ideal conducting, infinitely thin microstrip elements of arbitrary shape, located in the unit cell of rectangular grid (Fig. 2). Let's consider the Cartesian coordinate system with the origin placed on the microstrip elements arrangement plane, and z-axis directs perpendicularly this plane. Unit cells dimensions along axes x and y of Cartesian coordinate systems are equal accordingly d_1 and d_2. The angle between the vector $\vec{i}_z$ of Cartesian coordinate systems and vector $\vec{k}_0$ is equal to Θ, and the angle between vector $\vec{i}_x$ and projection of vector $\vec{k}_0$ on plane xy - φ_0. It is necessary to determine the current distribution on the radiators of array and scattering characteristic of the array.

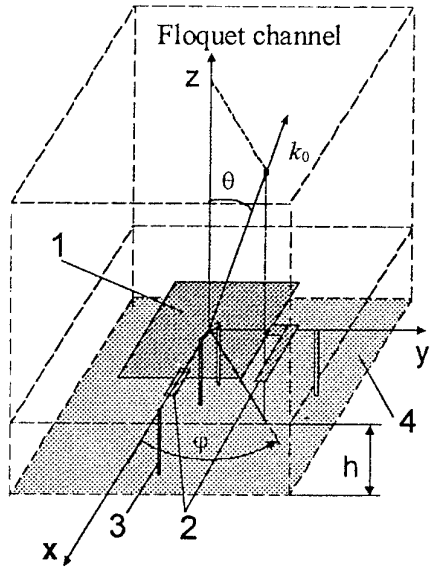


Fig.2

Apart from square microstrip radiators 1 with two transmission phased-delay lines 2, the array unit cell contains conducting shunts with impedance loads 3. These shunts are located between ground plane 4 and plane $z = 0$. They serve as a models of the controllable elements (crystal diodes). These array electrodynamic characteristics are controlled by diodes. For reaching a digital control all microstrip elements are divided into groups (modules). Each module can be as a minimum in two electrodynamic conditions. The condition of module is defined by condition of diodes (in open or closed stay). The array control is carried out by the microcomputer. The digital array probable conditions number is proportional to module number and number of each module allowable condition. This digital array has a set of radar-tracking images. The control of these images allows creating "intellectual" covers. These radiocovers capable to adapt for radar-tracking circumstances. Several possible ways of the microstrip elements excitation are considered including a plane wave excitation or periodic system of coaxial waveguides feeding. We consider the first case. In this case plane electromagnetic wave incidents on the array from the direction, which determined by wave vector $\vec{k} = -\vec{k}_0$. It is necessary to determine the current distribution on the reradiators of array and scattering characteristics.

Proposed mathematical model is based on the periodical structures conception and integral equation system solution. The vector integral equations are formulated by Lorentz lemma. The application of periodicity condition has allowed to reduce the solution area to one Floquet channel. The column matrix of magnetic current density components on the array aperture $J^M(q)$ ⟨ and the electrical currents in controllable elements $I_j^3(z')$ are determined from integral equation system based on the boundary conditions [4]:

$$\int_{S_A} \left\langle K^{MM}(p/q) \right\rangle \cdot J^M(q) \Big\rangle \, dS_q -$$

$$-i2\pi a \sum_{j=1}^{N} \int_{-h}^{0} I_j{}^{\Im}(z') \cdot \left\langle K^{M\Im}(p/q_j, z') \right\rangle dz' = \sum_{j=1}^{N} R_j{}^{(I)}(p) \Big\rangle ;$$

$$\int_{S_A} \left\langle K^{\Im M}(p_i, z/q) \right\rangle \cdot J^M(q) \Big\rangle \, dS_q -$$

$$- 2\pi a \sum_{j=1}^{N} \int_{-h}^{0} I_j{}^{\Im}(z') \cdot \left\langle K^{\Im\Im}(p_i, z/q_j, z') \right\rangle dz' =$$

$$= \sum_{j=1}^{N} r_{ij}(z) ,$$

where $i = 1, 2, \ldots, N$; $z \in [-h, \ 0]$, h – thickness of the array substrate, a – shunts radius; S_A – aperture surface. The kernel of an integral equation is a square matrix. This row matrix blocks $\left\langle K^{\nu\mu}(p/q) \right\rangle$ express interaction between unknown electrical and magnetic currents. Right parts of the equations system are the excitation fields [4]. The first equation represents the condition of fields tangential components continuity on the array aperture. The remaining equations are Poklington's equations on the controllable elements. The controllable elements are simulated by conducting shunts with impedance loads. Its distribution along each shunt is known. The moment method is used for integral equation numerical solution. The subsectional rooftop function set is used for current approximation [4]. The model does not impose restrictions on the microstrip element shape or substrate parameters. The crystal diodes are simulated by the loads with controllable surface impedance providing the digital control of microstrip array parameters. Every load is connected with the microstrip element's patch. Such loads can

execute a role either of phase shifters, or of switching elements. The substrate can be a crystalline semiconductor. In this case the diodes will be an integrated parts of a substrate. This electromagnetic structure is of a solid-state construction. There are proposed some ways of such microstrip array application.

NUMERICAL RESULTS

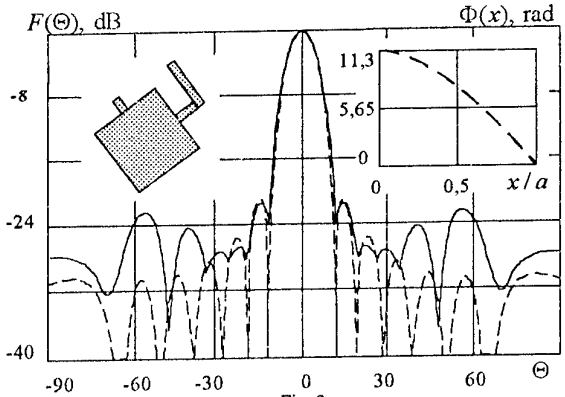


Fig. 3

This report section presents some numerical results, which shown the application of described model to computing of microstrip reflectarray element radiating and scattering parameters. The radiating pattern of a considered spiraphase microstrip array is shown in Fig. 3. The topology of an array unit cell is located in the left insertion. The phased-delay distribution along reflectarray is located in the right insertion. Thus this array is phased correcting reflector. The reflector has sizes: $2a \times 2a$, where $a = 3{,}55\lambda$. The focal length to diameter ratio F/D equals 0,46, where $D = 2a$. The calculated radiating pattern of this antenna has shown by solid line. In this case it has used the "element by element" technique. If the influence between array elements is neglected, then radiating pattern of this antenna has view, which is shown by dashed line in the Fig. 3.

REFERENCES

1. I. D.Gladkoskok, P.L.Tokarsky, Ya.S.Shifrin, "The analysis of spiraphase reflectarrays based on polarized scattering matrixes" *Proc. of 2-nd All-Union Conference "The devices and techniques of applied electromagnetics"*, Moscow-Odessa, 1991.
2. J. Huang, R.J.Pogorgelski, "A *Ka*-Band Microstrip Reflectarray with Elements Having Variable Rotation Angles" *IEEE Trans. Antennas and Propag.*, **AP-46**, N5, pp.650-656, 1998.
3. G. T. Markov, D.M.Sazonov, *Antennas*, [in Russian], Energiya, Moscow, 1975.
4. A.O. Kasyanov, V.A. Obukhovets, "Current control in a microstrip array with loaded elements" [in Russian], Radiotekhnika, **N12**, pp.32-36, 1995.

INVESTIGATION OF PARAMETERS OF LOOP OSCILLATOR WITH DISTRIBUTE REACTIVE LOAD

E. N. Kayashova, V. G. Slyozkin

Sevastopol State Technical University,
Studgorodok, 335053, Sevastopol, Ukraine
tel: 38-(0692)-23-5118, e-mail: rt.sevgtu@stel.sebastopol.ua

Loop antennas are widely used in antenna technology due to their simple construction. Recently, to overcome their main disadvantage, a narrow frequency band, modifications of such antennas have been developed. In particular, loop antenna with reactive loads based on a loop oscillator (LO) are known. There are concentrated capacitances that are connected into the circuit between passive arms and also between each active and passive arms in loop antennas. The principle of functioning of the loop oscillator with concentrated loads can be explained when considering an antenna input impedance with the inphase and antiphase excitation method [2].

Due to inphase currents in active and passive arms of LO a radiative electromagnetic wave is created. Conformal component of input impedance Z, has active and reactive parts which can be defined as components of the input impedance that are equvalent to the ones of "thick" oscillator with conductor radius re defined by the cross-section of conductors and distance between arms S. In particular, there is the expression for LO for the round conductor with radius R:

$$r_e = \sqrt{RS}\,.$$

The formula obtained for the case of the round and band conductors perimeters equality, can be used for LO band type conductor measured by thickness t and width B under condition of $t << B$, is as follows:

$$r_e = \sqrt{\pi BS}\,.$$

Antiphase currents create a non-radiative field near LO. The conformal component of input impedance Z_{op} is only reactive. Being an impedance of shorted twin feeder with wave impedance ρ_s this component for the oscillator with arm length l equals:

$$Z_{op} = j\rho_s \tan(kl)\,.$$

The total input impedance of unloaded loop oscillator is a result of parallel connection of the transformed impedance of equivalent oscillator and input impedance for antiphase regime excitation. Transformation coefficient N is defined by arms geometric parameters of LO and it equals two for identical arms.

There is a single concentrated capacitance included between passive arms in LOCL [2], the other one is connected between active and passive arms, moved off driving points for a defined distance. The first capacitance changes the correlation between inphase and antiphase currents, the second one — a value of Z_{op} as shunt loading of shorted feeder. It is evident that these two degrees of freedom enable a reactance of antenna input impedance to be compensated at least at a single frequency point, as to select a mean value of input impedance active component.

As a development of the proposed idea it is offered to use distributed reactive load in the form of a part of the open-circuited at the end twin feeder instead of the second concentrated capacitance. One conductor of this feeder is the active arm of LO and another one is located between active and passive arms of LO. Besides, one of its ends is connected with passive arm near the first concentrated capacitance and the other one is open — circuited. The scheme of the described loop oscillator with a distributed reactive load (LODRL) is depicted in Fig. 1:

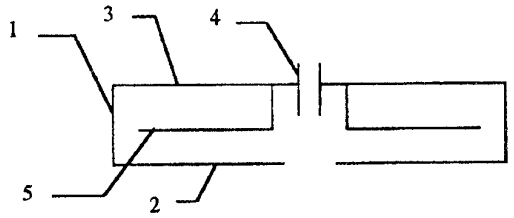


Fig. 1. The LODRL scheme

It is marked in the Fig. 1: 1 — loop oscillator; 2 — active arm; 3 — passive arm; 4 — concentrated capacitive load C_1; 5 — distributed reactive load.

The calculation of the feed impedance of LODRL Z_{inp} has been carried out with the equivalent scheme method taking into account the method of induced electromotive force:

$$Z_{inp} = \left(\frac{1}{Z_s N^2 + Z_1 N(N-1)} + \frac{1}{Z_p + Z_1 N} \right)^{-1} - Z_1(n-1)$$

where Z_1 is the reactive impedance of the capacitance C_1; Z_p is the impedance of antiphase excitation.

In this case, Z_p is defined as shunt connection of short and open-circuited parts of feeder with different wave impedances:

$$Z_p = \frac{Z_{op} Z_d}{Z_{op} + Z_d},$$

where $Z_d = -j\rho_d \cot(kl - l_z)$; l_z is a value of shortening of the open-circuited conductor.

Estimations have been carried out for the oscillator, in which the loop and distributed load had been in the form of strip. Wave impedances ρ_s and ρ_d of the strip twin feeder have been determined by the known formulae [3]. Plots of active (R, solid line) and reactive (X, dashed line) components of asymmetrical LODRL input impedance versus ratio l/λ are shown in Fig. 2.

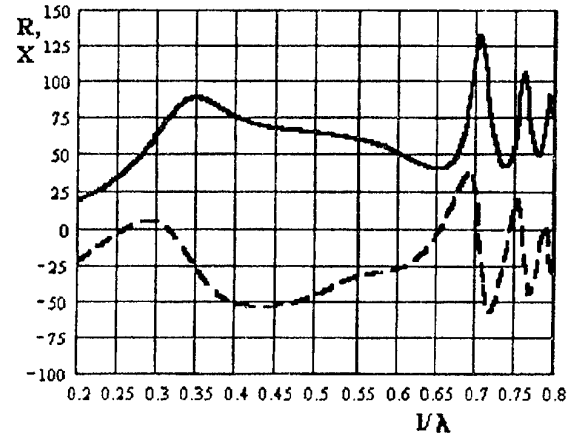


Fig. 2. Plots of feed impedance components of LODRL versus l/λ

One can see essential distinctions with respect to the LO input impedance frequency dependence: the active part of input impedance changes slightly for LODRL of $0.65 > l/\lambda > 0.25$ and it is limited by 40...80 Ω, whereas the reactive component of feed impedance mainly is of capacitive nature, and its absolute value doesn't exceed 50 Ω.

In order to illustrate the capabilities of LODRL matching, the dependence of input VSWR fed by 75 Ω feeder versus ratio l/λ is shown in Fig. 3.

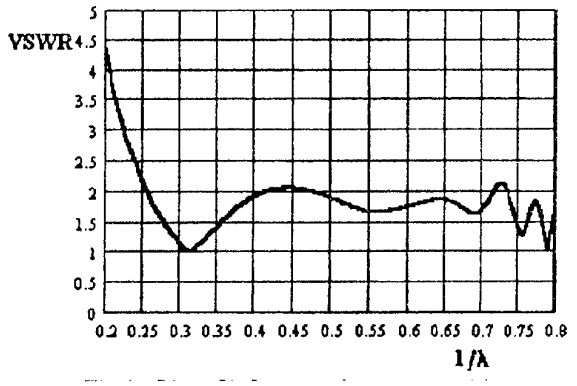


Fig. 3. Plot of LORDL VSWR versus l/λ

It is seen, that it is possible to attain optimal matching for LODRL (VSWR ≤ 2) in the frequency band 1:3 and more. In the high frequency domain the dependence is of oscillating nature, though sharp mismatching is not observed.

For experimental checking up there was a sample of asymmetrical LODRL with following parameters (mm): $l = 120$; $B = 28$; $S = 20$; $l_z = 1$; $S_d = 10$ (the distance between the active arm and a distributed load). Mesurments had been carried out for DMW band within limits of 450...800 MHz. Basing on the results. it has been found out that VSWR ≤ 2.0 can be reached at relative frequency band of about 42 % and besides, the middle frequency of this band is only 10 % above the resonance frequency of half -wave oscillator.

Basing on the theoretical and experimental results one can affirm that for the proposed loop oscillator with the distributed reactive load a sufficiently wider band of satisfactory matching with the feeder is provided than for the "classical" oscillators.

Nowdays, the theory of LODRL isn't developed enough and it needs to be specified.

REFERENCES

1. V. V. Ovsyannikov, *Oscillators with reactive loads*, Moscow: Radio I Svyaz, 1985 [in Russian].

2. G. Z. Aisenberg, S.P. Belousov, E.M. Zhurbenko, et al, *Short-wave antennas* / ed. G.Z. Aisenberg, Moscow: Radio I Svyaz, 1985 [in Russian].

3. A. L. Feldshein, L. R. Yavich, V. P. Smirnov, *Handbook on elements of waveguide engineering*, Moscow: Radio I Svyaz, 1969 [in Russian].

PECULIARITIES OF APPLICATION OF THE INDUCED EMF METHOD FOR DETERMINATION OF HELICAL ANTENNAS INPUT IMPEDANCE

L. M. Lobkova, M. V. Ivashina, V. V. Golovin

Sevastopol State Technical University
Streletskaya buhta, Sevastopol-53, 335053, Ukraine
Ph: +38(0692) 235-127, 235-118, e-mail: rt.sevgtu@stel.sebastopol.ua

ABSTRACT

The calculation expressions for the radiation resistance of a circular cylinder helix are deduced.

INTRODUCTION

The induced EMF method is of the most importance for determination of the radiation resistance and input impedance of helical antennas. However, it should be emphasized that there are two formulations of the method. One of them is based on the Poynting theorem; another other – on the mutuality theorem. The both formulations are suitable for consideration of helical antennas, but they characterize different physical phenomena, which can be described as the following:

$$Z_\Sigma(x)=\frac{P_\Sigma}{|I(x)|^2}=-\frac{1}{I(x)I^*(x)}\int_\ell E_\tau(\xi)I^*_{ex}(\xi)d\xi, \quad (1)$$

$$Z_A(x)=\frac{\varepsilon(x)}{I(x)}=-\frac{1}{I^2(x)}\int_\ell E_\tau(\xi)I^*_{ex}(\xi)d\xi, \quad (2)$$

where $I_{ex}(\xi)$ is the extraneous current distribution along an antenna wire, $I(x)$ and $I^*(x)$ are the direct and conjugate current values in the wire section, for which Z_Σ and Z_A are determined; $E_\tau(\xi)$ is the tangential component of the field near the antenna wire; Z_Σ and Z_A are the complex radiation resistance and the input impedance of the antenna, respectively.

Distinction of formulas (1) and (2) consist in that conjugate currents in (1) are replaced with the direct current values in (2). The expressions are the same only when the set current distribution $I(x)$ is described by a real function $I(x) = I^*(x)$, that is to say the current distribution is uniform. However, under $I(x) \neq I^*(x)$ for the travelling current distribution the calculation results of (1) and (2) are different. In this case an estimate of Z_A is more accuracy. In spite of this estimation of Z_Σ by (1) is used more often in practice. The paper deals with description of helical antennas according to the formula (1).

PROBLEM FORMULATION

Let us consider a helical antenna located on a circular cylinder as a model shown in Fig. 1.

According to Fig. 1 the cylindrical helical antenna represents the composition of two independent arrays: 1) the system of axial electrical dipoles for $h << \lambda$ and 2 the systems of parallel circular loops with finite sizes are located along the axis Z.

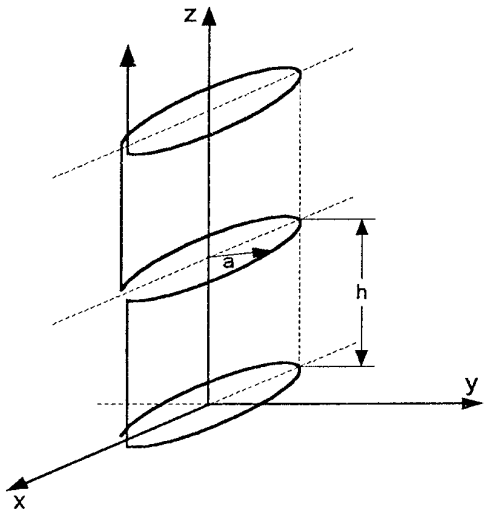


Fig. 1

Taking into consideration the orientation of dipoles and loops we can consider that $Z_\Sigma = Z_{\Sigma\bar{a}} + Z_{\Sigma\delta}$, where $Z_{\Sigma\bar{a}}$, $Z_{\Sigma\delta}$ are radiation resistances of arrays from dipoles and loops, respectively.

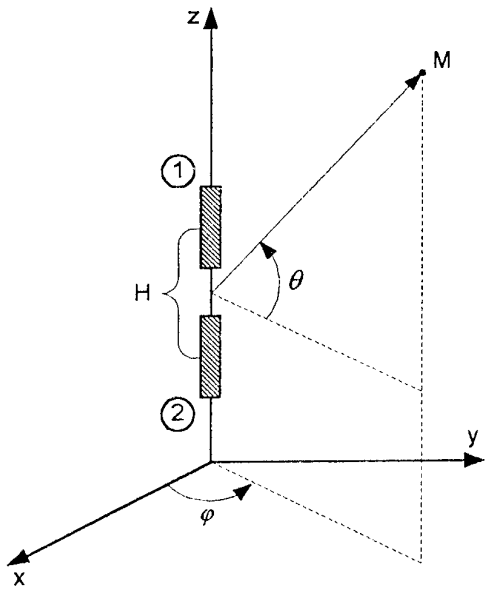
Let the helical antenna current distribution be travelling. Then, if we assume $2\pi a + h = \lambda$, elements of the array are inphase and with equal amplitudes in a first approximation.

Let us examine the interaction resistances for each array.

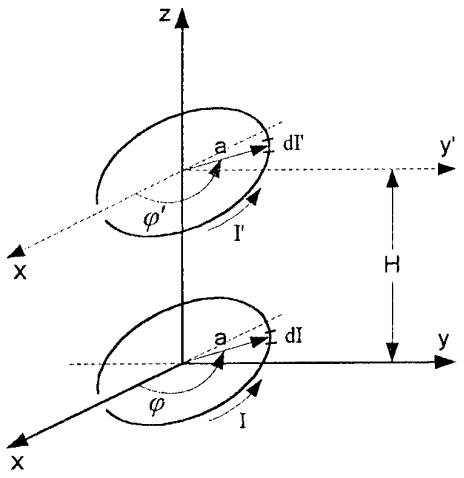
For axial electrical dipoles the investigation will be carried out for two dipoles located at the distance h (see Fig. 2a), which equals h for adjacent elements. Taking into account that the imaginary radiation resistance is very small for electrical dipoles, calculate the radiation resistance by the Poynting method for which it is necessary to know radiation field in the far-field zone

$$E_\theta = j\cdot 60kI_\ell\cdot\ell_{eff}\frac{\exp(-jkr)}{r}\cos\theta\cos\left(\frac{kH}{2}\sin\theta\right), \quad (3)$$

where I_ℓ is the current of the antenna inputs, ℓ_{eff} is the dipole effective length; $H_\varphi = 120\pi E_\theta$.



a



b

Fig. 2

Taking into account that

$$R_{\Sigma 12} = \frac{1}{|I_\ell|^2} \iint_S \left[E_\theta H_\varphi^*\right]_n dS, \qquad (4)$$

after calculations (4) we obtain

$$R_{\Sigma 12} = 60(k\ell_{eff})^2 \left[\frac{\sin(kH)}{(kH)^3} - \frac{\cos(kH)}{(kH)^2}\right]. \qquad (5)$$

The analysis for the radiation resistance of the array from loops was carried out similarly to [1].

GENERAL DESCRIPTION

In this case let us take advantage of the induced EMF method. The centers of the loops (in the planes XY and XY') are located in the center of the coordinate system and the distance between the centers equals h (see Fig. 2b). The current distribution of the loop is represented in the following way

$$I(s) = I_0 e^{jks},$$

where $S = a\cdot\varphi$, and the current element is given by

$$d\vec{I}(s) = aI_0 e^{jka\varphi}\left(\cos\varphi\cdot\vec{e}_y + \sin\varphi\cdot\vec{e}_x\right)d\varphi,$$

The current distribution for $I'(s)$ is the same, where $S = a\cdot\varphi'$.

Taking into account the coupling between the rectangular and polar coordinate systems for each loop:

$$\left.\begin{aligned} x &= -a\cos\varphi \\ y &= a\sin\varphi \end{aligned}\right\}, \quad \left.\begin{aligned} x' &= -a\cos\varphi' \\ y' &= a\sin\varphi' \end{aligned}\right\},$$

and writing the distance between the elements dl and dl' in term of

$$r = \sqrt{(x-x')^2 + (y-y')^2 + H^2},$$

the expression for $Z_{\Sigma 12}$ can be presented as

$$Z_{\Sigma 12} = -j\frac{30a^2}{k}\int_0^{2\pi}\int_0^{2\pi} \exp(-jka(\varphi-\varphi'))\exp(-jkr)\cdot$$
$$\cdot\left\{\left[\left(\frac{k^2r^2 - j3kr - 3}{r^3}\frac{(y-y')^2}{r^2} + \frac{k^2r^2 + jkr + 1}{r^3}\right)\cos\varphi\right.\right.$$
$$\left. + \frac{k^2r^2 - j3kr - 3}{r^3}\cdot\frac{(x'-x)(y'-y)}{r^2}\cdot\sin\varphi\right] +$$
$$+\left[\left(\frac{k^2r^2 - j3kr - 3}{r^3}\frac{(x'-x)^2}{r^2} + \frac{k^2r^2 + jkr + 1}{r^3}\right)\sin\varphi -\right.$$
$$\left.\left. - \frac{k^2r^2 - j3kr - 3}{r^3}\frac{(x'-x)(y'-y)}{r^2}\cos\varphi\right]\sin\varphi'\right\} d\varphi d\varphi'. \quad (6)$$

CONCLUSION

The radiation resistance research of circular cylindrical helical antenna represented as the two independent arrays allow to determine both the antenna input impedance and the directivity value in dependence on the helix geometrical parameters.

REFERENCE

1. L. M. Lobkova, M.B. Protsenko, O.A. Posniy, M.V. Ivashina, "Evaluation of the interaction impedance of the antenna array consisting from circular loops", Proc. of Int. Conf. on Antenna Theory and Techniques, Sevastopol, Ukraine, 1999.

ESTIMATION OF THE INTERACTION IMPEDANCE OF THE ANTENNA ARRAY CONSISTING OF CIRCULAR LOOPS

L. M. Lobkova, M. B. Protsenko, O. A. Posniy, M. V. Ivashina

Sevastopol State Technical University
Streletskaya buhta, Sevastopol-53, 335053, Ukraine
Ph: +38(0692) 235-127, 235-118, e-mail: rt.sevgtu@stel.sebastopol.ua

ABSTRACT

A wide application of MW band leads to the necessity of antenna arrays designing from the elements of small overall sizes. While designing these antennas the problem of interactive influence of the array elements and the interaction impedance is of paramount importance.

PROBLEM FORMULATION

Let us represent loop antennas as equivalent magnetic dipoles for calculation of the interaction impedance. Then using the principle of polarization duality the problem can be reduced to the examination of electrical dipoles with the antenna effective length l_{eff} equal to the dipole arm length. For small loops $l_{\text{eff}} = k \cdot S$, where $k = \pi/\lambda$, S is the loop area.

Small loop antennas in the plane XY and $X'Y'$ as well as their magnetic dipole moments q_M along the axis Z are presented in Fig. 1. The magnetic parallel dipole are located along the axis Y at the distance d. In order to calculate the interactive radiation impedance $Z\Sigma_{12}$ we take advantage of the induced EMF method. It is convenient to represent the radiation field components in the near-field zone by the vector potential of Hertz A

$$\vec{E}(x', y') = \frac{1}{j\omega\varepsilon_o\mu_o}\int_{-l}^{l}\left(\text{graddiv}\,\vec{A} + k^2\vec{A}\right)dl\,, \qquad (1)$$

where

$$\vec{A} = \frac{\mu_o}{4\pi}\int_{-l}^{l}\vec{I}(\xi)\cdot\frac{\exp(-jkr)}{r}d\xi\,, \qquad (2)$$

where ξ is the coordinate along the wire with the current; r is the distance to the observation point.

The interaction impedance of the input current I_1 is given as

$$Z_{\Sigma\ell} = -\frac{1}{|I_\ell|^2}\int_{-\ell}^{\ell}E_\tau(\xi)I^*(\xi)d\xi\,. \qquad (3)$$

On the basis of expressions (1), (2) for vertical Hertz dipole (see Fig. 1) the components E_θ, E_r and H_φ differ from zero. For further research we shall considere only the component E_θ

$$E_\theta = j30kI_\ell\ell_{eff}\left(1+\frac{1}{jkr}-\frac{1}{k^2r^2}\right)\frac{\exp(-jkr)}{r}\sin\theta\,. \qquad (4)$$

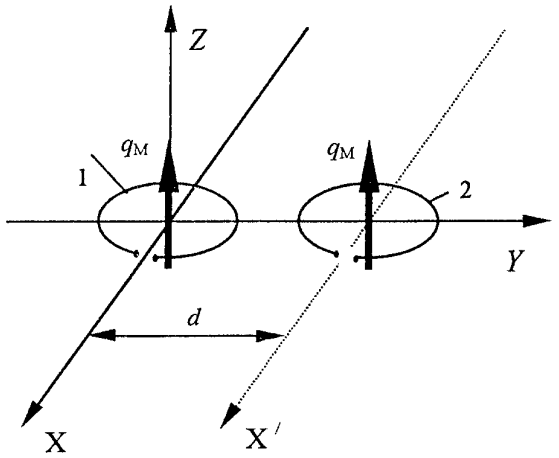


Fig. 1

Due to the dipoles located along the axis Z the component E_z can be written for the main direction $\theta = \pi/2$ in the rectangular coordinate system as the following

$$E_z = E_r\cos\theta - E_\theta\sin\theta = -E_\theta\,, \qquad (5)$$

and, therefore, $E_\tau = E_z = -E_\theta$.

Thus, on the basis of the formulas (4), (5) and under the condition that $I_{\ell 1} = I_{\ell 2} = I_\ell = const$ and $r \cong d$, we obtained

$$E_{\Sigma 12} = -j\cdot\frac{3R_{\Sigma\ell}}{2(kd)^3}\cdot\left(1+jkd-(kd)^2\right)\cdot e^{-jkd}\,, \qquad (6)$$

where $R_{\Sigma\ell} = 20\cdot k^4S^2$ is the self radiation impedance of the loop antenna.

On the basis of the result for magnetic dipoles we now turn to the consideration of the finite-sized circular loop with the radius a.

GENERAL DESCRIPTION

The loop antennas with the radius a are shown in Fig. 2. They are located along the axis (XY) and ($X'Y'$), respectively, and the distance between their centres

equals d. The loops inputs are on the axiases X и X', respectively, and the current distribution is assumed as the cosine-function. Then for the current element dl on the loop 1 we can write

$$d\vec{l}(\varphi) = I_o a \cdot \cos[ka(\pi - \varphi)] \cdot (\vec{e}_x \sin\varphi + \vec{e}_y \cos\varphi) \cdot d\varphi . \quad (7)$$

Corresponding expression can be given for $d\vec{l}'(\varphi')$ and the condition $I_0 = I_0'$. Therefore, $Z_{\Sigma 12} = Z_{\Sigma 21}$.

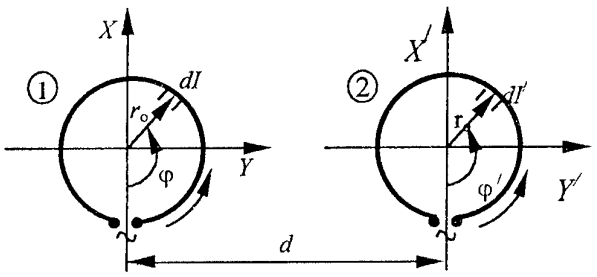


Fig. 2

For the further consideration the rectangular coordinates are substituted for angular ones (see Fig. 2):

$$\begin{cases} x = -a \cdot \cos\varphi \\ y = a \cdot \sin\varphi \end{cases},$$

$$\begin{cases} x' = -a \cdot \cos\varphi' \\ y' = d + a \cdot \sin\varphi' \end{cases}, \quad (8)$$

where $r = \sqrt{(x'-x)^2 + (y'-y)^2}$.

Thus, $Z_{\Sigma 12}$ is determined in terms of:

$$Z_{\Sigma 12} = -\frac{1}{I_0 I_0'^*} \int_0^{2\pi} \vec{E}(x', y') dl'^* , \quad (9)$$

The field components $\vec{E}(x', y')$ near the loop 2 are calculated according to the formulas (1) and (2). Thus, after substitution $\vec{E}(x', y')$ into (9) and transformation of the integrand for $Z_{\Sigma 12}$ we can write the following:

$$Z_{\Sigma 12} = -j\frac{30a^2}{k} \int_0^{2\pi}\int_0^{2\pi} \exp(-jka(\varphi - \varphi')) \exp(-jkr) \cdot$$

$$\cdot \left\{ \left[\left(\frac{k^2r^2 - j3kr - 3}{r^3} \frac{(y-y')^2}{r^2} + \frac{k^2r^2 + jkr + 1}{r^3} \right) \cos\varphi \right. \right.$$

$$\left. + \frac{k^2r^2 - j3kr - 3}{r^3} \cdot \frac{(x'-x)(y'-y)}{r^2} \cdot \sin\varphi \right] +$$

$$+ \left[\left(\frac{k^2r^2 - j3kr - 3}{r^3} \frac{(x'-x)^2}{r^2} + \frac{k^2r^2 + jkr + 1}{r^3} \right) \sin\varphi - \right.$$

$$\left. \left. - \frac{k^2r^2 - j3kr - 3}{r^3} \frac{(x'-x)(y'-y)}{r^2} \cos\varphi \right] \sin\varphi' \right\} d\varphi d\varphi' . \quad (10)$$

According to (10), $R_{\Sigma 12}$ and $X_{\Sigma 12}$ are computed and the results obtained are compared with the calculation (6) for small loop antennas.

CONCLUSION

The research of the interactive impedance for small loop antennas with the finite overall sizes allow to establish the application boundaries of the dipole representation of loop antennas as well as to analyze the behaviour of the interactive resistance $R_{\Sigma 12}$ and reactance $X_{\Sigma 12}$ in dependence on the ratios a/λ and d/λ.

REFERENCES

1. A. L. Drabkin, V.L. Zuzenko, A.G. Kislov // Antenna and feed devices / Moscow: Sovetskoe Radio, 1974. - PP. 536 [in Russian].

2. A. Z. Fradin.// Antenna and feed devices / Moscow: Svyaz, 1977. - pp. 440 [in Russian].

RADIATION FEATURES OF A FLAT Z - ANTENNA

L. M. Lobkova, M. V. Ivashina, A. F. Rozvadovsky

Sevastopol State Technical University
Streletskaya buhta, Sevastopol-53, 335053, Ukraine
Ph: +38(0692) 235-127, 235-118, e-mail: rt.sevgtu@stel.sebastopol.ua

ABSTRACT

The analysis of radiation characteristics for a zigzag antenna is represented. The obtained mathematical expressions of electromagnetic field components are given in an analytical form by the use of a Fourier's series for Bessel's functions. The numerical modelling results of radiation characteristics for zigzag antennas of an arbitrary configuration are discussed.

INTRODUCTION

The to-date requirements to antenna systems, a lot of existing research problems lead to necessity of the further improvement of the well-known antenna characteristics and to the search of new technical solutions. As for wire antennas the characteristics improvement is achieved by optimization of the antenna geometry on the polarization and directivity criteria [1], [2]. As it is shown in [3], zigzag radiators are more perspective from the point of view of potential directive features. The antenna allows to increase the directivity factor under the condition of its small overall sizes, for example, in comparison with various kinds of (director and log-periodic) antennas. However, frequently the radiation characteristics of zigzag antennas are calculated and analyzed approximately; and the fact doesn't allow to study and to realize the antennas potential features largely.

Therefore, the interesting for engineers problem appears, the solution of which is presented in this paper. This problem aim is to investigate radiation characteristics of zigzag antennas with various geometrical configurations in more general electromagnetic form.

GENERAL DESCRIPTION

The performance of antenna in terms of an elliptical helix[1] enables to solve a number of problems both for flat and volume geometry. For example, a zigzag antenna is a degenerate form of the elliptical helical antenna with the minor axis equal to zero. Further, we shall denote call the zigzag antenna as a Z-antenna.

The geometry of Z-antenna shown in Fig. 1 is described in parametric representation as follows:

$$\left.\begin{aligned} x &= a\cos\alpha \\ y &= 0 \\ z &= a\frac{2}{\pi}\alpha\,\mathrm{tg}\,\alpha \end{aligned}\right\}; \qquad (1a)$$

$$S = \frac{2}{\pi}a\alpha\sec\beta, \qquad (1b)$$

where x, y, z are the current coordinates in the rectangular coordinate system; a is projection of the antenna's arm on the plane XOY; β is the inclination angle of the antenna's arm to the plane XOY; S is the wire length of Z-antenna; α is the parameter changing from 0 to $2\pi n$, where n is the wraps number.

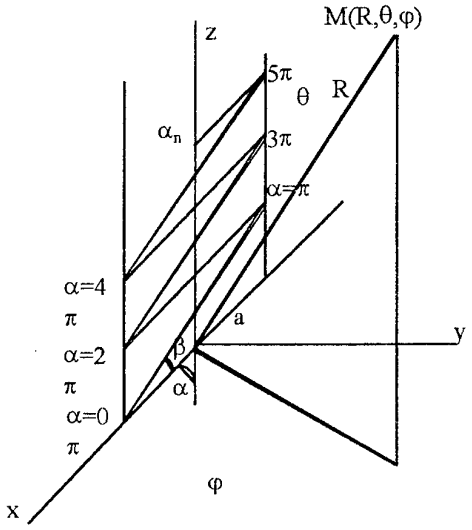


Fig. 1. Z-antenna

The expressions (1a) and (1b) are obtained on the basis of the asymptotical solution of the elliptical integral for the set antenna geometry as shown in [1].

In order to obtain the main expressions for radiation field of Z-antenna we take advantage of representation of the vector potential on the basis of which one can to determine electrical field density in asymptotical approximation of the far-field zone.

$$\bar{A} \cong \int_S I(s)\frac{\exp(-jkr)}{r}d\bar{s}, \qquad (2a)$$

$$\bar{E} \cong A_\theta\bar{e}_\theta + A_\phi\bar{e}_\phi, \qquad (2b)$$

where $\bar{e}_\theta$, $\bar{e}_\phi$ are the vector basises of the spherical coordinate system, $I(s)$ is the current distribution along the wire of the radiator, k is the wave number, r is the distance from an element with the current on

the radiator axis to a point of the antenna far-field zone.

According to the antenna geometrical configuration (1a) only two components of the vector potential (2a) differ from zero, namely A_x and A_z, therefore, the field polarization nature is given by the following equations

$$\left.\begin{aligned} A_\theta &= A_x \cos\theta\cos\phi - A_z \sin\theta \\ A_\phi &= -A_x \sin\phi \end{aligned}\right\}. \qquad (3)$$

Thus, the further analysis of Z-antenna radiation characteristics (2b) leads to investigation of corresponding components of the vector potential (3).

We assume the current distribution along the radiation wire to be

$$I(s) = I_0 \exp(-j\xi ks), \qquad (4)$$

where ξ is the coefficient characterizing the wave slowing under the condition of the wave propagation along the radiator, therefore it leads to improvement of the antenna directivity.

Then, taking into consideration the antenna geometry (1a), (1b) the vector potential components in the rectangular coordinate system are written in the following way:

$$A_x = A_0 \int_0^{\alpha_n} \exp(-j\xi ks) \times \times \exp\left[jk(x\sin\theta\cos\phi + z\cos\theta)\right]\sin\alpha d\alpha, \qquad (5a)$$

$$A_z = A_0 \operatorname{tg}\beta \int_0^{\alpha_n} \exp(-j\xi ks) \times \times \exp\left[jk(x\sin\theta\cos\phi + z\cos\theta)\right]\sin\alpha\, d\alpha, \qquad (5b)$$

where $A_0 = 30kI_0 a\exp(-jkR)/R$ is the multiplier describing of the spherical wave behaviour in the far-field zone; R is the distance from the coordinate system centre to a point in the antenna far-field zone.

In order to calculate the integrals in (5a), (5b) we use expansion into the Fourier series for exponential functions.

$$\exp(-jv\sin\gamma) = \sum_{M=-\infty}^{\infty} J_m(v)\exp(-jy); \qquad \exp(jv\cos\gamma) = \sum_{M=-\infty}^{\infty} j^m J_m(v)\exp(jm\gamma), \qquad (6)$$

where J_m is Bessel's function of the first kind of m-th order.

After complicated mathematical transformations of the expressions (5a) and (5b) the vector potential components can be presented as follows

$$A_x = A\sum_{m=-\infty}^{\infty} j^m J_m(ka\sin\theta\cos\phi)\times \times\left[\frac{\exp(jC\alpha_n)(jC\sin\alpha_n - \cos\alpha_n)}{C^2-1}\right]; \qquad (7a)$$

$$A_z = -jA\frac{2}{\pi}\operatorname{tg}\beta\sum_{m=-\infty}^{\infty} j^m J_m(ka\sin\theta\cos\phi)\times \times\left[\frac{\exp(jC\alpha_n)-1}{C}\right], \qquad (7b)$$

where $C = kh_1\gamma_1 - 2n + m$, $h_1 = a\left(tg\beta\cos\theta - \sec\beta\cdot\xi\right)$,

$$\gamma_1 = 1 - \frac{e^2}{4} - \frac{3}{64}e^4 + \frac{5e^6}{256} + \ldots,$$

m, n are the m-th and n-th orders of Bessel's functions, respectively.

RESULTS AND CONCLUSION

Thus, on the basis of the obtained expressions for the vector field components the analysis of Z-antenna radiation characteristics is made under the condition that the wave slowing along the radiation wire is insignificant ($\xi = 1.00\ldots1.11$ is obtained experimentally).

Note, that in the antenna plane (plane XOY), and also in the axial direction (the axis OZ) only one component of the vector field is excited, that is to say the field is linearly polarized.

The presented expressions for radiation field components allowed to carry out optimization of geometrical parameters of Z-antenna.

REFERENCES

1. L. M. Lobkova, M.B. Prozenko and M.V. Ivashina, A Methematical Model and Investigation Results of Field Polarization Characteristics of Elliptical Cylindrical Helical antennas // Proc. of 8-th International Conf. "CriMiCo'98"-Vol. 2 - Sevastopol, Crimea, Ukraine. - 1998. - PP. 486-487.
2. V. G. Ovetchkin, V.S. Pan'ko, Yu.P. Salomatov, Design of Non-Planar Wire Antennas // Proc. of 8-th International Conf. "CriMiCo'98"-Vol. 2 - Sevastopol, Crimea, Ukraine. - 1998. - PP. 449-450.
3. E. Machsshy Antennas Potential Directivity General Estimation // Proc. of 2-d International Conf. On Antenna Theary and Techniques. - Kyiv, Ukraine. - 1997. - PP. 27-28.

A COAXIAL SPIRAL ANTENNA WITH INCREASED GAIN

A. S. Mikryukoff, V. F. Korsak, Y. L. Maksimenko

Science Center of control, communications and Radio-Electronic Warfare
252149, Kyiv-149, Moscovskaya str. 45/1, phone (044) 291-23-65

The raise of the gain of cylindrical spiral antenna (CSA), which is excited in axial radiation mode, is usually reached by extension of axial length of the spiral [1]. However CSA gain at large (more than 15) number of coils depends on magnitude of the angle of the spiral winding [2]; when the angle of winding is close to 14^0, it is increased practically linearly with growth of coils number. Increasing of CSA gain of limited axial length is received by the putting of the metal cylinder inside of a spiral [3]. When common length of antenna is equal 1.58λ, gain is more than 13 dB.

Simultaneous reception and radiation of circular polarization waves with opposite (identical) field vectors rotation direction in two diverse frequency bands can be made in coaxial spiral antenna (CSA) containing two coaxial located spirals with opposite (identical) direction of winding and common screen.

Known CSA [4], containing two coaxial located tape spirals with identical direction of winding and the common screen operates in frequency bands of 750-900/1200-1300 MHz (λ_2/λ_1 = 1.47), has identical gain, that is equal 12 dB, in both frequency bands. The increasing of gain in a band of operational frequencies of an exterior spiral is obtained because of influence of an interior spiral. The substantiation of an obtained prize in gain of an antenna, and also limits of frequencies, at which the additional amplification is reached are not explained in [4].

The considered effect of gain extension is obtained by us at development of CSA containing two coaxial located regular cylindrical wire spirals with opposite direction of winding. CSA (Fig. 1) has gain that is not less than 13 dB in frequency bands of 3.4–3.9/5.72–6.25 GHz (λ_2/λ_1 = 1.65).

The substantiation of CSA additional amplification on the lower frequencies because of energization of an axial radiation wave in an interior spiral is insufficiently correct, because relative length of a coil of the spiral is $2\pi a/\lambda = ka < 0.6$ on these frequencies, where a - coil radius, $k = 2\pi/\lambda$. It is possible to explain extension of CSA gain on the lower frequencies, using a principle of antenna operation [3], taking into account the magnitude of the diameter of the exterior surface of the interior wire spiral ($2a_{1\ e.s.}$).

For the definition of regularity of a modification and the reasons of additional extension of the gain on the lower frequencies from relative geometric parameters of the CSA outcomes of experiments are shown in a table 1.

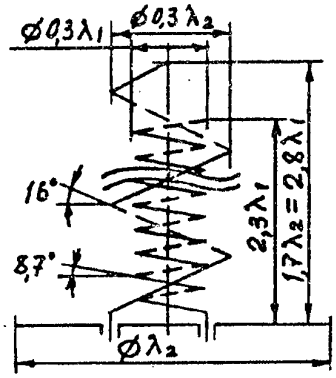


Fig. 1

Table 1

λ_2/λ_1 =1.47, a_2/a_1=1.62		λ_2/λ_1 =1.65, a_2/a_1= 1.83	
$2a_1/\lambda_2$	gain, dB	$2a_1 e.s./\lambda_2$	gain, dB
0.17	9.5	0.165	10
0.18	11	0.168	12
0.195-0.245	12	0.17-0.205	13
0.254	11	0.207	12
0.261	9.5	0.21	10

There are ratios of the tape interior spiral diameter $2a_1$ [4] and diameter $2a_{1e.s.}$ (Fig. 1) to the exterior spiral wavelengths l_2, where the gain extension is reached in 2 times, and also their boundary ratios, where the additional amplification is not observed, at ratios of average lengths of waves λ_2/λ_1 and angles of winding α_2/α_1 of considered CSA in the table. In gaps of these ratios the smoothly varying gain increment from 0 up to 2.5 ... 3 dB is observed.

The maximum gain extension on the lower frequencies is reached(achieved) at ratios $2a_1/\lambda_2$ = 0.195... 0.245 at tape CSA (at λ_2/λ_1 = 1.47, α_2/α_1 = 1.62) and $2a_{1e.s.}/\lambda_2$ = 0.17 ... 0.205 at wire CSA (at λ_2/λ_1 = 1.65 and α_2/α_1 = 1.83).

The increasing of the winding angles ratio α_2/α_1 reduces in a diminution of ratios $2a_1/l_2$, at which the gain extension is observed.

It is known [5], that in a beam dielectric antenna there is a sharp passage from a condition in which dielectric almost does not influence a phase velocity and it is equal to velocity of light (c), to a condition, when the phase velocity is close to $c/\sqrt{\varepsilon_r}$. If ε_r is small, the passage from one condition to another happens rather smoothly at large values of a ratio of the rod diameter to a wavelength. By this way the influence of an interior spiral, at which an additional amplification on the CSA lower frequencies is observed, similarly to a slowing down effect of a beam dielectric antenna with $\varepsilon_r \approx 30$ at a ratio of the rod diameter (interior spiral) to a wavelength $2a_1/\lambda_2 > 0.17$.

The influence of an interior spiral on CSA gain in the lower frequency band is not observed at ratios $2a_1/\lambda_2 < 0.17$.

The lower range of CSA operational frequencies with increased gain is narrowed down and the minimum frequency decreases at extension of a density (diminution of an angle) of the interior spiral winding. At the winding angle close to zero the antenna has increased gain in narrow frequency band [3].

The maximum frequency of the lower range of CSA operational frequencies with increased gain is determined by a upper bound of existence of an axial radiation wave at the exterior spiral and depends on a ratio of CSA spirals diameters [6]. When ratio of diameters of spirals is less than 1.75 the magnitudes of $ka < 1.25$, and the maximum value of ka decreases with a diminution of the ratio of diameters of the spirals.

The maximum ratio $2a_1/l_2$, at which the gain extension is observed, depends on the winding angles ratio and it does not exceed 0.25; at increasing a_2/a_1 the ratio $2a_1/l_2$ decreases.

The relative axial lengths of considered antennas practically are identical, but CSA gain (Fig. 1) is more than gain of an antenna on 1dB [4]. This prize is because the CSA spirals are cylindrical, but in [4] — with a conic termination. Besides the CSA spirals (Fig. 1) have unequal axial lengths distinguished on a quarter of a maximum wavelength. Length of a conic part of a metal rod [3] is also equal 0.25λ. It allows to improve the concordance of an antenna with the feeder.

CONCLUSIONS

The gain extension of the lower range of CSA operational frequencies at the expense of a slowing down effect of an interior spiral can be obtained only at indicated ratios of the interior spiral diameter to the exterior spiral wavelength.

The band of the CSA lower frequencies, when the additional amplification is observed, extends with a diminution of the ratio of spirals winding angles.

The concordance of CSA with the feeder is improved, if its spiral have unequal axial lengths distinguished on a quarter of a maximum wavelength.

REFERENCES

1. Yurtsev O.A., Runov A.V., Kazarin A.N. Helical antennas, Moscow, Sov. Radio, 1974, 224 p. [in Russian].
2. Samusenko A.I., Prigoda B.A. Maximal directivity of cylindrical helical antennas, Radiotekhnika, 1991, N1, p.85-86 [in Russian].
3. Prigoda B.A. Antenna systems of automatic space stations // Problems of antennas engineering. Edited by Bakhrahk L.D., Voskresenskij D.I., Moscow, Radio I Sviaz, 1989, 258 p. [in Russian].
4. Sultan N, and others. Design of concentric helical antennas for maximum gain and isolation over wide frequency separation.// National telesystems conference. IEEE,1983,11,- p.12...17.
5. Zhuk M.S., Molochkov Yu.B. Designing of antenna-feed devices, Moscow-Leningrad, 1966, 466 p.
6. Yurtsev O.A., Mikryukoff A.S. Band properties of cylindric coaxial helical antennas, Sbornik "Voprosy postrojenija antennykh ustrojstv", Is.2, Daugavpils, 1982, p.3-14 [in Russian].

ABOUT A NEW SMALL-SIZED LOOP ANTENNA WITH AN ISOTROPIC RADIATION PATTERN

V. V. Ovsyanikov

Dnepropetrovsk State University, Dnepropetrovsk 10, Pr. Nauchniy 13, korp. 12,
Tel. (0562) 43-36-30, Fax 46-55-23, E-mail: root@ap1.net-rff.dsu.dp.ua

ABSTRACT

A computational method of small-sized loop antennas of the meter and decimeter ranges with capacitive loads is considered. It is shown that a cascading of capacitive loads in antenna enables one not only to reduce the dimensions of antenna but also to obtain an isotropic radiation pattern in the horizontal plane. The offered antennas can find applications in TV broadcasting, and mobile and other kinds of radio communications.

INTRODUCTION

As it is known, in meter and decimeter wave bands under conditions of settlements and industrial objects the transmission quality of the television information, and also cellular phone mobile and other kinds of radio communication rises when using horizontally polarized waves, as compared to using vertical polarization [1]. In the given work the capability of creation of the small-sized antenna of horizontal polarization with the isotropic radiation pattern is regarded.

In the work [2], the method of integral equations (IE) for calculating stub and loop bent antennas of different form with sequentially connected concentrated loads has been set forth. Computing IE by this method, the authors managed to determine behavior in the frequency band of input impedance ($Z_{in} \approx R_{in} \pm X_{in}$) of the loop antenna of finite thickness with sequentially connected capacitive loads.

INVESTIGATION RESULTS

In Fig. 1, the charts R_{in} and X_{in}, obtained by IE method for the loop antenna in the form of a square are presented at change of electrical length of a closed loop P/λ within the limits of 0 ... 2. Dashed lines are for the customary antenna of finite thickness with parameter Ω = 10.3 without loads; solid ones - for input resistances of the same antenna with two symmetrically connected capacitive loads at distances $h_C = \pm 0.125P$. from the antenna excitation point

The chart in Fig. 1a illustrates originating in the antenna with capacitive loads of a padding (series) resonance of current ($X_{in} = 0$) at P/λ ≈ 0.5 symbolized in the figure as ①, whereas the resonance in the antenna without loads ensues only at electrical length of the antenna P/λ ≈ (1.1 ... 1.2) symbolized as ❶. Thus, at change of electrical length of the antenna in the range 0 < P/λ < 1.5 in the antenna without loads there is only one resonance (ordinaary property of loop antennas), and in the loop antenna with capacitive loads - there are two ones in points ① and ②.

A padding resonance of a current ① in the antenna with loads is of especial interest, for it can be utilised for the development of electrically small loop antennas, a resonance frequency of which can be controlled in the main with a value of a capacitive load. As is seen from the chart in Fig. 1a a resistance of the antenna lays within the limits of 50...200 Ohm, that is quite reasonable to matching such antennas with the feeder. The research [2] have shown, that the most favourable conditions for an antenna matching with the feeder take place at $|h_C| \le 0.2P$.

It is possible to determine the value of capacitive load depending on a place of its actuation (h_C), on a closed loop perimeter (P) and other parameters of the antenna with a reasonable accuracy rate by a method of an equivalent line [3]. After that it is possible computing by an integral equation method [2] to update a fissile component of an input resistance of the antenna R_{in} and distribution of a current, and also radiation pattern and other parameters.

Assuming the considered loop antenna to be in the form of short-circuited piece of lengthy waveguide, we shall obtain the expression for capacitive reactance of load to be defined [3]:

$$X_c = 0.5W\{tg[2\pi/\lambda*(0.5P-h_c)]+tg(2\pi/\lambda*h_c)\}, \quad (1)$$

$$W = 276\lg(P/4r_a), \quad (2)$$

where W is the wave resistance of the antenna, λ is the length of antenna operating wave.

As follows from (1), at a constance of parameters W, P and λ the change of points of connection of loads (h_C) entails a change of their capacitive reactance. Besides, the change of h_c results in R_{in} change [2]. Consider the small-sized antenna with loads produced from aluminium conductive of a tube a dia 16 mms with perimeter of a tube P = 1360 mm and h_C = 170 mms. An operational frequency 120 MHz. From the formula (1) is received X_C = -735 Ohm, that corresponds to capacitance with 1.9 pF. Calculation of this version of the

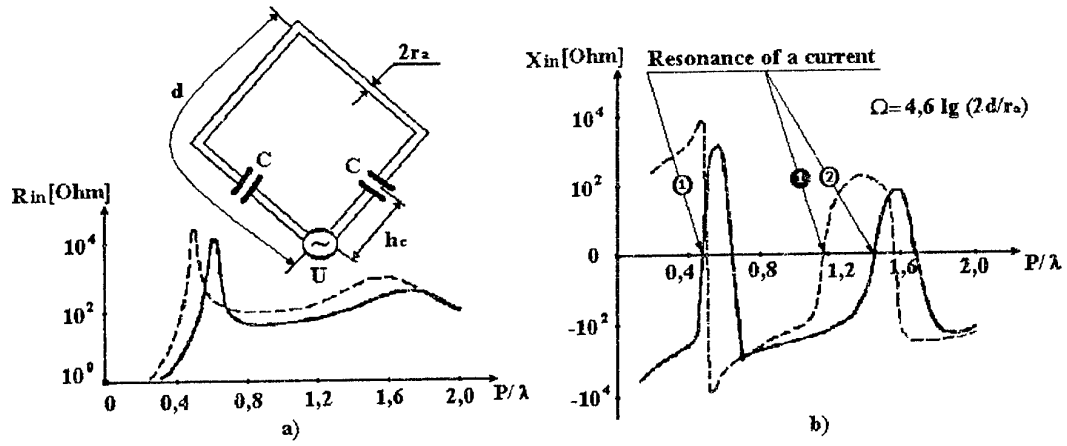


Fig.1

antenna by the integral equation method [2] has allowed to update a value of resonant capacitance from 1.9 pF to 2.03 pF and jointly to determine a value of resonance resistance: R_{in} = 47 Ohm. Note, that in the absence in the given antenna of capacitive loads its input resistance computed by the IE method [2] in the vicinity of the antiresonance is Z_{in} = 1522 - *i*4981 Ohm, and the corresponding value of a current module at voltage U = 1 V on an antenna input is 0.19 mA. Such data-ins are unacceptable for matching an antenna port with the feeding feeder.

Unlike this, under similar condition in the same antenna with connected capacitive loads the current module at a resonance sharply increases, approximately by two orders, and the antenna becomes serviceable with an input resistance close to 50 Ohm. We have considered the version of the loop antenna, diminished approximately twice relative to the classic sizes (P/λ = 1.1 ...1.2). If necessary, the antenna can be reduced by a greater factor at other values X_c of switched on capacitive loads, defined by the formula (1).

The research by an integral equation method [2] have shown, that in classic loop antennas of any configuration (circular, rhombic etc.) with an ordinary perimeter of a closed loop (1.1...1.2λ) without loads in the distribution of a current along a closed loop there are two diametrically opposite zero falls. These falls stipulate availability of the conforming two zero falls in the radiation pattern in a plane of such antennas. The connection of capacitive loads in similar antennas allows not only to reduce their sizes, but also to eliminate zero falls in the current distribution and, consequently, to obtain the isotropic radiation pattern in a plane of the antenna with capacitive loads [3, 4].

The version of implementation of a small-sized loop antenna with capacitive loads is depicted in Fig. 2. The loop antenna comprises a conductive closed loop 1, produced in the form of a bent tube, and terminals 2 on the opposite ends of a conductive closed loop for hooking up of a feeding channel. The loads 3, being of capacitive nature, are mounted in a closed loop 1 on both sides of terminals at distances from them no more than 0.2 perimeters of a conductive closed loop.

Each of loads 3 is implemented as metallic barrel 4, having a galvanic contact to one part of a conductive closed loop, inside of which one the iron core 5, galvanically bound by screwed joint with another part of a conductive closed loop, is introduced. The dielectric bush 6 is placed inside the barrel 4, inside this bush an iron core 5, and on its surface which is not entering inside of the dielectric bush freely slides, there is a thread. With the help of this thread the iron core 5 is twisted into a thread of shank bore of a handset 7, attached to isolator of load ,3, that enables a rod 5 to arbitrarily travel along internal space of the dielectric bush 6, changing with this reactance of load 3. The test leads of handsets 7 are closed by caps 8.

The antenna is attached to a dielectric crossbar 9 with the help of a grip 10 and the two grips 11 (one of them conditionally is not shown in Figure). Both grips 11, are welded to handsets 7, and simultaneously serve as removals for hooking up of the feeder 12 to terminals 2. Hooked up to terminals 2 feeder 12 is made on a crossbar 9 toward the receiver (transmitter). The final tuning of the antenna in a resonance of an iron implements at removed caps 8 by twist (unscrewing) core 5 screwdriver or special key entered into handsets 7. After tuning the situation of rods 5 is fixed with, for example, potting.

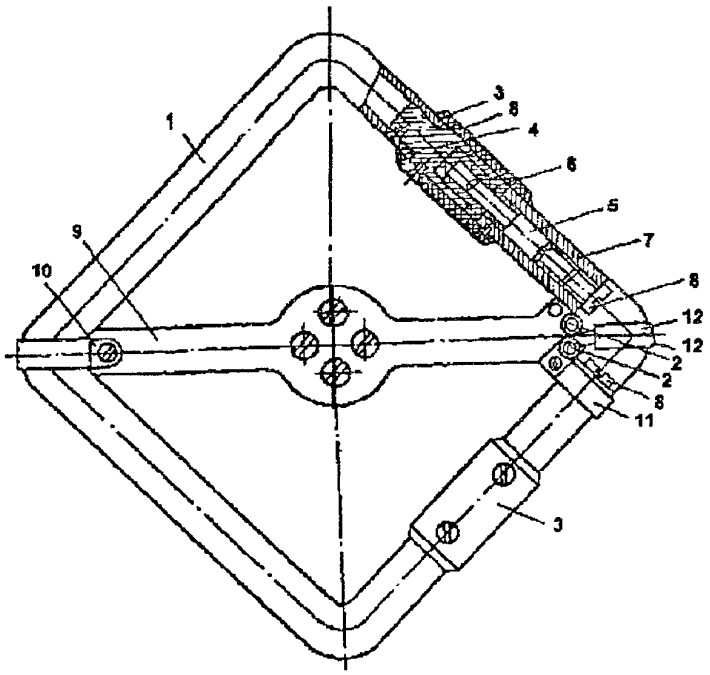


Fig. 2

CONCLUSION

The reported loop antenna can find applications in modern TV and radio communications, for it has a number of advantages with respect to ordinary stub antennas, namely there is a necessity for ground plane and the isotropic radiation pattern in the plane parallel to the Earth is provided at the horizontal polarization of radio waves.

REFERENCES

1. Kothergevsky G. N. The antenna-fiders arranfements. Moscow. Sviaz. 1968.
2. Ovsyanikov V. V. The investigation of linear antenna with loads in a curvilinear frame. Visnik DDU, series Physics and Radioelektronics, №. 3, vol 2, 1998, p.p. 103-108.
3. Ovsyanikov V. V. Wire antenna with reactive loads. Moscow. Radio i Sviaz. 1985.
4. Patent 624540 (USSR). Loop antenna / V. V. Ovsianicov. - Publ. 1983.

OPTIMIZATION OF GEOMETRIC AND RADIATION PARAMETERS OF A HEMISPHERE HELICAL ANTENNA

M. B. Protsenko, V. V. Molchanov

Sevastopol State Technical University, Streletskaya bukhta, UA-Sevastopol-53, 335053, Ukraine
Tel: + 380(692) 235-127, 235-118, e-mail: rt.sevgtu@stel.sebastopol.ua

ABSTRACT

The research of band properties of a hemisphere helical antenna with the optimum geometrical parameters has been carried out. Theoretical and experimental results of direction and polarization features of the antenna, and also the input impedance in a wide band are presented.

INTRODUCTION

A lot of up-date communication, radar and radiotelemetry system operate with signals of a various polarizations. Therefore, there are many problems concerned development of elliptical polarization of antennas operating in the set direction.

It is known that isotropic antennas are more suitable for such systems, since they provide the system reliable work due to that losses conditioned by the polarization anisotropy can be decreased by omni-directional helical antennas [1] which meet these requirements more fully because of they can radiate close to the isotropic patterns in the axial direction and to provide rather high values of the axial ratio in a wide band.

Possibilities of conical and cylindrical helical antennas application for different radio systems (including mobile ones) are restricted by their overall dimensions. The antenna axial size can be reduced by means of location of helical antenna wires on a hemisphere. However, there are engineering difficulties conditioned by the absence of full analytical and experimental results in research of such antennas.

GENERAL DESCRIPTION

Let us consider a hemisphere helical antenna, the geometry of which is shown in the Fig. 1 in Cartesian coordinate system. Radiation wires design in terms of regular helixon a hemisphere is a peculiarity of the antenna geometry. The maximum wavelength of the antenna radiation field is determined by the hemisphere radius R_{sph}.

Directional and polarization features of the presented antenna can be analyzed on the basis of the vector potential method, allowing to determine electromagnetic field in an asymptotical approximation of the antenna far-field zone as follows

$$\vec{E} \cong j\frac{k}{\sqrt{\varepsilon\mu}}\vec{A} = j30k\int_S \vec{I}(s)\frac{\exp(-jkr)}{r}ds, \qquad (1)$$

where k is the wave number of free space; ε, μ are the relative permittivity and permeability of environment, respectively; r is the distance between the observation point M in the far-field zone and an element dS on a radiation wire surface; $\vec{I}(s)$ is the current distribution function along this surface.

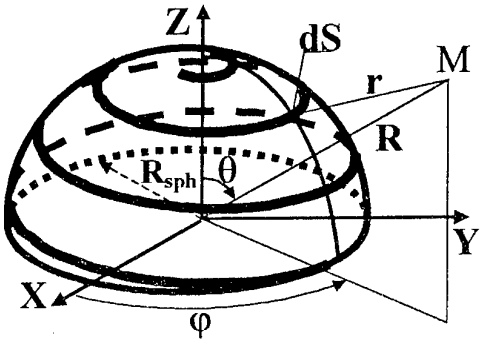


Fig. 1. Geometry of the hemisphere helical antenna

Let the antenna radiation be characterized by an 'active' area in the main. The current distribution along the area can be written as follows.[1]

$$\vec{I}(s) = \vec{s}\cdot I_0\exp(-jks), \qquad (2)$$

where $\vec{s}$ is the unit vector of a current direction; s is the length of a helixfrom the antenna center ($\theta = 0$) to the point ds to be considered; I_0 is the amplitude of the current distribution in the origin of the 'active' area.

As a result of numerical modeling of the antenna polarization and direction characteristics according to (1) and (2), the influence of the antenna parameters on these characteristics is evaluated in order to obtain optimum geometric parameters on the criteria of the axial radiation and elliptical polarization

Some results of theoretical research, for different number of antenna turns and arms are presented in [2].

The research of the antenna band properties in [2] fully agrees with the obtained experimental results in the paper.

RESULTS OF THE EXPERIMENTAL RESEARCHES

The frequency dependence describing direction and polarization properties at the following optimum antenna design is presented in Fig. 2.

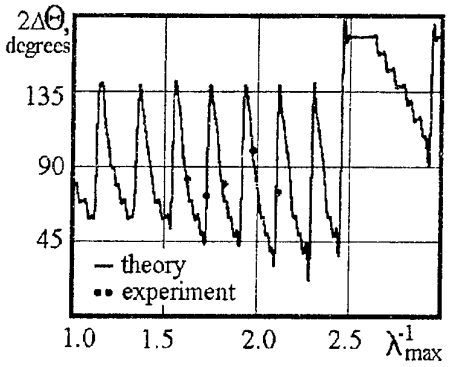


Fig. 2. Theoretical and experimental patterns widths of the hemisphere helical antenna

The two-arm helical antenna fed in antiphase in the sphere vertex, the turns number n equals 5.5. The geometry provides axial directional radiation with the main polarization component.

The presented frequency curve characterizes the pattern half-power width of the hemisphere helical antenna. Here the experimental results fully agreed with the shown theoretical data. The axial ratio is more then 0.7 in all band of the pattern width.

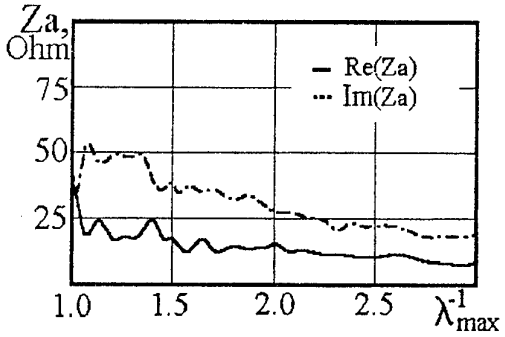


Fig. 3. The input impedance of the antenna

The experimental curves of the antenna input impedance in dependence on frequency values are shown in Fig. 3. According to it the antenna is a wide-band one as for the input impedance for the antenna optimum geometry and the assumed current distribution (2).

CONCLUSION

Thus, the obtained theoretical and experimental results of the hemispherical helical antenna with the optimum geometrical and radiation characteristics allow to come to the conclusion that the antenna application is a promising one due to its wide-band and elliptical polarization features. All of these allow to improve energy possibilities of communication channel.

REFERENCES

1. M. S. Juk, J. B. Molochkov Designing lens, scanning, broadband of antennae and feeder devices. - Moscow: Energia, 1973. - 440 p. [in Russian].

2. L. M. Lobkova, M. V. Ivashina, and V. V. Molchanov. Antenna optimization and radiation filed investigation results of hemisphere helical antennae // Proc. of 8-th International Conf. 'CriMiCo'98' -Vol. 2 - Sevastopol, Crimea, Ukraine. - 1998. - p. 490-491.

THE ESTIMATION OF THE RADIATION QUALITY OF THE FLAT ARCHIMEDEAN SPIRAL ANTENNAS

M. B. Protsenko, I. V. Tankov

Sevastopol State Technical University, Streletskaya bukhta, Sevastopol-53, 335053, Ukraine
Tel: + 380 (692) 235-127, 235-118, email: rt.sevgtu stel.sebastopol.ua

ABSTRACT

A research of the radiation quality of a flat Archimedean spiral antenna was carried out. The estimation of the radiation quality is made on the basis of the research of radiation complex impedance of the antenna calculated by the induced EMF method. The results of numerical modeling in a wide range of the radiator's design parameters are represented.

INTRODUCTION

The flat spiral radiating antennas [1] find wide application in the satellite radio communication systems because of their capability to form a radiation field of necessary polarization nature both in an axial direction and in a wide sector of corners, namely the electromagnetic field with the polarization close to the circular. All this raises stability and noise immunity of the radio communication channel. The mentioned radiators in service bands for the satellite radio communication systems are compact, that also allows to install them at the mobile objects.

A lot of investigations are devoted to the flat spiral antennas including the flat Archimedean spiral antennas [1]-[3]. For example, a monofilar spiral antenna is offered in [2], which distinguishes by compactness and relative design simplicity of feed system. Because of skew geometry it has tilted beam with respect to the axial direction that makes its directional characteristics worse. The marked lack is eliminated by twofilar variant of the spiral antenna described in [3]. However, both in [2] and in [3] there are no necessary dependencies allowing to optimize geometrical parameters of the investigated Archimedean antennas.

However, one of the important characteristics defining the antenna as a radiator (receiver) of electromagnetic power is radiation quality Q_Σ, which also characterizes band properties of the wire antennas. Therefore the consideration of a problem about potential band and power properties of the antenna is reduced to the research of Q_Σ and definition of its minimum values.

THE BASIC PART

According to [1], the radiation quality of the antenna can be presented as

$$Q_\Sigma = \frac{\omega_0 \langle W(\omega_0) \rangle}{P(\omega_0)}, \qquad (1)$$

where ω_0 is the resonance frequency; $P(\omega_0)$ is the active power, radiated by the antenna; $\langle W(\omega_0) \rangle = \langle W_e(\omega_0) + W_m(\omega_0) \rangle$ is the averaged power value of the electrical and magnetic fields, that is characterized by the "stored" power nearby the antenna. It is difficult to calculate Q_Σ by the expression (1) because of the complicated nature of the field. However, at the same time this is possible in a theoretical way, namely by such a characteristic of the antenna, as its radiation impedance. Resistance and reactance of the radiation impedance are proportional to the appropriate radiators power created by the antenna

$$Z_\Sigma(\omega) = R_\Sigma(\omega) + jX_\Sigma(\omega).$$

On the basis of the above mentioned, the approximate expression for calculation of the radiation quality of the wire antennas was obtained

$$Q_\Sigma \cong \frac{\omega_0}{2R_\Sigma(\omega)} \cdot \left. \frac{dX_\Sigma(\omega)}{d\omega} \right|_{\omega=\omega_0} = \frac{k_0}{2R_\Sigma(k)} \cdot \left. \frac{dX_\Sigma(k)}{dk} \right|_{k=k_0} \qquad (2)$$

where k is the wave number.

Thus, to determine the radiation quality Q_Σ it is necessary to investigate the frequency properties of the antenna, which is the more complicated the less its electrical sizes and the more complex geometry. The definition of antenna radiation impedance of the Z_Σ is a complex electrodynamic problem. To determine it we take advantage of the induced EMF method [2]. For this purpose generally we single out on an axis of a curvilinear conductor with a current element ds' and calculate a tangential component of a vector of the electrical field density in the specified point of the conductor s.

$$E_{tg}(s) = \int_L I(s') \cdot \exp(-jkR) \cdot G(R) \cdot ds', \qquad (3)$$

where $G(s) = 60\left(\frac{-j}{kR^3} + \frac{1}{R^2}\right) \cdot \cos^2(\vec{ds}, \vec{ds'}) +$

$$+ 30\left(\frac{-j}{kR^3} + \frac{1}{R^2} + \frac{jk}{R}\right) \cdot \sin^2(\vec{ds}, \vec{ds'});$$

L is the length of a conductor; R is the distance between the points of arrangement and integration of the elements on the surface of the antenna's radiating conductor; and $d\vec{s}, d\vec{s}'$ are the unit vectors of the line tangent to these points; $I(s')$ is the distribution of a current along the specified surface.

And further, according to the induced EMF method, let us write down the expressions for R_Σ and X_Σ

$$R_\Sigma = \mathrm{Re}\left(\frac{1}{I_0 I_0^*}\int_L I^*(s)\cdot E_{tg}(s)\cdot ds\right); \qquad (4a)$$

$$X_\Sigma = \mathrm{Im}\left(\frac{1}{I_0 I_0^*}\int_L I^*(s)\cdot E_{tg}(s)\cdot ds\right), \qquad (4b)$$

where I_0 is the amplitude of the current; * is the symbol denoting complex conjugate value.

After the concrete definition of the radiating conductor's shape, namely by means of its representation as an Archimedean spiral which is described in polar coordinates by the following equation

$$\rho(\alpha) = a\cdot\alpha,$$

where a is the geometrical parameter characterizing a lead of a spiral; α is the polar angle varying in limits $\alpha = 0...2\pi n$; n is the number of spiral's turns, the following expressions are derived:

$$ds = a\sqrt{\alpha^2+1}\cdot d\alpha;$$

$$s(\alpha) = \int_0^\alpha ds = \frac{a}{2}[\alpha\sqrt{\alpha^2+1} + \ln(\alpha+\sqrt{\alpha^2+1})];$$

$$L = s(\alpha)\big|_{\alpha=2\pi n};$$

$$\hat{d\vec{s}, d\vec{s}'} = arctg\frac{\sin\alpha+\alpha\cos\alpha}{\cos\alpha-\alpha\sin\alpha} - arctg\frac{\sin\alpha'+\alpha'\cos\alpha'}{\cos\alpha'-\alpha'\sin\alpha'}$$

$$R(\alpha,\alpha') = a\sqrt{\alpha^2+\alpha'^2+2\alpha\alpha'\cos(\alpha-\alpha')+r^2};$$

r is the radius of the antenna's radiating conductor.

THE RESULTS OF RESEARCH AND CONCLUSION

On the basis of the derived ratios the numerical calculation of the radiation quality of the flat Archimedean spiral antenna in a wide range of the antenna's design parameters are made. It is supposed that the distribution of a current along the "active" area corresponds to the form [1]

$$\vec{I}(s) = \vec{s}\cdot I_0\exp(-jks),$$

The integration of (3) and (4), and also differentition of (2) are made by numerical methods by the help of the package MathCAD 7.0 Professional.

The estimation results of the minimum value of the radiation quality and definition of them on the basis of optimal geometrical parameters of the radiator as the Archimedean spiral fully agree with the results in [1]. Some results determining the ratio of the optimum geometrical parameters of the radiating antenna as the Archimedean spiral, calculated on the criterion of minimum radiation quality are shown in table 1, where λ_0 is the element resonant length of the wave.

Table 1

n, turns	a_{opt}
2.00	$0.0225\lambda_0$
2.25	$0.0180\lambda_0$
2.50	$0.0167\lambda_0$
2.75	$0.0145\lambda_0$
3.00	$0.0134\lambda_0$
4.00	$0.0094\lambda_0$

The obtained results in the first approximation have been used during the experimental breadboarding of antennas, as the Archimedean spiral.

REFERENCES

1. *L.M. Lobkova, M.V. Ivashina, L. N. Stepanov, and I.V. Tanykov,* Methematical Model and Optimization of Geometrical Parameters for Flat Spiral Antennas of Diverse Configurations // Proc. of 8-th International Conf. "CriMiCo'98"-Vol. 2 - Sevastopol, Crimea, Ukraine. - 1998. - P. 458-461.
2. *H. Nakano, Y. Shiuma, and J. Yamauchi,* A Monofilar Spiral Antenna and Its Array Above a Ground Plane-Formation of a Circularly Polarized Tilted Fan Beam, IEEE Trans. Antennas and Propagat., - Vol.45 - Oct. 1997. - PP. 1506 - 1511.
3. *H. Nakano, K. Hirose, I.Ohshima, and J. Yamauchi,* A Integral Equation and Its Application to Spiral Antennas on Semi-Intinite Dielectric Materials, IEEE Trans. Antennas and Propagat., - Vol.46 - Feb. 1998. - PP. 267 - 274.
4. *L. M. Lobkova, L. I. Kalujniy, M. B. Potsenko,* The design principle of low-quality small sized band antennas for vessels communication // Proc. of Int. Conf. on technique and development in radio electromagnetic, Moscow: MAI 1991, PP. 102 [in Russian].
5. L. D. Bahrakh, L. F. Benenson, E. I. Zelkin, Antennas technique handbook, Moscow: IPRJR 1997 [in Russian].

AN IMPROVING OF ENERGY RADIATION CHARACTERISTICS OF AN CORNER REFLECTOR ANTENNA WITH FRANKLIN ANTENNA FEED

A. V. Seleznyov

National Technical University of Ukraine "Kiev Polytechnic Institute"
Ukraine, 254208, Kiev-208, Radyanskoi Ukraine Prospectus, Building 9, Flat 38, tel. (044) 462-89-27

There are two main requirements during antennas system researches and development – maximum adaptability to manufacture (for minimal cost) and required values of electrical parameters. There are contradictions between these requirements, therefore it is necessary to find acceptable technical solution. Thus it is necessary to prefer the completely defined characteristics depending on area of application, prospective consumers etc. For many practical tasks the modifications of the antennas system with a corner reflector will be optimal.

In the articles devoted to this problem [1–4], it is offered to use the half-wave vibrator as a feed for the corner reflector. The vibrator is necessary to install in a parallel way to an edge of a reflector. Changing a position of the vibrator in a bisectrix plane of a reflector and aperture angle of the reflector, it is possible to change the electrical characteristics antennas in a H-plane over a wide range. To change patterns in a E-plane it is necessary to increase the linear size of the aperture feed. It can be made by several ways.

The first: As the feed it is possible to use the linear phased antennas array. Thus the circuit of antenna power supply should be additionally realized. As a result the shadowing of the aperture increases (the efficiency is worsened) and the adaptability to manufacture is reduced.

A. I. Shalyakin offers another way [5]. He offers not to install the complex multidipole antenna as a feed, but simply to extend the symmetric vibrator. To preserve the co-phase field in antenna aperture, it is necessary to remove phase jump of originating in consequence transition through current nodes on the symmetric vibrator. Therefore it is necessary to change a corner reflector aperture angle. Such way gives the good electrical characteristics. However the necessity to manufacture reflector with several angles reflector aperture angle worsens it adaptability to manufacture.

In this article using the Franklin antenna (FA) (see Fig. 1) as a feed is offered. It consists of linear dipole array (1), connected through phase-specified loops (2). The antenna has one driving point (3). It's advantage is the simple matching and good repeatability with planar fulfillment. The loops for volumetric FA can be made as units of a construction for the mount of a feed in the aperture corner reflector. Besides using FA the distribution of electromagnetic energy on equivalent linear aperture automatically is falling down to edges. The latter additionally reduces the sidelobe levels in E-plane (that can be very useful in some cases).

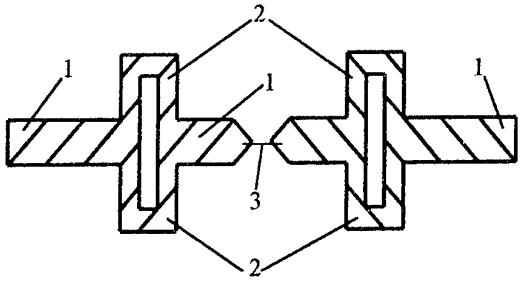
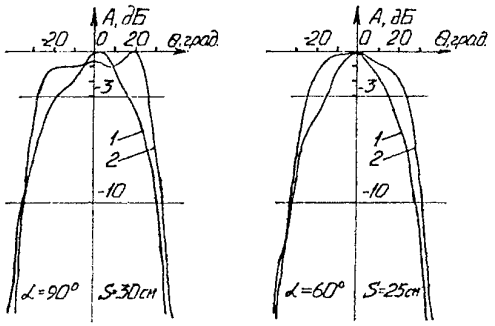


Fig. 1



a b

Fig. 2

For experimental check the sample of corner antennas was made. The corner reflector was made as a construction, with fixed aperture corners (45, 60, 90°). In this sample it is possible to change feed position in bisectrix plane. The feeds (half-wave dipole and three-element Franklin antenna) were made by a printed way and are matched with a measuring path with the matched and quarter-wave-closed stub.

During testing experimental sample the following characteristics were measured: radiation pattern in E- and H-planes, gain with various values of a corner reflector, its geometrical sizes, location of a feed in a plane of a bisectrix of the corner reflector. In Fig. 2 a,b radiation pattern in a E-plane for CRA with FA as the feed (curve 1) and with $\lambda/2$ dipole as the feed (curve 2) are represented. The measurements were made for fixed frequency 1530 MHz. The radiation pattern measuring

was executed according to a technique [1]. The gain was measured by a method of substitution. As a sample the measuring aerial of П6-23 type was used. In Fig. 3 dependencies of CRA gain with the FA feed (curve 1) and λ/2 dipoles (curve 2) as the function breadth of flasher side R, for an aperture angle $\alpha = \pi/3$ are given. From these results it is clear, that the application of FA as a feed is resulted in decreasing radiation pattern width at -3 dB level in E-plane on ~ 15° and increasing antenna gain on ~ 2÷3 dB. Thus a level of the nearest side lobes in a E-plane is equal to -17 dB. The radiation pattern performances in a H-plane during changing λ/2 dipoles on FA practically is not varied.

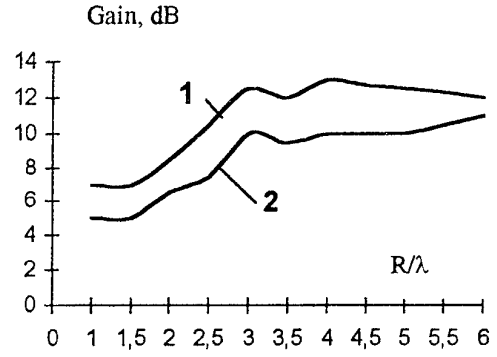


Fig. 3

Applying FA as the feed for CRA it is necessary to know it's optimal position. This is necessary to obtain the maximum gain. In [4] the results of experimental researches of this problem for λ/2 dipoles are given. On the basis of theoretical researches done for λ/2 dipole and FA the assumption of coincidence of optimal standings of a feed in both cases was made. To check this assumption when measuring gain of CRA the optimal position of a feed in bisectrix plane, (distance S_{opt} from top of a corner reflector up to a feed under condition of maximum gain) was determined. It has been determined, that S_{opt} depends on a reflector aperture angle, but practically does not depend neither on width of mirror facets (in a measurement range R from 6λ to 1λ) nor on a type of the feed. The values S_{opt} are given in table 1.

Table 1

Corner of aperture α,°	S_{opt}/λ	
	Dipole	Franklin antenna
45°	0.8	0.9
60°	0.7	0.75
90°	0.5	0.5

It is necessary to note, under manufacturing the feed substrate material influences strongly to power radiation characteristics. It occurs because it lays in area of concentration of an electromagnetic field and therefore the losses in it define antennas efficiency, and its gain correspondingly.

The FA used as the feed for CRA allows to increase gain by 2÷3 dB without noticeable increasing of system's cost.

REFERENCES

1. Drabkin A.A. Antenna - feeder devices -Moscow: Energija, 1974. - 467p.
2. Marcov G.T., Sazonov D.M. Antennas - Moscow, Energija, 1975. - 564p.
3. Ayzenberg G.Z. VHF Antennas / 2 parts - Moscow: Sviaz, 1977. - 354p.
4. Guk M.S., Molochcov U.B. Design of antenna - feeder devices -Moscow-Leningrad: Energija, 1966. - 365p.
5. Shalyakin A.I. About one way of increasing gain of corner-reflector antenna // Radiotekhnika. - 1985. - № 2. - p. 81 - 82.

ELECTRODYNAMIC MODELING OF TWO-PORT C-BAND FLAT ANTENNA

B. V. Sestroretsky, A. V. Dorofeev, A. N. Savchenko, M. A. Drize, S. A. Ivanov

Russia, Moscow, 117296, Universitetsky pr-t 5-358,
tel./fax (095)-938-15-14, const@glasnet.ru

ABSTRACT

The results of designing at an electrodynamics level of the case flat two-port antenna of a circular polarization for satellite communication system in 4/6 GHz band with the sizes 280×130 mm^2 and with printed emitters (9 for receiving and 18 for transmitting) are presented. The antenna has a dielectric plate with emitters, metal plate with rectangular slots, layer of air strip lines and two face coaxial inputs on the bottom metal plate. The general antenna thickness is 26 mm. The antenna has the −13 dB first sidelobes of a radiation pattern, ellipticity factor $K_e \sim 0.8$ and VSWR ≤ 1.7. The antenna analysis was made in a time domain without decomposition on the basis of the stream grid technique.

INTRODUCTION

The design variant of small-sized two-port flat antennas of a linear polarization of a Ku-band for satellite communication systems was considered in [1] (Fig. 1a). Two alternating systems of parallel waveguides were used in the antenna: rectangular ones with dumb-bell cross slots and П-figurative with longitudinal slots. The co-phase excitation of all cross slots on receiving frequencies (11.7÷12.2 GHz) and of all longitudinal slots on transmitting frequencies (14.0÷14.5 GHz) and low level of far sidelobes of the antenna radiation pattern were achieved by the choice of the geometrical sizes of waveguides (a_2b_2; $a_1h_1h_2$) and of exciting elements of slots (Fig. 1b,c). The general thickness of the two-layer flat antenna is 34 mm in view of introduction of a layer of exciting waveguides (Fig. 2a, b, c) in the antenna. That admits allocation of the developing twice antenna with an aperture 600×600 mm^2 in the case [1].

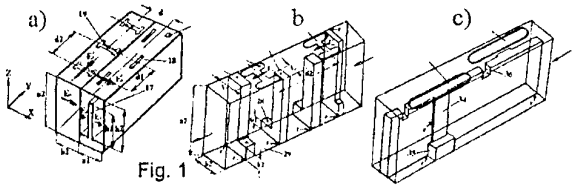


Fig. 1

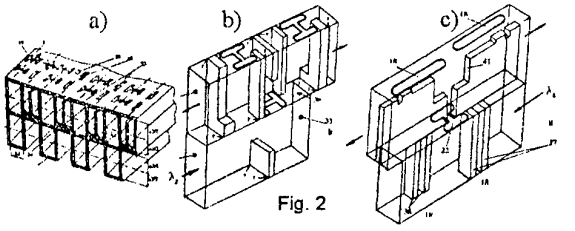


Fig. 2

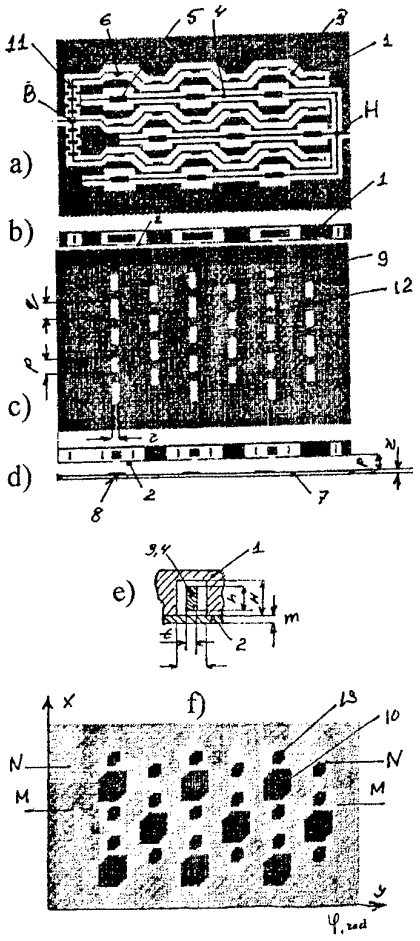


Fig. 3

The antenna thickness increases in 2÷3 times [2] with construction of the similar antenna in a C-band (receiving 4 GHz, transmitting 6 GHz) on the basis of waveguides Fig. 2a that excludes its use in a case variant. Various partition strip systems exciting patches through strip electrodes in which the orthogonal oscillations shifted on 90° use frequently instead of waveguides for decreasing the antenna thickness [3]. The printed strip systems bring in significant losses (decrease of the antenna gain G) and noise temperature of the receiver T. The technology of printed antennas is also undesirable on ecological reasons. Taking this into account, strip lines of high Q-factor with a vertically guided flat central electrode were used in the investigated flat antenna instead of printed strip partition systems.

ANTENNA DESIGN

The structure of three metal layers of the flat antenna is shown in Fig. 3. The view on the antenna with the removed top metal plate 2 with slot-hole coupling elements (Fig. 2c) is shown in Fig. 3a. In a plate 1 there are two systems of grooves in which the central electrodes 3 and 4 of strip lines with high Q-factor (Fig. 3c) are located. The lines have the sizes: h = 8 mm, H = 12 mm, t = 2 mm, m = 2 mm, n = 10 mm. The rectangular slots in a plate 2 (Fig. 3c) are guided across strip lines and are located above areas 5 and 6, where electrode width of lines is increased.

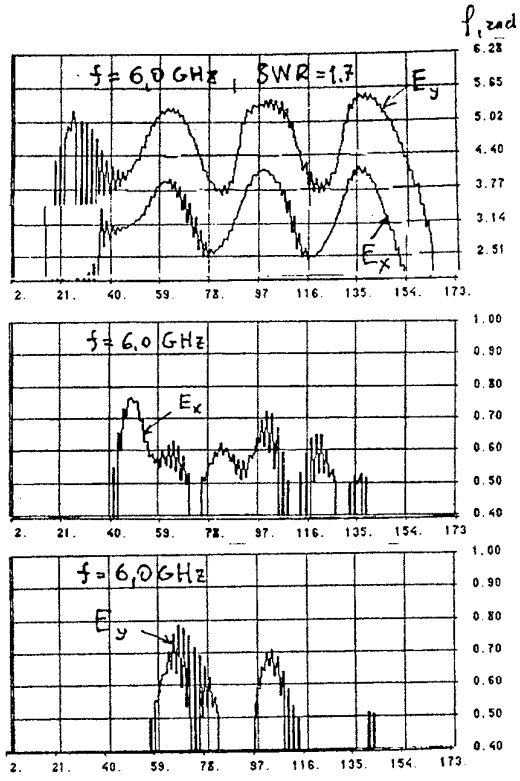


Fig. 4

The slot sizes (q = 18 mm, p = 14 mm, r = 6 mm) are chosen various for transmitting ($q \times r$) and receiving ($p \times r$). The electrodes of lines of the transmitting channel 3 are bent so that distances between thickenings 6 were equal to λ_h (f_h = 6 GHz). Similarly the distance between thickenings 5 of the receiving channel are equal λ_l (f_l = 3.57 GHz). The electrodes of all three lines of the transmitting channel are united in point B, to which the electrode with a coaxial socket located on an external surface of a plate 1 is connected. All electrodes of lines of the receiving channel are united similarly in point H. The dielectric plate (p = 8 mm, r = 2 mm, ε = 2.5, Fig. 3d), on which bottom side patch emitters 8 are placed, lays above a plate 2 with rectangular slots (Fig. 3c). The geometrical allocation of the receiving channel patches (9 patches) and of transmitting channel (18 patches) on plate 7 is shown in a Fig. 3f.

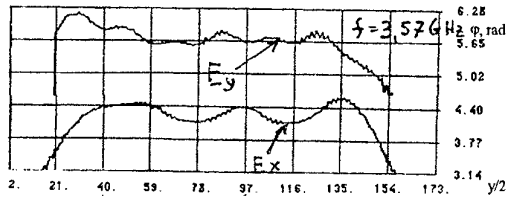


Fig. 5

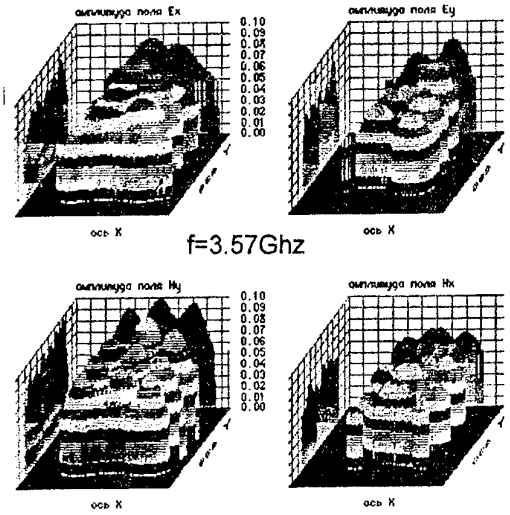


Fig. 6

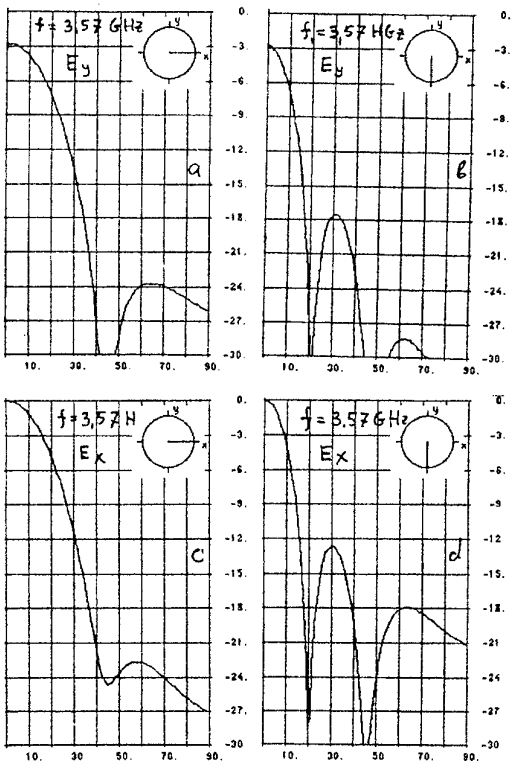


Fig. 7

ANTENNA PARAMETERS

The electrodynamic analysis of the antenna was carried out in a time domain without decomposition on the basis of a stream grid technique [4]. Parameters of separate radiating elements of the antenna in structure of a line Fig. 3e, of rectangular slot (9 in Fig. 3c) and patch emitter (10 in Fig. 3f) were previously investigated for receiving and transmitting bands. Strips with three (for receiving) and six (for transmitting) patch emitters further were investigated. Then the antenna with three strips separately for receiving and transmitting was investigated and the circular polarization radiation mode (left for transmitting and right for receiving) was achieved. With the analysis of the whole antenna Fig. 3a some correction of the patch sizes of receiving and transmitting channels was required, that was caused by interaction between patches of two channels (Fig. 3f). It was required to increase the electrical length of electrodes of strip lines (lines of the top and bottom strip) connected to the electrode B to provide a co-phase excitation of three strips of the transmitting channel. It was done introducing capacitor expansions 11 of electrodes of lines Fig. 3a.

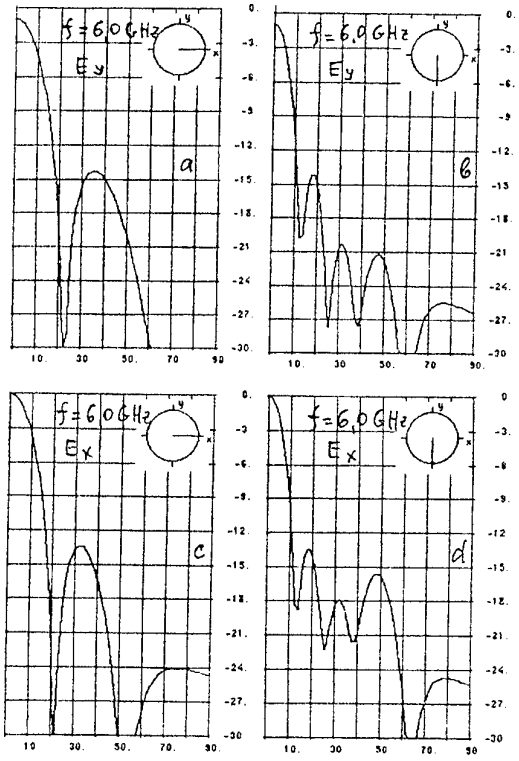


Fig. 8

Small VSWR values for receiving and transmitting channels was achieved by adjustment of expansions 6 and 5, allocation of rectangular slots 9 and 12, and patches 13 and 10 (Fig. 3). For receiving and transmitting frequencies 3.57 and 6.0 GHz VSWR equal to 1.5 and 1.7 were achieved. The phase (Fig. 4a) and amplitude (Fig. 4 b, c) distribution of fields E_x and E_y along axis Y on section M-M for receiving frequency 3.57 GHz is shown in Fig. 4. The distribution of E_x, E_y, H_x and H_y fields intensity over the whole antenna surface for the same frequency is shown in Fig. 6. The intensity and phase distribution of fields E_x, E_y, H_x and H_y over antenna surface was further used to calculate the antenna radiation pattern in far zone (Fig. 7,8) for two orthogonal fields E_x and E_y of circularly polarized wave. It is possible to make a conclusion about the rather high (~0.8) antenna ellipticity factor considering the insignificant difference of amplitudes of fields E_x and E_y for a maximum of radiation pattern ($\theta = 0$) and phase difference between fields E_x and E_y (Fig. 4a,5) which is more than 70°. The first sidelobes of a radiation pattern are −13 dB and less; the far sidelobes are monotonously reducing with increasing of a corner θ. To achieve this for distance between patches in strips equal to a wavelength λ, the next strips along axis Y are displaced on $\lambda/2$. In result the effective distance between patches decreases up to $\lambda/\sqrt{2}$, that eliminates increasing of radiation pattern sidelobes for corners $\theta \approx \pm 90°$.

RESUME

The topological synthesis carried out at an electrodynamics level has shown an creation opportunity of flat thin (thickness 26 mm) two-port circular polarization antennas of C-band with allocation of receiving and transmitting channels patch emitters on one aperture and by contactless excitation of patches by two not crossed systems of metal strip lines with high Q-factor.

REFERENCES

1. B.V. Sestroretsky, B.A. Prigoda, S.A. Ivanov, M.A. Drize. Electrodynamics optimization of flat two-input VSAT antenna. Proceedings of XXVIII Scientific Conference on Antenna Theory and Technology. September, 22-24, 1998, Moscow, Russia, JSC "Radiophisika".

2. J. Hirokawa, L. Manholm, P.S. Kindal Analysis of an Untilted Wire-Excited Slot in the Narrow Wall of a Rectangular Waveguide by Including the Actual External Structure. IEEE transactions, vol. AP-45, №5, June 1997.

3. B.J. Jang, Y.K. Lee, H.W. Moon, Y.J. Yoon, H.K. Park. Analysis of Finite-Phased Arrays of Aperture-Coupled Stacked Microstrip Antennas. IEEE transactions, vol AP-45, №8, August 1997.

4. B.V. Sestroretsky. Balance RLC and Rτ-circuits of elementary volume. Problems of radioelectronics, ser. "General problems of radioelectronics", 1983, vol. 5, pp56-85.

RADIATION CHARACTERISTICS OF A MULTIPLE-ARM CONICAL HELICAL ANTENNAS WITH TWO POINTS EXCITATION

L. N. Stepanov, A.V. Lukyanchikov

Sevastopol State Technical University,
Streletskaya bukhta SevGTU, Sevastopol-53,Ukraine,335053
Phone: +380(0692)235-127, e-mail: rt.sevgty@stel.sebastopol.ua

Abstract: The theoretical and experimental investigations of two arm conical helical antennas are presented. Analysis of the antenna radiation features has been carried out in dependence on various methods of the helix excitation.

INTRODUCTION

Inconstancy of electromagnetic field polarization in a point of reception is the main nature of the most radio communication channels due to complicated nature of underlying surface. All that leads to use of antennas operating with signals of various polarization features.

In [1], [2] the possibility of polarization control in helical antennas with opposite turning was substantiated. However for more simple conical designs with one direction turning the problems of radiation characteristics in dependence on helix wires excitation have been not enough examined. So the problem is the presented paper's goal.

PROBLEM FORMULATION

As well known for helical antennas with one directional turning the polarization vector rotation direction (PVRD) is defined by direction of the helix turning. Therefore in order to change PVRD it is necessary to vary excitation points of helix arms.

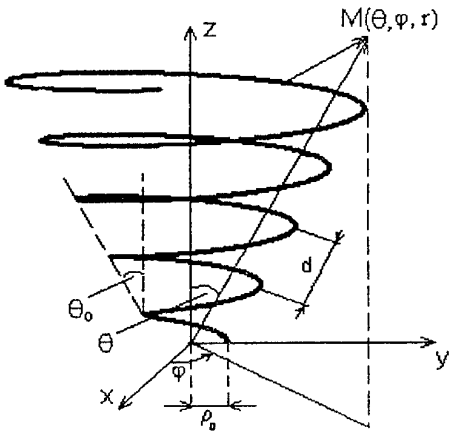


Fig. 1. The conical helical antenna

Therefore, multiparameter analysis of direction and polarization's features for two-arm conical helical antenna with one direction turning was carried out. The examined antenna represents infinite thin ideally conducting two-arm conical helix with cone's angle θ_0, the turning lead d. The excitation in the antenna inputs is antiphase. One of the antenna arms in the rectangular coordinate system is illustrated in Fig. 1. In order to calculate the antenna radiation field we used the vector potential method presented in [3],[4]

It was generalized for conical helical antennas with the prescribed geometry. It allowed to carry out electrodynamic analysis of antenna characteristics in the rigorous formulation of the radiation problem. The antenna's field research of the far-field zone case was carried out. Therefore the expression [3] for the calculation of the vector was used

$$\bar{E} \cong A_\theta \bar{e_\theta} + A_\varphi \bar{e}_\varphi, \qquad (1)$$

Where e_θ, e_φ are the unit vectors of the spherical coordinate system; A_φ, A_θ are the vectors potentional components in this system. These components were calculated taking into account the generalized vector potential for the helical antennas with the set geometry

$$\bar{A} = (\mu_0 / 4\pi) \cdot (e^{-ikr/r}) \int_S \bar{I}(S) \exp(ik(x \sin\theta\cos\varphi + y \sin\theta\sin\varphi + z\cos\theta))dS;$$

$I(s)$ is the current distribution helix wire, determined by the expression

$$I(S) = \vec{s} \cdot I_0 \exp(-jkS) \cdot \exp(-\eta \cdot S),$$

Where s is the unit vector of current direction on the antenna element, I_0 is the current amplitude; r is the distance between the coordinate system center and point M; η is the attenuation coefficient of the current amplitude, S is the helix length from the antenna input to the element ds.

INVESTIGATION RESULTS

The investigation results for the regular helix with various cone's angle are represented from the point of view of the geometrical parameters zones. These zones

meet the requirements shown in Fig. 2, where N is the number of helix turns.

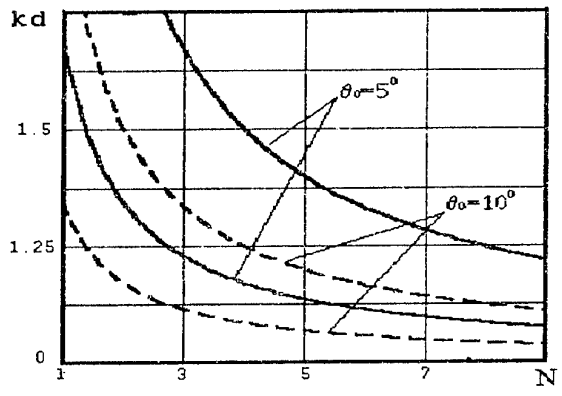


Fig. 2. The back radiation zones for the different cone's angles

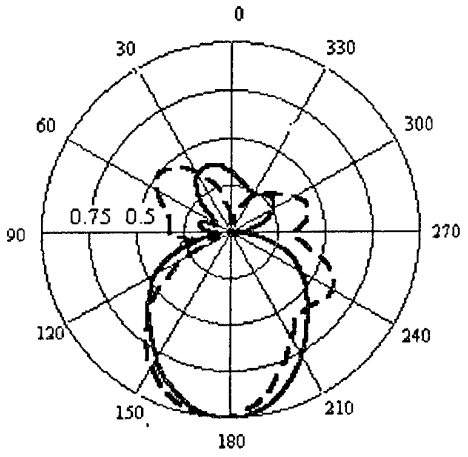


Fig. 3. The theoretical patterns of various excitation modes

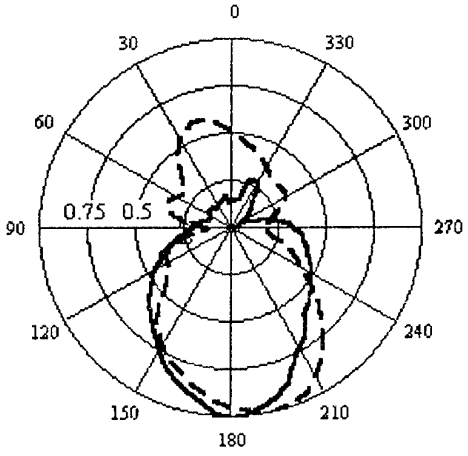


Fig. 4. The experimental patterns of various excitation modes

According to the vector potentional method the two-arm helical antennas were investigated by the modeling and experimental ways. So the theoretical and experimental patterns for the regular helical antenna illustrated in Fig. 3–4, respectively. the dotted curve is for the left-hand polarization with the following geometrical parameters: $N = 6$ measured at the frequency equal to 800 MHz. The antiphase excitation are in the corner vertex (for the solid line) and in the corner radix (for the dotted-line). Thus, the direction characteristics for the different PVRD are about the same except the back radiation. It can be eliminated by screen. The experimental radiation characteristics of the conical helix were investigated for the two-point excitation in the corner vertex. The peculiarity of excitation is the fact that it is possible to change axial ratio by means of the amplitude and phase selection of the current. Then one can to obtain the impedance and pattern constant features in a wide band.

CONCLUSION

The presented theoretical and experimental investigations of two-arm conical helical antennas and their excitations allow to solve the problem of design of antennas systems operating with different polarization signals in a wide band under conditions of the simple design.

REFERENCES

1. Yurtsev O.A., Runov A.V., Kazarin A.N..Helical antennas. - Moscow.: Sov. radio,1974. -224 pp. [in Russian].

2. V. Ramzey Frequently independent antennas: Moscow: Mir, 1968. - 176 pp. [in Russian].

3. Prozenko M.B., Stepanov L.N., Lukyanchikov A.V. Investigation of polarization characteristics of conical helical antennas with the set geometry // Pros. Int Conf. CriMiCo'98. - Vol 2. - Sevastopol, 1998. - pp. 492-493.

4. Prozenko M.B., Stepanov L.N., Lukyanchikov A.V. Analysis of directional and polarization characteristics of conical helix. Pros. of SevGTU, № 18.

MEANS OF RADIO–ACOUSTIC ANTENNAS INTERFERENCE IMMUNITY IMPROVING

Yu. N. Ulyanov, V. S. Bedin, and S. V. Butakova

Terminal Ltd. Box 10744, 310140, Kharkov, Ukraine. Tel. +380 0572 472457, 272409

Strong wind shears in the lower atmosphere constitute a major hazard for modern aeroplanes takeoffs and landings. At least one aircraft disaster per year is caused by this factor. Our investigations are focused on the sodar–radio-acoustic-sounding-system (RASS) to be developed in order to be used for monitoring low–level wind shears over airports. When getting such an information air–traffic–controllers might assist pilots to avoid disasters conditioned by this reason (Fig. 1). With the developed by us ground–based sodar–RASS complex all the weather changes might be registered without using balloons, towers, kites, ets. Penetrating clouds, heavy pollution, snow and low level inversions, it enable one to obtain temperature and wind vertical profiles in real time as well as the space–time turbulence structure reliably.

The concept used in RASS is the tracking of a sound waves packets with a doppler radar. In such a way it is possible to measure a sound velocity in any direction. Since a sound velocity is connected with the air temperature and the wind parameters, the latters might be measured too. This system continuously yields the quantitative data about the dynamics and the structure of wind and temperature fields in the lower atmosphere over a run-way. The incorporated in the hybrid bistatic acoustic sounding engineering is applied for increasing accuracy of measuring weather data. Using acoustic impulses for atmosphere sounding, this techniques detects the acoustic energy scattered by the atmospheric turbulence. [1–3]

The sodar–RASS complex deals with specific periodical air density structures formed by acoustic sounding signals propagating with a sound velocity. In this case aircrafts, birds, conjections of insects and other flying objects can not cause false alarms because their speeds are much less than a sound velocity. Owing to a sizeable radioacoustic cross–section (this value for RASS is four orders greater than that for the clear air) the accurate values of the wind and the temperature might be measured with a high probability. The high promptitude of the radioacoustic temperature and wind sounding at the runway area are achieved by using the sodar wind data off the runway [3].

This hybrid system could be incorporated in an automated airport weather station providing in real time data from 30 m up to 1 km above runway surface in order to detect dangerous wind shears and microbursts. Note that the system could be completed with a radar wind profiler that measures at high altitudes and can not provide data at lower layers. [4–6]

When location a sodar–RASS at airport it is essential to solve the problem of its interference immunity, as well as of its electromagnetic and acoustic compatibility (EMC and AC) with airport equipment. In this paper we consider ways of these problems solution.

In order to ensure the frequency isolation of the sodar–RASS antenna system we have analyzed the information [7–10] about frequency bands occupied by aviation electronics. Basing on the results of this analysis, the aviation frequency scale has been plotted (Fig.2), and the vacant frequency interval for the sodar–RASS has been found out. As it can be seen in Fig. 2 it is from 1215 to 1240 MHz. The lower of these frequencies is the upper limit of the near navigation system hardware band, the higher one is the bottom limit of the tracking radars. In Europe there are a few radar–acoustic temperature–wind sounding complexes operating at frequencies close to specified [5,6,11]. Among them there are French LT–radar «Degrean» (1300 MHz), German radars LT and LT–Rass named WTR–89 and TST WTR–83 (1235 MHz) and Austrian LT–radar (1280 MHz). Only Austrian LT–radar is placed directly at airport (Wienna).

The acoustic noise of surrounding aircfaft engines presents a serious problem for sodar, when the latter is situated close to a runway. Fig. 3 [2] shows acoustic noise levels near a runway at a wide frequency band (~15 kHz) under the heavy noise conditions (during aeroplanes of «Boyeing»–type takeoff or landing). As the sodar has a narrow bandwidth (~100 Hz), the ambient noise power affecting on the sodar decreases by ~40 dB as compared with Fig. 3. Since RASS is not acoustic noise sensitive, only aeroplanes crossing the sounding volume and breaking down the acoustic packet can be clutter sources. Such a clutter is missed when correcting placing the system at the airfield.

In solving the compatibility problem the antenna spatial isolation from extraneous radiations is important. Under airport area conditions characterized by radio hardware saturation it is not possible to move the sodar–RASS antenna system sufficiently far for isolation. The received power $P_{a\Sigma}$ in the input of the EM antenna might be present as follows:

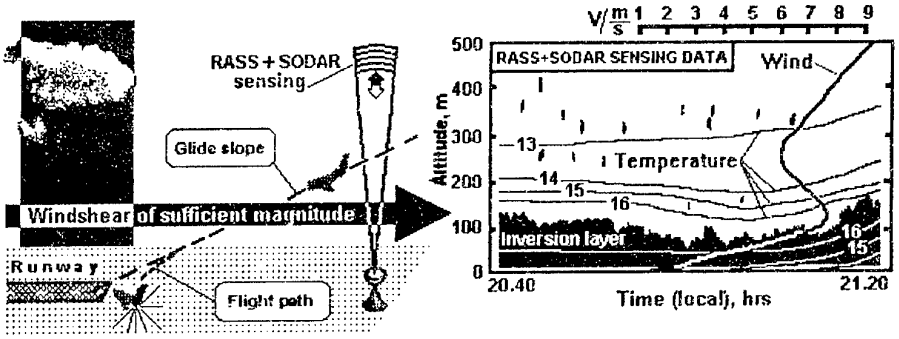


Fig. 1

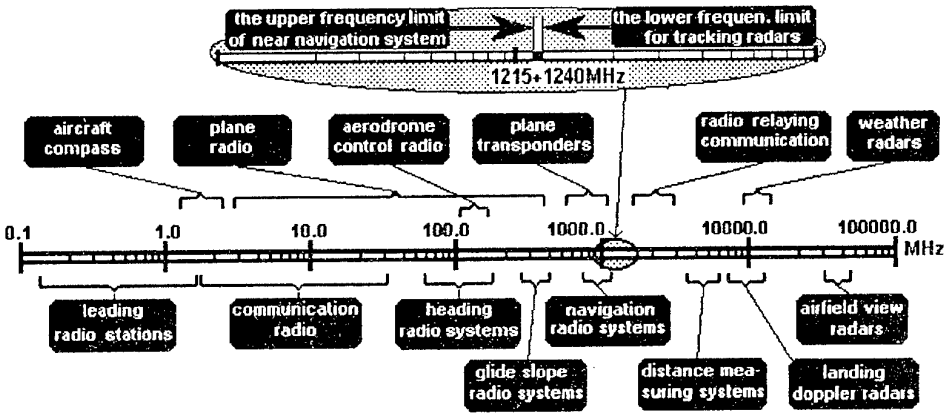


Fig. 2

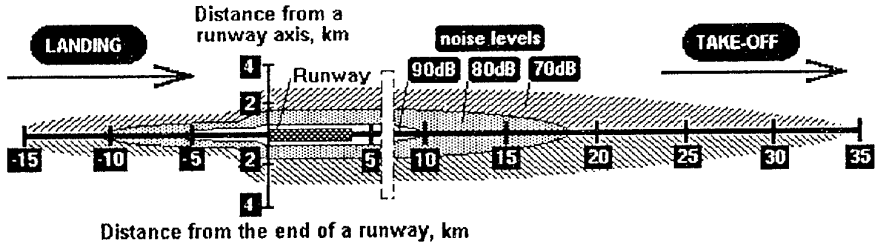


Fig. 3

$$
\left.
\begin{aligned}
&P\alpha\Sigma = P\alpha + \Delta P\alpha;\\
&P\alpha = \eta \int_{\Omega r} P_{sr}(\vartheta,\varphi) F(\vartheta,\varphi)\, d\Omega \Big/ \int_{\Omega r} F(\vartheta,\varphi)\, d\Omega;\\
&\Delta P\alpha = \eta \int_{4\pi-\Omega r} P_b(\vartheta,\varphi) F(\vartheta,\varphi)\, d\Omega \Big/ \int_{4\pi-\Omega r} F(\vartheta,\varphi)\, d\Omega.
\end{aligned}
\right\}
$$

where P_a is an echo signal power, ΔP_a is a sidelobe power associated with extaneous jamming P_b (ϑ,φ), $P_{sr}(\vartheta,\varphi)$ is a scattering pattern of an air perturbated volume, $F(\vartheta,\varphi)$ is a directional pattern of the receiving antenna, η is an antenna efficiency, Ω_r is an angle of perturbated volume vision from the antenna.

In order that the useful signal can be discerned against the ambient background that is $P_a >> \Delta P_a$, in the di-

rectional pattern of the receiving antenna the side and back lobes should be of a low level and the main lobe should intercept the angle of perturbated volume vision ($\Theta_a \leq \Omega_r$). The same requirements are imposed on the radiation pattern in order to provide the radio antenna efficiency and to reduce a level of the electromagnetic effect on the extraneous hardware. The requirements for the half-power beamwidth and for side and back lobes reduction of the RASS acoustic source follow from this.

Often the same means for creation the directional radiation are used in EM and acoustic antennas. There are horns and reflectors. As for these means, the origin causes of side and back lobes are identical. These causes are a diffraction on the aperture edge and a streaking of currents on a shadow side of antenna. In Acoustics the streaking «currents» are acoustic oscillations of the external panelling of the antenna and its edge exciting acoustic waves in the ambient space.

In order to decrease side and back lobes in directional radio–acoustic antennas, means reducing an illumination level on the edge and (or) scattering the diffraction wave are used. There are the selection of a reflector feed with a qualified radiation pattern, the use of absorber-lined tunnels (blends), the profile deformation of the horn or the blend (spaced as a broken line inscribed into an exponential curve) and working surfaces coating with material absorbing radio– or (and) acoustic waves. It is very productive to use the reachings in the side lobe suppression of radio antennas for acoustic directional radiators and on the contrary. On these grounds papers [12–16] are very useful.

When disposing sodar–RASS complex at an airport it is necessary to provide a low level of the radiation and the reception for acoustic and radio channels at all the directions near the earth surface around the antenna assembly in order to avoid interactions between the ground-based equipment with a surface-guided wave. For this a screening fence is installed around the antenna assembly [17, 18]. The action of the fence should not depend on a direction and polarization of the acoustic and radio waves. When antenna scanning the fence should decrease side lobes the most close to the earth surface from the first lobe to the greatest possible extent.

REFERENCES

1. M. A. Kallistratova, and A. I. Kon, Radioacoustic-sounding of the atmosphere. – Moscow: Nauka, 1985. 197 p. [in Russian].
2. M. F. Goldstane, Airacoustics. – Moscow: Mir, 1980. 294 p. [in Russian].
3. D. W. Beran, Acoustic: a new approach for monitoring the environment near airports. // J. Aircraft, 1971, Vol.8, no 11, 934–936.
4. E. E. Gossard, and N. Sengupta, Measuring gradients of meteorological properties in elevated layers with a surface–based doppler radar. // Radio Science , 1988. Vol 23, No 4, 1. P.625-639.
5. R. G. Strauch, D. A. Merritt, K. R. Moran, B. L. Weber, and D. B. Wuertz, Wind profilers for support of flight operations. // J. Aircraft, 1989, Vol.26, no 11, 1009–1016.
6. Wind profiler assessment report and recomendations for future use. // NOAA US Department of Commerce. – Silve Spring, Maryland, 1994. 141p.
7. L. Ya. Ilnitski, and A. A. Bolbot, Antenna essemblies of civil aircraft airports, Moscow: Transport. – 1983. 190 p. [in Russian].
8. P. S. Davidov, A. A. Sosnovski and I. A. Khaimovitsh, Air radio location., Moscow: Transport. – 1984. 223 p. [in Russian].
9. Air radio navigation. Handbook. Edited by A. A. Sosnovski, Moscow: Transport. – 1990. 264 p. [in Russian].
10. Air radio communication. Handbook. Edited by P. V. Olanuk, Moscow: Transport. – 1990. 208 p. [in Russian].
11. Wind profiler radar. Wienna / Austocontrol, Publicity materials, 1998. 9 p.
12. V. G. Yampolski, and O. P. Frolov, Antennas and electromagnetic copability. – Moscow: Radio I Sviaz, 1983. 272 p. [in Russian].
13. E. B. Dybdal, and Y. E. King, Performance of reflector antennas with absorber-lined tunnels. // Int. Symp. Dig.: Antennas and Propag.,1979, Vol. 2. 714-717.
14. N. P. Krasnenko, and A. G. Root, The protected parabolic antannas account of acoustic locators. // Dig. of 9th Symp. in lazer and acoustic sounding of the atmosphere. USSR, Tomsk, 1987. 225–229. [in Russian].
15. O. N. Steand, Numerical study of the gain pattern of a shielded acoustic antenna // IASA, 1971, Vol 49, No 6.
16. F. F. Hall Jr and J. W. Wescott, Acoustic antennas for atmospheric echo sounding. // J. Acoustic Soc. Am., 1974, Vol. 56, No 5. P.1376-1382.
17. IEEE Trans., 1985, Vol. AP-33. P.685-689.
18. The screens and SHF devices disign. Edited by A. M. Tshernushenko. – Moscow: Radio i sviaz, 1990. 351 p. [in Russian].

OPTIMIZATION OF THE POLYHEDRAL VEHICLE ANTENNA ARRAY CHARACTERISTICS

V. A. Voloshina, V. V. Shatskiy

Rostov Military Institute of a Missile Corps, Rostovs-on-Don, 344027, Russia

The optimization principle of polyhedral array radiator number and geometrical sizes of pyramid at a given gain on a scan sector boundary are considered in [1, 2]. This gain loss estimation is approximated because the diffraction effects on the object – carrier and mutual coupling of radiators are not taken into account [3]. Besides, the results [2] concern to the object-carrier as a regular truncated pyramid.

In the report the polyhedral antenna array (Fig. 1, a) is considered. It comprises a main subarray on an upper side (roof of the mobile object) and one or several additional subarray located on inclined sides. The following problems are considered:

- the main moments of the electrodynamics analysis of polyhedral antenna array, encompassing by to mathematical model development and realization of computing experiment are represented;
- the problems of the radiator matching are considered at wide-angle scanning (as radiators the symmetrical dipoles are selected);
- the array scattering characteristics are evaluated.

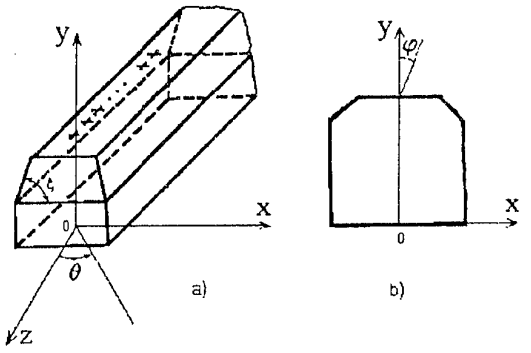


Fig. 1

In mathematical model of the dipole array the object-carrier is approximated by convex polyhedron. The solution is obtained by an auxiliary sources method. The numerical research results [3, 4] for a dipole array located on one of side walls of the mobile object-carrier are presented. For simplification of solution the two-dimensional model (Fig. 1, b) is used. It is accepted, that the identical dipoles of antenna array are rather thin cylindrical, surface of the object-carrier is perfectly conducting. The ground is the homogeneous dielectric medium. The linear dipole array with step $x0$ and dipole number N is located on upper and side walls of object-carrier. The object is represented by the cylinder of a trapezoidal cross-section. Each of dipoles has length $2l$ and is placed at the altitude h above the screen. The dipoles identical to substantial dipoles are utilised as auxiliary sources.

The system of the linear algebraic equations for definition of complex amplitudes of dipole currents, as well as in [5], is represented in a matrix form

$$|Z||I\rangle = |U\rangle \qquad (1)$$

where [Z] is a square matrix, whose elements are mutual coupling coefficients between harmonics of dipole currents; $|I\rangle$ is matrix-column composed from complex amplitudes of the dipole current harmonics; $|U\rangle$ is a matrix-column composed from voltages of exciting sources. The coefficient of [Z]- matrix (mutual coupling resistance) between m-th and m' -th current harmonics of dipoles with numbers n and n', is defined as

$$Z_{n,n'}^{m,m'} = \int_{-l}^{l}\int_{-l}^{l} E_{n,n'}^{e_3}\psi_{m'}(x')dx'\psi_m(x)dx, \qquad (2)$$

$\psi_m(x)$ is the current harmonics with number 1, 2, 3:

$$\psi_1(x) = \cos\frac{\pi x}{2l};\ \psi_2(x) = 1 - \sin\frac{\pi|x|}{2l};\ \psi_3(x) = \sin\frac{\pi x}{l};$$

$E_{n,n'}^{e_3}$ is the field strength of an auxiliary source;

$$E_{n,n'}^{e_3} = \frac{1}{i4\pi\omega\varepsilon_0}\left[k^2 + \left(\frac{d}{dx}\right)^2\right]\left[G_{n,n'} + \sum_{\nu=1}^{N_\nu} D_\nu^{n'} G_{n\nu}\right] \qquad (3)$$

$$G_{n,n'} = \frac{\exp(-ikr_{nn'})}{r_{nn'}} + k_s\frac{\exp(-ik\rho_{nn'})}{\rho_{nn'}}, \qquad (4)$$

$$G_{n\nu} = \frac{\exp(-ikr_{n\nu})}{r_{n\nu}} + k_s\frac{\exp(-ik\rho_{n\nu})}{\rho_{n\nu}}, \qquad (5)$$

k_s is a coefficient (Fresnel's) of reflection of a normally polarized plane wave, whose angle of incidence is β_0; $k = 2\pi/\lambda$, λ is a wave length; $r_{nn'}(\rho_{nn'})$ and $r_{n\nu}(\rho_{n\nu})$ are distances between the auxiliary dipole (its mirror image) located on n' -th dipole and actual (mirror image) dipole with number n, or actual (mirror image) auxiliary dipole with number ν, accordingly; $\dot{D}_\nu^{n'}$ is a complex amplitude of an auxiliary source with number ν.

The field-strength pattern of the dipole array is defined by expression

$$F_x(p) = \sum_{n=1}^{N_\Sigma}\sum_{m=1}^{M} I_n^m \{[\exp(ikz_n\cos\theta) + k_s\exp(-ikz_n\cos\theta)]\times \exp[ik\sin\theta(x_{0n}\cos\varphi + y_n\sin\varphi) + \sum_{\nu=1}^{N_\nu} D_\nu^{n'}[\exp(ikz_\nu\cos\theta) + k_s\exp(-ikz_\nu\cos\theta)]\times \exp[ik\sin\theta(x_\nu\cos\varphi + y_\nu\sin\varphi)]\}\times \int_{-l}^{l}\exp(ikx\sin\theta\cos\varphi)\psi_m(x)dx, \quad (6)$$

where $x_n, y_n, z_n; x_\nu, y_\nu, z_\nu$ are coordinate of center n-th dipole (ν-th auxiliary source).

Some calculating results for the dipole array with number of dipoles $N_\Sigma = 12 + N_l$ (N_l is a number of dipoles on a side wall) are shown in Fig. 2. The dotted curve corresponds to $N_\Sigma = 12$, curve 1 to $N_\Sigma = 14$, curve 2 to $N_\Sigma = 16$, curve 3 to $N_\Sigma = 18$ for the directivity D, the pattern width $2\theta_{0.5}$, the efficiency η and the gain G. Step between dipoles is selected $x_0 = 0.55\lambda$, length l of the dipole arm and altitude h are chosen 0.25λ, a maximum angle of scan sector $\theta_0 = 70^0$.

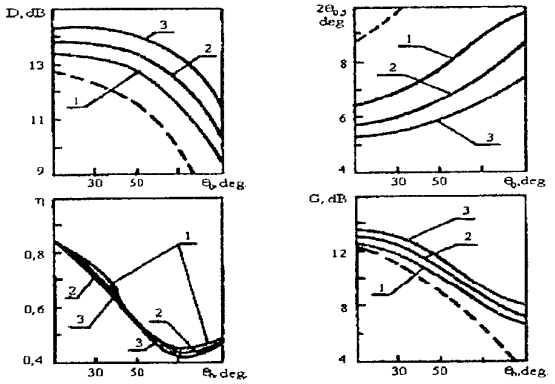


Fig. 2

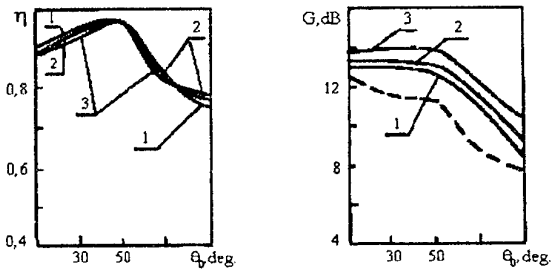


Fig. 3

The possibility of the dipole matching for a definite position $\theta_0 = \theta_{0c}$ of a pattern maximum is considered. The latter is produced with the help of matching devices, each of which includes the transformer and reactance. In Fig. 3 the dependencies for efficiency and gain of matched array ($\theta_{0c} = 50^0$) are shown. The denotation of curves corresponds to used in Fig. 2.

The evaluation technique for estimation of scattering characteristics polyhedral antenna array is considered in the report.

REFERENCES

1. Antennas and devices of a very high frequency (designing of antenna arrays) / Pod redaktsiei D.I. Voskresenskogo. - Moscow: radio i svyaz', 1981, 432 p. [in Russian].
2. Voloshin V. A., Shatskiy V. V. Calculation of pyramid-shaped antenna arrays // Voprosy radioelektroniki. Ser. "Obstshetekhicheskaya", 1976, vyp. 4, p.77-81 [in Russian].
3. Gabriel'yan D. D., Tarasenko O. M., Shatskiy V. V., Sevast'yanov Yu. V. Influence of the mobile object on the radiation pattern of the antenna system // Tekhnika sredstv svyazi. Ser. "Tekhnika radiosvyazi". -1989. -Vyp. 7.-pp. 112-119 [in Russian].
4. Voloshina V. A., Gabriel'yan D. D.. The influence of perfectly conducting surface on radiation of the dipole // Radiotekhika, 1998, v. 37, n. 3, pp. 29-31 [in Russian].
5. Gostyukhin V.L., Grineva K. I., Trusov V.N. Problems of designing of the phased arrays with use of a computer / Pod redaktsiei V. L. Gostyukhina. – Moscow: radio i svyaz', 1983.-248 p. [in Russian].

ELECTRODYNAMIC PARAMETERS OF NARROW SLOTS IN A RECTANGULAR WAVEGUIDE FILLED WITH THREE-LAYERED DIELECTRIC. THEORY AND EXPERIMENT

L. P. Yatsuk, A. F. Lyakhovsky, A. A. Lyakhovsky

Kharkov State University, 310077, Svoboda sq. 4,
E-mail: Ludmila.P.Yatsuk@univer.kharkov.ua

INTRODUCTION

Narrow slots in a waveguide surface are widely used in X-band techniques as coupling elements or radiators. The filling of waveguides with dielectric is utilised in order to miniaturise devices or slow down waveguide waves. The layered filling gives some additional opportunities to control output system parameters. Those are scattering matrix elements of a slot in a waveguide filled with layered dielectric. In order to obtain them it is necessary to solve an excitation problem for such a waveguide when a source is a magnetic current equivalent to the electric field in a slot. The main difficulty of solving this problem is due to the fact that in the description of magnetic current density the Dirac delta-function is present. The most traditional methods of solving this problem (the eigen waves method or Green's function one for the field) lead to the expressions for the H-field in the source region containing the series and the additional divergent term where the current density is present in an explicit form. As consequence of this a series which must compensate divergence of this additional term is also divergent. As a result the solution obtained in a such form is not suitable for calculations. This situation occurs in the following cases. Firstly, when we use the eigen-waves method for finding the field excited by a longitudinal slot. Secondly, when the direction used as a longitudinal one in the process of the Green's function construction is parallel to the magnetic current of interest. So for the narrow transverse slots we can use the eigen waves method without any difficulties. But in the case of longitudinal slots it is necessary to construct the Green's function using the direction perpendicular to the line of the magnetic current as a longitudinal one. For longitudinal slots this direction is perpendicular to the boundaries of adjacent dielectric layers. Such Green's functions were built in [1] and in B. A. Panchenko's works. This way specifies a representation of z-dependence of the field in the Fourier integral form. The same representation was used in [2] in the process of direct solving the Maxwell equations for obtaining an admittance of a longitudinal slot. The both above mentioned ways lead to very tedious computation formulas. The numerical results for a longitudinal slot in a waveguide with dielectric slab are given only in [3]. Another way of solving this problem, proposed in [4], permits to obtain more compact solution. The main idea of this method is expanding the magnetic current density over a set of potential vector functions and afterwards uniting this series with ones over LE- and LM-waves. The validity of this way is caused by the fact that the current density term in the solution has solely potential nature [5]. We call this way as a modified eigen waves (MEW) method.

The numerical results for the transverse slots, obtained with the eigen waves method, were described in [6]. In this paper we represent the numerical results obtained with the MEW-method for longitudinal slots and experimental results for both types of slots.

MAIN PART

The slots under consideration are cut in a broad wall of a rectangular waveguide 23×10 mm filled with the 3-layered dielectric. The layers are supposed to be parallel to the narrow or to broad walls of the waveguide. Their width are a_1, a_2, a_3 in the first case and b_1, b_2, b_3 — in the second one. Permittivities of the layers ε have the similar subscripts. When a dielectric slab is inserted into an empty waveguide it is convenient to use one of these subscripts for describing the width of the slab and its position (1-for the left or upper position). It was supposed that the slot of interest was cut on the left in the upper broad wall of the waveguide. Numerical and experimental investigations were performed for a case of a dielectric slab in a waveguide. Scattering elements were analysed in the one-mode regime for various permittivities of the slab, its dimensions and position in a waveguide. Usually waveguides are filled with dielectric in order to slow down a wave inside them. In antenna applications it is necessary to lessen the distances between adjacent equiphased resonance slots. Consequently, it is necessary to obtain resonance at the frequencies where the wavelength in a waveguide is less than one in an open space. So, we were interested how the presence of dielectric in a waveguide shifts resonance frequency of a slot and varies the level of radiation coefficient at this frequency. The most sufficient experimental and numerical regularities of slot scattering parameters behaviour are as follows.

In general presence of dielectric shifts the resonance frequency towards more long wavelengths. When a

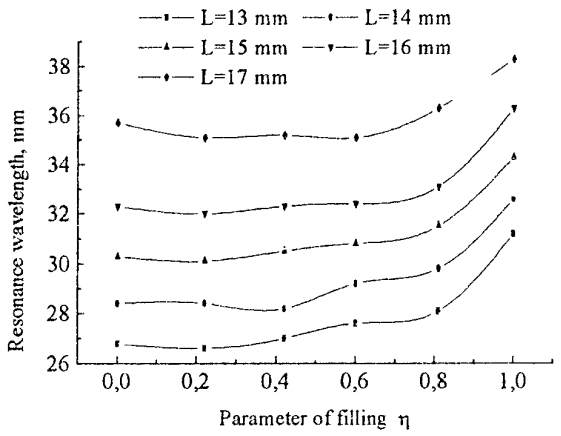


Fig. 1

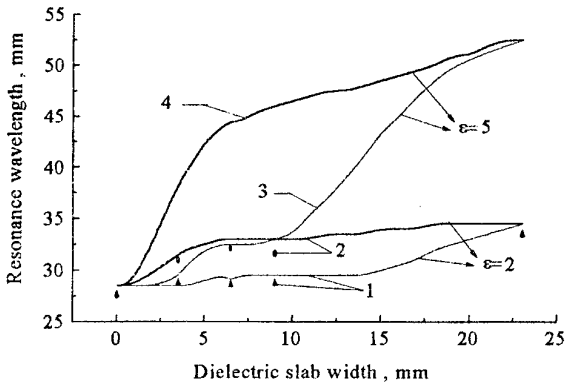


Fig. 2

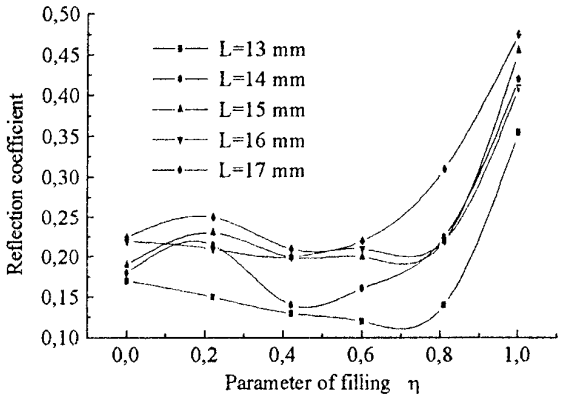


Fig. 3

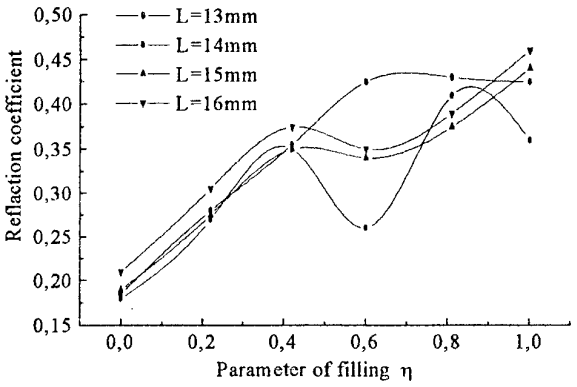


Fig. 4

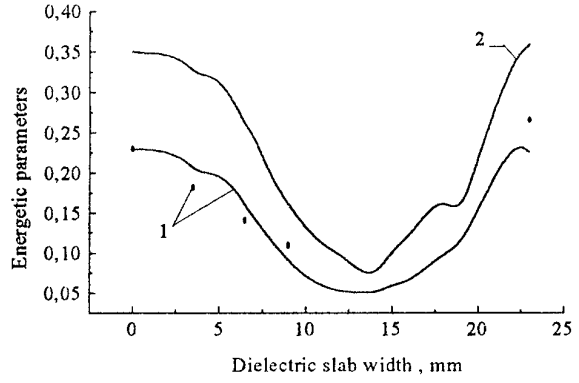


Fig. 5

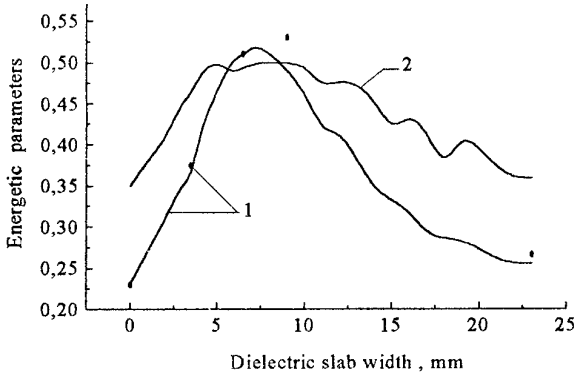


Fig. 6

dielectric slab is situated under a slot this shift is more rapid and less regular then in the case when it is displaced from the slot. The matching of a slot with a feeder line is better in the later case.

These regularities were confirmed by the experimental data for a transverse slot in a waveguide with dielectric slab parallel to both broad and narrow walls. Let us introduce a parameter $\eta = b_i/b$ or $\eta = a_i/a$ for slabs parallel to broad and narrow walls correspondingly. Subscript i is even to 1 when the slab is under the slot and $i = 3$ when it is displaced from the slot to the opposite wall. It is seen from Fig. 1 that in the case

$\eta = b_3/b$ resonance wavelength varies very slowly in the limits $0 \le \eta \le 0.6$ of this parameter and the reflection coefficient is practically the same as one in an empty waveguide (even less for short slots, see Fig. 3). When the slab is under the wall where the slot is cut the power reflection coefficient rises with the parameter $\eta = b_1/b$ within these limits rapidly enough (in average from 1.5 to 2 times, see Fig. 4), besides resonance frequency behaves unsteadily. These experimental data were obtained for $\varepsilon = 2$.

It must be noted, that the retarding of the dominant wave practically does not depend on the position of the slab parallel to broad walls. So it is preferable to displace the slab from the slot. The experimental results similar to ones in the Fig. 1, 3, 4 were obtained for longitudinal slots in both cases of the slab position, parallel to broad and narrow walls of a waveguide. In the case of a transverse slot in a waveguide with a centrally positioned slab parallel to narrow walls (most applicable position for obtaining effective slowing down) power reflection coefficient rises with η rapidly (approximately two times in limits $0 \le \eta \le 0.4$). Because of that such geometry is undesirable.

Numerical calculations have been performed for longitudinal slots using MEW-method under assumptions that the electric field along a slot is described with a half wave of sinusoid and is constant across the slot. Calculations were performed using two values of slab permittivity $\varepsilon = 2$ and $\varepsilon = 5$, slot length (L) and width (d): L = 13.7 mm, d = 1.5 mm, slot centre displacement from the narrow wall $x_0 = 2.5$ mm. (the slot length was chosen because the rectangular slot of length L = 13.7 mm has practically the same resonance frequency as the slot of length L = 14 mm with rounded ends, used in experiments). Dielectric slab was supposed to be parallel to narrow walls. The main numerical results are in a good agreement with experimental data and with data given in [3]. These results are as follows.

When permittivities of all dielectric layers are supposed to be $\varepsilon = 1$ (an empty waveguide) the data calculated coincide fully with experimental ones. Dielectric slab positioned under a slot shifts a resonance wavelength much more effectively than when a slab is displaced from the slot (see Fig. 2, curves 2,4 - for a slab under a slot and 1, 3 ones — for a slab displaced from it, the round and triangular black points are experimental data). These results are qualitatively the same as in the case of dielectric slab parallel to broad walls. We can see a good enough agreement between the numerical data and experimental ones. Very interesting behaviour of reflection and radiation coefficients depending on a slab width was observed. Results presented in Fig. 5 correspond to the position of dielectric slab, displaced from the slot, in Fig 6 — to a slab under the slot. The black points in the figures represent experimental data. The curves 1 in these figures represent reflection coefficient, curves 2 — radiation one. The numerical results concerning the reflection coefficient are in a good agreement with experimental data. As to the radiation coefficient there were observed some discrepancies between numerical and experimental results. The value of radiation coefficient $S2$ calculated exceeds the level 0.5 for a_1 = 6.5 mm and for the full waveguide filling with dielectric. These results could not be obtained under assumption of symmetric E-field distribution in the slot accepted in our theory. Thus we have come to the conclusion that the field distribution is not symmetrical in the presence of dielectric under the slot, therefore it is necessary to use more precise one. In [3] 30 spatial harmonics were used for description of E-field distribution in the slot. On our opinion it is too much. But it is obvious that one harmonic is not enough for description of the E-field in longitudinal slot when dielectric is under it.

CONCLUSION

Analysing the results obtained we come to the conclusion that MEW-method provides the results which are in a good agreement with experimental data. It is only necessary to use greater number of space harmonics for description of the E-field in a longitudinal slot. For the antenna applications it is better to use slots displaced from a dielectric slab.

ACKNOWLEDGEMENT

The authors are grateful to D. I. Ivanchenko for experimental studies fulfilled.

REFERENCES

1. Felsen L.B., Marcuvitz N. Radiation and Scattering of Waves, Prentice-Hall, Inc., Englewood Cliffs, New Jersey, 1973, v.1, 547 p.
2. Yatsuk L.P. Internal Admittances of longitudinal slots in a waveguide with layered magneto-dielectric // Radiotekhnika. All Ukr. Sci.Interdep.Mag.1997. N 101. P. 109-121 [in Russian].
3. Joubert J., McNamara D.A. Longitudinal slots in broad wall of rectangular waveguide inhomogeneously loaded with dielectric slab // Electronics Letters, August 1991, vol.27, N 16. P. 1480-1482.
4. Yatsuk L.P. Modified eigen waves method and Green's function method in the excitation problem of a waveguide with dielectric by magnetic current// Proceedings of 7 International Crimean conference "Superhigh technique and telecommunication technologies". Sevastopol. 1997. V2. p.573-575 [in Russian].
5. Collin R.E. On the incompleteness of E- and H-modes in waveguides // Canadian Journal of Physics. 1973.V.51. P. 1135-1140.
6. Yatsuk L.P. Physical properties of transverse slots in a rectangular waveguide filled with layered dielectric //Radiotekhnika. All Ukr. Sci. Interdep. Mag. 1997. N 104. P. 12-20 [in Russian].

ABOUT PLANE SCREEN SPIRALS NEAR FIELDS INFLUENCE ON RADIATION AND SCATTERING CHARACTERISTICS

K. P. Yatzuk, R. R. Shvelidze

Kharkov State University, 310077, Kharkov, sq. Svobody, 4
tel. (0572) 45-71-33, e-mail: Ludmila.P.Yatsuk@univer.kharkov.ua

ABSTRACT

Two problems of circular waveguide E_{01}-wave scattering on spiral obstacles were solved. One is for an obstacle in a form of spiral with substrate on a boundary of two semi-infinite dielectric media, another is for a spiral with metallic screen. It was shown that an existence of thin layer near a spiral caused a decreasing of reflectivity in both cases.

INTRODUCTION

Antennas constructed on the plane spirals base are frequency independent. When it is necessary to take unidirectional radiation a plane screen is arranged parallel to spiral. The spiral-screen distances a establish a radiation power. It is maximal if $a \approx \lambda / 4$, where λ is the working passband middle wavelength, and it is minimal if $a \to 0$. The frequency band decreases to one octave, but radiation field circular polarization preserves. It was shown in [1] that if two spirals with opposite spiral parameters $\pm u$ are used and distances between spirals b and screen a are small ($b \approx a \approx \lambda / 10$) than the radiation power increases. It's value achieves the same level as in the case of one spiral and screen with $a = \lambda / 4$. The problem solution in [1] was carried out by integral transformation method for non-symmetric wave with azimuth dependence $\sim e^{in\varphi}$, where $n = 1$. But a reason of such radiation power growing was not considered.

The aim of the present paper is to investigate the influence of thin layer near the spiral on E_{01}-wave scattering in circular waveguide on spiral obstacle.

PROBLEM SOLUTION

There are two problems to observe: 1) E_{01}-wave scattering on spiral in three layered dielectrics one of which is thin spiral substrate, and 2) E_{01}-wave scattering on spiral with metallic screen arranged on a small distance from spiral. In the first case the problem is solved in two wave approximation for incident E_{01}-, scattered E_{01}- and excited on spiral H_{01}-waves. The influence of symmetric surface wave excited on spiral on reflectivity is investigated in the second case.

Problem 1. There is infinite circular waveguide in which a plane logarithmic spiral with substrate is located in the plane $z = 0$ of cylindrical coordinates ρ, φ, z. The spiral described by the curve $\rho = \rho_0 \exp(\varphi / u)$, where ρ_0 is the starting spiral radius, $u = \operatorname{ctg}\psi$ is spiral parameter, ψ is the twirl angle of the spiral. The mode matching method have been used. There are three regions: I – $-\infty < z < -l$, $\varepsilon = \varepsilon_1$; II – $-l < z < 0$, $\varepsilon = \varepsilon_2$; III – $0 < z < \infty$, $\varepsilon = \varepsilon_3$. From $-\infty$ the incident E_{01}-wave with unit amplitude falls on the I – II regions boundary. Here it is scattering for the first time. Then it is scattering on spiral (boundary of the I – III regions). H_{01} is excited on the spiral. As spiral substrate is thin, H_{01}-wave penetrate in the first region also. So the fields in I, II, III regions are expressed by electric and magnetic Hertz vectors and they may be described by 8 unknown coefficients as the results.

The boundary conditions are formulated as conjugate conditions on two dielectrics boundary and as anisotropic sheet model form on spiral. The unknown coefficients are defined from 8 algebraic equations.

Results 1. The calculations for waveguide of radius 1.5 cm, various spiral parameters u, substrate thicknesses l and permittivities $\varepsilon_1, \varepsilon_2, \varepsilon_3$ in 2 – 3.5 cm wavelength were carry out.

The calculations showed that in the case of single spiral without dielectrics reflectivity (R) rushed to 0 for $u \geq 10$, and to 1 for $u \approx 1$.

The case of two dielectric regions ($\varepsilon_1 = \varepsilon_2 = 1$, $\varepsilon_3 \neq 1$) with spiral without substrate on dielectrics boundary is presented in Fig. 1. Solid lines are for $u = 10$, $\varepsilon_1 = \varepsilon_2 = 1$, ε_3 – var, the curves 1, 2, 3 are for $\varepsilon_3 = 2$, 10, 50, respectively. It is seen that growing of permittivity ε_3 causes the increase of R.

Another picture can be seen when substrate exists. In Fig. 1 the dashed lines for $u = 10$, $l = 1$ mm; curves 1, 2, 3 are for $\varepsilon_1 = 1$, $\varepsilon_2 = \varepsilon_3 = \varepsilon_\Sigma$ equal to 2, 10, 50, respectively. From Fig. 1 one can see, that for small ε_Σ the existence of thin layer besides spiral causes a some decrease of R in all frequency band. In the case of large ε_Σ the existence of thin substrate causes the more decreasing of R, but in the smaller frequency band. Curve 4 corresponds to $\varepsilon_1 = 1, \varepsilon_2 = 5, \varepsilon_3 = 50$. We see that in this case R becomes smaller then in the case of substrate absent.

Fig. 2 shows the dependencies of R versus λ for the same parameters as in Fig. 1, but for bigger substrate thickness ($l = 2$ mm). Curves 1, 2, 3 are for $\varepsilon_\Sigma = 2, 10, 50$, curve 4 is for $\varepsilon_\Sigma = 20$. It is seen that decreasing of R is observed for small ε_Σ in same frequency band. For $\varepsilon_\Sigma = 2$ and 10 R < 0.3 exists in 40% frequency band, but for $\varepsilon_\Sigma = 20$ this regime is remarked in 20% frequency band only. For $\varepsilon_\Sigma = 50$ (curve 3) in mentioned frequency band the region with small R does not exist. For thick layers or large $\varepsilon_\Sigma > 50$ the standing wave regime is observed.

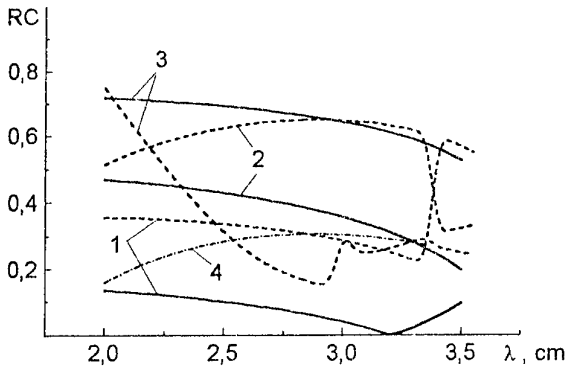


Fig. 1

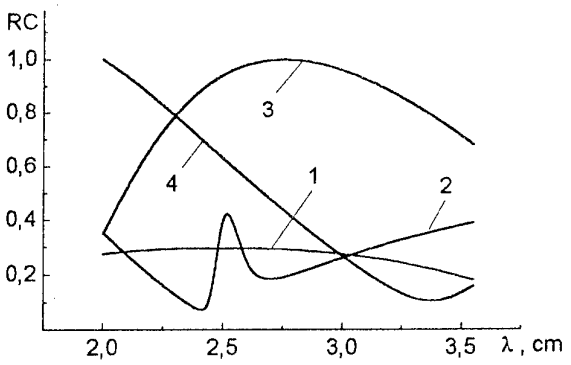


Fig. 2

Problem 2. In this case we have the obstacle in a plane spiral with screen form. We picked out two regions: I – $-\infty < z < 0$, II – $0 < z < d$. The spiral is arranged in plane $z = 0$, screen is located in $z = d$. The permittivities are equal to 1 in both regions. Incident form $-\infty$ E_{01}-wave scattering on spiral and existing the symmetric surface wave on it. The problem solution is carried out in two wave approximation: E_{01}-wave and symmetric surface wave. The boundary conditions are taken in approximation of anisotropic sheet model on spiral and in common form on the screen.

Results 2. The calculations showed that small R are observed then the distances between spiral and screen are also small ($d \le \lambda / 10$). On the Fig. 3 the curves 1, 2, 3, 4, correspond to $d = 1$, 2, 3, 5 mm, respectively. It is seen that for $d = 1$ or 2 mm the near field in form of surface wave also is gating R smaller. For $d \ge 5$ mm the standing waves in region spiral screen have been observed.

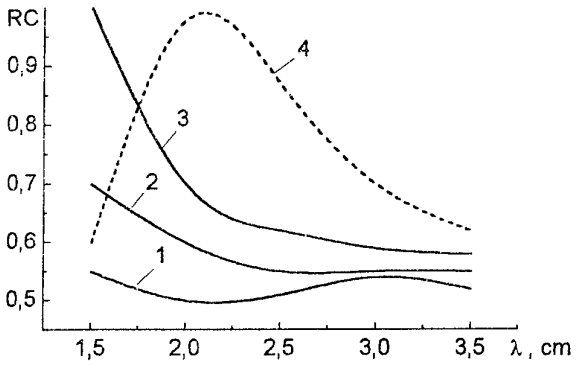


Fig. 3

The theoretical data have been confirmed by experimental results in both cases.

CONCLUSION

The thin layer near the spiral investigations shows its significant influence on the reflectivity. This effect may be explained by two facts: 1) the same waves re-reflection in layer and 2) surface wave excitement in it.

These result may be used in hyperthermia investigations and under working out of nonreflection surfaces.

REFERENCE

1. K. P. Yatzuk, V. P. Krivokhiga, O. F. Selenina. Calculation and experimental investigation of coupled logarithmic spiral with screen radiation characteristics. Radioelectronika, 1968, v.21, № 8, p. 3 – 8, (Izv. vissh. uchebn. zaved.) [in Russian].

INFLUENCE OF DIFFRACTION EFFECTS ON DIRECTIVITY OF THE CORNER ANTENNA OF ARBITRARY APEX ANGLE

N. P. Yeliseyeva

Kharkiv State University,
4 Svoboda Sq., Kharkiv, p.o.310077, Ukraine
Phone:0572+45-71-75; Fax: 0572+47-18-16; e-mail: Nadezhda.P.Yeliseyeva@ univer. kharkov.ua

INTRODUCTION

The corner antenna, being widely used in practice in the UHF band, is the classical model for illustrating the influence of the electromagnetic waves diffraction on the reflector edges on the directivity D of the radiating system. The experimental measurements of the directivity of finite — size corner-reflector antenna have been carried out by the authors [1] for numerical combinations of the width L and height W of the reflector under varying each from 0.4λ to 5λ. These measurements were made with a half-wave dipole, oriented parallel to the interior edge of the corner, for the first three optimal positions, providing the maximum directivity $D_{\max}$, when changing the dipole distance from the reflector apex s from 0.07λ to 2.5λ. The aperture angle β was adjustable from 20° to 180° to maximize the directivity. Using the uniform geometrical theory of diffraction a solution for the three-dimensional radiation problem in the far field zone of a finite - size corner antenna with an arbitrary aperture angle, excited by an arbitrary oriented electric dipole, has been obtained in [2]. Efficient algorithms and computer codes for calculating the directivity of the corner antenna have been worked out on its basis to conduct more delicate and full, then in the experiment, investigation of the optimal dipole positions in dependence on reflector dimensions at different aperture angles, to study the possibility to maximize the directivity by means of choosing optimal combination of the reflector dimensions , orientation and dipole position under fixed angle aperture. Such an analysis, conducted in [3] for the plane screen ($\beta = 180°$), determined the first maximum value $D_{max} = 8.61$, when dipole was oriented parallel to the square screen with $L_{opt} = 1.2\lambda$ at a distance $S_{opt} = 0.1\lambda$ from it. Just as the first D_{max} in the case of infinite plane screen is $D_\infty = 7{,}07$. The second maximum was achieved at $S_{opt} = 0.75\lambda$ being equal $D_{max} = 9$ ($D_\infty = 6$) under $L_{opt} = 1.5\lambda$ and in the case of the third maximum $D_{max} = 9.2$ ($D_\infty = 6$) at $S_{opt} = 1.25\lambda$, $L_{opt} = 2\lambda$. The calculated S_{opt} coincided with the experiment [1]. The purpose of the present paper is to determine the optimal combination of the reflector dimensions and dipole position providing the maximum directivity with the calculation of the diffraction effects on the reflector edges at an arbitrary angle aperture.

PROBLEM FORMULATION AND ANALYSIS OF NUMERICAL RESULTS

Consider a corner antenna consisting of two infinitely thin perfectly conducting plates with the width L and the height W, intersecting at an arbitrary angle β. A half-wave vibrator, used as the excitation source, is located in the bisector of the corner plane at the distance s from the interior edge in parallel to the latter (vertical vibrator) or perpendicular to it (horizontal vibrator). The no-loss power directivity of this antenna there have been calculated using the expression

$$D = 4\pi P_\Sigma(0,0)/ P_\Sigma,$$

where $P_\Sigma(0,0)$ is the power, radiated in the forward direction from the antenna, P_Σ is the total power radiated over the surface of the observation sphere. The developed programs allow to combine the study of the size of reflector with the value of aperture angle, required to maximize the directivity.

First of all, analyze the effect of the aperture angle on the value $D_{\max}$ and the vibrator position, providing it, under constant reflector dimensions. Fig.1a, b shows the dependencies D on the vibrator distance s, calculated by the mirror image method, which assumes infinite dimensions of the faces, for the corner antenna having values of aperture angle, obtained by dividing 180 degrees by an integer. The directivity improves as the vibrator is brought very close to the apex; however, the radiation resistance becomes quite low and the losses reduce the directivity. If the position of the vibrator is displaced from the optimum in the direction away from the apex, the directivity is reduced. The second and higher order maxima D correspond to points at which the direct radiation and reflected radiation add inphase in the forward direction. As seen the values $D_{\max}$ are greater in the second and higher order optimal positions.

For finite-size corner antenna, by analogy with the experiment [1], the various optimal vibrator positions S_{opt} and the changes in the values $D_{\max}$ with continuous variation of aperture angle β from 30° to 150° when s varied from 0.1λ to 1.1λ have been calculated. The calculated S_{opt} coincided with the experiment [1]. In the case of excitation by the vertical vibrator (Fig.1c) the dependence of the optimal values S_{opt} is a continuous function of the angle β. The distance S_{opt} increases as

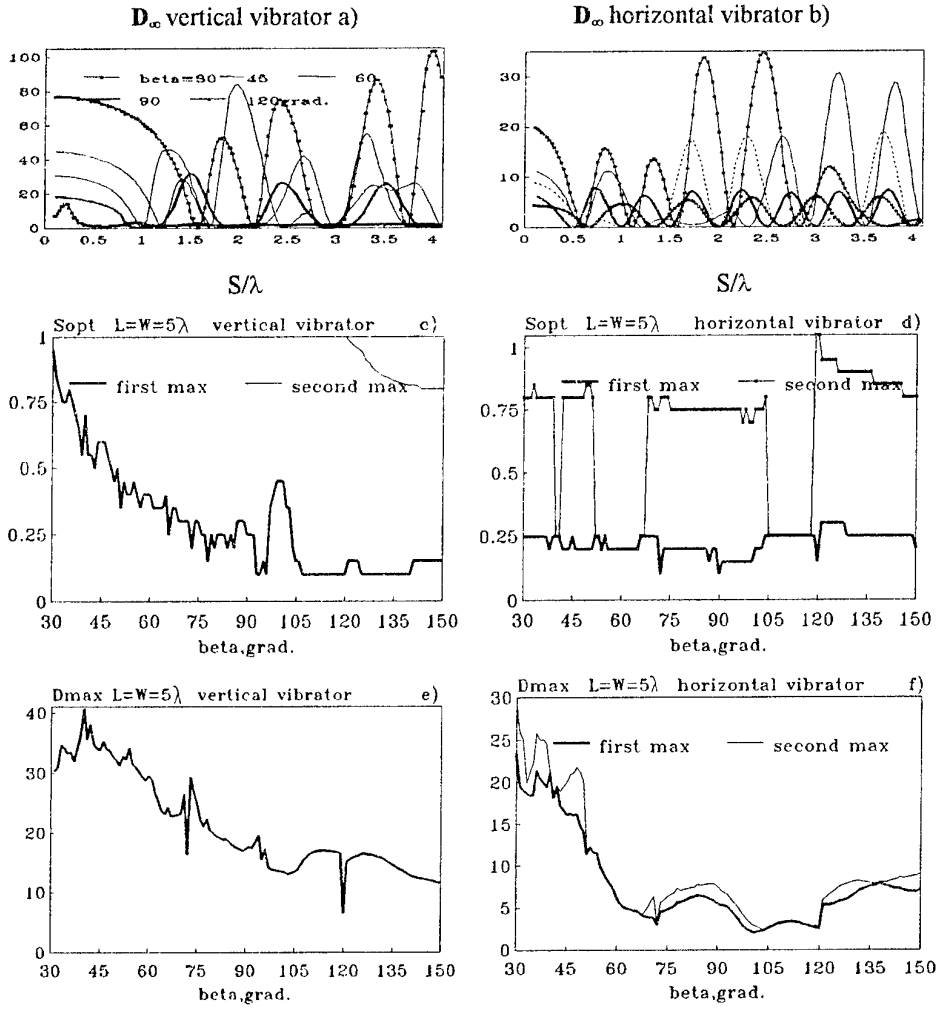


Fig. 1. The optimal vibrator positions S_{opt} and corresponding values D_{max} as the functions of the aperture angle β

the aperture angle is made smaller. The second maxima of D in given interval of changing s are only for β = 120°...150°. In the case of excitation by the horizontal vibrator (Fig. 1d) the first optimal positions practically coincide under all apex angle at S_{opt} = 0.25λ. The second maximum of D is near S_{opt} = 0.75λ at β =30°...55° and 65°...105°, at β > 120° S_{opt} is equaled 1.02λ...0.75λ. The values D_{max} increase as the angle β is made smaller from 9 at β = 180° to 30.4 at β = 30° in the case of vertical vibrator, and from 9 to 25 for horizontal vibrator (Fig. 1e, f). From the comparison the first D_{max} for a corner with $L = W$ = 5λ (Fig. 1c) and an infinite corner (Fig. 1a) for different angles β we obtain: for β = 30° D_{max} = 30.4 and D_∞ = 65 at S_{opt} = 0.95λ; for β = 45° D_{max} = 34 and D_∞ = 39 at S_{opt} = 0.6λ; for β = 60° D_{max} = 29.57 and D_∞ = 28 at S_{opt} = 0.4λ; for β = 90° D_{max}= 17.24 and D_∞ = 17.62 at S_{opt} = 0.25λ. So the diffraction effects on the corner edges reduce the directivity in forward direction at small angles β even at large corner sizes at W/L = 1.

Then, let us consider the effect of reflector dimensions on the value D_{max}. The calculated directivities in the case of excitation by vertical vibrator realizable with a corner antenna having various combination of width and height are presented in Fig. 2 in the form of contours of constant D in the system coordinates L and W/L. In the case β = 30° (Fig. 2a) the directivities change from 5 to 70. The behavior of dependence D on W/L at different fixed L is various. When changing W/L from 0.1 to 0.5 the directivities reduce from 20 to 10 at L = 2λ and from 69 to 36 at L = 6λ. Under changing W/L from 0.5 to 2 the values D increase from 10 to 15 at L = 2λ and from 36 to 42 at L = 6λ. In the case β = 45° the isolines are presented for s = 0.6λ and s = 0.9λ (Fig. 2c, d). The values D change from 12 to 42. For L = 3λ at s = 0.6λ the values D reduce from 26 to 24 when W/L are small; when W/L > 0.75 ones increase from 20 to 26. At s = 0.9λ for L = 3λ the values D practically don't depend from the height W and for L =

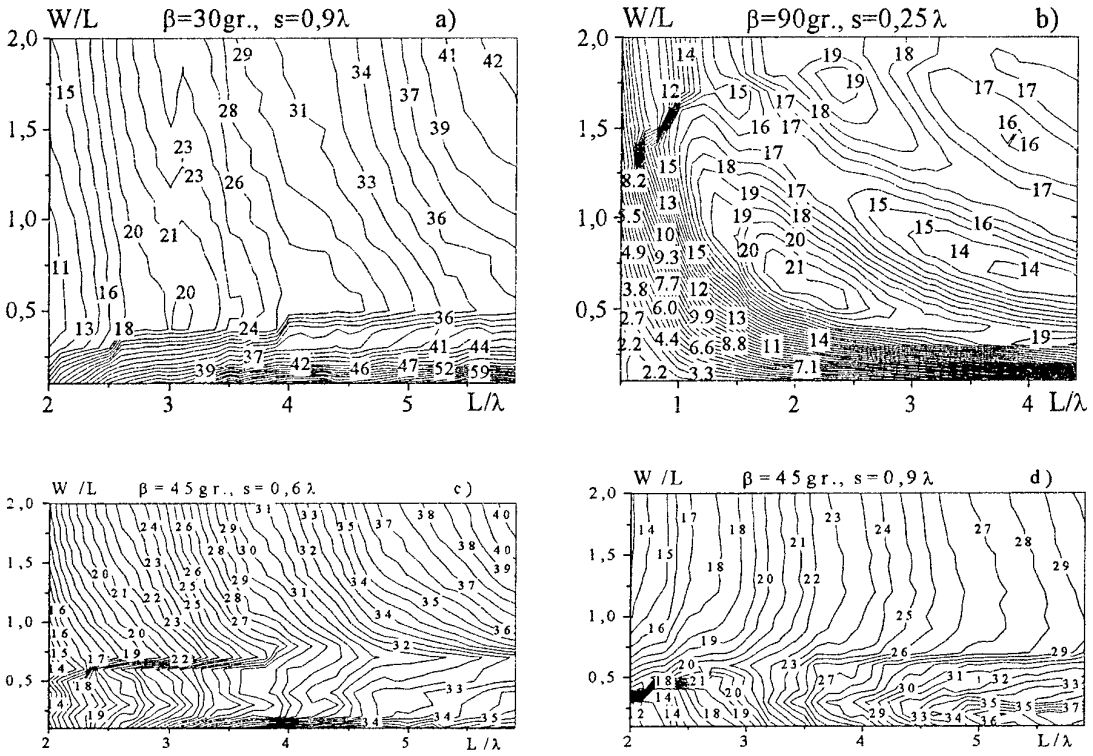


Fig. 2. The contours of constant directivity D with vibrator in first position for various reflector sizes

6λ ones reduce from 39 to 30 when W/L = 0.1...0.75 and being constant then. In the case β = 90° (Fig. 2b) the values change from 0 to 21.7. The extreme value D_{max} = 21 is at L_{opt} = 1.9λ and $(W/L)_{opt}$ = 0.7 (D_{∞} = 17). The changes in D prove, that the field, diffracted at the corner edges are essential in the forward direction to antenna in the fixed interval of side length ratio, which is depended from the β, L, s.

CONCLUSIONS

The diffraction of the electromagnetic waves on the corner edges leads to essential dependence of the directivity of the corner antenna on the height under fixed width and the vibrator distance in the defined interval of the side lengths ratio. It allows to maximize the directivity for each apex angle of the corner antenna by choosing the optimal combination of the reflector dimensions.

REFERENCES

1. Cottony H.V., Wilson A.C. IRE Trans. on Antennas and Propagation, 1958, AP-6, pp.366-369.
2. Gorobets N.N., Yeliseyeva N.P. Journal of Communication Technology and Electronics, V38, N6, 1993, pp. 99-107.
3. Gorobets N.N., Yeliseyeva N.P. Proc. of the VI Int. Conf. on Mathematical Methods in Electromagnetic Theory, Lviv, 1996, pp.513-516.

A MULTIBEAM HYBRID PRINTED ANTENNA BASED ON A STRIP PERIODIC STRUCTURE

A. P. Yevdokimov, V. V. Krizhanovsky, P. N. Melezhik, and A. Ye. Poedinchuk

A. Ya. Usikov's Institute of Radiophysics and Electronics NASU
Ul. Proskury 12, Kharkov 310085 Ukraine,
Ph.: 38 (0572) 44 83 26, fax 38 (0572) 44 11 05, e-mail: yevdok@ire.kharkov.ua

The present – day trend in automobile radar is toward the millimeter – wave technology which have the effect of increasing visibility in the road traffic. But despite the obvious benefits for the traffic safety, the high cost presents a serious deterrent to this millimeter – wave application. Even with a certain improvement in cost of some signal processing and functional units utilizing solid – state components, the planar small – size antennas remain too complex and expensive, sending us in search of new millimeter – wave antenna designs and calculation algorithms.

Historically there have been formed the two completely different lines in the radiating aperture design: waveguide engineering (hollow metal waveguides) and printed antenna technology. In the millimeter region, the waveguide antennas are very expensive and difficult in manufacture, such as slot – waveguide arrays, for one. Nevertheless they find their application which owes to the small loss. The antennas based on printed – circuit components and utilizing microstrip/slot transmission lines are impracticable because of the high loss in the short – wave part of the millimeter region. In this connection, apertures larger than ten wavelengths are not allowed. Besides, the required dimensional accuracy is often beyond the technology possibilities. An alternative to the traditional approaches is the so – called hybrid printed antenna [1, 2]. Its distinguishing feature is a metallized dielectric layer associated with printed – circuit radiating elements excited by the waveguide modes: TEM modes propagating in the metal – dielectric structure [1] or eigenwaves of the single dielectric waveguide [2]. In the first case, a quite compact construction is reached. However dictated by the single – mode propagation condition, the dielectric thickness (i. e. the spacing of the metal layers) is too small, which causes the loss increase. In the second case, the antenna loss is determined by the dielectric waveguide, which is at a loss minimum in this antenna class.

In the present work, an attempt will be made to combine the strengths and eliminate the weaknesses of both designs by employing H waves of the metallized dielectric layer. The strengths are amplified, as will be seen below, by the fact that the antenna suggested need not a separate radio – transparent shielding screen when exposed to rainfall.

The basis structure of the hybrid printed antenna is shown in Fig. 1 and represents a dielectric layer which is metallized on both sides and has permittivity ε_1. A strip periodic structure with period ℓ and slot width d is embodied in the upper metal layer. If $d = 0$, the metallized dielectric layer changes into the two – plane metal waveguide with dielectric filling. Its H_1 mode serves as an incident wave. The H_1 choice owes to the absence of longitudinal currents, with the result that the attenuation is only a trifle over that in the single dielectric layer. So the loss of the discussed antenna is comparable with the loss of the antenna built around a planar dielectric waveguide. The slots of the upper metal screen radiate into free space in the direction $\theta_{-1} = \arccos\left(U - \frac{\lambda}{\ell}\right)$ [3], where U is the wave slowing factor, ℓ is the grating period, and λ is the free – space wavelength. The upper dielectric layer with permittivity ε_2 acts as a shielding screen. In the general case, $\varepsilon_1 \neq \varepsilon_2$ as a choice of the layers materials is guided by different criteria: a loss minimum for the bottom layer and mechanical characteristics for the upper one.

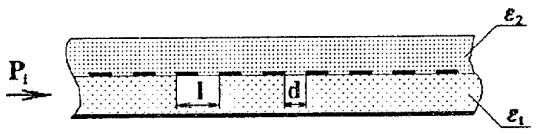


Fig. 1

The electrodynamical structure shown in Fig. 1 is quite difficult to analyze. The problem is that at $d \neq 0$ the phase velocity depends on the slot width and depth and the permittivities of the dielectric layers. Evidently the synthesis of the amplitude distribution in the radiating aperture along the slow surface wave propagation brings serious phase errors when performed only on a slot width basis. For the error compensation, every particular d value requires the period ℓ correction. So the synthesis of amplitude / phase distribution in the radiating aperture is governed by the knowledge of the real and imaginary parts of the propagation constant depending on all the structure parameters, but primarily on d. In addition, it is necessary to meet the propagation condition of most of the power in the bottom

dielectric layer. This means that the upper layer has to work as a screen rather than a surface wave line.

In view of all general physical considerations, the antenna design data have been determined using the rigorous mathematical methods of diffraction theory with the following experimental verification. For the considered periodic waveguide, a numerical analytical method has been developed, which is a generalization of the earlier technique [4] for finding complex propagation constants. By this method the initial eigenwave and propagation problem is equivalently reduced to the dispersion equation. For its solution, a set of computer programs has been devised to calculate the normalized real and imaginary parts of the propagation constants of the eigenwaves and leaky waves in a wide range of ℓ, d, λ, ε_1, ε_2, and thicknesses of the dielectric layers. At a satisfactory (no worse than 1 %) agreement with the experimental data, the slot width d and period ℓ are calculated depending on the coordinate coinciding with the slow surface wave propagation direction.

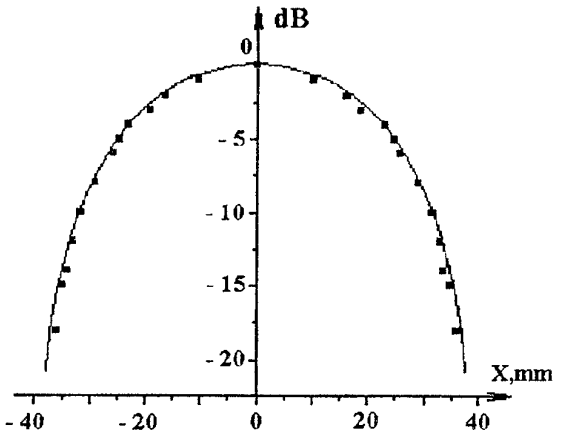


Fig. 2

For the sake of comparison, on Fig. 2 and 3 we indicate the desired cosine and Gaussian field distributions in the radiating aperture (solid lines). The corresponding field strength in the aperture of the experimentally tested structures is shown with dots; the aperture length is 78 mm, the operating wavelength λ = 3.92 corresponds to the center frequency of the operating range 76 – 77 GHz set off for automobile radar assisting the traffic safety. A quite good agreement between the desired data and measuring results is evident. The radiation pattern width is 3.5° for the cosine distribution and 3.0° for the Gaussian one. The radiation efficiency is 87 % for both. The total ohmic loss including the strips, metal substrate and dielectric layers is no more than 0.5 dB (excluding the excitation units). For both cases, the side lobe levels –20 dB and –22 dB exceeds the calculation values –23 dB and –27 dB. It should be mentioned that the side lobes are essentially asymmetrical. For the cosine distribution, they tend to the near – complete degeneration, suggesting the uncompensated phase distortions. The nature of the distortions is not as yet understood and requires further studies.

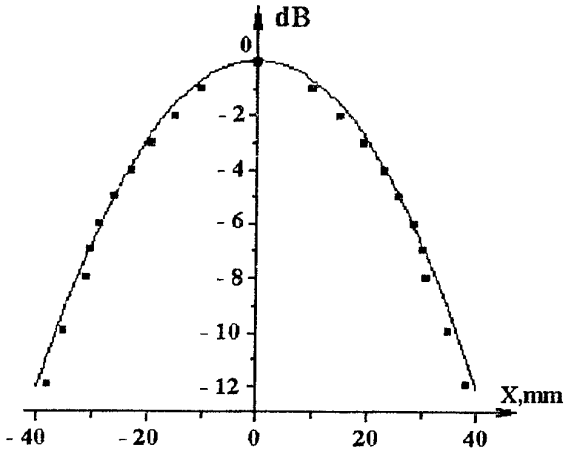


Fig. 3

Based on the investigated electrodynamical structure, a transmitting antenna combined with a three – beam receiving antenna has been constructed for automobile radar assisting the road traffic safety. The main characteristics of the antenna are listed below – combined if they are common for both receiving and transmitting antenna and separated if differ:

Common:

Operating frequency, GHz	76.5 ± 0.5
Polarization	linear horizontal
Pattern width in vertical plane, deg.	3.5
Side – lobe level in vertical plane, dB	- 20
Side – lobe level in horizontal plane, dB	- 18
Combined construction size, mm ^{3}	150 × 97 × 17
Waveguide flanges	1 for transmitting antenna 3 for receiving antenna

Transmitting antenna:

Pattern width in horizontal plane, deg.	9
Gain, dB	29

Receiving antenna:

Pattern width of each of the three beams in horizontal plane, deg.	3
Meeting level of neighbouring beams, dB	–3
Gain, dB	32

The antenna is usable either with a separate three – beam commutator in the receiving antenna or with a three receivers, which gives a certain gain in the radar system potential.

The antenna has been put through the modeling and testing stages. After a little refinement of the waveguide turns and bends the suggested construction can be available for manufacture.

REFERENCES

1. S. A. Zelubowski. " Low Cost Antenna Alternatives for Automotive Radars " . Microwave Journal, 1994 , № 7, p.p. 54-63.
2. A. P. Yevdokimov and V. V. Krizhanovsky. Hybrid printed antenna. – In Proc. ICATT'95, Kharkov, Ukraine, 1995, p 48.
3. S. D. Andrenko, N. D. Devyatkov, V. P. Shestopalov. Millimeter wave antenna arrays. – Doklady AN SSSR, 1978,vol.240, No.6, pp. 1340-1343.
4. P.N. Melezhik, A.Ye. Poedinchuk. Electrodynamical characteristics of two – dimensional open resonators with Internal inhomogeneities. Electromagnetics, v. 13, n. 3, 1993.

MULTI-BAND ELECTRONICALLY SCANNED ANTENNAS OF SANTIMETER AND MILLIMETER RANGE WAVES

N. A. Bei

Moscow State Technical University named after Bauman,
5, 2-Baumanskaya Str., Moscow 107005, Russia
E-mail: bei@mx.bmstu.ru

INTRODUCTION

The capabilities of construction of electrically scanning antennas, working at several frequency bands, are determined basically by appropriate characteristics of phasing devices and radiators. Lenses with the electronically controlled refraction index have a number of advantages in comparison with multi-element phased array, their application allows to considerably simplify a design and manufacturing technology of millimeter wave range antennas with electrical beam scanning in wide angle sector [1,3].

Controlled lenses are constructed on the basis of medium with electronically controlled refraction index, such as ferrite, liquid dielectric, having metallic and dielectric particles in suspension, and metallic delay structures. The creation of such antennas requires solution of problems both in the theoretical area and in manufacturing new antenna components. In many cases controlled lenses have many similarities with deflectors widely used in optical systems, mainly when solid environments are using for their construction. In considered below radiolenses, as well as in optical deflectors, diffraction grating is formed with parameters corresponding to the given angle of a beam deviation, the one basic of the them is the period of a refraction index change in the orthogonal direction to the electromagnetic wave propagated in the lens. The basic feature of considered system is the presence of strong distributed interaction via high-frequency electromagnetic field between areas of a lens with different refraction index. Such distributed interaction in a big extent determines the characteristics of controlled lenses.

STRUCTURE OF A CONTROLLED LENS

In general case an inhomogeneous controlled lens should perform two main transformation of waves passing through it: the transformation of a wave radiated by a feed horn to a wave with a plane phase front (i.e. focusing) and then changing a slope of the plane phase front by a required angle. Both surfaces of a controlled lens can be plane and the lens in this case is a layer of inhomogeneous dielectric. Let's consider just such lenses.

Consider a controlled lens, excited by a wave with a plane phase front. In general case such a controlled lens consists of several layers differed by the patterns of refraction index change. Consider the transformations of plane homogeneous wave I_0 to a wave with inclined phase front I_{+1}. Functioning of a two-layer lens (Fig. 1) is explained as follows.

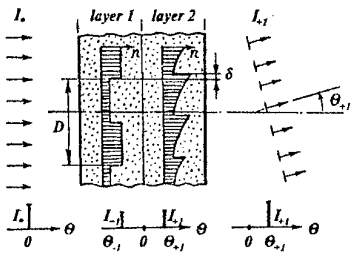


Fig. 1. Two-layer lens

A plane homogeneous wave, propagating along axis of lenses, is transformed to a wave with inclined phase front in two stages. The first layer 1 (next to the focal device) transforms the incident wave into two plane homogeneous waves I_{+1} and I_{-1}, which propagating with equal angles in module, but of opposite signs. Combination of these waves on boundary surface of layers 1 and 2 gives an "odd" wave. Then layer 2, playing the role of Bragg's deflector, changes the direction (only the angle sign) of one of these waves. The indicated transformations of plane waves correspond to the scheme: $I_0 \rightarrow I_{+1}+I_{-1} \rightarrow I_{+1}$. A necessary condition of such transformations is that period D of refraction index change in the first layer should be twice more than period of index change in the second layer. The order of layers arrangement is principal value. At the refraction index change saw tooth law, as results of theoretical research have shown, a relative arrangement of an refraction index jumps in layers 1 and 2 depends on a ratio between values I_{-1} and I_{+1} and varies with changing of a scanning angle of a beam.

In general case the lens scatters a incident wave into a set of plane waves, i.e. the electromagnetic field in the output of lens has complex spectral structure of spatial harmonics. The smaller part of energy of the exciting field goes into parasitic spectral components, the greater the lens efficiency is. The indicated criterion is decisive in the process of lens optimization consisting in selection of the layers number and of the refraction index change pattern. The number of longitudinally

homogeneous layers is determined by sector of beam scanning and generized parameter C/P, where C is a distributed coupling coefficient characterizing the medium, and P is a coefficient of media activity.

The analysis of equations (Fig. 2), describing at a wide band of wave lengths activity of medium as periodic systems with various geometrical parameters shows, that in area $d = (0.6...0.7)\lambda$ the value P varies in rather small limits. It creates the premises for construction wide band controlled lenses of such media. Maximum values of activity are achieved at diameters of transversal-magnetized ferrite rods $a = (0.25...0.28)\lambda$. It is also the fact, that with the decrease of a distance between rods ($d < 0.6\lambda$) at transversal magnetization the activity quickly decreases. Sharp activity reduction with reduction of rods diameter or period of a system coincides with the beginning of fast increase of the interaction coefficient. For systems of ferrite rods in the field of small diameters a and periods d the coupling coefficient essentially depends on a wave polarization.

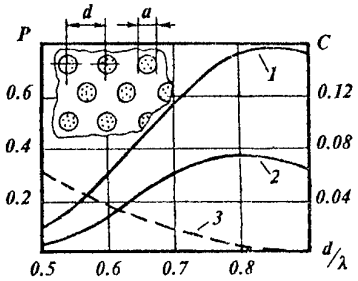


Fig. 2. Characteristics of controlled media: *1* — *P*, longitudinal-magnetized ferrite rods, $\varepsilon_f = 10$, $d = 3a$, $\mu_z = \pm 0.25$; *2* — *P*, transversal-magnetized ferrite rods, $\varepsilon_f = 10$, $d = 3a$, $\mu_a = \pm 0.25$; *3* — C, longitudinal-magnetized and transversal-magnetized ferrite rods

Liquid dielectric and semiconductors are associated with solid medium with a controlled refraction index. The change of a refraction index of ferrite medium happens under action of a magnetic field. It is known, that at longitudinal magnetization in such a medium the effect of polarization planes rotation is observed. In this connection ferrite lenses with longitudinal magnetization (along an optical axis of a lens) work on waves with circle polarization. Polarization distortions of a field in the output of such lenses are absent only in the case, if the refraction index in layers varies under the harmonic law. When changing according to the saw tooth law the distortions might be rather essential. At magnetization transversal with respect to the direction of distribution of an electromagnetic wave propagation, control of refraction index is also possible, if the propagating wave is polarized in planes, orthogonal to a direction of magnetization. In [2] characteristic artificial fluid dielectric with suspended smallest metal particles are described. For working frequencies of millimeter wave range, liquid dielectrics as n-nonane and other similar substances are used. The refraction index can be controlled by system of electrodes, diving through dielectric conductors or by passing ultrasonic waves. In order to prevent sticking of metal particles together fluid should circulate, and the controlling voltage should be alternative.

ANTENNAS WITH CONTROLLED LENSES

Two-Band Antenna with a Controlled Lens

The antenna operates at two frequency bands: in band $F1$ it forms one scanning beam, and in band $F2 < 0.5F1$ it forms one or more non-controllable beams. The frequency $F1$ corresponds to the K-band (12...27GHz); the scanning is carried out within the sector of 70°. The operating frequency band of the antenna in the K-band is more than 25%.

The ferrite rods forming the controlled medium are fixed directly on the wall of an H-sectorial horn. Conductors of the system controlling magnetization of the ferrite rods are located in a gaps, cut in the horn wall under the ferrite rods along their axes. The wall of the horn is a part of the iron circuit and it provides short circuit of magnetic currents flowed through the rods. The conductors of the control system are connected through a hole in the horn wall to the distributing system made as a printed circuit board with chips placed on it and located on the extenal surface of the horn walls. The matching of a lens is provided by conic tapers made on both ends of ferrite rods. In the H-sectorial horn there a metal-air lens is placed made as a convolution with a parabolic phase corrector.

Effective vending of warm from ferrite rods, ensured by their contact with the wall of a horn, allows to use such a lens in radiators with a high level of mean power. One more essential advantage of a considered lens in comparison with lenses with gradient refraction index change law, stipulated by periodicity of refraction index change law, is absence of any basic restrictions on the sizes of emanating aperture.

Antenna with a Ferrite Lens of a Reflective Type

The antenna consists of a feed horn and mirror with a controlled reflection coefficient. The mirror formed by multilayer slices touching each other by their sides. The phase of the reflected electromagnetic wave from the slices varies in the plane of aperture according to the law providing focusing and deviation of beam. Such a device is a reflective lens with a controlled refraction index. Each of slices represents a multilayer design including a screen with controlling plate, and a matching transformer in the form of a dielectric plate. By drilling the phase-controlling plate to partial depth,

a periodic lattice is formed which consists of cylindrical rods and magnetic circuit.

The same scanning device functioning at the whole 35 ÷ 70 GHz frequency range has been made and tested (Fig. 3). The module is constructed in the form of monolithic ferro-magnetic block with 100 × 100 mm aperture size. Sector of scanning at 37 GHz is 60×60°, at 60 GHz — no less than 40×40°, at 70 GHz — no less than 30×30°. Root mean square deviation from calculated phase distribution on the aperture is no more than 12°. Time of change of beam direction is 10 mcs when energy of switching (calculated on 1 cm^2 of the aperture area) is no more than 40 mcJ.

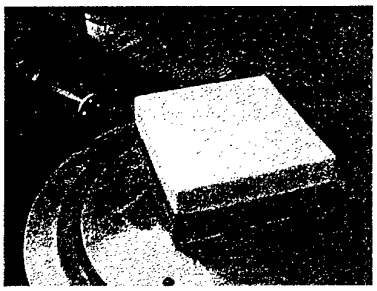


Fig. 3. Ferrite lens of a reflective type

The constructed block is intended for making controlled reflection coefficient lenses for multy-frequencies antennas. The used technology of producing blocks allows constructing such antennas for the frequency range up to 120...140 GHz.

CONCLUSION

The lenses made on the basis of media with electrically controlled refraction index are a new type of antennas that might scanning in a wide angle sector. By their principal electrical characteristics they, potentially, are no worse than the phased array antennas, and by their wide band capabilities they exceed the phased arrays. The controlled lenses can be realized at the whole millimeter wave range. They have a simpler design in comparison with phased array antennas, and are characterized by a high degree of integration of elements in the process of production.

REFERENCES

1. Lens Antennas with electrically controlled radiation patterns. / S.M.Avdeyev, N.A.Bei, A.N.Morozov. Ed. by N.A.Bei. Moscow: Radio & Svyaz Press.

2. Buscher H.T. Electrically Controllable Liquid Artificial Dielectric Media. IEEE Trans. on MTT, 1979, v.27, N5, p.540-544.

3. Bei N.A. Antennas with controlled lenses. XXVIII Scientific Moscow International Conference on Antenna Theory and Technology. 22-24 September 1998, Moscow, Russia.

DUAL-BAND ANTENNAS ON THE BASE OF SURFACE WAVE LINES

N. A. Bei, V. L. Khandamirov, A. A. Volkov, A. V. Pantelcev

The Moscow State Technical University named after Bauman, 107005,
Moscow, 2-d Baumanskaya 5, ph. (095) 2636144,
E-mail: bei@mx.bmstu.ru; Khandami@rl1.bmstu.ru

The antennas of surface waves, such as dielectric rod radiators, helix and impedance structures, have a number of features making expedient their application in a number of multiband antennas. Among these features it is necessary first of all to mark the following: rather weak coupling between inputs of antennas located at small distances (for example, in the phased array), existence of interaction between surface waves of the close located antennas, to great extent determining their pattern, capability of functioning on waves with various polarization and small cross-sectional overall dimensions. Taking into account these features the possibility of using such radiators for a construction of dual-band antenna array and reflector feed are considered.

In antenna systems for receiving signals of a satellite television in frequency bands (10.9 ... 12.75) GHz and (3.65 ... 4.2) GHz now it is used the expensive waveguide feeds with control of polarization of a signal by an electromechanical turn of connection loops of coaxial lines with waveguides. The representative of such feeds is, for example, a feed of the Chapparal corporation.

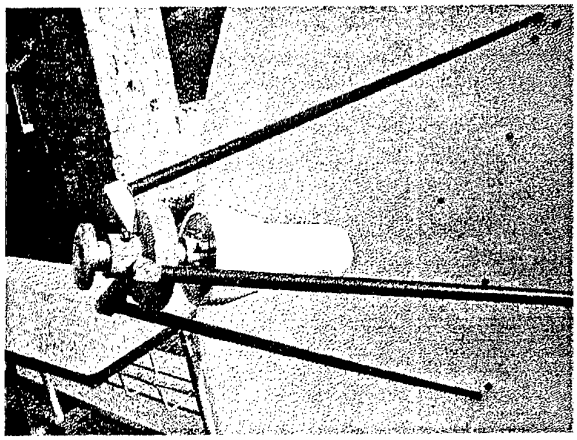


Fig. 1

Developed feed is designed to be used in antennas with f/d = 0.4, where f is focal distance, d is a reflector diameter. The feed design is shown in Fig. 1, and draft of a construction – in Fig. 2. Feed consists of two antenna elements with coinciding phase centres: dielectric rod antenna, working in frequency band (10.9 ... 12.75) GHz, and axial located with it helical antenna for band (3.65 ... 4.2) GHz.

The rod dielectric antenna is excited by the circular waveguide of diameter 17 mm with a flange for connection of the antenna amplifier with two electrically commuted probes ensuring receiving of two signals with orthogonal linear polarizations. In the waveguide the capability of the installation of a dielectric plate polarizer for a receiving signals of two orthogonal linear polarizations is stipulated. VSWR of a channel in all an effective band of frequencies does not exceed 1.5.

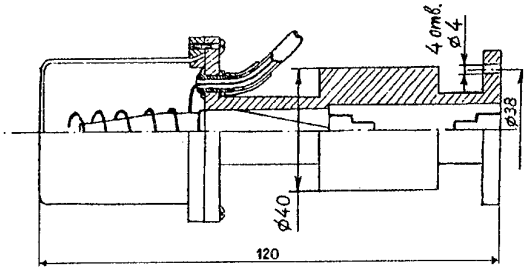


Fig. 2

The antenna of low-frequency band is made of two helixes with opposite directions of winding. When developing the two-helix radiator the basic difficulties were connected with ensuring of a good isolation between helixes. The value of an isolation, as it has been determined, depends on two major factors. The first factor is an effectiveness of helix exciters, i.e. transition from coaxial lines to opened helix waveguides. The second factor is the reflection from the ends of helix. In order to reduce coupling between exciters, diameter of the first coils of an external helix and their step were increased. The reduction of reflections from the ends of helix is reached by the increase of a step of the last two coils. If helixes are excited through a switch, with the help of which the phase shift $\pi/2$ between them is introduced, the linear polarization of a radiated field turns into orthogonal. The use of one helix is possible. Every helix radiates a wave with circular polarization with an ellipticity no more than 1.5 dB. The coaxial connectors which the wires of helixes are connected with, are located on a special flange. On the same flange the protective radiotransparent radome is fixed. In a case of use of the converter with waveguide input the connection is made through waveguide-coaxial transition.

The capabilities of a construction of electrically scanning antennas, working in several frequency bands, are determined basically by appropriate characteristics of phasing devices and radiators. At a construction of dual-band antenna arrays, for example, two independent working systems of radiators and phase shifters are used practically. Such a design, representing "array in array", is both rather complex and not always satisfies the requirements first of all because of significant mutual coupling between radiators of various frequency bands. In order to solve this problem in many cases dielectric rod radiators should be used.

On the base of the above considered helix-rod antenna the radiators of the two-frequency phased array can be made. It is clear that only in a part of radiators it is necessary to use helixes. Due to weak mutual coupling between helixes and dielectric rods it is possible to achieve not only rather good isolation between frequency channels, but also to optimize the pattern of array radiators.

The more simple design might be realized, if dielectric rod antennas is used as radiators of an array working at higher frequency, and between them on a screen of a array, slot radiators of a low-frequency channel is situated. The presence of slots, if parameters of dielectric radiators are selected correctly, practically will not affect the characteristics of a high-frequency channel, as the field in the area of a screen, as it has been established theoretically and experimentally, is concentrated mainly inside and near to a surface of a dielectric rod. The mentioned circumstance allows also to reduce considerably (in a comparison with a two-frequency array of waveguide radiators) coupling between high-frequency and low-frequency channels. It is possible to assume also, that the presence of dielectric rods in aperture will not significantly influence on the pattern of an array of slot radiators due to their small electrical sizes at low frequency.

To check the mentioned supposition the measurements of the pattern of the single slot radiator in environment of dielectric rods were carried out. For measurements the fragment of a dielectric rod array was used, in which the slot radiator was enclosed by three rings of dielectric rod radiators. In Fig. 3 the measured patterns of the slot radiator in two main planes are given. For a comparison measurements of the pattern of the slot radiator on a screen without dielectric rod radiators also were carried out.

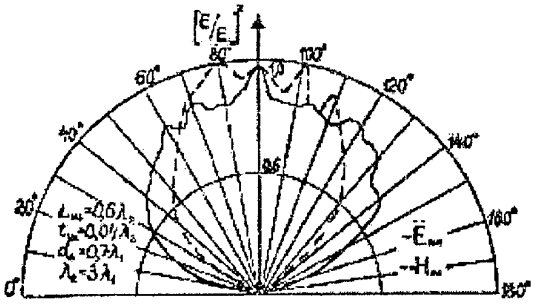


Fig. 3

The measurements have shown the absence of any essential features of the pattern of the slot radiator, enclosed by dielectric rods.

REFERENCES

1. Walter C. Travelling wave antennas. Moscow,"Energija", 1970, 447 p.p. [in Russian].
2. Voskresenskiy D.I., Ponomarev L.I. Multifrequency scanning antenna arrays//Radioelectronika.-1981, V.24, №2.-p.p. 4-15. [in Russian].
3. Bei N.A., Khandamirov V.L., Feed for communication antennas, Proceedings of The XXVIII Moscow International Conference on Antenna Theory and Technology, Moscow, 1998.

TIME-DOMAIN ANTENNA STUDIES FOR VIDEOPULSE SUBSURFACE RADARS

A. A. Boryssenko

Scientific research company Diascarb, P.O. Box 370, Kyiv, 253222, Ukraine,
E-mail: diascarb@public.ua.net

ABSTRACT

The results of time-domain theoretical and experimental studies of ultra-wide band antennas with impulse excitation in radiating and receiving modes are presented. The antennas under consideration, like a monopole antenna, a dipole antenna and a horn-like antenna, are used widely for high-resolution videopulse subsurface (ground-penetrating) radars and should be operated near the border between two medias with different electrical properties.

PROBLEM MOTIVATION AND DESCRIPTION

Subsurface (ground-penetrating) radars of the 30 MHz – 5 GHz operation frequency band are at present a rapidly growing smart technology of remote noninvasive sensing and probing applied to study the Earth interior regions, as well as others opaque matters with non-strong attenuation of sounding electromagnetic signals [1]. In order to achieve high level of spatial resolution in radars, ultra-wide band sounding signals are used implemented in time-domain region by videopulse signals (signals without frequency carrier or nonsinusoidal signals) which form by shock excitation of antennas.

The antennas are ones of the key elements of radar's equipment that determines main system features like performance factor, receiver-operating-characteristics etc. In contrast to common radars of free-space operation, radars discussed should be operated near the border of the two half-spaces «air media - subsurface media (Fig. 1), that causes serious perturbation of antenna's features:

1) energy and pattern working properties of antenna are formed under strong influence of operation environment;
2) searching objects in media under investigation may be located in the near-region of antenna and should be detected by radar also;
3) there are some statistical roughness of surface of border between two media and heterogeneity of media under investigation that disturbs antenna's features;
4) localized scatters in subsurface region, as well as ones in outer air space caused distortion of antenna operation features also;
5) complex modes of wave propagation and scattering may be appeared near the border between two media like multipath propagation, lateral waves, dispersion events and so on.

The radar's antennas should be maintained their main operation function in radars under influence of discussed working conditions, i.e. to radiate and to receive electromagnetic signals of given spatial-temporal performances, for instance, a short-duration videopulse electromagnetic signal to obtain a high-resolution radar's features for definite angular survey sectors of controlled media etc.

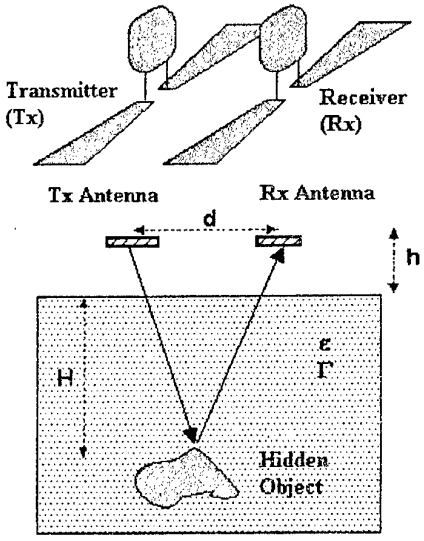


Fig. 1. Schematic presentation of problem of noninvasive studying of matter with a hidden object in it by subsurface radar with impulse Tx/Rx antennas

PROPERTIES OF VIDEOPULSE ANTENNAS

Let consider firstly the main regularities that are common for ultra-wide band impulse antennas with shock excitation, which operate in air-filled free space as well as near a border between two dielectric half-spaces. At the same time, those regularities are quite different to ones that are peculiar to ordinary antennas with sinusoidal excitation:

1) there is a time-dependent or transient operation mode of impulse (videopulse) antenna when its working features are implemented in act of short-timed shock excitation;

2) shock excitation of transmitting antenna is due to source of impulse driving signal, while excitation of receiving antenna is realized by an external incident electromagnetic field of impulse nature;

3) a key moment of impulse antennas operation is given transformation of signal's waveform due to inherent physics of transient electromagnetics in radiating and receiving antennas [2,3];

4) transmitting and receiving antennas demonstrate principal different features and a reciprocity principle, used widely for sinusoidal antennas, is not applied in this case at all and both antennas demand special cares to explore them [4];

5) waveforms of radiating and receiving signals by antenna are strictly dependent on distance and direction, especially for the near-range operation modes that is common for subsurface radars;

6) directivity features of impulse antennas in the far-range can be described by energy patterns that are determined by the auto-correlation functions of excitation signals entirely [2];

7) practical implementation of impulse antennas is realized, as a rule, by their integration with electronics component of transmitter and receiver units and a concept of active antenna is used;

A time-domain consideration of impulse antennas is more adequate to the physical nature of events studied in contrast to more commons, traditional in some degree, investigations in a frequency-domain. While from general point of view a impulse response and a complex spectral frequency response are mathematically equivalent, but corresponding time-domain theoretical models and experimental techniques applied to problems under investigation in this work are more easy by their implementation in time-domain than similar ones in frequency-domain [5].

A some classification of operation modes of impulse antennas in subsurface radars can be based on the features of their excitation determined by impedance matching of both the arms of antenna achieved like it is shown in Fig. 2 for a simplest monopole antenna.

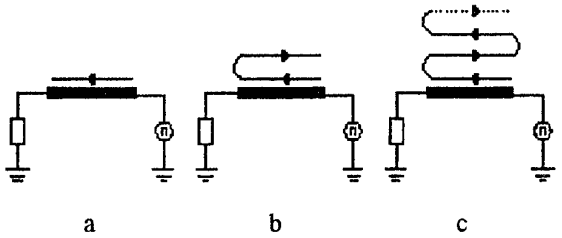


Fig. 2. Operation modes of impulse monopole antenna due to its matching achieved: a single-pass excitation or travelling-wave mode (a); a two-pass excitation mode (b); multi-pass excitation or standing-wave mode (c)

Let note that a match of opened end of antenna is provided by a lumped or distributed resistive adsorber, while match of antenna terminal port is put into practice by special means of microwave electronics circuits in an output stage of transmitter and an input stage of radar receiver.

For example, an elevation electric component of the far-region radiated electromagnetic field produced by a monopole antenna in the free space (Fig. 3) with the travelling-wave excitation mode (Fig. 2a) by a signal with given waveform s(t) can be expressed [4]:

$$E_{\Theta}(\rho,\Theta,t,La) \cong \frac{\sin\Theta}{1-\cos\Theta} \cdot \left\{ s(t-\frac{\rho}{c}) - s(t-\frac{\rho}{c}-\frac{La}{c}(1-\cos\Theta)) \right\} \quad (1)$$

and similarly, a load current of monopole receiving antenna with travelling-wave excitation mode also that excited by external incident impulse electromagnetic field with given impulse waveform $E(t)$ is determined by the following analytical expression [4]:

$$I_{\Pi}(t,\Theta,La) \cong \frac{\sin\Theta}{1-\cos\Theta} \cdot \left\{ e(t-La/c) - e(t-La/c\cdot\cos\Theta) \right\} \quad (2)$$

where $e(t) = \int E(t)dt$, c is the light velocity constant.

Note, that the presented expressions (1) and (2) demonstrate quite principal difference in radiating and reception cases concerning various regularities of transformation of primary waveforms of applied exciting signals due to integration in (2) [4]. Among antennas' structures used in videopulse subsurface radars those ones shown in Fig. 4 are applied namely.

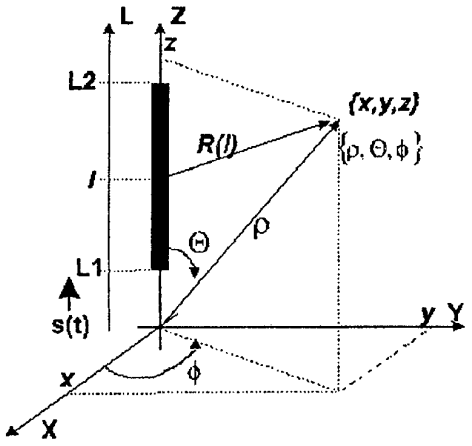


Fig. 3. General geometry of radiation problems under consideration for monopole of length $La = L2 - L1$

Environmental effects on antenna's features caused by a sounding media with quite different its electrical properties in contrast to air-filled half-space ones are significant aspect to study the impulse antennas of

subsurface radars. In general, this problem is complex electromagnetics one, but there is some opportunities to solve it approximately based on an approach discussed later. It is possible to estimate a slow-wave factor to describe some decelerating of electromagnetic signal in antenna considered as some equivalent transmission line (Fig. 5). A magnitude of this factor obtained can be used to modify a velocity of excitation signal in (1)-(2) and analogous expression, as well as to evaluate focussing effects, produced by a redistribution of electromagnetic field energy in a cross-section of equivalent transmission line (Fig. 5). The last causes finally a some modification of antenna pattern doing it inward to a sounding media in most degree.



a b c

Fig. 4. Antenna's structure: dipole antenna (a); bow -tie antenna (b); horn-like antenna (c)

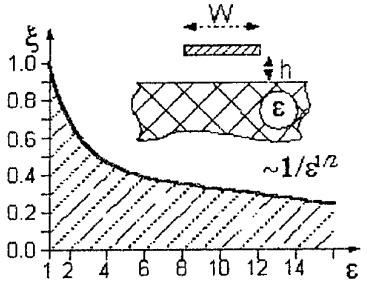
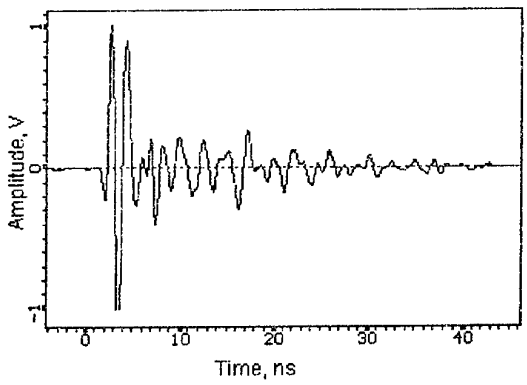


Fig. 5. Estimation of a slow-wave factor of electromagnetic signal propagation along antenna that is presented by an equivalent strip line spaced over a dielectric hulf-space

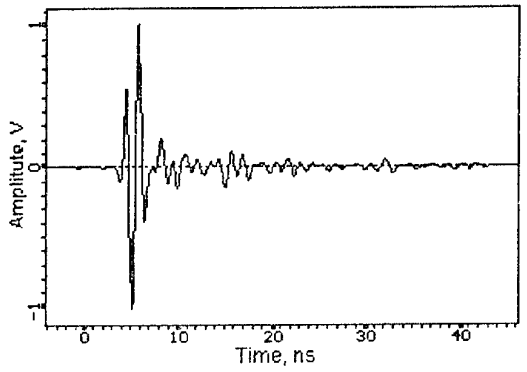
EXPERIMENTAL STUDIES

A time-domain experimental technique has sufficient benefit in comparison with frequency-domain experimental investigations due to the fact that the time-domain examinations can be accomplished in ordinary laboratory rooms without necessity to use special very expensive anechoic chambers. In this case, interference scattering electromagnetic events caused by various external objects, laboratory's walls etc. can be eliminated by a simple temporal range gating applied to a signal received [5].

In order to present the author's time-domain experimental studies, the waveforms signals measured in an radio link formed by a pair of the identical bow-tie antennas in a transmitter and receiver subassemblies of radar to detect hidden objects in vegetation is shown in Fig. 6. The corresponding testing procedures were being conducted by a special own-designed antenna's test bench based on a nanosecond pulse generator and a stroboscopic receiver unit with digital data registration by computer ADC/DSP card.



a



b

Fig. 6. Measured waveform in a radio link formed by the two identical bow-tie antennas like one in Fig. 4b: without reflector (a); with reflector (b)

REFERENCES

1. Proceedings of the 7th International Conference on Ground Penetrating Radar, Lawrence, USA, May 1998.

2. Boryssenko A.A., Analytical time-domain model of impulse antenna, Proceedings of International Symposium on Electromagnetic Theory, Thessaloniki, Greece, May 1998, Vol. 2, pp. 545-547.

3. Boryssenko A.A., Analytical research of impulse antennas for GPR applications, In [1].

4. Boryssenko A.A., Time-domain studies of ultra-wide band antennas, Proceedings of the 1999 IEEE Canadian Conference on Electrical and Computer Engineering, Edmonton, Canada, May 1999.

5. Boryssenko A.A., Time-domain experimental studies of ultra-wide band antennas, Proceedings of 22nd ESTEC Antenna Workshop on Antenna Measurements, ESTEC, Noordwijak, Netherlands, May 1999.

MODELING THE PROBLEM OF PULSE RADIATION FROM A SLOTTED CONE PLACED ON THE INHOMOGENOUS PLANE

V. A. Doroshenko

Kharkov Technical University of Radioelectronics,
14, Lenin av., Kharkov, 310726, Ukraine
tel.: (0572)409-372, e-mail: nerukh@anish.kharkov.ua

Abstract: The time dependent Green's function boundary problem for a semi-infinite perfectly conducting slotted cone placed on the impedance plane is considered. This geometry can be regarded as a suitable three-dimensional model of slotted cone antennas and wire antennas situated on the imgomogenous plane. The solution method is based on using the Laplace transform, the Kontorovich-Lebedev transform and the Rieman-Hilbert method. The Green's function representations are derived for the "partly penetrable" cone. The boundary problem spectrum and the plane contribution are investigated.

INTRODUCTION

The problem of electromagnetic pulse radiation and excitation of open structures placed near inhomogenous bodies is of great interest for many applications such as antenna technology, communications and others. In fact, the problem solution needs to construct the adequate mathematical model of the physical process. It's well known that the dyadic Green's function is a useful tool for researching the interaction of electromagnetic fields with several physical geometries. The purpose of this study is to find the time-dependent Green's function for a semi-infinite circular perfectly conducting periodically slotted cone placed on the impedance plane. The cone structure under consideration is a model of wire and slot wide-band antennas with controlled radiation diagram and polarization.

FORMULATION AND METHOD

In spherical coordinate system r, ϑ, φ the infinite circular cone Σ_1 with N periodical slots cut along generatricies is defined by the equation $\vartheta = \gamma$ and the impedance plane Σ_2 $\vartheta = \pi/2$. The cone structure period $l = 2\pi/N$ and the slot width d are values of dihedral angles formed planes passing through the cone axis and cone strip edges.

The Green's function $G(\vec{r}, \vec{r}_0, t, t_0)$ satisfies:

1) the four-dimensional partial differential equation

$$\left(\Delta - \frac{1}{c^2}\frac{\partial^2}{\partial t^2}\right) G(\vec{r}, \vec{r}_0, t, t_0) = -\delta(\vec{r} - \vec{r}_0)\delta(t - t_0);$$

2) the Dirichlet boundary condition on the cone strips

$$G(\vec{r}, \vec{r}_0, t, t_0)|_{\Sigma_1} = 0$$

and the boundary condition on the plane Σ_2

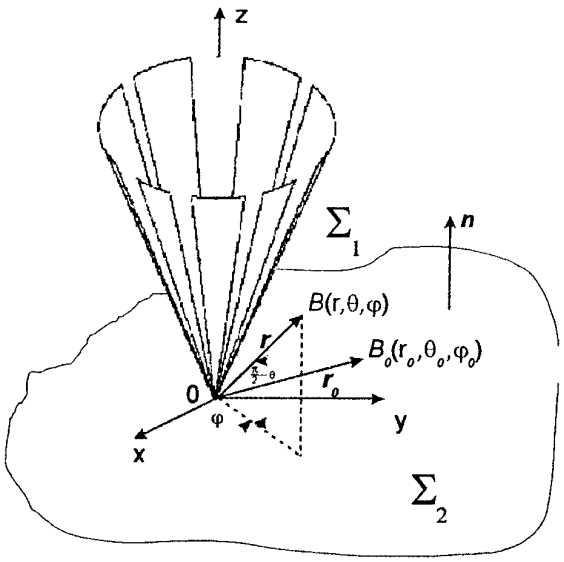
$$\left(G + \zeta(\vec{r})\frac{\partial}{\partial n} G\right) = 0,$$

where $\zeta = \zeta(\vec{r})$ is the given function;

3) initial conditions $G = \frac{\partial G}{\partial t} \equiv 0$, $t < t_0$;

4) infinity condition at $r \to \infty$;

5) singularity conditions (the cone tip, strip edges).



The solution for G can be written as the sum of a free-space field $G_0(\vec{r}, \vec{r}_0, t, t_0)$ and a scattered field $G_1(\vec{r}, \vec{r}_0, t, t_0)$, due to the presence of the cone and the plane:

$$G(\vec{r}, \vec{r}_0, t, t_0) = G_0(\vec{r}, \vec{r}_0, t, t_0) + G_1(\vec{r}, \vec{r}_0, t, t_0),$$

$$G_0(\vec{r}, \vec{r}_0, t, t_0) = \frac{\delta[\hat{\tau} - R/c]}{4\pi R}, \quad R = |\vec{r} - \vec{r}_0|,$$

$$\hat{\tau} = t - t_0,$$

c is the light velocity. The plane impedance ζ is assumed to be $\zeta(\vec{r}) = \chi r$, $\chi = const$. The time-dependent

response due to a point source in the presence of the slotted cone on the impedance plane can be found through the Laplace inversion of the time-harmonic Green's function [1,2]. The stationary boundary problem solution is based on using the Rieman-Hilbert method and the Kontorovich-Lebedev transforms [3,4]

$$F(\tau)=\int_0^{+\infty} f(r)\frac{K_{i\tau}(qr)}{\sqrt{r}}dr,$$

$$f(r)=\frac{2}{\pi^2}\int_0^{+\infty}\tau sh\pi\tau F(\tau)\frac{K_{i\tau}(qr)}{\sqrt{r}}d\tau,$$

where $K_\mu(y)$ is the Macdonald function. It follows, that

$$G_1=\frac{c}{4\pi r r_o}\eta\left(\hat{\tau}-\frac{r+r_o}{c}\right)\times$$

$$\sum_{m=-\infty}^{+\infty}e^{im\varphi}\int_0^{+\infty}a_{m\tau}U_{m\tau}P^{m}_{-\frac{1}{2}+i\tau}(chb)d\tau,$$

$$a_{m\tau}=\frac{(-1)^{m+1}}{ch\pi\tau}e^{-im\varphi_o}\frac{\Gamma\left(\frac{1}{2}-m+i\tau\right)}{\Gamma\left(\frac{1}{2}+m+i\tau\right)}\times$$

$$P^{m}_{-\frac{1}{2}+i\tau}(\cos\theta_o)P^{m}_{-\frac{1}{2}+i\tau}(-\cos\gamma),$$

$$chb(\hat{\tau})=\frac{\hat{\tau}^2c^2-r^2-r_0^2}{2rr_0},$$

$$U_{m\tau}=\begin{cases}\sum_{n=-\infty}^{+\infty}\alpha_{mn}(\tau)P^{nN+m}_{-\frac{1}{2}+i\tau}(\cos\vartheta)e^{i(nN+m)\varphi}, 0<\vartheta<\gamma\\ \sum_{n=-\infty}^{+\infty}\Phi_{mn}(\tau)e^{i(nN+m)\varphi}, \gamma<\vartheta<\pi/2\end{cases}$$

$$\Phi_{mn}(\vartheta,\tau)=\beta_{mn}(\tau)P^{nN+m}_{-\frac{1}{2}+i\tau}(\cos\vartheta)+$$

$$\xi_{mn}(\tau)P^{nN+m}_{-\frac{1}{2}+i\tau}(-\cos\vartheta),$$

$P^m_\mu(y)$ are associated Legendre functions, $\Gamma(z)$ is a gamma-function, $\eta(x)$ is the Heviside function, $\alpha_{mn},\beta_{mn},\xi_{mn}$ -unknown coefficients. Applying boundary conditions and continuity conditions for G and $\partial G/\partial\vartheta$ in slots gives connections between β_{mn},ξ_{mn} and α_{mn}. The coefficients α_{mn} satisfy the infinity system of linear algebraic equations [4]. The system solution can be obtained via the reduction method for any problem parameters and with the iteration one in case of a "partly penetrable" cone too.

RESULTS

For the "partly penetrable" cone that is defined by existence of the limit

$$\lim_{\substack{N\to\infty\\ d/l\to 1}}\left[-\frac{1}{N}\ln\left(\frac{l-d}{l}\right)\right]=Q,$$

we obtain

$$G_1=\frac{1}{r}\eta\left(\hat{\tau}-\frac{r+r_0}{c}\right)\times$$

$$\sum_{m=-\infty}^{+\infty}e^{im\varphi}\int_0^{+\infty}\tau th\pi\tau d^m_{i\tau}W^m_{i\tau}P^m_{-\frac{1}{2}+i\tau}(\cos\vartheta)P_{-\frac{1}{2}+i\tau}(chb)d\tau-$$

$$\frac{1}{r}\eta\left(\hat{\tau}-\frac{r+r_0}{c}\right)\sum_{m=-\infty}^{+\infty}e^{im\varphi}\int_0^{+\infty}\tau th\pi\tau d^m_{i\tau}\frac{A^m_{i\tau}}{2Q+A^m_{i\tau}}\times$$

$$\left[W^m_{i\tau}P^m_{-\frac{1}{2}+i\tau}(\cos\vartheta)-P^m_{-\frac{1}{2}+i\tau}(-\cos\vartheta)\right]d\tau,$$

$$\gamma<\vartheta<\pi/2,$$

$$W^m_{i\tau}=\frac{P^m_{-\frac{1}{2}+i\tau}(0)+\chi\frac{d}{d\vartheta}P^m_{-\frac{1}{2}+i\tau}(\cos\vartheta)\Big|_{\vartheta=\pi/2}}{P^m_{-\frac{1}{2}+i\tau}(0)-\chi\frac{d}{d\vartheta}P^m_{-\frac{1}{2}+i\tau}(\cos\vartheta)\Big|_{\vartheta=\pi/2}},$$

$$B^m_{i\tau}=W^{N(n+\nu)}_{i\tau}\frac{P^m_{-\frac{1}{2}+i\tau}(\cos\gamma)}{P^m_{-\frac{1}{2}+i\tau}(-\cos\gamma)},$$

$$A^m_{i\tau}=(-1)^m\frac{\pi}{ch\pi\tau}\frac{\Gamma\left(\frac{1}{2}+i\tau-m\right)}{\Gamma\left(\frac{1}{2}+i\tau+m\right)}\left(1-B^m_\tau\right)\times$$

$$P^m_{-\frac{1}{2}+i\tau}(\cos\gamma)P^m_{-\frac{1}{2}+i\tau}(-\cos\gamma),$$

To simplify the general result, we assume that the source point is located on the cone axis, i.e., $\vartheta_0=0$, $\varphi_0=0$

$$G_1=-\frac{c}{4\pi r r_0}\eta\left(\hat{\tau}-\frac{r+r_0}{c}\right)\times$$

$$\int_0^{+\infty}\tau th\pi\tau W_{i\tau}P_{-\frac{1}{2}+i\tau}(\cos\vartheta)P_{-\frac{1}{2}+i\tau}(chb)d\tau$$

$$+\frac{c}{4\pi r r_0}\eta\left(\hat{\tau}-\frac{r+r_0}{c}\right)\int_0^{+\infty}\tau i h\pi\tau\frac{A_{i\tau}}{2Q+A_{i\tau}}\times$$

$$\left[W_{i\tau}P_{-\frac{1}{2}+i\tau}(\cos\vartheta)-P_{-\frac{1}{2}+i\tau}(-\cos\vartheta)\right]d\tau\,,$$

$$\gamma<\vartheta<\pi/2\,,$$

$$A_{i\tau}=A^0_{i\tau},W_{i\tau}=W^0_{i\tau}\,.$$

By using the residue theorem we can derive series representations for G_1 [2]. The boundary problem spectrum for the "partly penetrable" cone placed on the impedance plane is defined by roots $\mu_j=\mu_j(\gamma,Q,\chi)$ of the equation $A_{\mu_j}+2Q=0$. One may determine these roots asymptotically for cases of the "partly penetrable" cone

$$Q<<1$$

$$\mu_j^+=\alpha_j^+-2Q\frac{\cos\pi\mu_j}{\pi P_{-\frac{1}{2}+\mu_j}(-\cos\gamma)\frac{d}{d\mu_j}P_{-\frac{1}{2}+\mu_j}(\cos\gamma)}$$

$$+O\left(Q^2\right),P_{-\frac{1}{2}+\alpha_j^+}(\cos\gamma),$$

$$\mu_j^*=\varsigma_j-$$

$$2Q\frac{\cos\pi\varsigma_j\left[P_{-\frac{1}{2}+\varsigma_j}(0)-\chi\frac{d}{d\vartheta}P_{-\frac{1}{2}+\varsigma_j}(\cos\vartheta)\Big|_{\vartheta=\pi/2}\right]}{\pi P_{-\frac{1}{2}+\varsigma_j}(\cos\gamma)\frac{d}{d\varsigma_j}V_{\varsigma_j}}$$

$$+O\left(Q^2\right),$$

$$V_\mu=\left[P_{-\frac{1}{2}+\mu}(-\cos\gamma)-P_{-\frac{1}{2}+\mu}(\cos\gamma)\right]P_{-\frac{1}{2}+\mu}(0)-$$

$$\chi\left[P_{-\frac{1}{2}+\mu}(-\cos\gamma)+P_{-\frac{1}{2}+\mu}(\cos\gamma)\right]\times$$

$$\frac{d}{d\vartheta}P_{-\frac{1}{2}+\mu}(\cos\vartheta)\Big|_{\vartheta=\pi/2},V_{\varsigma_j}=0,\varsigma_j=\varsigma_j(\gamma,\chi);$$

$$Q>>1$$

$$\mu_j=\upsilon_j+\frac{1}{2Q}\frac{\pi P_{-\frac{1}{2}+\upsilon_j}(\cos\gamma)}{\cos\pi\upsilon_j\frac{d}{d\upsilon_j}\sigma_j}\left[P_{-\frac{1}{2}+\upsilon_j}(\cos\gamma)\right]^2\times$$

$$\left[P_{-\frac{1}{2}+\upsilon_j}(0)+\chi\left(\upsilon_j^2-\frac{1}{4}\right)P^{-1}_{-\frac{1}{2}+\upsilon_j}(0)\right]+O\left(Q^{-2}\right),$$

$$\sigma_\mu=P_{-\frac{1}{2}+\mu}(0)-\chi\left(\mu^2-\frac{1}{4}\right)P^{-1}_{-\frac{1}{2}+\mu}(0),\sigma_{\upsilon_j}=0;$$

The term with $W^m_{i\tau}P^m_{-\frac{1}{2}+i\tau}(\cos\vartheta)$ in the integral representation for G_1 describes the effect of the impedance plane on radiation from the slotted cone.

CONCLUSIONS

The algorithm for finding the time-dependent Green's function of the pulse excitation problem for the semi-infinite circular perfectly conducting periodically slotted cone placed on the impedance plane is proposed. The solution method is based on using the Laplace transform, the Kontorovich-Lebedev transform and the Rieman-Hilbert method for a unit circle arc. It is shown that the boundary problem is reduced to solving the infinite system of algebraic equations. For the "partly penetrable" cone the time-dependent Green's function representation is obtained in integral form.

REFERENCES

1. Chan K.-K., and Felsen L.B. "Transient and time-harmonic diffraction by a semi-infinite cone.". IEEE Tr. Ant. Propagat., vol.AP-25, no.6, 1977, pp. 802-806.
2. Doroshenko V.A., "Transient radiation from longitudinal slots cut on the cone". Proc. of 2nd International Conference on Antenna Theory and Techniques, Kyiv, 1997, pp.8-9.
3. Shestopalov V. P., "Summary equations in modern diffraction theory", Naukova dumka, Kiev, 1988 [in Russian].
4. Doroshenko V. A., Klimova N.P., "The solution algorithm of electromagnetic wave scattering problem on a symmetric bicone with longitudinal slots", Kharkov, Radiotekhnika, № 101, 1997, pp. 148-154 [in Russian].

EFFECTS OF RADIATION PATTERN DISTORTIONS OF SLOT ANTENNAS WITH FINITE LATERAL METALLIZATION

F. F. Dubrovka and V. M. Tereshchenko*

National Technical University of Ukraine "KPI", Laboratory of Antennas and Telecommunications,
2110D, Radio Engineering Faculty, Polytekhnichna st., 12, Kyiv, 252056, Ukraine
Tel./Fax: +380-44-241-7223 e-mail: dubrovka@ucl.kiev.ua * a_tlab@ucl.kiev.ua

ABSTRACT

A theoretical study of radiation patterns distortions caused by lateral metallization truncation in open longitudinally inhomogeneous slot structures on dielectric substrates is presented. The study is carried out on the base of mathematical models obtained by Hybrid Finite Element Method and Galerkin method in spectral domain with taking into account all surface waves.

INTRODUCTION

Large frequency bandwidth, compatibility with microwave integrated circuits, light weight and geometric simplicity are among the most crucial requirements for antennas designed for some specific applications, such as airborne radars and communication systems. The tapered slot antenna (TSA) is one of the most desirable candidates, which can satisfy these demands. The most attractive features of the TSAs, in contrast to other kinds of planar antennas, are capability to work over a large frequency bandwidth and producing a symmetric endfire beam.

The use of endfire tapered slot antennas for wideband/wide-scan phased arrays was proposed more than two decades ago [1]. These arrays offer one of the best opportunities for realizing wide-bandwidth, wide-scanning phased arrays, but their development has not progressed nearly as rapidly as the initial promising results suggested. Although several arrays [2–4] of tapered slot antennas have been built and tested, propagation and radiation physical phenomena of electromagnetic waves in single TSA were not yet well understood. An attempt to identify and explain these phenomena in open longitudinally inhomogeneous slot structures on dielectric substrates was made in [5]. Investigations [5] are carried out on the base of mathematical model [6], which ideally valid for infinite lateral metallization, but, nevertheless, gives sufficiently accurate results when the half lateral dimension of metallization is at least three free space wavelengths. It has been observed experimentally [7], that the radiation pattern exhibits some interesting features as the antenna is truncated laterally.

The purpose of this paper is a theoretically study of radiation patterns changes, caused by lateral metallization truncation in open longitudinally inhomogeneous slot structures on dielectric substrates.

RESULTS AND DISCUSSIONS

Owing to the surface nature of wave propagation the radiation mechanism of slot antenna on dielectric substrate corresponds to the radiation mechanism of surface-wave antennas. It is well-known from the general theory of traveling wave antenna, that slight change in the phase velocity can have considerable influence on radiation characteristics. Influence of phase velocity on radiation characteristics of tapered slot antennas on dielectric substrates has been investigated for LTSA and "Vivaldi" performed on the substrate 0.23 mm ($0.0092\lambda_0$) thick with 62.5 mm ($2.5\lambda_0$) aperture width, 25.0 ($1.0\lambda_0$) taper length at the frequency of 12.0 GHz for different dielectric permittivities. One can see (Fig. 1), that for electrically "thin" substrate the phase velocity is only slightly less than velocity of light and within taper length practically does not alter (the change is only 1.5%), while for electrically "thick" substrate the phase velocity is considerably less than velocity of light and changes more than 8.0 %.

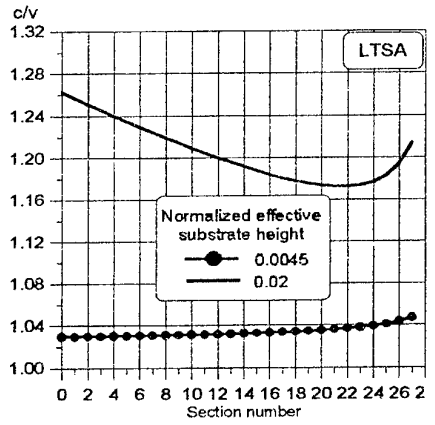


Fig. 1

Study of contribution into radiated far zone field from individual sections and relationship of these contributions in terms of length for different normalized effective substrate width (i.e. phase velocities) is of great interest. The normalized values of the contribution into radiated far zone field (Fig. 2) much less along the whole taper for greater value of normalized effective substrate width, because of the field is close to the unit

and radiation occurs mainly from the aperture. This results in the fact, that the first sidelobe level in E-plane (Fig. 3) changes by about 71 percent for a 15 percent change in the phase velocity for LTSA, caused by varying dielectric permittivity from 2.2 to 9.8.

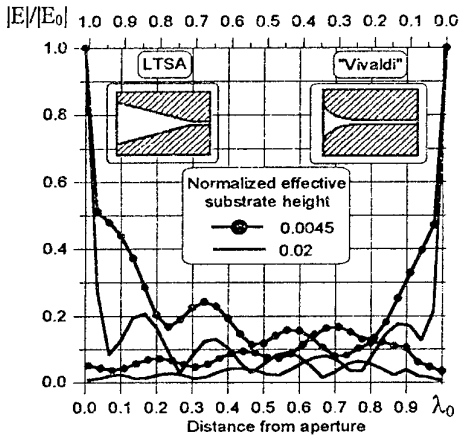


Fig. 2

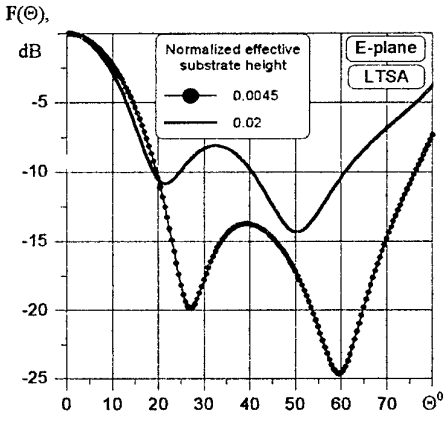


Fig.3

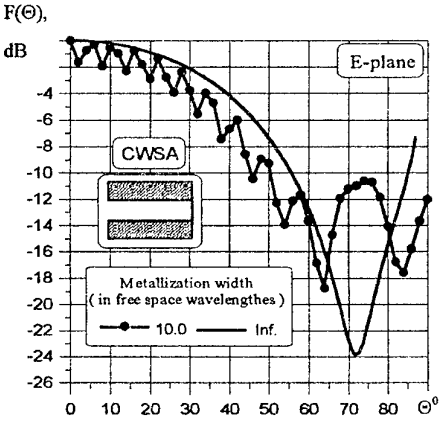


Fig. 4

The radiation mechanism of the "Vivaldi" antenna and other tapered slot antennas on dielectric substrates is highly dependent on the diffraction of the electromagnetic waves at the end of the aperture. This important phenomenon is taking into consideration by the mathematical model [6]. Such a diffraction also occurs when the metallic plane of a slot antenna is finite. The correct modeling of these phenomena is needed for a correct modeling of the endfire radiation.

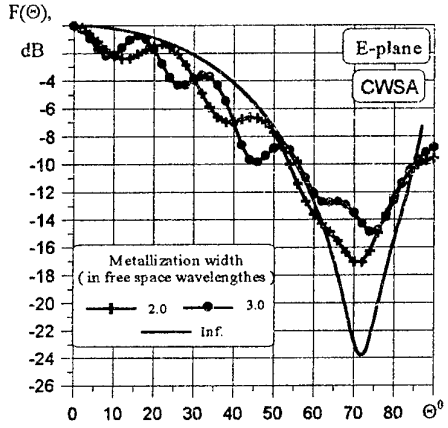


Fig. 5

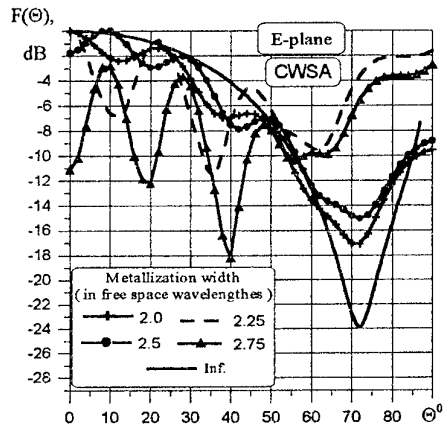


Fig. 6

To illustrate the effect of radiation characteristics distortions, caused by lateral metallization truncation, we consider air case of CWSA (Fig. 4–7) and LTSA (Fig. 8, 9) with 20.0 mm aperture width, 2.0 mm input slot width, 30.0 mm taper length at the frequency of 10.0 GHz for various dimensions of metallization. *E*-plane radiation patterns for CWSA with finite metallization are compared with those, obtained by using mathematical model of [6], which assume infinite lateral metallization (bold solid curve). Agreement with the bold solid curve changes from good to sufficient for CWSA with half metal width which equal to ten (Fig. 4) or two-three (Fig. 5) free space wavelengths respectively. It has been found, that when the half metal width greater than one free space wavelength and doesn't equal to integer number of wavelength, radiation pattern can has gap in endfire direction (Fig. 6). This phenomenon can be partially explain using the theory of radiation of vibrators. Lateral truncation results mainly in an E-

plane beamwidth that is, in most cases, considerably narrower than the one obtained using an antenna with a large metallization width (Fig. 7). LTSA shows analogous dependencies.

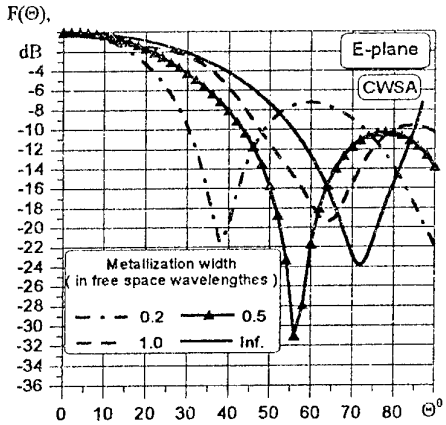


Fig. 7

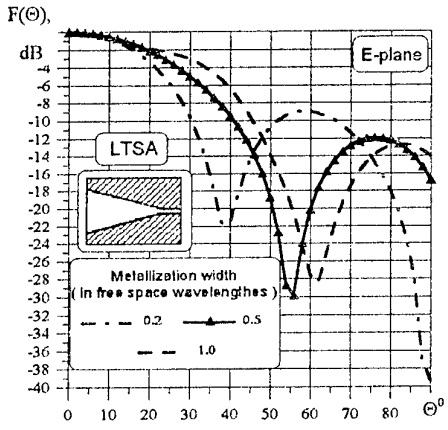


Fig. 8

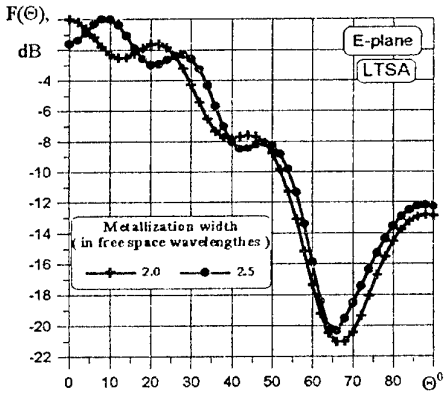


Fig. 9

CONCLUSIONS

The effects of radiation patterns distortions caused by lateral metallization truncation in open longitudinally inhomogeneous slot structures on dielectric substrates are observed. Radiation characteristics of the slot antennas are strongly dependent on lateral dimensions of metallization. A deep study of physical phenomena and reasons, that cause the strong radiation pattern changes, is in progress. At present we can conclude, that only slot antennas with a wide lateral metallization are capable to work in the endfire radiation mode over multi-octave frequency band.

REFERENCES

1. *Lewis L. R., Fasset M., Hunt J.* A broadband stripline array element // Digest of 1974 IEEE Ant. & Prop. Sym. - P.335-337.
2. *Choung Y. H., Chen C.C.* 44 GHz slotline phased array antenna // in Dig. IEEE Symp. Antennas Propagat., San Jose, CA. - Vol.3. - P.1730-1733. - June 1989.
3. *Lewis L. R., Pozgay J. H., Hessel A.* Design and analysis of broadband notch antennas and arrays // in Dig. IEEE Int. Symp. Antennas Propagat., Amherst. - MA. - P.44-47. - Oct. 1976.
4. *Pepe C. D., Povinelli M. J., Komiak J. J.* Wideband active phased array // presented at Proc. Antenna Applicat. Symp., Robert Allerton Park, Univ. Illinois. - Sept. 1987.
5. *F. F. Dubrovka,V. M. Tereshchenko* Features of propagation and radiation of electromagnetic waves by open slot endfire irregular structures on dielectric substrates // Radioelectronics and Communications Systems . - Vol.41. - No. 7, pp.14-22, 1998, Allerton Press Inc., New York.
6. *F. F. Dubrovka, V. M. Tereshchenko* Full surface waves analysis of radiation characteristics of tapered slot antennas on dielectric substrates // Proc. of 7-th. International Conference on Mathematical Methods in Electromagnetic Theory (MMET'98), Kharkov, Ukraine, 1998, p.p.547-549.
7. *Janaswamy R.* Radiation pattern analysis of the tapered slot antenna // Ph.D. dissertation, Univ. Massachusetts, Amherst, 1986.

A VHF-UHF LOGPERIODIC V-DIPOLE TV ANTENNA

F. F. Dubrovka, O. M. Kupriy, V. V. Zaskalniy

National Technical University of Ukraine "KPI", Laboratory of Antennas and Telecommunications,
2110D, Radio Engineering Faculty, Polytekhnichna st., 12, Kyiv, 252056, Ukraine
Tel/Fax: 380-44-2417223 e-mail: dubrovka@ucl.kiev.ua

INTRODUCTION

The rapid development of TV broadcasting, increasing a number of operating channels, improving of TV programs quality and availability of high quality TV receivers put the problem of developing dual-band VHF (174–230 MHz) and UHF (470–790 MHz) antennas with high gain and good matching in both operating frequency bands.

The paper gives one possible way to solve the problem, namely, using a combined dual-band logperiodic antenna with V-dipoles providing required radiation performances in VHF range at the basic harmonic and in UHF range at the third one.

RESULTS AND DISCUSSIONS

The antenna consists of vibrators located in one plane under a definite angle to each other. The antenna operates at 6–12th TV channels (174–230 MHz) and at 21–60th TV channels (470–790 MHz). A central vibrator's length is approximately equal to $\lambda/2$ at the average frequency of the 6–12th TV channels and to $3\lambda/2$ an the average frequency of the 21–60th channels.

At the third harmonic input impedance of a dipole of an active zone is approximately equal to its impedance at half-wave resonance that provides rather good matching with a feeder. An angle between the vibrators is chosen to be approximately $120°$. The necessity of providing such angle is caused by the following. Radiation pattern of a linear dipole of length $\lambda/2$ in horizontal plane looks like an "eight" directed along the axis of the antenna. For the 21–60th channels at the dipole length equals $3\lambda/2$ main lobe of the radiation pattern is bifurcated and in the axial direction a gap in radiation pattern arises. To obtain end-fire radiation pattern dipoles must be inclined towards the antenna's axis. This provides not only the filling the gap in the main lobe, but decreasing backward radiation as well and, as a result, the dipole at the 21–60th TV channels has higher directivity than at the 6–12th ones.

The theoretical investigation of antenna's performances have been carried out by utilizing the program NEC [1] designed to calculate wire antennas of various types. The program allows to calculate antenna's directivity, radiation pattern and matching in an operating frequency band. The 12th , 11th , 10th , and 8th element antennas with parameters σ and τ varying within some limits have been studied.

Note that parameter σ is a distance (in wavelength) between half-wave and neighboring dipoles and parameter τ is determined by the formula $\tau = 1 - \frac{4\sigma}{\mathrm{ctg}\alpha}$, where α is an angle between antenna axis and a line passing through dipoles ends.

Results of the parametric study show that directivity grows with increasing value of parameter σ and becomes stable in a frequency range when the parameter τ = 0.94–0.96. For τ = 0.90, 0.92 and 0.98 directivity is non-stable in UHF band and has its maximum at the boundaries of the frequency band. For τ = 0.98 the highest directivity is achieved (up to 14 dB) but in a narrow frequency range. In VHF band more stable directivity can be provided when σ = 0.04–0.08 and τ = 0.90–0.96. For τ = 0.98 there is a essential decreasing of directivity at the end of VHF band. This leads to optimal values of σ = 0.04–0.06, and τ = 0.94–0.96.

Radiation characteristics of the antenna also depend on the angle α. Decreasing the angle α and increasing structure period cause increasing the antenna gain and decreasing back and side lobes levels. However, it stipulates increasing overall dimensions and weight of the antenna. Thus, the angle 2α and the period of structure should be chosen proceeding from the condition of compromise between overall dimensions and weight, from one hand, and radiation characteristics from the other. So, the parameters α and τ, which define dimensions and geometric structure of the logperiodic antenna, are chosen in such a way to provide a sufficient gain and low side lobes levels for permissible overall dimensions and weight of the antenna.

In order to verify the results of theoretical investigations an antenna prototype having 12 dipoles has been designed and fabricated. The antenna prototype characteristics are stated below.

The parameters τ and σ have been chosen proceeding from the theoretical optimal values, namely σ = 0.06 and τ = 0.94. This values of parameters τ and σ should provide near uniform directivities 10dB in UHF band and 7dB in VHF band.

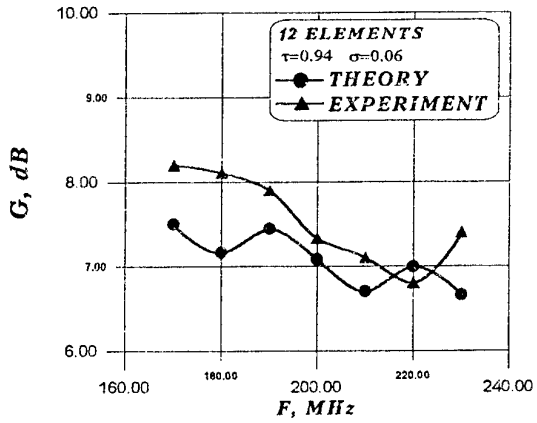


Fig. 1

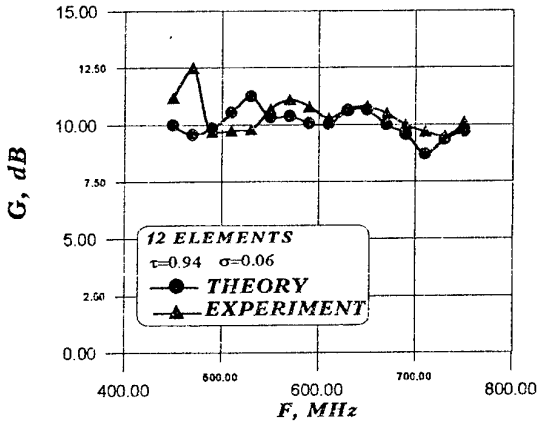


Fig. 2

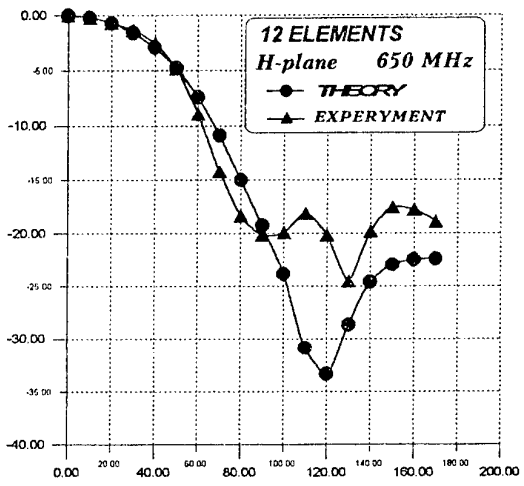


Fig. 3

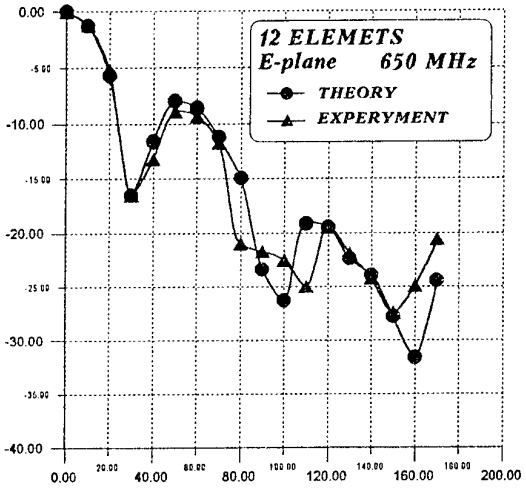


Fig. 4

Directivities of the antenna prototype versus frequency in VHF band and in UHF band are shown in Fig. 1 and Fig. 2 respectively. One can see in these figures that directivities in both frequency bands are fairly stable and theoretical and measured results are in reasonable agreement.

Radiation patterns of the antenna prototype has also been measured. Calculated and experimental results of radiation patterns in *H*- and *E*-plane at 650 MHz are shown in Figs. 3–4.

The theoretical and experimental results are found to be in general agreement.

REFERENCE

1. Barke G.J., Poggio A.J. The numerical Electromagnetics Code (NEC2), Lawrence Livermore Laboratory, Livermore, CA, 1980.

TRANSIENT EXCITATION OF COAXIAL CONE ANTENNA

A. N. Dumin, S. N. Pivnenko

Kharkov State University, 310077, Kharkov, Svobody Sq.,4,
Phone: (0572) 45-75-48, E-mail: Alexander.N.Dumin@univer.kharkov.ua

In relation to the using of ultrawideband signals in radar and radiocommunication there appeared a variety of mathematical methods for solving the problems for such signal radiation and propagation. One of them is the method of evolutionary equations relating to the analytical methods in time domain.

The essence of the method is that the basis for electromagnetic field expansion is constructed in cross-section. This permits to represent the field in waveguide or free space as a package of the modes and to trace their changes with longitudinal coordinate and passage of time. This requires to solve the evolutionary equation system that represents the second-order partial differential equations of Klein-Gordon type with given initial and boundary conditions. It is convenient to use the method for solving transient problems of radiation and propagation of waves excited by sources with arbitrary time dependencies in layered nonhomogeneous and nonstationary media.

In work [2] the characteristics of the coaxial cone antenna (CCA) with a infinite screen are studied theoretically and experimentally in receiving mode. The radiator is the cone antenna excited by step of current. However, at theoretical analysis there considered only one specific case of time current dependence and used the Fourier transform of the solution for sinusoidal waves.

The goal of this work is to investigate the videopulse radiation from coaxial cone antenna theoretically by means of the methods of Evolutionary Equations and Duhamel integral as well as to check experimentally the obtained results.

THEORETICAL PROBLEM

The source of a non-stationary electromagnetic field in the form of the coaxial cone antenna with infinite flange excited by TEM-wave is located on the plane $z=0$ (Fig. 1). We will solve the problem in Kirchhoff approximation regarding that the field in the antenna aperture is the same as in infinite coaxial waveguide. Consequently, the problem of interest is reduced to the problem of radiation from the open end of coaxial waveguide. It was shown in [3] that TEM-wave excited in the waveguide with arbitrary time dependence generates E-wave in free space:

$$\vec{E}(\rho,\varphi,z,t)=\int_0^\infty d\xi\nabla\phi\frac{\partial}{\partial z}e;$$

$$\vec{H}(\rho,\varphi,z,t)=\int_0^\infty d\xi\left[\vec{z}^0\times\nabla\phi\right]\varepsilon_0\frac{\partial}{\partial t}e;$$

$$E_z(\rho,\varphi,z,t)=\int_0^\infty \xi^2 d\xi\phi e,$$

where $\phi(\rho,\varphi;\xi)=J_0(\xi\rho)/\sqrt{\xi}$, $e(z,t;\xi)$ is the evolutionary coefficient that satisfies the evolutionary equation

$$\left\{\frac{1}{c^2}\frac{\partial^2}{\partial t^2}-\frac{\partial^2}{\partial z^2}+\xi^2\right\}e(z,t;\xi)=0$$

as well as zero initial conditions and boundary conditions at $z=0$ and $z=\infty$.

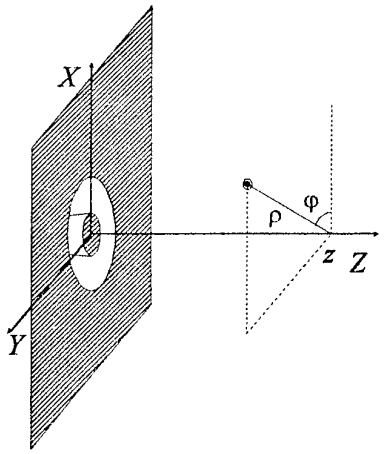


Fig. 1. The problem geometry

For the case of the unit step time dependence of TEM-wave amplitude in the coaxial waveguide taking into account the energy normalization of a field [1] and using the separation of variables method it was obtained in [3] the evolutionary coefficient expansion:

$$e(z,t;\xi)=\left(\frac{2C(\xi)}{-\xi}\right)\sum_{m=0}^{\infty}\left(\frac{ct-z}{ct+z}\right)^{m+\frac{1}{2}}J_{2m+1}\left(\xi\sqrt{c^2t^2-z^2}\right),$$

where

$$C(\xi)=\left(c\mu_0\left[J_0(\xi R)-J_0(\xi r)\right]\sqrt{R^2-r^2}\right)\Big/\sqrt{2\xi\ln(R/r)}.$$

The radiated field at an arbitrary time dependence of the source $f(t)$ one can find by taking the Duhamel

integral. Let $F_0(\vec{r},t)$ be the time dependence of any field component in the observation point $\vec{r} \equiv \vec{r}(\rho,\varphi,z)$ at the antenna excitation by the unit step of current. For the sake of simplicity assume that the point of observation is not arranged in the antenna, and $f(t)$ has no discontinuities. Then the corresponding component of the field at arbitrary time dependence $f(t)$ can be found, according to [4], from formulas:

$$F(\vec{r},t) = \int_0^t f(t-\tau)\dot{F}_0(\vec{r},\tau)d\tau ; \qquad (1)$$

$$F(\vec{r},t) = \int_0^t \dot{f}(t-\tau)F_0(\vec{r},\tau)d\tau . \qquad (2)$$

Formula (2) can be obtained easily from (1) with the help of integration by parts. It is of value to choose from formulas (1) and (2) the most convenient one for numerical calculation in accordance with the form and duration of exciting pulse $f(t)$ and with the form and duration of the transition diagram $F_0(\vec{r},t)$.

EXPERIMENTAL RESEARCH

The block scheme of the experimental set is depicted in Fig. 2. Generator of short pulses (GSP) forms a sequence of triangular videopulses with the amplitude controlled in the range from 1 to 6 kV on the load of 50 Ohm, with duration of 1.2 ns and with the frequency of repetition up to 30 kHz. GSP feeds the coaxial cable with wave impedance of 50 Ohm loaded to CCA with the length of 10 cm and the following aperture sizes: outer diameter is equals to 67 mm, inner diameter is equals to 2 mm.

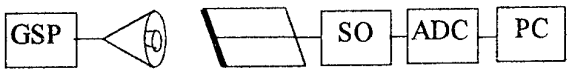


Fig. 2. Block scheme of the set

Radiated videopulse signal is received by special sensor, namely dipole-slotline probe. It is a stub of a slotline on dielectric substrate ($\varepsilon = 4.25$, 1.5 mm thickness) with width of 0.1 mm connected at one end to the coaxial cable with wave impedance of 50 Ohm and soldered at other end to tinmade dipole with sizes 3×20 mm. The over-all dimensions of the probe are 40×90 mm. The necessity of using the dipole-slotline probe consists in the fact that it effectively receives the transversal field component and suppresses the longitudinal one. Several ferrite rings are slipped over the coaxial cable for matching the transition from the slot line to the coaxial cable.

Stroboscopic oscilloscope (SO) C7-13 with the working range from 0 to 10 GHz is exploited in the set to observe and scale the pulses under study. Scaled signal from SO is digitized by ADC and transferred into computer for the processing.

Radiated longitudinal component has a maximum along the axis, whereas the transversal component of the field equals zero along the axis because of the symmetry of the investigated structure about the axis of the coaxial waveguide. The TEM-field structure have the symmetry as well. If the point of observation deflects from the axis in the opposite directions the polarity of the longitudinal component of field does not change but the polarity of the transversal one varies. The specified peculiarities of radiating field are used as the basis for algorithms of the experimental data processing.

Despite the using of the tailormade probe, it receives the longitudinal and the transversal components of field simultaneously. However, one can pick out the transversal and the longitudinal components from received signal by account the above mentioned peculiarities of the field. The points of observation are offset by 6 cm from the aperture of CCA and by ± 1, ± 3 и ± 6 cm from the axis. If two signals received in the points with the opposite deflections from the axis are added (averaged), we get the longitudinal component of the field. If one of them is subtracted from another we obtain the transversal component.

RESULTS

Experimental (thin lines with signs) and corresponding calculated curves (solid lines) obtained by formula (2) for the transversal electric component of the field radiated by CCA are depicted in Fig. 3. The experimental and computed time dependencies of the longitudinal electric component in the same points are illustrated in Fig. 4.

Notice that minor chaotic deviations of the estimated dependencies are not connected with computation errors. Since the measurements are carried out in the near zone of radiator, the amplitude of the longitudinal component of the field is comparable or greater than the transversal one. It can be some explanation of a weak dependence on ρ connected with size and excessive sensitivity of the sensor for the longitudinal component of field.

CONCLUSIONS

For the first time a theoretical solution obtained by Method of Evolutionary Equations is verified experimentally.

Satisfactory agreement of experimental and calculated curves demonstrates the validity of using the model of waveguide aperture with infinite flange for the description of the radiation from waveguide aperture without flange.

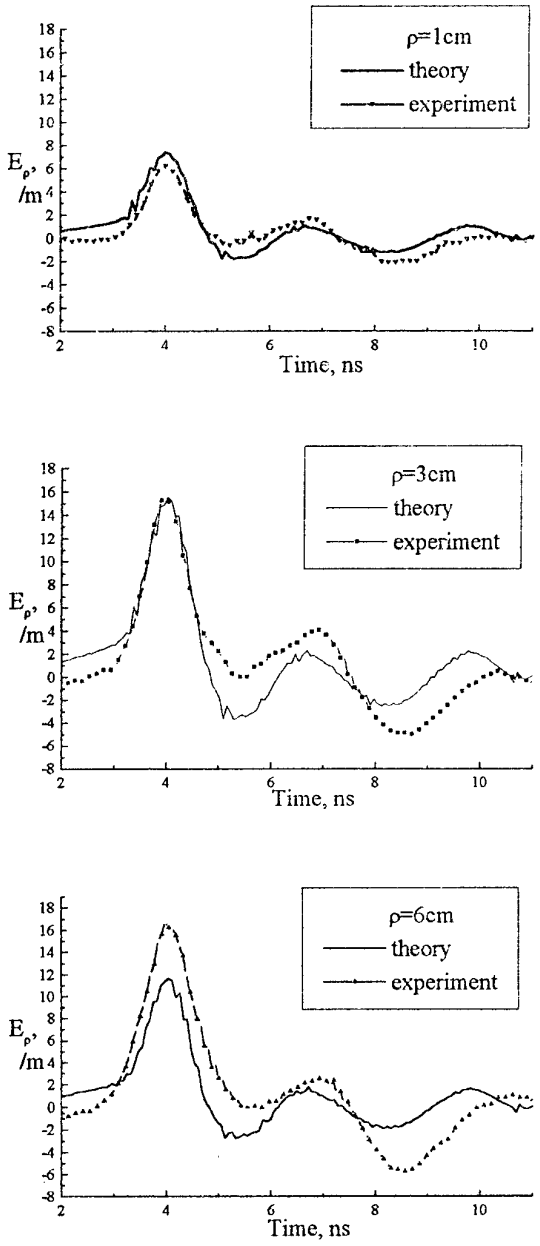


Fig. 3. Time dependencies of the transversal electric field strength in points $z = 6$ cm, $\rho = 1,3,6$ cm. Experimental curves are denoted by signs

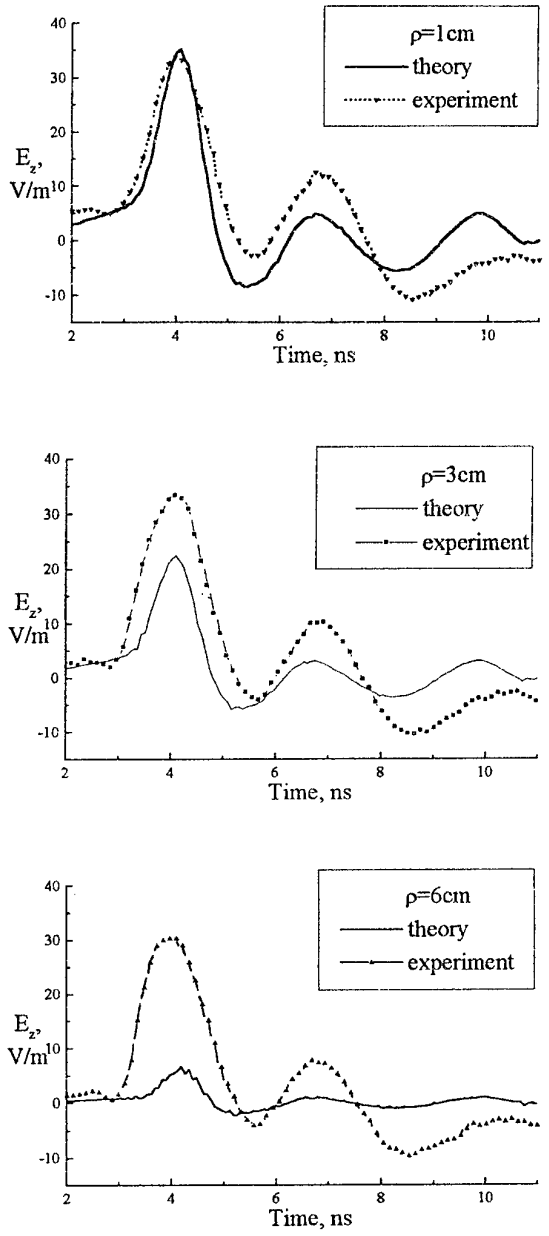


Fig. 4. Time dependencies of the longitudinal electric field strength in points $z = 6$ cm, $\rho = 1,3,6$ cm

Application of Duhamel integral for solving the problem of videopulse radiation by known transition diagram of radiators is the rather suitable technique provided that the time dependence of exciting current is given precisely.

REFERENCES

1. Tretyakov O.A. Modal Basis Method // Radiotehnika i elektronika, 1986, v.31, P. 1071-1082 [in Russian].
2. Lamensdorf D. The Transient Response of the Coaxial Cone Antenna // IEEE Trans. On Antennas and Propagation, 1970, vol.AP-18, N6, P. 799-802.
3. Dumin A.N. Transient field radiation from the aperture of coaxial waveguide with infinite flange // Vestnik Khar'kovskogo universiteta. Radiofizika i elektronika, 1998. P. 52-55 [in Russian].
4. Kharkevich A.A. Transient wave phenomena, Gos. izd-vo teh.-teor. lit-ri, Moskow, 1950, 202 p. [in Russian].

PROPAGATION OF SHORT PULSES IN LOSSY LONG LINES

A. L. Gutman, A. N. Manko

Voronezh State Forest Engineering Academy, Physics Chair
394613, Voronezh, Timirjazev Street, 8
E-mail: olc@ns.vglta.ac.ru

INTRODUCTION

The present work is the continuation of the investigations performed by the authors [1,2] of the processes of the electromagnetic waves oscillations in different media.

Passing of the short pulses through the elements of the antenna-feeder devices (AFD) presents particular interest, when the pulse duration becomes commensurable with the characteristic times of setting the processes of the electromagnetic wave propagation in the long lines.

For the investigation of these processes the authors use the traditional parameters of the long line; *R, L, C, G* – line, corresponding to impedance, inductance, capacity, conductivity of the long line, predestining the functional purpose of the path elements.

SHORT PULSE PROPAGATION

The general definition of the space-time Green function [3] is given by the following expression

$$g(z,t)=\frac{1}{2\pi}\int_{-\infty}^{\infty}e^{i[h(\omega)z-\omega t]}d\omega \qquad (1)$$

In order to take into account the dispersion and attenuation by the function $h(\omega)$ in (1), it is necessary to introduce the complex frequencies ($\omega = \omega + {}^{3}\alpha$, i = v-1), i.e.

$$h(\omega)=\frac{\omega+i\alpha}{c}\sqrt{1+\frac{\gamma^2}{(\omega+i\alpha)^2}},\quad (\alpha\ge\gamma\ge 0), \qquad (2)$$

where

$$\alpha=\frac{1}{2}\left(\frac{G}{C}+\frac{R}{L}\right)\qquad ;\gamma=\frac{1}{2}\left(\frac{G}{C}-\frac{R}{L}\right).$$

The expression of the pulse and its propagation in antenna-feeder devices is connected with Green function in the following way [3].

$$f(z,t)=\int_{-\infty}^{\infty}g(z,t-\bar{t})f(0,\bar{t})\,d\bar{t}, \qquad (3)$$

where

$$f(0,t)=f(z,t)\,|_{z=0}. \qquad (4)$$

is the form of the signal at the input of the antenna-feeder devices.

The explicit expression for the Green function in the long line is

$$g(z,t)=\delta(t-\frac{z}{c})e^{\alpha t}+\frac{\gamma z I_1(\gamma\sqrt{t^2-z^2/c^2})}{c\sqrt{t^2-z^2/c^2}}e^{\alpha t}, \qquad (5)$$

where $g(0,t)=\delta(t)$, $\delta(t)$ is the Dirac (delta) function, $t = z/c$.

According to (3) the ratio of the pulse duration is obtained

$$f(z,t)=f(0,t-\frac{z}{c})e^{-\alpha\frac{z}{c}}+ \qquad (6)$$
$$+\int_{0}^{t-\frac{z}{c}}\frac{\gamma z e^{-\alpha(t-\bar{t})}f(0,\bar{t})}{c\sqrt{(t-\bar{t})^2-z^2/c^2}}I_1\left(\gamma\sqrt{(t-\bar{t})^2-z^2/c^2}\right)d\bar{t}$$

Each term in (6) contributes to the distortion of the initial signal form to different extent, at different time moments, at different distances from the antenna-feeder devices feed point, i. e. two mechanisms of setting the oscillation process can be investigated.

The first term in (6) in the form of the product of two functions (the input signal and attenuation) corresponds to mechanism of signal distortion and characterizes the quality factor (α) of the line. Structurely one and the same antenna-feeder device changes the signals under consideration of different forms and durations to different extent.

The second term in (6) describes the distortions, depending on α and selectivity (γ) of antenna-feeder device.

The analysis of the signal form change in the setting phase can be simplified, when considering the three-dimensional representations as a set of particular independent sections:

$$f(z,t)=f(z)|t=ti\ ,\ f(z,t)=f(t)|z=zj\ ,$$

where $i=0,1,2...N$; $j=0,1,2...M$; $ti=\Delta t.i$; $zj=\Delta z.j$; N and M – the number of the particular sections $f(z,t)$.

PROPAGATION OF RECTANGULAR PULSE

Let's consider one form of short videopulse:

$$f(0,t)=\begin{cases}0, & t<0,\\ \sigma(t)-\sigma(t-T), & t\geq 0,\end{cases} \tag{7}$$

where $\sigma(t)$ is the Heaviside function.

If the following non-dimensional parameters:

$$\theta=\gamma t,\xi=\gamma\frac{z}{c},\eta=\frac{\alpha}{\gamma},\tau=\gamma T, \tag{8}$$

are introduced, the relationship can be obtained for the pulse propagation in the long line, taking into account the losses (η) :

$$f(\xi,\theta)=\sigma(\theta-\xi)e^{-\eta\xi}-\sigma(\theta-\tau-\xi)e^{-\eta(\xi-\tau)}+$$
$$+\xi\int_{1}^{\frac{\theta}{\xi}}e^{-\eta\xi x}\frac{I_1(\xi\sqrt{x^2-1})}{\sqrt{x^2-1}}dx- \tag{9}$$
$$-\xi\int_{1}^{\frac{\theta-\tau}{\xi}}e^{-\eta\xi\chi}\frac{I_1(\xi\sqrt{x^2-1})}{\sqrt{x^2-1}}dx$$

From (9) it is seen, that the symmetry of the pulse is violated due to the distortion of the back front of the pulse at its propagation.

The computation results for the rectangular pulses propagation (τ=2.7, η=1.1) in the long line are shown in figures. In Fig.1 the set of function is shown (9) in the form of the equal field levels, illustrating the dynamics of the propagation process of the pulse in the non-dimensional coordinates (ξ,θ).

In Fig. 2 the fragment of those parts of the surface $f(\xi,\theta)$ is presented, where the most essential changes of the initial form of the rectangular pulse can be observed. The differences of the level forms of the equal field in Fig. 1 and Fig. 2 are explained by diminishing (by same times) of the step at calculation of $f(\xi,\theta)$.

CONCLUSION

The possibities of using the space-time Green function for the examination of the short pulse propagation in long lines were discussed. The Green function application reduces a boundary-initial problem to an integral calculation. The usefulness of this way is determined by the possibility of exact construction of simple enough Green function and by the convenience of calculation of the obtained integrals. For the long line an explicit form of Green function can be expressed exactly through the known functions. The rectangular pulse propagation was observed. Two peculiar parts of the field are here: the first part propagates with light velocity. The magnitude of the first part may be essentially more than second one. The field decays at great enough range and time, but a sharp field growth itself detected in some interval of the range despite of the losses. This is stipulated by an interference. The pulse form noticeably changes with attenuation change.

REFERENCES

1. A. L. Gutman. Space-time Green Function and short pulse propagation in different media. 11 th. International Conference on High-Power Electromagnetics: EUROEM'98, Tel Aviv, Israel, june 1998.
2. A. L. Gutman, A. N. Manko. Propagation of short pulses in wave guides and long lines. The materials of the IV-th International scientific-engineering conference "Antenna-feeder devices, systems and techniques of radiocommunication". Voronezh, may 1999 (in print) [in Russian].
3. L. A. Vainstein. Propagation of pulses. UFN, 1976, v. 118 is 2, pp. 339-367 [in Russian].

ANTENNA SYSTEM FOR GEORADAR "ZOND - 10" CONSISTING OF A PAIR OF CURVED LOADED WIDEBAND DIPOLES[1]

S. A. Masalov, G. P. Pochanin, P. V. Kholod

Usikov's Institute for Radiophysics and Electronics of National Academy of Sciences of Ukraine,
12 Acad. Proskury St., Kharkov 310085, Ukraine. Tel. (0572) 448634. Fax. (0572) 441105
E-mail: masalov@ire.kharkov.ua; gpp@ire.kharkov.ua; kholod@ire.kharkov.ua

INTRODUCTION

The main characteristics defining a resolution and penetration depth of modern ground penetrating radar (GPR) are wide frequency band of radiated signals and high efficiency and uniformity of radiation through the whole working frequency range. Electrical parameters of a ground vary within a wide range. However, the main part of them has such a value that the pulse signals of nanosecond duration range corresponding to the frequency range from tens MHz to units GHz are optimal for several meters depth of sounding. On the one hand, such a signals allow to obtain a resolution about 10 cm, on the other hand to sound down to the several meters depth. As a rule, it suffice to solve a wide range of problems.

A design of an improved antenna system for GPR "Zond 10" produced by firm "Radar, Inc.", Riga, Republic of Latvia is discussed in the presentation. Advantage of the new antenna system is decreased duration of the after pulse oscillation with the energetic characteristics of the ground penetrating radar remaining the same.

ANTENNA DESIGN

There is a number of requirements to the antenna system. These are high efficiency of radiation/reception of electromagnetic waves combined with low level of after pulse oscillations. (Directivity of the radiation pattern is not relevant hence the depth of sounding is limited by several meters.) In order to satisfy these contradicting requirements we have developed and fabricated and experimentally tested a wide band dipole antenna system loaded with a matching load at the ends (Fig. 1).

This antenna system may be classified as an electromagnetic type antenna [1]. The main advantage of this class antennas is the possibility to generate a traveling wave mode in spite of relatively small dimensions of antenna. It is the mode that provides the one way traveling for the driving current wave and thus decreasing the amplitude and duration of after pulse oscillations.

The curved shape of the dipole elements, each of them being a half-circle, enables one to increase the lengths of the dipole arms. These allowed decreasing the low working frequency of the antenna significantly. The matched load (resistor R = 360Ω) at the ends of the dipole allows to absorb the whole non-radiated energy and significantly decrease the amplitude of the reflected wave. For the most efficient driving of the antenna the dipole arms were made in form of plates of varying width.

A pulse generator circuit with avalanche transistor switch with transistor 2N2222 was used to drive the transmitting antenna.

The ultra wide band transformer on transmission lines was used to match the antenna impedance and output impedance of the pulse generator. The frequency band of this transformer ranges from 10 MHz to 300 MHz. The transformation ratio on impedance is 4. Energy losses are less then 0.8 dB. The efficiency of radiation was enhanced and the amplitude and duration of the after pulse oscillations decreased owing to the correctly chosen design of the antenna arms.

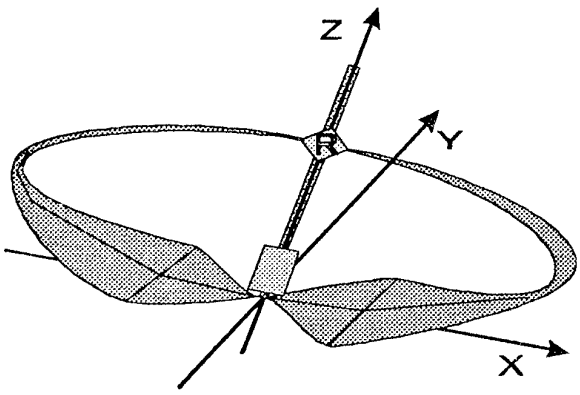
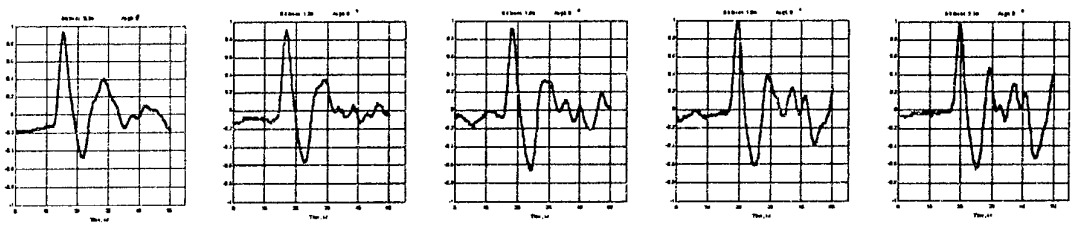


Fig. 1. Antenna system for the ground penetrating radar

[1] This work was supported by Science and Technology Center in Ukraine (project no.366).



$D = 0.9$ m $D = 1.2$ m $D = 1.5$ m $D = 1.2$m $D = 1.5$ m

Fig. 2. The dependence of shape of the radiated signal from distance to radiating antenna in direction of maximum energy radiation. (Horizontal scale is 10 ns/div)

SPATIAL CHARACTERISTICS OF ANTENNAS

Relations between the shape of the radiated signal and the distance between the sensor and radiating antenna are shown at Fig. 2.

The impulse of radiated electromagnetic wave has a form of a damped oscillations with a period about 10 ns and consist of 3 half periods of a sinusoid. In the near zone of antenna the amplitude of the first half period exceeds that of the second half period larger twice as much. The amplitudes of the first and the second half periods tend to 1 with a larger distance and at a distance more then 1.5 m they equal 1.

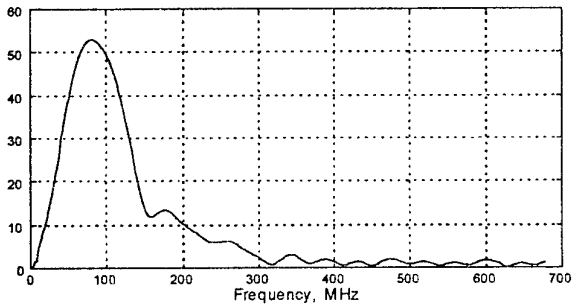


Fig. 3. The amplitude spectrum of radiated signal

The maximum of the amplitude spectrum of the radiated signal comes near 80 MHz. The lobe of the high frequency component is about 0.1 of the maximum amplitude. A distinction of this spectrum is absence of the gaps in the frequency response in the frequency band more then 300 MHz.

Relations between the radiated field shape and the direction of radiation by rotation of radiator in XZ- and YZ-planes (Fig. 4) show that this radiator behaves similarly to the electrical dipole, but this antenna unlike an ordinary dipole has a directional properties conditioned by the curved arms. The corresponding radiation patterns are shown at Fig. 5.

The shape of the radiated signals at Fig. 4b are similarly to the oscillations because of reflection from walls and floor following just after pulse radiated SP signal. This confirmed by distinction between the shapes of signals corresponding to angles 0° and 180° and clear pulses at Fig. 2.

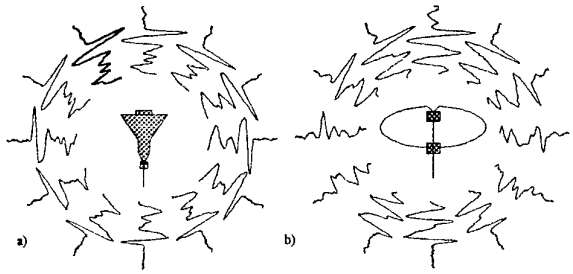


Fig. 4 Relations between the radiated field shape and direction of radiation at the distance 1.5 m in a) YZ-plane, b) XZ-plane

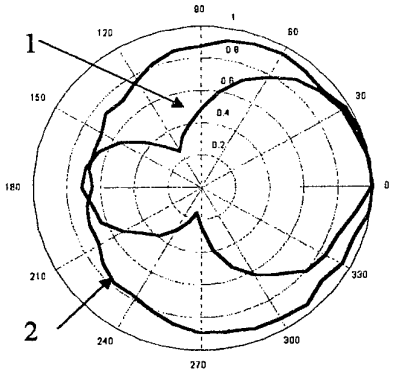


Fig. 5. Amplitude radiation pattern for loaded wide band dipole in XZ (line 1) and YZ (line 2) planes

The same design of the antenna is used for receiving reflected signals. The main advantage of such an antenna in the receiving mode is a decreased level of the after pulse oscillations owing to good matching both at the driving area and at the ends of the antenna.

The signal induced at the output of the receiving antenna after receiving the signal radiated by the transmitting antenna which located at the distance 2.2 m with the antennas being directed by the maximums of radiation patterns is shown at Fig. 6. The pulse signal

beginning at about 35 ns is conditioned by reflections of radiated signal from the walls of laboratory. The after pulse oscillations are negligible.

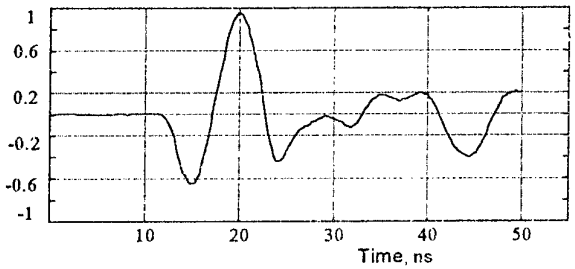


Fig. 6. The shape of signal received by receiving antenna of radar

Fig. 7 shows the signals at the output of the receiving antenna of the ground penetrating radar which were recorded while sounding. The dot line corresponds to the signal from "Zond's 10" antennas and the solid line corresponds to signal from loaded wide-band dipole antenna system. As the transmitting and receiving antennas are disposed in parallel planes at a distance 2 m (see Fig. 1), the coupling between these antennas is significant. It causes an additional half period of oscillation in the received signal. Therefore, the signal shapes at Fig. 6 and Fig. 7 are different.

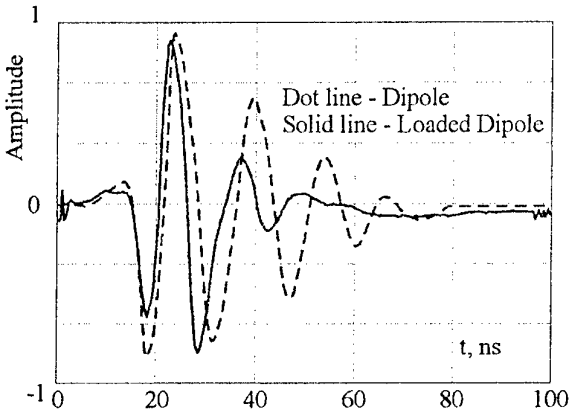


Fig. 7. Dot line correscponds to signal from "Zond's 10" antennas, and solid line — to signals from the loaded wide band dipole antenna system

Nevertheless, it is evident, that the loaded dipoles suppress the after pulse oscillations and promote improving the resolution of the ground penetrating radar.

CONCLUSIONS

The design of the loaded wide-band dipole antenna system with a matching load at the ends (Fig. 1) was fabricated and experimentally tested. The spatial distribution of the shape of radiated signals in the near and far zones is measured and shown.

The antenna is characterized by:

- VSWR in frequency band from 10 MHz to 300 MHz never exceeding 3;
- input impedance is 200 Ω;
- output impedance is 50 Ω;
- width of radiation pattern at the level 0.5 of the amplitude value:
- in XZ plane is 170°;
- in YZ plane is 360°;
- the signal radiated has a form of 3 half periods sinusoid of 10 ns duration;
- overall dimensions are 1100×230×500 mm.

Antenna system consisting of the loaded wide band dipoles was used in practice for mapping the subsurface communications. The antenna system demonstrates enhanced resolution and penetration depth.

REFERENCE

1. Pochanin G.P. UWB/SP antennas classification. / International Symposium "Physics and Engineering of Millimeter and Submillimeter Waves.", June 7-10, 1994, Kharkov, Ukraine, conference proceedings, v.3, p. 549-550.

NOVEL APPROACHES TO THE ANALYSIS AND MODEL SYNTHESIS OF ULTRA-WIDE-BAND HORN-TYPE ANTENNAS

A. O. Perov, Yu. K. Sirenko, A. E. Yaldiz*

IRE of National Academy of Sciences of Ukraine, 12, Acad. Proscura St., Kharkov, 310085, Ukraine
Tel.: 38(0572)448475. Fax: 38(0572)441105. E-mail: sirenko@ire.kharkov.ua
* GYTE, Gebze/Kocaely, PK 141, 41400, Turkey
Tel.: 90(0262)6538497. Fax: 90(0262)6538490. E-mail: yaldiz@yunus.mam.gov.tr

Model problems in the theory of ultra-wide-band horn-type antennas are initial boundary value problems in infinite domains with locally inhomogeneous and perfectly conducting compact scattering objects. The key to their efficient solution lies in the correct truncation of a computational domain, which on the one hand, reduces the fundamentally open problem to the closed one, and on the other hand, has little or no effect on the accuracy and reliability of resulting numerical data. The above-listed criteria are consistent and practicable as clearly demonstrated by the results of the papers [1, 2] devoted to a study of a similar issue in classical problems of nonstationary electrodynamics (waveguide inhomogeneities and periodic structures) and in some model problems of video pulse sensing (locally inhomogeneous objects in a free space or near a locally irregular boundary between two homogeneous media). Developing this topical subject for the modern computational electrodynamics, we turn in our work to the problems of the analysis and model synthesis of ultra-wide-band horn-type antennas (see Fig.).

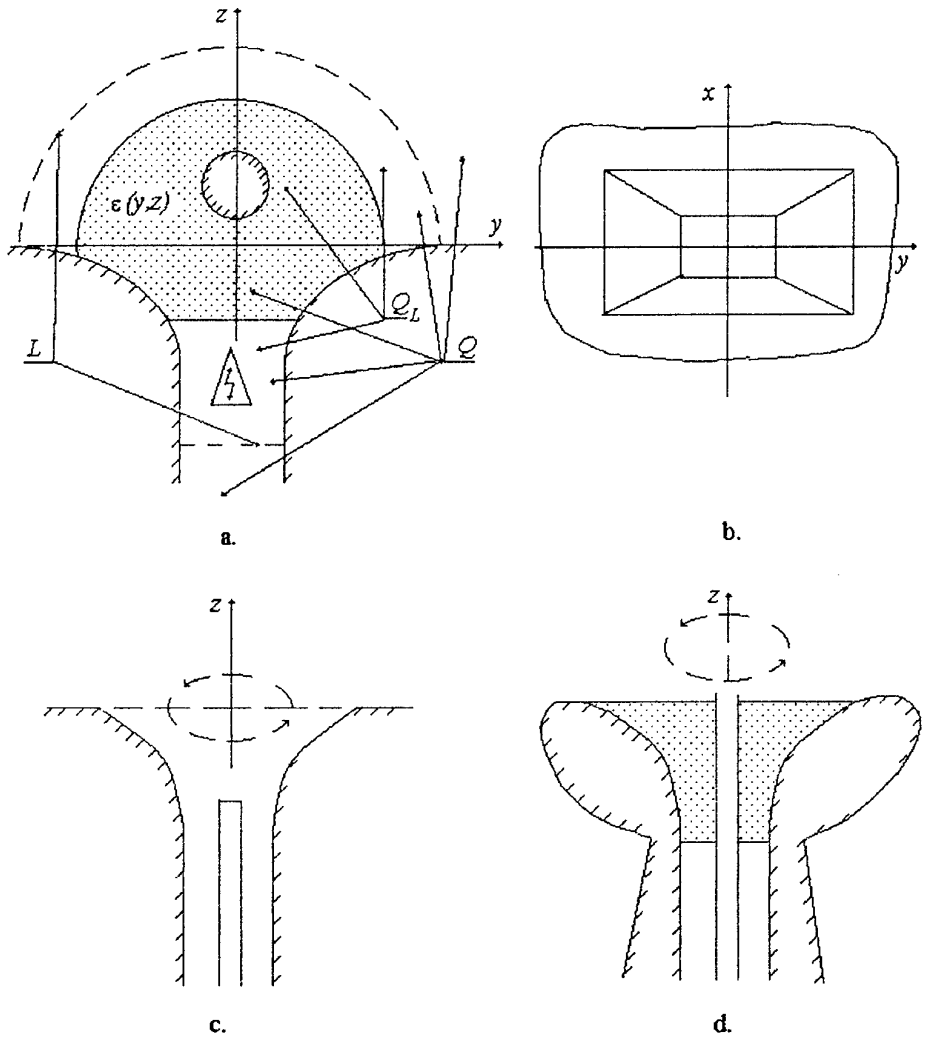


Fig. The model problem geometry

The first and the crucial step in their solution is connected with the formulation of exact radiation conditions for nonsinusoidal waves «outgoing» from the region $Q_L \subset Q$, where the efficient sources and scatterers are concentrated. Q is an infinite domain in two- or three-dimensional space where the initial boundary value problem is posed. The first step is largely based on integral transformations in a space of «evolutionary bases» [3] of nonstationary signals. The constructed exact radiation conditions are used then as additional boundary ones (on virtual coordinate boundaries L of the regions Q_L), which truncate efficiently a computational domain in conventional finite-difference methods. An important point is that the reformulated initial boundary value problem is fully equivalent to the original one. Not only does the theorem about single-valued solvability remain valid, but also the solutions coincide. The additional conditions on virtual boundaries are included correctly into a computational scheme of a finite-difference method without making it more complicated or distorting its stability and convergence. As a result we obtain the algorithm, which is every bit as simple and «fast» as in the case of classical closed problems. The problem of a truncation of a computational domain (in distinction to the approaches using Absorbing Boundary Conditions of different approximation orders [4]) is solved without distortion of physical essence of the processes simulated mathematically. The computational error is conditioned only by the discretization of the initial boundary value problem and can be estimated either «roughly» analytically or precisely by the results of specially aided computational experiments.

This work was partly supported by the Grant №336 of STCU.

REFERENCES

1. A.O. Perov and Y.K. Sirenko, "Nonstationary model problems in electrodinamic theory of grattings", Radiofizika i Elektronika, Vol. 2, № 2, pp. 66-86, 1997.

2. N.N. Naumenko, A.O. Perov, H. Akdogan and E. Yaldiz, "Exact conditions for the truncation of the computational domain of finite-difference methods in model problems of pulse sensing", Electromagnitye Volny i Electronnye Sistemy (to be published).

3. Y. K. Sirenko, V.P. Shestopalov, and N.P. Yashina, "New Methods in the Dynamic Linear Theory of Open Waveguide Resonators", Comp. Math. And Math. Physics, Vol. 37, № 7, pp. 869-877, 1997.

4. K. L. Shlager and J. B. Schneider, "A Selective Survey of the Finite-Difference Time-Domain Literature", Ant. and Prop. Magazin, Vol. 37, № 4, pp. 39-57, 1995.

MULTIBAND ANTENNAS ON LOOP RADIATORS

Y. A. Rensh

State Enterprise "Vector"
Gagarina str. 28, Ekaterinburg, 620078, Russia
Phone (3432) 754248, e-mail: vector@vector.mplik.ru

INTRODUCTION

In this paper the results are presented of designing multiband antennas on the base of a main model with loop radiating elements intended for functioning in very-high frequency range (VHF) and ultrahigh frequency range (UHF) in of communication and TV systems.

The base model is performed in the form of loop-slot antenna (LSA) comprising two identical loop radiators (LR) located in one plane in opposition to each other.

The LRs have a common axis of symmetry and are connected by a section of symmetrical slot line (SSL) with length L. At $L \approx 0$ the LSA is analogous to a "zigzag" antenna.

Points of the connection of the coaxial feeder are situated in the middle of SSL; slot gap is excited with a coupling loop. Matching of LSA performed by the choice of length L and SSL wave resistance, as well as by the distance to the reflector. With the bandwidth relation up to 1.6:1 it is possible to obtain VSWR <1.5 .

DESIGN AND CHARACTERISTICS

1. Loop-dipole antenna

The antenna functions in the first and second separated subranges with average wavelengths $\lambda_1 > \lambda_2$. It comprises base LSA of the second subrange, in which SSL is in the orthogonal plane and a flat wideband dipole (Fig. 1). The arms of the dipole are oriented perpendicularly to axis of vibration of LSA, connected to the middle of SSL and are antiphase with respect to LR conductors [1].

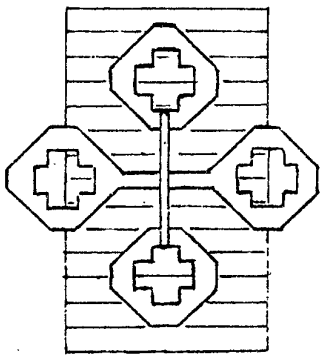


Fig. 1

LSA does not radiate in the first subrange because the perimeter of LR is less than λ_1. That is why in the first subrange the LR may be in the form of short-circuited segments of a 2-conductor line with variable distance between the conductors and with length of half the perimeter, that is 0.5 λ_2.

When condition $\lambda_1 \approx 2L + 2\lambda_2$ is satisfied, the input impedance of LR re-calculated according to the middle of SSL is equal to infinity, and LSA does not affect the function of the dipole in the first subrange.

A value of L can change within the limits of $\lambda_2 < L < 0.8\,\lambda_2$ what enables to choose the relation between λ_1 and λ_2.

The dipole does not radiate in the second subrange because the field of these frequences is closed between dipole arms and LR antiphase conductors. The input impedance of the dipole in the second subrange is much higher than that of SLA. The dipole influences on the LSA functioning when the antiphaseness is broken, i.e. at peripheries of the second subrange bandwidth. Various forms of the dipole arms may be used, but the form similar the loop radiators is preferable.

Fig. 2 presents the frequency dependence of the matching of a loop-dipole antenna intended for functioning in VHF and UHF of TV band. In the second subrange (UHF) at the bandwidth of 450 to 800 MHz, VSWR < 1.8. In the first subrange (VHF) at the bandwidth of 150 to 250 MHz, VSWR < 2.0. The gain in the second subrange is not less than 7 to 9 dB (with a reflector), and in the first one equals to the dipole gain (without reflector).

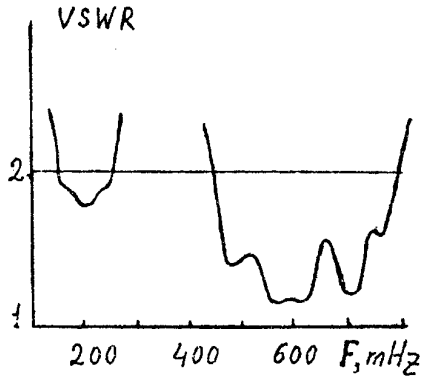


Fig. 2

2. A dual-band loop-slot antenna

The antenna functions in the first and second separated subranges with average wavelengths related as $\lambda_1 \approx 2\lambda_2$.

It comprises the base LSA of the first subrange. In the LR conductors at points of current loop there is a gap. A short-circuited piece of a double line with the length of about $0.25\lambda_2$ is connected in the gap (Fig. 3).

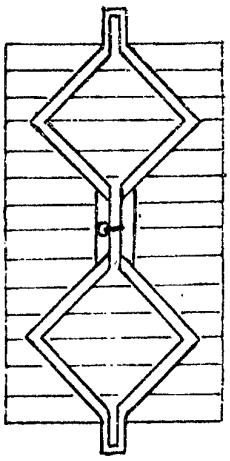


Fig. 3

In the second subrange LRs have a dual-mode perimeter and the LR conductors radiate inphase. In the first subrange LRs have a single-mode perimeter with capacitive inhomogeneity at current loop.

The bandwidth in the second subrange is limited on the side of high frequences due to gin drop. On the side of lower frequences the bandwidth is limited due to the VSWR increase which one can not compensate by choosing SSL parameters. In the bandwidth of up to relation 1.5:1 the gain drop does not exceed 1 to 2 dB. The matching values in both subranges are interconnected and depend on SSL dimensions and the distance to the reflector.

Fig. 4 shows the frequency dependence of matching. In the subranges of 210 to 330 MHz and 410 to 630 MHz VSWR is less than 1.8.

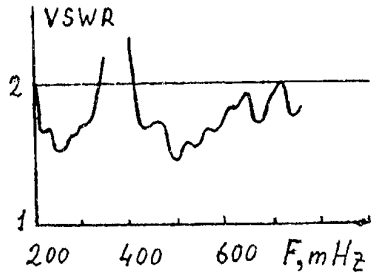


Fig. 4

3. Multiband loop-slot antenna

The antenna is intended for functioning in N separated subranges with average wavelengths $\lambda_1 > \lambda_2 > \ldots > \lambda_N$. It is designed in the form of N base LSAs of different dimensions with common SSL (Fig. 5). LRs with even numbers are connected in SSL antipsahe relative to the neighbouring odd LRs. In this case the axial symmetry of all LRs is observed [2].

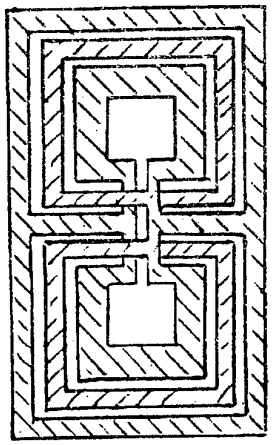


Fig. 5

The antenna functions as follows. The maximum bandwidth of one LSA does not exceed 1.7:1. This limit is kept in the case of several LRs of different sizes connected in phase in SSL. In the case of antiphase connection in SSL of neighboring LRs of different sizes the limit of summary bandwidth is eliminated. And the maximum bandwidth attained by individual LRs is maintained.

Fig. 6 presents the frequency dependence of matching multiband LSA comprising three LSAs (three subranges) with individual LSAs located at different distances from the reflector.

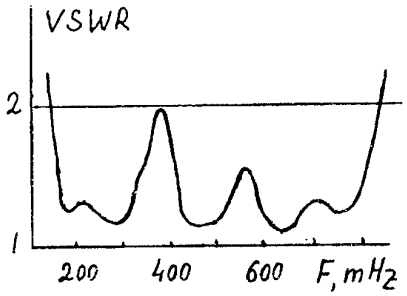


Fig. 6

The frequency coverage of 4.5:1 (from 170 to 770 MHz) with VSWR < 2 is provided.

CONCLUSION

The given above material illustrates great possibilities of loop-slot antennas for extension of working frequency range. The simplicity of design, the possibility of calculation and modeling make them indispensable for different areas of application.

REFERENCES

1. Patent No 8527 (Russia). The useful model. Joint dipole-loop antenna.
2. Patent No 8527 (Russia). The useful model. Multiband loop antenna.

FDTD ANALYSIS OF LOG-PERIODIC FLAT DIPOLE ANTENNAS

A. E. Shrenk

National Technical University of Ukraine "KPI", Laboratory of Antennas and Telecommunications,
2110D, Radio Engineering Faculty, Polytekhnichna st., 12, Kyiv, 252056, Ukraine
Tel/Fax: 380-44-2417223 e-mail: a_tlab@ucl.kiev.ua

INTRODUCTION

LPDA are now widely used for TV, broadcasting and communication in frequency range 100MHz...4GHz. The stand-point of the advantages of this type of antennas is the possibility to achieve permanently high gain in broad band. Up to the early 90th full-series production of LPDA use the technology of welding of metal tubes of different length and diameters. Obtained metal contacts were not reliable or otherwise were too expensive. Especially this regards to the cases when antenna gain is 10dB and more in broad band. The step forward in LPDA-building was made by proposal of new technology [1], which allows to increase reliability of antenna and to reproduce the geometry parameters of LPDA with precision not worth than 0.1 mm. Before, most of investigators used method of moments for LPDA modelling. Antenna model was consist of infinitely thin wires connected by hypothetical transmission line in free space. Results were obtained by numerical solution of integral equation for the currents and voltages on vibrators.

In this paper a new analysis based on FDTD method is presented. No specific simplification in antenna simulation were made. All geometrical features of LPDA, such as exact forms of dipoles and transmission line, the excitation (which is found to be non-symmetrical towards the transmission line in reality), part of transmission line between point of excitation and the smallest dipole, geometry of electrical short, have been taken into account. This was the main reason for applying FDTD method.

Application of FDTD method. Maxwell's curl equations in the lossless, source free, isotropic region can be expressed as:

$$-\mu\frac{\partial\vec{H}}{\partial t}=\nabla\times\vec{E},\quad \varepsilon\frac{\partial\vec{E}}{\partial t}=\nabla\times\vec{H},$$

where ε,μ are the constitutive parameters, and $\vec{E},\vec{H}$ are the electric and magnetic fields, respectively. In rectangular coordinates the two vector equations can be decomposed into six scalar equations for E_x,E_y,E_z,H_x,H_y,H_z components. For example, for the first component:

$$\frac{\partial E_x}{\partial t}=\frac{1}{\varepsilon}\left[\frac{\partial H_z}{\partial y}-\frac{\partial H_y}{\partial z}\right]. \qquad (1)$$

According to FDTD method the computational domain is discretised, partial derivatives are changed by central differences using standard Yee notification [3]. In this work the non-uniform mesh grading is used to reduce the memory storage and computer run-time. As it has been shown in [4] if the mesh grading factor $q < 1.2$ the accuracy of non-uniform mesh is close to the accuracy of fine uniform mesh. Fundamental equations for FDTD method can de deduced from equations like (1) as follows:

$$E_x^{n+1}(i,j,k)=E_x^n(i,j,k)+\frac{2\cdot\Delta t}{\varepsilon\left(\Delta y_j+\Delta y_{j-1}\right)}\times$$

$$\left[H_z^{n+1/2}(i,j,k)-H_z^{n+1/2}(i,j-1,k)\right]$$

$$-\frac{2\cdot\Delta t}{\varepsilon(\Delta z_k+\Delta z_{k-1})}\left[H_y^{n+1/2}(i,j,k)-H_y^{n+1/2}(i,j,k-1)\right];$$

$$H_x^{n+1/2}(i,j,k)=H_x^{n-1/2}(i,j,k)-\frac{\Delta t}{\mu\cdot\Delta y_j}\times$$

$$\left[E_z^n(i,j+1,k)-E_z^n(i,j,k)\right]+\frac{\Delta t}{\mu\cdot\Delta z_k}\times$$

$$\left[E_y^n(i,j,k+1)-E_y^n(i,j,k)\right];$$

where i, j, k are the numbers of cells in x, y and z directions respectively. Other four equation to be rearranged similarly. Courant stability criterion for the smallest values of $\Delta x,\Delta y,\Delta z$ defined the maximum possible value of time step Δt. The "soft" voltage source was implemented to the delta gap between the contact pin and the upper part of transmission line. Current and voltage trough the source in the non-uniform mesh grading case can be found according to the formulas:

$$I_S^{n+1/2}(i,j,k+1/2)=\frac{\Delta y_j+\Delta y_{j-1}}{2}$$

$$\left[H_y^{n+1/2}(i+1/2,j,k+1/2)-H_y^{n+1/2}(i-1/2,j,k+1/2)\right]-$$

$$\frac{\Delta x_i+\Delta x_{i-1}}{2}\left[H_x^{n+1/2}(i,j+1/2,k+1/2)-H_x^{n+1/2}(i,j-1/2,k+1/2)\right]$$

$$E_S^n(i,j,k)=V_S(n\Delta t)/\Delta z+I_S^{n-1/2}R_S/\Delta z,$$

where R_S is a internal impedance of voltage source and the E_S is the electric field on antenna at the delta-gap of excitation. In this simulation the excitation voltage of the source $V_S(t)$ is chosen to be two periods of sinusoid on desired frequency.

To truncate the computational domain the Mur's second order absorbing boundary conditions for the non-uniform mesh were used. Modelling object was surrounded by the closed surface, the running Fourier transform is done during time domain calculations to obtain the distribution of tangential E and H fields on desired frequency on this surface. The time shift of half time step between the E and H fields in formulas (2) is taken into account. Then after the standard near-to-far zone transformation in frequency domain [5] the radiation characteristics of LPDA were found.

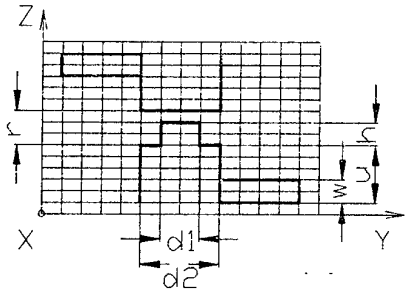


Fig. 1. Front view of novel LPDA
(only the smallest pair of dipoles is shown)

NUMERICAL RESULTS

Above analysis was implemented to the high efficient 10 element LPDA (see Fig. 1 and [1]) with parameters: $\tau = 0{,}935$, $\sigma = 0{,}186$, the length of the longest dipole is 140 mm, the geometry of transmission line $d2$ = 21 mm, r = 18 mm, u = 21 mm, the width of the contact pin $d1$ = 6 mm, the height of contact pin h = 15 mm, the width of dipole w = 15 mm. The "soft" voltage source was used with internal impedance 50Ω. Non-uniform mesh was used with q = 1.1 and total dimension $120\Delta x \times 330\Delta y \times 120\Delta z$. The finest resolution corresponds to the metal edges of LPDA. Antenna is based on elements which are physically highly resonant. Of course the implementation of "soft" voltage source decrease the required number of time steps. But as it seen from Fig. 2 nearly 18 thousands of time steps need to vanish the FDTD fields. Theoretically this curve can be obtained after the frequency domain analysis of LPDA, when the it is known the complex input impedance of LPDA in frequency range $Z(\varpi)$, according to the formula:

$$E_S(t) = F^{-1}\left(\frac{V_S(\varpi)}{\Delta z} \cdot \frac{Z(\varpi)}{R_S + Z(\varpi)}\right) \qquad (2)$$

here $V_S(\varpi)$ is spectrum of excitation and F^{-1} indicates backward Fourier transform. In time domain this also can be calculated after convolution of $V_S(t)$ and $F^{-1}\left(\frac{Z(\varpi)}{Z(\omega)+R_S}\right)$. Physically last function is delta-pulse response of LPDA, excited by "soft" voltage source.

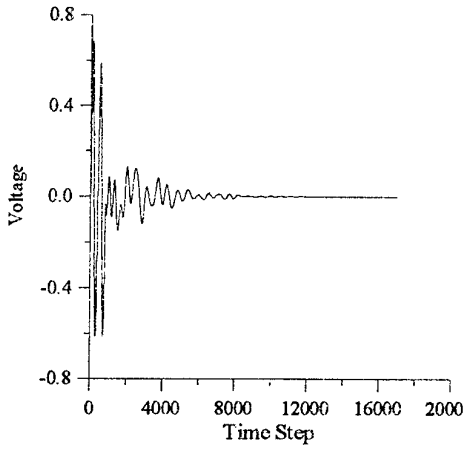


Fig. 2

Calculated after FDTD method values of VSWR in frequency range are compared with measurement and results after NEC on Fig. 3, obtained radiation patterns for the frequency 500 MHz in E- and H-plane given on Fig. 4 and 5 respectively.

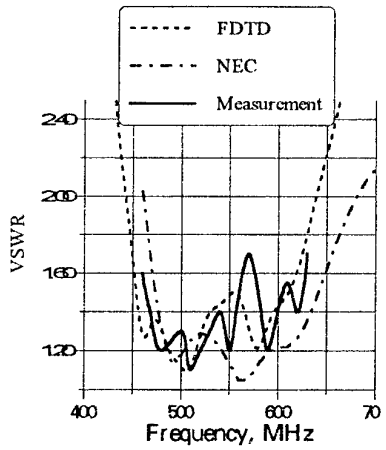


Fig. 3

Values of VSWR obtained by FDTD method is closer to experimental values than obtained by NEC program due to taking into account exact shapes and dimensions of dipoles and transmission line. Calculated by FDTD method radiation patterns show good agreement with experimental values for the main beam. Back lobe is higher than measurement. This may be caused by numerical errors of near to far zone transformation and reflections from non-ideal absorbing boundary conditions. Coincidence between FDTD method, measurement and NEC program prove the high accuracy of new analysis of LPDA developed right for the new technology proposed in [1].

This analysis required nearly 14 hours run-time on Pentium II-400 based computer and nearly 240MB RAM.

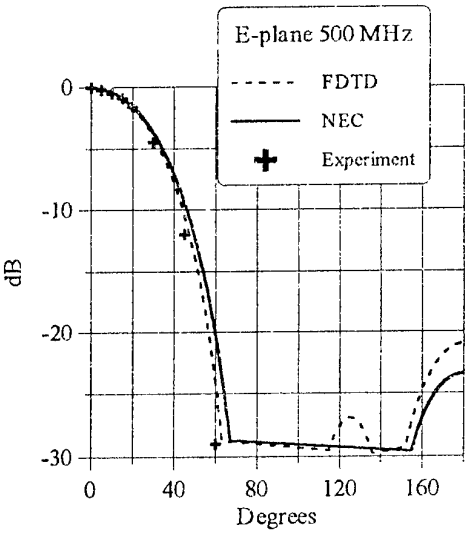


Fig. 4

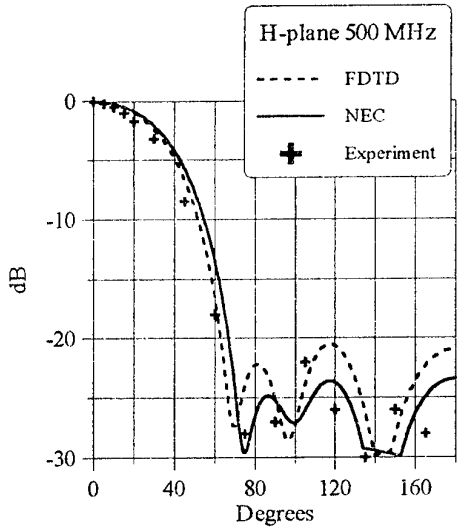


Fig. 5

CONCLUSIONS

Although the exact solution of Maxwell's equation for the complex structures is difficult and tedious, finite-difference time-domain method give the opportunity to analyse such structures relatively easy and accurate. The only problem is that it requires large memory storage and run-times. But this problem will be overcome by the progress in computer technics.

REFERENCES

1. Dubrovka F.F., Glushenko V.M., Kuprij A.M. Patent of Ukraine N1.
2. G. J. Barke, A.J. Poggio The Numerical Electromagnetic Code (NEC2), Lawrence Livermore Laboratory, Livermore, CA, 1980.
3. K. S. Yee. Numerical solution of initial boundary value problems involving Maxwell's equations // IEEE Trans. on AP, Vol. 14., pp302-307, May 1966.
4. G. Mur, Absorbing boundary conditions for the finite difference approximation of the time-domain electromagnetic field equations // IEEE Trans. on EMC, vol. EMC-23, pp 377-382, November 1981.
5. R. J. Luebbers, K.S. Kunz. A finite-difference time-domain near zone to far zone transformation // IEEE Trans. on AP, vol. AP-39, pp 429-433, April 1991.
6. V. N. Hlushenko, F. F. Dubrovka, A. M. Kuprii, S. E. Martynyuk, and A. E. Shrenk. New Log-Periodic and Quasi-Periodic Dipole Antennas of the VHF-UHF Range // Radioelectronics and Communications Systems, Vol. 41, No. 8, pp. 7–17, 1998.

MILLIMETER WAVE CHARACTERISTICS OF GLASS PLASTICS FOR ANTENNA COVERS

E. E. Chigriai, V. V. Meriakri

Institute of Radioengineering and Electronics, Russian Academy of Sciences
Vvedensky sq. 1, Fryazino, Moscow Reg. 141120, Russia
Phone: (095) 5269266, FAX (095) 7029572, (095) 2038414
E-mail: ask@ms.ire.rssi.ru, ask138@ire216.msk.su

Permittiyity ε and loss tangent tanδ of glass plastics and their components used for antenna covers were investigated in the 30–350 GHz band.

For glass plastics and their component testing in the frequency range 10-75 GHz we have used panoramic network analyzers R-2-61, R-2-65, R-2-68, R-2-69 with special horns. The measurements in the frequency range 75–350 GHz were carried out with help quasioptical beam wavequide spectrometers, interferometers, and open resonators [1].

The methods of determination permittivity ε and loss tangent tan δ are based on measuring the dependences of transmittance t and reflectance r moduli and phases as well the dependences of resonator quality factor Q and resonant frequency f for wavelength λ and sample thickness l.

The block diagram of spectrometer for wavelengths λ = 4–0.5 mm is shown in Fig.

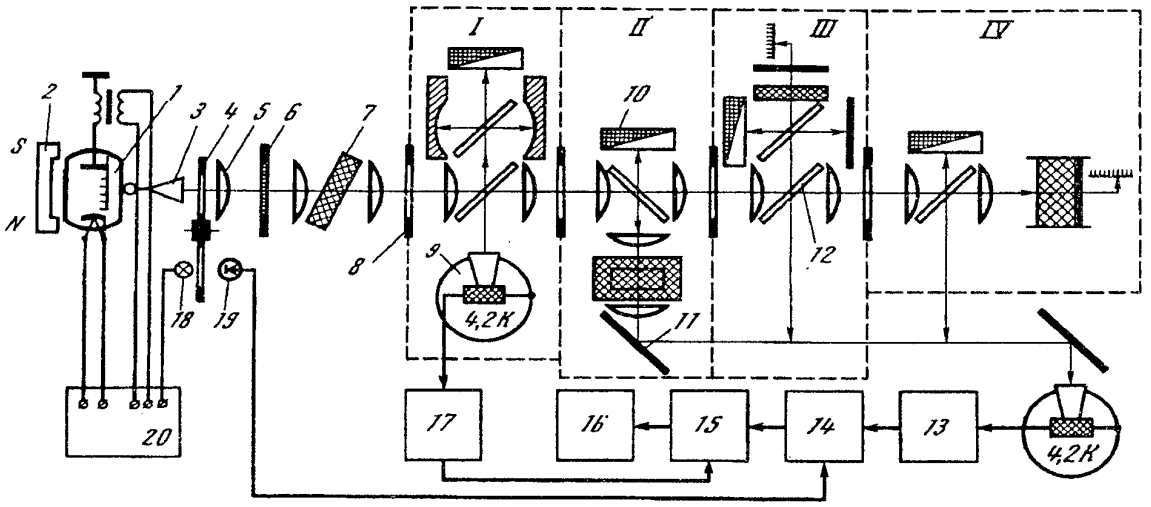


Fig.

Here I – resonator for low loss material properties measurement, II – transmission measuring circuit, III – Michelson or Max–Zender interferometer, IV – reflectometer. *1* – BWO, *2* – magnet, *3* – horn, *4* – modulator, *5* – lens, *6* – polarizer, *7* – attenuator, *8* – iris, *9* – receiver, *10* – absorber, *11* – mirror, *12* – beam splitter, *13* – amplifier, *14* – synchronous detector, *15* – digital voltmeter, *16* – storage unit, *17* – voltmeter, *18* – light source, *19* – LED, *20* – power supply.

To determine tan δ of low-absorption materials with $n \approx 1.3$ to 1.6, the $|t|$ value is measured in immersion liquids featuring identical refractive indices [3]. Materials with higher values of n for wich there are no low-absorption immersion liquids were investigated by measuring $|t(l)|$ in a «pile» containing various numbers of samples.

The second (in terms of its applicability) method consist in measuring arg $t = \varphi_t$ and arg $t = \varphi_r$ in an interferometer. In such measurements the authors used primarily the frequency sweeping technique [4] wich eliminates spurious interference effects in the sample and beam path and thus provides unambiguous determination of the interference order. The magnitude of n is related to the zero-order extremum displacement d_0 for samples of thickness l

$$n = 1 + d_0/l\,.$$

Errors in determination l, moduli t and r, arg t, arg r, Q, f were: Δl = 0.01 mm, t and r moduli 5 %, arg t and arg r 5–10 degrees, Q – 5 %, Δf = 0.2 GHz.

The resulting accuracy of determination ε and tanδ was (1–2) % for ε and (20–30) % for tan δ.

We have investigated many types of glass cloths and resins used for preparing glass plastics [2]. These materials and glass plastics were let us by I. G. Gurtovnik and V. N. Sportsmen.

Cloths based on nonalkaline and quartz glass fibers have ε =3.6–6.3 and tan δ from $\{0.2 - 2\}\ 10^{-3}$ at frequencies 30 – 35 GHz to $\{0.3 - 4\}\ 10^{-3}$ at frequencies 300 – 350 GHz.

Resins used for glass plastics (epoxy and silicon-bonded types) have ε from 2.8 to 3.1 and tan δ from $(1.2 - 2.5)\ 10^{-2}$ at frequencies 30 – 35 GHz to $(2.5 - 3.5)\ 10^{-2}$ at frequencies 300 – 350 GHz.

Table 1 presents characteristics of the best glass plastics, glass cloths and resins.

Table 1

No	Material	ε	tanδ·10³	λ, mm
1	Plastic based on TS-8/3-K-TO cloth and epoxy resin	2.60	5.9	8.4
		2.61	15.6	1.98
		2.62	28.5	0.87
2	Plastic based on TS-8/3-K-TO and SPE-25/3 resin	3.23	7.3	10.7
		3.30	10.0	4.6
		3.20	22.2	0.87
		3.26	4.4	29.9
3	Plastic based on nonalkaline glass and SPE-25/3	4.3	13.0	8.7
		4.37	16	4.3
		4.35	35.7	0.87
4	Silica glass	3.77	0.3	10.0
		3.77	0.6	6.0
		3.77	1.3	2.0
		3.76	2.2	0.82
5	Nonalkaline glass	6.11	7.4	8.4
		6.32	9.8	5.0
		6.20	32	2.0
6	Resin SPE - 25/3	2.88	13.5	9.9
		2.86	19.0	2.0
		2.86	41.0	0.88

Our investigations of more than 50 version of materials testified that ε for each sample practically invariable at frequencies 10 – 350 GHz and depends only on technology, tan δ.

Is slowly grows up (in interval 20 – 30 %) in frequency range 10 – 35 GHz, at higher frequencies tan δ increases more rapidly.

The measurements of the dependence of ε and tan δ on water content W in glass plastics show for W = 2–4 % the increase of ε not more than 0.1, tanδ becomes twice more.

Table 2 presents dielectric properties of antenna cover materials based on popous SiO_2 and Al_2O_3 in near millimeter region.

Table 2

No	material	ε	tanδ·10³	λ, mm
1	$Al_2O_3$and DS-150 resin	2.07	5	2.0
2	SiO_2 and Cr (o.5%)	3,35	1.2	1.1
3	SiO_2 and TiO_2 (15%)	3.80	1.6	1.25
4	SiO_2 - 107	1.15	4.0	2.0

REFERENCES

1. Meriakri V.V.,Apletalin V.N., Kopnin A.N. et al., Submillimeter beam wavequide spectroscopy and its application, in book Problems of modern radioengineering and electronics, edd. by V. A. Kotelnikov, Nauka, Moscow,1985, pp. 179-197.
2. Gurtovnik I.G.,Sportsmen V.A., Stekloplastiki dlj radiotekhniki, Moskwa, Khimia, 1987. [in Russian].
3. Meriakri V.V., Chigriai E.E., Pribory i tekhnika experimenta, 1976, No.1, p. 216. [in Russian].
4. Meriakri V.V., Ushatkin E.F., Pribory i tekhnika experimenta, 1973, No.2, p. 143. [in Russian].

A RESEARCH OF ELECTROMAGNETIC WAVES ABSORPTION IN FOAM AND LAYERED STRUCTURES

L. A. Filinskiy, V. M. Morozov

Dnepropetrovsk State University,
Ukraine, 320050, Dnepropetrovsk, per.Naukoviy, 13, phone. (38-0562) 46-79-95

Abstract. In the summary the results of experimental research of electromagnetic wave reflection of microwave - band (7.8 – 12.3 GHz) by samples of foam and layered structures, located in free space on a metal substrate are presented. The characteristics of reflection by foam structures in a range of sample thickness 10 – 84 mm with foaming ratio 30 – 170 as well as by layered structure with foam layer are investigated. The opportunity of the wave matching improvement of quasihomogeneous layered structures by means of foamed layer is shown.

INTRODUCTION

The radar absorbers find wide application to solve problems of antenna measurements, as well as other tasks, where the decrease or complete absorption of microwaves is important. Despite of a variety of used radar absorbers there is a constant need to create new materials with large value of absorption and wide operating bandwidth.

The number of ideas, used for development, has been considerably extended, when to solve problems it has begun to use achievements, obtained by research of foam structures [1].

The experiments, which have been carried out, have shown, that the appearance of foam formations and splashes on the surface of sea result in sharp change of the characteristics of own and scattered radiation of the sea in microwave band. So, foamed surfaces have microwave brightness temperature on tens Kelvins above, than clean agitated surfaces of the sea. Thus the value of radiation coefficient depends not only on the relative square of foam cover, but also on its structural features.

Among experimental researches it is need to note the works of the soviet-american program "Bering" (1973) [2]. They have shown, that in microwave band 0.8 – 21 sm microwave brightness temperature linearly grows with the increase of wind speed and its increment depends on percentage of foam on the surface of the sea.

The effect of sharp increase of sea emissivity due to foam formations required an explanation. In this connection the various theoretical estimations were fulfiled, however, the complexity of theoretical models has not allowed, especially at an early stage, to estimate adequately this phenomenon, though the appeared models predicted sharp increase emissivity till 1 for centimetric microwaves with a rather thin layer of a mix and small concentration of water in it [3].

The practice has shown, that variety of types and mobility of the foam formations, and also not always favorable hydrometeorological conditions on the sea, – considerably complicate statement purposeful and nsiderably complicate statement purposeful and besides expensive experiments in nature. Therefore, to understand physics of the phenomenon and to carry out detailed measurements in rather controllable conditions we have done laboratory researches.

In this work the frequency dependences of electromagnetic waves reflection by dispersion materials such as foam samples, layered samples, and also a combination of quasihomogeneous and foamed layers are investigated.

EXPERIMENTAL RESEARCH

For realization of investigation the measuring installation of blocks of microwave devices of a type ФК and P2 was assembled "on reflection". In measuring installation the signal of the basic channel was used as calibrated one, and the signal of the measuring channel was used as probe channel to be applied for direction to the object of research.

The signal from the generator, proportional to "falling microwave power ", is applied to the basic channel, and the signal reflected by the sample is applied to the measuring channel. The values of the ratio of the "reflected signal" to the "incident" were fixed in decibels. For "zero" value the reflection on a metal sheet was accepted. On the metal sheet the researched sample was placed, and its reflection was measured in the researched band of frequencies. Thus, by the way, the frequency reflective characteristics of researched samples were obtained.

The dispergation way was used to obtain the foam samples, which essence is the passage of the jet of gas (air) through foam generator with grids. In case the grids are watered by foaming liquid, the samples of the foam will be formed at the foam generator's output. In foam generator some partitions from grids with a various diameter of apertures were used, and they were placed in such sequence in direction of the movement of gas and liquid, that last grid was with the minimal cell and corresponded to necessary average diameter of bubbles.

Foaming liquid passes in turn through all grids with the help of the jet of gas, and creates at the output of the foam generator foam samples of necessary dispersion. Foaming ratio of foam - value representing the ratio of volume of foam to volume of the liquid, which was used to prepare the foam. Foaming ratio depends on the established values of the gas and the liquid expense. Before the beginning of measurements the calibration of foam generator was carried out with respect to foaming ratio of derived foam. The samples of foam structures were prepared from 6 % of the foaming water solution ПО-1 at the room temperature.

The samples were prepared as flat layers of necessary thickness in foam rubber tray with the base size 270×290 mm. On the distance which is equal to thickness of the sample from the top of the tray, the metal plate was placed on the substructure of necessary thickness. The tray was filled by foam, the surplus was removed precisely on the top edge of the tray. Thus, identical distance from the aperture of the antenna up to forward plane of the foamed sample was provided, which was equal to 140 mm. The size of the antenna aperture was equal to 80×80 mm.

ANALYSIS OF RESULTS

Based on obtained results of the reflectivity dependence on thickness of the sample it should be noted, that for thickness of the sample of 10 mm the reflectivity is within the limits of 0 – 12 dB, average reflectivity is in the order of –7 dB in researched band of frequencies. For thickness of the sample of 47 mm reflectivity is in limits of 4, ..., –35 dB, on the average it is not worse than –10 dB. For thickness of the sample of 84 mm reflectivity is within the limits of –5.3, ..., –30 dB, on the average it is not worse than –10 dB in the band 9 – 12 GHz.

From the diagrams of Fig. 1 it is easy to see, that the dependence of reflectivity on thickness has oscillating character. It indicates that a resonance of the reflected power on thickness of the sample has place, so the foamed sample for the researched band of frequencies is quasihomogeneous material, as the size of unhomogeneous (bubbles), having the diameter of 0.1 – 2 mm, is considerably less than the used wavelength.

From the Fig. 1 it is easy to see that larger thickness of the sample corresponds to smaller reflectivity (larger value in decibels). So, for thickness more than 84 mm reflectivity in a band 9 – 12 GHz is not worse than –10 dB, and for some frequencies its value achieves –20 dB and less.

The dependences of the reflectivity on frequency for samples with various foaming ratio are presented in Fig. 2 (thickness of samples – 45 mm, dispersion 0.1 – 2 mm). From the obtained results we shall note, that for the sample of foam with foaming ratio 30 value of the reflectivity is within the limits of –2.9, ..., –17 dB.

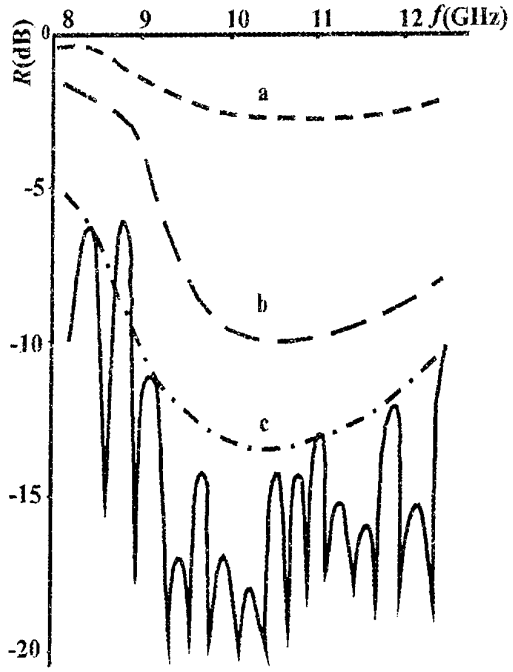


Fig. 1. Dependences of the reflectivity on the sample thickness (foaming ratio = 35)
a) Thickness of the sample - 10 mm;
b) Thickness of the sample - 47 mm;
c) Thickness of the sample - 84 mm.

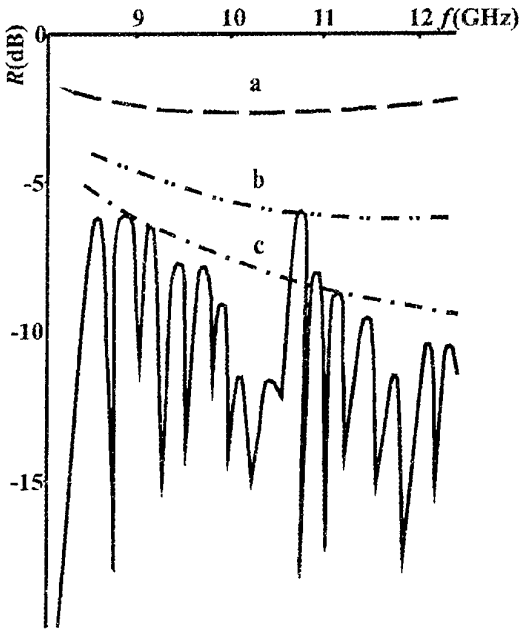


Fig. 2. Frequency dependence of the reflectivity for samples of various foaming ratio
a) Foaming ratio of the sample 30;
b) Foaming ratio of the sample 60;
c) Foaming ratio of the sample 170

In the considered band for frequency 10 GHz the reflectivity is not worse than –10 dB. Reflectivity for samples with foaming ratio 60 is within the limits of –5.7, ..., –28 dB. The reflectivity for frequency 10 GHz is no worse then –11 dB. For samples with foaming ratio 170 reflectivity is within limits of –2.3, ..., –13 dB. Reflectivity around 10 GHz is not worse than –6 dB.

From the Fig. 2 it is easy to see, that with the increase of foaming ratio (that is equivalent to increase of samples "dryness"), changes boundary (for example, maximal) value of the reflectivity. So, with foaming ratio of the samples of 30 its values are not worse than –2.5 dB, with increase of foaming ratio up to 60 reflectivity is not worse than –5, ..., –9 dB, and with the further encrease of foaming ratio, the value of the reflectivity has intermediate value, so it oscillates in limits from the minimal up to the maximal value with the certain direction change of foaming ratio, for example, from the minimal up to the maximal value.

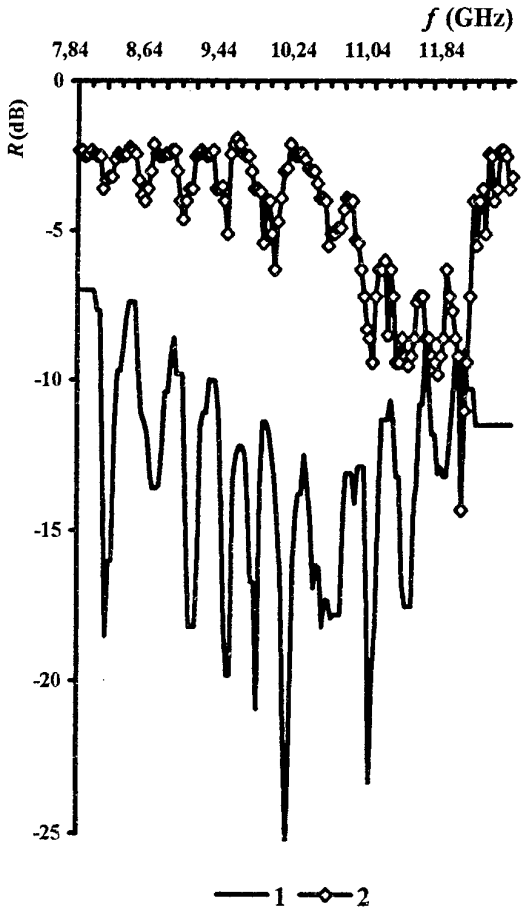


Fig. 3. Frequency reflection characteristics of layered structures

It is necessary to take into consideration that modeling of absorbing structures by means of foam is possible only in initial, more or less long period of its existance.

In common case, the foam is a dynamic structure. With substantial growth of time of its existence its natural disintegration begins, which is connected with flowing out liquid from its film skeleton. After the certain time of existence the foam structure becomes more and more radiotransparent and ceases to render appreciable influence on distribution of electromagnetic waves.

In Fig. 3 the results of experimental research of the reflectivity dependence on frequency for layered samples are presented.

In the diagram 1 the dependence of the reflectivity for three – layer elastic sample with thickness of layers 2, 1 and 3 mm and volumetric concentration of electroconductiv additive 14, 11 and 45 % accordingly for the 1-st, the 2-nd and the 3-rd layers are shown. The 1-st layer is foamed, the 3-rd layer of the layered structure was placed on the metal substrate. In the diagram 2 the values of the reflectivity for the same layered structure are presented, but without foamed layer.

From the diagrams it is easy to see that the sample with a foamed layer has considerably better characteristics of absorption. So if the two-layer sample had the bandwidth 1280 MHz with the reflectivity at a level not worse than –5dB with the minimal value of the reflectivity –14 dB, three-layer sample with the first foamed matching layer had the bandwidth 3584 MHz with the reflectivity at a level not worse than –10 dB and obtained minimal value of the reflectivity –25 dB.

CONCLUSIONS

Using the foam structures as an absorbing material, the required reflective characteristics can be obtained at the expense of correct selection of foaming ratio of foam and sample thickness. The obtained experimental data give new understanding about influence of foaming ratio and thickness of a sample on electromagnetic waves reflection from the foam structure in the band 8 – 12 GHz. As an absorbing material the layered structure can be effectively used, in which one of the layers is a foamed one.

REFERENCES

1. Williams, G., Microwave radiometry of the ocean and the possibility of marine wind velocity determination from satellite observations, J. Geophys. Res, 74 (18), 4591, 1969.
2. The Soviet-American experiment "Bering". Proc. of the simposium, Leningrad, 12-14 May, 1974.
3. Matveev D. T. Izv. AN SSSR, FAO, 1971, 7, 10, 1070.

TO ASYMPTOTICS OF A FIELD OF OVERREVERBERATED BEAMS IN THE APERTURE ANTENNA WITH RADOME

I. V. Sukharevsky, S. E. Vashinsky

Kharkov military university,
maidan Svobody 6, Kharkov 310043, Ukraine

The problem of existence and calculation of coordinates of stationary phase points in an overreverberated field, appearing in the aperture of antenna with dielectric radome, is investigated (in three-dimensional case) in report. Our research is based on works of authors [1–3], which include the two-parametrical theory of diffraction on layered structures and the generalization of the mirror images principle.

Let aperture S_0 be located on plane $x_3 = h > 0$ and radiates in half-space Ω^- ($x_3 < h$), in which dielectric radome, bounded by smooth convex surfaces S, S_1, is disposed.

Complex radiation pattern $\vec{E}(\vec{R}^0)$ in approximation of physical optics has ([1]) the following representation:

$$\vec{q}\cdot\vec{E}(\vec{R}^0) = \int_{S_0}\left[\vec{E}^T_{CT}(\vec{x})\cdot\vec{H}^{\perp}_0\left(\vec{x}\middle|\vec{R}^0,\vec{q}\right) - \vec{E}^T_0\left(\vec{x}\middle|\vec{R}^0,\vec{q}\right)\cdot\vec{H}^{\perp}_{CT}(\vec{x})\right]dS, \qquad (1)$$

where $\vec{q}$ is an arbitrary unit vector, $\vec{E}_{CT}, \vec{H}_{CT}$ is the field of extraneous sources (allocated at $x_3 > h$), and $(\vec{E}_0, \vec{H}_0)$ is the field, excited by coming from Ω^- plane wave:

$$\vec{E}_0 = \left(\vec{q} - \vec{R}_0(\vec{q}\cdot\vec{R}_0)\right)e^{-jk_0(\vec{R}_0\cdot\vec{x})};\ \vec{H}_0 = \frac{1}{j\omega\mu_0}\vec{\nabla}\times\vec{E}_0. \qquad (2)$$

Parameters $k_0, \varepsilon_0, \mu_0$ correspond to free space.

From the formula (1) and from amplitude-phase representations of entering here fields, the following expression is obtained:

$$\vec{q}\cdot\vec{E}(\vec{R}^0) = \int_{S_0}\vec{U}\left(\vec{x}\middle|\vec{R}^0,\vec{q}\right)e^{jk_0\Phi(\vec{x})}dS. \qquad (3)$$

In this case the amplitude vector $\vec{U}$ and the phase function $\hat{\Phi}$ are presented by the following beam design.

We select in an incident plane wave beams, piercing the surface S in a direction $-\vec{R}^0$ and forming sharp angles with unit vector $\vec{n}$ in points of S; we designate by $\overline{S}$ a part of surface S, "illuminated" by these beams (see Fig. 1).

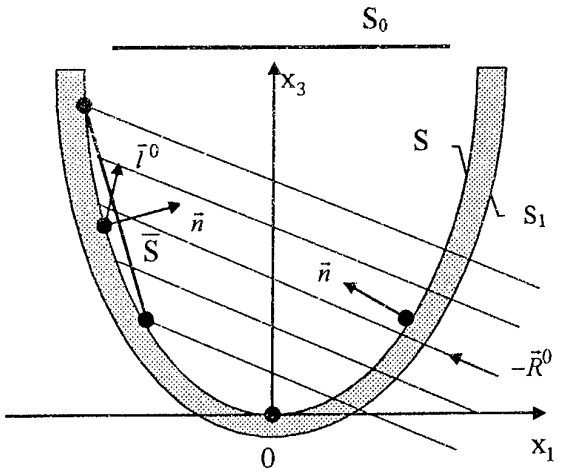


Fig. 1

Applying some asymptotical technique ([2]) to a problem of beams passing through the S_1 and fitted to S_1 layer, as well as to the subsequent reflection from $\overline{S}$, we obtain (in general asymptotic approximation) formulae for the $\vec{U}$ and Φ in the aperture.

In particular

$$\Phi = \Phi(\vec{x};\vec{\xi}) = \vec{p}^0\cdot\vec{x} + \left|\vec{x}-\vec{\xi}\right| - \vec{R}^0\cdot\vec{\xi}, \qquad (4)$$

where $\vec{p}^0 = (\sin\psi\cos\alpha; \sin\psi\sin\alpha; -\cos\psi)$ is a unit vector of scanning; $\vec{\xi} = (\xi_1, \xi_2, g(\xi_1,\xi_2)) \in \overline{S}$;

$$\vec{R}^0 = (\sin\vartheta\cos\varphi; \sin\vartheta\sin\varphi; -\cos\vartheta).$$

It is assumed, that $\vartheta \in (0; \frac{\pi}{2}]; \psi \in [0; \frac{\pi}{2})$.

Unit vector of reflected beam direction:

$$\vec{l}^0 = -\vec{R}^0 + 2\vec{n}(\vec{R}^0\cdot\vec{n}). \qquad (5)$$

This asymptotic method based on simultaneous infinitesimal of layer thickness and wavelength, relatively to curvature radii of surfaces S, S_1.

Further, the points, laying on one reflected beam $\vec{\xi} \in \overline{S}$ and $\vec{x} \in S_0$ are defined through by relations:

$$x_1 = \xi_1 - (h-g)\frac{l^0_1}{l^0_3};\ x_2 = \xi_2 - (h-g)\frac{l^0_2}{l^0_3};\ x_3 = h. \qquad (6)$$

In the vicinity of points , in which yakobian

$$\det\left(\frac{\partial x_i}{\partial \xi_j}\right) \neq 0,$$

the system of the equations (6) is convertible: there are functions $\xi_1 = \xi_1(x_1, x_2), \xi_2 = \xi_2(x_1, x_2)$, inversed to (6). Therefore,

$$\Phi(\vec{x}; \vec{\xi}) = \Phi(\vec{x}; \vec{\xi}(\vec{x})) = \Phi[x_1; x_2],$$

and our purpose consists in searching such points (x_1^0, x_2^0) ("stationary phase points"), in which

$$\frac{\partial \Phi[x_1^0, x_2^0]}{\partial x_1} = \frac{\partial \Phi[x_1^0, x_2^0]}{\partial x_2} = 0. \qquad (7)$$

In the given report the following not quite trivial result is established- system of identities:

$$\frac{\partial \Phi[x_1, x_2]}{\partial x_i} = p_i^0 + l_i^0(\xi_1, \xi_2), \ (i = 1; 2). \qquad (8)$$

From (8) follows

The theorem. If the system of equations

$$l_1^0(\xi_1, \xi_2) + p_1^0 = 0; l_2^0(\xi_1, \xi_2) + p_2^0 = 0 \qquad (9)$$

has some solution (ξ_1, ξ_2) and point, $(\xi_1, \xi_2, g(\xi_1, \xi_2)) \in \bar{S}$, then values (x_1, x_2, h), expressed by the formulae (6), are coordinates of stationarity of phase function $\Phi[x_1, x_2]$.

Thus, our problem is reduced to the effective solution of the system (9). Let's find this solution for such a practically important case, when azimutal angles of vectors $\vec{p}^0$ and $\vec{R}^0$ are coincide: $\alpha = \varphi$, we also designate: $\cos\varphi = c$; $\sin\varphi = s$.

Then, the system of relations (5), (9) is reduced to equations:

$$\frac{2g_{\xi_i}}{1 + g_{\xi_1}^2 + g_{\xi_2}^2}\left[\left(g_{\xi_1} c + g_{\xi_2} s\right)\sin\vartheta + \cos\vartheta\right] = A_i, (i = 1; 2), \qquad (10)$$

where $A_1 = c(\sin\vartheta - \sin\psi)$; $A_2 = s(\sin\vartheta - \sin\psi)$.

For system (10) it is necessary to add condition, stipulated by a geometrical configuration of problem: $l_3(\xi_1, \xi_2) > 0$. This condition ensures uniqueness of the solution. Then, we have:

$$\left.\begin{aligned} g_{\xi_1}(\xi_1, \xi_2) &= -\cos\varphi \cot\frac{\vartheta + \psi}{2}, \\ g_{\xi_2}(\xi_1, \xi_2) &= -\sin\varphi \cot\frac{\vartheta + \psi}{2}. \end{aligned}\right\} \qquad (11)$$

Hence, there can be obtained coordinates ξ_1, ξ_2 of reflection point and then, by formulae (6), coordinates of stationary phase point in aperture S_0.

The practical importance of the proposal research consists in that a grid of stationary phase points is obtained. In the local vicinity of these points significant part of the contribution brought by overreverberations from S to antenna sidelobe radiation is generated.

Thus, there is the principal technical possibility to compensate these contributions.

REFERENCES

1. Sukharevsky I. V., Sukharevsky O. I. Calculation of the field, generated by the radiating aperture at the presence of arbitrary system of scatterers. Radiotekhnika and electronika, 1986, № 1 [in Russian], p. 8-13.
2. Sukharevsky I. V. Asymptotical solution methods of some classes of waves diffraction problems. Radiotekhnica, 1996, № 100. -p. 19-41 [in Russian].
3. Prof. I. V. Sukharevsky, S. E. Vashinsky. About the stationary phase points and caustic influence on lateral radiation of antenna systems with radomes. International conference on mathematical methods in electromagnetic theory. Conference proceedings. Kharkov, Ukraine. 1998, vol.2 . -p. 537-539.

DISSIPATION FIELDS IN FLAT WAVEGUIDE WITH A TRIPLE BIFURCATION AND DIELECTRIC FILLING

V. Antyfeev, A. Borsov, A. Sokolov

Moscow, Russia

The generalized (Fig. 1), representing a concatenation of flat waveguides A, B and C, filled by isotropic dielectric is considered. Such frame appears for convenient determination of parameters of the equivalent circuit of the multi-mode slotted radiator [1], covers practically all internal and external problems: the step changing of cross-section at $\varepsilon_c \to \infty$; the radiation of aperture $L \to \infty$ etc. Thus it is possible to take advantage of modern methods of an electrodynamics, which allows to use the previous results at finding out of the scattered field by each subsequent modification of the generalized wave-guide frame, that dramatically reduces a computing time for numerical calculations.

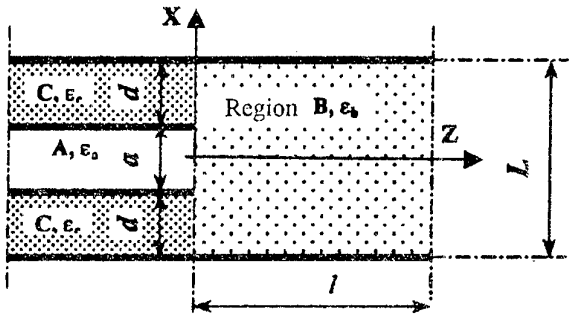


Fig. 1. Wave-guide frame

The calculation of parameters of an equivalent circuit and directional properties of the radiator requires consideration of a number of internal and external problems of an electrodynamics having essential differences. It is bound up that it is always practically possible to present the solutions of Maxwell equations determining an electromagnetic field in closed area, as decompositions on eigenwaves for which the discrete spectrum of eigenvalues is characteristic. In a case of unlimited area the spectrum of eigenvalues becomes continuous.

The part of problem indispensable for determination of parameters of the equivalent circuit is now resolved: radiation of aperture [1], the consideration of final width of waveguide walls [2] etc. However calculation of all units of an equivalent circuit and PP of the radiator is necessary to unite by the unified approach permitting to find scattered fields in open and closed areas, thus having provided probable filling of cavities of the radiator by dielectric.

The basic method of calculation is the modified method of the deductions given in [3]. In the essence of a method there is an obtaining of an infinite system of simple equations, which is in process of seaming fields subject to boundary conditions, and the solution of this system by means of application of the mathematical methods of the theory of complex variable functions. The introduction of preliminary analytical transformations results in essential reduction of computing time.

Let the H_{po}-wave drops from A-area, which one can be described by a function $\varphi^{(i)}$. Distinct from zero components of H_{po}-wave can be recorded as:

$$E_y^{(i)} = \varphi^{(i)} = \cos\left(\frac{p\pi}{a}x\right)\exp\left(-\gamma_{pa}\cdot Z\right),$$

$$H_x^{(i)} = \frac{j}{\omega\mu}\frac{\partial}{\partial z}\varphi^{(i)},$$

$$H_z^{(i)} = \frac{1}{j\omega\mu}\frac{\partial}{\partial x}\varphi^{(i)}.$$

The scattered field in areas A, B and C is possible to present as decompositions on eigenwaves. As the frame is uniform in a Y-direction, in decomposition there will be only waves such as H_{no}, and subject to a symmetry in areas A and B there will be only odd waves such as H_{no} (n = 1,3,5...). All component of scattered field can be expressed through appropriate component electrical fields E_y = φ, and the function φ should satisfy the wave equation:

$$\left(\frac{\partial^2}{\partial x^2}+\frac{\partial^2}{\partial z^2}+k^2\right)\varphi(x,z)=0$$

and boundary conditions:

1. meets radiation's condition at $Z \to \infty$;
2. φ = 0 at $|x| = \frac{a}{2}$ in area $Z \le 0$ and at $|x| = \frac{L}{2}$ for all Z;
3. In a plane Z = 0 tangent component of full electrical fields $\varphi^{(t)} = \varphi^{(i)} + \varphi$ and tangent component of full magnetic field, proportional $\frac{\partial\varphi^{(t)}}{\partial z} = \frac{\partial\varphi^{(i)}}{\partial z} + \frac{\partial\varphi}{\partial z}$, should be continuous.
4. φ – should meet condition on an acute edge at $|x| = \frac{a}{2}$, Z = 0.

5. $$\varphi \sim \rho^{-1+\tau}, \tau = \begin{cases} \frac{1}{2} + \frac{1}{\pi}\arcsin\left[\frac{\varepsilon_r - 1}{2(\varepsilon_r + 1)}\right] \text{ at } \varepsilon_r > 1, \\ \frac{1}{2} - \frac{1}{\pi}\arcsin\left[\frac{\varepsilon_r - 1}{2(\varepsilon_r + 1)}\right] \text{ at } 1 > \varepsilon_r > 0, \end{cases}$$

$$\rho = \left\{\left(|x| - \frac{a}{2}\right)^2 + Z^2\right\}^{1/2}$$

$$\rho \to 0,$$

and ε_r is permittivity of dielectric near to an acute edge in area $Z \le 0$.

The index (i) marks components of a dropping field, (t) — those one of a full field and without an index — components of the scattered field. The first three boundary conditions are known and are closed to geometry of considered frame. The fourth condition is additional encompassing by the requirement of finiteness of energy of an electromagnetic field accumulated in any final volume in a neighborhood of an acute edge. This requirement results in a statement that any component of electromagnetic field in a neighborhood of an acute edge can not increase faster than r^{-1+t} ($\tau > 0$) at $\rho \to 0$ [3]. In particular, for a number of private problems the parameter ($-1 + \tau$) attain following values: for discontinuous changing of cross-section (at $\varepsilon_c \to \infty$) is 1/3, and for triple bifurcation of the waveguide is 1/2 [3].

The conditions (1) and (2) will be executed if the scattered field in areas A, B and C presents as decompositions on eigenwaves, missing from a plane $Z = 0$. Thus, we have decompositions

At $Z < 0$ (area A) $\varphi = \sum_{n=1}^{\infty} A_n \cos\left(\frac{n\pi}{a}x\right)\exp\left(\gamma'_{na}Z\right)$

At $Z < 0$ (area C)

$$\varphi = \sum_{n=1}^{\infty}{}^{*} C_n \sin\left(\frac{n\pi}{\alpha}\left(x - \frac{a}{2}\right)\right)\exp\left(\gamma'_{nd}Z\right)$$

At $Z > 0$ (area B) $\varphi = \sum_{n=1}^{\infty} B_n \cos\left(\frac{n\pi}{L}x\right)\exp\left(\gamma'_{nL}Z\right)$

Here propagation coefficients:

$$\gamma'_{na} = \left\{\left(\frac{n\pi}{a}\right)^2 - k_a^2\right\}^{\frac{1}{2}}, \gamma_{na} = \left\{\left(\frac{n\pi}{a}\right)^2 - k_L^2\right\}^{\frac{1}{2}},$$

$$k_a = k\sqrt{\varepsilon_a}, k = \frac{2\pi}{\lambda}\sqrt{\varepsilon_0\mu_0}.$$

$$\gamma'_{pa} = \left\{\left(\frac{p\pi}{a}\right)^2 - k_a^2\right\}^{\frac{1}{2}}, \gamma'_{nd} = \left\{\left(\frac{n\pi}{d}\right)^2 - k_d^2\right\}^{\frac{1}{2}},$$

$$k_d = k\sqrt{\varepsilon_c},$$

$$\gamma_{nL} = \left\{\left(\frac{n\pi}{L}\right)^2 - k_L^2\right\}^{\frac{1}{2}}, \gamma_{nd} = \left\{\left(\frac{n\pi}{d}\right)^2 - k_L^2\right\}^{\frac{1}{2}},$$

$$k_L = k\sqrt{\varepsilon_b}.$$

The third boundary condition allows to conduct seaming fields on boundary $Z = 0$ and in an $\left(0 \le x \le \frac{L}{2}\right)$ interval. This procedure results in necessity of solution of sets of equations, which admits any number of the solutions, each is mathematically correct. However only one of these solutions meets condition (4) for functions φ and thus is true solution of a considered problem having physical sense. For this purpose it is enough to study an asymptotical behavior of unknown factors of decomposition of the scattered field A_i, B_n and C_n at large n.

At fulfillment of practical calculations the infinite sets of equations were reduced into end-systems of equations. The justification of such transformation follows from an asymptotics of behavior component scattered field at large n. The solutions of reduced sets of equations can be found by different methods, e.g.: the method of the direct reversal, with usage of the theory of continuants etc. In this case, most effective is a modified method of deductions requiring of a minimum volume of calculation [3]. The basis of a modified method of deductions is the construction of a holomorphic complex variable function $f(\omega)$, satisfying to a number of conditions. The fulfillment of these conditions allows to substitute all members of a set of equations by the sum of deductions of a constructed function.

Then the amplitudes of elapsed waves in area B are determined as:

$$B_n = \frac{\mathrm{Res}\{f(\gamma_{nL})\}}{\cos\left(\frac{n\pi a}{2L}\right)}, \quad (1)$$

Amplitudes of waves scattered in area A:

$$A_m = (-1)^{\frac{m+1}{2}} \frac{\left(\gamma_{ma} + \gamma'_{ma}\right)n\pi}{\gamma_{ma}\gamma'_{ma}a^2}\left\{f(-\gamma_{ma}) + \rho_{ma}f(\gamma_{ma})\right\} \quad (2)$$

After applying a similar procedure, scattered field in area C looks like:

$$C_m = \frac{\left(\gamma_{md} + \gamma'_{md}\right) m\pi}{\gamma_{md}\gamma'_{md} d^2}\left(1 + \rho_{md}\right) f\left(-\gamma_{md}\right). \qquad (3)$$

Thus, if it will be possible to construct $f(\omega)$, satisfying five above-mentioned conditions, by means of formulas (1-3) it is easily possible to find out amplitudes elapsed and scattered field in areas A, B and C.

In particular, in a case of a triple wave-guide bifurcation without dielectric factors ρ_{ma} and ρ_{mb} becomes equal zero and the function $f(\omega)$ looks like:

$$f(\omega) = (-1)^{\frac{p-1}{2}} \frac{\gamma_{pa} a^2}{2p\pi} \times$$

$$\times \exp\left\{\frac{\gamma_{pa} - \omega}{2\pi}\left[a \ln\left(\frac{2a}{d}\right) + L \ln\left(\frac{d}{2L}\right)\right] - \frac{2a}{p}\right\} \times$$

$$\times \prod_{n=1}^{\infty}{}^{(p)} \frac{\gamma_{na} - \omega}{\gamma_{na} - \gamma_{pa}} \exp\left(\frac{\left[\omega - \gamma_{pa}\right] a}{n\pi}\right) \times$$

$$\times \prod_{n=1}^{\infty} \frac{\gamma_{nL} - \gamma_{pa}}{\gamma_{nL} - \omega} \exp\left(\frac{\left[\gamma_{pa} - \omega\right] L}{n\pi}\right) \times$$

$$\times \prod_{n=1}^{\infty}{}^{*} \frac{\gamma_{nd} - \omega}{\gamma_{nd} - \gamma_{pa}} \exp\left(\frac{\left[\omega - \gamma_{pa}\right] d}{n\pi}\right).$$

The given modification of the generalized frame does not describe any of units of the equivalent circuit of the radiator, but has the relevant practical value, as the constructed function $\tilde{f}(\omega)$ can be used at calculations of all subsequent modifications of the generalized wave-guide frame.

REFERENCES

1. Antyfeev V., Borsov A., Sokolov A. Radiation of the multi-mode slotted radiator. The article in the given collection.
2. Vainstein L. The theory of diffraction and method of a factorization. M.: Soviet radio, 1966.
3. Friedberg P., Gorb H., Levinson I. The taking into account walls thickness in slotted problems of an electrodynamics. – R&E, 1968, V.13, I.12, pp. 2152-2161.
4. Mythra R., Lee S. Analytical methods of the theory of waveguide. - M., Mir, 1974.

NEW METHOD OF AERIALS CALCULATION

V. V. Artemiev, V. L. Danilchuk, J. J. Radzig, S. I. Eminov

Department of Theoretical and Special Physics, Novgorod State University,
41, St. Petersburg St., Novgorod, 173003, Russia.

STRUCTURE OF THE INTEGRAL EQUATION

The initial equation for the impedance dipole has a form [1]:

$$E_z(j_z)+E_z^o=Z\,j_z \qquad (1)$$

where $E_z(j_z)$ is the secondary field induced by the current j_z.

For the case when $Z = 0$, the structure of the equation (1) has been studied by the authors in the papers [2, 3]. Using the results from these works, the equation (1) can be written in a more obvious form as follows:

$$\alpha(AI)(\tau)+\frac{1}{2\pi a}ZI(\tau)+(KI)(\tau)= \qquad (2)$$

$$\alpha\frac{1}{\pi}\frac{\partial}{\partial\tau}\int_{-1}^{1}I(t)\frac{\partial}{\partial t}\ln\frac{1}{|\tau-t|}dt+\frac{1}{2\pi a}ZI(\tau)+$$

$$+\int_{-1}^{1}I(t)K(\tau,t)dt=e(t)$$

where α is a constant value, $I(\tau)=2\pi a\,j_z(l\tau)$, $e(\tau)=E_z^0(l\tau)$, $2l$ and a are the vibrator length and radius, correspondingly.

The equation (2) will be investigated in the power domain H_A of the positively-defined operator

$$(AI)(\tau)=\frac{1}{\pi}\frac{\partial}{\partial\tau}\int_{-1}^{1}I(t)\frac{\partial}{\partial t}\ln\frac{1}{|\tau-t|}dt \qquad (3)$$

The orthogonal normalised basis of H_A can be written as: $\varphi(\tau)=\sqrt{\frac{2}{n\pi}}\sin[n\arccos(\tau)], n=1,2,\ldots$ (4) In the papers [2, 3] it was proved that the operator $A^{-1}K$ is entirely continued in H_A. The operator $A^{-1}Z$ is the Gilbert-Schmidt operator, i. e. it satisfies the following condition :

$$\sum_{m,n=1}^{+\infty}\left|\left[A^{-1}Z\varphi_m,\varphi_n\right]\right|^2<+\infty, \qquad (5)$$

where $[\cdot,\cdot]$ means a scalar multiplication in H_A domain and $(\cdot\ ,\cdot\ )$ means a scalar multiplication in $L_2[-1,1]$. To prove this, it is enough that the equation (2) is the Fredholm equation of the second kind in H_A, where Z is the operator of the multiplication on $Z(\tau)$ function. Define the scalar multiplication in H_A as follows:

$$\left[A^{-1}Z\varphi_m,\varphi_n\right]=\left(Z\varphi_m,\varphi_n\right) \qquad (6)$$

When the impedance Z is a constant value, the matrix elements (6) are found analytically. In the case when $m = 2i - 1$, $n = 2i - 1$ (the even problem) we found the matrix elements as following:

$$\left(\varphi_{2i-1},\varphi_{2j-1}\right)=\frac{2}{\pi}\frac{1}{\sqrt{(2i-1)(2j-1)}}\cdot \qquad (7)$$

$$\cdot\int_{-1}^{1}\sin[(2i-1)\arccos(\tau)]\times\sin[(2j-1)\arccos(\tau)]d\tau=$$

$$=\frac{\sqrt{(2i-1)(2j-1)}}{2\pi(i+j-\frac{1}{2})(i+j+\frac{3}{2})(i-j+\frac{1}{2})(j-i+\frac{1}{2})}$$

By means of the expression (7) the condition (5) can be checked. In conclusion of this paragraph, note that in the case of the varying impedance the function $Z(\tau)$ is added to the integral (7). If $Z(\tau)$ is the partially-smooth function (and this condition is assumed for all the considered mathematical models of the impedance structure) then it is possible to extract the asymptotic solution of the integral by partial integration, and it can be proved that $A^{-1}Z$ is entirely continuous in H_A too.

UNIQUENESS OF THE GENERAL SOLUTION

As the alternative Fredholm equation is used for the equation (2), the equation should have only one solution or the correspondent uniform equation should have a non-zero solution. We shall show that the uniform equation

$$-E_z(j_z)+Z\,j_z=0 \qquad (8)$$

for $\mathrm{Re}(z)\geq 0$ has only zero solution. Write the expression for the secondary field

$$E_z(j_z)=\frac{1}{ik}\sqrt{\frac{\mu}{\varepsilon}}\left(\frac{d^2}{dz^2}+k^2\right)\cdot$$
$$\cdot\iint_S j_z\frac{e^{-ikR}}{4\pi R}dS \qquad (9)$$

Using the expansion of Green's function into the sum-integral in the cylindrical coordinate system [1] the following can be obtained:

$$E_z(j_z) = \frac{-a}{4\pi}\sqrt{\frac{\mu}{\varepsilon}}\int_{-\infty}^{+\infty}(-h^2+k^2)F(h)\cdot \cdot\int_{-1}^{1} j_z(z')e^{-ih(z-z')}dz'dh, \quad (10)$$

where $F(h) = J_0\left(-i\sqrt{h^2-k^2}a\right)H_0^{(2)}\left(-i\sqrt{h^2-k^2}a\right)$,

J_0 is the Bessel function and $H_0^{(2)}$ is the Hankel function.

Note that the function F(h) is of imaginary value when $h^2 > k^2$. When $h^2 \le k^2$ then $\mathrm{Re}(F(h)) \ge 0$.

Multiply (8) on the complex conjugate $\bar{j}$ and integrate the product. It is the same with a scalar multiplication of j_z in L_2 [-1,1]

$$-(E_z(j_z), j_z) + (Z j_z, j_z) = 0 \quad (11)$$

The relation $\mathrm{Re}\left(-(E_z(j_z), j_z) + (Z j_z, j_z)\right) \ge 0$ can be proved easily when we transverse from the function j_z to its Fourier transformation (11) in accordance to (10) and the condition $\mathrm{Re}(z) \ge 0$. The equality to zero takes place only when $j_z(z) \equiv 0$ and then it is proved that the general solution is uniqueness.

THE NUMERICALLY-ANALYTICAL METHOD

In theory of dipole antennas there is a problem to calculate a current and an input resistance for active antennas. Assume that the incident field E_Z^0 is localised at a small region and has a sharp extremum. The correspondent functions are called particular ones. The characteristic mathematical property of the particular function is that it can be extended into the slowly increasing series. Solution of the integral equations with the particular right-hand part by the Galerkin's method is very ineffective. A new numerically-analytical method is proposed which is based on the presented analysis. According to this method the solution is found in the following form:

$$I(\tau) = \sum_{i=1}^{N} C_i \varphi_i(\tau) + \sum_{i=N+1}^{+\infty} C_i \varphi_i(\tau) \quad (12)$$

The first N unknown variables are found by soling the system

$$C_i + \sum_{j=1}^{N} C_j I_{ij} + \sum_{i=1}^{N} C_j K_{ij} = e_i, \quad (13)$$

$$1 \le i \le N$$

and the last unknown variables are found by the analytical method

$$C_i \le e_i, \; N+1 \le i < +\infty \quad (14)$$

It is necessary to take into account N terms to achieve the necessary precision. N is found from the results of the numerical experiments.

REFERENCES

1. Veinstein L.A. Theory diffraction and method factorization. 1966. - P. 431.
2. Danilchuk V.L. "Optimization Of Band Properties Of A Short Impedance Vibrator On The Basis Of The Complex Analysis". Proc. Of Progress in Electromagnetics Research Symposium. Nantes, FRANCE, July 13 - 17, 1998, volume 3, p. 1199.
3. Danilchuk V.L., Eminov S.I. "Theory of the impedance dipole". Proceedings of the 1995 International Symposium on Electromagnetic Theory (URSI-1995). - St. Petersburg, 1995. - P. 498 - 500.

ANALYSIS OF MICROSTRIP ANTENNAS BY NUMERICAL–ANALYTICAL METHOD

V. V. Artemiev, S. I. Eminov, I. A. Jukovskaya

Department of the Theoretical and Special Physics;
Novgorod State University by Y. Mudry; 41, St. Petersburg st., Novgorod, 173003, Russia;
Phone: (816-2) 11-68-91; E-mail: vav@info.novsu.ac.ru

INTRODUCTION

In the field of antenna technology a lot of attention has been paid to microstrip antennas (MSA) recently. Many papers are devoted to this problem. But the theoretical part of these investigations has not been carried out sufficiently yet. Nowadays the construction of effective methods of integral equation solution for such problems is very important.

This paper gives a new numerical and analytical method of integral equation solution for linear plane multilayer dielectric substrate vibrators. The analysis of electrodynamic microstrip antenna characteristics is made on the basis of this method.

TWO-DIMENSIONAL INTEGRAL EQUATIONS

Let's assume that the strip width d is much smaller than its length ℓ and the wavelength λ, then the density of surface current j can be expressed through one component. The two-dimensional integral equation relative to this component is written as

$$\iint j_x(x',y')K(x',y',x,y)dS = -E_0(x,y), \quad (1)$$

where

$$K = \frac{i}{8\pi^2\omega\varepsilon_0}\left[\int_{-\infty}^{+\infty}\int\left(\chi_1^2 f_1(\chi_1,\chi_2) - k^2 f_2(\chi_1,\chi_2)\right)\frac{e^{-i\chi_1(x-x')-i\chi_1(y-y')}}{\beta}d\chi_1 d\chi_2\right],$$

$$\beta = \sqrt{\chi_1^2+\chi_1^2-k_0^2}\ , \quad k_0 = \omega\sqrt{\varepsilon_0\mu_0}\ ,$$

E_0 – antenna exciting initial field.

For free space the functions $f_1(\chi_1,\chi_2)$ and $f_2(\chi_1,\chi_2)$ are equal to unit.

When antennas are placed directly on the boundary of two mediums (Fig. 1) these functions have the following form

$$f_1 = \frac{2\beta^2\varepsilon_0\beta_1}{(\varepsilon_0\beta_1+\varepsilon_1\beta)(\chi_1^2+\chi_2^2)},$$

$$f_2 = \frac{2\chi_2^2\mu_1}{\mu_0\beta_1+\mu_1\beta},$$

where

$$\beta_1 = \sqrt{\chi_1^2+\chi_1^2-k_1^2}\ , \quad k_1 = \omega\sqrt{\varepsilon_1\mu_1}\ .$$



Fig. 1

The analysis of the integral equation (1) shows that the equation structure is defined by behaviour of the function f_1. When $\chi_1^2+\chi_1^2 \to \infty$, the function is $f_1 \to \frac{2\varepsilon_0}{\varepsilon_0+\varepsilon_1}$. Let's denote it as $\frac{2\varepsilon_0}{\varepsilon_0+\varepsilon_1} = \widetilde{\varepsilon}$.

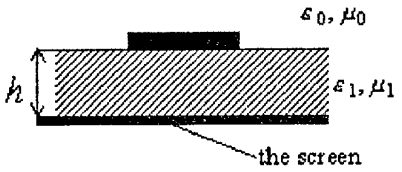


Fig. 2

When an antenna is placed on a dielectric substrate having thickness h and a screen (Fig. 2), these functions are as follows

$$f_1 = \frac{2\beta^2\varepsilon_0\beta_1 th(\beta_1,h)}{(\varepsilon_0\beta_1 th(\beta_1,h)+\varepsilon_1\beta)(\chi_1^2+\chi_2^2)},$$

$$f_2 = \frac{2\chi_2^2\mu_1\beta}{\mu_0\beta_1 th(\beta_1 h)+\mu_1\beta}.$$

And the function behaviour f_1 is the same as when an antenna is placed on the boundary of two mediums

$$f_1 \xrightarrow{\chi_1^2+\chi_2^2\to 0} \frac{2\varepsilon_0}{\varepsilon_0+\varepsilon_1}.$$

The same regularity is characteristic of a multilayer dielectric substrate antenna (Fig. 3).

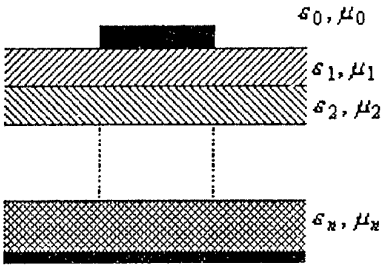


Fig. 3

In this paper the general method is offered for all the structures mentioned above.

ONE-DIMENSIONAL INTEGRAL EQUATION

Using the method developed by the authors we reduce the integral equation (1) to the following one-dimensional integral equation

$$\gamma(AI)(\tau)+(KI)(\tau)=i\sqrt{\frac{\varepsilon}{\mu}}\frac{1}{k}E_0(\tau)\,, \qquad (2)$$

where

$$\gamma=\frac{\widetilde{\varepsilon}}{\pi(k\ell)(kd)}\,,$$

$$(AI)(\tau)=\frac{1}{\pi}\int_0^{+\infty}\chi\int_{-1}^{1}\cos[\chi(\tau-t)]I(t)dtd\chi\,,$$

$$(KI)(\tau)=\frac{k\ell\widetilde{\varepsilon}}{2\pi^2}\int_0^{+\infty}\left[\chi^2 I_0\left(\frac{\chi kd}{4}\right)K_0\left(\frac{\chi kd}{4}\right)-\right.$$

$$\left.-\frac{2\chi}{kd}\right]\int_{-1}^{1}\cos[\chi k\ell(\tau-t)]I(t)dtd\chi+\frac{k\ell}{2\pi^2}\times$$

$$\times\int_0^{+\infty}\int_0^{+\infty}\left[\chi_1^2(f_1(\chi_1,\chi_2)-\widetilde{\varepsilon})-f_2(\chi_1,\chi_2)\right]\times$$

$$\times\int_{-1}^{1}\cos[\chi k\ell(\tau-t)]I(t)dtd\chi\,.$$

I – is the function of antenna surface current, I_0, K_0 – are modified Bessel functions.

NUMERICAL-ANALYTICAL SOLUTION METHOD FOR INFINITE SETS OF LINEAR ALGEBRAIC EQUATIONS

Let's define the function of current as

$$I(\tau)=\sum_{n=1}^{+\infty}\varphi_n(\tau), \qquad (3)$$

where

$$\varphi_n(\tau)=\sqrt{\frac{2}{\pi n}}\sin[n\cdot\arccos(\tau)]\,,\quad n=1,2,...$$

$$(A\varphi_m,\varphi_n)=\begin{cases}0, & m\neq n,\\ 1, & m=n,\end{cases}$$

and reduce the equation (2) to the infinite set of equations

$$c_n+\sum_{m=1}^{+\infty}c_m K_{mn}=b_n,\quad 1\le n<+\infty\,, \qquad (4)$$

The authors have proved that the set of equations (4) is a set of Fredholm equations of the second kind. Besides they have developed some effective calculating method for matrix elements K_{mn} in consideration of poles of integrands. These poles correspond to surface waves propagating in a dielectric substrate.

We can use the numerical-analytical method for solution of the set of algebraic equations (4). We obtain the solution in the form of decomposition

$$u(\tau)=\sum_{n=1}^{N}c_n'\varphi_n(\tau)+\sum_{n=N+1}^{+\infty}c_n'\varphi_n(\tau)\,, \qquad (5)$$

and besides the first unknowns N are defined by Galerkin method from the cut off set of equations

$$c_n'+\sum_{m=1}^{N}c_m' K_{nm}=b_n,\quad 1\le n\le N\,. \qquad (6)$$

This set of equations is deduced from the integral equation by Galerkin method. The other unknowns are calculated analytically

$$c_n'=b_n,\quad N+1\le n<+\infty\,. \qquad (7)$$

That is, the continuous operator K is substituted for an approximate operator and a term in the right-hand side of the equation is given a definite value. This principle peculiarity differs this method from the known modifications of the Moment Method.

The approximate solutions $c'=\{c_n'\}_{n=1}^{+\infty}$ have been calculated by the numerical and analytical method, they have the following speed of convergence to the exact solutions $c=\{c_n\}_{n=1}^{+\infty}$

$$\|c-c'\|\le\frac{const}{N^2}\,. \qquad (8)$$

This paper gives the detailed analysis of electrodynamic characteristics of microstrip antennas on the base of the present method. We have investigated the influence of geometrical dimensions of microstrip antennas, parameters of excitation field, parameters of dielectric mediums on microstrip antenna characteristics. We have offered the effective measures for improvement of bandwidth of antennas.

PROPAGATION OF THE ELECTROMAGNETIC WAVES IN DOUBLE RING WAVEGUIDE WITH DIELECTRIC LAYERS

A. V. Bezugliy, V. V. Khoroshun*

Kharkov Technical University of Radioelectronics
Lenina Ave., 14, Kharkov, 310726, Ukraine, Fax (0572) 409345
*Kharkov State University, Svobody Sq. 4, Kharkov, 310077, Ukraine, Tel. (0572) 126727

In this paper the problem of electromagnetic wave propagation in periodical structure consisting of coaxial metallic rings separated by a homogeneous isotropic dielectric layer with complex dielectric permittivity is considered.

It is assumed that the rings are infinitely thin and perfectly conducting. Dielectric layer forms cylindrical cover with thickness b - a, where b is the radius of external ring; a is the radius of internal ring.

Since the system is periodic to axis x with period l (the distance between rings - slot width is d, the ring height is (l - d) accordingly), fields are also periodic functions on z and are expressed in form of Fourier series, which coefficients are the Bessel functions of first and second kinds.

On the boundary surface $r = a$, $r = b$ exact boundary conditions are formulated, namely: tangential electric fields are zeroing, on rings, continuities of electric and magnetic fields on slots. In case of symmetric waves propagation, a set of equations obtained by sewing together fields is broken up into E- and H-types.

Due to results obtained in [1], both sets of equations are reduced to the boundary Riemann-Hilbert's problem that allows us to express the solution in terms of infinitely sets of linear algebraic equations, which permit to use the reduction technique applic.

In case of $\chi = l/\lambda << 1$ (λ is the wavelength) when zeroth space mode propagates only and assuming a parameter $\nu = \frac{h_0 l}{2\pi} << 1$ (h_0 is propagation constant along system axis), as well as the slots be narrow ($u = \cos\frac{\pi d}{l} << 1$), dispersion equation, describing E_{0n} and H_{0n} - modes propagation, is obtained.

$$\frac{1}{\Delta(1+\varepsilon)(p_0 a)}\left[A - B - \varepsilon\frac{p_0}{\bar{p}_0}(\bar{A}-\bar{B})\right] + \frac{2i\varepsilon}{\Delta\pi(1+\varepsilon)(\bar{p}_0 a)^2} C = -\ln\frac{1-u}{2}, \quad (1)$$

$$\frac{\Delta(p_0 a)}{2}[A^{-1} - B^{-1} - \frac{\bar{p}_0}{p_0}(\bar{A}^{-1} - \bar{B}^{-1})] - \frac{\Delta i}{\pi} C' \ln\frac{1+u}{2} = -1, \quad (2)$$

where

$$A = \frac{J_0'(p_0 a)}{J_0(p_0 a)},\ B = \frac{H_0^{(1)'}(p_0 b)}{H_0^{(1)}(p_0 b)},\ \bar{A} = \frac{J_0'(\bar{p}_0 a)}{J_0(\bar{p}_0 a)},$$

$$\bar{B} = \frac{H_0^{(1)'}(\bar{p}_0 b)}{H_0^{(1)}(\bar{p}_0 b)},$$

$$C = \frac{\frac{J_0(\bar{p}_0 b)}{J_0(\bar{p}_0 a)} + \frac{a}{b}\frac{H_0^{(1)}(\bar{p}_0 a)}{H_0^{(1)}(\bar{p}_0 b)}}{J_0(\bar{p}_0 a)H_0^{(1)}(\bar{p}_0 b) - H_0^{(1)}(\bar{p}_0 a)J_0(\bar{p}_0 b)},$$

$$p_0 a = \frac{1}{\Delta}\sqrt{\chi^2 - \nu^2},\ \bar{p}_0 a = \frac{1}{\Delta'}\sqrt{\chi^2\varepsilon - \nu^2},$$

$$p_0 b = \frac{1}{\Delta'}\sqrt{\chi^2 - \nu^2},\ \bar{p}_0 b = \frac{1}{\Delta'}\sqrt{\chi\varepsilon^2 - \nu^2},$$

J_0, $H_0^{(1)}$ are Bessel functions of first and second kinds, J_0', $H_0^{(1)'}$ are theirs derivatives;

$\Delta = l/2\pi a$, $\Delta' = l/2\pi b$ are dimensionless parameters.

C' looks like C, but Bessel functions are replaced with their derivatives.

Dispersion equations (1), (2) permit passing to the limit:

1) to a ring waveguide in boundless dielectric (under condition $b \to \infty$);

2) to a ring waveguide, situated in free space (under conditions $b \to \infty$, $z = 1$);

3) to a double ring waveguide, situated in free space.

Directing $b \to \infty$ in equations (1), (2) we obtain expressions:

for H-waves:

$$\frac{2iJ_1(p_0 a)H_1^{(1)}(\bar{p}_0 a)}{J_0(p_0 a)H_0^{(1)'}(\bar{p}_0 a) - \frac{\bar{p}_0}{p}J'_0(p_0 a)H_0(\bar{p}_0 a)} = -\left(\ln\frac{1+u}{2}\right)^{-1}, \quad (3)$$

for E-waves:

$$\frac{2iJ_0(p_0a)H_0^{(1)}(\bar{p}_0a)}{\varepsilon\frac{p_0}{\bar{p}}J_0(p_0a)H_0^{(1)'}(\bar{p}_0a)-J'_0(p_0a)H_0^{(1)}(\bar{p}_0a)} = -\ln\frac{1-u}{2}. \quad (4)$$

Assuming in equations (3), (4) $\varepsilon = 1$ we get expressions:

for *H*-waves:

$$\frac{\Delta i}{\pi\nu}\frac{1}{J'_0(p_0a)H_0^{(1)'}(p_0a)}\ln\frac{1+u}{2} = -1,$$

for *E*-waves:

$$\frac{\nu i}{\Delta\pi(p_0a)}\frac{1}{J_0(p_0a)H_0^{(1)}(p_0a)} = -\ln\frac{1-u}{2},$$

which coincide with equations, obtained in [3]. Finaliy, assuming in expressions (1) $\varepsilon = 1$ we obtain equations for the double ring waveguide in free space

for *E*-waves:

$$\frac{\frac{i}{\Delta\pi(p_0a)^2}\left[\frac{J_0(p_0b)}{J_0(p_0a)}+\frac{a}{b}\frac{H_0^{(1)}(p_0a)}{H_0^{(1)}(p_0b)}\right]}{J_0(p_0a)H_0^{(1)}(p_0b)-J_0(p_0b)H_0^{(1)}(p_0a)} = -\ln\frac{1-u}{2},$$

for *H*-waves:

$$\frac{\frac{\Delta i}{\pi}\left[\frac{J'_0(p_0b)}{J'_0(p_0a)}+\frac{a}{b}\frac{H_0^{(1)'}(p_0a)}{H_0^{(1)'}(p_0b)}\right]}{J'_0(p_0a)H_0^{(1)'}(p_0b)-J'_0(p_0b)H_0^{(1)'}(p_0a)} = \left(\ln\frac{1+u}{2}\right)^{-1},$$

which coincide with corresponding equations, obtained in [3].

REFERENCES

1. V.P. Shestopalov. The method of the Riemann-Hilbert problem in diffraction theory and electromagnetic waves propagation [in Russian]. Kharkov: Kharkov university's publish., 1971.
2. N.N. Smirnov. The electromagnetic waves propagation in the round waveguides with periodical slots. Zhurnal Technicheskoy Phiziki [in Russian], vol.28, No 7, p. 1494, 1958.
3. S.S. Tretiyakova. Dispersion equations of double ring waveguide. Radiotechnika, [in Russian], vol.1, Kharkov university's publish., 1965.

METHOD OF REGULARIZATION IN NUMERICAL SIMULATION OF AXIALLY SYMMETRIC DIELECTRIC PATCH ANTENNA EXCITED BY VED

N. Bliznyuk, A. I. Nosich

Institute of Radiophysics and Electronics NASU
Ulitsa Proskury 12, Kharkov 310085, Ukraine
Tel.: 380 572 326129, Fax: 380 572 377380, e-mail: natali@info.kharkov.ua

INTRODUCTION

In the design of microstrip monolithic integrated circuits and millimeter-wave printed antennas, accurate numerical modeling becomes important as the operating frequency becomes higher. Besides of metallic patches, dielectric antennas are actively studied as alternative radiating elements. Our solution of the scattering by a circular dielectric patch is based on the Method of Regularization combined with the Galerkin's Method. This method has a controlled accuracy in the resonant range, and a much smaller matrix size in comparison to solutions obtained by direct applications of the Method of Moments.

PROBLEM FORMULATION

We consider a circular dielectric disk placed ontop a grounded dielectric substrate. This structure shown in Fig. 1. It is excited by a vertical electrical dipole (VED) located at the axis of symmetry, on the perfectly conducting ground plane. Such a source simulates a coaxial probe feed.

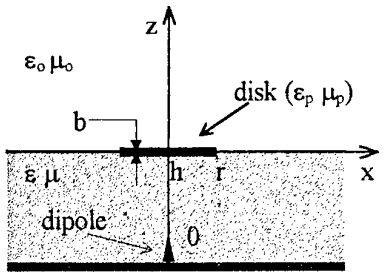


Fig. 1. Geometry of the problem

The full-wave problem formulation involves Maxwell's equations and boundary, edge and radiation conditions.

The field components are expressed via the Fourier-Bessel transforms. Due to the presence of the metal ground plane and the dielectric layer, the kernel functions are determined by the Green's function of the stratified medium This enables us to account rigorously for the surface and leaky wave effects [1]. Then, the approximate boundary conditions for the thin penetrable material sheets [2] are used due to the presence of the dielectric disk:

$$\left[E_t^e + E_t^o\right] = 2Z_o R n \times \left[H_t^e - H_t^o\right],$$
$$\left[H_t^e + H_t^o\right] = -\frac{2}{Z_o} S n \times \left[E_t^e - E_t^o\right],$$

where $Z_o = \sqrt{\mu_o/\varepsilon_o}$, $Z_p = \sqrt{\mu_p/\varepsilon_p}$,

$$R = \frac{i}{2} Z_p \cot\left\{\frac{1}{2}\sqrt{\varepsilon_p \mu_p} k_o b\right\}, \quad S = R/Z_p^2.$$

In terms of the normalized coordinate r and $ka = 2\pi\frac{a}{\lambda}$, $\gamma_i = \sqrt{\kappa^2 - \varepsilon_i ka^2}$, two coupled sets of the dual integral equations (CDIE) are derived:

$$\begin{cases} \int_0^\infty J_1(\kappa r) a_R(\kappa) d\kappa = 0, & r > 1 \\ \int_0^\infty J_1(\kappa r)\left\{\beta_R(\kappa)\alpha_R(\kappa) + D^-(\kappa)\alpha_S(\kappa)\right\} d\kappa \\ \qquad = \int_0^\infty J_1(\kappa r)\Pi^o(\kappa)\gamma_o \kappa^2 d\kappa, & r \le 1 \end{cases}$$

$$\begin{cases} \int_0^\infty J_1(\kappa r)\alpha_S(\kappa) d\kappa = 0, & r > 1 \\ \int_0^\infty J_1(\kappa r)\left\{\beta_S(\kappa)\alpha_S(\kappa) + D^-(\kappa)\alpha_R(\kappa)\right\} d\kappa \\ \qquad = \int_0^\infty J_1(\kappa r)\Pi^o(\kappa)\kappa^2 d\kappa, & r \le 1 \end{cases}$$

where α_R and α_S are the unknown functions; β_R, β_S and D^- are the known functions depending on the layered medium parameters. Right hand part integrand $\Pi^o(\kappa)$ is determined by the excitation, e.g. by the location of the VED source.

The weight functions β_R and β_S have a number of real and complex-value poles corresponding to the surface-wave and leaky-wave modes of the substrate, respectively.

METHOD OF REGULARIZATION

Each of the CDIE obtained consists of two IE. Unlike by the Method of Moments, we propose to invert analytically the singular parts of them, that results in the infinite matrix equation of the Fredholm 2-kind, and guarantees convergence of numerical solution. To obtain a matrix equation, we discretize CDIE by using a

Galerkin projection scheme with a set of judiciously chosen basis functions. The unknown functions of each pair of CDIE are expandedin terms of different basis functions depending on the patch properties and the edge conditions.

Consider the first set of the IE. We expand the unknown function α_R as it was proposed in [3]:

$$\alpha_R(\kappa) = \sum_{n=0}^{\infty} a_n^R \phi_n(\kappa),$$

where the expansion functions are

$$\phi_n(\kappa) = \sqrt{4n+5} \cdot J_{2n+5/2}(\kappa) \frac{1}{\sqrt{\kappa}},$$

so that they are orthogonal eigenfunctions of the static limit of this equation. Such a choice of the basis functions allows to invert the singular part of the dual integral equations analytically and provides satisfying the edge condition on the patch rim. Furthermore, the first equation is satisfied identically.

Extracting the free-space disk static (singular) part of the dual integral equations is done by introducing the function $\Omega_R(\kappa)$, such that

$$\beta_R = \frac{2\kappa}{1+\varepsilon}\{1 - \Omega_R(\kappa)\}.$$

Note that analytical inversion of a part of original operator essentially exploits the circular shape of the patch.

The second of CDIE can be easily converted to an integral equation of the Fredholm 2-nd kind by the the inverse Furier-Bessel transform. It does not require the analytical regularization. However, a good choice of basis functions allows to simplify a numerical solution of the problem and to decrease the CPU time expenses. We consider two sets of the basis functions [4]:

$$\alpha_S(\kappa) = \sum_{n=0}^{\infty} a_n^S \chi_n(\kappa)$$

where $\chi_n(\kappa) = \sqrt{\frac{2}{n+1}} e^{-\frac{\kappa^2}{2}} \kappa^2 L_n^1(\kappa^2)$ are proportional to the generalized Laguerre polynomials; and

$$\alpha_S(\kappa) = \sum_{n=0}^{\infty} \tilde{a}_n^S \tilde{\chi}_n(\kappa),$$

where $\tilde{\chi}_n(\kappa) = 2\sqrt{n+1} J_{2n+2}(\kappa)$, $J_{2n+2}(\kappa)$ are the Bessel function of the integer order. We made the comparison of advantages and disadvantages of these functions when solving the matrix equation.

On using the orthogonality of the chosen functions and the fact that they diagonalize the operators of the CDIE, the infinite block matrix equation (IBME) of the Fredholm 2-nd kind is obtained like it was done in [5] for a perfectly conducting disk.

$$\begin{cases} a_m^R - \sum_{n=0}^{\infty} a_n^R \Theta_{mn}^R(\kappa) + c_R \sum_{n=0}^{\infty} a_n^S \Psi_{nm}(\kappa) = b_m^R(\kappa) \\ a_m^S - \sum_{n=0}^{\infty} a_n^S \Theta_{mn}^S(\kappa) + c_S \sum_{n=0}^{\infty} a_n^R \Psi_{nm}(\kappa) = b_m^S(\kappa) \end{cases},$$

where

$$c_R = \frac{1+\varepsilon}{2}; c_S = \frac{ika}{2S}; \Theta_{mn}^S = c_S \int_0^{\infty} \frac{\chi_m(\kappa)\chi_n(\kappa)}{\kappa} \Omega_S(\kappa) d\kappa;$$

$$\Theta_{mn}^R = \int_0^{\infty} \Omega_R(\kappa)\phi_m(\kappa)\phi_n(\kappa) d\kappa; \Psi_{mn} = \int_0^{\infty} \frac{D^-(\kappa)\phi_m(\kappa)\chi_n(\kappa)}{\kappa} d\kappa;$$

$$b_m^R = c_R \int_0^{\infty} \Pi^o(\kappa)\gamma_o \phi_m(\kappa)\kappa d\kappa; b_m^S = c_S \int_0^{\infty} \Pi^o(\kappa)\chi_m(\kappa)\kappa d\kappa;$$

$$\Omega_R(\kappa) = 1 - (1+\varepsilon)\left(\frac{\gamma_o\gamma_\varepsilon \sinh(\gamma_\varepsilon h)}{\kappa D_m(\kappa)} - i\frac{ka}{\kappa}R\right); \Pi^o = \frac{1}{\pi D_m(\kappa)};$$

$$D^-(\kappa) = \frac{\gamma_\varepsilon \sinh(\gamma_\varepsilon h) - \gamma_o \varepsilon \cosh(\gamma_\varepsilon h)}{D_m(\kappa)}; \Omega_S(\kappa) = \frac{\varepsilon \cosh(\gamma_\varepsilon h)}{D_m(\kappa)};$$

$$D_m(\kappa) = \gamma_\varepsilon \sinh(\gamma_\varepsilon h) + \gamma_o \varepsilon \cosh(\gamma_\varepsilon h).$$

Here, the IBME elements have rapidly decaying integrands due to the choice of the basis functions and are efficiently computed by a numerical procedure. However, in the case of the Bessel functions it is necessary to expand the kernels and make some analytical integrations if wish to reach the machine precision in our computations.

CONCLUSIONS

We have proposed a full-wave approach to the analysis of the axially symmetric dielectric patch antenna excited by a vertical electrical dipole. Based on this approach the efficient numerical techniques were developed.

REFERENCES

1. N. Yu. Bliznyuk, and A. I. Nosich, "Basic properties of the fields excited by VED and HMD located in a dielectric substrate backed by a perfectly conducting ground plane," *Microwave and Optical Technology Letters,* vol. 15, no. 5, 1997, pp.316-320.
2. E. Bleszynski, M. Bleszynski, and T. Jaroszewicz, *IEEE Antennas Propagat. Magazine*, vol.35, no.6, pp. 14-25, 1993.
3. A. N. Khizhnyak, "Diffraction of a plane wave by a thin disks," *Sov. Physics Acoustics,* vol.25, no. 6, 1989.
4. M. Abramovitz, I. A. Stegun, "*Handbook of Mathematical Functions,*" Washington, DC: NBS, Ch. 10, 11, 1964.
5. N. Yu. Bliznyuk, A. I. Nosich, "Accurate Analysis of Fundamental Wave Phenomena in the Printed Antennas", IRMM-97 Digest, Wintergreen, July 1997, pp. 342-345.

RIGOROUS CALCULATION OF ACTIVE ANTENNAS

V. L. Danilchuk

Department of the Theoretical and Special Physics, Novgorod State University,
41, St. Petersburg st., Novgorod, 173003, Russia

Problems of development of compact antennas (in short-wave band, ultra-short or higher frequencies wave band) with a high sensitivity and/or a wide passband attend a stable non-reducing interest. As a rule, this problem is solved by one of the following ways:

- development of short inductively loaded antennas;
- design of antenna-amplifiers (active antennas) (AA).
- The first problem was considered in Ph.D. thesis [1] of one of the present paper authors within the frame of parametric synthesis.

The second problem is a destination of the present paper. As a rule, such a problem is subdivided into two ones with sufficient features of approaches to each problem: design of resonant AA and nonresonant AA. High level of the external noises within the range 30÷70 MHz provide a possibility to develope antennas of very short electrical length and obtain a wide AA passband when using the antenna with an active element. However, for very small dimensions of the antenna and high dis-matching of its output with the aqmplifier input (for non-resonant AA) the amplifier noise can be a factor which needs to be taken into account in such devices in spite of the high external noise. So, most of researchers in this field use different principles of AA constructing depending on the wave band.

The resonant AA solution stages so are the following:

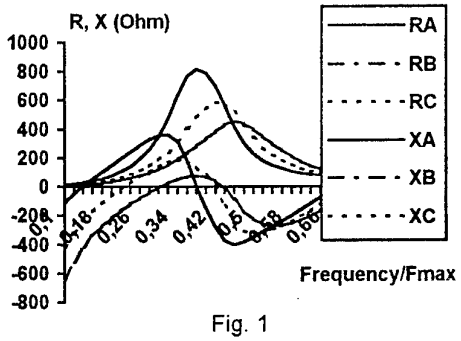


Fig. 1

a) choice of AA structure;

b) solution for the antenna itself: calculation of passband (which is a dominant one in the system "antenna-amplifier") (Fig. 1)

c) solution for the amplifier (Fig. 2) (calculation of its stability, nominal gain factor (Fig. 3), nominal differential factor of noise, nominal noise value (if the operating frequency is more than 100 MHz), input and output impedance);

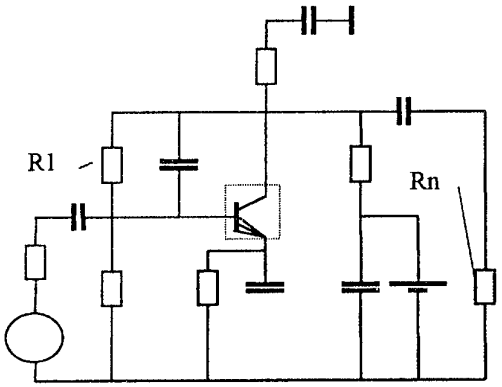


Fig. 2

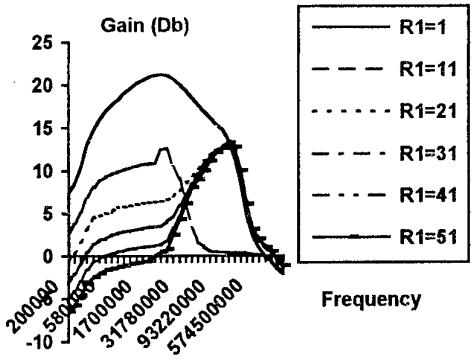


Fig. 3

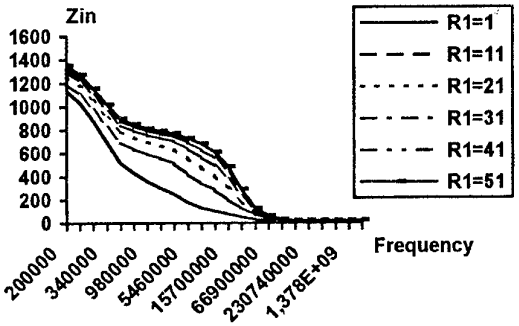


Fig. 4

d) solution of the problem on possibility of the antenna optimal matching with the amplifier (Fig. 1, 4);

e) correction of the antenna output parameters and the amplifier input ones.

The main stages of non-resonant AA calculation are the same, with only one correction, consisting in that the passband is calculated for the amplifier as well, and the noise characteristics of the amplifier are taken into account for any frequency band.

Calculation of the antenna electromagnetic parameters is carried out by means of a rigorous numerically-analytical method considered in [2, 3] in details.

Conventional calculation of AA was carried out by a graph-analytical method, where the calculation for the antenna itself was out of the consideration (only its static output characteristics were considered) and for the amplifier calculation a theory of two-ports [5] was used. It resulted in rather an approximate result, and consequently the experimental operational development of such AA was almost the main stage of work. The authors of the report propose more rigorous solution on their opinion, without the mentioned above subdivisions of the whole algorithm for solving the problem. Along with the rigorous calculation of electromagnetic characteristics ofthe antenna itself, the conventional two-port of the active element of the scheme is replaced with the following adapted models [6, 7]:

- for a bipolar transistor - with the Gummel-Pun model (or Ebers-Moll one in simplified case) (Fig. 5);

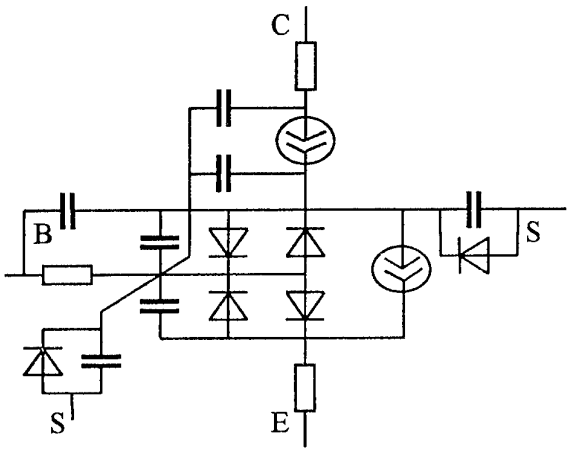


Fig. 5

- for a field transistor with a controlling p-n - transition - with the Shihman-Hodzes model;

- for a field MOH-transistor of LEVEL=4 models (or LEVEL=3, LEVEL=2, LEVEL=1in simplified case).

Due to SAPR, elements of the active circuit can be operatively corrected at any stage of development.

The main attention when choising, calculating and measuring the amplified and noise parameters of the amplifier is paid to system-invariant initial parameters (Y, Z, H, S parameters) of the amplified and noise characteristics, and which is more, the basic expressions are appropriate for absolutely steady, as well as for conditionally steady amplifiers.

The proposed approach and wide application of SAPR enables one to realise AA with a high reliability on the basis of computer designing as well as to achieve minimal experimental operational development.

REFERENCES

1. Zibaev B.G., Romanov B.S. Aerials - amplifiers, 1980.- P. 240. [in Russian].

2. Red. E. The Help allowance on a high-frequency circuitry. 1990.- P. 256.

3. Danilchuk V.L., Eminov S.I. The theory of a integrated equation of a impedance vibrator. JTP. - 1995. - V. 65(5), -P. 204.

4. Danilchuk V.L. "New Approach In A Problem Of Account Of Active Aerials" , Proc. of Progress in Electromagnetics Research Symposium. Nantes, FRANCE, July 13 - 17, 1998, volume 2, p. 633.

5. Etkin V.S. Semi-conductor source devices A MICROWAVES. 1975 - V. 1.

6. Rezvig V.D. Application of P-CAD programs and Pspice for circuit engineering modeling on PC, issue 1-4 [in Russian].

7. Popov V.P. Application of a package of the applied programs MICRO-CAP III for automated analysis of circuits, 1994 [in Russian].

NUMERICAL ALGORITHM FOR CALCULATING THE ELECTRIC CHARACTERISTICS OF WIRE ANTENNAS USED TO ANALYSE THE ELECTROMAGNETIC COMPATIBILITY PARAMETERS OF A RADIO SYSTEM

A. S. Ilinski, I. V. Berezhnaya, O. Ju. Perfilov

Faculty of Computational Mathematics and Cybernetics,
Moscow State University, Vorobievy Gory, Moscow, 119899, Russia
Tel./fax: (095)939-1776 / (095)939-2596, E-mail: celd@cs.msu.su

ABSTRACT

The authors have developed a numerical algorithm for analysing the electric characteristics of the system of vibrators arbitrarily located above the ground. The algorithm allows one to calculate the antenna radiation patterns corresponding to the harmonics (subharmonics) of the fundamental radiation, the frequencies of intermodulation interference, the pattern distortions, and the input impedance change caused by the installation of additional antennas on a given object. The votage induced by the nearby transmit antennas can be calculated as well.

INTRODUCTION

To analyze the electromagnetic compatibility (EMC) of radio systems (RSs) located inside an object it is necessary to find the channels that support the influence of electromagnetic field on these systems. Electromagnetic field may propagate over the communication lines of RSs connecting individual blocks, circuit wires and transmit and receive antennas of RSs. This paper does not consider connection lines between blocks and circuit wires of radio systems.

The estimation of the EMC inside the object involves the estimation of the electromagnetic field influence on the antenna systems. The key electromagnetic field characteristics depend on the source, the surrounding medium and the distance from the source to the observation point. It is worth noting that under certain conditions, the ground conductivity can affect the formation of the general electromagnetic situation.

The classic transmission equation is often used for estimating the input receiver noise levels:

$$E_n = P_t + G_t + G_r - \Delta G_{tr} - L_{tf} - L_{rf} - L + \delta + CF, \quad (1)$$

where E_n is the noise level, P_t is the transmitter power, G_t is the transmit antenna gain, G_r is the receive antenna gain, ΔG_{tr} is the transmitter-receiver isolation, L_{tf} is the transmitter antenna-feeder losses, dB; L_{rf} is the receiver antenna-feeder losses, L is the propagation path losses (losses in the coupling circuit), δ is the polarization isolation, CF is the frequency transmitter–receiver isolation.

However, parameters L, δ can be determined only empirically. Moreover, parameters $G_t, G_r, \Delta G_{tr}$ lose their physical sense when the antenna is located in the near or transition zones. The ground influence is not taken into account in formula (1). Therefore, formula (1) yields only an estimate of E_n, which does not take into account the pattern distortions and the antenna input impedance change in the regions spaced at electrically small distances. In order to elaborate the aspects of the object EMS, one needs to develop an algorithm for calculation of the electric characteristics of vibrator systems arbitrarily located above the ground.

As one can see from the current scientific and technical publications, there are no suitable and effective numerical algorithms intended for this purpose. Therefore, it was necessary to create a new algorithm for solving the EMC analysis and synthesis problems. The proposed algorithm is the result of the development of the methods published in [1, 2, 3]. A detailed description of the algorithm is given in papers [4, 5]. The key aspects of the developed algorithm are presented below.

METHOD APPLIED

The analysis of the excitation of the system of vibrators (Fig. 1) arbitrarily located above the semiconducting ground with relative permittivity ε_2 magnetic permeability μ_2 and conductivity δ_2 involves solving the inhomogeneous Maxwell equations

$$\begin{cases} \nabla \times \vec{H} = i\omega\tilde{\varepsilon}\vec{E} - \vec{j}_{ext} \\ \nabla \times \vec{E} = i\omega\mu\vec{H} \end{cases}, \quad (2)$$

where $\tilde{\varepsilon} = \varepsilon_m - i\sigma_m/\omega, \mu = \mu_1 = \mu_2$,

$$\varepsilon_m = \begin{cases} \varepsilon_1 z > 0, \\ \varepsilon_2 z < 0, \end{cases} \quad \sigma_m = \begin{cases} \sigma_1 z > 0, \\ \sigma_2 z < 0, \end{cases}$$

satisfying the boundary conditions on the vibrators' surface S_l

$$\left[\vec{E}^{tot}(Q), \vec{n}_l\right] = 0, \; Q \in S_l, \; l = 1,2,...N \quad (3)$$

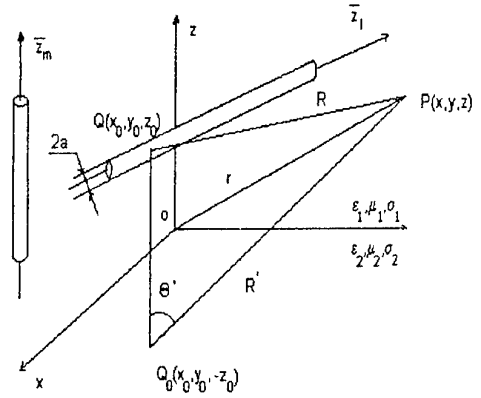


Fig. 1

and on a planar interface separating two media

$$[E_\tau]_{z=0}=0,[H_\tau]_{z=0}=0\,, \tag{4}$$

and the radiation conditions

$$\lim_{R\to\infty} R\vec{E}, \qquad \lim_{R\to\infty} R\vec{H}\,. \tag{5}$$

Usually, the initial vector problem described by the following equations

$$\vec{E}=-\frac{i}{\omega\tilde{\varepsilon}}\left(\nabla(\nabla\cdot\vec{A})+k^2\vec{A}\right),\ \vec{H}=\frac{1}{\mu_1}\nabla\times\vec{A}, \tag{6}$$

$$\nabla^2\vec{A}+k^2\vec{A}=-\mu_1\vec{J}_{ext}, \tag{7}$$

where

$$\vec{A}(Q)=\frac{1}{4\pi}\sum_{l=1}^{N}\int_{S_l}\vec{I}_l(Q)\hat{G}(P,Q)\,ds_l\,, \tag{8}$$

$$k^2=\omega^2\mu_1\tilde{\varepsilon},$$

reduces to the system of the Hallen-type integral equations for antennas current

$$\sum_{n=1}^{N}\int_0^{L_n} I_n(t_n)K_{ln}(t_n,z_l')dt_n=\tilde{C}_1^l\sin k_1z_l'+\tilde{C}_2^l\cos k_1z_l'-$$

$$-\frac{i\omega\varepsilon_1}{k_1}\int_0^{z_l'}E_{z_l}^{ext}(t_l)dt_l\,, \tag{9}$$

with the additional conditions at the antenna free ends and branch points.

This system is solved by the method of moments where the current is approximated by step basis functions

$$I_n(t)=\sum_{m=1}^{N_n}I_m^n\omega_m^n\,. \tag{10}$$

The system of the algebraic equations

$$\sum_{n=1}^{N}\sum_{m=1}^{M_n}b_{qm}^{ln}I_m^n=f_q^l, l=1,...,N, q=1,...,M_l \tag{11}$$

is solved by the iterative multistage minimal discrepancy method [6]

$$I_{i+1}=I_i-\sum_{s=1}^{p}\tau_{is}B^{s-1}r_i\,, \tag{12}$$

$$r_{i+1}=r_i-\sum_{s=1}^{p}\tau_{is}B^{s}r_i\,, \tag{13}$$

where B^s is the linear function and r_i is the inner parameter of this method on i iterative step.

The calculation of the inner integrals in expression (9) involves determining the components of Green's tensor function

$$\hat{G}(P,Q)=\begin{bmatrix} G_{11}(P,Q) & 0 & 0\\ 0 & G_{11}(P,Q) & 0\\ \dfrac{\partial g(P,Q)}{\partial x} & \dfrac{\partial g(P,Q)}{\partial y} & G_1(P,Q)\end{bmatrix}. \tag{14}$$

In the proposed algorithm the calculation of the Sommerfeld integrals

$$G_{11}(P,Q)=\frac{e^{-ik_1R}}{R}+\int_0^\infty J_0(\lambda\rho)\frac{\eta_1-\eta_2}{\eta_1+\eta_2}\frac{e^{-\eta_1|z+z_0|}}{\eta_1}\lambda d\lambda,$$

$$G_1(P,Q)=\frac{e^{-ik_1R}}{R}+\int_0^\infty J_0(\lambda\rho)\frac{\eta_1\varepsilon-\eta_2}{\eta_1\varepsilon+\eta_2}\frac{e^{-\eta_1|z+z_0|}}{\eta_1}\lambda d\lambda,$$

$$\frac{\partial g(P,Q)}{\partial x}=2\frac{x-x_0}{\rho}\int_0^\infty J_1(\lambda\rho)\frac{\varepsilon-1}{\eta_1\varepsilon+\eta_2}\frac{e^{-\eta_1|z+z_0|}}{\eta_1+\eta_2}\lambda^2d\lambda,$$

$$\frac{\partial g(P,Q)}{\partial y}=2\frac{y-y_0}{\rho}\int_0^\infty J_1(\lambda\rho)\frac{\varepsilon-1}{\eta_1\varepsilon+\eta_2}\frac{e^{-\eta_1|z+z_0|}}{\eta_1+\eta_2}\lambda^2d\lambda,$$

where $J_0(\lambda\rho)$ is the zero-order Bessel function, $J_1(\lambda\rho)$ is the first-order Bessel function,

$$\rho=\rho(P,Q)=\sqrt{(x-x_0)^2+(y-y_0)^2}\,,$$

$$R=R(P,Q)=\sqrt{\rho^2+(z-z_0)^2}\,,$$

$$\eta_1=\sqrt{\lambda^2-k_1^2}\,,\ \eta_2=\sqrt{\lambda^2-k_2^2}\,,$$

$$k_1^2=\omega^2\mu_1\varepsilon_1,\ k_2^2=\omega^2\mu_1(\varepsilon_2-i\sigma_2/\omega),$$

$$\varepsilon=(\varepsilon_2'-i\sigma_2/\omega)/\varepsilon_1,$$

is performed by the saddle-point method followed by expanding the integrand about the saddle point into the Laurent series

$$G_{11}(P,Q)=\frac{e^{-ik_1R}}{R}+\frac{e^{-ik_1R'}}{R'}r_h(\theta')-$$
$$-\frac{1}{\sqrt{2}}\frac{e^{-ik_1R'}}{k_1R'^2}r_{h_1}(\theta')+\ldots$$

$$G_1(P,Q)=\frac{e^{-ik_1R}}{R}+\frac{e^{-ik_1R'}}{R'}r_v(\theta')-\frac{e^{-ik_1R'}}{k_1R'^2}r_{v_1}(\theta')+\ldots,$$

$$\frac{\partial g(P,Q)}{\partial x}=2\frac{|x-x_0|e^{-ik_1R'}}{R'^2}r_{h_2}(\theta')-\sqrt{\frac{2ik_1}{\pi}}r_{h_3}(\theta')+\ldots,$$

$$\frac{\partial g(P,Q)}{\partial y}=2\frac{|y-y_0|e^{-ik_1R'}}{R'^2}r_{h_2}(\theta')-\sqrt{\frac{2ik_1}{\pi}}r_{h_3}(\theta')+\ldots,$$

where r_h, r_{h_1}, r_{h_2}, r_{h_3}, r_v, and r_{v_1} are the horizontal and vertical ground reflection coefficients.

Thus, the current distributions along the vibrators are determined.

Known the voltage and current at the excitation points, we can determine the input antenna system impedances. In order to determine the electromagnetic field intensity produced by the system of vibrators under consideration, we employ the method of potentials. To this end, we calculate the sum of the electromagnetic field vectors excited by each elementary oscillator placed at the collocation points. The total field at the observation point is the superposition of the electromagnetic fields of the elementary oscillators. If necessary, we can calculate patterns (distortions of the pattern) in any fixed cross section at any radiation frequency, including harmonics, subharmonics, etc.

RESULTS

The authors created a package of applied programs on the basis of the described algorithm. The input data of the program package are the geometry of the oscillators, the current sources, the number of the collocation points on each vibrator and in the desired pattern cross section, the ground parameters (permittivity and conductivity) and the required accuracy of the solution which is determined through the relative discrepancy. The algorithm enables one to calculate the key electric characteristics of the vibrator system arbitrarily placed above the semiconducting ground: such as the current distribution, the input impedance, traveling wave ratio, the electromagnetic field intensity at an observation point (the pattern), and the antenna gain.

The calculation results of the electric characteristics of the vibrator system are in good agreement with experimental data and the results presented in other papers. A number of applied problems, including the problem of optimizing the design of the wideband mast antennas [7, 8], were solved using the proposed algorithm.

REFERENCES

1. Zaharov E.V., Pimenov Ju.V. *Numerical Analysis of Radiowave Diffraction*.- Moscow: Radio and Communication, 1982, 184 p. [in Russian].
2. Ilinski A.S., Berezhnaya I.V. "Mathematical models of the Thin Wire Antennas", Mathematical models and Culculational Methods, Moscow State University, 1987, pp.103-125 [in Russian].
3. Alkhovski E.A., Berezhnaya I.V., Grishin K.V., Ilinski A.S., Kondratev A.G. "Registration of Conductive Ground Influence on Current and Radiation Pattern Distribution of Linear Antennas", Mathematical Methods and Culculational Diagnostic, Moscow State University, 1990, pp.199-207 [in Russian].
4. Berezhnaya I.V., Grishin K.V., Ilinski A.S., Kondratev A.G., Perfilov O.Ju. "Mathematical Modeling Method of many vibrator antennas placed near real ground", Mathematical Models of nature.- Moscow State University, 1993, pp. 35-41 [in Russian].
5. Alkhovski E.A., Berezhnaya I.V., Ilinski A.S., Kondratev A.G., Perfilov O.Ju. "Investigations of HF and VHF Antennas Located Near the Ground", Proceeding of the 1995 URSI Int. Symposium. on Electromagnetic Theory, St. Petersburg, Russia, May 23-26, 1995, pp. 492-494.
6. Ilinski A.S., Perfilov O.Ju., Samohin A.B. "Iterative Method of Solution Integral Equations of Theory Wire Antennas" *Mathematical Modeling*, 1994, v.6, No. 3, pp.52-59 [in Russian].
7. Alkhovski E.A., Kondratev A.G., Perfilov O.Ju., Teplyashin V.I. "Wide Range Mast Antenna", Patent, Russia № 2073943, 20.02.97 (H01 Q9/44) [in Russian].
8. Alkhovski E.A., Berezhnaya I.V., Grishin K.V., Ilinski A.S., Kondratev A.G., Perfilov O.Ju., Teplyashin V.I. "Investigation of HF wide range mast antennas for mobile radiostations", *Electrocvya*, 1994, № 3, pp.25-26 [in Russian].

SYSTEM OF LINEAR WIRES IN ANISOTROPIC PLASMA

E. A. Jatsenko, N. M. Jatsenko, N. A. Khizhnyak

Department of Radiophysics, Kharkov State University,
Svoboda sq. 4, Kharkov 310077, Ukraine
tel: (8-0572) 404232; e-mail: khizh@.khizh.kharkov.ua

STATEMENT OF A TASK

In anisotropic plasma, described by permittivity tensor $\hat{\varepsilon}$

$$\hat{\varepsilon} = \begin{pmatrix} \varepsilon_1 & 0 & 0 \\ 0 & \varepsilon_1 & 0 \\ 0 & 0 & \varepsilon_3 \end{pmatrix},$$

two parallel thin linear wires and a component any angle γ with an axis of anisotropy (the axis OZ) are located. Lengths of wires are $2L_1$, $2L_2$, radii are b_1, b_2, a distance between wires is d. It is necessary to find current distributions of each wire, radiation electromagnetic fields and power flux density in the far zone.

The solution of a task is carried out within the framework of the integral equations method of electromagnetics. It is shown, that anisotropy of medium essentially changes dependence of an input current (or a current distribution) in one wire on the length of other wire and on the distance d between wires. The influence of anisotropy is displayed in change of amplitude and period of these characteristics, which also depend on orientation of the wires system with respect to an axis of anisotropy. The influence of medium anisotropy and orientation of wires in medium on a function's period of current distributions established in each wire, is united by such integral characteristic, as equivalent permittivity of medium $\varepsilon_{eq} = \delta^2 \cos^2\gamma + \delta\sqrt{\varepsilon_1}\sin^2\gamma$, where $\delta^2 = \varepsilon_3 \sin^2\gamma + \varepsilon_1 \cos^2\gamma$. In wires located under angle γ in uniaxial anisotropic medium, the current distribution is established, whose space period is the same, as it was, if the wires are in isotropic medium with permittivity $\varepsilon = \varepsilon_{eq}$.

It is known, that for wires located in isotropic medium, the input current's amplitude of each wire is periodic dampted function of the distance d between wires. In anisotropic medium the character of this dependence is kept, excluding a case for the distance d, and for some equivalent distance d_{eq}, including the distance d, the dielectrical parameters ε_1, ε_3 of anisotropic medium and orientation of wires in this medium. For example, for wires located in one plane with the axis of anisotropy, d_{eq} has the kind $d_{eq}^2 = d^2 \varepsilon_1 \varepsilon_3 \delta^2$. By each concrete system of wires with the given geometry in anisotropic medium one can put in conformity some equivalent antenna system in isotropic medium, by choosing in appropriate way its geometrical sizes (this conclusion concerns only currents, instead of radiation fields).

The electromagnetic field of antenna system in far zone represents ordinary and non-ordinary waves. The power pattern in the plane, perpendicular to wires, practically does not depend on medium anisotropy. Anisotropy essentially influence on patterns in the plane of wires. The character of this influence is similar to the change of distance between wires and depends on orientation of wires in medium.

THE SOLUTION OF THREE – DIMENTIONAL ELECTRODYNAMIC PROBLEMS BY THE INTEGRAL EQUATION METHOD

V. M. Morozov, V. I. Magro

Dniepropetrovsk State University
13 Nauchny pereulok Dniepropetrovsk, 320050 Ukraine,
tel. (38) 0562-46-79-95

ABSTRACT

Solution of three-dimensional problems of radiation of infinite waveguide antenna array is considered, investigating the antenna array with subarray as matching elements. The antenna system possess triangular spacing of radiation elements. The study method is based on using the integral equation with separation of the piercing domain.

INTRODUCTION

Among other, the method of integral equation is very effective for solving three-dimensional problems. The subject of the paper is an application of the method of integral equation to the calculation of waveguide antenna array with triangular spacing of radiation elements. The whole domain of the field determination is subdivided into a piercing domain and partial domains. The theorem of vectorial theory of diffraction is used for the total field in the piercing domain. Theoretical investigation of antenna array, composed of open-ended rectangular waveguides and finite subarray with the purpose of obtaining the impedance matching with free space is presented.

PROBLEM FORMULATION AND METHOD OF SOLUTION

For unit cell the whole domain of the field determination is subdivided into three domains (Fig. 1):

I – waveguide extended to infinity (piercing domain)

$$-\frac{wx}{2} \le x \le \frac{wx}{2};\ -\frac{wy}{2} \le y \le \frac{wy}{2};\ -\infty \le z \le \infty;$$

II – "channel of Floker"

$$-\frac{Px}{2} \le x \le \frac{Px}{2};\ -\frac{PA\sin(A)}{2} \le y \le \frac{PA\sin(A)}{2};$$
$$-z2 \le z \le z1;$$

III – semi–infinite "channel of Floker"

$$-\frac{Px}{2} \le x \le \frac{Px}{2};\ -\frac{PA\sin(A)}{2} \le y \le \frac{PA\sin(A)}{2};$$
$$0 \le z \le \infty.$$

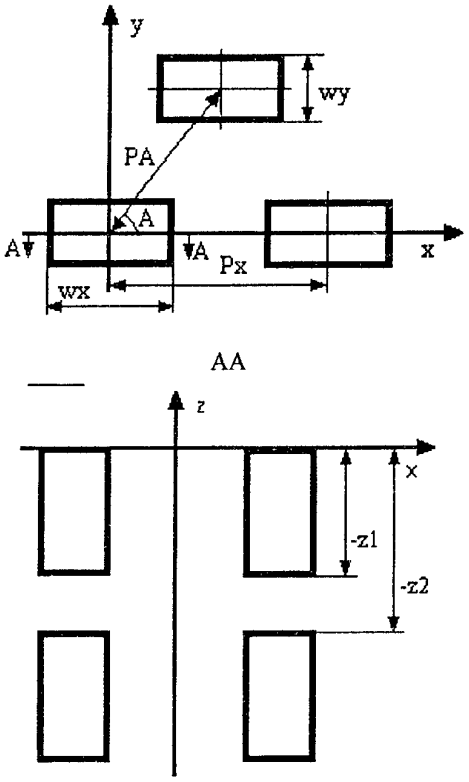


Fig. 1

On the strength of the theorem of vectorial theory of diffraction, one can write integral representation for the total field in the piercing domain as

$$\vec{\vec{E}}^{1}(x,y,z) = \vec{\vec{E}}^{1}_{EXC}(x,y,z) +$$
$$+[\vec{\nabla}\int_{S^1}(x,y,z;x`,y`,z`)[\vec{n}\vec{\vec{E}}^{1}(x`,y`,z`)]dS`].$$

Here $\vec{n}$ is inner normal to the boundary S^1; $\vec{\vec{G}}^{1}(\vec{r},\vec{r}`)$ is the affinor Green's function of potential type of the second kind which is reduced of the Helmholtz equation

$$\Delta\vec{\vec{G}}^{1}(\vec{r},\vec{r}`)+k^2\vec{\vec{G}}^{1}(\vec{r},\vec{r}`) = -\vec{\vec{I}}\delta(\vec{r},\vec{r}`)$$

and boundary condition on conductor surface S^1

$$[\vec{n}[\vec{\nabla}\vec{\vec{G}}^{1}(\vec{r},\vec{r}`)]] = 0;$$

$$(\vec{n}\vec{\vec{G}}(\vec{r},\vec{r}`)) = 0;\ \ \vec{r},\vec{r}` \in S^1 .$$

Let's locate the observation point on $z = -z2, -z1, 0,$ and take into consideration the boundary condition for tangential component of vector of intensity electric field. Then we obtain the system of Fredholm integral equations of the second kind. An application of the Galerkin`s method finally yields system of linear algebraic equation which can be solved by the reduction's technique.

The numerical results coincide well with other available data. The influence on geometrical parameters of the reflectivity in a waveguide is investigated.

COMPUTER MODELING OF ELECTROMAGNETIC WAVE PROPAGATION IN A TIME–VARYING MEDIUM

A. G. Nerukh, K. M. Yemelyanov*, F. V. Fedotov

Kharkov Technical University of Radio Electronics, 14, Lenin Ave., Kharkov, 310726, Ukraine
tel.: +380-572-409372, e-mail: nerukh@ddan.kharkov.ua
* Kharkov State University, 4, Svobody Sq., Kharkov, 310077, Ukraine
tel.: +380-572-457257, e-mail: k.yemelyanov@univer.kharkov.ua

INTRODUCTION

The purpose of the paper is to consider the transformation of electromagnetic wave in a medium with permittivity and conductivity changing in time as the finite sequence of rectangular periodic pulses.

Parametric phenomena in active media have been attracted attention for a long time in connection with the possibility of electromagnetic wave generation and amplification both by the interaction of charges with a spatially periodic medium [1], [2] and by the time modulation of the medium parameters [3–7]. In the systems with distributed parameters, nonstationarity of the medium caused by the moving of sinusoidal wave of the permittivity disturbance has mainly been considered. In this case, the solution to the problem is obtained approximately as an expansion in powers of a small parameter.

The investigation of transient electromagnetic phenomena is of importance for the problems of electromagnetic signal controlling by the temporal adjustment of medium parameters, i.e. in optoelectronic systems [8]. One of the possible ways of such an adjustment is the changing of medium parameters by a finite sequence of pulses.

The problem of the electromagnetic wave propagation in a time–varying medium is formulated as a Volterra integral equation of the second kind [9]. The temporal variation of medium parameters is considered as a finite sequence of the periodic rectangular pulses. The solution to the problem is obtained by the Direct Numerical Calculation Method [10]. On the basis of the proposed method an original software for numerical modeling of the wave propagation in a time–varying medium has been created. The structure of the program is created allowing for the further developing and extending its functionality. In general, the software enables us to consider an initial field with an arbitrary time–spatial dependence. Here we consider two initial fields, a plane wave and a gaussian beam.

PROBLEM FORMULATION AND BASIC RELATIONSHIPS

Let us consider an unbounded dielectric dissipative medium with an electromagnetic field defined by the function $E_0(t,x)$. The changes in medium permittivity $\varepsilon(t)$ and conductivity $\sigma(t)$ are a finite sequence of N rectangular periodic pulses originating under the action of external forces at the zero moment of time. We assume that the permittivity and the conductivity of the medium acquire the values ε_1 and σ_1 respectively on the disturbance intervals $(n-1)T < t < T_1 + (n-1)T$, $n = 1,...,N$ and the values ε and σ on the quiescence intervals $T_1 + (n-1)T < t < nT$, $n = 1,...,N$. Let us consider $\sigma = 0$.

$$\varepsilon(t) = \varepsilon + (\varepsilon_1 - \varepsilon)\sum_{k=1}^{N}\left\{\theta(t-(k-1)T) - \theta(t-T_1-(k-1)T)\right\}$$

$$\sigma(t) = \sigma_1\sum_{k=1}^{N}\left\{\theta(t-(k-1)T) - \theta(t-T_1-(k-1)T)\right\}. \quad (1)$$

Here, $\theta(t)$ is the Heaviside step function, T is the duration of the period of change in parameters, T_1 is the duration of the disturbance interval.

In the one-dimensional scalar case, the initial nonstationary electromagnetic problem is formulated in terms of a Volterra integral equation of the second kind [9], i.e.,

$$E(t,x) = E_0(t,x) - \frac{1}{2v\varepsilon}\int_0^{\infty} dt' \int_{-\infty}^{\infty} dx' \left\{\sigma_1(t') + (\varepsilon_1(t') - \varepsilon)\frac{\partial}{\partial t}\right\} \times \quad (2)$$
$$\times \delta\left(t - t' - \frac{|x-x'|}{v}\right) E(t',x')$$

where $\delta(t)$ is the Dirac delta function, $v = c/\sqrt{\varepsilon}$.

Let us introduce the new dimensionless variables $\tau = \kappa v t$, $\xi = \kappa x$ where κ is a scale factor with the wave-number dimension. The using of the properties of the delta function and transition to the differentiation with respect to the variable ξ simplify the equation (2) and yield the following equation for the further numerical calculations:

$$E(\tau,\xi)=a^2(\tau)\{E_0(\tau,\xi)-$$

$$\frac{\partial}{\partial\xi}\int_0^{\tau}d\tau'\frac{1-a^2(\tau')}{2a^2(\tau')}[E(\tau',\xi+\tau-\tau')-E(\tau',\xi-\tau+\tau')]-$$

$$-\frac{1}{2}\int_0^{\tau}d\tau' b(\tau')[E(\tau',\xi+\tau-\tau')+E(\tau',\xi-\tau+\tau')]\} \qquad (3)$$

where $a^2(\tau)=\frac{\varepsilon}{\varepsilon_1(\tau/v\kappa)}$, $b(\tau)=\frac{\sigma_1(\tau/v\kappa)}{\varepsilon v\kappa}$.

This equation describes the evolution of the process and determines explicitly the field magnitude at the point (τ,ξ) in terms of its magnitudes at preceding time points along the lines $\xi'=\xi\pm(\tau-\tau')$. We find the structure of the field after N jumps in the medium parameters when they change from the initial values to the values $a=const$, $b=const$. The algorithm allows to consider the initial field with an arbitrary time-spatial dependence.

NUMERICAL CALCULATIONS

For the numerical calculation we use a uniform grid on the time-space plane, i.e. $\Delta\tau=\Delta\xi$. Such a grid is chosen according to the stability condition [11]. The plane wave $E_0(\tau,\xi)=\exp[i(\tau-\xi)]$ and the gaussian beam $E_0(\tau,\xi)=\frac{\exp\left((\tau-\xi)^2/2u^2\right)}{\sqrt{2\pi}\,u}$ are considered as an initial field. The essence of the proposed methodology is the sequence of resolving of the equation (3) in time step by step. We find the electromagnetic field in the specified temporary layer $\tau=\tau_n$ using the solutions for the previous layers. The repetitive calculations of integrals along the same overlapping time intervals have been avoided. For the differentiation with respect to the spatial coordinate the smoothing scheme has been used [12]. The estimates of accuracy have been done by comparing the numerical solution and analytical solution of the test problems.

For all the cases listed below, the grid spacing has been selected as $\Delta\tau=\Delta\xi=0.05$, the initial value of the undimensional medium parameters has been chosen as follows: $a=1$, $b=0$. In all the cases, $\xi=0$. The time dependence of electromagnetic field for the plane wave as an initial field is presented in Figures 1, 2. As a test problem, we consider the problem of the plane wave propagation in a medium with parameters changing in time as the finite sequence of rectangular periodic pulses.

The dependence of relative errors in the numerical calculations with the calculation step is presented in Fig. 3. In Figures 4, 5 the time dependence of electromagnetic field for the gaussian beam as an initial field is presented.

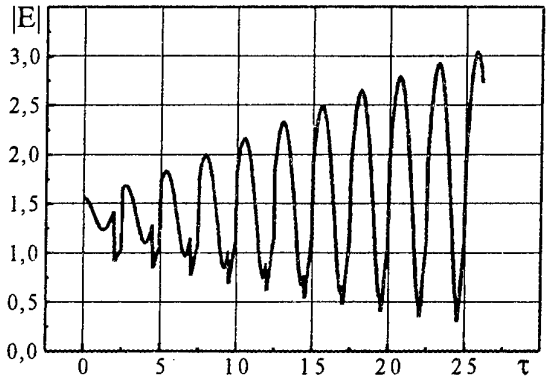


Fig. 1. Time dependence of electromagnetic field for $a=1.25$, $b=0.01$, $\tau_1=2$, $\tau_2=0.5$ and a plane wave as an initial field

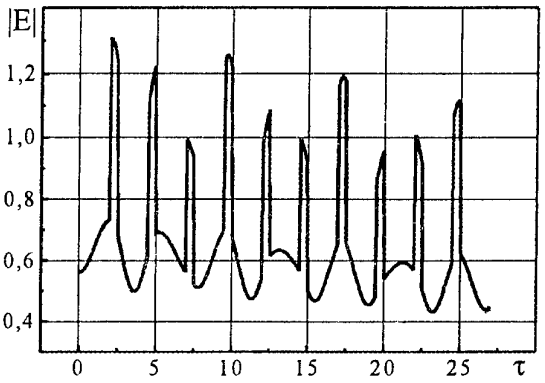


Fig. 2. Time dependence of electromagnetic field for $a=0.75$, $b=0.01$, $\tau_1=2$, $\tau_2=0.5$ and a plane wave as an initial field

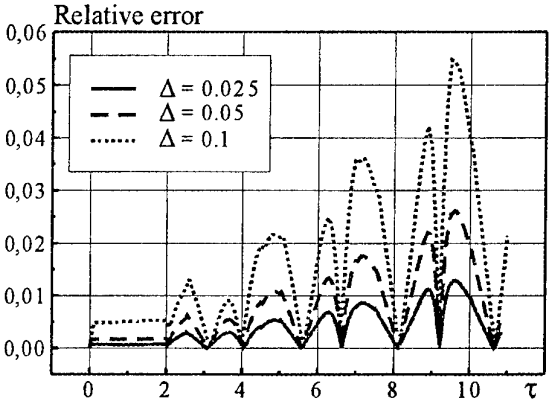


Fig. 3. The relative error of the test problem for $a=1.25$, $b=0.01$, $\tau_1=2$, $\tau_2=0.5$

In Fig. 4, 5 we assume $u=0.5$. It should be noted that the shape of the field can be radically changed by varying the value of u parameter.

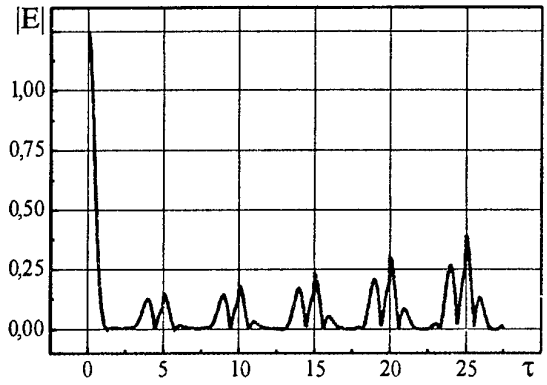


Fig. 4. Time dependence of electromagnetic field for $a = 1.25$, $b = 0.01$, $\tau_1 = 2$, $\tau_2 = 0.5$ and a gaussian beam as an initial field

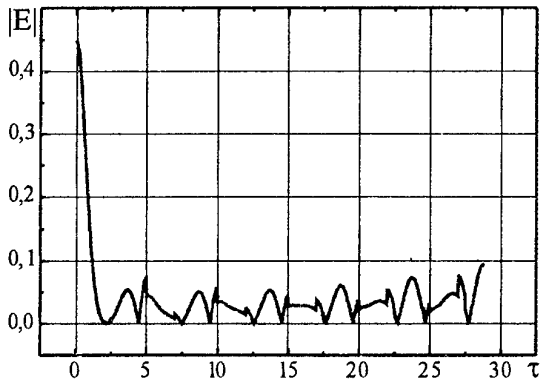


Fig. 5. Time dependence of electromagnetic field for $a = 0.75$, $b = 0.01$, $\tau_1 = 2$, $\tau_2 = 0.5$ and a gaussian beam as an initial field

CONCLUSION

The transformations of a plane electromagnetic wave and a gaussian beam in a medium with the permittivity and conductivity changing in time as a finite sequence of periodic rectangular pulses has been considered. The solution to the nonstationary electromagnetic problem has been obtained by using the Direct Numerical Calculation Method. Comparison with the exact solution of the test problem has been also performed. Numerical results for the different pulse parameters and initial fields have been presented. An original software for the computer modeling of electromagnetic wave propagation in a time–varying medium for arbitrary initial fields and different laws of changing in medium parameters has been created.

REFERENCES

1. Ya.B .Fainberg, N.A. Khizhnyak, "Energy Losses by the Charge Passing through the Slaty Dielectric", *Journal of Experimental and Theoretical Physics*, Vol. 32, 1957, pp. 883–895, [in Russian].
2. G. Bekefi, J.S. Wurtele, and I.H. Deutsch, "Free-Electron-Laser Radiation Induced by a Periodic Dielectric Medium", *Phys. Rev.*, Vol. A–34, 1957, pp. 1228–1236.
3. F. R. Morgenthaler, "Velocity Modulation of Electromagnetic Waves", *IRE Trans .Microwave Theory Tech.*, Vol. MTT-6, No. 4, 1958, p 167–172.
4. S. I. Averkov, V.P. Boldin, "Waves in Nondispersive Nonstationary Inhomogeneous Media", *Radiophysics Quantum Electron.* (English transl.), Vol. 23, No. 9, 1980, pp. 1060–1066 [in Russian pagination].
5. L. A. Ostrovsky, N.S. Stepanov, "Nonresonant Parametric Phenomena in Distributed System", *Radiophysics Quantum Electron.* (English transl.), Vol. 14, No. 4, 1971, pp. 489–529 [in Russian pagination].
6. S. N. Stolyarov, "Resonant Wave Transformation in the Periodically Nonstationary Media" *Radiophysics Quantum Electron.* (English transl.), Vol. 26, 1983, pp. 514–516 [in Russian pagination].
7. F. A. Harfoush, A. Taflove, "Scattering of electromagnetic Waves by a Material Half–Space with a Time–Varying Conductivity" *IEEE Trans. Antennas Propagation* , Vol. 39, 1991, pp. 898–906.
8. J. Wiesenfeld, Wavelength conversion technology, 1998 *Proc. of "COST 240 Management Committee Meeting"* (Warsaw Poland) April 23–25.
9. A. G. Nerukh and N.A. Khizhnjak, *Modern Problems of Transient Macroscopic Electrodynamics*, Test-Radio Publ., Kharkov, 1991 [in Russian].
10. A. G. Nerukh, I. V. Scherbatko, O. N. Rybin, "The Direct Numerical Calculation of an Integral Volterra Equation for an Electromagnetic Signal in a Time–Varying Dissipative Medium", *J. of Electromagnetic Waves and Applications*, Vol. 12, No 1, 1998, pp. 167–176.
11. N. N. Kalitkin, *Numerical Methods*, Nauka Publ., Moscow, 1978 [in Russian].
12. G. Korn, T. Korn, *Mathematical Handbook for scientists and engineers*, McGraw-Hill Book Inc., New-York, 1961.

EQUIVALENT SURFACE IMPEDANCE OF SLOTTED IMPEDANCE LOAD MADE AS SEMI-CYLINDRICAL CAVITY FOR INFINITE ARRAY. THE CASE OF E-POLARIZATION

B. M. Petrov, V. G. Koshkidko, O. V. Alpatova

Taganrog State University of Radio Engineering, department of Antennas and Radio Transmitters, TSURE, Nekrasovsky,44, GSP-17A, Taganrog, 347928, Russia,
phone (863-44) 6-17-33, fax (863-44) 6-50-19, e-mail: airpu@tsure.ru

INTRODUCTION

The problem of electromagnetic waves diffraction on an perfectly conducting open-ended cylindrical surface is of great practical importance. The metal screens of a similar configuration are used as reflectors at the linear radiator, as screens for protection of instrumentation against external electromagnetic fields, as the device for decreasing mutual influence of low directional antennas and for other purposes. With the help of impedance loads it is possible to obtain the specific diagram of conductive objects scattering. In the impedance loads used nowadays (such as a ridge structure, the rectangular groove) there is a strongly marked dependence of an impedance size on an angle of incidence of electromagnetic waves. It is known [1], that in the semicylindrical concavity this dependence is not pronounced.

Note, that the essential change of a scattering field with the help of single impedance loads can be achieved only for objects with small electrical sizes. At sizes of object, considerably exceeding a wavelength, a great deal of impedance loads or allocated impedance must be applied, that is eventually one is forced to deal with arrays of impedance loads.

STATEMENT OF A PROBLEM

In free space a periodic structure of slotted impedance loads with periodicity T is located, each element of which represents two parallel slots, cut out in ideally thin conductive screen, each of width S_0, divided by a strip conductor of width d. Unlimited space is divided by a screen into two areas V_1 and V_2. The area V_1 with parameters $\tilde{\varepsilon}_{a1}, \mu_{a1}$, contains exciting sources. Area V_2 with parameters $\tilde{\varepsilon}_{a2}, \mu_{a2}$ is without exciting sources. Area V_1 occupies the whole upper half-space and is limited by surface S_1. Area V_2 coincides with an internal volume of a semicircular cavity of radius a, bounded by surface S_2. From the upper half-space there falls a plane electromagnetic wave under angle θ, counted from normal to a screen surface. Assume, the characteristic of exciting sources and design parameters are independent from coordinate z. Screen and internal walls of a semicircular cavity are perfectly conductive (Fig. 1). It is required to determine an equivalent surface impedance of a structure.

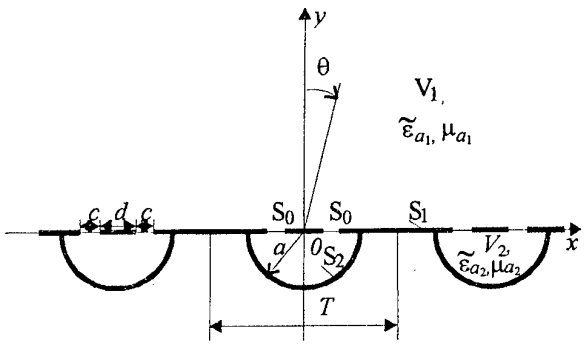


Fig. 1. Geometry of a problem

DERIVATION OF INTEGRO-DIFFERENTIAL EQUATION

We shall set a dropping field so that it satisfy the Flocket condition

$$E_z^{\text{п}} = \frac{1}{\sqrt{T}} \exp(ik_1(x\sin\theta + y\cos\theta)) \qquad (1)$$

where T is the period of the array.

By virtue of a structure periodicity the scattered field in area V_1 can be presented as the expansion into Flocket spatial harmonics. For waves in the direction of $\pm y$ they look like $\Psi_m(x)\exp(\pm i\Gamma_m y)$, where $\Psi_m(x)$ are functions, determining change of a field in a cross direction:

$$\Psi_m(x) = \sqrt{\frac{1}{T}} \exp\left(-i\left(2m\pi/T - k_1\sin\theta\right)x\right),$$

$$m = 0,\pm1,\pm2,\ldots,\ \Gamma_m = \sqrt{k_1^2 - (2m\pi/T - k_1\sin\theta)^2}$$

We shall present a scattered field in area V_1 as expansion into Flocket harmonics

$$E_{z1}^{\text{расс}}(x,y) = \sum_{m=-\infty}^{\infty} Z_m I_m \Psi_m(x) e^{-i\Gamma_m y}$$

$$H_{x1}^{\text{расс}}(x,y) = -\sum_{m=-\infty}^{\infty} I_m \Psi_m(x) e^{-i\Gamma_m y}$$

where $Z_m = \Gamma_m / \omega\tilde{\varepsilon}_{a1}$, I_m are the factors of current expansion.

Since it is possible to present the falling field as a zero Flocket harmonics, that is

$$E_z^n(x,y) = Z_0\Psi_0(x)\exp(i\Gamma_0 y),$$

then the entire electrical field will look like

$$E_{z1}(x,y) = \sum_{m=-\infty}^{\infty} Z_m I_m \Psi_m(x) e^{-i\Gamma_m y} + Z_0\Psi_0(x)e^{i\Gamma_0 y}.$$

And entire magnetic field will be as follows

$$H_{x1}(x,y) = -\sum_{m=-\infty}^{\infty} I_m \Psi_m(x) e^{-i\Gamma_m y} + \Psi_0(x)e^{i\Gamma_0 y}.$$

In the aperture that is at $y = 0$, we shall have

$$E_{z1}(x,0) = \sum_{m=-\infty}^{\infty} Z_m I_m \Psi_m(x) + Z_0\Psi_0(x), \qquad (2)$$

$$H_{x1}(x,0) = -\sum_{m=-\infty}^{\infty} I_m \Psi_m(x) + \Psi_0(x). \qquad (3)$$

Using an orthogonality of Flocket harmonics, we shall obtain from (2) and (3)

$$I_m = -\delta_m + \frac{1}{Z_m}\int_{-T/2}^{T/2} E_z(x',0)\Psi_m^*(x')dx' \qquad (4)$$

where $\delta_m = 1, m = 0$; $\delta_m = 0, m \neq 0$ (δ_m is the Kronecker delta).

Substituting (4) in (2), we shall finally obtain

$$H_{x1}(x,0) = -\int_{-T/2}^{T/2}\left\{\sum_{m=-\infty}^{\infty}\frac{1}{Z_m}\Psi_m(x)\Psi^*{}_m(x')\right\}\times \times E_x(x',0)dx' + 2\Psi_0(x). \qquad (5)$$

Thus, the expression for a magnetic field in area V_1 in the aperture is obtained.

For obtaining an integral equation it is necessary to find an expression for a field in area V_2 and to use a boundary condition in the aperture. The magnetic field in area V_2 looks like

$$H_{x2}(x,0) = \int_{-T/2}^{T/2}\{-i\omega\tilde{\varepsilon}_{a2}G_e(x',x) + , + \frac{1}{i\omega\mu_{a2}}\frac{\partial^2 G_e(x',x)}{\partial x^2}E_z(x',0)dx' \qquad (6)$$

where

$$G_e(x,x_1) = \frac{1}{2}\sum_{m=0}^{\infty}(\pm 1)^m \varepsilon_m J_m(k_2|x_1|)J_m(k_2|x|)\times \times \frac{Y_m'(k_2 a)}{J_m'(k_2 a)} - \frac{1}{2}Y_0(k_2|x-x_1|), \begin{matrix}\varphi=\varphi_1\\ \varphi\neq\varphi_1\end{matrix},$$

$\varepsilon_m = 1$ at $m = 0$ and $\varepsilon_m = 2$ at $m \neq 0$, $J_m(x)$, $J_m'(x)$ are Bessel's function and its derivative, $Y_m(x)$, $Y_m'(x)$ is a Neumann's function and its derivative.

Taking into account a property of the kernel $\frac{\partial G_e(x,x')}{\partial x} = -\frac{\partial G_e(x,x')}{\partial x'}$ and carrying out an x' integration in the second integral we shall obtain the following expression for a magnetic field in the second area

$$H_{x2}(x,0) = \int_{-T/2}^{T/2}\{-i\omega\tilde{\varepsilon}_{a2}G_e(x',x) - , - \frac{1}{i\omega\mu_{a2}}\left[\frac{\partial G_e(T/2,x)}{\partial x} - \frac{\partial G_e(-T/2,x)}{\partial x}\right]\}\times \times E_z(x',0)dx'. \qquad (7)$$

Further, satisfying a condition of a continuity of tangential components of fields in the aperture, from (5) and (7) we shall obtain an integro-differential equation (IDE) for the tangential component to be found of the electric field in the aperture

$$\int_{-T/2}^{T/2}\left\{\sum_{m=-\infty}^{\infty}\frac{1}{Z_m}\Psi_m(x)\Psi^*{}_m(x') - i\omega\tilde{\varepsilon}_{a2}G_e(x',x) - \frac{1}{i\omega\mu_{a2}}\left[\frac{\partial G_e(T/2,x)}{\partial x} - \frac{\partial G_e(-T/2,x)}{\partial x}\right]\right\}\times \times E_z(x',0)dx' = 2\Psi_0(x). \qquad (8)$$

We apply the scheme of a collocation method to IDE (8), using piecewise constant approximation of a unknown quantity of the solution by characteristic functions [2]. To enter this system of functions, we shall choose on an interval $[-T/2, T/2]$ some system of points x_i $(x_0 = -T/2, x_1, x_2, \ldots, x_n = T/2)$, whose interval $[-T/2, T/2]$ is broken into partial intervals of length $h = T/n$ where n is the number of intervals. As characteristic functions we shall choose piecewise constant, and as trial ones — the Dirac delta-function.

Taking into account the above explained, we come to following IDE

$$\sum_{i=1}^{n} C_i \int_{x_{i-1}}^{x_i}\left[\sum_{m=-\infty}^{\infty}\frac{1}{Z_m}\Psi_m(x)\Psi^*{}_m(x') - i\omega\tilde{\varepsilon}_{a2}G_e(x',x) - \frac{1}{i\omega\mu_{a2}}\left[\frac{\partial G_e(T/2,x)}{\partial x} -\right.\right.$$

$$-\frac{\partial G_e(-T/2,x)}{\partial x}\Bigg]\Bigg]dx' = 2\Psi_0(x) \qquad (15)$$

where C_i are the factors of expansion.

Choosing then as points of collocation $\xi_j = (x'_j + x'_{j-1})/2$, $j = 1,2,...,n$, we obtain the following system of linear algebraic equations

$$\sum_{i=1}^{n} C_i K_{ji} = 2\Psi_0(\xi_j)$$

where

$$K_{ji} = \int_{x_{i-1}}^{x_i}\left[\sum_{m=-\infty}^{\infty}\frac{1}{Z_m}\Psi_m(\xi_j)\Psi^*{}_m(x') - i\omega\tilde{\varepsilon}_{a2}G_e(x',\xi_j)\right]dx' -$$
$$-\frac{1}{i\omega\mu_{a2}}\left[\frac{\partial G_e(T/2,x)}{\partial x}\Big|_{\xi_j} - \frac{\partial G_e(-T/2,x)}{\partial x}\Big|_{\xi_j}\right]$$

After the IDE (8) solution, the equivalent surface impedance is determined by the formula [3]

$$Z^{\ni} = \frac{\int_0^T E_x(x)H_z^*(x)dx}{\int_0^T |H_z(x)|^2 dx}$$

where $Z^{\ni}$ is the equivalent surface impedance, T is the period of the array.

NUMERICAL RESULTS

For the problem solution, the software package is developed, permitting to calculate dependencies of an equivalent surface impedance on the design data of the array and on an angle of incidence of an electromagnetic wave. With the help of this package these dependencies are found for an infinite periodic array slotted impedance loads made as semi-cylindrical cavity. They are of less expressed character, than ones of an array produced from rectangular grooves of the equivalent sizes [4].

REFERENCES

1. V. G. Koshkidko, O.V. Alpatova, Equivalent surface impedance of slot impedance load on the basis of a cylindrical cavity. // Radiotekhnika i elektronika, 1999, V. 44. № 1, pp. 25-28 [in Russian].
2. Zaharov, Yu.V. Pimenov, Numerical analysis of waves diffraction, Moscow: RiS. 1982. p. 183 [in Russian].
3. Tsaliev, V.S. Cherenkov, Excitation Возбуждение individual ditch and equivalent surface impedance of ribbed structures. // Radiotehnika i elektronika. 1985. V. 30, № 9, pp. 1689- 1694 [in Russian].
4. B. M. Petrov, V.G. Koshkidko, O.V. Alpatova, Characteristics investigation of slot impedance loads as semicircular form included into infinite arrays. LII Research session devoted to the Radio day, Proc. V.1, Moscow, 1997, p. 188 [in Russian].

NUMERICAL SOLVING OF THE INTEGRAL EQUATION FOR THE ELLIPTIC LOOP ANTENNA

A. A. Schekaturin

The Sevastopol State Tecnical University,
335053, Studgorodok SevGTU, Sevastopol, Ukraine
Ph. +38(0692) 23-51-52, e-mail rt.sevgtu@stel.sebastopol.ua

INTRODUCTION

Loop antennas represents an important class of wire antennas and are widely used in various communication systems.

In the theory of loop antennas in general circular loop ones are investigated ([1], [2], [3]). In the presented work the problem of current distribution along an elliptical loop antenna wire is solved according to the moments method.

MAIN BODY

Let us consider an elliptic loop antenna (Fig. 1).

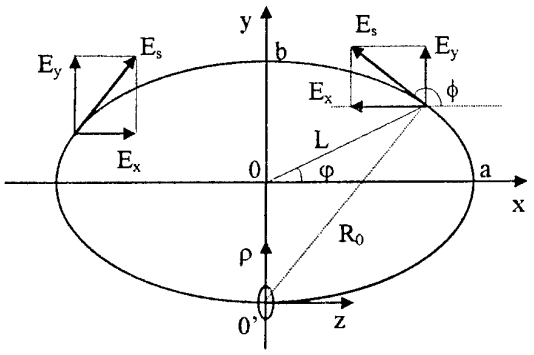


Fig. 1. The configuration of the loop antenna

The convenient form of the integral equation for a wire antenna is as follows

$$\int_o^l I(s')\{k^2 G(s,s')\bar{s}\cdot\bar{s}' - \frac{\partial^2 G(s,s')}{\partial s\cdot\partial s'}\}ds' = -i\frac{k}{z_0}E_s(s),$$

where $I(s')$ is the full current, $G(s, s')$ is Green's function, $\bar{s}, \bar{s}$© are the unit vectors which are tangent at the points s and s' of the wire in the curvilinear coordinate system, k is the wave number, z_0 is the wave impedance of the free space, $E_s(s)$ is the electrical tangent vector of the extraneous field in the point s, i is the imaginary unit.

We used the magnetic current loop shown with the local coordinate system z0'ρ in the bottom of the Fig. 1 as a primary source.

The product of $\bar{s}$ and $\bar{s}'$ is given

$$\bar{s}\cdot\bar{s}' = \frac{1}{A\cdot A'}(a^2\sin\varphi\sin\varphi' + b^2\cos\varphi\cos\varphi'),$$

where

$$A = \sqrt{a^2\sin^2\varphi + b^2\cos^2\varphi},$$

$$A' = \sqrt{a^2\sin^2\varphi' + b^2\cos^2\varphi'}.$$

For the second derivative of Green's function

$$G = \frac{e^{-ik|\bar{\Delta}r|}}{4\pi|\bar{\Delta}r|},$$

where

$$|\bar{\Delta}r| = \sqrt{a^2(\cos(\varphi)-\cos(\varphi'))^2 + b^2(\sin\varphi-\sin\varphi')^2 + a_2^2},$$

a_2 is the radius of a wire, we obtain

$$G_2 = \frac{e^{-ik\sqrt{f}}}{16\pi\cdot f^{5/2}}((3+3ik\sqrt{f}-k^2 f)f^{0,1}f^{1,0} + 2(-1-ik\sqrt{f})f\cdot f^{1,1},$$

where

$$f = a^2(\cos\varphi'-\cos\varphi)^2 + b^2(\sin\varphi'-\sin\varphi)^2,$$

$$f^{0,1} = -2b^2\cos\varphi(\sin\varphi'-\sin\varphi) + 2a^2(\cos\varphi'-\cos\varphi)\sin\varphi,$$

$$f^{1,0} = -2a^2(\cos\varphi'-\cos\varphi) + 2b^2\cos\varphi'(\sin\varphi'-\sin\varphi),$$

$$f^{1,1} = -2b^2\cos\varphi'\cos\varphi - 2a^2\sin\varphi'\sin\varphi.$$

For the tangent component of the electrical field vector, created by the radiator, we shall get

$$E_s(\varphi) = E_z\frac{1}{\sqrt{1+\frac{a^2}{b^2}\frac{1}{tg^2\varphi}}} + E_\rho\frac{b}{a}\frac{1}{tg\varphi\sqrt{1+\frac{b^2}{a^2}\frac{1}{tg^2\varphi}}}$$

$$E_z = k\frac{d^2-c^2}{8\ln(d/c)}\frac{e^{-ikR_0}}{R_0^2}V_0\{2(\frac{1}{kR_0}+i-$$

$$-\frac{i(d^2+c^2)}{2R_0^2})+\frac{\rho^2}{R_0}[(\frac{1}{kR_0}+i-\frac{i(d^2+c^2)}{2R_0^2})$$

$$(-ik-\frac{2}{R_0})+(\frac{-1}{kR_0^2}+i\frac{d^2+c^2}{R_0^3})]\},$$

$$E_\rho=-k\frac{d^2-c^2}{8\ln(d/c)}V_0\rho\frac{z}{R_0}\frac{e^{-ikR_0}}{R_0^2}\{k-$$

$$(\frac{3}{k}+\frac{k(d^2+c^2)}{2})\frac{1}{R_0^2}+i[\frac{2(d^2+c^2)}{R_0^3}-\frac{3}{R_0}]\},$$

where c, d are the interior and the exterior radii of the loop of the magnetic current, V_0 is the voltage in the driving point,

$$R_0(\varphi)=$$

$$=\sqrt{d^2+(c^2\cos^2\varphi+d^2\sin^2\varphi)+2d\sqrt{c^2\cos^2\varphi+d^2\sin^2\varphi}\sin\varphi},$$

$$z=\sqrt{c^2\cos^2\varphi+d^2\sin^2\varphi}\cos\varphi,$$

$$\rho=b+\sqrt{c^2\cos^2\varphi+d^2\sin^2\varphi}\sin\varphi.$$

When passing to new variables the integral equation to be found looks like

$$\int_0^{2\pi}I(\varphi')[G_2-k^2G(a^2\sin\varphi\sin\varphi'+b^2\cos\varphi\cos\varphi')]d\varphi'=$$

$$-\frac{ik}{z_0}\sqrt{a^2\sin^2\varphi+b^2\cos^2\varphi}E_s(\varphi). \qquad (1)$$

The desired function I(φ') is replaced with the appoximated $I_1(\varphi')$ function, represented as a sum of the linear - independent basic functions $f_p(\varphi')$:

$$I_1(\phi')=\sum_{p=1}^{N}I_pf_p(\phi'), \qquad (2)$$

where I_p are the unknown weight factors.

We used bit-constant functions as the basic ones

$$f_p(\phi')=\begin{cases}1,\phi_p-\Delta<\phi\le\phi_p+\Delta,\\0,\phi\le\phi_p-\Delta;\phi>\phi_p+\Delta,\end{cases}$$

where Δ is the interval between points φ_p.

After substatituation of (2) in (1) the integral equation (1) is transformed in a functional equation

$$\sum_{p=1}^{N}I_p\int_0^{\phi_{max}}f_p(\phi')K(\phi,\phi')d\phi'=-i\frac{k}{z_0}E_s(\phi), \qquad (3)$$

where $K(\varphi,\varphi')$ is the cernel of the integrated equation (1).

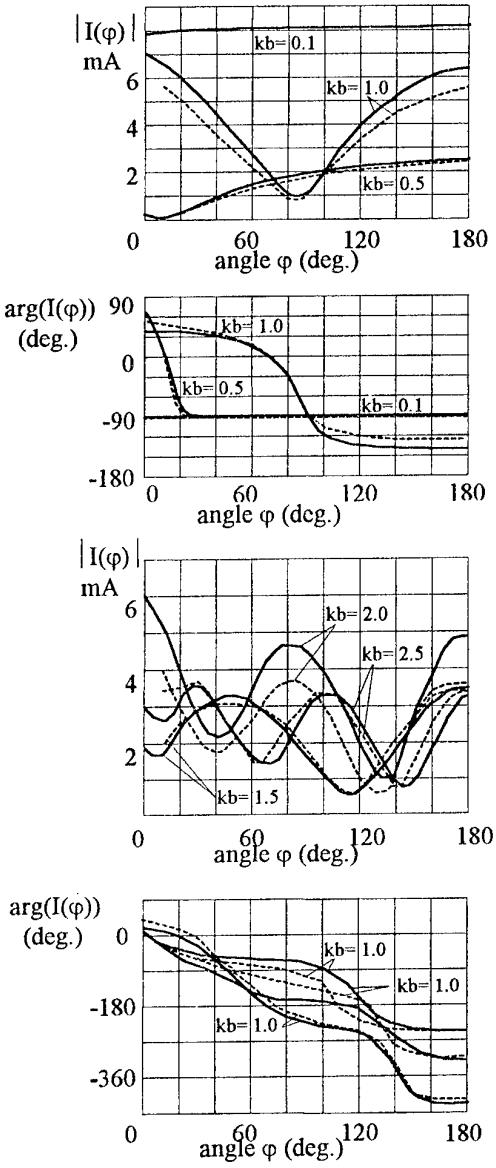


Fig. 2. Current distribution at frequency

After multiplication of both parts of the equation (3) on the delta-function $\delta(\varphi-\varphi_k)$, integration and according to (2), we obtain a set of the linear algebraic equations of a matrix form

$\tilde{Z}\cdot\bar{I}=-\frac{ik}{z_0}\bar{E}_s$. Elements of the matrix $\tilde{Z}$ $z_{ij}=\int_{\phi_{j-\Delta}}^{\phi_{j+\Delta}}K(\phi_i,\phi')d\phi'$ are evaluated numerically. The input impedance of the antenna is $z=V_0/I_1$.

The program in language FORTRAN was developed and the current distribution along the wires of the loop antenna was computed.

The integration was made by the Simpson method, the set of the linear equations was solved by the method of Newton.

For testing the program the calculation for a circular loop ($a = b$) was made at Ω=10.0, where Ω is the parameter of thickness, defined as $\Omega = 2\ln(2\pi b / a_2)$.

The results of calculation are given in Fig. 2. The dotted line shows the numerical results of the presented analysis, the solid line is according to the theory of Ronold W. P. King and Glenn S. Smith [1]. For kb = 0.1 the calculated magnitude value of the current is within the limits 11 to 12 mA.

CONCLUSION

The obtained equation allows to evaluate numerically the current distribution and therefore to find the input impedance and the radiation field.

REFERENCES

1. Ronold W. P. King, Glenn S. Smith Antennas in matter. Fundamentals, theory, and applications.- Cambridge, Massachusetts, and London .: The Mit press, 1981.- 824 pp.
2. A. Z.Fradin Antenna devices. - Moscow.: Svyaz, 1977, 440 pp.
3. L. M. Lobkova, M. B. Prozenko, O. A. Posnyj, "Frequency characteristics of input impedance of loop antenna" Izv. vusov Radioelektronika, KPI, No.12, 20-25, 1998. [in Russian].
4. Computer techniques for electromagnetics/ Edited by R. Mitra.-Oxford, New Yorc, Toronto, Sydney, Braunschweing.: Pergamon press, 1973.- 488 pp.

A CAD SOFTWARE FOR DESIGN AND ANALYSIS OF A RECTANGULAR MICROSTRIP ANTENNA

K. Y. Yazdandoost, D. C. Gharpure

Department of Electronic Science, University of Pune,
Pune 411 007, India
Tel: +91-20-359841, e-mail: dcgrs@electronics.unipune.ernet.in

ABSTRACT

A computer program is developed for design and analysis of a Rectangular Microstrip Patch Antenna. The program is based on cavity model and slot theory. The effect of substrate and surface wave has been taken into account.

INTRODUCTION

The microstrip antenna finds increasingly extensive application in microwave systems, ranging from Military to Medical, in view of its importance mathematical methods of electromagnetics have been applied for the microstrip antenna analysis. The papers and books [1–6] have analyzed the microstrip patch for CAD programming.

The computational time to find parameters of such an antenna is generally high. Hence, a Computer Aided Design (CAD) are required for practical circuit development and optimization.

The reasons for developing an accurate model for an antenna is to provide a tool for designer to design of antenna without costly trail-and-error experimental. The number of CAD packages which are available for microstrip antenna is too less. It can be because of

i) geometries of microstrip antenna, which is difficult to model because of the presence of substrate

ii) ii) it is new kind of antenna and need time for software development.

Most of the CAD software tools have placed emphasis on the design of microstrip line and few CAD software tools were developed for microstrip patch elements.

There are numbers of models which can be used for antenna modeling i.e. Transmission line model [2], Cavity model [4], Finite Difference Time Domain (FDTD) method [7], Moment method [8], Finite Element (FE) method [9]. But a good antenna model should calculate all necessary electrical parameters, with enough accuracy in less computational cost. The Moment, FDTD, FE methods are computationally costly and have low level of user confidence as experimental or other independent validation is absent [6]. A computer program name RMPA has been developed for design and analysis of rectangular microstrip patch antenna.

THE MAIN PART

RMPA is an acronym for Rectangular Microstrip Patch Antenna. RMPA computes design parameters as well as other parameters which are necessary for analyzing of this type of antenna. Figure 1 shows rectangular patch with its four slots.

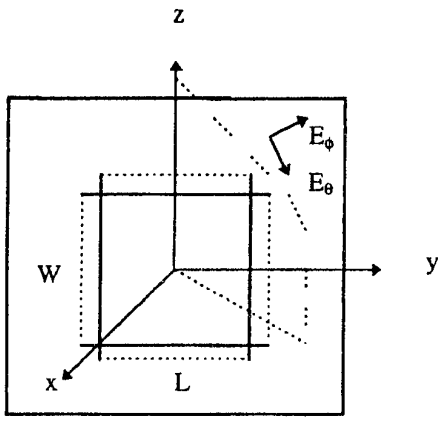


Fig. 1. Rectangular patch with it slots

The software is based on the cavity model and uses slot theory to Simulate the rectangular patch antenna considering the effect of substrate and surface wave. The overall structure of RMPA is showing in Fig. 2.

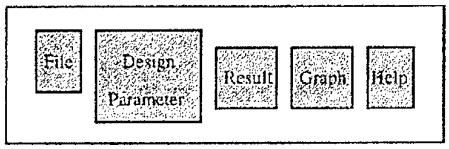


Fig. 2. The overall structure of RMPA

The design parameter module asks for input data:

Resonant frequency; the range of frequency which calculation should be done (lower frequency and higher frequency); substrate relative dielectric constant; loss tangent; patch conductivity; patch width; tolerance in patch length; tolerance in patch width; tolerance in substrate permittivity; tolerance in substrate thickness.

The outputs are: radiation resistance; resistance at feed point; input impedance; patch length; surface wave modes and No. of modes; far field pattern; directivity; efficiency; VSWR; bandwidth; and error in resonant frequency.

The far field pattern is calculated for dominant mode.

The graphs have been plotted for input impedance, VSWR, efficiency, E and H planes.

The help provides information on microstrip antenna and a substrate and conductor library.

Figure 3 shows the flowchart of whole program. Through flowchart we can see there are number of steps which have to be solved for antenna analysis.

To design any kind of antenna initial point is resonant frequency. Because it is necessary to know antenna should work for which band of frequency. In case of microstrip antenna, the bandwidth is very narrow, hence the exact value of resonant frequency is important [10]. Value of resonant frequency depends on the length of patch. Therefore knowing the resonant frequency the length of patch is obtained and displayed in result.

DESIGN AND ANALYSIS USING RMPA

For microstrip antenna the size of patch width (W) is important too. It affects the value of impedance and also it maybe considered that small values of W result in low antenna efficiency, while large values support higher order modes. If input impedance of patch and impedance of transmission line does not match, RMPA helps the user to obtain the optimum feed point position by displaying the impedance every time packaged is involved.

Most microstrip antenna are fabricated using photo-etching techniques. In the fabrication of such an antenna there are two types of tolerances, manufacturing tolerance and etching accuracy. Error in resonant frequency because of manufacturing and fabrication errors is also calculated.

The surface modes and number of surface modes is also calculated.

The bandwidth of antenna depends to the thickness of substrate. Therefore the kind of substrate depends to the designer choice. Low or high relative permittivity have different tolerance in substrate thickness and relative permitivity.

CONCLUSIONS

An improved cavity model has been developed that form an accurate tool for the analysis of rectangular microstrip patch antenna. As microstrip antenna is based on solid science [6], it needs strong understanding of antenna behavior to solve the problems. There are many direction where antennas can be designed more practically, with better achievement and less experimental repetition, when the proper CAD software tools are available.

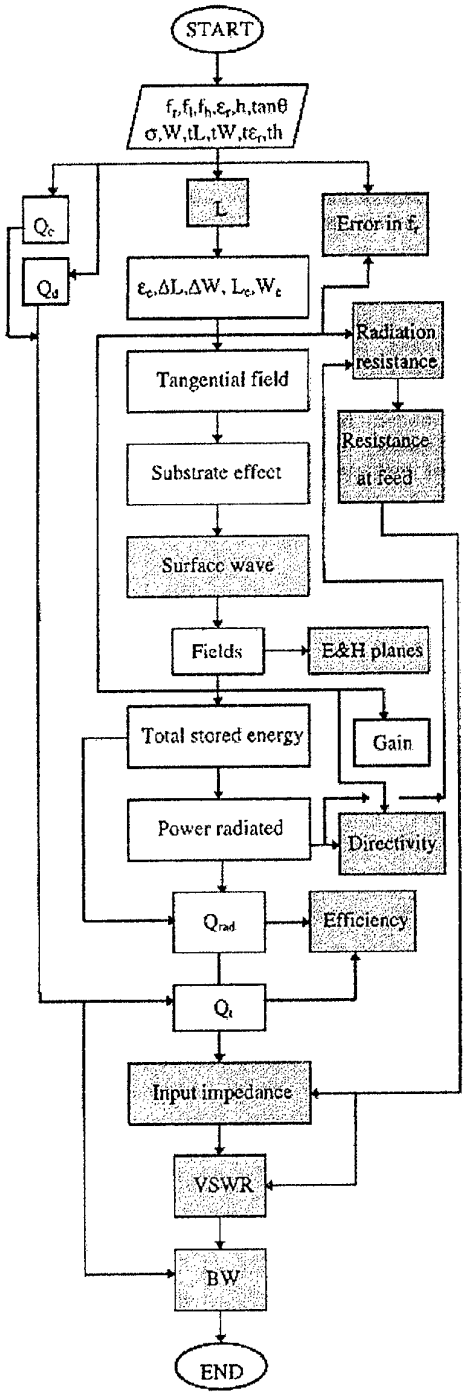


Fig. 3. Flowchart of program

To achieve more sophisticated solution, the tolerance in substrate and patch also taken in to account. The resonant frequency [10] and radiation resistance calculated by RMPA shows better agreement with the experimen-

tal data compare to other theories. The radiation quality factor [11] has been calculated by the electrical size of patch to achieve better result for efficiency as well as input impedance, VSWR, and bandwidth. Due to RMPA results, RMPA seems to be well suited for design purpose.

REFERENCES

1. K. C. Gupta, R. Garg, and R. chadha, Computer-Aided Design of Microwave Circuits, Artech House, 1981.
2. H. Pues and A. van de Capelle, " Accurate Transmission-Line model for the Rectangular Microstrip Antenna," IEE proceeding, vol. 131, No. 6, pp. 334-340, December 1984.
3. Vincent F. Fusco, Microwave Circuits Analysis and Computer-Aided Design, Prentice-Hall International (UK) Ltd., 1987.
4. D. Thouroude, M. Himidi, and J.P. Daniel, " CAD-Oriented Cavity Model for Rectangular Patches," Elec. Lett., vol. 26, No, 13, pp.842-844, June 1990.
5. Kazuhiro Hirasawa, Misao Haneishi, Analysis, Design, and Measurement of Small and Low Profile Antenna. Artech House 1992.
6. David M. Pozar and Daniel H. Schaubert, Microstrip Antenna, The Analysis and Design of Microstrip Antenna and Array, IEEE Press, New York 1995.
7. A. Taflove, Computational Electrodynamics: The Finite Difference Time Domain Method, Artech House, Norwood, 1995.
8. R. F. Richmond, Field Computations by Moment Methods, Macmillan, New York, 1968.
9. Keith R. Carver and James W. Mink, " Microstrip Antenna Technology, " IEEE Transaction on Antennas and Propagation, vol.AP-22, No.1, pp.2-24, January 1981.
10. Kamya yekeh Yazdandoost, D.C. Gharpure, " Simple Formula for Calculation of the Resonant Frequency of a Rectangular Microstrip antenna," IEEE 5th international Symposium on Spread Techniques and Applications, 2-4 September 1998.
11. Kamya Yekeh Yazdandoost, " Radiation Quality Factor of Rectangular Microstrip antenna," 8th International Crimean Conference: Microwave and Telecommunication Technology," vol.2, pp.470-471, September 1998.

DISTORTING INFLUENCE OF HORN ANTENNA ON MEASUREMENTS BY MULTIFREQUENCY RADIOINTERFEROMETER

M. V. Andreev

Dniepropetrovsk State University,
13 Nauchny pereulok, Dniepropetrovsk, 320050, Ukraine

The applied possibilities of multifrequency microwave measurements in a free space induce a large interest to creation of multifrequency radiointerferometers permitting to determine parameters of layered structures [1]. The operation of the multifrequency radiointerferometer is based on a measurement of a frequency characteristic of a reflectivity from researched structure, on transition from frequency in time (space) area and analysis of reflection peaks from the structure interfaces in time domain. It is supposed, that the reflection from researched structure with sufficient exactitude is described by expression:

$$R(\omega) = \sum_{m=1}^{M} r_m \cdot \exp(-j\omega t_m), \qquad (1)$$

where r_m is reflection from m-th layer interface (discontinuity), $t_m = 2z_m/c$ is time location m-th layer interface (discontinuity). In this case in time domain the reflection characteristic from structure is equal to:

$$R(t) = \sum_{m=1}^{M} r_m \cdot S(t - t_m), \qquad (2)$$

where $S(t)$ is a function which determines the form of reflection peak in time domain.

However, the actual scheme of measurements based on waveguide reflectometer (as a rule), for a measurement of reflection characteristic in a free space assumes usage of horn antennas. The segment of a measuring tract containing a horn antenna and a connective segment of a waveguide brings amplitude and phase distortions to a result of a measurement. In this case the measured performance can be described by expression:

$$R(\omega) = R_A(\omega) + T_A(\omega) \cdot \sum_{m=1}^{M} r_m \cdot \exp(-j\omega t_m), \qquad (3)$$

where $R_A(\omega)$ is the described reflection from the horn antenna, $T_A(\omega)$ is the described transmission characteristic of horn, which also determines amplitude and phase distortions brought by horn. The availability of the indicated distortions carries on that the time signal is equal:

$$R(t) = R_A(t) + \sum_{m=1}^{M} r_m \cdot \tilde{S}(t - t_m), \qquad (4)$$

where function $\tilde{S}(t - t_m)$ is describing a form of m-th time-domain reflection peak and for case of measurement on N frequencies located on grid ω_n (n = 1,...,N) with discreet Δf is determined as

$$\tilde{S}(t - t_m) = \sum_{n=1}^{N} T_A(\omega_n) \cdot \exp[j\omega_n (t - t_m)]. \qquad (5)$$

The purpose of this work is the experimental research of distortion components $R_A(\omega)$ and $T_A(\omega)$ and path of their diminution. For this purpose the outcomes of measurements on the measuring-computer complex of the radiowave non-destructive testing of layered dielectrics RIMCH-04 [1] were used.

The measuring complex RIMCH-04 works on basis of the vector reflectometer, in which primary measuring converters are the directed detectors with cross-section of waveguide transmission line 7.2×3.4 mm^2. The pyramidal horn of length 55 mm with the sizes of the aperture 42×36 mm^2 was used as radiator. The measurements were carried out in frequency band 26÷37.4 GHz in N = 58 equidistant frequency points. Reference plane of vector reflectometer was placed in a place of connection horn antenna with measuring waveguide tract.

The measurement of reflection performances in a lack of a researched structure in front of horn antenna (calibration on a free space) was carried out, that allows to learn a behavior of a frequency characteristic of a reflectivity for an analyzable antenna $R_A(\omega)$. In fig. 1 module and phase of a frequency dependence $R_A(\omega)$ are represented. Fig. 2 represents the module of appropriate time-domain signal $R_A(t)$, which are obtained using the Fourier transform.

One can see, several typical reflection peaks are predominated in time-domain signal $R_A(t)$. For detection of characteristic reflections in a horn antenna its frequency dependence of reflectivity was approximated by method of least squares with using a model:

$$R_{\text{mod}}(\omega) = \sum_{m=1}^{M_{\text{mod}}} \hat{r}_m \cdot \exp(-j\omega \hat{t}_m). \qquad (6)$$

Model order M_{mod} was determined from the analysis of discrepancy between a model data $R_{mes}(\omega)$ and measured data $R_{\text{mod}}(\omega)$:

$$\rho = \sum_{n=1}^{N} |R_{mes}(\omega_n) - R_{\mathrm{mod}}(\omega_n)|^2 \Big/ \sum_{n=1}^{N} |R_{mes}(\omega_n)|^2 \,. \quad (7)$$

It allowed to inspect adequacy of a selected model to the measured data.

In Fig. 3 the dependence of ln ρ from model order M_{mod} is represented. The represented dependence demonstrates, that the exponential model already of rather low order gives good approximation of the measured data.

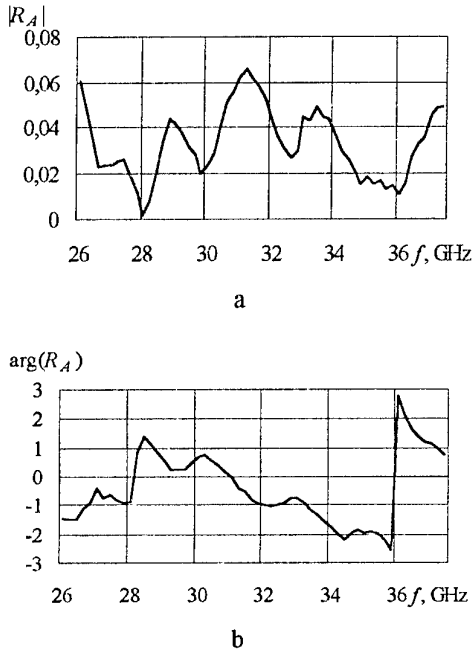


Fig. 1. Module (a) and phase (b) of reflectivity of horn antenna

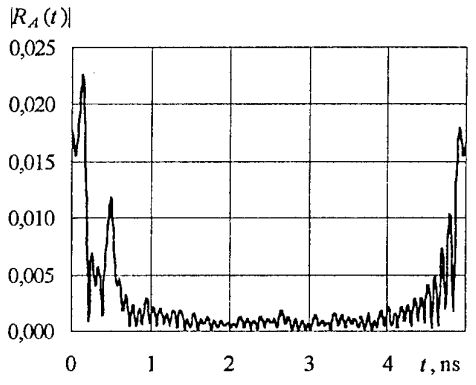


Fig. 2. Time-domain signal of reflection from horn $R_A(t)$

At M_{mod} = 1 discrepancy makes 59%; at M_{mod} = 2 discrepancy makes 17%; at M_{mod} = 3 discrepancy makes 6.6%; at M_{mod} = 6 discrepancy makes 1.1% (that is compared to noise level in the measured data). The outcomes of estimation of parameters of a model (6) at M_{mod} = 10 are represented in the table 1. In the first column of a table 1 number of a reflection m is indicated, in second one – estimation of its location $z_m = c \cdot \mathrm{Re}(\hat{t}_m)/2$, in third one – appropriate time-domain location $t_m = \mathrm{Re}(\hat{t}_m)$, in fourth one – imaginary part of estimation of location $\theta_m = \mathrm{Im}(\hat{t}_m)$, in fifth one – estimation of reflection amplitude $|\hat{r}_m|$, and in sixth one its phase in radians is indicated.

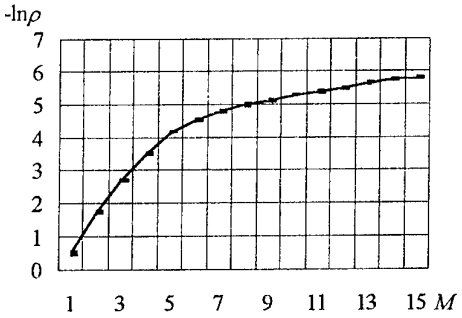


Fig. 3. Dependence of discrepancy between exponential model and measured horn reflectivity from model order

Table 1

Parameter estimations of model (6) for $R_A(\omega)$

m	z_m, mm	t_m, ns	θ_m	$\lvert r_m \rvert$	$\arg(r_m)$
1	-33	-0.22	0.030	0.002	-0.52
2	-13	-0.09	-0.012	0.009	-2.99
3	-2	-0.01	-0.020	0.023	-0.41
4	18	0.12	-0.002	0.029	-0.43
5	48	0.32	-0.004	0.005	-1.51
6	73	0.49	-0.005	0.013	-1.76
7	91	0.61	0.008	0.004	-2.06
8	99	0.66	-0.012	0.003	1.39
9	143	0.95	-0.036	0.001	2.84
10	403	2.68	0.002	0.001	2.85

Errors of measurements and singularities of work of the vector reflectometer stipulate first three components in a table 1. The component m = 4 is determined by a reflection from a port of horn, and m = 6 — from horn aperture. The model with indicated parameters ensures a discrepancy between the model and measured data less than 0.5%.

For determination of transmission characteristic $T_A(\omega)$ from (3) series of measurements of frequency characteristics of reflections from a metal plate 500×500 mm^2, located on a defined distance from aperture of horn in parallel to it were carried out. The reflection of a plane wave from a metal plane is determined by expression

$r_1\exp(j\omega t_1)$, but use of this model ($M_{mod} = 1$) for adjustment under the measured data gives a discrepancy between model and measured data more than 17 %, that considerably exceeds a level of a casual error of measurements. It confirms the supposition about presence of systematic error of measurements. Frequency dependences of module and phase of reflection characteristic from metal plate, and also appropriate curves for a model, adjusted under these data ($M_{mod} = 1$; $z_1 = 179$ mm; $t_1 = 1.19$ ns; $\theta_1 = -0.004$; $|r_1| = 0.196$; $\arg(r_1) = 2.05$) are represented in Fig. 4.

The appropriate time-domain signal for the measured data and for a model is represented in a Fig. 5. As it can been seen from the represented characteristics, the time-domain signal of peak of reflection from metal plane is extended and distorted, in comparison with model peak. And there is a decomposition of this peak, which is confirmed by estimations of exponential model obtained at $M_{mod} = 2$ ($z_2 = 166$ mm; $t_2 = 1.11$ ns; $\theta_2 = 0.133$; $|r_2| = 0.028$).

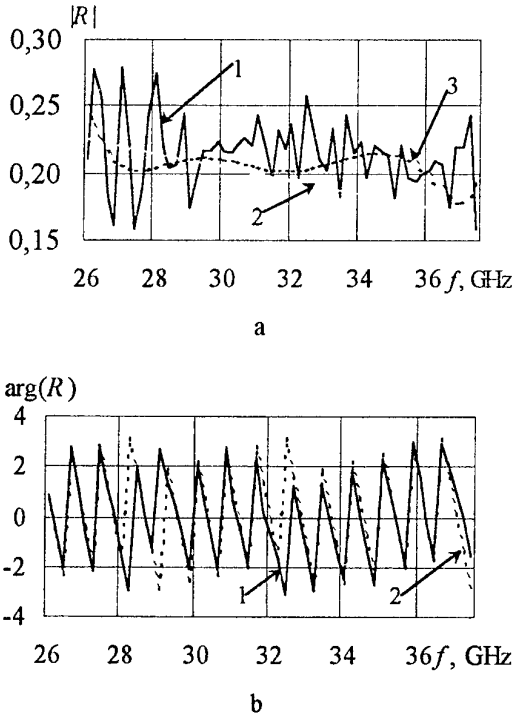


Fig. 4. Module (a) and phase (b) measured (1) and model (2) reflection characteristic for metal plate

These distortions are caused by amplitude and phase (in the greater degree) distortions introduced by a horn antenna and a part of measuring waveguide tract, located up to reference plane of the vector reflectometer. Additional research has shown that reference plane transition inside the waveguide measuring tract with magnification of its length has resulted in the even greater extension and distortion of peak. In this case, except the second additional peak, the third additional peak is found out about the principal peak. Besides, in the range 0 ÷ 0.6 ns there are peaks of a reflections caused by a reflection from the itself horn antenna.

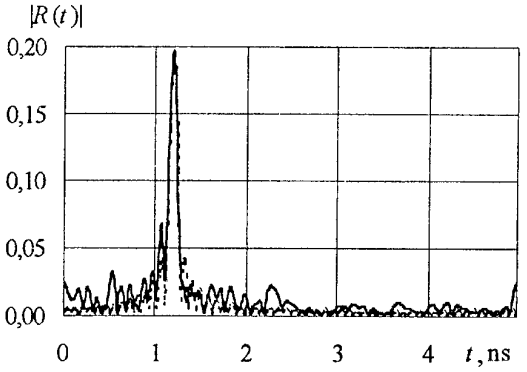


Fig. 5. Time signal of reflection from metal plane for measured data (solid line) and for model (dot line)

The estimation of distorting component $T_A(\omega)$ was produced by adjustment under the measured data of the model in form:

$$R_{pol}(\omega) = \exp(-j\omega t_1)\cdot\sum_{k=0}^{K} a_k \cdot P_k(\omega), \qquad (8)$$

where $P_k(\omega)$ is orthogonal degree polynomial of a degree k, specific on a discrete point set $\{\omega_n\}$. The following estimations of coefficients were obtained: $a_0 = 0.196$; $a_1 = 0.038$; $a_2 = 0.093$; $a_3 = 0.087$; $a_4 = 0.035$; $a_5 = 0.036$. In this case the discrepancy made 9%. Curve 3 in Fig. 4a demonstrates model dependence $R_{pol}(\omega)$. In Fig. 6 the phase of the measured characteristic and polynomial model $R_{pol}(\omega)$ after division on $\exp(-j\omega t_1)$ is represented.

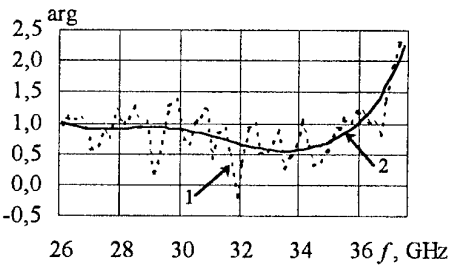


Fig. 6. Phase characteristic of reflection for experimental data (1) and for polynomial model (2)

The further research has shown, that the division of the measured data on a sum of polynomials $P_k(\omega)$ with the found values of coefficients a_k allows to remove the distortions introduced by a horn antenna. The time peak of a reflection from a metal plane ceases to be distorted and extended. This is confirmed by outcomes of estimations of parameters of exponential model (6),

adjusted under obtained data: $t_1 = -0.01$, $|r_1| = 0.13$; $t_2 = 0.13$, $|r_2| = 0.08$; $t_3 = 0.27$, $|r_3| = 0.05$; $t_4 = 0.51$, $|r_4| = 0.09$; $t_5 = 0.78$, $|r_5| = 0.08$; $t_6 = 1.19$, $|r_6| = 1.0$; $t_7 = 1.85$, $|r_7| = 0.11$; $t_8 = 2.29$, $|r_8| = 0.13$ (the discrepancy is equal 2%).

Also some the reduction of phase distortions introduced by a horn antenna and waveguide measuring tract, was possible to reach at multiplication of the measured data on a factor of an aspect:

$$T_\varphi(\omega) = \exp\left[j2\left(\varphi_w + \varphi_h\right)\right], \tag{9}$$

where

$$\varphi_w = \int_0^{l_w} \sqrt{\left(\frac{\omega}{c}\right)^2 - \left(\frac{\pi}{a}\right)^2}\, dx,$$

$$\varphi_h = \int_0^{l_h} \sqrt{\left(\frac{\omega}{c}\right)^2 - \left(\frac{\pi}{a + (a_p - a)x/l_h}\right)^2}\, dx,$$

l_w is the length of waveguide measuring tract from reference plane to the port of the horn, l_h is the horn length, a is a dimension of a broad wall of a waveguide and a_p is a dimension of the horn aperture.

REFERENCE

1. V. F. Borulko, O. O. Drobakhin, V. A. Karlov, "The measuring - computer complex RIMCH-04 for the non-destructive testing of layered dielectrics", Russian Non-destructive Testing [in Russia], No. 6, pp. 70-78, June 1993.

METHOD OF ESTIMATION OF REQUIREMENTS TO THE INPUT INFORMATION WHEN DETERMINING ANTENNAS CHARACTERISTICS WITH NEAR-ZONE METHODS

O. D. Anohina, A. V. Nechosa*

Kharkov Military University, 6 Svoboda Sq., Kharkov-310043, Ukraine
Phone(380-572)40-41-41-(2-85)
* Kharkov State University,4 Svoboda Sq., Kharkov-310077, Ukraine
Phone(380-572)45-71-75,Fax:47-18-16

Methods of the antenna parameters determination based on the near field measurements and transformation results of measurements in the far zone are the most perspective now. The essence of these methods is to measure field tangent components on a certain closed surface around the investigated antenna and to re-calculate the measured field in the far zone.

When estimating capabilities of these methods the analysis of the radiation pattern (RP) restoration accuracy are of essential significance.

Both methodical errors being of mainly systematical character and instrumental errors (of random nature in the most of cases) are main sources of errors of near-zone methods of the antenna parameters determination [1].

The methodical errors occur because the surface of the near field measurement is not closed and measurements are carried out not continuously on the surface but in separate points. These errors are named limitation and digitization errors.

The instrumental errors are conditioned by the near field measurements: errors of amplitude and phase measurers, inaccuracies of the probe movement on the measured surface, etc.

The methodical errors significantly depend on the size of the area of the near-zone measurements, chosen digitization step, position of the measurement area origin with respect to the antenna. In any realization the distinction between RP F obtained as a result of the treatment and real RP F_0 have an oscillating character caused by methodical errors. Limits of this distinction are presented for example in [2, 3].

Random errors of the antenna characteristics determination depend on the near field measurements accuracy. Calculated values of errors dispersions of the antenna restored main parameters are presented in [1].

When estimating the resulting error of the antenna characteristics determination by the near zone measurements all components of the error have to be considered as the random values of various magnitudes in any realization. The summation of these errors with other random errors has to be carried out according to the rule of the resulting error components one [4].

In order to sum separate components of errors they have to be presented by their root-mean-square σ. All computing operations of the errors summation are to be carried out only with these values.

Let us present the method of a choice of measurements conditions and estimate of requirements to the accuracy of the near field measurements for the restoration of the side lobe level with the given accuracy because the requirements to parameters of the measurement complex are the most rigid in this case.

Systematic errors of the RP ΔF determination are caused by the limitation of the measurement area ΔF_{lim} and digitization F_d. Assume that these errors are of the random values uniformlly distributed in the interval $[-|\Delta F_{lim}|,|\Delta F_{lim}|]$, $[-|\Delta F_d|,|\Delta F_d|]$. Hence, $\sigma_{lim}=|\Delta F_{lim}|/\sqrt{3}$, $\sigma_d = |\Delta F_d|/\sqrt{3}$. The magnitudes $|\Delta F_{lim}|,|\Delta F_d|$ are found by the relation presented in [2].

The resulting dispersion of the restored RP is as follows:

$$\sigma^2_F = \sigma^2_d + \sigma^2_{lim} + \sigma^2_{rand}. \qquad (1)$$

The comparatively high relative accuracy of the side lobe levels restoration (about 20–25% that corresponds to power RP measurements with the accuracy of ±2 dB) and the high reliability ($P_{cr} \geq 0.95$) are provided for those RP levels which meet condition [1].

$$\left[\frac{|F_0|}{\sigma_F}\right] >> 1. \qquad (2)$$

When the condition (2) is met, the amplitude of the restored RP is distributed by the normal law $N(|F_0|, \sigma^2_F)$. The probability of the difference between the amplitude of the restored RP $|F|=R$ and the true RP $|F_0|=R_0$ being no more than about $\pm V$

$$P_{cr}=P\{-V=|R-R_0|=V\}$$

is found from the equation

$$P_{cr}=2\Phi(V/\sigma_F), \qquad (3)$$

where $\Phi(\delta) = \frac{1}{\sqrt{2\pi}} \int_0^{\delta} e^{-t^2/2} dt$ is the Laplacian function.

The technique of requirements determination for the parameters of measuring set under given requirements to the antenna RP restoration consists in the following:

The admissible value of the dispersion σ^2_F is found by (2) and according to the requirements to the RP determination accuracy.

By giving the relation between errors components σ^2_d, σ^2_{lim}, σ^2_{rand} entered into (2) and stipulated by different sources, we determine the admissible contribution of every source of errors to the summary value of dispersion σ^2_F. The possibility of a choice of errors different sources contribution to the restored RP summary error σ^2_F allows to provide optimum measurement conditions from the point of view of economic expenses, time expenses, etc. In the most simple case the contribution of considered sources to the summary dispersion σ^2_F can be assumed to be equal. Measurement area sizes and the measurement step are found by the relation presented in [3] if values σ^2_d, σ^2_{lim}, σ^2_{rand} are known. And, at last, requirements to dispersions and correlation radii are to be found basing on the known relation between the dispersion σ^2_{rand} and statistical characteristics of errors of the measurements. If the correlation radii are unknown, requirements to dispersions of measurement errors are to be determined when assuming that correlation radius is of the value corresponding to the maximum magnitude of the dispersion.

Let us consider the methodical example.

Let it be necessary to restore the linear antenna RP with the uniform amplitude distribution in the angular sector comprising three first side lobes with the probability $P_F = 0.95$ and with the error no more than 25%. In this case $R_0 = 9\times10^{-2}$ (the third side lobe level). The equation (3) is solved using tables of the Laplacian function [5], hence, $(V/\sigma_F) = 1.96$. Since the error value is $V = 0.25R_0$ than $\sigma_F = V/1.96 = 1.14\times10^{-2}$. Assuming contributions of errors components to the summary error σ^2_F to be equal, we obtain the following: $\sigma_d = \sigma_{lim} = \sigma_{rand} = 6.5\times10^{-3}$. Intervals $|\Delta F_{lim}|$, $|\Delta F_d|$ are to be $|\Delta F_{lim}| = |\Delta F_d| = \sqrt{3}\,\sigma_{lim} = 1.1\times10^{-2}$ (this corresponds to the relative error $|\Delta F_d/F_0| = |\Delta F_{lim}/F_0| = 2$ dB). Measurement conditions are to be found using known intervals $|\Delta F_d|, |\Delta F_{lim}|$, and charts and equations presented in [3]. Thus, if the measurement area is placed at the distance $Z_0 = 10\lambda$ from the antenna, than measurement area size is $D = L + 8\lambda$, the interval between the near field measurement points is $\Delta x = 2\lambda$ and according to this the number of measurements is about $N \approx 20$.

Let measurement errors in the neighbor measurement points be independent, dispersions of amplitude measurement errors σ^2_β and phase measurement errors σ^2_φ be equal. Then the random errors dispersion of the amplitude RP restoration is as follows:

$$\sigma^2_{rand} = \frac{(\sigma^2_\beta + \sigma^2_\varphi)\Delta x}{L},$$

hence, $\sigma_\beta = \sigma_\varphi = 2.7\times10^{-2}$. That is the phase admissible measurement error of the near field amplitude is about $\approx 3\%$, and of phase — $\approx 1.5°$. Requirements to the accuracy characteristics of the measurement equipment can be not so rigid if the measurement step Δx is reduced (simultaneously the error component σ^2_d is less) or a number of independent measurements of the near field are carried out and their results are averaged.

Errors components of the RP determination σ_{lim} and σ_d [3] grow up in the case of the aperture antenna characteristics determination. At the same time requirements to the near field measurements accuracy $\sigma^2_\beta, \sigma^2_\varphi$ become less because of $\sigma^2_{rand} \sim \frac{\Delta x \Delta y}{L_x L_y}$.

This method of a choice of the measurement condition and the estimation of requirements to the measurement equipment accuracy can be used as well in the case when requirements to the antenna differeny parameters determination accuracy are given. In this case the corresponding proximity criteria of the restored and true RP are to be used [1].

REFERENCES

1. Bakhrakh L.D., Kremenetskiy S.D., Kurochkin A.P. ets. Measuremments Methods of Radiating Systems Parameters in the Near Zone. - L.: Nauka, 1985, 272 p. [in Russian].
2. Tseytman N.M. Methods of Microwave Antenna Characteristics Measurements. M.: Radio and Sviaz, 1985 [in Russian].
3. Bakhrakh L.D., Kurochkin A.P. Golography at the Microwave Techniques. - M.: Sov. radio, 1979, 320p. [in Russian].
4. Novitskiy P.V., Zograf I.A. Estimation of Errors of Measurements Results.-L.: Energoatomizdat, 1991.-304p. [in Russian].
5. Yanke E., Emde F., Lesh F. Special Functions. Equations, charts, tables. - M.: Nauka, 1977, 344p. [in Russian].

ABOUT NECESSITY OF CREATION OF THE ADDITIONAL SPACE SAR CALIBRATION POINTS AND EXPEDIENCE OF THEIR INTEGRATION INTO THE INTERNATIONAL CALIBRATION NET

V. S. Blinov

Kharkov-145 poste Restante, 310145, Ukraine
E-mail: vnt.@crse.kharkov.ua

ABSTRACT

Scientific, technical and organization aspects of shortening intercalibration period of space-borne synthetic aperture radar (SAR) are considered. In this paper it is proposed to use for calibration of SAR antennas groundbased antennas of space radio comunicaton, radio telescopes, meteo radars, etc. in the additional (background) regime at pauses in main work. Recommendations on integration of calibration means in nets of different level are created.

THE EXTERNAL CALIBRATION AND SIZING RESOURCES

Dynamics of the object's characteristic information changing — the radar cross-section (RCS), studied at radar Earth remote sensing (RERS) with using space synthetic aperture radar (SAR) is determined during the intersession analysis (monitoring) of radar images (RI) of one and the same terrain site. In this case the exact knowledge of the object reflection characteristics is required. This is impossible without performing external absolute through calibration of the SAR by standard calibration point reflectors or natural testing sites. The external calibration is required also in cases of one-time measurement. On the expert's opinion, it should be done as frequently as possible, better before each work session. For the absolute calibration of the through amplitude characteristic and certification of SARs in the dynamic range part the external standards of the RCS are need. Usually as the primary standard of the RCS there are used passive radar reflectors: Luneberg lenses, spheres, cylinders, trihedral, bihedral corner reflectors (CR), dipole, flate [1] and also active radar's calibrators (ARC). Passive reflectors can be classified as for their complexity of their manufacturing in the following way: dipole, plate, corner reflector (CR), cylinder, sphere, lens. The last one almost always is used as primary standard for calibration of other calibrators under laboratory conditions due to its complication and expansiveness. The plate is simple, but it has narrow radiation pattern (RP). This complicates the calibration. The RCS of the small sized CR doesn't correspond to calculated value and the CR should be replaced with spheres or lenses, or possibly, with the plates [2.3]. For the high values of the RCS even the CR becomes bulky, moreover it concerns sphere or lens. ARC overlaps the wide range of values, but they operate in one frequency range and require servicing.

TESTING SITES AND PERIOD OF CALIBRATION. PROPOSALS

The classified primary standard reflectors of different design parameters represent the testing site for calibration. This testing site is used not only for calibration but also for certification of space radars.

The time interval between the visits to just the same testing site is different for different space systems. For example, for systems with the geometry of observation as at "ERS-1", "ERS-2" it is 35 days. It is too much for the intercalibration period.

Therefore there is the problem of increasing the number of testing sites or we have to find another idea.

The construction of the additional testing site in favour of one national space system RERS is economically inexpedient, because it leads to rising up of the expenses for RI, which are already extremely heave. As a consequence, there is lack of possibility to carry out the external calibration of space radars by the primary standard reflectors as often as is needed. This weakens the confidence of the radar parameters as well as reduces the precision of measurement of calibration wedge steps between sessions. This makes doubtful the interpretation of different session radar images (RI) of the same "picture" obtained with functioning RERS systems.

Using of natural calibrators, such as Amazon forests and deserts, does not solve the problem completely. At the same time all over the world (in particular, in Ukraine) there are enough points of space radio communication and radio telescopes with full rotation antennas of different size (from 1 to 70...100 m indiameter). Some of them are occupied only episodically. They could undertake additional functions.

For calibration and certification of SAR of different classes one mast have the collection of primary standards of wide range of values. For space SAR the time of waiting for calibration is to be decreased. That demands to increase the number of calibration points. In this paper it is proposed to use the mentioned above antennas as additional calibrators (mini testing sites).

The expedience to create calibration net of local, regional and global levels is analyzed.

An essential shortening of intercalibration periods of the space-borne SAR is possible, when expanding the calibration net. Additional points can be created at places where full rotation antennas of different purposes and sizes are located. After simple completion the antenna becomes a single standard reflector with high or average value of RCS [2]. It functions between working sessions of the ground based equipment operation, when the antenna is not used for the main purpose it is intended.

SUBSTANTIATION OF THE SIZING RESOURCES INTEGRATION

The operational system of the external sizing should provide the calibration at any time wanted and for any trajectory of SAR carrier flight around Earth-orbit within the line-of-sight distance from a point, with approximate radius of 1000 km. (This value is corrected in the course of the experimental investigations). Hence, the necessity follow of joining separate calibrators (points) into nets of regional and international levels. The main requirement to this joining is the one of continuity of chain of windows in work, which are necessary for calibration.

With appearance of a number of such national calibration nets (it is better to join them into the international one) there'll be possible to calibrate space SAR several times a day. This periodicity can not be achieved with concentrated testing sites in the customary knowledge. The preliminary work for realization of this project is lead by us. The difficulties in operating with narrow RP make us to use the passive-active schedule of work.

The range of values of isolated standards of the RCS can be from 10 to 80...100-dBm^2 [3]. The expected error of standard is not worse than it is for ARC. The confidence is not worse than the one of passive reflectors. When using the insession and intersession statistical processing of the calibration results, the accuracy of the calibration wedge determination can be increased [4].

INVITATION TO COOPERATION. PROSPECTS OF CALNET

We hope, this project represents interest, because it proposes to decrease the range between calibration that is desirable for any acting RERS system. We invite anyone who is interested to take part in the project realization in any form.

We also hope that any space agencies or oters. related to the development, creation, exploitation of the onboard RERS systems and with the application of the obtained RI will support us in the idea of joining the calibrating resources into international calibration network (INTERCALNET) [5]. In future this net can be used for receipt and fast delivery of RERS material, for example RI to consumers.

REFERENCES

1. Kobak V.O.: Radar reflectors. - Sov. Radio, Moscow: 1975. -p 247 [in Russian].
2. Blinov V.S./ Proc.4-th'Ukr. - Russ. - Chin. Simp. Kiev: Sept.1996, -p 57-59.
3. Blinov V.S./ Proc. European Conference on SAR. EUSAR'96, Koenigswinter, Germany, March 1996, -p 547-548.
4. Blinov V.S. / Proc. NPO "Planeta", S-Peterb.:GMI,v.42- 1993. –p 38-57 [in Russian].
5. Blinov V.S.: The summary directed to the Conference RADAR-97. Kharkov: December 1996.

EM-PROPERTIES MEASUREMENT AND ERROR ANALYSIS OF PLANAR AND CONVEX SURFACE SAMPLES USING FINITE FLANGE OPEN-ENDED COAXIAL PROBE

A.-K. A. Hassan, D. Xu, and Y. Zhang

School of Communication and Information Engineering, Shanghai University
Jiading, Shanghai 201800, China

ABSTRACT

In this paper, open-ended coaxial probe is studied to make nondestructive EM-properties of planar and convex surface coating material testing. An error analysis was performed to investigate the influence of the flange diameter and the radius of convex sample variation on the reflection coefficient. A cylindrical 2-D FDTD code was developed and used for this analysis. It is found that the reflection coefficient affected for small radii of convex sample. Comparing with the analytical solutions based on the spectral-domain model, the FDTD modeling results of the constitutive parameters ε^* and μ^* for planar and convex samples were in agree-ment with the published data by companies. Results of the FDTD simulations and experiments are presented.

INTRODUCTION

Open-ended coaxial probes have been investigated by many researchers for non-destructive characterization of dielectric materials [1–2]. However, most of these studies are limited to measuring the complex permittivity only. In general, the properties of the materials such as microwave compound are required to be characterized by complex permittivity ε and permeability μ. Thus it is necessary to extend the open-ended coaxial probe technique to measure ε^* and μ^*. Until now, in most applications, the use of open-ended coaxial probe is restricted to the planar sample testing. But in the practical cases, especially on the worksite testing it is required to test the curved samples such as convex surfaces. Also for *in-situ* testing of material, it is more convenient to use open-ended coaxial probe with finite flange. Therefore, numerical techniques can be used for modeling the open-ended coaxial probe to obtain material properties iteratively from the measured reflection coefficients. Recently, a paper has been published [3] to quantify errors on the input reflection coefficient due to air gaps between the coaxial probe and the surface of the material under test. This paper focuses on quantifying errors due to air gaps between the coaxial probe and convex sample as shown in Fig. 1 (b). For air gaps under consideration, the use of the analytical procedure is rather difficult. Therefore, errors created by these air gaps are analyzed using Finite-Difference Time-Domain (FDTD) method. The effect of the flange diameter on the measurement is investigated. Also, the FDTD modeling technique is used to obtain both ε^* and μ^* of planar and convex surface coating materials. Modeling results are compared with the analytical solutions based on spectral-domain model and the available data recently published by companies to demonstrate the feasibility of FDTD-method in such problems.

SPECTRAL-DOMAIN MODEL OF THE PROBE

Admittance: It is not lost generality to consider the situation when material under test is coated on metal surface as shown in Fig. 1 (a). The inner and outer radii of air filled coaxial line are a and b respectively. The material under test whose EM properties are characterized by the relative complex permittivity ε and permeability μ is assumed to be linear, isotropic and homogenous in nature with thickness d. The spectral-domain model, which takes into account only the principal TEM mode, is formulated to relate the measured reflection coefficient with the EM-properties to be determined. The obtained normalized admittance model is given as follow [2]

$$Y = \frac{Y_{in}}{Y_0} = \frac{1-\Gamma}{1+\Gamma} = \frac{jk_0\varepsilon}{\ln(b/a)} \int_0^\infty \frac{\coth\left(d\sqrt{\lambda^2 - k_0^2\varepsilon\mu}\right)}{\lambda\sqrt{\lambda^2 - k_0^2\varepsilon\mu}} [J_0(\lambda a) - J_0(\lambda b)]^2 d\lambda , \quad (1)$$

where, Y_0 is the characteristic admittance of the coaxial line, Γ is the measured reflection coefficient, k_0 is the wave number in free space.

NUMERICAL ANALYSIS OF FDTD MODELING

To assist in the modeling of the air gaps on the order of 0.05 mm with the curved surfaces, a cylindrical FDTD code is developed to calculate the input reflection coefficient of finite flange coaxial probe terminated with planar and convex samples. The model is 2-D with the center of inner conductor forming line of symmetry as depicted in Fig. 1 (b). First-order absorbing boundaries are placed around the probe to limit the computational domain and increase the computational efficiency. The singularity in the coordinate system along Z-axis is handled with technique described in [4]. Effective average values of constitutive parameters are used to calculate field components at different interfaces. A stair-

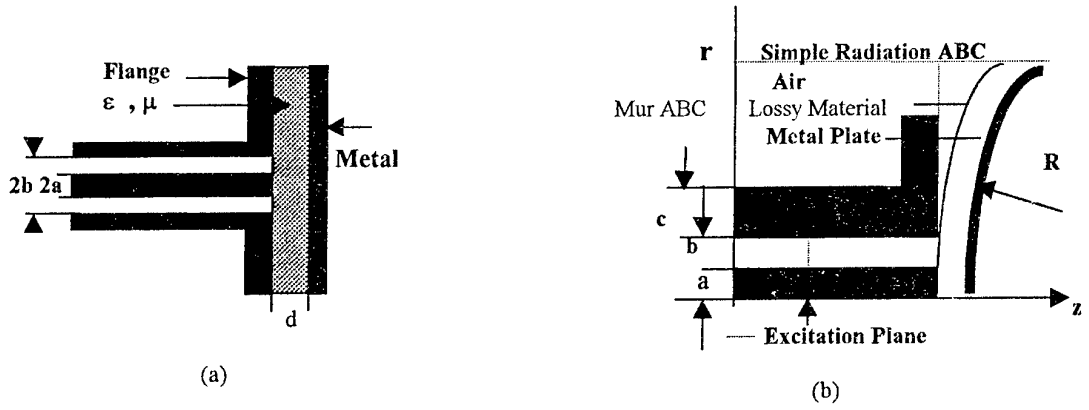


Fig. 1. Schematic presentation of the coaxial probe, a = inner conductor radius, b = outer conductor inner radius, c = outer conductor outer radius with convex sample of radius R. (a) Planar Sample (b) Convex Sample

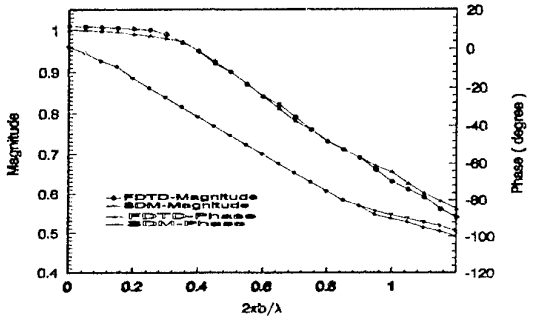


Fig. 2

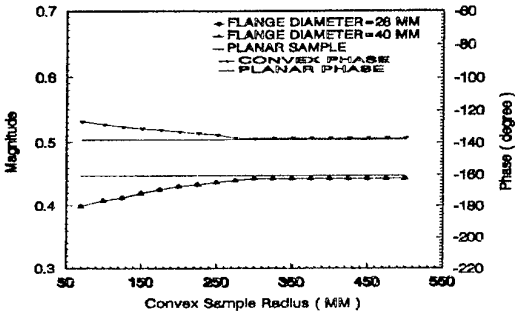


Fig. 3

Fig. 2. Comparison of the spectral-domain model and FDTD code results (Teflon)

Fig. 3. Variation of reflection coefficient of the coaxial probe with convex sample radius

stepped approximation technique is used to calculate field components at curved media between the probe and the sample under test. A forward moving toward the measurement end TEM wave is launched at the excitation plane located inside the coaxial line. Field distributions in the sample, air gap and the coaxial probe are calculated using Yee procedure [5]. Sampling of the fields occurs away from the aperture to avoid higher order TM modes excited by the aperture and other discontinuities. The reflection coefficient is computed at the sampling point using technique described in [6].

RESULTS

A number of tests were conducted for samples of different lossy materials of planar and convex surfaces to determine both ε^* and μ^* using spectral-domain model and FDTD-method. Measure-ments corresponding to the selected flange diameters and convex radii are performed using HP-8510B automatic network analyzer at 10 GHz. Thickness varying method is used to achieve the two reflection coefficients required to extract ε^* and μ^* using the admittance model as in equation (1) and FDTD technique. ε^* and μ^* are obtained by implementing an algorithm which finds the roots of the error functions between the measured and the calculated reflection coefficients. To check the accuracy of our FDTD code, we first compared the FDTD results with the data published in [7] as shown in Fig. 2, where it may be seen good agreements between them. It is also seen that at lower frequencies, the amplitude of the reflection coefficient obtained by FDTD-method is slightly longer than unity due to round off error arising from the use of absorbing boundary condition. As the field in the materials having losses decay much faster, the conclusions obtained by considering materials with no losses such as Teflon, is the worst case conclusion. To quantify the influence of air gaps between the coaxial probe and the convex sample, on reflection coefficient, different flange diameters and convex sample radii are simulated and the results are shown in Fig. 3.

Table 1

Comparison of the calculated ε^* and μ^* for different flange diameters (Planar sample)

Flange Diameter	Method	Value			
		ε_r	$\tan\delta_\varepsilon$	μ_r	$\tan\delta_\mu$
60 mm	Spectral	11.10	-0.021	1.36	0.65
60mm	FDTD	10.63	-0.005	1.29	0.65
13 mm	Spectral	11.53	-0.016	1.24	0.83
13mm	FDTD	10.74	-0.006	1.33	0.64
Reference [8]		10.40	-0.005	1.35	0.64

Table 2

Comparison of the calculated ε^* and μ^* for different convex sample radius (Flange diameter = 28 mm)

Convex Radius	Method	Value			
		ε_r	$\tan\delta_\varepsilon$	μ_r	$\tan\delta_\mu$
100 mm	Spectral	13.20	-0.12	1.59	1.10
100 mm	FDTD	14.89	0.023	1.28	1.21
150 mm	Spectral	13.67	-0.01	1.59	1.08
150 mm	FDTD	14.92	0.022	1.26	1.22
Reference [8]		1495	00222	135	122

The calculated reflection coefficient for the convex sample decreases for small radii as compared to the measured reflection coefficient of the planar sample, which may be due to the nature of convex surface. Also, it can be observed from the Fig. 3 that the flange diameter has negligible effect on the reflection coefficient measurement. It is clear from the FDTD results that the reflection coefficient is substantially affected for small radii of convex sample. To explore the limits of the analytical solution based on the spectral-domain model, we use the FDTD-method to simulate ε^* and μ^* measurement with open-ended coaxial probe for different lossy materials. Again, a series of tests and simulations are conducted to obtain both ε^* and μ^* simultaneously for the planar and convex surfaces samples using coaxial probe with its finite dimension of the flange. The measured values of ε^* and μ^* of planar sample using the spectral-domain model and FDTD-method for two different flange diameters of the coaxial probe are compared in Table 1. It is clear that the error in the measured values is higher in the case of using spectral-domain model compared to the reference data [8]. Also the error increases for smaller flange diameter of the probe. This error in the measurement is reasonable since the assumption of the infinite flange of the probe was made. In the FDTD-method, the results for both flange diameters agree well with the reference data. The small discrepancy between the FDTD results is due to using finite flange diameter by which the reflection coefficient is higher for the small flange. This could be caused by the presence of additional scattering edges near the aperture. The measured ε^* and μ^* using another lossy material for two radii of convex sample are given in Table 2. Again, it can be an error in measurement caused by using spectral-domain model and the error increases for small radii of convex sample. For the FDTD-method, the measured values of ε^* and μ^* are agree well with the reference data which may be due to geometry being modeled. Despite, the errors in the two methods are reasonable since the reflection coefficients are affected by the air gaps between the probe and the convex sample. But this error is more serious in the spectral domain model. The radii of the sample considered in the analysis herein represent the worst case. For

practical purposes, the radius is larger and accurate results can be obtained. For the cases examined, the results clearly demonstrate the feasibility of using FDTD method for modeling the open-ended coaxial probe to determine both ε^* and μ^* of lossy materials. The thickness varying method, which makes two reflection coefficients measurement with two samples of different thicknesses is not convenient for testing coating materials *in-situ* and errors are introduced in the measurement process. Therefore, the technique described in [9] can be used which simplify and speeds up the measurement process as well as improves the accuracy.

CONCLUSION

In this paper, an error analysis is done to investigate the influence of non-uniform air gaps and the flange diameter on the EM-properties measurement. Results of FDTD modeling and the analytical solutions have shown that it is quite difficult to extend the theoretical models developed for the flanged open-ended coaxial probe to include the effect of finite flange and the curved surfaces materials. Therefore, in planar and curved surface material testing, using the FDTD-method is essential to obtain accurate inversion results.

REFERENCES

1. J. R. Mosig, J. C. E. Besson, M. Gex-Fabry, and F. E. Gardiol," Reflection of an open-ended coaxial line and application to nondestructive measurement of materials," IEEE Trans Inst. Meas., Vol. IM-30, pp. 46-51, Mar. 1981.
2. P. D. Langhe, K. Blomme, L. Martens, and D. D. Zutter,"Measurement of low-permittivity materials based on a spectral domain analysis for open-ended coaxial probe," IEEE Trans Inst Meas Vol. 42, No.5 pp.879-886, Oct. 1993.
3. J. Baker-Jarvis, M. D. Janezic, P. D. Domich, and R. G.Geyer," Analysis of an open-ended coaxial probe with lift-off for nondestructive testing," IEEE Trans Inst Meas Vol. 43, pp.711-718, Oct. 1994.
4. B. G. Colpitts," Thru characteristics of a coaxial gap (FDTD model and measurement)," IEEE Trans. Micro. Theory Tech., Vol. 44, No. 1, Jan. 1996.
5. K. S. Yee,"Numerical solution of initial boundary-value problems involving Maxwell's equations in isotropic media,"IEEE Trans. Antennas Propagat., Vol. AP-14, may 1966.
6. M. Okonieweski, J. Anderson, and S. S. Stuchly," A technique to compute reflection coefficient in FDTD method," IEEE Antennas Propagat. Soc. Int. Symposium Digest Seattle, June 1994, Vol. 3, pp.1446-1449.
7. P. D. Langhe, L. Marteans and D. D. Zutter,"Design rules for an experimental setup using an open-ended coaxial probe based on theoretical modeling," IEEE Trans. Inst. Meas., Vol. 43, No. 6, Dec. 1994.
8. M. Niu, Y. Su, J. Yan, C. Fu, D. Xu , "Simultaneous measuring ε^* and μ^* of compound materials on-site using open-ended waveguide sensor," IEEE Inst. Meas. Tech. Conf. Ottawa, Canada, May 19-12, 1997, pp. 482-486
9. S. Wang, A. K. A. Hassan, M. Niu, and Deming Xu,"A swept-frequency technique with an open-ended wave-guide sensor for nondestructive simultaneous determination of thickness, permittivity, and permeability of radar obsorbing coatings,"1998 Asia-Pasific Microwave conference APMC'98, pp. 129-132, Dec.8-11 1998,Yokohama Japan.

COMPLEX REFLECTIVITY METER IN MICROWAVE PATHS

L.Y. Ilnitskiy, L. V. Sibruk, M. I. Fuzik

Kyiv international university of civil aviation.
Kyiv-58, str. Komarova 1. 484-97-45.

Complex reflectivity characterizes mode of operation of a transmission line and enables to evaluate parameters of a transmission line load. Therefore methods and measurement devices of reflection factor always causes the certain interest of the experts working in the field of antennas and microwave devices.

In known methods of reflection factor measurement either three – four probes, or rotating probes, or complex constructive couplers are used. For simplification of the measuring device, increasing its reliability and accuracy two-probe complex reflectivity meter of is designed. (Fig.)

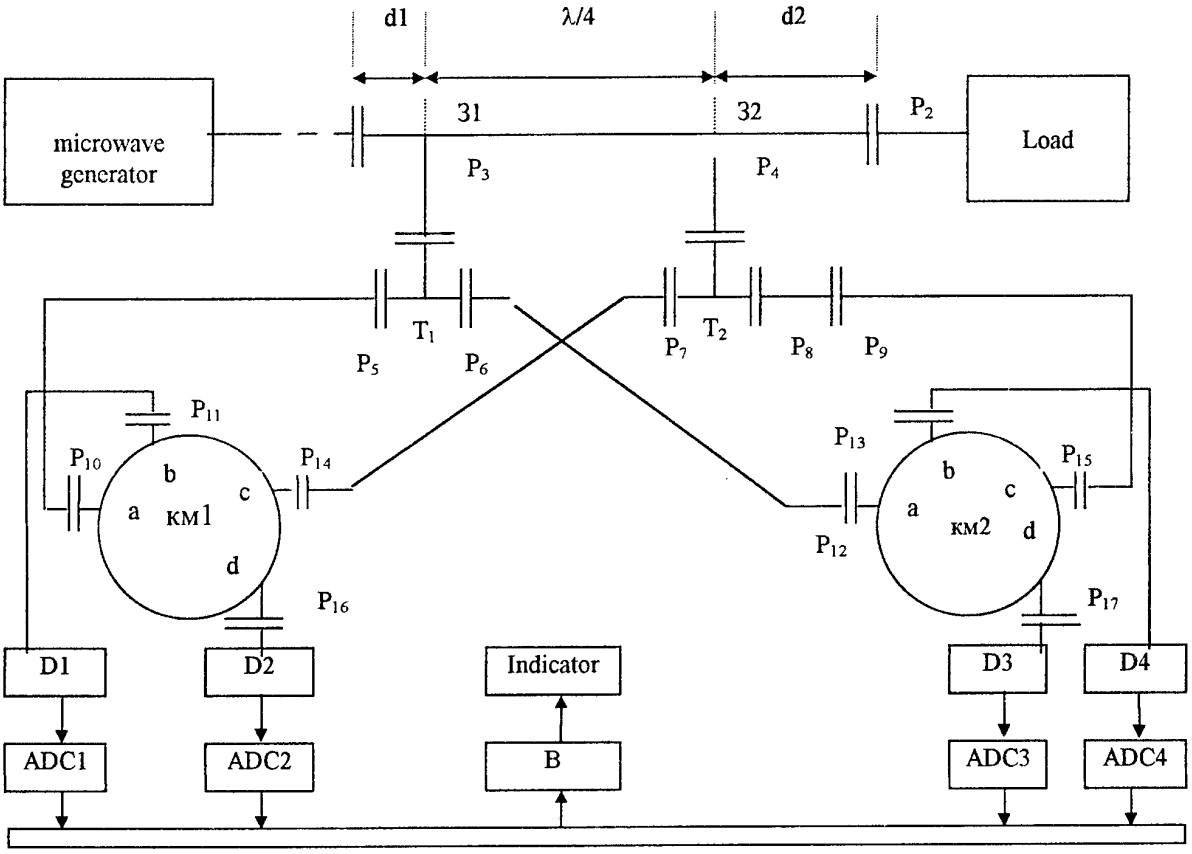


Fig. Complex reflectivity meter

The device connected by plugs (P) P1 and P2 is included in a microwave path connecting the a microwave generator with a load. In measuring section of a transmission line on distance λ/4 from each other there are probes (3) 31 and 32. Voltages, measured by these probes, by T-bends (T) T1 and T2 are divided in two synchro-phase and equal by wave power, which are made to ring bridges (KM) KM1 and KM2. In ring bridges the distance $d_{ab} = d_{bc} = d_{cd} = \lambda/4$ and the distance by an arc 'ad' counter-clockwise is equal $d_{ad} = 3\lambda/4$, therefore shoulders 'a' and 'c' are mutually untied and to them the waves from T-bend outputs P5, P6, and P7, P8 are made up. By means of that in shoulders 'b' the total waves, and in shoulders 'd' - difference waves are derivated.

If you count coordinate Z from a load up to the probe 32, voltage on plugs P5 and P6 of the T-bend T1 is determined as

$$\dot{U}_1 = \dot{U}_{\Pi}\, \ell^{\,i\beta(Z+\lambda/4)} + \dot{U}_0\, \ell^{\,-i\beta(Z+\lambda/4)} \qquad (1)$$

And on plugs P7 and P8 of the T-bend T2

$$\dot{U}_2 = \dot{U}_{\Pi}\, \ell^{\,i\beta Z} + \dot{U}_0\, \ell^{\,-i\beta Z}, \qquad (2)$$

$U_П$ – an amplitude of a falling wave, $\beta = 2\pi/\lambda$ – a constant of distribution in a transmission line, λ – the length of a wave in a microwave path; $\dot{U}_0$ – a complex amplitude of a reflected wave.

Using significance complex reflectivity $\tilde{\Gamma} = \tilde{A}\ \ell^{i\gamma}$, expression (1) and (2) can be shown as.

$$\left.\begin{aligned}\dot{U}_1 &= \dot{U}_П\ \ell^{i\beta(Z+\lambda/4)}[1+\tilde{\Gamma}\ \ell^{-i2\beta(Z+\lambda/4)}]\\ \dot{U}_2 &= \dot{U}_П\ \ell^{i\beta Z}[1+\tilde{\Gamma}\ \ell^{-i2\beta Z}].\end{aligned}\right\} \quad (3)$$

For the inclusion of measuring section could not cause changes to mode of a transmission line operation, its length from the plug P1 up to the plug P2 is selected equal to an integer of half-waves. Therefore distance d1 and d2 should satisfy to conditions.

$$d1 = S\frac{\lambda}{2} + \lambda/4 \quad (4)$$

And

$$d2 = q\frac{\lambda}{2}, \text{ where } s,q \in N.$$

In this connection $\exp(i\beta z) = 1$ and the expression (3) becomes simpler

$$\dot{U}_1 = i\dot{U}_П(1-\tilde{\Gamma})$$

and

$$\dot{U}_2 = \dot{U}_П(1+\tilde{\Gamma}) \quad (5)$$

The lengths of sections of a line from P5 up to the plug P10 of the bridge KM1 and from P7 up to the plug P14 should be such, that the phase parities of voltage $\dot{U}_1$ and $\dot{U}_2$ would not be destroyed, then in a shoulder 'b' (in the plug P10) the total wave is formed which can be characterized by voltage:

$$\dot{U}'_b = \dot{U}_1 + \dot{U}_2 = \dot{U}_П[1+i+\tilde{\Gamma}(1-i)] \quad (6)$$

On the same conditions difference wave in a shoulder 'd':

$$\dot{U}'_d = \dot{U}_2 - \dot{U}_1 = \dot{U}_П[1-i+\tilde{\Gamma}(1+i)]. \quad (7)$$

To the shoulder 'a' of the second bridge KM2 the voltage U1 (5) is made in the same phase, as to the shoulder 'a' of the bridge KM1. The wave of voltage $\dot{U}_2$ acquires additional phase shift 90^0 in the fixed phase shifter connected between the plugs P8 and P9, therefore voltage of a total wave in a shoulder 'b' of the second bridge is

$$\dot{U}''_b = i2\dot{U}_П \quad (8)$$

And the voltage of the difference wave

$$\dot{U}''_d = i2\dot{U}_П\tilde{\Gamma} = i2\dot{U}_П\tilde{A}\ \ell^{i\gamma}, \quad (9)$$

All four the voltages (see fig.) come to the detection sections with a straight-line characteristic of transformation, therefore constant voltage on output clips of detectors are:

$$U_1^{\partial} = f_{\partial}(U'_b) = \sqrt{2}\,k_{\partial}\sqrt{1+\Gamma^2+2\Gamma\sin\varphi}\ U_П; \quad (10)$$

$$U_2^{\partial} = f_{\partial}(U'_d) = \sqrt{2}\,k_{\partial}\sqrt{1+\Gamma^2-2\Gamma\sin\varphi}\ U_П \quad (11)$$

$$U_3^{\partial} = f_{\partial}(U''_d) = 2k_{\partial}\,\Gamma U_П; \quad (12)$$

$$U_4^{\partial} = f_{\partial}(U''_b) = 2k_{\partial}\,U_П. \quad (13)$$

All these voltages will be transformed to the digital form by means of analog-to-digitial converters (ADC).

In the computing device (B) "B" the magnitude of reflection factor is calculated as the division of voltage U_3^{∂} (12) to voltage U_4^{∂} (13).

$$\Gamma = U_3^{\partial}/U_4^{\partial} \quad (14)$$

The parameters δ and γ are calculated

$$\left.\begin{aligned}\delta &= \frac{U_1^{\partial}}{U_4^{\partial}}\frac{\sqrt{1+\Gamma^2+2\Gamma\ \sin\varphi}}{\sqrt{2}}\\ \gamma &= \frac{U_2^{\partial}}{U_4^{\partial}}\frac{\sqrt{1+\Gamma^2-2\Gamma\ \sin\varphi}}{\sqrt{2}}\end{aligned}\right\} \quad (15)$$

Values δ and γ are erected in a square and define the unit and phase of the reflectivity

$$\Gamma = \sqrt{\delta^2+\gamma^2-1}, \quad (16)$$

$$\gamma = \arcsin\left(\frac{\delta^2-\gamma^2}{2\sqrt{\delta^2+\gamma^2-1}}\right). \quad (17)$$

The value Γ, obtained from the expression (16) is compared to the value (14) and used for a control measurement accuracy.

Main source of errors are the breaks of phase parities, instability and disorder of transmission factors of detectors, the inaccuracies in definition of detected voltage significances.

For checking of accuracy of operation and calibration the measuring section of a transmission line is loaded on an agreed load. Here (2 = (2 = 0,5. If output is disconnected (2 = 2, (2 = 0 and if output of section is shorted.

Let's consider influence of a wave length change on accuracy of measurement of the magnitude of reflectivity. Let's accept, that the phase shift on 90^0 is realized by passing a wave of the waveguide section of length 'a', then from the formula (14) with the help of expressions (8), (9) and (1), (2) we can define the measured significance of reflection factor.

$$\Gamma_{rad} = \frac{\ell^{i\beta\ (Z+a)} + \Gamma\ell^{-i\beta\ (Z+a)} - \ell^{i\beta\ (Z+a)} - \Gamma\ell^{-i\beta\ (Z-a)}}{\ell^{i\beta\ (Z+a)} + \Gamma\ell^{-i\beta\ (Z+a)} + \ell^{i\beta\ (Z+a)} + \Gamma\ell^{-i\beta\ (Z-a)}},$$

where Γ_{rad} – reflectivity from a load. Getting rid of identical factors and components, we obtain

$$\Gamma_{rad} = \Gamma f(\lambda),$$

where

$$f(\lambda) = i\frac{\sin(\frac{2\pi\ a}{\lambda})}{\ell^{i\frac{2\pi\ a}{\lambda}} + \Gamma\cos(\frac{2\pi\ a}{\lambda})}. \qquad (18)$$

Assume, that the magnitude of reflectivity from a load little depends on a length of a wave, we find

$$\frac{\Delta\Gamma}{\Gamma} = \Delta f(\lambda)\Delta\lambda .$$

Using expression (18), we define a comparative error of calculation of the magnitude of reflectivity

$$\delta\Gamma = \pi\delta(\lambda) \qquad (19)$$

As it follows from (19) error $\delta\Gamma$ stipulated by change of of the wave length, increases inπ times. For example the range of frequencies 10 000 MHz error 0,03 is possible to ensure the error 0.03 in a bend of frequencies up to 100 MHz.

THE MEASUREMENT OF A POWER FLOW IN TWO-MODE WAVEGUIDE WITH USING GALVANOMAGNETIC TRANSDUCERS

P. V. Ivkin

National Technical University of Ukraine "Kyiv Politechnical Institute",
KPI-2110, Peremohy prospect, 252056 Kyiv, Ukraine,
tel. 441-12-71

The most widespread method of power measuring in multimode waveguide supposes using of multiprobe section [1], [2]. Such a section contains gauges of electrical field in shape of thin wire probes. The probes are situated in several reference and measuring sections. It is possible to measure amplitudes and phases of wave composition with use of such a section. The power of each wave is calculated from the obtained amplitudes of fields.

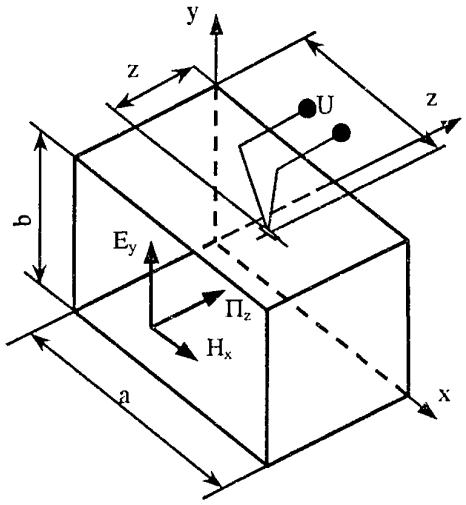


Fig. 1. Situating of gauge on the waveguide's wall

The method of determination the power of waves in two-mode waveguide with using galvanomagnetic transducers of microwave power flow on the base of ferromagnetic films [3] (later on – galvanomagnetic gauges or simply gauges) is presented by us. The principle of galvanomagnetic gauges' operation is in using galvanomagnetic phenomenons – magnetic-resistance and anomalous Holl's effect. These phenomenons appear in ferromagnetic films, operating in the mode of ferromagnetic resonance. At that microwave magnetic field excites alternative magnetization, that changes film's resistance. If in such a medium microwave current of the some frequency flows additionally, than converted field arises in the result of parametric detection in the volume of film. The mean of this field is proportional to a real part of Poynting's vector.

Thus, the signal from the gauge which is situated on a waveguide's wall will be proportional to the real part of Poynting's vector of a total electromagnetic field (see Fig. 1):

$$U = K \cdot \mathrm{Re}(\dot{\Pi}_z). \tag{1}$$

K — calibration factor of the gauge. The Poynting's vector represents product:

$$\dot{\Pi}_z = \frac{1}{2}\left[\dot{\bar{E}}_\Sigma \times \overset{*}{\bar{H}}_\Sigma\right]_z. \tag{2}$$

In the given expression $\dot{\bar{E}}_\Sigma$ and $\overset{*}{\bar{H}}_\Sigma$ represent the sums of transverse component of all waves, including incident and reflected ones.

Let's write field strengths for the two-mode case, in which there are only H_{10} and H_{20} waves:

$$\begin{aligned}
\dot{E}^{\pi}_{ym0} &= -j \cdot W_{m0} \cdot H^{\pi}_{xm0} \cdot \sin\frac{m\pi x}{a} \cdot e^{j\left(-\Gamma_{m0} \cdot z + \varphi^{\pi}_{m0}\right)} \\
\dot{E}^{o}_{ym0} &= j \cdot W_{m0} \cdot H^{o}_{xm0} \cdot \sin\frac{m\pi x}{a} \cdot e^{j\left(\Gamma_{m0} \cdot z + \varphi^{o}_{m0}\right)} \\
\overset{*}{H}^{\pi}_{xm0} &= -j \cdot H^{\pi}_{xm0} \cdot \sin\frac{m\pi x}{a} \cdot e^{-j\left(-\Gamma_{m0} \cdot z + \varphi^{\pi}_{m0}\right)} \\
\overset{*}{H}^{o}_{xm0} &= -j \cdot H^{o}_{xm0} \cdot \sin\frac{m\pi x}{a} \cdot e^{-j\left(\Gamma_{m0} \cdot z + \varphi^{o}_{m0}\right)}, \quad m = 1,2.
\end{aligned} \tag{3}$$

Here, W_{m0} — characteristic impedance of the wave H_{m0} in the waveguide; Γ_{m0} — propagation constant of the wave H_{m0} in the waveguide; H_{m0} and φ_{m0} — amplitude and phase of magnetic field strength of the wave H_{m0}. The superscripts **п** and **о** denote belonging either to incident or to reflected wave, respectively.

Thus, the multipliers in equation (2) represent values:

$$\begin{aligned}
\dot{\bar{E}}_\Sigma &= \left(\dot{E}^{\pi}_{y10} + \dot{E}^{o}_{y10} + \dot{E}^{\pi}_{y20} + \dot{E}^{o}_{y20}\right) \cdot \vec{y}_0 \\
\overset{*}{\bar{H}}_\Sigma &= \left(\overset{*}{H}^{\pi}_{x10} + \overset{*}{H}^{o}_{x10} + \overset{*}{H}^{\pi}_{x20} + \overset{*}{H}^{o}_{x20}\right) \cdot \vec{x}_0.
\end{aligned} \tag{4}$$

By substituting these values in (2), and then (2) in (1), we shall find, that

$$\begin{aligned}
U = K \cdot \Big(& \Pi_{10} \cdot \sin^2\frac{\pi x}{a} + \\
& + \Pi_{20} \cdot \sin^2\frac{2\pi x}{a} + C \cdot \sin\frac{2\pi x}{a} \cdot \sin\frac{\pi x}{a} \Big),
\end{aligned} \tag{5}$$

where

$$\Pi_{10} = \frac{1}{2} \cdot W_{10} \cdot \left(\left(H_{10}^{n}\right)^2 - \left(H_{10}^{o}\right)^2 \right), \quad (6)$$

$$\Pi_{20} = \frac{1}{2} \cdot W_{20} \cdot \left(\left(H_{20}^{n}\right)^2 - \left(H_{20}^{o}\right)^2 \right), \quad (7)$$

$$\begin{aligned} C = \frac{1}{2} \cdot \{ & H_{10}^{n} \cdot H_{20}^{n} \cdot \cos\left(\left(\Gamma_{20} - \Gamma_{10}\right) \cdot z + \varphi_{10}^{n} - \varphi_{20}^{n} \right) - \\ & - H_{10}^{o} \cdot H_{20}^{o} \cdot \cos\left(\left(\Gamma_{20} - \Gamma_{10}\right) \cdot z + \varphi_{20}^{o} - \varphi_{10}^{o} \right)] \times \\ & \times \left(W_{10} + W_{20}\right) + \\ & + [H_{10}^{o} \cdot H_{20}^{n} \cdot \cos\left(\left(\Gamma_{20} + \Gamma_{10}\right) \cdot z + \varphi_{10}^{o} - \varphi_{20}^{n} \right) - \\ & - H_{10}^{n} \cdot H_{20}^{o} \cdot \cos\left(\left(\Gamma_{20} + \Gamma_{10}\right) \cdot z + \varphi_{20}^{o} - \varphi_{10}^{n} \right)] \times \\ & \times \left(W_{20} - W_{10}\right) \} \end{aligned} \quad (8)$$

How it is seen from (6) and (7), the components Π_{10} and Π_{20} represent absolute value of Poynting's vectors of waves H_{10} and H_{20} separately. These values should be determined to us.

There are three unknown values in the equation (5): Π_{10}, Π_{20}, and C. Therefore, having defined with a certain value of coordinate z, and having arranged three gauges in points x_i, it is possible to make the system of equations:

$$\begin{aligned} K_i \cdot \Bigg(& \Pi_{10} \cdot \sin^2 \frac{\pi x_i}{a} + \\ & + \Pi_{20} \cdot \sin^2 \frac{2\pi x_i}{a} + C \cdot \sin \frac{2\pi x_i}{a} \cdot \sin \frac{\pi x_i}{a} \Bigg) = U_i, \end{aligned} \quad (9)$$

$i = 1,2,3.$

The given system is easily solved with the help of computer.

It should be noted, that value C represents a combination of products of all existing field strengths, and it depends on many variables:

$$C = C\left(H_{m0}^{n,o}, \varphi_{m0}^{n,o}, z\right) \quad (10)$$

The computer experiment, in which the dependence of Π_{m0} values' determination accuracy on the coordinates of gauges and on changing of waves' phases is investigated, was carried out by us. The magnetic field on frequency 4.5 GHz in the rectangular waveguide 72×34 mm was simulated. The amplitudes of field strengths were chosen:

$$H_{10}^{n} = H_{20}^{n} = 2 \cdot 10^{-3} \text{ A/m}; \; H_{10}^{o} = H_{20}^{o} = 1 \cdot 10^{-3} \text{ A/m}.$$

Longitudinal coordinate z was chosen:

$$B\,z = \frac{\pi}{3 \cdot \left(\Gamma_{20} - \Gamma_{10}\right)} = -0.022 \text{ m}.$$

It is supposed, that all the calibration factors are equal to unit.

The random values of coordinates x_i were generated with the random numbers generator. The phases φ_{m0} were also generated on the each set of coordinates. In the result, the data array was obtained (Table 1).

The results of computation are shown in the Table 2.

Table 1

The coordinates of gauges and the phases of waves

	x_1	x_2	x_3	φ_{10}^{n}	φ_{10}^{o}	φ_{20}^{n}	φ_{20}^{o}
№	M			rad			
1	0.008	0.059	0.020	5.218890	0.665913	0.462310	2.605526
2	0.008	0.059	0.020	3.465766	4.826006	3.557480	4.609133
3	0.008	0.059	0.020	5.417168	3.605163	1.887281	0.918405
1	0.056	0.040	0.063	1.138081	5.708012	1.908881	3.833564
2	0.056	0.040	0.063	1.725076	0.474110	3.786074	6.149724
3	0.056	0.040	0.063	4.494238	2.183859	3.522023	2.971317
1	0.006	0.029	0.007	3.403746	4.362166	6.231033	1.896779
2	0.006	0.029	0.007	5.710009	2.844226	1.195885	4.374097
3	0.006	0.029	0.007	5.915627	6.083404	5.268354	4.108367

Table 2

The results of computation

	Computational values of unknowns			Computational values of the gauges' signals			Values of unknowns, obtained from solving the set of equations.		
	Π_{10}	Π_{20}	C	U_1	U_2	U_3	Π_{10}	Π_{20}	C
№	Wt/m^2			V			Wt/m^2		
1	0.000638	0.001497	0.002531	0.001119	0.000181	0.003734	0.000640	0.001496	0.002531
2	0.000638	0.001497	0.001234	0.000865	0.000817	0.002757	0.000635	0.001499	0.001234
3	0.000638	0.001497	-0.000364	0.000551	0.001599	0.001554	0.000640	0.001496	-0.000364
1	0.000638	0.001497	0.001896	0.000515	0.000167	0.000326	0.000639	0.001498	0.001898
2	0.000638	0.001497	0.001538	0.000742	0.000283	0.000422	0.000641	0.001503	0.001549
3	0.000638	0.001497	-0.001131	0.002437	0.001151	0.001136	0.000639	0.001498	-0.001130
1	0.000638	0.001497	-0.000512	0.000352	0.000768	0.000500	0.000699	0.001554	-0.000652
2	0.000638	0.001497	0.003470	0.000869	0.002865	0.001246	0.000888	0.001725	0.002904
3	0.000638	0.001497	-0.000730	0.000323	0.000653	0.000459	0.000477	0.001350	-0.000366

As it is seen from the results, the value of Poynting's vector (power flow) of each wave does not depend on their phases. Furthermore, the results, which are founded from the set of equations, are in agreement with the computation values. However, there is some divergence in the determining of waves' power flow under a close arrangement of gauges. This divergence is connected only with the computational error. The following task of researching will be determining of an optimum arrangement of gauges.

REFERENCES

1. Burlachuk V. V., Geyvandov A. N., Daniluk V. S. Automatized measuring-calculating system for the multimode measuring in the microwave waveguide sections. – in the book: Transactions of III Republican scientific and technical conference "The methods and means of measuring in area of electromagnetic compatibility." – Vinnitsa, 1991, pp. 126–133.
2. Taub J. J. A new technique for multimode power measurement. — IRE Transactions On Microwave Theory and Techniques, 1962, v. 10, pp. 496 - 505.
3. Vuntesmeri V. S. Ferromagnetic-film galvanomagnetic transducers of microwave power flow. – Proceedings of higher educational institutes of USSR, – sec. Radioelectronics, 1980, v. XXIII, № 3, pp. 28–34.
4. Nikolskiy V. V., Nikolskaya T. I. Electromagnetics and propagation of radiowaves. – Moskow: «Science», – 1989, pp. 231–233.

RADIOHOLOGRAPHIC CORRELATIONAL MEASUREMENTS OF LARGE REFLECTOR ANTENNAS

A. V. Kalinin

Radiophysical Research Institute,
Bolshaya Pecherskaya, 25, Nizhny Novgorod 603600, Russia
fax: 7+ 8312 369902; e-mail: kalinin@nirfi.sci-nnov.ru

ABSTRACT

The results of radioholographic correlational measurements of the characteristics of several large Russian reflector antennas are discussed. Some features are considered of measurements with using of signals of natural radiosources and geostationary satellites. The techniques and results of the measurements on the 64-meter antenna at the deep space communicational centre "Medvezhy Ozera" near Moscow are detailed submitted. These measurements were carried out in 1996-1998 with the 4 GHz signals of geostationary satellites and discrete radio source Cygnus-A. The form of a reflecting surface of the main mirror was restored with accuracy about 0.1 mm (rms) and resolution along the aperture near of 90 cm. By results of measurements the adjustment of mirror system of this antenna was executed. Besides the thermal deformations of a mirror caused by daytime solar heating were investigated as well as dependence of the mirror form on elevation (gravitational deformations). In the report the most of experimental results may be demonstrated in the form of color maps of field distributions.

INTRODUCTION

Nowadays antenna measurements are effectively done by some modifications of the holographic method (for example, see [1,2]). The correlational radioastronomical antenna measurements with extraterrestrial sources [3,4] is a variant of the holographic method. Fig. 1 demonstrates the block-scheme of this method of antenna measurements.

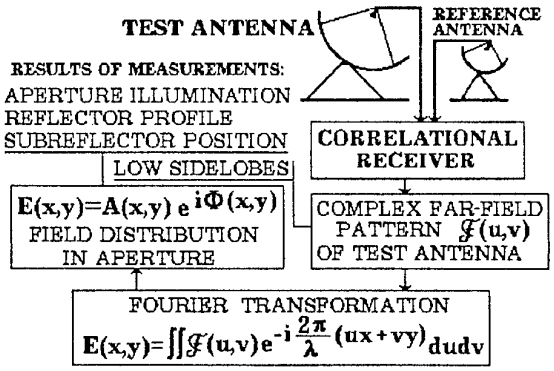


Fig. 1. Diagram of correlation antenna measurements

Measurements need the special two-channel correlation receiver and also additional reference antenna incorporated with tested in small-base interferometer and tracking the radiosource. The advantage of a considered method above a usual radio astronomical antenna measurements is an ability to measure the far-field pattern in significantly greater dynamic range, because an output signal of the correlational receiver is proportional to a field strength pattern of the tested antenna. This method is also suitable for measurement of phase and polarization parameters of the antenna pattern. The measurement of complex far-field pattern in a large angular region and Fourier transformation of the measured data allow to restore a complex field distribution in aperture.

Similar technique was used at several large radiotelescopes for determination and alignment of mirror's panels positions and subreflector displacements, for example [1,5]. Such measurements with a high degree of accuracy require development of the appropriate techniques, equipment and software and also careful analysis of opportunities and errors [8].

The correlation radioastronomical method was developed during a number of years in the Nizhny Novgorod Radiophysical Research Institute (NIRFI) for antennas with mirrors from 7 up to 70 meters. The measurements were carried out with signals of discrete radiosources, geostationary satellites and Sun in frequency ranges from 500 MHz up to 11 GHz. The antennas with mirrors from 1 up to 25 m. were used as reference. Some results received recently are presented below.

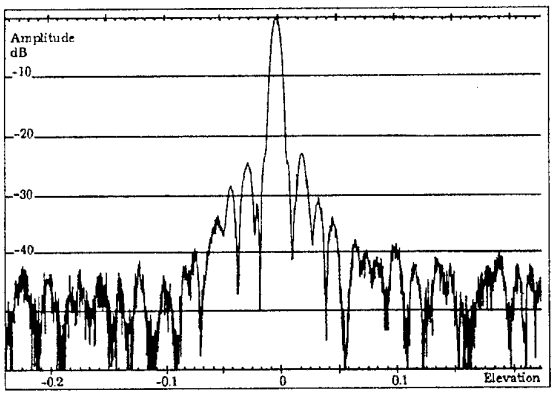


Fig. 2. Cross section of the 25-meter antenna far-field

EXPERIMENTAL RESULTS

The measurements with discrete radio sources Cygnus A and Cassiopeia A were carried out for 25-meter tested antenna and 25-meter reference one with a distance about 100 meters at the wavelength 10 cm [6]. The Fig. 2 demonstrates as an example of far-field pattern cross-section of the 25-meter antenna, obtained through the correlational measurement method with the radio source Cygnus A.

The measured dynamic range was about 50 dB, while in modulational radioastronomical measurements it did not exceed 25 dB.

At the radioholographic measurements with space radio sources one should exclude from the data being measured an interferometric component, caused by the source displacement. We used additional calibrations data for determine of size and the orientation of the interferometre baseline, after that an amplitude and phase distributions in aperture were restored.

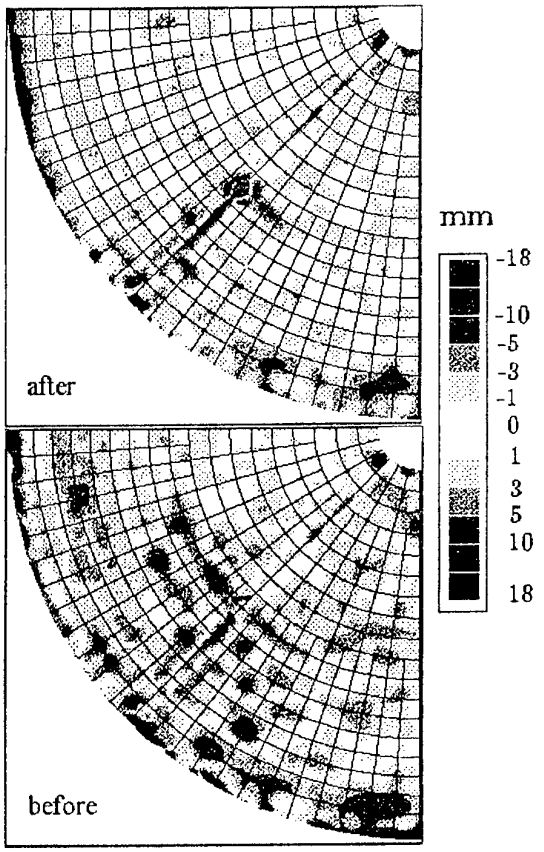


Fig. 3. Comparison of TNA-1500 aperture maps before and after adjustment

In 1996-1998 the holographic measurements were fulfilled for one of largest Russian fully steerable radiotelescopes — 64-meter mirror antenna in space communication center "Medvezhy Ozera" near Moscow [7, 8]. 4 GHz signals of geostationary satellites and discrete radio source Cygnus-A were used. A reference 90-cm antenna was installed at the tested mirror near of subreflector support. The dynamic range of measurement was near of 70 dB. High-resolution 90-cm map of mirror distortions was restored with use of 4 GHz satellites signals. A surface rms deviation was near of 2 mm. Rms difference of the maps measured under identical external conditions was about 0.1 mm. A stability of surface form was investigated for this antenna by means of comparison of surface maps measured under different external conditions. The mirror form dependence of elevation (gravity deformations) was investigated with Cygnus-A signal at different source elevations.

With using of the high-resolution map obtained, a partial adjustment of mirror surface was made for 405 points with displacement more than 2 mm. Fig. 3 demonstrates a comparison of mirror maps measured before and after partial adjustment. The rms surface deviation has made after adjustment about 0.8 mm. As a result of this the antenna efficiency at 5-cm band was increased from 0.51 to 0.65.

REFERENCES

1. Proceedings of the International Workshop "Holography testing of large radio telescopes", Nizhnij Arkhyz, September 10-13, 1990, Leningrad, "Nauka", 1991, 135pp.
2. L. N. Zakhar'ev, A. A. Lemanskij, V. I. Turchin, et al. Methods of measurements of VHF antenna characteristics. Ed. N. M. Tseitlin, Moscow, Radio i Svyaz, 1985, 368 pp.
3. P. F. Scott, M. Ryle. A rapid method for measuring the figure of a radio telescope reflector. Royal Astronom. Soc. Monthly Notices, v.178, pp.539-545, 1977.
4. Smith P. Measurement of the complete far-field pattern of large antennas by radio sources.-IEEE Trans. 1966, v.AP-14, n.1, p.6-16.
5. D. J. Rochblatt and B. L. Seidel, "Microwave antenna holography", IEEE Trans. on MTT, v.40, n.6, 1992, p.1294-1300.
6. A. V. Kalinin, V. P. Mal'tcev, V. S. Beagon, and G. A. Kislyakov. Interferometric Measurements of Mirror Antennas with Extraterrestrial Sources, Proc. of PIERS 1997, July 7-11, 1997, Cambridge, Ma, USA, p.600.
7. A. V. Kalinin, B. A. Poperechenko. Radioholographic measurements of the 64-meter mirror antenna TNA-1500 in Bear Lakes. Proc. of the Antenna Conference JINA'96,12-14.11.97, Nice, France, p. 559-562.
8. A. V. Kalinin, B. A. Poperechenco. Radioholographic Measurements and Surface Adjustment of the 64-meter Reflector Antenna in Medvezhy Ozera (Russia), Digest of IEEE Antennas and Propagation Sosiety Int. Symp., July 13-18, 1997, Montreal,Canada, Volume 1, pp. 564-567.
9. A. V. Kalinin. Radioholographic method of of measurements of radiotelescopes antennas characteristics. In col. "Antennas", Ed. L.Bakhrakh, Moscow, 1998, v.2 (41), p. 51-67.

PHASE SHIFT MEASUREMENTS FOR ANTENNA SYSTEMS

L. D. Ogorodnijchuk

National Technical University of Ukraine "Kiev Polytechnical Institute"
37, prospekt Pobedy, Kiev, 252056, Ukraine

INTRODUCTION

The necessity to create the high accurate antenna systems for radio systems and complexes [1] requires to provide this sphere of science and engineering with a high accurate phase-metering equipment. It's used to measure phase characteristics of units and blocks of antenna feeding systems, feeds, and antenna in the full sense [1-3], and to receive signals (phase radio direction finders, monopulse radars), and to control the operation (phase antenna arrays) as well. Also it's used for periodical attestation of antenna feeding systems. The accuracy of the equipment for antenna phase measurements has to be a subject of the requirements of the national standards [4,5]. These requirements are satisfied by methods of phase measurements and appropriate microwave phase-meters.

The present paper shows the analysis of errors of the proposed wide band, high speed, and accurate microwave phase-meter (below - a phase-meter) ant its peculiarities with respect to the analogues. As a prototype the phase-meter [6] has been used. The block diagram has been calculated in 1991 for the Laboratory of Antennas Systems and Telecommunication (headed by Dr. F.Dubrovka) of the National Technical University of Ukraine "Kiev Polytechnical Institute".

BLOCK DIAGRAM

The block diagram of the phase-meter is shown in Fig. 1. It consists of a directional coupler (DC), transmission line (TL), matched load (ML), probes (P), summer (S), detectors (D), differential sections (DS), and computer (C). A phase shift (FS) φ is measured between signals a and e with amplitudes A, E that arrive at system input.

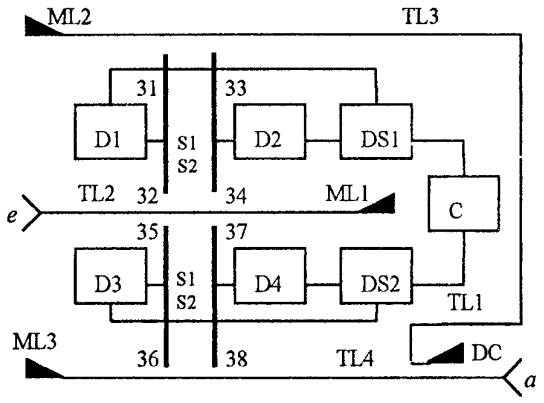


Fig. 1

The phase-meter belongs to a group of multi-probe phase-meters. It has diversed microwave channels, signal phasing is ensured by DC and diversing the probes along TL on $\lambda/4$, where λ - wavelength in the middle of operational frequency band.

The peculiarity of the method of measurements consists in the following. The signals are propagating along TL as travelling waves. The phasing is ensured by DC and probes placing. The mixed waves are formed in inter-probe circuits. Analysing them the informational voltages are formed

$$u_1 = kAE\sin\varphi,\ \ u_2 = kAE\cos\varphi, \qquad (1)$$

where k - a coefficient.

From (1) we pass to

$$u_3 = tg\varphi \text{ or } u_4 = ctg\varphi \qquad (2)$$

In (2) the functions are sufficiently non-linear. Thus we use the intervals $0...\pm 1$ with lesser non-linearity which permit FS measuring over the range of a natural phase cycle by measuring cycle intervals $m90° \pm 45°$, where $m = 0; 1; 2; 3$. For $m = 0; 2$ the expression (2a) is used, and for $m = 1; 3$ - (2b). These measurements are equivalent to each other. To evaluate an indetermined form the sign parameters in (1) and quantative ones in (2) are used.

Let consider the errors being characteristic for the circuit with diversed channels.

The standard deviation caused by reflectivity Γ of ML1, ML2, and ML3 can be determined as

$$\Delta\varphi_\Gamma \approx 1.7\Gamma. \qquad (3)$$

For $\Gamma = 0.01$ $\Delta\varphi_\Gamma$ doesn't exceed 1°.

The standard deviation caused by isolation I between channels, i.e. in DC, can be determined as

$$\Delta\varphi_I \approx 1.4I\Gamma. \qquad (4)$$

For $\Gamma = 0.01$ and $I = 0.1...0.03$ $\Delta\varphi_I$ doesn't exceed 0.09...0.03°. In inter-probe circuits better isolation can be ensured by using evanescent waveguides [7] or DC. The latter permits to improve sensitivity of the measurements.

The error caused by signal dephasing in DC can be determined according to

$$\Delta\varphi_\delta = arctg[\sin\varphi/\cos(\varphi-\delta)]-\varphi. \qquad (5)$$

For $\delta \le 1°$ in waveguide frequency band error (5) doesn't exceed 1°.

The error caused be a change of δG in directivity G of DC can be computed according to

$$\Delta\varphi_{\delta c} = arctg\left(\sqrt{\frac{2}{1+\delta G/G}-1}\ tg\varphi\right)-\varphi\,. \qquad (6)$$

For $\delta G/G$=0.05 the error (6) is 1.4°.

The analysis of the errors shows that the phase-meter can provide a high accuracy of the measurements in a wide frequency band.

DEVELOPMENT OF THE BLOCK DIAGRAM

Let consider two ways to measure FS in the event of number of probes is being reduced. Let assume that only probes 1, 2, 5, 6 or 3, 4, 7, 8 are used. The first way consists in switching signals *a,e*. Data is obtained during three cycles of measurements. They correspond to the mode when: both switches are opened; the first one is opened, the second - closed; the first one is closed, the second - opened. The experimental investigations of p-i-n- and mechanical switches have been carried out. They provided signal attenuation 50..70 dB in a closed state, and have loss 0.2...2 dB depending on a switch type. Mechanical switches can provide the highest (0.5°...1°) identity of phase characteristics. A corresponding error can be commensurable with the ones mentioned above.

The second way requires the detectors to measure signal amplitudes to be placed in TL 1, 2 or TL 2, 3, 4. For both methods joint data processing permit the voltages (1) to be obtained. These methods, as well as method based on transformation (1), allow to obtain the normalized value (1)

$$u_3 = \sin\varphi\,,\ u_4 = \cos\varphi\,. \qquad (7)$$

CHARACTERISTIC LINEARIZATION

To measure quickly changing FS it's expedient to use functions with small non-linearity. In [3] it has been proposed to compensate the non-linearity peculiar to (2) with one of the opposite sign taking place in (7). The corresponding functions are

$$u_5 = tg\varphi + N\sin\varphi \text{ or } u_6 = ctg\varphi + N\cos\varphi\,, \qquad (8)$$

where N ≥ 0 - parameter being, according to a physical sense, a gain. If the components in (8) to represent as trigonometric series and to compare terms with corresponding numbers, it can be noticed that the weight of the second (the 3rd order) and other even terms of the functions (3) is being reduced with respect to (2). Since the parameter N is a varying one, then it's expedient to normalize (8). On the proper intervals of the scale using of characteristics of the functions (8a) and (8b) is identical. Thus below let consider only function (8a). The normalized voltage (8a) is

$$u_7 = (tg\varphi + N\sin\varphi)/(N+1)\,. \qquad (9)$$

Its non-linearity with respect to $u = \varphi$ is determined as

$$\xi = 100(tg\varphi + N\sin\varphi - (N+1)\varphi)/(N+1)\varphi\,, \qquad (10)$$

which is a trigonometric series without a linear term.

There are two main linearization modes. For the first one parameter N has been fixed before measuring and isn't changed during measurements. For $N = 2$ in (8a) the component of the 3rd order is being excluded; practically there is no non-linearity on the scale interval ±5°, and on the interval ±10° it's less than 0.007%. If it's necessary to obtain the minimal non-linearity on the interval ±45° then $N \approx 2.6$ is being chosen. A Table 1 shows the calculation results for this interval of the scale. It's obvious that after linearization is taken place the non-linearity does not exceed 0.41 %, and there is an advantage in linearity from 13 up to 187 times in compensation with (2a).

Table 1
Linearization of the phase-meter scale

Non-linearity of the scale	FS, degrees					
	10	20	30	40	45	50
$\xi_{(N=0)}$, %	**1.03**	**4.27**	**10.26**	**20.19**	**27.33**	**36.56**
$\xi_{(N=2.6)}$, %	**-0.08**	**-0.27**	**-0.41**	**-0.12**	**0.39**	**1.33**
$\xi_{(N=0)}/\xi_{(N=2.6)}$	**13.05**	**15.75**	**25.3**	**187**	**69.8**	**28.43**

The second mode consists in changing the parameter N during measurements. For the ideal case ($\xi = 0$), from (10) the following expression can be obtained

$$N_0 = (\varphi - tg\varphi)/(\sin\varphi - \varphi)\,. \qquad (11)$$

A Table 2 shows N_0 for the interval of scale 0...±89°.

Table 2
Requirements for N_0

FS, deg.	10	20	30	40	50
N_0	2.03	2.12	2.28	2.55	2.99
FS, deg.	60	70	80	89	
N_0	3.78	5.41	10.39	100.7	

On the intervals ±50° it's required to change N_0 in range of 3 dB, i.e. very small variations of the parameter ensure the full linearization of the characteristic. The scale intervals can be expanded by changing the parameter on 34 dB. This value can be easily realized.

The obtained results are true for: 1) the function (8b); 2) normalization with respect to the straight lines with greater rate of change, i.e. $u=2\varphi$ and $u=3\varphi$. This permits the sensitivity of measurements to be increased. The linearization of the scale provides improvement of resolution and accuracy of FS measurements in a real time, permits to expand scale intervals in comparison with (2).

CLASSIFICATION

A classification makes it possible to place the described phase-meter in a group of multi-probe phase meters,

and to place the latter among other groups of microwave phase-meters. To carry out the classification it's expedient to use generalized signs. S the first one it's expedient to consider the presence of frequency conversion and intermediate frequency (IF) value. For such approach phase-meters can be divided into ones with IF greater than signal frequency and those with IF less than signal frequency. The second group is more wide spread one. As to criteria of IF value phase-meters belonging to this group can be divided into ones with IF > 0 and IF = 0. The first variant is ensured by applying modulation or heterodyning. In modulation phase-meters converting on IF is carried out by various types of modulation of one or two signals. These phase-meters are divided into two groups: with and without filtration of composite signal. Let note that for some modulation phase-meters the data about FS is in IF voltages, amplitudes of which are (1). For them the proposed methods to linearize characteristics can be used. In microwave phase-meters with heterodyning double heterodyning as well as single and multiple ones are used.

The realization of the second variant is provided without auxiliary signals. As a reference signal one of the signals is used. The multi-probe phase-meters belong to this group. Their classification is shown in Table 3.

Table 3
Classification of multi-probe phase-meters

Signs, characteristics	Realization of signs and characteristics
Peculiarities of methods of measurements	Providing travelling wave (TW) mode of the signals, their mutual phasing, forming and analysis of mixed waves (MW)
Variants of method realization	Joined channels (one TL), probes and detectors of MW; joined channels (two TL) DC, splitter, MW probes and detectors; diversed channels (two TL), TW probes, MW probes and detectors; diversed channels (three TL), DC, TW probes, MW probes and detectors
Waves	TW, MW
Place of forming TW MW	 TL TL, inter-probe circuits
Number of TW probes	No; eight
Number of MW probes and detectors	Four; two (in a combination with switches or amplitude detectors)
Number of TW amplitude probes and detectors	Two; three
TW switching	No; yes
Probes characteristic	Electrical; magnetic
Probes placement in TL	Diversed along TL (electrical, magnetic); in section of TL (magnetic)
Dependence of results on probe angle	Invariant to the angle (electrical); dependent on angle (magnetic)
Phasing 90°	DC; diversing electrical probes; rotation and diversing magnetic probes
Phasing 0°, 180°	Splitter; double DC; diversing electrical probes along TL; diversing magnetic probes or/and their rotation
Informational voltages processing	Analogous; digital
Peculiarity of linearization	Non-linearity (2) is compensated by one of the opposite sign (7)
Application of linearization	No; yes
FS indication	Analogous (cathode-ray tube, pointer display); digital (indicator, matrix)

CONCLUSION

The microwave phase-meter based on DC with diversed channels has been proposed and analysed. It preserves the advantages of the prototype - wide band and quick response. Due to its distinguished peculiarities and partially or full linearization of characteristic it permits to reduce errors of measurements up to 1..3°.

The system of criteria, which include the ones describing the considered phase-meter, has been formulated. On their basis the classification of microwave phase-meters with respect to IF has been carried out. It shows that multi-probe phase-meters belong to the group of phase-meters with zero IF. The classification of multi-probe phase-meters showing the place of the proposed one is presented. The multi-probe phase-meters can serve as a basis for the further development of waveguide detecting devices of modulation phase-meters that expands the sphere of their application.

REFERENCES

1. Problems of antenna engineering // L.D.Bachrach, D.I.Voskresenskiy, Moscow, Radio i sviaz, 1989, 368 p.
2. GOST 23066-78, Moscow, 1978, 10 p
3. GOST 23282-78, Moscow, 1978, 9 p.
4. GOST 8.192-76, Moscow, 1976, 4 p.
5. GOST 8.415-81, Moscow, 1981, 4 p.
6. Bova N.T. Phase shift meter. A.s. USSR, N176614, 1965.
7. Bondarenko I.K., Dejnega G.A., Magrachev Z.V. Automatization of measurements of the parameters of microwave lines, Moscow, Sov.radio, 1969, 304 p.
8. Ogorodnijchuk L.D. Method to measure phase difference. A.S. USSR, N991326, 1983.

REQUIREMENTS TO THE ACCURACY OF PAA PHASE METERS

L. D. Ogorodnijchuk

National Technical University of Ukraine "Kiev Polytechnical Institute"
37, prospekt Pobedy, Kiev, Ukraine

The development and application of phased antenna arrays (PAA) require a lot of types of phase characteristics to be measured. As a rule large PAA consists of thousands and ten thousands of modules. For them phase characteristics measurements distinguish by their mass character. To carry put these measurements a lot of phase meters are used. They belongs to PAA, because depending of their purpose, they are he part of PAA as its units or (and) devices of PAA complex.

One of the main characteristics of PAA is a word length of phase meters of its modules or PAA word length. It is expedient to use this characteristic to evaluate the requirements to the accuracy of PAA phase meters. As it is known a discrete level of phase shift variation in a phase rotator of PAA module is

$$\Delta = \frac{2\pi}{2^p}, \qquad (1)$$

and maximal value of phase shift setting error is

$$\Delta\varphi_m = \pm\frac{\pi}{2^p} = \pm\frac{\Delta}{2}, \qquad (2)$$

where p - a phase meter word length.

To ensure the reliability of phase shift measurements it is necessary to set more strict requirements to PAA phase meter with respect to (2). For this purpose in (2) it is necessary to add a coefficient $q > 1$. Then, the formula permitting to evaluate the requirements to PAA phase meter accuracy will be the following

$$\Delta\varphi_{tm} = \pm\frac{\Delta\varphi_m}{q} = \pm\frac{\Delta}{2q}. \qquad (3)$$

Also it is expedient to take into account the peculiarities of error adding for units being connected across FAR circuits. For example, in modules a branch of a splitter, a phase rotator, a matching element and an antenna radiator are connected in series; a frequency converter can be also included into a module.

There are several possible variants of modules matching: each of its devices are matched separately, according to groups or module in whole. The peculiarities in (3) can be taken into account with a coefficient of a number of measured objects $n \geq 1$. The requirements to the PAA phase meter accuracy can be determined as

$$\Delta\varphi_{tm} = \pm\frac{\Delta\varphi_m}{nq} = \pm\frac{\Delta}{2nq}. \qquad (4)$$

For estimation calculations let's $q = 3$, $n = 1$ (module is matched in a whole). Then

$$\Delta\varphi_{tm} = \pm\frac{\Delta}{6}. \qquad (5)$$

The calculated requirements to the accuracy of phase shift setting in modules and results of measurements with the help of PAA phase meters (5) is shown in Table 1.

Table 1

p, bit	2	3	4	5	6
2^p	4	8	16	32	64
Δ, deg.	90	45	22.5	11.2	5.6
$\Delta\varphi^m$, deg.	45	22.5	11.2	5.6	2.8
$\Delta\varphi_{tm}$, deg.	15	7.5	3.7	1.9	0.9
p, bit	7	8	9	10	
2^p	128	256	512	1024	
Δ, deg.	2.8	1.4	0.7	0.35	
$\Delta\varphi^m$, deg.	1.4	0.7	0.35	0.18	
$\Delta\varphi_{tm}$, deg.	0.5	0.2	0.12	0.06	

For many practical cases PAA are realized with word length $p = 3, 4, 5$. For such PAA the requirements to the phase meters accuracy can be easily satisfied. PAA with $p = 6$ are used as well. In literature there are the recommendations about purposefulness or using PAA with $p = 7, 8$ in scientific experiments. The requirements to phase meters of these PAA are more difficult to realize. The calculations carried out for PAA with $p = 9, 10$ shows a possible perspective concerning the requirements the accuracy of PAA phase meters. For $n \geq 2$ the requirement (4) to the accuracy of PAA phase-meters become essentially more strict.

CHARACTERISTICS OF ANTENNAS, RECORDING SYSTEMS AND PROCESSING ALGORITHMS USED IN THE RADAR SYSTEMS FOR MEASURING PROJECTILE MOVEMENT PARAMETERS AT THE TIME OF SHOOTING

S. V. Porshnev

Nizhny Tagil State Teachers' Training Institute,
622031 Nizhny Tagil, Krasnogvardeyskaya 57, tel. (3435) 256-433,
E-mail: ntr20@ntgpi.e-burg.ru

One of the main problems of experimental ballistics is the problem of measuring projectile movement parameters (PMP) (movement, velocity, and acceleration) at the time of shooting [1-4]. In so doing the developers of artillery systems and ammunition are mostly interested in the functional time dependence of kinematic parameters measured at separate sections of the trajectory and not their individual values, only in this case it is possible to get the complet analysis of the ammunition behavior at the time of shooting and to find out the reasons of a non-standard functioning emerges. The problem of continuous measuring projectile movement parameters from the starting point of the projectile movements in the barrel and further on the trajectory has not been solved to date. Therefore the investigations carried out in this direction is aimed at solving three independent problems:

1. Measuring PMP at the internal ballistic stage of shooting (the projectile movement in the bore of an artillery system barrel).
2. Measuring PMP at intermediate ballistics stage (from the moment when the projectile leaves the bore of a barrel till the moment when powder gases stop affecting the projectile).
3. Measuring PMP on the external ballistic trajectory.

In the practice of proving ground tests microwave CW radars are used for solving these problems. Their application is based on the fact that the phase of a radar signal (RS) emitted in the radar mixing section, when comparing an electromagnetic wave (EW) reflected from a moving target and a reference EW, are compared is determined by its movement, and the frequency is determined by velocity. The analysis of their change with time makes it possible to determine PMP.

In order to measure PMP at the internal ballistic stage of shooting a radar measuring system "Ariel-7" is used [7]. The system consists of a radar, RS amplifying and filtering units, an analog-digital converter, a personal computer (PC). A horn-lens has the following performance data: the lens diameter is equal to 30 cm, the beamwidth is equal to 2×2°, the radar operating frequency is equal to 10.5 GHz, 33.0 GHz, the radiated power is equal to 20 mW, the power gain is equal to 36 dB. An electromagnetic wave is directed into the barrel by neans of metal reflector fixed at the barrel at a distance of 1÷2 m from the front side of the barrel. Short duration of the process under study (≈5÷20 msec) allows us to digitize the analog radar signal and to transfer the digitized values of the signal amplitude to PC for further processing. If we use the known RS phase-to-movement (frequency-to-velocity) ratio [1] the time dependence of instantaneous radar signal values u(t) can be described in the most general form using

$$u(t) = A(t)\sin\left(\frac{4\pi}{\lambda}x(t) + \vartheta(t)\right) + \xi(t) =$$

$$= A(t)\sin\left(\frac{4\pi}{\lambda}\int_0^t v(\tau)d\tau + \vartheta(t)\right) + \xi(t), \qquad (1)$$

where x(t), v(t) are the functions describing time dependencies of the projectile movement and the projectile velocity respectively; A(t) is the function describing the RS signal amplitude modulation (AM appears due to the barrel recoil at the time of shooting and due to the gunpowder gases breaking into the space ahead of the projectile), $\vartheta(t)$ is a phase noise, $\xi(t)$ — is an additive noise. Studying the causes of the phase noise we have readed to a conclusion that when there are no gunpowder gases in the space ahead of the projectile the phase noise value is so insignificant that it can be neglected [3–5]. If the gunpowder gases break through, either EM waves are fully attenuated ahead of the projectile in the gas lock which is a low-temperature plasma or phase and amplitude distortions of the signal are so significant that the RS processing is impossible. It permits us to consider a simpler signal model without considering the phase noise. It should be also noted that the energy of the additive noise is not great in the case when the gunpowder break through. Under these conditions the signal-to-noise amplitude ratio is typically equal to 7.5–10 dB.

Thus in order to estimate the PMP (movement, velocity and acceleration) it is necessary to determine the the phase or frequency time dependence on the basis of can be reduced instantaneous signal values. From expression (1) one cab see that the problem of finding the function f(t) to the problem of signal parameter estima-

tion and noise filtering [6], which is well known in statistical radio engineering. Different statistical methods are developed for solving such problems, they make it possible to synthesize optimal and asymptotically optimal algorithms of signal parameters estimating [7]. However, the RS which we considered by us and the problem of its parameters estimating are not typical for the "classical" radar, since we have to estimate the parameters of the signal whose frequency varies from 0 Hz to 100÷300 KHz by a non-linear law during ≈10 msec at the shooting time, and our task is to use one signal only. The indicated reasons despute for the applicability of the well-know signal processing algorithms for solving the formulated problem, and these reasons determine the necessity of developing some new RS processing algorithms which do not use statistical methods. However, if we do not apply statistical methods of estimating it will be impossible to prove rigorously that these algorithms are optimal. So in order to prove the applicability of the processing algorithms and to estimate their accuracy it is quite natural to use an approach which is based on the processing of signals with the known time and frequency responses. Since there are no analog frequency-modulated signals whose frequencies vary like the obtained RS signal if the problems of measuring PMP in the barrel has been solved, the RS model has been developed in [8]. The model developed allowed it possible to develop and estimate frequency and time responses of the RS whose results were used the processing algorithms and to estimate their accuracy [9]. It has been found out that the least error of the PMP measuring was provided by an algorithm based on the concept of "the instant frequency of an analytical signal" [10] (the measured movement values exhibit the following errors: in the velocity range 0÷30 m/sec – 2.5%, 30÷50 m/sec – 0.28%, 50÷100 m/sec – 0.1%, ≥ 100 m/sec – 0.02%, and the measured velocity values exhibit the following errors: in the velocity range 0÷30 m/sec – 15%, 30–50 m/sec — 1.4%, ≥100 m/sec - 0.1%).

PMP measuring on the external ballistic trajectory is performed by a radar station "Luch-83" [11]. The radar station consists of a radar, an analog tracking filter and an RS processing unit. The performance data of the radar antenna (of revoloution paraboloid) are the following: the reflecting surface diameter is equal to 1 m, the beamwidth is equal to 2×2°, the radar operating frequency is equal to 10.5 GHz, the radiated power is equal to 600 mW, the power gain is equal to 36 dB. The external ballistic radar system "Luch-83" is based on the signal analysis method depending on measuring time intervals, which corresponds to the passage of the measure base of a certain length. Since one period of RS corresponds to the projectile movement by $\lambda/2$ (λ is the length of the probing electromagnetic wave), the number of RS periods counted by the number of passages of the signal through the zero level in the processing unit is a measure of the distance covered by the projectile. Timing of the passages through the measuring base allows to form a table time dependence of the projectile movement and to determine the velocity and the function of the projectile head resistance further differentiation and the least-squares smoothing.

We conclude that the method of RS analysis realized in the external ballistic stations has several obvious drawbacks, the main ones are the following: 1) impossibility of determining the values of kinematic characteristics inside the measuring base; 2) piecewise approximation of the projectile movement law (it means the equality of the value of the projectile average velocity on the measuring base and the value of the real velocity which is correct when the base length is shorter than 1 m only); 3) impossibility of selecting multiple targets (which is quite actual in measuring kinematic characteristics of rocket launcher projectiles and separating ammunition); 4) impossibility of using up-to-date methods of signal processing.

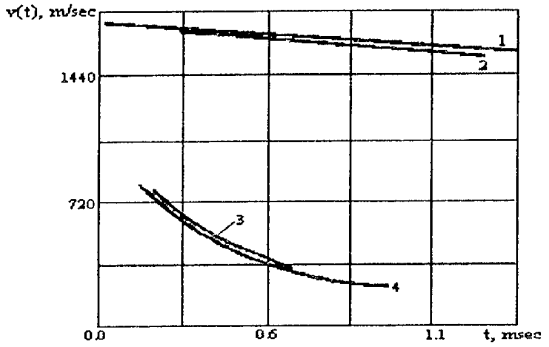


Fig. 1. The dependency of the APHCP components velocity on the external ballistic trajectory. (The digital processing method: 1 – the core, 3,4 – the sectors; the number of RS periods counting method: 2 – the core)

In order to get rid of the above-listed drawbacks we suggeste to registere the signals in a digital form and to apply the method of instant spectrum RS processing [12]. The proofs that the RS digital registration and that the new RS processing methods work were obtained we have measure the movement parameters of an armour-piercing hard-core projectile (APHCP) for a tank cannon D-81 (caliber 125 mm). This choice was determined by the following circumstances: 1) by the practical coincidence of the projectile trajectory velocity and the projectile radial velocity, and the relatively short flight time (≈1.2 sec); 2) by the presence of the APHCP sectors besides the core in the radar pattern (namely RS is analogous to the signal received in the case of measuring movement parameters of multiple targets). The results of the RS processing are presented in Fig. 1. Analysis of the presented results shows:

1. The projectile movements velocity measuring in the case of digital registration and RS processing

starts at more high movement velocities (that is nearer to the front side of the barrel) – 1767.4 m/sec, as it using when a standard registration method 1725.0 m/sec.

2. The projectile tracking is carried out up to the velocities 1350 m/sec (1489 m/sec – in the case of a standard registration method).

The efficiency of the digital registration and RS processing have been confirmed when the movement parameters of other types of ammunition were measured, and in particular when of high-explosive projectiles and passive and active rockets were used.

In order to carry out continuous measuring of the projectile movement parameters at the initial stage of shooting (the PMP measuring in the barrel and in the aftereffect period) we proposed a measuring technique which is a combination of the above-described radar measuring methods [13]. The standard radar applied to used in the PMP measuring in the barrel was replaced by the radar which is a part of an external ballistic radar station. A metal screen 3×3 m was used as a metal reflector directing the wave into the barrel. The distance from the front side of the barrel to the screen was 50-70 m, from the radar to the screen ≈ 8–10 m. An algorithm based on the property of the RS instant spectrum was used for the RS processing. The algorithm development of an RS proceeding and the error estimation have been carried out in [14]. For the first time in the practice of experimental ballistics, the use of this measuring technique allowed to pursue:

- an investigation of characteristic movement properties of the projectiles with separating and non-separating parts at the intermediate ballistics stage and to establish the dependence of the aftereffect period length and the velocity increment value of the projectile after its leaving the bore of a barrel on the mass of the powder charge for different types of projectiles [15].
- an investigation of the APHCP component parts movement on the initial section of the external ballistic trajectory and to time determine the dependence of the projectile movement kinematic characteristics at the initial of shooting (movement, velocity) and the movement dependence (velocity), and also to obtain the estimates of the parameters characterizing the properties of the projectile movement at the initial stage of shooting: the time of the projectile movement in the barrel, the front side velocity, the maximum projectile velocity at the time of shooting, the aftereffect period length, the time from the moment the projectile leaves the bore of a barrel up to the moment of its separating into component parts, the corresponding trajectory section length [16].

REFERENCES

1. A New Method of Measuring Parameters of Projectile Movements along the Bore of a Barrel/O.A. Buzhinsky, V.Y. Kvasov, V.A. Kovshov, V.I. Charitonov// Bojepripasy, 1979. № 11 [in Russian].
2. Finkelstein M.I. The Principles of Radar. –Moscow, 1983 [in Russian].
3. Kvasov V.Y. Determination of Projectile Movement Parameters in the Bore of a Barrel in the Process of Shooting by the Method of Microwave Interferometry//A Doctor Thesis. –Nizhny Tagil, 1986 [in Russian].
4. Buzhinsky O.A., Kvasov V.E., Porshnev S.V. The Model Adequacy Estimation of The Interaction Between Microwave Radiation and The Gases in The Space Ahead of The Projectile On The Basis of Experimental Results// Bojepripasy . 1990. № 2. [in Russian].
5. Kochkar N.I., Porshnev S.V., Shakirov M.R. The Barrel Wear Effects on The Microwave-range Radar Measuring of The Projectile Movement Parameters in The Barrel at The Time of Shooting//Voprosy oboronnoj tekhniki. In the print. [in Russian].
6. Levin B.R. The Theoretical Principles of Statistical Radio Engineering. Moscow, 1989. [in Russian].
7. Van Tress H.L. Detection, Estimation, Modulation Theory. Part. 1-3. Moscow, 1975. [in Russian].
8. Porshnev S.V. Simulation of A Radio Interferometric Signal in The Problems on Measuring the Projectile Movement Parameters in The Barrel at The Time of Shooting// Bojepripasy.1996. № 5-6. [in Russian].
9. Porshnev S.V. Algorithms for Processing Radar Signals Received when Measuring Projectile Movement Parameters in The Barrel of an Artillery System//The XXVII Moscow International Conference on Antenna Theory and Technology. 22–24 September 1998, Moscow, Russia: Materials of a Conference, 1998. [in Russian].
10. Buzhinsky O.A., Porshnev S.V.Application of Hilbert Transform for Processing the Radio Interferometric Signals// Bojepripasy, 1992. № 8. [in Russian].
11. A ballistic Station "Luch-83". Technical Description. ASHV. 1.400.003.TO. – Nizhny Tagil, 1984. [in Russian].
12. Kovzel A.V., Porshnev S.V., Shakirov M.R. Digital Methods of Registering and Analyzing Doppler Signals of External Ballistic Radar Station When Measuring Projectile Kinematic Characteristics on the Trajectory// Bojepripasy, 1996. № 5-6. [in Russian].
13. Kovzel A.V., Porshnev S.V., Shakirov M.R. Radiolocation Method of Measuring Projectile Movement Parameters at the Beginning Stage of Shooting// Bojepripasy, 1996. № 5. [in Russian].
14. Porshnev S.V. Investigation on Methods Increasing Accuracy and Information Content of Doppler Radar Meters for Measuring Movement Parameters of Projectiles and Barrels of an Artillery System at the Time of Shooting//A Doctor Thesis. –Nizhny Tagil, 1997[in Russian].
15. Kovzel A.V., Porshnev S.V., Shakirov M.R. Investigation of Projectile Movement Properties of the Tank Cannon D-81 in the Aftereffect Period//Voprosy oboronnoj tekhniki. In print. [in Russian].
16. Kovzel A.V., Porshnev S.V., Shakirov M.R. Investigation of Movement Properties of an Armour-Piercing Hard-Core Projectile at the Beginning Stage of Shooting by Means of the Counter Location Method//Voprosy oboronnoj tekhniki. In print. [in Russian].

STATISTICAL ASPECTS OF THE THEORY FOR DEFINING ANTENNA CHARACTERISTICS BY THE FIELD MEASUREMENTS IN THE NEAR ZONE

Y. S. Shifrin, V. A. Usin*

Kharkov State Technical University of Radioelectronics, Lenin Av.,14, Kharkov 310166, Ukraine,
Tel.: (38) 0572 409430, Fax.: (38) 0572 409113, E-mail: shifrin@ kture.kharkov.ua.
*Kharkov Military University, Svoboda Sq.,6, Tel.: (38) 0572 404141 (2-85)

The paper being of a review nature considers a complex of problems connected with the influence of random errors in the near field measurements on the antenna characteristics restoration precision.

It should be noted that in the general case the errors of the antenna parameters definition (restoration) by the field measurements in the near zone can be divided into three groups: methodical, instrumental and processing errors. One can single out systematic and random ones in every group.

Methodical and processing errors will not exceed admissible values with a correct choice of measurement conditions (the domain size and measurement step). Then the instrumental errors will mainly influence on the radiation pattern (RP) restoration accuracy.

Practically all elements involved in the process of the near field measurement, i.e. generators, antenna signal and reference signal transmission lines, amplitude-phase meters, mechanisms realizing mutual movement of the probe and the antenna, extraneous radiation sources, ambient objects etc., are the sources of the instrumental errors.

Selecting the measuring circuit elements with appropriate characteristics it is possible to ensure negligible small values of the systematic errors.

We have a completely different situation in the case of measurements' random errors. The possibilities to decrease them are limited.

Therefore the analysis of influence of the measurements' random errors in the near zone on the antenna parameters restoration errors is a highly important problem. The statistical antenna theory [1,2] provides the foundation for similar investigations.

Using this theory it is possible to estimate the potential of the available equipment for the antenna parameters restoration when measuring the field in the near zone, advisable fields of its application, to formulate requirements to the equipment for the near field measurements of the antennas under investigation and recommendations how to decrease the errors in the near zone methods.

The paper presents the foundations of the statistical theory of antenna measurements (STAM) which can be regarded as one of the general statistical antenna theory (SAT) aspects.

The STAM problems classification is considered and the tests of proximity of the restored RP and the true one are introduced.

It is noted that in accordance with the aims of the antenna measurements, the chosen method of these measurements, the equipment being used (in particular, whether it is an autonomous one or it is an element of a device), time allotted for measurements, whether the measurements are being carried out during the antenna development or in the process of its operation etc., the problems of antenna measurements can be formulated in a variety of fashions. Nevertheless, it is convenient to divide all these problems into two groups depending on whether we have to deal with the application of the available measuring equipment with known precision characteristics or these equipment should be developed. These groups of problems represent direct and inverse ones of the statistical theory of antenna measurements (STAM) [2].

The direct STAM problem is aimed at defining the available equipment capability to measure one or another antenna parameters, i.e. to define the area of the available equipment application.

The goal of the inverse STAM problem is defining the ways of creating the measuring equipment (with one or another measurement method) allowing to measure the desired antenna parameters with a given precision.

Both the direct and the inverse STAM problems can be divided into the internal and external problems.

The direct internal STAM problem consists in determining sources (mechanisms) of random errors of the field measurements in the near zone, inherent in the method being studied and the equipment being used, and in estimating these errors statistics, i.e. in finding their correlation functions or, as a minimum, errors' dispersions and correlation radii.

Random errors of the measuring equipment can be found, in particular, comparing the results of field measurements, obtained with this equipment, with the

results of the same field measurements, obtained with the high-precise equipment. One can also use a calibrated field for these purposes.

The direct external STAM problem is being formulated as follows: there are the measuring means with the known (found as a result of the internal problem solution) errors characteristics, it is necessary to define what type of the RP and in what angles sector one can measure (restore) it with the given precision using the measuring means data.

The inverse external STAM problem consists in finding the measuring equipment tolerated errors allowing to ensure the given precision of the antenna characteristics restoration in a definite angular sector. The given problem should be solved for a set of typical nominal (non-disturbed) amplitude-phase distributions (APD) which are assumed to be known when developing the equipment.

The inverse internal STAM problem consists in providing the equipment being developed with the total measurement errors non-exceeding the admissible ones (found as a result of the inverse external problem).

It should be noted that when solving the inverse external problem it is necessary to be aware of the following.

Any measuring circuit has a number of mechanisms of amplitude and phase errors in near field measuring. Amplitude and phase errors exert different action on the antenna parameters. Furthermore, every of the mechanisms is characterized by its own errors' dispersions and correlation radii. With the given errors dispersion their action on the antenna characteristics depends significantly on their correlation radius value. That is why, when solving the inverse internal problem, it is necessary to determine the range of tolerable values of dispersion and correlation radii of the amplitude and phase errors V_{iol} where the given precision in definition of the antenna desired characteristics is ensured. Knowing this range and taking into account that different mechanisms of errors bring different contribution into statistical characteristics of the RP being restored and the "action" on every of the mechanisms (their controlling) is achieved by various ways, one should formulate appropriate requirements for the concrete elements of the measuring circuit.

In the general case the inverse STAM problem solution in the above statement present great difficulties. At present to solve the inverse external problems a simplified approach based on a set of results of the direct external STAM problems solution with a partial "a priori" information on the statistics of the equipment being developed (correlation coefficients form, relations of errors' dispersions and correlation radii for different mechanisms of their origin) is commonly used.

The question of the restored and the true RP "proximity criterion" is significant when solving the direct and inverse STAM problems.

When choosing the "proximity criterion" the following approaches are typical ones:

- comparison of the true and restored mean power RP [3];

- comparison of the true amplitude RP and the possible scattering of the restored RP in separate angular directions ("local" criterion) [4];

- comparison of the true amplitude RP and the possible scattering of the restored RP as a function in a definite angular sector ("integral" criterion) [5].

Depending on the chosen proximity criterion the direct and inverse STAM problems are formulated in a different manner.

When applying the first approach, the direct external STAM problem consists in defining to what extent the true power RP (its envelope) will differ from the restored mean power RP when using the given equipment. In this case the inverse external problem consists in formulating requirements to precision of the equipment being developed, the restored mean power RP is sufficiently close to the true one if these requirements are met. An obvious shortage of the first criterion consists in the necessity to find the mean RP, i.e. a long time of the RP measuring. Often there is no this time and the judgment on the true RP should be formed on the basis of the examination of one (or several) of the restored RP realizations. In this case one should follow the local or integral criteria.

The local criterion of proximity in the direct external STAM problem solution is the probability P_{kc} that in one or another angular direction ψ_k the true value of the amplitude RP is in the given confidence interval relative to the restored (with the available equipment) RP value $R(\psi_k)$. The inverse external STAM problem, when using the local criterion of proximity, consists in formulating such requirements to the equipment that in meeting them in a definite angular direction ψ_k the difference of the restored PR $R(\psi_k)$ from its true value $R_0(\psi_k)$ with the given probability P_{kl} is in the given limits. The direction corresponding to the maximum of k-th side lobe is more often chosen as ψ_k direction. Application of the local criterion is a step forward as compared to the one using the mean power RP, since here the true RP is evaluated to a certain extent by its separate realization.

A shortage of the local criterion consists in the fact that the true RP is estimated only in separate directions.

The integral criterion of proximity enables to conclude about the true RP in the whole angular sector, when analysing a separate restored RP realization. In this

case the direct external STAM problem consists in defining to what extent the antenna RP envelope $R_0(\psi)$ is close in the desired angular sector Ω to the envelope $R(\psi)$ of a separate RP realization restored with the available equipment. The information to be found is given as the confidence region plotted around the envelope of the restored RP. The integral criterion of proximity is characterized by the probability P_{Rconf} that the envelope of the true RP is "covered" by the confidence region. The aim of the inverse STAM problem, when using the integral criterion, is to formulate such requirements to the equipment that meeting them the envelope of the restored RP $R(\psi)$ in the desired angular sector Ω should be with a prescribed probability in the given region relative to the true RP $R_0(\psi)$. In the SAT this probability is named as the difference functional distribution of the RP P_{Rdif} [5].

Difference in formulations of the direct and inverse STAM problems with different criteria of proximity of the restored and true RPs leads to different results of these problems solutions, i.e. the estimates of the measuring equipment capabilities or the requirements imposed on it are different. The question as for what criterion of proximity is to be chosen, should be solved by a user or a designer of the measuring equipment depending on the following: the aims of the antenna measurements; time alotted for them; whether measurements are carried out while developing antenna or its operating (control); either it is of need to know the nature of the whole antenna RP or its possible radiation in separate directions; reasonable cost of the equipment being developed, etc.

Depending on the chosen criterion of proximity the results of the SAT, concerning either the mean power RP calculations, or the ones of the RP fluctuations in separate directions ψ_k, or those of the whole RP fluctuations (its distribution functionals), should be used when solving the STAM problems.

Note that in dependence on the version of the method for defining the antenna characteristics in the near zone (whether amplitude and phase of the near field or its quadrature components are being measured; the surface shapes, where the field values are being measured, etc) the statistical theory of the antenna parameters measurement has these or those peculiarities. But the general approach to the STAM problems solution remains the same for all versions of the method.

The paper successively presents the STAM foundations for the case when the amplitude and phase of the field on the antenna plane aperture is being measured. The results of calculating the restored RP statistical characteristics, the mean power RP, the RP fluctuations, the RP correlation characteristics are given. The basic attention in the report is paid to the consideration of the normalized RPs and their fluctuations. It is stipulated by that when restoring RP it is of especial interest to evaluate a level of their sidelobe radiation, which might be estimated only when studying normalized RPs. Methods for the direct and inverse STAM problems solution are set forth. Formulae and figures illustrating results of the external problems solution are given.

Results features when measuring the near field on the cylindrical surface enveloping the antenna and on the plane surface in the Fresnel zone are given. It is shown, in particular, that measuring a near field in the Fresnel zone the correlation of fluctuations in symmetrical (with respect to a main maximum) angular directions depend on a position of the measurements area. It leads to that when registering a near field in the Fresnel zone, the requirements to measuring means will differ from the ones for the case of the measurement of a field in an antenna aperture.

Further, statistical aspects of the near zone methods when measuring not the antenna RP but its parameters, i.e. the RP width, the main maximum direction etc., are considered. It is noted that the requirements to the measuring equipment in these cases are less strict.

In conclusion the urgent directions of the STAM development are formulated.

REFERENCES

1. Shifrin Ya.S. Statistical antenna theory problems. –M. Sov.Radio,1970,383 p.[in Russian].
2. Shifrin Ya.S. Statistical antenna theory. Chapter 9. In book: : "Handbook on antenna engineering". V. 1. –M.: "Radiotekhnika", 1997. [in Russian].
3. Gueruny P.M., Aratunjan G.S. Radio holography and modern methods of antenna measurements. In the book: "Radio and acoustic holography". –L. Nauka, 1976, 85-98p [in Russian].
4. Kaplun I.V., Kurochkin A.P. Investigation of random errors of holographic methods for defining antenna directivity characteristics. Radiotekhnika i elektronika.1975, v.20, issue 46,71-76p [in Russian].
5. Shifrin Ya.S. Usin B.A. On precision of holographic method for antenna radiation patterns measurement. In the book Antennas/ Edited by Pistolkors A.A. –M.: Svijaz, 1979, issue 27, 26-38p. [in Russian].

MULTIREFLECTOR RESONANCE SYSTEMS IN MILLIMETER WAVE RANGE

D. G. Afonin, A. K. Malyshkin

Physics Department of Moscow State University,
Vorob'evy Gory, Moscow, 119899, Russia
phone: 095-9392094; e-mail: afonin@radi1.phys.msu.su

The application of multireflectors electromagnetic systems in devices of millimeter region and in antenna techniques is known.

Here are presented the results of investigation in millimeter waveband of resonance systems, comprising in series located and diffractionally coupled 4-8 reflector open resonators with spherical, cylindrical and circled reflectors.

These systems are performed as two blocks, where a chain of in series located reflectors was made mechanically. The coupling with outer devices is made by means of circular holes in reflectors. One of the OR was excited with the help of generator, and the signal was directed to the analysing devices. through the similar hole of one of the neighbouring coupled OR.

For the investigations an automatic complex was used [1]. It allowed to study the spectrum of the excited oscillation types of fields distribution in millimeter range, to measure Q-factor using a computer. The complex of devices comprised: a millimeter waveband generator, microwave detector, oscillograph, digital voltmeter and elements of automatization: personal computer, 2 outside controllers, digital-to-analog converter, 2 step-by-step motors. The signal is transmitted through the connecting waveguide and through the other connecting elements to the resonator system.

This signal is detected, amplified and comes to the outside controllers: to the PC and oscillograph simultaneously. It is transmitted to the oscillograph in order to control voltage. The transmission coefficient is defined by the changes of voltage.

One of the reflector blocks of the system under investigation is immovably mounted on the optical bench, the other reflector block is located on the table with micrometric serves, that is fastened on the optical bench. Transferring of this reflector block is made with the help of the step-by-step motor, controlled by computer.

The excited oscillation types distribution can be studied placing a sample body into the resonance volume of the system under investigation and replacing it with the help of another step-by-step motor. The analysis of the transmission coefficient allows to account Q-factor by knowing the width of the resonance curve. The frequency sweep is carried out also using IBM PC.

The spectrum of the OR with circular reflectors is consequence of types of oscillation, excited while changing the distance (L) between reflector blocks. It was rared very fast with increasing L and when $L > 3\lambda$, it was the only one across oscillation type excited.

An effective excitation of the circular OR system was achieved in a very small interval of variation of the distance between reflectors.

Q-factor of this system was decreasing with L increasing; the maximum value of Q-factor was: $2 \cdot 10^2$.

Coupled OR with cylindrical reflectors were investigated for the symmetrical geometry (both reflectors of the OR are cylindrical) and for the semi-cylindrical geometry (one of the reflectors was flat). The spectrum of such a coupled OR, consisted from 3-5 semicylindrical OR included, as a rule, three or more oscillation types.

The investigations of field distribution along the axis of the system have shown that the oscillation types with several field maxima in the region of one cylindrical reflector are excited.

Q-factor was equal to $2 \cdot 10^2$. Coupled ORs with symmetrical reflectors were effectively excited only when $L > R$ (R is the radius of the reflectors); the spectrum of these OR is thick enough, Q-factor~10^2.

Coupled OR with spherical reflectors were investigated with consecutive increasing of the exciting ORs number: at first a single OR was studied, then two-OR system and so on [2].

The spectrum of the single OR with short distances between reflectors consisted of 6-8 oscillation types; Q-factor was $5 \cdot 10^3$. With the increasing of ORs number, the distance between reflectors at which the system could be effectively excited was decreasing; Q-factor was also decreasing.

While studying a spectrum of the system under condition of changing a distance between reflector blocks at fixed excitation frequency, as a rule, an equidistance of excited oscillation types was found (Fig. 1).

Changing the distance between reflectors, we succeded in the excitation of four-five cell system with exciting area near concentric geometry of resonators.

Spectrum of the investigated system for excitation of three coupled ORs at fixed distance between reflector edges (L = 1 mm) (the signal was taken from the 3rd resonator) is presented in Fig. 2. Such a system have shown a rather rare spectrum. Factor Q of individual oscillation types reached a value of $5 \cdot 10^2$. The hole size did not allow the system to excite at frequencies of less than 63 GHz.

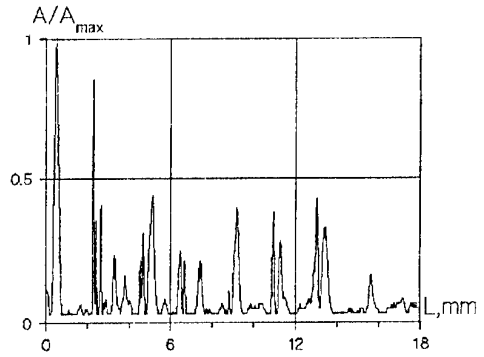


Fig. 1. Dependence of the transmission coefficient on distance between resonators

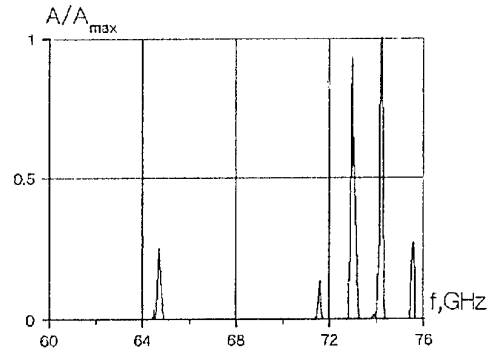


Fig. 2. Dependence of the transmission coefficient on the frequency

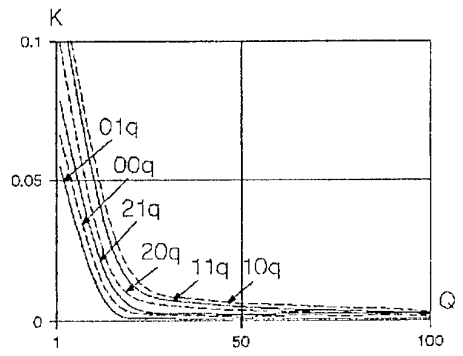


Fig. 3. Dependence of the transmission coefficient on the Q-factor

Using solutions to parabolic equation for several oscillation types, let us estimate possible values of the transmission coefficient for two diffractionally coupled ORs with spherical reflectors at fixed reflector aperture and different beam width.

Consider the simplest model of interaction between two identical spherical OR with parallel optical axes and which reflectors touching each other by edges. Assume, we know type field distribution on the first OR reflector and out of its limits for corresponding oscillation. For this purpose let us use well known analytical solutions to a problem of self oscillations of OR with spherical reflectors, expressed in terms of Gauss-Lagger's polynomials [3].

The results, obtained for several lowest oscillation types are presented in Fig. 3 (the transmission coefficient versus Q -factor plot).

From Fig. 3 it is clear, that the increase of transmission coefficient is accompanied by the fast decrease of Q-factor, and asymmetric oscillations excitation (particularly for 10q oscillation) is traded off for effective power flow from one OR to another.

The numerical model has confirmed the supposition about the predominant excitation of highest and asymmetrycal oscillation types in such a system, as has been shown by the results of experiment.

The experimental results have show effectiveness of functioning of diffractionally coupled two-reflector ORs with spherical reflector systems near a concentric geometry.

REFERENCES

1. Afonin D.G., Malyshkin A.K. Automatizirovannaya ustanovka s upravleniem chastotoi dlia issledovania rezonansnych sismem v millimetrovom diapazone (Automated device with frequency monitoring for studying resonant systems in the millimeter wave range) Pribory i tekhnika eksperimenta, 1999, N3, p.77-80 [in Russian].

2. Afonin D.G., Kazakov A.V., Malyshkin A. K. Investigation of open resonators with diffractional coupling. Proceedings of International conference NATO "Optical Resonators - Science and Engineering", Slovac, 1998, p. 281-287.

3. Vainshtein L.A. Otkrytye resonatory i otkrytye volnovody (Open resonators and open waveguides), 1966, izd. "Sov.Radio", Moscow [in Russian].

ACTIVE INTEGRATED ANTENNA AMPLIFIER FOR HANDSET RECEIVER FRONT END

A. S. Andrenko, Y. Ikeda, M. Nakayama, K. Horiguchi, T. Fukasawa, O. Ishida

Information Technology R&D Center Mitsubishi Electric Corporation
5-1-1 Ofuna, Kamakura, Kanagawa 247-8501, Japan
E-mail: andrey@isl.melco.co.jp

INTRODUCTION

Fast developments in the field of wireless mobile communications increase the demand for novel antennas and MMIC RF front end circuitry addressing the requirements of compactness, efficiency, and low cost. Recently, the active integrated antenna (AIA) approach became one of the most promising innovative designs in minimizing of interconnects and power consumption as well as increasing the efficiency of RF amplifiers [1-3]. Unlike the conventional configuration of receiver/transmitter front ends where the antenna and active circuit are separate components, their tight integration in AIA systems makes also possible the realization of broadband performance including efficient high-harmonics tuning [4]. Here we present a compact AIA receiver front end as a candidate for applications in the third-generation mobile communications handsets.

Size reduction becomes a key issue in designing antenna elements for integrated wireless handheld terminals, however the choice of dielectric rod helical antenna provides quite compact configuration of AIA amplifier. Because of direct integration of amplifier circuit and antenna in AIA approach, proper impedance matching proves to be a major condition for increasing the gain and minimizing the system's noise. The design and simulation of low-noise amplifier (LNA) for integrated receiver front end is presented and the measured results of AIA radiation pattern are demonstrated in this study.

AIA AMPLIFIER CONFIGURATION

Typical block diagram of AIA receiver front end is depicted in Fig.1. Unlike the conventional design where an antenna and receiver amplifier are separated by a standard 50 Ohm transmission line and interconnects, in AIA approach an antenna is directly attached to the input of amplifier circuit. It results in obviously much more compact design and smaller losses as well as increases the operational bandwidth, that are required in modern high-performance communication systems. One of the main challenges in realizing AIA design is the effective impedance matching of antenna element and amplifier depending on the antenna type used. Spiral helical antenna is characterized by complex input impedance with its high imaginary part at the design frequency of 2.1 GHz. Because of importance of both gain impedance matching, which provides the maximum gain of AIA device, and noise figure (NF) minimum impedance matching, which minimizes the NF value, an amplifier has to be designed according to the impedance characteristics of antenna used.

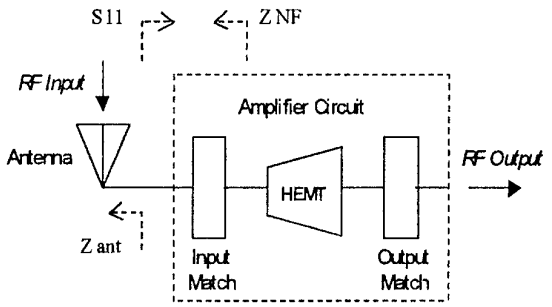


Fig. 1. Block diagram of AIA amplifier front end

AMPLIFIER DESIGN

As is well known, the condition of perfect gain impedance matching as applied to AIA device is expressed by

$$S_{11} = \overline{Z}_{ant}, \qquad (1)$$

where $S_{11} = \mathrm{Re}\,S_{11} + i\,\mathrm{Im}\,S_{11}$ is the reflection coefficient of an amplifier at its input port while $Z_{ant} = \mathrm{Re}\,Z_{ant} + i\,\mathrm{Im}\,Z_{ant}$ is the normalized input impedance of an antenna. The relation (1) simply implies that $\mathrm{Re}\,S_{11} = \mathrm{Re}\,Z_{ant}$ and $\mathrm{Im}\,S_{11} = -\mathrm{Im}\,Z_{ant}$ are the conditions that result in obtaining the maximum gain of AIA amplifier front end. Fig. 2 shows the input measured impedance of helical antenna made by rectangular dielectric rod sized 2.0×2.0×4.1 mm with $\varepsilon_r = 4$.

In designing the low noise active systems, on the other hand, the noise reduction and NF matching become very important issue [7]. In an ideal case for AIA system, the minimum NF is observed when the antenna input impedance is equal, or at least close, to the so-called active device NF minimum impedance Z_{NF} looking back into the input of an amplifier

$$Z_{ant} + Z_{input} = Z_{NF} \qquad (2)$$

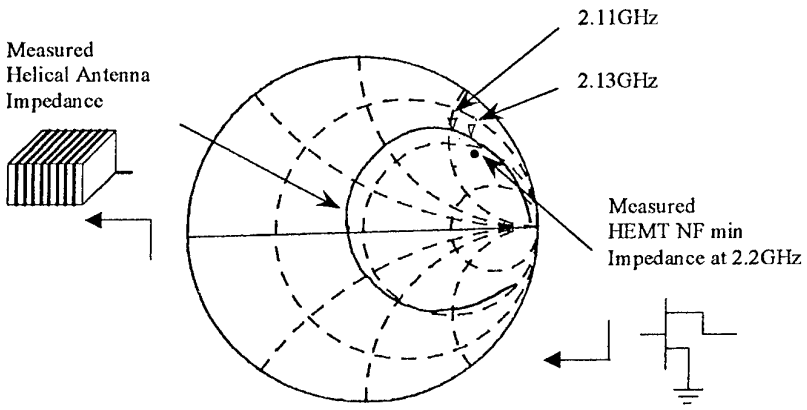


Fig. 2. Configuration of helical antenna and its input impedance

Nevertheless, the condition (2) is often difficult to realize since the NF minimum impedance is a given specification parameter of an active device while antenna impedance is defined by the required radiation characteristics of antenna. To remedy this, an input circuit can be tuned to change Z_{input}, i.e. to shift the left-hand side of (2) closer to the NF minimum impedance. However, it may simultaneously lead to the change of S_{11} value and, therefore, to an undesired amplifier gain degradation. It should be noted that a small NF mismatch does not essentially affect the system performance while the maximizing of receiver front-end gain is considered as the main design factor.

Mitsubishi Electric's high electron mobility transistor (HEMT) MGF4919G has been selected as a device providing the very low NF, 0.5 dB. The modeling of amplifier has been done using the Hewlett Packard's Libra circuit simulator. As a result, the stability factor of amplifier has been obtained as $K > 2.0$, which satisfies the critical condition $K_{\min} = 1.0$ over the entire frequency band from 0 to 4.5 GHz. Simulation results have shown the amplifier gain $|S_{21}| = 8.5$ dB at $f = 2.1$ GHz.

Tuning of the amplifier's input circuit has been carried out in matching the amplifier input impedance, i.e. adjusting its S-parameter S_{11} to the value close to a complex conjugate of the antenna input impedance Z_{ant} at the design frequency shown in Fig. 2. Then, the output circuit of amplifier has been designed to provide standard 50 Ω match, so that the simulation of S_{22} parameter shows that the output impedance of LNA is equal to 50 Ω.

The amplifier has been assembled as a single layer substrate with dimensions 10.3×6.0 mm. To test the performance of the LNA without antenna, we have measured its *S*-parameters on HP 8510 network analyzer and compared the experimental data with those of simulation. The obtained simulation and experimental results are presented in Fig. 3. The deep minimum of S_{22} parameter corresponds to the design frequency of 2.1 GHz of AIA amplifier. The results show good agreement between simulation and measured data, which confirms the design procedure. We have also tested the matching properties of amplifier's input circuit attached to the antenna used. Frequency dependence of measured reflection coefficient of helical antenna with LNA input circuit is consistent with the design requirement.

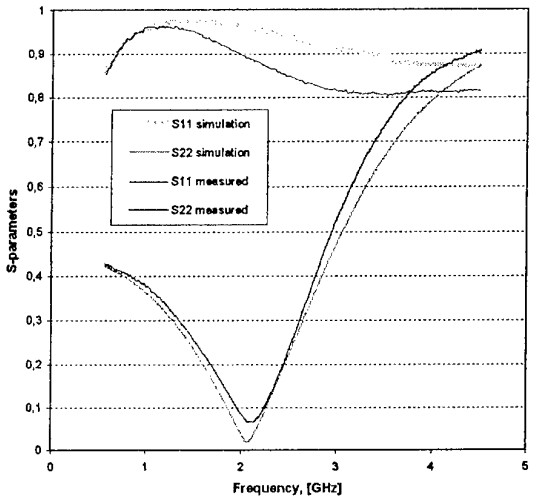


Fig. 3. Measured and simulated S-parameters of LNA

Finally, the radiation characteristics of AIA receiver have been obtained by measuring the radiation patterns of helical antenna attached to the LNA. Length sensitivity of a small spiral antenna has been experimentally proved. Typically, the longer the helix, the lower the resonant frequency of antenna becomes. As an example, Fig. 4 shows the pattern functions at 2.04 GHz

measured in the plane perpendicular to the axis of helix. The decrease of pattern level is observed in the direction of a ground plate used in the measurement setup.

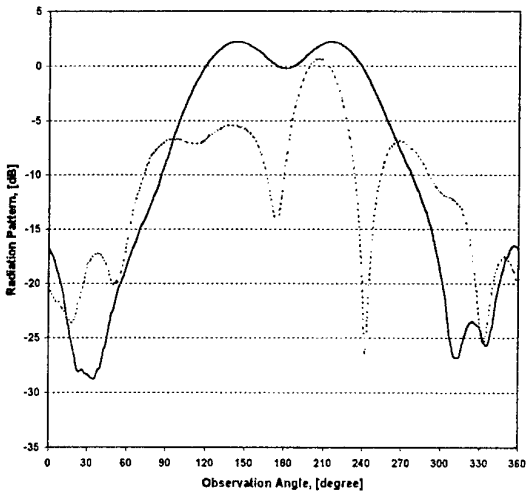


Fig. 4. Measured radiation patterns of helical AIA, solid line: E_ϕ field, dotted line: E_θ field

CONCLUSIONS

The design of AIA amplifier front end for the next-generation mobile communications handsets has been presented. The importance of the principle of both gain impedance matching and NF matching in increasing the efficiency of integrated device operation has been emphasized. Simulation results and measured data have demonstrated good agreement in testing the designed LNA. The compactness of AIA amplifier front end would allow its applications in the design of novel handheld wireless terminals and adaptive antenna systems. It is demonstrated that circuit integration of antenna and amplifier makes possible new RF configurations with greatly reduced size and increased efficiency.

REFERENCES

1. Y. Qian and T. Itoh, "Progress in Active Integrated Antennas and Their Applications," *IEEE Trans. Microwave Theory Tech.*, vol. 46, pp. 1891-1900, Nov. 1998.

2. W. Menzel, "Low-Noise Active Receiving Antennas," in Proc. of M+RF 97 Conference, London, UK, 1997, pp. 83-88.

3. P. S. Hall, P. Gardner, M.J. Cryan, D. Singh, and C. Kalialakis, "Novel Integrated Active Antennas for Microwave and Millimeter Wave Applications," in Proc. of M+RF 97 Conference, London, UK, 1997, pp. 76-82.

4. W. R. Deal, V. Radisic, Y. Qian, and T. Itoh, "Power Measurements for Push-Pull Integrated Antenna Power Combiner," in Proc. of 1998 Asia-Pacific Conference, Yokohama, Japan, 1998, pp. 703-706.

NUMERICAL SIMULATION OF TRANSVERSE-PLANAR STRUCTURES IN WAVEGUIDE

R. V. Antipenko, S. E. Yukhno

Design bureau "Storm", National Technical University of Ukraine "KPI"
12, Politechnichna str., Kyiv, 252056, Ukraine, Tel.:+38-(044)-441-17-69
E-mail: rus@rtus.ntu-kpi.kiev.ua

Planar antennas for the coupling of active element (AE) with waveguide section are of great practical interest as alternative for coaxial- and post-waveguide electrodynamic structures [1]. These structures have high recurrence of parameters, low cost and allow monolithic integration with AE. Application of slot antennas (SA) in such equipment allows to simplify AE connection and to use microstrip line to match and design power circuit [2].

The given paper offers a method of partial regions investigation of transverse-planar structures with SA.

Transverse-planar structure being analyzed is shown in Fig. 1, where 1, 3 are waveguides, 2 – dielectric substrate, S_1 – slot, S_2 – dielectric-waveguide 3 boundary.

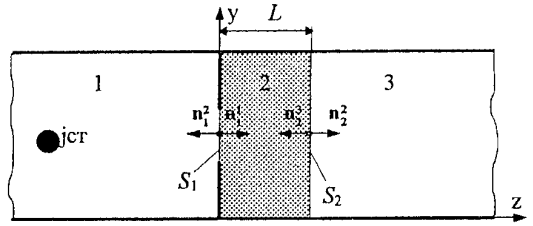


Fig. 1

Loss in metal walls of waveguides and thickness of SA metal were not taken into account in simulation.

The following system of equations is obtained basing on continuity of tangential components of magnetic field on S_1 and S_2 boundaries.

$$\begin{cases} n_1^1 \times H^1\{0, E_{\tau 1}\} + n_1^2 \times H^2\{E_{\tau 1}\} + n_1^2 \times H^2\{E_{\tau 2}\} = \\ = H^1\{j_{cr}, 0\} \times n_1^1 \\ n_2^2 \times H^2\{E_{\tau 1}\} + n_2^2 \times H^2\{E_{\tau 2}\} + n_2^3 \times H^3\{E_{\tau 2}\} = 0 \end{cases} \quad (1)$$

Galerkin's method is used to determine distribution of electromagnetic fields. According to this method electric field on S_1 and S_2 boundaries is approximated in the form of series

$$E_{\tau 1} = \sum_{p=1}^{P_1} e_p^1 \cdot \Theta_p^1, \quad E_{\tau 2} = \sum_{p=1}^{P_2} e_p^2 \cdot \Theta_p^2. \quad (2)$$

System of linear algebraical equations for amplitudes of tangential electric field on S_1 и S_2 boundaries is obtained from formulas (1) and (2)

$$\begin{cases} \sum_{p=1}^{P_1} e_p^1 \cdot (Y_{pm}^{1,1} + Y_{pm}^{2,1}) + \sum_{p=1}^{P_2} e_p^2 \cdot Y_{pm}^{2,2} = h_m, \\ \sum_{p=1}^{P_1} e_p^1 \cdot Y_{pl}^{2,1} + \sum_{p=1}^{P_2} e_p^2 \cdot (Y_{pl}^{2,2} + Y_{pl}^{3,2}) = 0. \end{cases} \quad (3)$$

Where

$$Y_{pm}^{1,1} = \sum_a Y_a^1 \cdot n_{ap}^1 \cdot n_{am}^1, \quad (4)$$

$$Y_{pm}^{2,1} = \sum_a Y_a^2 \cdot n_{ap}^1 \cdot n_{am}^1 \cdot \mathrm{cth}(K_a^2 \cdot L), \quad (5)$$

$$Y_{pm}^{2,2} = -\sum_a Y_a^2 \cdot n_{ap}^2 \cdot n_{am}^1 \cdot \frac{1}{\mathrm{sh}(K_a^2 \cdot L)}, \quad (6)$$

$$Y_{pl}^{2,1} = -\sum_a Y_a^2 \cdot n_{ap}^1 \cdot n_{al}^2 \cdot \frac{1}{\mathrm{sh}(K_a^2 \cdot L)}, \quad (7)$$

$$Y_{pl}^{2,2} = \sum_a Y_a^2 \cdot n_{ap}^2 \cdot n_{al}^2 \cdot \mathrm{cth}(K_a^2 \cdot L), \quad (8)$$

$$Y_{pl}^{3,2} = \sum_a Y_a^3 \cdot n_{ap}^2 \cdot n_{al}^2, \quad (9)$$

$$h_m = 2 \cdot U_1^+ \cdot Y_1^1 \cdot n_{1m}^1. \quad (10)$$

In (1)–(10) denotations are the same as in [3].

Described method can be used to analyse structures with different form of SA. In this case functions Θ_p^1 (2) can be derived using the methods from [3,4].

Analysis of interior convergence of the method in the calculations of slot radiator with rectangular form in waveguide 28.5×12.6 (L = 0.1 mm, ε = 4.3) showed that the difference of calculated values of $|S_{11}|$ reflection ratios at $P_1 = 1$ and $P_1 = 4$ does not exceed 0.7 %.

Such method provides coincidence of calculated and experimental values with error not more than 3 %. Experiment error is 8 %.

REFERENCES

1. A.R. Adams et al., "A metod-of-moments study of strip dipole antennas in rectangular waveguide," IEEE Trans. Microwave Theory Tech., vol. 45, №10, pp. 1756-1766, Oct. 1997.
2. N.A. Pershin et al., "Microstrip antennac for open resonators excitation," Proc. of the 2nd International Conference on Antenna Theory and Techniques, 20-22 May 1997, Kyiv, Ukraine, pp. 312-313.
3. Mashkovtcev B.M., Tcybyzov K.N., Yemelyn B.F. Waveguide theory, Moscow, Nauka, 1966. [in Russian].
4. Zargano G.F. et al. Waveguides of complex cross-sections, Moscow, Radio i Sviaz, 1986.

THE ANALYSIS OF THE IRRECIPROCITY OF THE SIGNALS DELAY OF IN THE ANTENNA–FEEDER DEVICES OF ACTIVE COMPARISON SYSTEMS

V. V. Bavykina, Yu. A. Koval, O. L. Troshchin

Kharkov State Technical University of Radioelectronics
Ukraine, 310166, Kharkov, avenue Lenin, 14, KTURE, ORT
Tel.: +380 (572) 409479; faks: +380 (572) 409113; e-mail: ort@kture.kharkov.ua

On the basis of the high precision radio meteor comparison method (RCM) with the time of radio signals propagation between corresponding points in direct and return directions as a first approximation is considered to be equal (the signal reflected by the "useful" meteor trail exists tens-hundreds of seconds).

At present the RCM along with the methods using transportable quantum clock (TQC) and satellite radio navigation systems (GPS, GLONASS), ensures the comparison error of the order of tens of nanoseconds.. In this case the RCM surpasses the indicated methods in such characteristics as the measurements productivity, self-sufficiency, operativeness, efficiency, concealness, stability to ionospheric perturbations [1].

To reduce the equipment systematic errors (ESE) depending on the difference of signals delay in the sections of reception and radiation of the radiometeor comparison complex (RMCC) signals, a number of methods were offered for their measurement, correlation and compensation. But these methods do not allow to measure the ESE sources resulted from the instability of the signal formation devices and irreciprocity of the signals delay in the antenna-feeder devices (AFD). The latter source is identified and studied quite recently and it deserves a special consideration.

In the active comparison systems the combined AFD are used for radiation and reception to exclude the errors caused by different angular coordinates of the trajectories of signals passage between the points. Here, on the basis of the known antenna reversibility property, the signals delay in the AFD in radiation and reception are assumed to be equal and, hence, not affecting the ESE.

The AFD delays irreciprocity was established experimentally with "detection and ranging in succession" of two RMCC of "METKA-8" type. The cable length variation, the AFD change and elements replacement in the commutator led to the ESE up to 20...30 ns.

Irreciprocity of delays in the AFD is explained by the signal form variations due to differences in regimes of the cable matching in reception (the antenna – cable – commutator – receivers input resistance) and in radiation (the transmitter – commutator – cable–antenna).

As an ideal matching of the AFD (that ahould be the simplest solution of the problem) is impossible, experimental investigations were continued and theoretical analysis of the signal form distortions with mismatchings in the AFD and subsequent anomalies in the delays was also carried out.

Fig. 1 shows the simulation block diagram of the signals delays irreciprocity in the AFD. For the predetermined parameters of the signal source [$s_1(t)$, Z_i], the load [Z_l] and the cable [Z_w, V_p, α, L] the real delay of the signal τ_d was defined. The influence of the cable mismatching on the ESE was estimated with an abnormal delay τ_A defined as the difference between the real and ideal delays: $\tau_A = \tau_d - (L/v_p)$.

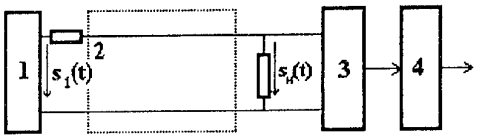


Fig. 1. Block diagram of simulation of delays irreciprocity in AFD
1 – source of the known form signal $s_1(t)$; *2* – cable; *3* – detector; *4* – device for measuring the signal's temporal position; Z_i – the source internal resistance; Z_l – load resistance; Z' – cable wave resistance; V_p – phase velocity in the cable; α – decay coefficient in the cable; L – the cable length

In the case of active resistances of the circuit [R_i, R_l, R_w] the temporal method of analysis was used. Here the output signal had the following form

$$s_l(t) = \frac{R_l}{R_i + R_l}\left\{[1 - \sum_{k=1}^{\infty}(p_i p_l)^k \cdot \exp(-k\alpha L)]s_1(t - L/V_p) + \right.$$

$$\left. + \sum_{k=1}^{\infty}(p_i p_l)^k \cdot \exp(-(2k+1)\alpha L)]s_1(t - (2k+1)L/V_p)]\right\},$$

where $p_i = (R_i - R_w)/(R_i + R_w)$, $p_i = (R_l - R_w)/(R_l + R_w)$ are the coefficients of reflection from the source and the load, respectively.

As $|p_i\, p_l| << 1$ is real, we can confine ourselves to the first component in the sums ($k = 1$) when performing calculations.

In the case of a random nature of resistances [Z_i, Z_l, Z_w] the frequency method of analysis was used, here the complex coefficient of the circuit transmission was converted to the form:

$$K(j\omega) = Z_l/(Z_l + Zi)[\mathrm{ch}(\gamma L + Z'\mathrm{sh}(\gamma L)],$$

where $\gamma = \alpha + j\beta$ is the coefficient of propagation in the cable, $\beta = \omega/V_p$ is the coefficient of the phase; $Z' = Z_w/Z_l + Z_2/Z_w$ is the relative resistance, $Z_l = Z_l + Z_w$, $Z_2 = Z_1 Z_i /(Z_l + Z_i)$.

The relative distribution Z' represents the dimensionless parameter characterizing mismatching of the cable both on the part of the load and on the part of the source. If $Z_i = Z_w$ or $Z_l = Z_w$, then $Z' = 1$. Here the abnormal delay does not depend on the cable's length, it is defined by the signal distortion in the circuit with a complex coefficient of transmission:

$$K(j\omega) = Z_l/(Z_l + Z_i).$$

Not only the abnormal delays of the signals envelopes but the abnormal delays of the coherent carrier frequency phases were analysed. In this case the real signal's delay was defined as

$$\tau = \varphi(\omega_0)/\omega_0,$$

where $\varphi(\omega_0)$ is an argument $K(j\omega)$ on the frequency ω.

Simulation was carried out for the main types of signals, different types of loads and resistances, the main methods of the signals temporal position measurement. Figs. 2 and 3 show the dependencies of the abnormal delays on those in the cable with the use of the relative dimensionless ones τ'_a, τ'_c [$\tau'_a = \tau_a/\tau_s$, $\tau'_c = L/(V_p\tau_s)$, τ_s is the signal duration].

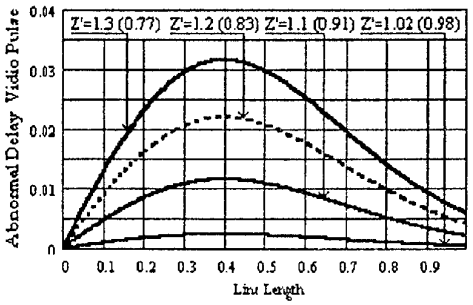


Fig. 2. The dependencies of the abnormal video pulses delays on the cable's length

The main results of the simulation are as follows:

1) for the real values of the active resistances R'∈ 0.7...1.3 the abnormal delays are negligible small for $0.8 < \tau'_c < 0.01$ and the maximum absolute values of abnormal delays correspond to the relative delay of the cable $\tau'_c \in 0.3...0.5$;

2) the dependencies of the abnormal radio pulses delays on the cable's length are of quasi-harmonic nature with a period corresponding to the cable's delay for a half-period of the signal carrier frequency;

for the complex Z' the abnormal radio pulses delays dependencies on the cable length have the constant component and the auxiliary "amplitude modulation";

4) three methods (subtraction of the delayed signal, by two fronts, by FFCh slope) of the main methods of the signal temporal position measurement are practically equally sensitive to the abnormal delays; the measurements by the gravity center have the largest values of the abnormal errors and the measurements by the maximum of the signal and by the leading edge have the smallest values of the abnormal errors.

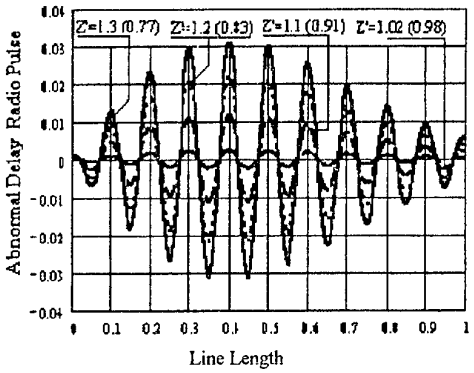


Fig. 3. The dependencies of the abnormal radio pulses delays on the cable's length

The simulation results are confirmed experimentally. The measurements were carried out for three types of antennas four synphased waveguide channels array; single four-elemental waveguide channel; shortened oscillator.

The dependencies of the abnormal delays measured values on the normal delay in the cable τ_c were studied. The plots' period $\tau_a(\tau_c)$ (≈8 ns) corresponds to the half period of the carrier frequency – 57.3 MGz. The array with $\tau_{amax} \approx 25$ ns had the maximum values of abnormal delays, the shortened oscillator had the minimum values ($\tau_{amax} \approx 3$ ns), then it was used as a measuring antenna for the ESE identification. The abnormal delays measurements in the receiving channel were carried out by the analogous methods. Here, the abnormal delays level within 1...2 ns was obtained at the expense of a more careful matching of the receiver input circuits.

Thus, for the cable real lengths and the AFD matching quality the abnormal delays can reach units of percents of the pulses duration, this amounts to tens of a nanosecond. This can lead to the ESE of the same order.

REFERENCE

1. Dudnik B.S., Kashcheyev B.L., Koval Yu.A., Pushkin S.B. High-precision comparison of the state and secondary time primary standards // Izmeritelnaja tekhnika, 1982. N 1.- P.30-32.

CREATION OF LOCALIZED HIGH INTENSITY ELECTROMAGNETIC FIELD PULSES IN OPEN RESONATOR

I. N. Belobaba, D. M. Sazonov

Moscow Power Engineering Institute, Krasnokasarmennaja 14,
111250, Moscow, Russia. Email: dsazonov@postman.ru

We propose a new type of open resonator, a resonator with focused travelling wave pulses. Our first paper about such resonators was published in 1996 [1]. This non-sinusoidal travelling wave is of the form of a radio pulse, compressed in space and time. The open resonator is formed by means of two identical confocal parabolic mirrors (Fig. 1). A use of spherical mirrors is also possible, though the result would be somewhat worse. A mathematical model for computing near electromagnetic fields inside the resonator is developed. This model uses a new representation of mirrors as antenna arrays with special elements performance. Model is based on the matrix theory of antenna arrays with arbitrary geometry, published earlier [2]. The algorithm is realized on personal computer with opportunities of numerical evaluation of characteristics of the focal region, where the total electromagnetic field represents a wide-angle short-pulse wavebeam. The electromagnetic field in focal region is approximately in the form of travelling electromagnetic wave.

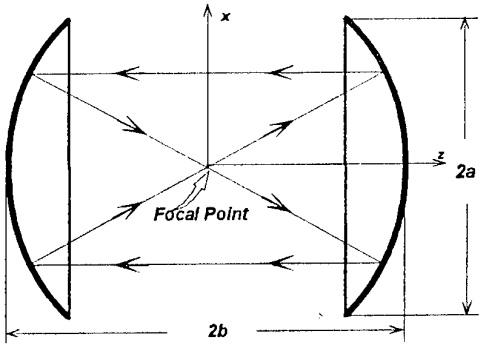


Fig. 1

In contrast to the known Gauss wavebeams with angular spectrum less than 10 degrees, we realize in our case wide-angle beams with the width of the angular spectrum up to 90 degrees and more. The waist width of beam may be reduced practically to the Rayleigh limit (half of the wavelength in the medium). We can provide coherent addition of waves and accumulation of energy of many phase-controlled generators in the focal region, using a special multi-element and multi-frequency excitation by means of an antenna array located at the surface of one or both mirrors. There are three variants of devices with various degrees of complexity. In the most powerful and complex variant it is necessary to use a system of many coherent generators, controlled both on phase and on the temporal pulse position on the set of resonance frequencies of the open resonator (Fig. 2). In a more simple variant with passive antenna arrays and beam forming networks it is possible to use one or several short pulse transmitting devices from the microwave radar; and in the simplest devices it is possible to apply the simple beam waveguide excitation (Fig. 3).

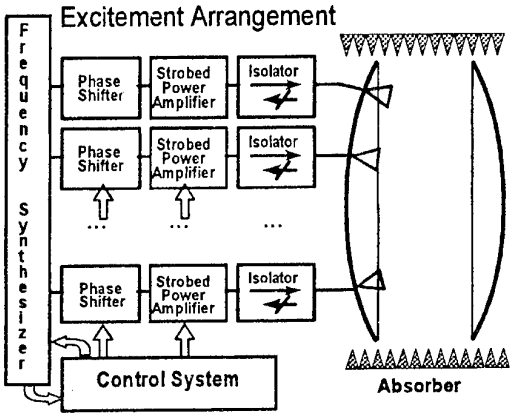


Fig. 2

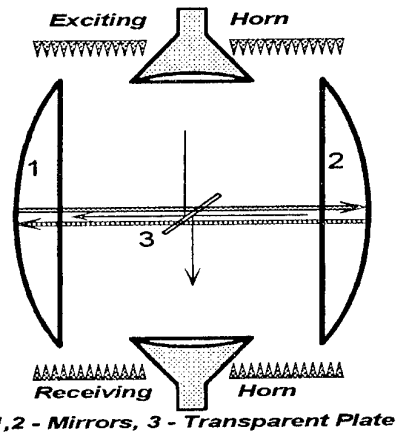


Fig. 3

The necessary sizes and optimal configuration for realization of the system within the given volume limits were found. A special non-equidistant arrangement of launchers on resonator mirrors was chosen. The potential use of the new type of open resonators and the localized pulses created in these is very wide: from investigation of the action of localized high intensity electromagnetic field pulses on samples of various

media (including radio-absorbing materials as in the well known Stealth technology), up to creation of plasma objects, its compressing and heating. It follows from the results of investigation of electromagnetic performance of such resonators that two necessary principles of achievement of high concentration of electromagnetic field must be fulfilled:

- The principle of coherent space summation of output powers of many microwave mutually phased generators of many various frequencies;
- The principle of time compression of radiopulses in space.

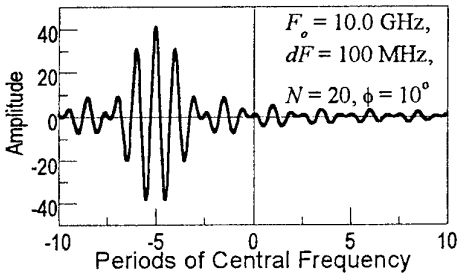


Fig. 4

According to these principles in vicinity of the focus we provide synchronous passing in various directions of properly phased extended coherent relatively long radiopulses with distinct carrier frequencies. The length of each partial pulse can in tens and hundreds of times exceed the length of the required synthesized short pulse. It means respective narrowing of individual spectra of partial pulses (to several hundreds or even to tens of MHz), which considerably facilitates realization of resonant microwaves amplifiers. Coherence means that the central frequencies of radiopulses should be fixed by a frequency synthesizer with high stability of the primary local oscillator. Synchronization of passing radiopulses in vicinity of the focus point means the necessity of individual strobing of the output stages of microwave amplifiers. The correct phasing means that converging to the focus point partial radiopulses should have at this point the same phases of its middles. The form of compressed electromagnetic pulse with frequency bandwidth 9.0–11.0 GHz is demonstrated in Fig. 4. In such device the maximal electromagnetic power density is in the focus: it is a so-called creative interference, giving a narrow burst of intensity of the field. Away from the focal point, along the main direction of propagation of the wave packet there is destructive interference, resulting in fast recession of the field intensity and electromagnetic power density. An important note: it is possible to organize the fast moving of the middle of synthesized pulse in vicinity of the focal region by fast adjusting of the phase distribution of the outputs of microwave amplifiers. The results of computations of distributions of electromagnetic fields around the focal point for a resonator with parabolic or spherical mirrors with a = 0.5 m, b = 0.4 m are demonstrated in Fig. 5.

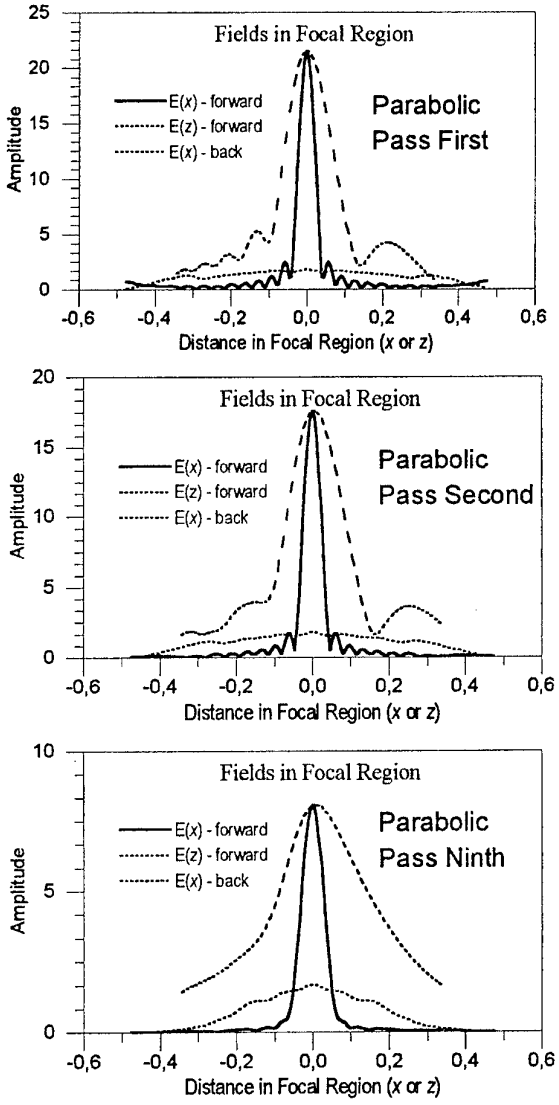


Fig. 5

You may see, how field distributions changed after first, second and ninth sequential passes electromagnetic wave between mirrors. In case of paraboloidal mirrors we use focal distance $Foc = b$ and in case of spherical mirrors we use sphere radius $R = 2b$.

REFERENCES

1. Sazonov D.M., "The Creation of Concentrated Electromagnetic Field Pulses by Means of Open Resonators", *Abstracts of Papers on* LI *Scientific Session of Russian PopovSociety,* May 1996, Pt.1, pp. 48-49 [in Russian].
2. Sazonov D.M., "Basics of Matrix Theory of Antenna Arrays ", *The Applied Electrodynamics*, High School (USSR), 1983, No.6, p.111-162.

PHASE STABILIZED FIBER CHANNEL WITH REMOTE HETERODYNING: SRECTRAL – NOISE ANALYSIS AND EXPERIMENT

A. N. Bratchikov, D. I. Voskresenskii, T. A. Sadekov

Moscow State Aviation Institute (MAI-Technical University)
Faculty of radioelectronics of flying vehicles. Division 406
Russia 125871 Moscow Volokolamskoye Sh., 4.
E-mail: alexbrat@aha.ru

INTRODUCTION

Information technologies have many current and future applications dealing with signals transmission to antennas and antenna systems which are removed from each other in space, but have to be fed by inphase analog signals or digital signals without mutual delays.

In fact big antenna arrays, radiointerferometers with long base line, multipositional radars, systems of hydroacoustical and seismological monitoring, geological systems of row materials search and mobile comunication systems realize holographic principles of signals transmission and especially of signal registration and processing, which demand correct knowledge of both phase (time delay for digital signals) and amplitude distributions of electromagnetic and acoustic fields.

For this purpose removed in space antenna elements, separate antennas, radiotelescopes, acoustical sensors may be united by phase stabilized fiber links, providing phase difference at their outputs, which should not exceed 1...5 degrees. These kinds of transmission links are known as phase stabilized links (PSL). The problem of phase stability traditionally resolved by two principal methods. *Component approach*: manufacturing the transmission links with given phase stability properties; *system approach*: usage the feedback systems with controllable phase shifters (delay lines) for parasitic phase difference (delays) compensation. Both methods have obvious disadvantages due to technological complexity and bad mass–weight–cost characteristics of the integral system.

PHASE STABILIZATION BY LENGTHENED FILTERS

Recently the new method of PSL design was proposed [1] and experimentally verified, based on as known *structural approach*. Proposed method utilizes standard commercial fibers and does not require complex hardware, making use of pseudo–flat input–output phase characteristics of extended fiber optic filters of transversal and recurrent types and their combinations (Fig. 1). Mathematical model of phase stabilized fiber-optic link on the basis of lengthened filter may be developed in terms of Z–transformation and transfer characteristics of four pole networks.

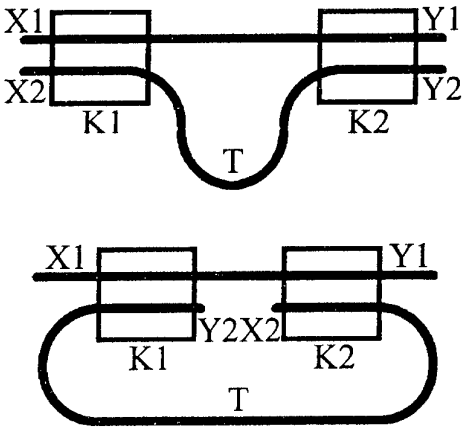


Fig.1. Transversal and recurrent optical filters

For example, complex transfer characteristic of optical field coupler with K as optical power coupling coefficient and of network, consisting of two parallel fibers with attenuation factors $\alpha_{1,2}$ and delays 0 and T, respectively, have the matrix form

$$H_c = \begin{bmatrix} \sqrt{1-K} & j\sqrt{K} \\ j\sqrt{K} & \sqrt{1-K} \end{bmatrix}, \qquad (1)$$

$$H_f = \begin{bmatrix} \alpha_1 & 0 \\ 0 & \alpha_2 e^{-j\omega T} \end{bmatrix}. \qquad (2)$$

Combining (1) and (2) by appropriate manner, transfer matrixes may be obtained for transversal and recursive filters of the first order. The H^{11} element of matrices is the transfer characteristic of basic first order filter elements, consisting in our case of two couplers and transversal or recursive filter element itself. For $\alpha_{1,2} \approx 1$ and $z^{-1} = e^{-j\omega T}$ one could write

$$H_{TF}^{11} = \sqrt{(1-K_1)(1-K_2)} - \sqrt{K_1 K_2}\cdot z^{-1}, \qquad (3)$$

$$H_{RF}^{11} = \sqrt{(1-K_1)(1-K_2)} \Big/ \left(1+\sqrt{K_1 K_2}\right). \qquad (4)$$

Cascading, for example, N transversal or recursive filters one could obtain filter of N–order with such given positions of zeros and in general case – poles of transfer characteristic function, that in certain region of

filter phase characteristic it will compensate parasitic phase shifts of fiber-optic waveguide

$$H_{TFN}(z) = D\sum_{j=1}^{N+1}\left[K_j\prod_{i=1}^{j-1}(1-K_i)\right]z^{-(2j-1)} = \\ = Dz^{-2(N+1)}\prod_{j=1}^{N+1}\left(z-z_{0j}\right)\left(z+z_{0j}\right), \quad (5)$$

where D is an amplitude factor, z_{0j} is the j-th zero of transfer characteristic and $K_{N+1}=1$.

SPECTRAL–NOISE CHARACTERISTICS OF UHF SIGNAL AT THE OUTPUT OF MULTICHANNEL FIBER FILTER WITH REMOTE HETERODYNING

Theoretical model is based on closed analogy between multimode fiber and single mode multi–channel fiber filter, so optical field $E_{out}(t)$ at the output is considered to be the weighted sum of appropriate input fields $E_{in}(t)$ with corresponding time delays along filter channels

$$E_{out}(t) = D\sum_{q=0}^{N}A_qE_{in}(t-qT). \quad (6)$$

Heterodyning photodetection mode means the presence of the two optical components at slightly different in optical scale frequencies ω_1 and $\omega_2=\omega_1+\Omega$, where $\Omega << \omega_{1,2}$ is the mentioned before UHF:

$$E_{in}(t) = E_0\left\{\exp j\left[\omega_1 t+\varphi_1(t)\right]+\exp\left[\omega_2 t+\varphi_2(t)\right]\right\}, \quad (7)$$

where $\varphi_{1,2}(t)=\bar{\varphi}+\Delta\varphi(t)$ – random phase and E_0 complex time–independent amplitude. Then the autocorrelation function of the photodetector output photocurrent $i(t)=\sigma E_{out}(t)E^*_{out}(t)$ might be determined as follows:

$$R_i(\tau) = \langle i(t)i(t+\tau)\rangle - \langle i(t)\rangle\langle i(t+\tau)\rangle \quad (8)$$

where σ is quantum efficiency of photodetector, asterisk stands for complex conjugation and $\langle\ldots\rangle$ denotes the averaging among photocurrent realizations.

Though phase fluctuation process in injection laser is not Gaussian, and corresponding field spectrum is not pure Lorentzian, the most practically applicable injection lasers have strong damping of relaxation oscillations, so it is accepted that $\Delta\varphi(t)$ have Gaussian probability density function [2,3] with zero mean value and dispersion $\langle\Delta\varphi\rangle^2$, which is proportional to delay τ and laser mode spectral line width $\Delta\omega$ [4]

$$\left\langle\Delta\varphi^2(\Delta\tau)\right\rangle = \Delta\omega|\Delta\tau|, \quad \Delta\omega = 2\tau_C^{-1}, \quad (9)$$

where τ_C – laser coherence time. Then one could write:

$$R_i(\tau) = 2\sigma^2D^4E_A^4\sum_{2q=-2N}^{2N}\sum_{2p=-(2N-|2q|)}^{2N-|2q|}\sum_{2r=-(2N-2x)}^{2N-2x}\sum_{2s=2y}^{4N-2z}\times \\ \times A_{\frac{p-q+r+s}{2}}A^*_{\frac{r+s-p+q}{2}}A_{\frac{p+q+s-r}{2}}A^*_{\frac{s-r-p-q}{2}}e^{-j(\omega_1+\omega_2)pT}\times \\ \times[\cos p\Omega T+\cos q\Omega T+\cos(r\Omega T+\Omega\tau)]\cdot f(\tau)$$

$$f(\tau) = e^{-\frac{\Delta\omega T}{2}x}\left\{e^{-\frac{\Delta\omega}{2}\left[|\tau+pT|+|\tau-pT|-|\tau-qT|-|\tau+qT|\right]}-1\right\}\otimes \\ \delta(\tau-rT) = f_{p,q}(\tau)\otimes\delta(\tau-rT), \quad (10)$$

where $f(\tau)$ is "characteristic" function determining the form of correlation function, that depends on parameters of a laser radiation source, and $\otimes$ – denotes the operation of convolution.

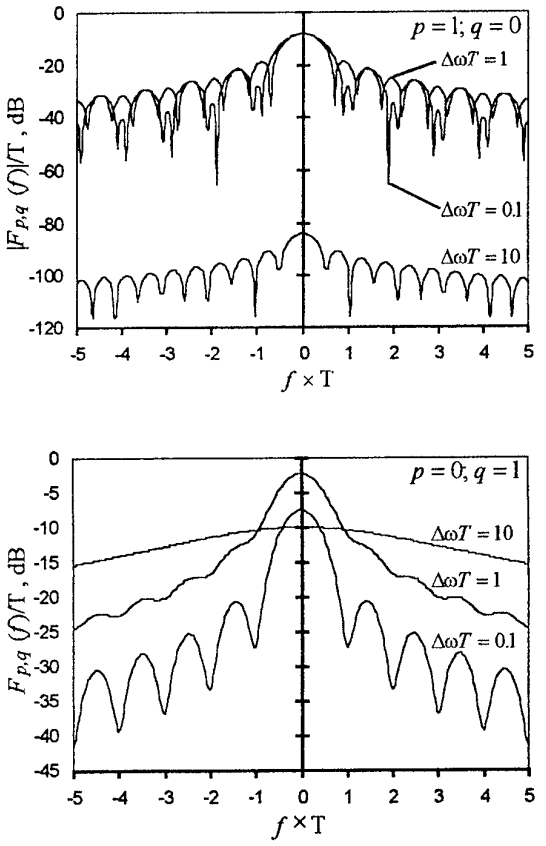


Fig. 2. The spectral functions $F_{p,q}(\omega)$.

Making Fourier transformation of autocorrelation function, the signal and noise spectra of output UHF signal may be obtained

$$S_S^2(\omega) = 2\pi\sigma^2D^4E_A^4\sum_{2q=-2N}^{2N}\sum_{p=|q|-N}^{N-|q|}e^{-j(\omega_1+\omega_2)pT}\times \\ \times\sum_{r=x-N}^{N-x}G_{p,q}(r)e^{-j\omega rT-\frac{\Delta\omega T}{2}x}\times \quad (11)$$

$$\times\{2[\cos p\Omega T+\cos q\Omega T]\delta(\omega)+\delta(\omega-\Omega)+\delta(\omega+\Omega)\}$$

$$S_N^2(\omega)=\sigma^2D^4E_A^4\sum_{2q=-2N}^{2N}\sum_{p=|q|-N}^{N-|q|}e^{-j(\omega_1+\omega_2)pT}\times$$

$$\times\sum_{r=x-N}^{N-x}G_{p,q}(r)e^{-j\omega rT}\{2[\cos p\Omega T+\cos q\Omega T]F_{p,q}(\omega)+$$

$$+F_{p,q}(\omega-\Omega)+F_{p,q}(\omega+\Omega)\},\qquad(12)$$

where $G_{p,q}(r)=\sum_{\substack{s=y\\ step\,2}}^{2N-z}A_{\frac{s+r+p-q}{2}}A^*_{\frac{s+r-p+q}{2}}A_{\frac{s-r+p+q}{2}}A^*_{\frac{s-r-p-q}{2}}$

$x=|p+q|+|p-q|,\quad y=\big||2r|+|p+q|-|p-q|\big|+x,$

$$z=\big||2r|-|p+q|+|p-q|\big|+x,\qquad(13)$$

and $F_{p,q}(\omega)$ are spectrum components at $\omega=0,\pm\Omega$, determined by Fourier transform of characteristic function $f_{p,q}(\tau)$:

$$F_{p,q}(\omega)=\begin{cases}\left\{-\frac{2\sin\omega T|q|}{\omega}+\frac{2\sin\omega T|p|}{\omega}e^{\Delta\omega T[|q|-|p|]}+\right.\\ +\frac{2e^{\Delta\omega T|q|}}{\Delta\omega^2+\omega^2}\big[\Delta\omega e^{-\Delta\omega T|p|}\cos\omega T|p|-\\ -\Delta\omega e^{-\Delta\omega T|q|}\cos\omega T|q|-\omega e^{-\Delta\omega T|p|}\sin\omega T|p|+\\ \left.+\omega e^{-\Delta\omega T|q|}\sin\omega T|q|\big]\right\}e^{-\Delta\omega T|q|},\quad |p|<|q|\\ \left\{-\frac{2\sin\omega T|p|}{\omega}+\frac{2\sin\omega T|q|}{\omega}e^{\Delta\omega T[|q|-|p|]}+\right.\\ +\frac{2e^{-\Delta\omega T|p|}}{\Delta\omega^2+\omega^2}\big[\Delta\omega e^{\Delta\omega T|p|}\cos\omega T|p|-\\ -\Delta\omega e^{\Delta\omega T|q|}\cos\omega T|q|+\omega e^{\Delta\omega T|p|}\sin\omega T|p|-\\ \left.-\omega e^{\Delta\omega T|q|}\sin\omega T|q|\big]\right\}e^{-\Delta\omega T|p|},\quad |p|>|q|\end{cases}\qquad(14)$$

The spectral functions $F_{p,q}(\omega)$ are depicted in Fig. 2 for two combinations of p and q and several relationships between channel delay T and laser coherence time τ_C.

SIGNAL–TO–NOISE RATIO ANALYSIS

In general case signal–to–noise ratio at the photodetector output may be calculated on the basis of (11)–(12)

$$SNR=\frac{\mathrm{Re}\left[S_S^2(\Omega)\right]_{\Omega+\pi\Delta f}}{\frac{1}{2\pi}\int_{\Omega-\pi\Delta f}\mathrm{Re}\left[S_N^2(\omega)\right]d\omega},\qquad(15)$$

where Δf–bandwidth of UHF–signal filter at photodetector output.

For coherent ($T/\tau_C\gg1$) and noncoherent ($T/\tau_C\ll1$) operating modes of PSL based on single transversal (TF) and recurrent (RF) filters *SNR* (15) may be derived in simple analytic forms. For noncoherent mode of operation

$$\mathrm{SNR}^{TF}=\frac{2\pi\left(\mathrm{A}_0^4+\mathrm{A}_1^4+2\mathrm{A}_0^2\mathrm{A}_1^2\cos\Omega T\right)}{\left\{\left[2\mathrm{A}_0^2\mathrm{A}_1^2+\mathrm{A}_0^4+\mathrm{A}_1^4\right]+2\mathrm{A}_0^2\mathrm{A}_1^2\cos\Omega T\right\}\tau_c\Delta f},$$

$$\mathrm{SNR}^{RF}=\frac{2\pi\left(1-K_1K_2\right)}{\left(1+K_1K_2\right)\tau_c\Delta f},\qquad(16)$$

where $K_{1,2}$ coupling coefficients of input and output optical couplers, $\mathrm{A}_0=\sqrt{(1-\mathrm{K}_1)(1-\mathrm{K}_2)}$; $\mathrm{A}_1=-\sqrt{\mathrm{K}_1\mathrm{K}_2}$. And for coherent mode of operation

$$\mathrm{SNR}^{TF}=\frac{\pi\left\{A_0^4+A_1^4+2A_0^2A_1^2\left(e^{-\Delta\omega T}+\cos\Omega T\right)\right\}}{A_0^2A_1^2\left(1-e^{-\Delta\omega T}\right)\tau_c\Delta f},\qquad(17)$$

$$\mathrm{SNR}^{RF}=\frac{\pi\left(1-K_1K_2\right)\left(1-K_1^2K_2^2e^{-2\Delta\omega T}\right)}{K_1K_2\left\{\begin{matrix}1-\left(1+2K_1K_2\right)e^{-\Delta\omega T}+\\ +\left(K_1K_2+K_1^2K_2^2\right)e^{-2\Delta\omega T}\end{matrix}\right\}\tau_c\Delta f}.$$

Expressions (16)–(17) for $\omega_1\to\omega_2$ convert to the well-known results [5] for one modulated optical carrier.

To increase SNR it is necessary to make $\mathrm{K}_1\mathrm{K}_2\to0$, that corresponds to the replacement of branched filter channel by nonbranched one. The worst *SNR* corresponds to the intermediate case $T/\tau_C\approx1$, when due to chromatic dispersion in single mode fiber the biggest distortions of signal and noise spectra occur.

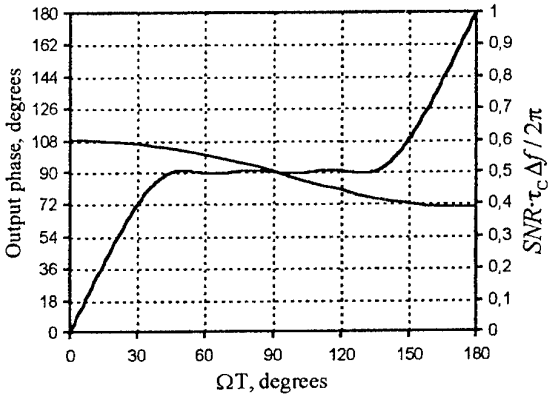


Fig. 3. Phase–frequency characteristic and signal–to–noise ratio variance versus the operating point factor ΩT

Conditions for optimum phase stabilizing and noise properties being independent from each other do not coincide in the same PSL. It may be illustrated by com-

parison of output UHF phase and *SNR* dependencies depicted in Fig. 3 for PSL used in experimental study (Fig. 4). Normalized *SNR* has maximum value at the left end of phase stability zone *SNR* (45°) ~ 0.544 and drops at the right end to *SNR* (135°) ~ 0.402. Thus, during phase stabilization of transmitted signal the displacement of operating point from the center of phase characteristic $\Omega T = 90°$ due to the temperature change of delay T in contours of the filter will cause the fluctuations of signal–to–noise ratio $\Delta SNR \approx 0.14 \cdot \tau_C \Delta f / 2\pi$.

EXPERIMENTAL INVESTIGATION

For experimental investigation of the model of phase stabilized fiber channel a scheme of three-link transversal filter was fabricated (Fig. 4). Calculations show, that such filter can ensure the level of phase stability of transmitted signal at frequency $\Omega = 2\pi f_0$ within $\Delta\varphi = \pm 0{,}98°$ in the area of phase stabilization $\Delta\theta = \Delta(\Omega T) = 90°$ (Fig. 3), where $T = 2Ln/c$ denote the delay in filter links. The given form of phase characteristic is ensured by optic couplers coefficients: K_1 = 0,494/0,506; K_2 = 0,661/0,339; K_3 = 0,831/0,169.

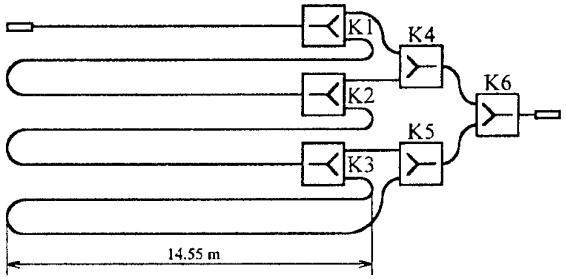


Fig. 4. Experimental configuration of third orders transversal optical filter

Construction of fiber channel consists of optical cable with seven fiber waveguides. At the one end of cable the fibers were welded in pairs and were formed the filter delay links. At the other end they are welded with optical couplers. The length of optical cable is 13,2 m, the full length of filter delay link is L=14,55 m, that corresponds to the frequency periodicity of phase characteristic f=1/T=7,06 MHz.

For experimental measurement of frequency characteristics of the proposed channel, an optical signal, whose intensity was modulated with chirped frequency $f = 0 \div 7$ MHz by amplitude-frequency analyzer, was coupled into the optical fiber. The output signal was detected by a photodetector. Then it was measured by differential phase-meter or amplitude detector, connected with analyzer. Therefore we can see amplitude- or phase-frequency characteristics of fiber-optic filter. This frequency characteristics registered by frequency analyzer are plotted in Fig. 3.

To measure the thermal phase shift by the frequency method, an optical signal, whose intensity was modulated with frequency f_0 = 399 MHz, was coupled into the optical filter set in an oven. The exact meaning of frequency f_0 was chosen on the basis of above mentioned experimental results as the central frequency of pseudoflat region of the 57th period of filter's phase-frequency characteristic ($\Omega T = \pi/2 + 56\pi$). The fiber temperature could be increased until the signal delay alteration at the filter links due to the thermal expansion of the fiber leads to the leaving an operation point $\Omega T = 90°$ out of stabilization zone $\Delta\theta$. That is

$$\delta L + L \cdot \Delta T \cdot S \le \frac{c \cdot \Delta\theta[degree]}{720 f_0 n}, \qquad (18)$$

where $\delta L \approx 5$ cm denote the possible mistake of channel length definition, and $S = 12 \times 10^{-6}$ 1/°C is a thermal coefficient of phase shift of optic multimode fibers, used in the filter construction. The fiber channel with above mentioned parameters ensures the phase stabilization of transmitted signal in the region of environment temperatures $\Delta T = 85$°C. That's why, the fiber-optic channel temperature was controlled from 15°C to 100°C.

The optic couplers unit was set out of the oven and didn't expose to the influence of high temperatures, because optic couplers have a very large thermal dependence of their coefficients. Figure 5 shows the thermal dependence of the phase shift in lengthened filter and optic waveguide with same geometrical and material parameters, relative to the phase shift at 15°C. The measured maximum phase shift was $\Delta\varphi = 2.1°$. This value is one of the same orders with that of the modern phase feedback systems.

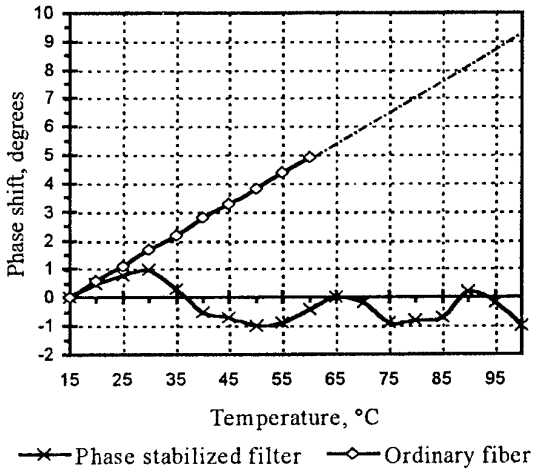


Fig. 5. Thermal dependence of transmitted signal phase shift in phase stabilized channel and ordinary single fiber

Then the thermal phase coefficient in stabilized channel is calculated as:

$$S = \frac{c}{2\pi f_0 Ln} \times \frac{\Delta\varphi[rad]}{\Delta T} = 2\times10^{-6}\ 1/°C, \qquad (19)$$

that is about 6 times less compared with ordinary single optical fibers, and two times less compared with experimental multilayered phase stabilized single fibers and optical cables. Further increasing of phase stability up to 10 times may be obtained in fiber filters of IV^{th} and V^{th} order.

REFERENCES

1. A.N.Bratchikov, S.A.Garkusha, T.A.Sadekov, "Phase stabilized fiber channel for UHF signal distribution based on an extended optical filter", *Photonics and Optoelectronics*, vol.4, No.2, pp.79-83, 1997.
2. J.A. Armstrong, "Theory of interferometric analysis of laser phase noise", *J. Opt. Soc. Amer.*, vol. 56, pp. 1024–1031, 1966.
3. K. Petermann and E. Weidel, "Semiconductor laser noise in an interferometer system", *J. Quantum Electron.*, vol. QE–17, pp. 1251–1256, 1981.
4. K. Petermann and G. Arnold, "Noise and distortion characteristics of semiconductor lasers in optical fiber communication systems", *J. Quantum Electron.*, vol. QE–18, pp. 543–555, 1982.
5. B. Moslehi, "Analysis of optical phase noise in fiber–optic systems employing a laser source with arbitrary coherence time", *J. Lightwave Technol.*, vol. LT–4, No.9, September, pp. 1334–1351, 1986.

RF SIGNAL SPECTRAL ANALYSIS AT THE OUTPUT OF ERBIUM DOPED FIBER AMPLIFIER IN THE REMOTE HETERODYNING MODE

A. N. Bratchikov, T. A. Sadekov

Moscow State Aviation Institute (MAI-Technical University)
Faculty of radioelectronics of flying vehicles. Division 406
Russia 125871 Moscow Volokolamskoye Sh., 4. E-mail: alexbrat@aha.ru

INTRODUCTION

Among the large quantity of possible optical fiber channel configurations for transmission and distribution of microwave and millimeter wave antenna signals the channels of great interest are the fiber links with optical fiber amplifiers operating in the remote heterodyning mode. These channels provide simultaneous decision of the two principal problems of analog fiber links: problem of insertion loss and problem of frequency bandwidth [1]. Insertion loss level in fiber channel with direct laser diode modulation is about 15-30 dB, that restricts the number of antenna elements, fed by one laser diode up to $M_{max} = 7...25$.

The basic restrictions on modulation bandwidth of analog signals in single mode fiber channels and devices on their basis arise mainly at the expense of frequency properties of the optical transmitter. Intensity modulation of injection laser in the optical transmitter can be performed at frequencies up to 5...20 GHz (commercial samples), and in special cases – up to 60 GHz. The ultrawide band modulation is accompanied by multimode oscillation and worsens the thermal and noise characteristics of the laser; therefore practically used modulation frequencies do not exceed 10 GHz. So when operating frequencies 10 GHz and higher are used in antenna system and insertion loss should not exceed 0 dB it is necessary to use another, different from basic, fiber channel configurations and modes of their operation, which provide mentioned specifications with guaranty.

Those are the fiber channels with Er-doped amplifiers (EDFA) [2], [3] operating in remote heterodyning mode, Fig. 1, distinguished by extremely high bandwidth, providing generation and transmission of microwave and millimeter wave signals without necessity of optical source modulation in these frequency domains [4]. In the fiber link, depicted in Fig. 1, the reference frequency $2nf_M$ is formed as result of remote heterodyning of the two optical carriers with frequencies $\nu_0 \pm nf_M$. For stabilization of reference (beat note) frequency the injection laser with direct frequency modulation (FM) at frequency f_M is used. As shown in Fig. 1, components of the FM radiation spectrum at frequencies $\nu_0 \pm nf_M$, perform external phase locking of appropriate optical carriers.

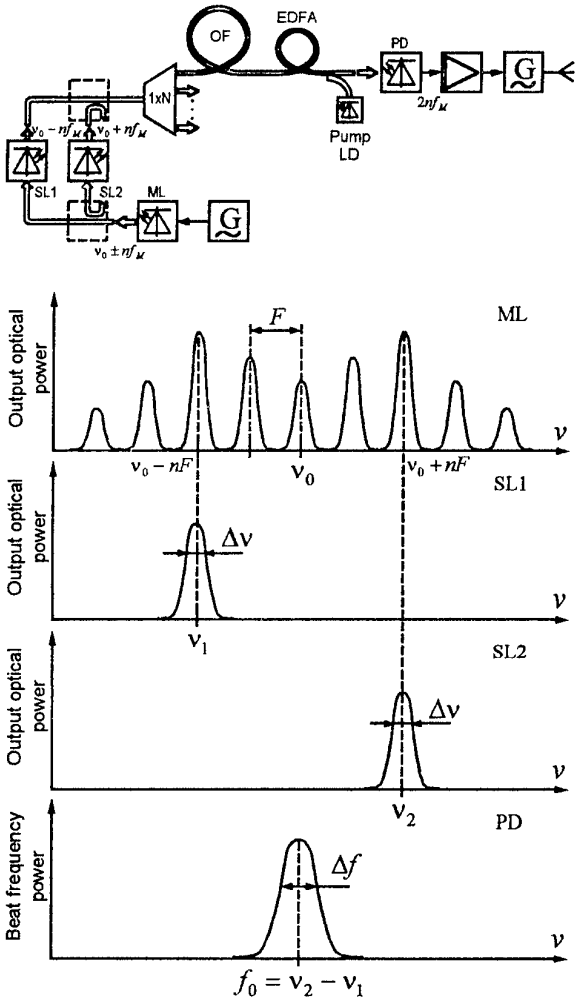


Fig. 1. Structural configuration of fiber-optic channel with Er-doped optical amplifier and spectra, explaining remote heterodyning mode: ML – master laser with FM, SL1,2 – slave lasers

In this paper the theoretical analysis of spectral characteristics of fiber channel with erbium doped fiber amplifier (EDFA) in remote heterodyning mode is considered. It allows estimating the performances and opportunity of its application in fiber-optic systems, transmitting and distributing the analog antenna signals.

SPECTRAL–NOISE ANALYSIS

Signal and noise wave components of optical field, incident upon the photodetector from the output of erbium doped fiber amplifier, can be expressed as follows

$$\begin{cases} E_S(t) = \sqrt{2GP_S^{in}}\left\{\cos(2\pi\nu_1 t + \varphi_1(t)) + \cos(2\pi\nu_2 t + \varphi_1(t))\right\} \\ E_N(t) = \sqrt{2Nh\nu_0\delta\nu}\sum_{k=-M}^{M}\cos\{2\pi(\nu_0 + k\delta\nu)t + \varphi_k\} \end{cases}, \quad (1)$$

where N is the quantity of amplified spontaneous emission (ASE) photons at the output of amplifier; P_S^{in} – average input signal power; $Nh\nu_0\delta\nu$ – average power of amplified spontaneous emission (ASE) within the frequency bandwidth $\delta\nu$; ν_0 – central frequency in optical domain ; $M = B_0/2\delta\nu$ – number of intervals $\delta\nu$ within the optical frequency bandwidth B_0; $\varphi_1(t)$, $\varphi_2(t)$, φ_k – random phase fluctuation processes of laser radiation and ASE noise spectral component at frequency $\nu_0+k\delta\nu$.

The instantaneous detector photocurrent through the photodetector with quantum efficiency σ is defined by the expression

$$\begin{aligned} i(t) &= \frac{\sigma e}{h\nu_0}\left[E_S(t) + E_N(t)\right]^2 = \\ &= \frac{\sigma e}{h\nu_0}\Big\{2GP_S^{in}\cos^2(2\pi\nu_1 t + \varphi_1) + \\ &+ 2GP_S^{in}\cos^2(2\pi\nu_2 t + \varphi_2) + \\ &+ 4GP_S^{in}\cos(2\pi\nu_1 t + \varphi_1)\cos(2\pi\nu_2 t + \varphi_2) + \\ &+ 2Nh\nu_0\delta\nu\left[\sum_{k=-M}^{M}\cos\{2\pi(\nu_0 + k\delta\nu)t + \varphi_k\}\right]^2 + \\ &+ 4\sqrt{GP_S^{in}Nh\nu_0\delta\nu}\left\{\cos(2\pi\nu_1 t + \varphi_1) + \cos(2\pi\nu_2 t + \varphi_2)\right\}\times \\ &\times\sum_{k=-M}^{M}\cos\{2\pi(\nu_0 + k\delta\nu)t + \varphi_k\}\Big\} \end{aligned} \quad (2)$$

The DC signal component of photocurrent is determined as time average of first and second terms in this formula

$$I_S = 2I_{S1,S2} = 2\sigma eGP_S^{in}/h\nu_0 . \quad (3)$$

Signal–signal beat frequency component. The third term in (2) corresponds to the result of interferention on the photodetector of two optical carriers, which can be rewritten as follows

$$\begin{aligned} i_{S1-S2}(t) &= \frac{2\sigma eGP_S^{in}}{h\nu_0}\left[\cos(2\pi(\nu_1 + \nu_2)t + \varphi_1 + \varphi_2) + \right. \\ &\left. + \cos(2\pi(\nu_1 - \nu_2)t + \varphi_1 - \varphi_2)\right], \end{aligned} \quad (4)$$

i.e. in form of two harmonic fluctuations at sum and difference frequencies with random phases $\varphi_+(t) = \varphi_1 + \varphi_2$ and $\varphi_-(t) = \varphi_1 - \varphi_2$, only one of which at difference (beat) frequency locates inside the pass-band of photodetector. Spectral density of this signal component can be found as the Fourier transformation of autocorrelation function

$$\begin{aligned} R_i(\tau) &= \langle i(t)i(t+\tau)\rangle - \langle i(t)\rangle\langle i(t+\tau)\rangle = \\ &= 2\left(\frac{\sigma eGP_S^{in}}{h\nu_0}\right)^2\left\langle\cos(\Delta\omega\tau + \Delta\varphi_-(t,\tau))\right\rangle, \end{aligned} \quad (5)$$

where the operation of time averaging is given by equation $\langle f(x)\rangle = \int_{-\infty}^{\infty} f(x)\cdot P(x)dx$.

It was noted before [1], that though the process of phase fluctuations of injection laser is not Gaussian [5], [6] and corresponding field spectrum is not pure Lorentzian, in the most of practically applicable injection lasers phase fluctuations $\Delta\varphi(t,\tau)$ are considered to have Gaussian probability density function [7]:

$$P(\Delta\varphi) = \frac{1}{\sqrt{2\pi}\sigma_{\Delta\varphi}}e^{-\frac{\Delta\varphi^2}{2\sigma_{\Delta\varphi}^2}}, \quad (6)$$

where $\sigma_{\Delta\varphi}$ – depends only on correlation time of injection laser $\Delta\tau$. And dispersion of Gaussian phase fluctuation process is linear function of time delay

$$\left\langle e^{j\Delta\varphi}\right\rangle = e^{-\frac{1}{2}\left\langle\Delta\varphi^2(\Delta\tau)\right\rangle} = e^{-\frac{\Delta\omega_0|\Delta\tau|}{2}}, \quad (7)$$

where $\Delta\omega_0$ is laser mode 3-dB bandwidth. Starting from these formulae, it might be shown that:

$$R_i(\tau) = 2\left(\frac{\sigma eGP_S^{in}}{h\nu_0}\right)^2\cos\Delta\omega\tau\cdot e^{-\frac{\Delta\omega_S|\tau|}{2}}, \quad (8)$$

where $\Delta\omega_S = 2\Delta\omega_0$ is 3-dB bandwidth width of beat frequency spectrum component. The spectral density of this signal is then:

$$S^2(\omega) = \frac{1}{\pi}\left(\frac{\sigma eGP_S^{in}}{h\nu_0}\right)^2\frac{\Delta\omega_S}{\Delta\omega_S^2/4 + (\omega - \Delta\omega)^2} \quad (9)$$

Signal–ASE beat noise component has the form:

$$\begin{aligned} \left\langle\left(i_{S1-ASE}(t)\right)^2\right\rangle &= \frac{4\sigma^2e^2GP_S^{in}N\delta\nu}{h\nu_0}\times \\ &\times\left\{\sum_{k=-M}^{M}\left[\left\langle\cos^2\{2\pi(\nu_0 - \nu_1 + k\delta\nu)t + \varphi_k - \varphi_1\}\right\rangle + \right.\right. \\ &\left.\left. + \left\langle\cos^2\{2\pi(\nu_0 + \nu_1 + k\delta\nu)t + \varphi_k + \varphi_1\}\right\rangle\right] + \end{aligned}$$

$$+\sum_{k=-M}^{M}\sum_{l=-M}^{M}\left[\left\langle\cos\left\{2\pi\left(2\nu_0+k\delta\nu+l\delta\nu\right)t+\varphi_k+\varphi_l\right\}\right\rangle+\right.$$
$$\left.+\left\langle\cos\left\{2\pi\left(2\nu_1+l\delta\nu-k\delta\nu\right)t+\varphi_l-\varphi_k+2\varphi_1\right\}\right\rangle\right]. \quad (10)$$

In this equation, the time average of cross–terms near doubled frequencies $2\nu_0$ and $2\nu_l$ vanish. The power spectrum of term with frequency $\nu_0+\nu_l$ falls outside the frequency bandwidth of photodetector and thus it can be neglected.

The time average of the remaining terms with frequencies $f=\nu_0-\nu_1+k\delta\nu$ is equal 0.5, and it is possible to show, that they contain two components within the frequency range from 0 to $f^I_{\min}=B_0/2-|\nu_0-\nu_1|$ and only one component within the range from $f^I_{\min}=B_0/2-|\nu_0-\nu_1|$ to $f^I_{\max}=B_0/2+|\nu_0-\nu_1|$. Hence, spectral power density of this signal is uniform within the specified intervals

$$\overline{\sigma}^2_{S1-ASE}=\begin{cases}\dfrac{4\sigma^2e^2GP_S^{in}N}{h\nu_0} & 0\le f\le f^I_{\min}\\ \dfrac{2\sigma^2e^2GP_S^{in}N}{h\nu_0} & f^I_{\min}\le f\le f^I_{\max}\\ 0 & f>f^I_{\max}\end{cases}, \quad (11)$$

and the total power of signal–ASE beat noise term $i_{S1-ASE}(t)$ in the electronic bandwidth B_e is then given by

$$\sigma^2_{S1-ASE}=\begin{cases}\dfrac{4\sigma^2e^2GP_S^{in}NB_e}{h\nu_0}, & B_e\le f^I_{\min}\\ \dfrac{2\sigma^2e^2GP_S^{in}N}{h\nu_0}\left(B_e+f^I_{\min}\right), & B_e>f^I_{\min}\end{cases}.$$

The similar expressions for $i_{S2-ASE}(t)$ photocurrent component can be obtained by replacement of frequency ν_l on ν_2.

ASE–ASE beat noise component. We focus next on the ASE–ASE beat noise component, which can be rewritten as

$$i_{ASE-ASE}(t)=$$
$$=\sigma eN\delta\nu\sum_{k=-M}^{M}\sum_{l=-M}^{M}\left[\cos\left\{2\pi\left(k-l\right)\delta\nu t+\varphi_k-\varphi_l\right\}+\right.$$
$$\left.\cos\left\{2\pi\left[2\nu_0+\left(k+l\right)\delta\nu\right]t+\varphi_k+\varphi_l\right\}\right]. \quad (13)$$

The terms oscillating at doubled optical frequency don't fall into the photodetector bandwidth, while the terms with frequencies $(k-l)\delta\nu$ yield nonzero contributions for $k=l$, corresponding to the mean DC photocurrent. The rest of spectral components oscillating at optical frequency $(k-l)\delta\nu$, determine the ASE noise power

$$\left\langle\left(i_{ASE-ASE}(t)\right)^2\right\rangle= \quad (14)$$
$$=2\left(\sigma eN\delta\nu\right)^2\sum_{k=1}^{2M}\sum_{\substack{l=1\\ l\ne k}}^{2M}\left\langle\cos^2\left\{2\pi\left(k-l\right)\delta\nu t+\varphi_k-\varphi_l\right\}\right\rangle$$

In this formula we assumed, that time average of terms with random uncorrelated phases is equal to zero. Further analysis shows that this equation contains 2M–1 terms at frequency $\delta\nu$, 2M–2 terms at $2\delta\nu$,..., one term at $(2M-1)\delta\nu$ and no terms are at frequency $2M\delta\nu$. The same number of corresponding terms with negative frequencies and opposite phases is also existing. Thus the spectral density near zero frequency takes the value:

$$\overline{\sigma}^2_{ASE-ASE}(0)=2\cdot 2M\left(\sigma eN\delta\nu\right)^2/\delta\nu=2\sigma^2e^2N^2B_0, \quad (15)$$

and decreases linearly with frequency to vanish at $\nu=B_0$. The total ASE noise power falling into the electronic bandwidth B_e of photodetector is then given by:

$$\sigma^2_{ASE-ASE}=I_N^2\frac{2B_e}{B_0^2}\left(B_0-\frac{\Delta\omega}{2\pi}\right). \quad (16)$$

The spectral density of different components of photocurrent, determined by above-stated equations, and their total sum are illustrated in Fig. 2. This result in particular case $\nu_1=\nu_2$, $\Delta\nu=0$ and absence of phase fluctuation of injection laser radiation coincides with expressions given in [2] for the case of single non-modulated optical carrier at the output of EDFA).

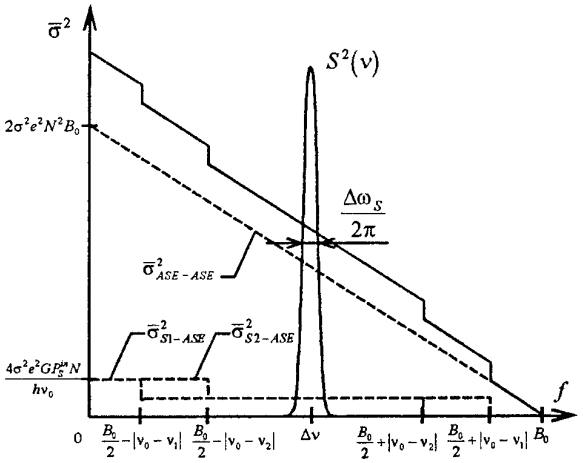


Fig. 2. Power spectral densities of photodetector signal and noise beat components at the output of EDFA

SIGNAL–TO–NOISE RATIO ANALYSIS

The signal–to–noise ratio (SNR) can be determined as follows

$$SNR=\frac{A_S^2(\Delta\omega)}{\sigma_d^2}, \quad (17)$$

where A_S is the magnitude of signal photocurrent at frequency $\omega = \Delta\omega$; σ_d^2 is the total noise power falling into the photodetector bandwidth. Noise power can be expressed as the sum of different noise components of EDFA and photodetector [1]

$$\sigma_d^2 = \sigma_{S1-ASE}^2 + \sigma_{S2-ASE}^2 + \sigma_{ASE-ASE}^2 + \sigma_{th}^2 + \\ + \sigma_{shot}^2 + \sigma_{beat}^2 \quad (18)$$

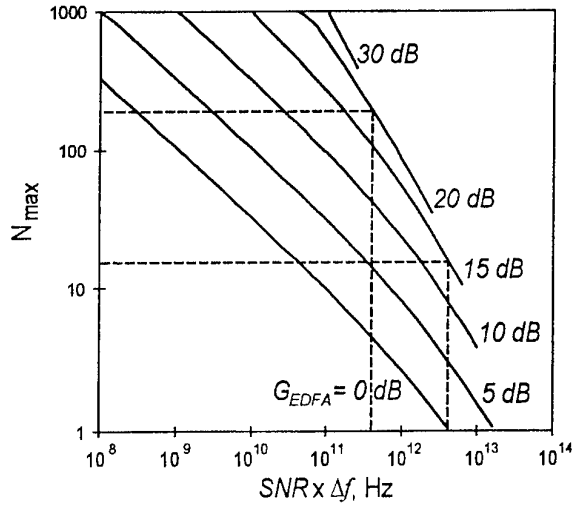


Fig. 3. Maximum number of channels in antenna signal distribution system, fed by single optical source

In this formula σ_{th}^2 denotes the photodetector thermal noise, and other two terms are associated with photodetector's shot and beat noise respectively. As was shown in [2], these terms are determined by the following expressions

$$\sigma_{shot}^2 = eB_e\left(I_S + 2mI_N\right), \quad (19)$$

$$\sigma_{beat}^2 = I_S I_N \frac{B_e}{B_0} + mI_N^2 \frac{2B_e}{B_0^2}\left(B_0 - \frac{\Delta\omega}{2\pi}\right), \quad (20)$$

where m is the number of amplifier ASE modes ($m = 2$ in case of single mode EDFA without polarizer between EDFA and photodetector). Substituting these formulae into expression for SNR, we can rewrite it as

$$SNR = I_S^2\left(\pi\Delta\omega_S\right)^{-1}\left[5I_S I_N \frac{B_e}{B_0} + I_N^2 \frac{2B_e}{B_0^2}\left(B_0 - \frac{\Delta\omega}{2\pi}\right) + \right. \\ \left. + \left(1+m\right) + \frac{4k_B T B_e}{R} + eB_e\left(I_S + 2mI_N\right)\right]^{-1}, \quad (21)$$

Plot of this function is shown in Fig. 4 as a function of EDFA gain factor G. To calculate it the following most typical values of parameters were taken: $\sigma = 1$, T =300 K, λ_S = 1.5 μm, P_S^{in} = 100 nW, B_0 = 10 GHz, B_e = 200 Hz, R = 50 Ω. Left half of the diagram illustrates the effect of each noise component on the total signal–to–noise ratio. The figure shows that the amplifier operates in two regimes: at low gains the SNR is determined by the dominant photodetector thermal noise; at high gains the signal where SE beat noise components are dominant.

This analysis allows calculating the maximum number N of channels in antenna signal distribution system, fed by single optical source [8]. Number of channels is the synthetic parameter, which is very important for antenna system designers. It determines the competition ability of fiber-optic distribution system, compared with traditional microwave transmission lines. For fiber link configuration of Fig. 1, N is given by

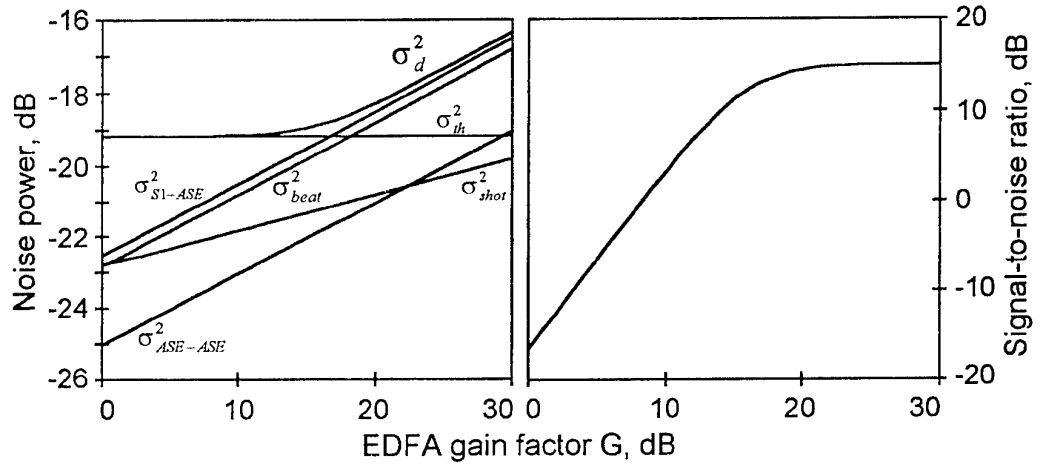


Fig. 4. Dependence of signal–to–noise ratio versus EDFA gain factor

$$N_{\max} = Int(P_{in}/P_{\min}), \quad (22)$$

where $Int(...)$ is an integer part operator; P_{in} is the input photodetector optical power; P_{min} is the photodetector sensitivity, defined as minimum P_{in}, proving $SNR = 1$. The dependence of N_{max} on SNR in antenna channel is depicted in Fig. 3. Figure shows, that fiber link of standard configuration without fiber amplifier with typical $SNR = 5 \cdot 10^{11} \ldots 5 \cdot 10^{12}$ in 1 Hz bandwidth provides $N_{max} \approx 7$. Configuration of Fig. 1 with EDFA gain factor $G = 15 \ldots 20$ dB allows to increase the number of simultaneously feeding channels up to $N_{max} = 20 \ldots 200$.

REFERENCES

1. A. N. Bratchikov, "Optical fibers and antennas. (Invited paper) ", *Proc. 10-th International symposium on antennas, Nice, France*, pp.275-289, 1998.
2. E. Desurvire, *Erbium–Doped Fiber Amplifiers. Principles and Applications,* A Willey–Interscience Publication, John Willey & Sons, Inc., New–York, 1993.
3. A. N. Bratchikov, A. P. Sheremeta, "Optical amplifiers on the basis of Er–doped fibers: present state", Modeling, Measurement & Control, AMSE Press, France, vol. 54, no. 3, pp. 1–25, 1994.
4. A. N. Bratchikov, I. P. Glukhov, "Interferentional fiber links for microwave signal transmission", presented at the XXIV Gen. Assembly, Int. Union Radio Sci. Kyoto, Japan, August, 1993.
5. K. Petermann and E. Weidel, "Semiconductor laser noise in an interferometer system", J. Quantum Electron. vol. QE–17, pp. 1251–1256, 1981.
6. K. Petermann and G. Arnold, "Noise and distortion characteristics of semiconductor lasers in optical fiber communication systems", J. Quantum Electron. vol. QE–18, pp. 543–555, 1982.
7. B. Moslehi, "Analysis of optical phase noise in fiber–optic systems employing a laser source with arbitrary coherence time", J. Lightwave Technol., vol. LT–4, No.9, September, pp. 1334–1351, 1986.
8. A.N.Bratchikov, "Fiber-optic systems for phased antenna arrays", Russian J. on Advances of Modern Radio Electronics, no. 7, pp. 3–15, 1997.

TUNABLE WAVEGUIDE BANDPASS FILTERS WITH A NEAR CONSTANT BANDWIDTH

F. F. Dubrovka and P. Ya. Stepanenko

National Technical University of Ukraine "KPI", Laboratory of Antennas and Telecommunications,
2110D, Radio Engineering Faculty, Polytekhnichna st., 12, Kyiv, 252056, Ukraine
Tel/fax: 380-44-241 72 23 e-mail: dubrovka@ucl.kiev.ua

INTRODUCTION

Tunable bandpass microwave filters are widely used in telecommunication systems. In transmit stations ferrite or mechanically tunable waveguide filters are commonly used due to capability to transmit high power levels.

The principal disadvantage of mechanically tunable filters built upon traditional inductive or capacitive discontinuities is a considerable alteration of bandwidth under the variation of resonance frequencies of the resonators. Bandwidth of filters with inductive discontinuities is becoming narrower under tuning to the lower operating frequencies. In contrary, a bandwidth alteration of filters with capacitive discontinuities has an inverse dependence under tuning and, what is more, its steepness is less then for the filters with inductive discontinuities. But in the event of capacitive discontinuities transmit power level is essentially decreased due to small gaps between their ridges.

In this paper a new approach to building mechanically tunable bandpass filters with a near constant bandwidth is proposed. The main feature of the approach is a combination of inductive and capacitive discontinuities to build resonators. In order to illustrate the new approach an adequate mathematical model for the filter has been developed and a tunable waveguide narrow bandpass filter prototype with near constant bandwidth has been designed, developed, constructed and tested.

THEORY

A key element to build the filter structure is a cascade connection of capacitive and inductive discontinuities shown in Fig. 1. The capacitive discontinuity is formed by two rectangular ridges of a certain length which are disposed symmetrically relatively to the vertical and horizontal symmetry planes of the filter. The inductive discontinuity is made in the form of septum dividing a standard rectangular waveguide into two equal below-cutoff rectangular waveguides. By combining dispositions of key element one can obtain different variants of the tunable filters.

To design the filter one should know a generalized scattering matrix of the key element waveguide structure. That matrix can be calculated by combining generalized scattering matrices of capacitive and inductive discontinuities and the regular waveguide section between them. We shall build an high efficiency algorithm to calculate a generalized scattering matrix of the single discontinuity by consideration all symmetry planes of the discontinuity. With taking into account longitudinal and transverse symmetry planes the models of the capacitive and inductive discontinuities are transformed to the form shown in Fig. 2 and 3 respectively. Taking into consideration the longitudinal symmetry planes allows to simplify the problem of calculating coupling coefficients of the eigenmodes of waveguides to be connected. Use of transverse plane of symmetry for the discontinuities allows to simplify essentially the calculation of generalized scattering matrices of the discontinuities.

To calculate the generalized scattering matrices we used the integral equation method [1]. Each single discontinuity is formed by three partial regions and has two common boundaries. Therefore, both discontinuities can be described by the same system of integral

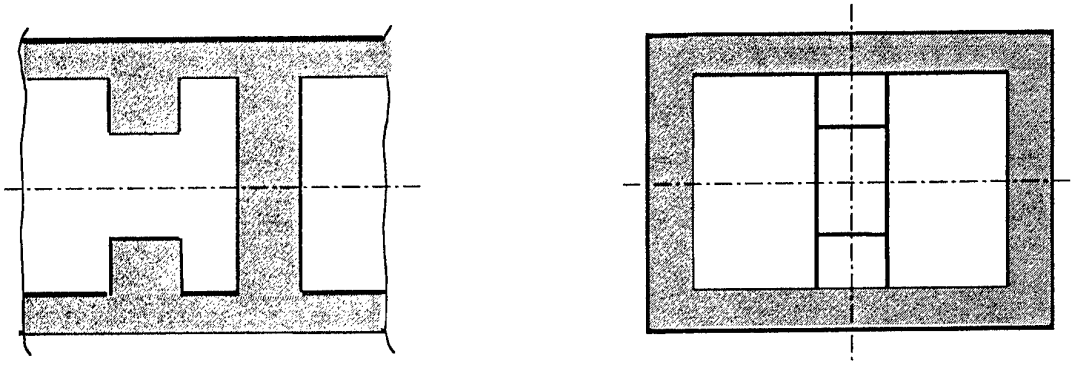


Fig. 1

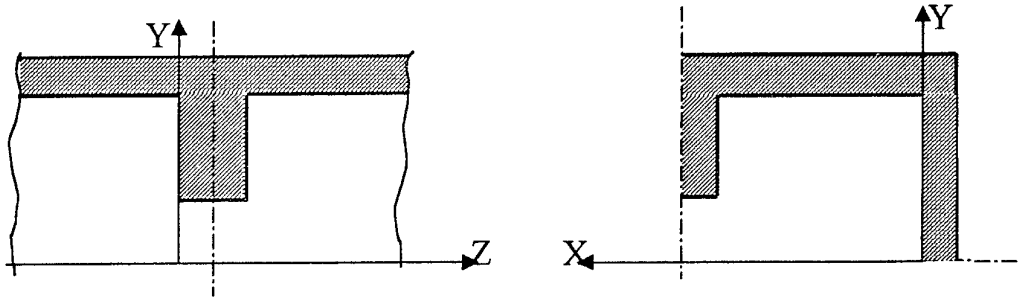


Fig. 2

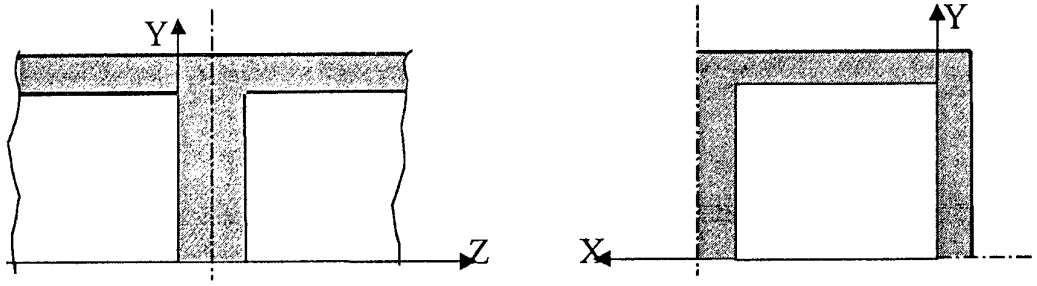


Fig. 3

equation. With taking into consideration identity of fields at both sides of each discontinuity we have obtained

$$\sum_{\nu=1}^{2}\sum_{m=1}^{M_\nu} Y_{\nu m}\vec{\Psi}_{\nu m}A_{1\nu m}+\sum_{\mu=1}^{2}\sum_{n=1}^{N_\mu}\vec{U}_{\mu n}\left(V_{\mu n}B_{1\mu n}-B_{2\mu n}\right)=$$
$$=2Y_{qp}\vec{\Psi}_{qp},$$
$$q=1,\ p=1,2,\ldots,P_1,$$
$$q=2,\ p=1,2,\ldots,P_2,$$
$$\sum_{\mu=1}^{2}\sum_{n=1}^{N_\mu}\vec{U}_{\mu n}\left(V_{\mu n}B_{2\mu n}-B_{1\mu n}\right)+ \quad (1)$$
$$+\sum_{\nu=1}^{2}\sum_{m=1}^{M_\nu} Y_{\nu m}\vec{\Psi}_{\nu m}A_{2\nu m}=0,$$

with

$$A_{k\nu m}=\int_{s_k}\vec{E}_k\vec{\Psi}_{\nu m}ds,$$

$$B_{k\mu n}=\int_{s_k}\vec{E}_k\vec{\Phi}_{\mu n}ds,$$

$$\vec{U}_{\mu n}=y_{\mu n}\vec{\Phi}_{\mu n}\Big/sh\gamma_{\mu n}l,$$

$$V_{\mu n}=ch\gamma_{\mu n}l,$$

where P_q is a number of modes of unity amplitude of magnetic (q = 1) and electric (q = 2) types which are alternatively incident onto the discontinuity from the left, $\vec{E}_k$ is an unknown tangential electric field at a k-th (k=1,2) coupling aperture for each mode incident onto discontinuity, $\vec{\Psi}_{\nu m}$ and $\vec{\Phi}_{\mu n}$ are orthonormalized vector eigenfunctions of a regular rectangular waveguide and a coupling section of magnetic $(\nu,\mu=1)$ and electric $(\nu,\mu=2)$ types, $Y_{\nu m}$ and $y_{\mu n}$ are modal admittances corresponding to the eigenfunctions, $\gamma_{\mu n}$ is a propagation constant of H_n-mode (μ = 1) and E_n-mode (μ = 2) in the coupling section (mode numbering is given by one index in order of cutoff frequencies increasing), M_ν and N_μ are numbers of eigenmodes of magnetic $(\nu,\mu=1)$ and electric $(\nu,\mu=2)$ types taking into account in the regular rectangular waveguide and the coupling section, s_k is a square of the k-th coupling aperture, l is a length of the coupling section.

For each mode incident onto discontinuity we transform system of equations (1) into two independent integral equations relatively to sums and differences of tangential electric fields at the coupling apertures. We form sum and difference of the first and second integral equations (1) for each mode incident onto discontinuity. This correspondents to the disposition at the symmetry

plane magnetic (r = 1) and electric (r = 2) walls. After some transformations we derived

$$\sum_{\nu=1}^{2}\sum_{m=1}^{M_\nu} Y_{\nu m}\vec{\Psi}_{\nu m}C_{r\nu m} + \sum_{\mu=1}^{2}\sum_{n=1}^{N_\mu} Q_{r\mu n}\gamma_{\mu n}\vec{\Phi}_{\mu n}D_{r\mu n} = 2Y_{qp}\vec{\Psi}_{qp}, \quad (2)$$

$$q=1,\ p=1,2,\ldots,P_1,$$

$$q=2,\ p=1,2,\ldots,P_2,$$

with

$$C_{r\nu m} = \int_{s_1} \vec{F}_r\vec{\Psi}_{\nu m}ds,$$

$$D_{r\mu n} = \int_{s_1} \vec{F}_r\vec{\Phi}_{\mu n}ds,$$

$$\vec{F}_1 = \vec{E}_1 + \vec{E}_2,\ \vec{F}_2 = \vec{E}_1 - \vec{E}_2,$$

$$Q_{1\mu n} = th(\gamma_{\mu n}l/2),\ Q_{2\mu n} = cth(\gamma_{\mu n}l/2).$$

To solve the system of equations (2) we applied Galerkin's method. We represented sum (r = 1) and difference (r = 2) tangential electric fields for each mode incident onto discontinuity by expansions into series of vector eigenfunctions of the coupling section

$$\vec{F}_r = \sum_{\mu=1}^{2}\sum_{n=1}^{N_\mu} S_{\mu n}\vec{\Phi}_{\mu n}, \quad (3)$$

where $S_{\mu n}$ are unknown coefficients, $\vec{\Phi}_{\mu n}$ are vector eigenfunctions of the Γ – region (Fig. 2) for capacitive discontinuity and those for below-cutoff rectangular waveguide (Fig. 3) for inductive discontinuity.

Substituting (3) in (2) and performing transformations in accordance with Galerkin's method we derived for each discontinuity the following two (r = 1,2) systems of linear algebraic equations with $P = P_1 + P_2$ right-side parts

$$\sum_{\mu=1}^{2}\sum_{n=1}^{N_\mu} S_{\mu n}\left[\gamma_{\mu n}Q_{r\mu n}\delta_{\mu u}\delta_{n\nu} + \sum_{\nu=1}^{2}\sum_{m=1}^{M_\nu} Y_{\nu m}\eta_{\nu m}^{(u\nu)}\eta_{nm}^{(\mu\nu)}\right] = 2Y_{qp}\eta_{vp}^{(uq)},$$

$$u=1,\ \nu=1,2,\ldots,N_1,$$

$$u=2,\ \nu=1,2,\ldots,N_2,$$

$$q=1,\ p=1,2,\ldots,P_1,$$

$$q=2,\ p=1,2,\ldots,P_2, \quad (4)$$

where $\eta_{nm}^{(\mu\nu)} = \int_{s_1} \vec{\Phi}_{\mu n}\vec{\Psi}_{\nu m}ds$ are coupling coefficients of eigenmodes, $\delta_{\mu u}$ and $\delta_{n\nu}$ are Kronecker symbols.

By solving the system of linear algebraic equations (4) with P right-side parts under r = 1,2 we determined distributions of tangential electric fields at the first and second coupling apertures of the corresponding discontinuity. After that we calculated elements of the discontinuity generalized scattering matrix using coefficients A_k.

The feature of the mathematical model of the inductive discontinuity is availability both magnetic H_{mn} and electric E_{mn} modes with index $n \neq 0$ in its mode spectrum which are caused by presence of capacitive discontinuity in the filter key element. This is a reason to consider diffraction problems of the modes with index $n \neq 0$ at the septum for each n = 1,2,... separately and then summarize obtained results.

RESULTS OF DESIGN AND TESTING

Using the derived formulas and equations an algorithm and a program package for calculation of frequency characteristics of the separate resonators and the whole filter have been developed. In order to confirm experimentally correctness of the developed theory a prototype of the narrow band 5-resonator bandpass filter (Fig. 4) with maximally flat frequency response of insertion loss has been designed, constructed and tested. Tuning the filter is performed by the rods introduced into each resonator.

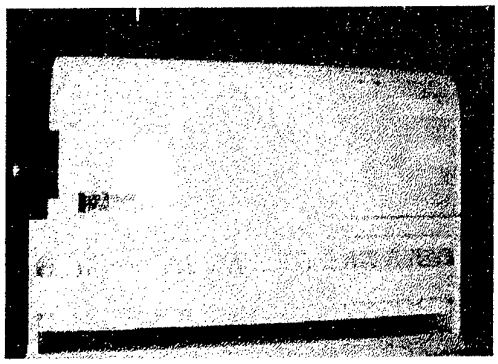


Fig. 4

The filter prototype insertion loss versus frequency at the three specified operating frequencies within tuning frequency range are shown in Fig. 5. Solid line relates to the lower operating frequency, dashed line – to the medium operating frequency and dashed-dotted line – to the upper operating frequency. Data of measurements are depicted by crosses.

Calculated (solid line) and measured (crosses) data of the filter prototype insertion loss near by pass band at upper operating frequency are shown in Fig. 6. One can observe in Fig. 5 and 6 that theoretical and experimental results are in a good agreement all over the tuning frequency range. The measured filter pass band at the level 0.5 dB from the level of insertion loss at the cen-

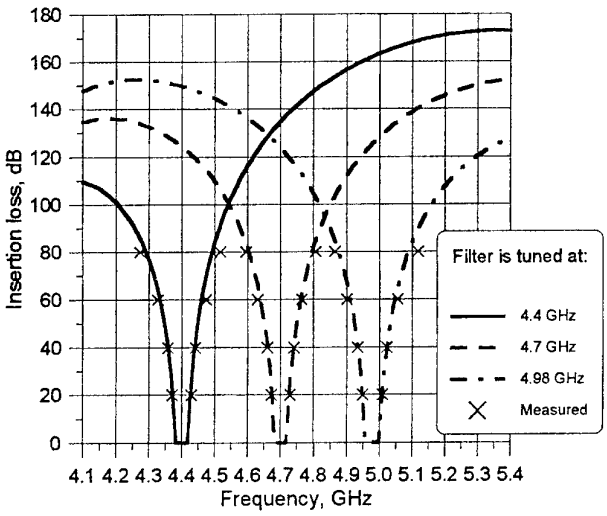


Fig. 5

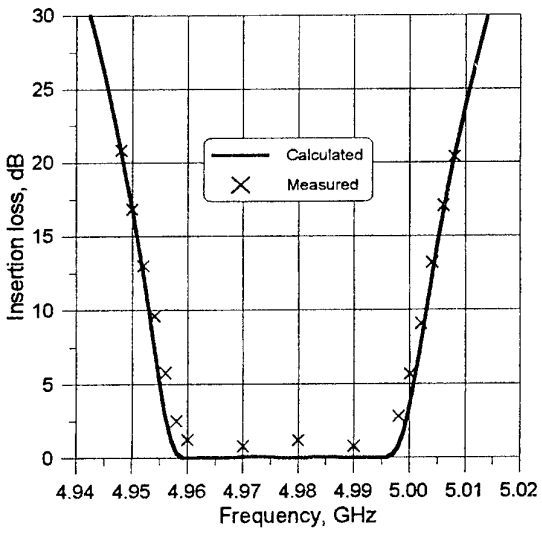


Fig. 6

tral frequency is equal 35 ± 2 MHz all over the tuning frequency range 13 %. Insertion loss in pass band all over the tuning frequency range is less then 1.2 dB. Measured VSWR is maximal at ends of tuning frequency range and is below 1.4. Insertion loss values at frequencies $f_0 \pm 60$ MHz are more than 50 dB and at $f_0 \pm 130$ MHz are more than 85 dB.

CONCLUSION

A new approach to building tunable bandpass filters with near constant bandwidth all over wide tuning frequency range has been proposed. The essence of the idea is in an successful combining inductive and capacitive discontinuities. An adequate mathematical model of the filter based on generalized scattering matrix, obtained by using the integral equation method for solving diffraction problems for single discontinuities, has been developed. A tunable bandpass C-band filter prototype with a near constant bandwidth in the tuning frequency range 13 % has been designed, constructed and tested. Testing the filter prototype has verified high accuracy of the mathematical model that exclude entirely necessity of any adjusting of tunable filter after fabrication. Due to a near constant bandwidth over a wide tuning frequency range the developed mechanically tunable waveguide filters open new possibilities in realization high efficient and cost effective frequency tunable transmit stations for various telecommunication systems.

REFERENCE

1. Mittra R. (Ed.) Computer techniques for electromagnetics, Pergamon Press, 1973.

NUMERICAL ALGORITHM FOR CALCULATION OF CAVITY MICROWAVE TRANSDUCER OF AN APERTURE TYPE

Y. E. Gordienko, A. Y. Panchenko, A. A. Ryabukhin

Kharkov State Technical University of Radioelectronics
14 Lenina pr., Kharkov-310726, Ukraine
phone: 0572-409362, e-mail: imd@kture.kharkov.ua

Microwave transducers gained a wide distribution at realization of non-destructive materials control, both during manufacture, and at output trials stage. The analytical measuring instruments based on their application allow to define a wide spectrum of parameters of dielectric materials. When designing such devices the essential difficulties arise during carrying out precomputations. At this stage, it is necessary to obtain transformation functions between required parameters of checked objects and transducer output parameters. For this purpose, it is necessary to find a rigorous solution of an electromagnetic problem, having rather intricate boundary conditions, as a rule. Therefore, the developers usually refuse from a solution of an inverse problem allowing to find an optimum transducer's construction, and use the multiple approach to a direct problem with different input conditions. Creation of convenient for use calculation algorithms of microwave transducers allows to essentially reduce period of designing.

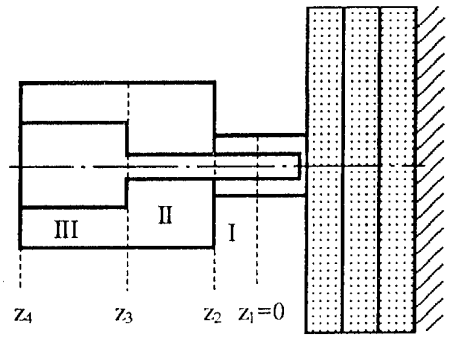


Fig. 1

In this report the numerical algorithm and the calculation program of a capacity cavity microwave transducers with a small aperture is presented. Advantage of these transmitters is absence of fields with multivalence in transformation functions, high responsivity, good resolution in space and construction simplicity. The transducer comprises the coaxial cavity, thin coaxial (with fast damping of higher modes) and measuring aperture in the flat screen (Fig. 1). Such transducers allow to define both electrophysical parameters of homogenous samples and integral characteristics of layered samples.

The calculations algorithm is based on the use of Galerkin's method ideas and different projection methods variants [1]. The problem algebraization is carried out by use of an approximate problem solution's orthogonality requirement to a zero-element of a function space, on which it is found. Usually as such zero-element pick the relations following from continuity condition of solution to be found on conditional division bounds of a system into regular areas [2].

Depending on desired solution's presentation it is possible to distinct variants of this method based on tensor Green's function application [3] and eigenfunctions of regular partial domain of simple shape.

In this case magnetic and electrical field's representation in explored domain through magnetic currents and corresponding Green's tensors for Maxwell's equations equivalent to tangential component of electric field is a common for method's variant based on application of Green's functions

$$\vec{H}(\vec{r}) = \int_S \Gamma_{22}(\vec{r},\vec{r}')\cdot\vec{J}^M(\vec{r})\,dS';$$

$$\vec{E}(\vec{r}) = \int_S \Gamma_{12}(\vec{r},\vec{r}')\cdot\vec{J}^M(\vec{r})\,dS';$$

$$\vec{J}^M = \left[\vec{n}\cdot\vec{E}_S\right],$$

where S is the conditionally selected section, in which there are magnetic currents; $\vec{n}$ is normal to this section; $\vec{E}_S$ is the unknown electrical field in the section.

Thus, it is convenient to represent a field in the separate conditionally selected regular parts of a system through equivalent magnetic currents on bound sections of these parts. The unknown field $\vec{E}_S$ can be expressed through the section eigenfunctions being solutions to the homogeneous two-dimensional Helmholtz equation under the corresponding boundary conditions

$$\vec{E}_S = \sum_{k=1}^{\infty} a_k \cdot \vec{e}_k$$

Using conditions of equality of electric field components on ideally conductive boundaries to zero and tangential components of electrical and magnetic fields on both sides of media interface, it is possible to obtain

$$\int_S \left(\vec{H}_{t|n=+0} - \vec{H}_{t|n=-0}\right)\cdot\vec{e}_k\,ds =$$

$$\int_S \sum_{k=1}^{\infty} a_k \int_{S'} \Gamma_{22}^{I}(\vec{r},\vec{r}')\cdot\vec{e}_k(\vec{r}')\cdot r'dr'd\varphi'\cdot\vec{e}_i^{*}(\vec{r})\cdot rdrd\varphi -$$

$$-\int_S \sum_{k=1}^{\infty} a_k \int_{S'} \Gamma_{22}^{II}(\vec{r},\vec{r}')\cdot\vec{e}_k(\vec{r}')\cdot r'dr'd\varphi'\cdot\vec{e}_i^{*}(\vec{r})\cdot rdrd\varphi = 0$$

The recurrent relations allow to reduce a solution of the problem both in a cavity volume, and in volume of a sample to one common surface. The choice of location of this surface and field on it will define an accuracy of all solution. For the resonator shown in Fig. 1 it is the most convenient to select section z_i in the middle of thin coaxial as such a surface, since the field in it the most precisely corresponds TEM wave.

The calculation algorithm scheme of a cavity microwave transducer loaded with a layered dielectric is shown in Fig. 2.

At the first stage of calculation the parameters of the cavity (radii and the length of the body and the central stub; the capacity clearance size, material of the resonator) and parameters of a layered sample (thickness of layers, value of a complex inductivity for each layer) are given. Further, using 4-th order's approximation the solution of the transcendental equation in the cavity's areas I-III for definition of the radicals and norms in each area is made. In this case the maximum accuracy of solution is assumed and equals 10–12 characters of a mantissa. The next step of the solution is the calculation of magnetic fields on the part of the cavity and sample separately in a frequency band. The recurrent relations based on equality of tangential components on areas boundaries, allow to represent a magnetic field as a particular integral, whose numerical solution, in our case, is obtained by the high-performance numerical method, which uses quadratures of Newton-Cotes. Thus, the accuracy is reduced down to 9 mantissa characters. After definition of magnetic fields the calculation of TEM-mode amplitude dependence on a frequency band is performed. At this stage the same program of integration is used again. The accuracy is already 8 characters of a mantissa. Further, TEM-mode amplitude dependence on frequency in sample $A_{sam}(f)$ and cavity $A_{cav}(f)$ are replaced with an approximating polynomial, whose degree is defined by a number of frequency points, it is usually 4-6. It allows to obtain results with an error in 6-7 sign of a mantissa. The similar reduction of accuracy at each stage allows to use software of automatic accuracy achievement without extra analytical research each time. For definition of resonant frequency f_0 the equation $A_{sam}(f) - A_{cav}(f) = 0$ is solved. Finally the magnetic field calculation of all system at frequency f_0 is performed.

In the program the application possibility of iterative methods of this equation solution with returning to initial calculation of fields is provided. However, test calculations have shown, that the exact solution is enough for obtaining accuracy, required in practice.

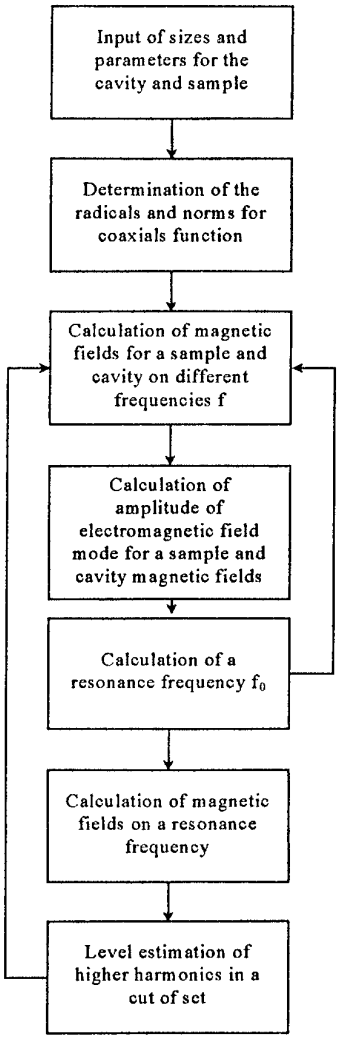


Fig. 2

The program is worked out in Borland C ++ Builder and works under the control of operating systems Windows 95/98/NT. The program has the convenient user interface and allows to calculate both a capacity microwave transducer of an aperture type, and cylindrical microwave transducer loaded with a layered dielectric sample.

REFERENCES

1. Nikolskiy V.V. The variant methods for internal electrodynamics problems. -M.: Nauka, 1967.- 460 p. [in Russian].
2. Williamson A.C. The resonant frequency and tuning characteristics of a narrow-gap reentrant cylindrical cavity.- IEEE Transactions on Microwave Theory and Techniques, 1976, vol. 24, N4, pp. 182-187.
3. Maxwell's equations tensor Green's functions for cylindrical areas / Panchenko B.A. - Radiotehnika, 1970, vol. 15, pp. 82-91 [in Russian].

MULTIELEMENT RESONANCE DIAPHRAGMS IN MICROWAVE ANTENNA-AND-FEEDER DEVICES

V. A. Katrich, A. A. Shmat'ko

Kharkiv State University,
Svobody Sq. 4, Kharkiv - 310077, Ukraine,
phone/fax: 8(0572) 47-18-16, e-mail: Victor.A.Katrich@univer.kharkov.ua

The resonance diaphragms are widely used in the antenna and microwave equipment as matching elements, filters, decoupling elements etc. As a rule the single-element resonance diaphragms or their serves along the direction of the wave propagation are used. Using the multielement resonance diaphragms may cause additional resonance couplings, changing the resonance frequency, matching the input and output of power electron microwave devices.

This paper focuses on the theoretical description of the wave propagation or excitation of oscillations in the resonance system with a limited number of the resonance diaphragms.

PROBLEM FORMULATION AND SOLUTION

The resonance system with volumes coupled by means of multielement resonance slot diaphragms of finite thickness h (Fig. 1) is considered. The number of slot elements is equal to N. The solution of the problem will be obtained with partial region technique using Floquet's theorem. The non-uniformity of the system leads to the necessity of solving a vector problem, because polarizations are not separated.

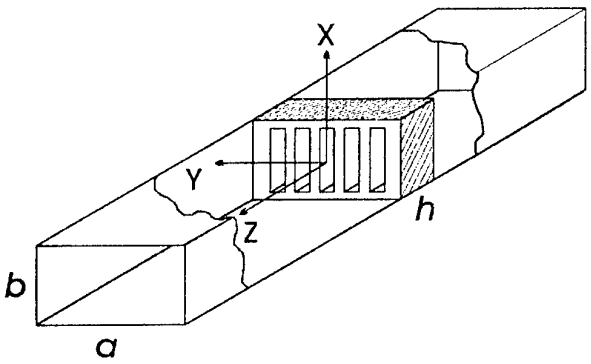


Fig. 1. Resonator with the multielement slot diaphragm

In each of the partial regions the fields are determined in the form of a combination of two Hertz's vectors – electrical $\left(\vec{\Pi}^e = \vec{x}^0\Pi^e\right)$ and magnetical $\left(\vec{\Pi}^h = \vec{x}^0\Pi^h\right)$. The Helmholtz equation solutions for Hertz's vector $\vec{\Pi}^e$ and $\vec{\Pi}^h$ are represented in the form of the expansion of eigenmodes of the infinite periodical structure consisting of the same elements as the resonance diaphragm. Such a method allows to represent the fields in the region of resonators in the form of the superposition of the limited number of oscillation modes. The number of these modes is connected with the index N. Furthermore, the field of every oscillation mode independently on the others is satisfying to all the necessary boundary conditions the use of which in the corresponding planes of the oscillating system leads to a uniform system of linear algebraic equations in relation to the amplitudes of the field harmonics. Equality of the determinant of this system to zero determines the resonance wave number values of the oscillation mode $\mu = 0,1,2...N$. In fact the wavelength λ is more than the one of the sizes of the resonance slot, the analytical expression of the characteristic equation may be written with the help of the second order determinant:

$$\begin{vmatrix} 1-\theta_1\theta_2 S\operatorname{ctg}\varphi_{10} & \theta_1\theta_2 S(\sin\varphi_{10})^{-1} \\ \theta_1\theta_2\hat{S}\sin\varphi_{10} & 1-\theta_1\theta_2\hat{S}\operatorname{ctg}\varphi_{10} \end{vmatrix} = 0,$$

where θ_1 and θ_2 are the slot sizes, which are normalized on the structure period ℓ; $\varphi_{10} = \frac{\pi h}{\ell}\sqrt{\kappa^2 - (\ell/2a)^2}$, $\kappa = \frac{2\ell}{\lambda}$. S and $\hat{S}$ are determined by the double series on transverse oscillation indices, the series converge quickly and hence may be represented explicitly.

ANALYSIS OF THE RESULTS OBTAINED

The multicoupled region causes the existence of LFM-waves in such a system at the selected frequency. Another peculiarity of the structure under consideration is practical coincidence of phase velocity of some spatial harmonics of different oscillation modes, which allows to excite the field with different spatial distribution without tuning the resonator. The multielement diaphragms cause the emergence of passbands and stopbands, the width of which depends on the correlation of the wavelength and geometrical dimensions of the system. A variation of the diaphragm thickness leads to displacement of short-wave limit of the passband in the direction of greater values of λ.

The obtained system of equations for determining the eigen resonance frequencies of different oscillation modes may be transformed into the form suitable for analysis of the problem of exciting the multielement diaphragm by the waveguide type of the wave.

THE FULL-WAVE MODEL FOR PLANE JUNCTION OF WAVEGUIDES WITH PIECEWISE LINEAR COORDINATE BOUNDARIES

A. A. Kirilenko, D. Yu. Kulik, L. A. Rud', and V. I. Tkachenko

Institute of Radiophysics and Electronics, National Academy of Sciences of Ukraine
12 Proskura St., 31085 Kharkov, Ukraine
Fax. 38 0572 441105, e-mail: kirilenko@ire.kharkov.ua

The algorithm of *S*-matrix calculation for generalized junction between complicated waveguides with arbitrary piecewise boundaries is described. The main goal is to generalize the mode-matching procedure on the wide class of objects to provide the possibility of exact electromagnetic analysis for the very complicated structures from microwave devices as itself up to multilayer integrated circuits.

The structures being considered can be treated as the junctions of several waveguides (WG) with piecewise coordinate boundaries (Fig. 1). From application point of view they may be broken into the following groups: 1) immediate fragments of microwave devices, 2) such fragments with smooth boundaries that are approximated by stepped surfaces [1, Orlov Electr Letters], and 3). the complex multilayer ceramic electronic circuits that have to be investigated at very high frequencies from point of view internal electromagnetic interaction and so on.

Consider the step junction of P different waveguides (numbered as p = "1", "2" ..."P ") with the "main "0"-waveguide.

It is supposed that cross-sections of all of P small waveguides are placed within the cross-section of the main waveguide. In the opposite case we may introduce an intermediate virtual waveguide of zero-length. A rectangular waveguide, the cross-section of which is formed by four "extreme" lines among all of cross-sections, including the "main " waveguide, is the most advantageous to play this role as its mode basis is the simplest one. After that the problem may be reduced to the calculation of two corresponding step junctions *S*-matrixes and using the well known generalized *S*-matrixes technique (GSMT).

The problem of *S*-matrix calculation for a junction being considered is reduced to two ones: search of WG's eigen-spectrums and the calculation of the matrix of coupling coefficients. Applying the Transverse Resonance Method (TRM) [2, 3] to find the set of eigen-frequencies and eigen modes we obtain the eigen-fields that is specified by the series of Fourier coefficients for each of sub-regions of WG cross-section (Fig. 1). It forces the definite way of describing the configurations of WGs that are joined. These configurations are naturally broken into the set of sub-regions in the form of rectangles. Let us number these rectangles for the "p"-waveguide cross-section from $j(p)=0$ up to $j(p)=J(p)$. In this manner the cross-section of "p"-waveguide may be specified completely by the matrix $\mathbf{G}_p = \{ G[j(p),k] \}_{j(p)=0,\,k=0}^{J(p),\;3}$, where

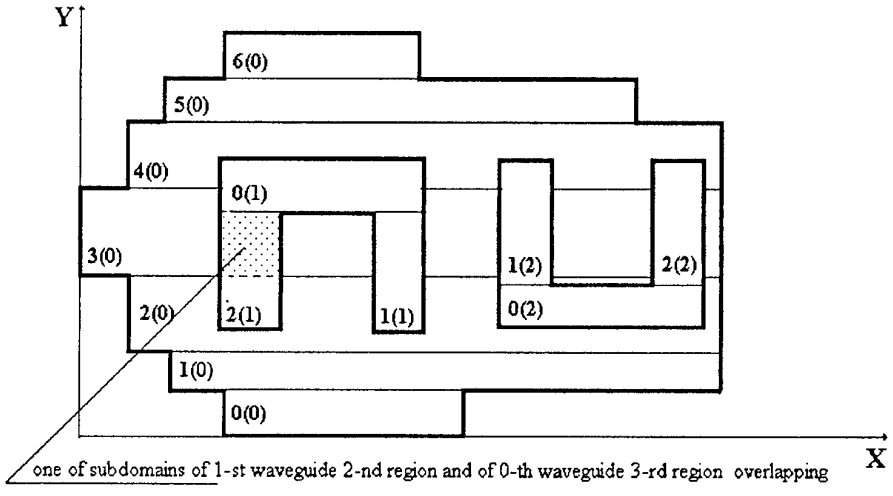


Fig. 1. Step junction of waveguides with piecewise linear boundaries and partitioning their cross-sections into the sets of rectangles

$$\mathbf{G}_p[j,0] = x^{(j(p))},$$

$$\mathbf{G}_p[j,1] = a^{(j(p))},$$

$$\mathbf{G}_p[j,2] = y^{(j(p))},$$

$$\mathbf{G}_p[j,3] = h^{(j(p))}$$

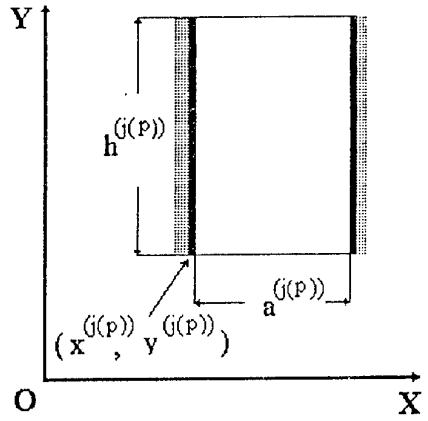


Fig. 2. Partial sub-region of "p"-waveguide cross-section and corresponding designations

The Herz potential functions $\varphi_{hn}(x,y)$ and $\varphi_{en}(x,y)$ in "j"-region of "p"-waveguide cross-section are presented in the following form

$$\varphi_{h(e)n}(x,y) = \sum_{m=0}^{M^{(j(p))}} \begin{matrix}\cos\\ \sin\end{matrix}\left(\beta_m^{(j(p))}(x - x^{(j(p))}\right) \times$$

$$\left[A_{nm}^{(j(p))} e^{i\omega_{nm}^{(j(p))}(y - y^{(j(p))})} + \right.$$

$$\left. + B_{nm}^{(j(p))} e^{-i\omega_{nm}^{(j(p))}(y - (y^{(j(p))} + h^{(j(p))})}\right]$$

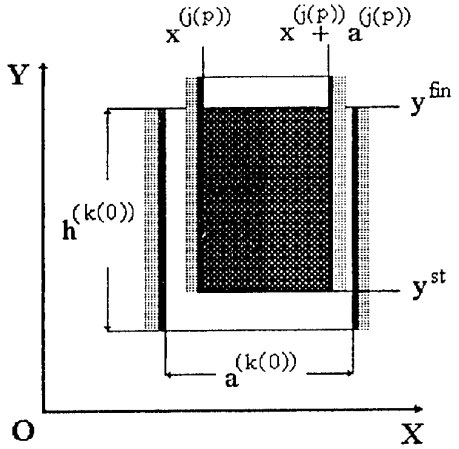


Fig. 3. Sub-domain of "p"- waveguide "j- region and "0"-waveguide $k(0)$-region overlapping

At using the mode matching method we have to calculate the set of coupling integrals $\mathbf{M}_{lq}$. As the eigen-fields of complicated waveguide modes are given by a piecewise manner, therefore the each coupling integral is reduced to the sum of partial integrals over the overlappings of "p"-waveguide sub-regions with "0"-waveguide sub-regions. As a consequence we obtain the following sum for each of coupling integrals

$$\mathbf{M}_{lq} = \sum_{k=0}^{J(0)} \sum_{j=0}^{J(p)} \int_{S^{(k(0))} \cap S^{(j(p))}} (....) dS = \sum_{k=0}^{J(0)} \sum_{j=0}^{J(p)} \mathbf{M}_{lq}(k,j)$$

where $S^{(j(p))}$ is the cross-section of "j"-sub-region of "p"-waveguide. In fact the sum contains only the integrals over some overlappings of corresponding sub-regions. In its turn the set of their geometry's may be specified by the "overlapping-matrix" $\mathbf{OL}_p$ that sets the coordinates of all sub-domains of overlappings: (see Fig. 3)

$$\mathbf{OL}_p = \mathbf{OL}_p[0 \le \nu \le (J(0)\,J(p) - 1),\ 0 \le \mu \le 5]$$

where

$$\mathbf{OL}_p[\nu,0] = x^{(j(p))},$$

$$\mathbf{OL}_p[\nu,1] = a(j(p)),$$

$$\mathbf{OL}_p[\nu,2] = y^{st},$$

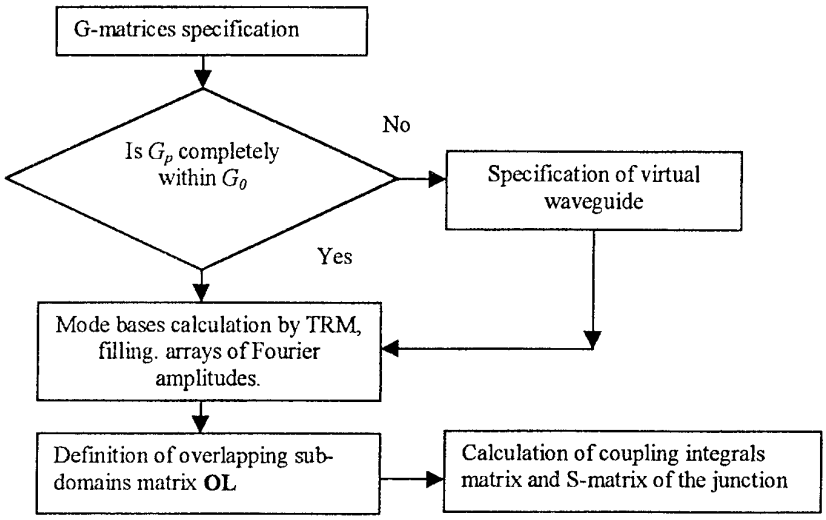
$$\mathbf{OL}_p[\nu,3] = y^{fin},$$

$$\mathbf{OL}_p[\nu,4] = j(0),$$

$$\mathbf{OL}_p[\nu,5] = j(p).$$

After specification of $\mathbf{G}_p$-matrixes for "0"- and all "p" waveguides $\mathbf{OL}_p$ matrixes may be found by a special algorithm that verifies simultaneously the type of junction and the necessity of above-mentioned virtual waveguide. Let us introduce the following set of designations for the sets of Fourier-amplitudes of field expansions within separate sub-regions : $\mathbf{A}_q^{(j)} = \{A_{qm}^{(j)}\}_{m=1(0)}^{M^{(j)}}$, $\mathbf{B}_q^{(j)} = \{B_q^{(j)}\}_{m=1(0)}^{M^{(j)}}$ and for the transversal and longitudinal propagation constants in these sub-regions $\beta^{(j)} = diag\{\beta_m^{(j)}\}_{m=1(0)}^{M^{(j)}}$, $\omega_q^{(j)} = diag\{\omega_{qm}^{(j)}\}_{m=1(0)}^{M^{(j)}}$, where $\beta_m^{(j)} = m\pi / a^{(j)}$ and $\omega_{qm}^{(j)} = \left(\chi_q^2 - \beta_m^{(j)2}\right)^{1/2}$. Introduce also the designation

$$\mathbf{CE}_{aa}^{(k,j)} = \{cc_{nm}^{(k,j)} e_{nm}^{(k,j)}(aa)\}_{n=1(0),m=1(0)}^{M^{(k)},M^{(j)}},$$



$$\mathbf{CE}_{ab}^{(k,j)} = \{cc_{nm}^{(k,j)} e_{nm}^{(k,j)}(ab)\}_{n=1(0),m=1(0)}^{M^{(k)},M^{(j)}},$$

$$\mathbf{SE}_{aa}^{(k,j)} = \{ss_{nm}^{(k,j)} e_{nm}^{(k,j)}(aa)\}_{n=1(0),m=1(0)}^{M^{(k)},M^{(j)}},$$

$$\mathbf{SE}_{ab}^{(k,j)} = \{ss_{nm}^{(k,j)} e_{nm}^{(k,j)}(ab)\}_{n=1(0),m=1(0)}^{M^{(k)},M^{(j)}}$$

for matrixes of expansion functions integrals on overlapping sub-region, where for example

$$cc_{nm}^{(k,j)} e_{\cdots}(ab) = \int_{x^{(j)},y^{st}}^{x^{(j)}+a^{(j)},y^{fin}} \cos(x - x^{(k(0))})\cos(x - x^{(j(p))}) \times$$
$$\exp(i(\omega_n^{(k)}(y - y^{(k)}) - \omega_m^{(j)}(y - y^{(j)} - h^{(j)}))ds$$

As the result the coupling integrals on a n overlapping sub-domain obtain the following form

$$\mathbf{M}_{lq}^{ee}(k,j) = \mathbf{A}_l^{(k)}\beta^{(k)} \times$$
$$\times \left\{C\mathbf{E}_{aa}^{(k,j)}\beta^{(j)}\mathbf{A}_q^{(j)} + C\mathbf{E}_{ab}^{(k,j)}\beta^{(j)}\mathbf{B}_q^{(j)}\right\} +$$
$$+ \mathbf{B}_l^{(k)}\beta^{(k)}\left\{C\mathbf{E}_{ba}^{(k,j)}\beta^{(j)}\mathbf{A}_q^{(j)} + C\mathbf{E}_{bb}^{(k,j)}\beta^{(j)}\mathbf{B}_q^{(j)}\right\} +$$
$$+ i\mathbf{A}_l^{(k)}\omega_l^{(k)}\left\{S\mathbf{E}_{aa}^{(k,j)}\omega_q^{(j)}\mathbf{A}_q^{(j)} - iS\mathbf{E}_{ab}^{(k,j)}\omega_q^{(j)}\mathbf{B}_q^{(j)}\right\} -$$
$$- i\mathbf{B}_l^{(k)}\omega_l^{(k)}\left\{S\mathbf{E}_{ba}^{(k,j)}\omega_q^{(j)}\mathbf{A}_q^{(j)} - iS\mathbf{E}_{bb}^{(k,j)}\omega_q^{(j)}\mathbf{B}_q^{(j)}\right\}$$

with similar expressions for $\mathbf{M}_{lq}^{hh}(k,j)$, $\mathbf{M}_{lq}^{he}(k,j), \mathbf{M}_{lq}^{eh}(k,j)$. Thus we have got the fully formalized relatively simple algorithm of *S*-matrix calculation for the junction of several waveguides with arbitrary piecewise linear coordinate boundaries. Its flowchart is shown above.

REFERENCES

1. A. A. Kirilenko, M.V.Orlov, V.I.Tkachenko, 'Stepped model of smooth irregularities corrected for location of equivalent reflection surface', Electronics letters, 1993, Vol.29, No. 25, pp. 2180-2181.
2. J. Borneman, 'Scaterring-type transverse resonance technique for the calculation of M(MIC) transmission line characteristics', 1991, MTT-39, pp.2083-2088.
3. Zhewang Ma, Eikichi Yamashita, Shanjia Xu, 'Transverse scattering matrix formulation for a class of waveguide eigenvalue problems', IEEE Trans., 1993, Vol. 41, No. 6/7, pp. 1044-1051.

BANDPASS AND LOWPASS FILTERS ON RIDGED WAVEGUIDE SECTIONS

A. A. Kirilenko, D. Yu. Kulik, L. A. Rud', and V. I. Tkachenko

Institute of Radiophysics and Electronics of the National Academy of Sciences of Ukraine
12 Acad. Proskura St., Kharkov, 310085, Ukraine
Tel. +38-0572-448518, Fax +38-0572-44105, E-mail: kirilenko@ire.kharkov.ua

Some aspects of designing lowpass and bandpass evanescent-mode filters based on single- and double-ridged waveguides are discussed. It is demonstrated that introduction the new type of transformers allows to obtain the lowpass filter configuration providing wide pass and stop bands. The improved procedure of initial synthesis of bandpass filters permits to obtain their geometry for pass bands up to 20 % and extended stop band.

INTRODUCTION

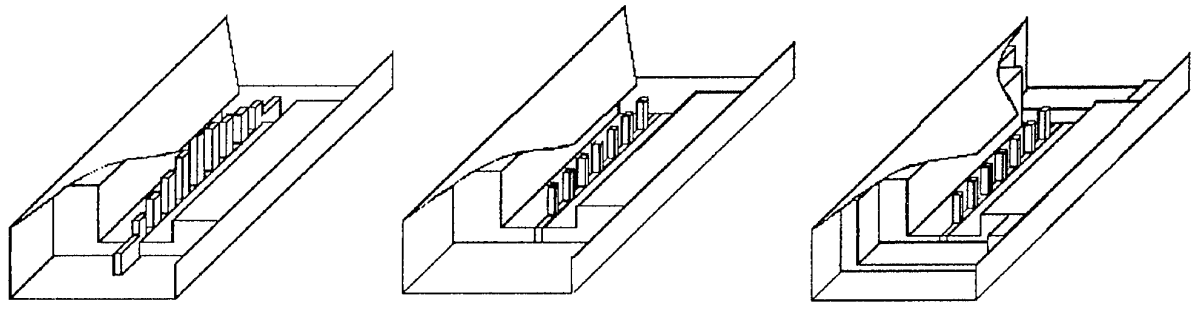
The design of evanescent-mode filters based on finned waveguides and printed-circuit technologies [1] and ridged waveguides with relatively wide ridges [2–4] has been discussed before. Nevertheless the development of CAD software, that provides the design and the optimization of filter geometry at a broad specification range, revealed some additional aspects of such a problem and the necessity to include new structural elements for provision of a wider range of possible specifications. The configurations of the filters being considered are presented in Fig. 1. They are sets of fins with varying gaps for lowpass filters (LPF) and a fixed gap for bandpass filters (BPF). In both cases the matching transformers in the form of sections of finned or rectangular (upper cutoff) waveguides can be used. Here matching transformers are not conventional transitions between rectangular and finned waveguides and simultaneously play the role of ended K-invertors LPF or BPF.

The exact full-wave mode-matching models are used for obtaining S-matrices of key elements. Analysis of separate parts of filters (as K-invertor scheme components) as well as analysis of filters as a whole is performed by the generalized S-matrix technique. Without emphasizing the details, note that the transversal resonance method was used at the calculation of ridged waveguide mode basis. Required S-matrices of bifurcation of plane waveguide by semiplate of finite thickness were calculated on the basis of moments method using basis functions that take into account the field behavior near the fin edges.

Two possible realizations for single- and double-ridged waveguides have been considered. In all cases the design algorithm has three stages: a). Definition of values of fin gaps and filter housing. b). Initial filter synthesis on the base of K-invertor lowpass prototypes according to Levy's scheme for LPF case and to Rhodes's scheme for BPF one. Possible correction of prototype K-invertors. c). Optimization of the filter geometry.

LOWPASS FILTERS

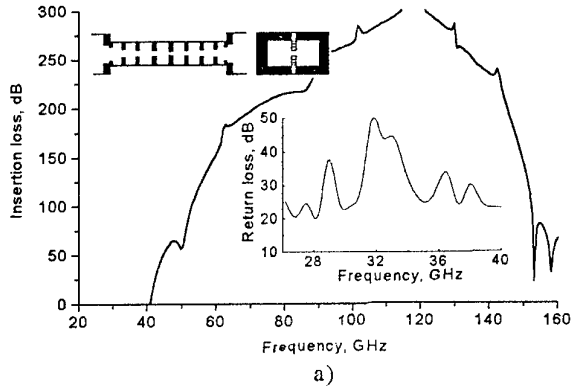
Search of ridged waveguide housing is done according to the given values of ridge thickness t, minimal gap size $w_{\min}$ for the central section, the specified frequencies of pass band beginning F_b and stop band edge F_s. The selection of width a_r and height b_r of ridged waveguide housing is based on two requirements [2]: 1) the cutoff frequency of dominant mode for the ridged waveguide with the specified minimal gap $w_{\min}$ must be below F_b ; 2) the next higher cutoff must be above the stop band upper limit F_s. The procedure of a_r and



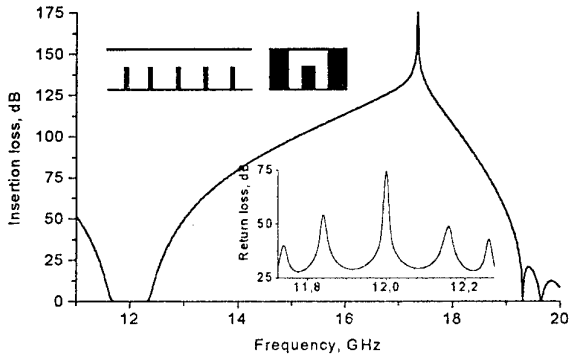
a *b* *c*

Fig. 1. Lowpass (a) and bandpass (b,c) evanescent-mode filters on single-ridged waveguides

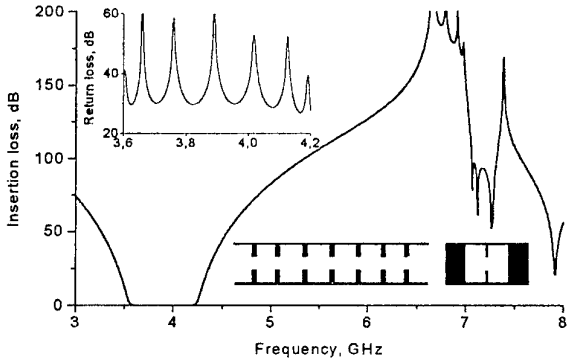
b_r definition is performed with the aid of preliminary calculated database. At that, the geometry with maximal a_r is considered as the best one.



a)



b)



c)

Fig. 2. Frequency responses for the optimized filters: 11-section LPF on double-ridge waveguide (a), 5-section BPF on single-ridged waveguide (b) and 7-section BPF on double-ridge waveguide (c)

The maximal gap size $w_{\max}$ is found reasoning from the requirements that the ridged waveguide with dimensions a_r, b_r, t, and $w = w_{\max}$ must be above cutoff within pass band. The waveguide sections forming notches between filter sections must be cutoff ones through the whole pass band however they should not be cutoff through the whole stop band. Rectangular cross-section notches provide simultaneously two advantages, shortening the total filter length and simplifying the calculations.

Notches model the internal K-invertors of lowpass prototype. The ended K-invertors have usually greater values than the internal ones, as they play a matching role. In the majority of cases the value of reflection coefficient for a junction between the main rectangular waveguide and the ridged waveguide of the first (last) filter section is too large. It has to be reduced by implementing an additional matching section of ridged waveguide with the cross-section of main rectangular waveguide. The search of transformer dimensions is performed by two steps: 1) the first global minimum of reflection coefficient within the range $w_{\max} \le w_{tr} \le b_r$ and different lengths $l_{tr} \ge 0$ is roughly defined; 2) the final dimensions are being found by exact estimation of l_{tr} to provide the required K-invertor value at the maximum possible transformer gap.

More often than not, the characteristics obtained after the synthesis, based on the circuit theory, are not completely satisfactory mainly within the stop band. To reach the specified response, the initial geometry is optimized on the base of full-wave exact model and the goal function that differs from conventional by taking into account some points on the slope of frequency response to avoid undesirable spikes of insertion loss.

As an example of the created software possibilities, the characteristics of the double-ridged lowpass filter with wide pass and rejection bands are presented in Fig. 2a. The filter has upper than 20 dB return loss within operating band of WR-28 and stop band up to 150 GHz.. It should be noted that other topologies, in particular based on single-ridged waveguides (see Fig. 1*a*), are suitable only for the design of lowpass filters with the narrower pass and stop bands. It happens first of all in consequence of the excitation of additional higher modes in single-ridge waveguide.

BANDPASS FILTERS

The peculiarity of the design of the filters being considered is born by capacitive character of filter section loads that is why the resonator length l may be chosen essentially less than $\lambda_g/2$. It is clear that at this condition the conventional procedures of circuit theory synthesis, that are oriented to $\lambda_g/2$ (K-prototype) or $\lambda_g/4$ (K-J prototype) resonators, will led to filter sections with too low Q-factors. The correction of K-invertor prototype is performed under the condition that Q-factor of shortened resonator must be equal to the one of $\lambda_g/2$ resonator. This correction ensures acceptable initial guess for the final optimization procedure

even though the filter pass band obtained by this manner turns out narrower than it is required.

As a rule the needed result can be reached at square ridge housing with a side size equals to the height of main waveguide and ridge gap providing the cutoff frequency near the one of input waveguide. However it is not always possible to obtain acceptable fin lengths at such a housing. In this case one has to reduce housing cross-section or increase ridge gap.

In Fig. 2b the example of designing the narrow-band filter in waveguide WR-75 (housing 9.525×9.525 mm^2, ridge thickness 3 mm, overall filter length ~51 mm) is presented. The broad-band filter in waveguide WR-229 (housing 32×29.083 mm^2, ridge thickness 1 mm, overall filter length ~160 mm) is illustrated by Fig. 2c. As it turned out the stop band is limited by the half-wavelength resonances in long notches when filter housing becomes upper cutoff.

The software is realized with Visual C++ tools as Windows (NT, 95, 98) application. The CPU time needed for synthesis and optimization of 5-resonator BPF equals about 1.5 hours with Pentium II-366.

REFERENCES

1. J. Bornemann, F. Arndt, "Modal *S*-matrix design of metal finned waveguide components and its application to transformers and filters", IEEE Trans. on MTT, Vol. 40, No. 7, pp. 1528-1537, 1992.
2. W. Chappel, "Waveguide low pass filter using evanescent mode inductors", Microwave Journal, Vol. 21, No. 12, pp.71-72, 1978.
3. C. Nanan, J. W. Tao, H. Baudrandt, B. Theron, and S. Vigneron, "A two-step synthesis of broadband ridged waveguide bandpass filters with improved performances", IEEE Trans. on MTT, Vol. 39, No. 12, pp. 2192-2197, 1991.
4. C. Husse, J. Herren, J. Cayrou, B. Cogo, J. Cazaux, and B. Theron, "Miniature tuningless filters for telecommunication active antennas applications", In EuMC-28 Conf. Proc., Vol. 2, pp.215-219, 1998.

ONE- AND TWO STOPBAND REJECTION SECTIONS BASED ON MULTIPLE RECTANGULAR APERTURE IRISES

A. A. Kirilenko, L. P. Mos'pan

Institute of Radiophysics and Electronics of the National Academy of Science. of Ukraine
Ulitsa Ac. Proskury, 12, Kharkov, 310085, Ukraine
phone 380(572)448-428, fax: 380(572)441-105, e-mail lyuda@ire.kharkov.ua

Multiple aperture rectangular irises are attractive for the scientists owing to their salient feature to form frequency response with clear total reflection resonance (rejection resonance). A difference of the dimensions of the iris apertures is the condition of the resonance. The simplest two aperture iris forms the frequency response with two resonances of total transmission and one resonance of total reflection, located between them. Numerical studies, carried by us on the base of solving appropriate diffraction problem, show that upper frequency resonance is defined by the slot with lesser width, whereas the resonance at the lower frequency is defined by the slot with larger width. Three aperture iris, cross-section of which contains a pair of equal slots and the other slot of different dimensions has similar frequency response. An influence of changing the geometry of the slots on the frequency response character was studied by us. All the numerical calculations were carried out in the frequency range, corresponding the operating range of the circuit, in which an iris was placed. Fig. 1 shows schematically the constant value plots for the reflection coefficient $|R|$ of the circuit dominant H_{10}-mode for three aperture iris placed in the waveguide WR-90 in the coordinates "frequency versus width of the slots being changed". The iris thickness is 0.38 mm. height of upper and bottom slots is 2.52 mm; their width is changed from 7 mm to 22 mm; dimensions of the central slot are 14.86×1.52 mm^2. From the figure we notice that a changing the ratio between the slot widths leads to a changing of location and quality factor of the rejection resonance. There is only one resonance of total transmission at the frequency response if dimensions of all the slots are equal.

Computational results show that as more as possible height of the slots is preferable from both the manufacturing point of view and loss level outside the stopband. So, three or more aperture irises is more preferable than two aperture ones.

As computational results shown that the rejection resonance, forming by multiple aperture irises, is defined by the ratio between slot dimensions, we carried out a number of numerical studies in order to make clear the assumption that multiple aperture irises can form a frequency responses with more than one rejection resonance. Three aperture iris, cross-section of which contained three different slots was chosen for such studies. There are two rejection resonances at the frequency response of such an iris, as predicted. Studies of the influence of changing the geometry of the slots on the frequency response were carried out. Some results of them are presented in Fig. 2. Fig. 2 shows schematically the plots for the reflection coefficient of circuit dominant H_{10}-mode for three aperture iris placed in the waveguide WR-90 in the coordinates "frequency versus width of the slots being changed". The iris thickness is 0.38 mm. height of the upper and the bottom slots is 2 mm; height of the central slot is 1 mm. The width of the upper slot is changed from 7 mm to 22 mm whereas dimensions of the central slot are constant. It turns out that the influence of changing the slot geometry on the frequency response has the same character with respect to one for the irises forming one stopband frequency response, namely a changing the ratio between slot widths leads to changing the location and quality factor of the rejection resonances. We also note that changing the height of the slots leads to steeper frontiers of the rejection resonances. Results of the studies allows to conclude that the frequency response with two rejection renounces and more can be obtained by using multiple aperture irises with a number of slots of different geometry.

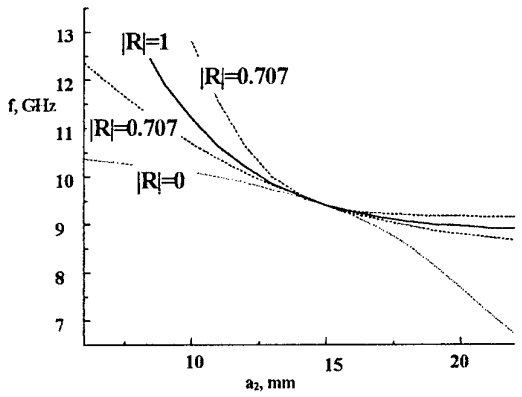


Fig. 1. Plots $|R|$ = const for three aperture iris with single stopband

A scheme of searching an approximate geometry of rejection cells based on multiple aperture irises, that use a specific character of rejection resonance nature, was proposed by us by the results of the studies carried out [1].

In order to verify the validity of our conclusions and to estimate the accuracy of obtained results a number of experimental measurements was carried out for three aperture irises, approximate geometry of which was obtained by the help of above-mentioned scheme. Fig. 3 presents calculated and experimental frequency response of three-aperture iris placed in WR-90 waveguide. Cross-section of the iris contains three horizontal rectangular slots, two of which were cut immediately adjacent to the upper and the bottom walls of the rectangular waveguide. Their dimensions are 14.91×2 mm^2. The third aperture was cut in the center of the circuit. Its dimensions are 12.94×2 mm^2. Iris thickness was 0.48 mm. Such an iris forms the rejection resonance at the frequency of 10.38 GHz. Transmission loss at its resonant frequency are -26 dB. The difference between calculated and measured data is 0.3 % and 8 % for the rejection frequency and its quality factor, respectively. The error for the bandwidth is explained by ideal theoretical model, in which the Ohmic loss are not taking into account. As "frequency error", it can be explained by relatively low quality of iris manufacturing. It should be noted that the left frontier of the rejection resonance is very steep and there is sufficiently even portion of the response, where transmission loss are close to zero, from the left side of the resonance. Probably, such a three aperture iris can be used not only as a rejection cell, locking the circuit in rejection stopband, and in order to improve filter response it can be used as additional rejection section of a low pass filter with a passband in above mentioned low loss frequency range.

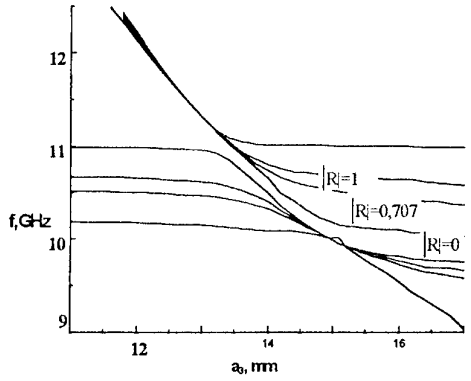


Fig. 2. Plots $|R|$ = const for three aperture iris with two stopbands

In order to verify our suggestions concerning a possibility to form multi stopband frequency response, demonstrative experiment with three different aperture iris in WR-90 waveguide was performed. Cross-section of the iris contains three different slots, two of which were cut immediately adjacent to the upper and the bottom walls of the rectangular waveguide. Their dimensions are 14.2×3 mm^2 and 15.2×3 mm^2. The third aperture was cut in the center of the circuit. Its dimensions are 13.1×1 mm^2. Iris thickness is 0.48 mm. Measured frequency response is presented in Fig. 4. As predicted, frequency response contains two rejection resonances at the frequencies of 8.93 GHz and 10.8 GHz. Transmission loss at the resonant frequencies are -13 dB and -16 dB, respectively. Stopband widths are 0.25 % and 0.6 % respectively. In contrast to single stopband rejection irises, a mechanism of the control of such multi stopband frequency responses is revealed not completely. However it is obviously that two stopband rejection irises with improved characteristics can be calculated and manufactured.

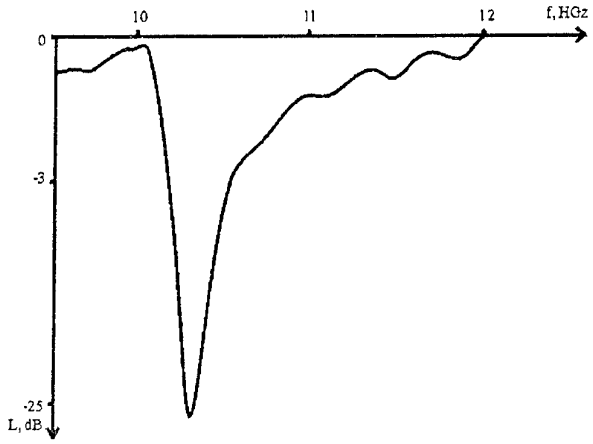


Fig. 3. Measured transmission loss of one stopband three aperture iris

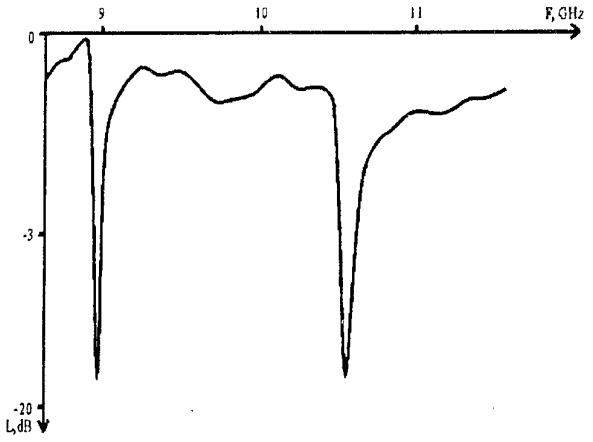


Fig. 4. Measured transmission loss of two stopband three aperture iris

Above mentioned one- and two stopband rejection cells can find an application both as separate frequency selective units and as additional elements of low pass filters, bandpass and bandstop filters. They will improve filter frequency response. An idea concerning to use such additional elements in filter was realized by

T. Sieverding and F. Arndt [2]. In this work the results of computational design of the bandpass filter with additional resonators placed on upper wall of the waveguide circuit and coupled with it by rectangular irises were presented. If two stopband rejection irises are used as such additional sections, the filter has less both transversal and longitudinal dimensions. Besides, such multiple aperture irises are very simple in manufacturing and low cost.

The author wish to acknowledge E. A. Sverdlenko for the help while carrying out the measurements.

REFERENCES

1. L. P. Mos'pan Numerical and analytical algorithm for the disign of rejection filters based on multiple aperture irises//Vesnik dnepropetrovskogo universiteta. Fizika, radioelektronika. [in Russian] N4.-1998.-pp.133-139.

2. T. Sieverding, F. Arndt Field theoretic CAD of open or aperture matched T-junction coupled rectangular waveguide structures// IEEE Trans. on MTT.-v. 40, N2.-1992.-pp.33-1992.

PORT REFLECTIVITY METHOD IN THE THEORY OF TEES WITH IRIS INSERTS

D. Y. Kulik

Institute of Radiophysics and Electronics of National Academy of Sciences,
12 Proscura St., Kharkov, 310085, Ukraine
Fax: 38-(0572)-441-105, e-mail: sem@ire.kharkov.ua

The problem of calculation of tees in rectangular waveguides has been discussed a lot of times. Except of the main geometry of conventional *H(E)*-tee [1] the tees with inserts of different kinds have been studied [2]. At that the dominant goal of real calculations was to investigate the possibility of ideal matching at the excitation of tee side arm. However there is another problem of tee tuning that arises at the frequency selective systems design. For example one of different schemes of dilplexer design is based on using so called *Y*-type three-ports. Such a three-port has to characterize by the *S*-matrix that is similar to *S*-matrix of symmetrical 120° *Y*-junction. To use an *E*- or *H*-tee as a common junction of diplexer we have firstly to design a special load in tee that equalizes the reflectivities in common port and in channel ports. It may be achieved for example by introducing the capacitive iris in the side tee arm [3]. However this way is not the best one, as such a unit usually has relatively high dispersion and is not available for broadband diplexers.

Another way consists in implementation of a tuning insert into internal tee region, that may be very convenient if an insert and the filter diaphragms are made by the same manner. In this report the iris inserts in *H*-tees are considered from point of view of the way of *S*-matrix calculation and possible properties corresponding tees as the common junctions of microwave diplexers.

The configurations that will be discussed are shown in Fig. 1. Taking into account that in the majority of cases the only dominant mode is propagating in common diplexer arm and the full-wave *S*-matrixes have to be found regarding the channel arms we have chosen the Port Reflectivity Method (PRM) [4] that make possible quick manipulation with different waveguide electromagnetic objects.

The main idea of PRM is the treatment of three-port networks through the triple consideration of two-ports, forming by shortening of one of the three-port arms. It reduces the problem of calculation of three-port *S*-matrix to relatively simpler multiply problems of a two-port. The latter may be considered as the sequence of plane junctions, the *S*-matrixes of which is calculated by *S*-matrix technique and for example by mode-matching method.

The configuration of *H*-tee with rectangular metal insert is shown in Fig. 1.

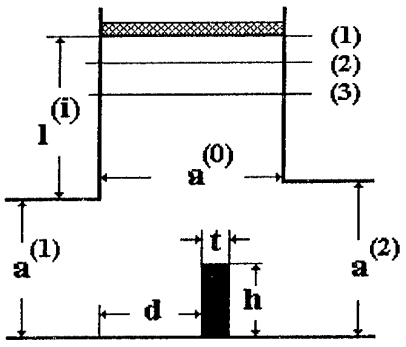


Fig. 1 Geometry of *H*-tee with rectangular metal insert

Below is used the following designations:

$\mathbf{S}^{\alpha\beta}$ are blocks of three-port scattering matrix; $\alpha,\beta = 0, 1, 2$.

$\mathbf{S}_j^{\mu\nu}$ are blocks of two-port scattering matrix for the j-th position of shortening; $\nu, \mu = 1, 2$ ($j = 1, 2, 3$).

$r(j) = -\exp\left(-2i\zeta_1^{(0)} l_j\right)$ is inverse value of reflectivity for shortening placed in 0-th waveguide at distance l_j $(l_1 < l_2 < l_3)$ from three-port reference plane; $\zeta_1^{(0)}$ is propagation constant of dominant mode in the 0-th waveguide. Then we have two possibilities: on the one hand, such a waveguide may be exactly calculated with the help of full-wave model for three different values of shortening position and on the other we may write a set of relations between three-port and two-port *S*-matrixes assuming only single-mode electromagnetic interaction between the shortening and the mouth of 0-tee arm. As three-port *S*-matrix coefficients have been previously calculated we obtain

$$S_{11}^{00} = \left(r(1)-r(2)\right)W^{11}(3\,1) - \left(r(1)-r(3)\right)W^{11}(2\,1) /$$
$$/\left(r(1)-r(3)\right)\left(R^{11}(1)-R^{11}(2)\right) - \left(r(1)-r(2)\right)\left(R^{11}(1)-R^{11}(3)\right) =$$
$$= \mathbf{A}/\mathbf{B} = \{a_{ik} \; / b_{ik}\}_{i,k=1}^{N}$$

where

$$\mathbf{W}^{\alpha\beta}(ij) = r(i)\,\mathbf{S}_{\div}^{\alpha\beta}(i) - r(j)\,\mathbf{S}_{\div}^{\alpha\beta}(j)$$
$$i, j = 1,2,3;\; i \neq j;\; \alpha,\beta = 1,2$$

The meaning of above expression is that the calculated value of S_{11}^{00} must be equal for all i and k. If it is not

then we have to place the shortenings further from three-port 0-th reference plane, as actual law of response dependence on shortening placements is not such for taking into account the dominant mode only. This reasoning is useful for internal control of calculation accuracy: comparing values of S_{11}^{00} at different i and k we may provide correct choosing of shortening's positions. For the rest of coefficient we have, for example,

$$\mathbf{S}^{11} = (r(1)-r(2))^{-1}\left(S_{11}^{00}\left(\mathbf{R}^{11}(2)-\mathbf{R}^{11}(1)\right)-\mathbf{W}^{11}(21)\right)$$

$$\mathbf{S}^{21} = (r(1)-r(2))^{-1}\left(S_{11}^{00}\left(\mathbf{T}^{21}(2)-\mathbf{T}^{21}(1)\right)-\mathbf{W}^{21}(21)\right)$$

As to transmission matrixes between the 0-th and the 1-st port (relative the dominant mode in the 0-th port only!) they may be found from

$$\mathbf{S}^{10}\mathbf{S}^{01} = \left(r(1)-S_{11}^{00}\right)\left(\mathbf{R}^{11}(1)-\mathbf{S}^{11}\right) = \mathbf{Q}^{11}$$

Using this expression one can find the elements of "0-to-1" and "1-to-0" transmission matrixes to common sign before matrixes.

As reciprocity relation $\mu^{(1)}\Gamma_1^{(1)}S_{11}^{10} = \mu^{(0)}\Gamma_1^{(0)}S_{11}^{01}$ takes a place we have

$$S_{11}^{01} = \pm\sqrt{\frac{\mu^{(1)}\Gamma_1^{(1)}}{\mu^{(0)}\Gamma_1^{(0)}}Q_{11}^{11}}\ ;$$

and consequently $S_{i1}^{10} = \dfrac{Q_{i1}^{11}}{S_{11}^{01}}$, i=1,2,...; $S_{1j}^{01} = \dfrac{Q_{1j}^{11}}{S_{11}^{10}}$, j=2, 3, ...

The frequency responses for tees without tuning irises that have been calculated by exact model [1] and for tees with an insert being created with using tools of [5] have been compared for the created algorithm testing. The role of initial two-port has played corresponding H-plane widening of WR-75 waveguide. In Fig. 2 the reflectivity response of an H-tee at the excitation from side arm and the difference between two solutions (scale axis is placed on right) are presented.

As one can see the solutions coincide all over operating range (absolute difference of reflectivity is not worse than $\pm 10^{-4} \div 10^{-5}$). At moving to the single mode range end (but out of operating range) diversification of conditions that are background of PRM becomes. On one hand the reactive attenuation of H_{20} mode within side arm is decreasing essentially and on the other hand the level of this mode excitation is increasing. It is caused by the features of H-tee having the resonance at the end of single-mode range.

The created model allows setting that a thin tuning inductive iris is similar to filter irises and can solve radically the problem of creating Y-type common

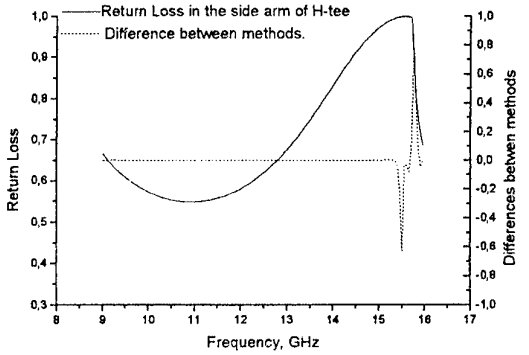


Fig. 2 Difference between two methods of calculation of H-tee junction

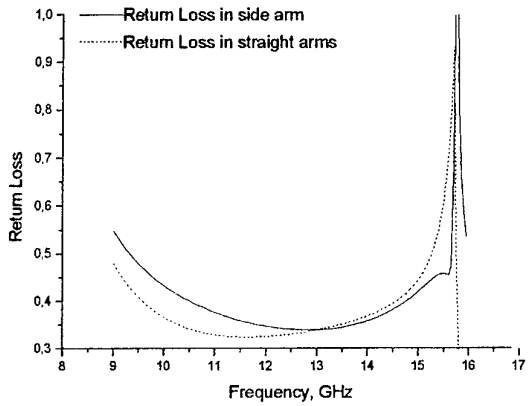


Fig.3 Return loss in common junction's arms

junction on H-tee. Reflectivities in straight and side arms are presented in Fig.3 for the common junction being designed at the frequency 13.01 GHz with the condition $\min\left|S_{11}^{00}-S_{11}^{11}\right| \,\&\, \min\left|S_{11}^{00}\right|$. As one can see this condition is satisfied not only at the given point, but within all over operating range practically.

REFERENCES

1. Rud' L.A., Wave diffraction on H-plane tee-junction of rectangular waveguides, Radiotechnica and electronica, v. 29, No. 9, pp. 1711-1719, 1984 (in Russian).
2. Kirilenko A.A., Onufrienko L.M., Chumachenko V.P., Matching of H-plane tee by metal strip, in "Radiophysics and electronics of mm and submm waves", IRE NANU, Kharkov, 1988, pp. 89-84. [in Russian].
3. Kirilenko A.A., Tkachenko V.I., Rud' L.A., Design of E-tee diplexers having closely spaced frequency channels in the upper band of operating range, Proc. of 12-th Int. Conf. on Microwaves and Radars (MICON-98), Krakov, Poland, 1998, v.1, pp. 23-26.
4. Z.Ma, E. Yamashita, Port reflectivity method for solving multiport microwave network problems, IEEE Trans. on MTT, v. 43, No. 2, 1995, pp. 331-337.
5. A.A. Kirilenko, V.I. Tkachenko, System of electromagnetic simulation for microwave devices. Izvestija vuzov, Radioelektronika, 1996, v. 39, No. 9, pp. 17-28 [in Russian].

FDTD ANALYSIS OF METAL PLATES IN RECTANGULAR WAVEGUIDE

A. M. Kupriy, S. E. Martynyuk

National Technical University of Ukraine "KPI", Laboratory of Antennas and Telecommunications,
2110D, Radio Engineering Faculty, Polytekhnichna st., 12, Kyiv, 252056, Ukraine
Tel/Fax: 380-44-2417223

INTRODUCTION

Waveguide sections are now widely used both for commercial and military purposes. The trend of investigations in this field is to decrease the insertion loss and overall dimensions of microwave devices. But if high power of propagating waves is required (100W or more) it is impossible to use waveguide circuits based on the dielectric discontinuities or semiconductor active devices. In such a case the metal discontinuities (irises, plates, posts etc.) become alternatives. Metal plates are especially easy to manufacture and maintain into metal waveguide. The possibility of creation of phase shifters with excellent parameters on the base of such type of discontinuities was shown in [5].

This paper presents new results of FDTD analysis of such structures well described in [1–2]. Actually, it's hybrid method combining the implementation of impedance boundary conditions to standard FDTD technique with generalised scattering matrix modelling. This algorithm proves its efficiency for rigorous analysis of different types of complex waveguide discontinuities.

GEOMETRY MODELLING

Two types of waveguide structures based on rectangular symmetrical plates are analysed. They have similar construction but different geometry so their separate analysis is given here.

Waveguide section with four plates. It consists of four rectangular metal plates (Fig. 1, 2), each one is placed symmetrically in cross-section and fixed by thin metal shaft. The structure dimensions are a = 72 mm, b = 28 mm; the first and the third plates are equal 36×16.8 mm^2; the second and the fourth ones are also equal 36×17.1 mm^2; the diameter S of metal shaft is 1.5 mm. All geometry is subdivided into five parts and analysed separately to reduce memory requirements and computational time. As it seen from Fig. 2 all discontinuities are symmetrical in the respect to excitation ports. There are two pairs of identical plates. Part III is a simple hollow waveguide. Its general scattering matrix parameters are found analytically. So it is necessary to implement FDTD procedure only for parts I and II and then final general scattering matrix is defined from cascade connection of five discontinuities. This also gives the opportunity to avoid the analysing of standing waves in resonators (as a result, decrease the quantity of time steps).

FDTD procedure with impedance boundary conditions is used (value of characteristic impedance is 500Ω). All geometry is refined to the standard uniform Yee lattice [3]. During this simulation metal shafts of circular cross-section is substituted by rectangular one with the same overall dimensions in order to simplify the implementation of boundary conditions. Different parameters $\Delta x, \Delta y, \Delta z$ are chosen for each part for the finest geometry modelling. Courant-Friedrichs-Lewy type stability condition is used to define Δt parameter. The results of modal voltages in time domain [1] then converted to the frequency domain using discrete Fourier transform. Then the standard procedure [1] is followed to obtain the generalised scattering matrix parameters in the frequency band 2.8...3.3 GHz.

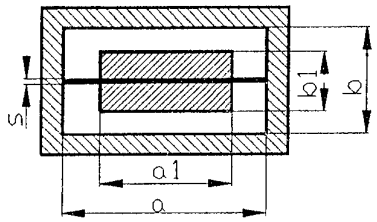


Fig. 1. Cross section with metal plate on a shaft

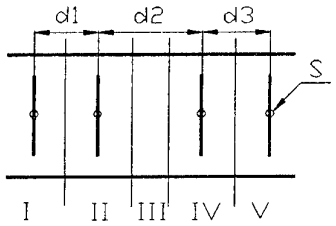


Fig. 2. Four metal plates along waveguide

Waveguide section with two plates. It consists of two equal rectangular metal plates placed symmetrically in rectangular waveguide with such parameters: a = 72 mm, b = 28 mm, $a1$ = 36 mm, $b1$ = 17.2 mm. All statements in geometry modelling are similar to waveguide section described above. In this case the only FDTD analysis for the single symmetric metal rectangular plate in waveguide is required.

NUMERICAL RESULTS AND MEASUREMENTS

For electromagnetic simulation of vertically located thin metal plate in waveguide cross section the method of moments (MOM) was used earlier. The plate was considered to be infinitely thin and without supported

metal shaft. The results obtained by FDTD method, MOM and experiment for the second structure are shown in Fig. 3, 5, and for the first on Fig. 4, 6 respectively. In fact, phase characteristics on Fig. 5, 6 are the differential phase shifts of given structures calculated with respect to the simple hollow waveguides of the same length as cross-section. Three waveguide modes TE_{10}, TE_{30}, TH_{12} were taken into account in hybrid FDTD analysis. However, taking first two modes are sufficient for both structures.

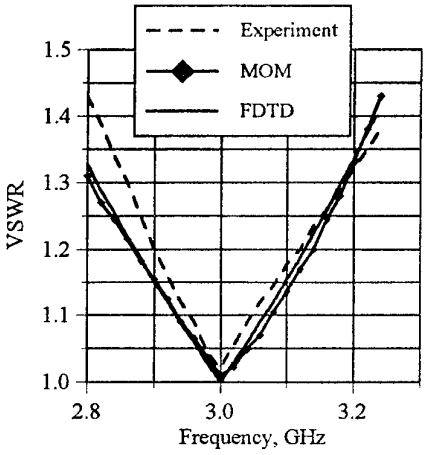


Fig. 3

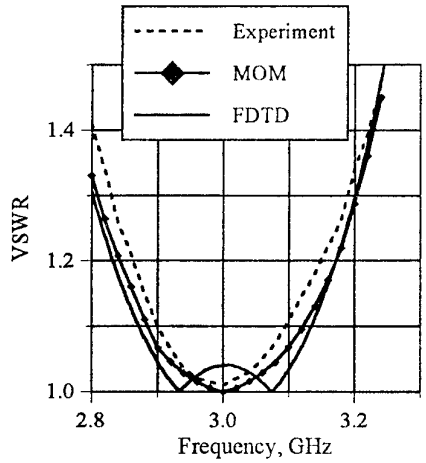


Fig. 4

As it seen from Fig. 3–6 good agreement was achieved between two methods and experimental results. Small errors occurred in FDTD methods because of geometry quantisation error and some principal differs between numerical and experimental models (sharp edges of rectangular plates in reality were rounded to increase the limited transmitting power). MOM gives the opportunity to calculate this structure much more quickly. No errors caused by discretisation occurred. But specific problems, such as convergence of series expansion of current on metal plates, arise. Also little change in geometry very frequently makes this method be tedious or even helpless. FDTD method requires much more computational efforts, but it can be used for accurate and versatile analysis of more complex structures.

Note, that further optimization of proposed structures is possible by searching the optimal form of plates in order to increase the frequency range and to reduce error of differential phase shift.

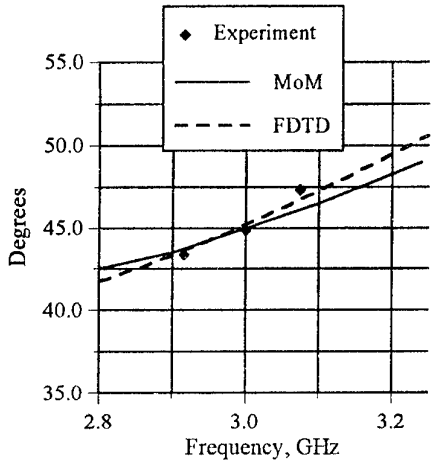


Fig. 5

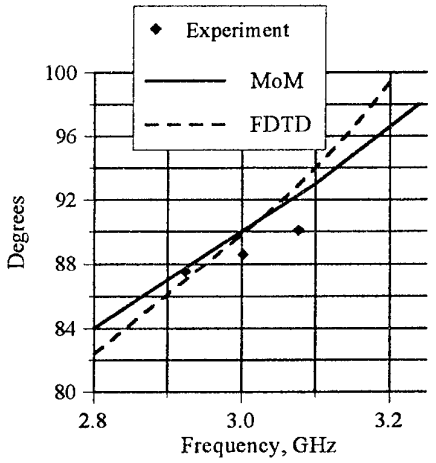


Fig. 6

REFERENCES

1. T. Shibata, T. Itoh. Generalized-Scattreing-Matrix-Modelling of Waveguide Circuits Using FDTD Simulations // IEEE Trans. on MTT, vol.46, No. 11,pp. 1742-1751, November 1988.
2. T. Shibata, Y. Qian, T. Itoh. An FDTD Imppedance Boundary Condition and It's Application to Waveguide Discontinuity Analyses // IEEE MTT-S Int. Microwave Symp. Dig., Denver, CO, June, 1997.
3. K. S. Yee. Numerical Solution of Initial Boundary Value Problems Involving Maxwell's Equations // IEEE Trans. on AP, Vol. AP-14, pp. 302-307, May 1966.
4. A. Taflove. Computational Electromagnetics, The Finite Diffrence Time Domain Method. Boston, MA: Artech House, 1995.
5. Kypriy A. M., Dubrovka F. F. A synthesis of microwave phase shifters based on reactive elements in waveguide // Izv. VUZov. Radioelectronika. -1982. -V. 25, No. 8.

HIGH-POWER MULTIPLEXER FOR AERIAL FEEDER OF TV AND RADIO BROADCASTING TRANSMITTERS

A. N. Lishchenko, A. A. Boryssenko

Scientific research company Diascarb, 253222, Kyiv, P.O. Box 370,
E-mail: diascarb@public.ua.net

ABSTRACT

Some ways of technical implementation of a high-power multiplexer for common operation of several broadcasting transmitters in the metric and decimetric waves band are considered. These transmitters pick up and carry a common aerial feeder that allows extending a net of TV and radio broadcasting by complete using opportunities of existing equipment. Engineering solutions proposed to build high-power multiplexers have been developed, designed, manufactured, tuned, tested in laboratory and under high-power operation mode. Some of those multiplexer are used now at TV and radio broadcasting centers in Ukraine since 1994.

INTRODUCTION

In the force of known economic reasons of the last times in Ukraine and some others countries of the former USSR, one of the most possible mean to extend a net of TV and radio broadcasting of the metric and decimetric waves band is complete capacity utilization of existing aerial feeder equipment by addition of new broadcasting channels.

To reach this goal, the corresponding additional devices, so-called, high-power (units and tens of kilowatts) multiplexer are necessary that demands special scientific and engineering approaches to fulfil principal technical and others requirements listed below:

1) providing with accurate requirements concerning terminal matching, insertion loss and inter-channel isolation;
2) taking into consideration electrical breakdown stability and thermal loads of device under high-power operation;
3) maintaining of non-complexity of manufacture and tuning;
4) ensuring of device easy installation, as well as, providing a serviceability of device due to its weight, overall dimensions etc.;

All operation conditions discussed above should be fulfilled rigorously during design procedures used that based on:

1) using of high-precise electrodynamics models of all components for their designing;
2) application of rigorous design procedures with model- prototypes for given approximations of amplitude-frequency responses etc.

The four designing variants of high-power multiplexer to provide operation of several broadcasting transmitters with common aerial feeder are considered here. All these devices have been developed, designed, manufactured and tuned, as well as, tested under high-power operation, and some of them are used at present at some Ukrainian broadcasting centers since 1994.

MULTIPLEXER BASED ON TWO 3 dB DIRECTIONAL COUPLERS

A multiplexer based on the two 3dB directional couplers provides summation of output powerful signals of two TV broadcasting transmitters of the decimeter waves band. This multiplexer was the first such device designing by authors that used since 1995 at the TV broadcasting center in Kryvoi Rog, Dnepropetrovsk region, Ukraine.

A designing aim was to obtain high-level technical performances of such multiplexer without necessity to apply any additional matching units connected to device terminals. A design of directional couplers implemented due to a coupled transmission lines concept has been accomplished by the known method [1]. After fabrication of the directional couplers, their laboratory adjustment and examination, a some correction of dimensions of coupled transmission line has been accomplished.

I order to access an inter-channel isolation that should be no less than 40 dB, the band-stop filters have been installed at the multiplexer's input terminals. Those filters have based on line-resonators formed by stubs with capacitance coupling. As results of multiplexer assembling and trimming of connecting lines, high-level performances of multiplexer have been achieved that shown in Table 1.

By its design the considered multiplexer has been manufactures by using a special frame which provided flat mounting of device's components. Both the directional couplers and the band-stop filters have been perform by application a symmetrical strip line with conductors of squared cross-section. The connecting lines have accomplished by a rigid feeder line.

Table 1

Input wave impedance	75 Ω
Output wave impedance	75 Ω
Input VSWR	1.04
Output VSWR	1.08
Inter-channel isolation	≥ 40 dB
Insertion losses of each channel	≤ 0.2 dB
Irregularity of amplitude-frequency response for each channel	≤ 0.1 dB
Maximum input power of each channel	5 kW

OPPOSING PROBES BAND-PASS FILTER MULTIPLEXER

An opposing probes band-pass filter multiplexer with output summation signal applied to central probe has been developed to provide common aerial feeder operation of the three TV broadcasting transmitters of the decimeters waves band (21, 34, 38 TV channels).

To design filters, as well as, dimensions of central output probe, special design procedures like ones presented in [2] have been adopted and used.

This multiplexer by its design had a T-shaped packaging in special metallic case (Fig. 1). Probe-opposing filter has been accomplished at each arm of device and the output central opposing probe has located at place where all arms are connected together.

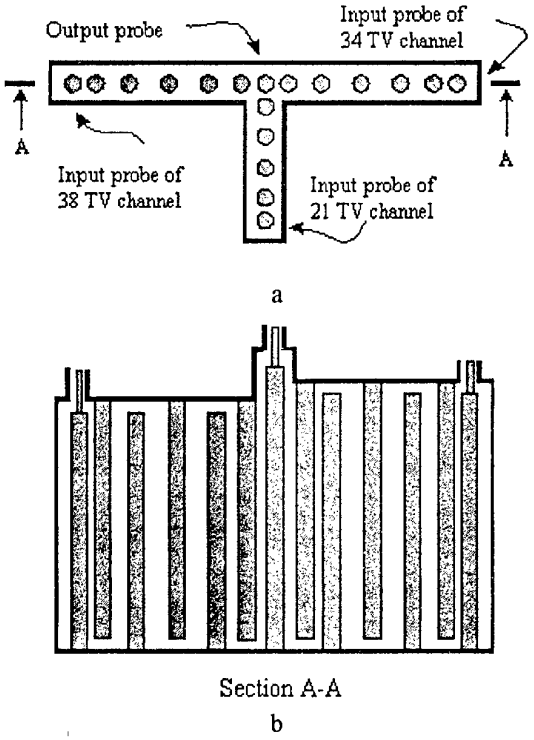


Fig. 1. Opposing probes band-pass filter multiplexer for the three TV broadcasting transmitters of the decimeters waves band (21, 34, 38 TV channels): horizontal section (a), section in the plane (b) of the filters of the 34 и 38 TV channels

The filter of the 21 TV channel includes four resonators, and the filters of 34 and 38 TV channels consist of five resonators each. The boundary probes of filter are served as impedance transformers.

The all filters used in this device are the opposing probes filters of the first kind with the short-circuit input probes. The first kind filters provides better technical performances of multiplexers, although the second and third ones are more preferable to put into practice them [2].

TRAVELLING WAVE RESONATOR MULTIPLEXER

A travelling wave resonator multiplexer has been designed for summation of the 5 TV channel (92–100 MHz) and a part of the European FM band (107.4–108.0 MHz).

To design such multiplexer a special procedure has been used that based on design of model-prototype low-frequency filter for some set of given approximations of amplitude-frequency response. Next step of design procedure has involved determination of quality factors of resonators that formed by directed filter with travelling wave mode [2, 4].

By using of the Chebyshov approximation of amplitude-frequency response of equivalent filters, multiplexer with given performances can be implemented by using of two travelling wave resonators.

The multiplexer for given TV channels has been accomplished by cascade connections of three directional couplers based on coupled transmission lines with crosstalk attenuation 13.07 dB, 31.01 dB and 13.07 dB correspondingly. The resonators of travelling wave formed by such connections have been tuned to resonance frequency of 107.7 MHz. Schematic presentation of this multiplexer is shown in Fig. 2.

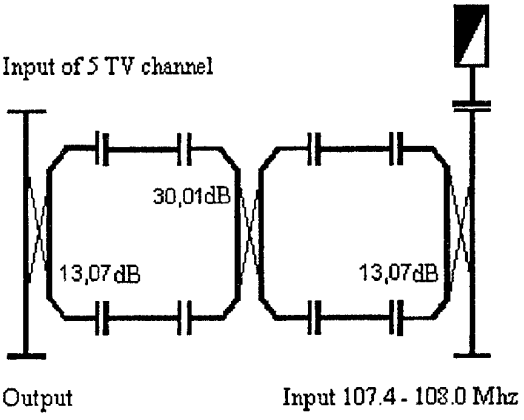


Fig. 2. Schema of travelling wave resonators for summation of signal of 5 TB channel (92-100 MHz) and a part of the European FM band (107.4-108.0 MHz)

Laboratory examination as well as testing under high-power operation have estimated that main difficulties to tune device properly is elimination of unwanted travelling wave propagated in opposite direction to main travelling wave operation mode.

This fact is forced due to presence of wave reflection from input terminals of the directional couplers due small but finite value of VSWR achieved. Such unwanted return wave is excited also due to finite value of directivity factors of directivity couplers used and decreases sufficiently inter-channel isolation and increases VSWR simultaneously. Some preventive measures to compensate return waves have been proposed and implemented effectively without a serious revision of total multiplexer.

To obtain device features closed to suitable ones demands exact setting of crosstalk attenuation magnitudes of the directional couplers. Tuning of crosstalk attenuation of the directional couplers has been made by tuning of each resonator separately. Note that amplitude-frequency response of each resonator should be setting under consideration of its internal loss.

MODIFIED BAND-STOP FILTER MULTIPLEXER

This type of multiplexer has been developed to give possibility of increasing number of broadcasting channels by adding new base modules for corresponding new channels without any revision existing before device of such architecture (Fig. 3). The considered before multiplexer have no such opportunities.

In order to reach declared goal a special kind of six-port microwave device has been developed and studied experimentally that based on modification of band-pass filter.

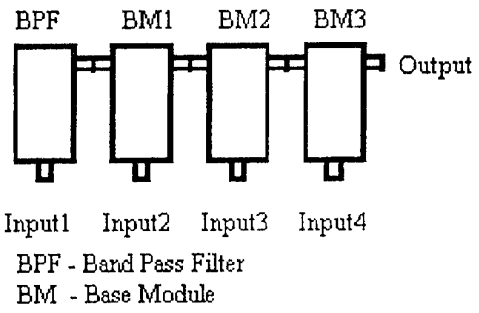


Fig. 3. Schematic presentation of multiplexer by using of six-port modified band-pass filters

The six-port microwave serves, as a base module to build necessary architecture of multiplexer with opportunities of its extending with new additional channels if is necessary.

As results of developing and studies of the six-port base module, a multiplexer of four TV decimeter wave channels has been designed, fabricated and tested. This device has been tuned to necessary performances like ones in table 1 without any principal problems and good agreement between given and measured figures has been achieved.

The multiplexer of such kind has been tested effectively and used at present at a broadcasting center in Ukraine.

CONCLUSIONS

Presented before the four variants of TV and radio broadcasting multiplexer of the decimetric and metric waves band have been developed and designed due to, firstly, precise electrodynamics models of device's components and, secondly, due to design procedures to get necessary device's performances like ones in table 1. The electrodynamics 2-D and 3-D models of much number of device's components that include thermal modes of device under high-power operation construction as well as tolerance and jitter of real manufacture processes have been involved in special software to make exactly, easy and faster design efforts. This software contains also synthesis procedures for total device that are adaptation and modification of known methods of filter design etc.

Besides developing and designing experience, some valuable practice of device' manufacturing, tuning and testing has been obtained also that allows to solve similar problems effectively.

REFERENCES

1. Feldstein A.L., Javich L.R., Design of microwave four-port and eight-port, Moscow, 1971. 388 p. [in Russian].

2. Mattey D.L., Young L., Jons E.M.Y., Microwave filters, matching and coupling circuits, Moscow, 1971, Part I, 439 p., Part II, 495 p. [in Russian].

3. Leonchenko V.P., Feldstein A.L., Sheljanskiy L.A.,. Strip opposing probe filter design, Moscow, 1975, 312 p. [in Russian].

4. Altman J.L, Microwave devices, Moscow, 1968, 487 p. [in Russian].

TRANSFER CHARACTERISTICS OF ULTRA HIGH FREQUENCY DEVICES BASED ON TWO SURFACE IRON-YTTRIUM GARNET FILMS

M. I. Lyashenko, V. M. Talalaevskii, L. V. Chevnjuk

Taras Shevchenko Kyiv University, radio physics department
Vladimirskaya 64 str., Kyiv, Ukraine, 252017, ph. (044) 2660580
E-mail: volodyat@boy.rpd.univ.kiev.ua

The devices based on the Iron-Yttrium Garnet (IYG) films are used in radio-location technique in UHF systems, particularly in the antennas. The examples of such devices are delay lines and filters. The transfer characteristics of such devices were considered in [1] where mostly single surface films were studied.

In this work we studied the transfer characteristics of the UHV devices based on two surface ferrite films. A two surface films were based on relatively thick (500 μm) substrate of Gallium Gadolinium Garnet (GGG). The 10 μm thick IYG film was epitaxially grown on this substrate (see Fig. 1). Eletrodynamically, the two surface film is a ferrite-dielectric-ferrite system. Mechanically, it is a three layer system with one layer significantly thicker than the others. Under such values of substrate and ferrite layer thickness, the film, deformed in the plane normal to its surface (bending deformation), has one ferrite layer stretched and another one squeezed. This results in effective internal magnetic fields of single axis crystallographic anisotropy H_a emerging in ferrite layers. The fields are of the opposite signs, The magnitude, direction and uniformity of the fields induced by elastic stresses are defined by deformation characteristics. It affects substantially the dispersion of magnetostatic waves in films, and, respectively, the transfer properties of devices with IYG ferrites.

The experiments were performed on the setup schematically shown in Fig. 1. A transmission line consists of electromagnetic-to-magnetostatic wave antenna transformer, a film, and a magnetostaic-to-electomagnetic wave antenna transformer. For effective transformation of electromagnetic waves into magnetostatic waves and vice versa, the antenna transformers were made in the form of loops around the film. The transfer characteristics of the line were studied in the range 2-4 GHz with the R2-53 detector. The antenna transformers and external magnetic field $\vec{H}_0$ were oriented such that only a surface magnetostatic wave (SMSW) was excited and propagated in the film. The SMSW reflections from various inhomogeneities resulted in indention of transfer characteristic (see Fig. 2). This adversely affected the precision of obtained transfer characteristics.

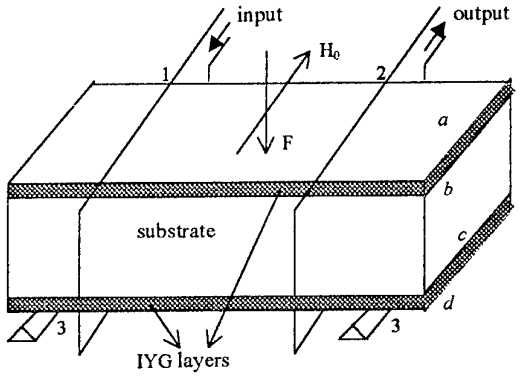


Fig. 1. Ferrite transmission line
1,2 – antenna transformers; 3 – dielectric supports;
F – transmission line deformig force;
H_0 – external field; *a*, *b*, *c*, *d* – ferrite layers surface.

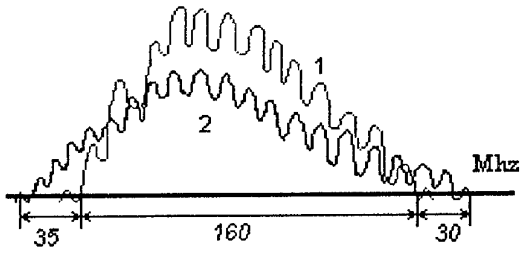


Fig. 2. 1 – non-deformed line, 2 – deformed line

Since the surface of SMSW propagation is defined by the direction of $\vec{H}_0$ and wave vector $\vec{K}$ [2], and they have same directions in both layers, the wave always propagated along the film air interface for one layer and along film-substrate interface for another layer. In our case (see Fig.1) the SMSW propagated along the "*a*" surface in the upper layer and "*c*" surface in the lower one. The reflected waves propagated along the "*b*" and "*d*" surfaces. The resulting transfer characteristic is a superposition of the transfer characteristic of each of film's sides. Thus, the transfer characteristic of transmission line depends both on the amplitudes of SMSW excited in each ferrite layer, and the propagation condition (air, dielectric) of these waves in waveguiding layers.

The influence of elastic deformation, external magnetic fields and temperature on the transfer characteristic of transmission line based on a two surface ferrite film was studied. The change of transfer characteristic caused by elastic deformations is shown in Fig. 2.

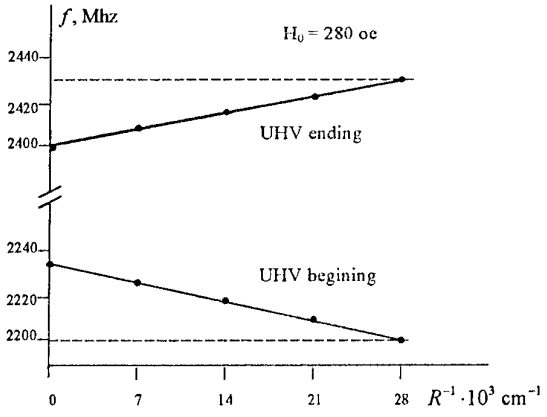


Fig. 3. The external field influence on the edge UHV shift

Such changes are resulted from emergence of single axis crystallographic anisotropy fields H_a in ferrite layers due to bending deformations. The films is place of dielectric supports and is bent by applying the force to its middle. As shown in [3], the anisotropy fields add up with demagnetizing fields $4\pi M_0$ (M_0 is saturation magnetization), and shift the dispersion characteristic of SMSW along the frequency axis, ω_k.

$$\omega_k^2 = \gamma^2(H_0 + 2\pi M_0 \pm H_a)^2 - \gamma^2(2\pi M_0 \pm H_a)^2 e^{-2|\vec{K}|d} \quad (1)$$

Since under the bending deformation one ferrite layer is stretched and another one is squeezed, the anisotropy fields H_a are of the opposite sign which is reflected in (1). In case of stretching, the H_a field added up to the internal films and the transfer characteristic was shifted toward higher frequencies. Squeezing reduces the internal field (negative sign before H_a) and shifts the transfer characteristic toward a low frequency range. Since the transfer characteristic of different layers are shifted to the opposite directions, the resulting curve is broadened. The dependence of the transfer characteristic edge on the film curvature R^{-1} (R is bending radius) is shown in Fig. 3. R^{-1} was chosen as an independent variable because it is proportional to H_a [4].

In our experiments, the anisotropy induced field $H_a << H_0$; $2\pi M_0$, and $2|\vec{K}|d << 1$. The last relationship is valid because the lower end of transfer characteristic corresponds to $|\vec{K}| = 0$ and the upper end corresponds to $|\vec{K}| < 40$ cm^{-1}. Thus, as seen from (1), $e^{-2|\vec{K}|d} \approx 1$, and $\omega_k \sim H_a$. The linearity of the dependence of the shift of transfer characteristic end on the elastic stress (H_a) is confirmed by the plot in Fig. 3. It is also seen from this plot, that the ends of transfer characteristic shifted differently because different physical processes are responsible for the exciting and damping of SMSW.

It was shown in [1] that inhomogeneous elastic stresses induced inhomogeneous fields of single axis crystallographic anisotropy in films that resulted in narrowing down of the transfer range of one surface films transmission line. In our case the film was rectangular, H_a fields were inhomogeneous and the transfer characteristic of each layer narrowed down. However, this narrowing was much less than the broadening due the elastic stresses.

We also studied the influence of external magnetic field and saturation magnetization on the transfer characteristic. The experiment showed that the change of both H_0 field and M_0 magnitude (M_0 was changed by film heating) resulted in shift of the transfer characteristic along the frequency axis, in accordance with eq. (1). Also, the width of transfer characteristic changed due to the shift in dispersion characteristic [1]. With the H_0 and M_0 increase, the transmission range of both ferrite layers narrowed down. The change of the transfer characteristic with $H_0(\Delta H_0)$ and $M_0(4\pi\Delta M_0)$ variation is much smaller than the change (broadening) caused by induced anisotropy fields H_a ($H_a = \Delta H_0, 4\pi\Delta M_0$).

Summarizing, the deformation of two surface ferrite transmission line as well as change of its temperature and external field affects the line transfer characteristic. This change affects the spectra of signals transferred along the line. As a result "amplitudno-fazovye xarakteristiki" of directivity pattern of multielement antenna systems, where these lines are used, are affected.

REFERENCES

1. Lyashenko M.I., Talalaevskii V.M., Chevnjuk L.V. Proceedings of the second international conference on Antenna theory and Techniques, Kyiv, 1997, p. 308.
2. I.V. Zavisyak, A.V. Tychinskij. Physical principles of functional electronics, Kiev, 1989, 106 p. [in Russian].
3. A.S. Beregov, E.V. Kudinov, Elektronnaja tekhnika, Ser. Elektronika SVCH, 1987, Is. 6, p. 8 [in Russian].
4. Lyashenko M.I., Talalaevskii V.M., Chevnjuk L.V.
5. Radiotekhnika i elektronika, 1994, v. 39, N 7, p. 1164-1169 [in Russian].

APPLICATION OF MW DELAY LINES IN COMBINED SAR CALIBRATION

A. Y. Matveyev

Center of Radiophysical Sensing of Earth
of NAS and NSA of Ukraine, Ul. Proskury 12, Kharkov, 310085 Ukraine,
Phone: 380-572-448-412, Fax: 380-572-441-012, E-mail: kalmykov@ire.kharkov.ua

This paper gives a description of the facilities for the combined calibration of the L- and VHF-band radars ($\lambda \approx 23$ cm, SAR-23 and $\lambda \approx 180$ cm, SAR-180, respectively) installed in the air-borne "MARS" system [1] where the MW delay lines are employed. The technique for the combined SAR calibration involves a periodic external calibration of point calibrated reflectors (transponders) being mounted close to the surfaces under study or on special testing sites as well as continuous internal calibration with indispensable recording of real carrier flight parameters [2].

The main feature in the implementation of SAR internal and external calibration of the air-borne "MARS" system is that the ultrasound MW signal delay lines are extensively used. These lines enable the transmitted SAR signals to be utilized for internal calibration (this tends to improve the accuracy of the latter) and adds up to new possibilities of measuring and checking SAR parameters.

The construction and procedure of the internal SAR calibration are highlighted by their peculiar features because of the differences in implementing antenna systems (controlled active phase antenna array [APhA] in the SAR-23 and non-controlled passive one [PhA] in the SAR-180). These differences make themselves evident both in selecting the ways of internal calibration and in tackling the most challenging issues of internal calibration, i.e. of checking the basic parameters of the SAR antenna array (gain, the width and configuration of a the radiation pattern). It is apparent that these parameters can only be measured in terms of the external-calibration results. However, as our experience suggests, the variation in gain caused by the external APhA (PhA) elements (radiators and their feeders) are unlikely, since it may be brought about by mechanical misalignment or damage of rigidly fixed antenna array radiators. Therefore, to ensure that the antenna array gain is properly checked it is necessary that the internal calibration should be able to check the amplitude-phase characteristics of the receiving-transmitting APhA channels to a sufficient accuracy.

The SAR-23 APhA is an electrically controlled multi-element (16 receiving-transmitting radiators) antenna array with a high gain ($\cong$ 19.4 dB). That system provides for receiving and transmitting the chirp-signals with vertical and horizontal polarizations and enables the spatial position of the combined pattern and the azimuthal plane ($\pm$ 10°) to be rapidly changed (1-3 μsec). Separate active feeding systems (16 receiving and 16 transmitting channels) of the overall antenna array are employed for the SAR-23 APhA. In addition to an increase in decoupling, this system makes it possible to construct a multi-functional system of calibrating and checking its working capacity (see Fig. 1).

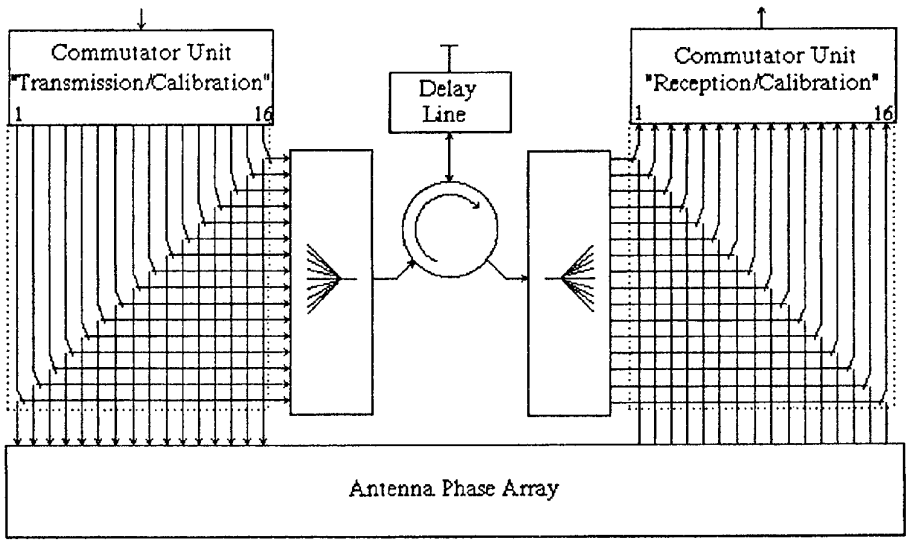


Fig. 1. Functional Diagram of SAR-23 APhA Calibration

The operating principle of this calibration system is that a certain fraction of the output power in each of the 16 transmitting channels arrives at the input of the MW delay line (it works based on the principle of repeated reflection) via the system of "receiving-transmitting" commutators, a summator and a circulator. The line-delayed radio pulses are fed by the circulator to the symmetrical-in-number input of the receiving phasing system (1-st to the 16-th, 2-th to the 15-th, etc.) through a divider and a system of the "reception/calibration" commutators. In the normal operation of the system, for phasing the receive/transmit APhA section at the receiver output, the radio pulses are equal in amplitude and phase (it is because they pass through the circuits having an equal electric length and attenuation). A difference in amplitude or phase in some of the receiving-transmitting channel pairs is indicative of errors in transmitter or receiver phasing systems. The accuracy of these measurements is largely determined by the stability of the MW delay line parameters. Therefore, the delay line is placed in a special thermostabilized box. The accuracy of these measurements is being checked using the data from in-situ measurements of the amplitude and phase characteristics of the receiving and transmitting APhA channels. The suggested technique enabled the transmission factors of the above-mentioned pairs of the receive/transmit channels to be compared within an accuracy of ≤ 0.15 dB and the phase difference between them to be determined with an error of not more than 3° to 5°. Using different modes of switching the high-speed MW-diode commutator ensures that routine information about the status of all the receiving/transmitting APhA channel pairs is collected both immediately during the radar surveying of the objects under study and in the course of adjusting the equipment and the pre-flight APhA checking.

The conditions under which various types of objects under study are being surveyed often require that the receiver amplification be fine-adjusted and the temporal automatic gain control (AGC) corrected. To perform a real-time checking of the receiver, a SAR calibration mode is provided. In this mode, a series of decreasing pulses generated by the MW delay line is delayed to be placed directly in a receiver band-width. The amplitudes of the pulses of this series are recorded twice, i. e. when the receiver temporal AGC is an on and off position. A comparison between these data makes it possible to restore the shape of the receiver temporal AGC and to estimate its dynamic range.

For the system of the SAR-180 internal calibration, the MW delay line is utilized to shape the calibration levels of signals in a special section of an image line. For this purpose a part of the output MW amplifier power enters the calibration system (see Fig. 2) via a directional coupler. The level of the coupled power is controlled by a steps attenuator (the number of step is 16, the magnitude of each step is $\cong 3$ dB). The step of the attenuator in combination with the MW delay line provides for the required level of linearity of the calibration signal transmission through the receiver. Of the train of pulses shaped by the MW delay line, the second pulse which is delayed by 30 μsec in relation to transmitted one passes through the switch at the delay line output to the receiver input. This signal is also amplified by a receiver and further processed using the same algorithm which is applied to process the signals being received from an object under study. To render the data handling more convenient the step attenuator is switched over to the next position within 3 sec. With a knowledge of the transmission factor of the calibration channel it is possible to determine the level of the transmitted signal power and make a check on its stability. Besides, the amplification and the dynamic range of the entire receiving channel can likewise be checked. To improve the measurement accuracy, the delay line is placed in a special thermostabilized box (similarly to the SAR-23 calibration system).

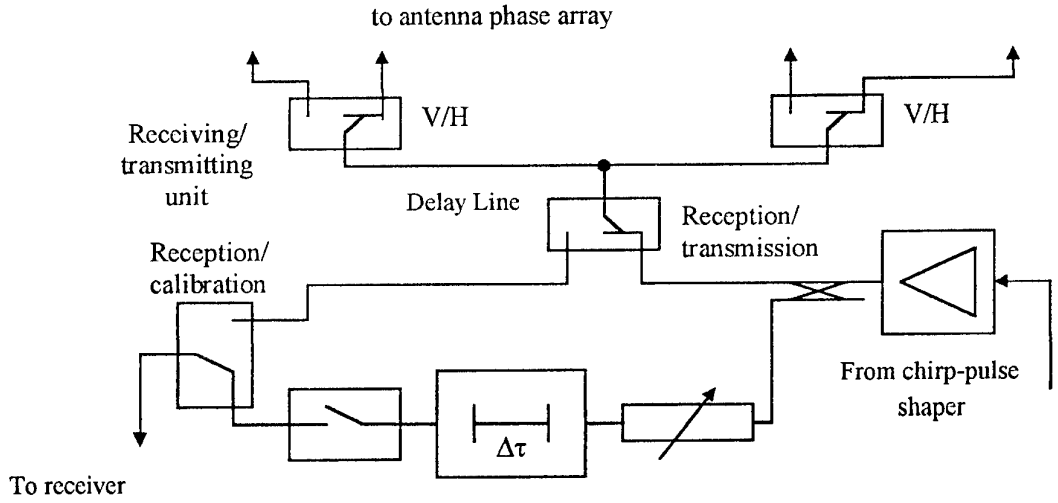


Fig. 2. The system of the SAR-180 internal calibration

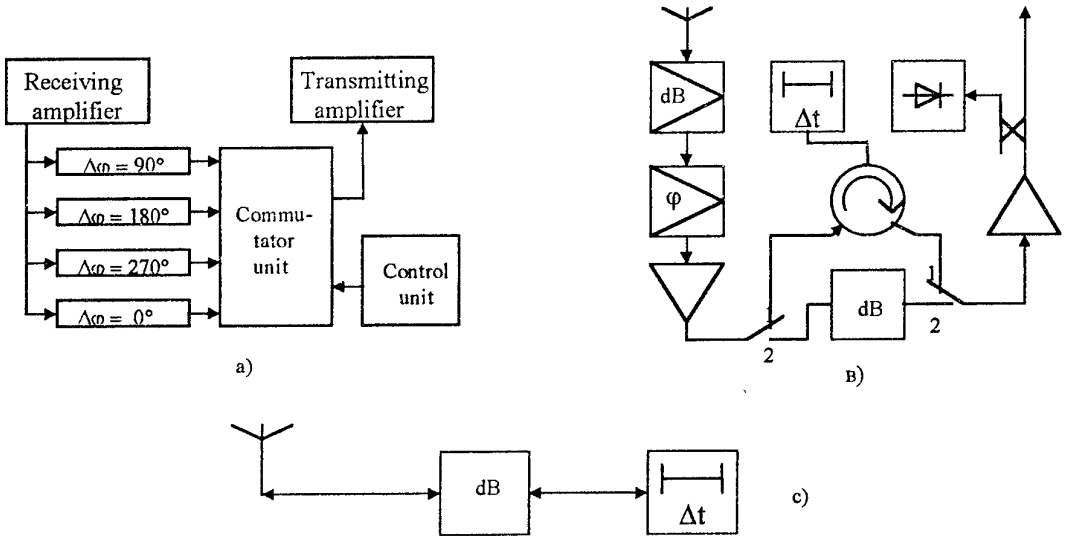


Fig. 3. Functional diagram of active (a,b) and passive (c) transponders for checking of the SAR parameters and the SAR calibration of the "MARS" system. (a) - with a phase modulator; (b), (c) - with a delay line; 1,2- switching versions of AT

The external calibration and checking of the SAR parameters of the "MARS" system were performed by using active (AT) and passive (PT) transponders (see Fig.3). Relatively to the conventional transponders [3], the ATs are complemented by a phase modulator (Fig. 3a) and MW delay line (Fig. 3b).

In the AT (Fig.3a), the phase modulator is realized as the sequentially switched speed-variable phase shifters with $\varphi = 90$ °, $\varphi = 180$ °, $\varphi = 270$ °, $\varphi = 0$ ° to simulate the spectrum the of pseudo-Doppler frequencies in the reflected signal. As a result, it can be efficiently utilized to run an on-ground check of the basic SAR parameters. The application of the phase-modulator transponder makes it possible to perform: polarization measurements of the radiation pattern, and the level of the APhA and PhA side lobes; adjusting the unit for measuring the Doppler frequencies of an APhA (PhA) beam, testing of the on-board signal processing system; evaluating the SAR potential.

Using the signals received from the AT with a turned-on delay line (Fig. 3b)(they are shown on a radar image as a series of amplitude-descending pulses spaced at $\tau = 6$ μsec) makes it easy to locate the AT against the background of any terrain. The presence of temporal reference points (and hence, the spatial ones) permits estimating the geometrical distortions of a radio image acquired.

The passive delay-line transponder was also used along with the AT to check the SAR parameters (Fig. 3c). This transponder served the purpose of supervising the pre-flight status of the SAR-23 antenna array components. In this case, the transponder was alternately positioned at a certain distance from the antenna array plane surface opposite to each of the radiators whereas the SAR-23 internal calibration system was set to perform switching of the corresponding receiving-transmitting channel pairs. The passive transponder reflected each pulse radiated by a transmission channel as a series of delayed pulses. The checking of the radiators condition was made while measuring the number of delayed pulses at the receiver output.

The use of the MW delay lines in the external and internal calibration devices of the "MARS" system SAR not only enabled the technique of combined calibration to be implemented right on an aircraft, but also provided for on-ground adjustment and checking of the parameters of basic SAR assemblies and the SAR facility as a whole.

REFERENCES

1. Kalmykov A. I., Tsymbal V. N., Kurekin A. S., Yefimov V.B., Matveyev A. Ya., Gavrilenko A. S., Igolkin V. V. The Multipurpose Airborne Radar System of the Earth's Remote Sensing "MARS"// Radiophysics and Radioastronomy, Vol.3, No.2, 1998, pp.119-129.

2. Matveev A.Ya., Tsymbal V.N., Gavrilenko A.S. et al. Peculiarities of the Calibration Methods for Air- and Spaceborne Synthetic Aperture Radar Systems//Proc. European Conf. on Syntheric Aperture Radar, EUSAR'96: 26 - 28 March 1996. - Königswinter(Germany).-VDE-VERLAG GMBH *Berlin*Offenbach. - 1996. pp. 511-514.

3. Freeman A. SAR Calibration: An Overview // IEEE Transactions on Geoscience and Remote Sensing. - 1992. - vol.30, No.6.- pp.1107-1121.

MILLIMETER WAVE DEVICES BASED ON DIELECTRIC, FERRITE AND SEMICONDUCTOR WAVEGUIDES

V. V. Meriakri, B. A. Murmuzhev, M. P. Parkhomenko

Institute of Radioengineering and Electronics , Russian Academy of Sciences
141120 Fryazino, Moscow region, Vvedensky sq. 1, Russia
E-Mail: ask@ms.ire.rssi.ru Tel. (095) 5269266 Fax (095) 2038414

ABSTRACT

A set of passive and active devices based on dielectric, ferrites and semiconductors for the frequency ranges 26 – 48, 80 – 120, and 115 – 145 GHz have been created and investigated. These devices use dielectric strip waveguides, image waveguides, nonradiative waveguides of rectangular cross-section and provide optical or magnetic control of attenuation, phase and polarization. The advantages of the reported devices are as follows: broad band, simple construction, small dimensions, low weight and price cost. Receiving, transmitting and measuring systems using above mentioned devices were realized.

INTRODUCTION

Dielectric strip waveguides (DSWs) are regarded as perspective transmission lines for the millimeter (MM) waves range because of lower losses, lower dimensional tolerance requirements and lower production costs compared with the traditional metal waveguides [1]. Being a kind of open transmission line, DSW is accessible to the influence of electric, magnetic and optical fields on its guiding characteristics. Presently, there are about a dozen types of DSWs. All these types consist of wave guiding dielectric strip placed inside or on top of dielectric substrate, or on top of metal plate, as well between two metal plates. Using such DSW it is possible to realize all devices and components similar to such circuit elements based on usual metal waveguides and microstrip lines [1–3]. Here, we present some results of investigation of the DSW made not only of dielectric but also of ferrite and semiconductors. Ferrites and semiconductors allow one to design DSWs with low propagation loss and with effective control functional elements [4].

MATERIALS FOR DSW

The parameters of low loss dielectrics, ferrites and semiconductors we used for DSW fabrication were presented in [4]. DSW sections made of TGS crystal were used as polarization filters. TGS crystal parameters for the wave propagation along three crystallographic axis were measured to be $n_1 = 2.74$, $\tan\delta_1 = 0.62$; $n_2 = 2.31$, $\tan\delta_2 = 8.4 \cdot 10^{-3}$; $n_3 = 2.91$, $\tan\delta_3 = 1.5 \cdot 10^{-2}$, respectively, at $\lambda = 1.1$ mm.

PASSIVE DEVICES

We used two types of DSWs: DSW with strip placed on dielectric substrate (refractive index $n_2 < n_1$) and dielectric image waveguide (DIW). Main components for frequencies 26 – 48, 80 – 120 and 115 – 145 GHz have been elaborated. Components are based on PTFE, SiO_2, AL_2O_3, Si, and ferrites. For the above mentioned frequency ranges DSW to rectangular waveguide transition sections, couplers, frequency and polarization filters, attenuators using rectangular DSW have been elaborated.

The transitions from metal rectangular waveguide to DSWs fabricated from AL_2O_3, NiZn ferrite or high resistivity semiconductor Si have matching taper of (15 – 20) λ and the total transmitted power loss changes from 0.2 dB to 0.8 dB in frequency range from 26 to 145 GHz, VSWR < 1.4. DSW section fabricated from ferrite (FDSW) and semiconductor (SDSW) usually have cross section $a \times b = 1 \times 2 = (0.2 \times 0.4)\ \lambda$, when a and b DSW wall dimensions. Usually we use E_{11}^{y} mode (electrical field strength vector E is parallel to greater wall).

The linear losses in all kinds of DSWs without metal plates were in good accordance with expression

$$\alpha[\text{dB/cm}] = 27.3 \tan\delta\, n / \lambda,$$

where n and $\tan\delta$ are values for strip materials. In cases of DIW and nonradiative dielectric waveguide (NDR) the total linear losses including conductivity losses amount to some dozen dB/cm at frequencies up to 150 GHz.

Passive components and devices (directional couplers, polarization and frequency filters, absorbers, interferometers) based on FDSW, SDSW, DIW and NDW have approximately the same parameters as in [3]. For example DIW directional coupler has in the frequency range 28 – 36 GHz the direct loss 16 ± 1.5 dB, the insertion loss 2 dB, the VSWR < 1.4. The rejection filter using GaAs DIW resonator coupled to the main DIW has maximum attenuation 26 dB at frequency 74.5 GHz, 20 dB rejection within 0.3 GHz band, VSWR < 1.2, and insertion loss less than 2 dB outside the stopband.

DEVICES WITH MAGNETIC AND OPTICAL CONTROL

Optically Controlled Devices

Optically controlled attenuators and modulators were elaborated using photoconducting Si with $\rho > 10^4$ Ohm cm in SDSW and IDW. Such SDSW attenuator with three standard light emitting diodes (LED) enable to change attenuation from 0.5 to 25 dB at the 26 – 37 GHz range. Broadband attenuator comprising a IDW made of AL_2O_3 with the contacting silicon IDW was for frequency region 80 – 120 GHz elaborated. When LED current changes from 0 to 0.5 A the insertion losses increase from 2.2 dB more than 20 dB level, VSWR < 1.35. The losses of the attenuator linearly depend on the LED current in the dynamic range up to 15 dB. We also studied operation of attenuators as modulators up to frequencies 80 kHz. The decrease in insertion losses for a constant current amplitude starts at the modulation frequency of 10 kHz and attains 80% at 50 kHz.

Magnetically Controlled Devices

A set of devices using magnetically controlled FDSW were created: isolators, phase shifters, polarization-plane rotators, channel switchers. We use nickel-zinc ferrite 1SCh4 of $n = 3.7$, $\tan\delta = 10^{-3}$, saturation magnetization $4\pi Ms = 5000$ G. Isolators used composite waveguide consisting of FDSW with a direct magnet and DSW. In such composite waveguide the energy concentration in FDSW and DSW depends on the direction of wave propagation. Isolators have insertion loss from 0.9 dB at frequencies 25 – 40 GHz to 1.8 dB at frequencies 115 – 145 GHz. Return loss is 12 – 15 dB. Longitudinally magnetized FDSW of aspect ratio $a/b = 0.5$ were used for preparing controlled phase shifters [5]. The FDSW was placed on the axis of a current coil. The coil of length of 20 – 30 mm consisted of 100 – 150 winds. At frequencies near 36 GHz depending on dimensions a and b the phase shift changes from 80 deg/cm to 120 deg/cm and the power losses vary from 0.4 – 0.5 dB to 0.45 – 0.9 dB respectively for coil current about 0.7 A and ferrite section length about 50 mm. Similar phase shifters were fabricated for frequency ranges up to 145 GHz with the maximum losses less than 2.0 dB for phase 2π or more. The same phase shifters using E_{11}^x mode had less phase shift and more losses than in the case E_{11}^y operating mode. And phase shift for E_{11}^x decreases as magnetic field increases contrary to E_{11}^y mode. In rotators of the plane of polarization, modulators, and switchers a FDSW of aspect ratio $a / b = 1$ was used. Faraday rotation angle θ for FDSW of cross section $a \times b = 2.8 \times 2.8$ mm^2 and length 28 mm was measured for frequencies 29 – 39 GHz. This rotation angle was practically independent on frequency in interval $\theta = 0 - 360^o$ and this dependence is well approximated by linear function $\theta = 189 \times I$, where θ is in degrees, and I is in amperes.

Three and four port switches based on FDSW Faraday rotators were fabricated. These devices used T-bridges based on square cross section FDSW with electrically controlled coil and metal grating into the bridges. Depending on coil current this grating passes or reflects power. Switching losses in such Faraday device are less than 0.6 dB, channel isolation is 20 dB.

SOME SUBSYSTEMS BASED ON DSW

Above mentioned devices and components were used for receiving, transmitting and measuring subsystems, e.g. set up for permittivity ε and $\tan\delta$ measurement of small cross section sample using NDW; transmitting and receiving module based on DIW with ferrite isolator, a directional coupler, an optically controlled attenuator and a modulator. The module had in the frequency range 80 – 120 GHz insertion losses < 3.5 dB, VSWR < 1.4, isolation > 14 dB, attenuation range 15 dB, the dimensions are $20 \times 40 \times 120$ mm^2, and the weight is 200 grams.

REFERENCES

1. T. Itoh, Inverted Strip Dielectric Waveguide for Millimeter Wave Integrated Circuits, IEEE Trans. on MTT, vol. MTT-24, pp. 821-830, Nov. 1976.
2. T. Yoneyama, IEEE Trans. on MTT, vol. MTT-29, pp. 1188-1192, Nov. 1991.
3. L. N. Vershinina and V.V. Meriakri, Dielectric Strip Waveguide for Short Millimeter Range, Radiotekhnika i Elektronika, vol. 27, no. 7, pp 1348--1351, 1980.
4. V.V. Meriakri, B.A. Murmuzhev, and M.P. Parkhomenko, Millimeter Wave Dielectric Strip Waveguides and Components Based on Ferrites and Semiconductors, Proc. of MIOP'95, Sindelfingen, pp. 211-213, 1995.
5. V. V. Meriakri and M.P. Parkhomenko, Millimeter Wave Dielectric Strip Waveguides Made of Ferrites and Phase Shifters Based on these Waveguides, Electromagnetic Waves and Electronic Systems, vol. 1, no. 1, pp. 89-96, 1996.

STUDYING OF RESONANT REJECTING AND ADSORBING CELLS BASED ON SECTIONS OF PARTIALLY FILLED WAVEGUIDES

L. Minakova, L. Rud'

Institute of Radiophysics and Electronics of the National Academy of Sciences of Ukraine
12 Acad. Proskura St., 310085, Kharkov, Ukraine
E-mail: rud@ire.kharkov.ua

Compact dielectric inserts, overlapping a waveguide cross-section completely or partially, received the name waveguide-dielectric resonators (WDR) and are widely used in microwave technique as filter resonant sections, scaled windows for vacuum tubes, terminal loads, and so on. The subject of studying in the given work is WDRs based on sections of partially filled rectangular waveguides in which a dielectric plate completely overlaps a waveguide cross-section through the height (Fig. 1). Results of calculations of both spectral and scattering characteristics with taking into account the dielectric loss as well as the comparison of the theoretical and measured data are presented in the work.

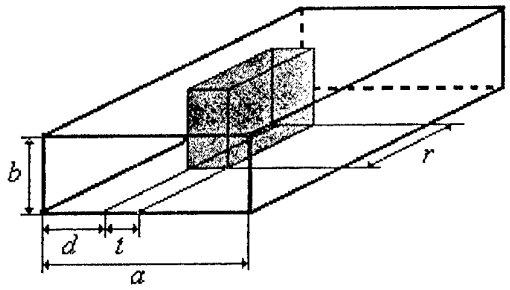


Fig. 1. WDR on a section of partially filled rectangular waveguide

The algorithm of scattering problem solution for a dielectric plate of finite length is based on the generalized scattering matrix technique with using a junction of hollow and partially filled waveguides as a key element. The generalized scattering matrix of key element was calculated by the mode-matching technique. Searching the mode basis of partially filled waveguide was performed at real frequencies on the base of dispersion equation obtained taking into account dielectric loss. The feature of spectral problem solution lies in the fact that the all above stages are needed to perform at complex values of spectral parameters. The latter is the propagating constants for partially filled waveguides and eigen frequencies for resonators on a section of a such waveguide. The spectral problem was considered in a strict formulation that allows for corresponding Riemann surface as a domain of spectral parameters varying.

The below presented results obtained for dielectric plates made from the organic materials (polystyrene filled with titanium dioxide): PT-5 (ε = 5, $\tan\delta$ = $1.1\cdot10^{-3}$) and PT-10 (ε = 10, $\tan\delta$ = $2.0\cdot10^{-3}$) The waveguide cross-section was 28.5×6.0 mm^2.

Analysis of the spectral characteristics of considered WDRs allows to obtain the complete information on an eigen oscillation that causes one or another resonant effect in the excitation problem. As an example, the real path of eigen frequency F' and quality factor Q of the H_{201}-oscillation dependence on the plate placement is presented in Fig. 2.

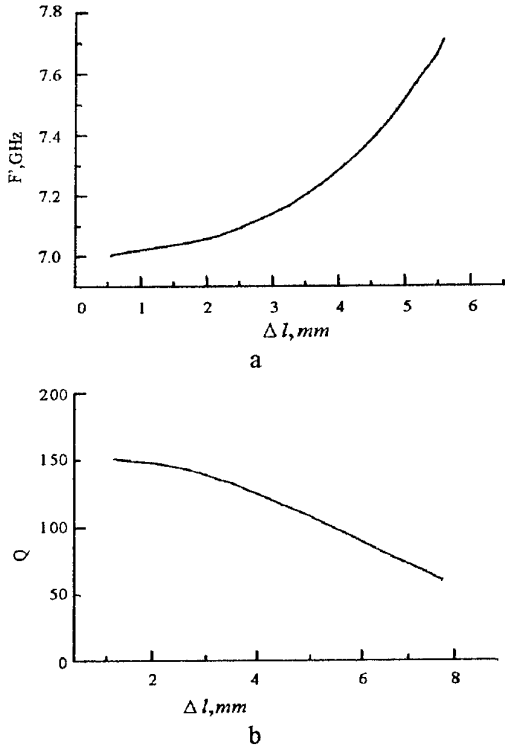
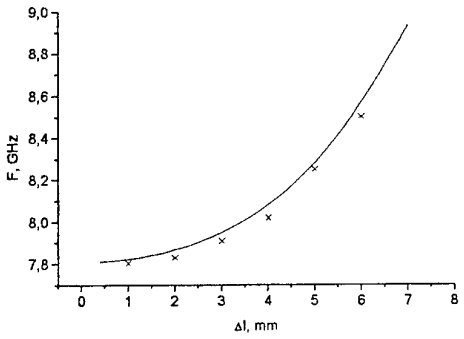


Fig. 2. Real part of H_{201}-oscillation eigen frequency (a) and quality factor (b) dependence on the plate placement

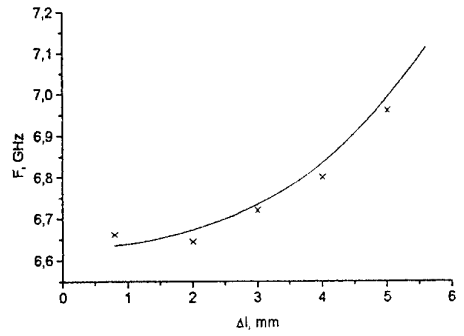
The geometrical parameters of structure are t = 17.2 mm, r = 10 mm, as a varying parameter is the excursion Δl of the plate axis from the waveguide one. It is significant that a quality factor Q of the H_{201}-natural oscillation is decreased in 3 times at shifting the plate from the central placement to the extreme one. It is explained by the fact that at increasingly plate shift the

level of coupling between the natural oscillation on H_{20}-mode and H_{10}-mode of the input waveguide (the power radiation is taken place on this mode) is changed. As it turns out, the knowledge of eigen-oscillation characteristics allows to define the authentic ranges of WDRs parameters and frequency where a resonant cell can perform the function of a rejecting or adsorbing waveguide element.

The comparison of resonant frequencies caused by the response on an excitation of H_{201} - oscillation in WDR and connected with the regimes of a maximal reflection of the incident H_{10}-mode is illustrated by the data in Fig. 3 (a — t = 10 mm, r = 17.2 mm; b — t = 17.2 mm, r = 10 mm). The theoretical results are marked by solid curves and measured ones by crosses. As one can see, the results of constructed numerical algorithm agree closely with the measured data.



a



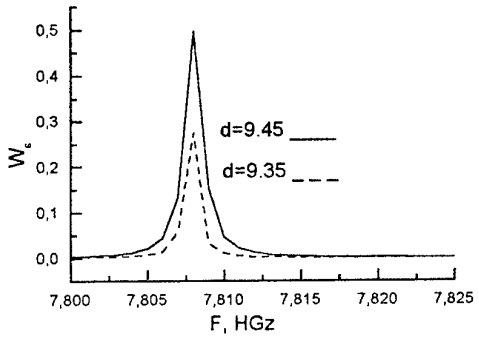
b

Fig. 3. Dependence of maximal reflection resonant frequencies for plates on PT-5 (a) and PT-10 (b)

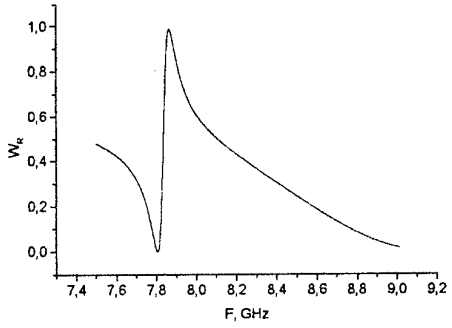
It should be noted that the reflection level at each frequency point is distinct. It is caused by a different quality of operating oscillation at each point and different level of adsorbed power correspondingly.

The comparative analysis of spectral and scattering characteristics allows to formulate a set of qualitative conclusions. In particular, it is possible to choose such a plate placement when the level of adsorption is $W_\varepsilon \approx 0.5$. At that parameters WDR can operate as an adsorbing cell (see Fig. 4a). The determining factor in choosing the optimal parameters (on maximal adsorption) is the relation between a eigen-oscillation quality and dielectric one. Unlike WDR completely overlapping a waveguide cross-section for which a maximum of adsorption was observed at $\eta_0 = Q\tan\delta \approx 0.5-0.6$, in WDRs on partially filled waveguides such a maximum takes a place at $\eta_0 \approx 1.0$. The maximal adsorption is observed for plates located near a waveguide axis and resonant curve is wider for WDRs on dielectric with a large $\tan\delta$.

It is clear that WDRs, having a large Q-factor of eigen oscillations, are conjectural in using as rejecting cells at $\eta \geq \eta_0$. However, it is not difficult to choose such parameters of WDR at which they can provide a regime of reflection close to a complete one (see Fig. 4b at d = 11.15 mm).



a



b

Fig. 4. Frequency response of adsorbed (a) and reflected (b) powers for WDRs on PT-5

As a rule, WDRs operating on H_{20}-mode is preferable for creating a rejecting cell when the plate is placed near a side wall.

The authors wish to thank Dr. A.G. Yuschenko for the submitted measured data.

RECONSTRUCTION OF MULTIPLE RECTANGULAR APERTURE IRIS RESPONSE BY ITS COMPLEX NATURAL OSCILLATIONS

L. P. Mos'pan

Institute of Radiophysics and Electronics of the National Academy of Science of Ukraine
Ulitsa Ac. Proskury, 12, Kharkov, 310085, Ukraine
phone 380(572)448-428, fax: 380(572)441-105, e-mail: lyuda@ire.kharkov.ua

The spectral theory of open waveguide structures is successfully employed over a period of years for studying electromagnetic properties of extended structures of waveguide type (waveguide broadening of finite length, finite length dielectric bifurcation of a waveguide etc.). Our work presents some results of applying the spectral theory to the analysis of waveguide unhomogeneities with small longitudinal dimensions, namely multiple aperture rectangular irises in a rectangular waveguide. Rejection frequency response is the salient feature of such irises if their cross-section contains at least two slots of different geometry. A number of works were devoted to studying frequency responses of rejection multiple aperture irises. A tool of their studying was or the circuit theory [1] or the diffraction theory [2]. In our previous works [3, 4] we have established, in particular, that the number of total transmission responses on the iris frequency response are coincident with the number of the slots having different geometry. Dimensions of these apertures define the location and quality factor of the total transmission resonances. However the reason of forming such a frequency response is not revealed yet. Employment of the spectral theory can give an answer for this question.

By a spectral problem is meant searching those values of the complex spectral parameter $\kappa=a/\lambda=\kappa'+i\kappa''$, for which homogeneous equation of Helmholtz has non-trivial solution. The Riemann surface with the cuts, that begin in the branching points, where propagation constant of input waveguide dominant mode $\tau=0$, is the definition region for the spectral parameter. All the studies were carried out on the first sheet of the Riemann surface between the first and the second cuts, that corresponds to the single mode regime of input and output waveguides. Complex frequencies of the structure under consideration were found as complex roots of the determinant of the homogeneous linear algebraic equations, when the frequency parameter changed. The values of the frequency parameter corresponding to the total transmission resonance on the frequency response are used as initial values. A pair of complex roots is the solution of the spectral problem in the complex frequency region. They correspond to two types of natural oscillations of two-aperture iris. One of them has low quality whereas the other hss high quality.

In according to the spectral theory frequency dependence of the reflectivity for the dominant mode of the waveguide circuit can be reconstructed by the set of natural frequencies of the waveguide unhomogeneity [5]:

$$|S^{11}|(\mathrm{Re}(\kappa)) = \frac{(\tau-\bar{\tau}_{1eig})(\tau+\tau_{1eig})(\tau-\bar{\tau}_{2eig})(\tau+\tau_{2eig})}{(\tau+\tau_{1eig})(\tau-\bar{\tau}_{1eig})(\tau-\bar{\tau}_{2eig})(\tau+\tau_{2eig})}+1$$

where $|S^{11}|$ is the module of the reflectivity for H_{10}-mode at the real frequency, $\tau=\sqrt{\kappa^2-1/4}$ is the propagating constant of H_{10}-mode, κ_{eig} is the pole, in the vicinity of which the expansion is carried out; the sign under τ_{eig} means the complex conjugation operation.

Figure 1 presents an example of such a reconstruction for a two-aperture iris. Cross-section of the iris contains two horizontal rectangular apertures with the dimensions of 13×1 mm^2 and 16×1 mm^2. The slots were cut immediately adjacent to the upper and the bottom walls of the rectangular waveguide WR-90. Iris thickness is 0.48 mm. The frequency response, reconstructed by above written formula (dashed line on the upper part of Fig. 1) is compared with the solution, obtained on the base of rigorous solution of the diffraction problem (solid line). The values of complex natural frequencies, by which the reconstruction was carried out, are marked in the bottom part of the Fig. 1. As usual, the location of total transmission resonance points are close to the real part of complex natural frequency only for high quality oscillations. It is obviously that all the peculiarities of the frequency response are explained well by the excitation of two natural oscillations of the iris. On order to make this conclusion it is sufficiently to compare the pair of solid and dotted curves from the Fig. 1. From the figure we notice that the curves are coincident qualitatively with high accuracy in the resonant region.

In order to verify the validity of our conclusions and to estimate the accuracy of obtained results a number of experimental measurements was carried out for the irises with different geometry of the slots. Fig. 2 presents calculated (solid line) and experimental (solid line with squares) frequency response for two-aperture iris of above-mentioned geometry. The frequency of the rejection resonance is 9.32 GHz. Its bandwidth is 9.6 %. The difference between calculated and measured

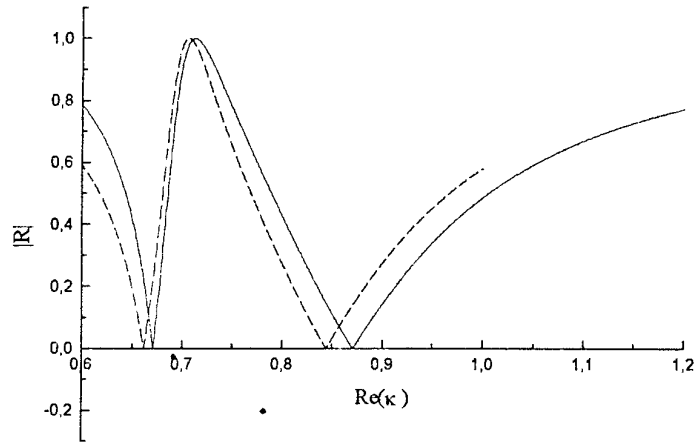


Fig. 1. Frequency response for two aperture iris. Iris thickness is 0.48 mm. Slot dimensions are 13×1 mm^2 and 16×1 mm^2

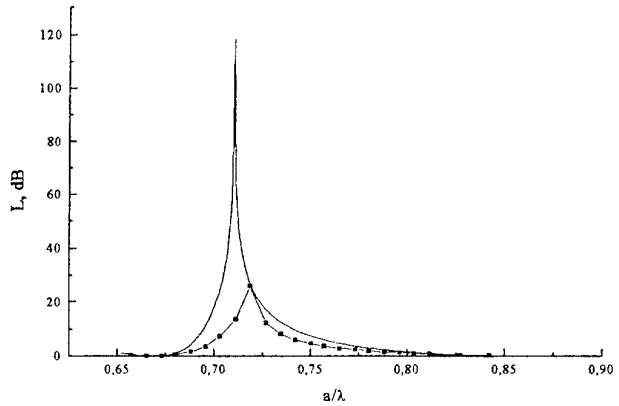


Fig. 2. Calculated and measured transmission loss characteristic for two aperture iris

data is explained by ideal theoretical model, in which the Ohmic loss are not taking into account, and by relatively low quality of iris manufacturing.

So, we conclude that specific character of the frequency response for the rejection multiaperture iris can be interpreted as a response for the excitation of the pair of natural oscillations in the iris. Using the spectral theory in the design of rejection irises with given characteristics is one of perspective lines of application for the obtained results. It decreases significantly the computing time for iris prototype calculations.

The author would like to express thanks to Prof. Anatoly A. Kirilenko for many helpful discussions during the course of this work.

The author wishes to acknowledge E. A. Sverdlenko for the help while carrying out the measurements.

REFERENCES

1. N.G.Paterson, I.Anderson Bandstop iris for rectangular waveguide, Electronics Lett., 1976, v.12, N22. pp. 592-594.
2. V.G. Alybin, N.M.Gordyuhina et. al. Double resonance waveguide iris, (Engl transl. in Radio Engn. Electron Phys) (in Russian), 1981, N.8, -pp. 1605-1613.
3. A. A. Kirilenko, L. P. Mos'pan, V. I. Tkachenko Numerical investigation of multiple rectangular aperture irises in a rectangular waveguide Proc. Int. Conf. Mathem. Methods in EM Theory (MMET*98), Kharkov, 1998, pp. 390-392.
4. A. A. Kirilenko, L. P. Mos'pan, L. A. Rud', V. I. Tkachenko Electromagnetic features of multiple rectangular and complicated irised in a rectangular waveguide// Proc. of XXYIII Moscow Int. Conf. on Antenna Theory & Technology, Sept.1998, Moscow, Russia, pp.528-530.
5. A. A. Kirilenko, B. G. Tysik Connection of S-matrix of waveguide and periodical structures with complex frequency spectrum, Electromagnetics, v.13, N3, pp.301-318.

PULSE CURRENT EXCITATION OF THE RECTANGULAR RESONATOR WITH DISTRIBUTED NONLINEAR LOADS

D. V. Semenikhina

Taganrog State University of Radio Engineering
Taganrog, 347924, Russia, GSP-17A, Nekrasovsky str., 44
Fax: (86344) 61685, airpu@tsure.ru

INTRODUCTION

The analysis of the mode in a rectangular microwave resonator with the distributed nonlinear loads located on a surface of walls can form the basis for designing and synthesis of generating modules, amplifiers, frequency multipliers, dividers and other microwave devices. The modelling such devices by means of the low-frequency equivalent circuits meets a number of difficulties, and the analysis of the equivalent circuits of the nonlinear loaded microwave device is limited usually by linear or quasi-linear approximation.

Besides urgency of research of the closed electromagnetic systems excited by pulse sources grows nowadays (for example, for designing a microwave generator). And if for linear systems the complex amplitude method application for study of these sources' fields is still justified, for nonlinear loaded object the direct time-domain analysis is required.

NONLINEAR BOUNDARY PROBLEM FORMULATION

Let $a \times b \times l$ rectangular resonator be excited by pulse sources with volume current densities $\vec{j}^{e,(m)pr}(p,t)(p \in V_j)$. The resonator has the distributed surface nonlinear loads as M narrow, in a general case, non-uniform nonlinear contacts.

To define fields excited by pulse currents in the time-domain integrated ratio for fields is applicable [1]. Let's choose as an auxiliary field $\vec{E}^{e,m}, \vec{H}^{e,m}$, one of the point magnetic (electrical) sources $\vec{j}^{a,e,(m)}(p,t) = \vec{b}(t)\delta(p,q)$ satisfying the boundary conditions on walls of the resonator without nonlinear loads (where $\vec{b}(t) = \vec{b}\delta(t-\tau)$). Then the integrated ratio for fields looks like

$$\vec{b}\begin{matrix}\vec{H}(p,t)\\ \vec{E}(p,t)\end{matrix} = \mp\int_{V_j}\int_{-\infty}^{\infty}\{\vec{j}^{e,pr}(t-\tau)\vec{E}^{e,(m)}(\tau) - \vec{j}^{m,pr}(t-\tau)\vec{H}^{e,(m)}(\tau)\}d\tau dV' \pm \pm\int_{S_l}\int_{-\infty}^{\infty}\vec{J}^{m}(t-\tau)\vec{H}^{e,(m)}(\tau)d\tau dS', \quad (1)$$

where S_l is area occupied by all nonlinear loads.

Nonlinear load is examined which mathematical model coincides with one given in [2], i.e. we assume that it is narrow along z. The electrical current flows through contact along z and magnetic one flows along x and y on wide and narrow walls of the resonator, respectively (Fig. 1). Let's divide contact on N_x elementary sites in wide and N_y ones on narrow walls, which sizes are $\Delta\aleph_m, \Delta z_m$ ($\aleph = x$ or y). Thus within the limits of a site of current amplitudes and contact V-I parameters are possible to be considered as constant ones. Then local nonlinear boundary conditions (NBC) on each site can be obtained according to a technique [2]:

$$J_z^e(p_m,t)\Delta z_m = \sum_{\nu=0}^{Q}\left(a_\nu(p_m)(\pm\Delta\aleph_m J_\aleph^m(p_m,t))^\nu + b_\nu(p_m)\frac{d}{dt}(\pm\Delta\aleph_m J_\aleph^m(p_m,t))^\nu\right),$$

where a_ν, b_ν are load V-I parameters being known as functions of co-ordinates.

Choosing $\vec{b} = \vec{i}_x$ we put the observation point on m_x th splitting site. We obtain the equation system as follows

$$\pm\sum_{\nu=0}^{Q}\left(a_\nu{}_{1/3}(x_{m_x},z_m)\frac{(\pm\Delta x_{m_x})^\nu}{\Delta z_m}[J^m_{x\,1/3\,m}(x_{m_x},t)]^\nu + b_\nu{}_{1/3}(x_{m_x},z_m)\frac{(\pm\Delta x_{m_x})^\nu}{\Delta z_m}\frac{d}{dt}[J^m_{x\,1/3\,m}(x_{m_x},t)]^\nu\right) =$$

$$= -\int_{-\infty}^{\infty}\int_{Vj}(\vec{j}^{e,pr}(t-\tau)\vec{E}^{mx}(\tau) - \vec{j}^{m,pr}(t-\tau)\vec{H}^{mx}(\tau))dV'd\tau +$$

$$+\sum_{m=1}^{M}\left\{\sum_{n_x=1}^{Nx}\{\int_{-\infty}^{\infty}J^m_{x1m}(x_{n_x},t-\tau)\rho^x_{1/3\,1m}(x_{m_x},x_{n_x},\tau)d\tau +$$

$$+\int_{-\infty}^{\infty}J^m_{x3m}(x_{n_x},t-\tau)\rho^x_{1/3\,3m}(x_{m_x},x_{n_x},\tau)d\tau\} +$$

$$+\sum_{n_y=1}^{N_y}\{\int_{-\infty}^{\infty}J^m_{y2m}(y_{n_y},t-\tau)\rho^x_{1/3\,2m}(x_{m_x},y_{n_y},\tau)d\tau +$$

$$+\int_{-\infty}^{\infty} J^{m}_{y4m}\left(y_{n_y}, t-\tau\right)\rho^{x}_{1/3\,2m}\left(x_{m_x}, y_{n_y}, \tau\right)d\tau\Big\},$$

$$m_x = 1...N_x, \qquad (2)$$

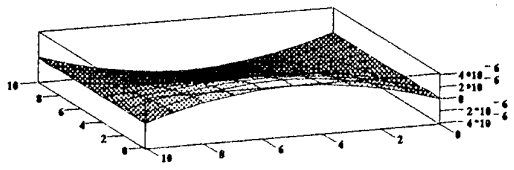
where for loads on the top wall (y = b) the mark "–" and on the bottom ($y = 0$) — "+" are used. For loads on the walls $x = 0$, a it is chosen $\vec{b} = \vec{i}_y$. In (2) there are the following designations: $i, j = 1, ..., 4$ are number of walls; m is number of cross loads; $\rho^{x,y}_{ijm}(\tau)$ are factors taking into account own and mutual influences of m-th load pieces.

We solve the equation system choosing unknown current weight functions as $W_{ij} = \delta(\aleph - \aleph_i)\delta(t - t_j)$ and assuming that up to the moment $t = t_0$ primary source was not included. We break an integration interval on τ into the sum of integrals to Δt site. On each step the equation system concerning unknown currents in the time site is solved.

NUMERICAL RESULTS AND CONCLUSIONS

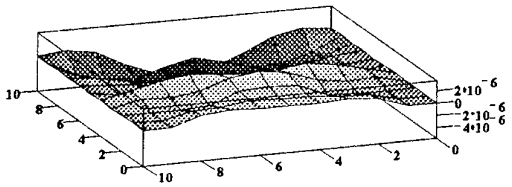
The mode in the resonator is not excited while spectral components getting in a resonator passband are absent in a primary current spectrum. Resonator bottom boundary frequency is determined by frequency of the fundamental mode. If resonator is exited by video pulse with pulse duration τ_p the reduction of the excited fields amplitude in the resonator at first grows, but in the resonator the fundamental mode is still excited, and then with the τ_p further reduction higher-order mode begins to be excited. When mode is excited by a radiopulse with signal frequency, close to mode frequency this results in excitation of quasi- harmonic mode with this mode frequency however a field structure reflects imposing some more several higher modes with close natural frequencies. The rectangular radiopulse duration in a much smaller degree influences to excited EM field structure in the resonator than gauss' one with identical signal frequencies.

We shall note that the presence of loads with large linear conductivity and with weak V-I nonlinearity does not bring in essential changes to field structure and mode frequency in the resonator as against loads with large linear resistance. For example, in Fig. 1 the H_z component distributions are shown when EM-field is excited by a radio pulse with signal frequency close to frequency of a 011-mode: in Fig. 1a load parameters are $a_1 = 0.01$, $a_2 = 0$, $a_3 = 0.0375$; in Fig. 1b — $a_1 = 0.00001$, $a_2 = 0$, $a_3 = 0.0375$.



Hz

a



Hz

b

Fig. 1

Thus, the electrodynamics solution of a pulse excitation problem of the nonlinear loaded rectangular resonator is found. The obtained ratio allows to define directly the time-domain characteristics of field raised by a source with any temporary dependence of a primary current in the resonator with nonlinear loads. The solution takes into account inertial properties of nonlinear loads and nonuniformity of the distributed loads.

REFERENCES

1. J. N. Feld Theorems and Problems of Electrodynamics Non-stationary Process //R&E, 1993. V.38, No. 1. PP.38-48.
2. D. V. Semenikhina, I. E. Dekalo The Electrodynamic Analysis of Microstrip Structure with Nonlinear Elements// Electrodynamics and Technique of Microwave and EHF, 1997.- V.5.- No. 4(20).- PP.83-87.

TRACTS OF KU AND C-BAND ANTENNAS FOR PERSPECTIVE COMMUNICATION SATELLITES

B. V. Sestroretsky, M. A. Drize, S. A. Ivanov, K. N. Klimov

Russia, Moscow, 117296, Universitetsky pr-t 5-358,
tel./fax (095)-938-15-14, const@glasnet.ru

ABSTRACT

The review of results of designing with the help of the topological synthesis technique and results of tract tests for the COUPON, YAMAL, LMI and other satellites is given in this paper.

INTRODUCTION

The necessary rate of researches and development of antennas-feeder devices for perspective satellite communication systems is impossible without creation of new information technologies of designing of devices practically of any topology at an electrodynamic level. The similar technologies, apparently, will not be reduced only to improvement of the widespread techniques of analytical (AS) and parametrical (PS) synthesis using for the computer analysis and optimization certain electrodynamic programs, obtained for specific device topology, on the basis of numerical solution methods of continuous Maxwell's equations for continuous vacuum. The alternative approach is the technique of a topological synthesis (TS) [1] with use of the universal electrodynamic programs (UEDP) based not on the solution of Maxwell's equations for a specific boundary-value problem, but on the impedance [2] or stream [3] operators of discrete (grid) vacuum.

THE REQUIREMENTS FOR THE TRACTS

The new requirements to antenna tracts are:

expansion of operating frequency band for receiving f_r and transmitting f_t up to $f_{t\max}/f_{r\min} = 1.78$–1.75 (Intelsat, YAMAL, LMI) and development of non-standard frequency bands of receiving and transmitting;

providing high values of an ellipticity factor (K_e=0.92÷0.97) and polarization isolation (30÷35 dB) for elimination of undesirable coupling in systems with receiving and transmitting channels multiplexing;

short terms of development of tract modifications (3-4 months for designing and creating the drawings of experimental samples), that practically excludes an opportunity of prototyping;

short terms and low cost of sample manufacturing of an experimental tract batch, that is achieved by use of automated machine tools, by excluding dielectrics, printed-circuit-boards, soldering, by excluding adjusting elements in tracts.

VARIANTS OF TRACTS

Three basic variants of construction of four-port tracts with circularly polarized signals are known (Fig. 1). In the circuit Fig. 1a at first L (left) and R (right) circularly polarized signals are received feed, then the L and R signals will be transformed in linear ones in the polarizer, then the polarizing divider divides linear polarizations, then the duplexer divides → (receiving) and ← (transmitting) frequencies. The and filters carry out an additional channel isolation of the receiver and transmitter.

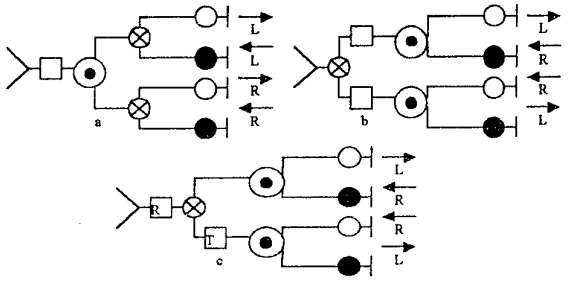


Fig. 1

In the circuit Fig. 1b unlike the considered above circuit Fig. 1b, frequency division in the duplexer is carried out, and then polarization division in the and is made. In the circuit Fig. 1c a polarizing filtration for receiving frequencies in an element is made, then there is a division frequency channel in to the subsequent correction operation of a polarizing filtration on the transmitter frequencies in and operations of polarization division on receiving and transmitting frequencies in polarizing dividers

TOPOLOGICAL SYNTHESIS RESULTS

With a topological synthesis of various Ku and C-band tracts the general approach ensuring performance of the requirement of the maximal simplicity of a design with an manufacturing opportunity of all units on automatic machine tools (milling and electrosparking) and absence of adjusting elements was used. The operational development of the sizes including geometrical error is made during a topological synthesis. The basic sizes, structure and design of basic elements are resulted for

each tract. For major devices (filters, polarizers) invariant relationships allowing to find the most achievable parameter values have been obtained.

KU-BAND TRACTS

COUPON(P), COUPON (C) tracts ($\vec{V}, \overleftarrow{V}, \vec{H}, \overleftarrow{H}$).

The COUPON (P) tract configuration is shown in Fig. 2, where Φ_1 is a receiver filter (f_r frequency receiving), Φ_2 is a transmitter filter (f_t frequency transmitting), Φ_3 is duplexer (separating frequencies f_r and f_t).

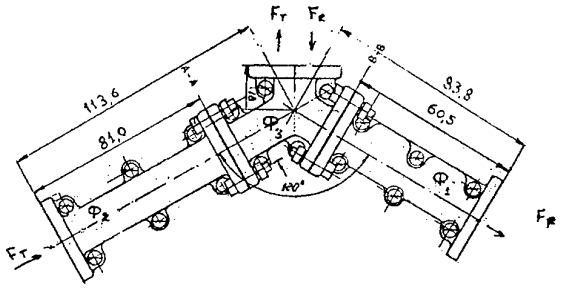


Fig. 2

The COUPON (C) is configured on the basis of a polarizing divider (Fig. 3), to which complect outputs 2 (Fig. 2) are connected. The basic parameters of elements are given in Tab. 1 and [5]. If the work of a tract with circularly polarized signals is provided, the polarizer Fig. 4 (a,b is a geometry of diaphragms, c is VSWR d is a phase shift) is connected between an emitter and divider.

Table 1

($f_r = 10.9-11.7GHz$, $f_t = 14.0-14.5GHz$)

N	Tract elem	Main chan loss, dB	Attenuation, dB	VSWR	Dimensions $L \times W \times m$	Inp. sections mm^2
1	⊖	≈0.1	>100	1.1	60.5×40×40	19×9.5
2	●	≈0.1	>70	1.1	81×40×40	19×9.5
3	⊗	≈0.1	>20	1.1	63×62×40	19×9.5
4	⊙	≈0.05	>35	1.1	60×50×40	19×19, 19×9.5
5	□	≈0.1	>35	1.0	35×35×93	19×19

LMI tract ($\vec{V}, \overleftarrow{V}$).

The configuration of two-port $\vec{V}, \overleftarrow{V}$ tract elements is shown in Fig. 5, where Φ_1 (⊖) is a receiver filter, Φ_2 (●) is a transmitter filter, Φ_3 (⊗) is a duplexer, 1 is an orientation device of a vertical polarization vector, 2 is an adapter from a rectangular waveguide into circular one, 3(⟩—) is an antenna feed. Design and the parameters of units are submitted in Fig. 6, 7, 8.

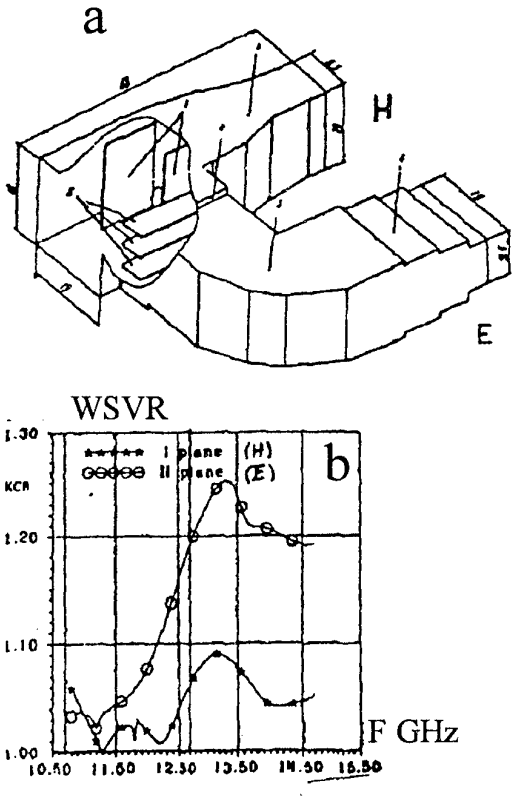


Fig. 3

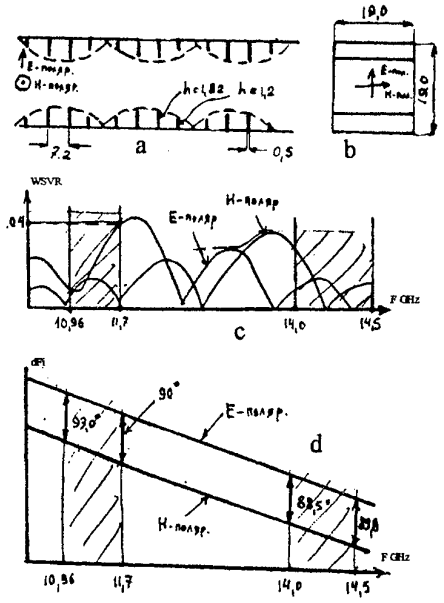


Fig. 4

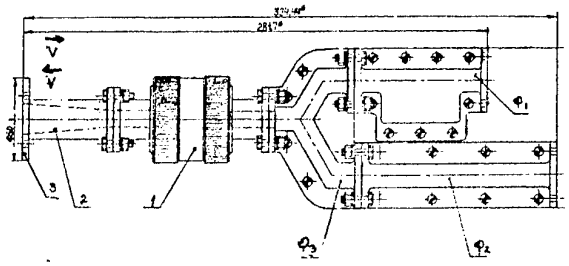


Fig. 5

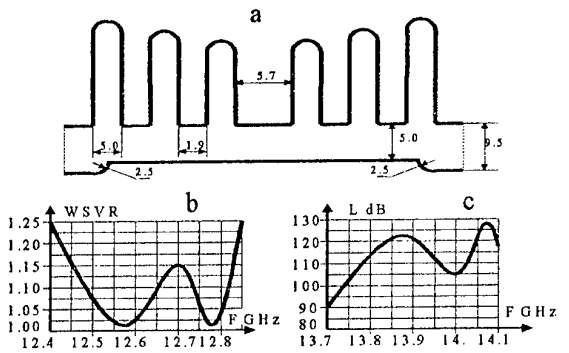


Fig. 6

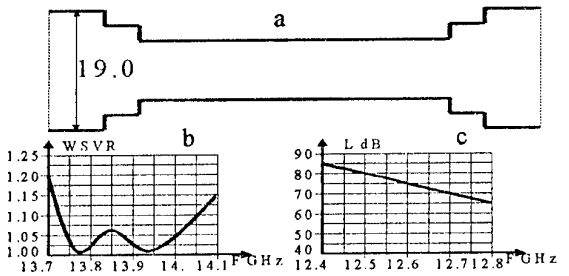


Fig. 7

C-BAND TRACTS

YAMAL (TV) tract ($\vec{L},\vec{R}$).

The tract is depicted in Fig. 12. The design of a polarizing divider and adapters is made as in Fig. 9a,b. Design and the parameters of transformers TR_1 (matching of circular and square waveguides) and TR_2 (matching of a joint of two semiaxis square waveguides turned on 45° around an axis) are shown in Fig. 10 a,b. In small-sized transformers the matching elements of a new type named as "concentrators" are used. For a polarizer based on a square waveguide $a\times a$ and thin diaphragms $a\times m$ (Fig. 4a, 11) the phase shift $\Delta\varphi$ and maximal broadbandness with work only in a receiving band are determined from invariant ratio [10]:

$$\Delta\varphi=\left(\frac{\pi}{2}\cdot\frac{2m}{a}\right)^2\cdot\left(\frac{\Lambda}{a}+\frac{2\cdot a}{\Lambda}\right)\cdot n\,;\ \Lambda_{min}=\Lambda_0\cdot\xi\,;\ \Lambda_{max}=\Lambda_0\cdot\xi^{-1};$$
$$\Lambda_0=a\cdot\sqrt{2}\,;\ \Delta\varphi_{min,max}/\Delta\varphi_0=1+2\cdot\Delta\,;\ \frac{1}{2}\cdot\left(\xi+\frac{1}{\xi}\right)=1+2\cdot\Delta \quad (1)$$

where $\Lambda_{0,min,max}$ are waveguide wavelengths, The index 0 corresponds to a minimum on a curve of Fig. 11b, min and max corresponds to a to values of the minimal and maximal frequencies f_{min} and f_{max}, for which $\Delta\varphi_{min,max}$ increase in $1+2\cdot\Delta$ times in comparison with $\Delta\varphi_0$, m is a width of diaphragms, n is number of diaphragms, $\Lambda^{-2}=\lambda^{-2}-(2\cdot a)^{-2}$, $m<<a$. For $\Delta<<1$ from (1) we determine $\xi\approx 1+2\sqrt{\Delta}$. Assuming $\Delta=0.02$ ($\Delta\varphi=90°\pm 2°$) we find $\xi\approx 1.28$ and $(\lambda_{min}-\lambda_{max})/\lambda_0=(\xi-1/\xi)/3\approx 0.67$, i.e. the least polarizer broadbandness is about 30%.

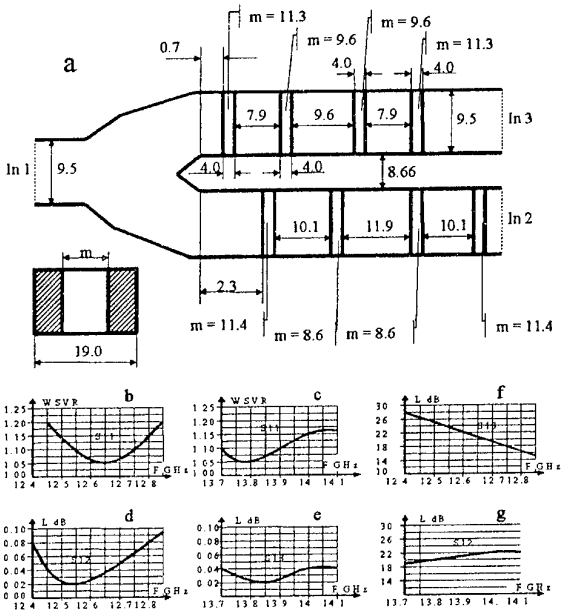


Fig. 8

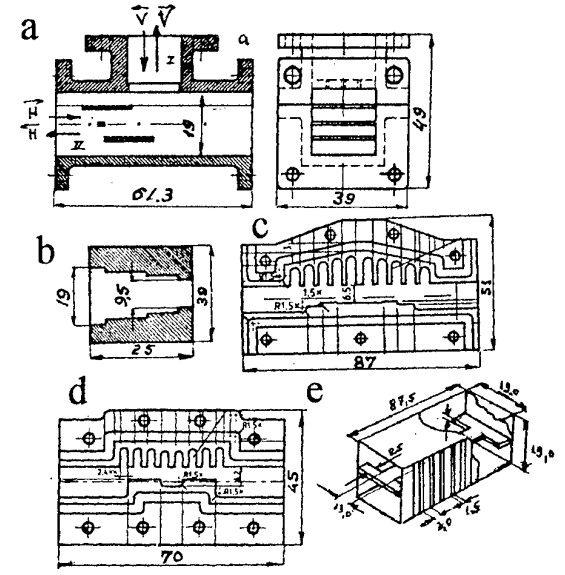


Fig. 9

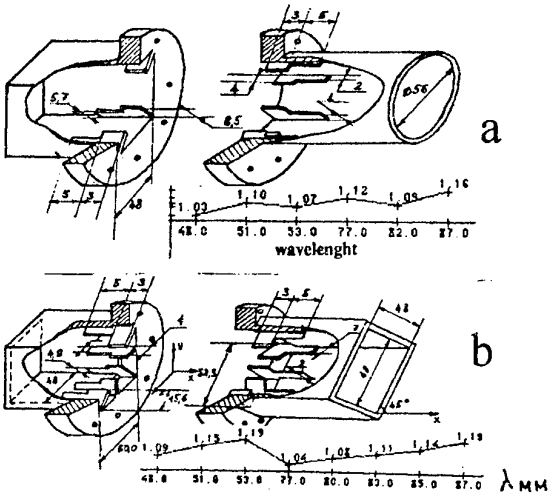


Fig. 10

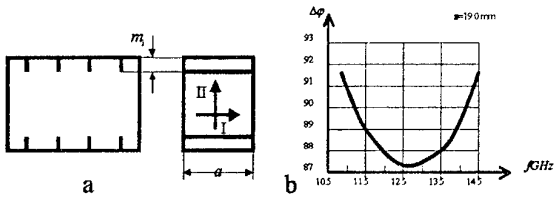


Fig. 11

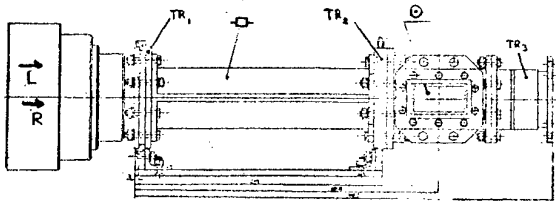


Fig. 12

The restriction of an operating frequency band of a polarizer Fig. 11a is the principle, since it is found from (1) that the width of a square waveguide is limited and is determined from a condition $a = \Lambda_0 / \sqrt{2}$. For a considered tract $f_r = 3.45 \div 4.15 GHz$ $f_0 = 3.8 GHz$ ($\lambda_0 = 79mm$, $\Lambda_0 = 136mm$) from (1) we determine $a = 63.5mm$ and a deviation $\Delta\varphi$ from 90° about ±2° within the limits of a operating frequency band. The following parameters of experimental tract samples Fig. 12 are found: an ellipticity factor K_e=0.90÷0.93 for angles of radiation pattern distinguished from a normal on ±10°, VSWR≤1.3. The VSWR of the feed together with the transformer *TR* is less than 1.2 that determines an isolation between inputs $\vec{L}, \vec{R}$ at a level 20÷30 dB. The radiation pattern width at a level of 10 dB is ±(50÷55°), level of sidelobes is less than 30 dB. The complex researches of tract parameters were carried out on the "Scientific Athlanta" automated stands. The YAMAL (TV) tract receives only signals of one polarization ($\vec{L}$ or $\vec{R}$). The second matched output of a divider allows to remove influence of the second polarization signals on the operating channel with an isolation more than 30 dB. The change of operating polarization direction is made by mechanical turn of units ⋋ and ⊣□⊢ on 90° or by connection of the receiver to the second divider output. The set-up and completion after designing and manufacturing of a tract batch was not made.

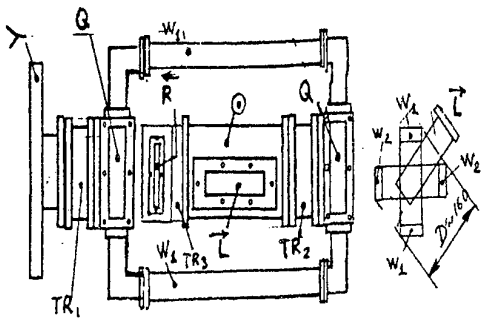


Fig. 13

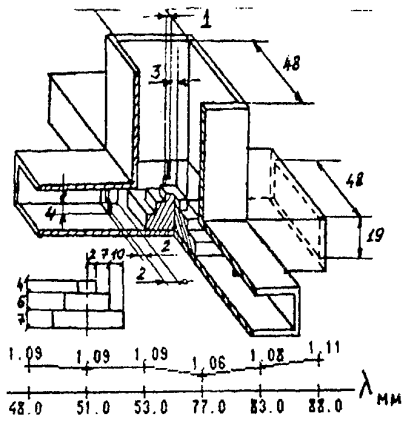


Fig. 14

YAMAL (P) tract ($\vec{L}, \vec{R}$).

The tract has two letter performances : a letter A: receiving of $3.45-3.80 GHz$, transmitting of $5.775-6.125 GHz$; a letter B: receiving of $3.80-4.15 GHz$, transmitting of $6.125-6.475 GHz$. The tract is two-port with operating frequency overlapping $\frac{f_{r\max}}{f_{r\min}} = 1.78$. The basic tract parameters (letter A) as: an ellipticity factor $K_e \geq 0.92$ in sector of radiation pattern 1 dB. The change of a circular polarization direction is carried out manually in severe conditions by turn on 90° of an emitter and polarizer of a tract.

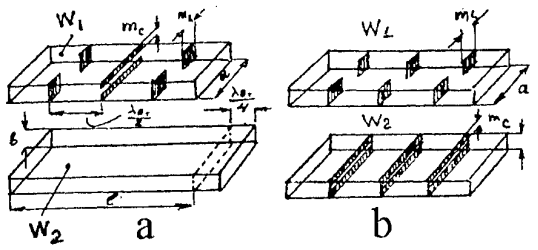


Fig. 15

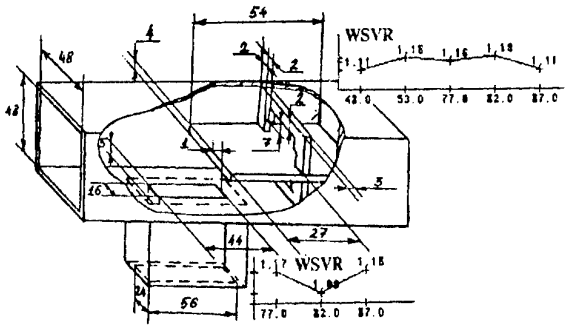


Fig. 16

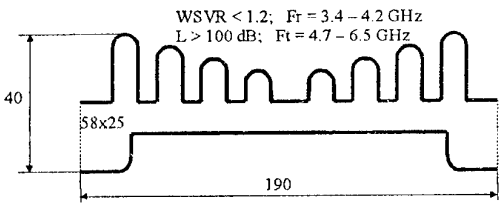


Fig. 17

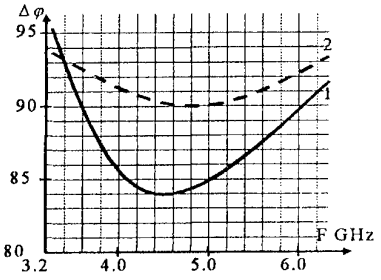


Fig. 18

The tract design is depicted in a Fig. 13, where the designations are used: $\succ$ is an emitter, TR_1 is a transition from round to a square waveguide (Fig. 10a), TR_2 is an element for matching of a joint of two square waveguides turned on 45° (Fig. 10b), Q is a turnstile (Fig. 14), W_1 is a piece of a waveguide containing inductive diaphragms m_L (Fig. 15a), W_2 is piece of a waveguide containing capacity diaphragms m_C (Fig. 15b), $\odot$ is polarizing divider (Fig. 16), TR_3 is adapter from square waveguide to a rectangular one. The rejective filter (Fig. 17) is connected to output flange of the receiver channel $\vec{R}$.

The circuits of three types were considered during a choice of the polarizer:1) using polarizer based on a square waveguide as a the YAMAL (TV) tract polarizer, 2) using two turnstiles and two pairs of waveguides with various length ($l_1 = l_2 + \Lambda_{min}/4$) and circuit of resonators in waveguides, 3) on the base of constructions of Fig. 13 with waveguides W_1 and W_2 with inductive and capacity diaphragms. For the polarizer of type 1 the square waveguide width a is unequivocally determined by sizes f_{min} and f_{max} that determines essential decrease of value $\Delta\varphi$ up to 84° in the area of curve 1 minimum in Fig. 34. The essentially smaller deviation from $\Delta\varphi = 90°$ (curve 2 in Fig. 18) has polarizers of type 2 and 3 with two W_1 and W_2 waveguide pairs. The polarizer of the second type was investigated in details at an electrodynamic level. The $\Delta\varphi = 90° \pm 2°$ performance in receiving $3.45 - 3.90 GHz$ and transmitting $5.725 - 6.475 GHz$ bands is confirmed. $\Delta\varphi = 90° - 3°$ is on $3.90 - 4.175 GHz$ frequencies. Essential disavantage of the polarizer of type 2 is the constructive complexity and length difference of waveguides W_1 and W_2. The polarizer of the third type is equivalent to the second one on electrical parameters and much easier on design. The polarizer of the first type has the most simple design and just it will be used in the first complete sets of a YAMAL (P) tract. The topological synthesis of the polarizer of the third type constructed on the square waveguide base is also carried out. In this design the independent non-interacting inductive and capacity diaphragms are used

RESUME

The technique of the topological synthesis with application of the universal electrodynamic programs based on the stream grid method allows to design all necessary set of waveguide elements which are included in structure of broadband two- and four-port polarizing tracts of antennas for perspective satellite communication systems. The designing is carried out without prototyping. All devices are made on automated machine tools and do not require adjusting operations. Heuristic procedures and the technique of topological invariants used with designing of devices with polarizing and frequency selections allows to provide the optimum values of parameters for the chosen circuit solutions. The new designing technology is illustrated on experience of development of Ku and C band tracts.

REFERENCES

1. B.V. Sestroretsky, E.S. Cuharkin. "Dialogue optimization of devices topology in electrodynamic CAD". Moscow, MEI, 1987.
2. B.V. Sestroretsky. RLC and Rτ analogues of ED space. Proceeding of MIREA "CAD of microwave devices and systems", MIREA, 1977, pp. 127-158.
3. B.V. Sestroretsky. Balance RLC and Rτ-circuits of elementary volume. Problems of radioelectronics, ser." General problems of radioelectronics",1983,vol.5,pp56-85.
4. B.V. Sestroretsky. Balance RLC and Rτ-circuits of elementary volume. Problems of radioelectronics, ser. "General problems of radioelectronics", 1983, vol.5, pp56-85.
5. B.V. Sestroretzkiy, K.N. Klimov, V.Y. Kustov, Yu.O. Shlepnev, Commutation theory and new technology of design of microwave filters. Proceeding of 5th International Symposium on recent advances in microwave technology. Vol. 2, Kiev, Ukraine, September, 11-16, 1995, pp621-626.
6. B.V. Sestroretzkiy, A.G. Nazarov, K.N. Klimov, Electrodinamical analysis and topological optimization of broad band polarized devices. Publication see [5], pp 711-713.
7. C. Zuffada, T. Cwik, G. Ditchman. Synthesis of Novel All-Dielectric Grating Filters Using Genetic Algorithms. IEEE Transactions, vol.AP-46, may 1998, N5, pp657-663.
8. E. Lier, T. Schaung-Petersen. An extremely broadband waveguide polarizer, AP-S Jnst. Symp., Syracuse, June, 6-10, 1988, vol. 3, N8,1988.
9. D.V. Vasiliev. Research and designing of broadband polarizing devices. The dissertation on competition of a scientific degree of Ph.D. Mosc. Tech. Uni. of Communication and Information. Moscow, 1994.
10. B.V. Sestroretzkiy, A.G. Nazarov, K.N. Klimov, Topological optimization of wideband polarized waveguide Tee. Publication see [5], pp 472-474.

ASPECTS OF IMPLEMENTING AN OPTICAL FIBER SOLITON SYNC-NETWORK FOR A COMPLEX OF PHASED ARRAYS

A. S. Shcherbakov, A. Yu. Kosarsky, and V. N. Zvegintsev

Radiophysics Department, Saint-Petersburg State Technical University,
29, Polytechnicheskaya Street, 195251 St. Petersburg, Russia
Phones: (812) 244-1379, (812) 534-3334, (812) 349-9022, E-mail: buzon@softhome.net

In order for operating a complex of phased arrays to be provided, individual arrays, comprising the complex, should be mutually synchronized. Naturally, the delta-function pulse is an ideal sync-signal, but in practice, it can be realized rather approximately. That is why some general requirements to the sync-signals have to be satisfied in the synchronously operating complex of phased arrays with an arbitrary arrangement. These signals should be precisely determined in the time scale as compared with a temporal interval, corresponding to the cut-off frequency in data flow, or to the time jitter conditioned by any internal instability as well as external perturbation. Consequently, the requirements to both the duration and the repetition period of sync-signals increase with growing the informative capacity and processing accuracy. A selection of these problems may be resolved by looking at the technique based on the application of ultrashort optical pulses, which are able to play the part of delta-function-like pulses under certain conditions. The objective in designing a report under proposal is to work out a radically new precise sync-network for synchronizing a medium-base complex of phased arrays. Therefore, we consider some aspects of implementing an optical fiber sync-network using ultrashort optical pulses as the sync-signal carriers. We take the simplest case when identical optical sync-signals are one-directionally distributed from the central processing unit all over the complex (see Fig. 1). These signals are concurrently directed to all phased arrays by different fiber channels, being just those fiber channels which are used for transmission of data signals. Later, after a passage over the arrays, these sync-signals come back at the central processor. The principal measurable value is the clock skew between the energetic centers of ultrashort optical sync-pulses passed in parallel through different fiber channels. However, this brings up the problem of estimating picosecond temporal intervals, suggesting that one needs ultrafast photon-to-electron conversion to be accomplished. Nevertheless, this difficulty can be successfully overcome if the repetition period inherent in the sync-pulses is sufficiently short. To keep a picosecond accuracy in electronic post-processing we rely on measuring the train-average clock skew.

Evidently, the preference should be given to the sync-signal carriers in the form of picosecond solitons being capable of passing through single-mode low-loss fibers at a short repetition period. As this takes place, the accuracy of synchronization is ultimately restricted by an error in determining the energetic center of a sync-pulse. In its own turn, such an error is no more than the sync-pulse width, so the application of soliton regime to transmitting the sync-signals through single-mode fibers is an essential prerequisite to create a complex of phased arrays with a picosecond accuracy of synchronization.

The phenomenon of the self-phase modulation is capable of compensating a dispersive broadening of ultrashort pulse in the anomalous dispersion region of single-mode fiber and thereby of shaping a stable carrier in the form of picosecond optical soliton. Unfortunately, evolution of optical soliton in a fiber is also conditioned by optical losses whose action may be defined by the parameter $\Gamma = 2\pi c\gamma\tau_0^2\lambda^{-2}D^{-1}$ (where c is the light velocity; γ and D are the coefficients of optical losses and dispersion, respectively; λ is the wavelength, lying in the anomalous dispersion region; τ_0 is the initial pulse width), which represents the ratio of the dispersion distance Z_d to the loss distance γ^{-1}.

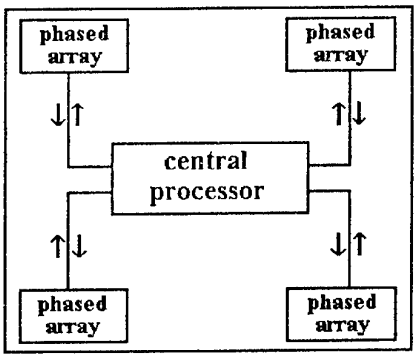


Fig. 1. The scheme of an optical fiber sync-network

If the parameter $\Gamma = 0$, the initial balance between dispersion and nonlinearity gives rise to the fundamental soliton when the initial energy of such a pulse is $E_f = \lambda^2 D\,(\pi c\sigma\tau_0)^{-1}$, where $\sigma = 2.7$ rad/W/km in standard single-mode silica fiber. When $\Gamma \ll 1$, a fundamental soliton cannot exist in an ideal sense, because optical losses induce adiabatical perturbation

due to broadening on the soliton pulse as $\tau(z)=\tau_0\exp(2\gamma z)$. In the case of $\Gamma \le 1$ or $\Gamma > 1$, to realize the soliton-like regime of pulse propagation in a lossy fiber the initial amplitude of a pulse should exceed the amplitude of fundamental soliton in the same but lossless fiber. The initial energy of soliton-like pulse is determined as $E_l = a_0^2 E_f$, where a_0 is the above mentioned excess of the pulse amplitude over the one of an ideal fundamental soliton with the same initial width τ_0. When propagating the soliton-like pulse exhibits self-compression up to the distance L_{min} and return of its own width to the initial value followed by broadening a pulse.

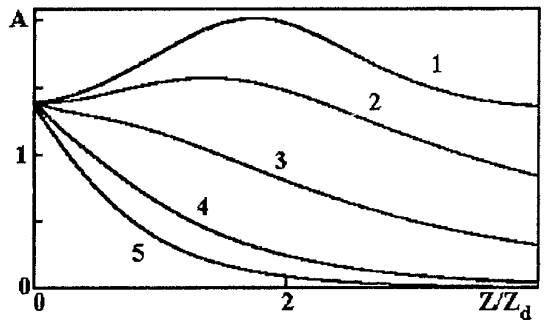


Fig. 2. Spatial dependencies of the amplitude, normalized to the amplitude of fundamental soliton in lossless fiber, for soliton-like pulses with $a_0 = 1.4$. The length of a fiber is normalized to the dispersion distance Z_d. The curves from 1 to 5 correspond to $\Gamma = 0.015$, 0.1, 0.3, 0.8, and 1.3, respectively

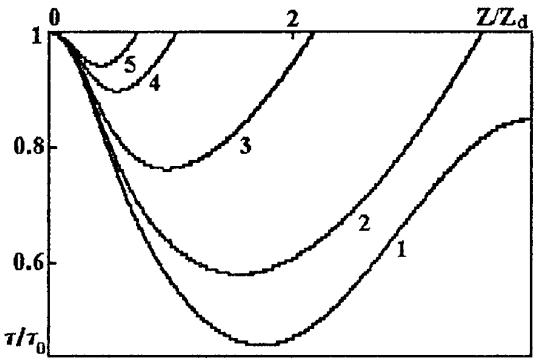


Fig. 3. Spatial dependencies of the width, normalized to its initial value, for soliton-like pulses. The magnitudes of all the parameters are the same as in Fig. 2

From the viewpoint of the maximum accuracy of synchronization, associated with the minimum magnitude of the width τ_s of sync-pulse arriving at the central processor, the designer of a complex gains two scopes for doing. The first scope is in using adiabatically perturbed fundamental soliton whose initial width is determined as $\tau_0 = \tau_s \exp(-4\gamma L_0)$, where L_0 is the arm length. The second one is in exploiting the soliton-like pulse with $\tau_0 = \tau_s$ as sync-signal carrier. The relation of initial energies E_f and E_l is the governing factor in deciding between adiabatically perturbed fundamental soliton and soliton-like pulse whose width are the same at the distance associated with twiced arm length $2L_0$. The soliton-like pulse is initially less energetic than fundamental soliton, i.e. $E_l < E_f$, when the following condition is true: $2L_0 > L_a = \gamma^{-1} \ln a_0$. For typical magnitudes $a_0 = 1.4$ and $\gamma = 0.5$ dB/km one can obtain $L_a = 9.2$ km. Consequently, the soliton-like pulse is energetically best suited carrier for a medium-base complex.

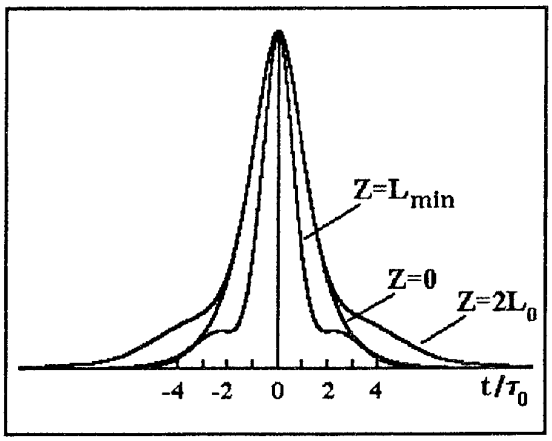


Fig. 4. Evolution of the soliton-like pulse as it passes the fiber arm ($a_0 = 1.4$, $\Gamma = 0.1$); here L_{min} means the distance in the fiber at which the pulse attaines its minimum width

Technically well-grounded parameters of both the sync-signal carrier and the single-mode fiber arm can be chosen using spatial dependencies of the amplitude and width for soliton-like pulses, presented in Figs.2 and 3. It is seen that the primary self-compression stage is accompanied by the increase in the amplitude only when Γ is small. In the other cases the monotonous lowering of the amplitude is observed. Fig. 4 shows that the energetic center of soliton-like sync-pulse has no temporal shift while a pulse is passing through a fiber arm. The above-considered return of pulse width to the initial value is also clearly seen.

Thus, key aspects of implementing a novel optical synchronization technique based on picosecond soliton-like pulses in single-mode fiber, being suitable for a medium-base complex of phased arrays, are considered in the report. Moreover, some properties of soliton-like sync-signal carriers under proposal are also discussed.

EXPERIMENTAL INVESTIGATION OF ANTENNA CHARACTERISTICS OF RADIOELECTRONIC ELEMENTS

A. V. Timchenko, V. I. Chumakov, O. I. Kharchenko*

Kharkov State Technical University of Radioelectronics
310726, av. Lenin, 14, Kharkov, Ukraine
* Kharkov Military University
310022, sqv. Svobody, 6, Kharkov, Ukraine

INTRODUCTION

Because of the difficulty and variety of designs of radioelectronics equipment (REE), analytical description of processes of interaction of electromagnetic wave (EMW) with REE can be carried out only in the most general case [1–3]. This is caused by that the process of interaction radioelectronic elements unit (REU) with the electromagnetic field is defined not only by parameters of radiating – a power, electrical and magnetic fields intensity, wavelength, a pulse duration (in the case of pulsed radiating), but as well as by features of object, to which EMW falls – geometric sizes, mutual orientation of object's elements with respect to vectors of electrical and magnetic fields, permittivity and magnetic permeability of object material.

Process of interaction of field with the object consideration is based on antenna model, according to which geometric object elements are presented by elementary antennas loaded on its internal structure elements. Thus, for instance, the semiconductor integrated circuit (IC) with the package leads length l is considered as an object, then the process of EMW incidence with arbitrarily oriented components of vectors E and H can be shown as in Fig. 1.

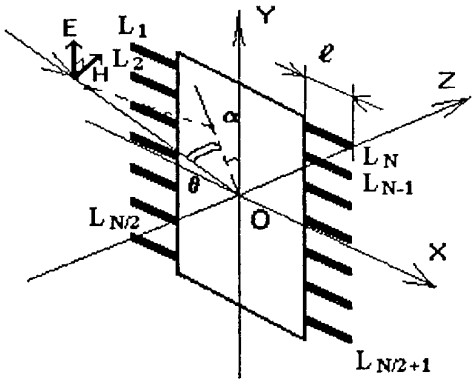


Fig. 1. IC antenna model
(package leads length is equal l)

Herewith, it is obvious that the energy, which escapes on internal structure elements of IC, is defined not only by the geometry of package leads, but also essentially depends on circuit engineering realization, because the load resistance of the elementary antenna can be of an arbitrary character (in general – complex resistance). Resistance schemes of planar IC periferic elements in Fig. 2 show possible form of the reaction on incident EMW. Experimental investigations of RE antennas characteristics allow to define its major electrodynamic parameters and choose the most optimum elements for designing REE operating under conditions of intensive electromagnetic irradiation.

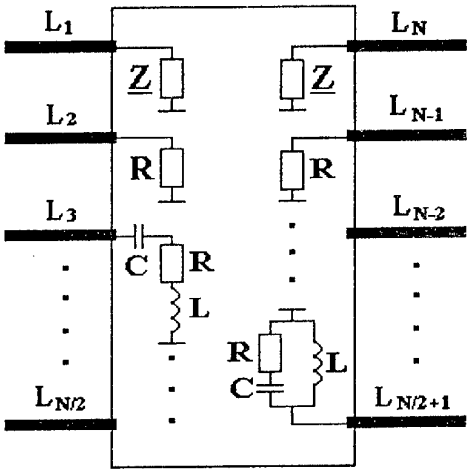
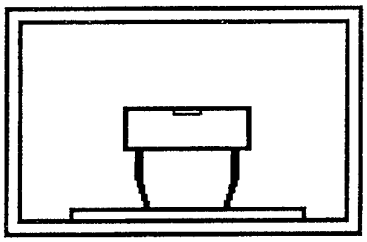


Fig. 2. Antennas loading model

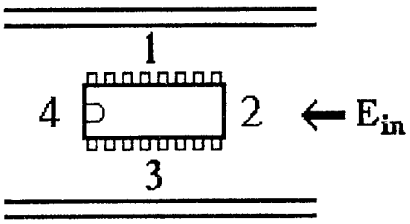
DESCRIPTION OF EXPERIMENTAL UNIT

The investigations of electrodynamics characteristics of REE were carried out by means of the panoramic rectangular waveguide standing-wave meter. As testing objects some different types of semiconductor IC and transistors were chosen, made in packages of several modifications (planar, metal-ceramic, plastic, metal-glass and others.). The REU under test was located into waveguide on dielectric base, ensuring galvanic uncoupling of metallic package and internal surface of the waveguide (Fig. 3a). The waveguide was matching loaded and calibrated beforehand. In such a position measurements of VSWR and reflectivity of the waveguide line with situated inside objects in the calibrated band 3.5–4.5 GHz with frequency response flatness of 0.25 dB were fulfilled.

For the influence study of mutual orientation of field vectors components and package leads the REU was rotated in respect of coordinate axes chosen in waveguide. Under changed position of REU new measurements of VSWR and reflectivity were carried out. Fig. 3b shows the scheme of location REU inside waveguide and distinctive positions, under which measurements were implemented.



a



b

Fig. 3. IC location inside waveguide

RESULTS OF EXPERIMENTS

REU types and main results of experiments are listed in Table. Fig. 4 shows frequency dependencies of VSWR (1, 2 – IC K1HT591 in positions 4 and 3 respectively, 3 – IC K1KT241 in the position 2, 4 – a transistor МП 26Б). As seen, transistors and IC in different packages have substantial differences in electrodynamics characteristics. The most important are resonant frequency dependencies of VSWR and reflection factor for different types of REU. Orientation of REU inside waveguide is of significant influence as well.

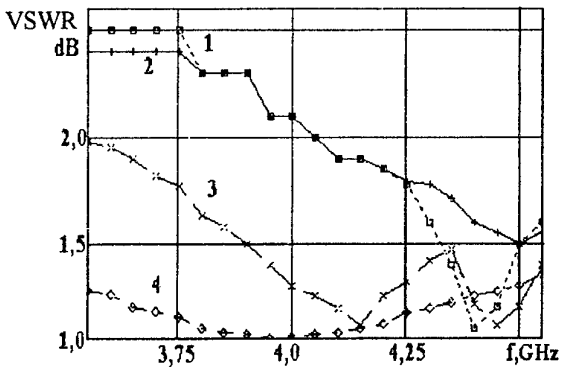


Fig. 4. VSWR frequency dependencies

Change of position of IC in DIP-type package, leads to both changes the absolute minimum of resonant curves and change of resonance frequency. Similar picture is observed for IC in round packages (TO-5 type), in spite of their symmetrical location under turn inside waveguide. Moreover, for some elements in round packages with symmetrical outputs the change of orientation leads to drastic changes of the frequency dependencies (resonant or uniform). Such an effect from the point of view of antenna model can be explained by more significant influence of frequency-selective characteristics of elementary antenna load. Resonance frequencies correspond to the load matching with elementary antenna regime, under which the efficient "extracting" of falling wave energy is observed [3].

CONCLUSION

Results of experiments show that interaction of electromagnetic field with radioelectronic elements and components, in general, are inserted in frames of antenna models. When scheduling, an elementary anten-

Table

Results of experiment

Radioelectronic elements	Type of IC and transistors	Package type	Frequency dependence of VSWR features	Resonant frequency, GHz	VSWR range, dB
Integrated circuit	TTL	Plastic, DIP	Resonant	3,83 3,58 3,87	0,8
	TTL	Metall-ceramic, planar	Uniform	–	
	Analog	Metall-glass, TO-5	Oscillating, resonant	– 4,16 4,4	0,4
Transistors	Low-power, HF	Metallic	Oscillating	–	

nas loads equivalent scheme it can be seen it is necessary to take into consideration both active resistors placed on the surface of IC chip which take into account dissipative characteristics of load, and reactive component, defining its selective properties. Reaction of IC in DIP packages on the direction of falling electromagnetic wave is also observed. Determination of electrodynamic characteristics of REE and resonant frequency measurement for different elements contain the auxiliary initial data for designing REE, that satisfy the electromagnetic compatibility, as well as allow to analyze reasons of REE failure, caused by electrical overstress.

REFERENCES

1. Radioelectronic facility and powerful electromagnetic interferences / V.I. Kravchenko, E.A. Bolotov, N.I. Letunova.- Moscow Radio i swjaz, 1987. - 256 p. [in Russian].
2. Mirova L.O., Chepizhenko A.Z. Resistance of communication equipment to ionazing and electromagnetic radiations. Moscow, Radio i swjaz, 1988.-296p. [in Russian].
3. Bludov S.B., Gadetski N.P., Magda I.I. et al. Generation of high-power UHF pulses and their action on radioelectronic equipment // Fizika plazmi, 1994, v.20, N.7,8, p.712-717 [in Russian].

RECTANGULAR WAVEGUIDE FILLED WITH BIANISOTROPIC MEDIUM

K. A. Vytovtov, I. V. Petrusenko

Dnepropetrovsk State University
Radiophysics Department, Naukova,13 str., Dnipropetrovsk–50, 320625, Ukraine, tel. 43–36–30,
E-mail: vytovtov@ap1.net–rff.dsu.dp.ua

STATEMENT OF PROBLEM

In resent years there have been a growing interest in new synthetic materials for special applications in applied electromagnetics [1–3].

In this work the rectangular waveguide filled with uniaxial bianisotropic medium $(x\in[0;a],\ y\in[0;b],\ z\in(-\infty;+\infty))$ is considered. Material relations describing this medium are [1]:

$$\begin{aligned}\vec{D}&=\overline{\overline{\varepsilon}}\vec{E}+j\overline{\overline{\xi}}\vec{B};\\ \vec{H}&=j\overline{\overline{\xi}}^{T}\vec{E}+\mu_0^{-1}\vec{B},\end{aligned}\qquad(1)$$

where

$$\overline{\overline{\varepsilon}}=\begin{vmatrix}\varepsilon_{xx}&0&0\\0&\varepsilon_{xx}&0\\0&0&\varepsilon_{zz}\end{vmatrix},\ \overline{\overline{\xi}}=\begin{vmatrix}\xi_{xx}&\xi_{xy}&0\\-\xi_{xy}&\xi_{xx}&0\\0&0&\xi_{zz}\end{vmatrix}.\qquad(2)$$

The expressions for the tensors elements are given in [1].

It is assumed that harmonic wave with frequency ω propagates within the considered waveguide.

Solutions to Maxwell's equations system

$$\begin{cases}\nabla\times\vec{H}=-j\omega\vec{D};\\ \nabla\times\vec{E}=j\omega\vec{B};\end{cases}\qquad(3)$$

may be written in form

$$\begin{aligned}\vec{E}(x,y,z)&=\vec{E}(x,y)e^{-jk_z z};\\ \vec{H}(x,y,z)&=\vec{H}(x,y)e^{-jk_z z},\end{aligned}\qquad(4)$$

as the waveguide is regular. The wave equations system for longitudinal components of the field is [1]:

$$\begin{cases}\nabla_t^2E_z+\gamma_{EE}^2E_z+\gamma_{EH}^2B_z=0;\\ \nabla_t^2B_z+\gamma_{HH}^2B_z+\gamma_{HE}^2E_z=0.\end{cases}\qquad(5)$$

Although material relations (1) are not general expressions but it is shown clearly that system(5) describes any bianisotropic guiding structure. Therefore, the proposed mathematical method is general. Additionally dependence of parameters on frequency is presented for this case in [1].

METHOD OF INVESTIGATION

The solution of the wave equations system (5) satisfying boundary conditions on the perfectly conducting walls of the waveguide can be written in the form

$$\begin{aligned}E_z=&\left(A_1\cos k_{x1}x+B_1\sin k_{x1}x+\right.\\&\left.+A_2\cos k_{x2}x+B_2\sin k_{x2}x\right)\sin k_y y;\end{aligned}\qquad(6)$$

$$\begin{aligned}H_z=&\left(Z_1A_1\cos k_{x1}x+Z_1B_1\sin k_{x1}x+\right.\\&\left.+Z_2A_2\cos k_{x2}x+Z_2B_2\sin k_{x2}x\right)\cos k_y y,\end{aligned}$$

where the constants A_1, A_2, B_1, B_2 depend on the wavenumber, frequency, value a, and are defined by following relations

$$A_2=-A_1\ ;\ B_2=-\frac{Z_1k_{x1}}{Z_2k_{x2}}B_1;$$

$$B_1=\frac{Z_1k_{x1}\sin k_{x1}a-Z_2k_{x2}\sin k_{x2}a}{Z_1k_{x1}\left(\cos k_{x1}a-\cos k_{x2}a\right)},\qquad(7)$$

where the wave resistences are

$$\begin{aligned}Z_1&=\frac{k_1^2-\gamma_{EE}^2}{\gamma_{EH}^2}+j\mu_0\xi_{zz};\\ Z_2&=\frac{k_2^2-\gamma_{EE}^2}{\gamma_{EH}^2}+j\mu_0\xi_{zz}.\end{aligned}\qquad(8)$$

From (6) we have the following expression for the transversal y–component of the wavenumber

$$k_y=\frac{\pi m}{b}.\qquad(9)$$

Taking into account (5) and (6) we obtain that the transversal x–components of the wavenumber are defined by the following relation

$$k_{x1,2}^2+k_{y1,2}^2=k_{1,2}^2,\qquad(10)$$

where

$$\begin{aligned}k_{1,2}^2=&\frac{\gamma_{EE}^2-\gamma_{HH}^2}{2}\pm\\&\pm\sqrt{\frac{\left(\gamma_{EE}^2-\gamma_{HH}^2\right)^2}{4}-\left(\gamma_{EE}^2\gamma_{HH}^2-\gamma_{EH}^2\gamma_{HE}^2\right)}.\end{aligned}\qquad(11)$$

From (10) and (11) it is seen that the x–components of the wavenumber are the functions of the longitudinal

component k_z as the γ_{EE}^2, γ_{EH}^2, γ_{HE}^2, γ_{HH}^2 are the functions of the k_z [1] if frequency is constant.

At given values a and b the longitudinal component can be defined as the solution of the trancendental equation

$$2Z_1Z_2\sqrt{\left(k_1^2-k_y^2\right)\left(k_2^2-k_y^2\right)}\times$$
$$\times\cos\left(a\sqrt{k_1^2-k_y^2}\right)\cos\left(a\sqrt{k_2^2-k_y^2}\right)+$$
$$+\left[Z_1\left(k_1^2-k_y^2\right)-Z_2\left(k_2^2-k_y^2\right)\right]\times \qquad (12)$$
$$\times\sin\left(a\sqrt{k_1^2-k_y^2}\right)\sin\left(a\sqrt{k_2^2-k_y^2}\right)=2.$$

Thus, the magnitudes $k_{x1,2}$, k_y, k_z are bound and they are functions of frequency and dimensions of the rectangular waveguide filled with uniaxial bianisotropic medium. *TEM*-, *TE*- and *TM*-waves can not exist within this waveguide. Only hybrid waves propagate. Since (5) we can consider resulting wave as superposition of two waves with x–component of wavenumber k_{x1}, k_{x2}. These waves are analogous to anomalous waves within waveguide filled with ferrite.

Analogously, we can show that the following solution of the system (5) satisfy boundary conditions on the perfectly conducting walls

$$E_z=\left(A_1\cos k_{y1}y+B_1\sin k_{y1}y+\right.$$
$$\left.+A_2\cos k_{y2}y+B_2\sin k_{y2}y\right)\sin k_x x; \qquad (13)$$
$$H_z=\left(Z_1A_1\cos k_{y1}y+Z_1B_1\sin k_{y1}y+\right.$$
$$\left.+Z_2A_2\cos k_{y2}y+Z_2B_2\sin k_{y2}y\right)\cos k_x x.$$

Solution of the equation (12) can be obtained only by numerical methods. However, accurate analytical solution exists in some particular cases.

Let us investigate the solution (6) when $Z_1k_{x1}=Z_2k_{x2}$. Analysis of this case gives an idea about general regularity of wave behavior within the considered waveguide. The transversal x–component for this case are

$$k_{x1}=\frac{2\pi n}{a}\frac{Z_2}{Z_1-Z_2}\ ;\ k_{x2}=\frac{2\pi n}{a}\frac{Z_1}{Z_1-Z_2}, \qquad (14)$$

and longitudinal component is to be defined from 4–th order algebraic equation

$$k_z^4+pk_z^2+jqk_z+r=0. \qquad (15)$$

The coefficients p, q, r are not written down here because of their bulk.

The equation (15) may be solved analytically, therefore analysis of wavenumbers may be carried out analytically. Existence of four longitudinal wavenumbers is the result of analysis of (15).

If $\xi_{xy}=0$ in (2) than $q=0$ and (15) is biquadratic equation. One or two waves may be propagating within waveguide. In this case phase velocities of direct waves are equal to the ones of back waves.

If $\xi_{xy}\neq 0$ in (2) then $q\neq 0$ and the following cases are possible:

1. Four wavenumbers are real values. Two waves can propagate within waveguide. Phase velocities of direct waves are not equal to the ones of back waves.
2. Two wavenumbers are real values and two are imaginary values. Real wavenumbers have opposite signs. One wave can propagate within the waveguide. Phase velocity of the direct wave is not equal to the one of back wave.
3. Two wavenumbers are real. Sings of wavenumbers are equal. In this case back waves do not exist.
4. Four wavenumbers are imaginary values. Both waves are unpropagating.

Each of these cases may be obtained for certain medium parameter, frequency, and dimensions of waveguide.

CONCLUSIONS

Analytical solution of Maxwell's equation that describe wave behavior in rectangular waveguide filled uniaxial bianisotropic medium are presented. That is particular case but not general solution. It is shown that two waves with different phase velocities exist within this waveguide. It is show also that phase velocity forward wave is not equal phase velocity of back wave if $\xi_{xy}\neq 0$.

REFERENCES

1. I. P. Theron, J. H.Cloete, The Electric Quadrupole Contribution to the Circular Birefringence of Nonmagnetic Anisotropic Chiral Media: A Circular Waveguide Experiment, IEEE MTT-44,No.8,1996,pp.1451-1459.
2. Y. Xu and R. G. Bosisio, An afficient method for study of general bi-anisotropic waveguides,IEEE Trans.Microwave Theory and Techniques, vol.43, pp.873–879, 1995.
3. R. D. Graglia, M. S. Sarto, P. L. E.Uslenghi, TE and TM Modes in Cylindrical Metallic Structures Filled with Bianisotropic Material, IEEE MTT-44, N8, pp.1470-1477, 1996.

INVESTIGATION OF THE COMPLEX PERMITTIVITY OF COALS AND OIL PRODUCTS BY THE RADIOPHYSICAL METHODS

S. V. Buharov, V. V. Ovsianicov, I. V. Petrusenko, A. G. Hundriga

Dnepropetrovsk State University, Ukraine 320625 Dnepropetrovsk, Naukova str. 13, Radiophysics Dep., phone (0562)433-630, e-mail: root@ap1.net-rff.dsu.ua

INTRODUCTION

Measurements of the complex permittivity $\varepsilon = \varepsilon' - i \cdot \varepsilon''$ allow to carry out fast control of the dielectric and semiconductor materials quality. Sometimes, this control measurement may complete or substitute the chemical, physical, optical and others types of analysises. Admixture, added into pure substance, change the significance of complex permittivity. The microwave measurements of ε' and $tg\delta$ may be used by the chemical, food and others industries to control technological processes, and by the research laboratories, which need in the information about the substance characteristics. The waveguide and resonant-cavity methods of dielectric constants measurements are the most widely used methods. They allow to comprise the wide band of values of Dielectric Constant and Loss Tangent and do not demand special equipment. For the complex permittivity measurements equipment for research of feed lines and antennas at microwave frequencies may be used. The Resonant- Cavity method provides relatively high precision of permittivity measurements for dielectric substance with low Loss Factor ($tg\delta < 0{,}01$) and Dielectric Constant , from 1 to 40. This method allow to measure parameters either of the separate specimen, or parameters of substance in the torrents (for the liquid and powder substances). The Waveguide method allow to measure ε' and $tg\delta$ practically of all dielectric materials. The specimen may be situated in the waveguide [1, 2] or in free space [5].

THE RESONANT-CAVITY METHOD

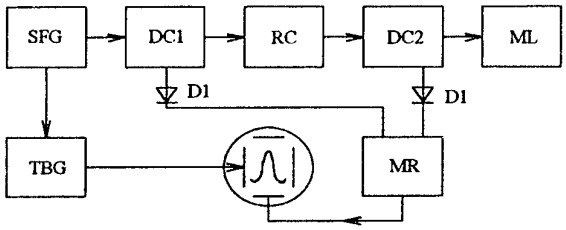
The Resonant-Cavity method is based on the determination of the resonance frequency and quality factor of the empty resonator (f_0 , Q_0) and the resonance frequency and Q-factor of the filled by the substance resonator (f_1 , Q_1). When resonant-cavity is full of the researched substance and relative magnetic permittivity is equal to unit ($\mu_r = 1$), we have

$$\varepsilon' = (f_0 / f_1)^2 \text{ , } tg\delta = 1/Q_1 - 1/Q_0.$$

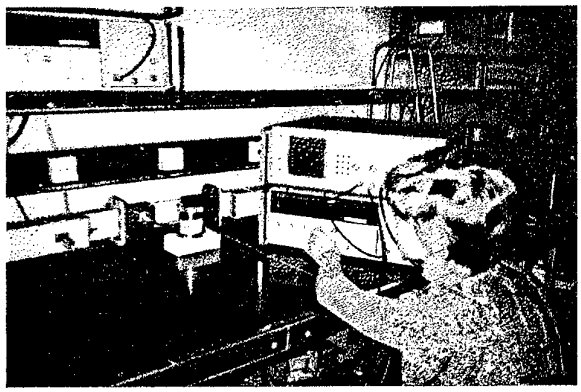
Some results of the complex dielectric permittivity measurements are given in Table 1. Scheme of the equipment used in the measurements, is shown in Fig. 1.

Table 1

Substance	ε'	$tg\delta$
oil	2.14	$8.5 \cdot 10^{-3}$
benzine A-76	2.05	$6 \cdot 10^{-3}$
toluol	2.37	$8 \cdot 10^{-3}$
benzol	2.28	$4 \cdot 10^{-3}$



a)

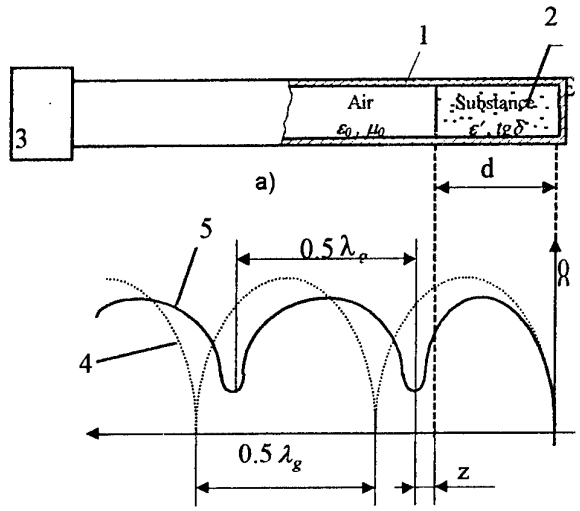


b)

Fig. 1. Measurement of the complex permittivity by resonant-cavity method:
a) Scheme of the set: SFG – sweep-frequency generator; DC – directional coupler; RC – resonant-cavity; ML – matched load; D – high-frequency detector; TBG – time-base generator; MR – meter of the ratio;
b) Appearance of the set.

THE WAVEGUIDE METHOD

The waveguide method is based on the interaction between electromagnetic wave directed by the feed line and researched substance. One of the more widely used methods is based on the impedance measurement of the filled by the specimen waveguide fragment. A value of the impedance is used for calculation of the dielectric constant and loss tangent, in accordance with the interaction model. The scheme of the equipment, realizing the waveguide method, is shown in Fig. 2.





c)

Fig. 2. Measurement of the complex permittivity by waveguide method:
a) The scheme of measurement set:
1– the waveguide; 2 – the specimen of the substance; 3 – the measurement device;
b) The diagrams of the standing wave in the waveguide: 4 – without the specimen; 5 – with the specimen;
Appearance of the set.

The specimen 2 is situated at the end of the measuring waveguide 1. Information about VSWR and phase angle $\theta = 2\pi \cdot z / \lambda_g$ (where z is the distance between the specimen surface and the first knot (minimum) of the standing wave in the waveguide, λ_g is the wavelength in the waveguide without specimen) is obtained with the measure apparatus 3. The waveguide fragment's (with specimen) impedance is

$$Z = Z_0 (1 - i \cdot S \cdot \mathrm{tg}\theta) / (S - i \cdot \mathrm{tg}\theta)$$

(where Z_0 is the wave impedance of the waveguide without the specimen, S is the VSWR). Significances of ε' and $\mathrm{tg}\delta$, we need in, are obtained from the solution of the following equation:

$$\frac{th(\gamma \cdot d)}{\gamma \cdot d} = -i \cdot \frac{\lambda_W (1 - i \cdot S \cdot tg\theta)}{2\pi d (S - i \cdot tg\theta)},$$

where $\gamma = i \cdot \frac{2\pi}{\lambda_0} \cdot \sqrt{\varepsilon' - i \cdot \varepsilon'' - (\frac{\lambda_0}{\lambda_C})^2}$,

γ is the constant of the wave spreading in the waveguide fragment with the specimen; λ_0 is the wavelength in free space; λ_C is the cut-off wavelength for type of wave used in measurements in the concrete waveguide.

If we introduce $\gamma d = a + i \cdot b$ and separate real and imaginary parts, we shall obtain the following system of equations:

$$\begin{cases} \dfrac{a \cdot sh\,2a + b \cdot \sin 2b}{(a^2 + b^2)(ch\,2a + \cos 2b)} - X = 0, \\ \dfrac{a \cdot \sin 2b - b \cdot sh\,2a}{(a^2 + b^2)(ch\,2a + \cos 2b)} - Y = 0, \end{cases}$$

where

$$X = \frac{-\lambda_g \cdot (1 - S^{-2}) \cdot tg\theta}{2\pi d (1 + S^{-2} \cdot tg^2\theta)},$$

$$Y = \frac{-\lambda_g \cdot (1 + tg^2\theta)}{2\pi d \cdot S (1 + S^{-2} \cdot tg^2\theta)}.$$

The obtained system of equation

$$\begin{cases} f1(a,b) = 0; \\ f2(a,b) = 0 \end{cases}$$

is solved by numerical methods at the computer. There are some methods of the analogous systems of equations solving. We used the following methods:

The 1-st: using the Newton's method:

$$a_{n+1} = a_n - \frac{f_1(a_n,b_n) \cdot \frac{\partial f_2(a_n,b_n)}{\partial b} - f_2(a_n,b_n) \cdot \frac{\partial f_1(a_n,b_n)}{\partial b}}{\frac{\partial f_1(a_n,b_n)}{\partial a} \cdot \frac{\partial f_2(a_n,b_n)}{\partial b} - \frac{\partial f_1(a_n,b_n)}{\partial b} \cdot \frac{\partial f_2(a_n,b_n)}{\partial a}};$$

$$b_{n+1}=b_n-\frac{f_2(a_n,b_n)\cdot\frac{\partial f_1(a_n,b_n)}{\partial a}-f_1(a_n,b_n)\cdot\frac{\partial f_2(a_n,b_n)}{\partial a}}{\frac{\partial f_1(a_n,b_n)}{\partial a}\cdot\frac{\partial f_2(a_n,b_n)}{\partial b}-\frac{\partial f_1(a_n,b_n)}{\partial b}\cdot\frac{\partial f_2(a_n,b_n)}{\partial a}};$$

where

$$\frac{\partial f_1(a_n,b_n)}{\partial a},\frac{\partial f_1(a_n,b_n)}{\partial b},\frac{\partial f_2(a_n,b_n)}{\partial a},\frac{\partial f_2(a_n,b_n)}{\partial b}$$

values of the partial derivatives when $a = a_n$,

$$b = b_n$$

As the first approach we used:

$a = 0{,}07$; b is the approximate solution of the equation

$$\frac{tgb}{b}=X.$$

The 2-nd method: the initial problem of the solving of the equations system is rediced to the one of the minimum searching of the two variable functions (problem of the optimization). We used the function

$$f(a,b)=(f1(a,b))^2+(f2(a,b))^2.$$

One of the descent methods is the one of the local variations was used for the solving of this problem. As the first approach we used the same magnitudes, as used in the Newton's method. The counting process was stopped, when the following conditions were obtained: $\left|\frac{a_{n+1}-a_n}{a_n}\right|<10^{-4}, \left|\frac{b_{n+1}-b_n}{b_n}\right|<10^{-4}$ (in the Newton's method) or $f(a,b)<10^{-8}$ (in the minimum searching).

After that found significances a and b, were recounted into parameters ε' and tgδ:

$$\varepsilon'=\frac{(b/d)^2-(a/d)^2}{(2\pi/\lambda_0)^2}+\left(\frac{\lambda_0}{\lambda_c}\right)^2;$$

$$\varepsilon''=\frac{0{,}5\cdot a\cdot b}{(\pi\cdot d/\lambda_0)^2};\quad tg\delta=\frac{\varepsilon''}{\varepsilon'}.$$

Theoretically, we obtain an interminable number of the system's roots (because periodical functions come in to the system), but practically correct value of ε' and tgδ are situated among the first five roots (depending on the thickness of the substance value). That is why preliminary information about ε' and tgδ values is important. Some results of the complex permittivity measurements for several liquids and powder substances are shown in Table 2.

Table 2

Substance	Parameter					
	Measurement			From [1,2]		
	ε	ε''	tgδ	ε	ε''	tgδ
Water	75.8	10.3	0.14	79.3	7.9	0.1
Acetone	22.3	2.23	0.1	21.3	16.7	0.78
Toluol	2.28	0.13	0.06	2.38	0.047	0.02
Coal	2.95	0.21	0.07	—	—	—
Ashes	3.17	0.4	0.13	—	—	—

Another type of the waveguide methods use the interaction between the irradiated to the substance surface (situated out of the waveguide (in free space)) and reflected signals. Radiating and receiving the electromagnetic signals are realized by the directional antennas. The reflected signal brings the information about the reflectivity value and phase. This information is used for the consequent searching of the complex permittivity.

CONCLUSION

These investigations have shown, that the resonant-cavity and waveguide methods may be widely used for rapid control of the different liquid and powder materials quality at the chemical, food (etc.) industries, and at the research laboratories. Realization of these methods allow to use resources more rationally to make more effective control of different industrial production's processes, where on information about substance parameters is required, to make research at synthesis of the dielectric materials with required values of the dielectric constant and loss factor.

REFERENCES

1. A. A. Brandt, Investigation of the dielectric at microwave frequencies, YIFML, Moskow, 1964 [in Russian].
2. A. F. Harvey, Microwave engineering, London and New York, 1963.
3. GOST 8.358-79.
4. GOST 8.544-86
5. Vicker R., Rose G. The use of complex dielectric constant as a diagnostic tool for the remote sensing of terrestrial materials., Dep. Elec. Eng.,Colorado State Univ., Project Themis Sci.,Rep.5,Sept. 1971.
6. V. V. Ovsianicov, Vibrator antenna with reactive loads, Moscow, Radio i Sviaz, 1985.

RATIONAL TECHNOLOGIES AND MICROWAVE DESIGNS FOR GYPSUM BINDER, CASEIN, FRUITS, VEGETABLES AND OTHER FOOD-STUFFS

A. I. Dokhov, V. V. Zhirnov, N. E. Lukyanenko

Kharkov-State Technical University of Radio-Electronics (KHTURE)
310726, Kharkov, pr. Lenina, 14

Electrothermal processing by microwave field is one of the perspective methods of exposure on materials, biological objects, agricultural and food-stuffs and so the investigations in this direction are rather urgent for national economy [1–2].

The authors developed economical technologies allowing to produce high-quality gypsum binder, casein and other building materials, as well as technologies and designs for drying grain, fruits, vegetables and other agricultural and food-stuffs using a combined multifunction method by the way of direct influence on the material by a hot air and microwave energy [3, 4].

In the report are stated rational, from the point view of economy, variants of construction of plants of combined type. Below main features of proposed technologies and designs of plants are given.

The proposed technology of gypsum binder production includes the thermal processing of gypsum stone by irradiating it with microwave field of microwave–field of Hmo range of 110-130 W/kg power during 20-30 minutes. The gypsum stone and electromagnetic field interaction is based on the mechanism of energy transmission to substance of high dielectric permittivity.

This interaction main peculiarity is that it takes place within the whole volume of substance (gypsum stone) simultaneous uses. As a result, thermal energy is radiated by the whole medium volume whereas interaction with environment is realized only through its surface. As a consequence of this a temperature rises in the sample center more intensively than on its surface. Owing to this, pressure is (up to 15-16 atm) created in gypsum stone middle and under its effect micropores are formed, through which water is pressed out to the sample surface and is evaporated (dehydration) due to additional absorption of microwave–energy. The heating of gypsum stone (bihydrate gypsum) with the purpose of its conversion into half-hydrate of α and β modifications is realized for no longer a 10 minutes (under condition of preliminary heating gypsum stone surface up to 120 ^{0}C). Without premilinary heating dehydration process is realized for 45-50 minutes.

The proposed technology of gypsum production enables to produce high quality gypsum binder (gypsum half-hydrate of α and β modifications) with high productivity and small power consumption as compared with known technology of gypsum production in autoclaves at the heated vapour pressure of 6 atm and following drying of steamed stone in the same autoclaves, where cycle lasts 29 hours and is not non-stop. At the proposed technology and plant a cycle of gypsum dehydration is 30 minutes and α–gypsum outcome efficiency runs to 25–35%, i.e. its productivity is raised approximately 20 times in comparison with the known technology.

The technology of casein and other building materials production includes thermal processing of raw material by means of electromagnetic radiation processing jointly with processing by hot air at 90...100 ^{0}C. For this there were incorporated a chamber of hot air wind and a one of water vapour extract.

Using of such multifunction method of processing cheeses by microwave energy and energy of hot air allows to reduce a consumption of microwave energy when producing 1 kg of casein 1.5...2 times and enlarge productivity approximately in 2 times as compared with processing with microwave energy alone.

As a basis of technology and design of combined microwave–system for drying grains, fruits, vegetables and other agricultural products and food-stuff was used the thermal processing by electromagnetic. microwave–energy irradiation of 50...130 W/kg power during 7...30 minutes with additional dehydration of working raw material by heated air and pneumatic withdrawal of air together with water vapour when withdrawal flow is controlled.

The technology on the base of the microwave–energy use for agricultural and food-stuff drying ensures high productivity with small power consumption, as well. The advantage is 2 times approximately.

Fields of using: Agricultural processing industry, food production. Practical importance in world is of wide scale: proposed technologies on the basis of microwave–energy use are ecologically pure as they are based on using only electric energy. Besides, the realization of technologies to be created will enable to replace power-consuming productions, which are based on using such energy sources as petroleum product and gas. For Ukraine daily economy may be hundred millions of USA dollars.

REFERENCE

1. Microwave power engineering. Vol. 2/Application of microwave energy in the industry/, M.: Mir, 1971, P.272. (in Russian) 2. Jacques Thuery. Microwaves Industrial, Scientific, and Medical Applications/ Edited by Edward H. Grant King's College London. London: Artech House, INC., 1992. 667 P. 3. Patent №2040498, registered in RF 25.07.95. 4. Patent №22036, registered in Ukraine 22.08.97.

BACK CHANNEL IN DIGITAL MMDS

A. I. Dolgonos, H. L. Baindurashvili*, A. M. Voychinsky

"Unique Broadband Systems, Inc.", *"Unique LLC"

The MMDS transmission system is a low cost television transmis-sion media. While the transmission of cable-television signals over coaxial lines has existed for many years, MMDS (known as "wireless cable") is gaining popularity for its easy maintenance and low cost.

MMDS systems are providing not only transmitting of broadcast analog TV channels now, but also are using as a basis for creating of complex digital systems. Besides of transforming analog signals to digital forms these systems allow to build wireless Internet delivery system for fixed and mobile wireless applications, telephone networks, systems of transmitting data with speed > 2 Mbps, and controlling systems. The portfolio of MMDS products offered by Unique Broadband Systems, Inc., Canada includes equipment to satisfy all systems requirements. The product includes transmitters and repeaters with equivalent output power capabilities ranging from 5 Watt to 1000 Watt. The outdoor equipment is designed to provide years of trouble free service and is robust, and can be configured in dual redundant broadband. A VHF band input signal is routed to a broadband PIN diode attenuator and upconverter assembly, were it is mixed with a low phase noise, local oscillator signal. A sample of the input signal is taken for monitoring purposes. A mixer output filter then selects the upper sideband signal, which is fed to the output power amplifier for amplification to the level required for transmission. A sample of the output amplifier signal is fed back to the PIN diode attenuator control circuitry closing the automatic level control loop. An additional RF sample is also taken and used for monitoring purposes. The transmitter output is protected from reflected signal power, lighting and corona dis-charge.

The front panel allows easy access to all system components for maintenance purposes. The transmitters are forced air-cooled and are able to operate over a wide indoor temperature range so they do not specifically require HVAC. The powering requirements are standard 115 Vac mains.

Front panel test points allow you to directly measure input and output signals and access the down-converter

VHF output. Voltage levels which represent input signal and local oscillator presence, ALC, output power amplifier temperature, power supply output and detected output power may be viewed at the front panel LCD display. All system parameters are internally monitored and in the event of a malfunction a summary alarm contact closure is provided. Transmitter output level is controlled from a front panel adjustment. A transmitter can also be equipped with an optional microprocessor board for remote monitoring and control using a host PC.

The Transmitter Redundancy Switch (TRSD) allows two transmitters to operate together in a dual redundant configuration. A dual redundant transmitter switch system finds application in locations were the modulator outputs are available and can be combined into two groups. During normal operation each of the two transmitters receives one half of the total number of channels. Under these conditions the output carrier power from each transmitter can be increased by 3 dB for a given intermodulation level. In the event either transmitter is taken off line, the switch transfers the total combined channel load to the remaining transmitter and it's internal automatic level control adjusts the output carrier power maintaining the same intermodulation level. If the channels cannot be combined into two groups a standby redundant transmitter switch system is required. TRSD systems are available for either indoor or outdoor applications.

Our experience shows that MMDS is truly infrastructural, it should give rise to many other industries within the Russian economy. Russia with its population 149 million and more than 30,000,000 homes has 4.6 million cabled homes, or only 15 %.

This is exactly our point: we believe that when driven by an infrastructurally-oriented business plan, MMDS will create hundreds of market niches, each representing opportunities for new industries to emerge. Free market economics can be unleashed to create both anticipated and unanticipated opportunities.

18th Session of the Board of the RCC Communications Administrations Heads-Ministers (Chisinau, September 30-October 1, 1997) and Sevastopol conference "Microwave and Telecommunications technology" have confirmed global solutions of UBS MMDS Systems for the former USSR:

- UBS which has been manufacturing products for more than 8 years is a leading Canadian designer and manufacturer of cable television equipment (5 MHz-1000 MHz). UBS' products for the CATV and LAN industries have won the award of the best RF passive items as commodity products in Russia. It was nominated by All-Russian Cable TV Association. This award was result of votes by both retailers, dealers and organizations of CATV and LAN industries, who com-

pare and recommend products by prices, terms of delivery and payment, specifications, quality and warranty;

- In 1993 its daughter company UBS-Russia, also known as UBS-R, was founded by UBS in St. Petersburg. UBS-R designs and manufactures products to meet the viewing and networking needs in the former Soviet Republics, Eastern Europe and Scandinavian. In addition to manufacturing and supplying products into the local markets, during the last two years UBS-R has shipped thousands of passives to UBS. They are being sold across the USA, Canada and abroad. Locally, UBS-R maintains a network of strategically situated dealers and distributors;

- UBS also does research, development and manufacturing of MMDS Transmitters and Downconverters for CIS and warrantees that the equipment meets published specifications and the international cable and broadcasting standards for this type of equipment. UBS-R with facilities in STP can provide turn key certified MMDS systems at low cost within 60-90 days. All repairs can take place at the UBS-R facility Service Center in St. Petersburg, UBS-R as usual may be responsible for the installation.

-The UBS MMDS Transmission System is a low cost television transmission media. A video and audio signal is fed to a modulator assembly. These signals can be from a downconverted satellite feed, a studio camera, a video recorder, or any similar device. The combined audio-video signal is modulated to comply to the SECAM format and upconverted to a frequency in the 200 MHz to 400 MHz frequency spectrum. The modulator frequencies are allotted in such way that no two signals occupy the same frequency slot. The modulator output goes to a broadband combiner. The combined signals are available at the output signal port.

The isolation of the combiner prevents signals generated in one modulator from adversely affecting the output of any other modulator. The combiner output is at a relatively low frequency when compared to the transmission frequency (10:1). Therefore, the signal can be distributed over distances of several hundred feet without severe insertion loss or signal degradation. This combined block of signals becomes the input to the transmitter. The transmitter upconverts and amplifies this information. Its frequency band is from approximately 2.5 GHz to 2.7 GHz. The amplifiers are ultra linear solid state Gallium Arsenide (GaAs) units. The high linearity is required to reduce the effects of cross modulation and composite triple beat from degrading the television signal. The transmitter is located in as close proximity as practical to the antenna since cable insertion loss increases with increasing frequency. The amplified signal is routed to the antenna assembly using the appropriate low loss transmission line. The antenna acts as a transformer allowing efficient radiation to space. The antenna pattern determines the direction of radiated energy thereby increasing the power density in a desired direction. This energy gained from the antenna patterns as compared to the transmitter amplifiers is a more cost effective way to increase the system output power. The radiated energy is received by the subscriber using a small antenna and downconvertor assembly. At this point the process is reversed and the information is extracted from the received energy and distributed to the desired locations.

As to single channel MMDS version, Metromedia International Telecommunications, Inc. has installed 10 systems in the former USSR, but it is very expensive equipment. The cost of Comwave made transmitters is about $500K. Only "new Russians" can afford to pay more than $30.00 per month for 24 channels. Of course, such expensive channels must be scrambled immediately.

UBS has another strategy: free advertiser-supported programming, educational television and distance learning.

To create economic growth and ensure widespread usage, technology must be affordable for a large number of users.

INFLUENCE OF NONLINEAR CAPACITANCE OF A MICROWAVE RECTIFYING DIODE ON RECTENNA CHARACTERISTICS

A. I. Luchaninov, M. A. Omarov, A. A. Konovaltsev

Kharkov State Technical University of Radio Electronics
Prospekt Lenina 14, Kharkov 310726, Ukraine
e-mail: tea@kture.kharkov.ua

Nowadays radio electronic devices are widely used in many fields of national economy. One of these fields is the space energetics, where systems of wireless power transmission by a microwave beam (WPT system) are rather viable and have good prospects for realization. A transmitting part of WPT system, radiating a required power and forming the microwave beam of a desired form, is maintained on a power satellite supplying energy to a few space vehicles. As receivers of energy on these vehicles arrays of antenna-rectifiers (rectennas) are used, which transform microwave energy into direct current by means of rectifying Schottky diodes.

Computation of main rectenna characteristics is performed by the methods of the theory of antennas with non-linear elements [1]. One of the computation stages is the selection of a simulation model of the rectifying Schottky diode. In [2] it is shown that when a WPT system is operating at the frequency of 2.45 GHz, the Schottky diode can be sufficiently represented as a nonlinear resistance assuming that the diode capacitance does not depend on the level of the input signal.

However the use of the mentioned above model leads to considerable errors of calculation when the dynamic range of an input signal is widening and the WPT system operating frequency is raising (for example to the frequencies of the millimeter wave range).

The paper presents the results of investigations of rectenna characteristics when the Schottky diode is simulated by a parallel connection of the nonlinear resistance with the following characteristic

$$i(u)=\begin{cases} I_S\left(e^{\alpha u}-1\right), \text{at } u \le U_\partial \\ D(u-U_\partial)+I_S\left(e^{\alpha u}-1\right), \text{at } u > U_\partial \end{cases} \qquad (1)$$

and the nonlinear capacitance $C(u)$ defined as

$$C(u)=\begin{cases} \dfrac{C_0}{\left(1-\dfrac{u}{\varphi_k}\right)^{\nu}}, \text{ at } u \le U_{\max} \\ C_{\max}\left\{k(u-U_{\max})+1\right\}, \text{ at } u > U_{\max}. \end{cases} \qquad (2)$$

In (2)

$$U_{\max}=\varphi_k\left\{1-\exp\left[\frac{1}{\nu}\ln\left(\frac{C_0}{C_{\max}}\right)\right]\right\},$$

$$k=\frac{\nu C_0}{\varphi_k C_{\max}\left(1-\dfrac{U_{\max}}{\varphi_k}\right)^{1+\nu}},$$

u is the input signal voltage; I_s is the saturation current; α is a constant; D is the parameter, determined experimentally for the good convergence of an iteration process to be provided; C_0 is the diode capacitance when $u=0$; $C_{\max}$ is the diode capacitance when $u=U_{\max}$; $U_{\max}$ is the voltage defined from $(\varphi_k-U_{\max})/U_{\max} << 1 \neq 0$, φ_k is the contact potential difference, $\nu=0{,}5$.

Numerical investigations of rectenna characteristics have been performed at frequencies of 2.45, 10 an 35 GHz taking into account the nonlinear dependence of the Schottky diode capacitance on the level of the input signal as well as ignoring it. It was clarified that when frequency increases the errors of rectenna characteristics estimation increase and can attain the value up to a few dozens of percent if dependence $C(U)$ is not taken into account. This dependence influences considerably on the course of a curve $P_0(S)$, where P_0 is a power of direct current in a rectenna load, S is a flux density of the microwave beam falling on the rectenna aperture.

In the paper the results of computation and experimental investigations of the dependence $P_0(S)$ of a specific rectenna are compared as well. This comparison confirms the possibility to use expressed as (1) and (2) model of rectifying Schottky diode in practice.

REFERENCES

1. Luchaninov A.I., Shifrin Y.S. Antennas with nonlinear elements // Chapter IX in "Reference book on antennas technique" / vol.1 Editors: Bakhrakh L.D. and Zelkin E.G., - Moscow, IPRZhR publishing, 1997 [in Russian].
2. Shifrin Y.S., Luchaninov A.I., Shokalo V.M., Shcherbina A.A. Methods for Increasing of Large Rectenna Efficiency // Turkish Journal of Phisics. – 1996. –v.20. –No.8. –pp.856-861.

TRANSMISSION OF AN E-MAIL FORMAT SIGNALS IN MF/HF RANGES IN A MARINE RADIO COMMUNICATION

V. N. Martynkin, Y. V. Malyarenko

Odessa State Marine Academy, Odessa, Didrichson Str. 8, Building 7

A transmission of E-mail format signals discovers more and more broad application for safe navigation in a marine radio communication.

The transmission of the E-mail format signals is carried out in ranges of average, intermediate and short waves. In comparison with a radio telephone a doubtless advantage of a radiotelex is in documenting the messages and saving them on a paper and magnetic carriers as a text files of an information. The special attention, in turn, is attracted by transmission of E-mail format signals on middle- and high- frequencies (MF: 1605-4000 kHz, HF: 4-27.5 MHz). It is stipulated by that the singular advantages are exhibited in a short-wave range, when the radio-frequency voice communication is unstable from various parasites and singularities of radio waves passing. In radio telex an influence of these parasites can be practically reduced to a minimum and irritant fadings, misses of connection, natural for a radio telephone being not appreciable for an operator of radio telex communication. In the field of an information of transmission by E-mail format signals it is reached by application of special methods of coding of an information permitting to discover and to correct errors.

Originally for radio telex communication between vessels or between vessels and coast servers the condition of direct printing was used at which in a radio channel the International telegraphic code (ITC-2) was applied. In this code each transmitted sign is represented by five binary elements. Such a condition is characterized by low reliability of transmission of an information, as the code ITC-2 does not ensure protection from hindrance of an information. The entrance into the communication is carried out manually.

Since the 70-th years an implementation of a new equipment of narrow-band direct-printing telegraphy (NBDP) starts, using improved methods of coding of an information. In correspondence with the requirements ICCR in radio telex, 7-element synchronous codes with constant ratio of number of "units" to number of "zero" equal to 3/4 are used. Each transmitted numeral is represented by a family of binary figures – bits, and only the combinations with three "units" and four "zero" are used. Such code in theory of coding is named as a code with constants of weight equal to three. The total number of code combinations have a weight equal to 3 being equal to number of permutations from three "units" and four "zero" that under the formula of a theory of combinations gives

$$C_7(3,4) = 7!/3!4! = 35 .$$

All these 35 combinations are enough for representing of all of the 32-nd numerals of a code ITC-2. The code with a ratio equal to 3/4 does not require start and stop bits because it is synchronous. Additional bit of check on evening is not required also because virtue of a constant ratio of number 1 to number 0.

For error detection at reception of each code combination its weight, or number of units is calculated. If the weight of an adopted code combination is equal to three or the ratio of number of units to number of zero is equal to 3/4, it is considered that the code combination is adopted correctly. Otherwise it is considered, that there was an error. Such code discovers all single errors (such as replacements 1 on 0 and on the contrary) and majority of errors of the greater multiplicity for which weight of a code combination is broken. In real digital channels with an error tending to grouping in packages, and besides inside one package the distortion is in one direction: the zero are substituted by units and on the contrary. For such asymmetric data links errors find out practically always and not undetected errors, for which the ratio is equal to 3/4 is constant, are very rare.

For an error checking in radio telex the following measures are adopted:

1) active method by recurring numerals adopted with an error (the condition ARQ);

2) transmission of each numeral twice with an offset through four numerals, without any re-request of transmission of the error block (condition FEC).

A condition ARQ (Automatic Repetition request – the Automatic demand of a recurring) provides retransmission of an information at a detection of an error on a receiving extremity. The station transmitting the message, is named conducting (Master) as the server, and receiving – driven (Slave) by the server. The master server transmits the block from three numerals. The slave server checks up if it is a ratio equal to 3/4 for each numeral in the block. After receptions of each block the driven server transmits confirmation about a regularity (or error). In a case when all three numerals are adopted correctly, the slave server transmits a sign of confirmation and readiness for reception of the following block. If even for one from numerals the ratio equal to 3/4 is defaulted, the driven server gives a demand for a recurring of the block. The retransmission of the block can be repeated up to 32 times. If all 32

attempts of transmission of the block are unsuccessful, the master server automatically initiates new call. If this call also appears unsuccessful the transmission of the message is also canceled and both servers pass in a condition Standby.

This process of block transmission, checking and repetition of transmissions of the deformed blocks happens automatically, it is imperceptible for an operator.

After transmission of the message in one direction the servers can interchange their roles and the transmission will be carried out in the opposite direction.

The given condition is characterized by the following features:

- correct message passing practically is guaranteed, if only the connection is generally possible;
- the connection is possible only between two servers;
- the guard from unauthorized reception of a telex is ensured;
- the driven server should use the transmitter.

The condition FEC (Forward Error Correction) is a condition without a demand of retransmission. The transmitting station transmits the message with a recurring of each numeral twice, with temporal gap through four positions. The interval between duplicates of the same numeral makes 280 ms at a transfer rate of 100 bauds. The receiving station checks up each numeral on the relation equality to 3/4, if this relation is withstand even for one from two numerals the adopted numeral is printed out and the relation 3/4 is not withstand for both numerals, instead of it the asterisk is printed. Thus, in a condition FEC only the error detection is practically ensured.

The condition FEC is characterized by the following features

- the message is addressed simultaneously to all servers, which can accept it;
- the accepting server works with the switched off transmitter;
- the confirmation in reception of the message is absent;
- there is no active error-checking;
- there is no guard from unpermitted reception of the messages.

Under the condition FEC the transmission of one concrete server (selective call – SEL/FEC) is possible by transmission of a telex code of the accepting server. Only server having such telex code receives the message. All other servers will ignore it.

As a rule the FEC condition is used for circular transmissions to all servers and is an ideal condition for transmission of an information to courts which cost in ports having no possibilities to work in transmission.

There are two possible basics in radio telex in essence of various mode of transmission, namely:

- base band signaling in real time (Direct);
- transmission with intermediate storage on the coast server (Store and forward, Mail).

At base band transmitting of signals each numeral of the text at once is received by the recipient and is printed out. The base band transmitting of signals is carried out both for the condition ARQ and for the condition FEC. At intermediate storage the message at first is completely transmitted to the coast server and then to final abonent (subscriber).

Through the 38 Rules of a radio communication for each ship station working under the NBDP condition the five-digit number of a selective call or nine-digit identifier of a marine mobile service (MMSI) in the correspondence with Application 43 PP are appropriated. For each coast station working in a NBDP condition four-digit identification number or nine-digit identifier of a marine mobile service (MMSI) in the correspondence with Application 43 PP are appropriated.

To be convinced, that the calling server has incorporated with the required coast server, ship station or subscriber of a coast telex web on installation of a radio telex line the procedure of interchanging by auto answering is provided. The auto answering of the ship server includes:

- telex number of selective call;
- call sign signal of ship radio station;
- the English letter 'X', indicating, that the server is the marine mobile one.

Example of auto answering of the ship server: 53248 UEUA X.

The auto answering of the telex abonent of a coast web includes:

- telex number of the subscriber;
- short word or group of the letters companies, designating a title;
- continuant of country (English letter/letters).

Example of auto answering of the telex subscriber of a coast web:

69789 SPRAD DK (S.P.Radio corporation, Denmark).

The installation of connection with use of conventional ground communication facilities including in a MF/HF range begins with call on a DSC system (digital selective call).

OPTIMIZATION OF ELECTROMAGNETIC FIELD EXCITATION FOR MICROWAVE INDUSTRIAL AND AGRICULTURAL APPLICATION

G. A. Morozov, I. E. Sedelnikov

The Research Centre of Applied Electrodynamics of Kazan State Technical University
420503, box 381, Kazan, Russia
E-mail: root@kaiadm.kazan.su

ABSTRACT

The aim of the paper is to discuss the modern approaches to the problem of electromagnetic field excitation efficiency improvement for operating chambers used for microwave industrial and agricultural applications.

Problems of microwave excitation optimization are divided into two classes: optimisation under requirements for electromagnetic field intensity and in accordance with the different kind requirements for the temperature field distribution. Optimization problems accordingly to these two classes are formulated and calculation methods are discussed.

INTRODUCTION

Recently the progress in the area of microwave industrial and agricultural application is closely approaching to the problem of efficient microwave radiators development. The principle consideration in microwave radiators design is to establish the electromagnetic or heat fields of the certain characteristics within the confines of the treated substance.

Typically a microwave radiator is made as a closed or semi-open partially filled resonator of different form whose dimensions are of the order of tens of the wavelength excited by some radiator. Electromagnetic field inside such a resonator, being a result of modes combining launched by the used exciter, is substantially non-uniform.

The promising idea is to use a multi-element resonator excitation with the aim to improve the field intensity distribution within the treated media. On the other hand, a theory of antenna array pattern synthesis has attained a high level of perfection by now. Advances in array synthesis theory and practice have led to a wider adoption of obtained results to allied applications. The objectives of this paper are different approaches for microwave radiators optimization based on array synthesis methods.

PROBLEMS OF EXCITATION OPTIMIZATION

Problems of microwave devices excitation optimization can be divided into two classes. Problems of optimization under requirements for electromagnetic field intensity can be classified within the E-class ./1/. For this cases the optimization problem can be formulated as finding the elements location ($\vec{r}_n$) and excitation

$$\dot{U}_n = U_n \times \exp\left(j\Psi_n\right),$$

n = 1-N under some requirements for the certain electromagnetic field intensity $E_g(\vec{R})$ within some part (V_s) of the internal volume of the microwave resonator:

$$A\left(\dot{U}_1 \ldots \dot{U}_N, \vec{r}_1 \ldots \vec{r}_N, \vec{R}\right) \rightarrow E_g\left(\vec{R}\right), \qquad (1)$$

$$\vec{R} \in V_s$$

where A is the direct problem operator describing the excitation-fied intensity distribution, $\vec{R}$ are the coordinates and N is a number of exciters.

The problem of excitation optimization in accordance with the different kinds of requirements for the temperature field distribution can be classified within T-class. The first type (T_1) of them consists in finding the excitation which minimizes the deviation of the steady-state temperature field from the certain temperature distribution within the treated media $T_g\left(\vec{R}\right)$:

$$B\left(\dot{U}_1 \ldots \dot{U}_N, \vec{r}_1 \ldots \vec{r}_N, \vec{R}\right) \rightarrow T_g\left(\vec{R}\right) \qquad (2)$$

$$\vec{R} \in V_s$$

where B is the direct problem operator describing the excitation-temperature steady-state field distribution.

The second type problem (T_2) consists in finding the excitation parameters as a function of time which minimizes the duration of transition to a steady-state temperature distribution:

$$t_{ss} \rightarrow \min_{U(t),r} \qquad (3)$$

under the conditions of the certain temperature distribution and limited input power

$$\left\| \lim_{t\to\infty} B(\dot{U}_1 \ldots \dot{U}_N, \vec{r}_1 \ldots \vec{r}_N, \vec{R} - T_g(\vec{R}) \right\| \le a_1 \qquad (4)$$

$$\max_n \max_t \left|U_n(t)\right|^2 \le a_2 \qquad (5)$$

where a_1 and a_2 are the specified known values.

Further we shall deal with solutions of the E-class problems.

SOLUTION OF THE MICROWAVE RADIATOR OPTIMIZATION PROBLEMS

The E-class synthesis problem statement in the form (1) seems being analogous with the array synthesis by a certain amplitude pattern. However, the E-class problems have some sufficient features . The first of them is a form of the direct problem operator, which describes the electromagnetic field within some resonator unlike far zone field for conventional array synthesis. Thus the expressions for the electromagnetic field are much more complicated. Moreover, the field intensity for the most cases can be calculated only numerically. This circumstance excludes any analytical approach application.

In the second, unlike the conventional array synthesis problem we deal with absolute values of the field intensity. Consequently, the model of resulted field should describe the absolute field strength excited by a certain source.

In the third, the resulted pattern always is essentially a linear sum of partial patterns for conventional array synthesis. The expression for the solution of the direct problem for microwave radiator may have one of three forms in accordance to the type of oscillators used for elements excitation: either coherent or non-coherent or mixed one.

The coherent excitation corresponds to the case where one powerful oscillator is used and its microwave energy is shared by the exciters according to some relation $(\dot{U}_1 \dots \dot{U}_N)$. The operator **A** is denoted as

$$A(U) = A_C(U) = \left| \sum_1^N \dot{U}_n \vec{E}_n(\vec{R}, \vec{r}_n) \right|^2 \qquad (6)$$

where $\vec{E}_n(R, r_n)$ is the electrical field corresponding to the n-th element by unity excitation.

Non-coherent excitation corresponds to the case when we use a number of oscillators each of which is connected with the only one exciter

$$A(U) = A_{NC}(U) = \Sigma |U_n|^2 \left| E_n(\vec{R}, \vec{r}_n) \right|^2 \qquad (7)$$

The mixed-type excitation means that several (N_g) non-coherent oscillators are used. Each of the oscillators is connected with some group of elements exited as coherent radiators:

$$A(U) = A_M(U) = \sum_{k=1}^{N_g} \left| \sum_{n=1}^{N_k} \dot{U}_{nk} \vec{E}_n(\vec{R}, \vec{r}_n) \right|^2 \qquad (8)$$

where N_k is element's number within the n-th group,

$$\sum_1^{N_k} |U_{nk}|^2 = P_k \qquad (9)$$

where P_k is the k-th oscillator output power.

Note that the equation (6) is an analogue to the conventional array synthesis direct operator's form. As for the expressions (7) and (8), there are no analogy with the expressions used in array synthesis theory.

PROBLEM SOLUTION

There are two key aspects of the E-class problem solution: the functions $\vec{E}_n(\vec{R}, \vec{r}_n)$ finding and excitation conditions definition. For the common case the problem of $\vec{E}_n(\vec{R}, \vec{r}_n)$ finding have not been well studied yet. An extremal complexity of this problem makes impossible to use some universal algorithms for resonators of an arbitrary shape. For particular cases a number of approaches can be successfully used including approaches which have been reported by the authors recently / 1 /.

It is of no use to try to find analytical solutions for the excitation conditions determination. The most prospective way is to reduce the synthesis problems (1) - (3) to the form of some minimization (maximization) problem:

$$Q(A(U, \vec{R}, \vec{r}_n)) \rightarrow \min_{U_1 \dots U_N, r_1 \dots r_n} (\max) \qquad (10)$$

where Q is some criteria corresponding to the definite requirements for field intensity, deviation from the given value for example.

We have the least difficulties for the case of in-coherent excitation under the given elements location because of that the problem operator is linear with respect to the values U_n. For this case we have the unique solution which can be successfully found by linear programming algorithms.

Problems in the form (6) and (8) under the given elements location cause much more difficulties as the criteria (10) can not garantee the unique solution finding. It is necessary to use some efficient procedures for the global extremum calculation.

The worst cases are when we try to find elements location as well as excitation. These problems also forced one to use some efficient numerical algorithms; do not garantee the global extremum definition. Besides, the corresponding calculations are exremelly clumsy because of continously changing the values $\vec{E}_n(\vec{R}, \vec{r}_n)$.

ILLUSTRATIONS

As an illustration we present the optimization problem solutions for the field intensity uniformity improvement within a partially filled rectaugular resonator. It is shown that the mentioned above values can be substantially improved by using the optimized multi-element excitation. Fig.1 shows the fields distribution within the half filled rectangular chamber (400×300×300 mm, the frequency - 2.45 GHz, W = 1kW, ε = 2.3, σ = 8 mSm). Fig. 1 corresponds to one-

Nonoptimized

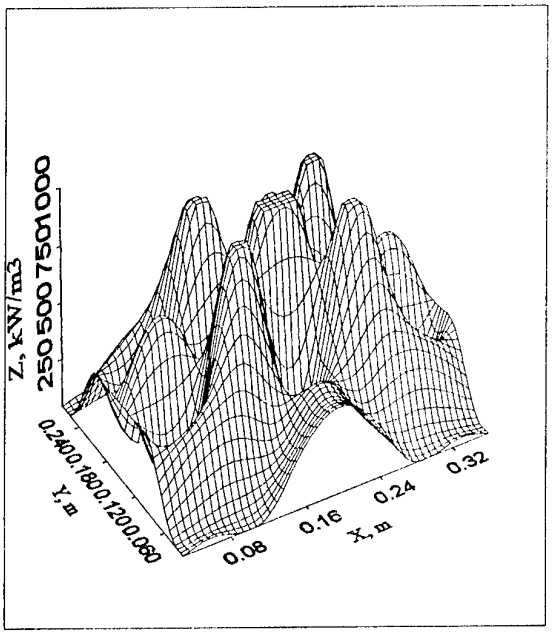


Fig. 1

Optimized

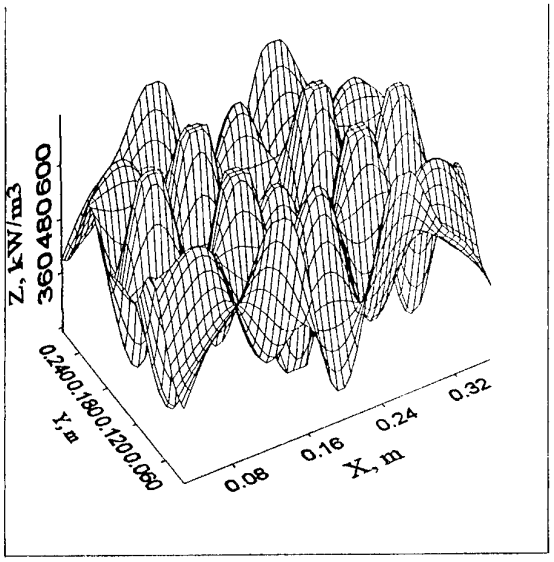


Fig. 2

elements excitation where the exciting slot is located at the centre of the upper wall. Fig. 2 illustrates a usage of the multi-element incoherent excitation (N = 8). Fig. 3 shows optimized elements positions and supplied power.

Optimized excitation

Slot	Supplied power, W
1	100
2	150
3	150
4	100
5	200
6	50
7	50
8	200

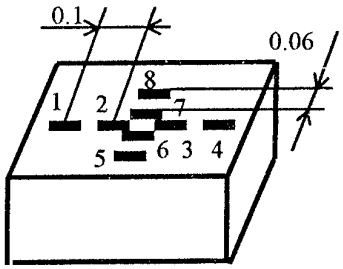


Fig. 3

REFERENCES

1. G.A.Morozov and Iu.E.Sedelnikov. Optimization of electromagnetic fteld excitation for microwave industrial and agricultural applications. The Fifth Scientitic Exchange Seminar. Munich, Germany 21 - 28 09. 1997. Lehrstuhl fur Hochfrequenztechnik Technische Universitat Munchen 1997

2. E.G.Vorobjeva, O.Sh.Dautov, O.V.Potapova, Iu.E.Sedelnikov. Focused array utilization for microwave agricultural application. Proceedings of the Second International Conference on Antenna Theory and Techniques, Kyiv, Ukraine, 20-22 May 1997, Kiev, p. 361-364.

IMPROVEMENT OF MICROWAVE EQUIPMENT EXCITATION EFFICIENCY USING METHODS OF FOCUSED ARRAYS

G. A. Morozov, O. V. Potapova, Y. E. Sedelnikov

Kazan State Technical University
Box 381, Kazan, 420503, Russia
Ph. 7-8432-3831620, Fax 7-8432-386924
E-mail root@kaiadm.kazan.su

ABSTRACT

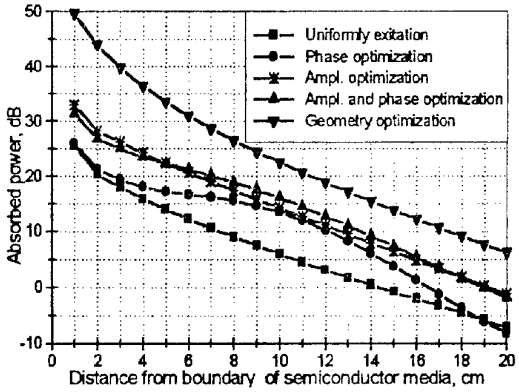
The problem of multielement excitation of exposed-type microwave equipment is studied. Optimization problem is formulated as amplitudes, phases and elements location definition to maximize the special efficiency criteria. Both coherent and noncoherent multielement excitation are considered. Substantial improvement of microwave field excitation can be achieved by proposed approach. A number of particular optimization procedures advantageous for practical use is presented.

INTRODUCTION

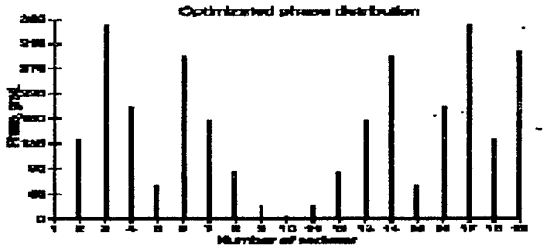
A number of cases such as soil disinfection, concrete slabs destruction, hyperthermia and others are classified among applications realized by exposed-type microwave equipment. So long as energy radiation is shielded partly or not shielded from surroundings for those cases, it is rather important to concentrate the electromagnetic energy efficiently within the given volume. On the other hand the field uniformity within the treating area are of great importance for quality of processing product. Presented paper seeks to review recent development have been carried out by Research

Small focused area

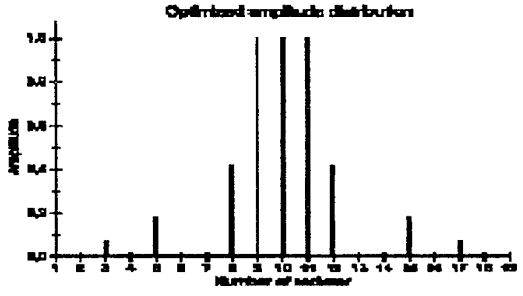
Coherent excitation



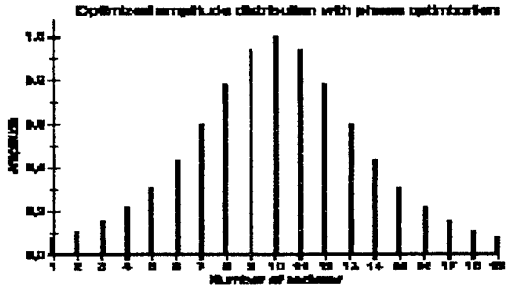
a) Field distribution



b) Optimized phase distribution (phase optimization)



c) Optimized amplitude distribution (amplitude optimization)



d) Optimized amplitude distribution (amplitude and phase optimization)

Fig. 1

Center for Applied Electrodynamics of Kazan State Technical University in the area of improvement an electromagnetic field excitation by using of modified focused arrays methods.

Small focused area

Noncoherent excitation

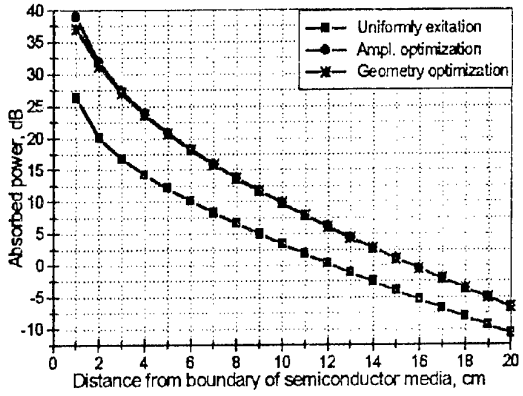


Fig. 2

MULTIELEMENT EXCITATION

Multielement electromagnetic field excitation is more efficient as against monoexcitation realized by alone radiator (applicator). The two principle excitation types are studied: multielement coherent and noncoherent manner one. The only powerful oscillator connected with radiators by some distribution circuit is trade off for the first of them. Noncoherent excitation means a number of relatively weak oscillators combined with the separate applicators are utilized. For excitation efficiency improvement both of the methods mentioned above are prospective.

OPTIMIZATION PROBLEM

Consider some criteria with reference to a exposed-type microwave equipment. The two criteria may be advanced:

energy efficiency criteria

$$\int_V P_{\text{real}}\left(|i\rangle,|r'\rangle,r\right)dV \to \max_{|i\rangle,|r'\rangle}, \tag{1}$$

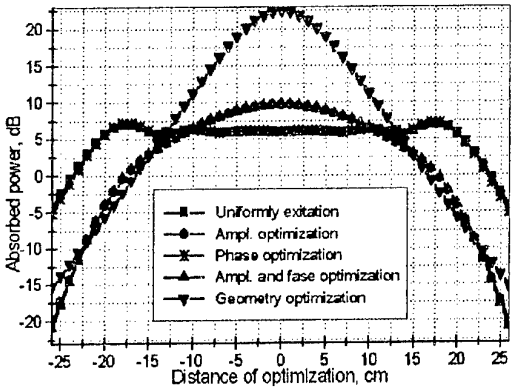
and energy uniformity criteria

$$P_{\min}\left(|i\rangle,|r'\rangle,r\right) \to \max_{|i\rangle,|r'\rangle}. \tag{2}$$

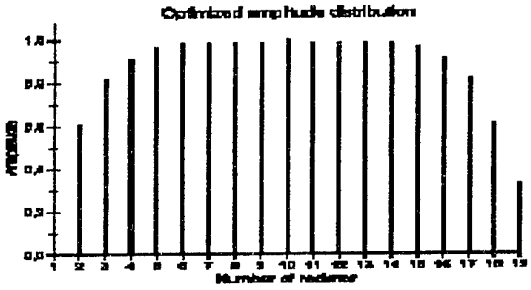
For the most common case we formulate the optimization problem as elements amplitudes, phases and displacement definition to maximize the criteria (1) or (2) value. Thus the problem of multielement excitation optimization for microwave application is analogous with that of antenna array synthesis. However unlike a conventional array synthesis, the electromagnetic fields used for microwave applications correspond to Fresnel zone and propagate into substantially absorbed media. So the direct operator as well as the optimization criteria for the optimization problem are rather specific.

Extended focused area, optimization according to criteria (1)

Coherent excitation



a) Field distribution



b)Optimized amplitude distribution

Fig. 3

Extended focused area, optimization according to criteria (1)

Noncoherent excitation

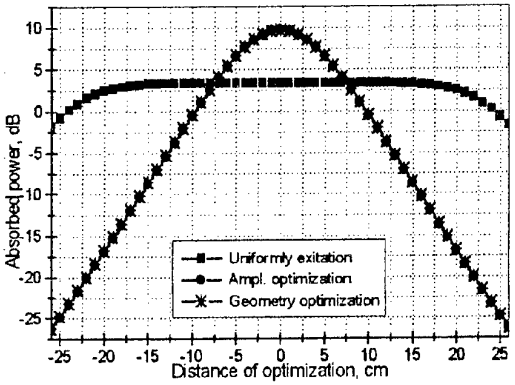


Fig. 4

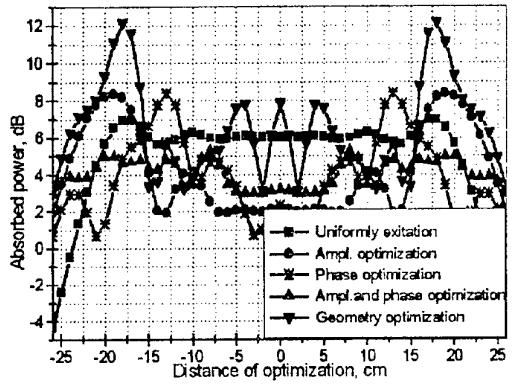
Also a number of particular optimization problems are of interest for practical use. Phase, amplitude or geometry optimization as well as amplitude or geometry optimization for noncoherent case can be noted among them. Here, the objective is two fold: to chose the intelligent algorithms and to estimate effects achieved by optimization under typical conditions.

SOLUTION AND NUMERICAL RESULTS

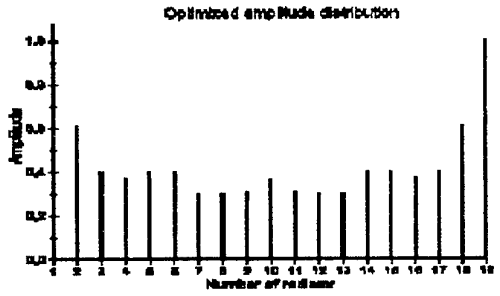
Formulated optimization problems are polyextremal predominantly. For numerical solution positive calculation methods are used for the global extreme finding. For this study we applied the modified Gauss-Seidel method. For a number of noncoherent excitation problems linear programming was also used.

Extended focused area, optimization according to criteria (2)

Coherent excitation



a) Field distribution



b) Optimized amplitude distribution

Fig. 5

Multielement exciter consists of N (N = 19) radiators located at one line on the plane boundary separating air and infinite semiconductor media (for f = 2.45 GHz, α = 11.8 1/m, β = 121.7 1/m, ε' = 6.0). For both coherent and noncoherent cases the amplitude, phase and geometry optimization problems are solved accordingly to criteria (1) and (2). The first of them corresponds to the case of a small focused area (sizes $<\lambda_{\tilde{n}}$), the second one to the extended area (sizes$>\lambda_{\tilde{n}}$) [1]. Substantial improvement of the excitation efficiency have been established by calculations. The field concentrating within the certain area can be greatly increased. So for the case of the small focused area the value of criteria (1) can be improved toward 12 dB for the coherent excitation with optimized geometry of array. For the extended area the criteria (2) value increases toward 0.25...7.5 dB in comparison with uniform exited uniformly spaced array both for the coherent and noncoherent cases [2]. Fig. 1-6 illustrate these results (the distance from boundary of semiconductor media to focused area is equal 10 cm).

Extended focused area, optimization according to criteria (2)

Noncoherent excitation

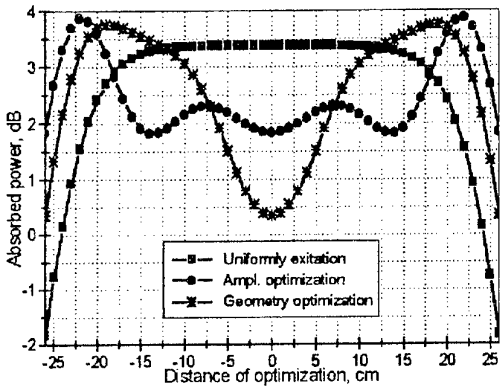


Fig. 6

CONCLUSION

Substantial improvement of exposed-type microwave installations efficiency by optimized multielement excitation can be achieved. For a number of cases particular optimization methods are also expedient for practical use.

REFERENCES

1. Anfinogentov V.I., Sedelnikov Yu.E., Stepanov V.V., Potapova O.V. Multielement excitation of electromagnetic fields for microwave industrial installations \ Proceedings of 7th International Crimean Conference "Microwave & Telecommunication Technology". – Crimea, Sevastopol, 1997. pp.200-201 [in Russian].

2. Vorobjova E.G., Dautov o.Sh., Potapova O.V., Sedelnikov Yu.E. Focused array utilization for microwave agricultural application \ Proceedings of the Second International Conference on Antenna Theory and Techniques.– Kiev, 1997. pp. 361-363.

A MODIFIED MICROWAVE TECHNOLOGY OF HEATING AND DRYING GRANULAR DIELECTRICS

V. I. Rudakov, A. V. Demchenko, Y. V. Zaichenko

Central Research and Development Institute of Armament and Military Engineering,
Kiev - 135, str. Andrushenko, 4, tel. 271-62-45

At the moment a power saving for power-intensive production processes is very actual in Ukraine. The microwave technologies known from [1–5] permit to reduce time of dielectric heating to a specified temperature and to achieve power consumption saving in 2–3 times. However, an application of only microwave energy to dry dielectrics is not effective enough [1], and thus, the technologies combining various types of power actions [5, 6] to dry dielectrics are used.

Thus the present paper is devoted to a theoretical backgrounds of modified microwave technology of dielectric drying which presents a combination of two types of power action towards dielectric being exposed simultaneously, namely: microwaves and hot air flow of specified temperature and humidity according to [1–5]. Here a process of dielectric-adsorbent (silica gel) performed in a specially designed cylindric adsorber shown in Fig. 1 is considered.

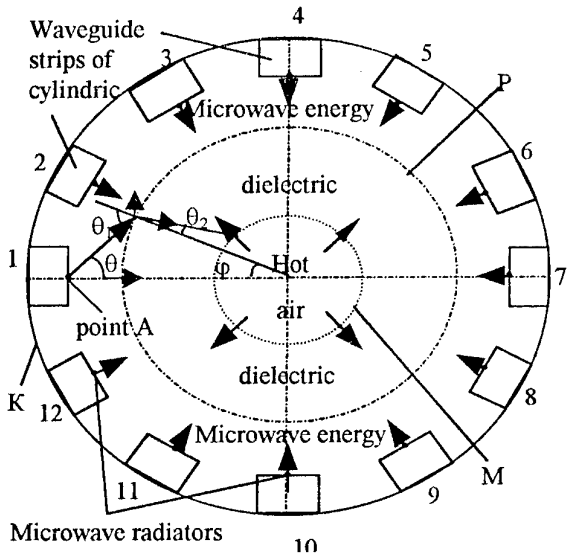


Fig. 1. A cross-section of the cylindric microwave adsorber

The microwave field in cylindric microwave adsorber is excited by cylindric antenna array formed of rectangular strips of waveguides with dimensions 45 × 90 mm placed on a line tangent to a generator of the outer cylinder — housing K of the adsorber, and is directed inside the microwave adsorber towards cylinders with slotted side walls P and M among which silica gel is placed.

The hot air flow is directed from inner cylinder M inside silica gel volume bounded by the cylinder P, and as a result, temperature fields of dielectric heating by microwaves and hot air flow are directed towards each other allowing an acceleration of dielectric heating and a required water withdrawal due to a simultaneous uniform heating of the whole dielectric volume [1–5]. In this event the uniform heating of the dielectric is ensured by high homogeneity of the electric field in microwave adsorber as a result a cylindric array of radiators, in a form of half-wave slots, placed in a distance not exceeding microwave generator wavelength [1–6] has been used.

It is necessary to note that the dielectric (silica gel) uniform heating is provided taking into account the fact that the silica gel properties depend on its humidity and temperature, and are subject to a sufficient variation under microwave heating [1–5].

Investigating the structure of the microwave field in a transversal cross-section of the adsorber it has been ascertained that for specified dimensions of microwave adsorber the required irregularity of electric field between cylinders P and M can be calculated according to [1-6]. The calculations have been carried out by geometrical optics method [6] (method of divergent and convergent rays) for the microwave adsorber shown in Fig. 1. To calculate the required parameters the geometrical construction presented in Fig. 2 have to be carried out.

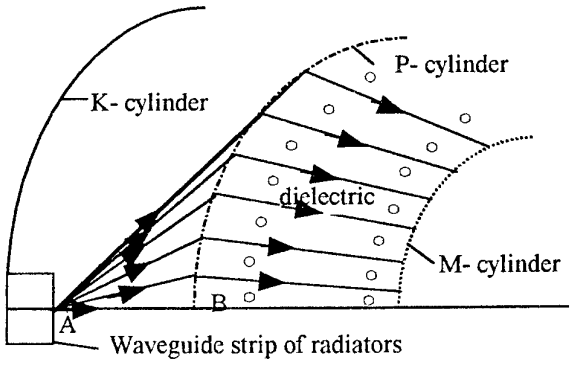


Fig. 2. A ray path in the microwave adsorber

Fig. 2 shows the path of a ray out coming from the radiating point A of one of the waveguide strips and being incident in the point B on the surface P in region of silica gel volume limited by dimensions $r_1 \le r \le r_2$.

The complex amplitude of the electric field in any point of silica gel volume is determined as [1–6]

$$E(\varphi, r_{\theta_2}) = E_{tr}(\varphi) \cdot f_1 \times$$
$$\times e^{-\frac{\pi\sqrt{\varepsilon_s}}{\lambda_0} r_{\theta_2}(\varphi) tg\delta_s - j[\Phi(\varphi)] - \frac{2\pi\sqrt{\varepsilon_s}}{\lambda_0} r_{\theta_1}(\varphi)}, \quad (1)$$

where $E_{tr}(\varphi)$ and $\Phi(\varphi)$ — amplitude and phase of a wave transmitted through dielectric; $f_1(\varphi)$ — function describing a variation of field amplitude due to a bundle of rays narrowing or enwidening; ε_s and $tg\delta_s$ — silica gel parameters.

According to [1–6]

$$E_{tr}(\varphi) = E_{ine}(\varphi) + E_{ref}(\varphi), \quad (2)$$

where $E_{ine}(\varphi)$ and $E_{ref}(\varphi)$ — electric field amplitudes of incident and reflected wave in the point B

$$E_{inc}(\varphi) = \frac{AE(\theta)}{\sqrt{r_\theta}}, \quad (3)$$

where $E(\theta)$ — radiation pattern (RP) of a slotted radiator;

$$A = \frac{1}{\rho_w}\sqrt{\frac{PK_{GA}}{2\pi H}},$$

where ρ_w — wave resistance of free space; P — power of microwave generator at waveguide input; H — height of adsorber cylinder; K_{GA} — gain of slotted radiator;

$$r_\theta = \sqrt{(x_A - r_a\cos\varphi)^2 + (r_2 + \sin\varphi)^2};$$
$$\theta(\varphi) = \text{arctg}\frac{r_2\sin\varphi}{x_A - r_2\cos\varphi}.$$

$E_{ref}(\varphi)$ is equal to [1–6]

$$E_{ref}(\varphi) = \frac{\cos\theta_1(\varphi) - \sqrt{\varepsilon_s}\cos\theta_2(\varphi)}{\cos\theta_1(\varphi) + \sqrt{\varepsilon_s}\cos\theta_2(\varphi)} E_{ine}(\varphi), \quad (4)$$

where $\theta_1(\varphi) = \theta(\varphi) + \pi\varphi$;

$$\theta_2(\varphi) = \arcsin\frac{\sin\theta_1(\varphi)}{\sqrt{\varepsilon_s}}; \quad \Phi(\varphi) = \frac{2\pi}{\lambda_\theta} r_\theta.$$

The calculation of synchronous and asynchronous excitation of the waveguide radiator strips has been carried out. For the synchronous excitation greater irregularity of electric field has been observed than for asynchronous one [1–5]. This permits to create more compact adsorber design and to achieve higher electric field uniformity along the whole silica gel volume excluding those regions laying near an outer surface of the volume ring M. This leads to a non-uniform silica gel heating [1–5]. The calculation results are shown in Fig. 3.

The non-uniformity of silica gel heating can be improved by warming up the adsorber silica gel by hot air flow directed radially from the cylinder M to cylinder P between which silica gel is placed. It is necessary to note that hot air flow is not only heating silica gel, but with drawing moisture from silica gel surface as well [1-5].

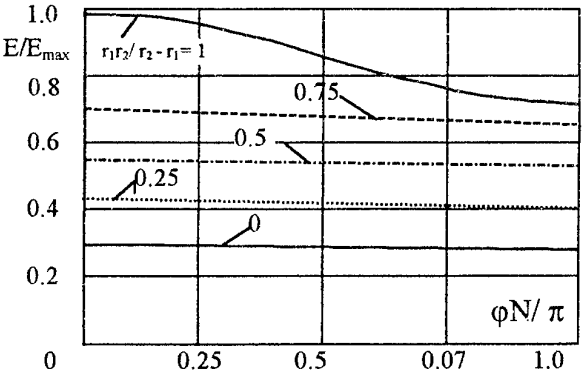


Fig. 3. A dependence of electric field normalized intensity vs azimuth

The variation of a heat flow in a unit of cylindric volume of the microwave adsorber for microwave radiation directed from the cylinder K through the cylinder P towards the cylinder M is determined as [1–6]

$$\frac{dQ}{dt} = 8\cdot 10^{-12} E^2 \cdot f_0 \frac{tg\delta_s}{\gamma_s \cdot C_s}\left[\frac{\text{deg}}{\text{min}}\right], \quad (5)$$

where E^2 — square of microwave field intensity; f_o — operational frequency of microwave generator; γ_s — silica gel density; C_s — silica gel specific heat.

The variation of silica gel heating temperature due to microwave radiation is determined as [5]

$$\Delta T = \frac{P_{MW}}{4.12 m_s C_s}, \quad (6)$$

where P_{MW} — microwave power; m_s — silica gel mass in the adsorber; C_s — silica gel specific heat.

The heat flow of the hot air being blown through silica gel in the microwave adsorber from the cylinder M through the cylinder P towards the cylinder K is determined as [1–5]

$$Q = \frac{T_{in} - T_{out}}{\frac{1}{\alpha_{in}F_1} + \sum_{i=1}^{n}\frac{S_i}{\lambda_i F_{im}} + \frac{1}{\lambda_{out}F_{n-1}}}, \quad (7)$$

where T_{in} and T_{out} — inner and outer temperatures of a conditional volume of cylindric *i*st silica gel ring between cylinders M and P; S_i — thickness of conditional *i*st silica gel ring between cylinders M and P; λ_i — thermal conductivity of volume 1st silica gel ring between cylinders M and P; F_{im} — mean design square of

the surface of volume *i*st silica gel ring between cylinders M and P; F_1 and F_{n-1} — design squares of volume 1st and $(n-1)$st silica gel ring between cylinders M and P; α_{in} and α_{out} — coefficients of convective heat transfer in the *i*st silica gel volume ring between cylinders M and P from the inner wall with temperature T_{in} towards the outer one with temperature T_{out}.

The characteristic feature of silica gel microwave heating is its receptivity to microwave field due to its parameters ε_s (permittivity) and $tg\delta_s$ (the loss tangent of a dielectric) which are equal to ε_s = 4.56–5.98 and $tg\delta_s$ = 0.069–0.15 [1–5]. At the first stage of the microwave heating quick processes are taken place; naturally silica gel heating and liquid phase transferring into a vapour from silica gel surface due to a thermobarrodiffusion process [1–5]. At the second stage hot air blowing arouses moisture withdrawing from silica gel surface with simultaneous reducing silica gel heating irregularity and lowing silica gel heating temperature permitting the adsorbent properties of silica gel to be preserved [1–5].

The calculated dependencies of temperature fields inside microwave adsorber between cylinders M and P are shown in Fig. 4.

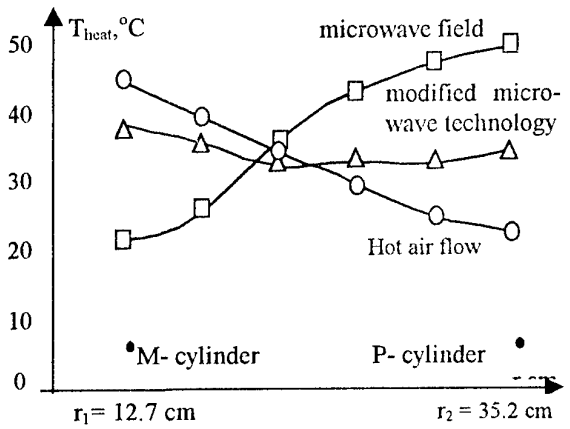


Fig. 4. The calculated dependencies of silica gel temperature heating in the microwave adsorber

The presented calculation dependencies of silica gel heating temperatures in the microwave adsorber permit to determine a design water withdrawal and power savings [1–5].

CONCLUSION

According to [1-5] the presented microwave technology of silica gel drying permits the 5% water withdrawal from silica gel with weight 164 kg to be carried out. The power consumption is 8–10 kW·h that makes it possible the power saving in 3 times with respect to the known methods [4, 5] which ensure the power consumption of 26.4 kW·h for the same water withdrawal percentage.

REFERENCES

1. Rudakov V.I. Application of microwave-technology in power-intensive productions, STS, ICATT-95, Kharkov, 1995 [in Russian].
2. Rudakov V.I. Multimode exitation of cylindrical resonator field with dielectric, STC, MWT-95, Kazan, 1995 [in Russian].
3. Rudakov V.I. Complex of storage of equipment as a closed thermodynamic system, STC, MWT-95, Kazan, 1995 [in Russian].
4. Puschner H. Heating with microwaves, Fundamentals, components and circuit technique, 1966 [in Russian].
5. Rudakov V.I. The microwave installation for drying of grain, ETR, SRI "KVANT", Kiev, 1993 [in Russian].
6. Nikolsky V.V. Electrodynamics and propagation of radiowave, M, S., 1978 [in Russian].

ABOUT ONE WAY TO DECREASE THE DIRECTIVITY OF RECTENNA SPURIOUS RADIATION

V. M. Shokalo, A. A. Konovaltsev, Yu. A. Luchaninov

Kharkov State Technical University of Radio Electronics
Prospekt Lenina 14, Kharkov 310726, Ukraine
E-mail: tea@kture.kharkov.ua

One of the promising alternative directions of modern energetics development is the creation of systems transmitting power by a focused microwave beam. The terminal of such a system is the rectenna (antenna-rectifier) that receives the microwave energy and converts it to the one of direct current. The rectenna is designed as the antenna array of a number of receiving-rectifying elements (RREs). Every RRE consists of an antenna loaded on a microwave rectifier with Schottky barrier diodes. The conversion of microwave energy in the rectenna is of non-linear nature and, consequently, is accompanied by the radiation at high-order harmonic frequencies [1].

In general, the power radiated by the rectenna at high-order harmonic frequencies is very small in comparison with the microwave beam energy incoming on its aperture. However, in some directions the rectenna like a phased antenna array is capable to produce the spurious radiation of a large intensity, and this causes the problem of the rectenna electromagnetic compatibility.

The decrease of the rectenna spurious radiation directivity can be achieved by means of dephasing the RREs in any known way at the harmonic frequencies. For example, it can be realized by changing in a random manner the parameters of elements in RRE low-pass filters or by displacing the rectrenna modules relatively each other, etc. The common shortcoming of the mentioned above ways is the complication of a rectenna design.

The paper presents the results of investigation of the possibility to decrease the directivity of a large rectenna array spurious radiation by a rather simple technique. The essence of the technique consists in achieving at the frequencies of high-order harmonics the anti-phased excitation of neighboring rectenna modules or lines of RREs in one module. The technical implementation of the technique does not entail the complication of rectenna module design. For example, at the frequencies of high-order harmonics the anti-phased excitation of the receiving-rectifying elements in neighboring lines in a rectenna module can be achieved by changing the direction of diodes connection in RREs to the opposite one (case b on Fig. 1) relatively to the case of phased excitation (Fig 1, a).

Preliminary the effect of decrease of the rectenna spurious radiation directivity that could be achieved with the proposed technique has been investigated analytically. As an initial model for the simulation the arbitrarily shaped flat periodical rectenna array with the triangular grid has been chosen.

The field of the spurious radiation can be found from the current distribution over the surfaces of RRE antennas at high-order harmonics frequencies. The rigorous way of stating the task of this distribution calculation requires to solve the boundary value problem taking into account the non-linearity of rectifying diode characteristics. However, since the rectenna is a large-aperture one, i.e. it has the large electric dimensions, the solution of such a rigorous boundary value problem is hardly feasible nowadays or in the nearest foreseeable future. That is why when developing the method of the rectenna spurious radiation calculation such simplifications were assumed:

- the rectenna is free of edge effects;
- all RREs have the same parameters that they would have in the infinite array.

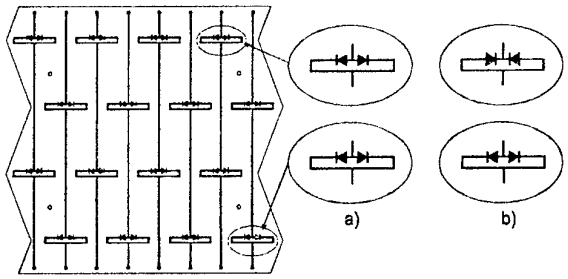


Fig. 1. The rectenna module design:
a) with phased excitation of lines of RRE;
b) with anti-phased lines excitation

Under such assumptions the method of calculation of rectenna energetic parameters stated in [2] can be applied. The first stage of this method includes the calculation of RRE antennas electromagnetic characteristics by the moments method. This calculation is carried out for the basic frequency as well as for the frequencies of high-order harmonics. The currents distribution over the RRE antennas surface at higher harmonics frequencies is approximated by the system of piecewise sine basis functions:

$$\vec{I}(\xi)=\sum_{n=1}^{M}\vec{I}_n(\xi), \qquad (1)$$

where M is the number of basis functions by which the currents distribution over the RRE antennas surface is approximated; $\vec{I}_n(\xi)$ is the basis piecewise sine function defined in two neighboring sections of the antenna as follows:

$$\vec{I}_n(\xi) = I_n \frac{\sin k(l_{mn} - \xi)}{\sin k l_{mn}} \vec{\xi}_{mn}, \quad m = 1,2. \qquad (2)$$

In (2) l_{1n}, l_{2n} are the lengths of the first and second sections of the antenna wire where the n-th basis function is defined; $\vec{\xi}_{1n}$, $\vec{\xi}_{2n}$ are the unit vectors describing the direction of the appropriate sections and ξ is the coordinate of their connection; $k = 2\pi/\lambda_i$ is the wave number of the i-th harmonic; I_n is an amplitude coefficient of the n-the basis function.

The second stage of the rectenna energetic parameters calculations [2] includes the developed in the theory of antennas with non-linear elements [3] procedure of computation of the currents flowing through the rectifying diodes at a basic frequency. Moreover, the currents at high-order harmonics frequencies formed as a result of the rectification process are also computed. Thus, after this procedure completion the amplitude-phase distribution of the currents at harmonics frequencies over the rectenna aperture becomes known. This distribution determines the values of the currents basis functions amplitude coefficients I_n in (2).

With the method [2] the rectenna spurious radiation field can be found in the following sequence. Initially the field created by the n-th current basis function is calculated. Then the field radiated by one RRE is determined by the coefficients I_n known from the solution of the rectenna excitation problem. The sum of all RRE fields gives us the resulting rectenna field at a chosen frequency of spurious radiation.

Generally the field of one half of the current basis function defined by (2) for $m = 1$ or $m = 2$ can be expressed as:

$$E_\theta(r,\theta,\varphi) = -\frac{j30I}{\sin(kl_{mn})}\frac{e^{-jkr}}{r} e^{jk\vec{r}_0\vec{r}} \times \frac{e^{jkl_{mn}(\vec{\xi}\vec{r})} - j(\vec{\xi}\vec{r})\sin kl_{mn} - \cos kl_{mn}}{1-(\vec{\xi}\vec{r})^2} \times (\cos\gamma_1\cos\theta\cos\varphi + \cos\gamma_2\cos\theta\sin\varphi - \cos\gamma_3\sin\theta), \qquad (3)$$

$$E_\varphi(r,\theta,\varphi) = \frac{j30I}{\sin(kl_{mn})}\frac{e^{-jkr}}{r} e^{jk\vec{r}_0\vec{r}} \times \times \frac{e^{jkl_{mn}(\vec{\xi}\vec{r})} - j(\vec{\xi}\vec{r})\sin kl_{mn} - \cos kl_{mn}}{1-(\vec{\xi}\vec{r})^2} \times (\cos\gamma_1\sin\varphi - \cos\gamma_2\cos\varphi). \qquad (4)$$

In (3) and (4) $\vec{r}_0$ is the radius vector, drawn from the origin of coordinates to the point of connection of two sections on which the current basis function is defined; $\vec{r}$ is the unit vector in direction to the point of supervision; r is a distance up to the point of supervision; $\cos\gamma_1$, $\cos\gamma_2$, $\cos\gamma_3$ are the directing cosines of the unit vector $\vec{\xi}$.

The screen presence was taken into account by introduction of mirror images of the current functions, whose fields were calculated with account of distinctions in their phases and locations.

Finally, the field of the complete current basis function with a number n can be expressed by

$$\left.\begin{aligned} E_{\theta n} &= E_{\theta n1} - E_{\theta n2} - E'_{\theta n1} + E'_{\theta n2} \\ E_{\varphi n} &= E_{\varphi n1} - E_{\varphi n2} - E'_{\varphi n1} + E'_{\varphi n2} \end{aligned}\right\}. \qquad (5)$$

Here the sign (') marks the fields of the mirror images of the first and second sections of the basis function.

Further, applying the principle of fields superposition it is not difficult to find the field radiated by the i-th receiving-rectifying rectenna element

$$E^{(i)}_{\theta,\varphi} = \sum_{n=1}^{M} E_{\theta,\varphi n}, \qquad (6)$$

and then to find the total field of the rectenna spurious radiation:

$$E^{\Sigma}_{\theta,\varphi} = \sum_{i=1}^{N} E^{(i)}_{\theta,\varphi}, \qquad (7)$$

where N is the number of RREs in the rectenna.

The described above calculation procedure had been used for the numerical investigation of the spurious radiation patterns of the rectenna array consisting of nine identical modules (one of such modules is presented in Fig. 1) and containing 144 RREs with loop vibrators. It was assumed that the rectenna aperture is excited by the field with the uniform amplitude distribution.

Fig. 2 shows the computed radiation patterns at the second and third harmonics frequencies. The curve 1 corresponds to the "traditional" case when the antennas of RREs are excited in phase at the harmonics frequencies. The rectenna radiation pattern for the case of the anti-phased excitation at higher harmonics frequencies is presented by the curve 2, and the curve 3 meets the case of the anti-phased excitation of lines in the rectenna modules. It can be concluded from the comparison of the calculated radiation patterns that:

- for the considered 144-element rectenna the anti-phased excitation of modules at the second and

third harmonics frequencies enables to decrease the maximum spurious radiation level only by 9.5 dB;

- the more substantial decrease of the rectenna directivity at higher harmonic frequencies is observed in the case of anti-phased excitation of the neighboring lines in every modules (up to -40 ... -43 dB).

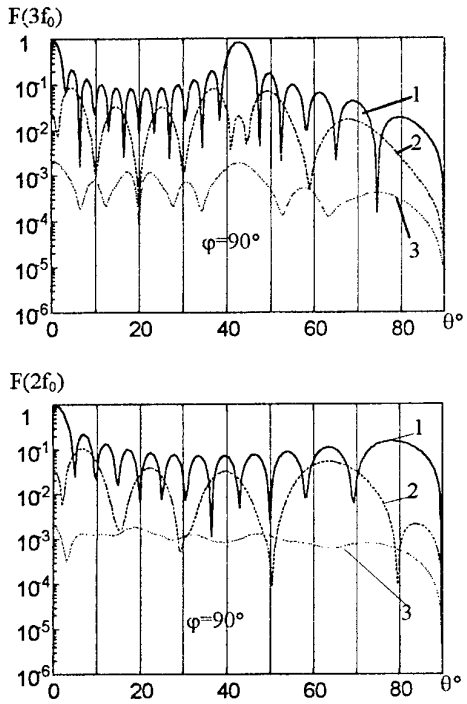


Fig. 2. The rectenna radiation patterns on the second and third harmonics frequencies

The effect of the spurious radiation directivity decrease in the case of anti-phased diode connection in neighboring lines of the rectenna modules (Fig. 1, b) has been confirmed experimentally as well. With this purpose the measurements of the harmonics radiation levels of the modules with anti-phased and phased diode connection has been carried out. The structure of the experimental set-up is shown in Fig. 3.

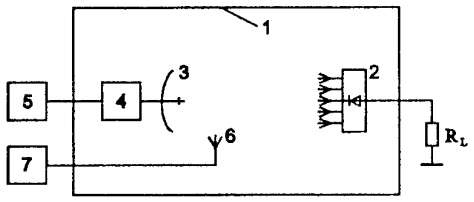


Fig. 3. Structure of the experimental set-up

The measurements has been implemented in the unechoic chamber 1. The investigated rectenna module 2 had the optimal direct current load resistance $R_L = R_{Lopt}$. The incident microwave beam was formed by the transmitting reflector antenna with the radius of 0.45 m. The magnetron generator 4 with the power supply unit 5 functioned as the powerful microwave source with working frequency of 2.45 GHz. The magnitudes of spectral components were measured with the help of the spectrum analyzer 7 with the remote sensor 6.

The main difficulty in measurements implementation was that magnetron generator 4 had a rather significant level of own high-order harmonics. In view of this only the relative level of the module higher order harmonics with respect to the level of generator harmonics had been measured. The results of these measurements are given in Table 1.

Table 1

Results of the rectenna modules spurious radiation measurements

Harmonic number	Harmonics level, dB			
	From generator	Diode connection in a module		The level decrease
		phased	anti-phased	
1	0	0	0	
2	-32.5	-26.3	-31.0	4.7
3	-52.3	-43.4	-52.3	>8.9

The measurements results given in Table 1 testify that the use of the principle of anti-phased diodes excitation at higher order harmonics frequencies only in one module with 16 RREs enables to obtain an appreciable decrease of the second and third harmonics radiation (4.7 dB and more than 8.9 dB, respectively).

CONCLUSIONS

In the paper the rather simple technique to decrease the spurious radiation directivity of a rectenna array is proposed. The principle of the technique consists in creation of such conditions when the neighboring rectenna modules or neighboring lines of RREs in a module are excited anti-phasely at higher harmonics frequencies. The proposed technique efficiency in the decrease of the spurious rectenna radiation have been shown by results of numerical and experimental investigations.

REFERENCES

1. Y. S. Shifrin, A.I.Luchaninov, V.M.Shokalo, A.A. Shcherbina. Spurious radiation of rectenna receiving-rectifying elements// International Wroclaw Symposium on Electromagnetic Compatibility, (EMC-94). -Wroclaw, Poland, 1994. -pp.67-72.

2. Y. Shifrin, A. Luchaninov, V. Shokalo, A.Sherbina Rectennas // JINA, Nice, France, Nov.1994. -pp.394-397.

3. Luchaninov A. I., Shifrin Y. S. Antennas with non-linear elements // Chapter IX in "Reference book on antennas technique" / vol.1 Editors: Bakhrakh L.D. and Zelkin E.G., - Moscow, IPRZhR publishing, 1997, [in Russian].

EFFICIENCY OF POWER TRANSMISSION SYSTEM BY A MICROWAVE BEAM WITH NON-AXIAL ARRANGEMENT OF TRANSMITTING AND RECEIVING APERTURES

V. M. Shokalo, S. V. Sevsky, A. M. Rybalko, A. A. Konovaltsev

Kharkov State Technical University of Radio Electronics
Prospekt Lenina 14, Kharkov 310726, Ukraine
E-mail: tea@kture.kharkov.ua

Systems of wireless power transmission by a microwave beam are prospective for remote energy supply of air and space flying vehicles, for transportation of the generated in space electric energy to the Earth, for wireless power transmission between on-ground points and for a number of other applications. For high efficiency of energy transmission to be achieved it is necessary to provide the optimal aperture illumination of a transmitting antenna as well as a co-axial arrangement and a polarization matching of transmitting and receiving antennas. However in practice, especially in cases when power transmission is organized between objects moving relatively each other, the co-axial arrangement of the antennas, as a rule, is disturbed. Therefore it is quite urgent to create a mathematical model of the wireless power transmission system that could take into account a dislocation of the transmitting and receiving antennas from the co-axial arrangement and allow to analyze and optimize the system with a sufficient accuracy at various values of system parameters.

Consider a system of power transmission by a microwave beam (Fig. 1) that consists of the circular transmitting and the square receiving antennas whose apertures are in parallel planes. The antennas are matched on polarization, but can be arranged non-axially. The field polarization is linear.

The electric field of the transmitting antenna on the plane of the receiving antenna situated in the Freshnel zone is described by the known expression:

$$\vec{E}(P)=\frac{jk}{2\pi}\int_{S_1}\vec{E}(Q)\frac{e^{-jkr(P,Q)}}{r(P,Q)}dS, \qquad (1)$$

where $r(P,Q)$ is a distance between a point $P(x',y',0)$ on the transmitting antenna aperture and a point $Q(x,y,D)$ on the receiving antenna aperture; D is a distance between the planes of the transmitting and receiving antenna apertures.

When assuming that the transmitting antenna illumination is circularly symmetrical, the expression (1) is reduced to

$$\vec{E}(x,y,D)=\frac{jke^{-jkD}}{D}e^{-\frac{jk}{2D}\left(x^2+y^2\right)}\times \times\int_0^{R_1}\vec{E}(u)e^{-\frac{jku^2}{2D}}J_0\left(\frac{ku\sqrt{x^2+y^2}}{D}\right)udu, \qquad (2)$$

where u is a radial coordinate on the plane of transmitting antenna aperture; j is the imaginary unit; $k=2\pi/\lambda$ is a wave number; R_1 is a radius of the transmitting antenna; J_0 is the Bessel function of the first kind of zeroth order.

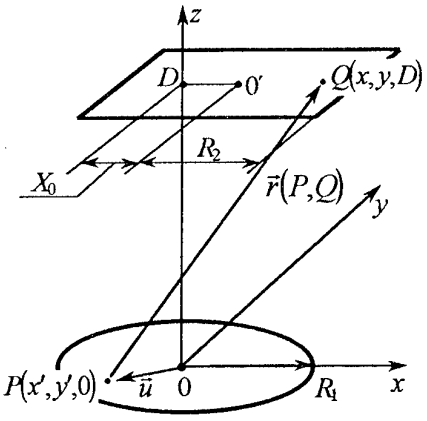


Fig. 1. Geometry of problem

On the basis of (2) it is possible to obtain the following expression for the efficiency of power interception that is introduced as a ratio of the power incident on the receiving aperture to the power radiated by the transmitting antenna:

$$\eta=\frac{P_{np}}{P_{us}}=\frac{k^2}{2\pi D^2}\frac{\int_{-R_2}^{R_2}\int_{-R_2+X_0}^{R_2+X_0}A^2(x,y)dxdy}{\int_0^{R_1}|E(u)|^2udu}, \qquad (3)$$

$$A(x,y)=\left|\int_0^{R_1}E(u)e^{-j\frac{ku^2}{2D}}J_0\left(\frac{k\sqrt{x^2+y^2}u}{D}\right)udu\right|,$$

where R_2 is a half of the receiving aperture width; X_0 is a value of the antennas dislocation from the co-axial arrangement.

After replacement in (3) of variables $u' = \frac{a}{R_1}u$; $x' = \frac{x}{R_2}$; $y' = \frac{y}{R_2}$ it is reduced to:

$$\eta = \frac{\int_{-1}^{1}\int_{-1+b}^{1+b}\left|\int_0^a E(u')e^{-jtu'^2}J_0\left(a\sqrt{x'^2+y'^2}u'\right)u'du'\right|^2 dx'dy'}{\frac{2\pi}{a^2}\int_0^a |E(u')|^2 u'du'}, \quad (4)$$

where $a = \sqrt{\frac{kR_1R_2}{D}}$ is a wave parameter; $t = \frac{R_1}{2R_2}$; $b = \frac{X_0}{R_2}$ is the relative antennas dislocation from the co-axial arrangement.

As it can be seen from (4) the efficiency of power interception is a functional of the amplitude-phase distribution $E(u)$ and depends on parameters of the system (a, b, t), which include the operating wavelength, the dimensions of the apertures and the distance between them, and the value of the antennas dislocation.

With the phase distribution of the transmitting aperture excitation field providing focusing of the microwave beam on the receiving aperture, the efficiency of power interception is given by:

$$\eta = \frac{a^2}{2\pi}\frac{\int_{-1}^{1}\int_{-1+b}^{1+b}\left[\int_0^a F(u)J_0\left(a\sqrt{x^2+y^2}u\right)udu\right]^2 dxdy}{\int_0^a F^2(u)udu}. \quad (5)$$

Under assumption that an effect of superdirectivity is ruled out the amplitude distribution $F(u)$ of the transmitting aperture excitation field can be approximated with the polynomial of the even order:

$$F(u) = \sum_{i=0}^{M} c_i u^{2i}. \quad (6)$$

Expanding the Bessel function into a partial sum with N members and integrating (5) it can be obtained:

$$\eta(a,b) = \frac{1}{\pi}\left[\sum_{i=0}^{M}\sum_{j=0}^{M} c_i c_j \frac{a^{2(i+j)}}{i+j+1}\right]^{-1} \times$$

$$\times\left\{\sum_{i=0}^{M}\sum_{j=0}^{M}\sum_{k=0}^{N}\sum_{p=0}^{N}\frac{(-1)^{k+p}c_i c_j a^{2[i+j+2(k+p)+2]}(k+p)!}{(k!)^2(p!)^2 2^{2(k+p)+1}(i+k+1)(j+p+1)}\times\right.$$

$$\left.\times\sum_{m=0}^{k+p}\frac{(1+b)^{2(k+p-m)+1}-(-1+b)^{2(k+p-m)+1}}{m!(k+p-m)![2(k+p-m)+1](2m+1)}\right\}. \quad (7)$$

The expression (7) allows to calculate the power interception efficiency with given coefficients c_i in (6) and parameters a and b. This expression can be represented as the ratio of two Hermit-square forms:

$$\eta = \frac{(\mathbf{GC},\mathbf{C})}{(\mathbf{HC},\mathbf{C})},$$

where $\mathbf{G}$ and $\mathbf{H}$ are the square symmetric matrices of the order of $M+1$; $\mathbf{C}$ is the vector of the order of $M+1$, whose elements are the coefficients c_i.

The elements of matrices $\mathbf{G}$ and $\mathbf{H}$ are as follows:

$$g_{i,j} = \sum_{k=0}^{N}\sum_{p=0}^{N}\frac{(-1)^{k+p}a^{2[i+j+2(k+p)+2]}(k+p)!}{(k!)^2(p!)^2 2^{2(k+p)+1}(i+k+1)(j+p+1)}\times$$

$$\times\sum_{m=0}^{k+p}\frac{(1+b)^{2(k+p-m)+1}-(-1+b)^{2(k+p-m)+1}}{m!(k+p-m)![2(k+p-m)+1](2m+1)};$$

$$h_{i,j} = \pi\frac{a^{2(i+j)}}{i+j+1}.$$

The maximum value of η is equal to the maximum eigenvalue of a matrix $\mathbf{L} = \mathbf{H}^{-1}\mathbf{G}$ and the eigenvector corresponding to the eigenvalue consists of the expansion coefficients c_i of the optimal amplitude distribution (OAD) in (6) [1]. The accuracy of OAD approximation depends on the number of members in partial sum (6). However, the use of $M > 3...4$ does not yield any noticeable change in a value of the calculated interception efficiency η.

The results of computations are presented in Fig. 1 and Fig. 2. It is seen (Fig. 1) that at dislocation of the antennas from the co-axial arrangement the OAD tends to be more uniform. When the relative dislocation is less than 20% the interception efficiency decreases slightly because with the antennas arranged co-axially the microwave beam is focused at the center of the receiving aperture.

Thus, the requirements to the accuracy of the microwave beam pointing as well as to maintaining the co-axial arrangement of the transmitting and receiving antennas are not very strict. When the dislocation from the co-axial arrangement is rather considerable (for example when providing the power supply of moving space vehicles), it is preferable to realize the illumination of the transmitting antenna with the amplitude distribution corresponding to the interception efficiency

values of $\eta = 60...80\%$. This enables to decrease the influence of the non-axial arrangement on the efficiency of the wireless power transmission system.

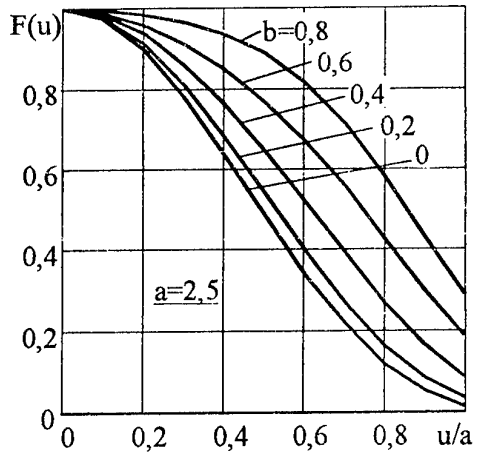


Fig. 2. Optimal amplitude distribution

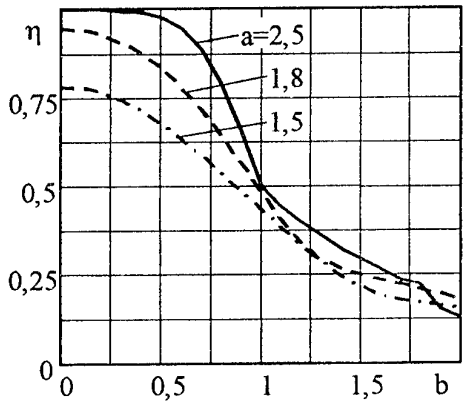


Fig. 3. Interception efficiency

REFERENCE

1. Shokalo V.M., Rybalko A.M. Efficiency of the power transmission system by a microwave beam, Kharkov Tech. University of Radio Electronics, Kharkov, 1995, 40p., Ref. num. 856-Uk95 on 13.04.1995 in State science-tech. library of Ukraine [in Russian].

PULSE HIGH-POWER ANTIBACTERIAL IRRADIATOR

S. N. Shostko, I. S. Shostko, U. F. Lonin,
V. I. Chumacov, U. L. Novoselov, O. S. Shostko*

Kharkov Military University, 6, Svobody sq., Kharkov, Ukraine
*Kharkov State University, 4, Svobody sq., Kharkov, Ukraine

The results of antibacterial irradiator efficiency research are adduced in this paper. The "plasma focus" formed at an end face of coaxial plasma accelerator at the discharge in an atmosphere is a source of powerful ultra-violet radiation in this irradiator.

Nowadays ultra-violet (UV) radiation sources, operating, as a rule, in a continuous mode [1], are widely used for the solving the problems of air, liquids and surfaces disinfection. It is possible to ensure an increase of UV radiation influence efficiency on microorganisms by the increase of radiation power density on the processable surfaces. UV sources of continuous action, with limited power can ensure such conditions only at rather small distances.

In this connection, the pulse sources of UV radiation which allow to receive considerably large power density on processable surfaces, can be more effective. It is possible to attribute Xenon pulse discharge lamps, widely used in laser engineering, or plasmodynamical lamps [2] to such sources.

However, the presence of a quartz vessel in such pulse UV radiation sources limits short-wave part (< 240 nm) of antibacterial radiation spectrum.

In this connection, the investigation of an opportunity to use magnetic plasma compressor (MPC) as a source of powerful UV radiation has been carried out. MPC is the coaxial plasma accelerator of a face type operating in a mode of plasma autofocussing (compression) with the own azimuth magnetic field.

The irradiators with various UV radiation power, distinguished by capacity values in which the electrical energy necessary for formation of "plasma focus" was accumulated, were created to research UV radiation power influence on the antibacterial processing efficiency. In table 1 the basic parameters of such irradiators are given.

It should be noted that the energy estimate in antibacterial band 0.2 - 0.3 μm has been made by calculation, using the ratio of voltage values in vacuum photocell "F-29" output for two spectral bands (0.12 - 0.3 μm and 0.28 - 0.3 μm) and Plank curves, because of absence of equipment for pulse UV radiation energy measurement. MPC output plasma is supposed behave as an absolutely black body.

The designed models of antibacterial irradiator based on MPC have been used for medical biological investigations.

Microorganisms Staphylococcus epidermis have been processed by UV radiation. The results of such acting have been compared with similar acting of a mercury lamp "DRT-230". The mercury lamp has been distanced on 0.2 m and 1 m from irradiated Petry caps with microorganisms. The samples of irradiators based on MPC with condenser capacity C = 200 μF and 600 μF have been distanced on 0.2 m.

The results of microbiological analysis are shown on the diagram of ratio N_{fin}/N_0 (N_{fin} is the number of survived microorganisms, N_0 - the early number of microorganisms) dependence upon summery irradiation dose D [J/m^2] in the band of 0.22 - 0.28 μm (Fig. 1).

Table 1

The energy store parameters	C = 200 μF U = 3 kV W_O = 900 J	C = 300 μF U = 3 kV W_O = 1350 J	C = 600 μF U = 3 kV W_O = 2700 J
Plasma discharge parameters	$I_{discharge}$ = 100 - 120 KA $T_{pl.\,rad.}$ = 11200 K	$I_{discharge}$ = 200 - 210 KA $T_{pl.\,rad.}$ = 12000 K	$I_{discharge}$ = 220 – 250 KA $T_{pl.\,rad.}$ = 12500 K
Parameters of radiation	$W_{0,33..10}$ = 112 J τ=24 μs $W_{rad\,\Sigma}$= 196 J $W_{0,2..0,3}$ = 46.1 J $P_{0,2..0,3}$ = 2 MW $\eta_{uv} = W_{0,2..0,3} / W_O$ = 0.051	$W_{0,33..10}$ = 229 J τ=30 μs $W_{rad\,\Sigma}$= 432 J $W_{0,2..0,3}$ = 109.1 J $P_{0,2..0,3}$ = 3.6 MW $\eta_{uv} = W_{0,2..0,3} / W_O$ = 0.081	$W_{0,33..10}$ = 478 J τ=40 μs $W_{rad\,\Sigma}$= 956 J $W_{0,2..0,3}$ = 248.6 J $P_{0,2..0,3}$ = 6.2 MW $\eta_{uv} = W_{0,2..0,3} / W_O$ = 0.092

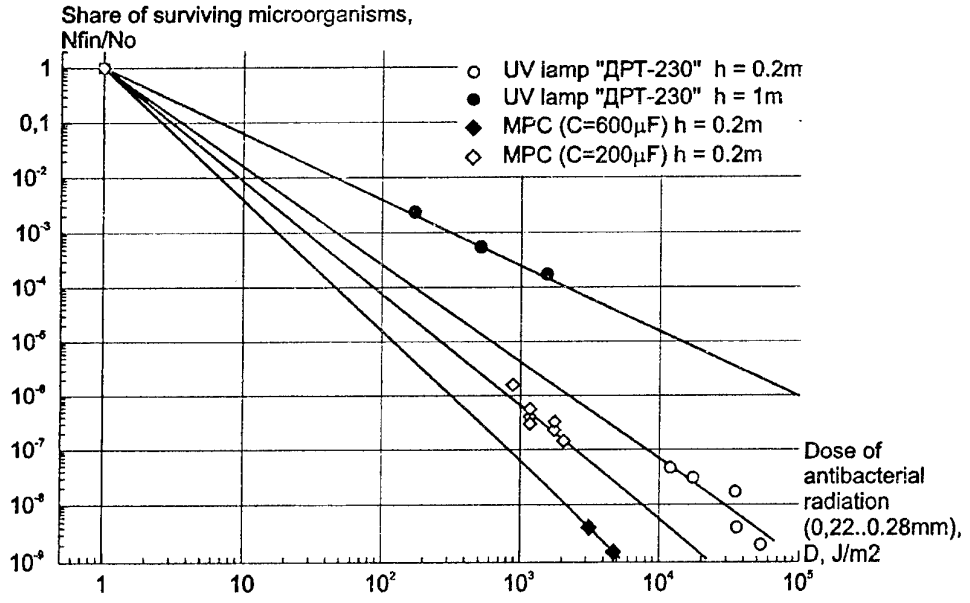


Fig. 1

For "DRT-230" the summery irradiation dose has been defined as product of radiation time and UV radiation power density in the band of 0,22 - 0,28 μm (has been measured by band spectroradiometer "SRP-85").

The summery radiation dose for irradiator based on MPC has been defined as a product of antibacterial radiation pulse energy (in the band of 0.22 - 0.28 μm) and number of MPC discharges.

It is easy to define that the change of necessary dose of radiation D depends on radiation power density q_p.

The necessary radiation dose D depending on radiation power density q_p for $N/N_0 = 10^{-6}$ and 10^{-8} is given in Fig. 2.

The increase of pulse power UV radiation as it has been shown leads to significant reduction of necessary radiation dose, time of disinfection and electric energy consumption.

It is necessary to compare UV irradiator based on MPC and mercury lamp "DRT-230". The distance from the processable surface is H = 0.2 m and disinfection level is $N_{fin}/N_0 = 10^{-8}$ (only one living organism left out of 10^8). Such values N_{fin}/N_0 have been realized in our research.

The irradiator allows to reduce radiation dose by 10 times as less, processing time by 8 times, and consumption of electrical energy by 20 times as less.

The usage of MPC as a UV radiation source has an

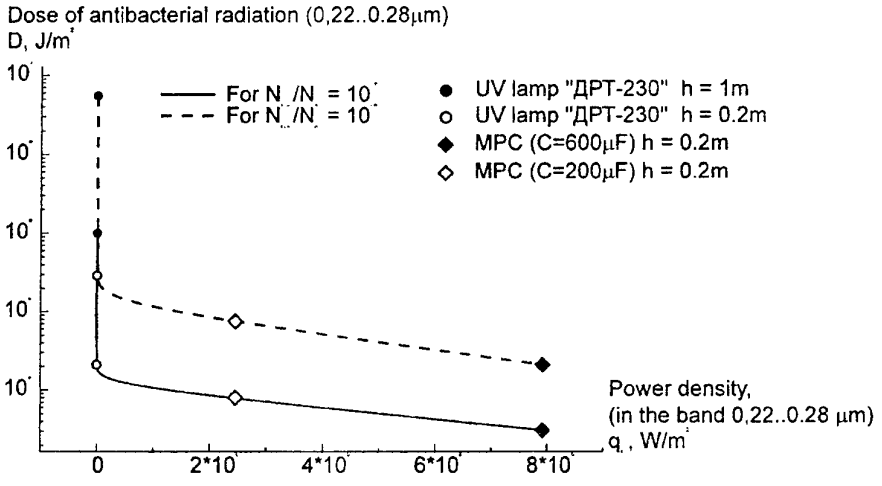


Fig. 2

additional antibacterial factor such as formation of ozone. Ozone content after 20 MPC discharges for C = 200 μF is 0.2 mg/m^3 .

The research shows that creation of high efficiency and economic antibacterial irradiator based on MPC is possible. It can be used for solving of such problems:

- air disinfection;
- disinfection of grain and vegetable storehouse;
- disinfection of packages and tanks at pharmaceutical and food-stuff industry;
- processing of food-stuff and agricultural products.

In conclusion it is necessary to note that antibacterial processing efficiency can be increased by the designing of combined UV and microwave radiation source. It was shown that simultaneous action of pulse UV radiation and pulse nanosec microwave radiation at 600 MHz and 1200 MHz allow to increase the efficiency of antibacterial processing.

REFERENCES

1. Meyer A., Zeyts E., Ultraviolet radiation. German Transl., Moscow, Foreign Literature Publish., 1952 [in Russian].
2. Kamrukov A.S. et al, Patent No RU 2001629 5A 61L 2/10, 30.10.93. Methods of desinfection and sterilization of open surfaces, liquids, and air [in Russian].

AN INCREASE OF POWER EFFICIENCY OF A MICROWAVE GENERATOR FOR MICROWAVE PROCESSING OF MATERIALS

V. I. Vodotovka, K. N. Gura, F. M. Repa

National Technical University of Ukraine,
Department of Theoretical Principles of Radio Engineering
12, Politechnicheskaja str., Kiev, 252056, Ukraine, Phone/Fax: 380-44-441-12-71

Now microwave energy is widely used for technological purposes – drying of vegetables, fruits, preparation of food, welding of dielectric materials, etc. The broad spectrum of experimental and plant installations realizing microwaves technological processes [1] is developed. Their wider spreading is stipulated by a possibility of deriving high quality final product with essential saving of power consumption.

To derive a high level of electromagnetic field intensity in the camera of technological heating the cavity resonators, through which treated materials are transported, are used. However, variable character of resonator load infringes matching of microwave generator with cavity resonator, reducing power saving of technological device.

The following methods to ensure the maximum intensity in a cavity resonator are known now:

– a three probes system to measure the electrical field heterogeneity along microwave tract and its alignment with the help of regulating device, for example, such as step drives ensuring [2] step by step immersing of a probe in a waveguide, achieving required compensatory phase and amplitude for a reflected wave;

– regulating system of a rotated slice transversally installed in a over-size waveguide of the П-cross-section to align phase and amplitude of reflected wave from cavity resonator, which smoothly realizes compensation for large reflections;

– systems of three-probes section placed on a distance of $\lambda/2$ from each other with three probes located from each other on a distance of $\lambda/6$ and being immersed in a waveguide by means of a controlling drives [3];

– using as the detector of a reflected wave a galvanomagnetic converter, analog signal of which, is used for operation of executive compensatory device.

These devices are not only the equalizers of the matching load and generator, but also serve to protect a high power microwave generator from overloads.

Fig. 1 represents the block diagram of system of automatic frequency control (AFC) of microwave generator on resonance frequency of cavity resonator promoting a maximum microwave power take off for technological purposes, realizing advantages of power saving.

The AFC system contains a microwave generator *1* with the block of frequency control *2*, to the output of which through the first quadrature phase shifter *3* the balance modulators of co-phase *4* and quadrature *5* signals are connected. The outputs of modulators are connected to arms of double waveguide T-junction *6*, one outputs of which through a circulator *7* is connected to cavity resonator *8*, containing a load *9* and a balance mixer *10*, the second input of which is connected to the second output of double waveguide T-junction *6*. To the output of the balance mixer *10* joint selective amplifier *11*, peak detector *12*, low frequency amplifier *13*, phase detector *14* and integrator *15*, which output is connected to the block *2* of frequency control of the microwave generator *1* are connected in series. The low frequency generator *16* through the second quadrature phase shifter *17* is connected to the biport switch *18*, controlling input of which is connected to an output of the generator *16* through a frequency divider *19*. The outputs of the biport switch *18* are connected to controlling inputs of balance modulators of co-phase *4* and quadrature *5* signals, and the controlling input of the phase detector *14* is connected to an output of frequency divider *19*.

The operation of the AFC system is as follows.

A microwave signal $U_1(t) = U_{m1}\cos(\omega t + \varphi)$ is modulated on amplitude by a low frequency harmonic signal $U_2(t) = U_{m2}\cos(\Omega t + \vartheta)$. Simultaneously microwave signal is shifted on phase on 90° $U3(t) = U_{m3} \cdot \sin(\omega t + \vartheta)$, and modulated on amplitude by shifted on 90° low frequency signal $U_4(t) = U_{m4}\sin(\Omega t + \vartheta)$. The low frequency is selected equal to an approximately half of passband $\Delta\omega$ of the loaded cavity resonator, that is $\Omega \approx \Delta\omega/2$.

So two amplitude-modulated signals are derived

$$U_5 = U_m\left\{\cos(\omega t + \varphi_1) + \frac{m}{2}\cos[(\omega \mp \Omega)t + \varphi \mp \vartheta]\right\}, \quad (1)$$

$$U_6(t) = U_m\left\{\sin(\omega t + \varphi_1) + \frac{m}{2}\cos[(\omega \mp \Omega)t + \varphi \mp \vartheta]\right\}, \quad (2)$$

where U_m – voltage of carrier oscillations; m – factor of depth of peak modulation.

The component of difference frequency $\omega_1 = \omega - \Omega$ with phase $\varphi_1 = \varphi - \vartheta$ represents a signal of the lower side band frequency of a resonator on characteristic

frequency $\omega_0 = \omega$ and component of sum frequency $\omega_2 = \omega + \Omega$ and phase $\varphi_2 = \varphi + \vartheta$ – signal of the upper side band frequency. The modulated signals (1) and (2) are being summarized and subtracted each other. As a result the signals with suppressed one of the side frequencies are derived

$$U_7(t) = U_m'[\cos(\omega t + \varphi_3) + \frac{m}{2}\cos(\omega_1 t + \varphi_1)], \quad (3)$$

$$U_8(t) = U_m''[\cos(\omega t + \varphi_4) + \frac{m}{2}\cos(\omega_2 t + \varphi_2)], \quad (4)$$

where U_m', U_m'' – amplitudes of carrier oscillations voltages; φ_3, φ_4 – initial phases of carrier oscillations.

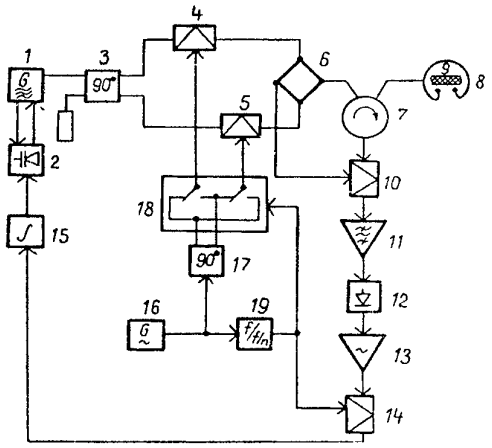


Fig. 1. A block diagram of the system of automatic frequency control

The depth of peak modulation of microwave oscillations is chosen in limits of m = 0.05...0.1, in this case the main power of microwave signal is concentrated in carrier oscillations of frequency ω.

At first the cavity resonator is being excited by sum signal (3), and reflected signal is being selected

$$U_9(t) = U_m'[\rho\cos(\omega t + \varphi_3 + \Delta\varphi_3) + \rho_1\frac{m}{2}\cos(\omega_1 t + \varphi_1 + \Delta\varphi_1)], \quad (5)$$

where ρ, ρ_1 – modules of reflectivity for frequencies ω and ω_1 correspondingly; $\Delta\varphi_1, \Delta\varphi_3$ – additional phase shifts of signals for their reflection from cavity resonator frequencies ω and ω_1 correspondingly.

The reflectivity module depends on cavity resonator mistuning on frequency ω and ω_1

$$\rho = \frac{\sqrt{4\rho_0^2 + (1+\rho_0)^2 a^2}}{\sqrt{4 + (1+\rho_0)^2 a^2}}, \rho_1 = \frac{\sqrt{4\rho_0^2 + (1+\rho_0)^2 a_1^2}}{\sqrt{4 + (1+\rho_0)^2 a_1^2}}, \quad (6)$$

where ρ_0 – reflectivity for a resonance ($\omega = \omega_0$); $a = 2Q\Delta\omega/\omega_0$ and $\Delta\omega = \omega - \omega_0$ – generalized and absolute cavity resonator mistuning on frequency ω_1; Q – quality factor of a cavity resonator; $a_1 = 2Q\Delta\omega_1/\omega_0$ and $\Delta\omega_1 = \omega_1 - \omega_0$ – generalized and absolute cavity resonator mistuning on frequency ω_1.

Further the microwave signal (5) reflected from the cavity resonator is mixed with the difference signal (4), and from resulting signal low frequency oscillations of the double modulation frequency are selected

$$U_{10} = S_1/4 \cdot \rho_1 K_1 m U_m' U_m'' \cos(2\Omega t + \varphi_5), \quad (7)$$

where S_1 – performance rate of change of the mixer; K_1 – factor of filtration by low frequency selective amplifier; φ_5 – resulting phase of low frequency signal.

Then the low-frequency signal (7) is detected and its voltage is measured

$$U_{11} = S_1 S_2/4 \cdot \rho_1 K_1 m U_m' U_m'', \quad (8)$$

where S_2 – transformation rate of change of the peak detector.

Then cavity resonator is excited by the difference signal (4), and the reflected signal is selected

$$U_{12} = U_m''[\rho\cos(\omega t + \varphi_4 + \Delta\varphi_4) + \rho_2\frac{m}{2}\cos(\omega_2 t + \varphi_4 + \Delta\varphi_4)], \quad (9)$$

where ρ_1, ρ_2 – reflectivity on frequencies and ω_2 correspondingly; $\Delta\varphi_2$, $\Delta\varphi_4$ – additional phase shifts for the reflections on frequencies ω and ω_2 correspondingly. The reflectivity for frequency ω_2 is

$$\rho_2 = \frac{\sqrt{4\rho_0^2 + (1+\rho_0)^2 a_2^2}}{\sqrt{4 + (1+\rho_0)^2 a_{21}^2}}, \quad (10)$$

where $a_2 = 2Q\Delta\omega_2/\omega_0$ and $\Delta\omega_2 = \omega_2 - \omega_0$ – generalized and absolute of cavity resonator mistuning on frequency ω_2. Further the microwave signal (9) reflected from the cavity resonator is mixed sum signal (3), and from resulting signal low frequency oscillations of double modulation frequency are selected

$$U_{13} = S_1/4 \cdot \rho_2 K_1 m U_m' U_m'' \cos(2\Omega t + \varphi_6), \quad (11)$$

where $\varphi_6 = \varphi_2 - \varphi_1 + \Delta\varphi_2$ – resulting phase of low frequency signal. Low frequency signal (11) is detected, and its voltage is measured

$$U_{14} = S_1 S_2/4 \cdot \rho_2 K_1 m U_m' U_m''. \quad (12)$$

Voltages of the low frequency signals (8) and (12) are compared, and a difference signal is formed

$$U_{15} = S_1 S_2 / 4 \cdot K_1 K_2 m U'_m U''_m (\rho_1 - \rho_2), \quad (13)$$

where K_2 – conversion (amplification) coefficient of resonance signal.

Changing the microwave generator frequency by difference signal up to the equality of voltages (8) and (12) being compared is reached, that is achieved for the equality reflectivities on side frequencies $\rho_1 = \rho_2$, or taking account cavity resonators reflectivities (6) and (10) on frequencies ω_1 and ω_2, we obtain

$$\frac{\sqrt{4\rho_0^2 + (1+\rho_0)^2 a_1^2}}{\sqrt{4 + (1+\rho_0)^2 a_1^2}} = \frac{\sqrt{4\rho_0^2 + (1+\rho_0)^2 a_2^2}}{\sqrt{4 + (1+\rho_0)^2 a_{21}^2}}. \quad (14)$$

From (14) it follows that the absolute values of generalized mistuning are equal to $|a_1| = |a_2|$ or

$$|\omega_1 - \omega_0| = |\omega_2 - \omega_0|. \quad (15)$$

As the side frequencies (ω_1 and ω_2) are changed synchronously with a changing of the microwave generator frequency, the last equality is satisfied under condition $|\omega - \Omega - \omega_0| = |\omega + \Omega - \omega_0|$, i.e. when the frequency of microwave generator ω coincides with characteristic frequency of cavity resonator ω_0.

Thus, frequency of microwave generator unequivocally follows the characteristic frequency of cavity resonator according to equality of products of two side frequencies microwaves signals, in which one of the signals is a reflected one from cavity resonator of one side frequency, the other – is a symmetrical one on frequency of the other side frequency. The inconstancy of absolute values of loaded cavity resonator reflectivities ρ_1 and ρ_2, and as well as inequality of amplitudes of mixed signals U'_m and U''_m, instability of mix (S1) and detecting (S2) performances and filtration factor (K1) do not influence to microwave generator tuning accuracy because the mentioned signals alternately are being processed by the same channel and amplifier.

The device operates as follows.

The microwave signal of the generator *1* is divided by 90° direct coupler *3* into two quadrature signals. Similarly low frequency signal of the generator *16* is divided by splitter *17* into two quadrature-modulating signals. In modulators *4* and *5* the peak modulation of microwave signals shifted on phase 90° by low frequency signals shifted, in its turn, also on 90° are carried out. As a result of summing of the modulated microwave signals in the double waveguide T-junction *6* signals with suppressed one-side frequencies will be derived. At one of the outputs of waveguide T-junction *6* sum signal with the lower side frequency will be derived, and at the other one – difference signal with the upper side frequency. The microwave signal modulated by such way, with one suppressed side frequency excites cavity resonator *8* with load *9*. Reflected microwave signal selected by circulator *7* is mixed up in the balance mixer (BM) *10* by microwave signal in which signal of other side frequency is suppressed.

With the help of automatic switch *18*, periodically, with a frequency of output voltage of frequency divider (FD) *19* the mutual substitution of modulating signals on the controlling inputs of modulators *4* and *5* is taken place. The mutual substitution of sum and difference microwave signals at the outputs of double waveguide T-junction *6* is occurred. As a results at FD output the packages of low frequency oscillations of the double modulation frequency will be derived, which amplitudes are proportional to reflectivity of cavity resonator *8* on different side frequencies. The packages of low frequency oscillations are selected and amplified by the selective amplifier *11*, adjusted on the double f modulation frequency. A series of oscillation packages with different amplitudes are detected by the peak detector *12*. The low frequency voltage with switching frequency of the switch *18* is amplified by the low frequency amplifier *13* and is compared on a phase with output voltage FD *19* by phase detector *14*.

Depending on a sign of cavity resonator *8* mistuning the envelope phase of the modulated signal selected by the selective amplifier *11* is changed. Therefore the polarity of output voltage of FD14, charging the integrator *15*, is determined by a sign of the loaded cavity resonator mistuning. The output voltage of the integrator influences to the frequency device controlling *2* of the microwave generator *1*.

As the frequency of the generator *1* coincides with the characteristic frequency of cavity resonator *8* (for example, resonance chamber for microwave heating) the peak modulation in signal of double frequency modulation is disappeared, and the charge of the integrator *15* by the voltage of this or that polarity is stopped, maximum microwave power take off from microwave generator for the technological purposes is ensured. For example, for microwave drying of fruits on average frequency 2.45 GHz with automatic frequency control the duration of process and, therefore, power savings were reduced in 2.7 times.

REFERENCES

1. Morosov G. A. Microwave technologies in industry and agriculture: modern achievement and new approaches // Antennas [in Russian]. – 1998. – № 1 (40). – P.88-95.
2. Van-Kafnet A.L. The automatic adjustment system for resonance systems of microwave heating //Journal of Microwave Power. – 1971. – V.6. – № 1. – P.25-30.
3. Yoshizako Yugi, Taniguchi Michelo. A microwave power source for the generator with automatic set-up of a transmitted power// Application UPV, MKI 5 H01 P5/04. – № 923047336. – Pub. 29.12.93.

PROBLEMS OF TECHNIQUE OF ORGANIZING ANTENNA LABORATORY COURSE

M. V. Andreev, O. O. Drobakhin, V. M. Morozov, D. Yu. Saltykov

Dnepropetrovsk State University,
13, per. Nauchny, 320625. Dnepropetrovsk, tel. (0562) 46-79-95

INTRODUCTION

Now our daily life is characterized by wide application of modern means of telecommunications. First of all satellite television and mobile communication means, including cellular ones, must be mentioned. The feature of this means is a wide usage of microwave electromagnetic waves especially of the range 11 – 12 GHz, which has elements with properties and construction distinct from more low frequencies ones in many respects. First of all, this fact concerns antenna devices. The pointed circumstances stipulate necessity of perfection of training the students of radiophysical specialty in the microwave antenna engineering. The learning of antenna engineering can not be restricted by only lecture course and requires such educational component as a laboratory experimental work. This situation is coursed by the following fact that the theoretical approaches allow only common tendencies of antenna devices behavior to be considered, but the problems of their practical tuning and application require experimental skills. In the paper the review of the contents of laboratory exercises with microwave antennas which have received implantation in educational process at a chair of microwave physics of Dnepropetrovsk State University is displayed.

LABORATORY EXERCISES DESCRIPTION

The laboratory practical work contains the following components under investigation: horn antennas, open-ended rectangular and circular waveguides, horn antennas with lenses, dielectric rod antennas, linear antenna arrays, reflector antennas, slotted waveguide antennas, transformers for matching of feeders. Total amount of a laboratory practical work makes 36 hours.

The first laboratory task is devoted to problems of study of both parameters and characteristics of antennas and methods of their measurements, requirements to antenna range, calculation of electromagnetic interference of reflections from range obstacles in geometrical optics approximation and optimal choice of antenna positions with the purpose of antenna range reflections influence reduction, estimation of a far-field region. The students should perform the relevant estimates for each concrete type of antennas under test. Such estimates form the basis for interpreting results of laboratory experimental results since the laboratory antenna range does not satisfy completely to all requirements for all types of antennas under test. The choice of a source antenna, its polarization in accordance with the type of the antenna under test is very important. The pyramidal horn antenna P6-23A was used as a source antenna. The measuring bench is founded on a scalar network analyzer R2-54, having microwave coaxial output. Traditionally, the scalar network analyzer has two directional couplers. The signal from the fundamental output of the directional coupler for an incident wave moves to the source antenna. The signal received by a receiving antenna under test is detected with the help of a detector waveguide section, the signal from which output on a low frequency cable moves to the second input of the analyzer, thus the second directional coupler is not used. It has allowed to boost processing signal power. The useful effect reaches due to low frequency modulation of microwave signal and usage of a synchronous detection in analyzer.

Studying an open-ended waveguide is represented by measurements of antenna pattern for a standard rectangular open-ended waveguide with cross-section 23×10 mm with a flange and without a flange. Supplementary to traditional antennas an open-ended waveguide with additional scatter in the form of vertical vibrator are considered. The open-ended waveguide is used as a power gain standard. A particular interest represents comparison of antenna patterns of open-ended waveguide and *E*-sectorial horn, for their sizes in the relevant plane are identical. The study of the open-ended waveguide with additional scatter is basis for study of a linear antenna array, since the antenna of that type is a feeding antenna for array. The necessity of experimental study of the open-ended waveguide with a flange and without a flange is stipulated by the application of this antenna in probing of dielectric structures. The antenna without a flange is more typical, however the open-ended waveguide with a flange ensures more short synthesized time pulses without additional oscillations apart from the main peak.

The set of horn antennas consists of a *E*-sectorial horn with section of feed waveguide of 23×10 mm and the set of H-sectorial horns with the dimensions 200×40×200 (horn 1), 200×23×375 (horn 2), 200×23×545 (horn 3), 260×10×310 (horn 4) mm. The presence of such number of horns allows one to test a requirement for optimal horn length by calculating and experimental way.

On the basis of horn antennas (1) – (4) a study of lens antennas is performed. The horn antenna (4) has two lenses of two types: dielectric and metal-plate. It allows ones to compare variation of directivity, width of a main beam antenna pattern and gain of antennas. For the antennas (2), (3) there is a dielectric lens, and for the antenna (1) – a metal-plate one with an additional metal plate in a *H*-plane. It allows students to study experimentally an influence of a polarization of electromagnetic wave reflection against orientation of a metal plate and necessity of reduction of vertical dimensions of a cell with the purpose of preventing originating of parasitic wave types. For horn antennas with lenses matching becomes very important, therefore measurements of reflectivity against frequency and choice of optimum frequencies must be performed. The calculation task is to determine the geometrical profile of dielectric and metal-plate lenses.

The dielectric rod antennas are represented by antennas on the basis of a circular waveguide with radius equals to 25 mm. The length of a dielectric rod was 75 mm and radius of the least section was 8 mm. The special interest represents measurement of antenna pattern with consequent calculation directivity factor and comparison of calculated value with a value obtained according to

$$D = 33000 / \theta_x \theta_y ,$$

where θ_x and θ_y are the width of main beam at 3 dB level in two orthogonal planes (in degrees). The considerable notice is given to testing a linear antenna array, which consists of nine open-ended waveguides. A sliding short-circuit plunger is disposed in each of waveguides. The construction provides a presence of relevant holders for each of the plungers. The open-ended waveguide with scatter, having very wide antenna pattern, is used as a feeding antenna. Thus, there is a reflective array with supply of an optical type. The students should calculate positions of plungers in each of the waveguides to scan of the main beam on a given angle. The calculation of a position of the plungers is carried out for several distances of the feed antenna up to the aperture plane. Thus the students should watch the profile of the plungers, which is close to parabolic. For observation and installation of plungers the waveguides have longitudinal slots and rulers. The evolution of the profile of plungers allows students to make the conclusion about displacement of a feed antenna from focus of a reflector antenna to provide of a main beam orientation in a desirable direction, which is distinct from normal to the aperture plane. Students can watch the decreasing gain and growing of the main beam width with increasing of scanning angle. The pointed effect is easily watched on a background of side lobes of the array stipulated by immediate direct reception by a feed antenna. The calculated and experimental task can be complicated by displacement of the feed antenna from center of the array. Students examine experimentally also antenna pattern versa variation of distance between the feed antenna and the aperture plane with the purpose of a choice of optimum distance.

A development of a satellite television and microwave relay communication lines requires study of reflector antennas. The paraboloid with a focal distance 13.8 see is used. A feed antenna is *H*-sectorial horn. This antenna is investigated under an electromagnetic radiation of both polarizations. The focal distance is calculated by students due geometrical measurements of the antenna sizes. The experimental tasks are measurements of antenna pattern and gain if feed antenna displaces from focus. For extremely small distance between the feed antenna and reflector the width of a main beam antenna pattern increases and beam splits itself. For distances more than focus one the reduction gain is displayed. Further subject of measurements of antenna pattern is measurements under displacement of the feed antenna from focus in the side. Thus the students should be convinced, that the main beam of antenna pattern is scan in the opposite side. The similar measurements have to be carried out for a reflector with larger sizes and with the same focal distance. The purpose of such experiment is to be convinced, that increasing the reflector sizes courses growing power gain.

Naturally the slotted waveguide antenna can be considered as an array of discrete radiators. The beam scanning is ensured by frequency sweeping. Measurement of VSWR versa frequency is important for such antenna.

The laboratory exercises are completed by study of the matching with the help of 4-element waveguide and strip transformers. The capacitive elements are used as discontinuities.

CONCLUSIONS

The generated laboratory practical work on microwave antennas allows the students to familiarize with the fundamental types of antennas, methods of their experimental investigation, to study the requirements to antenna ranges, to receive skills of operation with microwave equipment. To fix the material the testing questions are appeared at the end of each instruction. Feature of an arrangement of testing questions is their accidental order in comparison with presentation in theoretical part that induces the student more carefully to study a theoretical material.

ARCHITECTURE OF THE TEXTBOOK "ANTENNAS "

L. Y. Ilnitskiy, L. V. Sibruk, M. I. Fuzik

Kyiv international university of civil aviation. Kyiv-58, str. Komarova 1. 484-97-45

Learning antenna and feeder devices it is necessary to come from with certain classification. It is caused by that variety of construction aeriales devices is so great, that the learning of all existing aerials within the period of time, limited for educational discipline, simply is impossible. Besides it is not so necessarily, because for the certain groups of aerials by their correct selection it is possible to select general electrodynamic properties, principle of operation, characteristic design features, that enables to be limited to learning the separate specimens of a group.

The definition of such groups and detection of belonging of this or that aerial to a group, that is considered, depends on classification principles. A classification for a principle of operation now is widly used which in matching with other kinds of classifications allows precisely to relate aerials to various kinds and unambiguously define qualifying tags. Besides in such a system the qualifying tags are more homogeneous, than on the other principles of a classification. So for example, fulfilment of the qualifying system, which bases on division of aerials on ranges of waves causes misapprehend definitions which are stipulated by a working rang of waves, principle of operation, design features, by functional belonging and so on.

For much attention in this textbook is drawn to passive antennas so in a futher passive antennas radiating systems are considered. The readers inerested in active antennas, can acquaintance with the more complete classifications, which are resulted in the appropriate monographies.

The figure showes a classification, in which a principle of operation and design feature is the main tags.

According to this figure the contents of the textbook is offered:

- Definition of a radiation field on the given sources;
- Parameters and characteristics of aerials;
- Elementary radiators;
- Dipole antenna;
- Antenna system;
- Theory of aperture antennas;
- Influence of reflecting surfaces on antennas radiation;
- Theory of receiving antennas;
- Antennas synthesis;
- Linearly polarized linear antennas;
- Horn antennas;
- Lens antennas;
- Reflector antennas;
- Surface waves antennas;
- Circular polarization antennas ;
- Antenna with statistical amplitued – phase distribution (APD);
- Scanning arrays;
- Antennas with signal processing ;
- Aircraft antennas characteristics.

The textbook is base on the textbook by the authors of the theses "The theory of antennas".K.:KIUCA, 1996 and textbook by Ilnitskiy L.Y., Sibruk L.V. "Antennas".-K.:KIUCA, 1998. and is used for the students of radio engineering faculties of institutions, but will be useful to the scientists, post-graduate students and experts, which solve for problems aerial devices.

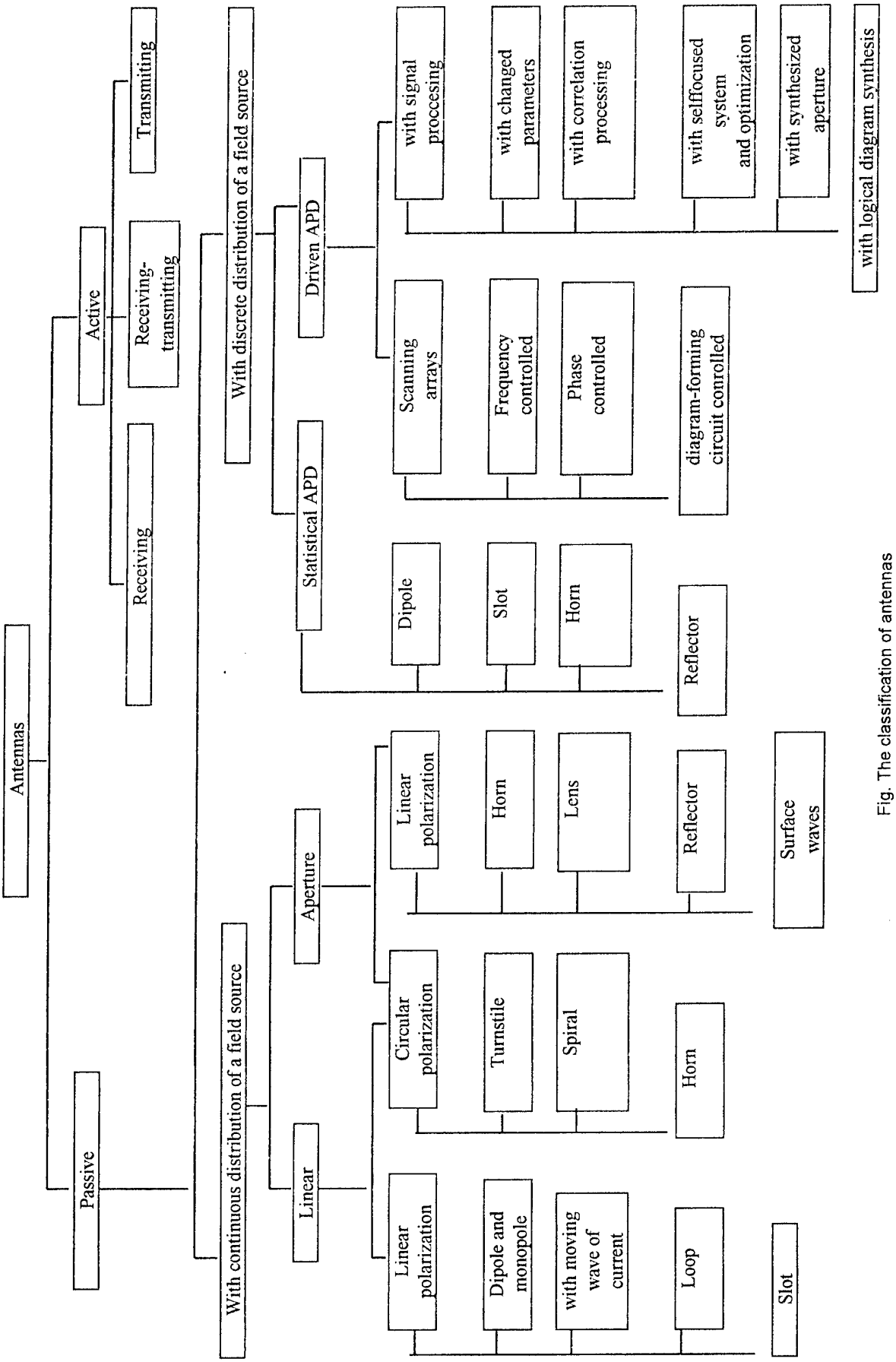


Fig. The classification of antennas